UNIVERSAL
LIBRARY

OU_158051

UNIVERSAL
LIBRARY

PEACEFUL USES OF ATOMIC ENERGY

UNITED NATIONS

OSMANIA UNIVERSITY LIBRARY

Call No. 539.96/In61P Accession No. 3609

Author International Conference --- Peaceful uses of Atomic Energy.

Title Proceedings. Vol. 5. 1956.

This book should be returned on or before the date last marked below.

PROCEEDINGS
OF THE
INTERNATIONAL CONFERENCE ON THE PEACEFUL USES OF ATOMIC ENERGY

Volume 5

PHYSICS OF REACTOR DESIGN

Proceedings of the International Conference

on the

Peaceful Uses of Atomic Energy

Held in Geneva

8 August-20 August 1955

Volume 5

Physics of Reactor Design

UNITED NATIONS

New York

1956

UNITED NATIONS PUBLICATIONS

Sales No. 1956.IX.1.Vol. 5

A/CONF.8/5

Price: US $9.00.; 63/–stg.; 39.00 Sw. frs.
(or equivalent in other currencies)

PREFACE

The Proceedings of the International Conference on the Peaceful Uses of Atomic Energy are published in a series of 16 volumes, as follows:

Volume Number	Title	Sessions Included
1	The World's Requirements for Energy; The Role of Nuclear Power	2, 3.2, 4.1, 4.2, 5, 24.2.
2	Physics; Research Reactors	6A, 7A, 8A, 9A, 10A.1.
3	Power Reactors	10A.2, 3.1, 11A, 12A, 13A, 14A.
4	Cross Sections Important to Reactor Design	15A, 16A, 17A, 18A.
5	Physics of Reactor Design	19A, 20A, 21A, 22A, 23A.
6	Geology of Uranium and Thorium	6B, 7B.
7	Nuclear Chemistry and the Effects of Irradiation	8B, 9B, 10B, 11B, 12B, 13B.
8	Production Technology of the Materials Used for Nuclear Energy	14B, 15B, 16B, 17B.
9	Reactor Technology and Chemical Processing	7.3, 18B, 19B, 20B, 21B, 22B, 23B.
10	Radioactive Isotopes and Nuclear Radiations in Medicine	7.2 (Med.), 8C, 9C, 10C.
11	Biological Effects of Radiation	6.1, 11C, 12C, 13C.1.
12	Radioactive Isotopes and Ionizing Radiations in Agriculture, Physiology and Biochemistry	7.2 (Agric.), 13C.2, 14C, 15C, 16C.
13	Legal, Administrative, Health and Safety Aspects of Large-Scale Use of Nuclear Energy	4.3, 6.2, 17C, 18C.
14	General Aspects of the Use of Radioactive Isotopes; Dosimetry	7.1, 19C, 20C.
15	Applications of Radioactive Isotopes and Fission Products in Research and Industry	21C, 22C, 23C.
16	Record of the Conference	1, 24.1, 24.3.

These volumes include all the papers submitted to the Geneva Conference, as edited by the Scientific Secretaries. The efforts of the Scientific Secretaries have been directed primarily towards scientific accuracy. Editing for style has been minimal in the interests of early publication. This may be noted especially in the English translations of certain papers submitted in French, Russian and Spanish. In a few instances, the titles of papers have been edited to reflect more accurately the content of those papers.

The editors principally responsible for the preparation of these volumes were: Robert A. Charpie, Donald J. Dewar, André Finkelstein, John Gaunt, Jacob A. Goedkoop, Elwyn O. Hughes, Leonard F. Lamerton, Aleksandar Milojević, Clifford Mosbacher, César A. Sastre, and Brian E. Urquhart.

The verbatim records of the Conference are included in the pertinent volumes. These verbatim records contain the author's corrections and, where necessary for scientific accuracy, the editing changes of the Scientific Secretaries, who have also been responsible for inserting slides, diagrams and sketches at appropriate points. In the record of each session, slides are numbered in numerical order through all presentations. Where the slide duplicates an illustration in the submitted paper, appropriate reference is made and the illustration does not appear in the record of the session.

Volume 16, "The Record of the Conference," includes the complete programme of the Conference, a numerical index of papers and an author's index, the list of delegates, the records of the opening and closing sessions and the complete texts of the evening lectures.

TABLE OF CONTENTS

Session 19A: Integral Measurements

			Page
P/661	Antonov *et al.*	Neutron Diffusion by the Impulse Method	3
P/662	Geraseva *et al.*	Beryllium as a Neutron Moderator	13
P/359	Koechlin *et al.*	Thermal Diffusion Length of BeO	20
P/872	Ramanna *et al.*	Measurements of L^2 and τ for H_2O and Be	24
P/358	Duggal, Martelly	Slowing Down of Neutrons in Graphite	28
P/928	Bustraan, Van Duuren	Neutron Density Distribution in Cylinder	37
P/360	Raievski, Horowitz	Measurements of λ_{th} in a Solid	42
P/789	Sjöstrand	Pulsed Measurements on a Subcritical Reactor	52
P/933	Barendregt, Bustraan	Capture to Fission Ratio in Uranium	55
P/597	Wilkins *et al.*	Neutron Slowing Down in Hydrogeneous Media	62
P/357	Jacrot *et al.*	Inelastic Scattering of Slow Neutrons	77
Record of Session			82

Session 20A: Resonance Integrals; Fission Product Poisoning; Criticality of Solutions

P/659	Spivak *et al.*	Resonance Integrals and Resonance Fission	91
P/833	Macklin, Pomerance	Resonance Capture Integrals	96
P/427	Crocker	Resonance Absorption in U^{238}	102
P/883	Eriksen *et al.*	Measurements of the Resonance Integral of Uranium	105
P/948	Van der Held	Computation of the Resonance Integral	107
P/5	Hurst	Characteristics of the NRX Reactor, Part I	111
P/6	Ward	Characteristics of the NRX Reactor, Part II	119
P/835	Spinrad *et al.*	Reactivity Changes in Fixed Fuel Thermal Reactors	125
P/432	Littler	Long Term Reactivity Changes	141
P/834	Callihan *et al.*	Criticality in Solutions	145
P/428	Horton, McCullen	Plutonium-Water Critical Assemblies	156
P/602	Snyder	The Critical Assembly—A Nuclear Design Tool	162
Record of Session			172

Session 21A: Zero Energy and Exponential Experiments

P/600	Kouts *et al.*	Exponential Experiments in Light Water	183
P/601	Krasik, Radkowsky	PWR Critical Experiments	203
P/603	Chernick	Theory of Uranium Water Lattices	215
P/604	Radkowsky, Krasik	Physics Aspects of the PWR	229
P/790	Persson *et al.*	An Exponential Pile of Uranium and D_2O	239
P/791	Hellstrand *et al.*	The Swedish Heavy Water Reactor	242
P/361	Horowitz	Neutron Studies in Heavy Water	256
P/605	Cohen	Exponential Experiments on D_2O Uranium Lattices	268
P/920	Gallone, Salvetti	Calculations for a D_2O—Natural U Reactor	279
P/429	Mummery	Experimental Basis of Lattice Calculations	282
P/607	Gast	Normal Uranium, Graphite Moderated Reactors	288

			Page
P/606	Kaplan, Chernick	Uranium Graphite Lattices– The BNL Reactor	295
P/599	Davenport	Exponential Experiments in Graphite Systems	309
Record of Session			317

Session 22A: Zero Energy Experiments on Fast Reactors and Reactor Kinetics

P/404	Holmes *et al.*	Experimental Studies on Fast Reactors	331
P/598	Beyer *et al.*	Fast Exponential Experiment	342
P/609	Okrent *et al.*	Fast Reactor Physics	347
P/775	Lipkin, Thieberger	Stability Conditions for Heterogeneous Reactors	364
P/934	Pelser	Transfer Function of a D_2O Reactor	367
P/334	Braffort	Kinetic Problems of a Power Reactor	369
P/610	Welton	Kinetics of Stationary Reactor Systems	377
P/612	Gast	Experimental Checks of Control Rod Theory	389
P/434	Cox *et al.*	Reactor Instrumentation Systems	393
Record of Session			401

Session 23A: Reactor Theory

P/611	Cohen	Neutron Thermalization Theory	405
P/433	Tait	Fine Structure of Thermal Flux	417
P/608	Hurwitz, Jr., Ehrlich	Theory and Experiment for Intermediate Assemblies	423
P/430	Mandl, Howlett	Critical Mass of Intermediate Reactor	433
P/665	Bat	Heterogeneous Reactors with Few Blocks	437
P/937	Woldringh	Fermi Age Treatment for Homogeneous Reactor	440
P/916	Schmid	Diffusion Theory for Multiple Reflector Spherical Reactor	444
P/647	Galanin	Moderating Neutrons in Two-Group Theory	448
P/664	Galanin	Effective Boundary for Calculating Critical Dimensions	451
P/431	Ackroyd	Critical Size, One-Group Diffusion Theory	454
P/663	Galanin	Critical Size of Heterogeneous Reactor	462
P/649	Gurevich, Pomeranchouk	Resonance Absorption in Heterogeneous Systems	466
P/613	Goertzel	Doppler Effect in Intermediate and Fast Reactors	472
P/666	Galanin	Thermal Coefficient in Heterogeneous Reactor	477
P/669	Feinberg	Heterogeneous Methods for Calculating Reactors	484
P/1003	Gamba *et al.*	Uranium-Beryllium Lattices in Cylindrical Reactors	501
P/656	Ussachoff	Neutron Reactor Kinetics and Perturbation	503
P/668	Galanin	Thermal Reactor Regulators' Efficiency	511
P/796	Trlifaj	Solution of Milne's Problem	515
P/655	Bat, Zaretsky	Solution of Generalized Milne Problem	519
P/667	Zaretsky	Effective Boundaries for "Grey" Bodies	525
Record of Session			531

Session 19A

INTEGRAL MEASUREMENTS

LIST OF PAPERS

		Page
P/661	A study of neutron diffusion in beryllium, graphite and water by the impulse method ..... A. V. Antonov *et al.*	3
P/662	The study of beryllium as a neutron moderator ..... L. A. Geraseva *et al.*	13
P/359	Measurements of the diffusion length of thermal neutrons in beryllium oxide ..... J. C. Koechlin *et al.*	20
P/872	On the determination of diffusion and slowing down constants of ordinary water and beryllium oxide using a pulsed neutron source ..... R. Ramanna *et al.*	24
P/358	A study of the slowing down of neutrons in graphite ..... V. P. Duggal and J. Martelly	28
P/928	Thermal neutron density distribution inside and outside infinite long cylindrical samples ..... M. Bustraan and K. van Duuren	37
P/360	Determination of the mean transfer free path of thermal neutrons by measurement of the complex diffusion length ..... V. Raievski and J. Horowitz	42
P/789	Measurements on a subcritical reactor with a pulsed neutron source ..... N. G. Sjöstrand	52
P/933	Determination of neutron capture to fission ratio in various uranium samples ..... T. J. Barendregt and M. Bustraan	55
P/597	Status of experimental and theoretical information on neutron slowing down distributions in hydrogenous media ..... J. E. Wilkins *et al.*	62
P/357	Time-of-flight spectrometry equipment for slow neutrons in use at the Saclay reactor—its application to a study of the inelastic scattering of cold neutrons ..... B. Jacrot *et al.*	77
P/1132	Production and neutron absorption of nuclear graphite (This paper appears in Session 16B.2, Vol. 8.) ..... K. Wirtz	

A Study of Neutron Diffusion in Beryllium, Graphite and Water by the Impulse Method

By A. V. Antonov, A. I. Isakoff, I. D. Murin, B. A. Neupocoyev, I. M. Frank, F. L. Shapiro, and I. V. Shtranich, USSR

Up to recent times most of the investigations of thermal neutron diffusion were carried out by studying the stationary distribution of the density of neutrons obtained from constant sources. The diffusion length, L, was the quantity directly measured in these studies, the diffusion coefficient D or neutron free lifetime T usually being determined indirectly.

Direct measurements of the lifetime of free neutrons in matter are sparse and often are of the nature of control measurements.[1,2]

Only in recent years some investigations have been carried out independently of us[3,4,5] in which pulsed-neutron sources were used to study neutron diffusion. In these experiments water was the substance investigated.

The quantity directly measured in experiments with pulsed-neutron sources is the decay of the neutron density. In these cases the experimental results depend on the diffusion coefficient D. This enables one to measure the diffusion coefficient with an accuracy of several per cent and the method is, therefore, not only simpler but also considerably more accurate than the conventional stationary diffusion methods.

The non-stationary diffusion method, moreover, permits one to approach the problem of investigating the final stage of slowing down of neutrons and to study the dependence of the diffusion coefficient D on the conditions under which the neutron gas exists. These features of neutron diffusion have not been extensively investigated as yet, although they are of importance for a number of problems in neutron physics.

A second characteristic feature of the non-stationary diffusion method is related to the dimensions of the experimental system. It will be seen from the following exposition that requirements similar to those encountered in the well known exponential pile method concerning the distance between the source and detector also exist in the given case; in this case, however, they apply to the time interval between generation of the neutrons and their detection. Therefore the dimensions of the system need not be large along any of the three coordinate axes. Thus the usual prism can be replaced by a cube. In some cases the possibility of reducing the amount of substance necessary for the experiments may be of practical importance.

Original language: Russian.

In the present investigation measurements were carried out on the diffusion coefficients of beryllium, carbon and water. Simultaneously, the dependence of D on the dimensions of the moderator could be determined; this dependence is caused by displacement of the thermal equilibrium of the neutron gas due to escape of the neutrons from the moderator. For water, the dependence of D on temperature of the water was also determined. The neutron absorption cross section in water is quite large and thus the neutron lifetime T, and the diffusion length L could be reliably measured in this substance. In order to measure these quantities in substances which absorb neutrons weakly (such as Be or C) the dimensions of the system must be correspondingly increased. Nevertheless the amount of material necessary for the measurements still remains much smaller than that required in the pile method. L and T could also be determined from the experimental data obtained for graphite; in the beryllium experiments the dimensions employed were insufficient to permit accurate evaluation of these constants.

THEORY OF THE METHOD

It will be assumed that the sample of the slowing-down substance is irradiated by a short (practically instantaneous) burst of fast neutrons. After a certain interval of time the neutrons in this sample will be slowed down to velocities close to thermal values and their behaviour will then be described by the diffusion equation

$$D\Delta n - \frac{n}{T} = \frac{\partial n}{\partial t} \qquad (2.1)$$

Here T is the mean neutron lifetime which is determined by absorption in the medium. For the substances investigated in the present work the $1/v$ law for the neutron absorption cross section can be considered valid and therefore T should be constant (at any rate as far as slow neutrons are concerned). The diffusion coefficient D may be considered a slowly varying function of time.

In order to separate the variables we seek a particular solution of Equation 2.1 in the form

$$n(x, y, z, t) = S(x, y, z)e^{-\frac{t}{T}}f(t) \qquad (2.2)$$

Thus, instead of Equation 2.1 we obtain

$$\frac{d}{dt}f(t) = -\Omega D(t)f(t) \tag{2.3}$$

$$\Delta S(x, y, z) = -\Omega S(x, y, z) \tag{2.4}$$

The general solution should therefore be of the form

$$n(x, y, z, t) = \sum_{l=1}^{\infty}\sum_{m=1}^{\infty}\sum_{n=1}^{\infty} A_{lmn}S_{lmn}(x, y, z) \times e^{-\left(\frac{t}{T}+\Omega_{lmn}\int_0^t D(t)dt\right)} \tag{2.5}$$

where the A_{lmn} depend on the initial conditions and S_{lmn} and Ω_{lmn} are, respectively, the eigen functions and eigenvalues of Equation 2.4 for the given boundary conditions. The boundary conditions are obtained by assuming that the neutron density and hence $S_{lmn}(x, y, z)$ are zero on the extrapolated boundary of the moderator, that is, at a distance $0.71\lambda_t$ beyond the geometrical borders of the sample. Thus for a given transport mean free path λ_t possible values of Ω_{lmn} are determined by prescribing the size and form of the investigated substance.*

As can be seen from Equation 2.5 the neutron density can be represented as the sum of a series of exponential terms; in each of these terms the exponents contain (with a minus sign) the following quantity

$$\alpha_{lmn}t = \Omega_{lmn}\int_0^t D(t)\,dt + \frac{t}{T} \tag{2.6}$$

For the future it will be important to separate out the first term of the expansion of Equation 2.5 which contains the smallest α and therefore which decays slower than any other term. It is not difficult to determine the necessary conditions for such separation to be possible. Let us suppose that slowing down of neutrons in the investigated substance can be described by Fermi's Age Equation

$$\Delta q = \frac{\partial q}{\partial \tau} \tag{2.7}$$

where q is the neutron slowing-down density.

Neglecting the dependence of λ_t on energy, the solution of Equation 2.7 will have the form

$$q(\tau) = \sum_{l=1}^{\infty}\sum_{m=1}^{\infty}\sum_{n=1}^{\infty} B_{lmn}S_{lmn}(x, y, z)e^{-\Omega_{lmn}\tau} \tag{2.8}$$

where as before $S_{lmn}(x, y, z)$ and Ω_{lmn} are the proper functions and proper values of Equation 2.4 for the same boundary conditions. Coefficients B_{lmn} are defined by the initial distribution of the fast neutrons. As the neutron slowing-down density at age τ (corresponding to slowing down to nearly thermal velocities) is the initial diffusion distribution one should put

$$B_{lmn}e^{-\Omega_{lmn}\tau} = A_{lmn} \tag{2.9}$$

Inserting Equation 2.9 into Equation 2.5 we find that the relative magnitude of the terms of the series defining $n(x, y, z, t)$ is proportional to the quantities B_{lmn} and depends on the power exponents

$$\alpha_{lmn}'t = \Omega_{lmn}\tau' + \frac{t}{T} \tag{2.10}$$

where τ' is the generalized neutron age

$$\tau' = \tau + \int_0^t D(t)\,dt \tag{2.11}$$

As one can evaluate the relative magnitude of coefficients B_{lmn} it should not be difficult to find such τ' and therefore such $t \geq t'$ which make all terms of the expansion negligible relative to the first term containing the lowest-valued $\Omega_{lmn} = \Omega$.

In this case

$$n(x, y, z, t) = C(x, y, z)e^{-\left(\frac{t}{T}+\Omega\int_0^t D(t)dt\right)} \quad (t > t') \tag{2.12}$$

If the investigated system has the form of a parallelepiped the quantity Ω will be given by the relation

$$\Omega = \frac{\pi^2}{4}\left(\frac{1}{a^2}+\frac{1}{b^2}+\frac{1}{c^2}\right) \tag{2.13}$$

where $2a$, $2b$ and $2c$ are the extrapolated lengths of the parallelepiped edges.

For a system of cylindrical shape

$$\Omega = \left(\frac{2.405}{R}\right)^2 + \frac{\pi^2}{4h^2} \tag{2.14}$$

where R is the extrapolated radius and $2h$ the extrapolated height of the cylinder. It can be seen from Equation 2.12 that at a time t, not sufficient for establishment of equilibrium between the neutron gas and the medium, ($D(t)$ still depends on time) the density will decay in accord with a law that differs from an exponential one. The process of establishment of equilibrium between the neutrons and the medium can be studied by investigating the initial phase of the decay process, as coefficient D is related in a definite manner to the velocity spectrum of the neutron gas.

With increasing time, D approaches a certain constant value, which is the equilibrium value for a given set of experimental conditions. This equilibrium quantity not only depends on the composition and temperature of the moderator substance but also on the escape of neutrons from the medium. Indeed, the quantity $D(v) = \lambda_t(v)v/3$ is a function of the neutron velocity and therefore the relative leakage of neutrons from the system will be different for neutrons of different velocity. This leads to the result that the neutron spectrum in the moderator will contain fewer neutrons for which the value of $D(v)$ is maximum. On the other hand, energy exchange between the neutrons and medium will tend to restore the thermal equilibrium distribution corresponding to the given temperature.

* If the sample dimensions are large compared with λ_t (only in this case are the equations written above valid) a knowledge of the precise value of λ_t will not be required beforehand. For the same reason, in determining the boundary conditions it may be considered that within certain limits λ_t is independent of velocity.

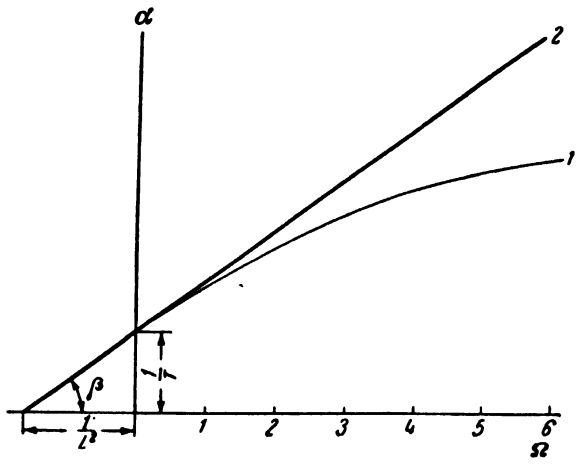

Figure 1. (1) Parabola $\alpha = 1/T + D_0\Omega - C\Omega^2$; (2) tangent to parabola 1 at point $\Omega = 0$ ($y = 1/T + D_0\Omega$). Angle coefficient of this straight line (tan β) is D_0

The equilibrium which is established as a result of the simultaneous action of these two factors leads to the result that in a finite medium the quantity D will be slightly smaller than the quantity D_0 for neutrons in thermal equilibrium. Neutron leakage is proportional to Ω (because $\Delta n = -\Omega n$, see Equation 2.4) and therefore D must be a function of Ω. It will be shown below that if D is close to D_0 the former will decrease linearly with increasing Ω. Thus in a finite system

$$D(\Omega) = D_0 - c\Omega \tag{2.15}$$

It follows from the foregoing that after $D(t)$ reaches its stationary value $D(\Omega)$ the neutron density will decrease exponentially as $e^{-\alpha t}$ and (see Equations 2.12 and 2.15)

$$\alpha = \frac{1}{T} + \Omega(D_0 - c\Omega) \tag{2.16}$$

In good moderators the exponential decay law becomes established in a sufficiently short time. If the measured value of α is plotted against Ω for various dimensions of the system one should expect from Equation 2.16 to obtain a quadratic relationship. With decreasing Ω (i.e., increasing dimensions of the system) this relation should tend to a linear one. The tangent of the slope of this asymptotic line should yield D_0, the ordinate intercept $1/T$ and the abscissa intercept $1/L^2$ (see Fig. 1).

As a matter of fact at large dimensions and for the substances investigated by us (Be, C and H_2O) the dependence of α on Ω was found to be almost linear. The quantities D_0, L^2 and T can be accurately obtained by α extrapolating as a function of Ω to zero, allowance being made for deviations from linearity. Simultaneously, the quantity can also be determined (see Equation 2.16).

Qualitatively, the question of dependence of $D(\Omega)$ on Ω can be elucidated if one considers the slowed down neutrons as a mixture of two groups of neutrons possessing different diffusion coefficients D. This means that as a first approximation one-group theory is replaced by a two-group theory.

In this case the diffusion equations take the form:

$$\left(D_1\Delta - \frac{1}{T} - \beta_1\right) n_1 + \beta_2 n_2 = \frac{\partial n_1}{\partial t} \tag{2.17}$$

$$\left(D_2\Delta - \frac{1}{T} - \beta_2\right) n_2 + \beta_1 n_1 = \frac{\partial n_2}{\partial t} \tag{2.18}$$

Here D_1 and D_2 are respectively the diffusion coefficients (D) for neutrons of the first and second groups, β_1 is the probability per unit time that, as a result of interaction with the medium, a neutron of group 1 makes a transition to group 2; β_2 is the probability of the inverse transition.

It will be assumed that the boundary conditions for neutrons of both groups are the same, namely, that the density is zero on the same extrapolated boundary that is considered in the one-group treatment.

Equations 2.17 and 2.18 can therefore be solved by using the same functions $S_{lmn}(x, y, z)$ and the same eigenvalues Ω_{lmn}.

At larger values of t it can be expected that the neutron density will be defined by partial solutions of Equations 2.17 and 2.18 corresponding to a minimal Ω. Then

$$n = n_1 + n_2 = S_0(x, y, z)e^{-\left(\frac{1}{T} + \frac{D_1+D_2}{2}\Omega + \frac{\beta_1+\beta_2}{2}\right)t} \times \{C_1 e^{-qt} + C_2 e^{+qt}\} \tag{2.19}$$

$$q = \frac{1}{2}(\beta_1 + \beta_2) \sqrt{1 + \frac{(D_1 - D_2)^2\Omega^2 + 2(D_1 - D_2)(\beta_1 - \beta_2)\Omega}{(\beta_1 + \beta_2)^2}} \tag{2.20}$$

Thus, variation of the neutron gas density can be described by the sum of two exponential terms of which one (having the exponent $-qt$) decays more rapidly than the other (with the exponent $+qt$). As can be seen from Equations 2.19 and 2.20, the rapidity of establishment of equilibrium between the two groups and the decay decrement in the exponential term (after equilibrium is reached) are related quantities and depend on D_1, D_2, β_1, β_2, Ω.

Let us suppose that equilibrium between the two groups is established, i.e., that the second exponential term can be neglected compared with the first. Assume now that equilibrium is established so rapidly that such values of Ω, are possible for which

$$\frac{|D_1 - D_2|\Omega}{\beta_1 + \beta_2} \leq 1 \tag{2.21}$$

This means that difference in neutron leakage of both groups is small compared with the rapidity of mixing of the two groups. In this case the quantity q can be expanded into a power series in Ω. For the decay coefficient in Equation 2.19 we then obtain

$$\alpha = \frac{1}{T} + \frac{\beta_2 D_1 + \beta_1 D_2}{\beta_1 + \beta_2}\Omega - \frac{\beta_1\beta_2(D_1 - D_2)^2}{(\beta_1 + \beta_2)^3}\Omega^2 + \frac{\beta_1\beta_2(\beta_1 - \beta_2)(D_1 - D_2)^3}{(\beta_1 + \beta_2)^5}\Omega^3 + \cdots \tag{2.22}$$

If Equation 2.21 is fulfilled the term involving Ω^3 will be small compared with the quadratic term and therefore can be neglected. The coefficient of the term involving in the first power Ω

$$D_0 = \frac{D_1\beta_2 + D_2\beta_1}{\beta_1 + \beta_2} \tag{2.23}$$

is simply the diffusion coefficient for thermal equilibrium as then $n_1/n_2 = \beta_2/\beta_1$. The function $D(\Omega)$ which thus follows from Equation 2.22 is the same as that encountered in Equation 2.15 if we put

$$c = \frac{\beta_1\beta_2(D_1 - D_2)^2}{(\beta_1 + \beta_2)^3} \tag{2.24}$$

The quantity c therefore essentially depends on the spread of D in various parts of the thermal neutron spectrum and is inversely proportional to the velocity of energy exchange between the neutrons and medium.

The linear relation between D and Ω obtained here is not connected with the validity of the two-group approximation. The same result qualitatively holds for a many-group treatment. The only essential assumption is that the neutron spectrum differs only slightly from the equilibrium spectrum.

Before proceeding to the experimental part of this work it should be mentioned that the pulsed-neutron method may yield useful results not only for moderators of finite (in all three directions) dimensions but also in connection with the large prism method. Suppose that the fast neutron source is located at $x = y = z = 0$ on the axes of a prism of rectangular cross section which is infinite along the x axis. The extrapolated prism dimensions along y and z are $2b$ and $2c$. It will be easy to find the dependence of the neutron density on the coordinates and time. We shall assume that slowing down of the neutrons in the prism material can be described by the age theory. Then after a certain time subsequent to initiation of the burst the dependence of the neutron density on the coordinates and time will be expressed by the equation

$$n(x, y, z, t) = \frac{A}{\sqrt{4\pi\tau'}} e^{-\left(\frac{x^2}{4\tau'} + \frac{\pi^2}{4}\left(\frac{1}{b^2} + \frac{1}{c^2}\right)\tau' + \frac{t}{T}\right)} \cos\frac{\pi}{2b} y \cos\frac{\pi}{2c} z \tag{2.25}$$

where τ' is the generalized neutron age (see Equation 2.11). As can be seen from Equation 2.25, for large x the relation between the neutron density and time is quite peculiar. For small values of time for which $x^2/4\tau' \gg 1$ the density will be small. At larger values of t it reaches a maximum and then begins to decrease due to an increase of the second and third terms in the exponent. This result shows that in prism studies the main role at any given distance from the source is played by neutrons whose generalized age is close to some definite value.

Let us suppose that the measurements are carried out in the same way they are performed in the usual type of exponential pile experiments, that is at two points but at a single time. From Equation 2.25 one then obtains

$$ln\frac{n(x_1)}{n(x_2)} = \frac{x_2^2 - x_1^2}{4\tau'} \tag{2.26}$$

Such measurements thus permit one to determine the neutron age. The dependence of t' on t should be linear for large values of t and $d\tau'/dt = D$, extrapolation of this straight line to $t = 0$ yields the effective age τ of neutrons slowed down in the given substance.

Simultaneously, from measurement of the neutron density decay at a given point the quantity T can easily be obtained. Thus the pulsed-prism method yields all the principal parameters describing the neutron behaviour in a moderator, i.e., τ, D and T.

EXPERIMENTAL ARRANGEMENT AND MEASUREMENTS

The neutron source was a high voltage (400 kev) pulsed ion accelerating tube which generated neutrons by the $D + T$ reaction. The duration of the fast neutron burst was about 6 μsec the repetition frequency 50–1000 cycles/sec. The system to be investigated was located in the vicinity of the target and a boron proportional counter was situated near the system. Cadmium sheets surrounding the system and counter shielded the latter from stray neutrons; in the water measurements B_4C shields were added. A proportional counter filled with BF_3 enriched with B^{10} was used to count the neutrons. The outer diameter of the counter was $d = 14$ mm, the counter length was 300 mm. In some of the measurements (with beryllium) a boron ionization-chamber was used.

The amplified counter pulses were fed to a pulse-height discriminator which removed the noise; the pulses were then shaped and fed into two identical one-channel time-analyzers. Both analyzers were synchronized with the pulsed-neutron source so that each of them began to operate simultaneously with initiation of the fast neutron burst. Counter pulses could be measured by each of the analyzers during a time interval t_2 which was delayed with respect to the fast neutron burst by t_1. The neutron counting time t_2 could be varied over a wide range; the usual values were $t_2 = 50$–200 μsec. Interval t_1 could be changed from 10 to several thousand microseconds. A special time-calibration circuit was used to measure t_1 and t_2, absolute accuracy of the measurements being 1%.

From the time-analyzers the pulses were fed into fast scalers and were finally recorded by an electromagnetic counter. Corrections for counting losses were introduced in the experimental results; the magnitude of this correction was determined experimentally. Even at the highest rates it did not exceed 3–4%.

Measurements with Beryllium

In the beryllium experiments the system had a rectangular shape. The target of the accelerating tube was placed opposite the center of the lateral surface of the prism at the distance of 5–7 cm from it. This ar-

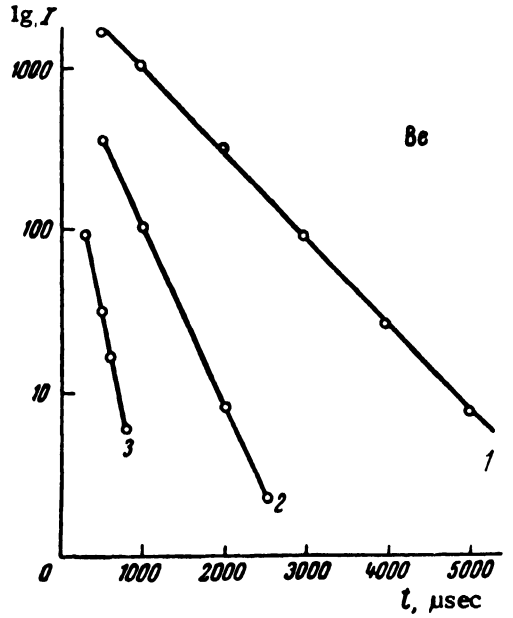

Figure 2. Density attenuation curves of thermal neutrons with time in beryllium prisms of various sizes: (1) for 60 × 60 × 56 cm³ prism (τ = 830 μsec); (2) for 40 × 40 × 32 cm³ prism (τ = 400 μsec); (3) for 20 × 20 × 20 cm³ prism (τ = 185 μsec)

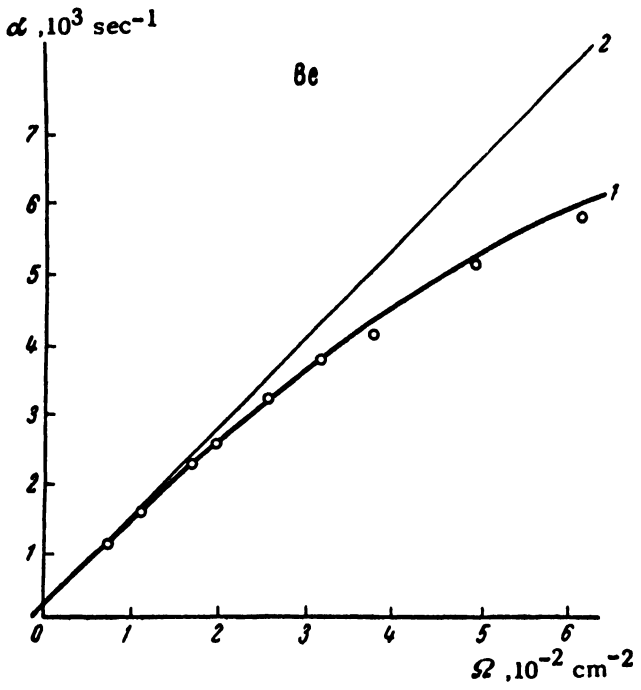

Figure 3. Dependence $\alpha = f(\Omega)$ for Be: (1) curve $\alpha = 1/T + D_0\Omega - C\Omega^2$; (2) tangent to 1 at point $\Omega = 0$. Experimental values for various sizes of prisms are shown by circles: 56 × 60 × 72, 56 × 60 × 60, 40 × 40 × 56, 40 × 40 × 40, 32 × 40 × 40, 32 × 32 × 32, 24 × 32 × 32, 20 × 32 × 32, 20 × 32 × 32, 20 × 20 × 20 cm³

rangement facilitated separation of the zero harmonic involved in Equation 2.5.

The density of the beryllium employed was ρ = 1.78 gm/cm³, deviations from this mean value being less than 0.5%. Prisms of 10 different sizes were used in the experiments (the dimensions are shown in Fig. 3 and also in Table I).

The time dependence of the counting rate (with respect to that of the monitor) is plotted in semi-logarithmic scale in Fig. 2 for prisms of three different sizes; corrections for counting losses were introduced in the curves.

In order to increase the accuracy, 4 or 5 measurements were made for each prism. As can be seen from Fig. 2 all experimental points satisfactorily lie on a straight line, even when the delay time is as small as 300 μsec. The graphs for other prisms differ from the one presented here only in respect to slope of the lines. This apparently signifies that 300 μsec (or even less) after the fast neutrons enter the prism all high harmonies die out and thus the solution of Equation 2 can be epresented by a single term—the zero harmonic; a stationary velocity distribution of the neutrons is already established by this time.

The mean thermal neutron lifetime $\tau = 1/\alpha$ for each prism was calculated from the slopes of the neutron density decay curves.

The values for the lifetime τ obtained in various series of experiments for prisms of the same size did not differ from each other by more than 1.5–2%.

In order to ascertain the effect due to stray neutrons an auxiliary experiment was carried out. In this experiment the distance between the target and prism was increased to 80 cm; however the slope of the graph did not change and this means that stray neutrons did not influence the experimental results. The graph of $\alpha = f(\Omega)$ (shown in Fig. 3) was plotted by

Table I

Substance and density	*Dimensions of system*	$D_0 \times 10^{-5}$ $\frac{cm^2}{sec}$	$c \times 10^{-5}$ $\frac{cm^4}{sec}$	T sec	L cm
Beryllium 1.78 gm/cm³	from 72 × 60 × 56 cm³ $\Omega = 0.730 \times 10^{-2}$ cm⁻² to 20 × 20 × 20 cm³ $\Omega = 6.118 \times 10^{-2}$ cm⁻²	1.22 ± 0.05	3 ± 1	4000*	22.1*
Graphite	from 200 × 180 × 140 cm³ $\Omega = 1.012 \times 10^{-3}$ cm⁻² to 20 × 20 × 40 cm³ $\Omega = 41.290 \times 10^{-3}$ cm⁻²	1.98 ± 0.03	12.0 ± 1.9	12200 ± 500	49 ± 2.0
Water 23°C	from 0.75 × 10³ ml to 5.6 × 10³ ml	0.35 ± 0.01	0.04 ± 0.01	207 ± 6	2.7 ± 0.1
Water 80°C	$\Omega = 0.086 - 0.94$ cm⁻²	$0.45^{+0.04}_{-0.02}$	$0.13^{+0.05}_{-0.07}$	212 ± 6	$3.1^{+0.2}_{-0.1}$

* The quantity was computed from $T = L^2/D_0$ where L = 22.1 cm is from the report of Gerasyeva *et al.*[6]

computing from Equation 2.13 the geometrical factor Ω for prisms of each given size.

From these data the numerical values of D_0 and c were evaluated by a least-squares calculation, it being assumed that the dependence of α on Ω was expressed by Equation 2.16. The first seven points corresponding to minimal Ω were used in the calculations. For these values of Ω one could be certain that stray neutrons could not be of importance. The quantity L^2 could not be obtained with a sufficient degree of accuracy from these curves. Therefore in the calculations of D_0 and c it was assumed that the curve $\alpha = f(\Omega)$ intersects the abcissae axis at $-1/L^2 = -2.06 \times 10^{-3}$. This additional point can be used to raise the accuracy of the diffusion coefficient computed from our data. The value $L = 22.1$ cm accepted by us was found by Gerasyeva[6] and others by employing the exponential method. It should be noted that an exact value of L is not required in our experiments. Thus a variation of 10% in L^2 changes the computed value of D_0 by only 3%. It can be seen from Fig. 3 that the smooth curve plotted by using the parameters determined in the described manner gives a good fit with the empirical dependence of x on Ω. Numerical values of the parameters thus obtained are presented in Table I.

Measurements with Graphite

The graphite measurements were also made with prisms of rectangular cross section; graphite bricks having a mean density 1.67 gm/cm³ were used. Density deviations of separate bricks from the mean value did not exceed $\pm 2.5\%$. Prisms of 10 different sizes were used. The results are presented in Figs. 4 and 5 which are similar to Figs. 2 and 3 obtained for Be. The values obtained for D_0, c, L and T are presented in Table I.

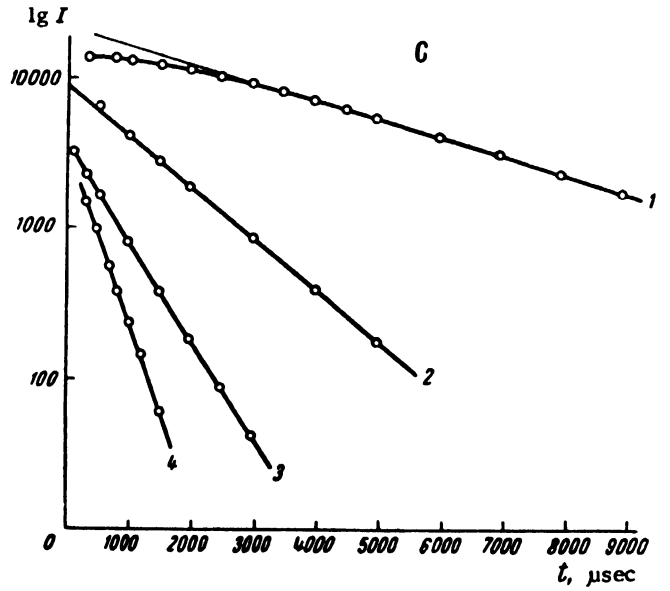

Figure 4. Density attenuation curves of thermal neutrons with time in graphite prisms of various sizes: (1) for prism 200 × 180 × 140 cm³ (τ = 3570 μsec); (2) for prism 120 × 80 × 80 cm³ (τ = 1310 μsec); (3) for prism 60 × 60 × 60 cm³ (τ = 680 μsec); (4) for prism 40 × 40 × 40 cm³ (τ = 350 μsec)

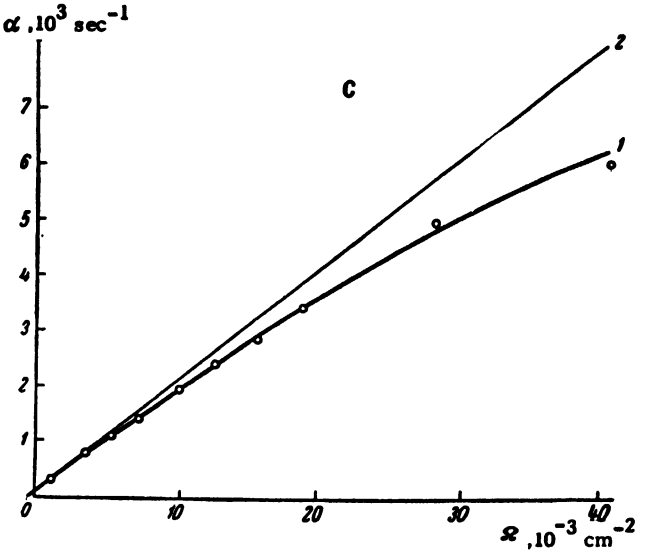

Figure 5. Dependence $\alpha = f(\Omega)$ for graphite: (1) curve $\alpha = 1/T + D_0\Omega - C\Omega^2$; (2) tangent to 1 at point $\Omega = 0$. Experimental values for various sizes of prisms are shown by circles: 200 × 180 × 140, 120 × 80 × 80, 80 × 80 × 60, 60 × 60 × 60, 60 × 60 × 40, 60 × 40 × 40, 40 × 40 × 40, 40 × 40 × 30, 40 × 20 × 20 cm³

Measurements with Water

The water was placed in a thin-walled cylindrical vessel 4 (Fig. 6) having a diameter $2R = 186$ mm and height $2h = 210$ mm. The lateral surface and bottom face of the cylinder were covered with 0.5 mm cadmium sheets. The cylinder was shielded from all sides by a four centimeter layer of B_4C.

During the measurements vessel 4 was filled with distilled water to the required level. The lowest amount of water used in the experiments corresponded to a height of 2.75 cm, the highest amount to 20 cm. An iron-constantan thermocouple, 5, placed within the vessel was used to check the water temperature. In experiments with heated water a heater coil was introduced into vessel 4 and for some calibration measurements a mercury thermoregulator was also introduced.

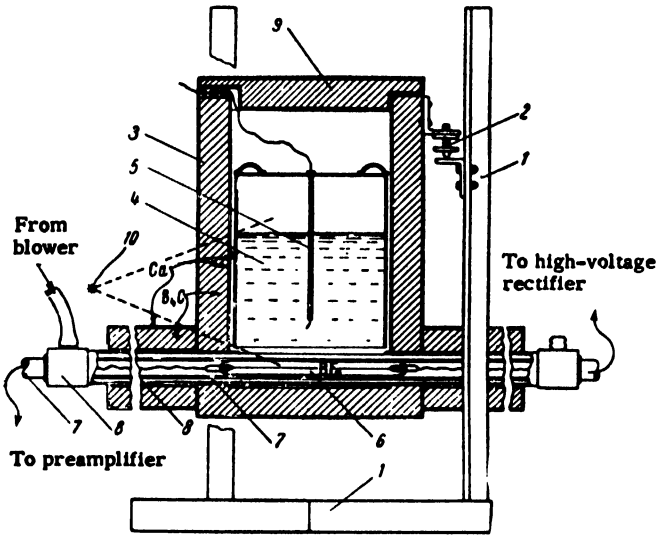

Figure 6. Installation for water measurements: (1) support; (2) setscrew; (3) boron protection; (4) cylinder with water; (5) thermocouple, (6) boron counter; (7) counter tube; (8) pipe for counter cooling; (9) boron protection cover; (10) fast neutron source

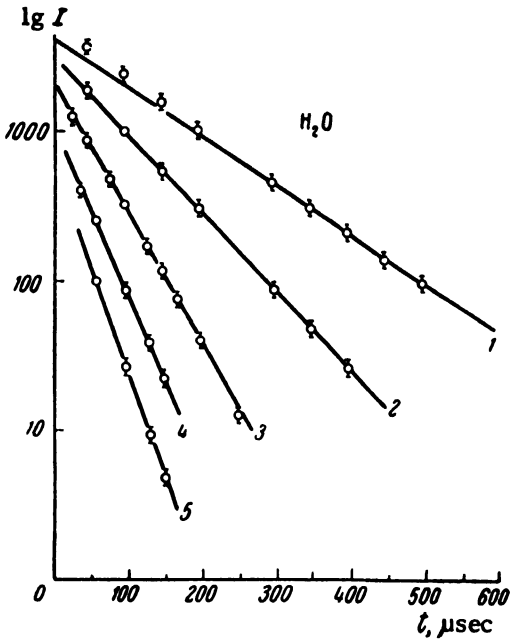

Figure 7. Density attenuation curves of thermal neutrons with time in water: (1) for $2h$ = 20 cm (τ = 127 μsec); (2) for $2h$ = 7.32 cm (τ = 81 μsec); (3) for $2h$ = 4.25 cm (τ = 48.9 μsec); (4) for $2h$ = 3.35 cm (τ = 38 μsec); (5) for $2h$ = 2.75 cm (τ = 29 μsec)

In the experiments with heated water the counter was cooled by blowing air through tube 8.

The time dependence of the neutron density for five different volumes of water at 23°C is plotted in a semi-logarithmic scale in Fig. 7. It can be seen from the curves in Fig. 7 that for Ω varying between 0.15 cm^{-2} and 0.94 cm^{-2} a linear dependence is attained in less than 50 μsec only in curve 1 which refers to a maximum water volume of 5.61 (Ω = 0.085 cm^{-2}) a time of 300 μsec was required.

Control experiments showed that there was almost no background, at any rate for delay times exceeding 50 μsec.

Water Measurements at Room Temperature

The value of α was determined in these experiments for nine different volumes of water (from 0.75 up to 5.6 liters). The quantity Ω was calculated from formula (2.14); the error in Ω due to errors in λ_t and to other factors was always smaller than 3%. (The magnitude of the error is denoted in Fig. 8 by triangles above the abscissae axes.)

The temperature of the water during the experiments was measured by a thermocouple. Changes in the water temperature never exceeded ±0.5°C. A graph of the dependence of α on Ω was plotted by using the measured values of α (Fig. 8). It can be seen from the graph that for $\Omega < 0.2$ cm^{-2} the experimental points approximately lie on a straight line while at larger values of Ω they appreciably lie below the line. Values of parameters T, D and c obtained by a least-squares fit are presented in Table I. The thick line in Fig. 8 is a parabola plotted for these parameters. As can be seen from the figure the experimental points satisfactorily fit this parabola. The errors of the points in Fig. 8 are mean square errors computed in the usual manner from the spread of values of α.

Experiments with Heated Water

In these experiments only five different volumes of water were investigated. The measurements were carried out at a temperature of about 80°C. The maximum temperature spread in various layers of the water was ±3°.

The method applied for measuring the neutron density decay curve was the same as that used in the previous series of measurements. In these experiments the thermoregulator was permanently located within the investigated volume. The total error in Ω (due to evaporation of the water during the measurements, to uncertainty in λ_t etc.) did not exceed 3–4%. The error in Ω is denoted in Fig. 9 by triangles above the abscissae axes (similar to Fig. 8).

Experimental points on the graph are designated by triangles. It would not be correct to directly determine the diffusion parameters from these points because the thermoregulator which was inside the investigated volume of water during measurements of the decay curves could absorb additional neutrons and thus lower the lifetime τ. A correction therefore had to be introduced into the measured value of α to account for neutron absorption in the material of the thermoregulator.

The points obtained after introduction of the correction are represented by circles in Fig. 9. In order to account for possible errors in this correction the error in α is increased by plus 50% and minus 20% of the magnitude of the introduced correction. It is not advisable to determine the values of the three diffusion parameters from the five experimental points obtained in these experiments as satisfactory accuracy cannot be attained in this way. Therefore only two diffusion parameters D_0 and c were evaluated from the experimental data and a value for T was assigned.

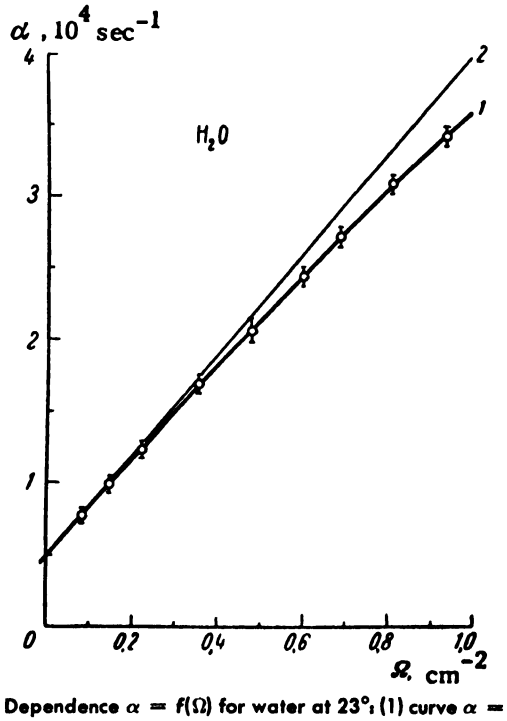

Figure 8. Dependence $\alpha = f(\Omega)$ for water at 23°: (1) curve $\alpha = 1/T + D_0\Omega - C\Omega^2$; (2) tangent to 1 at point Ω = 0. Circles denote experimental values for water which is poured into the reservoir up to the height of $2h$ = 20; 10.13; 7.32; 5.15; 4.25; 3.66; 3.35; 3.02; 2.75 cm

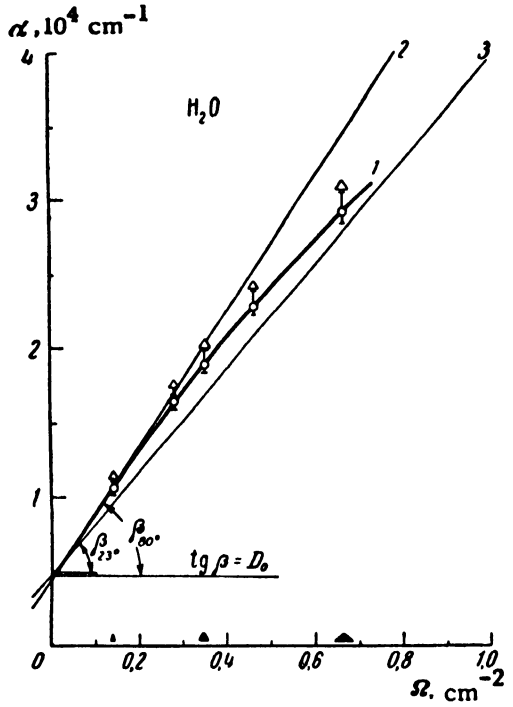

Figure 9. Dependence $\alpha = f(\Omega)$ for water at 80°: (1) curve $\alpha = 1/T + D_0\Omega - C\Omega^2$; (2) tangent to 1 at point $\Omega = 0$ (80°C); (3) straight line corresponds to 2 as shown in Fig. 8. Triangles and points indicate experimental values of α for water filling the reservoir to a height of $2h$ = 10.35; 6.02; 5.16; 4.28; 3.35 cm. The circles indicate corrections in absorption. Errors are indicated with consideration of correction inaccuracies

Apparently, the difference between the lifetimes T at 80° and 23° is due only to a decrease in density of the heated water. If this effect is taken into account and it be considered that at 23°C, $T = 207 \pm 6$ μsec (see Table I), then at 80°C, $T = 212 \pm 6$ μsec. This was the value inserted in Equation 2.16; the values of D_0 and c were then determined by the least-squares method.

Errors in the values of D_0 and c are considerably greater than those obtained in the cold-water measurements. This fact is in no way related to the essence of the method and is due only to the small number of experimental points and to the necessity for introducing a correction for absorption in the thermoregulator.

DISCUSSION OF THE RESULTS

A summary of the results is given in Table I.

Comparison of the data shows that in all of the cases investigated D depends on the dimensions of the system; the coefficient c which determines the dependence of D on Ω is quite large in Be and C. In Be, $c/D = 2.5$ cm² and in C, $c/D = 6$ cm². This means that in graphite the value of D is already about 5% too low for Ω approximately equal to 0.01 which corresponds to a cube of side $2a = 55$ cm.

The dependence $D(\Omega)$ for water was independently determined by von Dardel and Sjöstrand.[3] Our value, $c = (0.04 \pm 0.01) \times 10^{-5}$ cm⁴/sec is somewhat smaller than the value of c which follows from von Dardel's data, $c = (0.072 \pm 0.015) \times 10^{-5}$ cm⁴/sec. This discrepancy should not be considered important as the accuracy of measurement of this constant is not high.

Thus, if the diffusion coefficient is measured in a system of finite dimensions, its value due to neutron leakage may appreciably differ from that which one would expect for a neutron gas in thermal equilibrium.

We shall now separately consider the results obtained for different substances.

Beryllium

In Glasstone and Edlund's book[7] the value of $\lambda_t/3$ for Be is 0.70 cm at a density $\rho = 1.84$. Hence, if $\bar{v} = 2.5 \times 10^5$ cm/sec and $\rho = 1.78$, one obtains $D = 1.8 \times 10^5$ cm²/sec which considerably differs from our value, $D_0 = 1.22 \times 10^5$ cm²/sec.

Accord ng to Hughes[8] in Be $\lambda_t = 1.43$ for $\rho = 1.85$; the value of D for a density $\rho = 1.78$ will then be $D = 1.24 \times 10^5$ cm²/sec. This value, which agrees with ours, was computed by Sachs from the scattering cross section by taking into account the scattering angular distribution.

Graphite

By studying the transition effect at the boundary of two media Zipin (in 1950) obtained the value $D = (2.11 \pm 0.18) \times 10^5$ cm²/sec (the value refers to the same density as that encountered in our experiments, i.e., 1.67). The value cited in Glasstone and Edlund's book[7] is 2.2×10^5 cm²/sec. These values are in satisfactory agreement with the results of the present investigation. Our value for L satisfactorily agrees with the more precise value $L = 50$ cm obtained in graphite by the exponential method.

Water

Measurements with Water at 23 ± 0.5°C

The experimental value $T = 207 \pm 6$ μsec accords very well with the results of other authors obtained at room temperature. Thus, Manley[1] obtained 205 ± 10 μsec (1942), Whitehouse and Graham,[9] 205 ± 6 μsec, Hammermesh *et al.*,[10] 203 ± 6 μsec (1953), Harris *et al.*,[11] 206 ± 6 μsec (1953), von Dardel and Sjöstrand,[3] 204.4 ± 2.0 μsec (1954). Our value is in somewhat poorer agreement with the value measured by Scott *et al.*, $T = 216 \pm 4$ μsec.†[4]

Magnitude of Diffusion Coefficient

The value directly measured by us, $D = (3.50 \pm 0.10) \times 10^4$ cm²/sec is in good agreement with the value $D = 3.55 \times 10^4$ cm²/sec cited in Glasstone and Edlund's book[7] and also with the value $D = (3.634 \pm 0.075) \times 10^4$ cm²/sec, obtained by von Dardel and Sjöstrand.[3] If D is evaluated on basis of the data of Scott *et al.*[4] an appreciably higher value will be found: $D = (3.85 \pm 0.08) \times 10^4$ cm²/sec (for $\bar{v} = 2.5 \times 10^5$ cm/sec).

Calculating λ_t from our value for D_0 a value $\lambda_t = 0.420 \pm 0.013$ cm is obtained which satisfactorily ac-

† In their calculations of the geometrical factor these authors considered one of the dimensions of the system which equalled 70 cm to be infinitely large. If a correction is introduced to account for finity of this dimension then their value of T must be increased from 214 μsec to 216 μsec.

cords with that obtained by Fermi and cited in Tittle's paper:[12] $\lambda_t = 0.425 \pm 0.02$ cm.

Our value for the diffusion length, $L = 2.69 \pm 0.08$ cm, is in good agreement with the value $L = 2.72 \pm 0.04$ found in reference 3 and within experimental error accords with Fermi's value ($L = 2.76 \pm 0.03$ cm) quoted in Tittle's paper. The value ($L = 2.85 \pm 0.05$ cm) computed from Scott's data[4] considerably differs from our value. In references 7 and 8 the values $L = 2.89$ cm and 2.85 cm are cited.

As the quantity D was measured in the present work with a high degree of accuracy and there is practically no discrepancy between our value of T and those of other authors it seems correct to assume that our value of L is essentially correct. This would signify that the usually accepted value $L = 2.85$ cm is somewhat too high.

Measurements with Heated Water

For water heated to 80° the diffusion coefficient obtained by us is $4.52(+0.35 \text{ or } -0.20) \times 10^4$ cm²/sec. This value exceeds that for water at 23°C by approximately 30%. Changes in the diffusion coefficient $D = \lambda_t \cdot v/3$ may result from variation of the mean neutron velocity or of the transport path.

When water is heated from 296°K to 353°K the mean neutron velocity becomes $\sqrt{353/296} = 1.1$ times higher than it was initially, i.e., increases by 10%. Thus, an increase of $29(+14 \text{ or } -9)\%$ in D which we observed experimentally signifies that at 80°C λ_t is $18(+14 \text{ or } -9)\%$ higher that at 23°C. Heating increases the scattering mean free path by 2.6% due to a decrease in density. Moreover, the scattering cross section of water decreases with increasing neutron velocity. This will increase λ_t by approximately 6%. Apparently, these two factors are not sufficient to explain the observed increase of λ_t. It thus seems probable that heating of the water modifies the angular distribution of scattered neutrons. However the poor accuracy of the measurements does not permit one to consider this statement definitely proved.

The data presented in Table I show that with an increase of temperature from 23°C to 80°C the diffusion length increases from 2.69 ± 0.08 cm to $3.10(+0.17 \text{ or } -0.12)$ cm, that is, by 15%.

von Dardel[5] cites a formula from an unpublished paper of Fermi according to which the diffusion length depends linearly on the temperature of the medium:

$$L = L_0 + (T - 273) \times 0.0061 \text{ cm} \qquad (4.1)$$

Here L and L_0 are respectively the diffusion lengths for water at T°K and 273°K. Using the value for L at 23°C and applying this formula one can evaluate the value of L at 80°C. One thus obtains $L = 3.04 \pm 0.08$ cm in accord with our experimental value. von Dardel and Sjöstrand[3] have derived the temperature dependence of D and L for the interval 10°–35°. Their temperature coefficient is about half that obtained in the present investigation or in Fermi's work. The origin of this discrepancy is unclear.

In conclusion a few words will be said about the quantity c which defines the dependence of D on Ω. It was already mentioned that this dependence is due to violation of thermal equilibrium between the neutron gas and the medium. The nature of this violation may be quite diverse and is determined by the dependence of $D(v)$ on the neutron velocity. Let us assume, for example, that $D(v)$ is minimum for neutrons possessing velocities close to the mean thermal neutron velocity v and that it increases for higher or lower values of v. The neutrons, therefore, which remain in the medium will contain fewer fast and slow neutrons. This means that, in principle, the mean neutron energy in the medium may be constant and violation of equilibrium will consist in a change of the neutron velocity distribution which now differs from a Maxwellian. If $D(v)$ is a monotonic function the medium may become depleted in slow or fast neutrons depending on the character of the dependence. In this case violation of equilibrium will first of all lead to a change in the mean neutron energy in the medium whereas the velocity distribution may remain almost Maxwellian.

The dependence of the effective scattering cross section on the neutron energy in Be and graphite indicates that in these substances a change in the shape of the neutron spectrum resulting from neutron leakage may be quite important. The scattering cross section in water decreases with increasing neutron velocity and therefore it may be expected that $D(v)$ will monotonically increase with the velocity. Therefore one must not exclude the possibility that violation of thermal equilibrium of the gas in water can be sufficiently accurately described by a lowering of the mean neutron energy (temperature). This assumption was made by von Dardel in his analysis of the experimental results obtained in water which are similar to those obtained by us.

Following von Dardel[5,13] it may be assumed that in a finite moderator the neutron temperature T as a function of time should satisfy the equation

$$-\frac{3}{2}kT\frac{dT}{dt} = \left(\bar{E}_{en} - \frac{3}{2}kT\right)D\Omega + \frac{3}{2}k\gamma(T - T_0) \qquad (4.2)$$

Here $\bar{E}_{en}$ is the mean energy of neutrons escaping from the moderator. The first term accounts for variation of the mean neutron energy due to leakage. The second term $\frac{3}{2}k\gamma(T - T_0)$ accounts for the process of establishment of thermal equilibrium as a result of collisions between the neutrons and nuclei.

Applying relation 4.2 and using the experimental dependence $D(\Omega)$ the "heat transfer coefficient" γ may be estimated. This is a simple procedure if one assumes, as von Dardel does[5,13], that the transport path λ_t is independent of neutron energy. In this case the mean energy carried off by a neutron escaping from the medium is $\bar{E}_{en} = 2kT$, and the stationary ($dT/dt = 0$) temperature is related to the diffusion

coefficient by the simple formula $D/D_0 = \sqrt{T/T_0}$. The latter point is considered in more detail by von Dardel and Sjöstrand[3] who put $\lambda_t \sim \lambda_s$ that is, assume

$$\frac{D(\Omega)}{D_0} = \sqrt{\frac{T}{T_0}}\,\frac{\lambda_s T}{\lambda_s(T_0)}$$

where the dependence of the scattering mean free path λ_s on neutron temperature (i.e., mean energy) is deduced from known data on the energy dependence of the neutron scattering cross section in water.

The method for estimating γ described here is very inaccurate. First of all, as follows from our experiments λ_t varies with energy more rapidly than λ_s. Secondly, and what is more important, it is not permissible to neglect the dependence of λ_t on energy. Obviously, if λ_t increases with energy the neutron temperature outside the medium will be larger than that within the medium ($T_{en} > T$) otherwise $T_{en} < T$[1].

Information on γ (velocity of establishment of thermal equilibrium) can be obtained without applying the assumption made by von Dardel. To do this one must simply take $\bar{E}_{en}$ from the experimental data. Apparently, for water one may put $\bar{E}_{en} = 2kT_{en}$, where $T_{en} \cong 400°$ K. To obtain the relation between $D(\Omega)$ and T the dependence of D_0 on temperature (measured experimentally in the present investigation) may be utilized, it being assumed that this dependence is entirely conditioned by variation of the neutron gas temperature due to heating of the medium.

Computations carried out by this method lead to estimated values of γ lying between 1.5×10^5/sec and 4×10^5/sec. von Dardel[5,13] evaluated γ on the assumption that transfer of neutron energy to the water molecules takes place as if the water were a monoatomic gas with a mass number 18. This author also showed that this assumption accords with the results of measurements of the slowing down velocity of neutrons in water in the energy range lying somewhat above the thermal range.‡

Our estimated value of γ also does not contradict this assumption. However the value for γ which von Dardel and Sjöstrand[3] obtain from their data is about 3 times smaller than that which one would expect by assuming water to be equivalent to a monoatomic gas of mass number 18. This discrepancy is partly due to incorrectness of the method of estimating γ which we mentioned above and partly to the higher value of c obtained in the experiments of these authors.

The values of c in various media will now be compared. We rewrite Equation 2.4 defining the constant c by assuming for simplicity $\beta_1 = \beta_2 = \beta$,

$$c = \eta \frac{D_0^2 \lambda_s}{8v} \tag{4.3}$$

where

$$\eta = \frac{(D_1 - D_2)^2}{D_0^2} \Big/ \frac{\beta \lambda_s}{v} \tag{4.4}$$

In Equation 4.4 $(D_1 - D_2)/D_0$ is the relative difference between the diffusion coefficients for the two neutron groups and $\beta\lambda_s/v$ is the probability per collision of a neutron changing from one group to another. Thus, η is a dimensionless constant which characterizes the investiga.ed substance.

The value of η for H_2O, Be and C computed from the data presented in Table I with the aid of Equation 4.3 are very close to each other. Indeed, the values of c for water, beryllium and graphite are in the ratio as 1:75:300 whereas for these same substances, the values of $\eta = c \Big/ \frac{D_0^2 \lambda_s}{8v}$ are correspondingly $\eta_{H_2O} = 22$, $\eta_{Be} = 28$, $\eta_C = 24$. Thus we find that for all three substances $c/D_0 \sim \lambda_s \lambda_t$. It is clear from Equation 4.4 that the values of η for various substances should be approximately equal, at any rate by order of magnitude. For water η and γ from Equation 4.2 are connected by a simple relation.

‡ The problem of the temperature difference of neutrons in the moderator and of the neutrons escaping from it was considered earlier by K. O. Tolstov.[14]

REFERENCES

1. Manley, J. H., Haworth, L. J. and Luebke, E. A., Phys. Rev., *61*, 152 (1942).
2. Rainwater, J. and Havens, W. W., Phys. Rev. *70* 136 (1946).
3. Von Dardel, G. F. and Sjöstrand, N. G., Phys. Rev., *96*, 1245 (1954).
4. Scott, F. R., Tomson, D. B. and Wright, W., Phys Rev., *95*, 583 (1954).
5. Von Dardel, G. F., Trans. Royal Inst. Techn., No. 75, Stockholm (1954).
6. Geraseva, L. A., Kamayev, A. V., Krasin, A. K. and Morosov, I. G., P/662, "The Study of Beryllium as a Neutron Moderator," Vol. 5, Session 19A, these Proceedings.
7. Glasstone, S. and Edlund, M. C., "The Elements of Nuclear Reactor Theory," New York (1952).
8. Hughes, D. J., "Pile Neutron Research," New York (1953).
9. Whitehouse, W. J. and Graham, G. A. R., Canad. Journ. Res., *25A*, 261 (1947).
10. Hammermesh, B., Ringo, G. R. and Wexler, S., Phys. Rev., *90*, 603 (1953).
11. Harris, S. P., Muhlhause, C. O., Rose, D., Schroeder, H. P., Thomas, G. E., Jr. and Wexler, S., Phys. Rev., *91*, 125 (1953).
12. Tittle, C. W., Phys. Rev., *80*, 756 (1950).
13. Von Dardel, G. F., Phys. Rev., *94*, 1272 (1954).
14. Tolstov, K. D., Dissertation (1952).

The Study of Beryllium as a Neutron Moderator

By L. A. Geraseva, A. V. Kamayev, A. K. Krasin, and I. G. Morosov, USSR

A series of investigations into the properties of beryllium and beryllium oxide as neutron moderators have been carried out in the Soviet Union.

This report gives data on the measurement of the effective capture cross section of thermal neutrons by reactivity method and on the measurement of moderation length and diffusion length in beryllium, established by the authors in the periods between 1948 and 1952.

To carry out this work the authors had at their disposal 1500 kilograms of metallic beryllium of highest-grade purity, produced according to the technology developed in the Soviet Union.[1]

The purity of the beryllium is controlled in batches by spectral and chemical analysis methods for twenty-three of the most serious elements according to the total sum of impurities, and by measuring the effective capture cross section by the reactivity method (danger coefficient method).

MEASUREMENT OF CAPTURE CROSS SECTION OF THERMAL NEUTRONS IN BERYLLIUM AND BERYLLIUM OXIDE BY THE DANGER COEFFICIENT METHOD

The measurement of the capture cross section of thermal neutrons in beryllium and beryllium oxide was carried out in the physical graphite reactor of the Academy of Sciences in the USSR.

A method was applied in this work analogous to the one published earlier.[2] The basic principles of the method are simple but the detailed formulation of the measurements demands numerous additional investigations.

The basic principle of the method is that the sample of material under study is placed in the center of a critical reactor which is then brought back to critical. In capturing neutrons, the sample changes (reduces) reactivity. The effect caused by the sample is estimated from the position of the control rod graduated in units of reactivity. The change of reactivity caused by the sample is expressed as an effective capture cross section of the sample material in relation to boron, whose capture cross section is known. The control rod is calibrated against boron.

For samples of materials with small atomic weights and small capture cross sections (heavy water, graphite, beryllium, beryllium oxide) the change of reactivity depends not only on the capture of thermal neutrons, but also on the opposite effect—on the moderation of fast neutrons in the sample.

Moderation is caused by the presence in the pile neutron spectrum of neutrons which have energy higher than the lowest resonance level in uranium.

Samples of light elements placed in the reactor, due to their good scattering and moderation properties, increase the resonance escape probability and thus increase reactivity. For light low-absorbing materials, we compare the effect produced by neutron absorption with the effect caused by the moderation of fast neutrons in the sample. Therefore, the correct calculation of the second effect, which we shall henceforth term the "effect of additional moderation," constitutes the main difficulty in measuring the effective capture cross sections in the light low-absorbing materials.

The change of reactivity caused by placing the sample in the center of the reactor, which we shall henceforth term the "apparent effect," can be written in two-termed formulas:

$$S = N(\sigma_c - \sigma_T) \qquad (1)$$

where S is apparent effect, N is number of nuclei in sample, σ_c is effective capture cross section, σ_T is constant, characterizing the moderation capacity of the sample.

The constant σ_T is not only a function of the nuclear properties of the material under study but also depends on the parameters of the reactor and the place where the sample under study is situated. As pointed out earlier, for the materials interesting us, the effect of additional moderation gave approximately the same result as the capture effect, and therefore, when measuring, special attention is paid to the correct calculation of the effect of additional moderation.

Standards for additional moderation. In this work σ_T for beryllium and beryllium oxide was determined by comparing moderating capacities ($N_0\sigma_s\xi$) with other materials for which σ_T was known. Samples of graphite and heavy water were used as additional moderation standards. The graphite standards were made from the same batch of graphite, for which the diffusion length had been measured by the authors. Having the scattering cross section $\sigma_s = (4.8 \pm 0.2) \times 10^{-24}$ cm^2, the capture cross section was calculated and found to be equal to: $\sigma_c = (3.4 \pm 0.5) \times 10^{-27}$ cm^2.

Altogether several graphite standards were made, each of them consisting of small plates with a total weight $\sim$ 10 kilograms. As a controlling standard in

Original language: Russian.

Table 1. Results of Measurement of σ_T for Graphite and Heavy-Water Standards

Standard	Weight gm	$\sigma_c \times 10^{-27}$ cm²	$N\sigma_c$	S cm²	$\sigma_T 10^{27}$ cm²
1. Graphite	9300	3.4 ± 0.5	1.59 ± 0.23	−1.82 ± 0.03	(7.4 ± 0.6)
2. Heavy water	2340	4.5 ± 1.0	0.315 ± 0.07	−3.34 ± 0.03	(52.0 ± 1.5)

NOTE: The sign " − " in the apparent effect S indicates that when placing the graphite as well as heavy-water standards in the reactor, reactivity increased. An analysis of the errors in the value of σ_T for graphite and heavy water shows that in the first case the main contribution to the error is introduced by the inaccuracy in the value of σ_c of graphite, whereas, in the second case, due to the good moderation properties of heavy water, inaccuracy in the value of σ_c of heavy water no longer plays a decisive role. As the value of S can be measured with very high precision then subsequently $\sigma_T(D_2O)$ can be determined with great accuracy.

the experiment, one made from heavy water was used with a concentration of 99.75% and absorption cross section of: $\sigma_c = (1.5 \pm 1.0) \times 10^{-27}$ cm².

Altogether ~2.5 kilograms of heavy water were used for the standard. With the purpose of eliminating self-shielding in moderation, the heavy water was dispersed as much as possible in the volume occupied by the samples under study in the center of the reactor when measurements were carried out. σ_c was measured by the danger coefficient method and calculated according to Equation 1.

The results of measurements with graphite and heavy water standards are given in Table 1.

σ_T of the material under study (Be, BeO) was computed on the basis of the data on additional moderation in graphite or heavy water according to the following formula:

$$\sigma_T(X) = \sigma_T(A) \frac{\sigma_s(X)\xi(X)}{\sigma_s(A)\xi(A)} \qquad (2)$$

where $\sigma_T(X)$ is effect of additional moderation in beryllium or beryllium oxide, $\sigma_T(A)$ effect of additional moderation in graphite or heavy water, ξ average logarithmic decrement per collision, σ_s effective cross section of scattering for neutrons with energy ~1 ev.

In calculating σ_T for beryllium according to Equation 2 the following values of the constant were taken:

$$\sigma_s(\text{Be}) = (6.1 \pm 0.3) \times 10^{-24} \text{ cm}^2$$
$$\xi(\text{Be}) = 0.202$$
$$\sigma_s(\text{C}) = (4.8 \pm 0.2) \times 10^{-24} \text{ cm}^2$$
$$\xi(\text{C}) = 0.158$$
$$\sigma_s(D_2O) = (10.3 \pm 0.3) \times 10^{-24} \text{ cm}^2$$
$$\xi(D_2O) = 0.505$$

with these values we obtain:

(*a*) In calculating using the graphite standard: $\sigma_T(\text{Be}) = (12.0 \pm 2.0) \times 10^{-24}$ cm².

(*b*) From data according to the heavy-water standard: $\sigma_T(\text{Be}) = (12.5 \pm 1.2) \times 10^{-27}$ cm².

Elementary calculations show that the main error in σ_T(Be) is determined not by the error in measurements but by the low accuracy of scattering cross-section values.

The good agreement in the calculation of σ_T(Be) according to two different standards, shows that the method of calculating the effect of additional moderation, which was used is sufficiently accurate.

As will be shown later on, the main contribution to the error when measuring σ_c(Be) is due to the accuracy of the value of σ_T(Be). Therefore, in order to obtain more precise values of σ_c(Be) a heavy-water standard is used in measuring.

Standardization against boron was achieved by making standards from boron in the form of envelopes of aluminum foil, inside of which sheets of filter paper, soaked in borax solution, were inserted.

In order to eliminate self-shielding, the boron was distributed on a large surface. Boron with $N\sigma_c = 0.02$ cm² was distributed on 1 cm² of the surface of the standard.

The quantity of boron in the standard was determined within 0.5%. The standard made of envelopes was compared with the borax standard placed in graphite powder which filled the whole experiment volume. The data in both samples coincided. In the measurements for calibrating the control rod, borax standards were used with a total cross section $N\sigma_c$ ranging from 3 to 5 cm². The absorption cross section for boron was taken as equal to: $\sigma_c = 710 \times 10^{-24}$ cm².*

In using the above-mentioned method for measuring the effective absorption cross section in light low-absorbing materials, especially when samples of large volumes have to be used for obtaining high precision, it is necessary to control the conditions of the tests closely and introduce numerous corrections influencing the value of the apparent effect.

The following corrections were made:

(*a*) The calculation of self-shielding in the bulk samples of beryllium in relation to the moderation of the fast neutron spectrum. By way of experiment and theory it was shown that in samples of beryllium with a thickness exceeding 40 mm not all nuclei take part in moderation with equal effectiveness. Therefore, in our tests all samples of beryllium under investigation had a thickness of not more than 40 mm.

(*b*) It was shown by special tests that the "channeling" effect of the experimental hole for the sample or standard was within the statistical accuracy of the test. We shall note that the dimensions of the reactor were sufficiently large and, therefore, the solid angle at which the sample was seen from the reactor sur-

* Evaluation of results obtained with the use of the final values of σ_c(B) = 750 × 10^{-22} cm² a change in σ_c(Be) of 3%.

Table 2

Impurity	Content of impurity in % weight		Additional cross section per molecule in $cm^2 \times 10^{-27}$	
	BeO	Be	BeO	Be
Boron	5.8×10^{-5}	1×10^{-5}	0.346	0 060
Lithium	1.0×10^{-5}	3.4×10^{-5}	0.008	0.029
Silver	1.0×10^{-4}	1×10^{-4}	0.005	0.005
Lead	1.0×10^{-3}	1×10^{-2}	0.001	0.001
Manganese	1.8×10^{-3}	2.3×10^{-3}	0.027	0.048
Copper	1.0×10^{-3}	1.65×10^{-3}	0.004	0.007
Iron	6.0×10^{-3}	7×10^{-3}	0.024	0.028
Magnesium	2.0×10^{-2}	1×10^{-3}	0.030	0.001
Barium	5.0×10^{-3}	6.6×10^{-3}	0.004	0.006
Aluminum	1.0×10^{-2}	3×10^{-3}	0.008	0.002
Silicon	1.0×10^{-2}	2.4×10^{-2}	0.008	0.015
Cadmium	5.5×10^{-6}	5.9×10^{-6}	0.011	0.010
Cobalt	2.2×10^{-4}	1×10^{-4}	0.012	0.005
Nickel	3.3×10^{-4}	3×10^{-3}	0.002	0.021
Zinc	1.0×10^{-3}	1.6×10^{-2}	0.010	0.020
Titanium	1.0×10^{-3}	1×10^{-3}	0.010	0.009
Chromium	5.0×10^{-4}	8×10^{-4}	0.002	0.004
Calcium	5.4×10^{-2}	1.4×10^{-3}	0.055	0.002
Chlorine	5.5×10^{-4}	2×2^{-3}	0.050	0.200
Sulphur	1.0×10^{-3}	1×10^{-2}	0.001	0.011
Lead	5.0×10^{-3}	5×10^{-3}	0.001	0.002
Phosphorus	1.0×10^{-2}	1×10^{-2}	0.009	0.009
Fluorine	5.0×10^{-2}	5×10^{-2}	0 001	0.002
Total			0.629	0.505

face was insignificantly small. In addition, during the control tests, the experimental hole was closed with graphite plugs. The large dimensions of the reactor made it possible to create in its center a sufficiently large volume ($10 \times 10 \times 100$ cm), where the gradient of the neutron density was very small. It was also shown that the change in the neutron space-distribution as a result of a slight shifting of the sample under study from the center of the reactor (grad $n \neq 0$) within the limits of the statistical error did not influence the results of cross-section measurements.

(*c*) Special investigations were conducted and corrections made for the changes in atmospheric pressure, temperature and moisture content, i.e., for the parameters which influence reactivity. It must be pointed out, however, that the change of reactivity caused by the effects enumerated above does not constitute a fixed value but depends in some degree on the previous history of the reactor and on the nature of the change in atmospheric effects. Therefore, in this work the position of the control rod in the critical reactor without a sample was taken as "zero-reading." Such readings were repeated after every 20–30 minutes during the entire cycle of measurements.

In the interval between "zero-readings" measurements were carried out with the samples and standards under study.

Tests with Be and BeO were performed. The effective absorption cross section in beryllium and beryllium oxide was measured by the method described above. Two goals were pursued in this:

(*a*) Determination of the absolute value of σ_c for the beryllium nucleus.

(*b*) Control of the purity of beryllium produced by the factory.

It is known that several papers have been published on the measurements of the effective absorption cross section of thermal neutrons in beryllium[2,3,4] but the values obtained cannot be attributed to the true value of σ_c(Be). In fact as investigators point out, they represent the upper limit although the beryllium used in these experiments was of high purity. The authors point out that the quantitative composition of impurities in the sample under study was not known to them. Therefore, the determination of the true value of σ_c for beryllium is of certain scientific interest.

Tens of kilograms of beryllium oxide and highly purified beryllium were produced for solving the first problem. One can judge the degree of purity of the samples studied by the results of the spectral and chemical determination of impurities (Table 2).

As seen from the table, inpurities per nucleus according to the total sum of the 23 most wide-spread elements in beryllium as well as in beryllium oxide do not exceed 0.6×10^{-27} cm^2.

Taking into account the rare earths and other elements, impurities in these batches contribute to the absorption cross section $\Delta\sigma_c$ (impurities) not more than 1×10^{-27} cm^2 per beryllium nucleus.

In measuring the absorption cross section of beryllium and beryllium oxide for thermal neutrons all corrections described above, which are characteristic of this method, were introduced.

The metallic beryllium used in the tests was prepared in the form of cylinders with a mean density $\sim$1.78 gm/cm^3.

The results of measurements for one of the batches of beryllium are given in Table 3.

In substituting the values from Table 3 in Equation 1 we obtain

$$\sigma_c = \frac{(2.04 \pm 0.02) + 0.367 \times (12.5 \pm 1.2)}{0.367 \times 10^{27}} = (1.0 \pm 1.2) \times 10^{-27}\ \text{cm}^2$$

If one takes account of the fact that the total additional capture cross section from all impurities is 1×10^{-27} cm^2, then the effective thermal neutron capture cross section for beryllium equals: $\sigma_c = (6.0 \pm 1.2) \times 10^{-27}$ cm^2.

1% precision in determining the apparent effect S can be obtained for the samples used. Therefore, the main error is in the term σ_T(Be). Indeed, the relative error in the measurement of σ_c is determined by the expression:

$$\left|\frac{d\sigma_c}{\sigma_c}\right| = \frac{S}{S + N\sigma_T}\left|\frac{dS}{S}\right| + \frac{N\sigma_T}{S + N\sigma_T}\left|\frac{d\sigma_T}{\sigma_T}\right| \quad (3)$$

In substituting the data in Equation 3 we find that the first term accounts for an error of only 1%, whereas, the second one is ~18%. Beryllium oxide of high purity was produced for the tests in two batches of briquettes. The briquettes of the first batch had a density of 0.7 gm/cm^3, and the briquettes of the second batch, 2.0 gm/cm^3. The positioning of the sample of pure beryllium oxide in the center of the reactor increased the reactivity as in the case of the graphite standard.

Measurements with highly purified beryllium oxide confirmed that the beryllium nucleus has a considerably smaller capture cross section than was published earlier. In taking the average for several batches of highly purified beryllium oxide, the absorption cross section for a Be nucleus was obtained: $\sigma_c = (6.0 \pm 2.0) \times 10^{-27}$ cm^2.†

Table 3. Data on Measuring σ_c in Beryllium of Highest Grade Purity

Sample	Weight in grams	Number of nuclei in sample	S, cm^2	σ_T, 10^{-27} cm^2
Beryllium	5492	0.367	-2.04 ± 0.02	12.5 ± 1.2
Heavy water	2340	0.071	-3.34 ± 0.03	52.0 ± 1.2

In addition, control measurements for determining the purity of commercial beryllium were made. The measurements were conducted by this same method. Altogether ~1500 kg of beryllium were checked. The capture cross section for different batches varies from 8×10^{-27}–10×10^{-27} cm^2. The weighed mean of thermal neutron capture cross section for beryllium proved to be equal to: $\sigma_c = (8.8 \pm 1.5) \times 10^{-27}$ cm^2.‡

Simultaneously with the measurement of the capture cross section, each batch was subjected to quantitative control by spectral and chemical analyses for impurities. According to the results of chemical analysis, the batches of commercial beryllium contain impurities with $\Sigma\Delta\sigma_c = (2.5\text{–}3.5) \times 10^{-27}$ cm^2 per Be nucleus. Thus, the results of the chemical analysis confirm that the chosen method of measuring σ_c(Be) is highly sensitive and capable of detecting with practically adequate precision the changes in the capture cross section of several millibarns.

† The measurements were made by M. N. Lantsov.

‡ This value has been calculated on the basis that $\sigma_c(0) = 1.5 \times 10^{-27}$ cm^2 and impurities in beryllium oxide constitute 1.0×10^{-27} cm^2.

MEASUREMENT OF NEUTRON MODERATION LENGTH IN BERYLLIUM

The experimental determination of neutron moderation length consists of measuring the spatial distribution of neutrons with fixed energy around a point source of fast neutrons in the material under study.

The neutron moderation density for the point monoenergetic source in an infinite medium is expressed by the equation:

$$q(r,\tau) = \frac{Q}{(4\pi\tau)^{3/2}} e^{\frac{r^2}{4\tau}} \quad (4)$$

where Q is intensity of the source of fast neutrons, r is distance from the source, and τ is neutron age.

The moderation length is a function of the initial and final energy and therefore, depends on the neutron spectrum of the source and the resonance energy of the detector. In the case of a non-monoenergetic source, distribution can be presented as a result of the superposition of several gaussian curves.

The neutron age τ for a point source, in a rectangular prism of infinite height for a non-monoenergetic source is determined by

$$\tau = \frac{1}{6}\frac{\int_0^\infty A(z) z^4\, dz}{\int_0^\infty A(z) z^2\, dz} \quad (5)$$

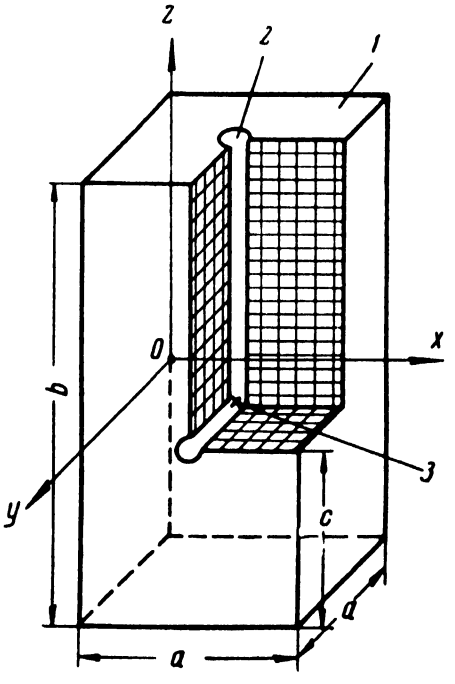

Figure 1. Experimental set-up for measuring neutron moderation length in beryllium: (1) beryllium prism; (2) vertical channel; (3) source of fast neutrons

where $A(z)$ is activity of indium foil, which is proportional to the neutron moderation density at this point of the prism.

The spatial distribution of neutrons was determined along the vertical axis OZ in the prism made of beryllium blocks 40 × 40 × 40 mm with a mean density of 1.78 gm/cm³. Dimensions of the prism are: 68 × 68 × 132 (Fig. 1). The chosen cross-sectional dimensions of the prism did not affect the neutron density along the central axis.

The detectors and source were placed in a vertical axial hole 28 mm in diameter.

Two series of measurements were made: one with a (Ra + Be) source and one with a mock fission source (Po + Be).

The source was positioned in the vertical hole 50 cm from the base of the prism.

Indium foils 25 mm in diameter covered with cadmium plates 0.5 mm thick were used as detectors. All of the measurements were carried out with five different detectors, which were compared with each other by activating them in standard conditions. One of the detectors was used as a monitor.

τ was calculated from Equation 5.

Curves were plotted z^2 *vs* $A(z)$ and z^4 *vs* $A(z)$. The areas under these curves were measured. From the relation of the areas the mean values of τ were found to be equal to: $\tau(1.44\text{ ev}) = (95 \pm 11)$ cm² for the mock fission source and $\tau(1.44\text{ ev}) = (120 \pm 23)$ cm² for the (Ra + Be) source.

The points far from the source were determined by extrapolating the curve z^2 *vs* $A(z)$; which at large distances from the source is exponential.

The value of τ for the (Ra + Be) source is given taking into account the (γ,n) reaction on beryllium.

The corrections were made according to the effect observed for the Ra-source. The experimental curves of the distribution of neutron moderation density from the point source are given in Figs. 2 and 3. The continuous line indicates the gaussian curves calculated for the mean values of τ, which were obtained from the relative areas. The error in τ was determined by the statistical errors and the errors in measuring the areas. The considerable increase of the error in τ for the (Ra + Be) source is explained by the small activity of radium (100 mc), used for the calibration of the (γ,n) reaction in beryllium.

MEASUREMENT OF THE THERMAL NEUTRON DIFFUSION LENGTH IN BERYLLIUM

The measurement of the thermal neutron diffusion length in beryllium was accomplished by the prism method.

The thermal neutron density for any point in a rectangular prism of sufficiently large dimensions is determined by the expression

$$n(x, y, z) = \sum_{lk} C_{lk} \cdot \cos\frac{\pi l}{a} x \cdot \cos\frac{\pi k}{a} y \cdot \operatorname{sh}\frac{c - z}{L_{lk}} \quad (6)$$

where a is length of the side of the prism base, c height of the prism, and L_{lk} relaxation length.

Representing $\operatorname{sh}(c - z)/L_{lk}$ as the difference of two exponents we obtain:

$$n(x, y, z) = \sum_{lk} C_{lk} \cdot \cos\frac{\pi l}{a} x \cdot \cos\frac{\pi k}{a} y \times e^{-\frac{z}{L_{lk}}}\left(1 - e^{-\frac{2(c-z)}{L_{lk}}}\right) \quad (7)$$

In addition to the main term $l = k = 1$ this expression contains terms of a higher order (higher harmonics). Each term of Equation 7 decreases with its own relaxation length. Higher harmonics attenuate faster with distance as the relaxation length decreases with an increase of l and/or K.

If the prism is very large along the axis OZ, then the value in the brackets of Equation 7 is nearly unity.

Hence, at great distances from the source, neutron

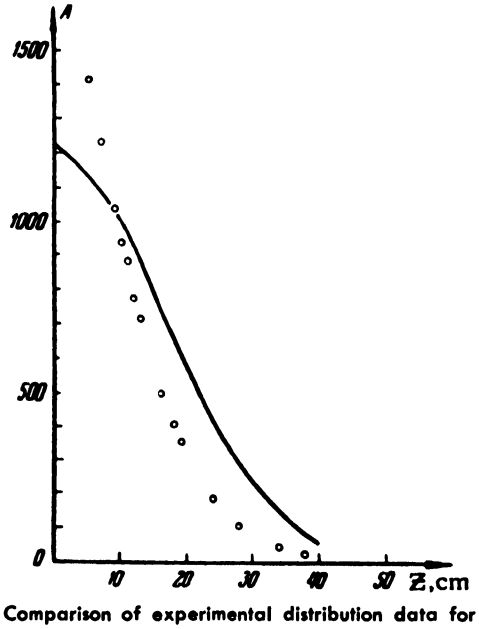

Figure 2. Comparison of experimental distribution data for neutrons of 1.44 ev in beryllium with that obtained under Gauss function (imitating source)

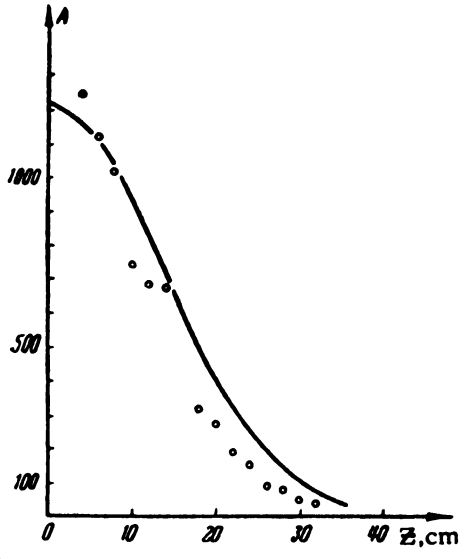

Figure 3. Comparison of experimental distribution data for neutrons of 1.44 ev in beryllium with that obtained under Gauss function ((Ra + Be) — source)

density decreases according to the exponential law with the relaxation length L_{11}

$$n(x, y, z) = A_{11} \cdot \cos\frac{\pi}{a}x \cdot \cos\frac{\pi}{a}y \cdot e^{-\frac{z}{L_{11}}} \quad (8)$$

where

$$\frac{1}{L_{11}^2} = \frac{1}{L^2} + \frac{2\pi^2}{a^2} \quad (9)$$

For measuring the diffusion length, a prism 100 × 100 × 84 cm with a total weight of 1500 kg was made of beryllium blocks.

Such dimensions are quite sufficient for measuring as the error in L due to the finite dimensions of the prism are much less than the error due to accuracy in measuring the relaxation length.

The prism was placed on a metal support at a height of 60 cm from the floor and about two meters from the walls of the room. For eliminating the influence of reflected thermal neutrons on the distribution of neutrons from the source, the whole prism was covered with a layer of cadmium 0.8 mm thick.

Four holes were made for positioning the indicators in the prism—each 28 mm in diameter. The first (I) hole passed along the main axis of the prism and holes, II, III, IV perpendicularly to this hole at a distance of 14, 34, 54 cm from the surface of the beryllium prism (area ABC Fig. 4). Beryllium cylinders 27 mm in diameter and 60 mm high were made to fill the holes during the irradiation of the detectors. Slots were made in several cylinders for the indicators.

(Ra + Be) placed in the beryllium multiplier [(γ,n) reaction on beryllium from the γ-rays of the source were used] served as the source of fast neutrons.

The activity of the sources was ~3×10^7 n/sec.

A graphite prism with a cross section of 220 × 220 cm was used for moderating fast neutrons.

As the measurement of neutron density by indium indicators in cadmium screens showed there were practically no fast neutrons at a distance of 14 cm from the plane ABC in the beryllium prism.

The distribution of neutron density in the prism was determined by dysprosium detectors. The detectors were made by covering an aluminum plate with a layer of dysprosium oxide ~100 mg/cm². Near the detectors the thermal neutron density is distorted, but as the measurement is relative, the errors, connected with this distortion are practically excluded.

The activity induced by neutrons was measured by a Geiger-Müller counter.

π_c, a 64 scaler, was used for registering the impulses from the counter. The stability of the apparatus was controlled by a uranium standard. The resolving time of the apparatus was measured periodically. The resolving time was equal to 2×10^{-4} sec. The thermal neutron density was measured along the central hole of the prism after every 6 cm on a section 20-62 cm from the plane ABC (Fig. 4).

The values of activity were expressed in saturation activation values to compare the results of the measurements by different detectors.

The role of higher harmonics of the spatial-distribution was studied by measuring the neutron

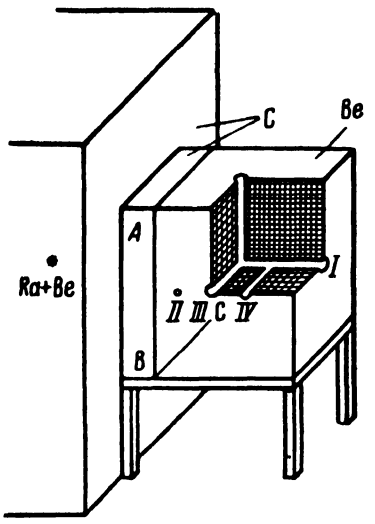

Figure 4. Experimental set-up for measuring diffusion length in beryllium

density in the holes perpendicular to the main axis at distance 14, 34, and 54 cm from the plane ABC. To lessen the influence of the higher harmonics of the neutron distribution, a layer of graphite 30 cm thick and with a cross section of 100 × 100 cm was placed between the graphite and beryllium prisms.

The neutron distribution curves along the cross holes showed that already at a distance of 14 cm, the distribution follows the cosine law, which was an indication of the absence of higher harmonics. The absence of higher harmonics is also confirmed by measurements along the central hole, along which the decrease of density corresponds well to the exponential law.

The results of the measurements are given in Fig. 5.

The value of L_{11} has been obtained from the curve (Fig. 5) equal to: $L_{11} = (16.0 + 0.3)$ cm.

The diffusion length $L = (22.1 + 1)$ cm has been calculated from Equation 9.

The error in measuring the diffusion length is given by the following equation:

$$\left|\frac{dL}{L}\right| = \left(\frac{L}{L_{11}}\right)^2 \left|\frac{dL_{11}}{L_{11}}\right| + 2\left(\frac{\pi L}{a}\right)^2 \cdot \left|\frac{da}{a}\right| \quad (10)$$

The least-squares method was applied to the curves of neutron density distribution. As a result, the error in determining L_{11} was 2%. We obtain the error for the diffusion length equal to 4.5% from Equation 10.

DISCUSSION OF RESULTS

Simultaneously while carrying out the experiments described above for determining σ_c and L the diffusion coefficient D for the same beryllium was measured by an independent method and shown to be equal to: $D = (1.22 \pm 0.04) \times 10^5$ cm²/sec.

We are able to compare the results obtained by the known relations connecting these values.

The weighed mean of the absorption cross section for commercial beryllium has been measured by the danger coefficient method: $\sigma_c = (8.8 \pm 1.5) \times 10^{-27}$ cm².

On the other hand σ_c can be calculated by the formula

$$\sigma_c = \frac{D}{NVL^2} \qquad (11)$$

where N is number of Be nuclei in 1 cm^3, and V = 2200 m/sec.

Substituting value $D = (1.22 \pm 0.04) \times 10^5$ cm^2/sec from other work[5] and $L = 22.1 \pm 1.0$ from this work in Equation 11 we obtain: $\sigma_c = (9.5 \pm 1.2) \times 10^{-27}$ cm^2. Thus, the value of the effective absorption cross section for commercial beryllium being measured by two different and independent methods (according to danger coefficient method and diffusion tests) are in good agreement.[1]

As pointed out above, a number of works were published on the measurement of σ_c, L for beryllium. Therefore, it is of interest to compare the results obtained in this work with those of other authors.

However, only the works of Anderson and Fermi with their collaborators[2] and Hughes[3] with his collaborators can be used for comparison.

Other authors[4,5] give the values σ_c, L without indicating the methods used and accuracy obtained and therefore, cannot be used for comparison.

For convenient comparison, the values given by other authors have been related to beryllium of γ = 1.78 gm/cm^3 density. Comparative data is given in Table 4.

As shown by the data in this table, the results of present measurement of $\sigma_c L$ are in agreement with the data of other authors.

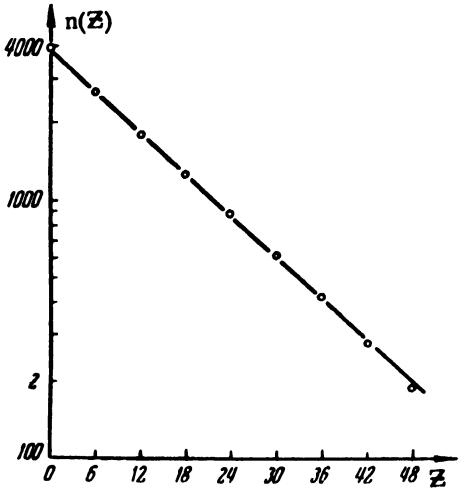

Figure 5. Distribution of thermal neutron density along the central channel in beryllium prism

Table 4

Authors	Values	L, cm	τ, cm^2
This work	8.8 ± 1.5*		
	9.5 ± 1.2†	22 1 ± 1.0	95 ± 11‡
Anderson, Fermi *et al.*	8.5*		--
Hughes *et al.*	10.2 ± 0.5†	21.6 ± 0.5	86.7 ± 2
Palevsky and Smith	10.0 ± 3.0		—

* Values obtained by direct measurement according to reactivity.
† Value of σ_c obtained by diffusion tests.
‡ Value for the imitating source.

CONCLUSION

The results obtained in this work allow us to make the following conclusions:

1. Metallic beryllium has a very small absorption cross section $\sigma_c = (6.0 \pm 1.2) \times 10^{-27}$ cm^2.

2. The mass production of highly purified beryllium (with the total sum of impurities per beryllium nucleus corresponding to an absorption cross section of less than 1 mb) presents serious technological difficulties. Beryllium, however, can be produced in large quantities with a total sum of impurities corresponding to 2–3 mb.

This beryllium has: σ_c(Be) = $(9.0 \pm 1.2) \times 10^{-27}$ cm^2.

According to its nuclear properties, commercial beryllium is a good moderator and can be used as material for thermal reactors.

The problem of the practical use of this material for constructing a real reactor can be solved after a study of the physical, mechanical and corrosion properties of beryllium at in-pile conditions.

REFERENCES

1. Kaplan, C. E., *et al.*, P/636, "Metallurgy of Thorium," Volume 8, Session 15B, these Proceedings.
2. Anderson, H. L., *et al.*, Phys. Rev. *72*, 16 (1947).
3. Hughes, D. J., "Pile Neutron Research" (1954).
4. Palevsky and Smith, Phys. Rev. *86*, 604 (1952).
5. Antonov, A. V., *et al.*, P/661, "A Study of Neutron Diffusion in Beryllium, Graphite and Water by the Impulse Method," Volume 5, Session 19A, these Proceedings.

Measurements of the Diffusion Length of Thermal Neutrons in Beryllium Oxide

By J. C. Koechlin, J. Martelly,* and V. P. Duggal,† France

SUMMARY

The diffusion length of thermal neutrons in beryllium oxide (BeO) was obtained by studying the spatial distribution of the neutrons in a massive parallelepiped of this compound which was constructed at the thermal column of the Saclay reactor.

The mean density of beryllium oxide is 2.95 gm/cm^3, that of the experimental sample 2.92 gm/cm^3.

The diffusion length, as derived from the measurements effectively carried out, is: $L = 32.7 \pm 0.5$ cm (probable error).

Comments are presented about the influence of the spectral distribution of the neutron flux used.

PRINCIPLE OF THE MEASUREMENT

A current of thermal neutrons is introduced into one side of a BeO block which scatters the incident neutrons in its interior.

According to elementary diffusion theory the neutron density ρ is defined in any volume which does not contain a source of thermal neutrons, by the equation

$$\nabla^2\rho - \frac{\rho}{L^2} = 0 \qquad (1)$$

where L is the diffusion length.

All that is needed, in order to determine L, is to analyze the spatial distribution of density ρ in the block used for the experiments, which, in our case, is a right parallelepiped, the dimensions of which are a_0, b_0, c_0. Axes $0x$, $0y$, $0z$, which are needed in order to specify the position of a point in space, are chosen parallel to the sides; the origin of the coordinates is at the center of the side $z = 0$ opposite to the point at which the neutrons enter the block.

The boundary conditions can be written:

$$\rho = 0 \quad \text{with} \quad \begin{matrix} x = \pm a/2 \\ y = \pm b/2 \\ z = -e \end{matrix} \qquad (2)$$

e being the extrapolation distance given by transport theory.

Thus one can write:

$$a = a_0 + 2e$$

$$b = b_0 + 2e$$

The general solution of Equation 1 then can be written:

$$\rho = \sum_{l,m} A_{lm}(z) \cos\frac{l\pi x}{a} \cos\frac{m\pi y}{b} \qquad (3)$$

$$A_{lm}(z) = A_{lm}' Sh\gamma_{lm}(z + e) \qquad (4)$$

when only the first harmonic is kept in the computation, which is a good approximation for our experiment. One can derive L from expression

$$\frac{1}{L^2} = \gamma_{11}^2 - \left(\frac{\pi}{a}\right)^2 - \left(\frac{\pi}{b}\right)^2 \qquad (5)$$

This leaves us with the need to determine γ_{11}.

From an experimental study of the distributions of neutron densities in three equidistant planes, at heights Z_1, Z_2, Z_3, coefficients $A_{11}(Z_1)$, $A_{11}(Z_2)$, $A_{11}(Z_3)$, can be derived, from which γ_{11}, in turn, can be computed by means of the formula:

$$Ch\gamma_{11}(Z_1 - Z_2) = \frac{A_{11}(Z_1) + A_{11}(Z_3)}{2A_{11}(Z_2)} \qquad (6)$$

EXPERIMENTAL SETUP

Beryllium Oxide Block

Since the axis of the thermal column of the Saclay reactor is horizontal, the block is irradiated on one of its vertical sides.

Its horizontal axis of symmetry, $0z$, coincides with that of the thermal column. The surface is separated from the wire, which is the source of neutrons used, by a 4 m thickness of graphite.

The sample consists of a regularly formed pile of 1800 beryllium oxide bricks, $100 \times 100 \times 50$ mm (tolerance ± 0.1 mm), which take up a total volume of 0.9 m^3 and weigh 2.655 tons, since the average density of sintered beryllium oxide is 2.95 gm/cm^3.[1]

The variations in the weight of the individual bricks are about 2% at the most.

As the bricks were being laid, care was taken to alternate in regular fashion between bricks from different lots, in order to avoid any important loss of homogeneity in the density inside the sample.

Original language: French.

* Experimental Neutronic Service, C.E.A.
† Indian Atomic Energy Commission.

The dimensions of the sample are: $a_0 = 100$ cm, $b_0 = 101$ cm, $c_0 = 90$ cm (see Fig. 1).

It was not possible, in the manufacture of the bricks, to provide space for detectors. The measurements are made in 36 horizontal channels having a 50 × 5 mm rectangular cross section, provided between the rows of bricks, two channels per course, and arranged in the pole according to the schematic shown on Fig. 1. Under these conditions, the average density of the mass is 2.92 gm/cm³.

Between the outlet extremity of the thermal column and the beryllium oxide mass, a block of graphite having the same vertical cross section (100 × 101 cm) and a length of 60 cm is interposed. It serves to damp out the upper harmonics of the neutron density, in order for the measurements carried out in the beryllium oxide to be made with the utmost precision.

The mass is covered on all sides, except for the one which faces the neutron source, with cadmium sheets 0.4 mm thick, in order to rule out their being penetrated by thermal neutrons.

Measuring Equipment

The thermal neutron detectors used are leaves of a manganese-nickel alloy (90% Mn, 10% Ni), the area of which is 8 cm², having a thickness of 0.1 mm.

The detectors are mounted in plexiglass frames, the possible error in their position being 0.3 mm.

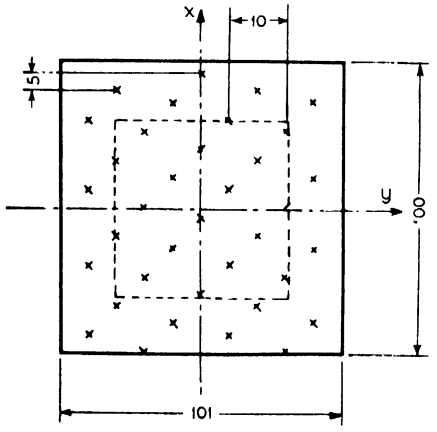

THE CROSSES (×) SHOW THE POINTS WHERE MEASUREMENTS ARE MADE
DISTANCES IN CM

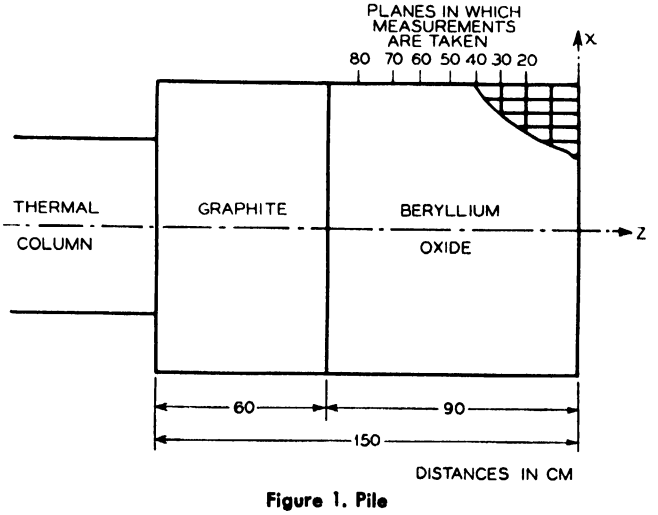

Figure 1. Pile

Activation of the isotope Ni^{62} (incidence 3.6%) entails no drawback, since the half-life of Ni^{63} (2.6 hr) is equal to that of Mn^{56}.

The activities of the detectors are counted by means of ten circuits of the conventional type: GM counters for β-rays (parallel connected counter pairs)—preamplifier—high voltage and scale of 100 or 1000. Each detector, which is first calibrated by means of a standard neutron source is studied by means of each one of the ten calibrated sets of instruments. The usual corrections for dead time and independent motion are applied, and the efficiency of the counting installations is checked by means of uranium standards.

The fluctuations in the power of the reactor and the counting equipment are eliminated by relating all the activities measured to those of the control detector which is placed, for each irradiation, at the same point in the reactor.

MEASUREMENTS

Seven measuring planes have been explored: they are those parallel to face $0xy$, with heights $z = 80$, 70, 60, 50, 40, 30 and 20 cm respectively.

In order to control possible perturbing influences, a series of measurements was made while blocking out the source of thermal neutrons from the reactor by interposing a cadmium sheet between the mass and thermal column.

The residual neutron density observed under these conditions, is approximately 0.3% of the normal density, and spatial distributions are similar.

This shows that, under the conditions of this experiment, no parasitic source (external fast neutrons, neutrons created in the mass by a (γ,n) reaction on beryllium, etc) can disturb the measurements.

Another control measure consists of blocking or plugging the measuring channel with graphite plates: it will be noted that the neutron density observed is slightly lower than that measured with the channel open, but the distribution is not modified appreciably (the near uniform reduction of the densities is about 0.5%).

RESULTS OF MEASUREMENTS

In all planes, even close to the source ($z = 80$ cm), the distribution of the densities $\rho(x,y)$ is represented with very good accuracy by an expression of the form $A_{11} \cos \pi x/a \cos \pi y/b$, without any contribution from the harmonics of higher order (Fig. 2).

A systematic study of the argument of the cosine in all measuring planes leads to taking uniform values: $a = 103.4 \pm 0.4$ cm, $b = 104.4 \pm 0.4$ cm, and namely, $e = 1.7 \pm 0.2$ cm.

This magnitude is substantially larger than that computed with the help of transport theory.

In fact, by using a value of λ_t given by Stephenson[2] ($\lambda_t = 1.65$ cm for beryllium oxide having a density of 2.80 gm/cm³), the figures obtained are: $\lambda_t = 1.57$ cm and $e = 0.71\ \lambda_t = 1.1$ cm.

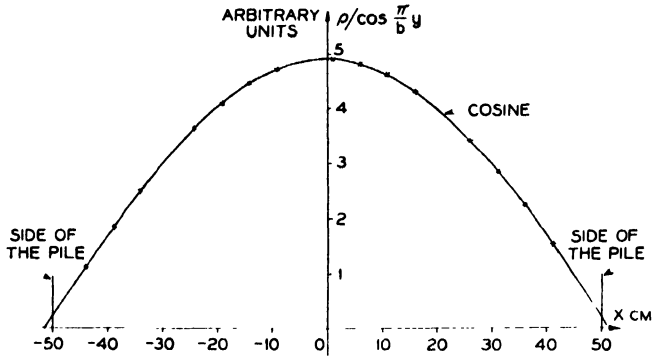

Figure 2. Distribution of the thermal flux in beryllium oxide along a vertical in plane Z = 80 cm

The same discrepancy already was mentioned by Hughes,[3] regarding a very similar experiment carried out with beryllium.

We shall come back to it in our discussion of the results.

In so far as, for beryllium oxide, no experimental value of λ_t, to our knowledge, has been published until now, it seemed to us that it would be more justified to take the empirical extrapolation distance (1.7 cm), which gives us the best representation of the density in the form $A_{11}(\pi x/a) \cos \pi y/b$.

From the distributions observed in the seven measuring planes, we were able readily to derive the seven values of coefficients $A_{11}(z)$.

Neutron density along axis Oz, $A_{11}(z)$ is represented by a function of the form $A_{11}' Sh\, \gamma_{11}(z + e)$ with good accuracy. It even practically coincides with an exponential function in $A_{11}'' e^{\gamma_{11} z}$ between planes $z = 80$ cm and $z = 50$ cm (Fig. 3).

By grouping the values $A_{11}(z)$ by sets of three, we derived γ_{11} and L with the help of Equations 6 and 5. The results so obtained are grouped in the table below:

$A_{11}(z)$ groups Z_1	Z_2	Z_3	γ_{11} in m^{-1}	L in cm
80	60	40	5.28 ± 0.03	32.3 ± 0.8
70	50	30	5.25 ± 0.03	32.8 ± 0.8
60	40	20	5.21 ± 0.04	33.6 ± 1.0
80	50	20	5.26 ± 0.02	32.7 ± 0.6

The average value is: $L = 32.7 \pm 0.5$ cm (probable error).

DISCUSSION OF RESULTS

The value of the diffusion length for thermal neutrons evidently depends on the spectral distribution of the neutron flux used in the diffusion experiment.

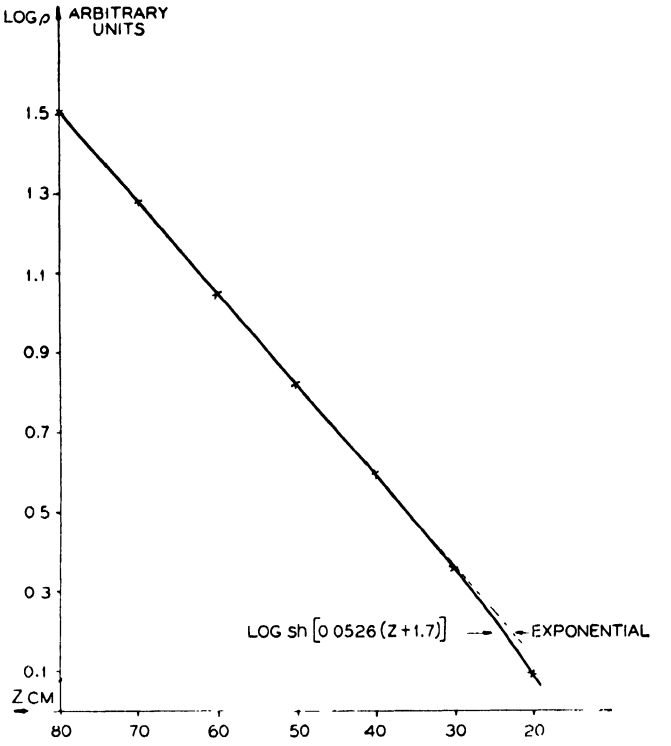

Figure 3. Distribution of thermal flux in beryllium oxide along the horizontal axis of the pile

This distribution, in turn, depends on the nature of the source and the form and dimensions of the experimental device.

On the one hand, the spectral distribution of the neutrons diffused by the graphite of the reflector and of the thermal column of the reactor may not be strictly Maxwellian, and, on the other hand, it is possible that it will be still further modified as the neutrons scatter in the medium in which the experiment is conducted.

In fact, a complete study of the experimental results shows that it is not possible exactly to represent the neutron density along axis Oz by a function $Sh(\gamma(z + e))$. Figure 4, in which the logarithm of the ratio of the density ρ to the function $Sh(0.0526(z + 1.7))$, has been drawn, illustrates the differences enhancing them considerably.

This anomalous situation (which cannot be reduced by adjusting the values of γ and e) is to be compared with a disagreement between the empirical value of a and quantity $a_0 + 2e$ (e as calculated by the transport theory).

Both effects show that low neutron densities are, in relative value, higher than those which are to be

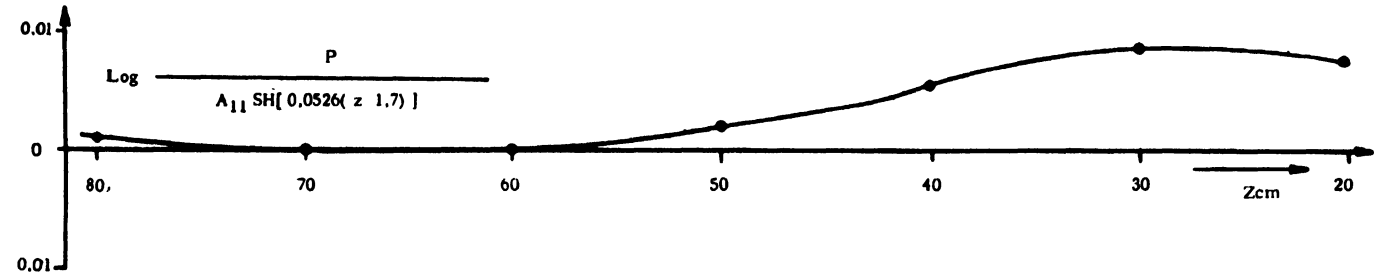

Figure 4

expected by the classical theory of thermal neutron diffusion.

This is expressed by an apparent increase in the diffusion length, when the neutrons progress into the sample.

Such an effect may be interpreted as a modification of the neutron spectrum which can be caused by a selective filtration phenomenon.

It thus appears that the regions in which the neutrons are in the highest densities would be least sensitive to this perturbation, and this consideration suggested to us that we ascribe a heavier weight to this region in our computation of the diffusion length.

A few complementary experiments are currently being carried out, for the purpose of determining the sensitivity with which a modification of the spectral distribution of the neutrons may influence the experimental value of the diffusion length.

ACKNOWLEDGEMENTS

We extend our thanks to Mr. Vendryès, Chief of the Experimental Neutronics Division, for his kind interest in our work, as well as for the suggestions that he made in the course of many consultations.

One of us (V. P. Duggal) wishes to express his warm thanks to the Department of Atomic Energy of the Indian Government for the financial help which made it possible for him to stay with the Nuclear Study Center at Saclay. He also wishes to thank the French Atomic Energy Commission for the kind welcome he has received.

REFERENCES

1. Caillat, R. and Pointud, R., P/345, *Sintering of Beryllium Oxide*, Volume 8, Session 17B.2, these Proceedings.
2. Stephenson, R., *Introduction to Nuclear Engineering*, McGraw-Hill Book Company, Inc., p. 377, New York (1954).
3. Hughes, D. J., *Pile Neutron Research*, Addison Wesley Publishing Company Inc., p. 221, Cambridge, Mass. (1953).

On the Determination of Diffusion and Slowing Down Constants of Ordinary Water and Beryllium Oxide Using a Pulsed Neutron Source

By R. Ramanna, G. S. Mani, P. K. Iyengar, S. B. D. Iyengar, and B. V. Joshi,* India

A method of obtaining the diffusion constants and the age to thermal energy of water and beryllium oxide using a pulsed neutron source is described. Such a method has been used by Haworth *et al.*[1] in the measurement of the mean life of thermal neutrons in water and by von Dardel[2] in the measurement of the diffusion length in water and heavy water. The main advantages of this method are that comparatively small quantities of the moderator material are required and it is possible to determine the absorption mean free path, transport mean free path and the age to thermal energy directly. In the case of water moderator of infinite dimensions the interpretation of the decay constants depends very much on the choice of the theory.

THEORY

The general equation for the time-dependent source in a non-multiplying medium on the age theory is given by

$$L^2\nabla^2\rho_s(\mathbf{r},t) - \rho_s(\mathbf{r},t) + \tau_c e^{\tau_0\nabla^2}S(\mathbf{r},t) = \tau_c\frac{\partial}{\partial t}\rho_s(\mathbf{r},t) \quad (1)$$

where L = diffusion length of thermal neutrons in the moderator, $\rho_s(\mathbf{r},t)$ = thermal neutron density at the point $\mathbf{r}$ and time t, $S(\mathbf{r},t)$ = source of fast neutrons at point $\mathbf{r}$ and time t, τ_c = mean life of thermal neutrons in the moderator, $e^{\tau_0\nabla^2}$ = "resolvant operator,"[3] and τ_0 = age of source neutrons to thermal energy.

On the two-group theory the equations become[4]

$$L_f^2\nabla^2\rho_f(\mathbf{r},t) - \rho_f(\mathbf{r},t) + \tau_{cf}S(\mathbf{r},t) = \tau_{cf}\frac{\partial}{\partial t}\rho_f(\mathbf{r},t) \quad (2)$$

$$L_s^2\nabla^2\rho_s(\mathbf{r},t) - \rho_s(\mathbf{r},t) + \frac{\tau_{cs}}{\tau_{cf}}\rho_f(\mathbf{r},t) = \tau_{cs}\frac{\partial}{\partial t}\rho_s(\mathbf{r},t) \quad (3)$$

where subscript f denotes "fast" group and s denotes "slow" group.

L_f^2 = square of slowing down length of source neutrons to thermal energy; in the two-group theory it can be shown to be equal to the "age."

L_s^2 = diffusion length of thermal neutrons, τ_{cf} = slowing down time of source neutrons to thermal energy, and τ_{cs} = mean life of thermal neutrons in the moderator.

* Atomic Energy Establishment, Trombay, India.

Finite Moderator

The thermal neutron distribution due to an instantaneous source of fast neutrons is given on age theory by

$$\rho_s(\mathbf{r},t) = S_0\sum_{lmn}B_{lmn}\phi_{lmn}(\mathbf{r})e^{-\tau_0\omega_{lmn}^2t}e^{-\left(\frac{1}{\tau_c}+D\omega_{lmn}^2\right)t} \quad (4)$$

For the case of a rectangular parallelepiped of sides a, b, c and origin of coordinates at one of the corners, with a point source at (x',y',z') and detector at (x,y,z),

$$B_{lmn} = \frac{8}{abc}\sin\frac{l\pi x'}{a}\sin\frac{m\pi y'}{b}\sin\frac{n\pi z'}{c} \quad (5)$$

$$\phi_{lmn} = \sin\frac{l\pi x}{a}\sin\frac{m\pi y}{b}\sin\frac{n\pi z}{c} \quad (6)$$

$$\omega_{lmn}^2 = \pi^2\left[\frac{l^2}{a^2}+\frac{m^2}{b^2}+\frac{n^2}{c^2}\right]; \qquad L^2 = D\tau_c \quad (7)$$

On the two-group theory the solution is

$$\rho_s(\mathbf{r},t) = S_0\tau_{cs}\sum_{lmn}B_{lmn}\phi_{lmn}(\mathbf{r})\frac{e^{-\lambda_{lmn}^s t}-e^{-\lambda_{lmn}^f t}}{\tau_{cf}\tau_{cs}[\lambda_{lmn}^s-\lambda_{lmn}^f]} \quad (8)$$

where $\lambda_{lmn}^s = (1+\omega_{lmn}^2L_s^2)/\tau_{cs}$ and $\lambda_{lmn}^f = (1+\omega_{lmn}^2L_f^2)/\tau_{cf}$. After a short time the fast term $e^{-\lambda_{lmn}^f t}$ becomes negligible and the two theories give the same decay in time. The two group expression is less convergent than the age theory expression.

From the expressions given by the age theory one can find the mean life of thermal neutrons, the diffusion length of thermal neutrons, and the age of source neutrons to thermal energy in any moderator, if the size of the moderator assembly is so chosen that only the first harmonic is important, the other harmonics dying out very rapidly with time. Under such conditions

$$\rho_s(\mathbf{r},t) = S_0B_{111}\phi_{111}(\mathbf{r})e^{-\tau_0\omega_{111}^2}e^{-\left(\frac{1}{\tau_c}+D\omega_{111}^2\right)t} = Ae^{-\lambda t} \quad (9)$$

Using Behrens formula 5 for exponential fitting one can find log A and λ. From λ_i's for various bucklings ω_i^2, one can get by least-squares fitting τ_c, D and L^2. If the source and detector positions are fixed, and the

source strength is normalised by a fast neutron monitor, S_0 and $\phi_{111}(r)$ are constants for all bucklings. Writing $S_0\phi_{111}(r) = K$

$$\log A - \log B_{111} = \log K - \tau_0\omega_{111}^2$$

From the values of $(\log A - \log B_{111})$ for various bucklings ω^2, τ_0 can be obtained by least-squares fitting.

Infinite Moderator

The thermal neutron distribution for an instantaneous point source of fast neutrons is given on the age theory by

$$\rho_s(r,t) = \frac{S_0}{8\pi^{3/2}} \exp[-t/\tau_c] \exp\left[-\frac{r^2}{4(\tau_0 + L^2t/\tau_c)}\right] (\tau_0 + L^2t/\tau_c)^{-3/2} \quad (10)$$

On the two-group theory we get

$$\rho_s(r,t) = \frac{\tau_{cs}S_0}{2\pi^2\beta r}[e^{-t/\tau_{cs}}I(\alpha_s,\mu^{1/2}) - e^{-t/\tau_{cf}}I(\alpha_f,\mu^{1/2})] \quad (11)$$

where

$$\beta = (\tau_{cs} - \tau_{cf}); \qquad \mu^{1/2} = \left[\frac{\tau_{cf}L_s^2 - \tau_{cs}L_f^2}{\beta}\right]^{1/2};$$

$$\alpha_s = \frac{L_s^2 t}{\tau_{cs}}; \qquad \alpha_f = \frac{L_f^2 t}{\tau_{cf}}$$

$$I(\alpha, \mu^{1/2}) = e^{\alpha/\mu}\left[e^{-r/\sqrt{\mu}}\left\{1 - \operatorname{erf}\left(\sqrt{\frac{\alpha}{\mu}} - \frac{r}{2\sqrt{\alpha}}\right)\right\} - e^{r/\sqrt{\mu}}\left\{1 - \operatorname{erf}\left(\frac{\sqrt{\alpha}}{\sqrt{\mu}} + \frac{r}{2\sqrt{\alpha}}\right)\right\}\right]$$

$$\operatorname{erf}(x) = \frac{2}{\sqrt{\pi}}\int_0^x e^{-u^2}\,du$$

$I(\alpha, \sqrt{\mu}) = e^{\frac{\alpha}{\mu}} e^{-\frac{r}{\sqrt{\mu}}}$ up to a time t_1, after which it decreases rapidly. Since $\tau_{cf} \ll \tau_{cs}$, after a time t_2, $I(\alpha_f, \sqrt{\mu}) \ll I(\alpha_s, \sqrt{\mu})$ and can be neglected. Hence between t_1 and t_2,

$$\rho_s(r, t) \approx \frac{\tau_{cs}S_0}{\pi^2\beta\gamma} e^{-\frac{\gamma}{\sqrt{\mu}}} e^{-\frac{t}{\tau_{cs}}\left[1-\frac{L_s^2}{\mu}\right]} \quad (12)$$

and

$$\frac{d}{dt}\log \rho_s(r, t) = -\frac{1}{\tau_{cs}}\left[1 - \frac{(\tau_{cf} - \tau_{cs})L_s^2}{\tau_{cf}L_s^2 - \tau_{cs}L_f^2}\right] \quad (13)$$

The age theory expression does not show such an exponential character in any interval of time.

EXPERIMENTAL ARRANGEMENT

The Neutron Pulsing System

The fast neutron bursts were produced from a cascade generator using the (D-Be) reaction. The generator was operated at about 900 kv with a steady current of 300 microamperes. The deuteron beam was modulated by pulsing the extraction voltage of the radio-frequency ion source. The pulse width was 30 microseconds and the repetition frequency was about 600 per second.

The Detector

The thermal neutrons were detected by means of a lithium iodide scintillation counter. The crystal was mounted at the end of a long perspex rod which was attached to the photocathode of a 6262 E.M.I. photomultiplier. The light guide arrangement was used so that the photomultiplier was as far away as possible from the moderator assembly, to avoid any interference in the neutron distributions. The LiI crystal detects thermal neutrons due to the reaction Li^6 (n,α) H^3. The disintegration products lose all their energy in the crystal and cause a scintillation pulse large compared to pulses due to the extraneous gamma radiation and from the activated iodine atoms in the crystal. The pulses from the disintegration of Li atoms are of nearly equal height and hence these pulses can easily be discriminated from the background radiations. The LiI crystal was a 1 cm cube. The fast neutrons were monitored by a stilbene scintillation detector placed at a large distance from the moderator assembly and directly above the fast source, so that small buckling changes do not affect the fast counts due to leakage neutrons. Figure 1 gives the complete diagram of the experimental arrangement.

The Time Analyser

A new type of time analyser was used to obtain the time distributions. The advantage of this method is its extreme simplicity and it easily satisfied the demands of the present experiment. The principle of this method is to make the ion pulse at the accelerator target initiate the time base of an oscilloscope and allow the thermal neutron pulses to intensify the oscilloscope spot. These spots are observed by a series of 20 photomultipliers on to which the oscilloscope trace is magnified and focussed by means of a simple optical system. The pulses from the photomultipliers after passing through a single stage of amplification

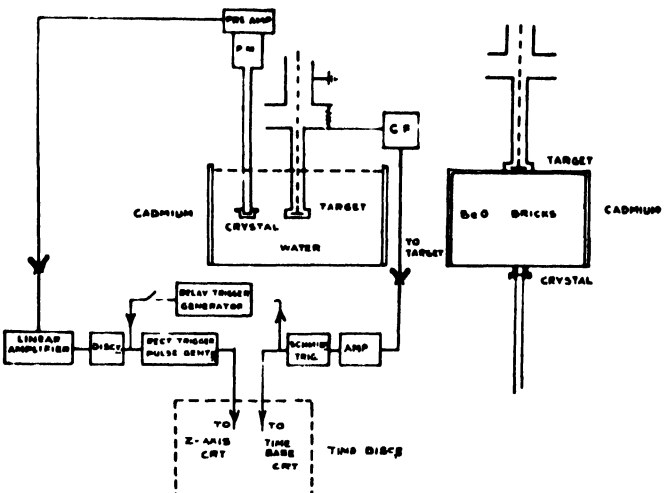

Figure 1. Block diagram of experimental arrangement

are recorded by 20 scales of 32. The widths of the various channels were determined from the number of counts in each channel due to a constant source of random pulses.

It may be mentioned that this instrument can be used as a pulse analyser without any additional circuits if the cancellation is produced by feeding the last dynode pulse of each succeeding tube to the collecting cathode of the previous tube by suitable integration circuits to allow for the time differences of the pulses.

ORDINARY WATER—INFINITE GEOMETRY

A cylindrical tank of aluminium of diameter 77 cm and depth 40 cm was filled with distilled water. The sides and bottom of the tank were lined with cadmium on the outside to absorb thermal neutrons entering or leaving the tank. The target tube of the accelerator and the detecting crystal were kept in the mid-plane of the water at a distance of 20 cm from each other (Fig. 1). The thermal neutrons were detected in a time range between 150 and 700 microseconds, a region in which the two-group theory predicts a nearly pure exponential decay to within 1%.

The experimental logarithmic neutron distributions as well as theoretical distribution on age and two group theories are shown in Fig. 2. It will be noticed that in a region between 200 and 500 microseconds the experimental logarithmic distribution is a straight line. The slope of the straight line in this region was determined by exponential fitting and was found to be 0.003386 ± 0.000018.

Calculations of the slope were made on both age and two-group theories. The constants used in the calculations were those given by Glasstone and Edlund.[6] Using for L the value 2.88 cm, for τ_0 the value 33 cm^2, for τ_{cs} the value 210 microseconds and for τ_{cf} the value of 10 microseconds, we get on the age theory a mean slope of 0.004145 between 200 and 500 microseconds. The two-group theory gives a region of approximately pure exponential decay between 150 and 700 microseconds, yielding a slope of 0.003592 which, as can be seen from Fig. 2 agrees better with the experimental value. If we use a value of 5.33 cm for the slowing down length instead of 5.74 cm, the two-group theory agrees with the experimental slope. The disagreement of age theory is to be expected since it is well known that age theory is inapplicable in the case of very light moderators like water and heavy water.

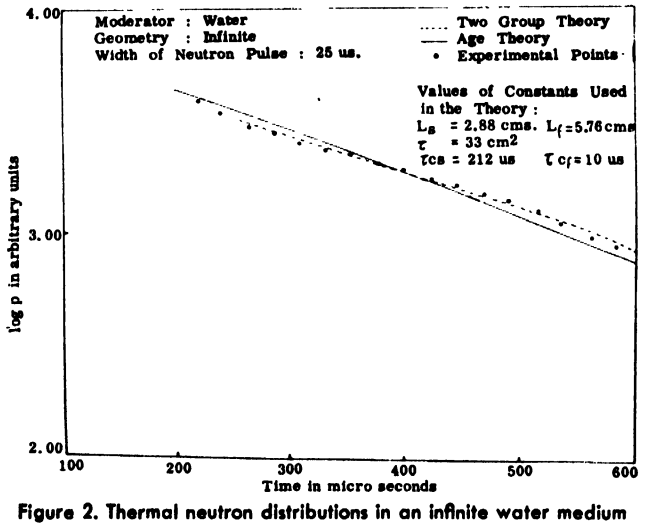

Figure 2. Thermal neutron distributions in an infinite water medium

The experimental curve disagrees with the theoretical curve in two respects. The region of pure exponential decay is only between 200 and 500 as against 150 and 700 microseconds, as predicted by theory. The theoretical slope is higher than the experimental slope by a factor which is larger than the experimental error. These two deviations could be explained on a three or four group model by fitting the group parameters to the experimental curve as was done by Fermi *et al.*[6] for the spatial distribution. Since this is an arbitrary method it was not attempted.

BERYLLIUM OXIDE

The material was available in the form of rectangular bricks of size 10 cm × 10 cm × 5 cm. The mean density was 2.96 gm/cc and the impurities as specified by the manufacturers was less than 725 ppm of iron equivalent by weight. The bricks were arranged in a rectangular pile. The source and detector were placed on opposite sides of the pile. In order to eliminate the effect of thermal neutrons reflected from the walls of the room the moderator assembly was covered on all sides except on the side facing the detector, by a cadmium sheet of 1 mm thickness. A sheet of cadmium was placed below the photomultiplier to stop neutrons reflected from the floor.

It is essential to perform the experiment under conditions such that the effect of the higher harmonics is negligible and only the fundamental mode of decay is important. By calculations made from existing values for the moderator constants and by making some trials it was found that the best sizes to work with were those around about a 35 cm cube. The higher harmonics die down very rapidly with time, and it was found that between 500 and 1000 microseconds only the fundamental mode is excited. If the sizes of the assemblies are very much reduced it was found that the counting rates become very low and the wall reflection effects of fast neutrons due to the large leakage become appreciable.

The calculation of bucklings involve a proper choice of the extrapolation length and since our results yield a value of D and hence λ_r, an approximate value of λ_r was chosen leading to a first value of λ_r (experimental). This was used in a process of successive approximations to get the final correct value of D.

Figure 3 shows the variation of the decay constant with buckling. The points within the region of investigation lie on a straight line. The slope of this straight line gives D and the intercept gives the value of $1/\tau_{cs}$. The diffusion length L is given by $(D\tau_{cs})^{1/2}$. It can be seen from Fig. 3 that a small error in λ causes a large error in τ_{cs} because the choice of the bucklings

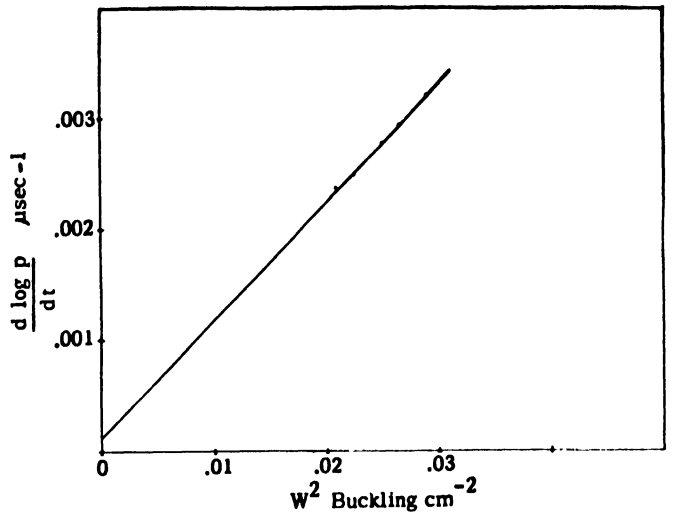

Figure 3. Neutron decay constants for various bucklings in BeO. The slope and intercept give D and $1/\tau_c$ respectively

is restricted to between 0.02 to 0.03 to avoid higher harmonics on the one hand and large leakage on the other.

The measured decay constants with their statistical errors are given below.

Size	ω^2	λ	$\Delta\lambda$
30 × 30 × 30 cm	0.028790	0.003214	0.000019
30 × 30 × 35 cm	0.026376	0.002949	0.000018
30 × 30 × 40 cm	0.024770	0.002782	0.000019
30 × 35 × 40 cm	0.022356	0.002481	0.000015
30 × 40 × 40 cm	0.020750	0.002378	0.000014

$L = 28.6 \pm 0.3$ cm (density 2.96 gm/cm^3)
$D = (0.1069 \pm 0.0006) \times 10^6$ cm^2-sec^{-1}
$\tau_c = 7661 \pm 119$ microseconds.

The value of L obtained for BeO is in reasonable agreement with that published in an AECD report[7] and by Stephenson[8] who give a value of 30 cm for a density of 2.8 gm/cm^3 and unspecified purity. No error is mentioned in their value.

The value of D obtained by us is slightly lower than that quoted by above authors. We find that even after allowing for "diffusion cooling" the value of D does not increase above statistical error.

A value of 156 cm^2 was obtained for age to thermal energy in BeO. This is in agreement with the value of 151 cm^2 calculated from microscopic data. Further experiments are in progress to confirm this value.

ACKNOWLEDGEMENTS

Our thanks are due to Mr. P. N. Rama Rao and Mr. M. P. Navalkar for their assistance in the design and construction of the time analyser and pulsing system and to Mr. C. S. Somanathan and Mr. S. K. Amberdaker for running the cascade generator.

REFERENCES

1. Haworth, L. J., Luebke, E. A. and Manley, J. H., *The Mean Life of Neutrons in Water and the Hydrogen Capture Cross-Section*, Phys. Rev. *61*, 152.
2. von Dardel, G. F., *The Interactions of Neutrons with Matter Studied with a Pulsed Neutron Source*, Thesis Goteborg (1953).
3. Salvetti, *Symbolical Calculation Methods Applicable to Neutron Multiplication*, Il Nuovo Cimento *7*, 482; *Time Dependent Neutron Sources in Multiplying Media*, Il Nuovo Cimento *8*, 960.
4. Glasstone, S. and Edlund, M., *The Elements of Nuclear Reactor Theory*, D. Van Nostrand Co. (1952).
5. Behrens, *The Fitting of Exponential Decay Curves*, AERE report, T/R 629.
6. Cf. reference 4.
7. Abernathy, F. H., *et al. Reactor Design and Feasibility Problem Part II*, AECD/3557.
8. Stephenson, R., *Introduction to Nuclear Engineering*, McGraw-Hill Book Co. (1954).

A Study of the Slowing Down of Neutrons in Graphite

By V. P. Duggal* and J. Martelly,† France

AIM OF THE INVESTIGATION AND PRINCIPLE OF THE METHOD

It was undertaken to determine empirically an effective value of the slowing-down age of thermal neutrons in graphite, i.e., the value of τ_r which could be introduced in the conventional formula for the migration area:

$$M^2 = \tau_r + L_\theta^2$$

It will be necessary to explain accurately the meaning given to M^2. We have taken it to be the mean value of $\overline{r^2}/6$ for the neutrons captured according to a $1/v$ law. This is a measurable magnitude.

In order to minimize the term L_θ^2, to be subtracted, and to work on a medium of reasonable dimensions, we poisoned the graphite. For practical reasons, the poison is made up of iron sheets alternated with slabs of graphite. Since their separation is substantially less than the mean free path we consider the medium as homogeneous.

We refer back to indium resonance as the standard origin for all terms having age ($\overline{r^2}/6$). This offers the two-fold advantage of furnishing results that are independent of the neutron source and little affected by the insertion of iron sheets in the graphite mass. (The perturbation will mainly occur in the region above the indium resonance. It would be difficult to compute a correction for the effect of inelastic collisions with the iron.)

In order to rule out the effect of the resonance neutrons on the detector (manganese), it is necessary to make a study of the neutrons captured by cadmium (group C) by using the conventional method which consists of computing the difference between the activities measured with and without a filter.

One of us suggested,[1] as the final touch to a project which was completed ten years ago, that the method be generalized in such a way as to take advantage of the properties of gadolinium. It was used here concurrently with that of the cadmium screen. Gadolinium shows a resonance at 0.04 ev, with a width[2] of 0.1 ev.

The group of neutrons it captures yields a spectrum closer to a Maxwellian distribution than does group C.

Interpretation of the experiment will be seriously complicated by the fact that the epithermal capture following a $1/v$ law which adds up to the thermal capture, is no longer simply a corrective term. These terms are comparable to each other in magnitude, and it would be futile to attempt to make a distinction between them: in fact, we deal here with a neutron spectrum very far removed from Maxwell's spectrum. This interpretation is the subject of part three.

The distribution of the indium resonance neutrons was the subject of a special investigation.

At large distances from the source of fast neutrons the neutron density differs substantially from a Gauss' law distribution. We found qualitative agreement between the experimental curve and Holte's theory[3] which accounts for the variation of λ (mean diffusion free path) with the neutron energy.

We also checked the experimental value of the age of the neutrons, between 24 ev (Pd) and 1.45 ev (In); and the result agrees with Fermi's theory.[4]

PART I. EXPERIMENTAL SET-UP AND MEASUREMENT

The graphite pile has the following dimensions: vertically: 190 cm, horizontally: 210 cm × 210 cm; it is placed on a horizontal concrete platform. Part of this pile (which we shall call the poisoned medium) having dimensions of 120 × 120 × 120 cm is made up of graphite plates 1.4 cm thick, with a density of 1.65 gm/cm^3, which alternate with iron sheets 0.1 cm thick, the surface density of which is 0.78 gm/cm^2. We used a 6 curie source of Ra-α-Be, which was placed in the poisoned medium, at the point having coordinates (20,20,20), and we used the notations shown on Fig. 1.

DETECTORS

End detector used an area of 8 cm × 1.4 cm. The indium leaves had a thickness of 0.1 mm and were clad with cadmium 0.4 mm, each side. For the manganese detectors we used an alloy consisting of: 88% Mn, and 12% Ni, 0.12 mm thick. The gadolinium filters for the manganese detectors were prepared as follows.

A Gd_2O_3 powder was mixed with a solution of plexiglass + dioxane. The mixture was spread on a glass plate and solidified by evaporation. We prepared homogeneous leaves containing 3 mg/cm^2 of Gd_2O_3 each. Homogeneity was checked by activating a gold foil behind the Gd_2O_3 filter, in a spatially uniform flux of neutrons. The activation was observed by the blackening of a photographic plate, in accordance with the "autoradiographic" method of Zaleski.[5]

An approximation to the filter's absorption was obtained by means of a crystal spectrometer[6] for three

Original language: French.

* Indian Atomic Energy Commission.

† Experimental Neutronic Service at the C.E.A. (Centre d'Énergie Atomique) (Service de Neutronique expérimentale au C.E.A.).

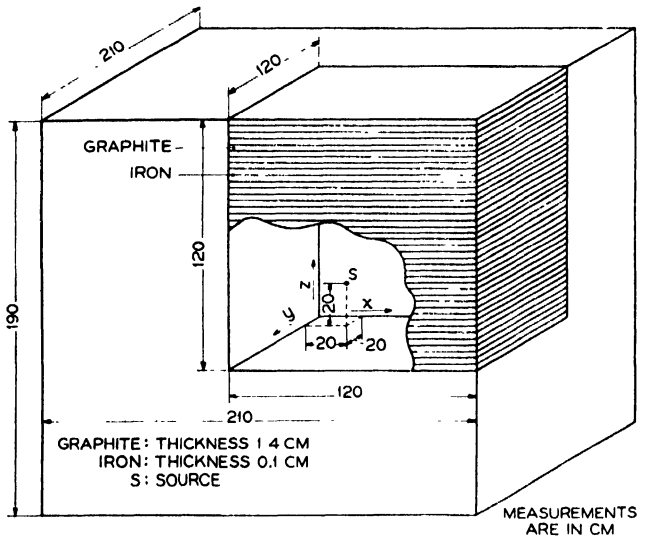

Figure 1

neutron energies as follows: 0.025, 0.04 and 0.08 ev. The corresponding absorption curve is shown on Fig. 2.

We also measured the Gd_2O_3 filter's absorption in an isotropic flux of thermal neutrons in the poisoned medium. For this purpose, we irradiated, in the thermal column of the Saclay pile, a sample of the poisoned medium in which we measured the activity of a manganese detector, with and without Gd_2O_3. The transfer coefficient was 36%. This value is in agreement with that computed by means of the Bothe formula[7] (34%), allowing for the absorption and flux depression caused by an absorber.

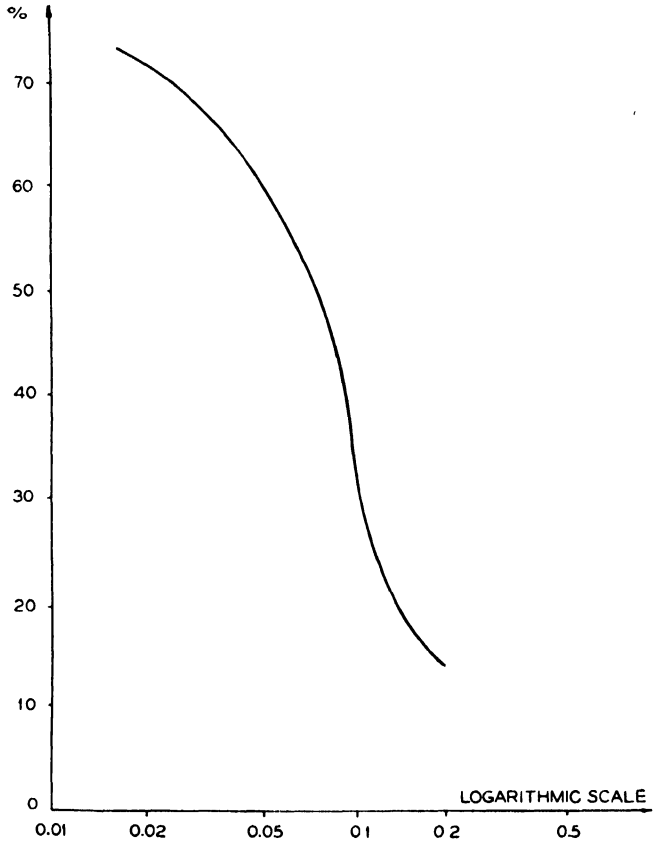

Figure 2. Gd-filter absorption coefficient for the neutrons detected by Mn, as a function of the energy in the thermal range

The palladium detectors (24 ev) are made up of sheets of 0.146 gm/cm² thickness. The other resonances are to be found in the very high energy range (about one Mev) and do not play any role.

EXPERIMENTAL RESULTS

Measure of $\overline{r^2}$: Mean Square of the Distance Covered by the Neutrons until They are Captured

We measured the activity at saturation, A, of the Cd-covered indium detectors in the poisoned medium, as a function of distance r to the source, up to $r = 140$ cm. Figure 3 shows the variations of the logarithm of A as a function of r^2.

The age theory calls for a linear variation which is well verified in the interval $500\ \text{cm}^2 < r^2 < 2500\ \text{cm}^2$. In the neighborhood of the source ($0 < r^2 < 500\ \text{cm}^2$) and for large distances ($r^2 > 2500\ \text{cm}^2$) the experimental points are to be found above the straight line.

At small distances, this phenomenon is in agreement with the fact that In possesses several high-energy resonances; the flux in this region, near to the source, is particularly rich in fast neutrons.[8]

For great distances, the results are better given by an exponential law: the logarithm of Ar^2 decreases as a linear function of r. The relaxation length is 14.3 ± 0.3 cm. This value is larger than that to be expected from the asymptotic theory[9] which yields.

$$A = \frac{Cte}{4\pi r^2} \exp\left(-r/\lambda_s\right) \qquad (1)$$

wherein λ_s represents the scattering mean free path for neutrons coming from the source. The scattering cross section for the neutrons produced by Ra-α-Be (average energy about ~5 Mev) is about 1.2 barns, and corresponds to a mean free path of 10.6 cm.

A comparison between the experimental distribution and the theoretical formulae will be given in greater detail in the discussion.

For the Mn detectors a relaxation length of 14.9 ± 0.4 cm was found experimentally.

Measurements with Gd- and Cd-clad Mn detectors have been made up to $r = 90$ cm. It has been assumed that the activity differences [Mn − (Mn + Gd)] and [Mn − (Mn + Cd)] will decrease exponentially where $r > 90$ cm, with the same length relaxation as for the case of Mn alone. The value of $\overline{r^2}$, for each detector, has been found from the formula

$$\overline{r^2} = \frac{\int_0^\infty Ar^4\,dr}{\int_0^\infty Ar^2\,dr} \qquad (2)$$

Integrations have been carried out graphically from the curves showing Ar^4 and Ar^2 as functions of r, up to a distance of $r = 90$ cm. Beyond 90 cm, the curves were extrapolated up to infinity by the use of Equation 1, in which λ_s represents the experimental relaxation length.

In order to correct for the effects of high-energy resonances, the experimental straight line (log A as a function of r^2), was extrapolated for values up to

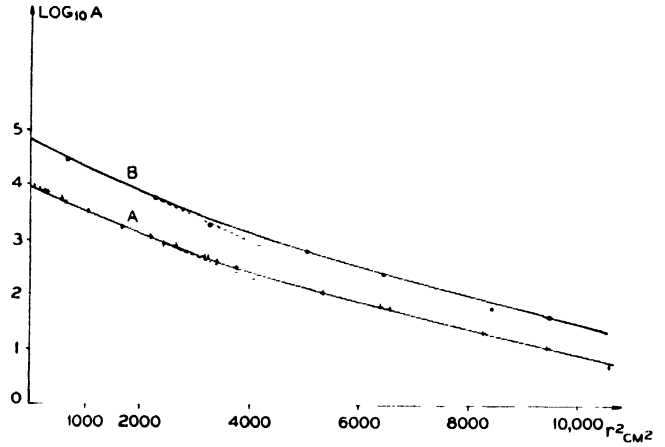

Figure 3. (A) In + Cd detector, energy 1.45 ev; (B) Pd + Cd detector, energy 24 ev. Curves of $\log_{10} A = f(r^2)$. (A) activity (counts/minute); (r) distance at the source (cm)

$r^2 = 0$. Table 1 shows the values of $\overline{r^2}/6$ computed according to these rules.

Table I. Value of $\overline{r^2}/6$ in the Poisoned Medium

Detector	$\overline{r^2}/6$, *from the source of Ra-α-Be*	$\overline{r^2}/6$, *from 1.45 ev on up (In resonance)*
Pd + Cd (24 ev)	307.2 ± 4 cm²	−36.4 ± 6 cm²
In + Cd (1.45 ev)	343.59 ± 2.5 cm²	
Mn (alone)	409.1 ± 2.7 cm²	65.5 ± 5.4 cm²
Mn (Mn + Cd 4/10 mm)	428.1 ± 3.0 cm²	84.5 ± 5.5 cm²
Mn (Mn + Gd)	452.1 ± 3.6 cm²	108.4 ± 6.0 cm²

Measuring of the Diffusion Length L_θ

The value of L_θ (diffusion length), for the poisoned medium, was determined by using the thermal column of the Saclay reactor in a conventional method of an exponential experiment, with the help of Mn detectors. The dimensions of the medium were $b_0 = 75.2$ cm, $a_0 = 72.3$ cm, $z = 103$ cm. In this experiment, the (1,1) harmonic decreases exponentially as a function of Z, with a relaxation length of 7.03 cm.

We may write:

$$\frac{1}{L_\theta^2} = \frac{1}{\gamma^2} - \frac{\pi^2}{a^2} - \frac{\pi^2}{b^2}$$

where

$$a = a_0 + 2\epsilon$$

$$b = b_0 + 2\epsilon$$

ϵ = extrapolation length

which gives:

$$L_\theta^2 = 58.6 \pm 2 \text{ cm}^2$$

$$L_\theta = 7.56 \text{ cm}$$

The age of the neutrons between 24 ev (Pd + Cd) and 1.45 ev (In + Cd) is 36.4 ± 6 cm² for the poisoned medium. For a graphite of 1.6 density, this slowing-down age becomes (the corrections will be discussed later on):

$$-\tau_{24\,ev} + \tau_{1.45\,ev} = 40.9 \pm 6 \text{ cm}^2$$

This is in agreement with the Fermi theory, which yields 42.6 cm².

The fifth group of neutrons: [Mn − (Mn + Gd)] is a very close approximation to the thermal group.

If we apply to it the conventional formula[10]: $\overline{r^2}/6 = \tau_\theta + L_\theta^2$ wherein τ_θ designates the slowing-down age of the neutrons all the way to the thermal energy, we find: $\tau_\theta = 49.8 \pm 6.5$ cm² (the origin of all ages being taken at the In resonance).

Correcting this value to get back to the case of graphite of density 1.6, we find:

$$\tau_\theta = 56 \pm 6.5 \text{ cm}^2$$

The interpretation of all experimental results is the subject matter of the third part of this paper.

PART II. DISCUSSION OF THE SPATIAL DISTRIBUTION OF THE INDIUM RESONANCE NEUTRONS

Role Played by Collisions with Iron Atoms

These collisions have a probability of 10%. At high energies (≥ 25 kev) the inelastic collisions affect all measured age terms in the same manner. We made no attempt to correct them by calculation. However, differences of ages are not affected. For these, the experimental results can be adapted to the case of graphite having a density of 1.6 by dividing them by

$$k^2 = \frac{\xi_0}{\xi_m} \cdot \frac{\lambda_m^2}{\lambda_0^2} \cdot \frac{1 - \cos\theta_0}{1 - \cos\theta_m} = 0.888$$

Index 0 relates to graphite having a density of 1.6; index m relates to the composite medium under study.

It is known that the Fermi theory is not valid in graphite for $r > 50$ cm. However, Fermi's three-term empirical formula[4] accounts with good accuracy for the distribution of the In resonance neutrons in graphite for a (Ra-α-Be) source. Our results, once they are corrected as explained above, are in good agreement with the formula (Fig. 4).

On the other hand, the asymptotic law, Equation 1, is valid only[11] where $r \gg M/2u^3$ where

$$u = -\log \frac{E}{E_0} \text{ (lethargy)}$$

and M is the atomic weight. In the case of graphite,

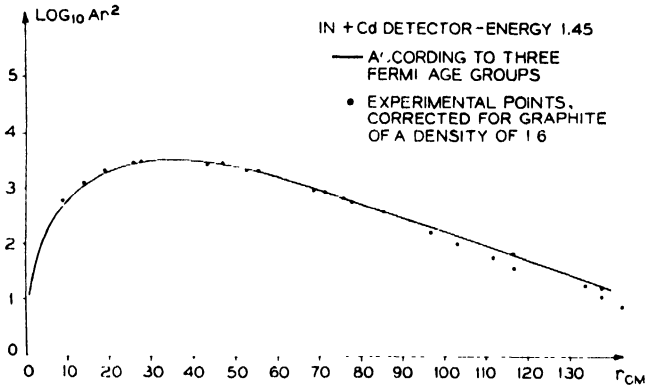

Figure 4. Curve $\log_{10} Ar^2 = f(r)$. In + Cd detector, energy 1.45 ev: dotted curve, according to three Fermi age groups; experimental points are corrected for graphite of a density of 1.6

with Ra-α-Be, neutrons the order of magnitude, for distance r, is about 3 km.

Using transport theory, Bethe[12] gave a formula for the intermediate distances, by assuming that λ_s was independent of neutron energy.

But this formula accounts for the experimental distribution only where $r < 70$ cm; beyond this, the values it gives are too small (see Fig. 5).

Holte[3] allowed for the variation of λ_s with neutron energy. For the case of graphite he proposed a formula of the following type:

$$\lambda(E)_{cm} = 2.65 + 2.35E_{(\text{Mev})}$$

$\lambda(E)$ is the mean free path for energy E (expressed in Mev). This law is a good approximation up to about 2.5 Mev.

Holte's theory leads to an expression which is valid for great distances:

$$A(r,E) = \frac{Q}{4\pi\lambda_m{}^3}\,\mu\,\frac{e^{u\theta m-\frac{r}{\lambda_m}}}{(r/\lambda_m)\rho} \qquad (3)$$

Q is the intensity of the source, λ_m is the mean free path of the neutrons emitted by the source; θ_m, ρ and μ are independent of r and u, and depend solely on M (atomic mass) and the variation of λ with energy.

For a source of 2 Mev neutrons, the values obtained are:

E	ρ	μ	θ_m
2 Mev	0.765	14.5	0.316

For a Ra-α-Be source, the neutron spectrum extends from 1 to 10 Mev, with maxima at 4 and 6 Mev[13]. We took 5 Mev as the average energy and adopted, for constants ρ and θ_m, the values: $\rho = 0.8$ and $\theta_m = 0.3$.

The value of λ_m at 5 Mev is equal to 10.6 cm; this corresponds to a scattering cross section of 1.2 barns.

We assumed that the scattering cross section varies regularly between 2 Mev and 5 Mev, but it is known that carbon shows resonances between these two limits.

The ratio of the scattering cross sections of iron and carbon is approximately the same at 5 Mev and at the epithermal energies. We assumed that both vary in the same manner with the energy of the neutrons.

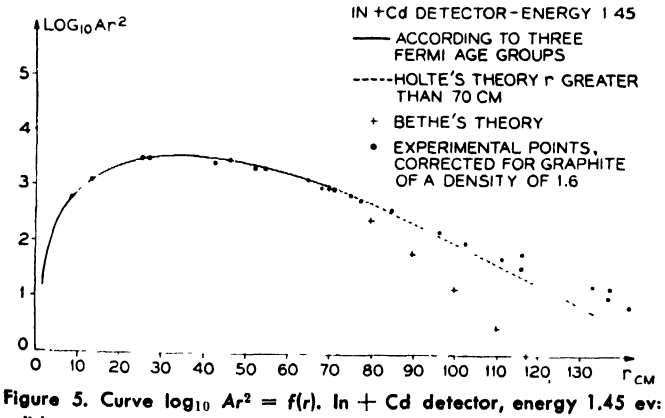

Figure 5. Curve $\log_{10} Ar^2 = f(r)$. In + Cd detector, energy 1.45 ev: solid curve, according to three Fermi age groups; dotted curve, Holte's theory, r greater than 70 cm; crosses, Bethe's theory; experimental points, corrected for graphite having a density of 1.6

We plotted the theoretical curve, Equation 3, which passes through the experimental point obtained at 70 cm from the source.

The experimental points, Fig. 5, are situated on this curve, between $r = 70$ and $r = 100$ cm; and above it for values $r > 100$ cm. This difference must be attributed to the neutrons emitted between 3 Mev and 10 Mev, which can travel exceptionally great distances both because of the minima in the scattering cross section at high energies and the possible anisotropies in elastic collisions.

PART III. DISCUSSION OF THE SLOWING-DOWN OF NEUTRONS BETWEEN INDIUM RESONANCE AND THERMAL EQUILIBRIUM: SEARCH FOR AN EFFECTIVE VALUE OF THE SLOWING-DOWN AGE (M. J. MARTELLY)

Definition of the Slowing-Down Age

The distinction between the slowing-down and thermal ranges, in any study of the energy changes suffered by the neutrons, is an artificial one. The average logarithmic loss of energy by collision decreases in the range of chemical and crystalline binding energies. This loss progressively tends to disappear as one gets close to thermal equilibrium. It is not possible, therefore, to determine exactly when this point has been reached.

However, the distinction is a convenient one. It is implicitly made by the formula used for the migration area, which is consistently used in reactor calculations:

$$\overline{r^2}/6 = \tau_r + L_\theta{}^2 \qquad (1')$$

$\overline{r^2}/6$ is the mean square of the distance covered by a neutron from its source until it is captured. $L_\theta{}^2$ is the thermal diffusion area, and τ_r the slowing-down age, which is assumed to be constant.

In fact, τ_r defined in this fashion is a function of $L_\theta{}^2$, for there exists, in the slowing-down range a capture which depends on $L_\theta{}^2$.

Equation 1′ holds true asymptotically for large values of $L_\theta{}^2$ (see Fig. 6).

We therefore propose to define the effective value of τ_r as the limit of $\overline{r^2}/6 - L_\theta{}^2$, for infinite $L_\theta{}^2$, in case that the capture law is of the $1/v$ form.

This boundary value is of practical interest, for it is achieved, to a good approximation, in the case of pure graphite, or even in graphite containing a quantity of absorbing substances comparable to that found in graphite moderated reactors ($L_\theta{}^2 \sim 300$ cm^2), to the extent that a point closer to thermal equilibrium is reached.

Remarks

The physical significance of this assumption can be seen as follows: it is supposed that the neutrons will diffuse, throughout the course of a slowing-down period, until age τ_r is reached, without being subject to capture; then, that they will then diffuse without change, during a second phase in the course of which they have the properties of thermal neutrons. The

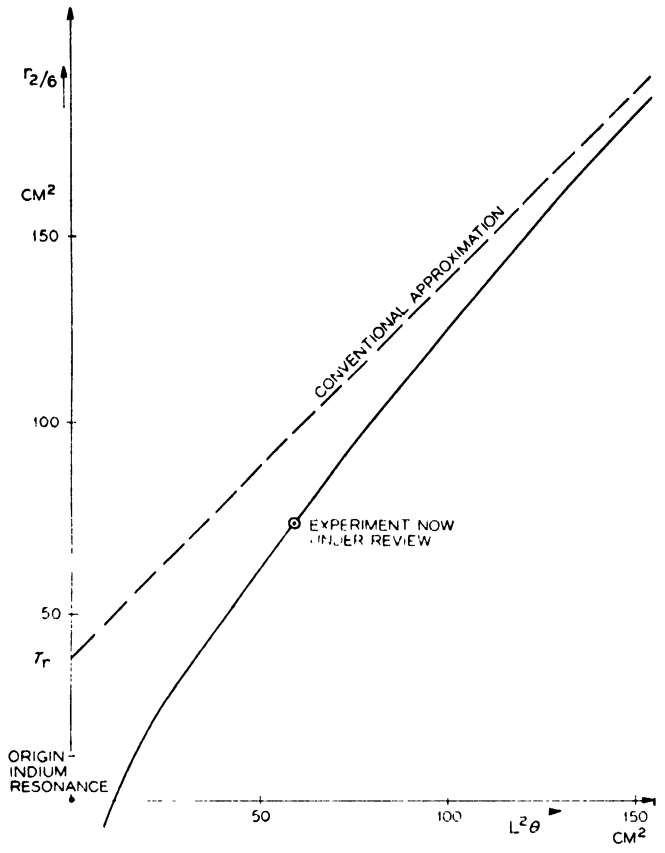

Figure 6. Ratio of the migration area to the capture properties of the medium

migration area calculated by means of this simplifying hypothesis is the same as that found in reality.

Since this *fictitious* thermal range contains all of the capture effects, it must begin before true thermal equilibrium is reached. Thus, should the slowing-down power remain unaltered up to a thermal energy of $\frac{3}{2}kT$ (extrapolation of Fermi's law), this thermal energy would be reached for an age of 55 cm² (the origin of τ being In resonance), whereas the effective age τ_r would be some 25 cm² (according to the calculations that will be developed below).

The thermal diffusion area L_θ^2 has a meaning, even in strongly capturing media, if the capture iron section is of the $1/v$ form. The probability of capture per unit time is then independent of the speed. Starting from a source of neutrons in thermal equilibrium, the spectral distribution of neutrons as a function of energy (independent of their position in the medium that is presumed to be infinite) will remain unaltered. In fact, it is not modified, neither by capture, nor by collisions. L_θ^2 may then be defined as a fraction of $\frac{1}{6}$ the mean square of the distance covered until capture.

One could evidently choose other definitions of the slowing-down age, for instance: the age of 0.039 ev neutrons (mean energy at ordinary temperature) in a medium in which the atoms are supposed to be motionless (or at least cooled down to a very low temperature).

In order to use the defined slowing-down age in practical computations (for instance for reactors), it would evidently be necessary to take account of an epithermal capture term proportional to $1/v$, which would depend on the slowing-down law.

The age difference τ_θ that has been pointed out earlier is closer to the latter definition than to the former; unfortunately, it is not an intrinsic property of graphite. It also depends on the concentration of "poison" and the peculiar properties of Gd.

Method of Discussion

For each neutron trajectory, we consider the parameter X: path covered (broken line), counted as positive or negative, from a given origin (In resonance energy).

Let $\bar{v}$ be the mean velocity of all neutrons of a given X, and v_0 the mean neutron speed in the Maxwellian distribution.

We will arbitrarily express the slowing-down law by a function $y(X) = \bar{v}_0/\bar{v}$, which must possess the following properties:

It is identical with Fermi's law for small values of X; $y = 1$ for large values of X.

By analytical methods, we are able to compute the magnitude which is observed experimentally.

Any comparison should, in principle, allow for the choice, among the laws tried out, of those which are acceptable, so as to deduce τ_r from them together with its limit of error.

The reverse process would strike us as being too ambitious and unnecessary since experimental data are not accurate enough to justify more than the hope of getting an over-all picture.

At any rate, the magnitude τ_r does not depend very substantially on this.

We tried out the laws shown on Fig. 10:

S_1 which was purposely chosen very close to curve S_0, which, in turn, is an extrapolation of Fermi's law:

$$y = 0.155 \exp(-X\xi/2) \qquad (2')$$

and S_2 which differs very substantially from it.

Experimental Magnitudes Which Must Be Mutually Correlated by the Theory

All of these have to do with the mixed graphite-iron medium used for our experiments.

1. Geometrical distribution of the various groups of neutrons characterized by their *diffusion areas* $r^2/6 = M/Q$ where:

$$M = \int r^2/6 A dv \qquad \text{(Time integral)}$$

$$Q = \int A dv \qquad \text{(Quantity integral)}$$

These groups are defined by the differences in activity A of a manganese detector, bare and covered by a filter on both sides respectively.

(*a*) Cd group (cadmium screen, 0.4 mm thick)

(*b*) Gd group (thin gadolinium screen: 3 mg/cm²).

In order to restrict the computation to the low energies, the indium age τ_{In} is taken out, which amounts to taking In resonance (1.45 ev) as the origin of the X-values and of the diffusion areas.

The results have been shown Fig. 7 by points of coordinates M and Q for each experimental situation

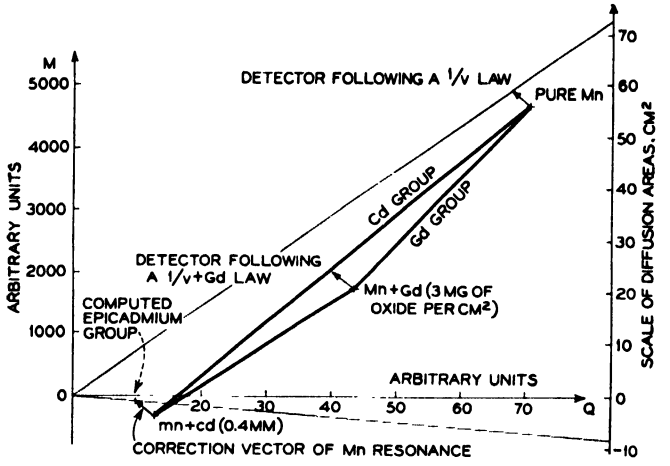

Figure 7. Graph of neutron groups

(bare and with Mn filter), according to this convention. The integrals for the Cd and Gd groups are represented by the components of the vectors which connect the various points. The slopes of these vectors represent diffusion areas $\overline{r^2}/6$.

We shall refrain from interpreting the group detected by Mn alone. The role played in it by the resonance in this nuclide is difficult to determine by calculation. (We shall determine it semi-empirically later.)

2. Ratio of the "quantity integrals" of groups Gd and Cd

$$R = Q_{Gd}/Q_{Cd}$$

3. The gadolinium cross section as a function of neutron energy,[15] and transmissive power of our gadolinium filter, as determined experimentally in a flux of thermal neutrons.

The first figure enables us to compute the law of variation of the transmissive power h_{Gd} of our filter as a function of y; the second datum allows us to adjust the curve for $y = 1$, i.e., in the area where calculation was most uncertain. (The semi-empirical law represented in Fig. 8 has thereby been reasonably justified.)

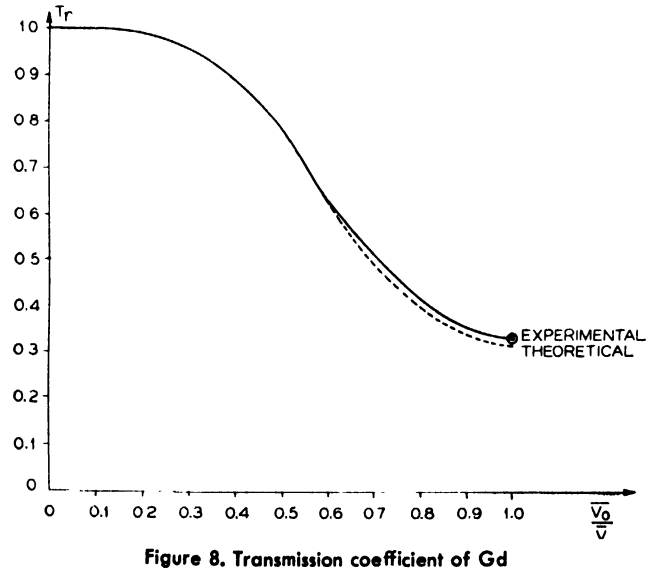

Figure 8. Transmission coefficient of Gd

This boundary value is the one that comes in mostly in the computation of ratio R as above.

4. Cadmium cross section as a function of neutron energy:[15] The transmission coefficient h_{Cd} of the cadmium filter has been derived from it as a function of y by a suitable application of the conventional computation of Amaldi and Fermi.[10] This led to a value of the "cadmium ratio" which agrees well with other data pertaining to this magnitude.

5. Transport mean free path (its variation as a function of $\bar{v}$ is of little importance in our computations). We assumed, throughout, that $\lambda_{tr} = 2.44$ cm.

6. Capture mean free path Λ_0 of the thermal neutrons in the medium.

This value is known from the analysis of its components and a measurement of L_θ^2. If a thermal mean free path of 2.36 cm be assumed, the value $\Lambda_0 = 74.5$ cm can be derived from these data. However, in order to know the influence of a possible systematic error on this determination, we have also tried another fictitious value which is probably too low: $\Lambda_0 = 62.5$ cm.

Computation of the Test Magnitudes and of τ_r by Means of the Slowing-Down Law

$$y = v_0/\bar{v} \tag{3'}$$

The factor of survival to capture from the moment of emission (practically $X = -\infty$) is:

$$p(X) = \exp\left(-\int_{-\infty}^{x} y\,\frac{dX}{\Lambda_0}\right) \tag{4'}$$

By derivation

$$-\frac{dp}{dX} = \frac{1}{\Lambda_0}\,py \tag{5'}$$

Function py (see Fig. 9) represents the spectral distribution, as a function of X: (a) of the neutron density; (b) of their capture by a nuclide which obeys a $1/v$ law; and, therefore: (c) of the absorption by the medium; and (d) of the detector activation.

In the presence of a filter this activation is to be multiplied by the transmission factor h.

To within a multiplicative factor, the integrals Q and M that have been defined above are:

$$Q = \int_{-\infty}^{+\infty} hpy\,dX \tag{6'}$$

$$M = \int_{-\infty}^{+\infty} \tfrac{1}{3}\lambda_{tr} X hpy\,dX \tag{7'}$$

$$r^2/6 = M/Q = \frac{\lambda_{tr}}{3}\,X\ (\text{mean}) \tag{8'}$$

Equation 7′ then is derived from 6′ by noting that the neutrons which had activated the detector over the interval $(X, X + dX)$ of their trajectory have a mean diffusion area of:

$$\overline{r_x^2} = \frac{\lambda_{tr}}{3}\,X$$

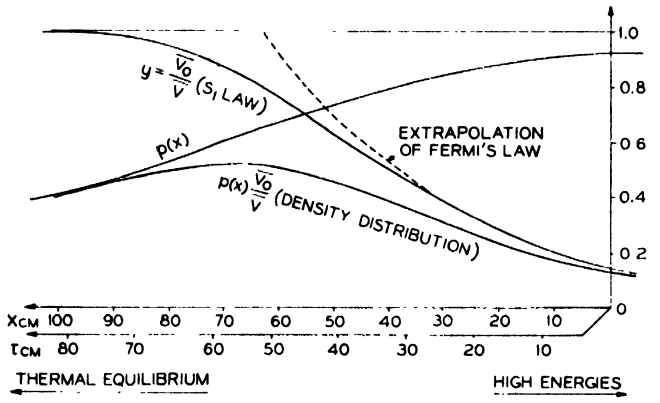

Figure 9

It should be remembered that passage through energy value 1.45 ev was chosen as the origin of the abscissae and of the $r^2/6$ values.

The characteristics of the Cd and Gd groups (diffusion areas, ratio R) are obtained by subtracting the magnitudes Q or M (see graph on Fig. 7, described above).

Computation of Effective Slowing-Down Age

The reasoning will start with the magnitude X_r, which is related to τ_r by a relation analogous to 8', i.e.:

$$\tau_r = \frac{\lambda_{tr}}{3} X_r \qquad (9')$$

X_r is the value of X at which the neutrons become thermal, in the fictitious case described above. This fictitious case has been defined in order to fit strictly with Equation 1' which, when expressed by means of parameter X, becomes:

$$\bar{X} = X_r + \Lambda_0 \qquad (10')$$

where $\bar{X}$ is the abscissa of the center of gravity of the spectral distribution (function py).

It will be shown that the boundary value of X_r for an infinite Λ_0 is:

$$X_r = \int_0^1 X\, dy$$

(the time integrals then are equal in the real as well as in the fictitious cases, the second order; the quantity integrals are equal to Λ_0 in both instances.)

From this:

$$\tau_r = \frac{\lambda_{tr}}{3} \int_0^1 X\, dy \qquad (11')$$

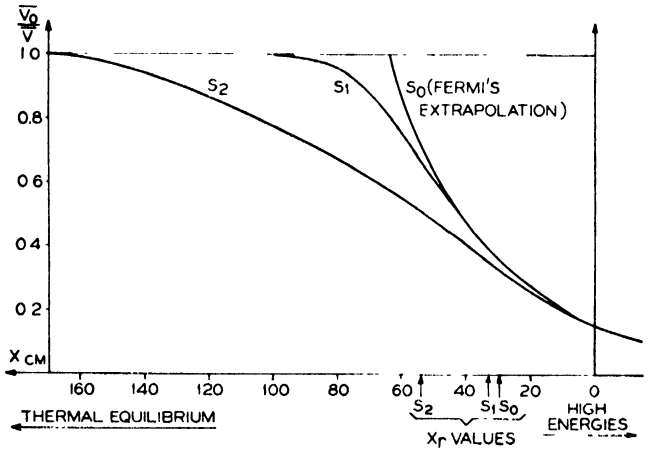

Figure 10. Tested slowing-down laws

Comparison of the Slowing-Down Laws with the Experimental Results

This comparison is shown in Table II.

In this discussion, it is advisable to use the parameter X_r for classification of the possible laws since it characterizes the order of magnitude of the path (therefore the number of collisions or impacts) which the neutrons must make in order to acquire reactivity ($\bar{v}_0/\bar{v}$) with respect to the nuclei.

It appears that, in this classification, the best law would be something between S_1 and S_2.

S_1 is too small due to the value for R (which depends on the neutron's probability of survival below 0.1 ev).

S_2 is too large because of the value of the diffusion area. In the limit it would be consistent with the experimental data where it is assumed that some systematic errors may have been made in certain magnitudes (Λ_0, λ_{tr}, diffusion areas, etc.), of which no account is taken in the accidental error margins that have been pointed out, which are due to parasitic effects in this borderline case (for instance filtration of the neutrons through the crystals, which makes the thermal group heterogeneous).

We do not make any choice between S_1 and S_2, but we feel that the actual result will be somewhere between the two, close to S_2, and that the difference between them gives an idea of what could be called, by generalization, the "margin of uncertainty."

Table II

		Theoretical values derived from the laws tested			
		Law S_0 $\lambda_0 = 74.5$	S_1 74.5	S_2 74.5	S_2 62.5
	Experimental values	X_r (cm) = 29.5 τ_r (cm²) = 24.4	33 26.8	54 44	54 44
$R = \frac{Q_{Gd}}{Q_{Cd}}$	0.47	0.59	0.58	0.49	0.48
Departure from experimental value		26%	24%	4%	2%
DIFFUSION AREAS					
Cd Group					
origin:					
1.45 ev	84.5	93	93.5	108	97
Ra-Be Source	428.1	436.6	437.1	451.6	440.6
Deviation		2%	2%	5.5%	3%
Gd Group					
origin:					
1.45 ev	108.4	100	101	128	113
Ra-Be Source	452.1	443.6	444.6	471.6	456.6
Deviation		−2%	−2%	+4%	+1%

Comparison of the Slowing-Down Laws with Gurney's Theory[14]

The writers computed the variation of the slowing-down power of graphite as a function of neutron energy down to the thermal-energy range.

It is interesting to compare the results with the variation of the expression $2d/dX$ (log $\bar{v}$), which is an approximation of ξ, although a fairly rough one, in the vicinity of thermal equilibrium (but this consideration would only come into the picture if we were to endeavor, with our method, to go down to finer details which we have not done as yet).

This comparison is shown in Fig. 11. It appears from it that Gurney's results are to be found between S_1 and S_2, closer to S_2. This is in agreement with the conclusions shown above.

Numerical Value Proposed for Magnitude τ_r from this Discussion

We endeavored to correlate various experimental magnitudes by a calculation based on the additive property of the quantities λ and λ_{tr}, by bringing in an "unknown" which is the slowing-down law.

We have shown that, by means of a suitable hypothesis about this "unknown," it was possible to obtain satisfactory agreement within the limits of accuracy of the experiment.

The law is applicable to the "unknown" with only limited accuracy; conversely, it is possible to derive the magnitude of τ_r from it, which has an experimental meaning, with an accuracy comparable to that of the other $\overline{r^2}/6$ magnitudes measured in our experiment. All of these show slight sensitivity with respect to this law (on the condition that it retains a form considered "reasonable" according to the present status of our knowledge). We offer, as the most likely value 38 cm^2 subject to a standard error of ± 9 cm^2.

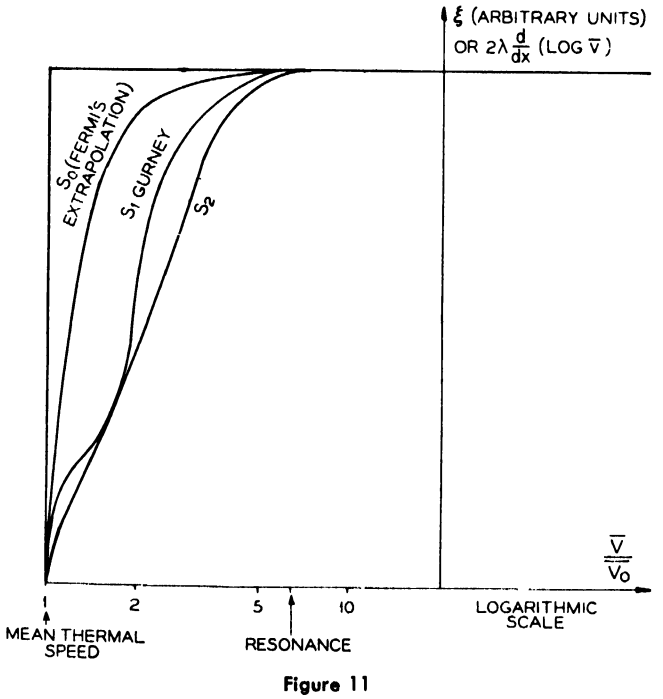

Figure 11

The result is obtained for graphite having a density of 1.6, by dividing through the coefficient k^2 which has the value $\lambda\lambda_{tr}/\xi$; although this ratio is a function of the energy, the value of 0.888 obtained earlier for the epithermal range remains an adequate approximation. From this, we can derive $\tau_r = 43 \pm 10$ cm^2 which is the effective value of the age for neutrons between 1.45 ev and the thermal range, according to the definition given in the introduction.

Value of $\overline{r^2}/6 - L_\theta^2$ in the Poisoned Medium

In order to reach $\overline{r^2}/6$ (when the capture cross section varies according to a $1/v$ law), it is necessary to compute the *correction of the resonance effects in manganese.*

In the graph shown on Fig. 7, this is a single vector for the entire polygonal contour. It is determined for the representative point of the epi-cadmium group, since Fermi's slowing-down relation is applicable to this group and is specified by: (*a*) the diffusion area: -8.5 cm^2; (*b*) the reciprocal of the "cadmium ratio"

$$\frac{Q_{\text{with cadmium}}}{Q_{\text{without filter}}} = \frac{1}{\Lambda_0}\int_{-\infty}^{+\infty} phy\, dX = 0.14 \quad \text{(cf. Equation 6')}$$

Remark

The integral appearing in this expression is not modified significantly by the presence of the "poison." The cadmium ratio, for a detector which obeys a $1/v$ law, is therefore proportional to Λ_0 and to L_θ^2. For our medium we have L_θ^2 Cd ratio $= 9.2$ cm^2. It is known that for a graphite pile the order of magnitude is of $^{30}\%_{33} = 9$ cm^2. This is good agreement.

After this correction the following is obtained for a detector in $1/v$, in the poisoned medium:

$$\overline{r^2}/6 = 73 \pm 8 \text{ cm}^2$$

$$\overline{r^2}/6 - L_\theta^2 = 14 \text{ cm}^2$$

i.e., a difference of 24 cm^2 from the asymptotic value

ACKNOWLEDGMENTS

One of us (V. P. Duggal) wishes to express his gratitude to the "Department of Atomic Energy" (Indian Government) for the financial assistance which enabled him to stay at the Nuclear Study Center, at Saclay. He would also like to express his thanks to the French Commissariat of Atomic Energy for the many courtesies extended to him.

ANNEX: DISCUSSION OF THE SLOWING DOWN OF THE NEUTRONS BETWEEN INDIUM RESONANCE AND THERMAL EQUILIBRIUM

Determination of an Effective Value of the Slowing-Down Age (M. J. Martelly)

We attempted to explain the experimental results by means of a slowing-down law ($y(x) = V_0/V$) which should be in keeping with the variation of ξ as foreseen by Gurney.

The computed values are: $R = 0.49$; diffusion area

of the Cd group = 446 cm²; diffusion area of the Gd group = 461 cm².

The differences, as compared to the corresponding experimental values, are, respectively: +4%, +4% and +2%. The agreement is, therefore, satisfactory.

The value of τ_r is the same as for the S_2 law, i.e., for the composite medium: $\tau_r = 44$ cm²; and, for pure graphite of a density of 1.6: $\tau_r = 49$ cm².

We believe that this value is the one to be chosen as the most probable one, since it brings our experimental results in agreement with those Gurney used for his theory (vibration quantum energy of the graphite lattice).

The theory we have developed is based on the assumption that the neutrons reach thermal equilibrium for large values of X. This postulate is not essential. We are entitled to assume that the capture, which has the effect of absorbing the slower neutrons, leads to a "hotter" thermal distribution. This can be allowed for by the use of an increased value of Λ_0. Now, the exponential experiment furnishes precisely a value of Λ_0 which has been altered in the same way by the same phenomenon.

REFERENCES

1. Martelly, J., Ann. de Phys. *12*, 2: 255 (1947).
2. Nuclear Data. NBS circular 499 (1950).
3. Holte, G., Ark. Fys. *3*, nr 14: 209 (1951).
4. Fermi, E., Nuclear Physics, *The University of Chicago Press* (1951).
5. Ertaud, A. and Zaleski, P., Jr., Phys. et Radium. *14:* 191 (1953).
6. Hubert, P., Auclair, J. M. and Vendryès, G., Jr. Physique & Radium (in press).
7. Bothe, W., Z. Physik *120:* 437 (1943).
8. Roberts, L. D., Hill, J. E. and McCammon, G., Phys. Rev. *80:* 6 (1950).
9. Weinberg, A. M., and Noderer, L. C., *Theory of Neutron Chain Reactions*, AECD—3.471 (1951).
10. Amaldi, E. and Fermi, E., Phys. Rev. *50:* 899 (1936).
11. Marshak, R. E., Rev. of Mod. Phys. *19:* 185 (1947).
12. Bethe, H. A., Tonks, L. and Hurwitz, H., Jr., Phys. Rev., *80:* 11 (1950).
13. Teucher, Z., Phys. *126:* 410 (1949).
14. Gurney, R., Declassified Report. AECD. 2449 (1949).
15. Neutron Cross-Section Compilation AECU. 2040 (1952).

Thermal Neutron Density Distribution Inside and Outside Infinite Long Cylindrical Samples

By M. Bustraan* and K. van Duuren,*† The Netherlands

NEUTRON DENSITY DISTRIBUTION INSIDE THE SAMPLES

The elementary diffusion equation

$$D\Delta\varphi(r) - \Sigma_a\varphi(r) + S(r) = 0 \qquad (1)$$

with the diffusion coefficient $D = \frac{1}{3}\Sigma_s$ and $S(r)$ the source density, cannot be used to describe the neutron flux near boundaries and concentrated sources due to the fact that this simple theory neglects the anisotropy in the flux distribution caused by those discontinuities.[1,2]

Under certain restricting conditions[3] one can deduce from the diffusion approximation of the rigorous transport equation the same differential Equation 1, with the diffusion coefficient

$$D = \frac{1}{3}(\Sigma_{tot.} - \bar{\mu}_0 \cdot \Sigma_s) \qquad (2)$$

Although the conditions for application of the diffusion approximation are certainly not fulfilled in the case of the f-calculation for a heterogeneous reactor, this approximation is extensively used because the mathematical complexity of the rigorous transport theory hinders applying more accurate theories.[4,5]

In order to find the accuracy of the diffusion approximation for the calculation of the thermal utilization factor f we measured the neutron density distribution in cylindrical samples.

The solution of Equation 1 for the radial part of the flux distribution inside such samples of non-multiplying material for infinite sample length is given by:

$$\varphi(r) = \varphi(0) \cdot I_0(\kappa r) \qquad (3)$$

$\varphi(0)$ being the flux on the axis of the sample, $I_0(\kappa r)$ being the zero order modified Bessel function of the first kind,‡ κ being the reciprocal diffusion length of the sample material

$$\kappa^2 = \Sigma_a/D \qquad (4)$$

Our measurements show that Equation 3 describes fairly well the actual flux distribution, provided the reciprocal diffusion length κ is adjusted.

Experimental Procedure

In all our experiments the sample was contained in cylindrical tubes of technical aluminum (2S), with a 2 mm wall thickness. In most of the cases the inner diameter of the tubes was 2.54 cm. Some experiments were done with samples of 3.00 and 5.07 cm diameter. The length was about twelve times the diameter in all cases.

The materials investigated were powders, solutions and metals, chosen so as to give a good range in Σ_a and Σ_{tr} (see Table 1).

The samples were irradiated in one of the horizontal irradiation channels of the JEEP[6] (with the exception of samples 13 and 14, which were irradiated in a vertical fuel rod hole). The location of the sample was chosen at the center of the reactor, where the flux gradient in all directions was minimum.[7]

For the powder and solution samples, copper wires 0.7 mm in diameter were used as detectors. The wires were stretched axially along the sample tube, at various distances from the axis (see Fig. 1). After irradiation, the center portion of the wire was counted for the 12.9 hr β-activity of Cu^{64}, by means of a Philips end-window counter. The purity of the copper was checked by following its radioactive decay after neutron irradiation. Assuming copper to be a $1/v$ absorber, the activities are directly proportional to the neutron densities.

By measuring also the activity at various points along the wires, it was shown that the flux is actually constant in axial direction in the center half of the sample.

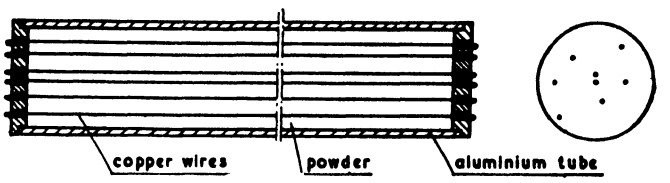

Figure 1. Container for powder sample

For the solid-metal samples electrolytic copper and natural uranium were used. The samples were 2.52 cm in diameter, 30 cm in length and were divided into two parts, each part being 14.5 cm in length, with a disk of 1 cm length in between. This disk was provided with holes parallel to the axis at various distances from the

* Joint Establishment for Nuclear Energy Research, Kjeller per Lillestrom, Norway.
† Now at the Philips Research Laboratories Synchrocyclotron, Amsterdam, The Netherlands.
‡ A table of $I_0(x)$ can be found in "Mathematical Tables, Vol. VI: Bessel Functions part I," Cambridge University Press.

Table I

No.	Sample material	Density gm/cm³	Σ_{tr} in cm⁻¹	Σ_a in cm⁻¹	Diam in cm	κ_1	κ'	κ_{th}††	κ_{th}‡‡	κ''
1*	B/SiO_2	1.632	0.184	0.347	2.54	0.86 ± 0.05	0.92	0.74	0.44	--
2*	B/SiO_2	1.712	0.194	0.636	2.54	1.31 ± 0.07	1.26	1.26	0.61	—
3*	B/SiO_2	1.613	0.183	0.685	2.54	1.27 ± 0.06	1.29	1.34	0.61	—
4*	B/SiO_2	1.645	0.187	0.778	2.54	1.45 ± 0.07	1.39	1.50	0.66	—
5*	B/SiO_2	1.748	0.201	1.186	2.54	1.59 ± 0.03	1.73	2.22	0.85	--
6*	Mn	4.616	0.106	0.491	2.54	1.10 ± 0.03	1.01	0.94	0.39	--
7*	MnO_2	2.164	0.162	0.147	2.54	0.57 ± 0.01	0.59	0.37	0.27	—
8†	H_3BO_3/H_2O	1.000	2.083	0.302	2.54	1.30 ± 0.09	1.36	1.47	1.35	—
9*	Cu	2.938	0.227	0.079	2.54	0.51 ± 0.07	0.46	0.27	0.23	—
10‡	Cu	8.92	0.676	0.232	2.54	0 91 ± 0.05	0.94	0.80	0.69	0.91 ± 0.05
11§	U	18.82	0.396	0.279	2.52	1.01 ± 0.04	0.97	0.75	0.60	1.09 ± 0.05
12¶	U	18.82	0 396	0.279	2.52	1.01 ± 0.04	0.97	0.75	0.60	1.09 ± 0.05
13**	U	18.82	0.396	0.279	2.52	0.97 ± 0.04	0.97	0.75	0.60	1.04 ± 0.05
14**	U	18.73	0.394	0.278	3.00	0.84 ± 0.04	--	0.75	0.60	0.83 ± 0.04
15*	MnO_2	2.017	0.149	0.136	5.07	0.44 ± 0 02	—	0.34	0.25	—
16*	B/SiO_2	1.709	0.191	0.342	5.07	0.70 ± 0 02		0.74	0.44	—

* Powders.
† Solution, 0.00876 gm B/cm³.
‡ Metal, Cu metal pins detector.
§ Metal, U metal pins detector, irradiated in isotope channel of JEEP.
¶ Metal, Cu pins detector, irradiated in isotope channel.
** Metal, U pins detector, irradiated while dipped in the reactor tank in normal fuel rod position 38 cm from the axis of the reactor.
†† κ_{th} = according to diffusion approximation.
‡‡ κ_{th} = elementary theory.

center. The bore of these holes was 2 mm. Pins of 1-cm length fitted accurately into these holes.

The neutron density distribution inside these metal samples was determined from the induced specific γ-activity of the pins. The detector materials were copper and uranium.

For the uranium detector, it was verified by decay measurements, that we actually measured the fission induced γ-activity. The influence of the soft γ-rays from the Np decay, could be neglected.

Corrections were made for the contribution of fast fission. For this it was sufficient to assume a constant distribution for the fast fission density.

Results

Figures 2, 3 and 4 show the radial neutron density distributions for the samples 5, 11, 12, 13 and 14 from

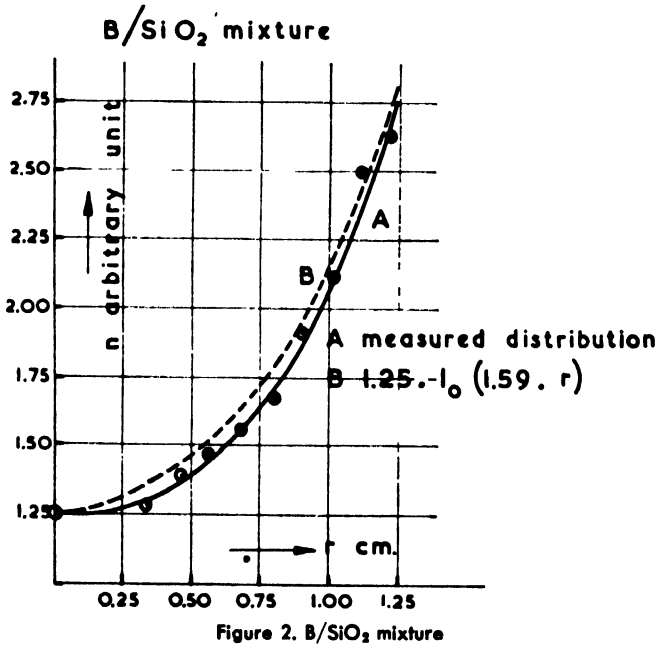

Figure 2. B/SiO_2 mixture

Table I. It is clear from these figures that a κ_1 can be found so that $I_0(\kappa_1 \cdot r)$ fits the experimental points.

The values of κ_1 found by fitting the Bessel function to the experimental curve in two points, viz., for the center and the surface of the sample are listed in Table I.

The Σ_a values in Table I are calculated from the 2200 m/sec cross sections taken from references.[8,9] In this calculation a Maxwellian neutron energy spectrum was assumed with a neutron temperature of 390°K, as measured for JEEP by Goedkoop and Pelser.[10]

The Σ_a's were also corrected for the presence of the copper detectors (for the cases where used). These corrections did not exceed 1%.

Discussion of the Results

It is clear from Table I that there is a large discrepancy between the κ_1 values and the κ values calculated on the basis of the elementary diffusion theory and of the diffusion approximation. Another striking fact is that κ_1 is much less dependent on the Σ_{tr} than predicted by diffusion theory.

The relation between the κ_1 and the sample materials cross sections mentioned in Table I can be described reasonably well for the sample diameter of 2.54 cm, by the formula:

$$(\kappa')^2 = 4.7 \times \Sigma_{tr}^{0.38} \Sigma_a \qquad (5)$$

For the 2200 m/sec cross sections Equation 5 becomes:

$$(\kappa')^2 = 3.6 \Sigma_{tr}^{0.38} \cdot \Sigma_a \qquad (5a)$$

The values of κ' are also listed in Table I.

As mentioned above, since copper is a $1/v$ absorber, we measured, with the copper detector, the real neutron density distribution independent of hardening effects. From recent measurements of Popović *et al.*[11] it has been shown that the fission cross section does not behave like $1/v$. The good agreement, however, of

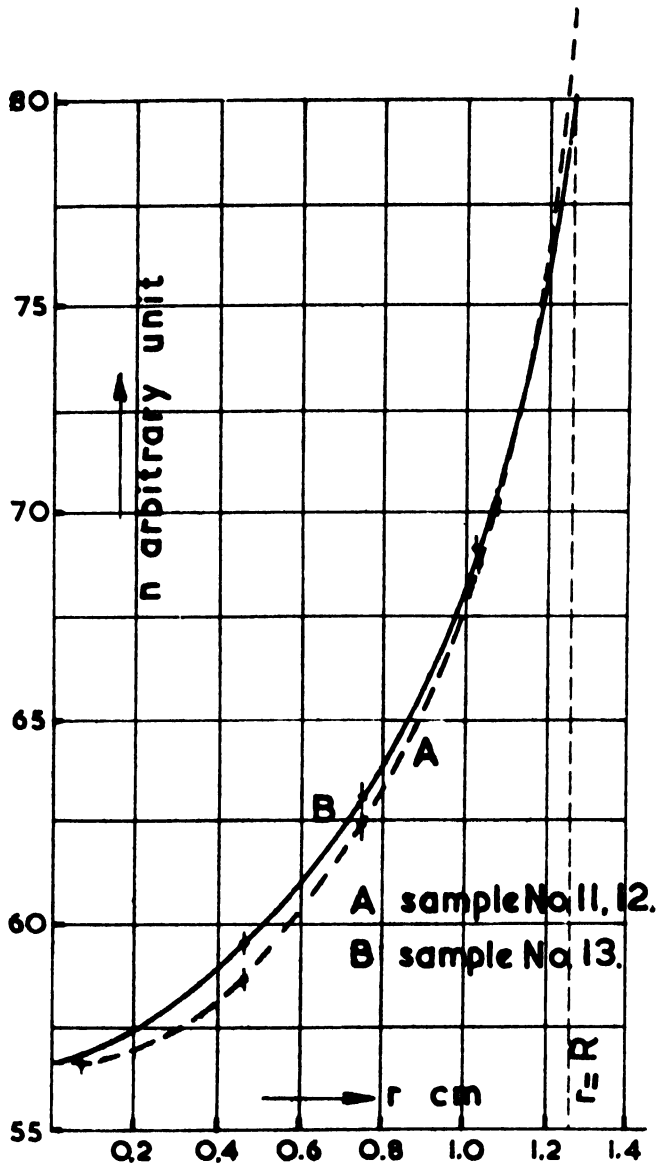

Figure 3. U sample, R = 1.26 cm

the κ_1 values for the uranium sample with copper and with uranium detector (sample 11, 12), shows that in our case this deviation does not play a significant role.

From the experiments with samples 11 and 13 it can be seen that it makes only a slight difference whether the sample in its container is irradiated directly in the heavy water in a position parallel to the fuel rods, or whether it is irradiated in an isotope channel, perpendicular to the fuel rods and where there is also an air gap of 1.9 cm and the 5-mm Al wall of the channel between the sample and the heavy water.

Comparison of the κ_1 of samples 1 and 16 respectively with 7 and 15 shows that a marked influence of sample diameter exists. The discrepancy between experimental and theoretical values of κ decreases with increasing sample diameter; this is partially due to hardening effects.

It may be somewhat preferable in some cases to define κ'' as the solution of[5]

$$\frac{\pi R^2 f(R)}{\int_0^R 2\pi f(r)\,dr} = \frac{\kappa R \cdot I_0(\kappa R)}{2I_1(\kappa R)} = G(\kappa R) \qquad (6)$$

where: $f(r)$ is the measured density distribution; and R is the outer radius of the sample. In the last column of Table I, some of the values obtained in this manner are given. The difference, however, of κ'' and κ_1 is only slightly greater than the error of the experiment.

THE NEUTRON DENSITY DISTRIBUTION IN THE MODERATOR OF AN ELEMENTARY CELL

The solution of Equation 1 for the flux in the moderator is:[11]

$$\varphi_1(r) = A \cdot I_0(\kappa_{D_2O} \cdot r) + B \cdot K_0(\kappa_{D_2O} \cdot r) + S/D \qquad (6a)$$

S being the slowing-down density of thermal neutrons in the moderator, $K_0(x)$ being the zero order modified Bessel function of the second kind,§ and D the diffusion coefficient of the D_2O.

By the boundary conditions, i.e., continuity of both neutron flux and current at the moderator fuel rod interface, and zero net current over the outer boundary of the cell, the constants A, B and S are fixed.

One may expect that the neutron density distribution in the moderator around a fuel rod will also differ

§ Tables of $K_0(x)$ are found in "Mathematical Tables, Vol. VI," loc. cit., or in "National Bureau of Standards, Applied Math Series 25" (Sept. 1952).

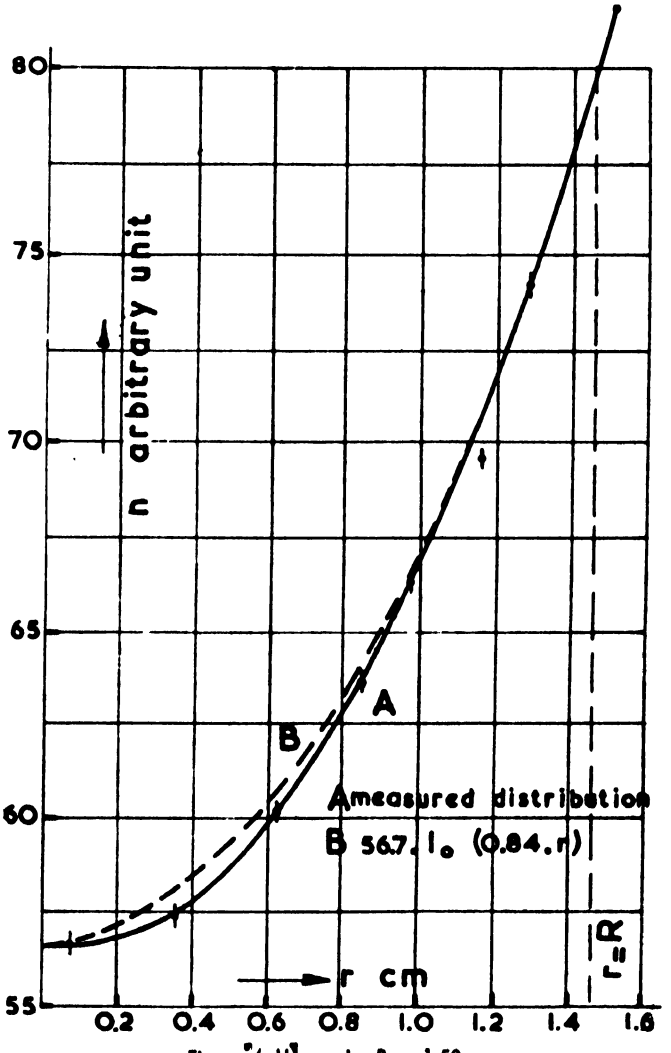

Figure 4. U sample, R = 1.50 cm

from the one calculated with diffusion theory, as a result of anisotropy of the flux distribution. Therefore, the neutron density distribution in the heavy water of an elementary cell was also measured.

Experimental Procedure

The experimental set-up is schematically drawn in Fig. 5. The uranium in the aluminum tube A consists of three slugs with a total length of 90 cm and 2.52 cm diameter. The whole set up is designed so that the tube A, with floater F in down position, can pass through a 72-mm hole in the top lid of JEEP at

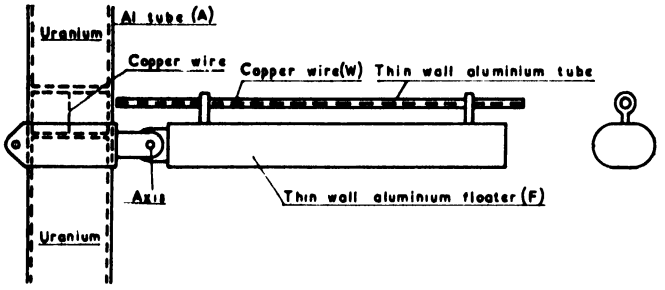

Figure 5. U-rod with floater assembly

a distance of 38 cm from the axis of the reactor. When the tube is lowered, the floater takes a horizontal position perpendicular to the rod. The floater is located at the point where the gradient of the vertical flux is zero. On top of the floater a copper wire W of 0.7 mm is fixed. Irradiation took place at a reactor power level of 20 kw for 10 minutes. Afterwards the copper wire was cut into pieces of about 1-cm length and the induced specific γ-activity is measured.

Results

The measured neutron density distribution in the unit cell is given in Fig. 6. In the same figure the distribution calculated on the basis of diffusion theory is given. We used the constants: $\kappa(u) = 0.75$; $\kappa(\mathrm{Al}) = 0.053$; $\kappa(\mathrm{D_2O}) = 1 \times 10^{-4}$; $D(u) = \frac{1}{3}\Sigma_{tot} = 0.5$; $D(\mathrm{Al}) = 3.83$; $D(\mathrm{D_2O}) = 0.83$.

For this calculation we assumed the lattice to be a square one with a pitch of 18 cm, like the JEEP lattice, and the fuel elements to be rods of 2.52-cm diameter. In fact, our uranium rod, around which we measured the flux distribution, is surrounded by the double rods of the JEEP, but this does not significantly influence the flux distribution around our rod.

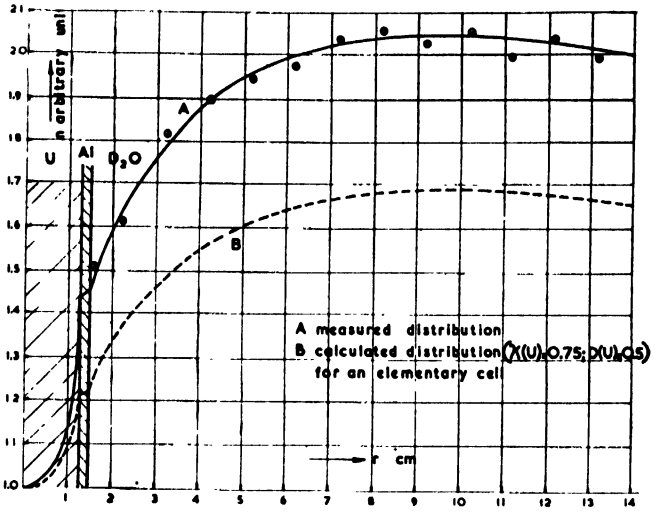

Figure 6. Neutron density in U-rod and moderator

For our measured distribution the thermal utilization factor was calculated to be $f = 0.949 \pm 0.001$. The calculation of this factor on the basis of the diffusion approximation yields the value: $f_{th} = 0.954$.

This means that calculation according to diffusion theory yields a K_{inf} value that is 0.5% too high. The pile diffusion length L was calculated to be: $L^2 = 286 \pm 5$ cm^2 while the diffusion approximation yielded: $L^2 = 260$ cm^2. This would mean for a reactor with a geometrical buckling of 4×10^{-4} cm^{-2} and a lattice like the assumed one a drop in K_{eff} of about 1.3%.

LIST OF SYMBOLS

n = thermal neutron density in neutrons/cm^3
φ = thermal neutron flux in neutrons/cm^2-sec
D = thermal neutron diffusion coefficient in cm
S = thermal neutron source strength in neutrons/cm^3 sec^1
Σ_a = macroscopic absorption cross section in cm^{-1}

Table II. Measured Neutron Density Distribution in Uranium

Sample diameter 2.52 cm						*Sample diameter 3.00 cm*	
Cu detector irrad in channel		*U detector irrad in channel*		*U detector irrad directly in tank*		*U detector irrad directly in tank*	
r cm	*n* arbitrary unit	*r* cm	*n* arbitrary unit	*r* cm	*n* arbitrary unit	*r* cm	*n* arbitrary unit
0.07	566 ± 3	0.07	566 ± 3	0.07	566 ± 2	0.07	569 ± 3.5
0.47	586 ± 3	0.47	587 ± 3	0.47	595 ± 3	0.35	574 ± 0.2
0.75	625 ± 3	0.75	624 ± 3	0.75	632 ± 3	0.62	602 ± 3
1.02	691 ± 4	1.02	690 ± 3	1.02	694 ± 3	0.85	637 ± 0.6
1.07	712 ± 3	1.07	713 ± 2	1.07	713 ± 2	0.98	664 ± 1.6
1.26	823*	1.26	823*	1.26	800*	1.16	697 ± 1.5
						1.28	743 ± 2.0
						1.50	815*

* Extrapolated value.

Σ_s = macroscopic scattering cross section in cm^{-1}

Σ_{tot} = total macroscopic cross section

Σ_{tr} = macroscopic transport cross section in cm^{-1}

$\bar{\mu}_0$ = averaged cosine of scattering angle

κ = the reciprocal diffusion length = $\sqrt{\Sigma_0/D}$ in cm^{-1}

f = thermal neutron utilization factor

A and B = arbitrary constants

REFERENCES

1. Glasstone, S. and Edlund, M., *The elements of nuclear reactor theory*. D. van Nostrand, New York (1952).
2. Weinberg, A. M. and Norderer. L. C., AECD Report No. 3471.
3. Reference (1) p. 391.
4. Rennie, C. A., AERE Report R/L 5, Harwell.
5. Guggenheim, E. A. and Pryce, M. H. L., AERE Report R/R 922, Harwell.
6. Dahl, O. and Randers, G., Nucleonics *9*, 11, 5 (1951).
7. Bogaardt, M., Hälg, W. and Pelser, J., JENER Publication No. 21 (1953).
8. Hughes, D. J., Pile Neutron Research, Addison Wesley (1953).
9. Neutron Cross-Sections Compilation, AECU 2040, Suppl. III (April 1954).
10. Goedkoop, J. A. and Pelser, J., *Proceedings of the Kjeller Heavy Water Conferences*, JENER Publication No. 7 (1953), pp. 163 and 174.
11. Popovic, D. and Rajšić, N., Journal of Nucl. Energy *1*, 170, (1954).

Determination of the Mean Transfer Free Path of Thermal Neutrons by Measurement of the Complex Diffusion Length

By V. Raievski and J. Horowitz,* France

The method which will be described is the result of a technique used routinely at Saclay, in the study of media in which neutrons are diffused and are moderated. In this technique, the continuously emitting sources used in the conventional experiments are replaced by modulated sources of a variable frequency.

This technique was first utilized in the oscillation method,[1,2] which was developed to measure the purity of the materials used in the construction of reactors. It is now used very widely with slight variations most of which are designed to attenuate the signal produced by the diffusion of neutrons in materials such as graphite, Be or BeO. The specific characteristics of the oscillation technique used at Châtillon[3,4] are covered in another paper submitted to this conference.[5]

The oscillation technique has been extended to permit the independent measurement of the mean life of the neutrons, and of the reactivity, by various authors.[6,7,8]

Recently, the shim plates of the Saclay reactor also were calibrated in this fashion.[9]

It is proposed, in this paper to describe the extension of the method to the measurement of the transport mean free path of thermal neutrons, and also to indicate possible applications to the measurement of other quantities such as the moderation length or the absolute value of the capture cross section of boron.

We should like to point out that Weinberg already had made a theoretical study of the case of a modulated source in a diffusing medium[10,11] and considered the principle of such measurements. Finally, von Dardel and Sjöstrand measured the transport and capture cross sections of ordinary water by a different method, using a pulsed accelerator.[12]

Determinations of mean free path have been made, starting from the measurements of extrapolation lengths.[13] It appears to be difficult, by this method, to obtain a precision of better than 5%. Recently, Kash and Woods used a different method for heavy water.[14] They poisoned the medium by introducing a known quantity of an absorbing material, and thus measured, the reduced diffusion length. This technique, while it is accurate, appears to be limited to the study of liquid, or possibly porous, media. The method used at Saclay[15] offers a means of determining the transport mean free path from the measurement of a complex diffusion length and is applicable regardless of the physical form of the medium under study.

Original language: French.

* Department of Mathematical Physics, C.E.A.

THEORY OF THE MEASUREMENT

Let us take an infinite diffusing and moderating medium, and let $f(\vec{r}, E, t)$ be the spatial and energy distribution of the neutrons at time t after their emission from source S, in the absence of a capture. If the capture cross section of the medium is proportional to $1/v$ and if τ_0 is the mean life of the neutrons, the distribution created by the stationary source S is:

$$g\left(\vec{r}, E, \frac{1}{\tau_0}\right) = \int_0^\infty f(\vec{r}, E, t) e^{-\frac{t}{\tau_0}} dt$$

By substituting a modulated source $Se^{i\omega t}$ for the stationary source S, we get a distribution

$$e^{i\omega t} g\left(\vec{r}, E, \frac{1}{\tau_0} + i\omega\right)$$

in which

$$g\left(\vec{r}, E, \frac{1}{\tau_0} + i\omega\right) = \int_0^\infty f(\vec{r}, E, t) e^{-t\left(\frac{1}{\tau_0} + i\omega\right)} dt$$

These few considerations show that it is easy to transpose the results obtained for stationary problems with a capture law of the $1/v$ form into the case of a modulated source.

For thermal neutrons, if the rate of capture is low ($\Sigma_c \lambda_t \ll 1$) and if the frequency of modulation is not too high ($\omega \lambda_t / v \ll 1$), we can apply the elementary diffusion theory, which, for a point source placed at the origin $S = S_0 + \delta S_0 e^{i\omega t}$ gives the distribution

$$\vec{n}(\vec{r}, t) = \vec{n_0}(\vec{r}) - \delta \vec{n_0}(\vec{r}) e^{i\omega t}$$

with

$$n_0 = \frac{S_0}{4\pi D r} e^{-\sqrt{\frac{\Sigma_a v}{D}} r}$$

$$\delta n_0 = \frac{\delta S_0}{4\pi D r} e^{-\sqrt{\left(\Sigma_a + \frac{i\omega}{v}\right)\frac{v}{D}} r}$$

$D = \lambda_t v/3$ is the diffusion coefficient; the speed v which comes into the picture here is the mean speed of the Maxwellian distribution and Σ_a is the macroscopic capture cross section which corresponds to that speed ($\Sigma_c \tau_0 v = 1$).

It will be seen that, while the stationary part n_0 is characterized by the customary diffusion length L, the

variable part of n, δn_0 depends on a complex diffusion length L_ω, given by

$$L_\omega^{-2} = \frac{v}{D}\left(\sum_c - \frac{i\omega}{v}\right)$$

If $\omega/v\Sigma_c \gg 1$ a power series in $v\Sigma_c/\omega$ can be set up, giving:

$$\frac{1}{L_\omega} = \sqrt{\frac{\omega}{2D}}\left\{\left(1 + \frac{v\Sigma_c}{2\omega} + \frac{v^2\Sigma_c^2}{8\omega^2} + \cdots\right) + i\left(1 - \frac{v\Sigma_c}{2\omega} + \frac{v^2\Sigma_c^2}{8\omega^2} + \cdots\right)\right.$$

Measuring the modulation rate $\delta n_0/n_0$ at a given point for various values of the frequency $f = \omega/2\pi$ makes it possible to determine diffusion coefficient D.

Observation

The modulus of the complex diffusion length decreases as the frequency increases; it is thus easy to have a medium of very large dimensions as compared to that diffusion length. The solution of the diffusion equation then is very close to that applicable to an infinite medium. We shall see, in the section on corrections what modifications must be made to this solution in order to allow for the finite size of the medium. For the distribution given by a constant source, the solution in an infinite medium is not generally valid, but this distribution [$(n_0 = S_0 f(\vec{r})$], does not have to be made explicit.

The method also can apply to the case in which the dimensions of the medium are comparable to the modulus of the complex diffusion length. The variable solution then must be developed in the eigenfunctions which correspond to the geometry of the medium. An additional damping term is then used to allow for the leakage. In the finite case the precision is not as high as for the infinite medium case. This situation is that met in the conventional measurements of the diffusion length.

Case Where the Source Is a Fast Neutron Emitter

If the source emits fast neutrons, but thermal equilibrium is practically reached in a time which is very short as compared to T_0 and $2\pi/\omega$, one can take, as a starting point the thermal sources given, for example, by the age theory, which are in phase with the fast sources. By placing one's self at distances greater than the moderation length, we can also determine λ_t by the measurement of $\delta n_0/n_0$.

The modulation method may be used for the measurement of the moderating length. The migration area $M^2 = \bar{r}^2/6$ from a fast point source is customarily taken to be equal to $M^2 = \tau - L^2$ in which L is the diffusion length and the age τ is supposedly independent of the capture. This approximation is valid for weak absorption.

One can readily measure the moderation length to the resonance energy of In, on the other hand, the moderation length to thermal energy, can only be measured by markedly reducing the effect of the diffusion phenomenon by poisoning the medium with absorbers. The modulation method offers an equivalent technique, which is also applicable to solid media.

Similarly, it is interesting to study the case in which there is sufficiently large capture to affect the evolution of neutrons at the end of the slowing down process. Here again, capture could be replaced by modulation by the device of operating at a high frequency.

Absolute Measurement of the Capture Cross Section

The formal analogy between the capture cross section and the modulation frequency provides a means of developing a method for the measurement of this cross section by comparison with a time standard, a comparison which is independent of the energy distribution of the neutrons, when the capture cross section measured varies according to a $1/v$ law.

VARIABLE DENSITY MEASURING METHOD

Since in general the neutron density is rather low, and the frequency high, one measures a number of counts rather than an ionization current.

We shall consider the case in which the source varies according to a periodic law with a period $T = 2\pi/\omega$:

$$S = S_0 - \delta S_0 \varphi(t)$$

the periodic function $\varphi(t)$ may be expanded in a Fourier series.

Let S_0, δS_1, δS_2 . . . be the coefficients of this expansion. The density produced by source S at point $\vec{r}$ becomes:

$$n(\vec{r},t) = S_0 F(\vec{r}) + \frac{\delta S_1}{4\pi D r} e^{-\frac{r}{L_\omega} + i\omega t} + \frac{\delta S_2}{4\pi D r} e^{-\frac{r}{L_{2\omega}} + 2i\omega t} + \cdots$$

The counting rate of a detector placed at $\vec{r}$ is proportional to the density, and, denoting the proportionality factor by K, one can write:

$$\frac{C}{K} = n(\vec{r},t)$$

The pulses from the counter then are separated into consecutive time intervals each of duration $T/4$. Now let n_j be the number of pulses in time $(j-1)(T/4)$ . . . $j(T/4)$.

The following sums will be considered:

$$N_1 = n_1 + n_5 + n_9 + n_{13} + \cdots$$
$$N_2 = n_2 + n_6 + n_{10} + n_{14} + \cdots$$
$$N_3 = n_3 + n_7 + n_{11} + n_{15} + \cdots$$
$$N_4 = n_4 + n_8 + n_{12} + n_{16} + \cdots$$
$$N = N_1 + N_2 + N_3 + N_4$$

Since the source varies periodically, $n_j = n_{j-4}$ regardless of j. This equality is true on the average;

later we shall include in the computations the errors due to statistical fluctuations.

Let us consider the ratios:

$$m_{90} = \Re\left\{\frac{(N_4 - N_2) + (N_3 - N_1)}{N}\right\}$$

$$m_0 = \Re\left\{\frac{(N_4 - N_2) - (N_3 - N_1)}{N}\right\}$$

in which $\Re$ means that the real part of the expression is taken. One takes as the origin of time, the instant when the amplitude of the source passes through its maximum. If t_0 is the moment when counting begins, one can write:

$$m_{90} = \Re\left\{\frac{\int_{t_0+\frac{T}{2}}^{t_0+T}\frac{C}{K}\,dt - \int_{t_0}^{t_0+\frac{T}{2}}\frac{C}{K}\,dt}{\int_{t_0}^{t_0+T}\frac{C}{K}\,dt}\right\}$$

$$m_0 = \Re\left\{\frac{\int_{t_0+\frac{T}{4}+\frac{T}{2}}^{t_0+\frac{T}{4}+T}\frac{C}{K}\,dt - \int_{t_0+\frac{T}{4}}^{t_0+\frac{T}{4}+\frac{T}{2}}\frac{C}{K}\,dt}{\int_{t_0+\frac{T}{4}}^{t_0+\frac{T}{4}+T}\frac{C}{K}\,dt}\right\}$$

$$m_0 = -\frac{1}{2\pi^2 Drf(r)}\,\Re\sum_{k=1} i^{k-1}[1-(-1)^k]\frac{\delta S_k}{S_0}\frac{e^{-\frac{r}{L_k\omega}+ik\omega t_0}}{k}$$

$$m_{90} = -\frac{1}{2\pi^2 Drf(r)}\,\Re\sum_{k=1}[1-(-1)]^k\frac{\delta S_k}{S_0}\frac{e^{-\frac{r}{L_k\omega}+ik\omega t_0}}{k}$$

m_0 and m_{90} thus come into the expression as the components of a vector ωt. The term $(1 - (-1)^k)$ remains equal to zero for all even values of k, so the detection method eliminates the contributions of the even harmonics and divides the odd harmonics by their rank k. We thus have selective detection.

EXPERIMENTAL ARRANGEMENTS USED IN THE MEASUREMENT OF THE MEAN FREE PATH OF GRAPHITE

The source consists of a beam of neutrons issuing from a radial channel of the reactor, and modulated by a cadmium disk. The beam is scattered by a nickel target placed in the axis of a graphite stack which has the shape of a parallelpiped having dimensions of 160 × 160 × 180 cm. The density along the axis is measured with a counter. The directions of the neutron beam and axis of the pile form an angle of 90 degrees (see Fig. 1).

Neutron Beam

The neutrons of an energy greater than cadmium cut off are not modulated, and accordingly form a continuous background which has no effect whatsoever on the measurements. One uses the neutrons coming directly from the lattice, in order to have maximum intensity. Now, a high, continuous background level does increase the size of the statistical fluctuations. Thus, it is necessary to collimate the beam carefully, not only the thermal neutrons (cadmium filters), but also the fast neutrons.

Practically, the beam comes from a conical channel drilled through a graphite brick of the reflector, a steel plug of the shield, and a paraffin plug between the shield and the cadmium disk. This channel goes through a second paraffin plug placed between the disk and the pile. The beam, defined in this way, passes down a channel, which is drilled completely through the whole of the pile, without touching the sides. One must be very careful in order that the sides of the channel do not scatter part of the beam so that no modulated sources distributed along the axis of the channel are generated.

The neutron beam is then scattered by a nickel target placed at the center of the channel. Nickel was chosen because of its large scattering cross section: $\Sigma_s = 1.6$ cm^{-1}; its capture cross section $\Sigma_c = 0.36$ cm^{-1} is small enough so as not to attenuate prohibitively the intensity of the scattered beam.

The nickel target is a cylinder having $h = 15$ mm, and $\phi = 18.5$ mm.

The target scatters 90% of the thermal neutrons and the attenuation due to the absorption in the target is 35%.

A polyethylene target may also be used, but the hydrogen nuclei have the drawback of scattering the neutrons very anisotropically.

The measuring channel is at 90 degrees to the channel used for the neutron beam. This selection is suggested by the following considerations:

(*a*) A position is sought, along the axis of symmetry of the pile, in order to be able to compute readily the corrections due to the finite size of the medium.

(*b*) No measurement can be carried out on the axis of the beam. In fact, the neutrons which were not scattered by the nickel target and which have not had a collision with the graphite interposed between the target and the counter will contribute to the count. This proportion is equal to $\alpha e^{-r/\lambda_s}$ where α is the fraction of the neutrons which have not had any collisions, λ_s is the average scattering mean free path of the neutrons in the graphite, and the rate of modulation decreases according to the relation $e^{-\sqrt{\omega/2D}\,r}/r$. Measurements can be taken only at distances for which

$$\frac{r\alpha e^{-r/\lambda_s}}{e^{-\sqrt{\omega r/2D}}} \ll 1$$

at the higher frequencies, the measurements can be carried out far from the source only.

In addition, since λ_s is larger for fast neutrons, the continuous background will be markedly increased.

The source made up of neutrons scattered by the target always exhibits some anisotropy, the contribu-

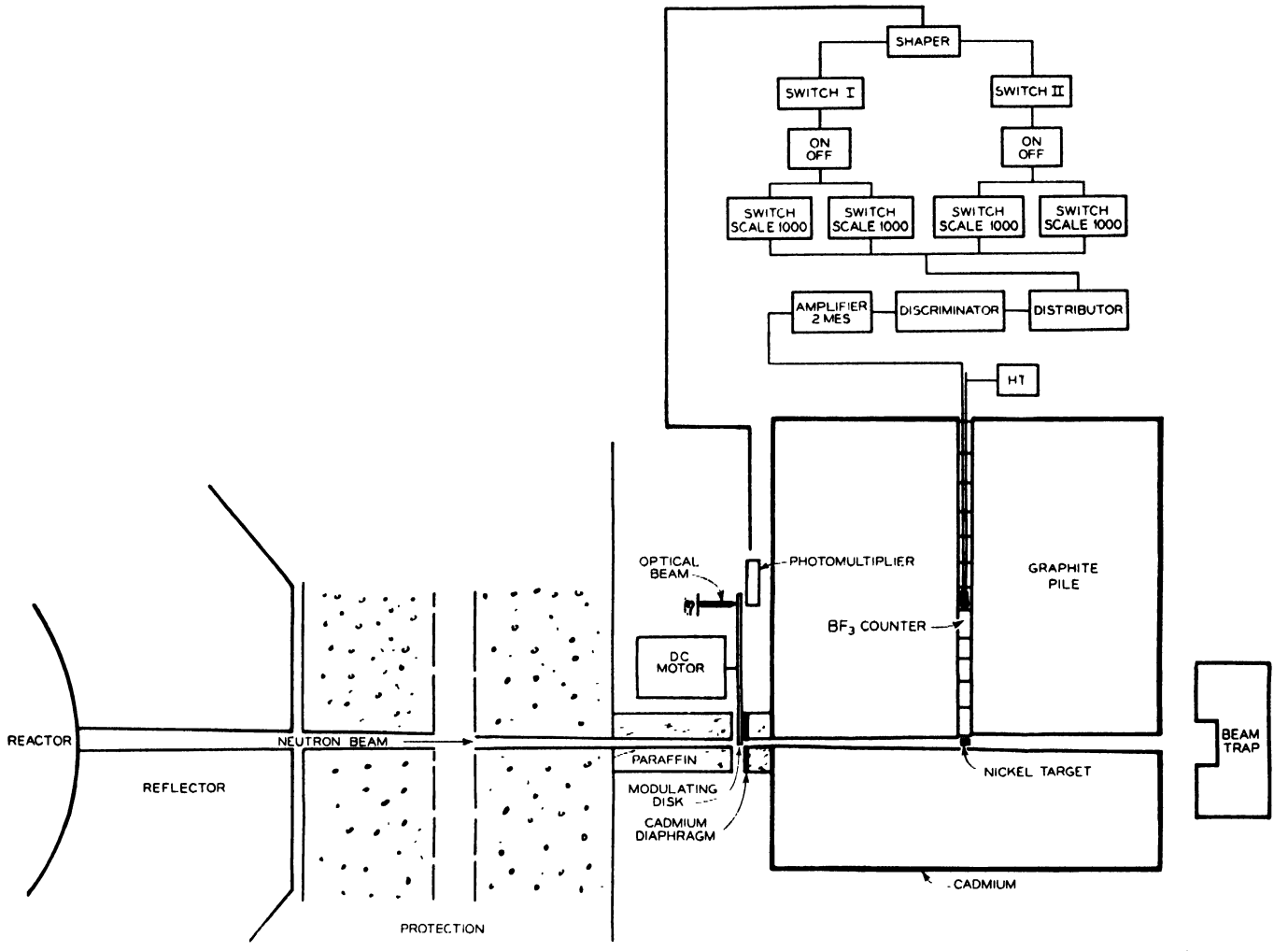

Figure 1. Experimental device used for graphite. This is a horizontal cross section of the channel used for the neutron beam, the collimator, the pile, the target and the measuring channel which receives the counter. Density modulation brought about by rotation of the disk in the beam, is measured in phase and in quadrature by groups of scalers synchronized by pulses from the photomultiplier

tion of the odd harmonics of the angular distribution is zero at 90 degrees from the direction of the beam.

Modulator

The disk is made up of a piece of cadmium sandwiched between two sheets of duraluminum. This design was chosen because of the ease with which it can be made; however, it has the drawback of introducing some higher harmonics, which must be allowed for in the correction terms. A better solution would be to machine the disk using a template, in order to have a modulated form as close as possible to a pure sine wave. The method of fabrication by drilling holes of various diameters in the disk must be ruled out because the resistance of such a disk, at a rotation speed of 6000 rpm, might be inadequate.

The whole system must be extremely rigid, and devoid of vibrations, which might introduce systematic errors which would be functions of the frequency.

The disk is driven by a 5-hp dc motor fed by a Ward Leonard system. A remote control system makes it possible to adjust the speed between 600 rpm and 6000 rpm at rates stable within 0.3%. The frequency is measured by using a stabilized heat frequency oscillator.

Use is made of a five-lobe disk for obtaining modulation frequencies between 50 cps and 500 cps. For other frequencies, other disks are used. The maximum frequency which can be obtained with this device is 10,000 cps (Fig. 2).

Detecting Device

Use is made of a counter of Swedish manufacture 3-cm long, 0.8 cm in diameter. The chamber is placed in an aluminum tube (Fig. 3).

Two coaxial cables make it possible to bring the high voltage to the counter and to receive the pulses.

The aluminum tube and the coaxial cables are embedded in graphite, in such a way that the volume of the cavity is reduced to that of the tube and its cable (Fig. 4).

The pulses from the counter are distributed to two scalers by an electronic switch which operates in such a way that one scaler is counting for one half of a period while the other one does not operate and vice versa. A second switch, having a delay of $T/4$ with respect to the former, feeds a second group of scalers.

The four scalers register the following counting rates: $(N_1 + N_2)$; $(N_3 + N_4)$; $(N_2 + N_3)$; $(N_1 + N_4)$. The switches are synchronized by pulses received from

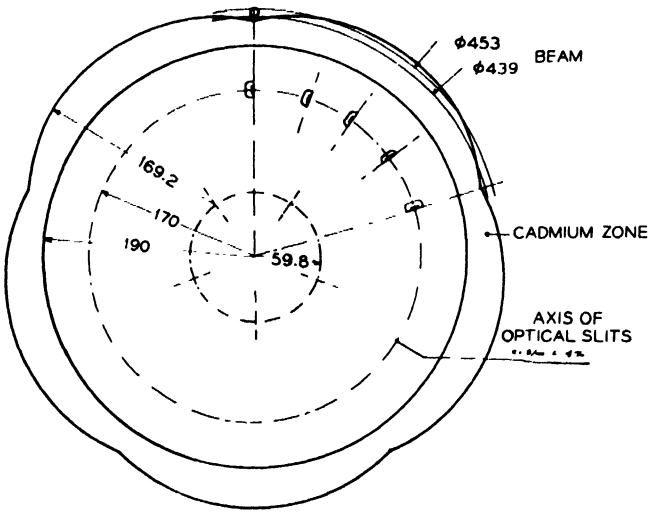

Figure 2. 5-lobe disk used in the experiment on graphite. The motor which drives the disk has a speed of between 600 and 6000 rpm which makes it possible to explore the whole frequency range (50 cps to 500 cps). The position of the optical slit which makes it possible to synchronize the counting scalers is shown. Alternate slits are longer, which make it possible, by observing the signals from the PM on an oscilloscope, to know which group of scalers are counting "in phase"

a photomultiplier operated by the luminous flashes coming from slits in the disk.

EXPERIMENTAL ARRANGEMENTS USED FOR MEASURING THE MEAN FREE PATH IN HEAVY WATER

The measurement was made in the experimental hole of the Saclay pile surrounded by its graphite reflector but with the uranium slugs removed.

The source consisted of a bar of radioactive antimony (ϕ = 5 mm) placed along the axis of two beryllium quadrants diametrically opposite one another (ϕ_{int} = 32 mm, ϕ_{ext} = 47 mm). A screen made of a very dense substance was needed to regulate the density of the γ-radiation striking the target, and it consisted in fact of two 12 mm-thick uranium quadrants rotating between the beryllium and the antimony. The outside dimensions of the source made up in this way were h = 100 mm, ϕ = 48 mm.

Since the Sb-Be source is less intense than a reactor beam, the counter employed had an effective volume about ten times larger than that used for the graphite experiment. The detecting device was generally similar to that used in the graphite measurement (see Fig. 5).

The heavy-water experiments have been described elsewhere.[15] The result obtained for heavy water at 13°C was λ_t = 2.45 ± 0.07 cm.

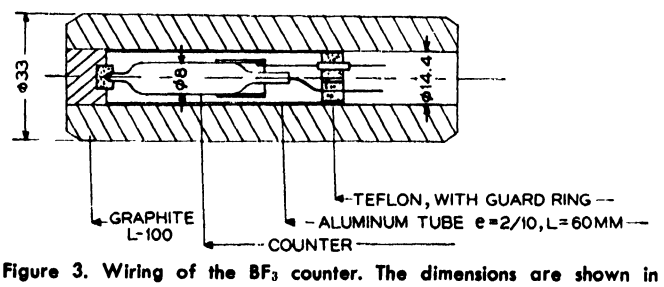

Figure 3. Wiring of the BF_3 counter. The dimensions are shown in millimeters; the graphite cylinder which contains the counter is placed in the measuring channel

EXPERIMENTAL SETUP

The frequency interval and position of the counter are suitably chosen.

The lower frequency limit to be used depends on the capture cross section of the medium under study. In the case of the graphite $v\Sigma_c \cong 80$ sec^{-1}, the corrective term $v\Sigma_c/2\omega$ has a value of 0.06 for a frequency of 100 cps.

When the frequency increases, for a given position of the counter, the modulation rate decreases, and the time necessary to carry out measurements with a preset statistical accuracy increases in inverse ratio to the square of the modulation rate. The higher frequency depends on the selected measurement time interval and, therefore, on the intensity of the source.

In the case of graphite, the measurements were carried out in the 80 cps to 50 cps range.

The minimum distance between source and detector must be such that the contribution of the harmonics due to anisotropy of the source is negligible. The maximum distance depends on the amplitude of the modulation rate, and, practically, the measurements are stopped at the distance at which the modulation rate is below 1%. In all cases, the farthest position must be set so that the distance from the counter to one of the sides of the pile is greater than one scattering length.

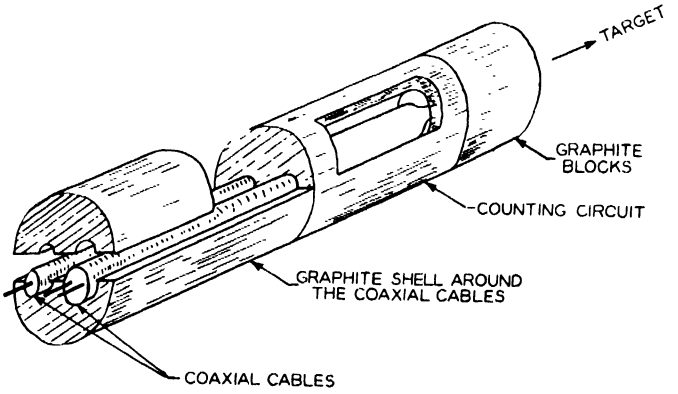

Figure 4. Coaxial cable exit. The outside diameter of the graphite shell is equal to the inside diameter of the measuring channel. This design eliminates empty spaces behind the counter

In the case of graphite, the length of the pile was 180 cm. The target was placed in the axis of the pile 50 cm from one side and the measurements were carried out on the line between positions 65 cm and 130 cm. The counter was located in the axial channel of the pile and the beam was then centered so that, in the absence of a target, the counting rate was a minimum.

The target then is set up, and the counting rate measured, for successive positions of the disk which correspond to a total rotation of 2π in time ωt. The third harmonic, which is the most disturbing, was allowed for in the correction computations.

The modulation rate is then measured to give the phase and the amplitude as a function of the frequency at a given position, after which the position of the counter is changed and the measurements taken again. For every measurement, that portion of the

channel between the target and the counter is blocked off by graphite cylinders.

This gives the components of the complex number which represents the modulation rate:

$$M = \frac{1}{2\pi^2 Drf(r)} \frac{\delta S_1}{S_0} e^{-\frac{r}{L_\omega} - i\omega t}$$

$$|M| = \frac{1}{2\pi^2 Drf(r)} \frac{\delta S_1}{S_0} e^{-r\sqrt{\frac{\omega}{2D}}\left\{1+\frac{v\Sigma_c}{2\omega}\right\}}$$

$$Arg\ M = -\psi_0 - r\sqrt{\frac{\omega}{2D}}\left(1 - \frac{v\Sigma_c}{2\omega}\right)$$

where $\psi_0 = \omega t_0$ is an angle, independent of ω, defined by the angle formed between the neutron beam and the optical beam which operates the photomultiplier.

The curve which represents $\log |M|$ as a function of $\sqrt{\omega}\{1 + (v\Sigma_c/2\omega)\}$ is a straight line, the slope of which is $p_m = -v/\sqrt{2D}$. Thus it is not necessary to determine function $rf(r)$ in this measurement.

The distance r between the target and the counter is poorly defined. On the other hand, the variations of r are known accurately; thus, the slope of p_m is defined as a function of r and this gives the value of $1/\sqrt{2D}$.

The function $rf(r)$ does not come into play in the argument of M and one can measure, either the slope of $Arg\ M$ as a function of $[1 - (v\Sigma_c/2\omega)]$ or of r. We shall see that the phase shift caused by the time-of-flight of the beam requires the second technique.

CORRECTIONS

Since the correction terms are small, those corrections which are superimposed on existing corrections are left out, in other words, corrections are made independently of one another.

Third Harmonic of the Source

The high harmonics can generally be left out. It was seen that, following detection, the complex number which represents the modulation rate can be expressed as:

$$M = \frac{1}{2\pi^2 Drf(r)} \left\{ \frac{\delta S_1}{S_0} e^{-\frac{r}{L_\omega} - i\omega t_0} - \frac{1}{3}\frac{\delta S_3}{S_0} e^{-\frac{r}{L_{3\omega}} - 3i\omega t_0} \right\}$$

which can be put in the form:

$$M = \frac{1}{2\pi^2 Drf(r)} \frac{\delta S_1}{S_0} e^{-\frac{r}{L_\omega} - i\omega t_0} \epsilon_{h3}\, e^{i\varphi_{h3}}$$

$$\text{with } \epsilon_{h3} = 1 + \frac{1}{3}\frac{\delta S_3}{S_1} e^{-0.73r\sqrt{\frac{\omega}{2D}}} \cos\left(0.73r\sqrt{\frac{\omega}{2D}} + 4\omega t_0\right)$$

$$\varphi_{h3} = -\frac{1}{3}\frac{\delta S_3}{S_1} e^{-0.73r\sqrt{\frac{\omega}{2D}}} \sin\left(0.73r\sqrt{\frac{\omega}{2D}} + 4\omega t_0\right)$$

an approximate value of D is taken, and the corrections required are made on M.

Finite Dimensions

The effect of the finite dimensions of the pile can also be computed by developing the variable density eigenfunctions of the rectangular parallelepiped; how-

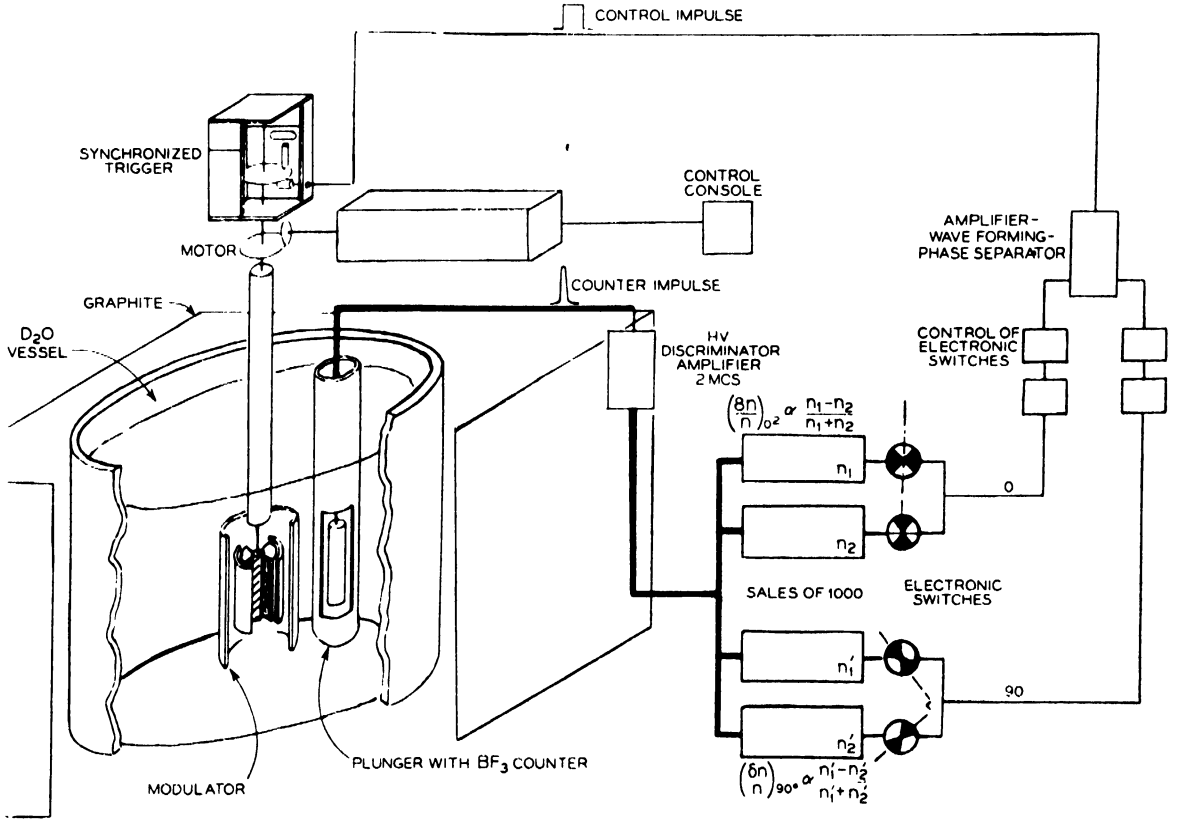

Figure 5. Experimental device used for heavy water. The uranium sectors driven by a variable speed motor modulate the gamma flux coming from radioantimony: a modulated flux of 25 kev neutrons then is emitted from the beryllium sectors. Density modulation is measured by a device similar to that shown on Fig. 1

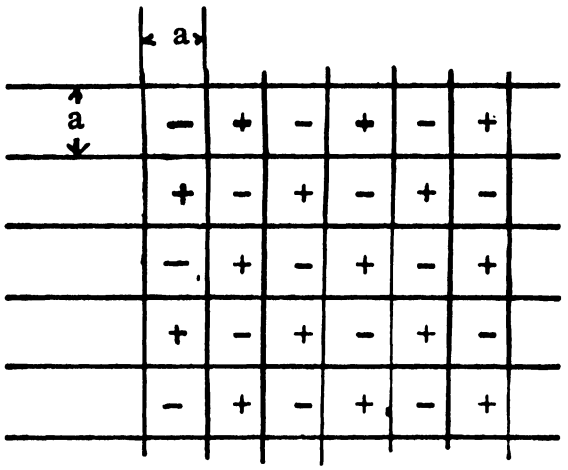

Figure 6

ever, the solution is very close to that obtained for an infinite medium, so that the series development does not converge rapidly. A more rapidly converging expansion can be obtained from the method of images.

If a is the length of the side of the parallelepiped plus twice the extrapolation length, then $a = 160 + 2 \times 0.71 \times \lambda_t = 164$ cm.

The position and sign of the image source points which give the same boundary conditions is given in Fig. 6, (the density becomes zero at a distance $0.71\lambda_t$ of the side of the parallelepiped).

If r_0 is the distance between the source and the counter (taken perpendicular to the plane of the figure, according to the axis of the pile) then, the distances from the counter to the image source points are:

$$r_1 = \sqrt{a^2 + r_0^2}$$

$$r_2 = \sqrt{2a^2 + r_0^2}$$

and the density at the point r_0 can be expressed by:

$$n_0 = \frac{S_0}{4\pi D}\left\{\frac{e^{-\frac{r_0}{L_\omega}}}{r_0} - \frac{4}{r_1}e^{-\frac{r_1}{L_\omega}} + \frac{4}{r_2}e^{-\frac{r_2}{L_\omega}} - \cdots\right\}$$

the series thus obtained converges rapidly, and it can be stopped at the second term.

The modulation rate then can be expressed as:

$$M = \frac{1}{2\pi^2 D r_0 f(r)}\frac{\delta S_1}{S_0}e^{-\frac{r}{L_\omega} - i\omega t_0}\epsilon_{df}\, e^{i\varphi_{df}}$$

$$\text{with } \epsilon_{df} = 1 + 4\frac{r_0}{r_1}e^{-(r_1 - r_0)\sqrt{\frac{\omega}{2D}}}\cos\left[(r_1 - r_0)\sqrt{\frac{\omega}{2D}}\right]$$

$$\varphi_{df} = -\text{Arctan}\left\{4\frac{r_0}{r_1}e^{-(r_1 - r_0)\sqrt{\frac{\omega}{2D}}}\sin\left[(r_1 - r_0)\sqrt{\frac{\omega}{2D}}\right]\right\}$$

Time of Flight

The time t_0, at which the photomultiplier is triggered, is defined by the passage of the optical slit on the disk. The neutrons modulated by the disk are delayed over a path which extends from this disk to the target; thus, the source is out of phase with respect to disk rotation, and this phase shift, which may become very large is a function of the frequency.

Since the neutrons are not monoenergetic, but rather are distributed according to a Maxwellian distribution with a mean temperature close to that of the core of the reactor from which they come, the amplitude of the source also depends on the frequency, an effect which is much smaller for the amplitude than for the phase.

Let

$$n(v)v\,dv = n_0 v_0 \frac{4}{\sqrt{\pi}}\left(\frac{v}{v_0}\right)^3 e^{-\frac{v^2}{v_0^2}} d\left(\frac{v}{v_0}\right)$$

be the distribution of the flux in the reactor core.

By writing $z = v/v_0$, the flux modulated on the right side of the disk can be expressed by:

$$\phi = \phi_0 \frac{4}{\sqrt{\pi}}\int_0^\infty z^3 e^{-z^2} dz e^{i\omega t} = \phi_0' e^{i\omega t}$$

if l is the distance between the disk and target, then, the flux scattered by the target can be expressed by:

$$\phi' = \phi_0' \frac{4}{\sqrt{\pi}}\int_0^\infty z^3 e^{-z^2 + \frac{i}{z}\varphi_0} dz e^{i\omega t}$$

where $$\varphi_{tv} = \omega l'/v_0$$

This integral can be computed by means of a series, which gives the modulus and phase of Φ'/Φ_0'

$$\frac{\Phi'}{\Phi_0'} = (\epsilon_{tv})e^{i\varphi_{tv}}$$

in which ϵ_{tv} and φ_0 depend on ω. ϵ_{tv} generally is close to unity, and can be allowed for as a corrective term. On the other hand, the phase shift due to the time of flight cannot be considered as a correction term (Fig. 7).

If the slope of the phase shift of the modulation rate can first be measured as a function of the distance, the effect of the phase shift due to the time of flight is eliminated.

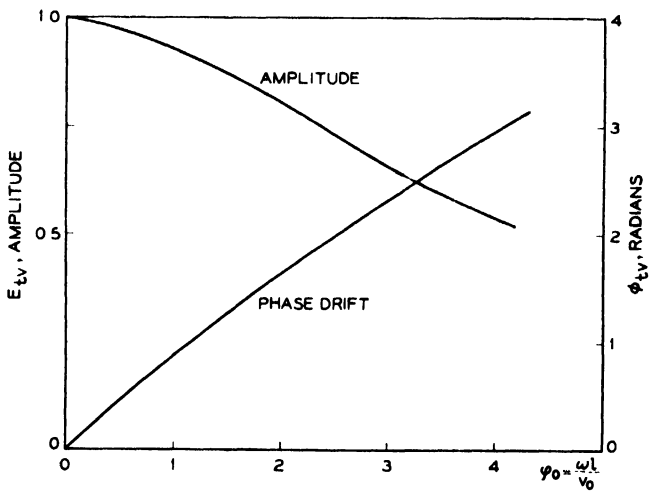

Figure 7. Times of flight. These curves, computed for a Maxwellian spectrum, give the attenuation due to a mixture of components of the spectrum and the phase shift due to the time of flight as a function of $\omega e/v_0$ in which $f = \omega/2\pi$ is the modulation frequency, l the distance between the disk and the target, and v_0 the most likely speed of the burst (that corresponding to the temperature of the neutrons in the core)

Influence of Anisotropy of the Source and Counter Dimensions

We take the case of a spherical source of radius a, in which case the distribution of the neutrons which come out at a given point of the sphere is isotropic, but the intensity is a function of the angle θ_λ between the directions of the point and incident burst. The radiation from the source can be exhibited in the form of a series of Legendre polynomials.

$$\delta S = \frac{\delta S_0}{2B_0} \sum_{n=0}^{\infty} B_n P_n (\cos\theta)$$

The solution of the diffusion equation is then:

$$\delta\phi_0 = \frac{\delta S_0}{4\pi Dr} e^{-\frac{r}{L_\omega}} \left\{ \frac{1}{1 - i\frac{a}{L_\omega}} + \sum_{n=1} i^n \frac{B_n}{B_0} \frac{2^n n!}{(n+1)(2n)!} \times P_n(\cos\theta) \sum_{m=0}^{m=n} \frac{(n+m)!}{m!(n-m)!} \left(\frac{iL_\omega}{2r}\right)^m \right\}$$

If the observation is made for $\theta = \pi/2$, the contribution of the odd terms is zero, and one can write:

$$\delta\phi_0 = \frac{\delta S_0}{4\pi Dr} e^{-\frac{r}{L_\omega}} \left\{ 1 + \left(\frac{a}{L_\omega}\right)^2 \left[1 - \frac{\beta_2}{18\beta_0} \left(1 + \frac{3L_\omega}{r} + \frac{3L_\omega^2}{r^2} \right) \right] + \epsilon \left(\frac{a^4}{L^4}\right) \right\}$$

in which ϵ is a term of order a^4/L^4.

The influence of anisotropy thus depends on the ratio a/L_ω if $r/L_\omega \gg 1$ and on a^2/rL_ω if $r/L_\omega \sim 1$.

This computation shows the need for a source of small dimensions. Let r be the distance between the centers of the source and counter. Let $2l$ be the effective length of the counter and $r + x$ the position of a point in the counter. If $x/r \ll 1$, the neutron density at point $r + x$ can be written:

$$\delta\phi_0 = \frac{\delta S_0}{4\pi Dr} e^{-\frac{r}{L_\omega}} \left\{ 1 - \left(1 + \frac{r}{L_\omega}\right)\frac{x}{r} + \frac{2 + \frac{r^2}{L_\omega^2}}{2} \times \frac{x^2}{r^2} + \cdots \right\}$$

then, the mean density for the counter is:

$$\overline{\delta\phi_0} = \frac{1}{2l} \int_{-1}^{+1} \delta\phi_0 \, dx$$

$$\overline{\delta\phi_0} = \frac{\delta S_0}{4\pi Dr} e^{-\frac{r}{L_\omega}} \left\{ 1 + \left(\frac{a}{L_\omega}\right)^2 \left[1 - \frac{\beta_2}{18\beta_0} \left(1 + \frac{3L_\omega}{r} + \frac{3L_\omega^2}{r^2} \right) \right] + \frac{2 + \frac{r^2}{L_\omega^2}}{6} \frac{l^2}{r^2} + \cdots \right\}$$

the terms which have been left out are of the order of $(a/L_\omega)^4$ and $(1/r)^4$. If a and r are suitably chosen, the correction thus applied to the slopes is negligible.

Influence of Dipole Emission of the Source

The method used to modulate the intensity of the beam of neutrons also brings about a periodic oscillation having the same frequency as its center of gravity. Then the equation for the source is of the form:

$$S = (S_0 + \delta S_0 e^{i\omega t})\delta(\vec{r} - \vec{\rho} e^{i\omega t})$$

an expression which can be developed formally, to give:

$$S = S_0 + \{\delta S_0 \delta(\vec{r}) - S_0(\vec{\rho}\cdot\Delta)\delta(\vec{r})\} e^{i\omega t}$$

where $\vec{\rho}\cdot\Delta$ is the directional derivative.

Then the solution takes the form:

$$n_0 + \delta n_0 = S_0 f(\vec{r}) + \left\{ \frac{\delta S_0}{4\pi Dr} e^{-\frac{r}{L_\omega}} - \vec{\rho}\cdot\Delta \frac{S_0}{4\pi Dr} e^{-\frac{r}{L_\omega}} \right\} e^{i\omega t}$$

$$\vec{\rho}\cdot\Delta \frac{S_0}{4\pi Dr} e^{-\frac{r}{L_\omega}} = \frac{S_0 \rho_r}{4\pi Dr} e^{-\frac{r}{L_\omega}} \left\{ \frac{1}{L_\omega} + \frac{1}{r} \right\}$$

where ρ_r is the component of vector $\vec{\rho}$ along the line of observation. Now the modulation rate can be written:

$$\frac{\delta n_0}{n_0} = \frac{\delta S_0}{4\pi Dr f(r)} e^{-\frac{r}{L_\omega}} \left\{ 1 + \frac{S_0 \rho_r}{\delta S_0} \left(\frac{1}{r} + \frac{1}{L_\omega} \right) \right\}$$

the term in parenthesis is very close to being equal to unity, so that one can still write:

$$\frac{\delta n_0}{n_0} = \frac{\delta S_0}{4\pi Dr} e^{r - \frac{S_0}{\delta S_0}\frac{\rho_r}{L_\omega} + \frac{S_0}{\delta S_0}\frac{\rho_r}{r}}$$

The dipole contribution of the source thus causes an apparent shift of the source with respect to the counter, having an amplitude $S_0\rho_r/\delta S_0$. This effect has no influence on the measurement of the diffusion coefficient, but it does indicate that the distance from the source and counter is poorly defined.

ρ_r is of the order of magnitude of the target radius,

$$\frac{S_0}{\delta S_0} \cong 1$$

so the apparent shift may reach 10 mm.

ANALYSIS OF THE RESULTS, COMPUTATION OF ERRORS

The results are analyzed by the method of least squares.

The numbers of counts N_1, N_2, N_3, N_4, are mean values. If we repeat the measurements we find numbers which are slightly different. The dispersion of the results is $\sigma_{N_i} = \sqrt{N_i}$ if there is no correlation between the numbers N_i, which is assumed to be the case. Since, in addition, the modulation rates are small, one can assume without any great error that the various σ_{N_i} are equal:

$$\sigma_{N_1} = \sigma_{N_2} = \sigma_{N_3} = \sigma_{N_4} = \frac{\sqrt{N}}{2}$$

The amplitude and phase of the modulation rate can be written as:

$$m = \sqrt{m_0^2 + m_{90}^2}$$

$$\tan \varphi = \frac{m_{90}}{m_0}$$

from which

$$m^2 = \frac{(N_4 - N_2)^2}{N^2} + \frac{(N_3 - N_1)^2}{N^2}$$

The expressions $x = N_4 - N_2/N$ and $y = N_3 - N_1/N$ are independent variables, so that

$$\sigma_{m^2}^2 = \sigma_{x^2}^2 + \sigma_{y^2}^2$$

The counting rates N_1, N_2, N_3, N_4, also being independent variables, we can write:

$$\sigma_x^2 = \frac{1}{N^2}(\sigma_{N_2}^2 + \sigma_{N_4}^2)$$

$$\sigma_y^2 = \frac{1}{N^2}(\sigma_{N_1}^2 + \sigma_{N_4}^2)$$

If we leave out the fluctuations of the source with respect to those of a difference in the counting rate, we can write: $\sigma_x = \sigma_y = \sqrt{N}/N$ by using the relationship between the dispersion of a variable and the dispersion of its square. We thus have:

$$\sigma_{x^2} = 2x\sigma_x$$

from which

$$\sigma_{m^2}^2 = 4(x^2 + y^2)\sigma_x^2 = 4\frac{m^2}{N}$$

then

$$\sigma_m = \frac{1}{\sqrt{N}}$$

The probable error (50 per cent reliability) thus will be:

$$\epsilon_m = 0.675\sigma_m = \frac{0.675}{\sqrt{N}}$$

Dispersion in the logarithm of the modulus: $z = \log m$ is given by the formula:

$$z \pm \sigma_z = \log(m \pm \sigma_m) = \log m \pm \frac{1}{m\sqrt{N}}$$

so that:

$$\sigma_{\log m} = \frac{1}{m\sqrt{N}}$$

Similarly, we find that the dispersion along the tangent can be expressed by:

$$\sigma_{\tan\varphi} = \frac{1}{N}\frac{m}{m_0^2}$$

The dispersion in the angle φ is given by relationship:

$$\tan(\varphi \pm \sigma\varphi) = \tan\varphi \pm \sigma_{\tan\varphi}$$

$$\tan\varphi \pm (1 + \tan^2\varphi)\sigma\varphi = \tan\varphi \pm \sigma_{\tan\varphi}$$

from which:

$$\sigma_\varphi = \frac{1}{m\sqrt{N}}$$

In conclusion, the dispersions in the phase shift and the logarithm of the modulus are equal and their common value is:

$$\sigma_{\log m} = \sigma_\varphi = \frac{1}{m\sqrt{N}} = \frac{dm}{m} = d\varphi$$

In the computation of slopes p_m and p_φ by the method of least squares, we shall take, as weight p_i of these measurements, the value:

$$\sqrt{p_i} = \frac{1}{m_i\sqrt{N_i}}$$

Experimental Results

A first series of measurements was carried out in cooperation with Messrs. Cherot, Lacour, Lebaud, Meunier of the Mathematical Physics Department.

Results Bearing on the Modulus

In Fig. 8, we show the experimental points which represent $\log|\delta n/n|$ as a function of $x_m = [1 + v\Sigma_c/2\omega]\sqrt{\omega}$ for various distances z between the source and the detector. The dispersions indicated are statistical dispersions ($\sigma_{\log m} = 1/m\sqrt{N}$) which are most significant in the present case. The straight lines shown were determined by the method of least squares. Their slopes p_m, marked on Fig. 9 as a function of z, are

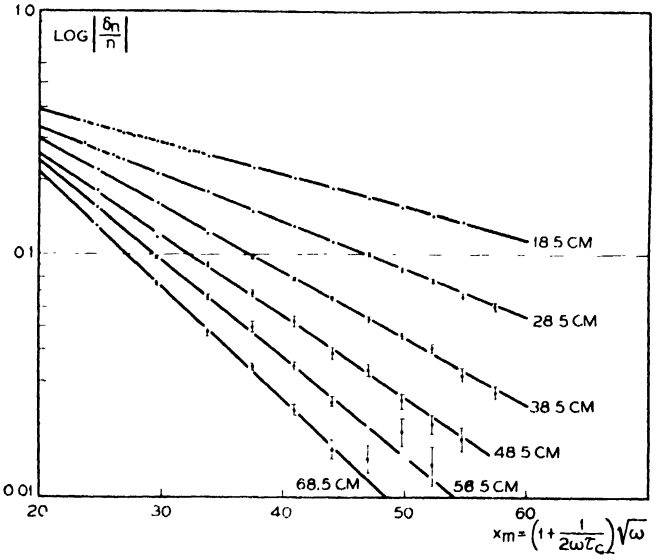

Figure 8. Modulus. Experimental points which represent log ($\delta n/n$) as a function of $x_m = \sqrt{\omega}\{1 + v\Sigma_c/2\omega\}$ are shown. We took $(v\Sigma_c)^{-1} = 13 \times 10^{-3}$ sec. The error bars are the standard deviations due to statistical fluctuation of the counting rate. The straight lines drawn for each position z and the counter were determined by the method of least squares, suitably weighting the points

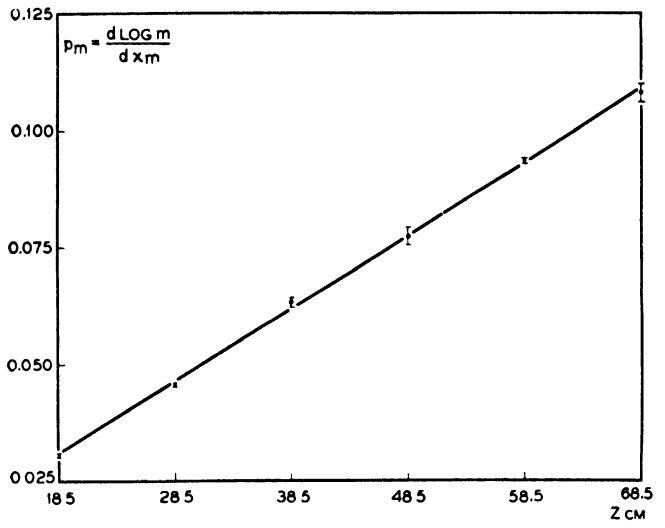

Figure 9. Modulus. The slope of the straight lines is shown on Fig. 8. $p_m = d \log (\delta n/n)/dx_m$ as a function of position z of the counter. The error bars were determined by the method of least squares. From the slope of straight line dp_m/dz the value of the diffusion coefficient can be derived

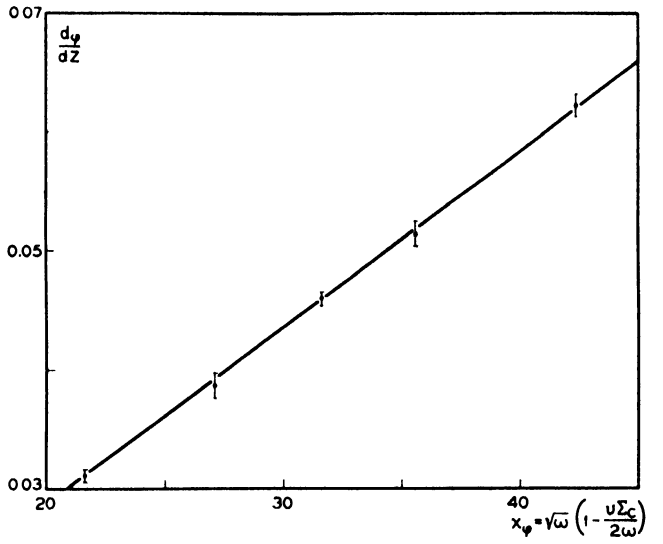

Figure 11. The slope of the straight lines is shown on Fig. 9: $p\varphi = d(\text{Arg } \delta n/n)/dZ$ as a function of $x\varphi = \sqrt{\omega}\,(1 - v\Sigma_c/2\omega)$. The error bars are determined by the method of least squares. From the slope of the straight line $dp\varphi/dx\varphi$ we compute the value of the diffusion coefficient

aligned on a straight line, the slope of which determines the diffusion coefficient $D = \lambda_t v/3$.

The mean temperature of the graphite was 20°C, and its density 1.625 ± 0.003. By making $v = 2.198 \times 1.128 \times 10^5$ cm/sec, the transport mean free path λ_t for graphite, for density 1.6, will be: $\lambda_t = 2.55 \pm 0.09$ cm.

It should be remembered that the straight line which gives p_m intersects the z axis at point $z_0 = -(13 \pm 5)$ mm, and not at the origin. This, as it seems, should be ascribed to the dipole term in the source.

Results Bearing on the Phase

The results are shown on Figs. 10 and 11. The fluctuations observed in the phase are greater than the statistical fluctuations. This might be due to fluctuations of the temperature of the neutrons in the burst, bringing about corresponding variations in the phase shift due to the difference in time of flight (this effect is less important in the case of the modulus). Experiments are under way in order to verify this hypothesis. The origin of the additional fluctuation is uncertain, so that the straight lines in Fig. 10 (φ as a function of z) were determined by the method of least squares without giving any weight to the experimental points. We thus obtain the value $\lambda_t = 2.70 \pm 0.18$ cm.

Other series of measurements are under way. They will be the object of an addition to this communication.

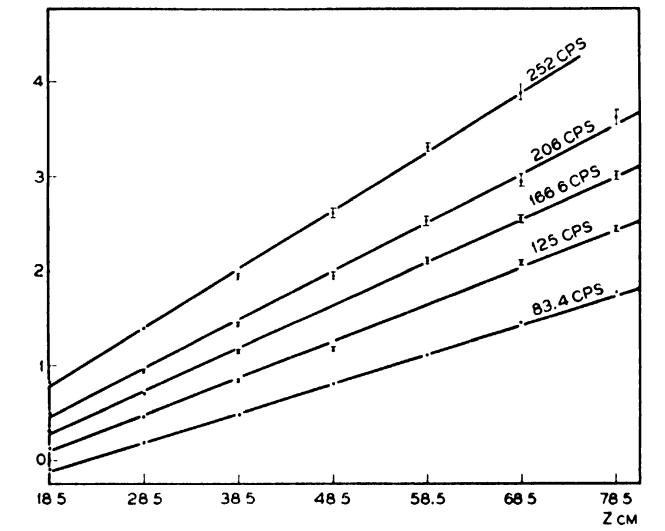

Figure 10. Experimental points are shown, which represent the phase shift of the bundle: Arg $\delta n/n$ as a function of position z on the counter. The error bars represent the statistical fluctuations of the counting rates, the straight line drawn for each modulation frequency was determined by least squares without any weighting of the points

REFERENCES

1. Langsdorf, Alexander, Jr., Bull. Am. Phys. Cos. *23*, No 3, 20 (1948).
2. Pomerance, H. and Hoover, J. I., Phys. Rev. *73*, 1265 (1948).
3. Raievski, V. and Yvon J., Comptes rendus *231*, p. 345 (1950).
4. Ertaud, A., Raievski, V. and Breton, D., J. Phys. Rad. 12, 784 (1951).
5. Breton, D.
6. Bentzen, F. L., Bridge, J., Fermi, E., Feynman, R. P., De Hoffmann, F., Derst, D. W., King, L. D. P. and Young, G. A., A.E.C.D. 3051 (1944).
7. Gilbert, C. W. and Fergusson, G. J., C.R.P., 377 (1948).
8. Raievski, V., Comptes rendus, *237*, p. 1513 (1953).
9. Raievski, V., Note C.E.A. No. 73 (1954).
10. Weinberg, A. M. and Schweinler, H. C., Phys. Rev. *74*, 851 (1948).
11. Weinberg, A. M., A.E.C.D., 3471 (1951).
12. von Dardel, G. and Sjöstrand, N. G., Phys. Rev., *96*, 1245 (1954).
13. Auger, P., Munn, A. M. and Pontecorvo, B., Can. J. Res., *125*, p. 143 (1947).
14. Kash and Woods, Phys. Rev., 90, p. 564, (1953).
15. Raievski, V. and Horowitz, Comptes rendus, *238*, p. 1993 (1954).

Measurements on a Subcritical Reactor with a Pulsed Neutron Source

By N. G. Sjöstrand,* Sweden

This paper describes a new method for determining some constants of a reactor in a subcritical state. The principle of the method is to pulse the reactor with a neutron source and study the time behaviour of the neutron flux. It is possible to determine the decay time of the prompt neutrons and the amount of reactivity by which the reactor is below criticality. From these results the reactivity equivalent of a safety rod or of a certain amount of heavy water and the mean life-time of thermal neutrons can be derived. Such quantities are otherwise difficult to determine without actually making the reactor critical, and it therefore seems that the method employing a pulsed neutron source will be of value as a complement to exponential experiments.

THEORY

The treatment given here is restricted to a bare, subcritical reactor containing a source, the strength of which is a periodic function of time, $S(t)$. It is further supposed that only the fundamental mode of the neutron distribution is important. The delayed neutrons, which in a D_2O reactor include photoneutrons, are represented by one group and are assumed to have the same age as the prompt neutrons. If the age of the source neutrons is called τ_s, the following equations are obtained:[1]

$$\frac{\partial C(r,t)}{\partial t} = -\lambda C(r,t) + \frac{k}{p}\beta\Sigma_a\phi(r,t) \tag{1}$$

$$l\frac{\partial\phi(r,t)}{\partial t} = -[1-(1-\beta)k_{eff}]\phi(r,t) + \frac{p}{\Sigma_a(1+L^2\beta^2)}[e^{-\beta^2\tau}\lambda C(r,t) + e^{-\beta^2\tau_s}S(r,t)] \tag{2}$$

If these equations are integrated over the period T, we get

$$\int_0^T \lambda C\,dt = \frac{k}{p}\beta\,\Sigma_a\int_0^T\phi\,dt \tag{3}$$

$$[1-(1-\beta)k_{eff}]\int_0^T\phi\,dt = \frac{p}{\Sigma_a(1+L^2\beta^2)}\left[e^{-\beta^2\tau}\int_0^T\lambda C\,dt + e^{-\beta^2\tau_s}\int_0^T S\,dt\right] \tag{4}$$

Elimination of $\int_0^T\phi\,dt$ between the equations gives

$$\frac{e^{-\beta^2\tau_s}\int_0^T S\,dt}{e^{-\beta^2\tau}\int_0^T\lambda C\,dt} = \frac{\rho}{\beta} \tag{5}$$

where ρ is the amount of *negative* reactivity

$$\rho = \frac{1-k_{eff}}{k_{eff}}$$

Since β is a known quantity, it is possible to determine the reactivity if the ratio of the number of thermal neutrons arising from the prompt multiplication of source neutrons and those coming from the delayed neutrons can be derived from a measurement.

From Equation 2, we further find that the time constant for the prompt neutrons is

$$l_p = \frac{l}{1-(1-\beta)k_{eff}} \quad \text{or} \quad l_p = \frac{l}{\beta+\rho} \tag{6}$$

The latter expression is valid close to criticality. If the reactivity is known, the mean life-time of thermal neutrons in the reactor can also be found.

APPARATUS

The Swedish heavy-water reactor in a subcritical state was pulsed by means of a 150 kv neutron generator.[2] The acceleration tube was placed horizontally in front of the reactor, and a 4-m long target-tube was extended into the reactor tank through a horizontal channel (see Fig. 1). When the deuterium ions struck the Zr-T target 14 Mev neutrons from the T-D reaction were produced. By modulation of the ion source a pulsed-neutron source was obtained about 30 cm from the centre of the reactor. A movable BF_3 proportional counter was situated in another horizontal channel. The pulses from the counter were fed into a 40-channel time-analyser,[3] by means of which it was thus possible to study the time variation of the neutron flux in the reactor.

DETERMINATION OF THE REACTIVITY EQUIVALENT OF THE HEAVY WATER

Reactivity measurements were made at several D_2O levels down to 18 cm below the critical level with all safety and control rods pulled out of the reactor.

* Aktiebolaget Atomenergi, Department of Physics, Stockholm, Sweden.

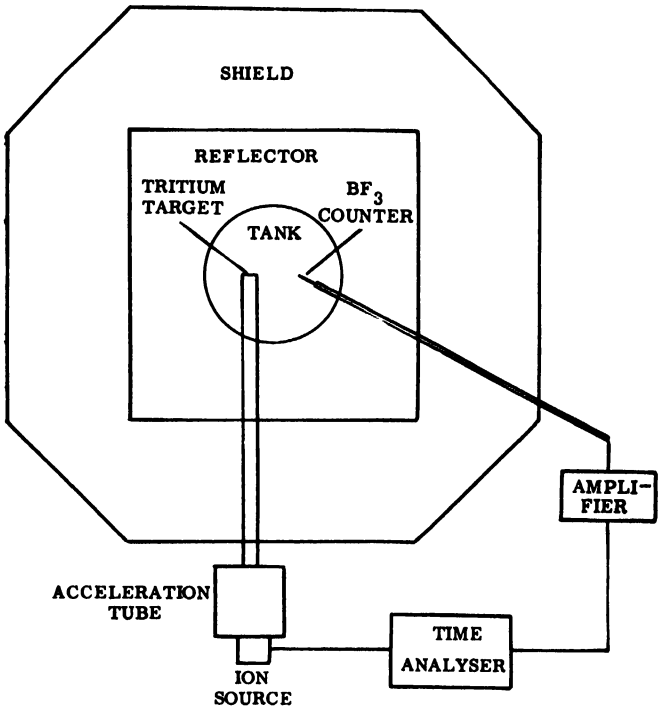

Figure 1. A schematic view of the experimental arrangement

The repetition time was 0.5 or 1 sec, and the neutron pulse-length half this period.

Up to the time of these measurements the reactor had only run at a very low-power level. Photoneutrons were therefore negligible, the background mainly arising from spontaneous fission neutrons. It was always less than one per cent during the present measurements.

Before commencing a measurement with the time-analyser, the neutron generator had to run for 10 minutes in order to reach a steady state as regards the delayed and photoneutrons.

The heavy-water level was read on the gauge glass and corrected for temperature effects. The critical level was determined by running the reactor at a power of a few watts and then pulling out a control rod while the water level was lowered to the critical level.

A typical curve from the measurements is shown in Fig. 2. The ratio ρ/β is obtained from Equation 5. According to the one group theory of a bare reactor we have

$$\rho = \frac{1 - k_{eff}}{k_{eff}} = \frac{M^2\pi^2}{1 + M^2B_c^2}\left(\frac{1}{H^2} - \frac{1}{H_c^2}\right) \qquad (7)$$

where H is the effective height of the reactor, and H_c the critical height. When ρ/β is plotted as a function of $1/H^2 - 1/H_c^2$ we get a straight line. From the slope we find that one mm D_2O corresponds to a reactivity of 7×10^{-5} at the critical level, if β is assumed to be 0.79×10^{-2}.[4] This agrees with results of measurements by Jonsson.[5]

The migration area M^2 is found to be 320 cm^2. This high value is due to the influence of the reflector (Equation 6), which has not been taken into account in the derivation of Equation 7.

CALIBRATION OF THE SAFETY RODS

The calibration of the safety rods was carried out in a manner similar to the reactivity measurements described above. The D_2O level chosen was close to the critical level, and measurements were made with safety rod number one, number two, or both rods in the reactor. The background was relatively higher for these measurements, as the reactor was farther from criticality, but it never amounted to more than 5 per cent. The preliminary result is that each safety rod corresponds to a reactivity of 1.7 per cent and both together to 3.2 per cent. These values are also consistent with the measurements made by Jonsson.[5]

DETERMINATION OF THE MEAN LIFE OF THE THERMAL NEUTRONS

According to Equation 6 the mean life of the thermal neutrons in the reactor can be obtained from measurements of the decay time of the prompt neutrons. In order to examine this possibility a series of measurements were made with the neutron pulse-length $\frac{1}{10}$ of the repetition time, which was 0.25 or 0.5 sec. As the repetition time was not short compared to the shortest periods of the delayed neutrons, the neutron flux due to the delayed neutrons decreased appreciably during the off time of the pulse. In evaluating the results the decay curves therefore had to be fitted to a sum of two exponentials, one corresponding to the decay of the prompt and one to the delayed neutrons. The time constant of the former gives the mean life of the thermal neutrons, when the

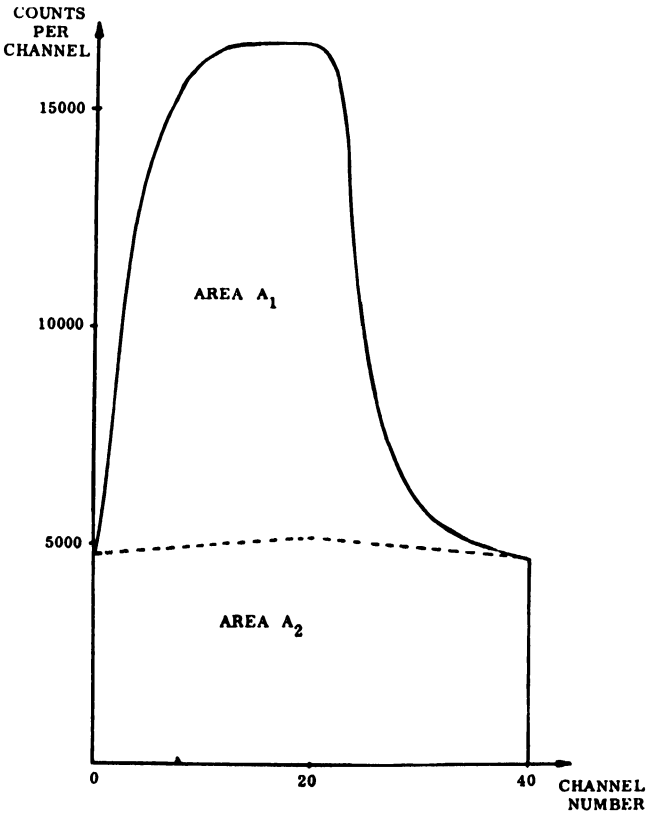

Figure 2. A curve obtained with the reactor subcritical by about one per cent. According to Eq. 5, $A_1/A_2 = \rho/\beta$

reactivity is known. A preliminary value of 0.7 msec has been obtained, in agreement with measurements by Hellstrand.[5]

INVESTIGATION OF THE INFLUENCE OF THE DETECTOR POSITION

The formulae used for getting the above results are all derived on the assumption that the higher harmonics in the neutron distribution can be neglected. In order to investigate the validity of this assumption, the time constant was measured with the detector in five different positions, from close to the centre of the reactor tank to the middle of the reflector. The five values agree within ± 4 per cent and no clear trend can be seen.

The reactivity equivalent of each safety rod was also measured with the detector in two different positions, but no effect from the higher harmonics could be found.

REFERENCES

1. Glasstone, S. and Edlund, M. C., *The Elements of Nuclear Reactor Theory*, D. Van Nostrand Co., Inc., New York, pp. 295ff (1952).
2. Blomsjö, E. and von Dardel, G., *A Versatile 150 kv Neutron Generator*, Appl. Sci. Res. B 4: 49–67 (1954).
3. Von Dardel, G., *A Multichannel Time-Analyzer for Precision Work*, Appl. Sci. Res. B 3: 209–229 (1953).
4. Johns, M. W. and Sargent, B. W., *Photoneutrons in a Heavy-Water Pile*, CRP-416 (1949).
5. Hellstrand, E. *et al.*, P/791 *Characteristics of the Swedish Heavy-Water Reactor*, Volume 5, Session 21A, these Proceedings.
6. Rumsey, V. H., *On the Analysis of Experiments Involving the Kinetics of Piles with Reflectors*, Can. J. Phys. *32*, 435–449 (1954).

Determination of Neutron Capture to Fission Ratio in Various Uranium Samples

By T. J. Barendregt and M. Bustraan,* The Netherlands

A great deal of attention has been paid to reactor designs in which the metallic-uranium fuel elements are replaced by solutions or suspensions. Such designs circumvent problems in the production of metallic uranium, which must withstand repeated thermal cycling and irradiation. Further, they make it possible to consider removing the fission products continuously. On the other hand neutron absorbing materials are often introduced into reactors and it will never be possible to reach the same density of fissile material without enriching the uranium in the fuel element. According to Wigner *et al.*,[1] the resonance absorption of lumps embedded in a moderator can be divided into two parts; the mass absorption and the surface absorption. The mass absorption, which is the main part of the total resonance absorption, is proportional to the total number of U^{238} atoms present in the lump. It also depends on the scattering cross section per U^{238} atom. It is obvious that one can expect a considerable difference in the neutron absorption of U^{238} between metallic uranium and uranium-oxide lumps. We have been interested in the magnitude of the neutron absorptions in various fuel element designs. Since little was given in the literature about the neutron absorption in uranium lumps when we started our investigations,[2,3,4] we decided to determine the distribution of the neutron absorption in 2.5 and 3-cm natural-uranium rods. The results have been compared with experiments carried out with U_3O_8 and UO_2 rods.

EXPERIMENTAL CONDITIONS

In natural uranium, neutrons can be captured in U^{238} according to the reaction:

$$U^{238} + n \rightarrow U^{239}$$

U^{239} is a beta-emitter and will decay as follows:

$$U^{239} \xrightarrow[23.5\ \text{min}]{\beta^-} Np^{239} \xrightarrow[2.33\ \text{d}]{\beta^-} Pu^{239}$$

Table I. U^{239} and Ba^{139} Activities as Determined in a U-Rod, Diameter 3.0 cm

Distance from rod centre	*U^{239} activity in c/min/gm U_3O_8*	*Ba^{139}-activity in c/min/gm U_3O_8*	*Neutrons absorbed/sec*	*Neutrons which caused fission/sec*
0.00 cm	388.400	39.990	5.89×10^6	7.21×10^6
0.35 cm	393.400	41.440	5.97	7.47
0.60 cm	403.500	42.550	6.12	7.67
0.94 cm	446.500	46.860	6.77	8.45
1.14 cm	497.900	49.790	7.55	8.98
1.26 cm	528.900	54.890	8.02	9.90
1.50 cm	843.400	60.580	12.79	10.92

Correction for fast fission (F_2): $0.052F_1$

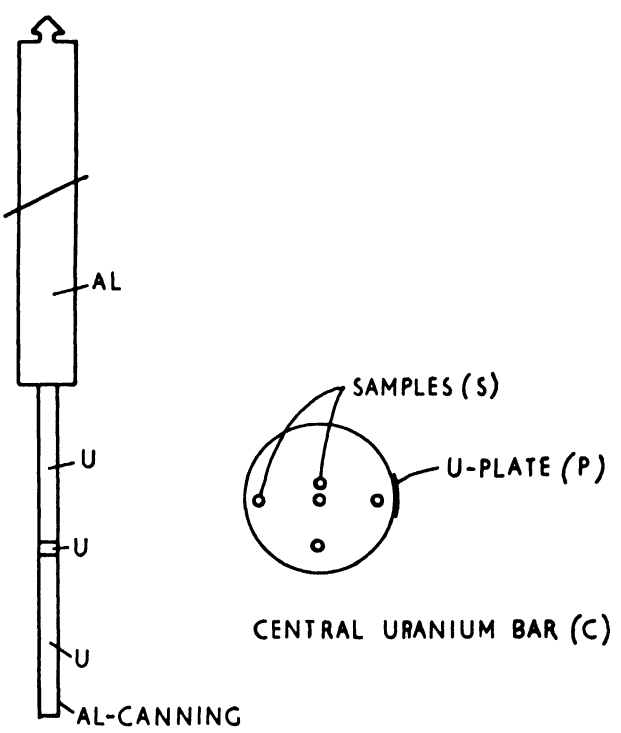

Figure 1. Fuel-element assembly; central uranium bar (C)

* Joint Establishment for Nuclear Energy Research, Kjeller, near Lillestrøm, Norway.

Table II. U^{239} and Ba^{139} Activities as Determined in a U-Rod, Diameter 2.5 cm

Distance from rod centre	*U^{239}-activity in c/min/gm U_3O_8*	*Ba^{139}-activity in c/min/gm U_3O_8*	*Neutrons absorbed, sec*	*Neutrons which caused fission/sec*
0.00 cm	454.100	46.090	6.88×10^6	8.31×10^6
0.43 cm	467.600	48.650	7.09	8.77
0.94 cm	556.300	57.560	8.46	10.38
1.07 cm	591.300	60.980	8.97	11.00
1.25 cm	906.600	71.950	13.75	12.97

Correction for fast fission (F_2): $0.047F_1$

For the determination of the neutron capture in U^{238}, the activity measurements of both U^{239} and Np^{239} have been suggested.[3,5] Since the isolation of neptunium from neutron-irradiated uranium is difficult without appreciable losses, we decided to measure the neutron capture in uranium by means of determination of the U^{239} activity. Loss of uranium during chemical treatment is of no importance as the yield of the separated uranium is indicated by its weight. Furthermore, the energy of the beta-rays of U^{239} is much higher than that of the beta-rays of Np^{239}, the corrections involved in the determination of the total activity are much smaller in the former case than in the latter.

It is possible to exclude all thermal absorption in U^{238} by embedding the uranium lumps in cadmium. We decided not to use this cadmium cut-off for two reasons. First, we were interested in the neutron capture-to-fission ratio in the chosen fuel elements and furthermore, the introduction of a large amount of material absorbing, thermal neutrons would prevent criticality of JEEP, the reactor in which the experiments have been carried out.

The fission in neutron-irradiated uranium can be determined by means of measurement of the activity of Ba^{139}. We have chosen this fission product since the known fission yield, is sufficiently accurate,[6] and owing to their half-lives, Ba^{139} and U^{239} will have comparable intensities.

Under the mentioned experimental conditions, it is obvious that the U^{239} activity will represent the total neutron absorption, but we can make a tentative calculation of the resonance absorption in the irradiated uranium in the following way:

Let C be the total capture per unit time and unit volume, then:

$$C = \frac{1}{\Delta v}\int_{\Delta v}\int_{0}^{E(\mathrm{Cd})} \Sigma_a^{238}(E)G(E,\vec{r})\,dE\,dv + \frac{1}{\Delta v}\int_{\Delta v}\int_{E(\mathrm{Cd})}^{E_0} \Sigma_a^{238}(E)G(E,\vec{r})\,dE\,dv + \frac{1}{\Delta v}\int_{\Delta v}\int_{0}^{E_0} \Sigma_a^{235}(E)G(E,\vec{r})\,dE\,dv \quad (1)$$

where $G(E,\vec{r})$ is the neutron spectrum inside the samples as function of energy and space, Δv the volume part under consideration, E_0 averaged energy of the fission neutrons, $E(\mathrm{Cd})$ the energy of the Cd-cut-off, and $\Sigma_a(E)$ macroscopic absorption cross section as function of energy. Under the same assumption one

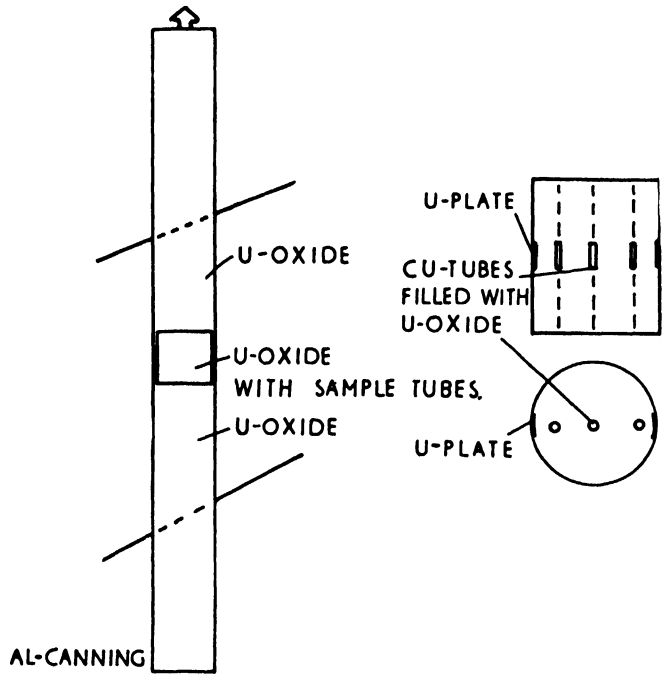

Figure 2. Fuel-element assembly

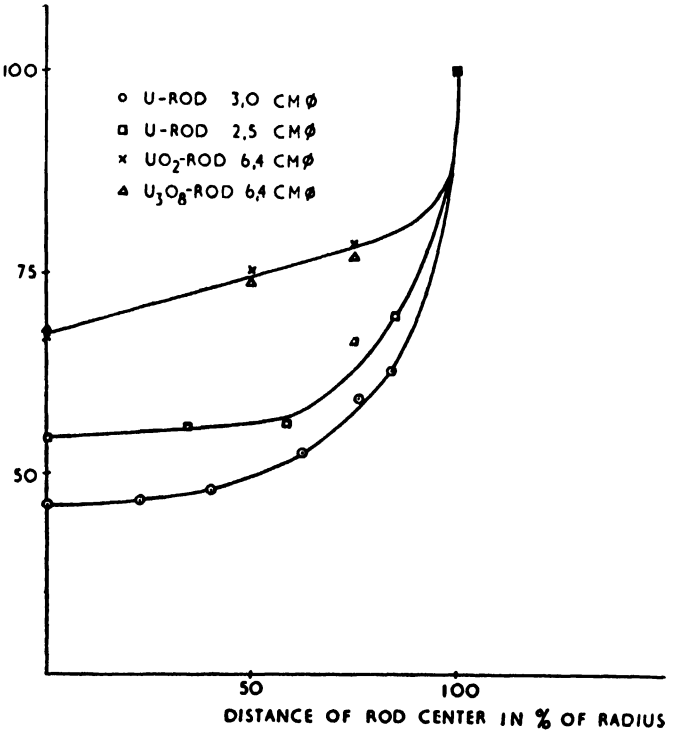

Figure 3. Neutron capture in different U samples

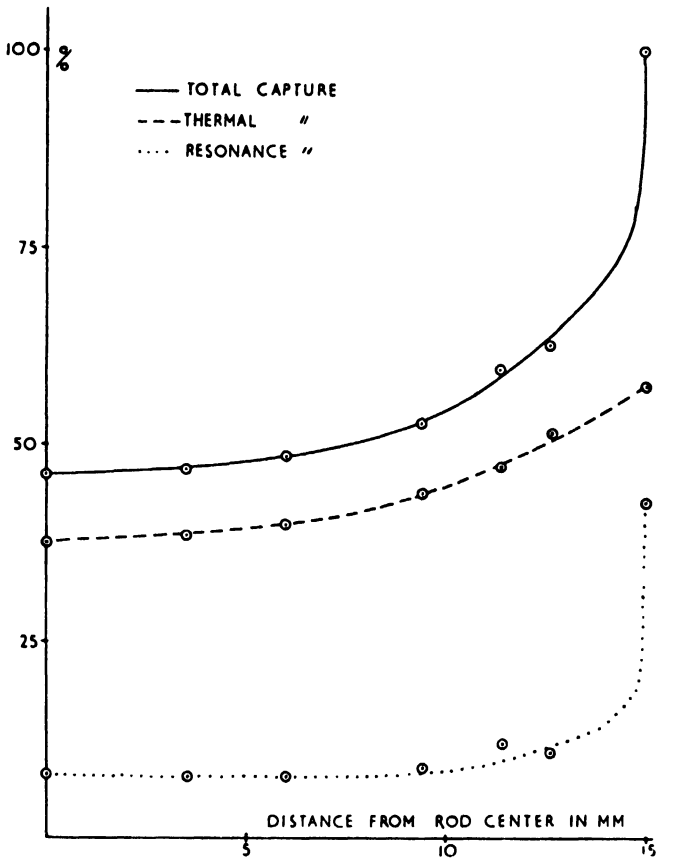

Figure 4. Contribution of thermal and resonance capture to the total neutron capture in a U rod, ϕ 3.0 cm

has for the total fission rate, or number of fission per unit time and unit volume:

$$F = \frac{1}{\Delta v}\int_{\Delta v}\int_{0}^{E(\mathrm{Cd})} \Sigma_f^{\mathrm{U}}(E)G(\vec{E,r})\,dE\,dv + \frac{1}{\Delta v}\int_{\Delta v}\int_{E(\mathrm{Cd})}^{E_0} \Sigma_f^{\mathrm{U}}(E)G(\vec{E,r})\,dE\,dv \quad (2)$$
$$= F_1 + F_2$$

where $\Sigma_f^{\mathrm{U}}(E)$ is the macroscopic fission cross section as function of energy. F_1 is the thermal fission contribution, F_2 the contribution by the fast fission. Assuming fission cross section and capture cross section of U in the thermal region to vary as $1/v$ one finds the thermal absorption in U^{238} to be equal to $0.668F_1$, since $\sigma_a = 2.8$ b and $\sigma_f = 4.18$ b.[7] Since the fast fission distribution is more nearly constant, we introduced one value for F_2 for each investigated case. We choose for the 3.0 cm rod $F_2 = 0.052\ F_1$, for the 2.5 cm rod $F_2 = 0.047\ F_1$ and for the oxide rods $F_2 = 0.015\ F_1$. The resonance absorption is then found from $C - 0.668(F_1 - F_2)$, since the correction for the last term due to the U^{236} activity can be neglected.

PROCEDURE

Experiments with the 2.5 and 3.0 cm Diameter Natural Uranium Rods

Two uranium bars, each 140 mm long with a third bar 10 mm long in between them, were pressed into an aluminium tube with a wall thickness of 2 mm. Holes were drilled in the middle of the small centre bar and at different distances from the centre. The holes were filled with small uranium bars (2 mm diameter) and a uranium plate (thickness 0.1 mm) was mounted on the surface of the entire centre bar (Fig. 1). The filled aluminium tube was then irradiated in JEEP for three minutes. Care has been taken that the irradiation was carried out with the reactor critical without any control plates in, to avoid distortions in the flux distribution near the sample due to these control plates. Since a low-power level (100 w) was required, the D_2O level had to be dropped. The samples were irradiated in a fuel rod position (38 cm from the axis of the reactor) and by means of the rod construction shown in Fig. 1, we were able to have the samples at the place where the vertical flux gradient is zero and so we had an almost flat flux distribution at the place of the sample.

Immediately after irradiation, the aluminium tube was taken out of the reactor tank, the samples (*s*) were taken from the centre uranium bar (*c*) and dissolved in concentrated nitric acid. Furthermore, one or more samples were taken from the uranium plate (*p*). All samples had been weighed before the irradiation was carried out.

Both Ba^{++} and Cs^{+} ions were added as carriers to the nitric acid, and at the end of the dissolving procedure, bromine was added to ensure that all the uranium would be present in the (VI) state. After cooling, the solution obtained was divided into two parts for uranium and barium determinations.

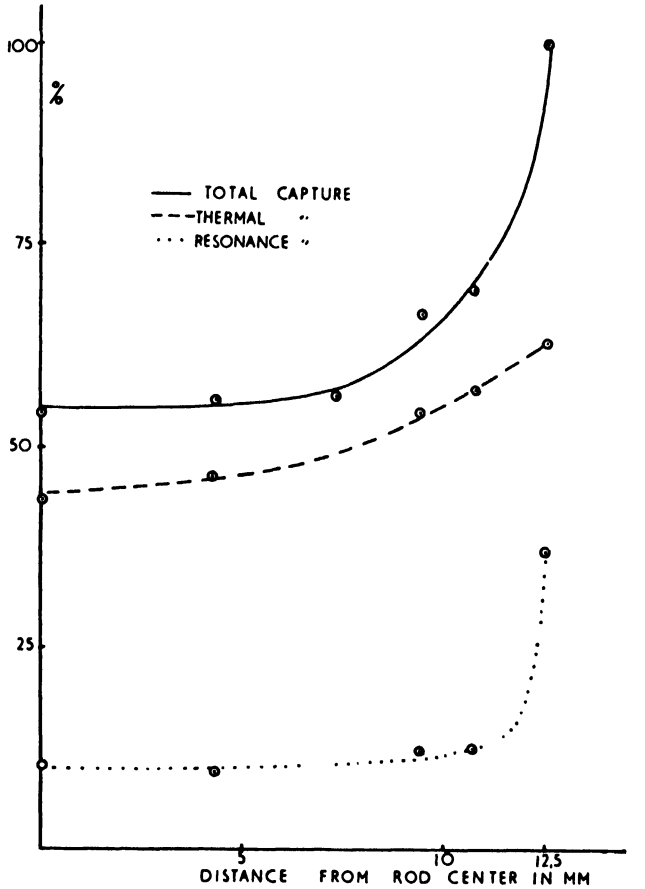

Figure 5. Contribution of thermal and resonance capture to the total neutron capture in a U rod, ϕ 2.5 cm

Determination of U^{239}

The solution was mixed with a few mg Ba^{++} and La^{+++} ions, and poured into a hot solution of sodium acetate, which was saturated at room temperature. The precipitate of sodium uranyl acetate was filtered off and washed with saturated sodium-acetate solution. The precipitate was dissolved in concentrated nitric acid, saturated calcium nitrate solution added, and the solution extracted two times with diethyl-ether, and afterwards re-extracted with water. The final water fraction containing the purified uranyl nitrate was made strongly ammoniacal, the precipitated UO_4 filtered off, washed and ignited at 850°C. The U_3O_8 obtained was ground to a fine powder and the activity counted with a G-M end-window counter (Philips 4100-11). After correction for the growth of UX_2 and Np, the samples showed a reproducible decay with a half-life of 23.5 minutes.

The determination of the geometrical factor has been performed by means of activity measurements on thin layers of uranium oxide[8] and the absorption factor for U^{239} is calculated on the assumption that the sample of uranium oxide is infinitely thick for the beta-rays of U^{239}. If the uranium layer was not sufficiently thick, an additional "individual factor" has been introduced.

The measurements were carried out on Al dishes, diameter 1 cm. Auxiliary experiments indicated that the thick layer of uranium oxide used emits a quantity of beta-radiation of U^{239} equal to that which the radiation would be in the absence of self-absorption from 75 mg/cm^2. Due to our counter arrangement and because we shall be interested in the activity of the U^{239} in 1 gram of U_3O_8, which would equal 318 mg/cm^2 in our dishes, the total activity of the U^{239} samples will be the "measured" activity multiplied by 0.771×10^2. (Efficiency of the counter 5.498%.)

Determination of Ba^{139}

An aliquot of the uranyl nitrate solution was mixed with 38 mg barium nitrate, dissolved in 2 ml water. The barium chloride was separated according to the method worked out by Glendenin.[9] The correction factors introduced have been described elsewhere,[10] the total correction factor to convert the measured activity in the total activity (which means the total number of decaying nuclei per unit time) being calculated as 15.98.

Experiments with UO_2 and U_3O_8 Rods, Diameter 6.4 Cm

To be able to take samples at various distances from the rod centre, we made an arrangement which is shown in Fig. 2. In a 10-cm long aluminium tube, boxes made of thin copper foil filled with the uranium oxide were mounted in the centre of the tube and at arbitrarily chosen distances from the centre. Small uranium plates (thickness 0.1 mm) were mounted on the inside of the aluminium tube to measure the neutron absorption on the surface. The entire tube was filled afterwards with UO_2 or U_3O_8, of densities 3.5 and 2.5 respectively, taking into account the filling factor. The aluminium tube was closed on both sides with thin aluminium foil and placed in the centre of a large

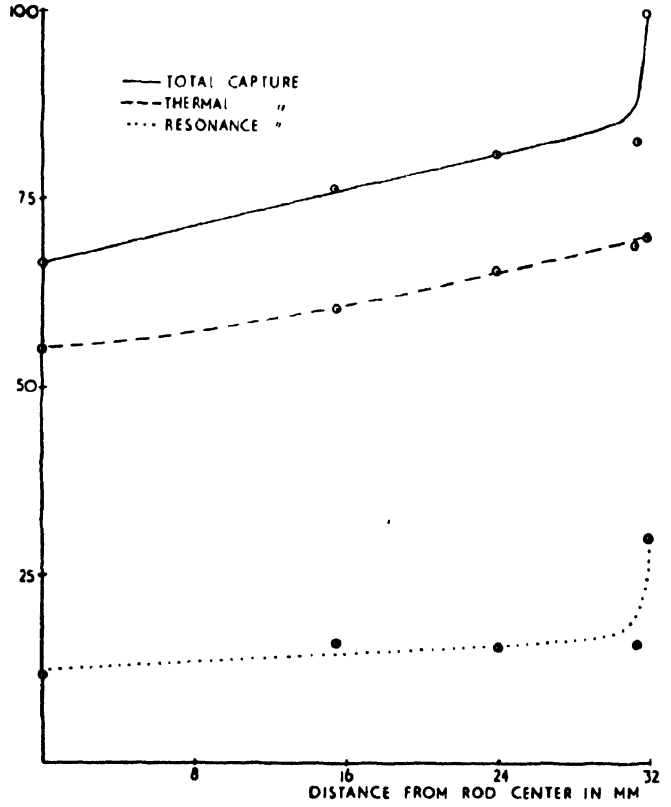

Figure 6. Contribution of thermal and resonance capture to the total neutron capture in a UO_2 rod, ϕ 6.4 cm

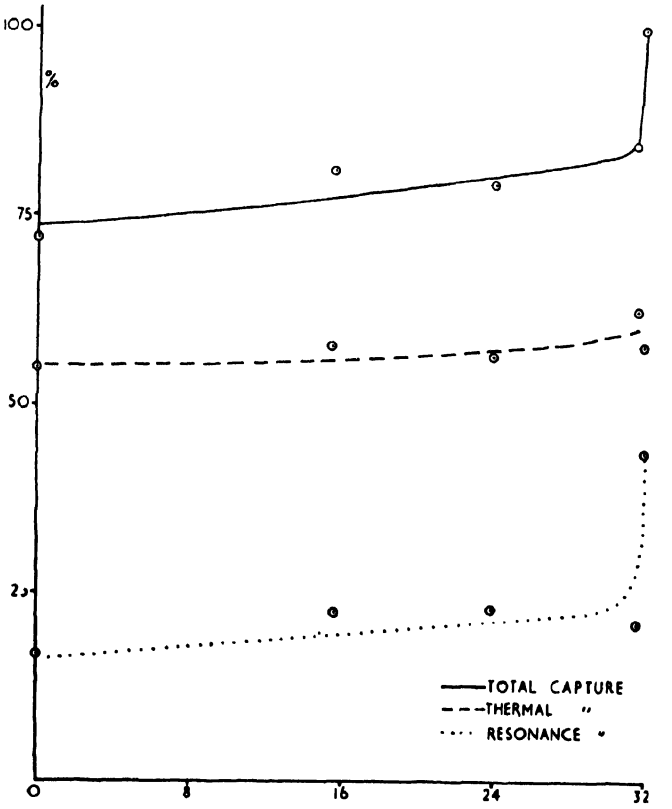

Figure 7. Contribution of thermal and resonance capture to the total neutron capture in a U_3O_8 rod, ϕ 6.4 cm

Table III. U^{239} and Ba^{139} Activities as Determined in a UO_2-Rod, Diameter 6.4 cm

Distance from rod centre	*U^{239}-activity in c/min/gm U_3O_8*	*Ba^{139}-activity in c/min/gm U_3O_8*	*Neutrons absorbed/sec*	*Neutrons which caused fission/sec*
0.00 cm	306.500	31.000	4.65×10^6	5.59×10^6
1.50 cm	343.600	34.200	5.21	6.17
2.40 cm	362.500	37.200	5.50	6.71
3.15 cm	374.300	37.500	5.68	6.76
3.20 cm	437.600	39.200	6.63	7.07

Correction for fast fission (F_2): $0.015F_1$

aluminium tube in such a way that the inner tube was covered by a UO_2, or U_3O_8 layer on both sides (Fig. 2).

The irradiation, the separation and determination of the activities of U^{239} and Ba^{139} have been carried out in an identical way as in the experiment with the metallic U-rods.

RESULTS

All irradiations have been carried out for a period of three minutes. To calculate the activity after an infinitely long time of irradiation (A_∞ the "saturation activity"), when the number of decaying atoms equals the amount formed by absorption or fission, we used the formula:

$$A_t = A_\infty(1 - e^{-\lambda t})$$

in which the activity (A_t) of a radioactive species with a decay constant λ, after an irradiation time t is given.

For U^{239}, the total activity has to be multiplied by 0.118×10^2 in order to obtain the amount formed per unit time, which is equal to the amount of neutrons absorbed.

As Ba^{139} is formed in 6.1% of all fission reactions,[11] the total activity of Ba^{139} has to be multiplied by 6.77×10^2 for total fission,[10] which is equal to the number of neutrons which caused fission.

All experiments were repeated several times under the same conditions. Due to statistical errors in the counting technique, the quality of the prepared samples and the uncertainty of several correction factors, the final data for the total number of decaying nuclei per unit time deviated.

Tables I–IV show the average values of the U^{239} and Ba^{139} activities measured and the conversion of the results into the amounts of neutrons absorbed and the amounts of neutrons which caused fission, all per unit time and per gram of U_3O_8.

In Fig. 3, the neutron capture on the rod surface in the different cases is normalized to unity and the graphs show the total capture (C) as a function of the rod radius.

In Figs. 4, 5, 6 and 7 the contributions of thermal absorption ($0.668\ F_1$) and resonance absorption ($C - 0.668\ F_1$) to the total neutron absorption (C) have been shown, the total absorption on the surface being normalized to 100%, using Equations 1 and 2.

In Figs. 8, 9, 10 and 11 the distribution of the neutron absorption as a function of the distance from the

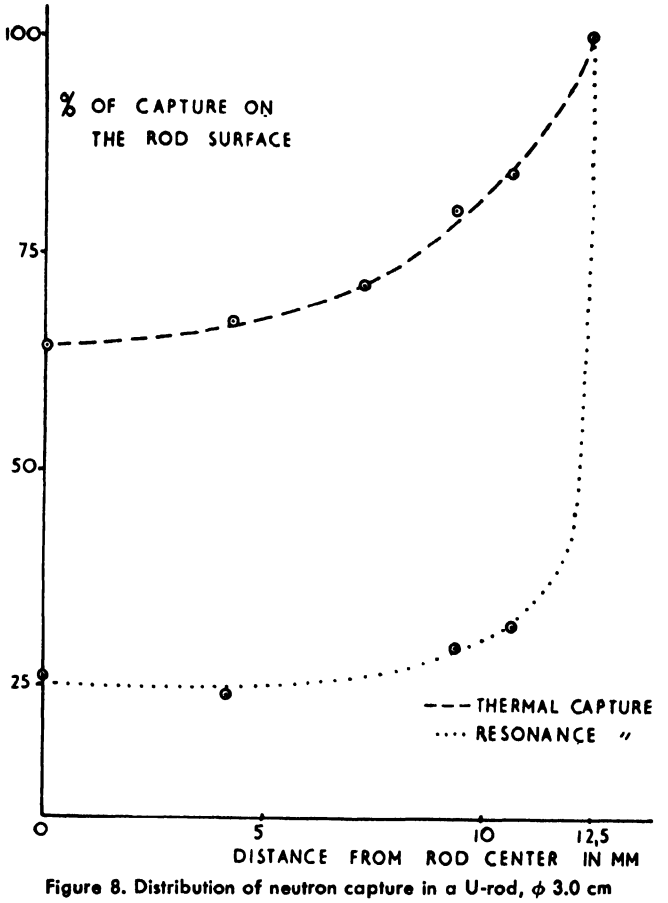

Figure 8. Distribution of neutron capture in a U-rod, ϕ 3.0 cm

Table IV. U^{239} and Ba^{139} Activities as Determined in a U_3O_8-Rod, Diameter 6.4 cm

Distance from rod centre	*U^{239}-activity in c/min/gm U_3O_8*	*Ba^{139}-activity in c/min/gm U_3O_8*	*Neutrons absorbed/sec*	*Neutrons which caused fission/sec*
0.00 cm	274.300	27.100	4.16×10^6	4.89×10^6
1.50 cm	285.600	25.800	4.33	4.65
2.40 cm	301.100	27.000	4.57	4 87
3.15 cm	325.300	28.100	4.93	5.07
3.20 cm	398.000	30.800	6.03	5.55

Correction for fast fission (F_2): $0.015F_1$

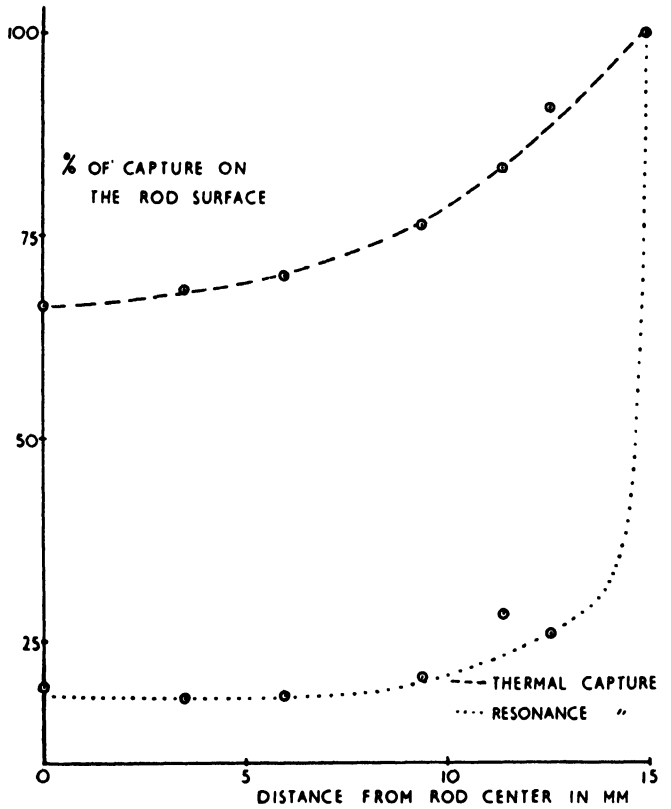

Figure 9. Distribution of neutron capture in a U-rod, ϕ 2.5 cm

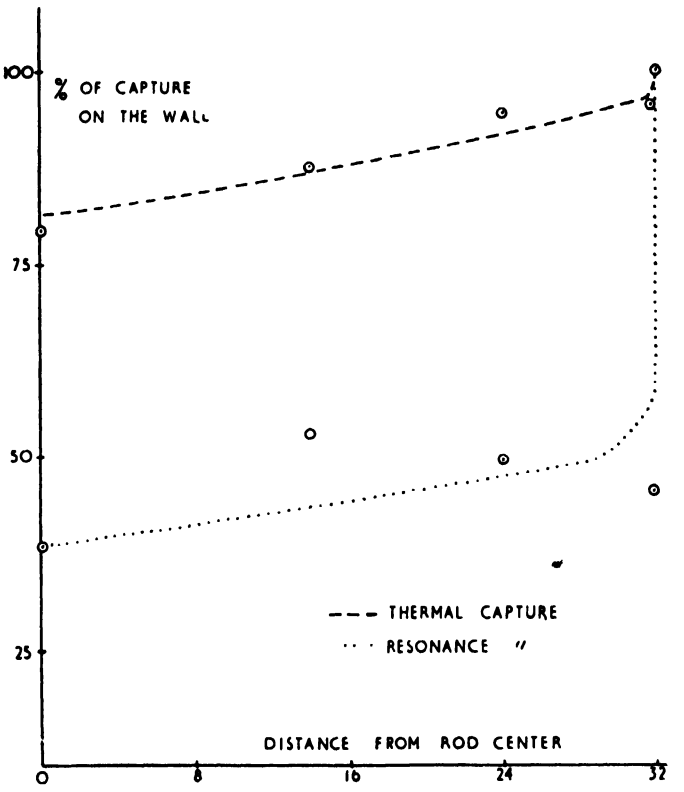

Figure 10. Distribution of neutron capture in a UO_2 rod, ϕ 6.4 cm
$D_{UO_2} = 3.5$

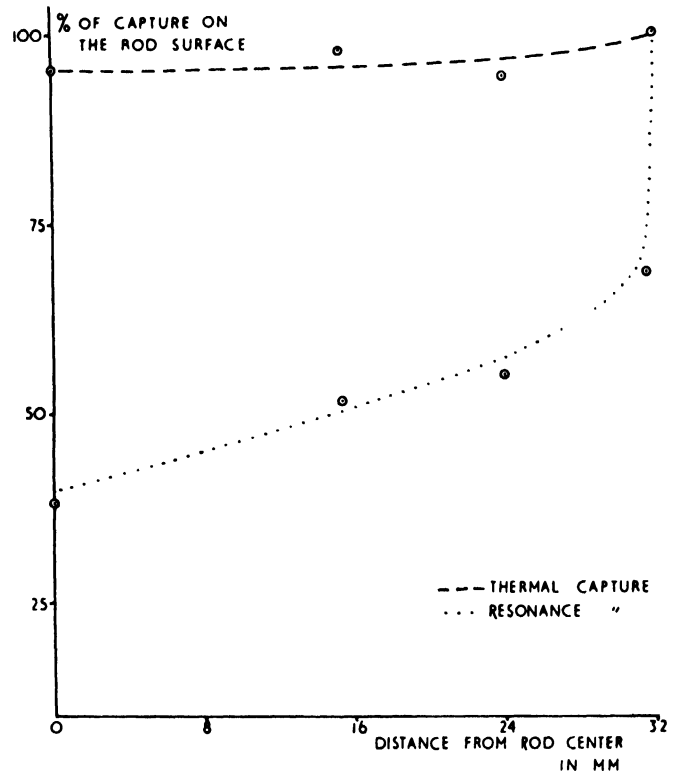

Figure 11. Distribution of neutron capture in a U_3O_8 rod, ϕ 6.4 cm
$D_{U_3O_8} = 2.5$

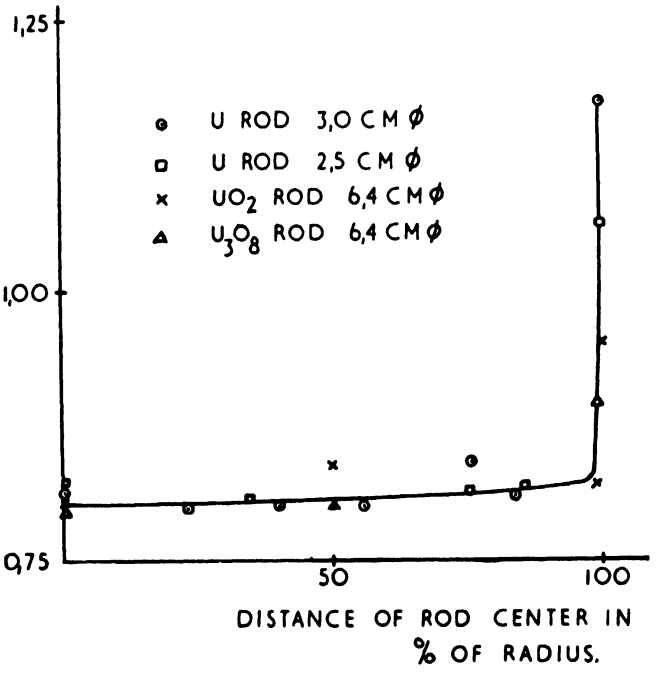

Figure 12. Neutron capture to fission ratio in different uranium samples

rod centre is shown, both thermal and resonance absorption on the rod surface being normalized to unity.

Finally, Fig. 12 gives the neutron capture to fission ratio in the various uranium samples.

CONCLUSIONS

Although the accuracy of the method is not very high (standard deviation of the data in the second and third rows in the tables is 5%), and the division into thermal and resonance absorption is arbitrary, the results still present a fairly good picture of the difference between metallic uranium and uranium oxide rods.

The radial distribution of the thermal absorption can be described by the function $I_0(0.95r)$, for the metallic rods and for the oxide cases by $I_0(0.2r)$, $I_0(x)$ being the zero order Bessel function of the first kind of imaginary argument, r being the distance to the rod centre.

Apart from the surface, little difference in the neutron capture to fission ratio could be detected in the rods investigated.

The ratio of the resonance absorption between centre and surface may be too low, due to the fact that plates of 0.1 mm thickness have been used for the determination of the surface conditions. As can be seen from the graphs, a considerable decrease in the resonance absorption already occurs within the 0.1 mm mentioned.

ACKNOWLEDGEMENTS

The authors would like to express their appreciation to Professor Dr. A. H. W. Aten, Jr., for his helpful advice and discussions, and to Dr. J. J. Went for suggesting the investigation. Also we thank Dr. K. van Duuren for his co-operation in the earlier part of this investigation. The authors are grateful to Miss M. Fürst for her assistance in the experiments.

REFERENCES

1. Wigner, E. P., Creutz, E., Jupnik, H. and Snyder, T., J. Appl. Phys. *26:* 260 (1955).
2. Creutz, E., Jupnik, H., Snyder, T. and Wigner, E. T., J. Appl. Phys. *26:* 257 (1955).
3. Creutz, E., Jupnik, H., Snyder, T. and Wigner, E. T., J. Appl. Phys. *26:* 271 (1955).
4. Creutz, E., Jupnik, H. and Wigner, E. T., J. Appl. Phys. *26:* 276 (1955).
5. A. B. Atomenergi, Stockholm (unpublished).
6. Grummit, W. E., Gueron, J., Wilkinson, G. and Yaffe, L., Can. J. Research, *258:* 364 (1947).
7. AECU-2040, Suppl. 3.
8. Kamen, M., Radioactive tracers in biology, 2nd edition, appendix.
9. Glendenin, L. E., N. N. E. S. IV: 9, Parts VI–VIII, 1657 (1951).
10. Barendregt, T. J., Rec. des Travaux chemie Pays-Bas, in the press.
11. Pappas, A. C., Technical Report No. 63: M.I.T., Cambridge (1953).

Status of Experimental and Theoretical Information on Neutron Slowing-Down Distributions in Hydrogenous Media

By J. Ernest Wilkins, Jr.,* Robert L. Hellens,† and Paul E. Zweifel,‡ USA

I. INTRODUCTION

The theoretical treatment of the neutron slowing-down problem in hydrogenous media is unique in two respects. The first is that in the simplest case of moderation by a single element in an infinite medium, an exact solution to the problem is available only if that element is hydrogen.[1] (An exact solution is also obtainable if the hydrogen is mixed with another, infinitely heavy element, in which case only the hydrogen is a "moderator.") The second unique feature of the hydrogen problem is, paradoxically, that for a practical case in which a mixture of moderators is present in a medium of finite extent, the presence of hydrogen in that mixture increases the difficulty of the calculation considerably. This is because the usual approximate methods of treating this problem based on a continuous slowing-down model[1,2] are not valid for the case of hydrogen moderation, since a neutron may lose an appreciable fraction of its energy in a collision with a hydrogen nucleus.

There are also some experimental difficulties encountered in measuring slowing down distributions which become particularly pronounced in hydrogenous media. These arise primarily from the rapid attenuation of both fast and slow neutrons in water. The large energy loss per n-p collision leads to a rather short slowing-down length, which in turn tends to accentuate the importance of the flux distribution in the neighborhood of the neutron source. In most slowing-down measurements the displacement of small volumes of the medium by both the neutron source and detectors is unavoidable. Since the scale of the experiment is proportional to the slowing-down length, measurements in water require much smaller neutron sources and detecting instruments than are customarily employed in nonhydrogenous mixtures. However, the same total neutron yield from the source is required in any case to attain comparable statistical uncertainties.

A second difficulty of some consequence, which is more or less unique to hydrogenous media, is encountered in using a fission plate and thermal column as a source of fission neutrons. The strong attenuation of the slow neutrons in water necessitates placing the fission plate close to the source of thermal neutrons, thereby distorting the slowing-down distribution in the important region close to the source plate. A third difficulty which is met in the interpretation of any slowing-down measurement is engendered by uncertainties in the energy distribution of the source neutrons. Here again, such uncertainties are particularly significant in hydrogenous media since the hydrogen cross section drops by a factor of four in the range 1–10 Mev and the resulting neutron slowing-down distribution spreads very rapidly with increasing source neutron energy. One helpful feature is the fact that the large energy loss per n-p collision allows one to ignore "flux depression corrections"[3] in measuring neutron distributions in hydrogen by the activation of resonance absorbers.

These points are discussed in some detail in Section IV, in connection with a review of the experimental evidence presently available. Some recent experiments are also described there which attempt, in their design, to avoid one or another of the difficulties mentioned.

Some of the very features which make the theoretical and experimental treatment of the hydrogen slowing-down problem unique also make hydrogen a desirable material to use in reactors. The rapid thermalization brings neutrons into the region of high fission cross section before too many have had a chance to escape. The fast neutron attenuation makes hydrogen a useful component in the construction of biological shields. The fact that hydrogen is readily available in the form of a liquid compound allows moderator and heat transfer agents to be the same. As a matter of fact, even if the reactor is not moderated by hydrogen, water is frequently present as a coolant, so that detailed reactor calculations must take the hydrogen into account.

The quantities whose calculation and measurement are discussed in this paper are the neutron flux distributions, the neutron slowing-down density, and the "moments" of the neutron flux from a point or plane source of neutrons. (The second moment, or the neutron mean-square slowing-down length is six times the neutron "age," τ, which is an important quantity for reactor calculations. Age calculations are discussed in detail in Section III.) Such quantities are often immediately applicable to shielding problems because of the nature of the information desired. For reactor ap-

* Nuclear Development Associates, Inc.
† Westinghouse Atomic Power Division.
‡ Knolls Atomic Power Laboratory, General Electric Company.

plications, however, in which one is interested in critical masses and dimensions, and flux distribution from a neutron source distributed throughout the reactor core, it is then necessary to use these quantities in further calculations. These are discussed in Sections III and IV, in which it is shown how the Fourier transform of the neutron slowing-down density may be applied to a criticality calculation by a modification of a variational principle originally derived by Greuling,[4] how it may be applied to multigroup analysis of hydrogen-moderated reactors by being used to obtain group averages of cross sections; and finally, it is seen how the neutron distribution from an arbitrary source may be constructed from a Fourier analysis of the source.

The moments calculations, which are particularly applicable to shielding problems, are discussed in Section II. In Section III, the theory of the calculation of the Fourier transform of the neutron flux and slowing down density is discussed, while in Section IV, a discussion of experiments and reactor calculations is given. In Section V, the various theoretical calculations and experimental results are compared, and the discrepancies present and the possible sources of these discrepancies are investigated in some detail.

II. MOMENTS METHOD

(a) General Explanation of Moments Method

A detailed picture of the penetration of neutrons in a slowing-down medium requires a knowledge of the distribution of the neutrons as a function of position $\bar{r}$, energy E and direction $\bar{\Omega}$. It is convenient here to choose as the fundamental function the angular number flux of neutrons,§ i.e., a function $F(\bar{r},E,\bar{\Omega})$ such that $F(\bar{r},E,\bar{\Omega})dEd\Omega$ is the number of neutrons which cross in unit time a unit area located at $\bar{r}$ whose normal is $\bar{\Omega}$, which have energies between E and $E + dE$ and directions in the solid angle $d\Omega$ about $\bar{\Omega}$. The corresponding lethargy dependent flux $N(\bar{r},u,\bar{\Omega})$ is simply EF.

If the source of neutrons is uniformly distributed over a plane ($x = 0$), the angular number flux will depend only on the distance x from the source plane, the energy, and the angle $\cos^{-1}\omega$ between the normal to the source plane and the direction of motion of the neutron, and so will be denoted as $F(x,E,\omega)$. The theoretical treatment will be confined to such plane sources, and even more particularly will generally be applied only to plane isotropic sources. A simple transformation[2] enables one to secure numerical results for point isotropic sources from those for plane isotropic sources.

The moments method[5] begins with a spherical harmonics expansion of the angular number flux

$$F(x,E,\omega) = \sum_{l=0}^{\infty} \frac{2l+1}{4\pi} F_l(x,E)P_l(\omega) \qquad (1)$$

The coefficients $F_l(x,E)$ in this expansion are of physical significance in their own right. Greatest interest attaches to F_0, which is called the number flux, and F_1, which is called the number current. In the moments method, the coefficients F_l are not determined directly. Instead, their spatial "moments"

$$F_{nl}(E) = \frac{1}{n!}\int_{-\infty}^{\infty} x^n F_l(x,E)\,dx = \frac{2\pi}{n!}\int_{-\infty}^{\infty}\int_{-1}^{1} x^n P_l(\omega)F(x,E,\omega)\,d\omega\,dx \qquad (2)$$

are calculated. Various techniques[6] may then be employed to determine the coefficients F_l. Almost all applications have been confined to the case when $l = 0$, but some work has been done[7] at NDA when $l = 1$.

One of the principle virtues of the moments method is that it is possible to determine a finite number of the moments F_{nl} exactly without making any assumptions as to the behavior of the neglected moments. This is in sharp contrast to the usual spherical harmonics approach for finding the coefficients F_l as a function of position in which it is necessary to make a specific assumption concerning the first neglected coefficient in order to determine a finite number of coefficients. (cf. Section III below.)

The moments themselves are occasionally of interest. For example, the age τ at energy E can be expressed as $\tau(E) = F_{20}/F_{00}$. The moment F_{00} calculated for a plane isotropic source can also be regarded as the number flux which would be generated by a uniform distribution of point isotropic sources throughout space.

(b) Results

Calculations of the moments for a plane isotropic source have been carried out using the National Bureau of Standards high-speed electronic computer (SEAC) for a number of interesting cases. From these moments the number flux $F_0(r,E)$ for a *point* isotropic source was determined making use of the relationship between plane and point isotropic sources already referred to. Results[8,9] for some typical situations are presented in graphical form in Figs. 1 and 2.

Most of the numerical calculations performed with the moments method lead to results describing the behavior of the high energy fluxes only. These furnish the relevant data for studying the effectiveness of biological shields since low-energy neutrons are more easily captured and are also less damaging to tissue. The moments method, however need not be restricted to high energies and the graph of Fig. 7 below illustrates a specific case in which calculations were carried down to the epithermal region. Other such calculations are in process.

A specific comparison of some of the results with experimental curves will be referred to Section V. In making such comparisons it is, of course, necessary to take account of the characteristics of the measuring instruments. One instrument frequently used for meas-

§ Other choices can be made of course. In particular the collision density has frequently been employed in the literature.

uring fast neutrons is the dosimeter. The dosimeter gives a reading (denoted as "dose") of

$$D(r) = \int F_0(r,E) f(E)\, dE$$

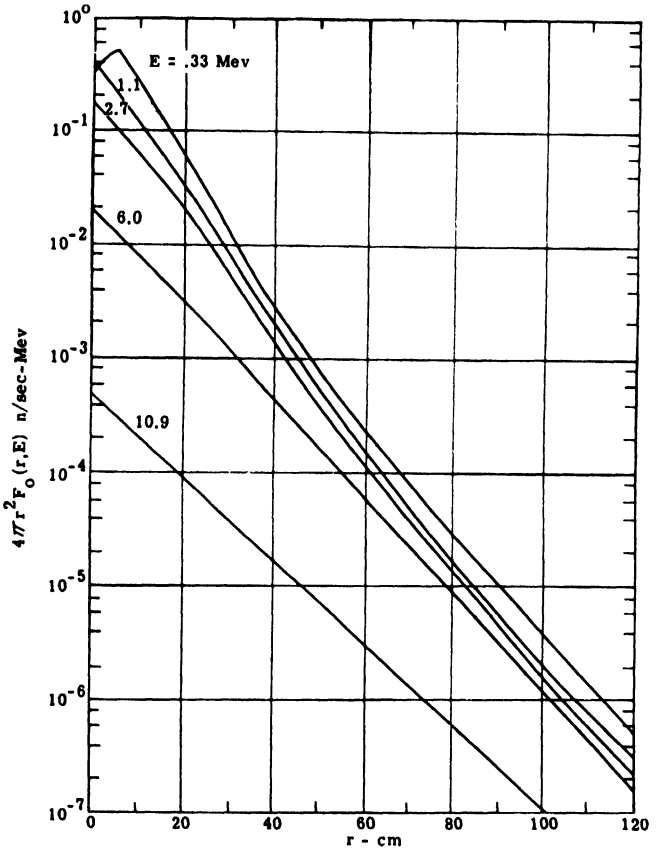

Figure 1. Flux distribution for fission sources in water

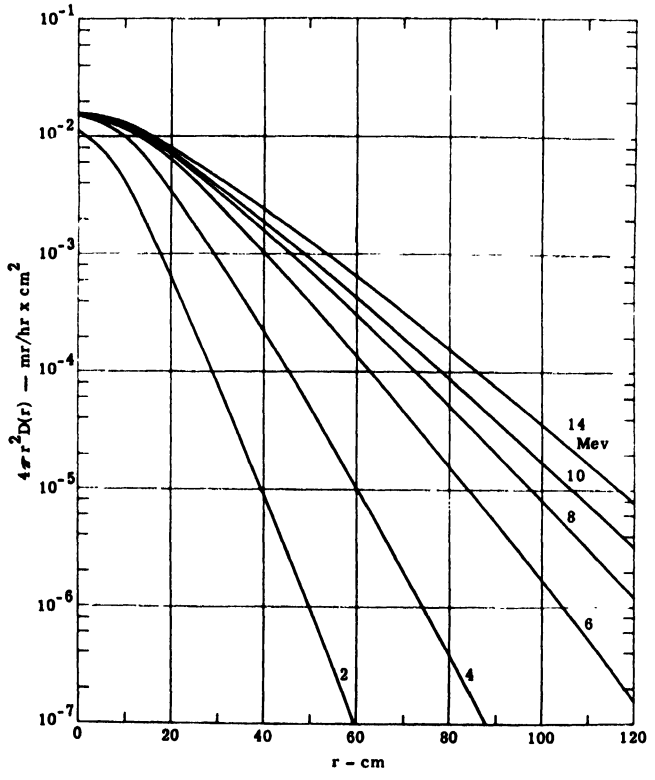

Figure 2. Fast neutron doses for various monoenergetic sources in water

provided the response function $f(E)$ is properly defined.[10] A table of values of the dose is presented in Table I, column C for fission neutrons in water and in Fig. 3 for various monoenergetic sources of neutrons in water.

The source strength in all the problems described in the graphs is one neutron per second. The penetration r is in centimeters and the energy E is in Mev. The number flux F_0 is in neutrons/cm^2-sec-Mev, and the dose $D(r)$ is in mrep/hr. It should be noted that the fluxes and doses are not shown directly, but rather as $4\pi r^2 F_0$ and $4\pi r^2 D$.

An important conclusion that has been drawn from a study of the numerical results is that the number flux in the intermediate energy range (2 ev–300 kev) for a hydrogenous moderator may be approximated rather closely in terms of the fast neutron dose $D(r)$ and the total hydrogen cross section $\Sigma_H(E)$ as

$$F_0(r,E) \propto \frac{D(r)}{E\Sigma_H(E)}$$

This approximation is valid to a few per cent for distances from the source greater than about 20 cm of water. For monoenergetic sources of neutrons with energy E_0 in water, the constant of proportionality may be roughly expressed as $30/E_0$.

(c) Calculation of the Moments

The moments $F_{nl}(E)$ satisfy an infinite sequence of integral equations which may be derived from

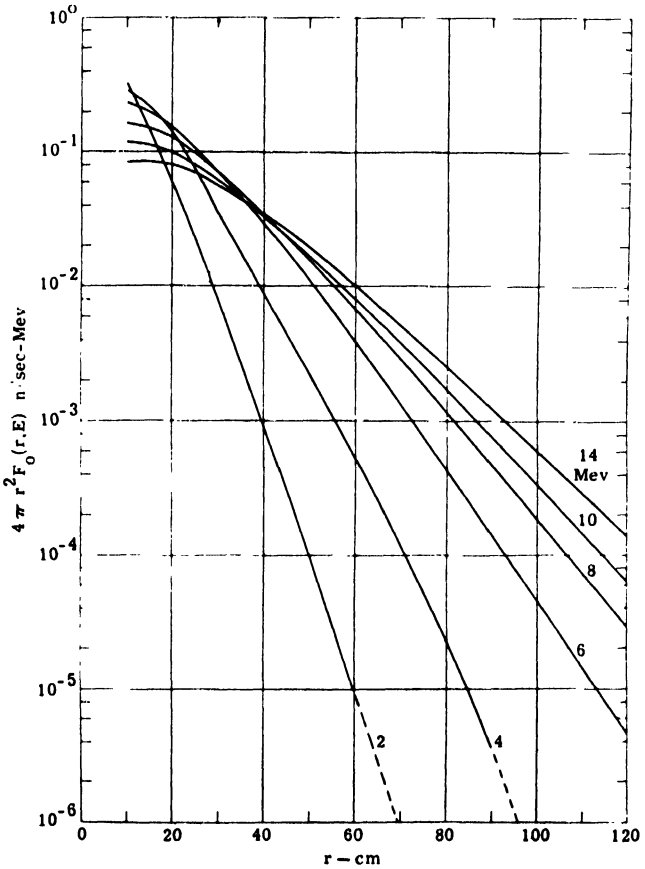

Figure 3. Flux distribution at 330 kev for various monoenergetic sources in water

the basic Boltzmann equation by multiplying by $x^n P_l(\omega)/n!$ and integrating over solid angle and x. The result[11] is that for a plane isotropic source

$$\sigma_T(E)F_{nl}(E) = \frac{(l+1)F_{n-1,l+1}(E) + lF_{n-1,l+1}(E)}{2l+1} \quad (3)$$

$$+ 2\pi \sum \left[CA \int_E^{E/\beta} \sigma_s(E')f(E',\mu)P_l(\alpha)F_{nl}(E') \times dE'/E' + S(E)\delta_{n0}\delta_{l0} \right]$$

In this equation σ_T is the total macroscopic cross section of the compound, C and σ_s are respectively the concentration and microscopic scattering cross sections of an individual scattering element, $f(E',\mu)$ is the probability per unit solid angle in the center of mass system that upon collision with a scatterer the neutron at energy E' undergoes an angular deflection of $\cos^{-1}\mu$, $\cos^{-1}\alpha$ is the corresponding angular deflection in the laboratory system, and $S(E)\,dE$ is the number of source neutrons created per second in the energy range from E to $E + dE$. If m is the atomic mass of a scatterer, then $A = (1+m)^2/2m$, $\beta = (m-1)^2/(m+1)^2$. The summation is extended over all scattering elements present.

The major problem is to find some way to express the scattering integral in Equation 3 in order to facilitate machine computation. Since scattering by hydrogen is isotropic in the center of mass system and since $\beta = 0$, the hydrogen integral is very much simpler than the others and no necessity for special treatment arises. The oxygen scattering integral has been handled in the following three different manners.

A. Assume that no energy loss occurs upon a collision with an oxygen nucleus. In this case the integral describing the oxygen collisions reduces to a single term and the equations assume the same appearance as (3) except that σ_T is replaced by a modified cross section and the sum of scattering integrals contains only the integral for hydrogen.

B. The oxygen scattering integral is expanded as a linear function of m^{-1}. A partial or approximate treatment of the slowing down by oxygen is thus obtained.

C. No physical assumptions are made and the integral is evaluated using a quadrature formula[12] which takes into account the oscillation of the factor $P_l(\alpha)$ in the integrand.

Table I. Fast Neutron Doses from a Point Isotropic Fission Source in Water ($4\pi r^2 D(r)$ mrep-cm²/hr)

	Method		
	A	B	C
r (cm)			
0	1.02×10^{-2}	1.02×10^{-2}	1.02×10^{-2}
10	3.88×10^{-3}	3.57×10^{-3}	4.06×10^{-3}
20	1.13×10^{-3}	9.97×10^{-4}	8.89×10^{-4}
30	3.31×10^{-4}	2.79×10^{-4}	2.74×10^{-4}
60	1.06×10^{-5}	8.44×10^{-6}	9.39×10^{-6}
90	5.20×10^{-7}	4.01×10^{-7}	3.83×10^{-7}
120	2.78×10^{-8}	2.13×10^{-8}	2.14×10^{-8}
$\bar{r^2}/6$ (cm²) at 330 kev	19.33	18.03	18.16

Procedures A, B and C are intended to be successively more accurate methods of handling scattering by oxygen. A comparison of the results using the three different procedures is made for the dose in Table I. For rough estimates it appears safe to neglect slowing down by oxygen, but even for careful work the differences between methods B and C are probably unimportant in view of uncertainties in the cross-section data.[13] The same conclusion can be drawn from a comparison of the ages $\bar{r^2}/6$ at 330 kev.

III. SOLUTION OF THE FOURIER—TRANSFORMED BOLTZMANN EQUATION

(a) General Description of Theory

As is pointed out in Section I of this paper, the solution of the Fourier transform of the Boltzmann equation is pertinent for several reasons. First, a source of arbitrary spatial distribution may be analyzed into its Fourier components, and the Boltzmann equation solved for each Fourier component; the transform may then be inverted to yield the flux distribution from the arbitrary source. Second, in many reactor applications the thermal flux is of the form $\cos Bx$, so that the source contains only a single Fourier component whose wave number, k, is equal to B (the "buckling" of the reactor is B^2).[1] Third, for a reflected reactor, critical masses and volumes may be found from a variational principle expressed directly in terms of the Fourier transform of the slowing-down density. Finally, the spatial moments of the flux distribution from a point source may be found by expanding the transform of the flux in a power series with respect to k, the $2n^{\text{th}}$ spatial moment being $(-1)^n(2n+1)!$ times the coefficient of k^{2n} in the expansion.

The details of the calculations are discussed elsewhere.[14] Essentially, the procedure is to expand the transforms $N(k,u,\omega)$ and $J(k,u,\omega)$ of the angularly-dependent flux and the degradation integral in series of Legendre polynomials. This yields an infinite set of simultaneous integral equations for the Legendre components of N:

$$\sigma_T(u)N_l(k,u) = \sum_{l=0}^{\infty} (2l+1)A_{jl}\left[\sum_\gamma J_l^\gamma(k,u) + S_l(k,u)\right] \quad (4)$$

Here σ_T is the total cross section and the S_l are the Legendre components of the transform of the source. The sum over γ goes over all moderators present. If the source is isotropic,

$$S_l(k,u) = S_0(k,u)\delta_{l0} \quad (5)$$

the problem is considerably simplified, as then $N_{2j}(k,u)$ is real and $N_{2j+1}(k,u)$ is purely imaginary. If the source is not isotropic, then all components of the flux-transform are complex. However, the equations for real

and imaginary parts couple in such a way that when the set of equations[4] is made finite by replacing the upper limit of the sum by some integer L, one need not solve a set of $2L$ simultaneous equations, but rather two sets of L simultaneous equations for the symmetric and antisymmetric components of the flux.

The coefficients A_{jl} in Equation 4 are defined by:

$$A_{jl}(k,u) = A_{lj}(k,u) = \frac{1}{2}\int_{-1}^{1} \frac{P_j(\mu)P_l(\mu)}{1-\eta(u)\mu}\,d\mu$$

$$= \eta^{-1}Q_j(\eta^{-1})P_l(\eta^{-1}) \qquad (l \leqq j) \qquad (6)$$

Here P_j and P_l are Legendre polynomials of the first kind, Q_j is a Legendre function of the second kind, and $\eta(u) = ik/\sigma_T(u)$. When the set of equations is made finite by assuming that $J_l = 0$ for $l > L$, (which corresponds to replacing ∞ by L in the sum) one obtains what is called the "B_L approximation".[15] The usual spherical harmonics "P_L approximation"[2] corresponds to performing the integration in Equation 6 by the $L+1$ point Gauss formula. (This is a consequence of the fact that the Gaussian integration procedure of Wick[16] is identical with the spherical harmonics method.) The P_L approximation is equivalent to assuming $N_{L+1} = 0$. Since J_{L+1} involves an integration of the product of N_{L+1} and a rapidly oscillating function,[17] J_{L+1} is a smaller quantity than N_{L+1}, and thus the B_L approximation, which ignores J_{L+1}, is superior to the P_L approximation which ignores N_{L+1}.

The familiar Selengut-Goertzel (S.G.) method[18] begins with the P_1 approximation, and evaluates J_1 by assuming the product of N_1 and the scattering cross section σ_s to be constant (Fick's law). This has the effect of reducing the two simultaneous integral equations to two coupled integral equations for the transform of the total flux (*i.e.*, flux integrated over angle) $N_0(k,u)$. The age-diffusion approximation[1,2] makes this assumption, and also approximates J_0 by assuming the product $N_0(k,u)\,\sigma_s(u)$ to be a linear function of lethargy. This yields a single differential equation for N_0. In general, such expansions are valid for heavy moderators, where the slowing-down process may be viewed as continuous, but for moderation by hydrogen, in which the neutron loses, on the average, 50 per cent of its energy in a single collision, these expansions yield poor results. In the work reported in this section, the age-diffusion approximation is always made for the integrals J_l^γ corresponding to heavy moderators. Thus, in referring to a particular method of solution, one is specifying only the manner in which the hydrogen integral is approximated, if at all.

The "modified S.G." method is obtained by making the S.G. approximation in the B_1 rather than the P_1 equations. Modified age-diffusion and "Greuling-Goertzel"[19] methods may be defined in the same manner. In each case, the same redefinition of the diffusion coefficient, D, serves to leave the form of the equations invariant.

For small values of k, the B_L and P_L cases give similar results. In particular, both approximations are correct through terms of the order k^{2L} in all components of the flux. Thus, for example, both the B_1 and P_1 approximations give the same (and correct) second moment, or neutron "age." As k increases the discrepancy between the two methods becomes larger, due to the inadequate representation of the integral in Equation 6 by the Gauss formula.

It is interesting to note from Equation 6 that since $P_{2j+1}(\mu)$ has a zero at $\mu = 0$, and since in the n-point Gauss formula, the integrand is evaluated at the zeroes of $P_n(\mu)$, in a P_L approximation with L even, $A_\infty(k,u)$ does not approach zero as $k \to \infty$. This prevents $N_0(k,u)$ from approaching zero as $k \to \infty$ and gives rise to the well-known delta function singularity in the spatial flux as calculated by an even P_L approximation. This difficulty does not arise in the B_L case—in fact, it may be shown that it is preferable to use even B_L approximations.[14]

(b) Numerical Results

The coupled integral equations[4] have been solved numerically in the B_L and P_L approximations for various values of L, and in the S.G. and "modified S.G." approximations. The quantities calculated include the transform of the total flux, $N_0(k,u)$, the transform of the slowing-down density, $q(k,u)$, and the neutron age, τ. Cases considered include a fission source[20] of neutrons, a Po-α-Be source,[21] and various monoenergetic sources; the slowing-down media are taken to be pure water and mixtures of water with aluminum, zirconium and uranium metals. Calculations have been performed which indicate the roles played by various nuclear characteristics of the moderator, such as anisotropic scattering in the center of mass system,[17,22] and inelastic scattering. (The inelastic scattering was considered only for moderation by water-uranium mixtures, in which case the energy spectrum of the inelastically scattered neutrons was estimated from a continuum model of the nucleus.[23] Zirconium and aluminum probably exhibit an appreciable amount of inelastic scattering also.[24] However, until further work is done towards finding the inelastic cross sections and the spectra of scattered neutrons for light elements, one has little choice but to omit the inelastic effects from the calculations, keeping them in mind, however, as a possible source of error.)

The additional effects of fast fission and resonance capture in the U^{238} were taken into account for the water-uranium calculations. Inclusion of the former effect, of course, tends to increase the value of the second moment, while the latter tends to decrease it. The resonance capture was calculated from the U^{238} resonance parameters as measured at BNL,[25] treating the mixture of metal and water as homogeneous.

The calculations which are directly susceptible to comparison with experiment are reported in Section V of this paper. These include neutron ages and spatial flux distributions (*i.e.*, the inversion of the transform of the flux). In this section, comparisons of the various calculational schemes are given.

In Table II, the integral over lethargy of the transform of total flux,

Table II. Comparison of B_L and P_L Approximations in Constant Cross-Section Case—Neutrons Slowing Down in Hydrogen

	$\eta = i$		$\eta = 5i$	
L	$N_0^*(B_L)$	$N_0^*(P_L)$	$N_0^*(B_L)$	$N_0^*(P_L)$
0	3.660	∞	0.3787	∞
1	1.660	1	0.2990	0.0400
2	1.831	2.067	0.3218	1.1067
3	1.831	1.794	0.3218	0.1514
4	1.832	1.839	0.3238	0.5422
5	1.832	1.832	0.3238	0.2313
6				0.4074
7				0.2781

$$N_0^*(k) = \int_{-\infty}^{\infty} N_0(k,u)\, du \qquad (7)$$

is given for neutrons slowing down in pure hydrogen, for the hypothetical case in which the hydrogen scattering cross section is taken to be independent of energy and absorption is absent. Solutions are given in the B_L and P_L approximations for two values of η. Note the more rapid convergence with L of the B_L case, particularly for large η.

In Fig. 4, we plot $q(k,u)$ for neutrons slowing down in water as a function of k at a lethargy corresponding to indium resonance energy (1.44 ev). The calculation was performed by means of a B_3 approximation for a source of fission neutrons. In Table III, values of $q(k,u)$ as calculated by means of B_1, B_2, P_1, P_2, P_3, and S.G. approximations are compared with the B_3 result for q. This is done for purposes of comparing the accuracy of the various calculational schemes.

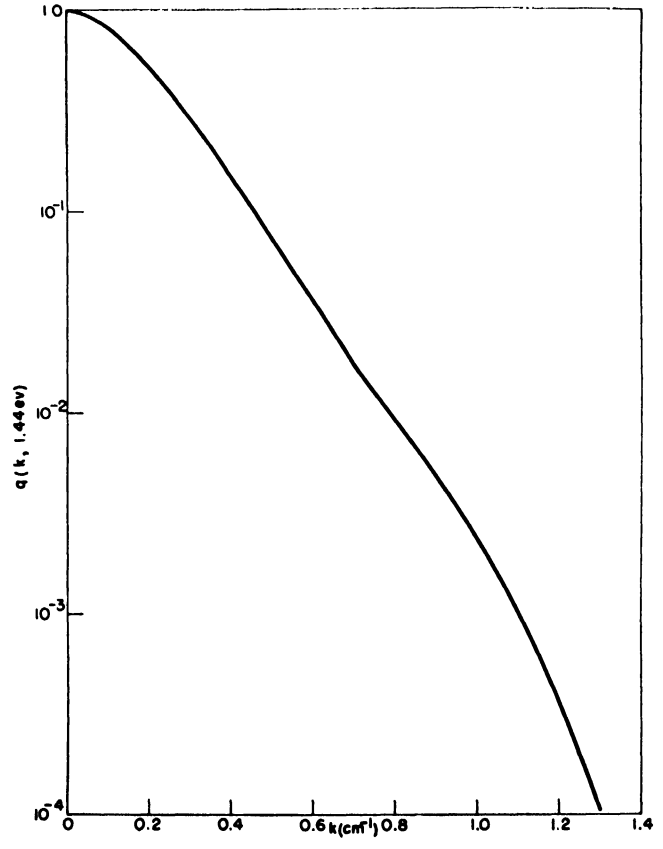

Figure 4. $q(k, 1.44\ ev)$ vs k-B_3 approximation for fission neutrons in water

Figure 5 is a curve of $q(k,u)$ *vs* u for $k = 0.1$, again in the B_3 approximation, for fission neutrons in water. Table IV compares $q(k,u)$ as calculated by the B_1, B_2, P_1, P_2, P_3, S.G., and "modified S.G." methods with the B_3 result.

In Table V, the ratio of $N_0(k, 1.44\ ev)$ as calculated by the B_3 and moments method (see Section II) is given. The series for $N_0(k,u)$ in terms of the spatial moments of the flux does not converge for k greater than approximately 0.1 (corresponding to a bare spherical reactor of radius less than approximately one foot). For this reason, the Fourier transform method is more applicable to reactor calculations than is the moments method. For extremely high penetrations, however, as are encountered in shielding problems, the moments method is superior. This is true because the moments method evaluates $N_0(k,u)$ as a power series about the origin, which is the nearest point on the real axis to the "saddle point" of $N_0(k,u)$. (The saddle point is on the imaginary axis, its distance from the origin depending upon the values of the total cross section.) Since the major contribution to the flux at deep penetration comes from the saddle point, the moments method would be expected to give better results for large distances.

A method of evaluating the spatial dependence of the flux at large distances by solving for the Fourier transform along the imaginary axis has been considered. However, due to the rapid change in the hydrogen cross section over the fission spectrum, the position of the saddle point changes drastically as the energy of the source neutrons changes, which complicates the problem to a considerable extent. (The spatial flux distribution obtained from Fourier transform calculations (quoted in Section V) has been found by straightforward numerical integration of $N_0(k,u)$ along the real axis. Because of the rapid oscillations of the integrand for large values of r, it is difficult to find $N_0(r,u)$ more than 30 or 35 cm from the source by this method.)

From all of these results, one may conclude that except at extremely large values of k, the B_1 approximation is sufficiently accurate for most applications. The P_1 and P_2 calculations, on the other hand, are quite poor except for very small k, and in particular, a P_3 calculation is not much better than a B_1, and significantly poorer than a B_2 calculation. Since the amount of labor involved in a B_1 calculation is perhaps two orders of magnitude lower than that involved in a P_3, the advantages of the B_L approximation over the P_L are apparent.

The S.G. approximation gives rather poor results, even for quite small k, although the "modified S.G." method is somewhat of an improvement over the ordinary S.G. approximation. Since the S.G. approximation is convenient because of the ease with which

Table III. Comparison of Calculational Methods: Ratios of Slowing-Down Densities at 1.44 ev as a Function of k

k (cm^{-1})	B_1/B_3	B_2/B_3	P_1/B_3	P_2/B_3	P_3/B_3	S.G./B_3
0.10	0.9978	1.0001	0.9894	0.9949	0.9935	0.9417
0.20	0.9864	1.0010	0.9219	0.9988	0.9818	0.8524
0.35	0.9584	1.0028	0.7474	1.3756	0.9519	0.7447
0.50	0.9190	1.0024	0.5253	1.0410	0.8797	0.6697
0.65	0.8672	0.9983	0.2796	1.0340	0.7848	—
0.80	0.8063	0.9890	0.04814	1.5560	0.8741	—
0.95	0.7418	0.9716	—	1.8938	0.8221	—
1.3	0.6878	0.7355	—	—	—	—

Table IV. Comparison of Calculational Methods: Ratios of Slowing-Down Densities at k = 0.1 cm^{-1} as a Function of Lethargy

u	B_1/B_3	B_2/B_3	P_1/B_3	P_2/B_3	P_3/B_3	S.G./B_3	"Modified S.G."/B_3
0.05	0.9934	1.0022	0.8750	1.0366	0.9907	—	—
0.50	0.9910	1.0020	0.9185	1.0182	0.9965	0.7459	0.9493
1.00	0.9953	1.0007	0.9658	1.0028	0.9964	0.8172	0.8696
1.50	0.9965	1.0003	0.9778	0.9960	0.9927	0.8567	0.9038
2.00	0.9970	1.0002	0.9832	0.9946	0.9924	0.9008	0.9339
2.50	0.9974	1.0002	0.9861	0.9948	0.9931	0.9247	0.9486
3.00	0.9976	1.0001	0.9872	0.9950	0.9935	0.9366	0.9583
3.50	0.9977	1.0001	0.9881	0.9951	0.9938	0.9465	0.9666
4.00	0.9978	1.0001	0.9884	0.9951	0.9938	0.9396	0.9575
5.00	0.9978	1.0001	0.9884	0.9951	0.9938	0.9414	0.9606
6.00	0.9978	1.0001	0.9884	0.9950	0.9937	0.9413	0.9606
8.00	0.9977	1.0001	0.9882	0.9949	0.9936	0.9432	0.9620
10.00	0.9977	1.0001	0.9882	0.9949	0.9936	0.9434	0.9625
12.00	0.9977	1.0001	0.9882	0.9948	0.9936	0.9946	0.9638
15.00	0.9977	1.0001	0.9881	0.9948	0.9935	0.9436	0.9643
19.50	0.9977	1.0001	0.9880	0.9948	0.9935	0.9452	0.9678

it may be calculated, and since the use of "modified S.G." introduces little additional computational difficulty, the "modified S.G." approach represents a reasonable method of performing calculations for hydrogen-moderated assemblies.

In Fig. 6 is plotted the age $\tau(E_0, 1.44\text{ ev})$ of neutrons slowing down to 1.44 ev from a point isotropic monoenergetic source of energy E_0, as calculated by the S.G. method. Also plotted is the product of the fission spectrum,[20] $\chi(E_0)$ and $\tau(E_0, 1.44\text{ ev})$ in order to demonstrate the large contribution to the age made by the relatively small number of neutrons born at energies appreciably higher than the mean fission energy, because of the low-hydrogen cross section at these high energies. This indicates the importance of knowing accurately both the high energy (>5 Mev)

Table V. Transform of Neutron Flux at 2.03 ev Ratio of Moments Results to B_3 Calculations

k (cm^{-1})	N_0 (Moments)/$N_0(B_3)$
0	1.000
0.025	1.007
0.050	1.007
0.0750	1.007
0.100	1.007
0.125	1.088

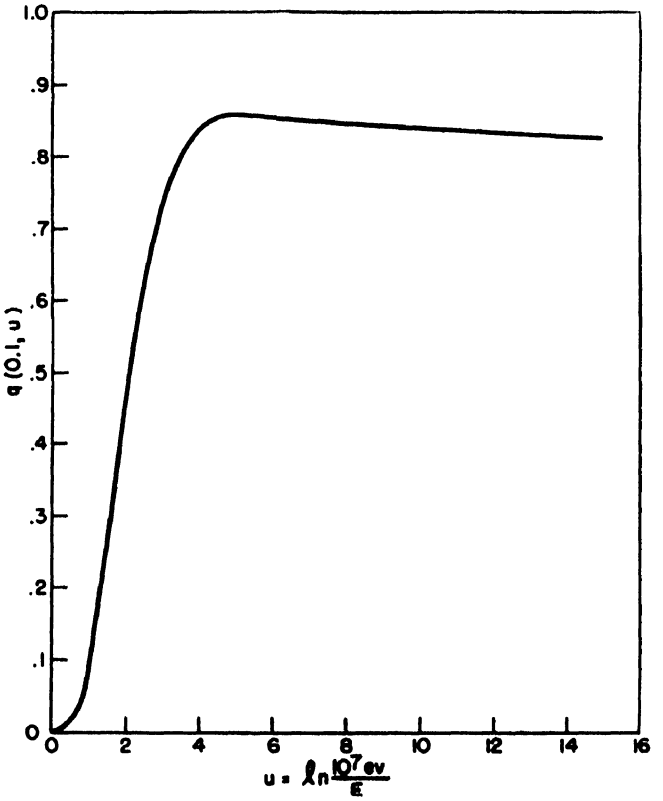

Figure 5. q(0.1 cm^{-1}, u) vs u-B_3 approximation for fission neutrons in water

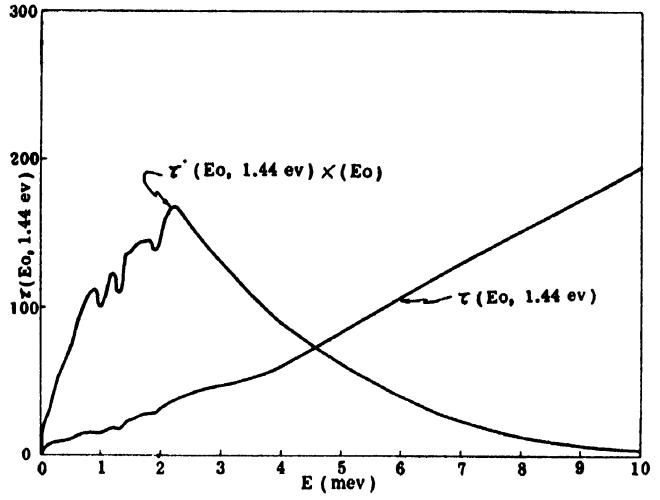

Figure 6. $\tau(E_0, 1.44\ ev)$ and $\tau(E_0, 1.44\ ev) \times (E_0)$ vs E_0-S.G. approximation for neutrons in water

part of the fission spectrum and the cross sections at these energies. The implications of these facts are discussed in Section IV in connection with certain experiments for measuring the age of neutrons in water.

(c) Reactor Calculations

The results of the Fourier transform calculations may be applied to reactor problems in a number of different ways. The simplest application is, of course, to a bare homogeneous reactor of buckling B^2, in which case the criticality equation may be written directly in terms of $q(k = B)$.[1]

In a more practical case, reactor problems must be solved by means of group-diffusion techniques.[26] In choosing group constants for such calculations, the

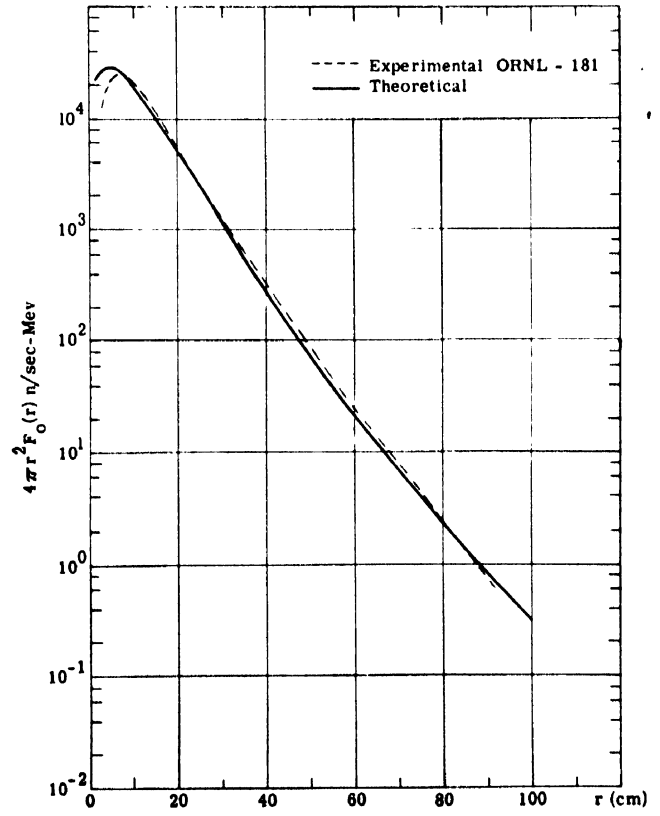

Figure 7. Flux distribution at 2.03 ev moments calculation for fission neutrons in water

Fourier transform calculations may be applied in two general ways:

1. The transform of the convolution of the slowing-down kernels for the individual groups must agree with the calculated transform of the slowing-down density at thermal energies and

2. In choosing group averages of cross sections and "ages," the calculation of the transform as a function of energy may be used as a general guide.

One further application of the Fourier transform calculations is to an assembly whose reflector may be taken to be infinite, and whose core and reflector have the same moderating properties (but different absorption). For such a case, Greuling[27] has developed a variational principle for finding critical masses and dimensions. This variational principle has been re-expressed[28] in terms of the Fourier transform of the slowing-down density. The results, for a spherical core of radius R may be summarized as follows.

Let the absorption cross section of the core be $\sigma_c + \sigma_H$ and that of the reflector be σ_H; σ_f is the fission cross section of the core, ν the average number of neutrons emitted per fission, and L is the thermal diffusion length. Then the equation to which the variational principle may be applied is

$$\int_0^R dr\,[r\phi(r)]^2 = \frac{\nu\sigma_f}{\sigma_H}\int_0^\infty dk\,[k\phi(k)]^2\left[q_{th}(k) - \frac{\sigma_c}{\sigma_f}\right]\frac{1}{1+L^2k^2} \quad (8)$$

Here $q_{th}(k)$ is the transform of the slowing-down density at thermal energies.

A convenient trial function to use in the variational principle is

$$\phi(r) = \frac{\sin \alpha r}{\alpha r}\sum_{n=0}^{\infty}\gamma_n r^{2n}$$

in which case

$$\phi(k) = \frac{(2\pi)^{-1/2}}{\alpha k}\sum_{n=0}^{\infty}\gamma_n[I_n(C_-) - I_n(C_+)]$$

$$C_+ = \alpha + k \qquad C_- = \alpha - k$$

$$I_n(C) = (-1)^n R\frac{\partial 2n}{\partial C^{2n}} j_0(CR)$$

where $j_0(x)$ is the spherical Bessel function of order zero.

IV. EXPERIMENTAL DETERMINATION OF THE SLOWING-DOWN DISTRIBUTION

(a) Introduction

Experimental evidence pertaining to the slowing-down distribution of neutrons in hydrogenous media is obtainable from a rather wide variety of measurements involving non-reproducing systems with fast neutron sources of several types and reproducing sys-

tems with, and without, external neutron sources. In this section those measurements which can be compared with reliable theoretical calculations are summarized, not with the intent of providing a critical re-evaluation of the experiments themselves but for the purpose of indicating the extent of the experimental information available for the comparisons with the theory discussed in Section V. This listing is by no means exhaustive since a number of experiments are not included on the basis that they involve neutron source energy distributions or cross sections which are so poorly known that any comparison with theory would be of questionable value.

For convenience, the descriptions of the experiments have been arranged according to the energy distribution of the fast neutron source and the experimental technique. In the first three groups of experiments the flux distribution in space at either indium resonance or thermal energies was measured, from which the moments of the distribution could be obtained. The first group comprises measurements made with a high intensity fission neutron source. In the second group, experiments with other broad source energy distributions are described, while in the third group, three experiments, designed to avoid some of the uncertainties encountered in earlier measurements, are described and some preliminary results listed. In the fourth group a series of reactor experiments are included in order to show how the theoretical calculations can be correlated with these indirect measurements of the slowing down distribution. This latter group demonstrates also the important role which is played by inelastic scattering in some mixtures.

(b) Fission Neutron Source

The slowing-down distribution from a source of fission neutrons in water is of particular importance since the theoretical treatment of this problem has been extensive. In the measurements made by Hill, Roberts and Fitch,[29] a source of fission neutrons was obtained by placing a plate containing U^{235} in a large tank of water. Fissions were induced in this plate by thermal neutrons entering the tank from an adjacent graphite thermal column. The neutron-flux distribution in the water was then measured by the activation of indium foils positioned along the perpendicular axis of the source plate.

Several rearrangements of the apparatus were necessary to provide adequate activation of the foils throughout the range of 2.35 cm to 90 cm from the source plate. First, both source and foil dimensions were increased with their separation. The corrections to attain the distribution for spherical geometry were, however, generally less than 10%. Secondly, although measurements up to 15 cm from the source were made with the fission plate 10 cm from the graphite, the fission plate was placed adjacent to the graphite for measurements at larger separations, in order to increase the source intensity (by a factor of roughly 35). By this procedure, sufficient activation of the cadmium-covered indium foils was obtained to permit measurements to 70 cm from the source. Additional measurements between 70 cm and 90 cm were made with uncovered indium foils and interpreted as being proportional to the indium resonance flux.

Because of the very high source intensity available from this combination of reactor, thermal column and fission plate it was possible to evaluate the first four even moments of the distribution with less than a 10% extrapolated contribution even to the eighth moment. However this advantage was obtained at the cost of locating the source near the graphite-water boundary thereby introducing the possibility of flux distortion, particularly near the source. Roughly, the effect may be thought of in terms of the spatial distribution of first collisions, from which the graphite is seen to behave as a displaced secondary source of slightly degraded neutrons. However, until a detailed calculation of the magnitude of the effect can be made, it is impossible to do more than point out this uncertainty, of which the experimenters were fully aware.

Further measurements, with only minor modifications of the experimental arrangement already described, were made in aluminum-water mixtures by Roberts, Hill and Fitch,[30] and in zirconium-water mixtures by Hoover and Arnette.[31] The results of these experiments are summarized and compared with theoretical calculations in Section V.

(c) Broad Energy Distribution Sources

A rather large number of slowing-down distribution measurements have been performed with Ra-α-Be and Po-α-Be neutron sources. Some of these results are not particularly suitable for the purposes of a summary such as this because of the considerable width of the source spectra and uncertainties in the detailed yield as a function of energy. It is readily seen from Fig. 6 that errors in the neutron yield at high energies are weighted very heavily in averaging the age to indium resonance energy since the age rises rapidly with initial neutron energy. Thus no rigorous calculations have been made for Ra-α-Be sources and only limited results are available for a Po-α-Be spectrum.

The energy spectrum of neutrons from Po-α-Be sources has been the subject of considerable investigation,[21,32] with the result that there appears to be a general agreement between several measurements by different methods, although the certainty attained is not comparable to that of the fission spectrum. A slowing-down distribution measurement for Po-α-Be neutrons has been made by Baer[33] in an aluminum tank, of dimensions 50 cm × 40 cm × 100 cm, filled with water. The thermal flux distribution was measured with a small BF_3 proportional counter, ¼ inch in diameter and 1 inch long, by taking the difference between bare and cadmium shielded counting rates. The source was placed on the long axis of the tank, 25 cm from the end; the data were taken along this same axis to a distance of 60 cm from the source. Further measurements were made of the same sort in a lattice of zirconium rods immersed in water.

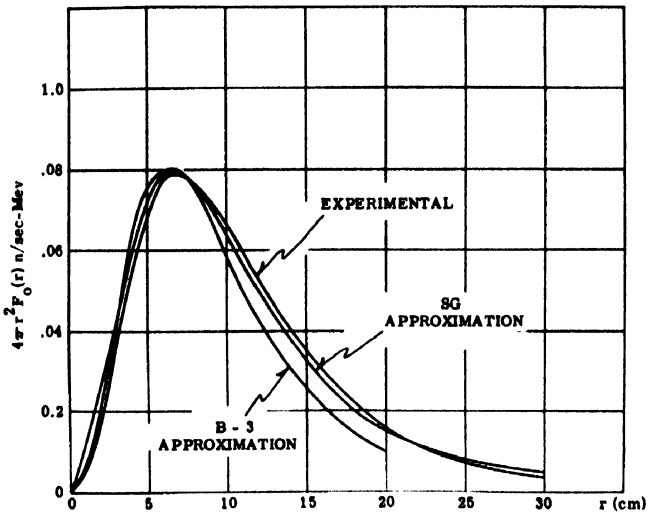

Figure 8. Flux distribution at 1.44 ev inversion of transform for fission neutrons in water

Two undesirable features occur in this experiment. The BF_3 counter differences measure thermal flux at a point integrated over the B^{10} absorption cross section. This in turn represents, roughly, the convolution of a diffusion kernel with the slowing-down distribution, which has the effect of averaging the slowing-down distribution over a region of space whose dimensions are of the order of the diffusion length. Taking the measured migration area to be the sum of an age and diffusion length (squared), the diffusion process is estimated to account for 12% of the migration area for pure water, 18% for a zirconium-to-water volume ratio of unity. The ages obtained by such an estimate are compared with theoretical calculations in Fig. 11. A further uncertainty is introduced by the large diameter (approximately ¾ inch) of the rods available for the experiment. Some finite rod size effects observed in the uranium-water experiments are mentioned later.

Measurements of a Ra-α-Be neutron spectrum[34,35] indicate a broad but rather uncertain yield extending to approximately 13 Mev. An S.G. approximation of the age, made for the source description of Teucher,[34] is in very poor agreement with 48 cm^2, the latter being the result of several measurements.[36,37]

(d) Narrow Energy Distribution Sources

Several slowing-down distribution experiments have been designed in the past several years with the intent of avoiding some of the uncertainties encountered in the interpretation of earlier measurements. None of these, as yet, has been fully described in the literature so that only a brief account of the experiments and some preliminary results can be given here.

Caswell[38] has measured the indium resonance flux distribution in water from an essentially isotropic source of 14 Mev neutrons obtained from a *D-T* reaction at low-incident deuteron energy. The source was located near the center of the water tank by directing the deuteron beam through a narrow tube leading to the tritium target. The magnitude of the flux was sufficient to permit cadmium-covered foil measurements as far as 60 cm from the source. Beyond this point measurements were extended to 125 cm by use of a B^{10} counter. In addition to these low-energy flux distribution measurements the fast neutron dose, shown in Fig. 9, was observed at distances from 15 to 55 cm from the source. As is mentioned in Section V both of these results are in rather good agreement with the theory. It should be noted that this experiment is nearly ideal in that the energy spectrum of the source and geometry of the system were well defined and the strength of the source was adequate for the determination of at least the second moment of the distribution.

More recently Caswell has obtained some, as yet, preliminary results from a *D-D* reaction (~2.5 Mev neutron energy) in much the same geometry. Here, however, because of the lower energy available from the reaction some dependence of energy and yield of neutrons on angle is to be expected. This does not, however, introduce any uncertainty into comparisons with theoretical calculations since the energy and yield of neutrons from the source can be calculated according to classical mechanics. With this information, the slowing-down distribution can be calculated rigorously. Plans have been made to extend the measurements to systems containing water and various metals of interest.

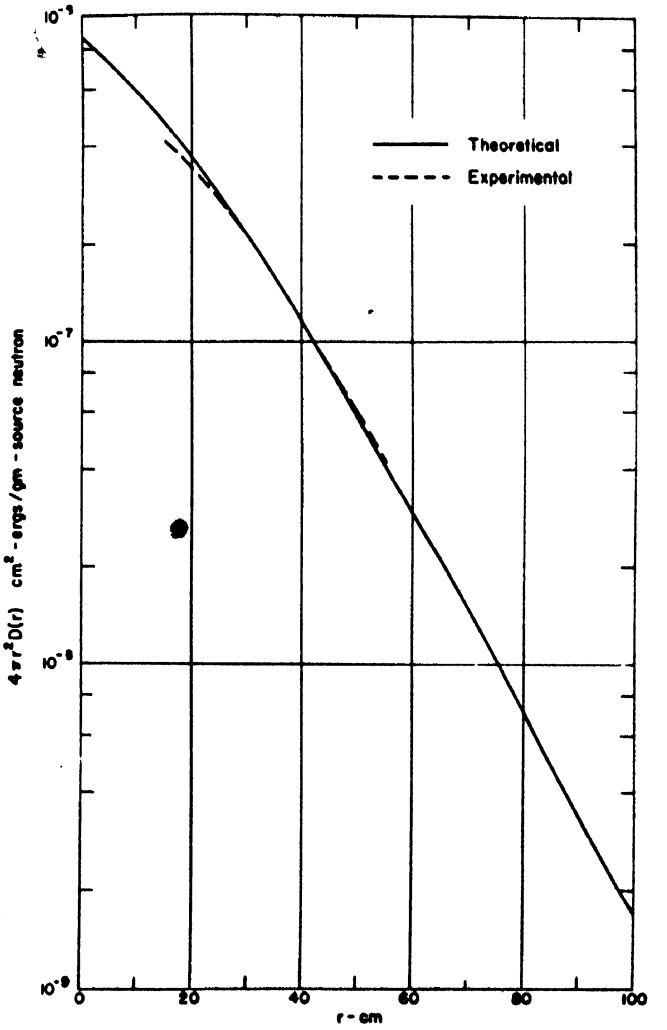

Figure 9. Single collision polyethylene dose from 14.1 mev neutron point source in water

A rather unusual experiment has been carried out by Shure[39] employing the delayed neutron emitter N^{17} as the source. The N^{17} is produced in the water of a closed loop by passing a section of the loop through the core of the Materials Testing Reactor. Upon emerging from the reactor the water is pumped rapidly to the center of a hydrogenous plastic source plate. The water then passes through spiral channels to the outer periphery of the plate and is piped back to the reactor core. Consideration of the geometry of these channels shows that the neutron yield as a function of the radius of the plate has the form of a truncated Gaussian. The thermal neutron flux distribution has been measured along an axis perpendicular to the plane of the disk. The distribution so obtained can be rigorously transformed to the corresponding distribution from an infinite plane source.

Because of the low source intensity provided by this scheme, it has not been possible to measure the indium resonance flux distribution over a distance sufficient to allow the evaluation of the second moment. The experiment has the advantage, however, of providing a well-defined source geometry with little perturbation introduced by the structure of the source itself. Since the shape of the flux distribution in the neighborhood of the source is a matter of considerable interest and a primary discrepancy in the measurements with fission neutrons, this experiment is capable of providing data in a rather crucial range.

The energy of the neutrons resulting from the decay of N^{17} has been observed to lie in the neighborhood of 900 kev, but the half-width of spectrum[40,41] (roughly 200 kev) is not well known.

(e) Reactor Measurements

In the conceptual description of thermal reactors the neutron migration area is related to the mean square distance a neutron travels from its birth in thermal fission to its subsequent absorption as a thermal neutron. Although clearly defined, the migration area is not amenable to calculation at the present time because of the theoretical difficulties encountered in describing the scattering of low energy or thermal neutrons. In highly absorbing systems however, the thermal diffusion length is small so that the predominant contribution to the migration area comes from the slowing-down process. Thus some comparison can be made of measurements of the migration area in reproducing systems and calculations of the neutron age by treating the thermal diffusion as an additive correction.

The extensive program of exponential experiments in slightly enriched, water moderated systems, conducted by Kouts[42], has provided sufficient data for the evaluation of the migration area through a range of water-to-uranium volume ratios. The experiments which have been most effective in determining the migration area are carried out by measuring the thermal utilization for a series of buckling values, the variation in buckling being obtained by poisoning the moderator with boron. If the results of these experiments are then fitted by one group diffusion theory the migration area, at zero buckling, is just equal to the logarithmic derivative of the thermal utilization with respect to the buckling. This procedure does not require that either the fast fission factor ϵ or the resonance escape probability p be independent of buckling, since, for example, it is the change in ϵ with buckling which represents the contribution of fast fission to the migration area.

Other methods can be applied to the determination of the migration area, such as observing the change in buckling with enrichment of the uranium. In critical assemblies the migration area can be inferred from the reactor period observed when the geometrical buckling of the system is changed. Thus far, however, the poison method has been the most successful in providing consistent data. The results of the BNL measurements for two uranium rod sizes are shown in Fig. 12.

V. COMPARISON OF THEORY AND EXPERIMENT

(a) Fission Neutrons in Water

As was mentioned earlier, the experimental and theoretical investigation of the slowing-down distribution from fission neutrons in water has been most extensively pursued. For this case alone, the actual spatial distribution of flux has been calculated in various approximations and can be compared in detail with measured distributions. The moments method which, as pointed out in Section III, is the most convenient method for obtaining spatial distributions, has been used to evaluate the first eight even spatial moments of the flux distribution (see Section II). In addition, the Fourier transform of the flux as calculated in the B_3 and S.G. approximations has been inverted to give the flux distribution at small distances ($\sim$30 cm) from the source. In Fig. 7, the spatial distribution at 2.03 ev, as calculated by the moments method, is compared with the experiment of Hill, Roberts and Fitch[29], for $2 < r < 90$ cm. Although the theoretical result is for 2.03 ev neutrons and the experiment for 1.44 ev neutrons, it is not expected that the shape of the spatial distribution will change appreciably in this small energy range. Absolute normalization has not been made in this experiment. In Fig. 8, the B_3 and S.G. transform inversions are compared with the same experimental results for smaller distances. The S.G. curve was first obtained by Nelkin,[43] and later modified by Shapiro, Clark and Preiser.[44]

It may be observed that of the three theoretical evaluations, only the S.G. result is in substantial agreement with the experiment in the region of small penetrations. The more nearly rigorous calculations yield a higher flux near the origin than is observed. This is consistent with the fact that the second spatial moment of the flux, if calculated exactly, is smaller than the experimental moment, while the S.G. second moment is in almost perfect agreement.

On the other hand, it will be observed from Fig. 7 that the theoretical flux distribution far from the

source exhibits essentially the same behavior as does the experimental distribution. This fact is more evident from Table VI, in which the calculated and measured spatial moments are exhibited. The "rigorous" results in Table VI were obtained by the moments method; a B_L or P_L calculation gives the first $2L$ moments rigorously, as is pointed out in Section III, and the higher moments approximately. Note that the higher B_1 moments are closer to the rigorous values than are the P_1 moments. Consistent with the good agreement between theory and experiment at deep penetrations, the $2L$-th rigorous moment approaches the $2L$-th experimental moment with increasing L.

In view of the discrepancy observed in the case of the second moment, a number of exploratory calculations have been made in an attempt to isolate the influence of various approximations and uncertainties. The approximations include the treatment of the oxygen degradation by age theory, and the complete neglect of the oxygen slowing down, while the major uncertainties are in the angular distribution of the neutrons scattered from oxygen[13,17] and in the fission neutron energy spectrum. The influence of the first three effects is indicated in Table VII, from which it is seen that none of them is large enough to explain the discrepancy. The minor differences between the rigorous values of τ or $\overline{r^2}$ are attributable to minor differences in data and group spacings. As far as uncertainties in the fission spectrum are concerned, the most recent spectrum measurements lead to an increase in the second moment of less than 0.5 cm^2 over the values quoted here.

A somewhat different comparison of theory and experiment can be made using the results of Caswell[38] referred to in Section IV. He measured, among other things, the single-collision polyethylene dose from a point isotropic source of 14.1 Mev neutrons in water at distances from 15 cm to 55 cm. A moments-method calculation of the same dose has been made and the results, independently normalized, are shown in Fig. 9. The agreement is much better than could have been predicted.

(b) Some Neutron Ages in Hydrogenous Media

The neutron age, which is related to the second spatial moment, is of particular interest in that it frequently appears in the description of reactor characteristics.[1] Furthermore, the relatively weak sources available for most slowing-down measurements permit determination of flux distributions over such a limited range of distance from the source that moments higher than the second can not be found. Thus, in most experiments, other than some of those employing fission sources, the neutron age provides virtually the only basis for comparison with theory. We compare here the results of some age measurements, described in the previous section for various metal-water mixtures and neutron sources, with some theoretical results.

Table VI. Comparison of Moments for Fission Neutrons in Water at 1.44 ev

$\overline{r^n}$ (cm^n)	$n=2$	$n=4$	$n=6$	$n=8$
Experiment[39]	185	1.222×10^5	2.270×10^8	8.642×10^{11}
Rigorous moments*	154	0.979	1.934	8.753
P_1	149	0.742	0.919	1.502
B_1	149	0.912	1.391	2.501
S.G.	184	1.422	2.542	4.924
S.G.M.	184	1.694	3.470	7.091

* Oxygen degradation neglected; calculations for 2.03 ev.

Table VII. Age of Fission Neutrons at 1.44 ev in Water

	Rigorous	*S.G.*	*Age-diffusion*
a. No approximations	25.3 cm^2	30.9 cm^2	—
b. Oxygen scattering assumed isotropic	23.6	28.7	—
c. Oxygen assumed not to slow down	26.8	32.8	17.5 cm^2
d. Approximations *b* and *c* both made	25.3	—	—

Figure 10 gives a comparison of theoretical and experimental ages[30] for aluminum-water mixtures as a function of metal-to-water volume ratio. It should be emphasized here that both inelastic scattering and anisotropic elastic scattering were ignored in the calculations for Al and Zr systems.

Several experiments made with Zr-water mixtures are summarized in Fig. 11, again plotted as a function of metal-to-water volume ratio. The upper curves refer to the Po-α-Be neutron source[45] measurements; the lower curves correspond to a fission neutron source. The experimental curve for the latter case is based on a single distribution measurement,[31] one critical assembly analysis[46] and the value for pure water. This paucity of data precludes any serious conclusions as to the agreement between theory and experiment. However, the tendency of the theoretical curves to lie below the experimental points, particularly for the larger metal-to-water volume ratios, indicates that for Zr and Al the anisotropy of the elastic scattering is more important than the effect of inelastic scattering.

Of the two experiments performed by Caswell[39] which were discussed in Section IV, the measurement with *D-T* (14.1 Mev) neutrons has been completed, while only preliminary data are available on his more recent experiment with *D-D* (2.5 Mev) neutrons. In the former experiment, the neutron age for 1.44 ev is measured to be 163 cm^2. Volkin's[22] result for the age of neutrons of this energy slowing down in water is 173 cm^2. This represents rather good agreement, although the calculations must be considered somewhat uncertain due to the lack of information concerning the differential scattering cross section of oxygen at the high energies involved here. In addition, Volkin has ignored the effect of the energy degradation which accompanies the oxygen scattering. Since this effect would serve to reduce the age, it would be in the correct direction, but its magnitude has, at the present time, not been estimated.

The experiment involving *D-D* neutrons is more difficult to analyze because the neutrons are not emitted isotropically. The measurements performed so far are for neutrons at 0 degree to the beam; clearly, a second moment obtained from such a measurement would be too large. The experimental age is of the order 47 cm², while the theoretical values, which averaged the source distribution over angle, are 33 cm² and 42 cm² as calculated rigorously and by the S.G. method respectively.

The experiment involving neutrons from N^{17} appears to be in good agreement with theory. The measured age is 14.3 cm², while the rigorously calculated value[22] is 13.0 cm², and the S.G. result is 14.4 cm². Here again, however, considerable uncertainty is present because the N^{17} neutron spectrum is not well known, and, in addition, the thermal rather than the indium resonance neutron distribution was measured.

(c) Reactor Measurements and Uranium-Water Mixtures

Because of the interest centered in slightly enriched uranium-water lattices of the type used in the measurements of Kouts *et al.*,[42] rather extensive calculations of their slowing down properties have been made. The Fourier transform of the slowing-down density has been calculated in the P_1, B_1 and S.G. approximations, including a homogeneous description of fast fission and resonance capture in U^{238}. The uranium inelastic scattering was treated by the continuum model and the anisotropy of the elastic scattering was estimated by a hard sphere model of the nucleus.[23] The thermal diffusion length was calculated according to a simple model[1] and found to be between 1–2 cm². The rigorous migration area so obtained is compared in Fig. 12 with the results obtained by Kouts for 0.60 inch and 0.75-inch diameter uranium rods.

It will be noticed that the results of the theory compare quite favorably with the measurements for the smaller rods except for the tight lattice with water-to-uranium volume ratio of unity. Although this experimental point may be in error it has been pointed out by Kouts that the strong increase in epithermal fission rate observed for this configuration may invalidate any simple correspondence between the present Fourier transform calculations and the experiment. The earlier measurements made with the 0.75-inch diameter rods indicate a very marked decrease in inferred migration area with increasing rod size. If this difference should prove to be real the curve for the homogeneous mixture of uranium and water should lie far above that obtained by the present calculations.

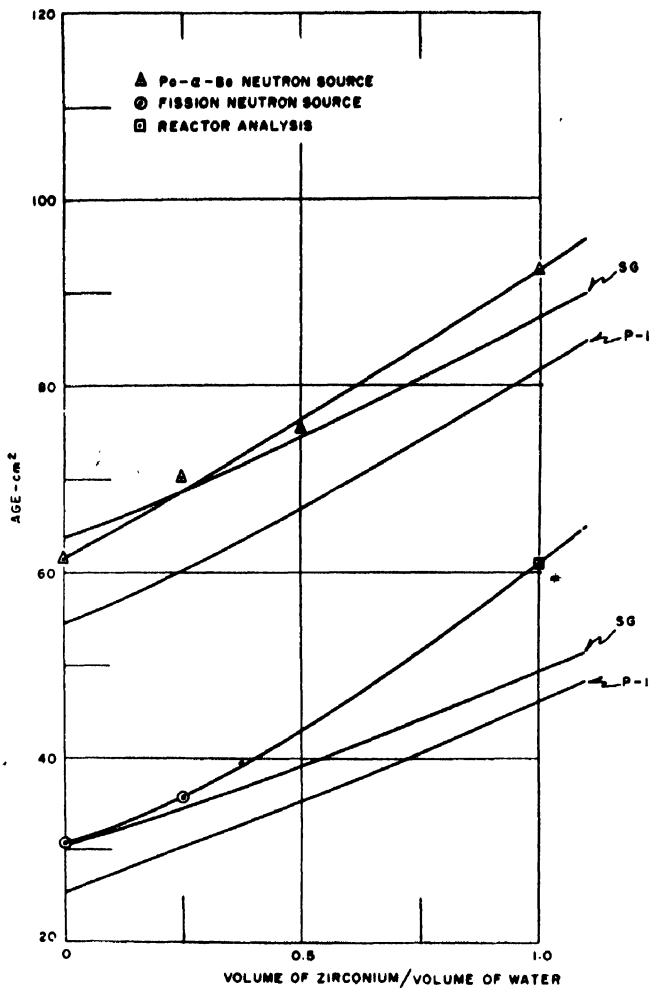

Figure 11. Age in zirconium-water mixtures of fission and Po-α-Be neutrons

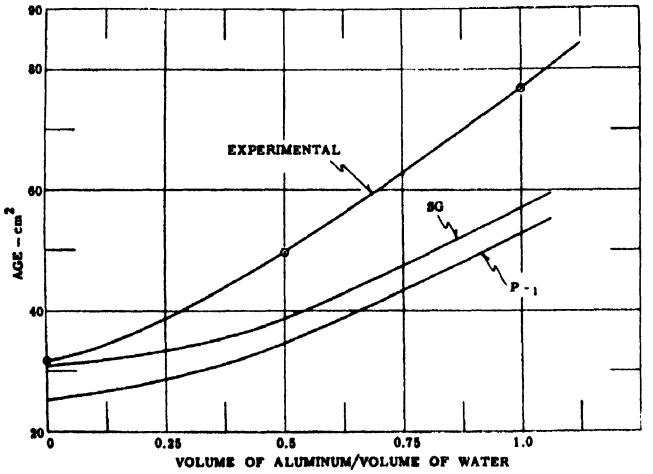

Figure 10. Age of fission neutrons to 1.44 ev in aluminum-water mixtures

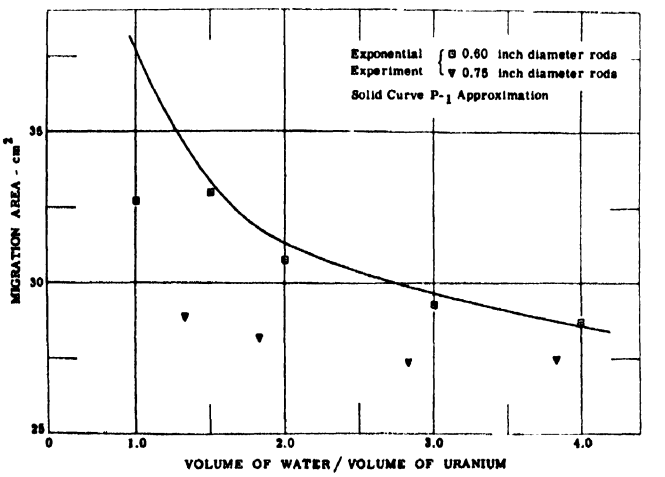

Figure 12. Migration area of fission neutrons in uranium-water mixtures

It is customary in a one-group theory of neutron diffusion to describe the probability of escaping fast leakage by either a group diffusion or exponential model,

$$P_0 = \frac{1}{1 + \tau_0^2 B^2} \qquad P_e = e^{-\tau_e^2 B^2}$$

The theoretical calculations permit the evaluation of both τ_0^2 and τ_e^2 as a function of buckling. It is seen in Fig. 13 that these quantities become appreciably different in the range of bucklings encountered in actual reactors. If the estimate of the 4-th spatial moment of the slowing-down probability given by these calculations is correct, neither simple description of the leakage should fit the experiments through the relevant range of buckling.

(d) Conclusions

It is rather apparent from the theoretical and experimental results reviewed so far that the agreement obtained is not extensive, nor is the amount of evidence sufficient to point with any degree of certainty to the source of this disagreement. There is some indication that the situation is relatively satisfactory at high (14 Mev) and low initial energies (1 Mev). However, even if this apparent agreement should prove to be real, the pronounced disagreement observed for intermediate energy neutrons can not be overlooked.

The tentative result of the *D-D* experiment seems to follow the pattern set by the earlier fission neutron measurement. This essentially monoenergetic experiment removes two of the conceivable difficulties encountered in the experiment of Hill, Roberts and Fitch, namely, the uncertainty in the fission energy spectrum and the proximity of the graphite thermal column to the neutron source. Thus, a confirmation of the tentative results of Caswell would indicate that the source of the discrepancy must be sought elsewhere.

In considering experiments which are capable of providing the answer to this dilemma, it becomes clear that there are three criteria which must be fulfilled:

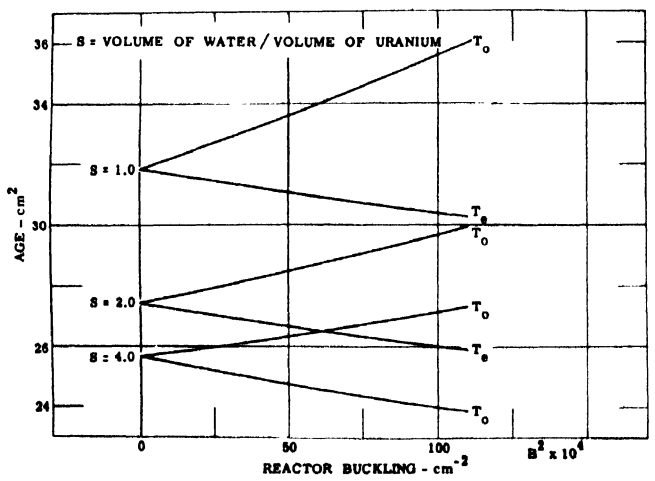

Figure 13. One group and exponential ages as function of buckling P_1 approximation

1. The source strength must be large enough to permit measurement of the neutron distribution with epithermal detectors such that at least the second moment is determined with negligible extrapolation contribution. Although it is desirable to determine some of the higher moments, the main discrepancies are apparent in the second moment alone.
2. The source of neutrons should exhibit a well-defined energy spectrum somewhere in the region of 1 to 5 Mev. This region is chosen because of the discrepancies which now exist for neutrons whose initial energy lies in this range and because this is the energy range of interest in reactor applications.
3. The boundaries of the medium in which the measurement occurs should be well removed from the source and detector.

These requirements are more or less obvious, but the number of experiments in which they are met is small.

It should also be emphasized that substantial uncertainties are still present in the evaluation of the theoretical results, even for pure water. It will be noticed that the estimated average cosine of the oxygen scattering angle,[17] although appreciably different from zero, changes sign several times in the fission neutron energy range. Thus the assumption of isotropic scattering introduces a decrease of only 1.7 cm² in the age (Table VII). However, this does not necessarily indicate that the effect of anisotropy in the oxygen scattering is small but rather that this particular average cosine, which has been widely used in most recent calculations, results in only a small net forward scattering of the neutrons. An upper bound for the effect is obtained by choosing an average cosine of unity, which leads to a calculated age of 43 cm². Thus it may be that small changes in the average cosine estimated for oxygen could account for the discrepancy now observed.

ACKNOWLEDGEMENT

It should be apparent that a survey article of this type must lean very heavily on the work of many people and that it is not always possible to acknowledge their assistance adequately. The authors wish here to express their appreciation to all those whose efforts have made a contribution to this paper.

REFERENCES

1. Glasstone, S. and Enlund, M. C., *The Elements of Nuclear Reactor Theory*, D. Van Nostrand Company, Inc., New York (1952). The solution is found for the case in which the source is distributed uniformly throughout space, so that the solution is independent of position.
2. Marshak, R. E., *Theory of the slowing down of neutrons by elastic collision with atomic nuclei*, Reviews of Modern Physics, *19:* 185–239 (1947).
3. Bothe, W., *Zur Methodik der Neutronensonden*, Zeitschrift für Physik, *120:* 437–439 (1942).
4. Greuling, E. (unpublished).
5. This method was first used for gamma-ray penetration problems by Spencer, L. V. and Fano, U., *Penetration and diffusion of X-rays. Calculation of spatial distributions by*

polynomial expansion, Physical Review 81: 464–466 (1951) and Journal of Research of the National Bureau of Standards *46:* 446–456 (1951).

6. Certaine, J., NYO-6270 (unpublished), Berger, M. J., *The penetration of gamma radiation from a plane monodirectional oblique source*, to be published in Physical Review.
7. The application of these techniques for gamma rays is more advanced and considerable work has been done on the entire angular distribution. See Certaine, J., NYO-3074 (unpublished) and Berger, M. J., *The angular distribution of multiple scattered gamma radiation from a plane isotropic source*, to be published in Physical Review.
8. Aronson, R., Certaine, J., Goldstein, H. and Preiser, S., NYO-6267 (unpublished).
9. Aronson, R., Certaine, J. and Goldstein, H., NYO-6269 (unpublished).
10. Hurst, G. S., CF 51-4-122 (unpublished).
11. Certaine, J., NYO-3081 (unpublished).
12. Certaine, J., NYO-6268 (unpublished).
13. The hydrogen cross-section data are taken from Neutron Cross Sections AECU-2040, 15 May, 1952 (unpublished) and the oxygen data are described by Goldstein, H., NDA Memo 15C-15 (unpublished).
14. Hurwitz, H., Jr. and Zweifel, P. F., *Slowing down of neutrons by hydrogenous moderators*, to be published in Journal of Applied Physics. Or see KAPL-1269 (unpublished).
15. The essential features of this method have been widely applied. See Waller, I., *On the theory of the diffusion and the slowing down of neutrons*, Arkiv för Matematik Astronomi och Fysik, 34A, No. *3:* 1–9 (1947); Wick, G. C., *On the space distribution of slow neutrons*, Physical Review, *75:* 738–756 (1949); Bethe, H. A., Tonks, L. and Hurwitz, H., Jr., *Neutron penetration and slowing down at intermediate distances through medium and heavy nuclei*, Physical Review, *80:* 11–19 (1950); Selengut, D. (unpublished); Price, J. P., Harwell report A.E.R.E. T/R 523 (unpublished). Waller gives a derivation of Equation 6.
16. Wick, G. C., *Uber ebene Diffusionsprobleme*, Zeitschrift für Physik, *121:* 702–718 (1943).
17. Zweifel, P. F. and Hurwitz, H., Jr., *Transformation of scattering cross sections*, Journal of Applied Physics, *26:* 127–128 (1955).
18. Goertzel, G., AEC Report TAB-53 (1950); Selengut, D. (unpublished).
19. Greuling, E., *Modified Fermi theory of neutron moderation*, Physical Review, *87:* 177 (1952).
20. Watt, B. E., *Energy spectrum of neutrons from thermal fission of* U^{235}, Physical Review, *87:* 1037–1041 (1952).
21. Elliott, J. O., McGarry, W. I. and Faust, W. R., *Energy spectrum of neutrons from Po—Be*, Physical Review *93:* 1348–1349 (1954); the calculations reported here employed the earlier spectrum measured by Whitmore, B. G. and Baker, W. B., *The energy spectrum from a Po—Be source*, Physical Review, *78:* 779–801 (1950) which is in good agreement with the later measurements of Elliott *et al.*
22. Volkin, H., *Effect of asymmetric oxygen scattering on the slowing-down lengths of neutrons in water*, Journal of Applied Physics, *26:* 127–128 (1955).
23. Blatt, J. M. and Weisskopf, V. F., *Theoretical Nuclear Physics*, John Wiley and Sons, New York (1952).
24. The work of Beyster, J. R., Henkel, R. L. and Nobles, R. A., *Inelastic collision cross sections at 1.0-, 4.0- and 4.5-Mev. neutron energies*, Physical Review *97:* 563–564 (1955) and Jennings, B. (private communication) seems to indicate that the inelastic cross sections for zirconium and aluminum are not insignificant. (There is some discrepancy between the results of Beyster *et al* and of Jennings, the latter measuring less inelastic scattering for zirconium than the former. This discrepancy is not yet resolved.)
25. Harvey, J., private communication.
26. Ehrlich, R. and Hurwitz, H., Jr., *Multigroup methods for neutron diffusion problems*, Nucleonics *12*, No. *2:* 23–30 (1954).
27. Greuling, E. (unpublished).
28. Francis, N. C. and Zweifel, P. F. (unpublished).
29. Hill, J. E., Roberts, L. D. and Fitch, T. E., ORNL-181 (unpublished).
30. Roberts, L. D., Hill, J. E. and Fitch, T. E., ORNL-294 (unpublished).
31. Hoover, J. I. and Arnette, T. I., ORNL-641 (unpublished).
32. Cochran, R. G. and Henry, K. M., ORNL-1479 (unpublished).
33. Baer, W., WAPD-99.
34. Teucher, M., *Über das Primärspektrum der schnellen Neutronen einer (Raα + Be) = Quelle und deren unelastische Stösse in Be, Bi und Pb*, Zeitschrift für Physik *126:* 410–421 (1949).
35. Schmidt-Rohr, U., *Ein Spektrometer für schnelle Neutronen und das Neutronenspektrum von Raα + Be*, Z. Naturforschung, *8A:* 470–479 (1953).
36. Munn, A. M. and Pontecorvo, B., *Spatial distribution of neutrons in hydrogenous media containing bismuth, lead, and iron*, Canadian Journal of Research, A, *25:* 157–167 (1947).
37. Fieno, D., NACA-RM-E 54H04 (1954) (unpublished).
38. Caswell, R., private communication.
39. Shure, K., private communication.
40. Alvarez, L. W., N^{17}, *a delayed neutron emitter*, Physical Review *75:* 1127–1132 (1949).
41. Hayward, E., *The energy spectrum of the delayed neutrons from* O^{17}, Physical Review *75:* 917–919 (1949).
42. Kouts, H., P/600, *Exponential experiments with slightly enriched uranium rods in ordinary water*, Volume 5, Session 21A, these Proceedings.
43. Nelkin, M. (unpublished).
44. Shapiro, M. M., Clark, F. H. and Preiser, S. (unpublished.)
45. Baer, W., WAPD-99 (unpublished).
46. Taylor, J. J., WAPD-RM-42 (unpublished).

Time-of-Flight Spectrometry Equipment for Slow Neutrons in Use at the Saclay Reactor—Its Application to a Study of the Inelastic Scattering of Cold Neutrons

By B. Jacrot, F. Netter* and M. Galula,† France

SUMMARY

The equipment uses a rotary mechanical shutter which absorbs the neutrons having energies up to values greater than 1 kev, a mechanical filter which makes it possible to retain only long wavelength components, and a 100-channel-pulse analyzer.

Its principal utilization is in the thermal energy region, where it made possible measurements of inelastic neutron scattering brought about by various substances, including H_2O, Be, and BeO.

EQUIPMENT

The machine described is the first of its type in France.[1] Its design characteristics were so chosen that it should give good results in the thermal neutron range, while remaining capable of making some measurements (with poor resolving power) up to 1000 ev. The requirements set by a compromise of this type brought the repetition rate down to the value required in measurements at low neutron speeds, but made it possible to take advantage, for the measurements in the thermal neutron range, of the absorbing qualities of a mechanical shutter designed to stop 1 kev neutrons.

The mechanical shutter (Fig. 1) is a thick steel flywheel, 1 m in diameter. A schematic cross section of the shutter is shown in Fig. 2.

Schematic Cross Section of the Shutter Cross Section

The shutter weighs 450 kg and rotates at 3000 rpm about a horizontal shaft, mounted on a carriage. Two rings of absorbing material each 2 cm thick are set into the shutter on its periphery. The absorbing material is a compound of boron carbide and araldite (a plastic material) which has been polymerized by a cold process after pouring, and contains ¾ of its weight as boron carbide. The cutting off of the neutron pulse thus is ensured by a total thickness of 4 cm of an absorbing material, plus 4 cm of steel. Protection against parasitic radiation is fairly efficient, thanks to the thickness of the steel used in the flywheel.

A recess is provided in the absorbing rings and the flywheel proper, for the mounting of the boron-carbide-araldite part (which was not molded, to give ¾ of its weight as boron carbide) where desired, in which a slot has been provided to allow a pulse of neutrons to get through each time the flywheel completes a revolution.

Three movable slots (with the three corresponding balancing counterweights) are available, 1.5, 6 and 16 mm wide, all of which are 50 mm deep. A fixed slot also is used, made of the same material and of similar dimensions, which makes it possible to define neutron impulses which are 10, 40 or 100 μsec in duration.

The precise moment at which the rotating slot passes before the fixed slot is indicated by an optical signal.

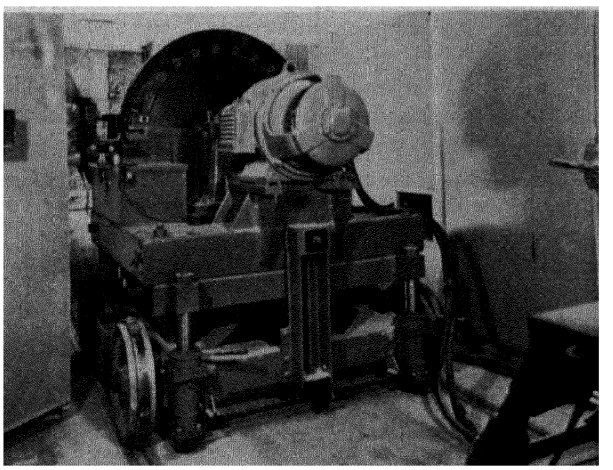

Figure 1

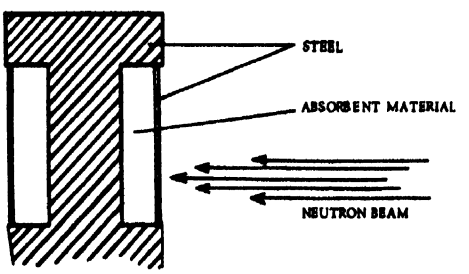

Figure 2. Schematic cross section of shutter periphery

Original language: French.
* Service de Physique Nucléaire du C.E.A.
† C.N.R.S. and Service de Physique Nucléaire du C.E.A.

The pulse of neutrons is taken directly from the reactor vessel, and passed through a collimator with an exit cross section of 20 × 100 mm.

The most frequently used flight path is 7 to 8 m.

The detectors are $B^{10}F_3$ proportional counters, or ionization chambers which contain one or two layers, either of boron, or of a fissionable material.

The pulses supplied by the detector are distributed according to their lengths between channels which correspond to the various times of flight by means of a suitable selector.

The deferred impulse selectors (Fig. 3) were supplied by the electrical manufacturing division of the C.E.A. (Laboratory of Mm. Désneiges and Guillon).

A first multi-channel selector, which gave only 10 simultaneous readings, was made by Mr. Bibron. It permits using very high counting rates.

A second selector, capable of giving 100 channels simultaneously, also using the ring principle, was built by Mr. Thenard. It is currently used for measurements at low counting rates.

The energy calibration is frequently checked by a study of the indium resonance and, for the slow neutrons, by determining the critical Bragg wavelength of various materials.

Spectrometer Applications

Aside from the determination of the spectrum of the neutrons which come out of a channel of the reactor which was studied between 0.002 and 100 ev, and from investigating the spectra emerging from the reflector and thermal column, most of the time available for this work was devoted to a measurement of the energy variation of the fission cross sections for slow neutrons, and of the slowing down of U^{233}, U^{235}, and Pu^{239}.

APPLICATION OF THE SPECTROMETER TO AN INVESTIGATION OF INELASTIC SCATTERING

Thanks to its large diameter, this spectrometer makes it possible to utilize high intensity neutron pulses with good resolution. In addition, its steel mass and boron-carbide rings considerably reduce the intrinsic background due to the epithermal neutrons.

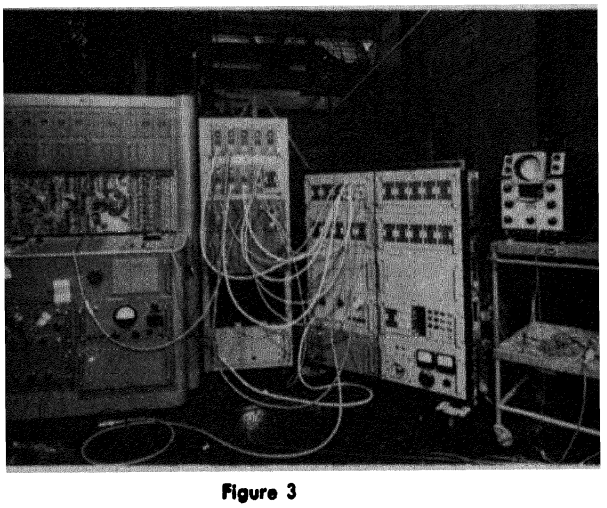

Figure 3

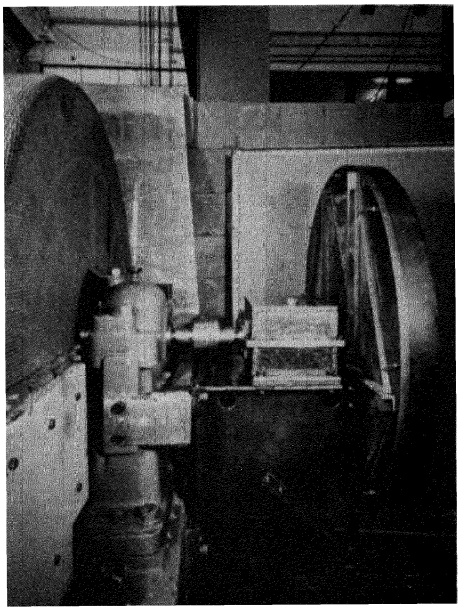

Figure 4

The spectrometer is set up at the end of a channel of the Saclay reactor so as to have unobstructed access directly to the heavy water vessel. It thus lends itself rather well to experiments which require a high intensity of slow neutrons, with as low as possible neutron background, outside of the pulse. These conditions have made it possible to conduct a direct study of the inelastic scattering of very slow neutrons.

For the purpose of these experiments, the main shutter was complemented by a second disk, so that the assembly made up a mechanical filter (Fig. 4).[2] This disk, placed 80 cm ahead of the shutter, uses two diametrically opposite cadmium sectors. It rotates in a direction contrary to that of the shutter, at half the shutter speed. This device makes it possible to observe only that part of the Maxwellian distribution beyond a predetermined wavelength, the value of which depends on the angular position of the cadmium sectors. The advantage of such a filter over a crystal filter, is that there is no loss of intensity, and that the cut-off wavelength may be varied continuously.

The filter however does not cut out the fast neutrons from the direct pulse. They must be eliminated, for they always contribute substantially to the scattering, particularly in the case of a material containing hydrogen. Accordingly, 6 cm of beryllium have been added. This filter attenuates the pulse of very slow neutrons only by a factor of some 1.4. It thus offers the advantage of bringing about a considerable reduction of the group motion. The presence of this beryllium causes, for some wavelengths, a distortion of the filtered spectrum which can be noted on Figs. 5 and 6.

The filtered spectrum is scattered by a sample which is placed as close as possible to the exit of the mechanical shutter. The scattered neutrons are then detected at a selected distance and scattering angle. The energy analysis of the scattered spectrum is carried out in the form of a measurement of the times of flight from the

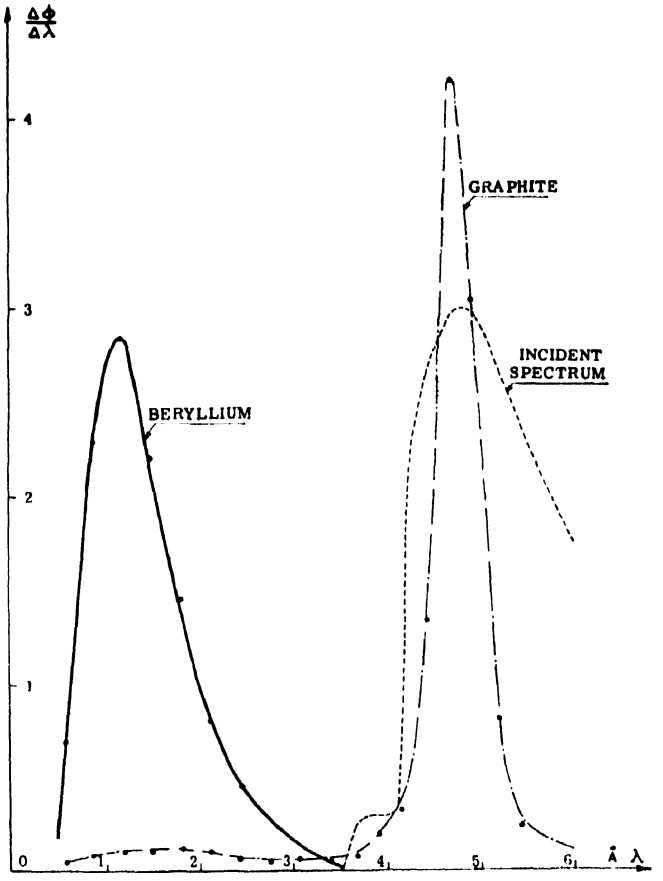

Figure 5. Scattering by graphite and beryllium

shutter and detector. A correction is applied for the path traveled between the shutter and sample. For the measurements which have been carried out, the angle was 90 ± 2.5 degrees with a 1-m travel path, or 90 ± 1.25 degrees with a 2-m travel path.

A typical example of the results obtained with the 1-m base is given in Fig. 5, where the spectrum which impinges on a polycrystalline sample of beryllium 60 mm thick‡ and the spectrum scattered at 90 degrees are shown. This case is of interest, for the inelastic scattering cross section is known[3] (0.5 barn at $T = 300$ degrees, for 3×10^{-3} ev neutrons); thus it can be used as a standard for the cross section.

Curves of the same kind were obtained for several polycrystalline substances, such as graphite, Al, V, Mg, Cu, Fe, Zn, Sn, Bi, Pb, U, and BeO. These substances give a scattered neutron spectrum which generally consists of an elastic scattering peak and one or more inelastic scattering peaks, the mean energy of which increases with the Debye temperature of the sample. According to some writers, the cut-off wavelength of the incident spectrum may be small enough to give a Bragg reflection. This, for instance, is the case of graphite where, with the incident spectrum shown in Fig. 5, a peak is observed, the width of which gives a good idea of the resolution, and the position of which makes it possible to calibrate the time-of-flight equipment (the thickness of the graphite sample is 6 cm).

‡ *Thickness* designates the dimension of the sample along the impinging bundle; *height* is dimension along the scattered bundle.

Work with polycrystalline substances, except where dealing with magnetic materials, is not generally likely to give much information other than the inelastic scattering cross section.§ In the case of the magnetic substances, experiments have been made by varying the temperature of the sample (Fe_3O_4).

We devoted most of our attention to single crystals, the study of which makes it possible to conduct a complete analysis of crystal vibrations, and to those of H_2O and D_2O, from which it is hoped some data may be obtained on the mechanism whereby the neutrons reach thermal equilibrium.

Diffusion in a Single Crystal

When the resolution is adequate, the scattered neutron spectrum must appear as a series of lines superimposed on a continuous background made up from the random vibrations. The position of these lines

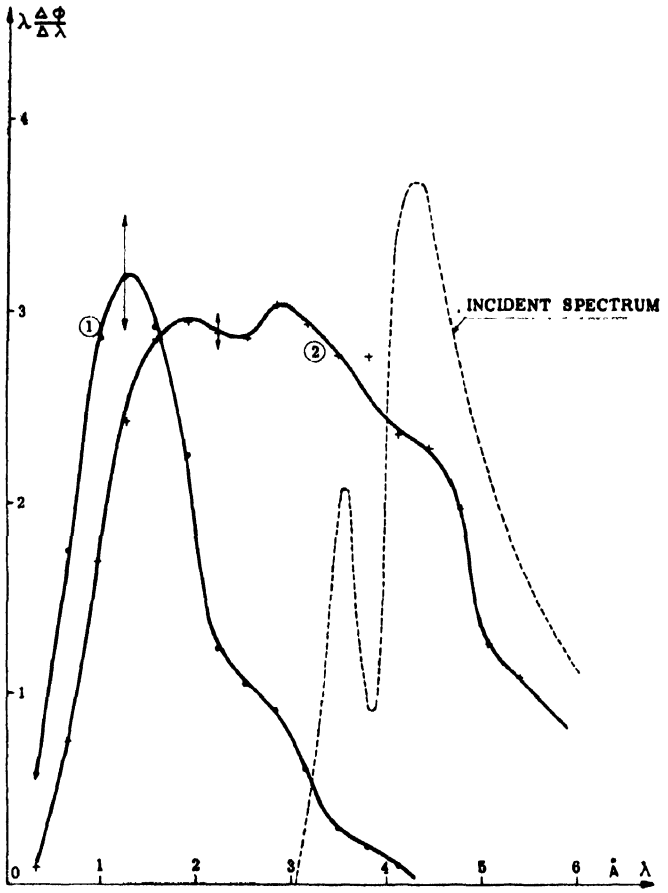

Figure 6. Scattering by H_2O

which is determined by the orientation of the crystal and the scattering angle, makes it possible, in principle, to determine the vibration characteristics of the crystal from geometrical analysis. In the work already carried out with a copper single crystal, a study of 90-degree scattering in a plane of symmetry (110) has been made for various positions of the crystal as it rotated about the binary axis. Unfortunately, it is not

§ The case of vanadium is most interesting since the scattering, which takes place entirely at random, would make it possible to determine the spectrum of the vibration frequencies of the vanadium crystalline lattice.

possible, with a copper crystal and the flux now available at Saclay, to achieve sufficiently good resolution to obtain well localized lines. Several peaks can be distinguished in the best cases, but no simple interpretation is ever possible. The cross section values thus have to be used. An interpretation of the results on that base is being made.

The resolution is improved, as the thermal neutron flux coming out of the reactor is increased. The new reactor to be built at Saclay (EL3) which will give a gain of at least a factor 20 over the flux used in the experiments described here, will make it possible to increase the resolution considerably. Development work is under way on equipment for use, in such projects, in the flux to be obtained from one of the channels of EL3.

Scattering by H_2O and D_2O

The demands placed on the intensity and resolution are much less critical in a study of scattering by ordinary water, heavy water and various hydrogen containing materials.

A systematic study was undertaken, in order to analyze the distortion of the spectrum made up of very cold neutrons after they have been passed through a certain H_2O or D_2O thickness at a temperature of 40°C.

The samples used had the same dimensions for water and heavy water. Three boxes were used, the height and thickness of which were, respectively:

Sample 1	15 × 40 mm
Sample 2	10 × 20 mm
Sample 3	7 × 10 mm

With such dimensions, in ordinary water, the distance covered would be large with respect to the mean free path of very slow neutrons (some 2 to 3 mm). Thus, there are many collisions and diffusion takes place isotropically. On the contrary, where heavy water is concerned, the dimensions are comparable to the length of the mean free path, and there is usually only one collision. The problem is narrowed down by studying 90 degree scattering.

The boxes are placed so that their height is completely exposed to the neutron flux.

The Case of H_2O

Most measurements were made with the spectrum shown in Fig. 6. It corresponds to a temperature of approximately 26°K. After scattering by sample No. 1, it gives nearly a Maxwellian spectrum (curve 1), with a temperature close to that of the medium (40°C). On the other hand, after scattering by sample No. 3 (curve 2), the spectrum is very different. Sample No. 2 gives an intermediate spectrum, not shown on the figure.

In order to try and get a closer approximation to the number of collisions needed in order to bring the incident neutrons to thermal equilibrium, a separate

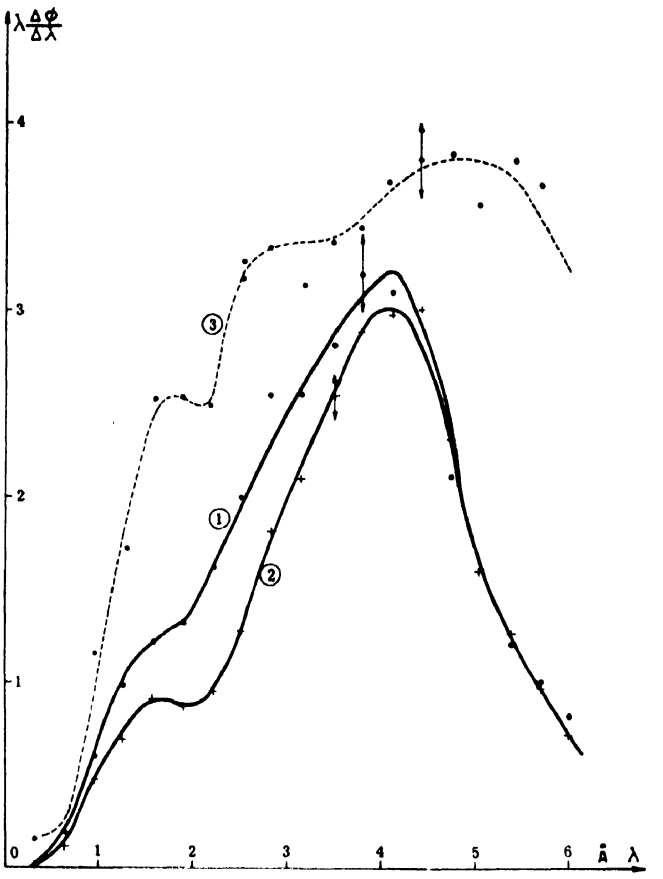

Figure 7. Scattering by D_2O

study was made of the spectrum of the neutrons coming out of successive layers of the box. Ideally, these layers should be some 2 mm thick and of the same height. The intensity is not sufficient for this purpose. Accordingly, 10 mm thick layers, 14 mm high, were defined. This led to the estimate that some ten mean free paths were needed in order to arrive at a near Maxwellian spectrum corresponding to 320°K. These measurements will be made more accurate by reducing the thickness of the layers and the height of water.

Some measurements were carried out with a lower initial temperature, about 11°K, and others with cadmium or indium filtered incident neutrons.

The measurements made with various hydrogen containing substances, such as paraffin, plexiglass and polystyrene, also give, for 6-cm thick samples, approximately Maxwellian spectra.

The Case of D_2O

Curves 1 and 2, of Fig. 7 show the spectra obtained with D_2O samples numbers 1 and 2 (98.4%). The incident spectrum was the same as that used for H_2O. The main feature of these curves is the existence of a very sharply defined peak toward the longer wavelengths. In all likelihood, one is dealing with Bragg-type scattering. In fact, the measurements taken with an incident spectrum having a much longer wavelength no longer give this peak (No. 3 curve). Measurements carried out with a better resolution give a 4.15 Å wavelength for this peak. It is difficult, with

heavy water, to carry out measurements on samples much larger than the neutron mean free path, since this would lead to the requirement for very large samples in order that the length of the neutron path may be well defined.

CONCLUSION

Measurements of the mean energy of neutrons scattered by hydrogen containing substances had been carried out earlier at Harwell by Egelstaff. Others had been made at Chalk River by Brockhouse, in which the scattered neutron spectrum was studied as a function of the angle for monokinetic neutrons having a wavelength of 1.4 Å. We feel that the work already carried out gives but a sketchy idea of the vast domain yet to be explored. We hope to clarify the analysis of H_2O and D_2O scattering, particularly by a study of scattering by liquids of simple structure.

REFERENCES

1. Galula, M., Jacrot, B. and Netter, F., *Journal de Phys. et Rad., 15,* 595 (1954).
2. Galula, M., and Netter, F., *Journal de Phys. et Rad., 16,* 233 (1955).
3. AECU 2040, *Neutron Cross Sections,* Supplement 3 (1954).

Record of Proceedings of Session 19A

THURSDAY MORNING, 19 AUGUST 1955

Chairman: Mr. A. de Shalit (Israel)
Vice-Chairman: Mr. B. Ferretti (Italy)
Scientific Secretaries: Messrs. J. Goedkoop and I. Ulehla

PROGRAMME

P/661 A study of neutron diffusion in beryllium, graphite and water by the impulse method ..... A. V. Antonov *et al.*

P/662 The study of beryllium as a neutron moderator ..... L. A. Geraseva *et al.*

P/359 Measurements of the diffusion length of thermal neutrons in beryllium oxide ..... J. C. Koechlin *et al*

P/872 On the determination of diffusion and slowing down constants of ordinary water and beryllium oxide using a pulsed neutron source ..... R. Ramanna *et al*

DISCUSSION

P/360 Determination of the mean transfer free path of thermal neutrons by measurement of the complex diffusion length .... V. Raievski and J. Horowitz

P/789 Measurements on a subcritical reactor with a pulsed neutron source ..... N. G. Sjöstrand

P/933 Determination of neutron capture to fission ratio in various uranium samples ..... T. J. Barendregt and M. Bustraan

DISCUSSION

P/597 Status of experimental and theoretical information on neutron slowing down distributions in hydrogenous media ... J. E. Wilkins *et al.*

P/357 Time of flight spectrometry equipment for slow neutrons in use at the Saclay reactor—its application to a study of the inelastic scattering of cold neutrons ..... B. Jacrot *et al.*

DISCUSSION

Mr. J. G. MOROTOV (USSR) presented paper P/662.

Mr. F. L. SHAPIRO (USSR) presented paper P/661 and added the following remarks:

Let us examine the question of the constant C in more detail.

The value of C is determined by the rate of energy exchange between a thermal neutron and the medium and by the dependence of the diffusion coefficient on the neutron energy. Knowing C and making certain assumptions, we can evaluate the rate of energy exchange. Following von Dardel, but refining his approach to some extent, we can write the following expression for the variation of the neutron temperature with time:

$$-\frac{3}{2}kT\frac{dT}{dt} = \left(\bar{E}_{en}' - \frac{3}{2}kT\right)D\Omega + \frac{3}{2}k\gamma(T - T_0)$$

Here T is the absolute temperature of the neutron gas, the spectrum of which is assumed to be Maxwellian, and T_0 is the absolute temperature of the medium. The first term characterizes the "diffusion cooling." $D\Omega$ is the portion of neutrons escaping to the outside per unit time. $\bar{E}_{en}$ is the mean energy carried off by one neutron. If the transport path λ_t is assumed independent of the energy, $\bar{E}_{en} = 2kT$.

In the general case, we can set

$$\bar{E}_{en} - 3/2\ kT = P \cdot 1/2\ kT$$

The second term takes into account the energy transfer to the medium, which transfer is assumed to be proportional to the temperature difference between the neutron gas and the medium. We can readily solve for the stationary state $dT/dt = 0$, particularly since it may be assumed in this case that $(T - T_0) \ll T_0$. In seeking the solution, it should be borne in mind that D depends on T, inasmuch as $D = \lambda V/3$, while $\bar{V} \approx \sqrt{T}$. We find

$$D = D_0 - C\Omega$$

where

$$C = P\left(1 + 2\frac{d\ln\bar{\lambda}}{d\ln T}\right)\frac{\bar{\bar{K}}D_0^2}{4\gamma}$$

But this is the same C we discussed above. Thus, from a measured value for C, we can obtain the coefficient γ, which may be termed the coefficient of heat transfer from the neutron gas to the medium. In the investigation covered by paper P/661, this coefficient was evaluated for the case of water. It is important in such cases to take account of the dependence of λ_{tr} on the neutron velocity. The product of P by the term in the parentheses has a value of approximately 3 for water, whereas with λ_{tr} = constant, it equals 1. Evaluation yields a value of γ in line (within the limits of the rather large experimental error) with simple assumption that, where energy exchange with

thermal neutrons is concerned, water is equivalent to a monoatomic gas with an atomic weight of 18.

So much for paper P/661; I shall now give a brief résumé of some supplementary results on graphite obtained by A. V. Antonov, A. A. Bergman, A. I. Isakov, I. D. Murin and B. A. Neupokoev.

In order to verify the relationship between T and t and to determine the parameters θ and γ, the investigators measured the variation of the neutron temperature with the time interval after the neutron burst. The quantity measured was the coefficient of transmission of a silver filter for a collimated neutron beam from the graphite box. The set-up described in paper P/661 was used for the measurements. The resultant curves are shown in Slide 1. The lower curve is for a 40 × 40 × 20 cm box; the middle curve is for a 180 × 140 × 120 cm box; the top curve is for a box of the same dimensions but containing natural uranium in the amount of about 0.013 atoms of uranium per atom of carbon. The same curves redrawn in a semi-logarithmic coordinates are shown in Slide 2. It will be seen that from 160 μsec after the neutron burst, the variation is exponential. In the range of shorter intervals the variation is in accord with the age theory of slowing-down, if the time of flight of the neutrons to the detector is taken into account. Processing of the results, taking into account the energy dependence of the scattering length and other corrective factors, yielded the data listed in Columns 2 and 4 of the following table:

Box	*180 × 140 × 120 cm*		*40 × 40 × 20 cm*	
1	*2*	*3*	*4*	*5*
Equilibrium T, °K	320 ± 30	295 ± 10	255 ± 50	225 ± 15
θ (μsec)	209 ± 30	191 ± 35	154 ± 65	145 ± 25
Mean transfer of energy in one collision, %	4.7 ± 0.7	5.1 ± 1.0	5.2 ± 1.7	5.9 ± 1.5

Columns 3 and 5 show the results of computations by the method I described earlier, using the value of the constant C from paper P/661. For graphite one can assume

$$p \approx 1 \quad \text{and} \quad \left(1 + 2\frac{d \ln \lambda + 2}{d \ln T}\right) \approx 0.94$$

As will be seen the results of the two methods are in satisfactory agreement. The values of θ for the large and small boxes differ somewhat; this is explained by different rates of neutron leakage. This difference can be taken into account by a more precise method of calculation, which I shall not discuss here.

It follows from the measurements made that in the energy region $E < 0.1$, the energy exchange between the neutrons and the graphite is about one third that for the theoretical case of a monoatomic gas with an atomic weight of 12.

Mr. MARTELLY (France) presented paper P/359 as follows: This paper is a joint presentation of India and France.

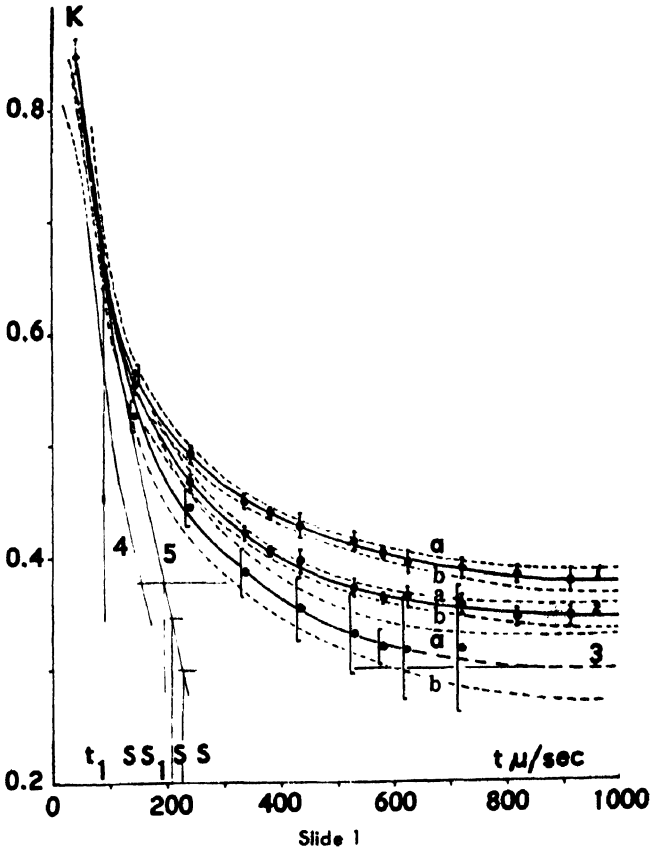

Slide 1

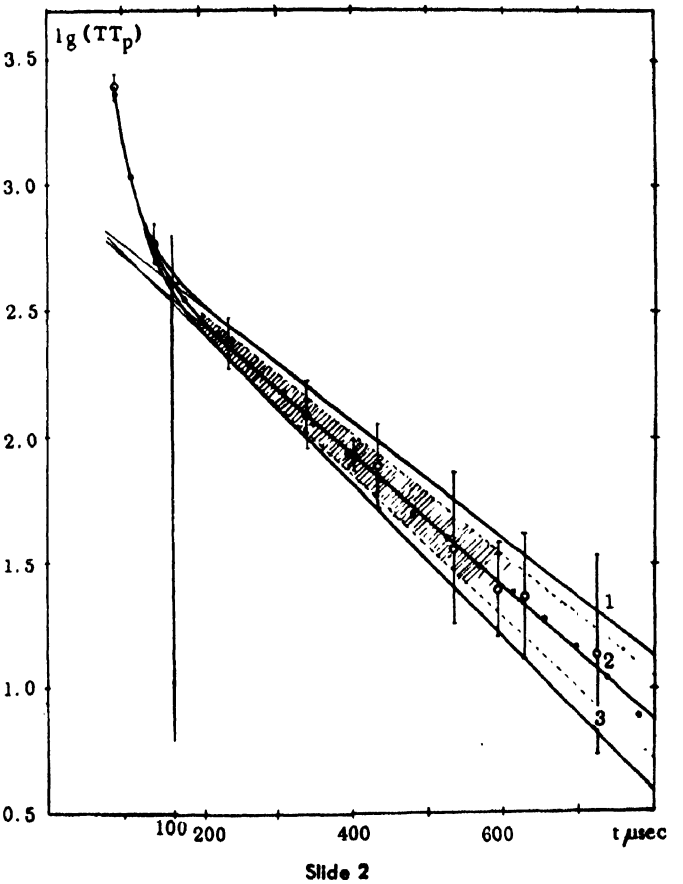

Slide 2

The diffusion length in beryllium oxide was measured by the classical exponential experiment method, the neutron source used being the thermal column of the Saclay reactor, limited by suitable neutron filters. The experimental medium was a box of square cross section—1 m × 1 m in the *OX-OY* axial plane and 0.90 m deep, along the *OZ* axis. The neutrons entered along the *OZ* axis. A graphite prism measuring 1 m × 1 m along the *OX* and *OY* axes and 0.60 m along the *OZ* axis was located between the neutron source (i.e., the thermal column) and the experimental medium.

The neutron density was surveyed by means of manganese detectors placed in 36 channels parallel to the *OX* axis. Measurements were made in seven planes spaced 10 cm apart.

The diffusion length in the beryllium oxide mass, which had a mean density of 2.92, was found to be equal to $L = 32.7 \pm 0.5$ cm. The density of the beryllium is 2.95.

A point to which I should like to call your attention is the small difference between the experimentally determined neutron distribution and the distribution predicted by elementary theory. This difference was brought to light through the great number of measurement planes used. Generally speaking, the measured density is relatively higher in the regions bordering on the sides of the box, i.e., in the regions of low neutron density.

The distribution along the *OX* and *OY* axes cannot be fitted to a cosine curve unless we assume an extrapolation length of 1.7 cm which is appreciably greater than that predicted by transport theory if we set $0.71\lambda = 1.1$ cm, in accordance with currently accepted data. Analysis indicates that this divergence cannot be attributed to higher harmonics.

Along the *OZ* axis the distribution of the fundamental term in the Fourier series diverges systematically from the hyperbolic sine function. This shows up in the curve of the logarithm of the ratio $P/\sinh \gamma(z + e)$ as a function of z (e is the extrapolation length).

If the theory is correct, there should exist a pair of values of γ and e which make this ratio constant. We tried three values of γ: 5.30 m^{-1}, 5.26 m^{-1} and 5.22 m^{-1}. We also tried two values of e: $e = 1.7$ cm and $e = 3.0$ cm. The value of e does not change the results much because it affects only the very last measurements and if we assume the most likely value of 1.1 cm, the difference is even greater. There is no value of gamma for which the curve is rectified; we adopted $\gamma = 32.7$. The disagreement is evidenced by an excess neutron density, far from the neutron source, amounting to as much as 3 per cent in relative value.

As for the distribution along the *OX* and *OY* axes, if we consider the normal distribution to be given by a sin function vanishing at an extrapolation distance of 1.1 cm beyond the sides of the box, we find that the actual distribution diverges from it by an amount which can be represented by curves of the same type as those for the divergence as a function of z, with amplitudes of the same order of magnitude.

The results of a series of additional experiments have lead us to reject the following suggested explanations for the discrepancies: perturbation of the measurements by the channels serving for introduction of the detectors; a photoneutron effect; and the effect of fast neutrons scattered by surrounding objects and entering the medium box though its lateral sides. We have reason to doubt the validity of the differential equation for the propagation of thermal neutrons:

$$\nabla_\rho^2 = \frac{1}{L^2}\rho$$

We feel that the explanation must be sought in the complexity of the thermal group: the capture free path and, to an even greater extent, the transport free path vary with the neutron energy, the latter increasing rapidly at low energies below the limit of the Bragg reflection.

The crystal medium, scattering the neutrons, produces a filtering effect as a result of which the neutrons having a greater scattering power show up farther from the source, i.e., in the regions near the sides of the box.

Under these conditions it is pertinent to ask how the diffusion length should be defined. The exponential experiment measures the length entering into the differential propagation equation. But this differential equation itself is questionable. We, therefore, propose a more general definition:

$$L^2 = \tfrac{1}{6}\bar{r}^2$$

where L is the diffusion length and $\bar{r}^2$ is the mean square of the distance traversed by the thermal neutrons from their source to their capture. In the hypothetical case of an experiment with an infinite plane source in an infinite medium the magnitude of L will be given by $L^2 = \tfrac{1}{2}\bar{z}^2$.

The exponential experiment differs from the ideal case in that the dimensions are finite. In both cases theory introduces an exponential distribution in z with relaxation lengths which are not markedly different (20 cm in one case and 35 cm in the other).

In the case of an infinite medium, the distribution curve will at first coincide with an exponential function and then diverge gradually.

In transposing the results obtained in the exponential experiment to the ideal case of an infinite medium, one can roughly evaluate the influence of this correction on the calculation of $\bar{z}^2$, and I believe that this evaluation will be pessimistic.

One can deduce $\bar{z}^2$ either from the initial exponential law or from the corrected distribution.

We have computed that these two different procedures lead to results differing by 2–3 per cent for $\bar{z}^2$, whence we have a difference of 1 to 1.5 per cent for L.

This difference corresponds to the margin of error we have quoted for our results.

Mr. RAMANNA (India) presented paper P/872 as follows: The method of determining diffusion and slowing down constants has already been described by the Soviet workers, and I shall not go into detail

and repeat what has been said. I shall concentrate on some of the differences and on the different approach which we made to the same problem.

I shall summarize the theoretical points concerning this method. The general equation for the time dependant source on the age theory is given by:

$$L^2\nabla^2\rho_s(r,t) - \rho_s(r,t) + \tau_{cs}\exp\left[\tau_0\nabla^2 - \tau_y\frac{\partial}{\partial t}\right]S(r,t) = \tau_c\frac{\partial}{\partial t}\rho_s(r,t)$$

The resolvent operator form was first given by Salvetti and Galoni, but it contains only the space dependent part. Here the operator contains a time dependent term $\tau_{cf}\partial/\partial f$ also. We have put this in. This does not change the decay constants but wherever t appears, it is changed into $(t - \tau_{cf})$. It also makes an important change in some other aspect with which I shall deal later.

On the two-group theory the equations become:

$$L_f^2\nabla^2\rho_f(r,t) - \rho_f(r,t) + \tau_{cf}S(r,t) = \tau_{cf}\frac{\partial}{\partial t}\rho_f(r,t)$$

$$L_s^2\nabla^2\rho_s(r,t) - \rho_s(r,t) + \frac{\tau_{cs}}{\tau_{cf}}\rho_f(r,t) = \tau_{cs}\frac{\partial}{\partial t}\rho_s(r,t)$$

where subscript f denotes "fast" group and s denotes "slow" group.

The method of obtaining D, T_c and hence L from the above solutions is described by von Dardel and others. I should like to point out that it is also possible to measure the age to thermal neutrons directly without the use of resonance detectors like indium etc. If the fast neutron source term is kept constant, by comparing the amplitude terms for various bucklings T_0 can be directly measured. Here the correction due to the finite time of the decay of fast neutrons becomes important.

We tried this only as a possibility, and I do not say that our results are final. Experiments are still in progress on this point.

I shall now deal with certain experimental arrangements which are different from those of previous workers. For our neutron source, we employed a generator using the (D-Be) reaction. We operated the generator at 900 kv with a steady current capacity of 300 microamperes to get as many neutrons as possible. The pulse width was 30 microseconds and the repetition frequency was up to 600 per second.

As regards the detector, the thermal neutrons were detected by means of a lithium-iodide scintillation counter. We were fortunate in using LiI because then we could have a point detector, as it was only a 1 cm cube. The source is actually dependent on the width of the beam of the neutrons falling on the beryllium. That must be quite small because it is focussed to a point.

I shall say a few words about our time-analyzer, not because it is one of the wonderful things which have been described by previous speakers at this Conference, but because it can be built very simply and one can get on with the results. It merely consists of an oscilloscope. The principle of this method is to make the deuteron ion pulse at the accelerator target initiate the time base of the oscilloscope and allow the thermal neutron pulses to intensify the oscilloscope spot. These spots are observed by a series of 20 photomultipliers on to which the oscilloscope trace is magnified and focussed by means of a simple optical system. There are certain corrections which have to be applied for purposes of calibration, but I do not have the time to deal with that now.

Slide 3 (Fig. 7 of P/872) is a block diagram of the experimental arrangement which we used. The diagram is not according to scale but is just schematic. This is the crystal and here is the target, which is covered with cadmium. The deuteron beam is taken directly as an initiator for the time base. For beryllium oxide it is practically the same arrangement, but the source is at the top and the detector at the bottom. The cadmium is placed below the photomultipliers, so as not to be too near the crystal.

In the case of ordinary water, we used a cylindrical tank of aluminium of diameter 77 cm and depth 40 cm filled with distilled water. The sides and bottom of the tank were lined with cadmium to absorb thermal neutrons.

Slide 4 (Fig. 2 of P/872) is the distribution given by the age theory for a given set of constants. The dotted line is given by the two-group theory. The interesting thing about this, although you cannot see it on the slide, is that there is no point at which the age theory shows a straight-line character, but in the two-group expression with water, in which the fast neutron lifetime is very small and the diffusion length is very much longer than slowing-down length—and we get a straight-line character between 150 msec and 500 msec to within 1%. These are the experimental points we plotted and you find that in this region it follows a straight line; it does not follow exactly the same slope as the two-group theory—in fact, the slope is less. The mean slope in the time limit between 200 and 500 msec given by the age theory is 0.00415 whereas in the two-group theory it is 0.003592 and the experimental slope is about 0.003386. I would like to stress the fact that in fitting the water data we have so many parameters that we can do exactly what we want. This is not meant to measure slowing-down length, but just to show the trend of the characteristics of these curves. You find in the case of a straight line given by the two-group theory that it falls off towards the end, and so do the experimental points.

Another thing one can see after closer analysis, although it is not clear on this slide, is that the region of straight-line dependence is less than predicted by theory. We therefore thought that a multi-group process would probably give a much better fit but we did not attempt it because it is a somewhat arbitrary procedure as we have to assume too many of the constants for slowing down.

Now I come to the last case of beryllium oxide. The material was very kindly given to us by the Commissariat à l'Energie Atomique de France and I

must congratulate them on the fine bricks they are producing. The material was available in the form of rectangular bricks 10 cm × 10 cm × 5 cm and the mean density was 2.96 gm/cm³. The impurities as specified by the manufacturers were less than 725 ppm of iron equivalent by weight. The bricks were arranged in a rectangular pile and the source and detector were placed on opposite sides of the pile. In order to eliminate the effect of thermal neutrons reflected from the walls of the room, the moderator assembly was covered on all sides except on the side facing the detector by a cadmium sheet of 1 mm thickness. A sheet of cadmium was placed below the photomultiplier to stop neutrons reflected from the floor.

It is essential to perform the experiment under conditions such that the effect of the higher harmonics is negligible and only the fundamental mode of decay is important. By calculations made from existing values for the moderator constants, and by making some trials, it was found that the best sizes to work with were about 35 cm³. The higher harmonics die down very rapidly with time, and it was found that in the period between 500 and 1000 microseconds only the fundamental mode is excited. This was verified by putting the detector at the bottom as well as at the side and getting the same decay constant. If the sizes of the assemblies are very much reduced it is found that the counting rates become very low and the wall reflection effects of fast neutrons due to the large leakage become quite appreciable.

The calculation of bucklings involves a proper choice of the extrapolation length, and since our results yield a value of D and hence λ_t an approximate value of X_I was first assumed and the final value obtained by a process of successive approximations.

In Slide 5 (Fig. 3 of P/872) we have plotted buckling against the various slopes obtained and we have these five points. We cannot work on this side because of the higher harmonics. It is true we have plotted a straight line whereas we should have plotted a parabola. At the time this paper was ready the only information on BeO in print was an American document, of which unfortunately no details were available. In this document the diffusion length is given as 30 cm for a density of 2.8. If we draw a straight line through the points we have obtained we get a value which agrees with this within statistical error, and also gives a value of ∂_0 for BeO as 8.3 mb. From this we conclude that the diffusion cooling constant was small for the sizes which we were using. However, until an experiment is carried out to specifically measure the cooling constant we cannot say anything definite. It is possible to make theoretical calculations, but I would not venture to do this as this would be somewhat arbitrary. I would like to point out that the value obtained in the previous paper for the diffusion length is very much more and the only discrepancy I can think of in this experiment as compared with theirs might be caused by our having neglected the diffusion cooling constant; but it seems that our value will be increased to that extent.

It is also possible that if one uses a pile spectrum of neutron the value comes out larger.

My last point concerns the question of age. As I pointed out earlier, we have obtained a certain value which is not inconsistent at all, but I would like to add now that in my discussions with Mr. Horowitz of France yesterday, he said that there might be a discrepancy because of the effect of the higher harmonics in the neutron distribution. However, I could probably make a calculation and show him that this would be very small. I would like to add that if one makes a correction for the age due to the finite lifetime of the fast neutrons the value becomes 164 cm² instead of 156 cm² given in the earlier version of the paper.

Our thanks are due to the Commissariat à l'Energie Atomique for the BeO bricks which were made in France under the General Agreement between the Commissariat and the Indian Atomic Energy Commission, for the study of beryllium as a moderator.

DISCUSSION OF P/662, P/661, P/359 AND P/872

Mr. SANDERS (UK): I would just like to make a short remark about the effect of fast neutron reactions in beryllium which I think has to be taken into account when considering beryllium as a moderator for a nuclear reactor.

There are two important fast neutron reactions in beryllium for a fission neutron source: the $Be^8(n,\alpha)$ reaction and the $Be^9(n,2n)$ reaction. The $Be^8(n,\alpha)$ reaction is a sink of fast neutrons, while the $(n,2n)$ reaction serves as a source of fast neutrons. The thresholds of the reactions are 0.6 Mev and 1.8 Mev respectively. Now, when fission neutrons are slowed down past the 0.6 Mev threshold there will be a net gain or net loss of neutrons, depending upon the relative magnitudes of the (n,α) and the $(n,2n)$ cross sections, and from the data that we have so far obtained it does seem that there will be a net gain of something between 5 and 10 per cent in the number of neutrons due to the competition of these two reactions. We are doing more experiments on this problem and we shall be very interested to hear if any other workers in this field have made similar calculations or measurements.

Mr. RADKOWSKY (USA): I note that in paper P/661 on methods of measuring diffusion lengths and their integral qualities the orators expressed some surprise at the increase in diffusion length of the water with temperature. I did some work at Argonne some time ago which has been reported in paper P/603 by Mr. Chernick, in which this fact could be explained by the change in the scattering area of the neutrons, and in fact by a simple model it is possible to get very good agreement with the experimental results.

Mr. MARTELLY (France): I refer to the disagreement between the experimental results obtained by Mr. Ramanna and by ourselves, concerning the diffusion length of beryllium oxide. If I am not mistaken, with the method used by Mr. Ramanna, the relative error in L^2 is greater than the relative error in the

magnitude T_e for the mean life of neutrons in an infinite medium.

I would like to ask Mr. Ramanna whether he thinks that the extrapolation of the results for the determination of T_e allows of the 2 per cent accuracy required to obtain an accuracy of 2 per cent for L^2, i.e., an accuracy of 1 per cent for L, the diffusion length.

Mr. RAMANNA (India): The errors in my paper are statistical errors and there is no mention of any systematic errors because this is not possible. As I say, the error in question is a statistical error and if you just multiply OC into D and take the square root you have the error that is given in the diffusion length, which is also a statistical error of 0.1 per cent.

Mr. V. RAIEVSKI (France) presented paper P/360.

Mr. N. G. SJÖSTRAND (Sweden) presented paper P/789.

Mr. T. J. BARENDREGT (Netherlands) presented paper P/933.

DISCUSSION OF P/360, P/789, P/933

Mr. RAIEVSKI (France): Mr. Sjöstrand took measurements at different points and has told us that they gave similar results to an accuracy of plus or minus 4 per cent. Now the effect from the harmonics which are aroused in a device of this nature is precisely of this order of magnitude. I should like to know whether Mr. Sjöstrand considers the measurements sufficiently accurate to support the contention that the deviations observed are really independent of the position of the detectors.

Mr. SJÖSTRAND (Sweden): I do not think that my measurement shows that the result is quite independent of the harmonic modes, but it does show another thing. It is sometimes assumed that one should find a longer time constant with the detector placed in the reflector. I think that the fact that this is not so is proved by my measurement.

Mr. SHAPIRO (USSR): I shall report on an investigation in which the pulse method was used for the study of neutron multiplication systems in a somewhat different way from that described by Mr. Sjöstrand. The work was carried out by A. B. Antonov, A. A. Bergman, A. I. Isakov, I. D. Murin and B. A. Neupokoev.

The measurements were carried out with the heterogeneous, uranium-graphite prism shown in Slide 6. The set-up used was the one described in paper P/661. Proceeding from the single velocity theory of diffusion and Fermi's age theory, it can be shown that if such a prism is exposed to a burst of neutrons the falling off of the neutron density in the prism over a sufficiently long time will be exponential:

$$n(t) = Ae^{-\alpha t}$$

$$\alpha = D\Omega + \frac{1}{T} - \frac{Ke^{-\Omega\tau}}{T} e^{\alpha S}$$

where K is the neutron multiplication factor in an infinite system, D is the thermal neutron diffusion coefficient, T is the neutron lifetime in an infinite medium, S is the slowing-down time of the neutrons to thermal energies, and Ω is the minimum eigenvalue of the Laplacian operator for a prism of the given size.

The values of α were determined from curves of the attenuation of the neutron density with time.

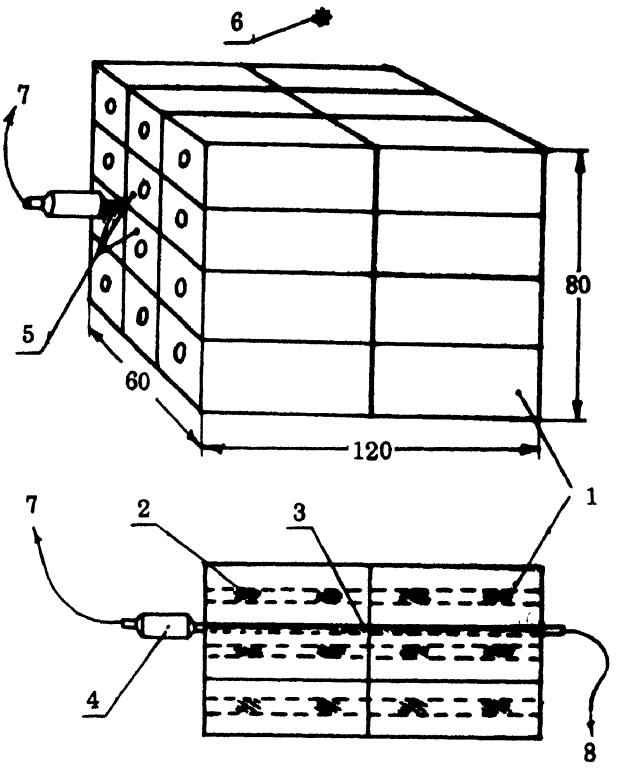

Slide 6

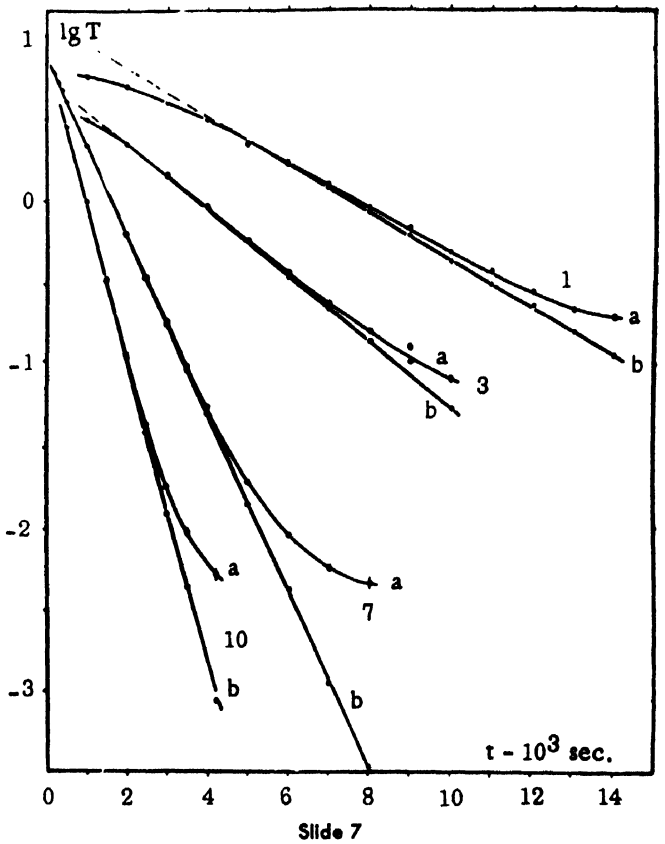

Slide 7

Measurements were made using prisms of ten different sizes (from 200 × 180 × 180 to 60 × 60 × 60 cm) and with two concentrations of uranium: $C_1 = 0.0132$ U-atoms/C-atom and $C_{1/3} = 0.0044$ U-atoms/C-atom.

The attenuation curves are shown in Slide 7, from which it may be seen that the decrease in neutron density departs from the exponential curve at high temperatures. This apparent departure is due to the background of delayed neutrons (produced under the influence of both fast primary neutrons and thermal neutrons) and spontaneous fission neutrons. After the introduction of the appropriate corrections for these effects, the $n = n(t)$ curves become very nearly exponential in form.

The experimental curves for $\alpha = f(\Omega)$ are shown in paper P/661. The values of K, D and T for both concentrations were computed on the basis of the determined values of α by means of Equation 2 taking $\tau = 350$ cm^2 and $S = 150$ μsec. (The value of S was determined from auxiliary measurements.)

The values obtained proved to be close to the values of the corresponding parameters determined by exponential methods in the investigation reported on at the July session of the Academy of Sciences of the USSR.

The differences in the values of K did not exceed 2 per cent, while the disagreement in the case of D and T was under 10–20%. It may be assumed that these small disagreements are at least partially due to the inadequate accuracy of the theoretical analysis of the problem. Specifically, the analytic procedure employed failed to take into account such factors as the dependence of the mean energy of the neutrons in the prism on the size of the prism. This size-dependence is due primarily to the constant presence of partially slowed-down neutrons in the systems.

A more detailed analysis of the problem is now under way.

The advantages of the pulsed method in question as compared with the exponential method are that the system can be of smaller size and that the constants D and T can be determined.

Mr. J. E. WILKINS (USA) presented paper P/597.

Mr. B. JACROT (France) presented paper P/357.

Session 20A

RESONANCE INTEGRALS; FISSION PRODUCT POISONING; CRITICALITY OF SOLUTIONS

LIST OF PAPERS

		Page
P/659	Measurements of the resonance absorption integrals for various materials and ν_{eff}—the multiplication coefficient of resonance neutrons for fissionable isotopes.....P. E. Spivak *et al.*	91
P/833	Resonance capture integrals.....R. L. Macklin and H. S. Pomerance	96
P/427	Studies on the neutron resonance absorption of U^{238}.....V. S. Crocker	102
P/883	Measurements of the effective resonance integral of uranium with the pile-oscillator.....V. O. Eriksen *et al.*	105
P/948	Computation of the effective resonance integral.....E. F. M. Van der Held	107
P/5	Experiments on some characteristics of the NRX reactor. Part I—Methods and prolonged fuel irradiation.....D. G. Hurst	111
P/6	Experiments on some characteristics of the NRX reactor. Part II—Temperature and transient poison effects.....A. G. Ward	119
P/835	Reactivity changes and reactivity lifetimes of fixed-fuel elements in thermal reactors.....B. I. Spinrad *et al.*	125
P/432	Long term reactivity changes in natural uranium reactors.....D. J. Littler	141
P/834	Small thermal homogeneous critical assemblies.....A. D. Callihan *et al.*	145
P/428	Plutonium-water critical assemblies.....C. L. Horton and J. D. McCullen	156
P/602	The critical assembly—a nuclear design tool.....T. M. Snyder	162

Measurements of the Resonance Absorption Integrals for Various Materials and ν_{eff}—the Multiplication Coefficient of Resonance Neutrons for Fissionable Isotopes

By P. E. Spivak, B. G. Erozolimsky, V. I. Lavrenchik, and G. E. Dorofeyev, USSR

In order to design a nuclear reactor it is essential to know the constants which determine the neutron balance. Such constants are, in the first place the capture cross sections σ_c and fission cross sections σ_f, as well as the number of secondary fission neutrons emitted per captured neutron, ν_{eff}.

To determine these constants experimentally it is convenient to use a system of neutron detection, whose sensitivity does not depend on either the neutron energy or the angular distribution of the neutron flux at a given point.

By placing a sample of the substance to be investigated at this point we can determine from the detector readings the required characteristic of the sample material with respect to the given neutron spectrum. The sample must be thin in order that the effect of self-shielding of the sample should not influence the results of the measurement and the detector must measure small changes of the neutron flux.

At one of the beams of the RPT pile there was mounted in 1952 an experimental arrangement which had all of the required properties and which was designed for measuring both the resonance absorption integrals of various materials and the number of secondary neutrons emitted per captured resonance neutron for fissionable substances.

THE MEASURING APPARATUS

The diagram of the measuring arrangement is given in Fig. 1. The graphite cube is 190 cm on a side with an internal cubic cavity 50 cm on a side. The samples under investigation are placed in a special holder at the center of the cavity in the path of the neutron beam. The beam enters the cavity through a boron collimator. In the walls of the cube at a distance of 50 cm from the cavity and located uniformly around it are 12 proportional counters filled with BF_3 (enriched with B^{10}) pressurized to 500 mm Hg.

The measurement consists of determining the change of the total counting rate of all counters, which occurs when the sample to be investigated is placed in the cavity.

The size and shape of the neutron beam in the cavity are determined by a collimating arrangement. A steel cylinder 25 cm long with a central hole of 25 mm diameter is mounted in the experimental channel (this cylinder serves as the first collimator); in the front wall of the prism there is fixed an entrance collimator consisting of a tube 60 cm long with an outer diameter of 100 mm, having an 8 mm diameter tube fixed along its axis, the space between them being filled up with boron carbide.

The beam size near the center of the cavity depends to some extent on the neutron energy, since the effective length of the entrance collimator is different for neutrons of different energies. For thermal neutrons the collimator arrangement insures a beam diameter not exceeding 15 mm at the cavity center. For faster neutrons the collimation grows worse, however. Up to energies of the order of thousands of electron-volts the main part of the beam penetrates the cross section of samples, whose diameter equals 22 mm. Along the whole path from the outlet opening of the pile channel to the front wall of the prism the beam is surrounded by a paraffin-boron shielding which serves to reduce the detector background arising from scattered neutrons. For the same reason the front wall of the prism is covered with a paraffin-boron shield 15 cm thick.

The spectrum of the beam used for measurements was determined by cadmium or boron filters of various thickness, which were placed in the way of the beam in a special cassete. The high energy neutrons (above 100 kev), a considerable number of which are present in the pile beam, do not contribute to the total neutron interaction for the sample being investigated. These fast neutrons penetrate into detector system leads and decrease the resolution of the measurements. Therefore it has been proved expedient to reduce the intensity of this hardest part of the slowing down spectrum by placing an aluminum filter 40 cm thick deep in the pile channel. The effectiveness of the filter is based on the fact that the total cross section of aluminum for neutron energies of 100 kev to 2 Mev (about 4.5 barns) is three times larger than for energies under 10 kev. Such a filter causes a 5–10 fold attenuation of the hard portion of the spectrum. To get a pure thermal neutron beam a 40 cm long graphite rod was placed deep in the channel. As a result, the epi-cadmium flux made up several per cent of the total flux.

Original language: Russian.

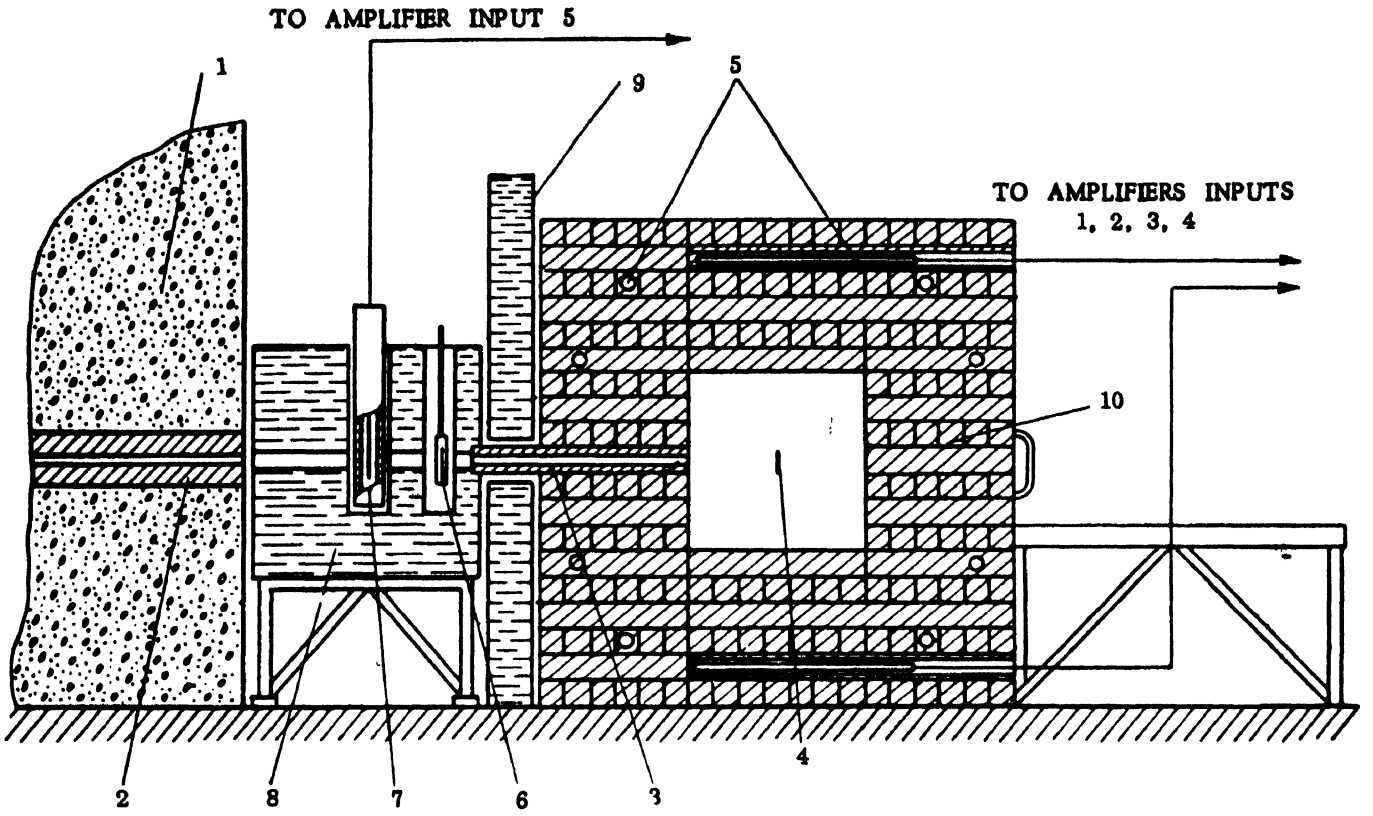

Figure 1. Schematic section of the measuring arrangement: (1) pile shielding; (2) first collimator (steel); (3) second inlet collimator (boron carbide); (4) investigated sample at the cavity center; (5) proportional boron counters (12 pieces); (6) cassete with filter; (7) fission chamber with U^{235} layer; (8) shield (paraffin-boron); (9) front wall shielding of the prism (paraffin-boron); (10) plug pulled out when replacing the sample

The pulses from all 12 counters are fed into four amplification channels by means of cathode-follower type preamplifiers mounted together with the counters; to each amplification channel three cathode followers are connected in parallel (Fig. 2).

Each amplification channel, using 6 ж 4 tubes has an amplification factor of about 2×10^4 with a four-fold negative feed-back including all the three stages. After being cut off by the diode discriminators which follow the amplifiers, the pulses enter a common pulse-shaping stage—the Schmidt circuit with a cathode follower, from the output of which they are fed into the scaling circuit with a total scaling factor 1:16,000. The resolving time of the detector system is 1 μsec, which permits counting up to 10^4 pulses per second without serious counting losses. The bias curve of the system— the dependence of the counting rate on the cut-off voltage of the discriminators—is shown in Fig. 3. In the working region it has a slope of 2% per 100 v. The small slope of the bias curve, the large negative feed-backs in the amplifiers, the stabilized power supply of the anodes and heaters of all the tubes—all these insure the stability of the detector system, permitting an accuracy in the measurements of the number of pulses to $\pm$(0.02–0.03%).

To eliminate the influence of reactor instability (the power is maintained constant within $\pm$0.5%) a fission ionization chamber with a layer of U^{235} is placed in the beam. The pulses from it are recorded by means of a similar amplifying and counting system. As a result, the number of pulses recorded by the boron counters is always referred to the same number of pulses of this control chamber.

The efficiency of the detector system is about 0.5% and the necessary number of pulses for getting the required statistical accuracy is gathered in a time not exceeding 10 minutes.

The insensitivity of the detector system with respect to neutron scattering in the sample was examined with the help of thick samples of scattering substances (graphite and bismuth). The absence of scattering due to the sample has been shown experimentally to be, within the limits of measurement accuracy, ($\pm$0.03%).

The independence of the detector system sensitivity on the neutron energy was examined with help of photoneutron sources of various energies. The numbers of neutrons emitted by these sources were compared in a special experimental arrangement to an accuracy of $\pm$1%. The counters in the prism were located in such a way that the sensitivity of the detector system was constant over the whole energy range investigated (up to several Mev).

It follows from the above that the change of the counting rate caused by placing the sample to be investigated into the cavity is rigorously related to the change in the number of neutrons in the cavity due to neutron absorption in the sample and, in case of a fissionable sample, to the emission of fission neutrons.

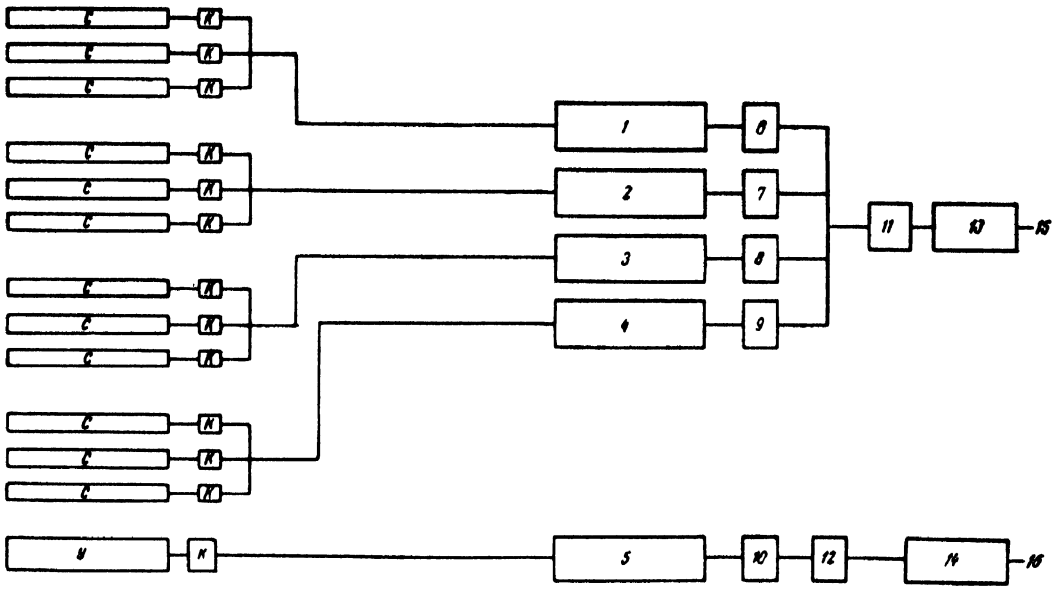

Figure 2. Block diagram of the electronic device: (C) counters; (K) cathode followers; (γ) fission chamber with uranium layer; (1,2,3,4,5) amplification channels; (6,7,8,9,10) diode discriminators; (11,12) stages of Schmidt circuit; (13,14) scaling circuits (1:16,000); (15,16) electromechanical registers

MEASUREMENT OF RESONANCE ABSORPTION INTEGRALS

When a sample of a non-fissionable substance is placed in the experimental cavity, the corresponding decrease of the counting rate ΔN_x can be expressed as follows:

$$\Delta N_x = N_x - N_0 = k \int f(E)(1 - e^{-n\sigma_x(E)})\, dE \quad (1)$$

where ΔN_x is the difference between the counting rates of the detector system: N_x in the presence of the sample and N_0 without the sample; $f(E)$ is the neutron flux in the energy interval from E to $E + dE$; $\sigma_x(E)$ is the neutron absorption cross section of the sample under investigation at the neutron energy E; n is the number of the absorber nuclei in the sample per 1 cm² of its cross section; and k is the efficiency of neutron detection (independent of energy).

The integration is performed over the energy spectrum of the neutrons in the beam.

If the beam is coming from the pile, and is cadmium filtered, one may assume $f(E) = F_0/E$ (F_0 is the normalization coefficient which is independent of neutron energy) and integrate between the limits 0.5 ev and 1 Mev. In the case of a thin sample, when $n\sigma(E) < 1$ over the whole neutron energy range, Equation 1 may be simplified as follows

$$\Delta N_x = kF_0 n \int_{0.5\,\text{ev}}^{\infty} \frac{\sigma_x(E)}{E}\, dE \quad (2)$$

Thus in this case the experimentally observed effect ΔN_x is proportional to the magnitude of the resonance absorption integral Σ_x of the given substance, since by definition

$$\Sigma_x = \int_{0.5\,\text{ev}}^{\infty} \frac{\sigma_x(E)}{E}\, dE \quad (3)$$

Carrying out these measurements for various substances including the substances with a known value of the resonance integral (e.g., with boron) we obtain the required values of the resonance absorption integrals for the investigated substances.

However, as has been mentioned, Equation 2 holds only in the case of the sample being sufficiently thin that $n\sigma_x(E) < 1$ for all E. Therefore the possibilities of this method depend to a large extent on the magnitude of the minimum effect $\Delta N_x/N_0$ which can be measured in the experimental equipment.

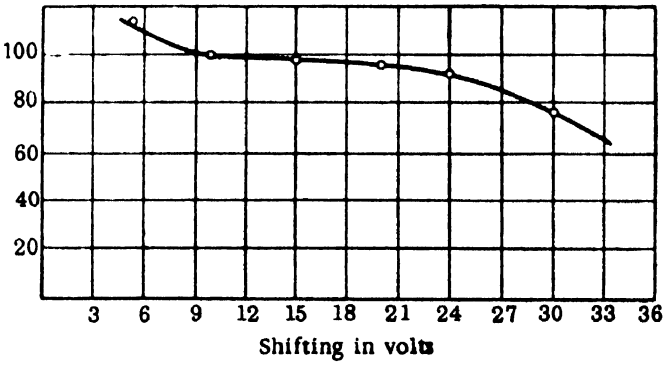

Figure 3. Bias curve of the indicator system

The quantity N_0—the counting rate in the absence of the absorbing sample—may be expressed for purposes of estimating in the following way:

$$N_0 = kF_0 \int_{E_{min}}^{E_{max}} \frac{dE}{E} \quad (4)$$

Performing the integration from $E_{min} = 0.5$ ev to $E_{max} = 10^6$ ev we obtain

$$N_0 \approx 15kF_0 \quad (5)$$

Using Equations 2, 3 and 5 we obtain finally:

$$\frac{\Delta N_x}{N_0} = \frac{n\Sigma_x}{15} = \frac{1}{15} n\sigma_{max} \frac{\Sigma_x}{\sigma_{max}} \quad (6)$$

where σ_{max} is the maximum absorption cross section in the whole energy range.

Setting $n\sigma_{max} = 1$ and taking into account that the sensitivity limit of the described measuring system is $\Delta N_{min}/N_0 \geq 0.03\%$, we get that the minimum values of the resonance integrals, measurable to an accuracy of 30% are:

$$\Sigma_{min} \geq 0.005\, \sigma_{max}$$

This limitation is not too hard to realize for most substances. When investigating a substance, for which the maximum cross-section values at the resonance are unknown, it is necessary to measure the effect ΔN_x from samples of various thickness in order to convince oneself of the absence of self-absorption.

On the other hand, the magnitude of the minimum measurable effect $\Delta N_x/N_0$ determines the limit for investigating weak absorbers. We cannot choose the thickness of a sample arbitrarily, since the scattering of the neutrons in the sample increases the mean path of the neutrons and thus affects the number of neutrons which are absorbed. Restricting ourselves to that thickness of the sample, for which $n\sigma_{scatt} \leq 0.3$ (then for any shape of sample the change of the mean path of the neutrons in going through the sample does not exceed 15%) and taking into account that the minimum allowable value $\Delta N_x/N_0$ is 0.03%, we obtain that the minimum absorption integral measurable to an accuracy of 30% is:

$$\Sigma_{min} \geq \tfrac{1}{20}\, \sigma_{scatt}$$

As an illustration of the possibilities of this method for investigating neutron resonance absorption, the results of measurement of resonance integrals for a number of elements are listed in Table 1. For some elements the results of the present work may be compared with the resonance activation integrals from other works.[1,2] The comparison shows that the resonance activation integrals (see Table 1) calculated from the data of the reference works 1 and 2, taking proper account of the relative abundance of particular isotopes, coincide within the limits of measurement accuracy, with the resonance absorption integrals obtained in the present work.

Table 1. Resonance Absorption Integrals for Some Elements

No.	Element	Results of the present work	Values of the resonance activation integrals computed from the data of references 1 and 2
1	Fe	2.3 ± 0.25	—
2	Cu	3.3 ± 0.3	3.35[1,2]
3	W	170 ± 20	—
4	Hg	73 ± 5	—
5	I	130 ± 18	119[1]
6	Sb	115 ± 12	138[1]
7	Nd	40 ± 6	—
8	Pr	7 ± 3	9.3[1]
9	La	5.5 ± 2	
10	Lu	720 ± 70	
11	Hf	2800 ± 600	

METHOD OF MEASURING ν_{eff} FOR FISSIONABLE SUBSTANCES

When placing the sample with the fissionable isotope into the prism the effect ΔN_1 of the change of the counting rate can be presented in the following form:

$$\Delta N_1 = -k_1 Q + k_2 Q \nu_{eff} \qquad (7)$$

Here Q is the neutron number of the primary spectrum absorbed by the sample per unit time; k_1 is the sensitivity of the detector with respect to neutrons of the primary spectrum; and k_2 is the sensitivity of the detector with respect to fission neutrons.

For determining ν_{eff} it is necessary to carry out a second measurement, the result of which would by the determination of a quantity containing Q and ν_{eff} in another combination. For this purpose a spherical filter of a paraffin-boron mixture having an entrance opening for the neutron beam is placed into the cavity of the prism. The filter is thick enough so that the sensitivity of the detection system to neutron absorption by a sample located inside the filter is negligible. Therefore, when a sample is placed inside the prism (within the filter) the change of the counting rate, ΔN_2, is given by

$$\Delta N_2 = k_3 Q \nu_{eff} \qquad (8)$$

where k_3 is the sensitivity of the detection system to fission neutrons in the presence of the spherical paraffin-boron filter in the cavity of the prism.

Denoting the ratio $\Delta N_1/\Delta N_2$ by x, we obtain finally:

$$\nu_{eff} = \frac{k_1}{k_2} \frac{1}{\left(1 - \frac{k_3}{k_2} x\right)} \qquad (9)$$

The coefficient k_3/k_2 may be measured easily by means of a thermal neutron converter. For such a converter one may use any sample of a fissionable substance, placed at the center of the prism across the beam of thermal neutrons and surrounded by cadmium from all sides, except for an entrance opening for the beam. The ratio of the effects from this sample in the presence of the spheric filter in the cavity and in the absence of it evidently equals the desired coefficient k_3/k_2.

To obtain the absolute value ν_{eff} it is necessary to determine the absolute value of the coefficient's ratio k_1/k_2 (which is very close to unity, since the sensitivity depends slightly on the neutron energy).

It is sufficient, however, to carry out the measurements of the relative variation of ν_{eff} in its dependence on the neutron spectrum of the beam and then normalize this dependence to the value of ν_{eff} for thermal neutrons. For this purpose the measurements of the effects ΔN_1 and ΔN_2 are carried out with various beam filters (cadmium or boron carbide of several thicknesses) and also for the case of the thermal neutron beam. For obtaining the variation in the dependence of ν_{eff} on the neutron spectrum from the data for the x-value variation it is necessary to determine only the

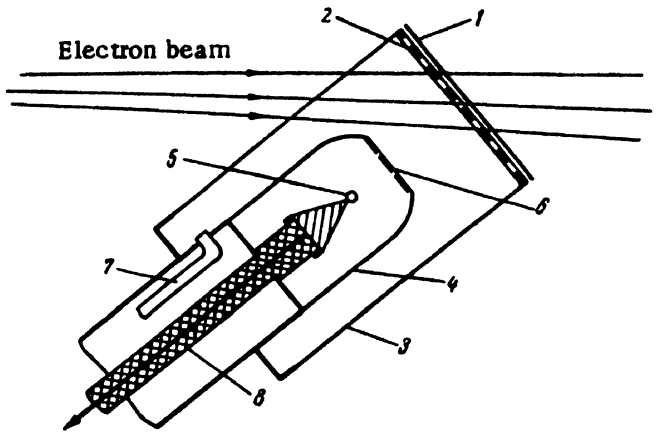

Figure 4. Construction of the proportional counter and its position relative to the neutron beam: (1) target; (2) aluminum cap with holes, covered with mica 1.2 mg/cm² thick; (3) counter body; (4) counter cathode; (5) counter anode (sphere 0.16 mm); (6) wire-net covered with thin collodium film; (7) copper tube for connection to the ballast gas volume (90% A + 10% methylalcohol at 30 mm Hg pressure); (8) insulator

exact variation of the coefficient k_1/k_2 or simply k_1 (since k_2 does not depend on the primary neutrons' energy).

The dependence of the coefficient k_1 on the neutron spectrum was determined in the following way. For all the neutron spectra, for which measurements with fissionable samples were performed, measurements were also carried out with a sample of boron carbide. The effect of the change of the counting rate caused by introducing the boron sample, ΔN_B is given by

$$\Delta N_B = -k_1 Q_B \qquad (10)$$

where Q_B is the number of neutrons absorbed by the boron sample per unit time.

A thin target of LiF was then set in the same place. The α-particles and the H^3-nuclei arising as a result of neutron capture by Li^6 hit the window of the proportional counter which is covered with a thin foil (Fig. 4). The number of counter pulses N_{Li} is proportional to the number q_{Li} of the neutrons absorbed in the thin LiF layer. Since the lithium target and the boron sample are set into the same place, and the capture cross sections of lithium and of boron depend similarly on the neutron energy, q_{Li} is proportional to Q_B. Therefore, the ratio $\Delta N_B/N_{Li}$ is a quantity, which is proportional to the coefficient k_1. The set of $\Delta N_B/N_{Li}$ values, measured for different neutron spectra, gives the required variation of the coefficient k_1. These measurements have shown that with appropriate placement of the counters the efficiency k_1 of the detecting device for the neutrons passing through the thickest of the filters used does not differ from the efficiency for thermal neutrons within the experimental error ($\pm 1\%$).

Having available data the variation of the coefficient k_1 and the value k_3/k_2, the variation of ν_{eff} of the sample of fissionable material can be inferred from the results of the measurements of the ratio X for different neutron spectra.

It should be said in conclusion that the experimental apparatus described has been used to measure the effective number of secondary fission neutrons from various substances for resonance neutrons and for neutrons with higher energies, obtained from the photoneutron sources.

Due to the high degree of stability of the measuring system which make it possible to carry out measurements of very small effects with high accuracy it has been possible to apply the described technique of investigation of the effective number of the secondary fission neutrons over a wide energy range up to 10^6 electron-volts.

REFERENCES

1. Harris, R. P., Muehlhause, C. O. and Thomas, D. E., Phys. Rev., *79*, 11 (1950).
2. Lichtenberger, H. V., Nobles, R., Monk, J. D., Kubitschek, K. and Dancoff, S. M., Phys. Rev., *72*, 164 (1947).

Resonance Capture Integrals

By R. L. Macklin and H. S. Pomerance,* USA

In the calculation of thermal neutron reactors, it is often convenient to consider the neutrons above thermal energies as a single group. It is then important to know the effective cross sections of many nuclei for the neutrons of this group. As the neutron flux distribution varies as the reciprocal of the neutron energy, a resonance integral is defined as $\int\sigma(E)\,dE/E$ for this purpose, with cross section σ and neutron energy E. The limits of the integral are some convenient energy above the Maxwellian thermal neutron energies (usually 0.4 ev, approximated by a cadmium absorber, though gadolinium at 0.2 ev or other absorbers may be used) and some high energy, such as 1 Mev, approximating the primary fission neutron energies.

For nuclei having only a $1/v$ (reciprocal neutron velocity) cross-section dependence over the limits of the integral (boron capture is the best known example) the integration can be carried out explicitly, and is just twice the difference in cross section at the lower and upper limits. For the usual cadmium absorber, this is equivalent to 0.44 times the thermal neutron cross section.

When there are also separate neutron resonances the contribution of each to the resonance integral can be computed from the Breit-Wigner formula and is very nearly $\pi\sigma_0\Gamma_\gamma/2E_0$ for resonances above a few ev. At lower energies the $1/v$ dependence and finite lower limit of the integral introduce small corrections.

It is usually assumed that any resonance integral can be separated into a sum of contributions from separate resonances and a single $1/v$ component. The effect of the $1/v$ component is separately computed from the thermal cross section. In a few cases resonances near or below one ev strongly influence the thermal cross section and prohibit the separation into a resonance and a non-resonance contribution.

Neutron resonance parameters have now been measured for many materials and provide estimates of the resonance integrals. The resolving power of the apparatus (principally neutron time-of-flight detectors) is generally proportional to $1/v$, leaving many resonances above a few hundred ev unresolved. While the effect of the higher energy unresolved resonances can be obtained from the average widths and spacings of the known resonances in many cases, the most accurate values are obtained for materials whose chief resonance integral contribution comes from a single level at low enough energy for good resolution.

Dresner has investigated the estimation of resonance capture integrals from measured average resonance parameters. Two cases must be distinguished: (*a*) the resonance is due to the cumulative effect of many separate resonances; for example, Th^{232}, U^{238}, I^{127}; (*b*) the resonance integral is primarily from a single large resonance; for example, Ag^{109}, In^{115}, Au^{197}. In the first case the resonance integral can be expressed in terms of a statistical average over many resonances, viz.

$$\int_{E_1}^{\infty}\sigma_a dE/E = (1.3\times 10^6/E_1)(2\pi\Gamma_\gamma/D^*)\frac{\beta-\ln(1+\beta)}{\beta^2}\ \text{barns} \quad (1)$$

$$\beta = E_1^{-1/2}(\Gamma_\gamma/\overline{\Gamma_n^0})$$

where E_1 is the energy of the first resonance in ev, Γ_γ is the average radiative width of resonances of zero neutron orbital angular momentum (to which this discussion is confined, since they provide the major contributions to the resonance integral), $\overline{\Gamma_n^0}$ is the average reduced neutron width ($\Gamma_n^0 \equiv \Gamma_n/E^{-1/2}$), and D^* is the average energy spacing of resonances of the same spin and parity.

The parameter $2\pi\Gamma_\gamma/D^*$ is a convenient one since it is virtually independent of neutron energy in the range 0–1 Mev. It rises with mass number, A, from small values of A to $A = 100$, and is approximately 0.02 for A between 100 and 200, except for sharp dips in the vicinity of the magic number nuclei. For the heavy nuclei ($A > 100$) the variations of the resonance integral caused by changes in the value of $2\pi\Gamma_\gamma/D^*$ are slight.

According to the continuum theory of nuclear reactions, $2\pi\overline{\Gamma_n^0}/D^* = 8.8\times 10^{-4}$ ev$^{-1/2}$ for low neutron energies.[1] According to Feshbach *et al*,[2] the quantity $2\pi\overline{\Gamma_n^0}/D^*$ should have peaks at $A = 11$, 55, and 155, where it rises to several times the value from the continuum theory; and valleys between these mass numbers, at which it is only a fraction of the continuum theory value. Carter and co-workers[3] have compared the theories with experimental values and

* Oak Ridge National Laboratory, Oak Ridge, Tennessee. Including work by G. Arfken, D. Caldwell, T. Cuykendall, L. Dresner, R. L. Macklin, H. S. Pomerance, J. Risser, R. J. Stephenson, Oak Ridge National Laboratory; L. J. Brown, A. C. G. Mitchell, E. D. Nering, J. R. Pruett, Indiana University; E. D. Clayton, Hanford Atomic Products Operation; C. Eggler, N. Goldstein, D. J. Hughes, C. O. Muehlhause, A. Radkowsky, S. Untermyer, Argonne National Laboratory.

find that $2\pi\overline{\Gamma_n^0}/D^*$ does have a peak near $A = 155$, but that the experimental peak is lower than the theoretical peak and the experimental wings are higher than the theoretical wings.

Equation 1 is meant only for purposes of estimation. Where the parameters $2\pi\overline{\Gamma_n^0}/D^*$ and $2\pi\overline{\Gamma_\gamma}/D$ are experimentally well known, the estimated and measured resonance integrals generally agree within about 50 per cent; for example, Ag^{107}, I^{127}, Ta^{181}, Re^{187}, Th^{232}, U^{238}. In other nuclides the average resonance parameters are less certain, and the estimates are correspondingly worse. Estimates based on Equation 1 are listed in the Summary Table where they are designated by *s*.

Where the resonance integral (and the thermal cross section) can be attributed to a single resonance well removed from thermal energy, the integral can be calculated as

$$\int \sigma_a \, dE/E = (2\pi\sigma_{th} \cdot E_{th}^{1/2} \cdot E_0^{1/2})/\Gamma \qquad (2)$$

where σ_{th} is the absorption cross section at thermal energy E_{th}, usually 0.0253 ev. E_0 and Γ are the neutron energy and width of the resonance. The estimates from this formula (designated by *th* in the Summary Table) suffer frequently from poorly known level widths.

EXPERIMENTAL METHODS AND STANDARDS

Resonance absorption integrals have been frequently measured from induced beta activities and by measuring changes of reactivity in a nuclear reactor. Both methods require a primary standard determined by another method. The boron (n,α) reaction with its $1/v$ cross-section dependence is sometimes useful for materials with little resonance contribution, although the difficulty of observing the boron reaction with its high cadmium ratio (30–70) often precludes accurate comparison. The cadmium ratio is defined as the ratio of neutron intensity measured by the uncovered detector to the intensity measured when the cadmium is interposed; resonance energy neutrons pass through 0.5 mm to 0.8 mm of cadmium and thermal energy neutrons are absorbed, so that as an equation:

$$\mathrm{Cd}R \equiv \frac{\text{thermal response} + \text{resonance response}}{\text{resonance response}}$$

Indium with its large resonance at 1.46 ev was used as a standard in much of the early activation work because of its convenient beta activity and low cadmium ratio. Its use suffers from the disadvantage of a strong dependence on the transmission curve of the absorber, particularly so where the experiments are done in an isotropic flux in which the attenuation of neutrons depends on the angle of incidence as well as on the energy.

In this work, we have adopted gold for the standard. The major resonance near 5 ev has recently been carefully measured[4] with the Brookhaven crystal spectrometer and small contributions from the next six resonances are known from neutron time-of-flight spectrometer studies.[5] These studies lead to a new value of 1513 barns resonance integral (resonance contributions only) accurate to ±4 per cent or less. In addition, a measurement will include the effects of the neutron absorber near its cutoff and the $1/v$ component of the gold, 45 barns for a 0.44 gm/cm² Cd absorber or 145 barns for a 0.061 gm/cm² Gd absorber in a collimated beam. In the Summary Table all values of measured integrals have been corrected to correspond to the 1513 barn value for gold and, somewhat arbitrarily, to the 45 barn addition for $1/v$ contribution which correctly should depend on whether a beam flux or an isotropic flux was used and exactly how thick the cadmium shield was.

ACTIVATION MEASUREMENTS

Most activation work has been the measurement of the cadmium ratios of a sample *x* and a standard *s*. The resonance integral, $RI(x)$, is computed including the thermal neutron capture cross sections σ_{th}, the definition of the cadmium ratio Cd*R* which makes the ratio of thermal neutron to resonance neutron activation just the cadmium ratio minus one, and the $1/v$ contribution of value $0.44\,\sigma_{th}$ in general.

$$[RI(x) + 0.44\,\sigma_{th}(x)] = [RI(s) + 0.44\sigma_{th}(s)] \frac{\mathrm{Cd}R(s) - 1}{\mathrm{Cd}R(x) - 1} \cdot \frac{\sigma_{th}(x)}{\sigma_{th}(s)} \qquad (3)$$

By this method the beta- or gamma-counting apparatus need not be calibrated absolutely. In effect the thermal cross sections are used to calibrate the counters and the errors in these cross sections become important. An extensive series of such measurements using gold for a standard was made at the Argonne National Laboratory.[6] Resonance integrals recalculated from their cadmium ratios and from more recent values of the thermal neutron capture cross sections[7] are listed in column 4 of the Summary Table.

Absolute counter measurements are possible for some beta emitters, thus allowing a more direct and accurate measurement of the resonance integral. The values for Th^{232} and U^{238} in column 4 were obtained in this way at the Oak Ridge National Laboratory last year. The absolute decay rates of a foil of irradiated gold and of a sample of 23.5 min U^{239} were determined by 4π beta-gamma coincidence counting. The same gold foil and another aliquot of the U^{239} sample were then used to establish the efficiency of the counter used with the 7 cm diameter samples.

In all these measurements, the samples must be thin. The requirement depends on the maximum value of the cross section at a resonance. Macklin and Pomerance at Oak Ridge used 0.015 mg Au/cm², 0.07 mg U^{238} cm², and 0.3 mg Th/cm². Harris, Muehlhause, and Thomas at Argonne used samples varying from 0.2 to 5 mg/cm².

The fission resonance integral of U^{235} offers an example of the interference of resonances near and below the cadmium cutoff to the usual computation. The measurement is simple because the fission counter has an efficiency of unity. Clayton used an enriched U^{235}

fission counter, a boron counter, and 0.5 mm cadmium shields. Boron is a $1/v$ absorber; its resonance capture integral is twice its capture cross section at the cadmium cutoff and serves as the standard for the measurement. His value of 271 ± 25 barns has been confirmed at Oak Ridge.

Extrapolation of the U^{235} fission cross section from thermal energy (0.0253 ev) to 0.5 ev is not proper. A negative energy resonance and a resonance at 0.29 ev are responsible for part of the thermal cross section; above 0.29 ev the cross section is not $1/v$. However, the contributions from these resonances are canceled by the deficit at higher energies, up to the cadmium cutoff, where the cross section decreases faster than $1/v$. The net result is only 7 per cent more than the integral for a $1/v$ absorber with the same thermal cross section. Numerically, the thermal fission cross section of 580 barns would, if it were a $1/v$ cross section, be 129 barns at 0.5 ev; the corresponding resonance integral of $2 \times 129 = 258$ barns is nearly as much as the measured value of 271 barns.

The fission cross-section curves, shown in BNL-325, can be integrated numerically, taking into account the transmission factor for the cadmium and the dE/E neutron flux. For 0.5 mm Cd with a cutoff energy of 0.49 ev, Clayton computed 302 barns for the fission of U^{235}, to be compared with his measurement of 271 barns. If the cutoff energy were 0.17 ev, the integral would be 172 barns larger. Calculation from the measured resonance parameters for the resonances above one ev gives a 260 barn resonance integral, but it is not clear how accurate the 62 barn estimate for the region above 35 ev is, nor how much more to add for the 0.29 ev resonance and the negative energy resonance. The latter resonance is responsible for most of the thermal neutron cross section.

ABSORPTION MEASUREMENTS

Resonance neutron absorption measurements with a cadmium absorber, without using activation, can be performed analogously to thermal neutron absorption measurements. The most sensitive method uses a sample oscillating in and out of a nuclear reactor with detection of the induced oscillating component of neutron flux having the same period. The necessary cadmium shielded flux region acts as a severe poison in the reactor and this precludes its use with natural uranium graphite reactors. Even with the excess reactivity available in a heavy water reactor, samples of materials with high resonance cross sections have been too thick to avoid self absorption corrections. There are also interferences due to the scattering cross sections of the sample, making the small integrals also rather uncertain. The work at Argonne National Laboratory by this method was not continued after about 1950. The often fragmentary results obtained, based on an indium standard, have been discussed by Langsdorf.[8] His data have been revised to the gold standard through the gold and indium-cadmium ratio comparisons of Harris, Muehlhause, and Thomas,[6] and the $1/v$ component taken from recent cross-section data as for the activation integrals. The results are shown in column 4 of the Summary Table. Later work of Harris, Muehlhause, Schroeder and Thomas led to tentative results for which the accuracy is not well established. Because some of the elements cannot be measured in activation, we have included these tentative values for lack of better information. The accuracy can best be judged by comparisons in those cases for which the activation value is also known. These values are in column 5 of the Summary Table.

EFFECTIVE CAPTURE INTEGRALS

For a nuclear reactor to operate, materials with significant resonance cross section are generally avoided. The important exceptions are the fertile materials Th^{232} and U^{238} which can be converted to fissionable nuclides through neutron capture. Natural uranium reactors of necessity contain large masses of U^{238} which absorb incident neutrons at resonance energies near the surface. Some of the neutrons above resonance energies penetrate deep within the mass where they may be slowed to resonance energy by elastic collisions and then absorbed. The early work on the behavior of the effective integral (an average over the region) as influenced by surface area, mass and thermal Doppler broadening has been treated in terms of the individual resonances by Wigner and co-workers in a recently published group of articles reporting work performed 13 years ago.[9]

Measurements on uranium and thorium metal rods and plates have been analyzed by Untermyer in terms of the approximate formula

$$RI(\text{eff}) = A\left(1 + \frac{\mu}{r + r_0}\right) \qquad (4)$$

where r is the mass to surface ratio (gm/cm²) and the three constants satisfy the relation imposed by setting the effective integral equal to the true integral for r equal to zero, the case where the material is infinitely dilute. In this respect the result is a better empirical formula than the older formula in which $r_0 = 0$.

The effective integrals for uranium were measured by Muehlhause, Radkowsky and Untermyer at the Argonne National Laboratory with the pile oscillator in a cadmium-enclosed region. The natural uranium rods were 5 cm long and of several diameters between 0.25 cm and 2.3 cm; the foil was 0.005 cm thick. The corresponding surface to mass ratios are from 0.07 gm/cm² to 8.9 gm/cm². At the Oak Ridge National Laboratory, Risser, Arfken, Cuykendall, Stephenson, and Caldwell measured the activations induced in U^{238} metal foils mounted as part of a cylinder of natural uranium. The cadmium-covered cylinder was irradiated in an exposure hole of the graphite-natural uranium reactor with gold foils for the resonance flux monitors.

Thorium rods were measured by Untermyer and Eggler by the danger coefficient method. In this method the samples are introduced into a reactor that is just critical and the control rod is readjusted to

bring the reactor back to criticality. For the thorium experiment the control rod was calibrated with uranium metal samples of the same size as the thorium samples; the samples were 9, 19 and 32 mm in diameter corresponding to 2.1 to 9.2 gm/cm², and the accuracy of measurement was estimated to be 20 per cent. In addition they irradiated foils of 0.01 to 0.2 gm/cm² which were placed against a 2.5 mm thick plate of thorium, the whole covered with cadmium, in an exposure hole of a reactor. The foil measurements were estimated to be accurate to 30 per cent.

The data from the two uranium experiments and the thorium experiment can be fitted fairly well, within about 15 per cent, by the constants in Table I for Equation 4. The $1/v$ contributions have not been included.

Table I. Parameters for the Effective Resonance Integral

	A (10^{-24} cm²)	μ (gm/cm²)	r_0 (gm/cm²)
Th^{232} metal	8.37	0.55	0.08
U^{238} metal	10.2	2.95	0.11

The temperature dependence of the effective resonance integral has been reported by Creutz, Jupnik, and Wigner[9] for uranium and uranium oxide, and is in the range of 10^{-2} per cent change per degree Celsius.

The effective resonance capture integral depends on the competition for neutrons between the absorbing atoms and the scattering atoms in the neighborhood which can change the neutron energy by elastic collision. The absorption per uranium atom and per unit flux density is

$$A = \int \frac{dE}{E} \frac{\sigma_a}{\frac{\sigma_a + \sigma_s}{\sigma_D} + 1} \tag{5}$$

The cross sections σ_a and σ_s are the absorption and resonance scattering cross sections of the uranium; σ_D is the scattering cross section of the diluent plus the potential (non-resonance) scattering cross section of the uranium, expressed as scattering cross section per uranium atom. When the absorber is infinitely dilute, $\sigma_D = \infty$, the integral becomes $\int \sigma_a \, dE/E$; the Summary Table is a list of such values, including values for thorium and uranium. When $\sigma_D = \sigma_P$, (σ_P is the non-resonance scattering cross section of the metal), the integral is for undiluted metal. The solution of the integral for the intermediate cases in terms of the resonance parameters assumes that the resonances are narrow and that the regions between resonances contribute hardly at all to the total.

$$\sigma_{eff} = \sum \frac{\pi}{2} \frac{\sigma_0 \Gamma_\gamma}{E_0} \left(\frac{\sigma_0}{\sigma_D} + 1 \right)^{-1/2} \tag{6}$$

where σ_0 is the peak total cross section.

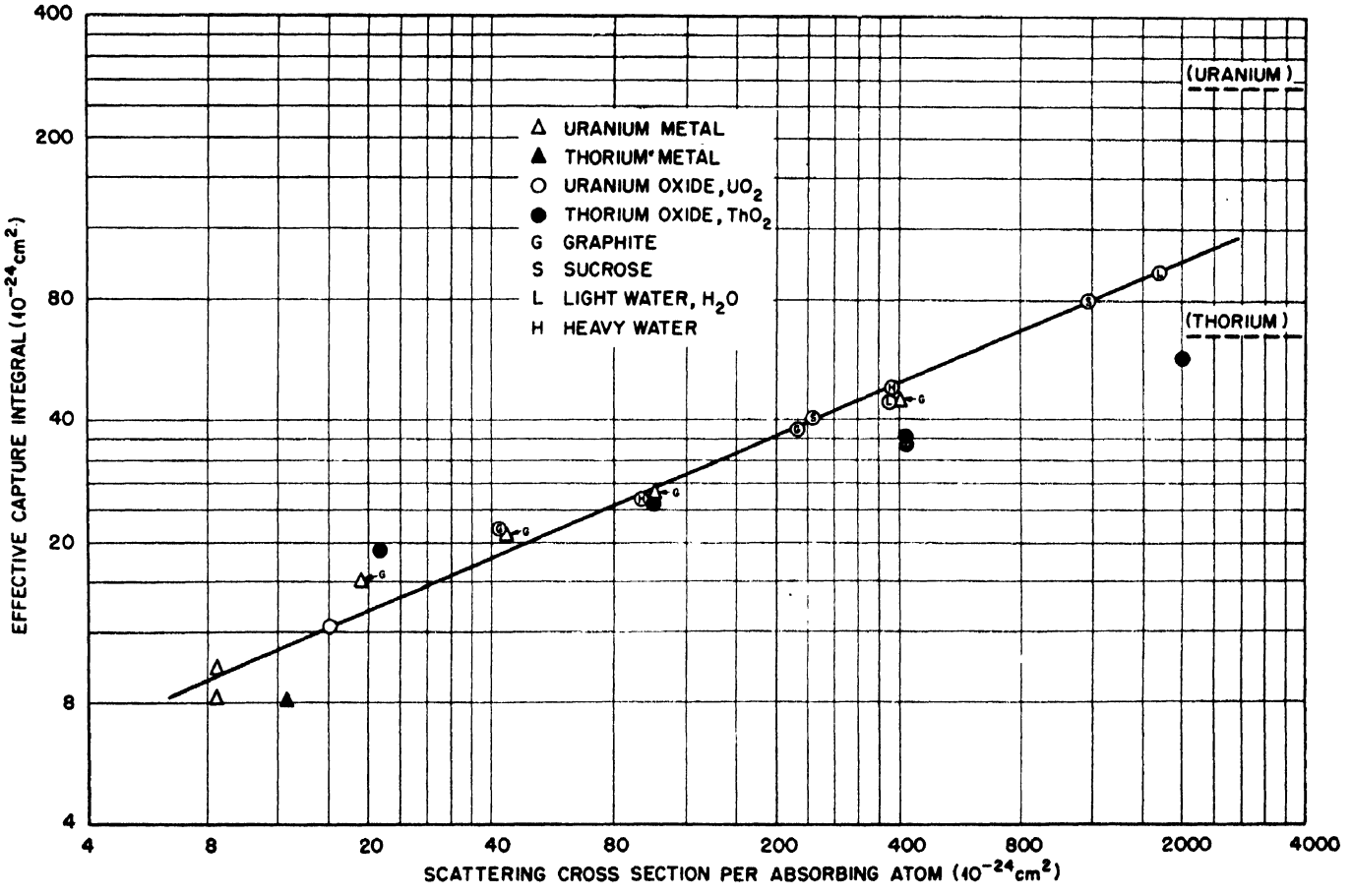

Figure 1. Effective resonance capture integrals of U^{238} and Th^{232} diluted with neutron scattering materials

Table II. Summary Table of Resonance Capture Integrals (10^{-24} cm²)

Nuclide or Natural element	Calculated		Measured	
	Resonance	1/v	Activation	Absorption
$_{3}Li$		31		28
$_{11}Na^{23}$	0.12[th]	0.25	~0.24	0.27
$_{12}Mg$		0.027		0.9
$_{13}Al^{27}$		0.095	~0.16	0.18
$_{14}Si$		0.06		0.5
$_{15}P^{31}$		0.084	~0.092	<2
$_{16}S$		0.22		0.6
$_{17}Cl$		14.3		12
$_{19}K$		0.89		1.1
$_{20}Ca$		2.0		2
$_{21}Sc^{45}$		10.6	~10.7	
$_{22}Ti$		2.5		3.0
$_{23}V^{51}$		2.2	~2.2	
$_{24}Cr$		1.3		1.9
$_{25}Mn^{55}$	12[th]	5.9	~11.8	10.8
$_{26}Fe$		1.1		2.1
$_{27}Co^{59}$	90[th]	16.3	49.3	48
$_{28}Ni$		2.0		4
$_{29}Cu$		1.6	3.7	4
$_{29}Cu^{63}$	0.8[s]	1.9	4.4	
$_{29}Cu^{65}$	0.8[s]	0.92	2.2	
$_{30}Zn$		0.48		2
$_{31}Ga^{69}$	20[s]	0.62	9.2	
$_{31}Ga^{71}$		1.58	15	
$_{33}As^{75}$	170[th]	1.8	36.8	33
$_{35}Br^{79}$	62[s]	4.8	147	
$_{38}Sr$		0.53		16
$_{39}Y^{89}$		0.62	0.91	
$_{40}Zr$				3
$_{41}Nb^{93}$		0.47	3.87	8.3
$_{42}Mo$		1.1		13
$_{45}Rh^{103}$	1080[th]	66	656	575
$_{46}Pd$		3.6		23
$_{47}Ag$		27		>650
$_{47}Ag^{107}$	82[s]	13	74	
$_{47}Ag^{109}$	1206[th]	37	1160	
$_{49}In^{113}$		26	1050	
$_{49}In^{115}$ (a)	1752[th]	87	2640	
$_{50}Sn$		0.26		4.3
$_{51}Sb^{121}$		3.0	162	
$_{51}Sb^{123}$		1.1	~138	
$_{52}Te$		2.0		36
$_{53}I^{127}$	150[s]	2.9	140	>90
$_{56}Ba$		0.53		7.5
$_{57}La$		4.0		11
$_{59}Pr^{141}$		4.9	11.3	
$_{62}Sm^{152}$ (a)		61	>1750	
$_{63}Eu^{153}$ (a)		1400 (b)	950	
$_{72}Hf$	2778[th]	51	~1750, (c)	1300
$_{72}Hf^{180}$		4.4	21.8	
$_{73}Ta^{181}$	555[s]	9.4	590	
$_{74}W^{186}$	180[th]	15	355	
$_{75}Re^{185}$	1630[th]	44	1160	
$_{75}Re^{187}$	310[s]	33	305	
$_{77}Ir^{191}$ (a)	7680[th]	420	3500	
$_{77}Ir^{193}$ (a)	976[th]	57	1370	
$_{78}Pt$		3.7		69
$_{79}Au^{197}$	1390[th]	45	1558 (d)	
$_{80}Hg$		(b)		31
$_{81}Tl^{203}$		4.8	129	
$_{81}Tl^{205}$		0.04	0.5	
$_{82}Pb$		0.08		0.1
$_{83}Bi$		0.014		0.5
$_{90}Th^{232}$	83[s]	3.2	69.8	
$_{92}U^{233}$ (f)	650[g]	234		
$_{92}U^{235}$ (f)	>260[s]	255 (b)	271	
$_{92}U^{238}$	290[s]	1.2	282	
$_{94}Pu^{239}$ (f)	250[g]	(b)		

[a] A near thermal resonance leads to considerable dependence on the details of the cadmium absorber that was used.
[b] The capture cross section is not 1/v near thermal energies.
[c] Capture gamma-radiation used to determine the cross section; some self-protection in the sample.
[d] Adopted as the standard, using $\sigma_{th} = 98 \times 10^{-24}$ cm².
[f] Fission integral.
[g] Graphical estimate. For Pu^{239}, a cutoff at 2.0 ev was used and no separate 1/v contribution.
[s] Estimated from average level parameters.
[th] Estimated from parameters of the first large resonance and the thermal cross section.

However, these values disagree with the measured values by as much as a factor of two. If the broadening of the resonance lines from the Doppler effect is considered, the error is reduced by about 5 per cent for 300°K.

Measurements of the effective resonance capture integral for thorium were made by Hughes and Eggler. A cylinder 7.5 cm in diameter and 7.5 cm high was filled with mixtures of ThO_2 and graphite powder. The activities of a cadmium-covered thorium foil and cadmium-covered indium foil irradiated at the center of the cylinder provided the necessary information. The material used to hold the foils in place probably perturbed the experiment and it is likely that the less dilute points are in error, but the experiment has not been repeated.

Hughes and Goldstein performed a similar experiment with uranium powder and graphite for the diluent. The irradiations were again in a nuclear reactor, but there was better control of the placement of the foils. Mitchell and co-workers at Indiana University used a cyclotron to generate neutrons, and a stack of graphite to moderate the neutrons. They mixed uranium dioxide with various scatterers—graphite, sucrose, light water, and heavy water—to eliminate any effect of the mass of the scattering atoms; also they used pure oxide and pure metal. The experimental points are plotted in Fig. 1.

CONCLUSION

For thermal neutron reactors the resonance integral is one of two average cross sections of great utility. For materials whose resonance parameters are well measured, the resonance integral can now be computed to fair precision. In reactors or regions of reactors where the flux is not distributed as $1/E$, direct model measurements or more detailed cross sections are required.

The Summary Table lists measurements of the resonance capture integrals, some previously published

and some not. The measurements depend on a standard, which in this table is gold and a secondary standard, indium, which was used to bring all the measurements to a common basis. The calculations of the resonance capture integrals separate the value into two components, a pure resonance contribution and a $1/v$ contribution. In this table, the $1/v$ contribution is 0.44 σ_{th} (σ_{th} is the cross section for neutrons of 2200 m/sec velocity); σ_{th} is also used in the computation of the resonance capture integral from cadmium ratio measurements.

REFERENCES

1. Blatt, J. and Weisskopf, V., *Theoretical Nuclear Physics*, John Wiley and Sons (New York, 1952).
2. Feshbach, H., Porter, C. E. and Weisskopf, V., *Model for Nuclear Reactions with Neutrons*, Physical Review *96:* 448–64 (1954).
3. Carter, R. S., Harvey, J. A., Hughes, D. J. and Pilcher, V. D., *Ratio of $\Gamma n^0/D$ for Slow Neutron Resonances*, Physical Review *96:* 113–4 (1954).
4. Wood, R. E., Landon, H. H. and Sailor, V. L., *Parameters for the Neutron Resonance in Gold*, Physical Review *98:* 639–45 (1955).
5. Seidl, F. G. P., Hughes, D. J., Palevsky, H., Levin, J. S., Kato, W. Y. and Sjöstrand, N. G., *"Fast Chopper" Time-of-Flight Measurement of Neutron Resonances*, Physical Review *95:* 476–99 (1954).
6. Harris, S. P., Muehlhause, C. O. and Thomas, G. E., *Low Energy Neutron Resonance Scattering and Absorption*, Physical Review *79:* 11–18 (1950).
7. AEC Neutron Cross Section Advisory Group, *Neutron Cross Sections (AECU-2040)*, Office of Technical Services, Department of Commerce, Washington, D. C. (1952–54).
8. Langsdorf, A., Jr., *The Thermal Neutron Reactor as an Instrument for Measuring Neutron Cross Sections*, AECD 3194, Government Printing Office, Washington, D. C.
9. Creutz, E., Jupnik, H., Snyder, T. and Wigner, E. P., *Review of Measurements of the Resonance Absorption of Neutrons by Uranium in Bulk*, Journal of Applied Physics *26:* 257–9 (1955).
   Wigner, E. P., Creutz, E., Jupnik, H. and Snyder, T., *Resonance Absorption of Neutrons by Spheres*, Journal of Applied Physics *26:* 260–70 (1955).
   Creutz, E., Jupnik, H., Snyder, T. and Wigner, E. P., *Effect of Geometry on Resonance Absorption of Neutrons by Uranium*, Journal of Applied Physics *26:* 271–5 (1955).
   Creutz, E., Jupnik, H. and Wigner, E. P., *Effect of Temperature on Total Resonance Absorption of Neutrons by Spheres of Uranium Oxide*, Journal of Applied Physics *26:* 276–9 (1955).

Studies on the Neutron Resonance Absorption of U^{238}

By V. S. Crocker,* UK

The absorption of non-thermal neutrons by U^{238} is of particular interest for from it is derived ρ, the resonance escape probability, for natural and near-natural uranium reactors. The absorption of non-thermal neutrons is partly determined by the first resonance level at 6.7 ev. This level has been studied using neutron time-of-flight spectrometers but at the time this work was begun no information was available concerning the variation with temperature of the characteristics of the level. The resonance absorption of spheres of uranium has also been studied[1] but only limited results were available. It was therefore decided to perform an experiment using the self-indication technique to determine the effective resonance integral $\int\sigma(E)\,dE/E$ for various shapes and masses of uranium. It was also hoped it would be possible to derive some temperature dependence from such experiments.

EXPERIMENTS

Characteristics of the First Resonance Level

The experiment was performed using a 2-in. diameter, well-collimated neutron beam from BEPO. U^{238} (containing one U^{235} atom/6000 U^{238}) detector foils were used. They were made by depositing U_3O_8 from a suspension in alcohol onto PTFE discs 2 cm diameter, 0.1 cm thick. The U_3O_8 ($\sim$3 mg/cm^2) was "fixed" by spraying on a very small weight ($\sim$0.2 mg/cm^2) of Zapon lacquer. The foils were used surrounded by 0.1 cm of cadmium to eliminate thermal neutron activation.

The transmission of the beam of neutrons, as defined by the activity of the detector foil, corrected for decay, etc., was measured as a function of the mass/unit area of uranium absorber, varying from 10–100 mg/cm^2. The absorbers, (U_3O_8 deposited onto thin aluminium sheets) were prepared from a suspension of U_3O_8 in water. To monitor the intensity of the neutron beam a thin foil of lead iodide was placed in the beam in front of the uranium. I^{128} and U^{239} have similar half-lives, 25 min and 23.5 min respectively, and thus any variations in beam strength were readily followed. The activities were measured using end-window Geiger-Muller counters.

To determine the temperature characteristics of the first level, the absorbers were placed inside an annular furnace with the detector outside at room temperature. The transmission was measured as a function of the absorber temperature over the range 300°A–700°A with an absorber thickness of 15 mg/cm^2.

Determination of the Effective Resonance Integral

This was essentially a continuation of the previous transmission experiment using absorbers up to 3 cm thick (55.8 mg/cm^2). The depleted uranium was deposited onto lead foils 0.025 cm thick. Lead was preferred to PTFE in the case of thick absorbers because its mass and scattering properties are similar to uranium. The detector foils were backed by 0.5 cm of uranium so that they were essentially measuring the activation at a given position in a mass of uranium.

RESULTS

The transmission curve for thin absorbers at room temperature is shown in Fig. 1. The initial shape of the curve is exponential and corresponds to a cross section of 5000 $\pm$ 200 barns. Figure 2 shows the temperature variation of the transmission of a 15 mg/cm^2 absorber. For a 400°C rise in temperature the transmission changes by $\sim$5%.

The activation curve for all the absorbers used is shown in Fig. 3. The detector in this curve always had 0.5 cm of uranium behind it. The tail of the curve is approximately exponential corresponding to a cross section of 9.48 barns.

DISCUSSION

First Resonance Level

The activity of a detector, cross section $\sigma(E)$, N atoms/cm^2, due to neutrons having traversed a thin absorber N' atoms/cm^2, of the same material can be shown to be

$$A = N\int[\phi(E) - N'\phi(E)\sigma(E)]\sigma(E)\,dE \simeq A_0e^{-N'\sigma_s}$$

where

$$\sigma_s = \frac{\int\sigma^2(E)\phi(E)\,dE}{\int\sigma(E)\phi(E)\,dE} \qquad (1)$$

A_0 is the activity of the detector with zero absorber thickness, $\phi(E)$ the neutron flux, σ_s is termed the self-indication cross section, its value as derived from the initial slope of the curve in Fig. 1 is 5000 barns. This is the effective cross section of the level using thin absorbers. It is in good agreement with the results of Anderson[2] 4600 barns $\pm$ 40% and Sauerwein[3] 4700 barns. After $\sim$30 mg/cm^2 the calculated transmission using $A = A_0e^{-N'\sigma_s}$ is less than the experimental value. This is due to the fact that the approximations assumed in deriving the formula are incorrect for "thick" absorbers and also that the higher resonance

* A.E.R.E., Harwell, England.

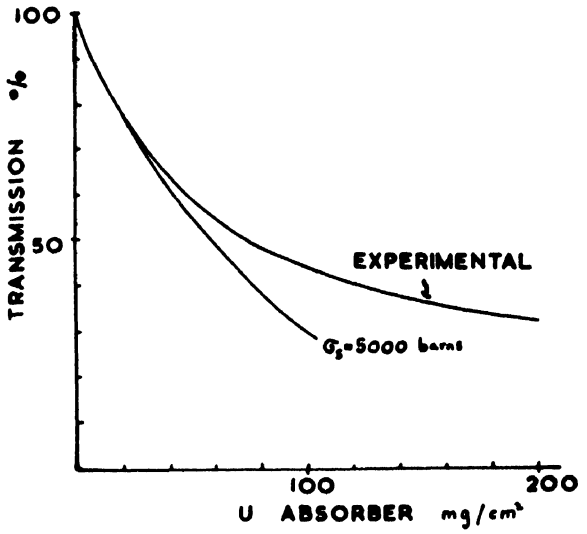

Figure 1. Transmission curve for thin uranium absorbers

levels in U^{238} are becoming effective. Even if the correct one-level formula is used the curves still do not fit indicating the effect of higher resonance levels.

In certain cases the velocities of the capturing nuclei are not negligible compared with the neutron velocities and Doppler broadening of the level occurs.[4] The Doppler width of the level is

$$\Delta = 2\,(mE_r kT/M)^{1/2}$$

where m is the neutron mass, M the mass of the capturing nucleus and E_r the resonance energy. For uranium $\Delta = 53$ millivolts (assuming a Maxwellian distribution of velocities for the nuclei). If the Doppler width is comparable with the natural width of the level, a variation in σ_s with temperature is to be expected.

The integral in the numerator of Equation 1 can be evaluated yielding

$$\sigma_s(a,b) = \tfrac{1}{2}\sigma_s F(c,0);\ c = 2ab(a^2 + b^2)^{-1/2}$$

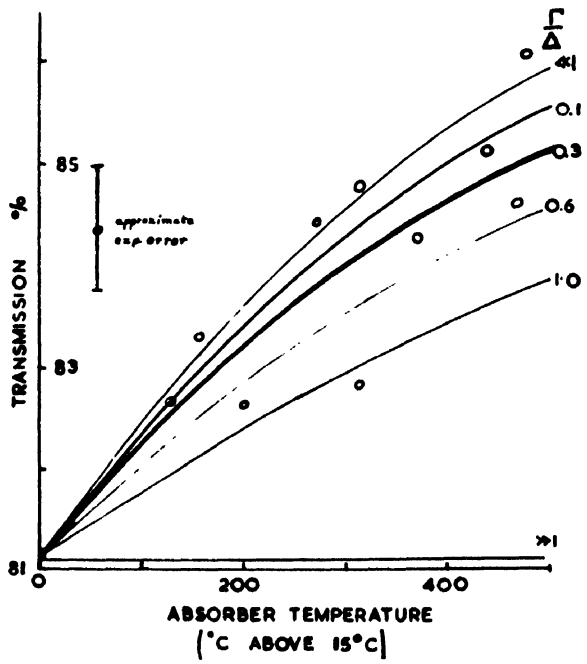

Figure 2. Variation of transmission with absorber temperature

where $a = \Gamma/\Delta$ and $b = \Gamma/\Delta'$, Δ being the Doppler width of the detector and Δ' that of the absorber.

$$F(c,0) = \frac{c}{2\pi^{1/2}} \int_{-\infty}^{+\infty} \frac{e^{-\frac{1}{4}c^2y^2}}{1+y^2}\,dy$$

where $y = (E' - E_r)/(\Gamma/2)$, E' being the relative neutron energy.

Figure 2 also shows the expected variation with temperature, of the transmission, for different values of Γ/Δ. It is seen that when $\Gamma/\Delta \to 0$, at high temperatures, only small differences in transmission cause large variations in Γ/Δ thus making it difficult to estimate accurately the value of Γ/Δ from the experimental points. However, the experimental points indicate that the Doppler width predominates and that $\Gamma/\Delta = 0.3 \pm 0.3$. From this value $\Gamma = 15.9$ mv.

The Effective Resonance Integral

The activation curve in Fig. 3 can be divided into two sections. The first portion, up to ~3 gm/cm² represents the absorption of the incident resonance neutrons. The second part corresponds to the absorption of non-resonance incident neutrons. The first portion is a surface effect, all the neutrons within a given energy range being absorbed. The second part has been called the mass term, because the cross section (9.48 barns) is such that all the U^{238} is effective. This mass absorption is due to absorption at the wings of the resonance level(s) and the absorption of neutrons which have been scattered into the resonance level(s). Those that are scattered into a resonance energy band travel only a short distance before being captured and the neutrons which are not scattered into a resonance band of energy have a high probability of escaping before being absorbed. The activation curve is thus typical of what would be expected from a narrow beam of neutrons incident upon a mass of uranium.

The activation curve can approximately be fitted to the formula

$$A = 5.1e^{-u_1 x} + 14.3e^{-u_2 x} + 80.6e^{-u_3 x}$$

where $u_1 = 0.445$ corresponds to a cross section of 9.48 barns, $u_2 = 9.48$ corresponds to a cross section of 201 barns, and $u_3 = 129$ corresponds to a cross section of 2750 barns.

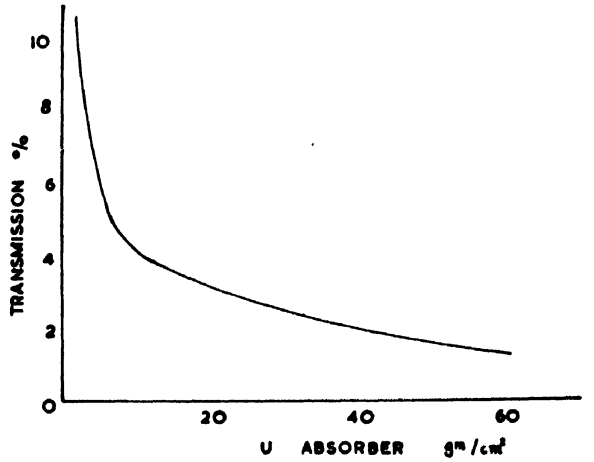

Figure 3. Transmission curve for thick uranium absorbers

This formula can be used to calculate the non-thermal neutron activation in slabs, spheres and cylinders of uranium, assuming an isotropic distribution of neutrons into the uranium. For this purpose it is assumed that the flux into the material is half the flux at an undisturbed position.

The formulae derived were:

Slab

Activity at a distance x from surface of an infinite slab of thickness t

$$A = \tfrac{1}{2} \sum_{i=1\,2,3} [e^{-u_i x} + e^{-u_i(t-x)} + u_i x Ei(-u_i x) + u_i(t-x)Ei(-u_i(t-x))]$$

Sphere

Activity at a distance x from the centre of a sphere of radius a

$$A = \sum_{i=1,2,3} \frac{e^{-u_i(a-x)}}{4x}\left(a + x + \frac{1}{u_i}\right) - \frac{e^{-u_i(a+x)}}{4x}\left(a - x + \frac{1}{u_i}\right) + \frac{(a^2 - x^2)}{4x} u_i[Ei(-u_i(a-x) - Ei(-u_i(a+x))]$$

Cylinders

Activity at a distance x from axis of an infinitely long cylinder of radius a

$$A = \frac{1}{\pi} \sum_{i=1,2,3} \int_0^{K_0} K_{12}[u_i(x+a)\,dnu] \frac{d}{du}\left[\arcsin(snu) + \arctan k' \frac{snu}{cnu}\right] du$$

where

$$K_{12} = \int_0^{\infty} \frac{e^{-y\cosh v}}{\cosh^2 v}\,dv \quad \text{and} \quad k' = \frac{a-x}{a+x}$$

snu, *dnu* and *cnu* are Jacobian elliptic functions.

Graphical integrations had to be performed for the cylindrical geometry case.

The activity at the surface of the uranium is composed of two parts: (1) the activity due to the neutron current into the uranium at the point under consideration; and (2) the activity due to neutrons which have entered the uranium except at the point under consideration. These neutrons have traversed varying thicknesses of uranium.

The surface activity due to (1) above, is by definition one-half of the activity which would be measured had the uranium been finely distributed. The resonance integral $\int \sigma_F$, for thin films of uranium has been measured. The effective resonance integral $\int \sigma(E)\,dE/E$ can thus be obtained for a given size and geometry of uranium by measuring the area under the activation curve (A_a) and comparing it with the corresponding area had the uranium been finely distributed (A_F)

$$\int \frac{\sigma(E)\,dE}{E} = \left(\frac{A_a}{A_F} \times \int \sigma_F\right) \text{barns}$$

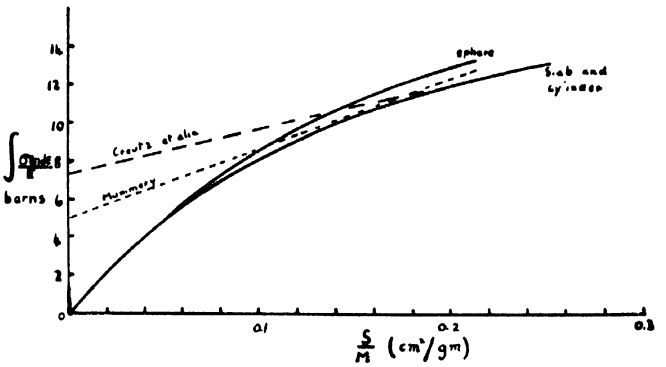

Figure 4. The effective resonance integral of uranium for various geometries

The value of $\int \sigma_F$ has been measured in the neutron beam used as 248 ± 18 barns, assuming the resonance integral for gold to be 1300 barns. The result was obtained from cadmium-ratio measurements on gold and uranium films.

Figure 4 shows $\int \sigma(E)\,dE/E$ plotted as a function of (Surface Area)/Mass of uranium for slabs, cylinders and spheres. A correction equal to 1.5 barns has been subtracted from the values of $\int \sigma(E)\,dE/E$ evaluated. This correction is due to the $1/v$ tail of neutrons extending above the cadmium cut off. It is seen that for a given value of (S/M), $\int \sigma(E)\,dE/E$ is greater for spheres than for cylinders or slabs. The cylinder curve actually lies slightly higher than the slab curve, but due to the smallness of the difference it is not shown separately on the graph. The slight differences are caused by the different geometrical shapes used, causing slight variations, for a given S/M, of the flux distribution through the uranium.

Also shown in Fig. 4 is the formula derived by Creutz *et al.*[1] $\int \sigma(E)\,dE/E = (7.3 + 23.5(S/M))$ barns and an approximate formula derived by Mummery[5] using solid and hollow cylinders of uranium. The agreement with the two curves is reasonable.

CONCLUSION

Using a self-indication technique, the principal resonance level in U^{238} has been studied and found to have an appreciable Doppler width. From a transmission curve using thick uranium absorbers, the effective resonance integral for uranium has been derived for slabs, cylinders and spheres of uranium. It was found that spheres for a given value of S/M, have a higher effective resonance integral, than cylinders and slabs.

REFERENCES

1. Creutz, E., Jupnik, H. and Snyder, T., *Effect of Geometry on Resonance Absorption of Neutrons by Uranium*, A.E.C.D. 3387.
   Creutz, E., Jupnik, H., Snyder, T. and Wigner, E. P., *Review of Measurements of the Resonance Absorption of Neutrons by Uranium in Bulk*, Journal of Applied Physics *26*, 257 (1955).
2. Anderson, H. L., *Resonance Capture of Neutrons by Uranium*. Physical Review, *80*, 499 (1950).
3. Sauerwein, Von Kurt, *Neutroneneinfang des Urans in verschiedenen Energiebereichen*, Zeitschrift Für Naturforschung *2a*, 73 (1947).
4. Bethe, H. A., *Nuclear Physics B*, Reviews of Modern Physics, *9*, 140 (1937).

Measurements of the Effective Resonance Integral of Uranium with the Pile-Oscillator

By V. O. Eriksen,* R. W. Meier,† and P. Schmid,† Norway

The effective resonance integral of uranium metal has been studied using the pile-oscillator in JEEP. A Cd-covered guide tube penetrates close to the centre of the reactor. The samples are oscillated inside this tube by a pneumatic system.

The effective resonance integral is generally assumed to consist of a surface and a mass effect. By using a thin-walled uranium box as container and by filling this box with discs of uranium, the effects have been studied separately.

Deviations from a linear dependence on the mass have not been observed. Thin In-foils have been used to calibrate the measurements.

INTRODUCTION AND EXPERIMENTAL PROCEDURE

The well-known empirical formula for the effective resonance integral of uranium lumps

$$\int \sigma_{eff} \frac{dE}{E} = 9.25 \left(1 + 2.67 \frac{S}{M}\right) \text{barns} \qquad (1)$$

where S = surface of lumps in cm² and M = mass in grams has been checked in Kjeller by using the pile-oscillator. The JEEP in its present state allows for a Cd-tube penetrating close to the centre of the reactor. For the samples of 22 mm, the tube has a diameter of 30 mm and surrounds a guiding tube. The Cd-tube is placed in one of the irradiation channels of the reactor, and there is an air-gap of 15 mm between the tube and moderator.

The driving mechanism for the samples is of the pneumatic type working with under-pressure. The Cd-tube is kept tight against thermal neutrons. The samples are shot in or out within 1 second and remain in the extreme positions for 27 seconds. This gives square-wave modulations of k_{eff}, the mean value being close to 1. The fundamental harmonic of the resulting periodic response of the thermal neutron flux is selected. This is done by multiplying the ac signal from the ionization chamber with a sine-function and integrating over at least 8 consecutive half periods.

The integration is performed by an integrating type velodyne system. Drifts in the mean neutron flux superimposed upon the periodic signal are eliminated by weighting the integrals over the first 4 half-periods with the numbers 1, 5, 11, 15, and the last 4 half-periods with the same numbers in the reversed order, whereas all the other half-periods of the same series are weighted by 16. This procedure can be shown to eliminate exactly a constant shift as well as a linear or a parabolic drift. Due to the continuous changes in the temperature of the moderator during one measurement, the magnitude of the shifts is comparable to the amplitude of the signal.

The effective resonance integral of uranium has not been discussed much in the open literature. A review of the work done during the war has been given by Creutz *et al.*[1]

It is reasonable to imagine that the integral can be divided into two terms, one proportional to the surface of the lump and another proportional to the mass.[1,2] The mass effect has been studied separately by making the sample in the shape of a thin-walled uranium box, which is filled-up successively with discs of uranium. Only one box has been used up to now. It was cylindrical and had dimensions 19 mm diameter and 60 mm in length. The wall thickness was 1 mm. The observed signal then consists of a constant contribution from the surface of the box and a part varying with the total mass. Fig. 1 shows that the predicted linear dependence on the mass is strictly fulfilled. This means that no change in the statistical weight of the region around the sample in position is observed.

By multiplying the signal with a cosine function it was shown that the loading of the box did not shift the phase.

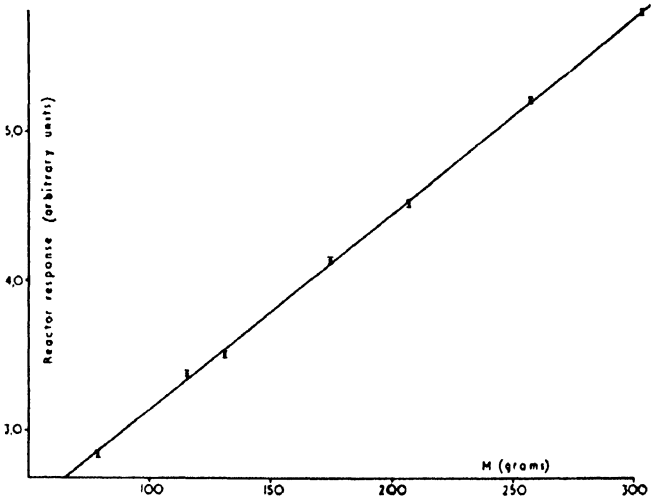

Figure 1. Mass dependence of effective resonance integral of uranium

* Joint Establishment for Nuclear Energy Research, Kjeller near Lillestrom.

† "Arbeitsgemeinschaft Kern reaktor," Switzerland.

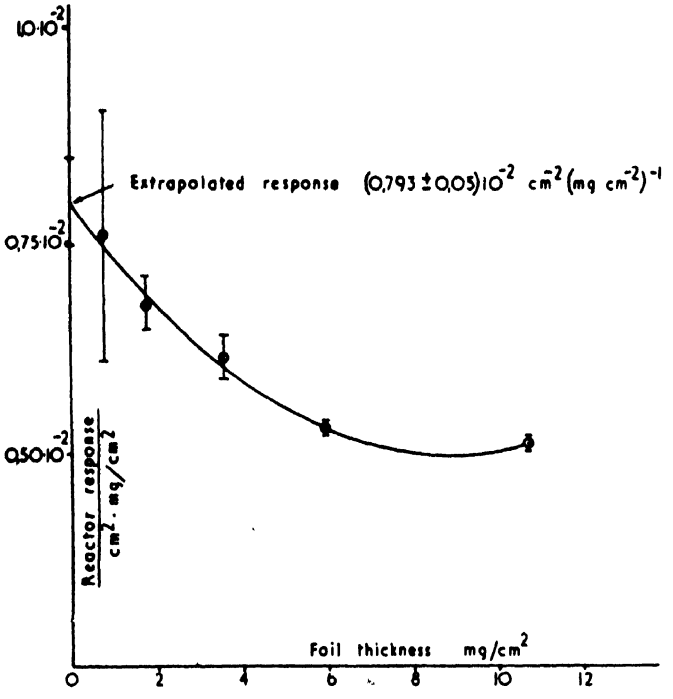

Figure 2. In calibration

CALIBRATION

The calibration of the measurements was performed with In-foils. As any practical thickness of In-foils will show self-protection, it was necessary to use a series of foils of varying thicknesses and extrapolate to zero thickness in order to obtain the correct reactor response per In-atom.

The foils were prepared by vacuum-evaporating pure In on to thin-walled Al-cylinders of dimensions: 90 mm length, 19 mm diameter. In-layer thicknesses of from 0.4 to 5 mg/cm² were employed. Foil area was 54 cm². The value of the resonance integral of In was taken from Hughes.[3] The value given there for In^{118} is 2800 barns (calculated). This is higher than the resonance activation integral of 2580 barns quoted by Hughes. We then adopt for the element In:

Resonance absorption integral = 2720 barns
Resonance activation integral = 2520 barns

The results of the calibration measurements are shown in Fig. 2. Here the reactor response to In-foils, per unit thickness and unit area is drawn against the thickness of the foil. The full-drawn curve is the best parabola found from a least-squares analysis according to M. E. Rose.[4]

RESULTS

Assuming the value 2720 barns for the resonance absorption integral of In, we find

$$\int \sigma_{eff} \frac{dE}{E} = (9.37 \pm 0.59) \left\{1 + (2.89 \pm 0.03) \frac{S}{M}\right\}$$

On the other hand, using the activation integral 2520 barns, we obtain

$$\int \sigma_{eff} \frac{dE}{E} = (8.66 \pm 0.56) \left\{1 + (2.89 \pm 0.03) \frac{S}{M}\right\}$$

If the difference between the resonance absorption and activation integrals is real, it is necessary to apply the first one. The second one should, however, give a lower limit to the measured effective resonance integral of uranium.

No correction has been applied due to a possible effect from fast fission. The work is still in progress.

A very good survey of the use of the pile-oscillator for measuring resonance integrals, is given by A. Langsdorf, Jr.[5]

ACKNOWLEDGEMENTS

The authors are greatly indebted to: T. Holm Hansen, F. Palm, R. Strand, A. Sunde, and S. Saether for their help in performing the experiments. Special thanks to B. Grimeland and A. Sunde who, in collaboration with W. Hälg, have constructed the pile-oscillator.

REFERENCES

1. Creutz, E., Jupnik, H., Snyder, T. and Wigner, E., *Review of Measurements of the Resonance Absorption of Neutrons by Uranium in Bulk.*
2. Glasstone, S. and Edlund, M. C., *The Elements of Nuclear Reactor Theory*, D. van Nostrand Company, New York (1952).
3. Hughes, D. J., *Pile Neutron Research*, p. 139. Addison-Wesley Publishing Company, Inc., Cambridge 42, Mass.
4. Rose, M. E., *The Analysis of Angular Correlation and Angular Distribution Data*, Phys. Rev. *91:* 610 (1953).
5. Langsdorf, A. Jr., *The Thermal Neutron Reactor as an Instrument for Measuring Neutron Cross Sections*, ANL 4342.

Computation of the Effective Resonance Integral

By E. F. M. van der Held,* The Netherlands

From the measurements of E. Hellstrand and R. Persson,[1] on the resonance absorption of neutrons by uranium the following conclusions can be drawn:

MEASUREMENTS AT THE RESONANCE LEVEL OF 6.6 EV

1. The Breit-Wigner formula for the variation, with the energy E of the incident neutron, of the nuclear cross section σ_a for resonance capture by uranium is represented by:

$$\sigma_a = \frac{\sigma_0}{1 + \frac{4}{\Gamma^2}(E - E_r)^2} \qquad (1)$$

σ_0 being the maximum of σ_a, Γ the total level width and E_r the energy of the incident neutron at resonance. The temperature of the uranium causes a Doppler broadening of the line. If $\Delta = 2[(m/M)EkT]^{1/2}$ is half the Doppler broadening, m the mass of the neutron, E its energy, M the mass of the nucleus, k the Boltzmann constant and T the absolute temperature of the medium, the energy dependence of the neutron cross section in the neighbourhood of a resonance level is:

$$\sigma_a = \sigma_0 \frac{a}{\sqrt{\pi}} \int_0^\infty \gamma e^{-\gamma^2} \arctan \left(\frac{4\gamma/a}{1 + \frac{4}{\Gamma^2}(E - E_r)^2 - \frac{4\gamma^2}{a^2}} \right) d\gamma \qquad (2)$$

with $a = \Gamma/\Delta$. This integral has been computed by the author.[2] The total absorption in a layer with n absorbing nuclei per cm² is given by:

$$A = J_0 \int_{-\infty}^{+\infty} (1 - e^{-n\sigma_a})\, dE \qquad (3)$$

The results of these integrations are given in the same article. For $a \geq 10$ the integrations can be carried out. One finds

$$A = \Gamma J_0 \frac{\pi}{2} n\sigma_0 \exp\left(-\frac{1}{2}n\sigma_0\right) \left\{ I_0\left(\frac{1}{2}n\sigma_0\right) + I_1\left(\frac{1}{2}n\sigma_0\right) \right\} \qquad (4)$$

I_p being the modified Bessel function of the first kind and the order p. The results of these computations are given in Fig. 1. For $n\sigma_0 < 0.1$: $A/\Gamma J_0 = (\pi/2)n\sigma_0$; for $a \geq 3$ and $n\sigma_0 > 1$, and for $a < 3$ and $n\sigma_0 > (2 - 2 \log a)$: $A/\Gamma J_0 = \sqrt{\pi n\sigma_0}$.

In a double logarithmic plot of the measured values of A/J_0 against the weight of UO_3(gm/cm²) the slope of the curve through the points (Fig. 1) is nearly ½, so there is self shielding. Adjustment of the measurements in Fig. 1 with the given accuracy is possible for different values of a. Because of the negative deviation of the lowest point from the line with slope ½ this measurement has to lie in the neighbourhood of the line

$$\frac{A}{\Gamma J_0} = \frac{\pi}{2} n\sigma_0$$

If we choose the highest value of a for which the measurements can be adjusted to the theoretical curve, we find a value which is nearest to values found by others. In Fig. 1 we have made this adjustment, the highest and at the same time best value of a is about 1. The relative absorption (A/J_0) on a logarithmic time-of-flight scale has been adjusted to the theoretical scale of log ($A/(\Gamma J_0)$) and to the logarithmic scale of the mass (gm UO_3/cm²) we have added the adjusted theoretical scale of log ($n\sigma_0$). From the first set we find Γ and from the second set σ_0, the value of n following from the grams of UO_3/cm² used.

Having stated that $a \approx 1$, we can get more accurate results in the following way:

For the thickest layer used and for $a \approx 1$ the corresponding point in Fig. 2 will be situated on the line $A/\Gamma J_0 = \sqrt{\pi n\sigma_0}$. In this case A/J_0 was found to be 1.42 μsec/m or 0.665 ev and after the adjustment $A/\Gamma J_0$ turned out to be 14.6. Thus $\Gamma = 0.0455$ ev. As $\Delta = 0.052$ ev, we find a to be 0.87. The given values of Γ and a are upper limits with an accuracy of about 30% (7% in the measurement for the thickest layer and about 20% in the adjustment).

The mass of the thickest layer is 5.46 gm UO_3/cm² with $n = 1.15 \times 10^{22}$ U-nuclei/cm². Reading $n\sigma_0$ for this layer from the adjusted scale in Fig. 2 we find 69 ± 21 for it. Then the maximum cross section is 6000 ± 1800 barns and the value of $\sigma_0\Gamma = 273 \pm 82$ barn-ev. The accuracy of this product will be better than the one of Γ alone because an increase of Γ causes a decrease of σ_0.

2. There are more resonance levels, which we shall designate with successive Roman numbers in order of increasing energy, thus $\sigma_I\Gamma_I = 273 \pm 82$ barn-ev. The

* The Netherlands Reactor Research Group of the F.O.M., Utrecht.

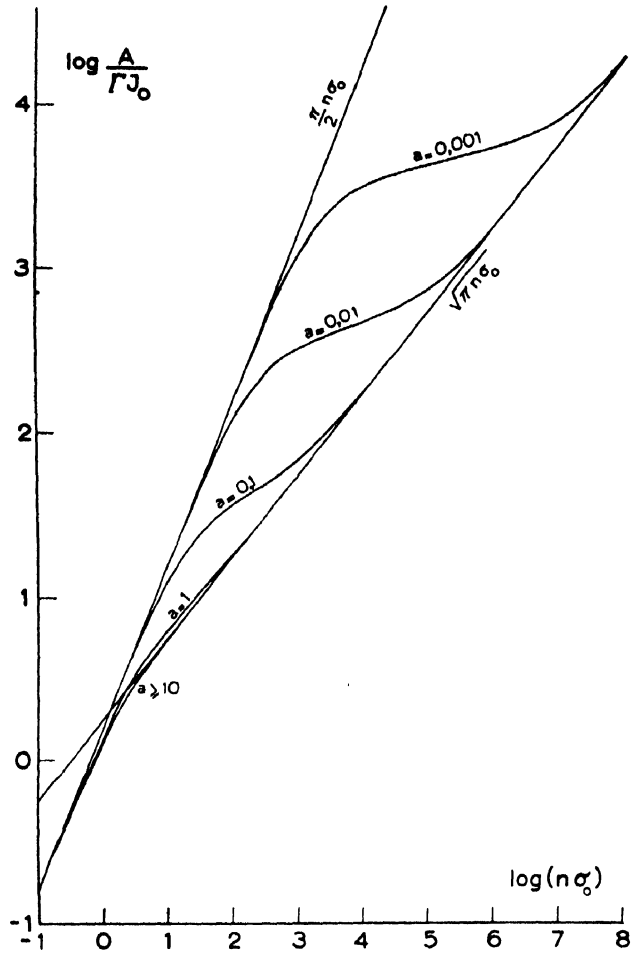

Figure 1

second level is at about 20 ev, and the third at about 38 ev. Hellstrand and Persson[1] assuming self-shielding, give $\sigma_{II}\Gamma_{II}^2 = 4.5$ barn (ev)^2 and $\sigma_{III}\Gamma_{III}^2 = 6.5$ barn (ev)^2. Neglecting the possibility of self-shielding one finds $\sigma_{II}\Gamma_{II} = 22.3$ barn-ev and $\sigma_{III}\Gamma_{III} = 26.8$ barn-ev. This is only possible if $\Gamma_{II} \geq 0.20$ ev and $\Gamma_{III} \geq 0.24$ ev, i.e., $\alpha_{II} \geq 4$ and $\alpha_{III} \geq 4.5$ (these measurements have only been made with the thickest layer of 5.46 gm UO_3/cm^2. Then with the aid of Fig. 1 one can find these limits). In the case of self-shielding $\Gamma_{II} < 0.20$ ev $<$ and $\Gamma_{III} < 0.24$ ev and thus $\sigma_{II}\Gamma_{II} >$ 22.3 barn-ev and $\sigma_{III}\Gamma_{III} >$ 26.8 barn-ev. The higher values for Γ being improbable, self-shielding is assumed. Γ_{III} and Γ_{II} being unknown we shall assume that they equal Γ_I. With this assumption $\sigma_{II}\Gamma_{II}$ becomes 100 barn-ev, $\sigma_{III}\Gamma_{III} = 140$ barn-ev and σ_{II} and σ_{III} 2200 and 3100 barns respectively. Resonances at higher levels than the three considered are unimportant with respect to the following computations. Summarizing, we remark that for more reliable results further measurements have to be supplied:

(*a*) A measurement at the first level with a still thinner layer than the thinnest one of Hellstrand and Persson. Therefore the resolving power of the apparatus has to be improved, if possible.

(*b*) Measurements at the second and third level. These have to be extended over such a range of thicknesses that the lowest one is at the proportional part of the curves of Fig. 1 and the highest one is on the line with slope ½. Then Γ_{II}, Γ_{III}, σ_{II} and σ_{III} can be calculated with a reasonable accuracy.

SLOWING DOWN DENSITY

The slowing down density in homogeneous materials with N different sorts of nuclei is given by

$$q = \sum_{i=1}^{N} \int_{E}^{E/\alpha_i} \frac{\Sigma_{si}}{\Sigma_s + \Sigma_a} \cdot \frac{E - \alpha_i E'}{E'(1 - \alpha_i)} \cdot F(E') \cdot dE' \quad (5)$$

with $\alpha = [A - 1/(A + 1)]^2$; A = mass of the nucleus, Σ_{si} = macroscopic cross section for scattering by nucleus i, Σ_s and Σ_a total macroscopic cross sections for scattering and for absorption respectively and $F(E)$ = the collision density given by:

$$F(E) = \sum_{i=1}^{N} \int_{E}^{E/\alpha_i} \frac{\Sigma_{si}}{\Sigma_s + \Sigma_a} \cdot \frac{F(E')}{E'(1 - \alpha_i)} dE' \quad (6)$$

The quantity

$$\int a(E) \frac{dE}{E} = \xi \sigma_s \ln \frac{q_0}{q}$$

is known experimentally in some cases, ξ being the mean value of the average logarithmic energy decrement per collision and q_0 the slowing down density at the higher energy and q that at the lower energy. We shall check the value of $\int a(E)\, dE/E$, computed from

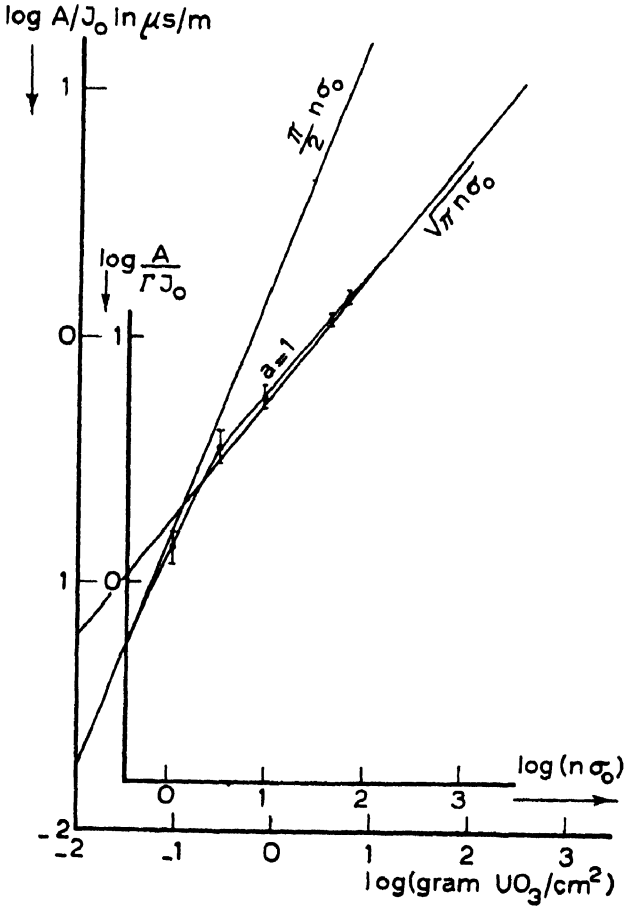

Figure 2

Table 1. (E_r = 6.6 ev)

E(ev)			E(ev)		
7.400	9.21×10^{-4}	6.50×10^{-2}	6.575	0.471	1.28×10^{-10}
7.375	9.85×10^{-4}	5.47×10^{-2}	6.550	0.313	1.98×10^{-11}
7.350	1.05×10^{-3}	4.61×10^{-2}	6.525	0.175	$3.07_5 \times 10^{-12}$
7.325	1.13×10^{-3}	3.62×10^{-2}	6.500	9.17×10^{-2}	5.06×10^{-13}
7.300	1.21×10^{-3}	2.93×10^{-2}	6.475	5.25×10^{-2}	1.02×10^{-13}
7.275	$1.30_5 \times 10^{-3}$	2.33×10^{-2}	6.450	3.34×10^{-2}	2.48×10^{-14}
7.250	1.41×10^{-3}	1.84×10^{-2}	6.425	2.36×10^{-2}	7.17×10^{-15}
7.225	1.53×10^{-3}	1.43×10^{-2}	6.400	1.76×10^{-2}	2.35×10^{-15}
7.200	1.66×10^{-3}	1.10×10^{-2}	6.375	1.32×10^{-2}	8.40×10^{-16}
7.175	1.81×10^{-3}	8.33×10^{-3}	6.350	1.02×10^{-3}	3.29×10^{-16}
7.150	1.98×10^{-3}	6.20×10^{-3}	6.325	8.36×10^{-3}	1.39×10^{-16}
7.125	2.18×10^{-3}	4.52×10^{-3}	6.300	7.05×10^{-3}	6.27×10^{-17}
7.100	2.40×10^{-3}	3.25×10^{-3}	6.275	6.04×10^{-3}	3.03×10^{-17}
7.075	2.67×10^{-3}	2.28×10^{-3}	6.250	5.21×10^{-3}	1.52×10^{-17}
7.050	2.98×10^{-3}	1.57×10^{-3}	6.225	4.55×10^{-3}	7.88×10^{-18}
7.025	3.34×10^{-3}	1.05×10^{-3}	6.200	4.01×10^{-3}	4.28×10^{-18}
7.000	3.78×10^{-3}	6.90×10^{-4}	6.175	3.57×10^{-3}	2.42×10^{-18}
6.975	4.30×10^{-3}	4.38×10^{-4}	6.150	3.19×10^{-3}	$1.40_5 \times 10^{-18}$
6.950	4.95×10^{-3}	2.72×10^{-4}	6.125	2.86×10^{-3}	8.38×10^{-19}
6.925	5.74×10^{-3}	1.64×10^{-4}	6.100	2.59×10^{-3}	5.14×10^{-19}
6.900	6.74×10^{-3}	9.56×10^{-5}	6.075	2.36×10^{-3}	3.24×10^{-19}
6.875	8.03×10^{-3}	5.35×10^{-5}	6.050	$2.15_5 \times 10^{-3}$	2.09×10^{-19}
6.850	9.83×10^{-3}	2.80×10^{-5}	6.025	1.97×10^{-3}	1.37×10^{-19}
6.825	1.28×10^{-2}	1.43×10^{-5}	6.000	1.82×10^{-3}	9.18×10^{-20}
6.800	1.52×10^{-2}	6.99×10^{-6}	5.975	1.68×10^{-3}	6.23×10^{-20}
6.775	2.30×10^{-2}	3.17×10^{-6}	5.950	$1.55_5 \times 10^{-3}$	4.37×10^{-20}
6.750	3.26×10^{-2}	1.43×10^{-6}	5.925	1.44×10^{-3}	3.09×10^{-20}
6.725	5.15×10^{-2}	5.31×10^{-7}	5.900	1.35×10^{-3}	2.21×10^{-20}
6.700	9.05×10^{-2}	1.84×10^{-7}	5.875	1.26×10^{-3}	1.61×10^{-20}
6.675	0.173	5.92×10^{-8}	5.850	1.18×10^{-3}	1.19×10^{-20}
6.650	0.311	1.67×10^{-8}	5.825	1.11×10^{-3}	8.92×10^{-21}
6.625	0.469	4.03×10^{-9}	5.800	1.04×10^{-3}	6.77×10^{-21}
6.600	0.545	7.65×10^{-10}			

the data of Hellstrand and Persson with the aid of Equations 5 and 6 for pure natural uranium.

As the level width is not known accurately we have used the value $\Gamma = \Delta = 0.050$ ev and thus $a = 1$.

We start with the resonance level at 6.6 ev, neglecting as yet the other levels at 20 and 30 ev. For energies higher than 8.4 ev the capture can be taken as slowly varying. Then according to G. Goertzel and E. Grueling[3] we can use the formula:

$$\frac{q}{q_0} = \exp\left(-\int_E^{E_0} \frac{\Sigma_a}{\xi\Sigma_s + \gamma\Sigma_a}\frac{dE'}{E'}\right) \qquad (7)$$

γ being $1 - \dfrac{\frac{1}{2}\alpha\epsilon^2}{1 - \alpha - \alpha\epsilon}$ and $\epsilon = \ln\left(\dfrac{1}{\alpha}\right)$

Then the collision density is:

Table 2. (E_r = 20 ev)

E (ev)			E(ev)		
21.00	6.10×10^{-4}	3.18	20.10	0.170	0.303
20.95	6.76×10^{-4}	3.10	20 05	0.277	0.191
20.90	7.55×10^{-4}	3.00	20.00	0.326	0.109
20.85	8.46×10^{-4}	2.89	19.95	0.277	5.31×10^{-2}
20.80	9.56×10^{-4}	2.77	19.90	0.170	2.05×10^{-2}
20.75	1.09×10^{-3}	2.63	19.85	7.9×10^{-2}	6.87×10^{-3}
20.70	1.29×10^{-3}	2.47	19.80	3.25×10^{-2}	2.43×10^{-3}
20.65	1.52×10^{-3}	2.30	19 75	1.43×10^{-2}	1.07×10^{-3}
20.60	1.76×10^{-3}	2.14	19.70	8.71×10^{-3}	6.02×10^{-4}
20.55	2.14×10^{-3}	1.97	19.65	6.24×10^{-3}	3.90×10^{-4}
20.50	2.59×10^{-3}	1.79	19.60	4.47×10^{-3}	2.81×10^{-4}
20.45	3.37×10^{-3}	1.60_5	19.55	3.44×10^{-3}	2.21×10^{-4}
20.40	4.39×10^{-3}	1.43	19.50	2.65×10^{-3}	1.84×10^{-4}
20.35	6.13×10^{-3}	1.23	19.45	2.20×10^{-3}	1.58×10^{-4}
20.30	8.58×10^{-3}	1.005	19.40	1.82×10^{-3}	1.36×10^{-4}
20.25	1.41×10^{-2}	0.807	19.35	1.55×10^{-3}	$1.19_5 \times 10^{-4}$
20.20	3.21×10^{-2}	0.618	19.30	1.33×10^{-3}	1.05×10^{-4}
20.15	7.9×10^{-2}	0.445			

$$F(E) = \frac{\Sigma_a + \Sigma_s}{\Sigma_a}\frac{dq}{dE} = \frac{q_0}{E}\frac{\Sigma_a + \Sigma_s}{\xi\Sigma_s + \gamma\Sigma_a} \exp\left(-\int_E^{E_0}\frac{\Sigma_a}{\xi\Sigma_s + \gamma\Sigma_a}\frac{dE'}{E'}\right) \quad (8)$$

From 7.4 ev to 5.8 ev we have used Equation 6 proceeding with steps of only 0.025 ev. From about 0.085 ev the integration-path is known from the preceding steps. Moreover, the values of the integrand at the lower energies are much smaller than at the higher ones. So a rough extrapolation will do. For energies lower than 5.8 ev we have used Equation 8 again, adapted to the value found with the step-by-step method. As we have now to use Equation 1 at greater distances from the resonance level we cannot neglect the factor $\sqrt{E_r/E}$. Then the integral in Equations 7 and 8 becomes:

$$G = \int_E^{E_0}\frac{\sigma_a}{\xi\sigma_s + \gamma\sigma_a}\frac{dE'}{E'} = \frac{\Gamma^2\sigma_0}{2\xi\sigma_s E_r^2} \int_{\sqrt{E/E_r}}^{\sqrt{E_0/E_r}} \frac{1}{\kappa^5 - 2\kappa^3 + \left(1 + \frac{\Gamma^2}{4E_r^2}\right)\kappa + \frac{\gamma\sigma_0\Gamma^2}{\xi\sigma_s 4E_r^2}}\frac{d\kappa}{\kappa} \quad (9)$$

with $\kappa = \sqrt{E/E_r}$ and E_r = resonance level. Now $\Gamma^2/4E_r^2 \ll 1$. We shall neglect this quantity. Moreover E_0/E_r is so great that we may substitute for $\sqrt{E_0/E_r}$ by ∞. Putting

$$P = \frac{\gamma\sigma_0}{\xi\sigma_s}\cdot\frac{\Gamma^2}{4E_r^2}$$

we find in the cases that $P < 0.01$:

$$G = \frac{3P}{4\gamma}\ln\frac{\kappa^2 + a_0\kappa + a_1}{(\kappa - c)(\kappa - d)} + \frac{2P^2}{\gamma}\ln\frac{(\kappa - b)^4}{(\kappa^2 + a_0\kappa + a_1)(\kappa - c)(\kappa - d)} + \frac{2}{\gamma}\ln\left(1 - \frac{b}{\kappa}\right) + \frac{\sqrt{P}}{2\gamma}\left(1 + \frac{77}{32}P\right)\ln\frac{\kappa - d}{\kappa - c} + \frac{\sqrt{P}}{\gamma}\left(1 - \frac{77}{32}P\right)\arctan\frac{\sqrt{a_1 - \frac{1}{4}a_0^2}}{\kappa + \frac{1}{2}a_0} \quad (10)$$

with:

$$a_0 = -2 - \tfrac{1}{2}P + \tfrac{35}{64}P^2 \ldots$$
$$a_1 = 1 + \tfrac{3}{4}P - \tfrac{23}{32}P^2 \ldots$$
$$b = -P - 2P^3 \ldots$$
$$c = -1 + \tfrac{1}{2}\sqrt{P} + \tfrac{1}{4}P + \tfrac{15}{64}P^{3/2} + \tfrac{35}{128}P^2 \ldots$$
$$d = -1 - \tfrac{1}{2}\sqrt{P} + \tfrac{1}{4}P - \tfrac{15}{64}P^{3/2} + \tfrac{35}{128}P^2 \ldots$$
$$\sqrt{a_1 - \tfrac{1}{4}a_0^2} = \tfrac{1}{2}\sqrt{P} - \tfrac{15}{64}P^{3/2} \ldots$$

We have used the following values: $E_r = 6.60$ ev; $\Gamma = 0.050$ ev; $\Delta = 0.050$ ev; $\sigma_0 = 6000$ barns; $\sigma_s = 8.3$ barns; $\xi = 0.00834$; $\gamma = 0.00557$. Starting with Equation 10 we have computed G and with Equation 8 $F(E)/q_0$ for some values of E in the neighbourhood of $E = 7.4$ ev and stated that these values are in accordance with Equation 6. Then we used this formula to proceed, step by step, to lower energies using the values of σ_a/σ_0 computed with Equation 2. The results of these computations are given in Table 2. Below $E = 5.8$ ev we can return to Equation 10 because the capture is then slowly varying again. The upper limit of the integration is now $\kappa = \sqrt{5.8/6.6}$. If we use ∞ as the upper limit we have to correct the value of G by adding the difference of G computed from the value $F(E)/q_0$ in Table 1 with the aid of Equation 8 and G computed with Equation 10. We find $\Delta G = 49.6 - 34.8 = 14.8$. For neutrons slowed down to thermal energy ($E = 0.026$ ev) we find, giving the values of the terms of Equation 10 in the same sequence, and at the end ΔG:

$$G = -0.225 - 0.184 + 37.595 + 0.5985 + 45.525 + 14.8 = 98.1$$

We see that 38.5% of G originates at energies where the capture is inversely proportional to the neutron velocity.

We repeat the calculations for the resonance level at 20 ev assuming as in part I that $\Gamma_{II} = \Gamma_I$, that Δ is now 0.10 ev, i.e., $a = \frac{1}{2}$, and that $\sigma_0 = 2000$ barns, we find the values of σ_a/σ_0 and $F(E)/q_0$ as given in Table 2. ΔG is now 2.96 and G for thermal neutrons:

$$G = -0.0044 - 0.00025 + 2.26 + 0.020 + 8.483 + 2.96 = 13.7$$

As these calculations take much time and as we have seen by the foregoing examples the trend of ΔG (I: $\Delta G = 15.1\%$ of G; II: $\Delta G = 21.6\%$ of G), we assume, for level III ($E = 38$ ev), ΔG to be 30% of G. Then:

$$G = (-0.0006 - 0.00004 + 1.245 + 0.0079 + 5.360):0.70 = 9.5$$

Thus the total value of G will be $G_{tot} = 98.1 + 13.7 + 9.5 = 121.3$ and $\int a\,dE/E = \xi\sigma_s G = 0.00834 \times 8.3 \times 121.3 = 8.4$ barns as against 9.25 barns, given by Glasstone and Edlund. In view of the accuracy with which σ_0 and Γ are known, this is a better agreement than could be expected.

The calculations given will, however, yield a still better agreement with the measured value of the resonance integral when Hellstrand and Persson's[1] data will have been completed by some additional measurements.

REFERENCES

1. Hellstrand, E. and Persson, R., Arkiv für Fysik *6*, 57 (1953).
2. Van der Held, E. F. M., Ztschr. f. Physik *70*, 508 (1951).
3. See Glasstone, S. and Edlund, M. C., *The Elements of Nuclear Reactor Theory*, van Nostrand, p. 168 (1952).

Experiments on Some Characteristics of the NRX Reactor Part I—Methods and Prolonged Fuel Irradiation

By D. G. Hurst,* Canada

DESCRIPTION OF THE REACTOR

The NRX Reactor, Fig. 1, is a natural-uranium heavy-water-moderated reactor with light-water cooling of the rod-assemblies. The uranium is in the form of long rods (Table 1). Each rod is sheathed in an aluminium tube having three fins for centering in an outer aluminium sheath. The light water flows through the annulus between the aluminium sheaths and carries away about 95% of the heat. The uranium assemblies hang vertically through tubes in the heavy-water vessel called the "calandria." This is of aluminium, and is cylindrical with diameter 8.75 feet (2.67 metres) and height 10.5 feet (3.2 metres). It is pierced by 198 vertical tubes 2.25 inches (5.72 cm) diameter for the fuel, control, and shut-off rods, Fig. 2. A central tube of larger diameter is called the "central thimble." The calandria is surrounded by a cylindrical graphite reflector and steel and concrete shields. Two graphite thermal columns terminated at the outer end by cadmium-lined lead doors extend through the concrete shield. Ionisation instruments for control and measurement are located near the outer boundary of the reflector and in a thermal column.

The level of the heavy water is controlled by flow over a weir and is adjustable over the full height of the calandria, thus providing the primary control and measure of reactivity. The mechanism for moving the weir box is sensitive to ± 0.01 cm, and consistency of low-power behaviour of the reactor indicates that the weir setting is reproducible to ± 0.02 cm. The flow over the weir is approximately 23 litres per minute; circulation of the heavy water at the rate of 900 litres per minute from the calandria through heat exchangers and pumps and back to the calandria causes no difficulty in control by the weir. A small oscillation in the neutron flux (amplitude 0.4%, frequency 0.82 cycles per second) is attributed to selective response of reactor power to the fundamental radial mode of the surface disturbance caused by this heavy-water circulation.

The temperature of the heavy water is not measured in the calandria, instead a recorder-controller is connected to a resistance thermometer element between the calandria and the heat exchangers. Reactivity tests during rapid temperature changes have proved that the indications of this instrument represent sufficiently well the effective moderator temperature. The temperature may be read to 0.1°F, and is controlled automatically through variation of the light-water supply to the heat exchangers. Under almost steady conditions the temperature remains within ± 1°F, and for transient conditions similar constancy can be realised by manual adjustment of the control point.

At present eighteen of the calandria tubes, arranged symmetrically in three rings of six, are assigned to shut-off rods. During operation these tubes are empty except for thin aluminium sheaths. A control rod located about two-thirds of the core radius from the centre operates in one tube and takes care of small reactivity drifts by automatic control. The fractional insertion of the control rod is used as a secondary measure of reactivity.

OPERATIONAL FEATURES

Power and Flux

The present operating power is 40 Mw, achieved in steps from the original design maximum of 20 Mw. With slight modifications 30 Mw operation was possible. During the restoration which followed an accident in 1952 the cooling of the top and bottom thermal shields was improved and the increase to 40 Mw total power was then made. The maximum power is permissible only with the calandria almost full. Before xenon poison builds up, the reactor operates at reduced heavy-water depth and the power is correspondingly reduced to keep the maximum heat flux approximately constant. Some values of the neutron flux at 40 Mw are tabulated (Table 2). By flux is meant the quantity nv where n = neutron density and $v = 2.2 \times 10^5$ cm/sec = 2200 metres/sec.

Weir-Box Control, Reactivity

The weir-box can be rapidly set to a new position after which some time is required for the moderator to reach the new level in the calandria. The readjustment is almost complete 15 minutes after a small change, but for high precision 30 minutes must be allowed.

For a bare cylinder the vertical Laplacian is π^2/h^2 where h is the extrapolated height. A flux survey showed that the extrapolated height of NRX can be written

* Assistant Director, Research and Development Division, Atomic Energy of Canada Limited, Chalk River, Ontario.

h = Weir-Box Setting + 22 cm

where the extrapolation distance of 22 cm is usually assumed to be constant.

The quantity π^2/h^2 and the difference $\delta(\pi^2/h^2)$ of two such quantities are useful measures of reactivity and will be used constantly in these papers. On account of the reflector the relationship between $\delta\kappa^2$, the change in Laplacian, and $\delta(\pi^2/h^2)$ is approximately

$$\delta\kappa^2 = 1.07\ \delta(\pi^2/h^2)$$

An alternative measure of reactivity change is $M^2\delta(\pi^2/h^2)$, a conventional expression for the change in effective multiplication, where $M^2 = 312$ cm^2. $10^3M^2\ \delta(\pi^2/h^2)$ is said to be in "milli-k units."

MEASUREMENT OF REACTIVITY

General

Reactivity measurements in NRX relate primarily to the critical value of weir-box setting and thus to h_0 the "critical height" which is found most directly by operating at critical. When the change in critical height due to substituting one rod for another or some similar operation involving shut down is to be measured, it is advisable to avoid complications arising from thermal effects and xenon-production by keeping the power below 50 kw. For some time after operation at high power there is a strong source of photoneutrons and the reactor is appreciably subcritical at these low powers. The weir-box setting for steady

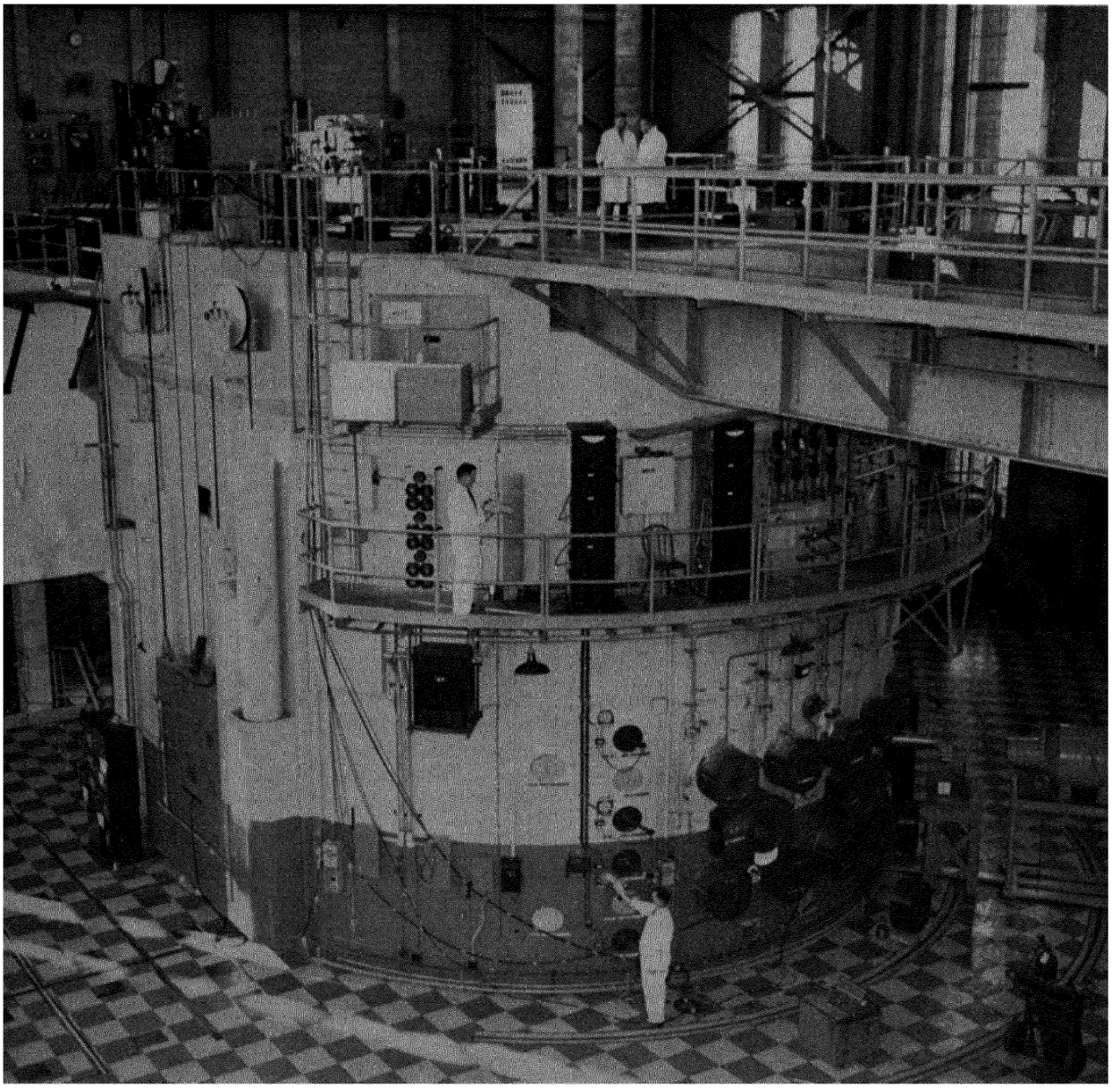

Figure 1. The NRX reactor. The mid plane of the calandria is about six feet from the floor and is marked by the boundary between the light and dark paint on the cylindrical concrete shield. To the right are beam exit ports where holes run through the shield and provide neutron beams for experimental purposes. To the left is the lead door (with pulleys and counter-weights) which covers the south thermal column

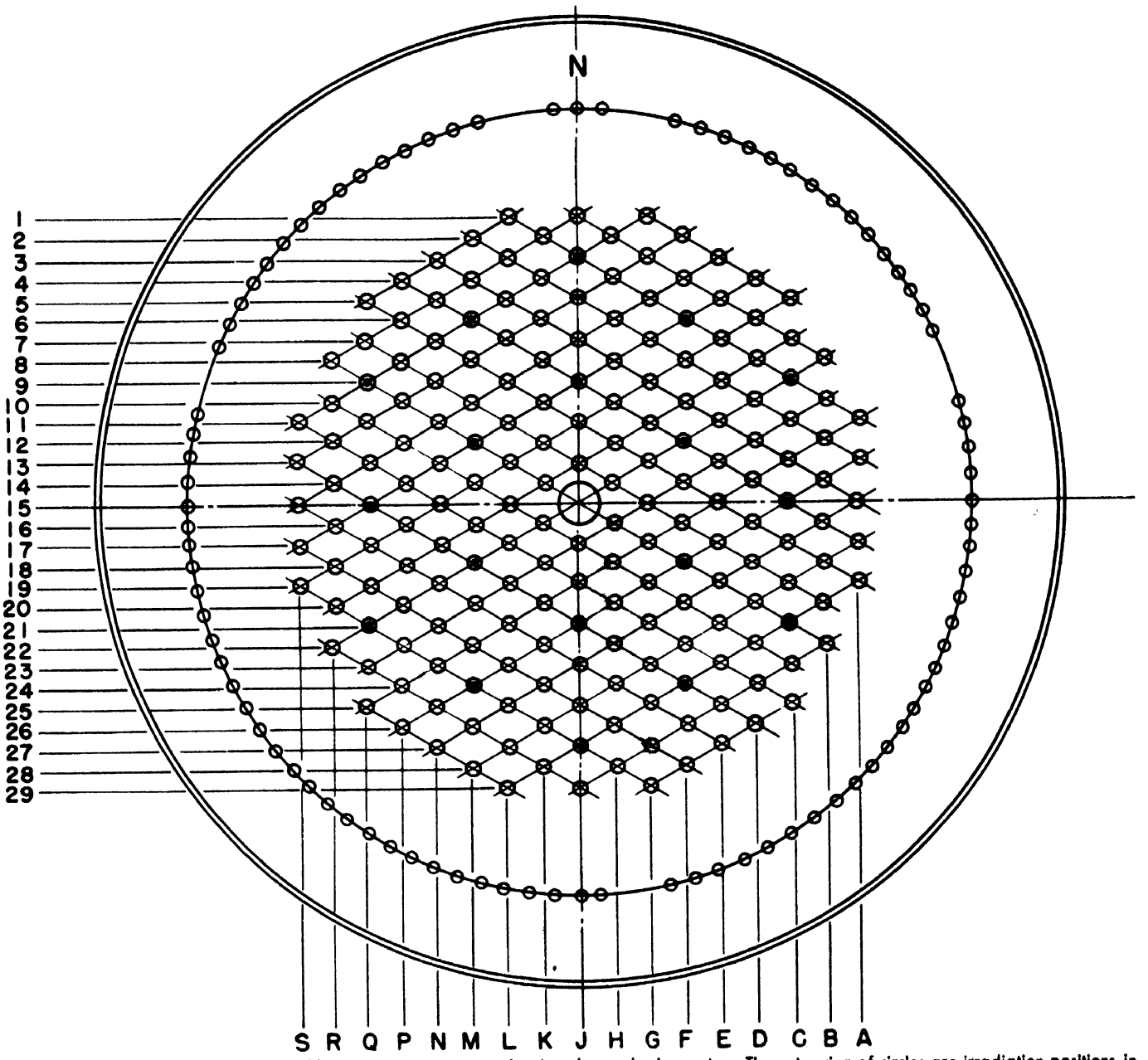

Figure 2. A schematic drawing of the NRX lattice arrangement showing the numbering system. The outer ring of circles are irradiation positions in the reflector. The large circle J-15 is the "central thimble." The control rod is at J-5 and shutoff rod positions are marked, for example as at J-3

power does not then represent a critical condition. Moreover the behaviour is sluggish, and to the extent that the photoneutron sources are decaying the equilibrium is secular. Consequently the direct method is unsuitable at low power if the uranium rods are not fresh. It was used when NRX was first started and again in 1954 especially for determination of temperature coefficients.

Three other methods giving the critical height during low-power conditions following normal operation will be outlined. These are the measurement of period, extrapolation to critical, and variation of the subcritical flux by a calibrated absorber.

Period

The use of period for reactivity determinations is standard practice with graphite reactors, involving the well-known "inhour" formula. Figure 3 shows the course of the flux during a period measurement. Without the photoneutrons the early part would be a straight line (the curvature late in the run is produced by thermal effects and sets an upper limit on

Table 1. Dimensions of NRX Rod-Assembly

Item	*Dimension*	*Magnitude*	
		English	*Metric*
Uranium	Diameter	1.36 inches	3.46 cm
	Length (approx.)	122 inches	3.10 metres
Aluminium sheath	Thickness	0.079 inches	0.20 cm
Outer aluminium sheath*	Internal diameter	1.66 inches	4.22 cm
	Thickness	0.040 inches	0.10 cm

* Early models had a slightly larger outer sheath. The light water annulus then had 1.5 times the present area.

the useful power range). The lower curve can be rectified by the addition of a constant, found by trial and error, with the result shown. In this way periods can be measured and used even when the source is too large for steady-state operation. The added constant varies as the source strength and inversely as the excess multiplication. A calibration curve (Fig. 4) obtained under suitable conditions can be used to transform periods determined in this way to excess height. There are difficulties in following a rapidly changing reactivity; for example, the weir must be set at a suitable height well in advance of the period run to permit the moderator to reach its equilibrium level. If a sensitivity of 0.01 cm is desired the period must be measured accurately. In practice periods from 100 to 200 seconds have been used, the accuracy aimed at being 1%. This method was applied in a study of the growth and decay of xenon following shut down from 1.4 Mw. It appears to be unsuitable for use after shut down from full power.

Extrapolation

Instead of finding the critical height from period measurements with excess reactivity, extrapolation may be made from a sub-critical condition. An approach to critical by raising the weir in steps at sufficiently long intervals for the power to level off at each step, permits an extrapolation to critical as in the common start-up procedure for new reactors. Over a range of many centimetres the graph of $(\text{flux})^{-1}$ *vs* π^2/h^2 is generally a straight line which may be extrapolated to meet the π^2/h^2 axis at π^2/h_c^2. Many measurements of this kind have been made in NRX, especially in determining reactivity effects of individual rods. The method is basically capable of good precision, but it is time consuming as at least two weir settings must be used and a single determination takes three or four hours. Drifts in the reactor over this interval can introduce errors; the extrapolation itself even with a source equivalent to 5 or 10 watts is accurate to ± 0.02 cm.

When measurements were attempted with the calandria nearly full, as described below, the points did not lie on a straight line. The curvature was ascribed to a dependence of upper extrapolation distance on heavy-water depth (a decrease of several centimetres is expected between low level and full depth but the manner of decrease is not known). The method was abandoned and replaced by a technique using a standard absorber. This has become the preferred method for sub-critical operation.

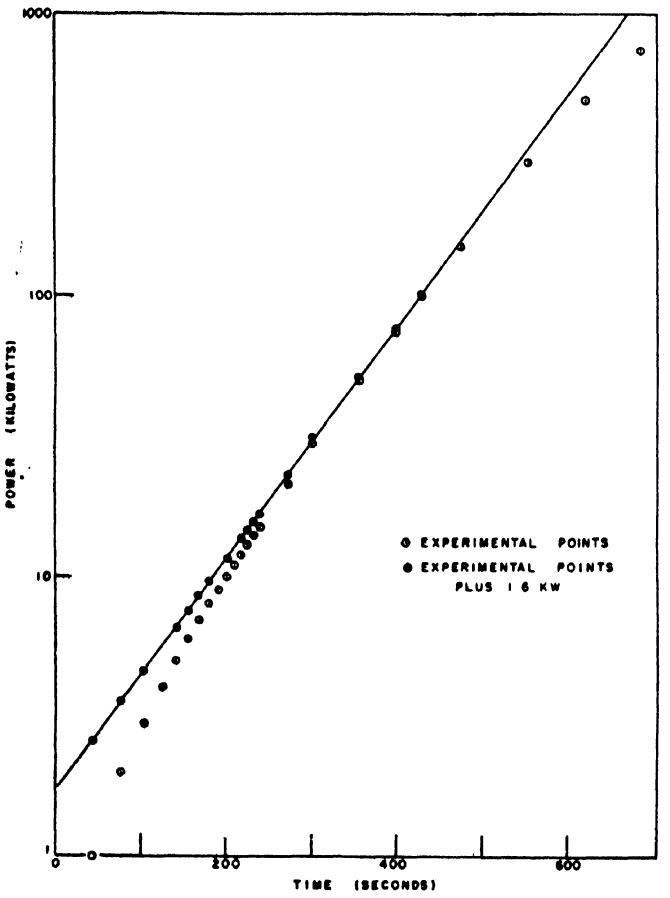

Figure 3. A typical period run. The curvature at low power is caused by the presence of photoneutron sources and can be removed by the addition of a constant power, in this case 1.6, to all the experimental points as shown. The curvature beyond 100 is due to thermal effects. The period obtained from the straight line is 104.5 seconds (doubling time 72.5 seconds)

Standard Absorber

In this method an absorber of known reactivity effect, R; is inserted into the already sub-critical reactor causing the flux to decrease. The initial flux, D_1, and the final flux, D_2, are measured at a location remote from the absorber. The initial amount below critical is given by $RD_2/(D_1 - D_2)$. Thus without moving the weir the reactivity deficit is obtained. It is important, particularly when several weir settings are involved, to use an absorber having radial symmetry and extending the full height of the core. Two applications of this technique have been made: a determination of reactivity changes of rods resulting from irradiation, and a study of xenon poison after shut down from 40 Mw. In the first application the light water in three fuel rods symmetrically located was used. Water was drained from the three rods, and the cooling was maintained by a downward flow of compressed air. Insertion of the absorber consisted of turning off the compressed air and flowing water into the rods from below. In the second application the absorber was an aluminium rod 3 metres long and

Table 2. Flux, (nv_{2200}) for 40 Mw Operation

Location	*Remarks*	*Maximum flux*
Empty Calandria tube	Based on 98 barns for gold	6.8×10^{13} neutrons/cm²/sec
Average across uranium rod at position of maximum flux	Based on $\sigma_f(U)$ = 3.91 barns and 198 Mev per fission	$2.9_5 \times 10^{13}$ neutrons/cm²/sec
Moderator	Maximum in a normal lattice cell	6.0×10^{13} neutrons/cm²/sec

3.75 cm diameter which could be inserted into the central thimble by an electric motor.

The light water was calibrated by measurements at several weir settings. The same procedure was used for the aluminium rod, in addition a direct measurement of the change of critical height was also possible.

In the first application the effects to be measured were small and drifts in the reactor were considered to be the major source of error as each operation took several hours.

In the study of xenon the standard absorber was operated on a regular schedule for six days; at first on a seven-minute half-cycle, then a ten-minute, and finally a twenty-minute half-cycle. Two similar ion chambers, one with a boron coating, were located side by side in a thermal column and connected in opposition to a recorder with an expanded scale. Gamma-ray and activation currents, which were in any case small, balanced each other—thus the reading represented the current produced in the boron-coated chamber by the neutron flux.

A number of errors and corrections applicable to the xenon study will be discussed.

The formula $RD_2/(D_1 - D_2)$ assumes equilibrium, whereas the cycles were short compared to many of the photoneutron lifetimes. The error due to lack of equilibrium has been calculated. It is less than 5×10^{-5} in k and has been ignored. This error is almost independent of the distance from critical, the apparent sluggish behaviour near critical being compensated by the greater magnitude of the flux.

The insertion of the standard absorber disturbs the flux distribution and increases the relative leakage by increasing the harmonics relative to the fundamental. A simple calculation of this effect was made for a bare rectangular pile with the one-group approximation by finding the third-harmonic leakage-current produced by insertion of an absorber along the axis. The result, 0.7%, was applied to the readings with the standard absorber inserted.

At its maximum the xenon poison amounted to more than 0.03 in k. The resulting flux perturbation causes the reactivity effects of xenon and standard absorber to be non-additive. A correction was calculated, again on a simple model of a bare reactor, and applied to that portion of the xenon which grew from iodine after the shut down. (The poisoning effect of the xenon already in the reactor at the time of shut-down was considered to be uniformly distributed as a result of burn-out and thus not to interfere with the standard absorber.) The maximum correction amounted at most to 1.2×10^{-3} in k and was appreciable only for a few hours near the poison peak.

A few other corrections, although not associated with the standard absorber, will be outlined at this time.

The calculated self-interference of the xenon was very small and was neglected.

In the course of the measurement the weir box was lowered in five steps from 259 cm, the level at which the iodine was produced, to 194 cm. The measuring flux did not match the poison distribution and with the "statistical weight theorem" a factor was calculated for each weir setting to reduce the measurements to a common basis. By chance the factor was the same at 259 cm as at 194 cm within 0.4%. The largest correction amounted to 2%.

The isotope-producing load was contained in three positions H-18, L-15 and H-12 symmetrically located. The loading was not quite uniform vertically and the change with weir setting was also calculated. This amounted to 2×10^{-4} in k between 194 cm and 259 cm.

Because the calculated interference corrections are so small, no attempt has been made to improve the accuracy by taking a model which would be a better representation of the reactor.

REACTIVITY LOSSES DUE TO IRRADIATION

Individual Rods

The latest measurements of the loss in reactivity of individual rods were carried out in 1952. Several ranges of irradiation were included, provisionally chosen as (*a*) 3000 (*b*) 1800 (*c*) 900 and (*d*) 250-megawatt days per tonne maximum in the rod. The actual values were determined by the material on hand. Group (*a*) represented the maximum then available, (*c*) lies near the predicted maximum reactivity when fission products are ignored, (*d*) is in the region where

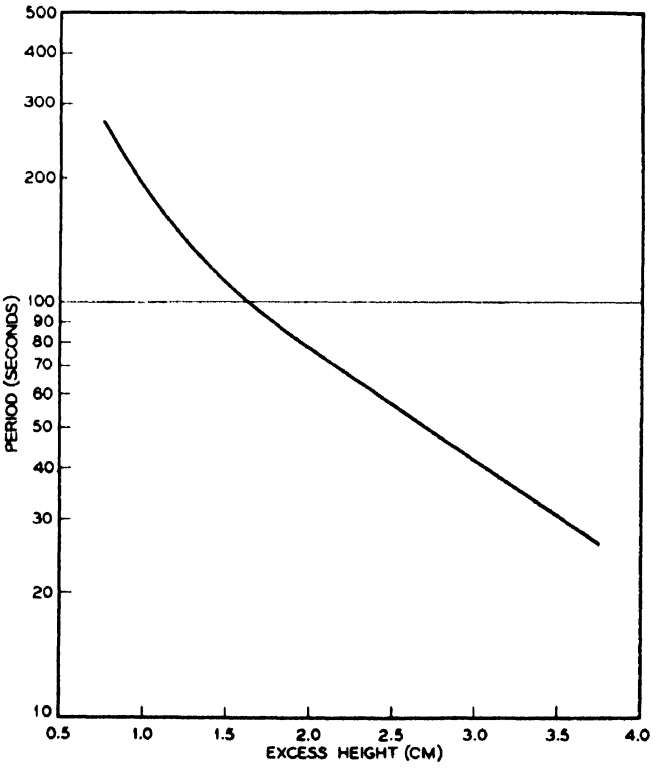

Figure 4. Reactor period versus excess height of the weir above a critical weir setting of 220 cm. Comparison of this curve with the curve calculated from separately measured photoneutron lives and intensities led to the choice of $M^2 = 312$ cm^2 as the value to be used in calculating changes of effective multiplication according to the conventional expression $\delta k = M^2\delta(\pi^2/h^2)$ mentioned in the text

stable fission products of large cross sections, e.g., Sm^{149}, are near equilibrium, and (*b*) is a suitable intermediate value. Six rods of group (*a*), five rods of group (*b*), and three rods of each group (*c*) and (*d*) were measured by comparison with unirradiated rods from the same batch of uranium having the same style of aluminium sheath. Lattice positions *L*-15, *H*-12, and *H*-18 (Fig. 2) were used.

The rods under test were air-cooled to eliminate uncertainties in the volume of light water arising from possible dimensional changes of the uranium. Six shut-off rods were left in the reactor at *C*-9, *C*-21, *J*-27, *Q*-21, *Q*-9 and *J*-3 to simulate xenon poison and raise the critical height to the usual operating level. In this way the measuring flux was matched to the irradiation flux. The advantages of this condition were considered to outweigh the disturbance of radial flux variation by the shut-off rods. All lattice positions inside the ring of lowered shut-off rods were occupied by uranium rods except for the control rod at *J*-5 and empty tubes at *F*-12, *M*-18, and *F*-18 (shut-off rods and a special control rod). Measurements were begun 14 days after the pile was shut down. Xenon had by then decayed to a negligible amount and Pu^{239} and Sm^{149} had reached final values.

The standard reactivity change was the water in the rod assemblies at *G*-15, *K*-12 and *K*-18. These are in the same circle as the test positions and are symmetrically located with respect to the thermal column containing the ion chamber. The standard was calibrated by measurements at two neighbouring weir settings. The calibration was carried out at both the high weir (distorted pile) and at low weir (undistorted, all shut-off rods out). The two values obtained are

$$\delta(\pi^2/h^2) \text{ distorted pile} = 0.0414 \text{ metres}^{-2}$$

$$\delta(\pi^2/h^2) \text{ undistorted pile} = 0.0327 \text{ metres}^{-2}$$

The results for the irradiated rods are shown in Table 3 where the irradiation is given in total megawatt days generated by the rod. The maximum irradiation in the rod in Mw days/tonne is roughly 30 times this quantity.

Errors are difficult to estimate because many factors are involved. Keeping in mind that the measured effects were in all but one case three times those in the third column of Table 3, these figures may be compared with the magnitude of certain changes required to produce 10^{-3} metres^{-2}, for example 2°F in moderator temperature, 0.15 cm in depth, 1.3°F in the temperature of the normal rod-assemblies. None of these factors is believed to have caused errors of this magnitude. The temperature of the air-cooled irradiated rods is not known but measurements with different air flow rates suggest a maximum error of 0.25×10^{-3} metres^{-2} per rod from this source.

The net reactivity loss includes several contributions, for example, losses due to burn-up of U^{235}, absorption by fission products, Pu^{240}, etc., and gains due to production of Pu^{239} and Pu^{241}. The net loss is sensitive to cross sections, neutron yields, conversion factor, and the characteristics of the lattice.

A formula appropriate to these measurements in NRX is

$$\delta\left(\frac{\pi^2}{h^2}\right) = 39.3 \frac{\int\{0.0772(\delta\sigma/\sigma) + (\delta\eta/\eta)\}x^2\,dV}{\int x^2\,dV} \text{ metres}^{-2}$$

where x is the flux, $\delta\sigma/\sigma$ is the fractional change in absorption cross section and $\delta\eta/\eta$ is the fractional change in η (i.e., primary fast neutrons per thermal absorption in the fuel) of the material which was originally uranium. The model used is the equivalent two-group homogeneous reactor with the same boundary conditions for both groups and the integration in the numerator is over the cells containing the rods under test. Values to be inserted for $\delta\sigma/\sigma$ and $\delta\eta/\eta$ are the averages across the rod weighted according to the flux distribution inside the rod. The integrations were carried out on the assumption that $\delta\sigma/\sigma$ and $\delta\eta/\eta$ can be represented by quadratic functions of the irradiation. Tables from which $\delta\sigma/\sigma$ and $\delta\eta/\eta$ can be derived as functions of irradiation were available. These tables are based on the constants of Table 4 and include fission product absorption. It is not possible to get good fits with quadratic expressions and a compromise favouring the long irradiations was made in all but one case where the coefficients were chosen to fit the low irradiations. The resulting calculated reactivity losses are shown in Table 3. They are presented to show the order of agreement with experiment, and they make evident the effect of small changes in η of Pu^{239}. No conclusions have yet been drawn from these results regarding the correct values of parameters. From other evidence the conversion factor is now thought to be slightly less than 0.8. It is clear from the agreement of the calculated effects for Case 2 with the measurements that if the conversion factor is less than 0.8 there must be a compensation and this may be achieved by a larger value of η for Pu^{239} than was assumed in Case 2.

Over-all Reactivity Loss of the Reactor

The course of the reactivity during the first 1000 Mw day's output of a charge of uranium was studied in 1954 as part of an extensive experimental programme. The reactor was operated under carefully controlled conditions, and special records were made. The loading for isotope production was constant and very nearly symmetrically arranged. The time-table included a 5-day run at 1.16 Mw, 25 days at 30 Mw, and 12 days at 40 Mw (all with minor interruptions), followed by 6 days of sub-critical measurements. During the high-power operation the principal effects are expected to arise from the growth of Sm^{149}, the burn-up of U^{235} and its partial replacement by Pu^{239}, and possibly a changing light-water content due to deformation of the fuel. This last effect is believed to be small. The net reactivity, expressed as equivalent π^2/h^2 in metres^{-2}, is plotted in Fig. 5 versus total energy output. This is the sum of $\pi^2/(\text{Weir setting} + 22 \text{ cm})^2$ plus corrections for control rod insertion, D_2O temperature variation, and xenon poison. The xenon poison was calculated with the parameters discussed above. Be-

cause of uncertainties in calculating critical height when the poison is changing rapidly, only cases where the xenon was not far from equilibrium are plotted in Fig. 5 and the curve has not yet been carried back to the beginning. (Another effect occurred which prevents the over-all reactivity change from initial to final low-power operation being ascribed solely to the effects listed. This was observed as an increase of the flux in the outer part of the calandria relative to the flux near the centre during the first 3 to 4 hours at high power, and is attributed to improved reflecting properties of the graphite as a result of heating. There is a concomitant improvement in reactivity. A similar effect, but of smaller magnitude (3 to 4% instead of about 13% flux increase), is observed on each start-up following a shut down of many hours duration. The large change may be due to drying out of the graphite, the regular change is due to an increased scattering relative to capture with increasing temperature.)

In the present state of the analysis it is not possible to list a preferred set of nuclear data to fit the results shown in Fig. 5. By way of illustration Fig. 6 shows a calculated curve for the parameters of Table 4, case 2, together with a Sm^{149} cross section of 75000 barns and yield of 0.011. Only changes due to U^{235}, Pu^{239} and Sm^{149} are included. The delay in production of Pu^{239} and Sm^{149} from precursors of mean life 3.3 days should be taken into account but will require detailed calculation not yet carried out. Roughly the effect of the delay in the Pu^{239} is to increase the loss by about 0.06 metres^{-2} beyond that shown. This is at first partly compensated by a lag in production of Sm^{149} but after the first few hundred Mw days the Sm approaches equilibrium.

The measured loss is estimated as 0.10 ± 0.02 metres^{-2}. The agreement with the curve of Fig. 6 is perhaps fortuitous partly on account of the neglect of the delays and also because the net change in Fig. 6 is the algebraic sum of larger quantities, a small change in which would destroy the agreement. For example the calculated net loss at 1000 Mw days is 0.100 metres^{-2} which results from a 0.199 loss due to Sm, a 0.487 loss due to U^{235} and a 0.586 gain due to Pu^{239}. However, as in the case of individual rods, these results suggest that if the conversion factor is less than 0.8, the value assumed for the calculations but now believed to be somewhat too large, then a compensation is required to maintain the agreement. The most obvious possibility is an increased η for Pu^{239}, but other possibilities have not been eliminated.

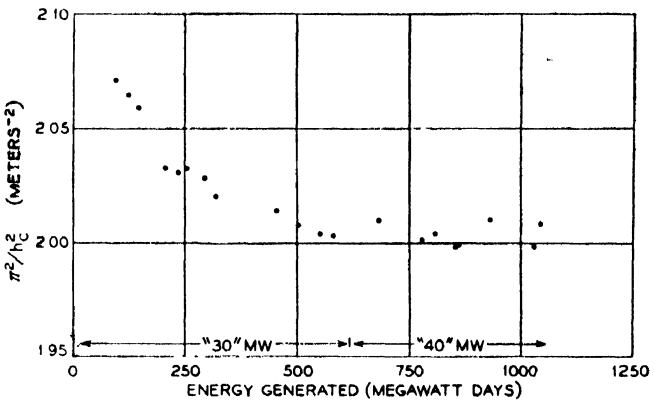

Figure 5. Measured change of reactivity. The measured trend of reactivity (π^2/h_c^2) in metres^{-2} during the first 1050 Mw days' output of a fresh charge of uranium. The points have been corrected for variations of moderator temperature, control rod insertion, and xenon poison. A correction has been applied, using the "prompt poison" data, for the sudden loss of reactivity which accompanied the increase of power from 30 to 40 Mw

Table 3. Reactivity Losses due to Irradiation

Irradiation Megawatt days per rod		*Measured reactivity loss per rod (based on 0.0327 metres^{-2} for the standard)*	*Calculated reactivity loss Metres^{-2}*			
Individual rods	*Average*	*Metres^{-2}*	*Case 1*	*Case 2**		*Case 3*
9.1 10.8 10.5	10.1	0.0013	0.0023	0.0016	0.0019	0.00063
28.8 29.6 35.1	31.2	0.0013	0.0028	0.0013	0.0012	−0.00032
61.4 60.3 —	60.8	0.0031	0.0050	0.0026	0.0027	−0.00007
67.9 67.9 67.9	67.9	0.0040	0.0058	0.0032	0.0035	0.0003
107.4 100.8 100.8	103	0.0072	0.011	0.0075		0.0034
107.4 107.4 107.4	107.4	0.0078	0.012	0.0082		0.0040

* In this case the constants in the quadratic were chosen to give an improved fit to the cross sections for low irradiation.

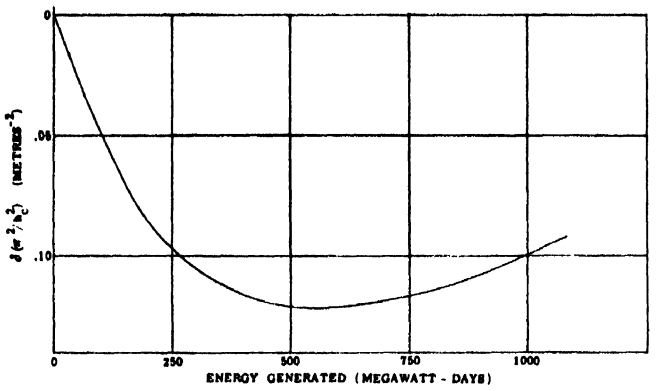

Figure 6. Calculated change of reactivity. The calculated loss of reactivity, $\delta(\pi^2/h_c^2)$ metres^{-2}, during generation of 1100 Mw days energy in NRX for contributions from Pu^{239} and U^{235} with parameters as in Table 4, case 2, and from Sm^{149} with 0.011 yield and 75,000′ barns cross section. Loss of reactivity is plotted below the zero line. Transient effects, although of considerable magnitude, are not included

CONCLUSION

The main result of these experiments has been to give confidence from information that is as direct as possible that reactors can be designed for a long irradiation of uranium metal without fear of any large unrecognized poisoning effect. Moreover, although exact fitting has not been achieved, it appears that adjustments of the nuclear constants required to fit the over-all measurements lie within the limits of error assigned to the data.

Table 4. Constants for Reactivity Calculations

Nuclide	σ_f *barns*	σ_a *barns*	*Case 1*	*Case 2*	*Case 3*
U^{235}	545	645	2.112	2.112	2.112
Pu^{239}	730	1060	2.00	2.05	2.10
Pu^{241}	1000	1400	2.35	2.35	2.35
Pu^{240}		600			
U^{236}		25			

Conversion factor (Pu^{239} atoms produced per U^{235} atom destroyed) = 0.8.

ACKNOWLEDGEMENTS

Members of several divisions of the Laboratory shared in the planning, execution, and analysis of the experiments. A major part of the work, preparing and operating the reactor, was the responsibility of the Reactors Branch of the Operations Division.

Experiments on Some Characteristics of the NRX Reactor Part II—Temperature and Transient Poison Effects

By A. G. Ward,* Canada

The design and operation of high flux natural-uranium heavy-water-moderated reactors requires a good understanding of the various effects which cause reactivity changes. In NRX, major reactivity changes are associated with the growth, radioactive decay and burn-up of Xe^{135} poison, while reactivity changes due to temperature effects and other causes are an order of magnitude less important. The studies of reactivity changes reported in this paper were made to verify the predicted reactivity changes based on knowledge of lattice theory, relevant cross sections and other experimental data, and to search for additional reactivity changes peculiar to high flux operation which might have been undetected in previous lower flux experiments.

Measurements were made during 1947 and 1948, at the time of the initial start-up experiments on NRX, and during February and March, 1954, when the reconstructed reactor was put back into service with a fresh charge of uranium. Many of the staff at Chalk River have contributed to these experiments.

Experimental results on the temperature coefficients and so-called "prompt poison" are discussed first; these effects cause relatively small reactivity changes in NRX but their values must be known accurately to allow for their effects in the analysis of the reactivity changes due to Xe^{135} poison.

TEMPERATURE COEFFICIENTS OF NRX

In the NRX reactor, reactivity changes due to changes of heavy-water moderator temperature, and changes of rod-assembly temperature, have been measured separately. The experimental results of measurements taken during 1948 are shown in Figs. 1 and 2. At weir-box settings of heavy-water moderator depth near 200 cm (see Part I for more detailed explanation), the inverse reactivity change is about 2.3 cm per mk. During the cooling of the heavy-water moderator, the power was kept nearly constant by adjustment of the weir-box to compensate for the reactivity change with moderator temperature. The scatter of the points is a good indication of the precision of the measurements. The points with circles are of lower precision since they have required rather large corrections (>0.05 cm) for the difference between the actual moderator level and the equilibrium level at the given weir-box reading. The smooth curve has been drawn to give a reasonable fit to the experimental points. The curvature results from the non-linear relation between heavy-water density and temperature. A preliminary experiment over a somewhat smaller range of temperatures agreed well with the data of Fig. 1.

The data in Fig. 2 were taken in a similar experiment in 1948 during the cooling of the rod-assemblies from 117°F to 37°F. A closed circuit on the light-water coolant was used for this experiment, with temperature control through a heat exchanger using steam for heating, and river water for cooling the light water in the closed loop.

The temperature coefficient of the rod-assemblies as measured in this experiment was much larger than had been expected. The difference between experiment and calculation has been attributed to the strong moderating properties of the light water in the cooling annulus surrounding each rod. Although the coolant annulus was only 0.1 inch thick, the temperature of the "thermal" neutrons in the uranium metal rods is at some mean temperature between the temperature of the heavy-water moderator and that of the light-water coolant.

Figure 3 shows measurements of the reactivity change with moderator temperature taken in February 1954. A smooth curve representing a fit to the 1948 measurements is also shown. It can be seen that the moderator temperature coefficients are markedly different, while the only change in the reactor which should affect the result is the use of a 0.071-inch cooling annulus for the rods in this experiment. Although the temperature coefficient of reactivity of the rod-assemblies was not measured at this time, on the basis of the above measurements it should be appreciably smaller with the thinner cooling annulus.

A comparison has been made of the over-all temperature coefficient of reactivity, the sum of the moderator and rod-assembly temperature coefficients, with that predicted from the lattice theory. Effects included in the calculations are: (*a*) the Eta-Effect—arising from the change in the ratio of the effective cross section of U^{235} to U^{238} with neutron temperature; (*b*) the Doppler broadening of the U^{238} resonances; (*c*) the change in thermal utilization arising from the flattening of the neutron flux distribution across a lattice cell as the neutron temperature rises; and (*d*) the changes in L_s^2 and L^2 with temperature.

* Reactor Research and Development Division, Atomic Energy of Canada Limited, Chalk River, Ontario.

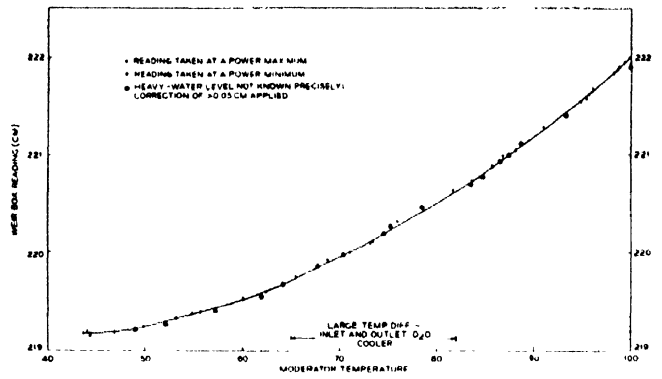

Figure 1. Variation of critical weir-box position with heavy-water temperature. Measurements taken during cooling of heavy water from 100°F to 44°F. Power kept nearly constant by adjustment of weir-box

The calculated temperature coefficient for NRX was

$$\left(10^7 \frac{d}{dT}(\pi^2/h^2) = \right.$$
$$-2.0 + 5.9 \times 10^3 \frac{1}{\rho_m}\frac{d\rho_m}{dT}$$
$$\left. - 1.08 \times 10^3 \frac{1}{\rho_w}\frac{d\rho_w}{dT}\right) \Bigg\} \begin{matrix} h(\text{cm}) \\ T(^\circ\text{C}) \end{matrix}$$

The experimental data give

$$\left(10^7 \frac{d}{dT}(\pi^2/h^2) = \right.$$
$$-2.05 + 5.0 \times 10^3 \frac{1}{\rho_m}\frac{d\rho_m}{dT}$$
$$\left. - 1.08 \times 10^3 \frac{1}{\rho_w}\frac{d\rho_w}{dT}\right)$$

where h = critical height (weir-box reading plus 22 cm); T = temperatures (°C); ρ_m = density of heavy-water moderator; and ρ_w = density of light-water coolant.

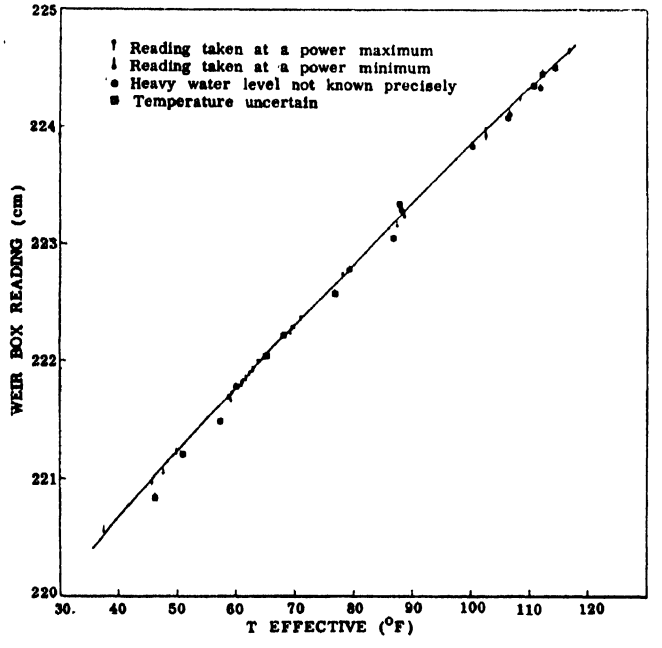

Figure 2. Variation of critical weir-box position with rod-assembly temperature. Measurements taken during cooling of light water coolant from 117°F to 37°F power kept nearly constant by adjustment of weir-box

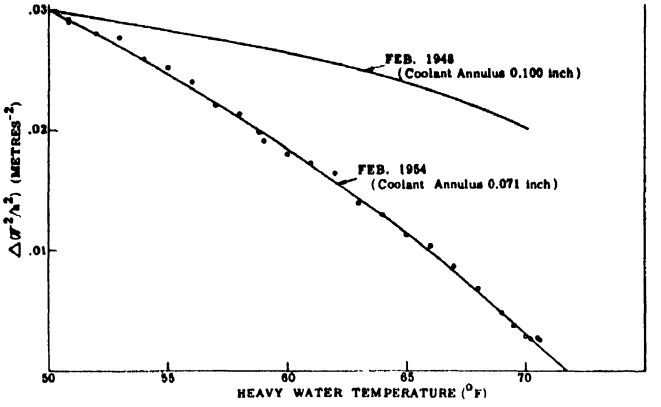

Figure 3. Change of reactivity (π^2/h^2) with heavy water temperature

The agreement is much better than is justified by the accuracy of the data used in the calculation. It should be mentioned that the last term in both equations, describing the effect of density changes of the light-water coolant, is semi-empirical in nature, being derived from lattice measurements with and without cooling water. It has been assumed in the analysis of the experimental measurements. A correction has also been made for the effect of the graphite reflector in calculating the measured reactivity changes with temperature.

Figures 4 and 5 show the experimental data plotted in a way that enables the density effects to be separated from the effects arising from neutron temperature only. The points plotted were derived from the smoothed curves through the experimental points, and the differential nature of this plot emphasizes the experimental errors.

The temperature coefficients of the NRX-type reactor are small and relatively unimportant in operation. In the design of power reactors, much larger changes of reactivity with temperature are possible, and correct estimates of temperature coefficients of reactivity are required.

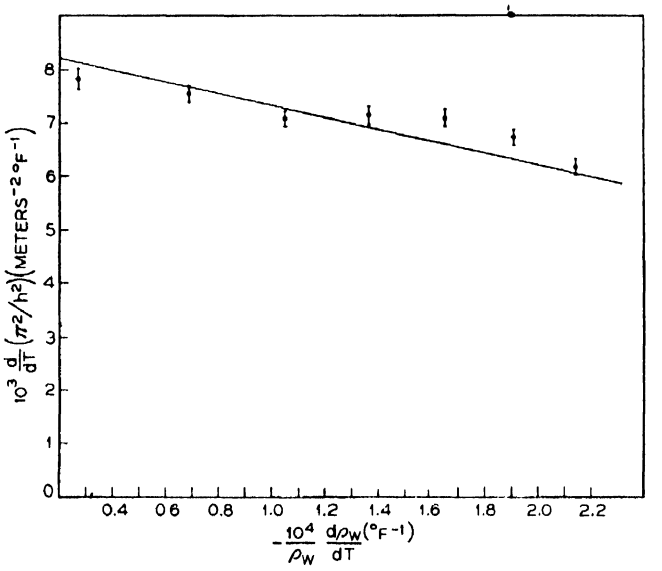

Figure 4. Temperature coefficient of reactivity for NRX rod assemblies. Rate of change of reactivity with light-water coolant temperature as a function of the rate of change of light-water density with temperature. Points derived from Fig. 2 slope of line calculated from lattice measurements with and without cooling water

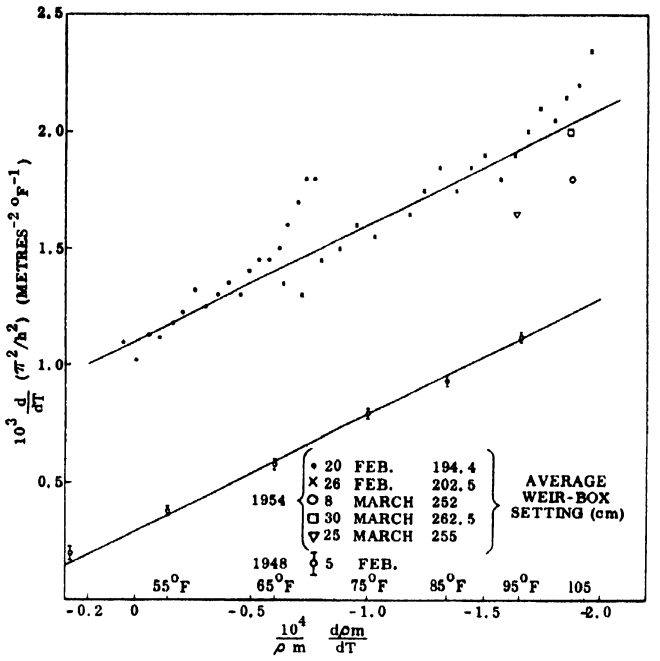

Figure 5. Temperature coefficient of reactivity for NRX heavy water. Rate of change of reactivity with heavy-water moderator temperature as a function of rate of change of heavy-water density with temperature. Points derived from Figs. 1 and 3 and from additional measurements in 1954

PROMPT POISON IN NRX

The immediate reactivity change accompanying a change of operating power in NRX is called "prompt poison." It is of importance in stabilizing the power level. It was first measured in 1948; effects contributing are: (*a*) the change in mean coolant temperature in the pile with change of power; (*b*) the change in Doppler width of the U^{238} resonances, and consequent change in the resonance trap, with change of metal temperature; and (*c*) differential expansion of the rod-assembly, and the consequent alteration of the thickness of the cooling annulus with the radial temperature gradients.

The measurements were made in the following way: the reactor was operated at a steady power level, and then the power level was rapidly altered to a different value and held constant. The control rod has normally been used to provide the necessary reactivity changes, and the control-rod position and moderator temperature recorded as a function of time.

Data from a typical experiment is shown in Fig. 6. (Expt. Feb. 27, 1954.) The operating power as a function of time is indicated at the top of Fig. 6. The reactivity changes calculated from the control-rod position are shown by the circled points. At the bottom of Fig. 6 are shown the reactivity changes resulting from changes in moderator temperature, delayed neutron sources and changes in xenon poison. The control-rod reactivity changes are corrected for these effects and the remaining change in reactivity with power is indicated by the crosses. The discontinuity at the times when power changes have been made are then interpreted as the changes in reactivity due to the "prompt poison."

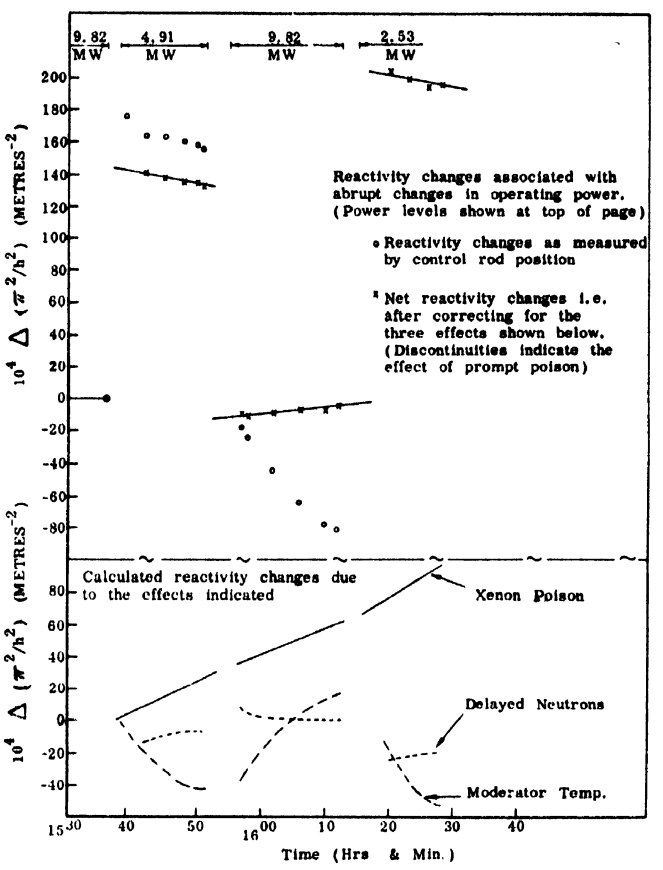

Figure 6. Prompt poison experiment. Reactivity changes associated with abrupt changes in operating power (Power levels shown at top)

Figure 7 shows the collected results of several such measurements plotted against the average power before and after the change. The results have been normalized to a weir-box reading of 250 cm on the assumption that the measured prompt poison per Mw is inversely proportional to the weir-box reading. It can be seen that the prompt poison/Mw decreases at the higher reactor powers.

The total prompt poison for operation at 40 Mw corresponds to about 2.2 mk in the usual notation.

XENON POISON, EXPERIMENTAL METHODS, AND THEORY

The behaviour of the xenon poison in the NRX reactor has been studied in three types of experiments.

1. The growth to equilibrium level during operation at power levels ~1 Mw. In this experiment the weir-box changes are relatively small and the interpretation of the results straightforward. Similar experiments to observe the growth of the xenon poison at higher powers have not been analysed since the complications in the analysis due to gross changes of weir-box level with poison are formidable.

2. Measurement of the equilibrium level of xenon poison at various power levels. Our data is not as precise as we would like it to be, since for many of the measurements it was not possible to measure the critical height without xenon poison at closely related times. In the experiments which have been made, the knowledge of the unpoisoned critical height has been obtained from measurements made either before or

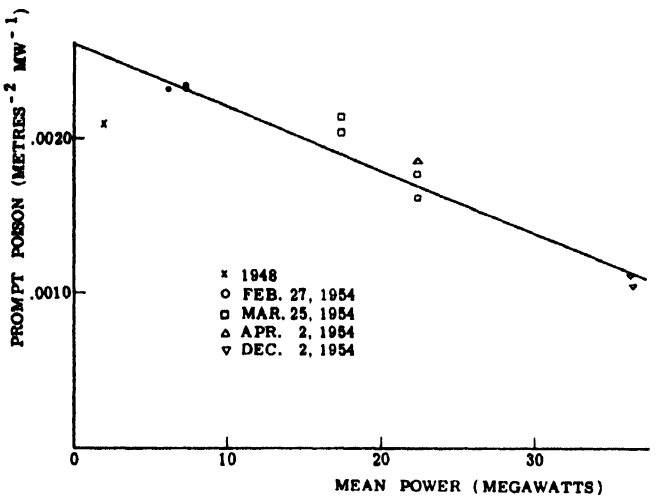

Figure 7. Prompt poison. Collected experimental results normalized to a weir-box setting of 250 CMS, assuming that prompt poison per megawatt is inversely proportional to weir-box setting

after the time at which the equilibrium xenon poison was measured.

3. Reactivity measurements of the transient behaviour of the xenon poison during a shut-down, subsequent to high-power operation under near equilibrium conditions.

Calculations of the reactivity change due to Xe^{135} in the NRX reactor have been based on the usual two-group diffusion theory applicable to lattice reactors.[1] Measurements of critical height are usually taken with no control rod in the reactor; the calculated critical heights are based on a pile model which includes the graphite reflector on the cylindrical surface only, and allowance for the vacant lattice positions assigned to the control rod and the shut-off rods. In the experiments of February-March, 1954, three further lattice positions contained no uranium rods and were occupied by relatively weakly absorbing samples for the production of isotopes.

The perturbation calculation of the effect of Xe^{135} on the critical height of NRX has been carried out as if the lattice were complete, but assuming that no heat and no xenon is produced at the empty lattice positions reserved for shut-off rods, or those occupied by the control rod or weak absorbers.

The calculated change in critical height is given by the equation

$$\left(\frac{\pi^2}{h^2}-\frac{\pi^2}{h_0^2}\right)=\frac{1}{R_1}\times\frac{1}{R_2}\times\left(\frac{k}{L_s^2+L^2+2\kappa^2L_s^2L^2}\right)+\frac{\int\left\{\frac{\Delta k}{k}-\left(\frac{\kappa^2L^2}{1+\kappa^2L^2}\right)\frac{\Delta L^2}{L^2}\right\}\phi^2\,dV}{\int\phi^2\,dV}$$

where h = critical height (weir-box reading plus 22 cm) (cm); h_0 = critical height without poison (cm); $R_1 = 1.07$ = reflector effect; $R_2 = 1.15$ = correction for "vacant" lattice positions; $L_s^2 = 114\ \text{cm}^2$ = slowing down area; $L^2 = 156\ \text{cm}^2$ = thermal diffusion area; $\kappa^2 = 4.07\times10^{-4}\ \text{cm}^{-2}$ = Laplacian or buckling of lattice; $k=(1+\kappa^2L_s^2)(1+\kappa^2L^2)$; ϕ = average thermal flux in the uranium.

The integrals are taken over the uranium rods in the pile.

$(\Delta k/k)$ and $(\Delta L^2/L^2)$ are then calculated from the effects of added absorption cross section in the rods using the normal diffusion theory calculations for the lattice cell.

For the NRX lattice

$$\frac{\Delta k}{k}=-0.940\frac{\Delta\sigma}{\sigma}$$

$$\frac{\Delta L^2}{L^2}=-0.528\frac{\Delta\sigma}{\sigma}$$

where $\Delta\sigma/\sigma$ is the fractional change in the absorption cross section of the rod (initially uranium only), due to the presence of the added absorber.

With these values, the relation becomes

$$\Delta(\pi^2/h^2)=\left(\frac{\pi^2}{h^2}-\frac{\pi^2}{h_0^2}\right)=-2.89\times10^{-3}\times\frac{\int\frac{\Delta\sigma}{\sigma}\phi^2\,dv}{\int\phi^2\,dv}$$

To evaluate $\Delta\sigma/\sigma$ as a function of time and position in the reactor we proceed as follows:

1. We can evaluate $\phi\,(r,t)$ from the record of operating power and weir-box height.

2. The concentration of xenon is assumed to be governed by the differential equations

$$\frac{dI}{dt}=K\phi-\lambda_I I$$

$$\frac{dX}{dt}=\lambda_I I-(\lambda_X+\sigma_X\phi)X$$

where I = concentration I^{135} (atoms/cm^3); X = concentration Xe^{135} (atoms/cm^3); t = time (sec); λ_I = radioactive decay constant of I^{135}; λ_X = radioactive decay constant of Xe^{135}; σ_X = Xe^{135} thermal neutron cross section; $K = N_U\sigma_f(1+\delta)Y$; N_U = atoms/cm^3 of uranium; σ_f = thermal fission cross section of uranium; $(1+\delta)$ = total number of fissions per thermal fission; Y = yield per fission of I^{135}; σ_U = thermal absorption cross section of uranium.

3. The value of $\Delta\sigma/\sigma$ is given by $X\sigma_x/N_U\sigma_U$.

The exact computation of $\Delta(\pi^2/h^2)$ as a function of time using the relations would be exceedingly tedious, and has not been carried out.

We have restricted our analysis to approximate solutions which are valid: (*a*) at low power, when the fractional change of heavy-water depth with poison is small; (*b*) at near equilibrium conditions at all power levels; (*c*) for the xenon transient behaviour, after shut down from operation at near equilibrium conditions.

XENON POISON—OBSERVED BUILD-UP

Figure 8 shows measurements of the change of xenon poison with time when the reactor was operated at low power and there was no xenon poison in the pile at the initial starting time. Two experiments of this kind were carried out during initial start-up experiments. The results were complicated by pile trips

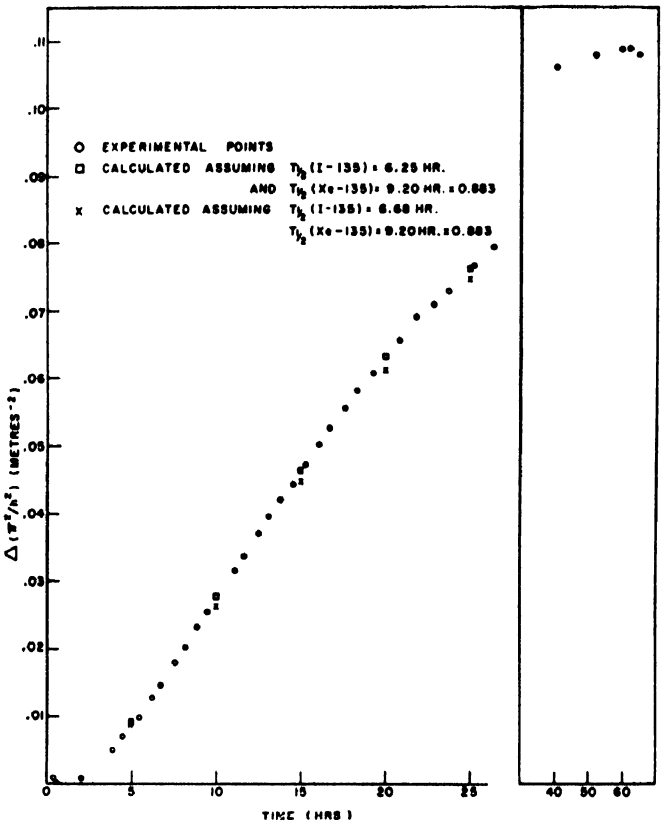

Figure 8. Growth of Xe^{135} poison. Low-power operation (1.4 megawatts). Equilibrium level taken at 0.110 metres^{-2}

before the equilibrium level was reached. Also shown in Fig. 8 are calculated points based on two sets of parameters. It should be emphasized that at this power level, the equilibrium xenon poison depends essentially on the product of the xenon yield in fission and the xenon cross section. The time-dependent behaviour depends on the assumed decay time constants of I^{135} and Xe^{135} in the mass 135 decay chain. At this power level the burn-up of Xe^{135} is small and the assumed xenon cross section has relatively little effect on the time-dependent behaviour.

In both sets of calculated points no direct production of Xe^{135} from fission has been assumed. The fit of the calculated points to the experimental points is not as good if as little as 3% of the xenon is assumed to be formed directly in fission; this is good experimental evidence that the direct production of Xe^{135} in fission is negligible.

It can be seen that the two calculated curves both provide a fair fit to the experimental data, but that the curve calculated using the value of 6.25 hr for the half-life of I^{135} rather than the "accepted" value of 6.68 hr gives a better fit to the experimental data.

Recent experiments at Chalk River indicate that the decay scheme may be more complex than assumed and that a somewhat shorter half-life may be appropriate.

MEASUREMENTS OF EQUILIBRIUM XENON POISON VS OPERATING POWER

The following table gives data on the measured values of equilibrium xenon poison at various power levels. For the first four items, the relative power measurements are reliable but there is an uncertainty estimated as 5% in their absolute value. For the remaining entries, the power measurements are reliable (~2%). For items 5 and 6, two values are given to indicate the uncertainty arising from lack of precise knowledge of the unpoisoned critical height. No measurements of this quantity were made at times close to those of the equilibrium poison measurements. The precision of items 7 to 10 is poor for the same reason.

Since the 1948 and 1950 data were not very accurate, two measurements were made in February and March 1954, with unpoisoned critical heights measured at closely related times. These data, items 11 and 12, are believed to be reliable.

If the reciprocal equilibrium poison is plotted against the reciprocal power per unit height, the theory predicts that the points should lie within 2% of a straight line.

The experimental data, plotted in this manner, are shown in Fig. 9. The intercept on the ordinate scale is inversely proportional to the yield of Xe^{135} in fission, while the slope of the line is inversely proportional to the product of xenon cross section times xenon yield. The scale factor appearing as a multiplying constant for both the intercept and the slope depends on the precision of our knowledge of the parameters such as L_s^2, L^2 used to calculate the change in (π^2/h^2) resulting from a change in the absorption cross section of the uranium in the reactor.

The two straight lines on the curve are calculated values of the equilibrium xenon poison with differing assumptions as to the effective yield and cross section of Xe^{135}. In this curve the agreement with the data appears good, but the method of plotting does not show clearly the errors of the high-power readings.

Figure 10 is another plot of the same data which shows the lack of agreement for the higher power readings. The precision of the 1954 data is believed to be good (±2%). The interpretation requires an assumed yield of 5.7% and does not agree with the measured value of 6.4%. The cross section of 3.5 × 10^6 barns is, however, in reasonable agreement with experiment.

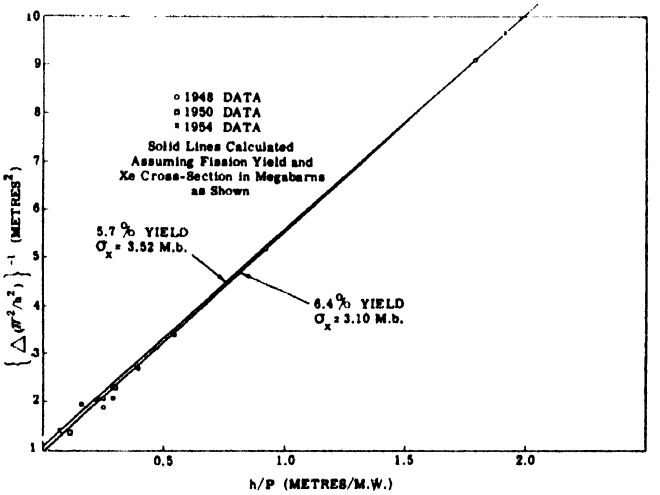

Figure 9. Equilibrium xenon poison in NRX

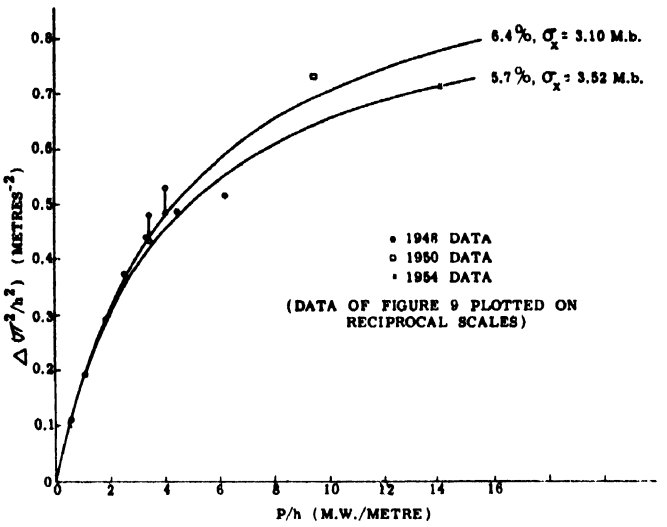

Figure 10. Equilibrium xenon poison in NRX

The calculated reactivity changes are based on the analysis described previously, and the following data:

$$\sigma_f/\sigma_U = 0.528 \text{ for natural U}$$

$$\sigma_f = 4.18 \text{ barns}$$

$$\text{Energy/fission} = 198 \text{ Mw}$$

and the measured flux distribution of the NRX reactor.

TRANSIENT BEHAVIOUR OF XENON POISON AFTER SHUT-DOWN

Experimental data from measurements on the xenon-poison transient after shut-down, following near equilibrium operation at 40 megawatts, are shown in Fig. 11. The measurements were made using an oscillating absorber, as described earlier, and with weir-box changes to maintain the reactivity near critical. Throughout this experiment the moderator temperature was kept near 60°F and only very minor corrections have been made for temperature changes.

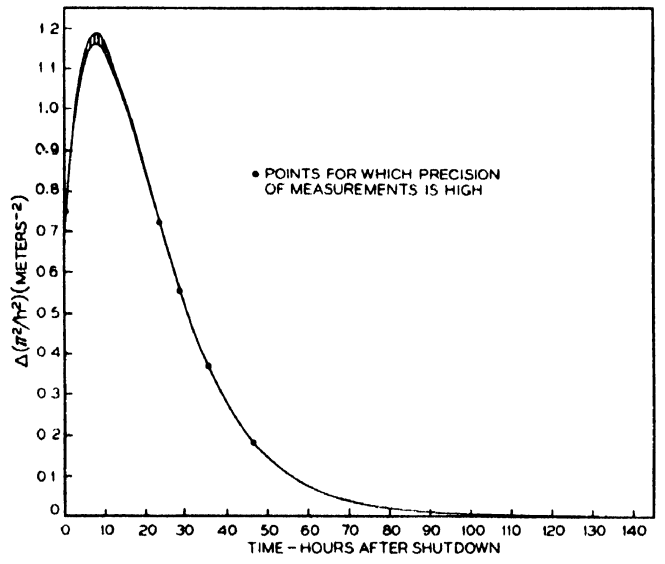

Figure 11. Reactivity transient after shutdown. Power near equilibrium at 40 megawatts before shutdown. Data taken using an oscillating absorber and weir-box changes. The double curve indicates the range of experimental uncertainty

Table I. Experimental Data on Equilibrium Xe^{135} Poison

Item no.		Critical height (Weir box + 22 cm)	Power (Mw)	h/P (metres/Mw)	Δ(π²/h²) (metres⁻²)
1	1948	250.9	1.4	1.79	0.110
2		258.5	2.8	0.923	0.193
3		268	4.9	0.547	0.293
4		277	7.0	0.396	0.372
5		291	10	0.291	0.480 0.433
6		299	12	0.249	0.531 0.484
7		300.5	10	0.300	0.440
8		312	14	0.223	0.487
9		322	20	0.161	0.516
10	1950	317.2	30	0.106	0.729
11	1954	222	1.16	1.91	0.1035
12	1954	285	40	0 0712	0.712

Where the weir box is relatively far from critical, the precision of the measurements is debatable since large corrections have been made for interference between the oscillating absorber and the xenon poison, and for the fact that the ion chambers measure neutron-leakage current. At the times indicated by circles, when the weir box is near critical, and when the xenon poison has nearly disappeared, the experimental data have good precision.

Since the fission yield and cross section of xenon can be considered as fixed by the equilibrium poison experiments, the only parameters adjustable to fit this data are the half-lives of I^{135} and Xe^{135}. The analysis of the experimental data has not been completed. Preliminary analysis has shown that the data are best fitted by a half-life of I^{135} appreciably smaller than the accepted value of 6.68 hrs. The shorter half-life of I^{135} is also required to fit the experimental data on the build-up of Xe^{135} poison discussed above.

Extrapolation of the data taken after shut down to the time of shut down gives a value for the Xe^{135} poison present at shut-down in good agreement with that calculated from the operating critical height with corrections for prompt poison and moderator temperature. The value of the poison present at shut down, corrected for the fact that the Xe^{135} is not quite the equilibrium value, has been used to obtain the equilibrium Xe^{135} poison at 40 Mw given in Table I.

CONCLUSIONS

The measured changes in reactivity of NRX agree reasonably well with predictions based on other experimental data. The measured reactivity changes due to Xe^{135} are about 10% smaller than the predicted changes based on a 6.4% fission yield. The measurements also favour a half-life for I^{135} less than the currently accepted value of 6.68 hours.

Since no marked discrepancy between calculation and experiment has been observed, some confidence can be placed in calculation of reactivity changes to be expected in higher flux reactors.

REFERENCES

1. Glasstone, S. and Edlund, M. C., *The Elements of Nuclear Reactor Theory*, van Nostrand, New York (1952).

Reactivity Changes and Reactivity Lifetimes of Fixed-Fuel Elements in Thermal Reactors

By B. I. Spinrad, J. C. Carter, and C. Eggler,* USA

SCOPE

We present in this paper those generalizations concerning the utilization of nuclear fuel which can be made, to a reasonable degree, independently of the choice of a specific reactor type. Common characteristics of nuclear fuels and the limitations on their use are illustrated. Specific fuel cycles are examined with regard to their behavior under limitations of nuclear reactivity. Experimental reactivity gains data are presented.

INTRODUCTION

Economical use of nuclear fuel is made more probable if high fuel burnups can be achieved. One limitation on high burnup is imposed by the condition that a reactor remain critical during the lifetime of a fuel charge. This limitation is examined in this paper with reference to specific fuel systems and operating procedures.

Statement of the Problem

As power is extracted from nuclear fuel, several changes occur in the nuclear species constituting the fuel: (1) fission introduces fission products (FP), which are nonfissionable isotopes and retard the chain reaction by absorbing neutrons; (2) fission and capture in fissionable isotopes reduce the number of fissionable atoms and thus lower reactivity; (3) capture in fissionable isotopes produces new isotopes, some of which are fertile, but all of which retard the chain reaction; and (4) capture in fertile isotopes produces new fissionable isotopes, which raise reactivity.

The balance between these effects results in a long-term reactivity trend. When this trend is uniformly negative, finite fuel lifetimes can only be obtained by removing parasitic material, such as control rods, or by introducing extra fuel. When the trend is initially positive, it may bend downward and finally become negative, giving a finite reactivity lifetime, whose value depends on the shape of the reactivity curve and the uses to which the initial excess reactivity is put; or reactivity may rise indefinitely, removing the limitation of nuclear reactivity from consideration.

The components of the nuclear system which must be considered are: (1) fissionable nuclei; (2) fertile nuclei; (3) parasitic nuclei; (4) fission products; and (5) higher chain nuclei formed by capture processes in fissionable nuclei.

Other significant factors which must be included for real systems are: (1) neutron leakage; (2) fast fission; and (3) non-uniform flux distributions.

Initial Conversion Ratio

The problems of long-range reactivity changes in fuel have been greatly simplified by considering as a parameter the initial conversion ratio (*ICR*), defined as the ratio of captures in fertile material to absorptions in fissionable material at the beginning of an irradiation history. The parameter thus provides a qualitative scale which can be used by the designer of a reactor to estimate the nuclear economy of a system; its usefulness in these studies is that the concentrations of all isotopes formed as a result of capture in fertile material are proportional to *ICR*, making possible simplification of the mathematics required.

Productivity

The reactivity of a system is commonly defined by the reactivity ρ, which is defined as the difference in rates of neutron production and loss per neutron lost. A critical system then has $\rho = 0$. For reactivity studies, a more useful parameter is the productivity, π, defined as the difference in rates of neutron production and loss per unit of flux-time. The use of this parameter enables one to ignore changes in fuel blackness during the course of irradiation. Thus, when $\pi = 0$, the system is just critical, and when

$$\frac{1}{\tau}\int_0^{\tau} \pi d\tau' = 0$$

the system will be critical if loaded with fuel of linearly graded irradiation up to flux-time τ; the latter relation does not hold for reactivity.

Neutron Leakage

Although neutron leakage is a completely different process from parasitic capture and is computed from different characteristics of a reactor, its effects on nuclear reactivity and productivity are identical with those of parasitic capture. We may lump the two phenomena together as losses to obtain a parameter which is a constant of a reactor.

* Argonne National Laboratory.

Fast Effects

Fast fission affects reactivity by making all thermal fissions appear to produce slightly more neutrons than they actually do; it affects productivity by being associated with fast neutron capture; it increases the relative rate of production of fission fragments per thermal fission; and it increases the power associated with a thermal fission. The first two of these effects make fast fission appear as a negative parasitic absorption, and it may be so treated. The only error associated with this substitution is due to the difference between the number of neutrons emitted per fast fission and the number of neutrons emitted per absorption in fissionable material. The difference is not great, and in view of the usual smallness of the fast fission effect, ϵ, it may be ignored. The error may be compensated by using as a parameter the true conversion rate of the system, calculated to include fast conversion, rather than the true parasitic effect. When this is done, the critical equation omitting the factor ϵ gives a recipe for determining effective losses (which may, in extreme cases, be negative). The power increment due to fast fission must be calculated individually for each reactor, and the extra fission fragments introduced by fast fission must be treated as perturbing reactivity lifetime.

Non-Uniform Flux Distribution

A fixed-fuel element does not have all of its parts subjected to the same neutron flux and therefore does not burn out uniformly. Its reactivity and productivity must be determined by an averaging process, such as is done in perturbation theory, which is quite satisfactory. In general, the most highly burned portions of an element are in regions of high statistical weight, so that they tend to control the lifetime. The studies in this paper do not take this effect into account.

As irradiation proceeds, the changing blackness of an element alters the flux ratio between fuel and other reactor constituents. This change, which is, fortunately, small in most cases, has been ignored here. In addition, such resonance absorbers as Pu^{239} and Pu^{240} have self-protection effects as they build up in concentrations, and these effects have also been ignored.

Enrichment

The enrichment of a fuel element has only a secondary effect on reactivity lifetime. It can, to some degree, make effective parasitic and fertile cross sections vary during irradiation for constant age τ, buckling B^2, and resonance escape probability p; it alters the relation between reactivity lifetime (as measured by fissions per original fissionable atom) and burnup (as measured by fissions per original fuel atom); and it also affects the relation between $\delta\pi$ and $\delta\rho$.

The most significant effects of enrichment occur when some such property as radiation damage limits fuel residence time to some arbitrary megawatt-day per ton (Mwd/t). This limitation may, for high enrichment, make for a system whereby the fuel is not efficiently used, in terms of the fraction of fissionable atoms burned; for low enrichments, a higher fraction of fissionable atoms may be burned before such a limit is reached. Thus, under these conditions, the throughput of fresh fissionable material is doubly high at high enrichment.

Separability of the Problem

To the extent that fast fission effects and non-uniform fluxes may be treated as perturbations, and spectral changes in cross-section ratios may be ignored, we can determine nuclear reactivity lifetimes for various schemes of fuel utilization in terms of choice of fissionable nucleus, choice of fertile nucleus, and *ICR*. The fission products and higher chain nuclei which must be considered as contributing to reactivity changes enter the problem as functions of *ICR*. The details of resonance escape, thermal utilization, and leakage, which must be considered in specific reactor design, may be ignored in this treatment, since their effects are all included in the specification of *ICR*. The problem is thus sufficiently separable from details of reactor concept so that a separate and general study is warranted.

SYSTEMS WITH U^{238} AS FERTILE MATERIAL

We now proceed to examine reactivity and productivity changes for reactors in which U^{238} is the major fuel constituent. Since U^{235} occurs naturally with U^{238}, the most important system is that for which U^{235} and U^{238} are the sole heavy elements initially loaded. Some consideration must also be given to systems in which the Pu formed is cycled back into the reactor. The highly artificial U^{233}-U^{238} system is not considered.

Reactivity Changes with Irradiation

We here present the equations governing concentration of fission products and higher isotopes, first when the U^{238} effective cross section (which includes fast and resonance capture) and the parasitic cross section (which includes leakage) are constant; and second, when resonance escape probability and fast leakage are constant.

We use the following nomenclature:

$28 = U^{238}$
$25 = U^{235}$
$26 = U^{236}$
$49 = Pu^{239}$
$40 = Pu^{240}$
$41 = Pu^{241}$
$S = N_{28}\sigma_{28}^{Eff}$
$X = N_{25}\sigma_{25}$
$Y = N_{26}\sigma_{26}$
$Z = N_{49}\sigma_{49}$
FP = fission products which do not rapidly saturate

ϕ = flux
t = time
α = capture/fission ratio
N = number of atoms per cubic centimeter
$U = N_{40}\sigma_{40}$
$V = N_{41}\sigma_{41}$
$W = N_{FP}\sigma_{FP}$

$$\tau = 10^{-21}\int_0^t \phi(t')\,dt'$$

If we express all cross sections (σ) in kilobarns (10^{-21} cm^2) σt is properly scaled.

We have terminated the higher isotope chains with U^{236} and Pu^{241} because the U^{237} formed from U^{236} rapidly delays into Np^{237}, which would be removed in chemical processing; and because Pu^{242}, as the capture product of a chain passing through two fissionable constituents, is not expected to be a major ingredient. We have also omitted all short-lived β precursors, such as U^{239} and Np^{239}, from our chain. This latter omission leads to a trivial effect on neutron economy at fluxes ca 10^{14} neutrons/cm^2-sec and may be considered chiefly as an inventory requirement on U^{235}.

Thus, we consider the following processes:

$$U^{235} \xrightarrow{(n,\gamma)} U^{236}$$

$$U^{235} \xrightarrow{(n,f)} \text{fission products (FP)}$$

$$U^{238} \xrightarrow{(n,2\beta^-)} Pu^{239} \xrightarrow{(n,\gamma)} Pu^{240} \xrightarrow{(n,\gamma)} Pu^{241}$$

$$\downarrow{\scriptstyle (n,f)} \text{FP} \qquad \downarrow{\scriptstyle (n,f)} \text{FP}$$

The following equations and initial values then apply:

$$S = S_0 \qquad S_0 = ICR \quad (1)$$

$$\frac{dX}{dt} = -\sigma_{25}X \qquad X_0 = 1 \quad (2)$$

$$\frac{dY}{dt} = \frac{\alpha_{25}}{1+\alpha_{25}}\sigma_{25}X - \sigma_{26}Y \qquad Y_0 = 0 \quad (3)$$

$$\frac{dZ}{dt} = \sigma_{49}(S - Z) \qquad Z_0 = 0 \quad (4)$$

$$\frac{dU}{dt} = \frac{\alpha_{49}}{1+\alpha_{49}}\sigma_{40}Z - \sigma_{40}U \qquad U_0 = 0 \quad (5)$$

$$\frac{dV}{dt} = \sigma_{41}(U - V) \qquad V_0 = 0 \quad (6)$$

$$\frac{dW}{dt} = FP\left[\frac{X}{1+\alpha_{25}} + \frac{Z}{1+\alpha_{49}} + \frac{V}{1+\alpha_{41}}\right] \qquad W_0 = 0 \quad (7)$$

The normalization of Equations 1 and 2 is arbitrary and chosen for convenience. In addition, we define:

$$\delta\pi = \text{excess productivity} = (\eta_{25} - 1)(X - X_0) - Y + (\eta_{49} - 1)Z - U + (\eta_{41} - 1)V - W \quad (8)$$

When $\delta\pi = 0$ then the excess reactivity is also zero.

The solutions of Equations 2 through 8 may be obtained by quadratures in a straightforward manner. It is then found that X and Y are directly proportional to X_0, as is the first term on the right-hand side of Equation 7, while Z, U, V, and the remainder of W are proportional to ICR. It becomes convenient to define W_g and W_h from the equations:

$$\frac{dW_g}{dt} = \sigma_{FP}\left[\frac{X}{1+\alpha_{25}}\right] \quad (7a)$$

$$\frac{dW_h}{dt} = \sigma_{FP}\left[\frac{Z}{1+\alpha_{49}} + \frac{V}{1+\alpha_{41}}\right] \quad (7b)$$

Clearly,

$$W = W_g + W_h \quad (7c)$$

It is also convenient to define two further functions g and h:

$$g_{25} = (N_{25} - 1)(X_0 - X) + Y + W_g \quad (9)$$

$$h_{25} = \frac{1}{ICR}\left\{(N_{49} - 1)Z - U + (N_{41} - 1)V - W_h\right\} \quad (10)$$

Solutions giving X, Y, and W_g as functions of τ are given in Fig. 1a; Z/ICR, U/ICR, V/ICR, and W_h/ICR are plotted in Fig. 1b. Figure 2 gives the

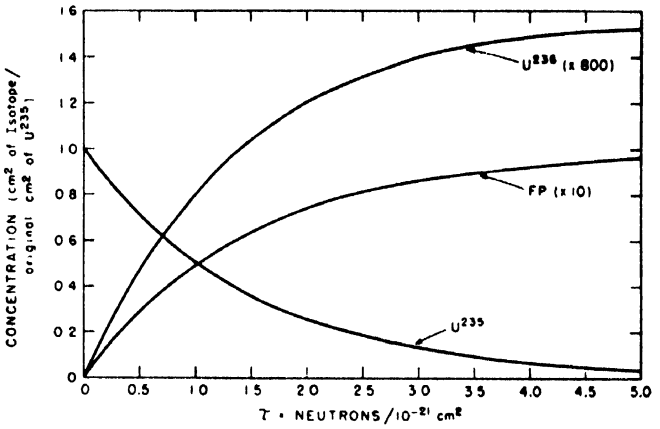

Figure 1a. Concentrations of materials derived from U^{235} plotted as cm^2 of product/original cm^2 of U^{235}, vs flux-time

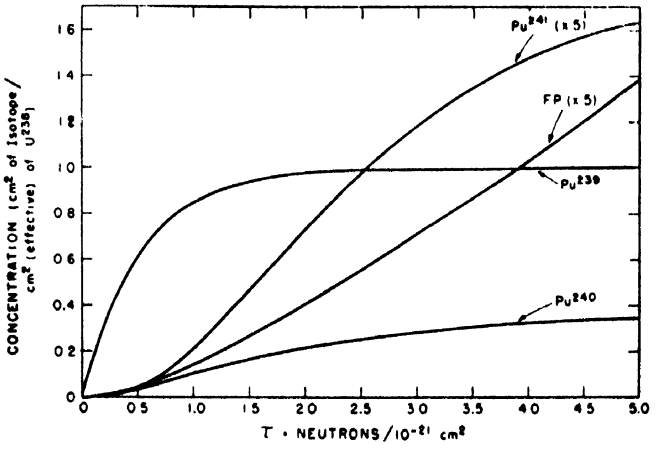

Figure 1b. Concentration of materials derived from U^{235}

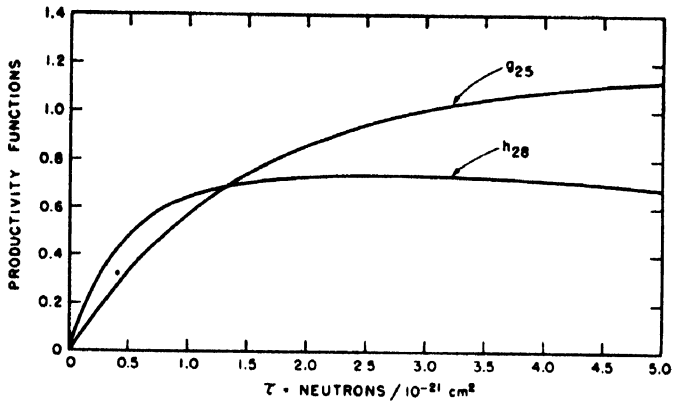

Figure 2. The productivity functions g and h for U^{235}-U^{238} systems; normalized to 1 cm^2 of U^{235} or U^{238} absorption and plotted vs flux-time

functions g_{25} and h_{25} against τ. Values used for nuclear constants are the "hot" values listed in Appendix I and are believed to be typical for thermal power reactors. Figure 3 gives, for several ICR, $\delta\pi$ vs $T \equiv \sigma_{25}/\sigma_{FP} W$; T is proportional to Mwd/t divided by enrichment (Mwd/t = 9400 ET, E being the enrichment in per cent) and measures the fractional burnup per fissionable atom loaded.

Although the actual curves are subject to error owing to the possibility of the assumed cross sections being in error, the shapes of the curves are certainly illustrative of general trends.

The previous equations were solved with constant S. If, instead of holding S constant, we hold p, ϵ, and fast leakage constant in a reactor, Equation 1 must be replaced by:

$$S^{Eff} = ICR + \epsilon l^{-\tau B^2}(1 - p)[\eta_{49}Z + \eta_{41} V - \eta_{25}(X_0 - X)] \quad (11)$$

Thus S^{Eff} tends to vary in such a way as to increase when η of the fuel increases, and decreases when it decreases. This means that the variation in productivity is largely taken up by variable U^{238} absorption.

When $(1 - p)$ is large, the change in S^{Eff} can become greater than the increase in productivity which caused it. Thus, for sufficiently high enrichments, reactivity will drop for all reasonable ICR, even though the fission neutron excess per fissionable atom destroyed may have increased.

To observe the consequence of this effect, we have plotted in Fig. 4a the variation of $\eta f/\eta_0 f_0$ with power-time (Mwd/t) for natural U at several ICR, with correspondingly variable p in systems whose thermal losses were constant at 5% of the initial thermal absorption. In Fig. 4b, we have plotted η/η_0 for uranium of three different enrichments and constant ICR = 1.0 under the same conditions. Figures 4 were computed with the "cold" nuclear constants of Appendix I and with fission products included in the expression for f; while this represents some changes in the details

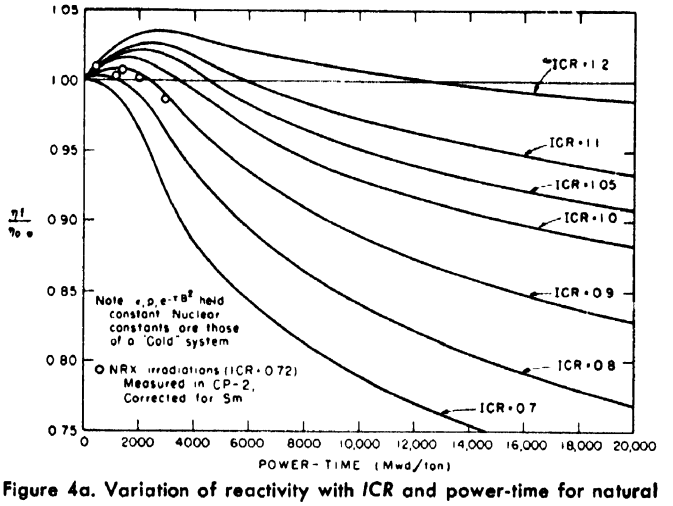

Figure 4a. Variation of reactivity with ICR and power-time for natural uranium fuel

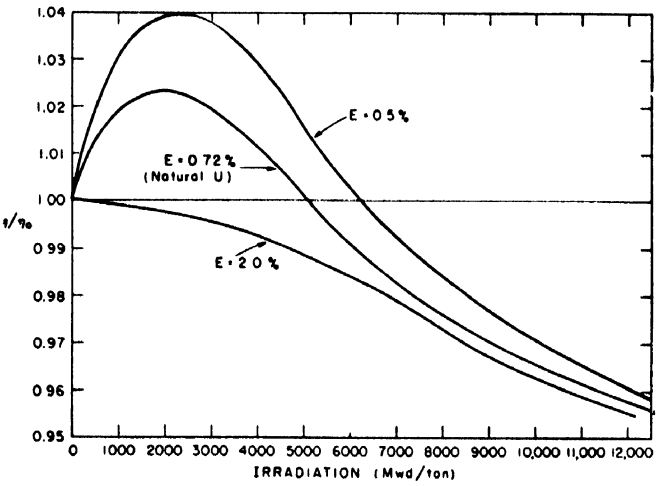

Figure 4b. Reactivity changes on irradiation as a function of enrichment (E) at ICR = 1.0 for the U^{235}-U^{238} system

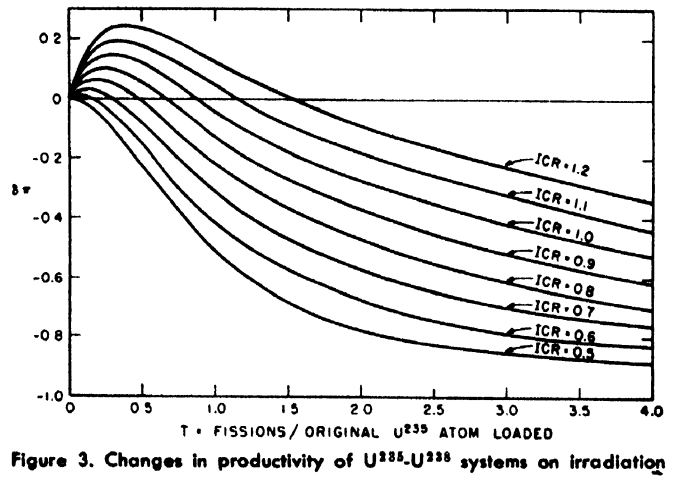

Figure 3. Changes in productivity of U^{235}-U^{238} systems on irradiation

of the corresponding curves, qualitative comparison of Figs. 3 and 4a leads to the valid conclusion that, for systems of low enrichment, productivity and reactivity changes show a rough correspondence, while Fig. 4b shows that enrichment tends to eliminate positive reactivity changes. Figure 4b also demonstrates the tendency of η/η_0 to approach a value independent of enrichment at ca 12,500 Mwd/t. The significance of this fact is not great, however, since it implies equivalent reactivity loss at widely varying

Table I. Results of Single-Pass System with Constant U^{238} Absorption

ICR	*Fractional burnup of 25*	*Final atoms per original 25 atom*				*No. of fissions per original 25 atom (T)*
		49	*40*	*26*	*41*	
0.574	0.127	0.065	0.005	0.020	—	0.116
0.656	0.238	0.125	0.018	0.037	0.001	0.235
0.738	0.335	0.180	0.039	0.051	0.005	0.361
0.817	0.420	0.229	0.006	0.064	0.010	0.494
0.892	0.493	0.271	0.098	0.076	0.018	0.635
0.962	0.558	0.309	0.133	0.086	0.027	0.782
1.029	0.614	0.342	0.169	0.094	0.039	0.933
1.083	0.663	0.370	0.205	0.101	0.052	1.100
1.138	0.706	0.394	0.241	0.108	0.066	1.270

fuel efficiency, as measured in fissions/per initial fissionable atom.

Experimental Data on η/η_0

Returning to Fig. 4a, we observe circled points up to 3000 Mwd/t. These points were obtained from measurements on sections of an NRX rod ($ICR \cong 0.72$) irradiated to a central value of 3000 Mwd/t. The sections were measured in CP-2, the original nuclear reactor, by the danger coefficient method. Because the response of the reactor to impurities embedded in natural U was unknown and difficult to predict theoretically, the samples were measured against samples of slightly enriched, depleted, and/or poisoned uranium. These calibrations indicated that the response of CP-2 to a change in η of the sample was independent of sample blackness over a large range of blackness, and so the measurements of the irradiated samples could be directly calibrated for η. Theoretical estimates of f/f_0 have been applied to the data. Corrections on the measurements to account for Sm^{149} in the samples have also been made, so that the curve of $\eta f/\eta_0 f_0$ will extrapolate to unity at zero time.

The experimental points do not fall on the curve for $ICR = 0.72$, even allowing for their obvious scatter. A rough check shows that they fall closer to the equivalent curve for the "hot" constants leading to the conclusion that even in a cold, well-moderated reactor the contribution of the 0.3-ev resonance to the Pu cross section, which is the main source of difference between the two sets of constants, must not be ignored.

Reactivity Lifetimes with Constant Effective U^{238} Cross Section

For systems of sufficiently high *ICR*, the reactivity of a fuel element increases for a short period and then drops below its initial value. Under the assumption that the lifetime of a fuel element is limited to the time during which its reactivity stays above the initial value (i.e., no extra reactivity needs to be added to maintain criticality), it is of interest to determine what this lifetime is. In this first scheme, we assume that the U^{238} concentration and cross section remain constant. We have also used in this and subsequent sections the "hot" nuclear constants of Appendix I.

We then may restate the problem as that of finding the time τ at which $\delta\pi$, the excess productivity, is zero for given *ICR*, and then deducing from the corresponding W the equivalent power-time, T. The condition that $\delta\pi = 0$ then becomes $g = (ICR)h$, which may be rearranged to $(ICR) = g/h$. Thus, the ratio g/h is the initial conversion rate for which $\delta\pi$ will be zero at flux-time τ.

Table I above lists the pertinent data for this method of operation. In Fig. 5, Curve 1 is a plot of T vs *ICR*. It is clear that this method of operation requires the reactivity rise initially for a positive residence time of fuel. This occurs for $ICR \gtrsim 0.5$. For lower values, excess reactivity must be continuously applied. The discussion of the influence of excess reactivity will, however, be deferred, and another, more appealing method of operation examined.

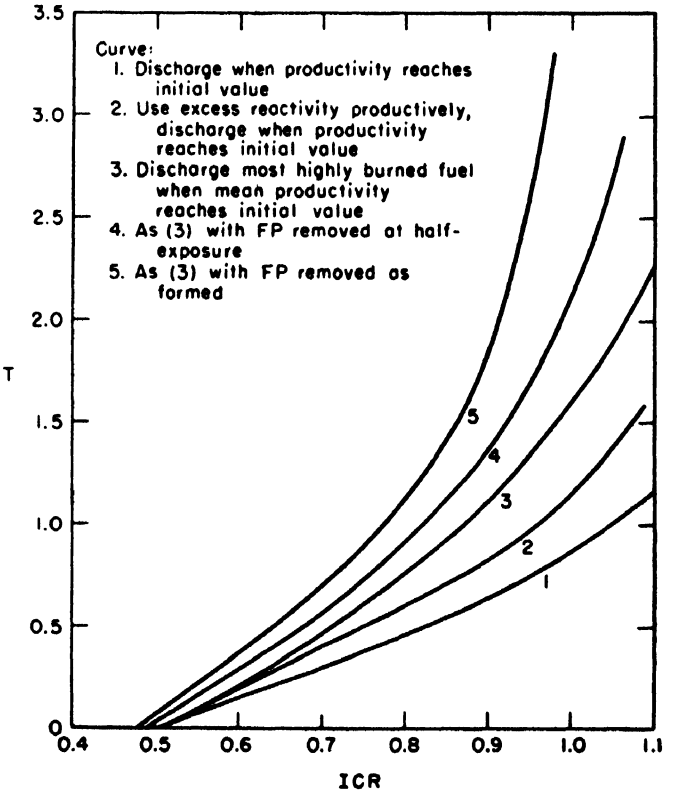

Figure 5. Fuel lifetime under various operating methods, plotted as fissions/U^{235} atom in feed (T) vs *ICR* (U^{235}-U^{238} systems)

Table II. Results of Single-Pass System with Variable U^{238} Absorption

ICR	Fractional burnup of 25	Final atoms per original 25 atom				No. of fissions per original 25 atom (T)
		49	40	26	41	
0.5	0	0	0	0	0	0
0.79	0.446	0.243	0.077	0.069	0.012	0.58
0.86	0.553	0.297	0.109	0.083	0.023	0.725
0.93	0.598	0.337	0.161	0.092	0.037	0.905
1.01	0.698	0.388	0.243	0.107	0.006	1.380

Single-Pass Operation with Variable U^{238} Absorption

The preceding results indicate that high burnup of fuel cannot be expected unless the *ICR* is high. An improvement is possible, however, provided that the effective cross section of U^{238} can be varied (for example, by varying moderator density and thereby increasing or decreasing resonance capture). It is assumed for this scheme that the U^{238} cross section can be varied by an amount required to soak up excess reactivity as it appears. Here, therefore, productive use of excess reactivity is made; in the previous scheme, reactivity is taken out nonproductively.

Equations 2 through 7 remain unchanged. However, instead of keeping S constant, its value is adjusted so that excess productivity is always zero; that is, in place of Equation 1 we use

$$S = (\eta_{25} - 1)X - Y + (\eta_{49} - 1)Z - U + (\eta_{41} - 1)V - W - L \quad (12)$$

where L is a constant parasitic cross section (losses). Since at zero time

$$\left.\begin{aligned} S = ICR, \quad X = X_0 = 1, \\ Y = Z = U = W = V = 0 \\ ICR = (\eta_{25} - 1)X_0 - L \end{aligned}\right\} \quad (13)$$

we may substitute Equation 13 into Equation 12 to obtain

$$S - ICR = (\eta_{25} - 1)(X - X_0) - Y + (\eta_{49} - 1)Z - U + (\eta_{41} - 1)V - W \quad (14)$$

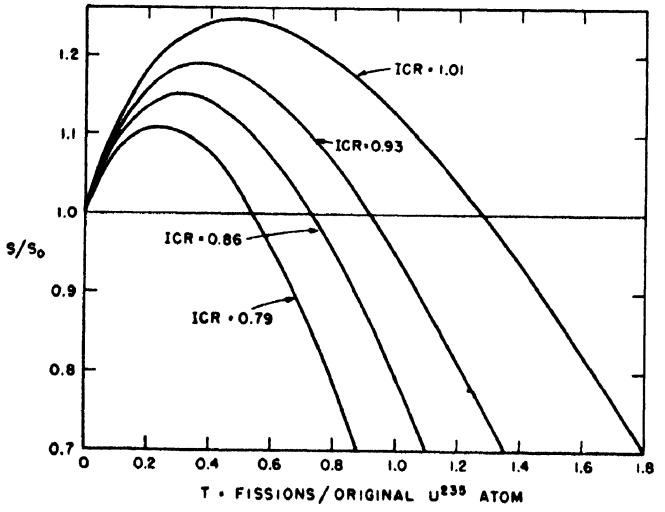

Figure 6. Variations in productivity (S/S_0) required to maintain criticality with constant neutron losses

Equations 2 through 7 and 14 may be most conveniently solved numerically, and the solutions for S/S_0 for four different values of *ICR* are given in Fig. 6. Excess productivity and reactivity are zero when $S/S_0 = 1$, and this limits the lifetime of the fuel. Figure 5, curve 2, gives T vs *ICR*. Pertinent data are summarized in Table II.

While curve 2 of Fig. 5 indicates that longer irradiation times than for the nonproductively controlled system can be achieved, Fig. 6 indicates that the required changes in U^{238} cross section are very large. Since the effective U^{238} cross section tends, in general, to increase with irradiation for constant p, this change is somewhat reduced in real cases. Control of p by changes in moderator density for large systems with low leakage is the immediate operating method which comes to mind, but the required changes are out of the question except for boiling or supercritical aqueous systems.

Of course, there is no need for stopping at $S/S_0 = 1$; if the means of varying S exist, the process can be extended to times for which S/S_0 reaches some practical minimum value. In the ultimate case, the system can be made to operate until it is no longer critical, even when all fertile material is removed.

Single-Pass Operation with Uniformly Graded Fuel Irradiation

One way of obtaining productivity control without reactivity change is to consider that the reactor is always loaded with rods of uniformly varying exposures. In such a system the reactor loading is frequently changed, the most highly irradiated fuel being discarded while fresh fuel is loaded. This system allows us to continue irradiation until the reactivity of the system *on the average* is equal to that of the feed. Since reactivity first increases, the material at the end of the cycle is considerably less reactive than the feed.

We again assume constant cross section for U^{238}. Since average productivity is just $1/\tau$ times the integrated productivity and is to be set to zero, we work with the integrals $G = \int_0^\tau g dT'$ and $H = \int_0^\tau h dT'$. The *ICR* which results in material being rejected at time τ is $ICR = G/H$. Figure 5, curve 3, gives T for this system, and Table III summarizes pertinent information.

Comparison reveals that this is a very fruitful way of extending the lifetime of a fuel charge, leading to residence times 50 to 100 per cent greater than for a

Table III. Uniformly Graded Irradiation

ICR	*Fractional burnup of 25*	*Final atoms per original 25 atoms*				*No. of fissions per original 25 atom (T)*
		49	*40*	*26*	*41*	
0.574	0.127	0.065	0.005	0.020	0.0002	0.112
0.611	0.232	0.116	0.017	0.037	0.0013	0.233
0.656	0.335	0.160	0.035	0.051	0.004	0.352
0.702	0.420	0.197	0.057	0.064	0.008	0.474
0.747	0.493	0.228	0.082	0.076	0.015	0.599
0.790	0.558	0.254	0.109	0.086	0.022	0.728
0.830	0.614	0.276	0.136	0.094	0.032	0.859
0.868	0.663	0.296	0.164	0.101	0.042	0.995
0.904	0.706	0.312	0.191	0.108	0.052	1.135
0.937	0.743	0.328	0.217	0.113	0.063	1.279
0.968	0.776	0.342	0.242	0.118	0.075	1.423
0.997	0.804	0.353	0.266	0.122	0.086	1.570
1.024	0.829	0.362	0.288	0.126	0.097	1.724
1.049	0.851	0.372	0.309	0.129	0.107	1.880
1.072	0.870	0.382	0.328	0.132	0.117	2.040

uniformly loaded system. The practical means of achieving this type of operation involves some switching of fuel elements in a reactor of varying flux pattern, until such time as the irradiation history of the reactor fuel is uniformly graded in each reactor zone; thereafter, fuel replacement according to program is required.

The effect of this scheme is to build up and maintain in the reactor a supply of plutonium which is at almost steady state. The operating range of Pu concentration is kept as small as the fuel-replacement schedule can allow. Under these conditions, it becomes more appropriate to speak of the mean conversion ratio (*MCR*) as the ratio of $Pu^{239} + Pu^{241}$ atoms recovered per U^{235} atom lost. A check on Table II will reveal that the *MCR* over the whole range of T quoted is very close to the limiting value (ca 0.5) of *ICR* for which the fuel has zero residence time; that is, the large gain in residence time is attained at the expense of over-all conversion efficiency. We shall see that this is also true of thorium systems, and, in fact, of all systems for which this method of operation is considered: to have a mean conversion ratio close to the minimum required for positive residence time.

Continuous FP Removal

The scheme just described gives adequate reactivity lifetimes for systems with $ICR > 0.85$. In order to get an idea of how far an original feed could be used in a given reactor, we now consider the same scheme, in which, however, *FP* are removed.

The equations used in the previous scheme may be used with the following changes:

$$\left.\begin{aligned} G_1 &= G - \int_0^T W_g\, dT' \\ H_1 &= H + \int_0^T \frac{W_h}{ICR}\, dT' \end{aligned}\right\} \tag{15}$$

$$ICR = G_1/H_1 \tag{16}$$

Results of this computation are summarized in Table IV and in Fig. 5, curve 5. It should be noted

Table IV. Complete FP Removal

ICR	*Fractional burnup of 25*	*Final atoms per original 25 atom*				*No. of fissions per original 25 atom (T)*
		49	*40*	*26*	*41*	
0.522	0.127	0.059	0.005	0.020	0.0002	0.115
0.553	0.238	0.105	0.015	0.037	0.0012	0.230
0.591	0.335	0.144	0.032	0.051	0.004	0.345
0.629	0.420	0.171	0.051	0.064	0.007	0.462
0.666	0.493	0.204	0.073	0.076	0.013	0.579
0.700	0.558	0.225	0.097	0.086	0.019	0.698
0.731	0.614	0.243	0.120	0.094	0.028	0.819
0.760	0.663	0.260	0.144	0.101	0.037	0.941
0.786	0.706	0.272	0.166	0.108	0.045	1.063
0.810	0.743	0.284	0.188	0.113	0.054	1.188
0.831	0.776	0.294	0.208	0.118	0.064	1.313
0.850	0.804	0.301	0.227	0.122	0.073	1.439
0.867	0.829	0.307	0.244	0.126	0.082	1.566
0.882	0.851	0.313	0.260	0.129	0.090	1.694
0.895	0.870	0.319	0.274	0.132	0.098	1.821
0.942	0.934	0.337	0.327	0.141	0.128	2.462
0.972	0.967	0.348	0.346	0.144	0.147	3.113

Table V. Fission Product Removal at Half-Irradiation

ICR	*Fractional burnup of 25*	*Final atoms per original 25 atom*				*No. of fissions per original 25 atom (T)*
		49	*40*	*26*	*41*	
0.582	0.238	0.111	0.016	0.037	0.0012	0.242
0.670	0.420	0.187	0.054	0.064	0.008	0.469
0.744	0.558	0.239	0.103	0.086	0.021	0.713
0.814	0.663	0.277	0.154	0.101	0.039	0.968
0.872	0.743	0.305	0.202	0.113	0.059	1.230
0.920	0.804	0.326	0.245	0.122	0.077	1.500
0.962	0.851	0.342	0.283	0.129	0.098	1.781
1.046	0.934	0.375	0.362	0.141	0.142	2.645

that the curves in Fig. 5 are numbered in the order of increasing reactivity life rather than in order of presentation.

Complete Fission Product Removal at Half-Irradiation

We consider a two-step *FP* removal to get a realistic idea of how many stages of fission-fragment removal are required to approximate continuous extraction. The method envisaged here is to irradiate material to time $\tau/2$; then its fission fragments are removed, and it is irradiated for another interval $\tau/2$, at which time it is discarded. We again ask ourselves what *ICR* exists such that this discarding after time τ is correct for constant reactivity. The answer is:

$$ICR = \frac{G(\tau) - \frac{\tau}{2}\left[g\frac{\tau}{2} - g_1\frac{\tau}{2}\right]}{H(\tau) - \frac{\tau}{2}\left[h\frac{\tau}{2} - h_1\frac{\tau}{2}\right]} \quad [g_1(\tau) \equiv G_1'(\tau)] \qquad (17)$$

Results are summarized in Table V and in Fig. 5, curve 4.

As seen in Fig. 5, curve 4 is close to the average *ICR*, for given T, between curves 3 and 5. This method of averaging would therefore seem to be appropriate for an n-step *FP* extraction.

Steady-State U-Pu Fuel Cycle

Plutonium produced in a uranium fuel cycle can be fed back into the reactor with large reductions in U^{235} feed rate and higher fractional burnup of the U^{235}. We must therefore examine steady-state systems in which the Pu present is maintained at equilibrium relative to the U^{238} concentration, and in which the Pu isotopic ratio is at steady state. At the beginning of a cycle, the Pu is mixed into depleted U; at the end of a cycle, the Pu is extracted from the U, which by this time is more highly depleted.

In order to furnish a basis for comparison with single-pass systems, we assume as the criterion for rejection of fuel that its time-averaged reactivity shall be that of the feed of the graded-irradiation system. We also match two other characteristics of that system: the total fissions per unit of U^{238} feed, and the ratio of leakage and parasitic capture to U^{238} absorption. The solution of the problem is presented in terms of a parameter X' which represents the concentration of U^{235} in the feed for a steady-state cycle relative to the concentration of U^{235} in the feed for the equivalent single-pass cycle.

At steady state, Equations 4 to 6 have the solutions

$$\left.\begin{aligned} Z &= S \\ U &= \frac{\alpha_{49}}{1+\alpha_{49}} S \\ V &= U \end{aligned}\right\} \qquad (18)$$

The condition that the average reactivity over time shall be the same as the initial reactivity for the feed of the equivalent single-pass system is:

$$0 = \int_0^\tau \{(\eta_{25})(X-1) - Y + (\eta_{49}-1)Z - U + (\eta_{41}-1)V - W - L - S\}\, d\tau' \qquad (19)$$

when concentrations are normalized so that $X_0 = 1$ in the single-pass system feed.

Since S and L are constant, and equal to the same value in the steady-state as in the single-pass system, Equation 19 becomes, after substitution of Equation 18,

$$\int_0^\tau \{(\eta_{25}-1)(1-X) + Y + W\}\, d\tau' = S\int_0^\tau \left\{\eta_{49} - 1 + \frac{\alpha_{49}}{1+\alpha_{49}}(\eta_{41}-2)\right\} d\tau' \qquad (20)$$

As before we may split W into W_0 and a term proportional to S, observing that W_0 is proportional to X', as are X and Y, and the *FP* term proportional to S is:

$$\frac{S\sigma_{FP}\tau}{1+\alpha_{49}}\left\{1 + \frac{\alpha_{49}}{1+\alpha_{41}}\right\} \qquad (21)$$

Substituting the definition of G, and performing some algebra, we get:

$$\frac{X'}{\tau}[G(\tau) - \tau(\eta_{25}-1)] = -(\eta_{25}-1) + S\left[\eta_{49} - 1 + \frac{\alpha_{49}(\eta_{41}-2)}{1+\alpha_{49}} - \frac{\sigma_{FP}\tau}{2(1+\alpha_{49})}\left(1 + \frac{\alpha_{49}}{1+\alpha_{41}}\right)\right] \qquad (22)$$

The number of fissions which have occurred to time τ per unit X is:

$$T = X'W_0(\tau)\frac{\sigma_{25}}{\sigma_{FP}} + \frac{S\tau\sigma_{25}}{1+\alpha_{49}}\left\{1 + \frac{\alpha_{49}}{1+\alpha_{41}}\right\} \quad (23)$$

Equations 22 and 23 permit us to eliminate X' so as to obtain a value of τ compatible with the choice of S and T. We may then solve either equation for X'. The results are presented in Table VI, in which the columns have the following significance:

S = ICR of equivalent single-pass feed.
X' = ratio of U^{235} concentration in steady-state feed to that in equivalent single-pass feed.
X'' = ratio of U^{235} concentration in steady-state reject material to that in equivalent single-pass feed.

We observe that, in recycling, we end up with no excess plutonium to replace the U^{235} system. We have, therefore, set up a system whose conversion ratio is zero, and whose finite reactivity lifetime we attain by using more U^{235} in the feed than is required for criticality. Of course, we have also fissioned many atoms which are originally U^{238}, so that, despite this, the efficiency of the system may be high.

Fuel Systems with Excess Reactivity in Feed

The previous studies, with the exception of the recycled Pu case, have been made with the condition that the initial reactivity of the feed will make the reactor into which it is loaded just critical. When fuel lifetime is computed on the assumption that the mean composition of fuel during its exposure will make the reactor critical, this condition is unnecessary. We therefore now examine fuel systems in which fresh feed has excess reactivity. Initial feed is assumed to have an excessive concentration of U^{235} given by a parameter X_0 the ratio of U^{235} concentration in reactive feed to that in just critical feed.

This extra fuel gives the system, initially, excess productivity of amount

$$\delta\pi = (\eta_{25} - 1)(X_0 - 1) \quad (24)$$

Table VI. U^{235} Requirements with Pu Feedback

S	X'	X''
0.574	0.483	0.445
0.611	0.476	0.400
0.656	0.458	0.353
0.702	0.429	0.304
0.747	0.400	0.261
0.790	0.372	0.222
0.830	0.344	0.188
0.868	0.316	0.158
0.904	0.289	0.132
0.937	0.262	0.109
0.968	0.235	0.089
0.997	0.209	0.072
1.024	0.185	0.058
1.049	0.163	0.047
1.072	0.142	0.037

The condition that mean productivity be zero over fuel lifetime is

$$SH(\tau) = X_0G(\tau) - \tau\,\delta\pi \quad (25)$$

Clearly, even when $S = 0$, the limiting value of τ is that for which $\delta\pi/X_0 = G(\tau)/\tau$, so that a simple "burning" of fuel can be achieved by building in excess reactivity.

For greater τ, the ICR required to achieve such lifetimes is

$$ICR' = \frac{S}{X_0} = \frac{G(\tau) - \tau\,\delta\pi/X_0}{H(\tau)} \quad (26)$$

It should be noted that the ICR of excessively reactive feed is less than the ICR of just-critical feed, because excess reactivity is achieved by increasing fissionable material concentration, thereby increasing its relative initial rate of destruction.

To determine T's, we use

$$T = (W_0 + ICR'W_h)\frac{\sigma_{25}}{\sigma_{FP}} \quad (27)$$

This value of T is the number of fissions per initial atom of fissionable material loaded, which includes the incremental fuel.

Results of these calculations are presented in Fig. 7 as parametric plots of T vs ICR for various X_0.

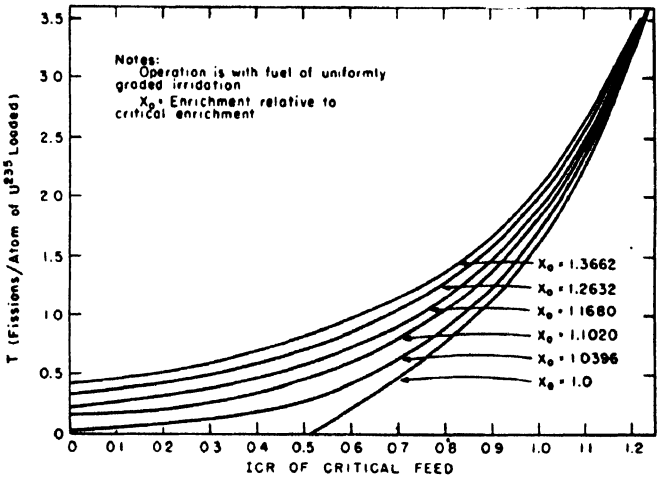

Figure 7. Influence of incremental fuel enrichment on lifetime (U^{235}-U^{238} systems)

ICR is used rather than ICR' as a running variable so that the effect of incremental loading of a given system can be evaluated. T is, however, as defined in Equation 27.

Th^{232} SYSTEMS

Th^{232} is a fertile material found commonly in nature; on neutron capture followed by double β^- emission, it yields, U^{233}, U^{233} is an interesting material because its thermal η, 2.33, is high enough to make thermal breeding possible.

Two possible fissionable materials have generally been considered as fuels for the Th systems. One is U^{235}, the only common fissionable isotope in nature, available as a separated isotope; the other is the reac-

tion product, U^{233}, which might be initially loaded into new reactors if its breeding is feasible.

Reactivity and Isotope Changes with Irradiation

The pertinent elements of the Th^{232} chain are sketched below:

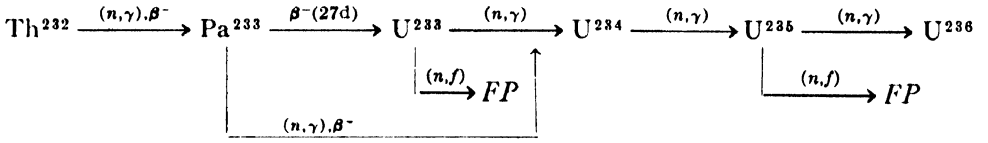

It is not necessary to sketch out the U^{233} or U^{235} chains, as they are imbedded in the Th^{232} chain.

The theory of reactivity change, enrichment effects, isotope changes, etc., is quite analogous to the theory of the U-Pu system. The only extra feature is the chain branching at Pa^{233}. The 27-day half-life of Pa^{233} allows the capture cross section of Pa^{233} to lead to significant bypassing of the β decay to U^{233} product.

Although this fuel is capable of breeding for $ICR > 1$, reactivity of a Th system will show a large initial drop due to holdup of bred material in the form of 27-day Pa^{233}. Since the material is recovered at shutdown, this reactivity change is not a long-term effect; we have omitted it here and taken the position that some fissionable material is required as excess inventory to produce the equilibrium Pa^{233}. Our initial loading is consequently assumed to consist of Th, fissionable material, and enough Pa^{233} to be in capture and decay equilibrium with the Th. This quantity is flux-dependent, and, for the purposes of illustration, we have taken only one typical case, namely, a neutron flux of 10^{14} neutrons/cm^2-sec at a temperature of 600°K.

At this flux, a fraction 0.97225, of the Pa atoms decay into U^{233}, and ICR is, for these systems, 0.97225 times the ICR which would exist if Pa had zero lifetime, or if the flux were very low.

The extra symbols and equations used in describing the chain are:

$$R = N_{Th}\sigma_{Th}^{Eff} \qquad m = N_{23}\sigma_{23} \qquad \Lambda = \lambda_{13}/\phi$$

$$l = N_{13}\sigma_{13} \qquad n = N_{24}\sigma_{24}$$

Subscripts: 13 = Pa^{233}; 23 = U^{233}; 24 = U^{234}.

$$R = R_0; \qquad ICR = 0.97225\ R_0 \tag{28}$$

$$l = l_0 = \frac{1}{1 + (\Lambda/\sigma_{13})} R_0 \tag{29}$$

$$\frac{dm}{d\tau} = \sigma_{23}\left(\frac{\Lambda l}{\sigma_{13}} - M\right) \tag{30}$$

$$\frac{dn}{d\tau} = \sigma_{24}\left(\frac{\alpha_{23}}{1 + \alpha_{23}} m + l - n\right); \qquad n(0) = 0 \tag{31}$$

$$\frac{dX}{d\tau} = \sigma_{25}(n - X) \tag{32}$$

$$\frac{dW}{d\tau} = \sigma_{FP}\left(\frac{X}{1 + \alpha_{25}} + \frac{m}{1 + \alpha_{23}}\right); \qquad W(0) = 0 \tag{33}$$

Initial conditions have been omitted from Equations 30 and 32 since they depend on whether U^{233} or U^{235} is the initial fuel. In addition, U^{236} builds up from U^{235} as described in Equation 3.

The solution of this set of equations is straightforward. (Constants used in these computations are listed in Appendix I.) As with the U-Pu systems, we get isotopic abundances which are sums of functions proportional to R or to initial values of n or X. We may combine these abundances, as before, to obtain the productivity functions g_m, describing contributions to productivity loss arising from isotopic changes in atoms which were originally U^{233}, and h_R, measuring contributions to productivity gain arising from atoms which were originally Th. These, and the g function for U^{235} (which we will henceforth denote by g_x), enable us to predict productivity changes in the Th-U^{233} and Th-U^{235} systems. For completeness, we display formulae for g_m and h_R:

$$g_m = (\eta_{23} - 1)(m_0 - m_m) + n_m - (\alpha_{25} - 1)X_m + I_m + W_m \tag{34}$$

$$h_R = (\eta_{23} - 1)m_R - n_R + (\eta_{25} - 1)X_R - I_R - W_R \tag{35}$$

In Equations 34 and 35, the subscripts on the abundance functions indicate the nuclide from which the given isotope is derived.

In Fig. 8, we have plotted the productivity functions, g_m and h_R, and in Fig. 9, the FP cross-section contributions, W_m and W_R.

For attainable ICR, replacement of U^{235} by U^{233} always leads to productivity loss at zero time. Therefore, none of the methods we have considered for operation of U-Pu systems will work for U^{235}-Th systems, except those which allow for excess productivity in the feed material. Thus, until we consider excess-productivity systems, we will concentrate on the breeding system, U^{233}-Th.

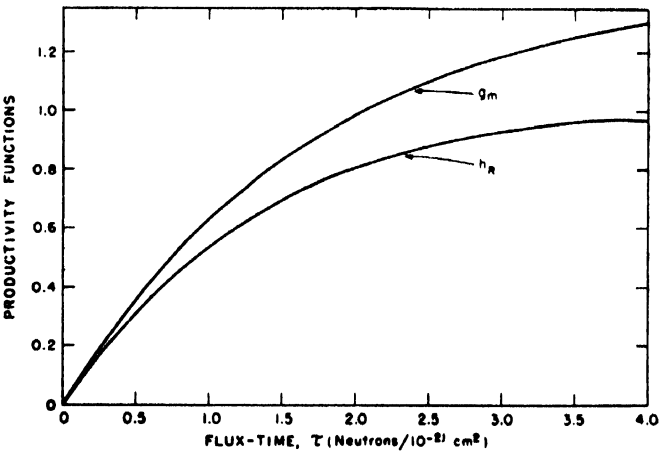

Figure 8. The productivity functions g_m and h_R for Th-U^{233} systems

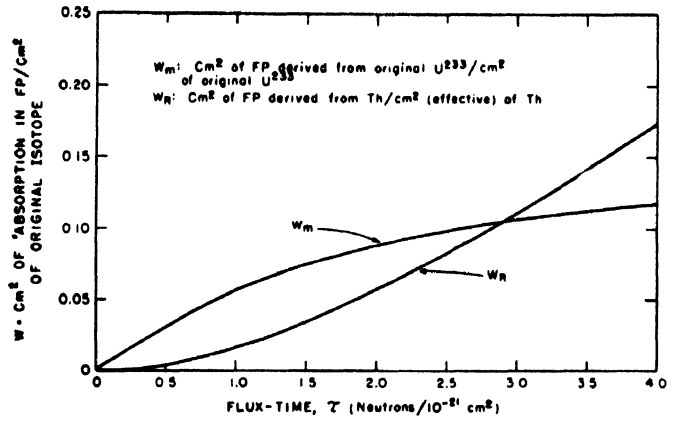

Figure 9. Fission product contributions to productivity change in Th-U^{233} systems

Systems with Reactivity Limited to Initial Value

For the Th systems with U^{233} as initial fuel, productivity will show a steady drop for $ICR < 1.115$, because the bred material must compete for neutrons with U^{234} and FP as formed. For higher ICR, reactivity rises and then falls off, because U^{234} and FP accumulate, while bred U^{233} is partially burned. Note also that as breeding takes place, the breeding ratio will drop for systems with constant effective macroscopic cross section for thorium, Σ_{Th}^{Eff}. The point at which reactivity returns to its initial value is determined by the same linear relation between g_m and h_R as was the case for the U-Pu system, as is apparent from consideration of the definition of productivity. We use:

$$ICR = 0.97225 \left\{\frac{R_0}{m_0}\right\} = \left\{\frac{g_m(\tau)}{h_R(\tau)}\right\} \qquad (36)$$

$$T = \frac{\sigma_{23}}{\sigma_{FP}} W_m(\tau) + R_0 W_R(\tau) \qquad (37)$$

Figure 10 contains the plot of ICR vs T for this system as curve I.

Graded Irradiation Histories

The graded fuel scheme, in which reactivity excess near the beginning of irradiation is balanced out against reactivity decrement toward the end of irradiation, may be evaluated by computing the integrals of g_m and h_R as G_m and H_R. Then, $ICR = 0.97225\, G_m/H_R$, and we may then obtain T as usual. Figure 10, curve 2, gives T vs ICR for this system.

Removal of Fission Products

The major contributor to the requirement of high breeding gain to attain initial reactivity gain of a Th-U^{233} system is the fission products. They give greater poisoning per fission than is contributed by the corresponding captures to give U^{234}. Moreover, the capture product of U^{234} is U^{235}, which builds up to such a concentration as to approximately cancel the productivity loss of the U^{234}.

As a consequence, if FP are removed, any breeding gain in excess of that required initially to cancel out U^{234} absorption will continue to override new U^{234}, while the U^{235} formed will override the old U^{234}. The result of this is a virtually infinite reactivity lifetime for $ICR > 1.1014$.

Recycled U at Steady State

The recycling of U produced in a U^{233}-Th fuel cycle will lead to an accumulation of higher U isotopes, which is mitigated by the fact that bred material, which is available for sale, contains some of these higher isotopes; the sale of bred material constitutes a slight purge on U^{234}, U^{235}, and U^{236}. The isotopic constitution of the recycled U thus varies slightly with ICR, but not rapidly enough to be an important variable.

A typical set of relative concentrations may be obtained by setting dm/dt, dn/dt, dx/dt, and dy/dt to zero in the differential equations for composition. If this is done, relative concentrations of U^{233}, U^{234}, U^{235} and U^{236} are obtained as $m:n:x:y = 1:0.1072:0.1072:0.0166$. With this material, U^{235} is responsible for 9 per cent of all fissions. To achieve the same reactivity as pure U^{233}, the U^{233} concentration in recycled feed must be 1.0078 times that in the original feed.

To obtain the breeding gain per cycle at steady state, we adopt the simplifying assumption that since U^{235} is responsible for 9 per cent of all fissions, the τ required to give the same T for given R as the pure U^{233} fuel is 91 per cent of the equivalent τ for pure U^{233} feed. We call this number τ'. We then solve Equation 30 for $m(\tau')/m_0$, obtaining

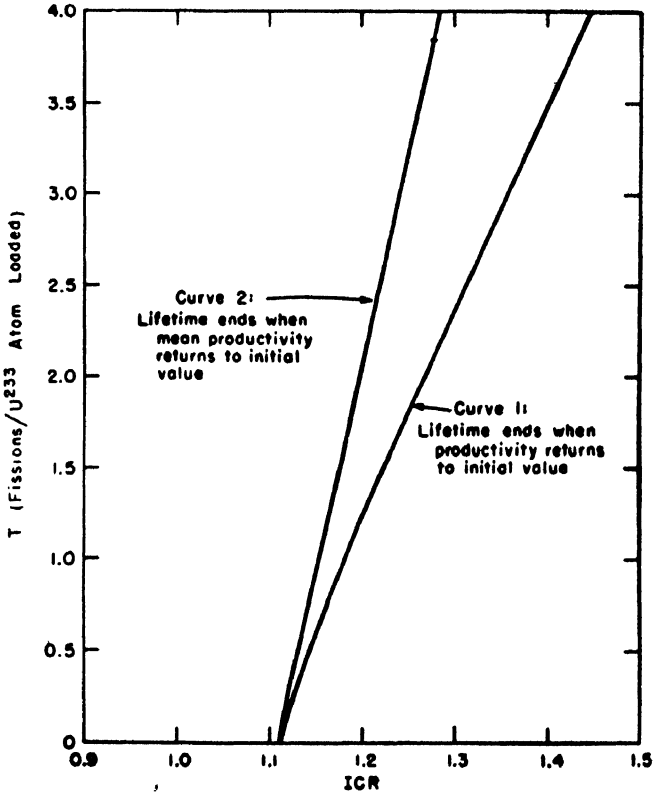

Figure 10. Reactivity lifetimes of U^{233}-Th systems for constant Σ_{Th}^{Eff}

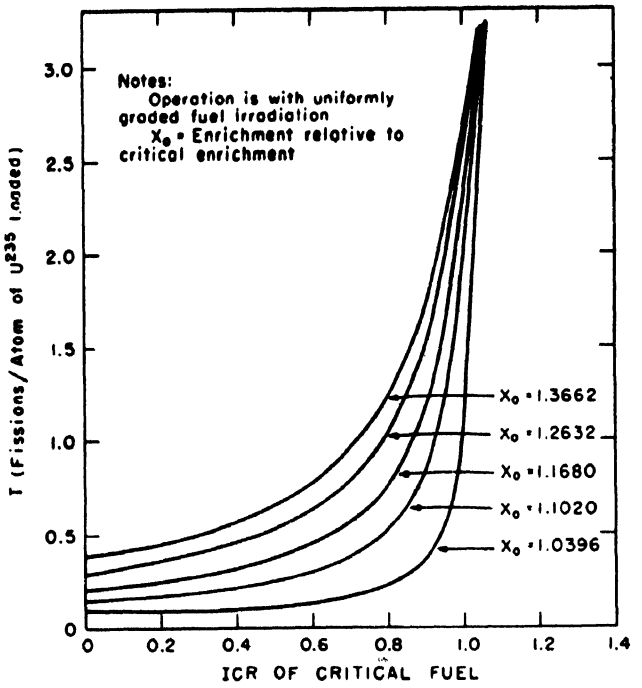

Figure 11a. Influence of incremental fuel enrichment on lifetime of U^{235}-Th systems

$$\frac{m(\tau')}{m_0} = \frac{T}{1+\frac{\sigma_{13}}{\lambda}} - \left[\frac{T}{1+\frac{\sigma_{13}}{\lambda}} - 1\right]\left[\frac{1-e^{-\sigma_{23}\tau'}}{\sigma_{23}\tau'}\right] \quad (38)$$

The breeding gain per cycle (BG) is given by

$$BG = \frac{m(\tau')}{m_0} - 1 \quad (39)$$

Table VII summarizes the results of the indicated calculations as BG (breeding gain/cycle) vs ICR of equivalent original loading.

Systems with Excess Initial Fissionable Material

The previous theory of fuel systems with excess reactivity in the feed may be extended without difficulty to obtain the reactivity lifetimes of systems whose feed contains more fissionable material than is required for criticality. This enables us to make an analysis of both Th-U^{235} and Th-U^{233} systems in an analogous fashion to that already presented for U^{235}-U^{238} systems.

Table VII. Breeding Gain Cycle of Steady-State Th-U Systems

ICR	BG
1.118	0.011
1.121	0.022
1.125	0.033
1.129	0.043
1.134	0.053
1.138	0.063
1.143	0.073
1.148	0.082
1.153	0.091
1.158	0.100
1.163	0.109
1.168	0.118
1.173	0.127
1.179	0.136
1.185	0.144
1.215	0.186
1.249	0.229

Results are presented in Figs. 11a and 11b for Th-U^{235} and Th-U^{233} systems, respectively, as plots of T vs ICR (where, as before, ICR is the value for critical feed) as a function of X_0. The Th systems are highly responsive to incremental loading at $ICR \cong 1$, because productivity changes in these systems are comparatively small.

Systems with Variable Effective Th Cross Section

With a reactor operated at constant p, ϵ, τ, and B^2, the thorium effective cross section will vary with time according to

$$R^{Eff} = ICR + \epsilon l^{-\tau B^2}(1-p)(\eta_{25}[X - X_0] + \eta_{23}[m - m_0]) \quad (40)$$

If we designate the product $\epsilon l^{-\tau B^2}(1-p)$ as a parameter μ, then

$$R^{Eff} = ICR + \mu(\eta_{25}[X - X_0] + \eta_{23}[m - m_0]) \quad (41)$$

is a constant of the reactor design.

Under this restriction, a change in productivity may be overcompensated by a change in R^{Eff} for large μ, and the reactivity and productivity curves lose their similarity. Plots of reactivity treating ICR, E and μ parametrically and presented in terms of integrated

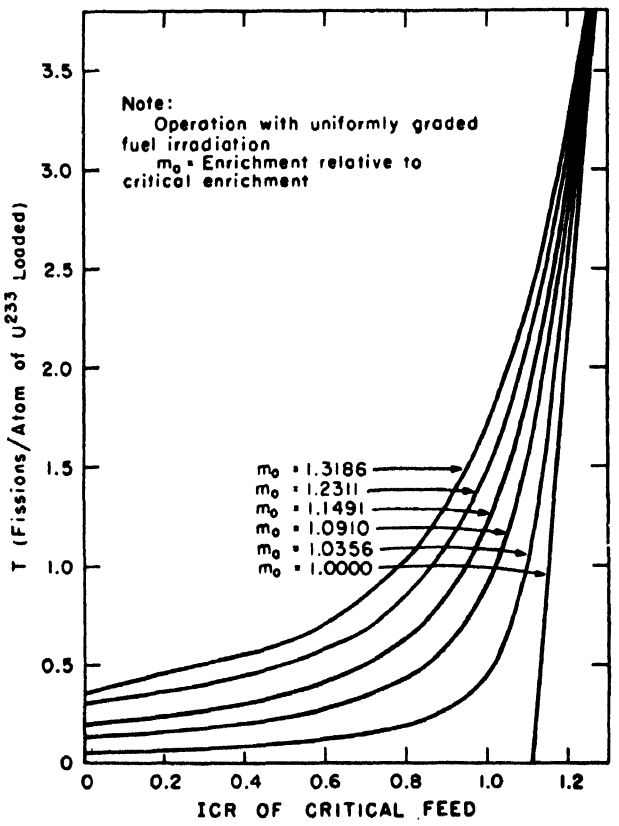

Figure 11b. Influence of incremental fuel enrichment on lifetime of U^{233}-Th systems

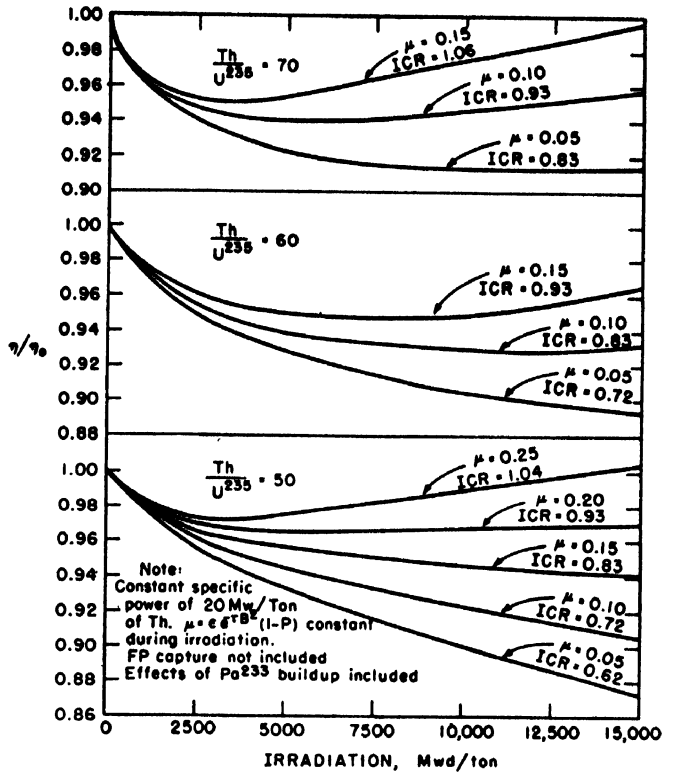

Figure 12. Variation of η for U^{235}-Th systems under irradiation

specific power (Mwd/t) are presented in Figs. 12 and 13, for the U^{235}-Th system. (In these figures, Pa-buildup at a specific power of 20 Mw/t has been included in η variations, while *FP* poisons have been omitted.) Figure 14 gives a corresponding set of productivity changes for constant R and variable *ICR* vs fuel efficiency, T.

GENERAL NOTES

In this section we shall discuss certain problems in the application of the data presented in previous sections.

Fast Fission Effects

Fast fission has three separate effects on the relationship between neutron economy and power life-

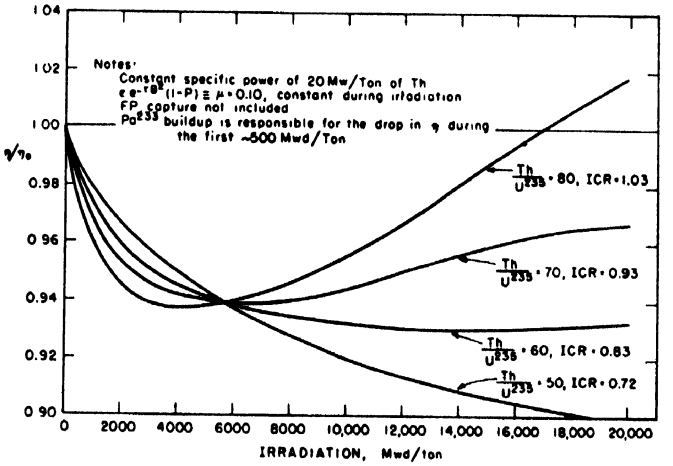

Figure 13. Variation of η for U^{235}-Th systems under irradiation, with enrichment as a parameter

time. Since there is associated with it some fast neutron capture, the true conversion rate, including fast capture, must be used in determining *ICR*. In addition, fast fission gives a power bonus to any system, which may be interpreted as a rescaling of the power-time coordinate of all graphs presented by a factor: 1 + Fast Fissions/Thermal Fissions. Finally, fast fission produces extra fission fragments, and these must be accounted for as cumulative poisons, decreasing reactivity lifetime. An estimate of the magnitude of this last effect may be obtained by reference to the discussion of the effect on lifetime of removing fission products: since it has been shown that removal of half the fission products yields a curve of T vs *ICR* which is midway between the no-removal and complete-removal curves, on the *ICR* scale, it may be expected that addition of a given fraction of fission products yields a curve which is obtained by extrapolation on the *ICR* scale from the complete-removal curve beyond the no-removal curve. Crude estimates have verified the reliability of this extrapolation.

Axial Flux Variations

In a reactor in which fuel elements have a major axis, it is not always possible to design so that flux is always constant throughout the length of the element. When this is so, a fuel element will have varying

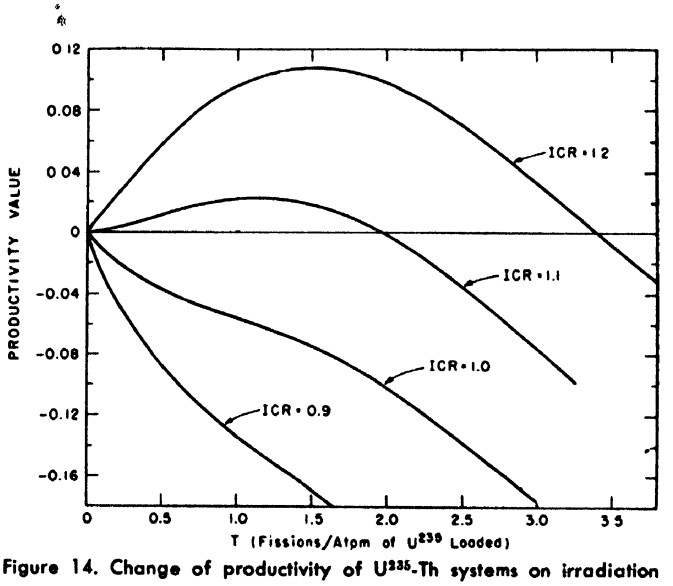

Figure 14. Change of productivity of U^{235}-Th systems on irradiation

irradiation history along its length. Since the more highly burned-out region generally has a high statistical weight for reactivity, little use can be made of the (usually) higher reactivity of the low-flux regions.

In order to see what sort of effect this has on lifetime, some sample calculations were performed in which a fuel element was simplified so as to consist of two pieces irradiated at two different fluxes. By adjusting the relative sizes and fluxes of the two pieces, it was possible to match both maximum-to-average fluxes and maximum-to-average statistical weights for one group theory with those of chopped-cosine distributions. For a few different *ICR*'s it was then possible to estimate how much burning of the high-flux

piece beyond its normal lifetime could be accomplished by using the excess reactivity of the low-flux piece. This excess burning was negligible in all cases.

Consequently, it is recommended that the lifetime be computed for the most highly burned section of an element, so that the mean lifetime of a rod will be down from that predicted for uniform exposure by a factor which is the average flux/maximum flux. The flux curve which should be used is that computed for the system when burned out, however, so that the flux flattening caused by high-irradiation reactivity loss can be properly included.

Reactivity vs Productivity

Although we have previously observed that the correlation between reactivity and productivity is not always very great, we have developed most of the conclusions concerning reactivity changes from observations on the productivity changes. This is despite the fact that we are interested in reactivities in designing reactors.

The reason for this discrepancy is that the productivity considerations yield a set of mathematical functions which are capable of linear combination to simulate many types of reactors and many modes of operation. Reactivity predictions must be based on a given initial enrichment, resonance escape probability, leakage, etc., and the reactivity changes of no two reactors are identical; moreover, the solution of problems for reactivity change is complex enough to require automatic computing machinery (the reactivity curves displayed in this paper were, for example, obtained by solving the differential equations on a Reeves Analog Electronic Computer (REAC)). While such machinery is coming into widespread use, and although ultimately the reactivity changes of a specific system must be mapped, productivity considerations offer the virtue of providing simple figures of merit for a reactor designer.

A high degree of applicability of the productivity lifetimes does exist whenever the graded-irradiation scheme of operation is used. Under this circumstance, it is true that the effective cross section of the fertile material remains constant throughout irradiation history. Since this operating method is, moreover, the most attractive of those considered (and has been assumed in all arguments concerning excess enrichment, fuel recycling, and fission-product removal), productivity lifetimes presented in the previous sections are correct reactivity lifetimes to use in evaluating fuel performance capabilities.

When we can use this argument, we must then be careful about our definition of *ICR* for "just-critical" fuel feed. Productivity changes are associated with changes in the thermal fissionability of the fuel, which are balanced against changed absorption. In general, thermal fissionability, as measured by Sum (η_i, Σ_i), where i represents the i'th isotope, increased initially and in many cases continued to increase throughout irradiation (as with the U^{233}-Th breeders). Under these circumstances, and for constant ϵ, p, and τB^2, the effective cross section of the fertile material is, on the average, greater than it is for a critical loading of fresh fuel. Because of this, the required enrichment of steady-state feed is greater than the required enrichment for a completely clean loading.

The significance of this observation is to point out that constant reactivity, under the graded irradiation scheme, using feed material which will be critical initially, corresponds to a system which, on the productivity scheme, has a negative excess enrichment (X_0 or $m_0 < 1$ on Figs. 7, 11a, and 11b). Where such operation is desired—it is not recommended in our conclusions—curves can be constructed according to the appropriate formulae to give T vs ICR.

U^{235}-Th Systems without Incremental Loading

The curves giving T vs ICR for U^{235}-Th systems with incremental loading show a very abrupt break near $ICR = 1.0$. This is due to the fact that at about $ICR = 1$, the initial productivity dip, due mainly to replacement of high cross-section U^{235} by low cross-section U^{233}, is a transitory change and the system becomes, on further irradiation, a long-lived U^{233}-Th breeder. Thus, although reactivity drops initially, there is excess reactivity available at later stages in the irradiation, and such systems can, in principle, be operated without incremental loading. Lifetime curves for such operation can be constructed from the functions listed in Appendix II.

CONCLUSIONS

The results of this study indicate that:

1. Operation of a reactor by the graded-irradiation method is an excellent way of attaining efficient use of the original fuel.
2. Removal of fission products during irradiation makes very large reactivity lifetimes possible.
3. Incremental enrichment of fuel increases reactivity lifetime, even when measured in fission/total atom of fissionable material loaded.
4. For systems using Th as fertile material, very large reactivity lifetimes are possible for ICR significantly less than the theoretical maximum ($\eta - 1$); for systems with U^{238} as fertile material, very large lifetimes can be achieved only in very efficient converters.
5. The recycling of product (Pu or U^{233}) can cause very great economies in the enrichment required of fresh feed material.
6. The attainment of a flat axial flux distribution in reactors with long fuel elements increases not only the mean specific power of the system, but also its mean reactivity lifetime.

ACKNOWLEDGEMENTS

The authors wish to acknowledge contributions to this study achieved by helpful discussion of the problems both with colleagues at Argonne National Laboratory and with members of the staff of the Chalk River Laboratory and the Massachusetts Institute of Technology. We would like also to ac-

knowledge the large amount of study on specific systems which has been contributed by the following individuals: John B. Sampson, Henry Hurwitz, and J. W. Weil of Knolls Atomic Power Laboratory; C. J. W. Wende and coworkers of the du Pont Corporation; W. R. Clancy, R. Creagan and coworkers of Westinghouse Atomic Power Division; E. R. Cohen, R. H. Sehnert, E. F. Weisner, and coworkers of North American Aircraft Company; L. B. Robinson and coworkers at Hanford Atomic Products Operation.

In this listing of persons whose work is known to the authors, we wish to emphasize that the literature on the reactivity changes of specific systems is vast indeed, and to apologize to those contributors to it whose work is not herein specifically acknowledged.

APPENDIX I: NEUTRON CROSS SECTIONS

The neutron cross sections used in the computations are listed below in Tables A.I, A.II, and A.III. Table A.I contains the "cold constants used to describe the U^{235}-U^{238} systems examined for changes in reactivity; Table A.II, the "hot" constants used for investigations on productivity of U^{235}-U^{238} systems; and Table A.III, the constants (in addition to those already listed in Table A.II) used in Th systems. The origins of the data are discussed following each table.

Table A.I. "Cold" Cross Sections and Fission Parameters for U^{235}-U^{238} Systems

Isotope	σ_a (*barns*)	σ_f (*barns*)	σ_c (*barns*)	η(*neutrons/absorption*)
U^{235}	640	540	100	2.12
U^{236}	9	—	9	—
U^{238}	2.7	—	2.7	—
Pu^{239}	1150	765	385	2.02
Pu^{240}	540	—	540	—
Pu^{241}	1420	1060	360	2.2
FP (fission products)	50 barns per fission	—	50 barns per fission	—

Here, σ_f = fission cross section; σ_c = radiative capture cross section; σ_a = absorption cross section = capture + fission.

To obtain other nuclear parameters,

$$\alpha = \frac{\text{captures}}{\text{fission}} = \frac{\sigma_c}{\sigma_f}$$

$$\nu = \frac{\text{neutrons}}{\text{fission}} = \frac{\sigma_a}{\sigma_f}$$

The values quoted above were obtained from the cross-section compilations which were standard at the time the work was performed (1953). These compilations are predecessors of reference 1. The numbers were 2200 meter/sec values, corrected for Maxwellian spectrum at 293°K, with the following exceptions: (1) η for Pu^{241} was chosen so as to make ν for Pu^{241} equal to ν for Pu^{239}; (2) σ_a for FP was obtained as private information from the Chemistry Division at Argonne National Laboratory.

Table A.II. "Hot" Cross Sections and Fission Parameters for U^{235}-U^{238} Systems

Isotope	σ_a (*barns*)	σ_f (*barns*)	σ_c (*barns*)	η(*neutrons/absorption*)
U^{235}	680	575	105	2.06
U^{236}	9	—	9	—
Pu^{239}	1900	1200	700	1.84
Pu^{240}	640	—	640	—
Pu^{241}	1480	1080	400	2.41
FP	80 barns per fission	—	80	—

Table A.III. Additional "Hot" Cross Sections Used for Thorium Systems

Isotope	σ_a (*barns*)	σ_f (*barns*)	σ_c (*barns*)	η (*neutrons/absorption*)	λ (*decay constant, sec*$^{-1}$)
U^{233}	564	514	50	2.32	—
Pa^{233}	135	—	135	—	0.294×10^{-6}
U^{231}	89	—	89	—	—
Th^{232}	7	—	7	—	—

These values were all obtained from reference 1.

These numbers were obtained from reference 1 with the following conditions and exceptions:

1. Neutron temperature 600°K, cross sections corrected to equivalent 293°K values by multiplying Maxwellian averages by $\sqrt{600/293}$.
2. η for U^{235} was obtained by independent evaluation of the data quoted in reference 1, which evaluation led to a 1% difference from that value.
3. For Pu^{239}, 150 barns were added to the values obtained by the procedure described for both fission and capture cross section to account for absorption in the 0.3-ev resonance before thermalization is complete.
4. For Pu^{240}, 110 barns were added to the values quoted in reference 1 to account for capture in the 1.2-ev resonance.
5. For Pu^{241}, the cross-section values are very slightly different, older values than those of reference 1. The η value was based on a ν of 3.3, which was tentative (private information (as of 1953) from Chalk River Laboratory).
6. The value for cross section of *FP* was obtained by combining fission-yields data[2] with cross-section data available for many of the fission products.[3] A sample of ca 50% of the fission products (weighted by yield) was obtained, whose yield-weighted average cross section was about 40 barns/atom. Since two atoms of *FP* are formed per fission, this yields 80 barns per fission. Isotopes of cross section >5000 barns, which saturate at high fluxes, were omitted, and these isotopes must be included as contributors to neutron losses in predicting *ICR*.

APPENDIX II: PRODUCTIVITY-CHANGE FUNCTIONS

The productivity-change functions described in this paper are tabulated here for reference. In this tabulation, the *g*'s, *h*'s, and *w*'s are listed with a subscript descriptive of the appropriate isotope: 23

Table A.IV. Productivity-Change Functions

Flux-time (neutrons/ 10^{-21} cm²)	g_{23}	w_{23}	g_{25}	w_{25}	h_{02}	w_{02}	h_{28}	w_{28}
0.2	0.15598	0.01378	0.14770	0.01265	0.13561	0.00076	0.25738	0.00163
0.4	0.29512	0.02610	0.27662	0.02369	0.25511	0.00297	0.42195	0.00608
0.6	0.41925	0.03713	0.38913	0.03333	0.36026	0.00644	0.52791	0.01236
0.8	0.52997	0.04696	0.49734	0.04174	0.45258	0.01107	0.59683	0.02000
1.0	0.62875	0.05576	0.57306	0.04908	0.53349	0.01671	0.74247	0.02867
1.2	0.71686	0.06364	0.64789	0.05549	0.60418	0.02328	0.67335	0.03812
1.4	0.79551	0.07067	0.71320	0.06108	0.66577	0.03067	0.69482	0.04821
1.6	0.86566	0.07698	0.77021	0.06597	0.71924	0.03878	0.71018	0.05882
1.8	0.92829	0.08263	0.81997	0.07023	0.75644	0.04756	0.72136	0.06985
2.0	0.98417	0.08768	0.86339	0.07395	0.80519	0.05692	0.72949	0.08129
2.2	1.03404	0.09221	0.90131	0.07720	0.83916	0.06682	0.73536	0.09305
2.4	1.07855	0.09627	0.93438	0.08003	0.86796	0.07720	0.73934	0.10509
2.6	1.11829	0.09991	0.96326	0.08250	0.89217	0.08800	0.74167	0.11741
2.8	1.15376	0.10318	0.98846	0.08466	0.91225	0.09919	0.74253	0.12995
3.0	1.18544	0.10611	1.01047	0.08655	0.92866	0.11069	0.75818	0.14270
4.0	1.29967	0.11690	1.08497	0.09293	0.96800	0.17241	0.72230	0.20886
5.0	1.36474	0.12334	1.12270	0.09616	0.95904	0.23886	0.68067	0.27771

= U^{238}; 25 = U^{235}; 02 = Th^{232}; 28 = U^{238}. All g's are normalized to one unit of absorption area of original fissionable material; h's are likewise normalized per unit of effective absorption area of fertile material; and w's are fission-product-absorption areas associated with various materials, also normalized.

Integral functions, G's and H's which were obtained by trapezoidal integration in this paper may be evaluated for use by the reader of this data.

REFERENCES

1. BNL-325, "Neutron Cross Sections," by the Brookhaven National Laboratory Neutron Cross Section Compilation Group.
2. Coryell, C. D. and Sugarman, N., "Radiochemical Studies: The Fission Products," Book 3, Appendix B. NNES, Div. IV, Vol. 9. McGraw-Hill Book Co. (1951).
3. AECU-2040: "Neutron Cross Sections," by the AEC Neutron Cross Section Advisory Group.

Long Term Reactivity Changes in Natural Uranium Reactors

By D. J. Littler,* UK

In most of the existing natural uranium reactors, the uranium is removed for chemical processing after only a small percentage of the U^{235} has been burnt up. However, it may be desirable in future natural-uranium power reactors, to leave the uranium in the reactor almost indefinitely, thereby lowering the fuel costs for such reactors.

There are two questions which must be answered before one can say whether such a scheme is feasible. The first is whether the uranium fuel elements can be made to withstand the metallurgical damage due to the production of a large quantity of fission products in them; no attempt will be made to answer this question in this paper. The second is whether the changes in cross section of the uranium, due to the build-up of plutonium and fission products, and the destruction of U^{235}, are such that the reactor can remain divergent for a long period; this paper deals with some research which has been done in an attempt to answer this latter question.

It will be clear at the outset that we need only consider changes in the effective cross section of the uranium which will produce long-term reactivity effects, i.e., we can neglect the effect of fission-product poisons such as Xe^{135}.

If the conversion coefficient (amount of Pu^{239} made divided by the amount of U^{235} destroyed) in a natural-uranium reactor is greater than about 0.6, then the reactivity of the pile will rise initially if we ignore the effect of fission-product poisons. However, as the amount of Pu^{239} builds up, its destruction by neutron capture increases, and the rate of increase of reactivity due to its production will be gradually reduced. Meanwhile the destruction of U^{235}, and the building up of non-fissile Pu^{240} and stable fission products with large cross sections, cause a loss in reactivity.

The net effect of these changes will depend on the type of reactor being considered. In some reactors, the effect will be to cause a continuous loss in reactivity. In reactors such as those at Windscale, after a small initial loss in reactivity caused chiefly by a rapid build up of Sm^{149} poison, the reactivity of the reactor will rise above its initial value for a time, and then steadily fall to and below that initial value. For a natural-uranium power reactor with a high conversion coefficient, therefore, there will be a certain period of time, depending on its conversion coefficient and flux rating, during which its reactivity will be greater than its initial value.

* Atomic Energy Research Establishment, Harwell, Berks.

It is quite a straightforward matter to obtain analytical expressions for such reactivity changes in a reactor. When, however, values are inserted for the nuclear constants, it is found that the expressions are extremely sensitive to the values used, and that the time during which the reactivity of a reactor with a high conversion coefficient is greater than the initial value can only be predicted within wide limits. Furthermore, it is evident from the formulae that it is impracticable to determine the individual nuclear constants sufficiently well for accurate predictions to be made; this is especially true when one considers the competition between the build-up of Pu^{239} and the destruction of U^{235}.

We have, therefore, made measurements of the apparent change in cross section of uranium bars due to irradiation in order to determine various combinations of the nuclear constants with sufficient accuracy for long-term predictions to be made.

MEASUREMENTS OF THE CHANGE IN CROSS SECTION OF IRRADIATED URANIUM BARS USING A PILE OSCILLATOR

The effective change in cross-sectional area of an irradiated uranium bar can be measured with a pile oscillator. As already mentioned, besides the building up of fission-product poisons in the bar, there will be a change in the amount of fissile material in the bar during irradiation (due to the destruction of U^{235}, and the build up of Pu^{239} and Pu^{241}). For a fissile isotope, its effective absorption cross section is given by $\sigma(1 - W'\eta)$, where σ is its actual absorption cross section, η is the number of neutrons emitted per thermal neutron absorbed, and W is a factor giving the relative changes in reactivity produced by the emission of a fission neutron and the absorption of a thermal neutron; all three quantities depend on the neutron spectrum in the reactor in which the oscillator measurements are being made.

So far, all the oscillator measurements we have done have been with the GLEEP oscillator, although we will shortly be making measurements in DIMPLE, since in this latter reactor we can easily change the ratio of uranium to heavy water, and thus alter the neutron spectrum. A derivation of the value of W' has been given by Littler,[1] and its numerical value for GLEEP is 0.877.

Thus, the change in effective cross section of an irradiated bar per U^{235} atom originally present in the bar will be given by:

$$X(nvt) = \sum \frac{\Delta N\sigma(1 - W\eta)}{N_{235}(0)}$$

where $X(nvt)$ is the measured change in effective cross section (a function of the integrated thermal neutron flux received by the bar, i.e., nvt), ΔN is the change in the number of atoms of a particular kind due to the irradiation, and $N_{235}(0)$ is the original number of U^{235} atoms in the bar.

The summation extends over all the elements and isotopes in the bar, and of course η is zero for any non-fissile isotope.

The procedure has therefore been to compare the effective cross sections of uranium bars with the cross section of a standard bar before irradiation, and to make further comparisons with the standard after known irradiations. Allowance had to be made for the self-shielding in the bars in order to convert the apparent cross-sectional change measured into a true cross-section change; this was done by making measurement with small copper absorbers embedded firstly in graphite and then in a uranium bar.

The irradiation dosages received by the bars were determined by using cobalt-wire monitors in the manner described by Littler and Thomas;[2] since the cobalt-wire monitors were wrapped round the bars, we had also to determine the ratio of the maximum to average neutron flux in the bars, in order to find the mean integrated dosages received by the bars.

Irradiations have been carried out in the BEPO, the Windscale and the NRX reactors. The Windscale measurements have been made up to irradiation dosages in excess of 1000 Mwd/ton, and the NRX measurements up to comparable dosages. Besides making measurements with natural uranium, some irradiations using thorium and some measurements with Pu^{239}, U^{235}, and U^{233} have been made, or are being made, in the Windscale and NRX reactors; in the case of the three fissile isotopes, bars have been made by alloying the fissile material with aluminum. All irradiations have been made with the bars occupying a normal lattice position in the appropriate reactor. It is worthy of mention that it is necessary to measure the change in total effective cross-sectional area of a bar to an accuracy of ± 0.3 mm^2, the overall total-absorption area of a uranium bar being of the order of 50 cm^2. This has to be done, for example, with bars which make two trips across the Atlantic Ocean and have, after irradiation, to be handled completely remotely.

By such measurements it is possible to analyse the long term reactivity changes in a reactor such as the NRX into elementary components. By allowing for the change in effective cross section from one reactor to another (using the DIMPLE oscillator measurements, for example) one can then synthesise these components in order to obtain the change in reactivity with time for any projected thermal reactor.

In such a short paper as this, it is impossible to quote all the results we have obtained so far, but the paper will be concluded by describing the typical piece of analysis of the experimental values.

THE THERMAL FISSION YIELD OF SAMARIUM-149

Let us consider how the effective cross section of uranium will vary with irradiation dosage for integrated neutron fluxes up to of the order of 10^{20} n/cm^2 (300 Mwd/t). We will first consider the effect of the build up of stable or long-lived fission-product poisons. On examining the fission-product tables (Coryell and Sugarman)[3] we find that the fission products listed in Table 1 have cross sections which are large enough to contribute an appreciable poisoning effect.

Table 1

	Isotope	*Cross section (barns)*	*Fission yield (%)*
	Sm^{149}	76,700	1.3
A	Gd^{157}	160,000	0.015
A	Gd^{155}	70,000	0.03
A	Eu^{155} (1.7 years)	14,000	0.03
A	Cd^{113}	25,300	0.012
B	Nd^{143}	240	5.4
B	Eu^{153}	420	0.15
B	Kr^{83}	205	0.586
B	Sm^{152}	150	0.279
B	Rh^{103}	150	3.7
B	Xe^{131}	120	2.8
B	Pm^{147} (4.4 years)	60	2.6
B	Cs^{133}	29	4.5
B	Cs^{135} (2×10^6 years)	15	5.6
B	Mo^{95}	13	6.0
B	Pr^{141}	11	4.6
B	La^{139}	8	6.3

The cross-section figures quoted in the table are taken from AECU 2040,[4] with the exception of Sm^{149} which is a value obtained by Lockett[5] by measuring a sample of natural samarium.

Sm^{149} is unique because it has a large fission yield as well as a large cross section. Because of its large cross section there will be appreciable neutron capture in Sm^{149} during the irradiation, and then its poisoning will grow approximately as the form $(1 - \exp(-nvt\sigma_s))$, where σ_s is the cross section of Sm^{149}. (This is not quite the accurate form of the growth since Sm^{149} is not formed directly in fission.)

At an integrated neutron flux $\sim 10^{20}$ n/cm^2, the Sm^{149} poisoning effect will reach saturation, and we will have,

$$S\sigma_s = \beta\sigma_f N_{235}(0)$$

Where S is the number of atoms of Sm^{149} in a uranium bar at saturation, σ_f is the fission cross section of U^{235}, and β is the fission yield of Sm^{149}.

Thus, at saturation, the poisoning effect of the Sm^{149} will be proportional to its fission yield and independent of its cross section.

The other fission-product poisons with cross sections greater than 10,000 barns (Group A) will tend towards saturation during the irradiation, but because of their low fission yields will not produce poisoning effects comparable with Sm^{149}. On the other hand, the fission-product poisons with cross sections less than 1000 barns (Group B) will not reach saturation but will produce a change in effective cross section of the uranium which will vary linearly with nvt.

We can thus say that, so far as the fission-product poisons are concerned, the change in effective cross section of the uranium is substantially due to the build up of Sm^{149} together with a linear change in cross section with *nvt*, the latter being the contribution of the other poisons.

Since Pu^{239} and U^{235} have cross sections of 1025 and 650 barns respectively,[4] the build-up of Pu^{239} and the destruction of U^{235} will also produce a linear change in the effective cross section of the uranium for integrated flux values up to $\sim 10^{20}$ n/cm^2. The amounts of Pu^{240} and Pu^{241} which are produced in irradiations up to these flux levels will be quite small.

We would therefore expect that the over-all change in effective cross section of the uranium could be considered as consisting of two components: (*a*) one due to the build-up of Sm^{149}; (*b*) A linear variation of cross section with *nvt* due to changes in all the other isotopes; including the fissile materials.

We will now consider the build up of Sm^{149} in more detail. It is produced in the fission chain,

$$Nd^{149} \xrightarrow{1.7\ hr} Pm^{149} \xrightarrow{47\ hr} Sm^{149}$$

Since the half-life of Nd^{149} is short compared with the half-life of Pm^{149}, we will assume that Pm^{149} is formed directly in fission. Allowing for the hold-up of Sm^{149} as Pm^{149} during the irradiation, and the build-up of Sm^{149} from Pm^{149} after the irradiation, it can be shown that the ratio of the number of Sm^{149} to U^{235} atoms present after a dosage *nvt* and irradiation time *t* is:

$$\frac{S}{N_{235}} = \frac{\beta\sigma_f\lambda_p t}{\sigma_s(\lambda_p t - nvt\sigma_s)}\left[1 - \exp(-nvt\sigma_s) - \left\{\frac{nvt\sigma_s}{\lambda_p t}\right\}^2\right]$$

where λ_p is the radioactive decay constant of Pm^{149}, and it has been assumed that the irradiation time and decay time are both long compared with the half-life of Pm^{149}.

Thus the ratio of the cross section of the Sm^{149} to the total fission cross section of the uranium is given by:

$$\frac{S\sigma_s}{N_{235}\sigma_f} = \frac{\beta\lambda_p t}{(\lambda_p t - nvt\sigma_s)}\left[1 - \exp(-nvt\sigma_s) - \left\{\frac{nvt\sigma_s}{\lambda_p t}\right\}^2\right]$$

$$= \beta \cdot \gamma(nvt) \qquad \text{say}$$

where $\gamma(nvt)$ is a calculable function of *nvt* since σ_s is known.

Recalling that $X(nvt)$ is the measured change in effective cross section per U^{235} atom originally present in the bar, we have:

$$\frac{X(nvt)}{\sigma_f} = \beta \cdot \gamma(nvt) + \alpha nvt$$

the second term representing the linear change in effective cross section with *nvt* due to all the other isotopes apart from Sm^{149} (α being a constant).

Figure 1 shows a plot of $X(nvt)/\sigma_f$ from the results of the irradiation of 42 uranium bars in one of the Windscale reactors. Since $\gamma(nvt)$ can be calculated, it

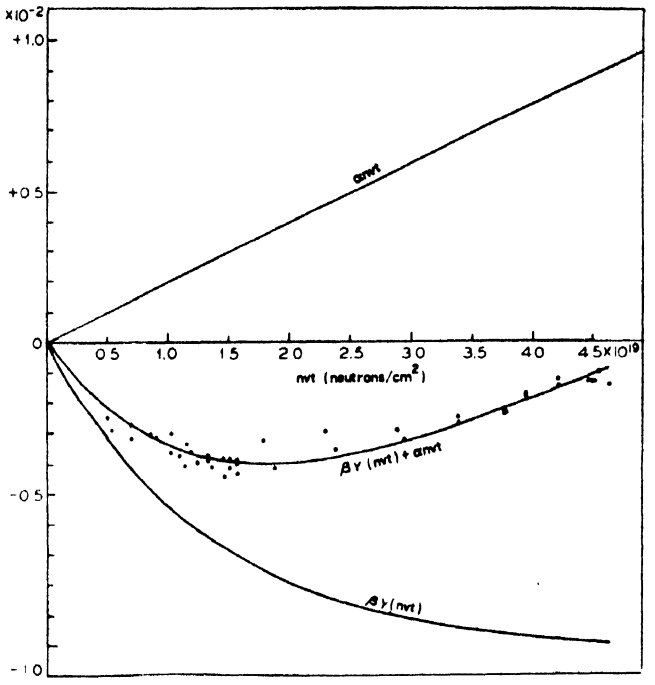

Figure 1. Cross section changes in irradiated uranium

is possible to analyse this curve by the method of least squares to find the best values of α and β. The functions αnvt and $\beta \cdot \gamma(nvt)$ are also shown in Fig. 1. The least-squares analysis for α and β gives the results:

$$\alpha = 1.963 \times 10^{-22}$$

$$\beta = -1.00 \times 10^{-2}$$

Thus the fission yield of Sm^{149} is shown to be 1.00 $\pm$ 0.07%. The value of 1.3% for the Sm^{149} fission yield quoted in Table 1 was determined by Marinsky and Glendenin.[6] They compared the β-emission from Pm^{149} with that from 12.8 day Ba^{140} (assumed yield 6.1%), and obtained a yield for the mass 149 chain of 1.3 $\pm$ 0.2%.

Ingrham, Hayden and Hess[7] report a value of 1.1% for the fission yield at mass number 149. They compared the relative yields of the neodymium isotopes on a mass spectrometer and assumed that the yield for mass number 143 was 5.4% (Katcoff, Finkle and Sugarman).[8]

Our value of 1.00% is in agreement with both of these values. It is of interest to note that the value we obtain is really the poisoning yield (i.e., the yield of Sm^{149} with a cross section of 76,700 barns) of Sm^{149}, and we have shown that this is the same as the fission yield of the mass 149 chain. Some early reactor poisoning measurements at Chalk River[9] had indicated that the poisoning yield of Sm^{149} was considerably less than its fission yield, and it had been suggested that some of the Sm^{149} resulting from the decay of Pm^{149} was formed in an long-lived isomeric state and had a low-absorption cross section. Our experiments disprove this hypothesis.

CONCLUSION

By measurements of the change in effective cross section of uranium with irradiation, supplemented by

measurements of the changes in effective cross sections of fissile materials and fission-product poisons with neutron spectra, it is possible to predict the long-term reactivity changes in a natural-uranium power-pile.

REFERENCES

1. Littler, D. J., "A Method of Calibrating Neutron Sources Absolutely," Proc. Phys. Soc. A, *64*, 638 (1951).
2. Littler, D. J. and Thomas, R. H., "Absolute Neutron Density Determinations using Cobalt, A.E.R.E." Report number R/R 1019 (1952).
3. Coryell, C. D. and Sugarman, N., *Radiochemical Studies of the Fission Products* McGraw-Hill Book Company, Inc. Book 3 (1951).
4. "Neutron cross-sections," American Atomic Energy Commission report A.E.C.U. 2040 (1952 and supplements).
5. Lockett, E. E., "The pile neutron absorption cross section of Sm^{149}," Unpublished work (1953).
6. Marinsky, J. A. and Glendenin, L. E., *Radiochemical Studies of the Fission Products*, McGraw-Hill Book Company, Inc. Book 2 (1951).
7. Ingrham, M., Hayden, R. and Hess, D. "U^{235} Fission Yields in the Rare Earth Region," Phys. Rev. *79*, 271 (1950).
8. Katcoff, S., Finkle, B. and Sugarman, N., *Radiochemical Studies of the Fission Products*, McGraw-Hill Book Company, Inc. Book 2 (1951).
9. Watson, W. H., "Poisoning in the N.R.X. Pile," Chalk River report T.P.I. 51 (1948).

Small Thermal Homogeneous Critical Assemblies

By A. D. Callihan, J. W. Morfitt, and J. T. Thomas,* USA

The term critical assembly refers to a neutron chain-reacting accumulation of fissionable and other material which usually operates at a nuclear power of the order of one watt. Experiments with such systems provide data to support the design of reactors and specialized process equipment for handling fissionable isotopes. Critical experiments yield, in addition to the critical mass, data on neutron flux and power distributions, and information on the reactivity effects due to neutron reflectors, and information on the reactivity effects due to neutron reflectors, reactor structural materials, temperature changes, and reactor control devices. They provide basic information for evaluating methods of reactor analyses and give empirical data on those reactor prototypes to which analytical methods are not applicable.

During the past few years several laboratories operated for the United States Atomic Energy Commission have carried on extensive experimental programs of this kind. It is the purpose of this paper to present a survey of the data obtained in three laboratories from measurements on critical arrays of aqueous solutions containing U^{233}, U^{235} and Pu^{239}. Representative results have been selected from an extensive accumulation of data and are intended to summarize the critical parameters for these isotopes. Typical experimental equipment and procedures are briefly described.

EXPERIMENTAL EQUIPMENT

Although these experiments have been done in different laboratories the equipment used in them is basically similar. A typical arrangement includes a reservoir for the fissionable material, a transfer mechanism to introduce the solution into the system under test, a source of neutrons, and other control equipment. In some installations the operating personnel have been located a few hundred meters from the reactor while in others the safety has been provided by concrete shields. In every case the reactivity is controlled by one or more remotely adjusted variables to further reduce potential dangers to personnel. Each experiment is equipped with at least two safety devices which reduce the reactivity by a large amount in case of an accident. One of these is usually a mechanism for inserting, by gravity or by a loaded spring, a material of high neutron absorption cross section. The second device opens a valve and allows the solution of fissionable material to drain into a less reactive shape. In a variation of the latter safety feature the liquid neutron reflector is rapidly drained from around the reactor vessel. These devices may be operated manually and are activated electronically if the radiation near the experiment exceeds a pre-set level. Safety equipment is always designed for "fail safe" operation, that is, the devices are actuated in case of a failure in the power supply or in the electronic circuits. It is also general practice to make the procedure by which the nuclear reactivity is increased readily reversible with the maximum rate of increase substantially less than the rate of decrease. This can be accomplished, for example, by making the solution inlet pipe much smaller than the outlet pipe.

The rate of change of reactivity may be controlled by altering the positions of neutron absorbing rods or by adjusting the quantity of fissionable material or neutron reflector. These adjustments must be adequately indicated at the control station. A source of about 10^6 neutrons per second, initially located near the center of the assembly, is attached to a mechanism whereby it can be removed after the system has become critical. An intimate mixture of polonium and beryllium serves as a satisfactory source.

The signals from several neutron and gamma-ray detectors, located near the assembly, are amplified and recorded as guides in the control of the reactivity. These signals also actuate the safety devices. Proportional neutron counters with scaling circuits provide quantitative measures of the apparent source neutron multiplication during the step-wise approach to criticality. In this startup procedure a plot is made of the reciprocal of this neutron multiplication as a function of the variable by which the reactivity is being increased. Extrapolation of this curve to zero reciprocal multiplication provides a preliminary estimate of the critical conditions and is, therefore, a guide in the addition of succeeding increments of reactivity. The criterion of criticality is the constancy of the neutron flux, in the absence of the source, as indicated by the recorded neutron level.

The critical experiments reported here have been operated at a nuclear power not greater than a few watts. These levels were found adequate for the activation of neutron flux detectors and for other measurements and permitted modifications of the reactor to be readily made. Except for secondary effects, such as fission product build up, the critical parameters of sig-

* Including work by J. R. Brown and associates, Westinghouse Electric Corp.; A. D. Callihan and associates, Oak Ridge National Laboratory; W. J. Ozeroff and associates, General Electric Co.

nificant interest are independent of the power level at which they are measured.

Neutron distributions within the solutions have been measured successfully with indium and other resonance detectors and with the fissionable materials themselves. It has been found possible to keep indium foils uncontaminated by sealing them with pressure between two pieces of fluorocarbon tape coated with an adhesive. These "sandwiches" are firmly attached to rigid rods and located in regions of interest. The distribution of neutrons producing fission has been observed by exposing small volumes of the solution of the fissionable element and counting the resulting delayed gamma activity. These samples were contained in cylindrical capsules, about 6 mm in diameter and 6 mm high, made from a methacrylate plastic and mounted in a re-entrant plastic tube in the core. Both the resonance detectors and the fission detectors could be covered by cadmium in order to obtain a measure of the energy distribution of the neutrons.

The effect on reactivity of a number of variables, such as changes in structure, composition, or temperature, can be measured by calibrated control rods. These calibrations are obtained by noting the time rate of change in reactivity following the displacement of the rods from their critical positions.

PARAMETERS OF HYDROGENEOUS CRITICAL SYSTEMS

Using the methods described, data have been obtained on the critical conditions of aqueous solutions of uranium and plutonium compounds. In most experiments the fissionable isotope was enriched to about 90%; included are a few measurements made with uranium of lower U^{235} enrichment. The properties of U^{235} have been investigated more extensively

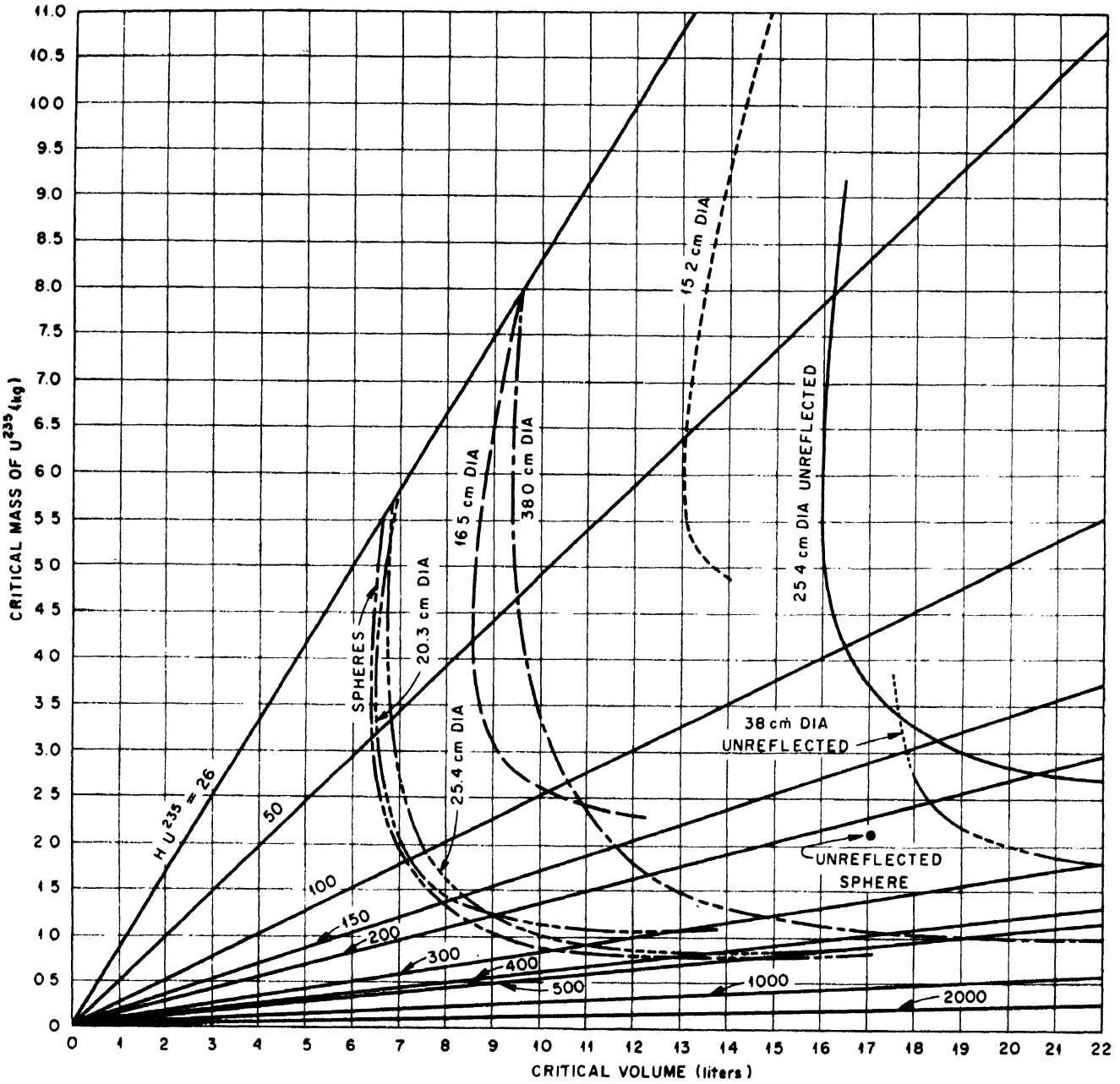

Figure 1. Critical mass and volume of U^{235} as a function of concentration for both reflected and unreflected spherical and cylindrical geometries

than those of U^{233} and Pu^{239} although the results from the latter two isotopes are representative. It is intended to present here a summary of the data obtained at about 25°C. The effect of water and stainless steel reflectors on the mass of critical aqueous solutions is summarized.

Figure 1 presents the values of the critical mass of U^{235} as a function of the corresponding volume for cylinders of solution of UO_2F_2 in the concentration range from about 50 to 800 gm U^{235}/l. The solution was contained in aluminum vessels and, in most cases, was surrounded by an infinite water neutron reflector. The critical data for a given cylinder is represented by a curved line on the graph. Similar results from critical spherical volumes form the envelope of these curves. The rays are lines of equal chemical concentration, or equal moderation, and range between hydrogen to U^{235} atomic ratios of 26 to 2000. The intersections of one of these radial lines with the curves represent systems critical at the same concentration. The effect of removing the infinite water reflector is shown by the displacement of the curves for the 25.4 cm and 38.0 cm diameter cylinders toward larger values of mass and volume. The critical mass of U^{235} in an unreflected 32.0 cm diameter sphere is 2.13 kg.

An extension of the experiments to larger volumes is shown in Fig. 2. These data represent relatively dilute solutions of $UO_2(NO_3)_2$. The experiments show that the minimum critical concentration corresponds to a $H:U^{235}$ ratio of about 2000. Since the dimensions of these systems are large compared to those presented in Fig. 1, the difference between the reflected and unreflected critical values is not as pronounced. The neutron absorption by the nitrogen is sufficiently small compared to that of the hydrogen to make a comparison between these data and those of the more concentrated UO_2F_2 solutions valid.

The results with the U^{233} isotope are limited, being restricted almost exclusively to cylinders of equal height and diameter and surrounded by a reflector. The curve for these equilateral cylinders is shown in Fig. 3. The few data presented for spherical geometry indicate critical values only slightly lower than those of the equilateral cylinders. The critical mass of U^{233} in an unreflected 32.0 cm diameter aluminum sphere is 1.15 kg. Presented in Fig. 4 are the values for Pu^{239} measured with $Pu(NO_3)_4$ solutions in reflected stainless steel cylinders and spheres. The solution contained about 20 per cent excess nitrate ion.

Figure 5 is included to illustrate typical neutron flux distributions in a spherical homogeneous reactor. The measurements were made in a water reflected sphere containing UO_2F_2 solution at a $H:U^{235}$ atomic ratio of about 500. The distribution of those neutrons producing fission and those activating indium foils fall on the curve representing a sine function obtained from a two-group calculation. A measure of the spectral distribution of the neutrons is given by a comparison of the activities of bare and cadmium-covered detectors. One such measure, the cadmium fraction, is defined as the fraction of all activations which is produced by neutrons in the energy range where

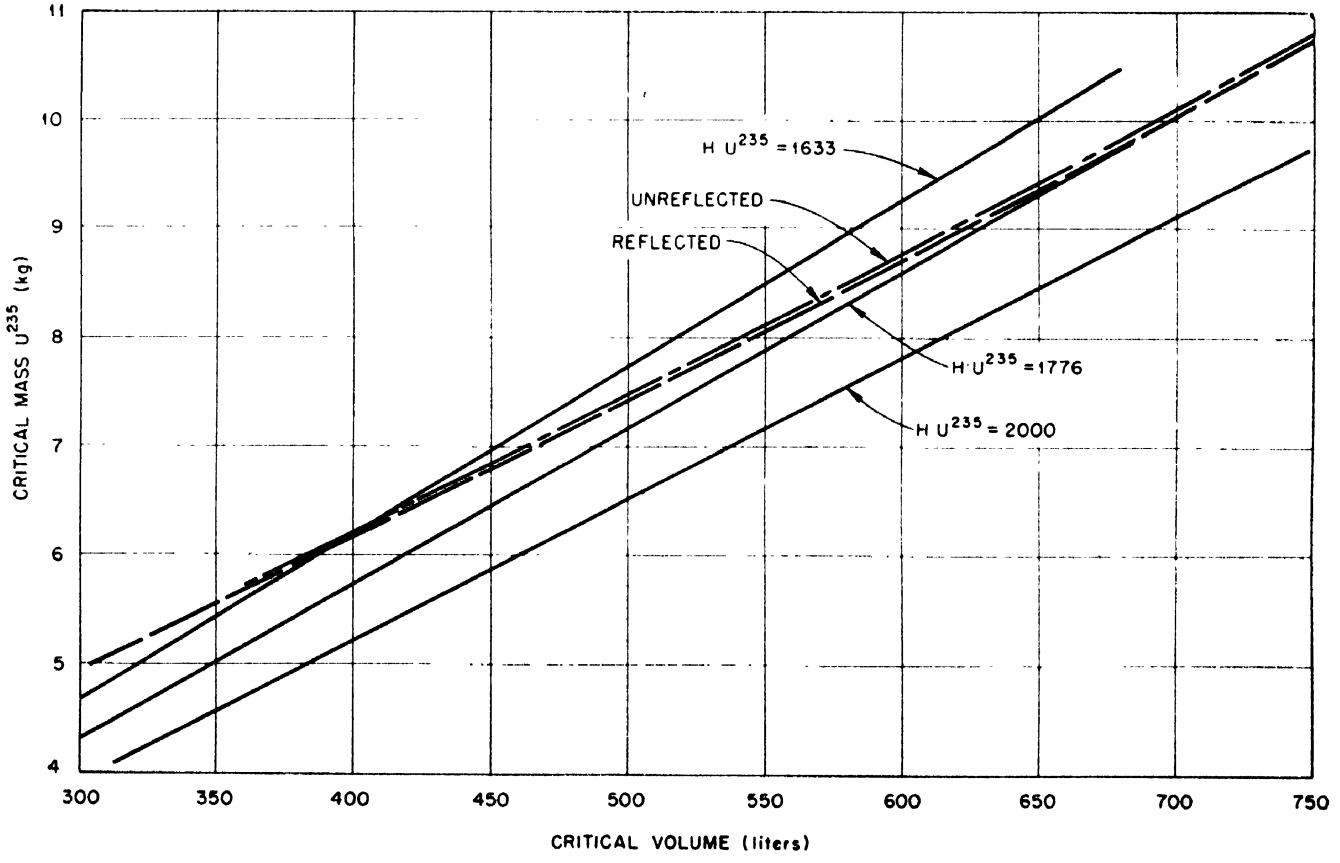

Figure 2. Critical mass and volume of U^{235} as a function of concentration for a reflected and unreflected 91.4-cm-diameter cylinder

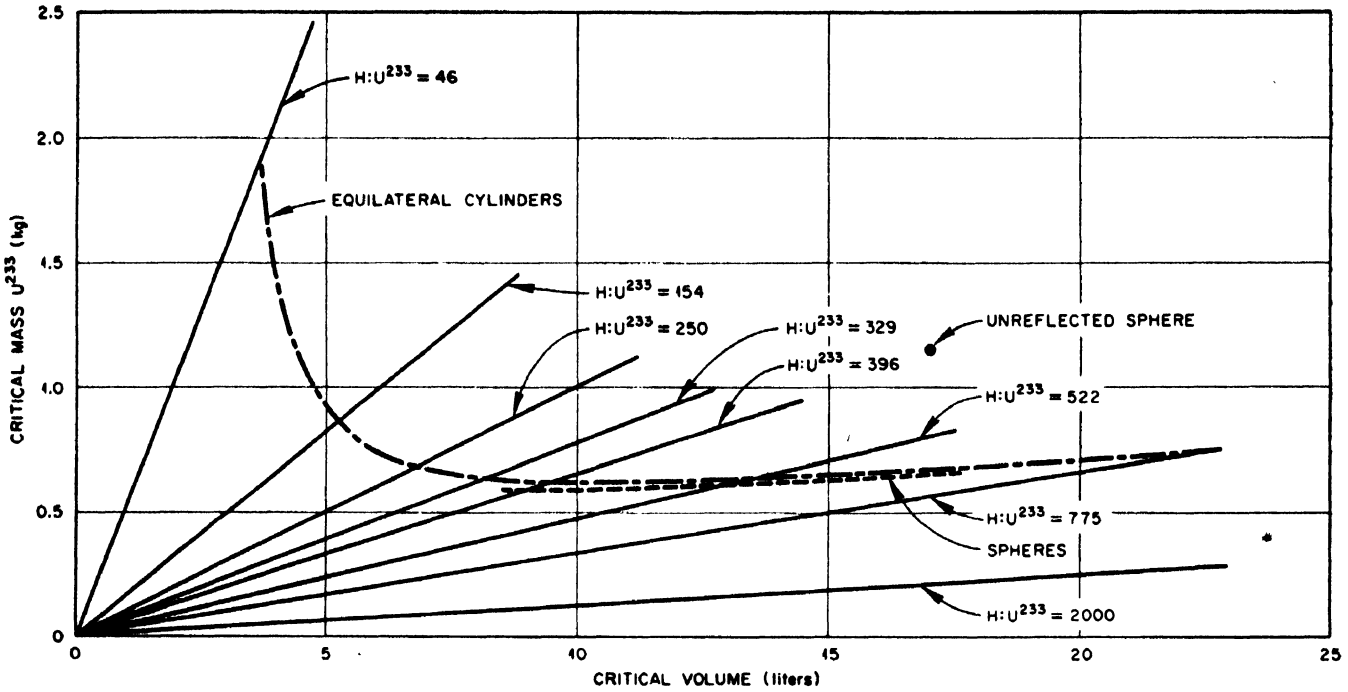

Figure 3. Critical mass and volume of U^{233} as a function of concentration in reflected equilateral cylinders and spheres

cadmium is strongly absorbing. This range extends below about 0.5 ev. The uranium activation curves indicate that approximately 92% of the fissions are produced by neutrons having energies less than 0.5 ev. The cadmium fraction measured with indium foils is about 54%. The values of these cadmium fractions are relatively constant in the central region of the core. About 65% of the fissions in the more concentrated solutions, $H/X = 45$, were produced by low energy neutrons.

The minimum critical parameters for uniform, homogeneous solutions of the three fissionable isotopes considered here have been estimated. It has been observed that the minimum critical mass and minimum critical volume for a particular isotope do not occur at the same concentration. Summarized in Table I are the experimental minimum critical masses for water-moderated, water-reflected, spherical geometries. Values of minimal volumes are given for the uranium isotopes. The uncertainty in the results is $\pm 5\%$.

A few definitive experiments have been performed with aqueous solutions of UO_2F_2 in which the uranium was enriched to 4.9% in the U^{235} isotope. The results

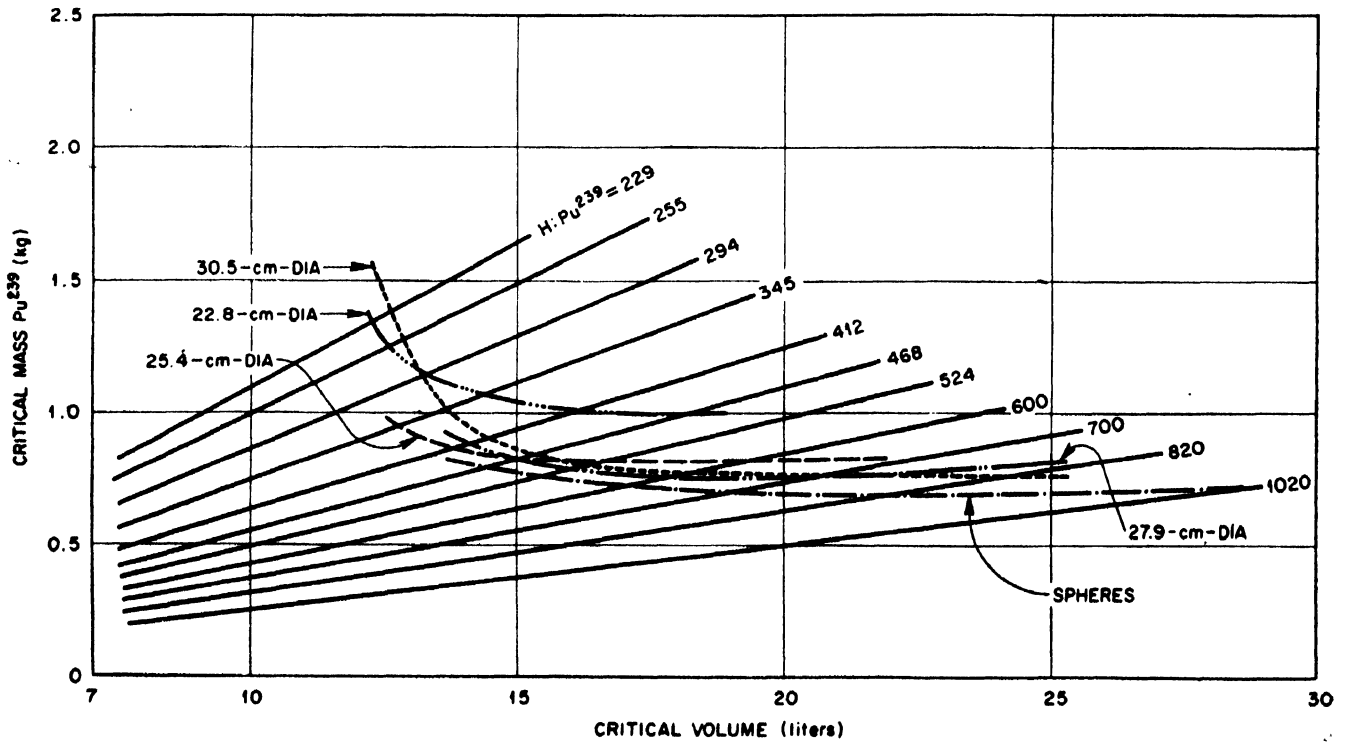

Figure 4. Critical mass and volume of Pu^{239} as a function of concentration in reflected spherical and cylindrical geometries

Table I. Minimum Critical Mass and Volumes

Isotope	*Chemical compound*	*Minimum mass, gm*	*Minimum volume, l*
U^{235}	UO_2F_2	800	6.35
U^{233}	UO_2F_2	588	3.50
Pu^{239}	$Pu(NO_3)_4$	690*	—

* When corrected for the presence of impurities and other isotopes of plutonium this value is estimated to be 510 gm.

are included here because of their application to the design of reactors employing partially enriched uranium as fuel and demonstrate the relatively small U^{235} requirement. Experiments have been done with the solution in an aluminum sphere 69.3 cm in diameter having a volume of 174 l. The critical mass was 3.78 kg U^{235} with the sphere surrounded by an infinite water reflector and 4.16 kg U^{235} with no reflector. Lower values of these masses can be obtained with solutions of somewhat higher chemical concentrations occupying smaller volumes. Data obtained from solutions of several concentrations in cylinders show that the minimum critical mass at this enrichment is somewhat less than 2 kg U^{235} occupying a volume of about 50 l. Results of fission rate distribution measurements along a radius of the sphere are in agreement with simple multigroup theory. Ninety-four per cent of the fissions in the center of the sphere were produced by neutrons having energies below about 0.5 ev.

In the design of reactors consideration must be given to the dimensions of the reflector and to the physical boundary separating the fuel and reflector regions. The effect on the critical mass of aqueous solutions of highly enriched U^{235} by various thicknesses of neutron reflectors has been examined. Some results are shown in Fig. 6 where critical mass is plotted as a function of the thickness of lateral surface reflectors. Measurements were made in aluminum cylinders of two diameters and with solutions of two concentrations. In general water and stainless steel are similar as neutron reflectors, particularly if the solution is dilute and is contained in large cylinders where the leakage neutrons are of more nearly thermal energy. With more concentrated solutions a thick layer of stainless steel is a more effective reflector than water.

In another experiment a study was made of the

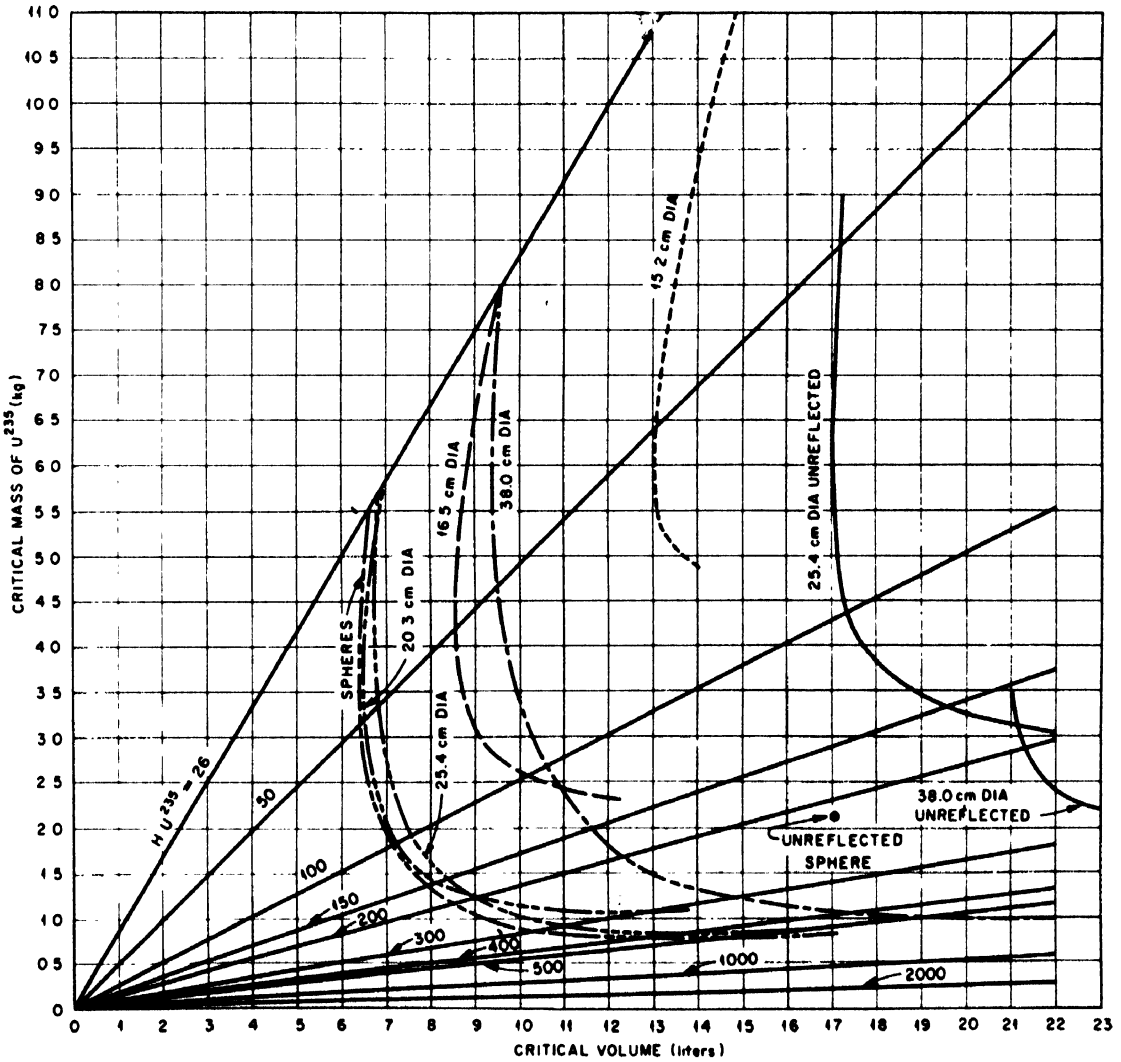

Figure 5. Fission rate and neutron flux distribution in the core of a critical water reflected spherical reactor

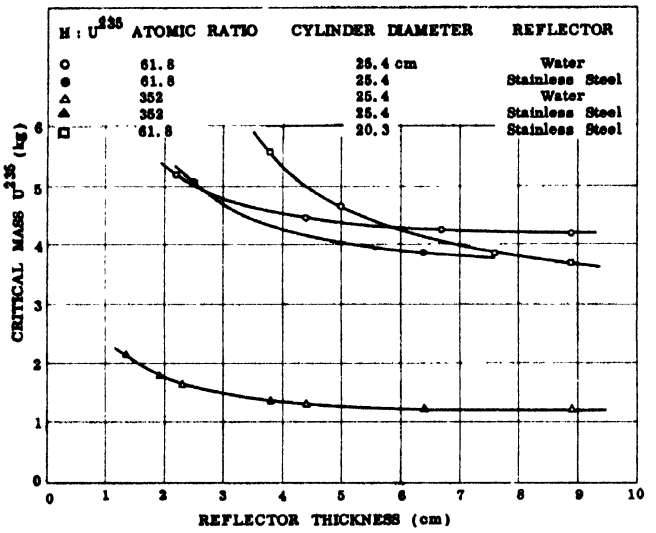

Figure 6. Comparison of the effect of water and stainless steel reflectors on critical mass

changes in reactivity produced by a composite reflector of stainless steel and water. A cylinder of U^{235} solution was surrounded by a closely fitting, cylindrical shell of steel which, in turn, was surrounded by an effectively infinite layer of water. The thickness of the steel could be increased from zero to several centimeters. The results are shown in Fig. 7 where the critical mass of U^{235} is plotted as a function of the thickness of the stainless steel layer in contact with the solution container. The value of the mass at zero thickness is, of course, that of a water reflected cylinder. Introduction of the steel first increased the critical mass by absorbing neutrons which would otherwise cause fission after reflection by the water. As the thickness of the steel layer was further increased the critical mass decreased because of the reflector properties of the steel itself. In the experiments with the solutions of higher uranium concentration, the steel is again shown to be a more effective reflector than water.

ANALYSIS OF HYDROGENEOUS CRITICAL SYSTEMS

An attempt has been made to compute, by a one-dimensional model, the critical parameters of the water-moderated, water-reflected, U^{235} cylindrical cores of finite length reported above. Since the critical equations for totally reflected cylinders are not separable, the finite cylindrical geometry was replaced by an equivalent spherical geometry which could be calculated by already existing computer programs.

Two programs were available which divided the neutron energy spectrum into 30 groups. These were an age-diffusion model and a Goertzel-Selengut variation of this model. The two models differ in their treatment of the slowing down density. In the age-diffusion model an average slowing down density is used for all the elements. In the Goertzel-Selengut calculation an average slowing down density is used for all the elements except hydrogen which is treated separately. Calculations of several reflected critical spheres were made by both methods even though the limitations of the age-diffusion model were recognized. The results are listed in Table II where the reactor size, critical concentration, and temperature are given with the two calculated values of the mutiplication constant, k.

Table II. Comparison of Age-Diffusion and Goertzel-Selengut Analytical Models

Spherical diameter cm	*Critical concentration gm U^{235}/l*	*Temp. °C*	*Effective multiplication constant*	
			Age-diffusion Model	*Goertzel-Selengut Model*
26.4	95.1	27.5	1.130	0.992
26.4	97.1	39.5	1.133	0.992
26.4	104.9	74.0	1.148	1.007
26.4	106.8	85.5	1.152	1.011
32.0	52.1	54.0	—	1.010
32.0	53.1	64.5	—	1.015

The results indicate an error of 1.5% in the Goertzel-Selengut model as compared to 14% in the age-diffusion model. The Goertzel-Selengut model was, therefore, used in the subsequent computations.

In order to find a suitable transformation from cylindrical to spherical geometry, the radii of critical reflected spheres were computed at various solution concentrations. The results of these computations are given in Fig. 8 where the critical spherical radii are plotted as a function of the concentration expressed as the $H:U^{235}$ atomic ratio. Also presented in the figure, for comparison, are the spherical experimental data from Fig. 1. Each sphere is characteristic of a particular concentration and is designated as being equivalent to the set of critical cylinders experimentally measured at that concentration. None of the calculations considered the effects of the containing vessels.

Four methods were used to transform from cylindrical to spherical geometry. The transformations considered are: (1) the volume of the cylinder is equated to the volume of the sphere; (2) neglecting the reflector, the buckling (the lowest eigenvalue of the solution to the wave equation for a critical reactor) of the cylindrical core is equated to the buckling of a spherical core; (3) the ratio of the surface area of the cylinder to its volume is equated to that of a sphere; (4) the linear dimensions of the cylinder are increased by an amount equal to the reflector savings, the buckling is calculated and equated to that of a bare sphere which is then converted to a reflected sphere by the reflector savings.

The results of the four methods of transformation are shown in Figs. 9 and 10 where the dimensionless ratio of the diameter of the calculated critical sphere to the diameter of cylinder, D/d, is plotted against the ratio of the height of the cylinder to its diameter, h/d. The curves labeled aluminum and stainless steel show the experimental obtained with cylinders constructed from the two materials.

One may conclude from these curves that the Goertzel-Selengut model, when used with the last of the above transformations, fits the experimental data over a large range of concentrations. The deviation from experimental data becomes greater for all four

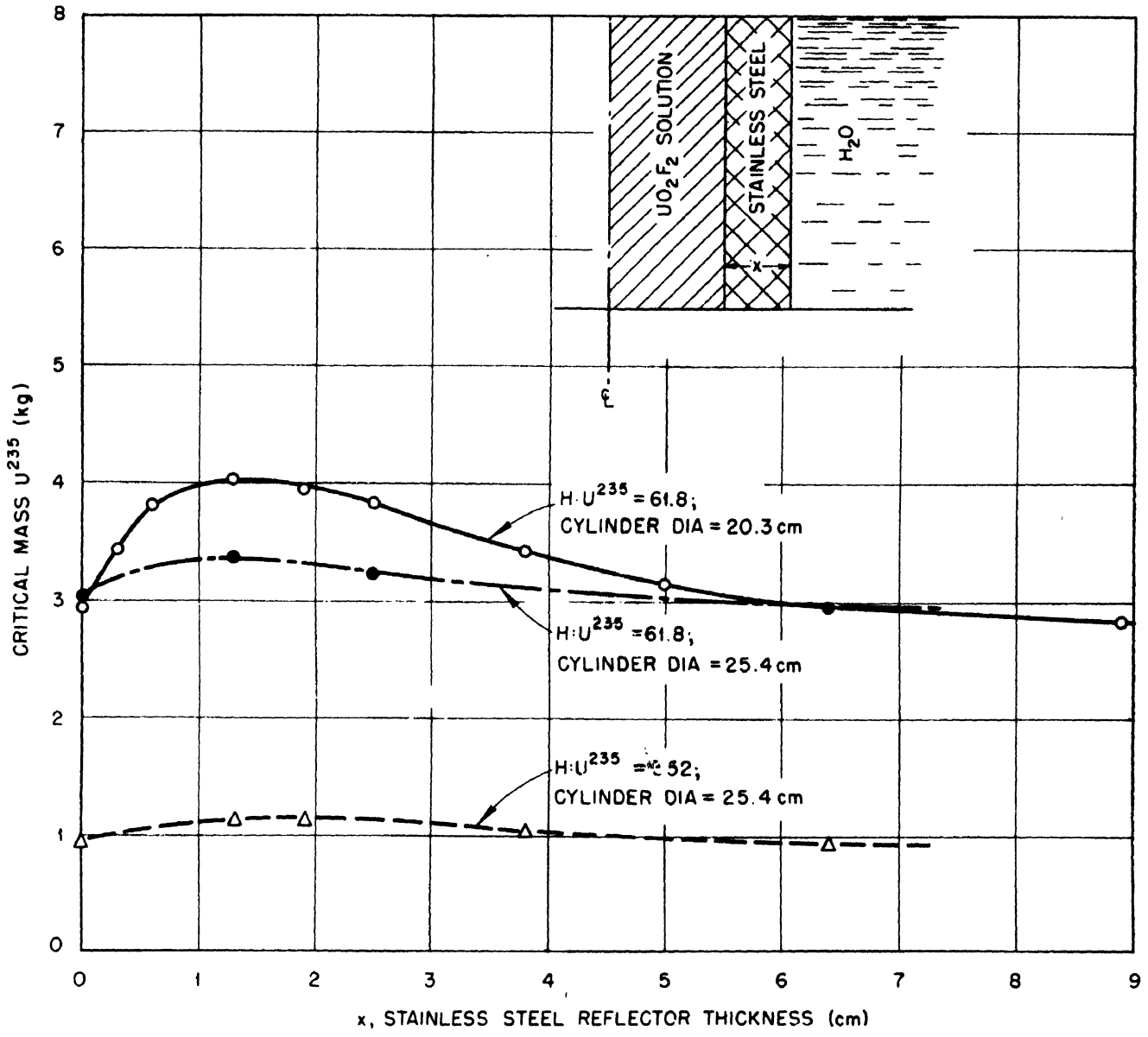

Figure 7. Effect of composite reflector of stainless steel and water on critical mass

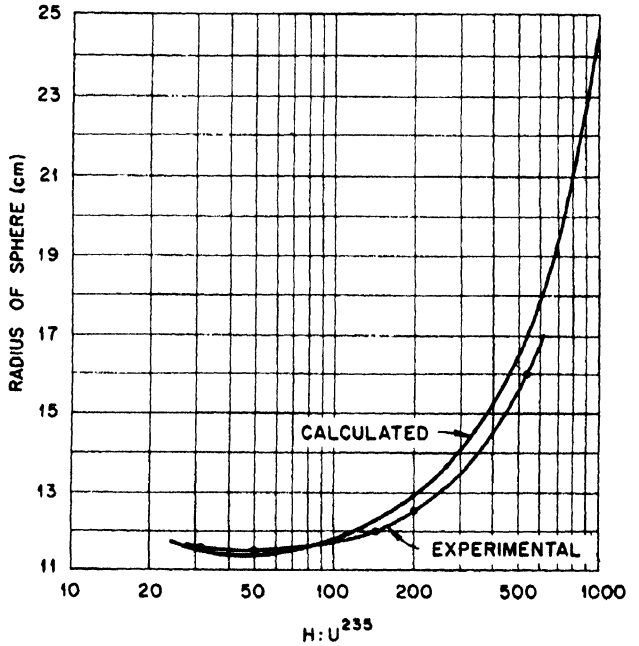

Figure 8. Effect of concentration on critical radius of water-reflected spheres

transformation methods as the height to diameter ratio increases.

FUNDAMENTAL INVESTIGATIONS

The experimental methods described above can be extended to examine a wide variety of problems. As an example in reactor design, consider the apparently independent requirements of minimizing the critical mass and flattening the thermal neutron flux in the core. These are problems of academic and practical interest which have been studied both theoretically and experimentally. The conditions can be achieved simultaneously by a particular fuel distribution in certain thermal reactors meeting the following requirements: (1) a single material serves as both moderator and reflector; (2) the fissionable material and the moderator are intimately mixed in the core but not necessarily uniformly distributed in it; (3) moderator atoms are not displaced from the core by the addition of the fissionable isotope; (4) all fissions are produced by thermal neutrons; (5) the extrapola-

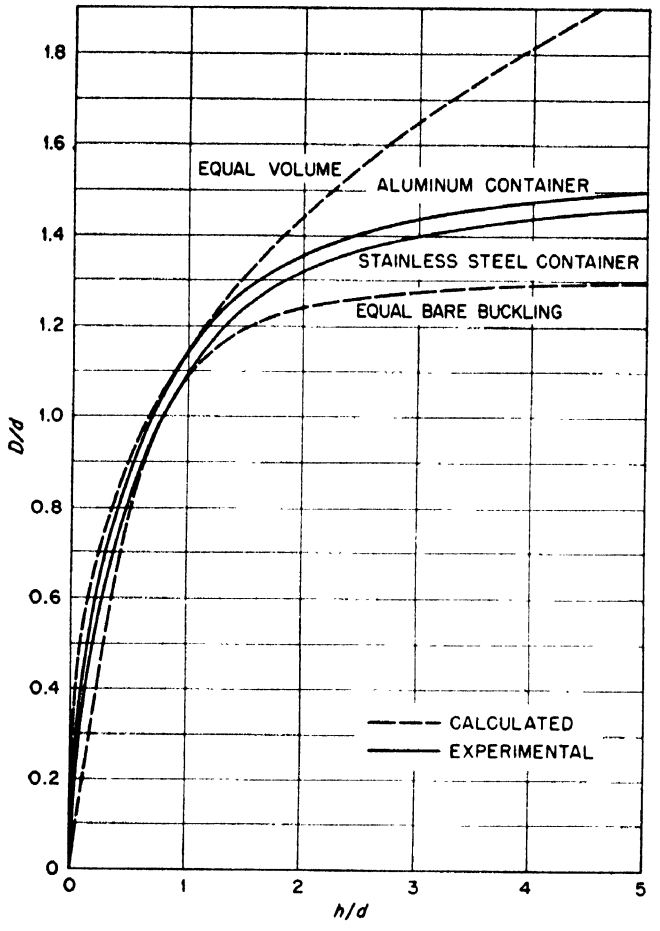

Figure 9. Comparison of geometric transformation methods with experimental data

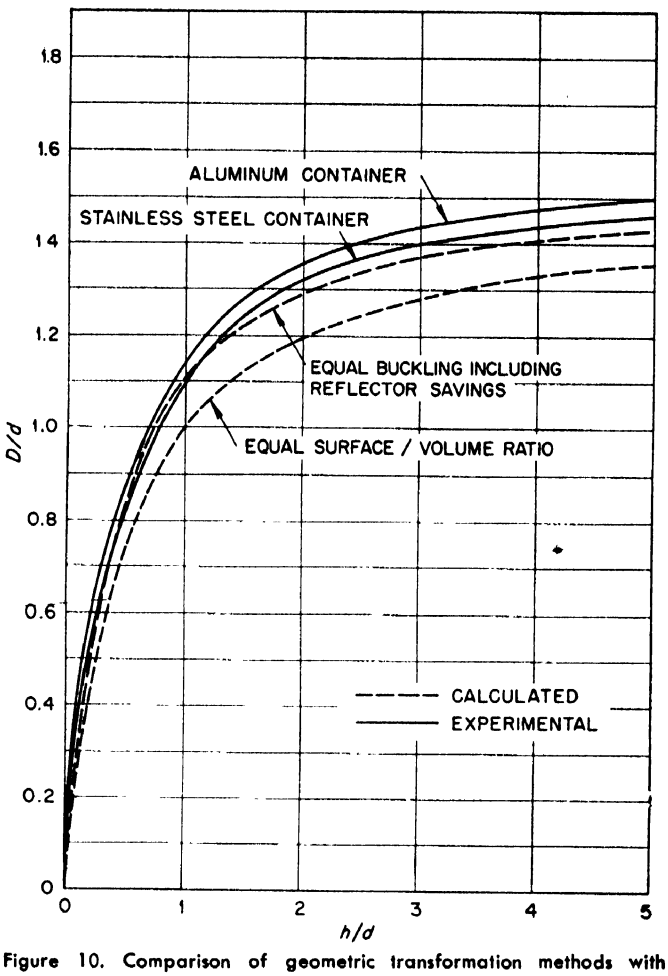

Figure 10. Comparison of geometric transformation methods with experimental data

tion distance is independent of the neutron energy. The desired parameters are calculated by a multigroup, two-region integral-equation method using a fourfold synthetic-slowing-down kernel. The method determines a unique fuel distribution, a unique geometry, and, hence, a unique critical volume and mass.

The relationship between minimum critical mass and uniform thermal neutron core flux was experimentally investigated in a water-moderated, water-reflected, cylindrical reactor. Uranyl fluoride solutions, prepared from uranium containing about 90% of the U^{235} isotope, were chosen as the fuel. To simplify mathematical computations the reactor had an infinite water reflector on its lateral surface and no end reflectors. The length was fixed at 41.6 cm since this was the shortest cylinder for which the corrections introduced into the parameters by the end effects were one order of magnitude less than the values of the parameters themselves. By the multigroup method the corresponding critical radius was 14.8 cm and the fuel concentration was found to vary along the radius in the manner shown by the continuous curve in Fig. 11. Calculated minimum critical mass was 1024 gm U^{235}.

Since the continuous concentration gradient of the theoretical fuel distribution could not be duplicated experimentally, it was approximated, as shown in Fig. 11, by one which changed stepwise over the core. The division of the core into five concentric regions was found to be a good compromise between theoretical and practical considerations. The widths of the steps were chosen to be inversely proportional to the concentration gradient and hence the boundaries of each region were uniquely located. The volume, mass, and average fuel concentration of each region could then be determined directly from the continuous curve in Fig. 11. A correction was made for the aluminum forming the partitions which increased the calculated critical radius to 15.1 cm and mass to 1038 gm U^{235}.

A comparison between theory and experiment was made by filling each of the core regions with solution of the calculated concentration, surrounding the core with a water reflector, and determining the common height of core and reflector at which the system became critical. The pertinent data are summarized in Table III. Measured masses are believed to be correct to within $\pm 0.4\%$.

Table III. Comparison of Calculated and Measured Reactor Parameters

Parameter	*Calculated value*	*Experimental value*
Height of core and reflector	41.6 cm	42.7 cm
Core volume	29.2 l	30.0 l
Mass of U^{235}	1038 gm	1061 gm

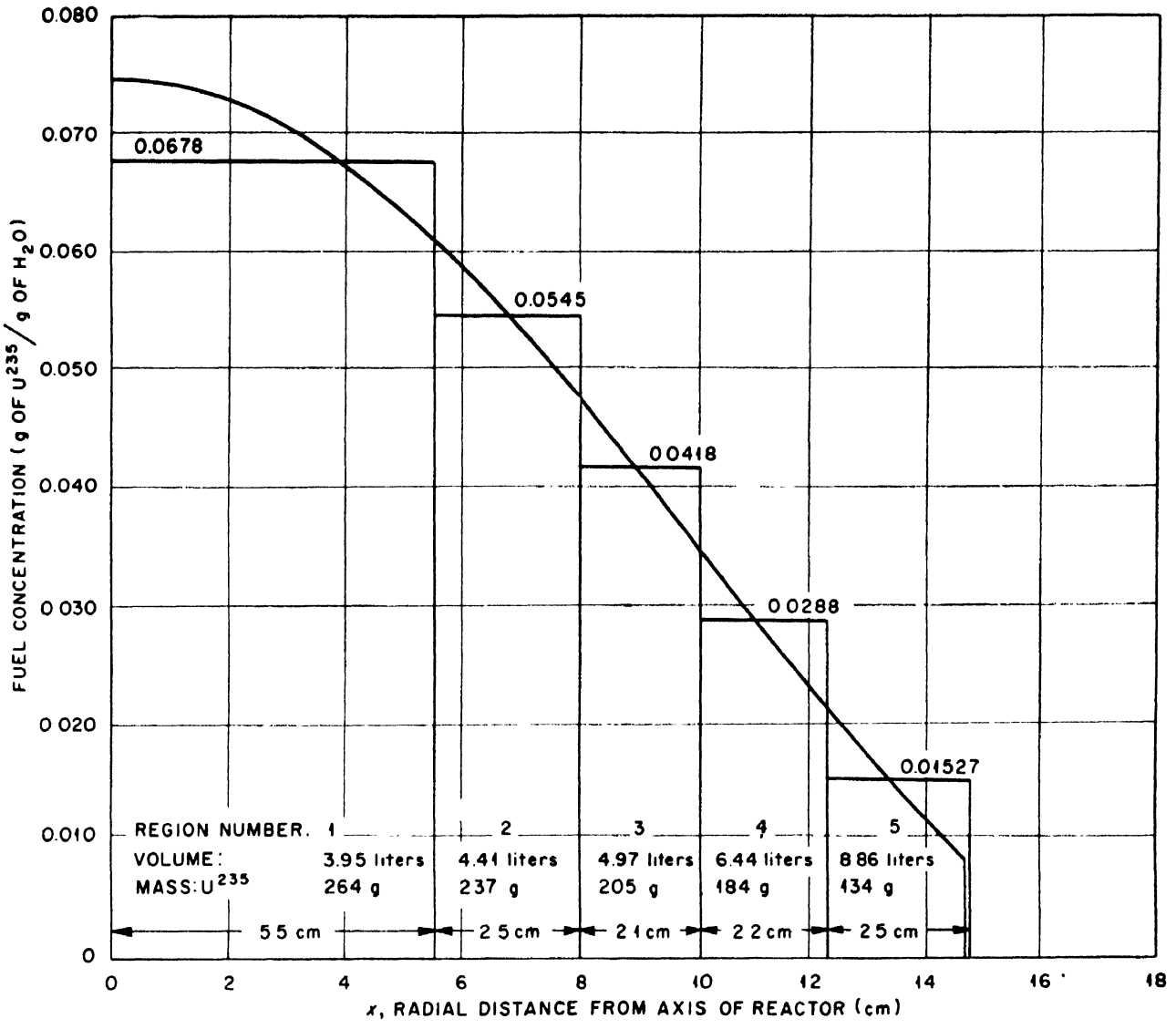

Figure 11. Comparison of fuel loading in the experimental reactor with that of a calculated reactor

Thus the calculated and measured critical masses agree within 2.5%. In order to establish that the agreement was more than fortuitous, the mass of U^{235} in a localized volume in each region was increased separately by the same amount and its effect on the over-all reactivity was determined. The results of these experiments demonstrated that the fuel importance function was uniform to within 5% of its average value. Additional experiments also showed that the importance function was insensitive to small changes in the fuel concentration.

A comparison of the fuel mass of the minimum loading with that of a uniformly loaded reactor is given in Table IV.

Table IV. Comparison of Calculated and Experimental Critical Masses

	Uniform loading U^{235}, *gm*	*Minimum loading* U^{235}, *gm*	*Reduction in Mass* (%)
Calculated values	1192	1038	12.9
Experimental values	1162	1061	8.7

Values obtained for the total, non-thermal, and thermal neutron fluxes along a radius at the midplane of the reactor have been plotted in Fig. 12. Indium detectors, with and without cadmium covers, were used for these measurements. The curves for the total and non-thermal fluxes were drawn through their respective experimental points. The curve for the thermal flux was plotted from differences between the smoothed curves of the non-thermal and total fluxes. The thermal-flux curve was found to be substantially flat in the core, deviations being less than 5% of the average.

In Fig. 13 the experimental thermal neutron flux data are compared with their theoretically predicted values on the basis of two-group neutron diffusion theory. The two-group model was chosen not only for its simplicity but because the division of all neutrons into thermal and non-thermal groups, although artificial, corresponds closely to the natural division inherent in the flux measuring method. Measured values of the thermal flux are believed to be correct to within $\pm 3\%$.

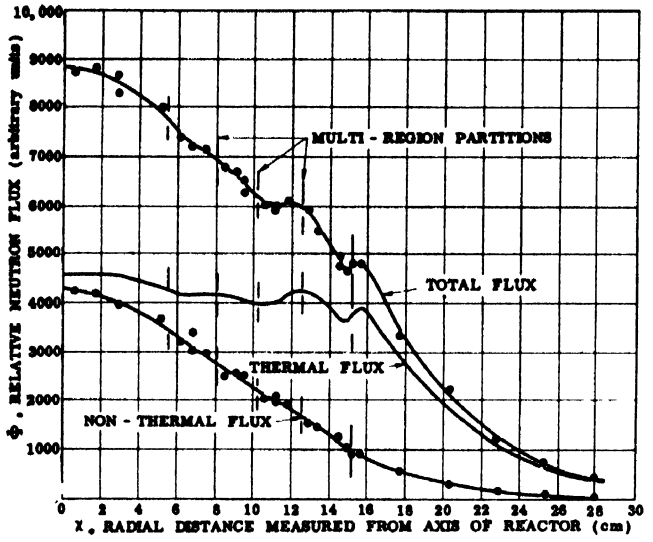

Figure 12. The radial neutron flux in the experimental reactor

It was shown in the experiment that, on the average, 96% of all fissions were caused by neutrons having energies less than about 0.5 ev. The effective water density in the core was approximately 99.4% of theoretical. Use of an infinite lateral reflector and a sufficiently long core obviated the requirement of an energy independent extrapolation distance. Thus the postulated requirements were satisfactorily met. The theoretical and experimental work are therefore in substantial agreement.

A second example of the utility of critical experiments is the evaluation of nuclear properties. Some constants of U^{233} and U^{235} have been compared in experiments with critical aqueous solutions in the same spherical vessels. The spheres were fabricated of aluminum and suspended in the center of reflector tanks containing water. The spheres were 26.4 cm and 32.0 cm in diameter. The thickness of water surrounding the spheres was such as to provide an effectively

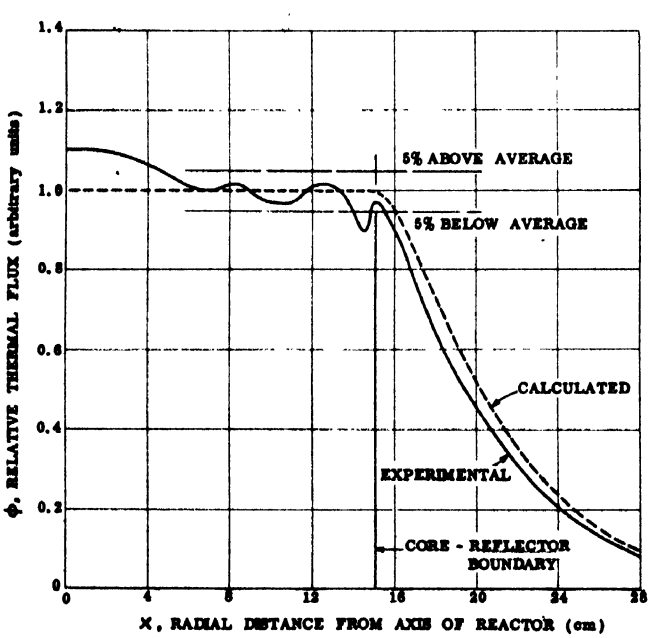

Figure 13. Comparison of theoretical and experimental values of the radial thermal neutron flux

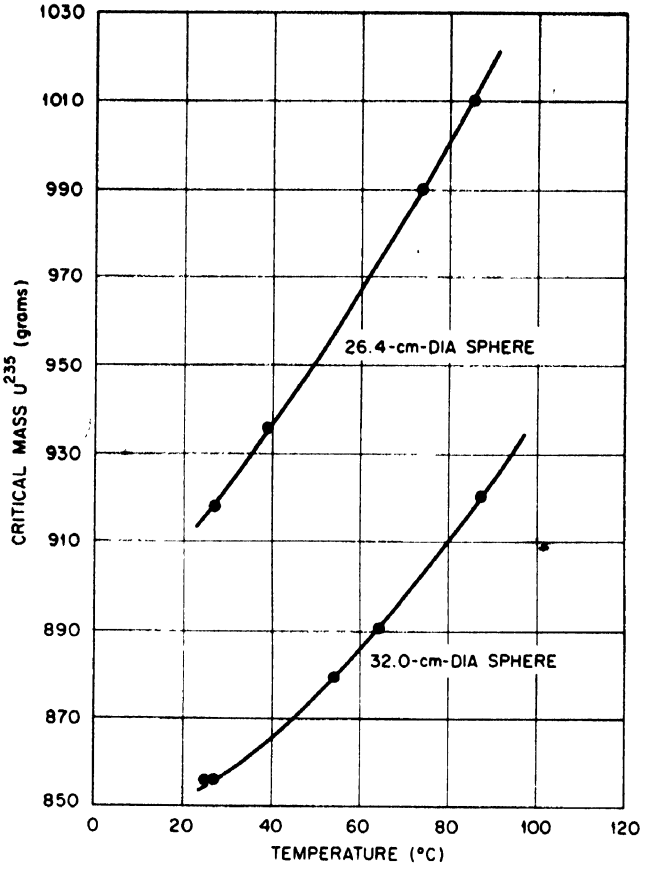

Figure 14. Critical mass of U^{235} in water reflected spherical reactors as a function of temperature

infinite neutron reflector. The observed critical masses of U^{235} and U^{233} over the temperature range 20°C to 100°C are presented in Figs. 14 and 15, respectively. The critical concentrations, measured at 25°C in the smaller sphere were $H:U^{233} = 421.2$ and $H:U^{235} = 269.8$; in the larger sphere the corresponding values were 663.8 and 516.0.

Using the nuclear constants for U^{235} and the assumption that the leakage spectra of the two solutions in the same critical reflected sphere are equal, the fission neutron yield per neutron absorbed, η, may be calculated for U^{233}. The results were obtained directly from the characteristic equation of the two-group model

$$\frac{k}{(1 + L^2B^2)(1 + \tau B^2)} = 1 \qquad (1)$$

In the same critical water reflected sphere the ratio of $\eta(233)/\eta(235)$ is then

$$\frac{\eta(233)}{\eta(235)} = \frac{f(235)[1 + B^2L^2(233)]}{f(233)[1 + B^2L^2(235)]} \qquad (2)$$

where f is the thermal utilization, L is the thermal diffusion length in the solution, and B^2 is the material buckling. The thermal utilizations and diffusion lengths were calculated from the experimentally determined critical concentrations of the two isotopes. The material buckling, B^2, was calculated from the U^{235} concentration and set equal to the geometric buckling for this critical system. The geometric bucklings for the two experiments were the same, thus establishing

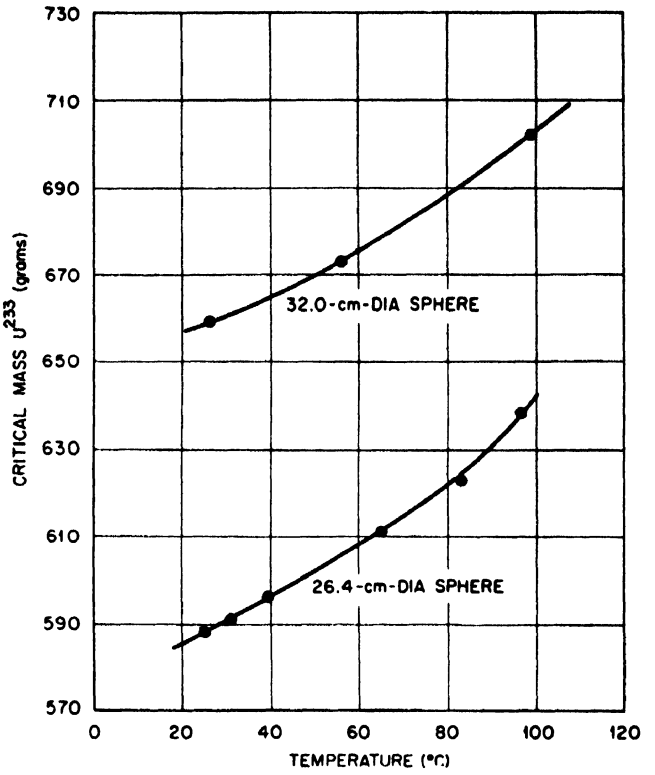

Figure 15. Critical mass of U^{233} in water reflected spherical reactors as a function of temperature

a value for the U^{233} material buckling in Equation 2. The resulting value of η for U^{233} is 2.32 ± 0.03 at 0.026 ev based on η for U^{235} being 2.08 ± 0.02. The associated error is directly attributable to the accuracy of the nuclear constants used in Equation 2.

The reactivity temperature coefficients were determined over the temperature range 25°C to 100°C, using Equation 1, and the data presented in Figs. 14 and 15. The results are compared in Table V for both reactor sizes.

The delayed neutron groups were compared by direct period measurements in the two solutions. A

Table V. Reactivity Temperature Coefficients

Reactor diameter	*Reactivity coefficients*	
	U^{233}	U^{235}
26.4 cm	-8.72×10^{-5}/°C	-1.24×10^{-4}/°C
32.0 cm	-3.54×10^{-5}/°C	-1.16×10^{-4}/°C

boron rod was inserted along the diameter of the sphere and displaced to produce positive periods. Identical displacements were made in the two solutions. The reactivity change is proportional to the measured period and hence to the total delayed neutron yield from the isotope. The total yield of delayed neutrons from U^{235} is about three times the yield from U^{233}. Comparison of the reactivities and the ratio of the delayed groups is given in Table VI for 2.5 cm and 5.0 cm displacements of the boron rod. The reactivity is defined by the expression

$$\rho = \frac{\sum_i \frac{\beta_i}{1 + \lambda_i T}}{\sum_i \beta_i} \tag{3}$$

where β_i is the fraction of delayed neutrons in the ith group; λ_i is the decay constant of the ith group; and T is the measured period in seconds.

Table VI. U^{233}:U^{235} Reactivity Comparison

Rod displacement	U^{233}		U^{235}		$\frac{\rho\ (233)}{\rho\ (235)}$
	T	ρ	T	ρ	
2.54 cm	77 sec	14.4	213.4 sec	4.8	3.08
5.08 cm	26 sec	28.2	106.7 sec	9.3	3.02

Plutonium-Water Critical Assemblies

By C. C. Horton and J. D. McCullen,* UK

The experiments described in this paper were carried out to provide data on which the design of storage vessels for plutonium solution could be based, and to check the validity of theoretical methods of critical size calculations on aqueous solutions of fissile material. Preliminary calculations showed that the variation of critical mass in aqueous solution should exhibit a minimum at a hydrogen to plutonium atomic ratio of about 600; experiments were therefore planned to measure the critical mass as a function of concentration in this region. Three concentrations were chosen, one at the expected minimum, and two at concentrations bracketing this value; the H/Pu^{239} ratios finally achieved were 397, 655 and 892.

In order that the experiment should use a small amount of fissile material, it was decided to use a water-reflected system, and the geometry of a cylinder reflected at the sides only was chosen as the most convenient shape. The solution was obtained in the form of plutonium nitrate dissolved in nitric acid, the free acidity of the solution was kept as low as possible in order to make the hydrogen concentration in the solution as near as possible to that in the reflector. The acidity used in the experiments was in fact 1.7*N*, a value considered necessary to avoid hydrolysis.

APPARATUS

Tank

Because of the health hazard associated with the manipulation of plutonium compounds the whole apparatus was enclosed in a dry-box and remotely controlled (Fig. 1). The reactor tank consisted of a stainless-steel cylinder 30.5 cm in diameter, 61 cm high, with walls 1.59 mm thick. The base of the tank was 6.35 mm thick and was dished so that the solution drained into a small cavity. The lid of the tank was provided with a gasket and all tubes and probes passing through it were fitted with glands; this enabled the solution to be transferred to and from the tank by suction. The solution was added via a 1 mm bore stainless steel tube; this diameter was chosen to give a small hold-up of solution in the tube and also served to restrict the maximum rate of addition to about 40 cm^3/min. The solution was extracted via a 3.2-mm bore tube which reached to the base of the cavity in the base of the tank; the solution could thus be extracted at a much greater rate than it could be added.

The depth of the solution was measured in two ways; a polythene float to which a long calibrated needle was attached, or a calibrated electric probe accurate to about 0.5 mm. Depth measurement was necessary because of the irregular shape of the tank base, and to enable the reflector height to be set to the correct value.

The solution tank was surrounded by a aluminium-sprayed steel tank open at the top and 76.3-cm diameter. Water could be admitted to the tank by a pipe from the main supply, the tank could be emptied quickly by a magnetically operated dump valve. Depth of water was measured by a calibrated gauge glass.

Neutron-Detectors

The neutron density in the system was monitored by six BF_3 proportional chambers 28 cm long by 1-cm diameter filled with BF_3 gas to 40 cm Hg pressure; these were screwed into re-entrant stainless-steel tubes in the base of the system. One chamber filled with natural BF_3 gas was placed in a tube along the axis of the central tank; two filled with natural BF_3 and two filled with enriched BF_3 were placed equally spaced in a ring just outside the solution tank in the reflector, and one enriched chamber was placed in the reflector at a radius of 40.6 cm. This arrangement of chambers was made so that the neutron density could be measured over many decades.

Pulses from the counter were detected and counted in a conventional way; in addition the output of the central counter was fed to a rate-meter, the output of which was connected to a simple trigger circuit which could energize the safety devices. The tank and counting equipment are shown in Figs. 2 and 3.

Safety Controls

In the event of the reactor becoming super-critical unexpectedly, it could be made sub-critical by (1) dropping a cadmium tube inside the core, (2) dropping a cadmium tube which surrounded the core, (3) dumping the water from the reflector.

Solution Handling Equipment

The quantity of solution in the tank was obtained by weighing each addition of solution. The solution was transferred from one vessel to another via a flexible polyvinyl chloride (P.V.C.) tube and the use of a suction pump. This technique was found to be very reliable, and transfers were reproducible to within a few tenths of a cm^3. The solution to be added was transferred to an 800 cm^3 vessel which was then weighed on a balance; a flexible tube connected to the tank was fitted with a stainless-steel "needle" which

* Atomic Energy Research Establishment, Harwell.

could be pushed through the rubber cap of the vessel into a depression at the base. The solution was then transferred to the tank by use of a suction pump, and the vessel reweighed to find the mass of solution added. The pump could be remotely controlled from behind a concrete wall about 1 metre thick for added safety. Hold-up of solution in the transfer pipes was negligible.

THEORY OF THE METHOD

It can be shown on simple one-group diffusion theory that for an unreflected cylinder of fissile material not too far from critical size

$$\frac{W^2}{I} \propto W_c^2 - W^2 \qquad (1)$$

where W is the mass of plutonium in the system; W_c is the critical mass of plutonium in the system; and I is the neutron density at the centre of the system.

One would expect this formulation to be modified for a system with a side reflector, and far from critical; however, in our experience it appears to be adequate over a wide range. As the experiment proceeds, W is increased, and if W^2/I is plotted as a function of W^2, a nearly linear variation is obtained which intersects the W^2 axis at the value of the critical mass.

Several corrections are needed for this formula in our geometry.

Effects of Fissile Counter Length

The flux variation given above applies for a small detector at the centre of the system, in fact, to avoid the difficulties of mechanical movement and the use of very small counters, long counters fixed in the axial direction were used. If we neglect the effect of neutrons incident on that part of the counter which is not submerged in the liquid, then a simple correction to Equation 1 may be deduced. If we assume that the first harmonic of the neutron distribution predominates throughout, then the shape of the axial flux distribution is constant and the total number of neutrons entering the counter is just proportional to the height of solution. Then Equation 1 becomes

$$\frac{W^2}{R} \propto W_c^2 - W^2 \qquad (2)$$

where R is the counting rate in the counter.

Unequal Length of Counter and Liquid Depth

The counter has a fixed length; thus for small depths of solution some of the counter is not immersed, and for large depths the counter will not record the neutron flux over the whole depth of solution. We define a function $\alpha(h) = n/n'$ where n = number of neutrons entering the counter; n' = number of neutrons entering the counter if it were the same length as the liquid depth.

Theoretical estimates showed that $\alpha(h)$ could take values up to about 2 for practical cases; a separate experiment was performed to deduce values of $\alpha(h)$ for use in this experiment. This was done by arranging the counter along the axis of a water tank in which fast neutron sources were placed above and below the liquid, in this way it was hoped to obtain an approxi-

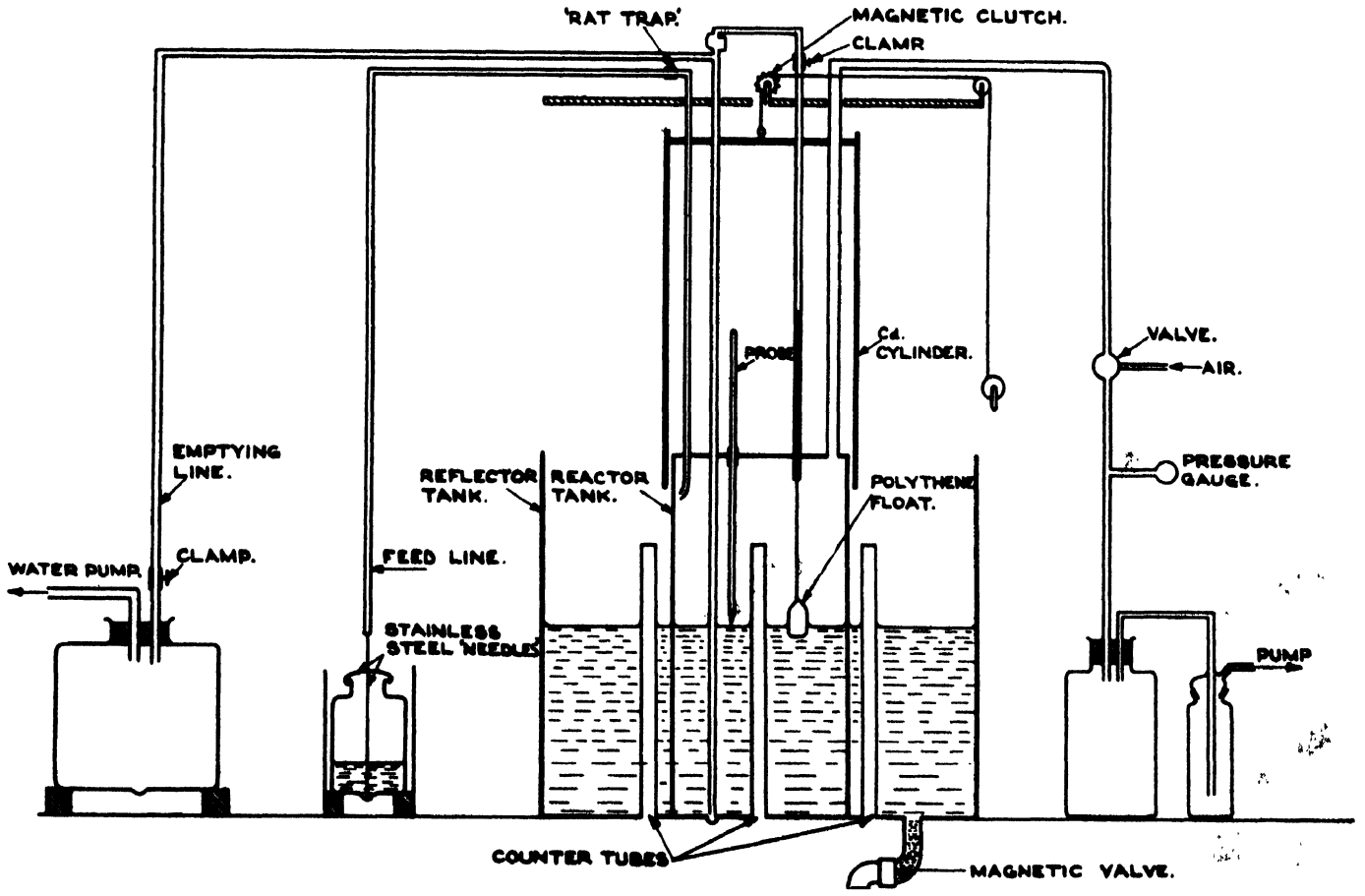

Figure 1. Reactor tank and accessories

mately uniform distribution of thermal neutron sources in the water. Values of counting rate were taken with and without a cadmium sleeve covering that portion of the counter which protruded from the water, and $\alpha(h)$ deduced as a function of liquid depth. We note here that $\alpha(h)$ need not be known with great accuracy; the introduction of this quantity merely reduces the curvature of the approach to critical graph and thus enables extrapolations to the value of W_c to be made with greater safety during the assembly. Theoretical estimates of $\alpha(h)$ were used for liquid depths greater than the counter length; in this region the theory should give reliable results.

Values of $\alpha(h)$ are shown in Fig. 4.

The final curve to be plotted in the approach is thus

$$\frac{W^3\alpha(h)}{R} \propto W_c^2 - W^2 \qquad (3)$$

Selection of Counter Sensitivity

In order to be able to follow the variation of neutron flux in the system from the lowest possible value of W it is necessary to calculate the large neutron-source strength existing in the solution (spontaneous fissions, etc.) and thus provide counters of the necessary sensitivity, or a separate source to give a flux of sufficient intensity. Calculations showed that the major source of neutrons in the solution was from (α,n) reactions between the oxygen present and Puα-particles. These calculations showed that this should provide a sufficiently large source (about 11 neutrons/ml/cm^3 in a 50 mg Pu/litre solution) to make an external source unnecessary, and on this basis the counters referred to above were chosen. Agreement between the predicted and observed fluxes was satisfactory.

TEMPERATURE EFFECTS

When the first assembly had been made, it was clear that sufficient plutonium was available to make a critical assembly at the second concentration, the effective reproduction constant k_E could thus be made as near to unity as we pleased. It was decided to use this facility to attempt to measure the variation in reactivity of the system with temperature; since the neutron flux in the system varies inversely as $(1 - k_E)$ a small change in k_E for $k_E \sim 1$ should produce a large change in the observed neutron flux. The reflector was therefore fitted with a 2 kw immersion heater.

EXPERIMENTAL METHOD

Approach to Critical

The experiments were performed in the following way. In the first run plutonium was added cautiously in batches of 800 ml until it became clear that the approach-to-critical curve was being followed. The procedure was then:

1. The safe quantity of solution to be added was deduced by an inspection of the approach-to-critical

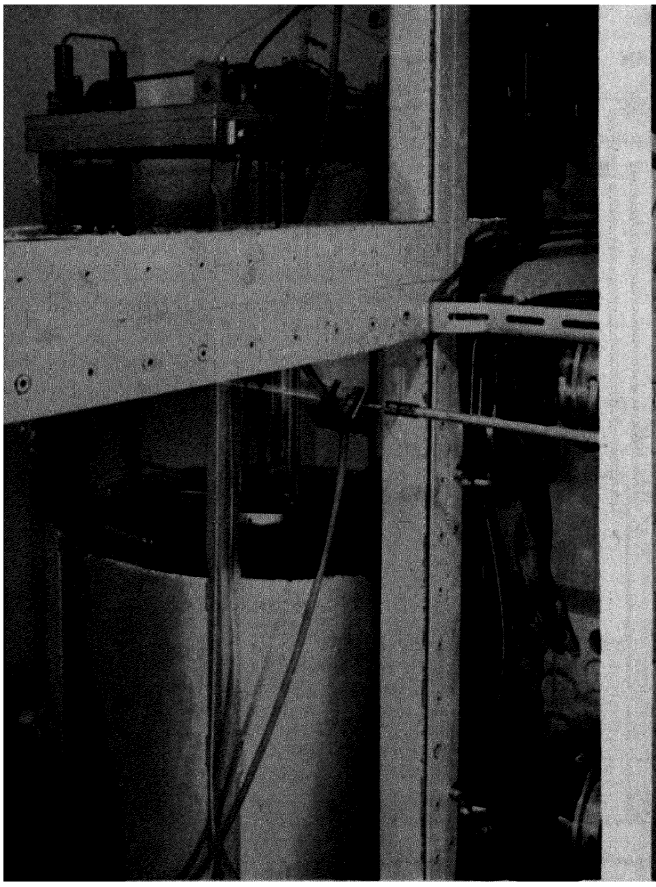

Figure 2. Reactor in position

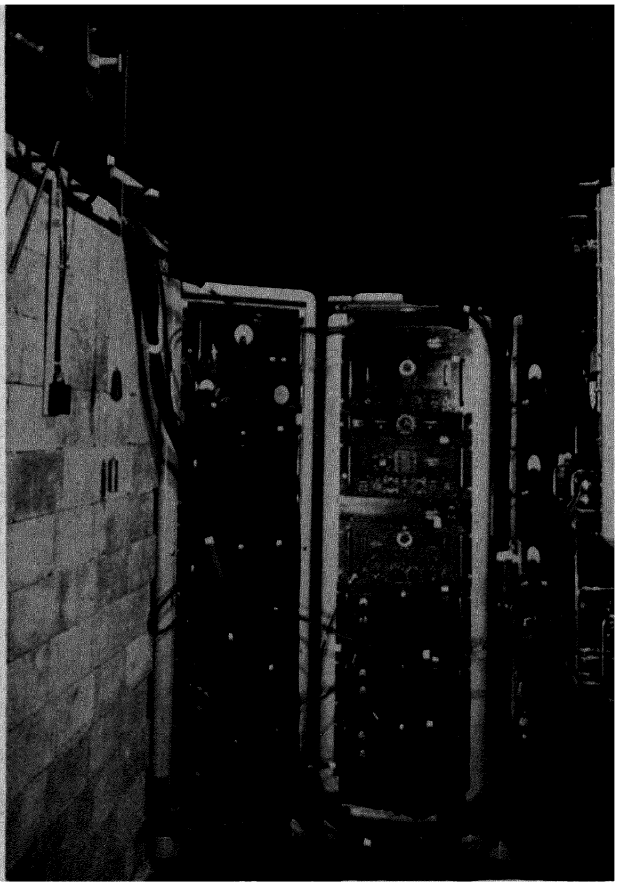

Figure 3. Counting equipment

curve. This was done by taking one-quarter of the difference in predicted critical mass and mass already added, or 800 ml, whichever was the smaller.

2. The amount thus decided was transferred to the transfer vessel from stock and weighed. The weighed bottle was then connected to the tank by the flexible tube, and the reflector height raised to correspond to the expected height of solution after the addition. The safety rod and tube were checked, and the next operation performed from behind the concrete safety-wall.

3. Plutonium was then transferred to the tank, this operation took about 30 min and rough checks of neutron density were made periodically to ensure that it was not rising faster than expected.

4. When all the solution had been added, a short time was allowed to ensure that the system was not diverging, and the depth of solution was then measured. The depth of the water reflector was adjusted if necessary, the neutron density was measured by taking two consecutive readings of the counter. The empty transfer vessel was reweighed and the mass of plutonium added, determined; the value of $W^3\alpha/R$ was computed and plotted, and a fresh estimate of W_c made. At several points measurements were made with the Cd-cylinder between the reflector and solution and also with the reflector removed, these were used to make estimates of the critical masses with fast reflection only, and with no reflection at all.

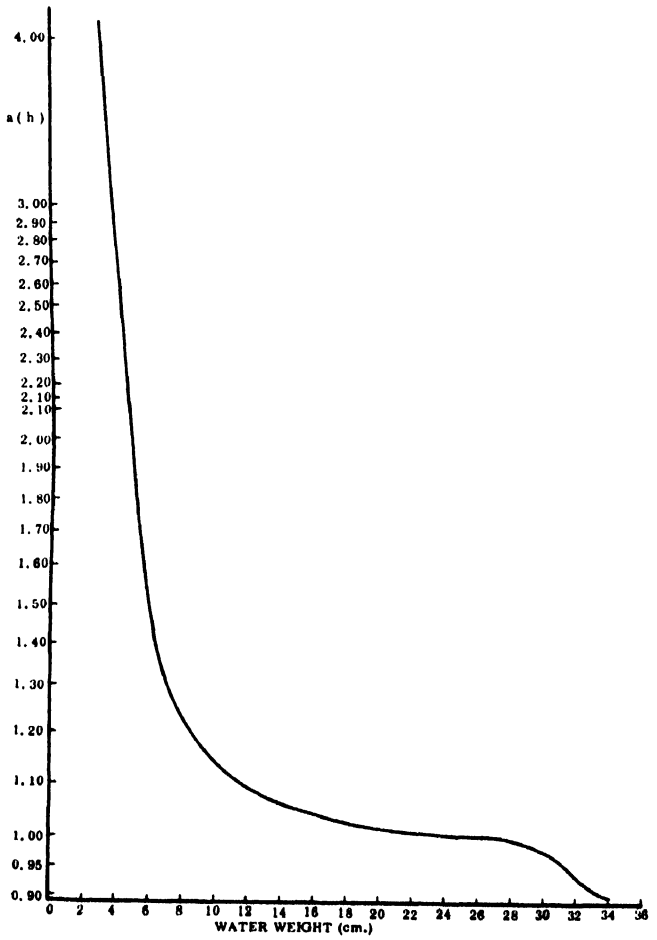

Figure 4. $\alpha(h)$ as a function of (h)

5. The procedure was then repeated for the next addition.

Measurement of Temperature Effect

At two points during the second assembly (multiplications of about 30 and 100), the amount of plutonium in the tank was held constant while the temperature was varied. It was difficult to make an accurate record of the time variation of temperature due to the large thermal capacity of the system, the temperature and the count rate in all counters was thus recorded in a cycle in which the temperature was brought to a maximum and the tank then allowed to cool. The maximum difference in count rate and the maximum temperature difference in the reflector were thus recorded. There was no provision for measuring the temperature of the plutonium solution directly, but theoretical considerations showed that due to the relatively small thermal capacity of the plutonium solution the temperature rise in it should have been the same as that in the reflector to within 10%. The temperature of the reflector was observed with a mercury-in-glass thermometer.

To check the magnitude of temperature effects due to the counters themselves, a separate experiment was performed in which a counter was heated in a beam of thermal neutrons from the Harwell pile. To provide a further check on the effect, a run was made during the progress of the third assembly at the same solution height; in this case the multiplication was very low, and any change in counting rate was therefore due to counter temperature effects.

The change in density with temperature of the plutonium solution used in these experiments was measured separately over the range of temperatures employed.

RESULTS

Critical Mass

The results obtained are set out in Figs. 5, 6 and 7. It was found that the curves obtained with each of the six counters were almost linear for values of $(W/W_c)^2 \gtrsim 0.5$; the accuracy of curve fittings and convergence of the approach curve was such that the critical mass could be deduced to within about 1%. Estimates of the fast-reflected system could be made in solutions I and II, an estimate of the bare system could only be made for solution I. No estimate of the fast-reflected or bare system is possible in solution III.

Table I

Quantity	Solution I	Solution II	Solution III
Concentration (mg Pu/ml)	62.86	38.63	28.55
Observed critical mass in grams Pu for reflected cylinder	1182	920	944
Observed critical mass in grams Pu for fast reflection only	1350	1200	—
Observed critical mass in gm Pu for bare system	1700	2200	
H/Pu atomic ratio	397	655	892

Table II. Estimated Effect on Critical Mass in gm Pu

Disturbance	Solution I	Solution II	Solution III
Counter tube displacement	2	—	—
Absorption in Pu^{240}	60	67	126

Table III

	Run 1	Run 2
Temperature rise (°C)	6 ± 0.6	9 ± 0.9
Observed change in counting rate	1.075 ± 0.01	1.44 ± 0.02
= counting rate at ambient/maximum temperature reached		
Observed change in counting rate due to temperature effect in counters	1.018 ± 0.006	1.027 ± 0.009
Net observed change	1.057 ± 0.01	1.413 ± 0.02

Table IV

		Water parameters	
σ (239)	1113 b	Thermal transport mfp	0.48 cm
σ (240)	1000 b	Fast transport mfp	3.2 cm
σ (N)	1.78 b	(slowing down length)^2	33 cm^2
σ (H)	0.34 b	(diffusion length)^2	7.129 cm^2

The chemical composition of the solution used is given in Table I; with these values, the results observed for critical mass variation can be summarized as follows. Effects due to absorption of neutrons in the counters and impurities were negligible; other effects are summarized in Table II. The plutonium used contained about 3% of Pu^{240} for which the absorption cross section was taken to be 1000 barns.

Temperature Effect

The results obtained on solution II are summarized in Table III.

CONSTANTS ADOPTED

In order to determine values of η, values for the nuclear constants of water, nitrogen, plutonium-239 and plutonium-240 had to be used. The values adopted are given in Table IV. The characteristic lengths quoted for water were adjusted in the core according to the observed hydrogen densities for the three solutions studied.

ANALYSIS OF RESULTS

From the concentration and quoted cross sections, the thermal utilization and characteristic lengths in the core were obtained. The observed values for the critical size and a two-group calculation gave values of K^2 for the three systems, and so k_∞ was deduced. The equation $k_\infty = \eta f$ then gave the values of η.

The results are given in the following Table V:

Table V

Solution	$1/f$	k_∞	η
I	1.165	1.853	2.16
II	1.251	1.728	2.16
III	1.329	1.610	2.14

DISCUSSION OF RESULTS

These values of η are about 10% higher than would be predicted from the published cross sections and ν value for plutonium. Epithermal fissions have been neglected in the calculations, and if due allowance is made for this a reduction of about 5% is obtained. However, there is considerable discrepancy between the experimental and theoretical slowing-down length in water, and if the latter value is used in the analysis, values of about 2.0 are obtained. In view of the existing uncertainties in the cross sections of Pu^{240} and more particularly as these results have been used in safety calculations for chemical plants, it has been considered advisable to retain the higher values of η in further work on these solutions.

As a guide to critical size problems in plutonium solutions, calculations have been made using a two-group theory and a value of η of 2.22.[1] This value is chosen to allow a margin of error in the safe direction. Two types of systems have been considered: the hypothetical case of Pu^{239} suspended in water without change of hydrogen density, and the more realistic one of plutonium nitrate in 5N nitric acid solution.

ANALYSIS OF TEMPERATURE EFFECTS

From the observed ratio of count rate for the subcritical reactor at two temperatures 9° apart, a value was calculated for the corresponding change in reactivity. This was based on the following theory:

Let H_e = extrapolated critical height of solution; h_e = extrapolated height of solution; R_e = extrapolated radius of tank; S = neutron source density; D = diffusion coefficient for thermal neutrons; λ_z = axial extrapolation length; λ_r = radial extrapolation length; C = count rate in centre counter; d = solution density; k_∞ = reproduction constant; L = diffusion

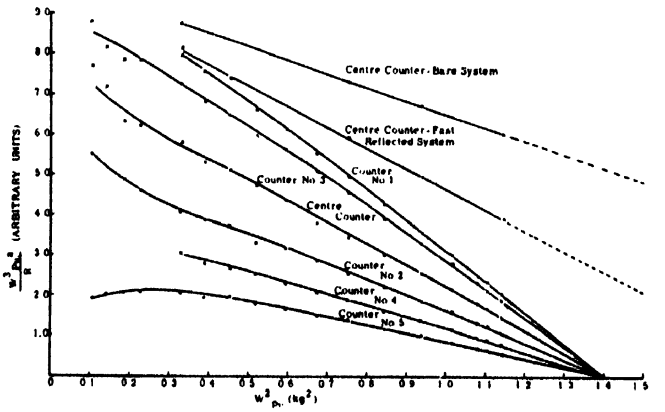

Figure 5. The approach to critical solution I

length in core; and L_s = slowing down length in core. Suffixes 0 and 1 refer to the initial and final temperatures respectively, and Δk_∞ is the change in k_∞ due to this temperature rise. Then

$$\frac{C_0}{h_0} = \frac{S_0}{D_0} H_{0e}^2 \frac{h_{0e}^2}{H_{0e}^2 - h_{0e}^2}$$

$$\frac{C_1}{h_1} = \frac{S_1}{D_1} H_{1e}^2 \frac{h_{1e}^2}{H_{1e}^2 - h_{1e}^2}$$

$$\frac{\pi^2}{H_{0e}^2} + \frac{2.405^2}{R_{0e}^2} = -\frac{1}{2}\left(\frac{1}{L_0^2} + \frac{1}{L_{s0}^2}\right) + \frac{1}{2}\sqrt{\left(\frac{1}{L_0^2} + \frac{1}{L_{s0}^2}\right)^2 + \frac{4(k_\infty - 1)}{L_0^2 L_{s0}^2}}$$

$$\frac{\pi^2}{H_{1e}^2} + \frac{2.405^2}{R_{1e}^2} = -\frac{1}{2}\left(\frac{1}{L_1^2} + \frac{1}{L_{s1}^2}\right) + \frac{1}{2}\sqrt{\left(\frac{1}{L_1^2} + \frac{1}{L_{s1}^2}\right)^2 + \frac{4(k_\infty + \Delta k_\infty - 1)}{L_1^2 L_{s1}^2}}$$

In these equations h_{e0}/H_{e0} is known, $\delta = d_0/d_1$ is known, and R_1/R_0 can be obtained by a knowledge of thermal expansion of the tank. This implies that

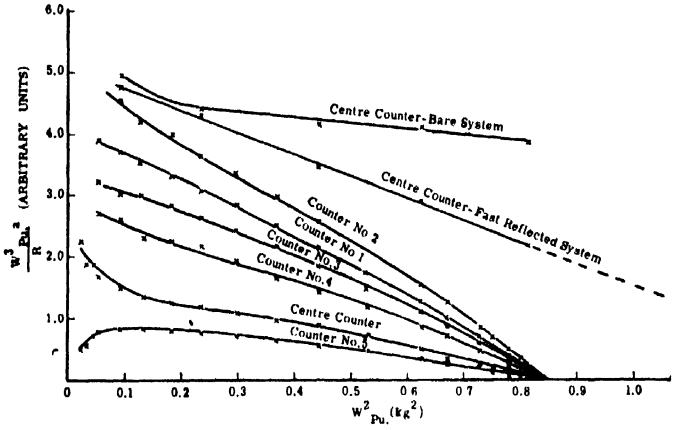

Figure 6. The approach to critical solution II

h_0/h_1 is known. Furthermore $\delta = S_0/S_1 = D_1/D_0$. Knowing the solution density changes in core and reflector it is possible to find L_1^2, L_{s1}^2 and λr_1 and λz_1. From this, it is possible to express $\Delta k_\infty/k_\infty$ in terms of the other parameters and for solution II the following value was obtained:

$$\frac{\Delta k_\infty}{k_\infty} = -0.00846\% \pm 0.003\%/°C.$$

DISCUSSION OF TEMPERATURE EFFECTS

$\Delta k_\infty/k_\infty$ as observed is the sum of the fractional changes in thermal utilization and η. The expected change in f can be deduced from figures given in a companion paper by Egelstaff. Assuming that the neutron spectrum in the core was pure Maxwellian cor-

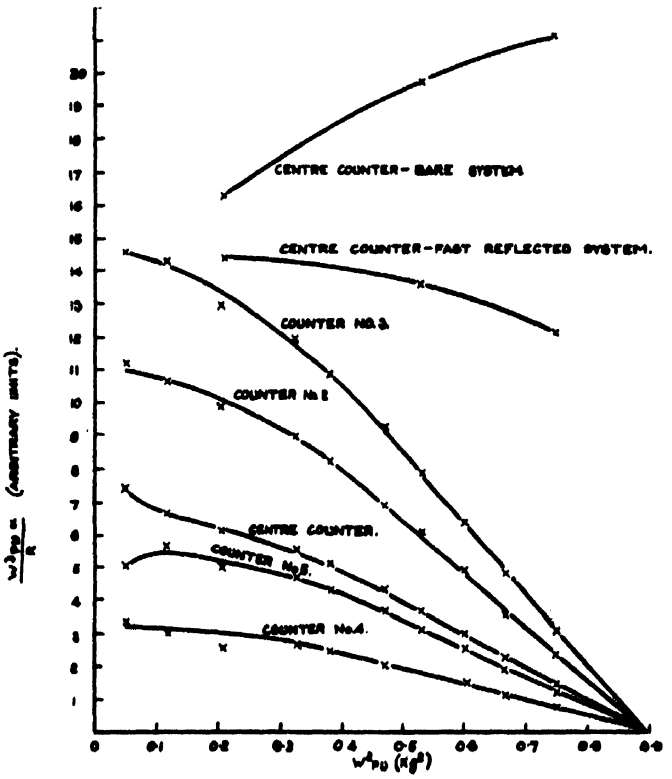

Figure 7. The approach to critical solution III

responding to 20°C, the expected change is

$$\frac{\Delta f}{f} = 0.0197\%/°C$$

This, with the experimental reactivity change, would give for the change in η

$$\frac{\Delta \eta}{\eta} = -0.0282\%/°C$$

This is in disagreement with the experimental values for the cross sections of Pu^{239} as a function of energy.[2] These suggest that η is constant up to 0.5 ev within the experimental uncertainty of about 3½%. As discussed before, the Pu^{240} cross section is an uncertainty, and more so the temperature variation of this cross section. The Pu^{240} concentration is low in these experiments and so its effect is unlikely to explain the discrepancy.

ACKNOWLEDGEMENTS

This account covers the Physics work carried out for these assemblies by V. S. Crocker, J. D. McCullen and C. C. Horton. No attempt has been made to describe the considerable chemical work ably carried out by I. L. Jenkins, B. A. Lister and N. J. Keen in the preparation and use of the solutions.

REFERENCES

1. Fenning, F. W., Horton, C. C. and McCullen, J. D., *A Two Group Analysis of Z.E.T.R. Experiments*, A.E.R.E. R/R 1225 (1953).
2. Egelstaff, P. A., *The Slow Neutron Cross Sections of Pu^{239}*, NRDC52 (1954).

The Critical Assembly—A Nuclear Design Tool

By T. M. Snyder,* USA

A zero-power or critical assembly has been constructed and operated by the Knolls Atomic Power Laboratory since early 1948. This assembly was designed with the objective of permitting study of as many of the nuclear characteristics of a wide variety of reactors as possible. The experience through 1950 was concerned with studies of intermediate neutron energy reactors using highly enriched U^{235}. The object of these studies was to explore the possibility of breeding with plutonium in an intermediate spectrum. For this type of reactor the laboratory chose sodium as a coolant and beryllium as a moderator.

At that time there was very little available knowledge of neutron cross sections; therefore calculations of the neutron energy spectrum, critical masses, power distributions, control properties, etc., were especially difficult and uncertain. The KAPL "preliminary pile assembly" was built to supply answers to these problems.

Its primary purpose was to obtain information used in the early stages of design work. However, improvements in technique have made it possible to use the PPA for accurate check of the nuclear performance of a final reactor design. An additional function of the apparatus has been to determine parameters and properties of materials useful for future power reactors in further development programs.

The desired reactor information in the intermediate power breeder development program primarily concerned the following:

1. Critical mass, composition and dimensions as affected by various design parameters.
2. Effect of reactivity of proposed control and safety mechanisms.
3. Power generation contour determination.

These items are strongly influenced by the following design parameters: (*a*) dilution ratio of moderator and of coolant to fuel; (*b*) disposition of fuel with particular reference to self-absorption; (*c*) thickness of beryllium reflector; (*d*) thickness of natural uranium blanket (blanket arrangement) and (*e*) disposition of coolant channels and manifolds.

The following additional properties of the assembly were needed and studied:

4. Effect on reactivity of iron and sodium in various locations in the reactor, also of possible impurities, and stable fission products.
5. Temperature coefficients.
6. Delayed neutrons and contribution of photoneutrons to the delayed neutron source, related transient effects and control problems.
7. Distribution of plutonium production in the blanket.

The materials used in the experimental studies were adapted to the special features of the intermediate power breeder. The fuel material was fabricated into thinner pieces than had been used in previous assemblies in order to avoid undue self-absorption. Special means had to be developed to include sodium in the assembly.

The work was undertaken in full cooperation and close contact with the theoretical physics and pile technology groups and the problems of an intermediate spectrum reactor were sufficiently different from those of thermal and fast piles that a considerable amount of know-how and understanding had to be developed by these groups. The experimental physics group was set up to tackle the large number of associated experimental problems.

EXPERIMENTAL MEASUREMENT PROGRAM

The information that may be obtained from any reactor assembly consists of the following: criticality conditions, neutron distributions, distribution of various radioactivities, gamma fluxes and transient behaviors.

A series of criticality measurements gives most of the information needed on effectiveness of controls, safety mechanisms, poisoning effects and effects of variation in distribution and inhomogeneity of component materials. The distributions of fissions, neutrons and gamma- and beta-fluxes together give the distribution of heat generation.

One important measurement to which considerable attention was given was the determination of the neutron spectrum. This is a parameter in terms of which all other data can be interpreted. It affects the neutron economy of the assembly chiefly through parasitic capture in the fuel, but also through capture in structure and coolant materials and in fission products. Measurement of the high-energy portion of the spectrum was done using various threshold detectors. However, the most sensitive test of theory is provided by measuring the low-energy end of the spectrum since this represents the product of all of the interactions which must be survived by a neutron. This

* Knolls Atomic Power Laboratory. Including work by H. B. Stewart, H. F. Schulz, F. G. LaViolette, Knolls Atomic Power Laboratory; G. Dessauer, E. I. DuPont de Nemours & Co.; J. F. Coneybear and Associated 1951 Group at ORNL.

portion of the spectrum was studied with sandwich test foils in which the difference between inside and outside induced activity strongly emphasized captures at a single resonance.

Another important measurement that was desired was the conversion ratio, i.e., plutonium produced in the blanket per unit fuel consumed in the core. It was found, however, that a more accurate value of the conversion ratio could be obtained by study of the individual losses: parasitic fuel capture, fission products, structural material and coolant capture. These were measured by reactivity coefficient methods.

LABORATORY AND FACILITIES

The objectives of design were safety, flexibility and precision. The achievement of safety starts with the laboratory building design (Fig. 1). Remote control approach to criticality was the adopted philosophy with provision for low reactivity during any manual operations. In addition, a heavy-shielding wall (5 ft of concrete) was provided between the operating console and the assembly. Other walls of the assembly room were thinner with a labyrinth entrance on one side. A light roof sloping down away from the direction of personnel minimized roof scatter. Sky shine was not serious because of wall light. This arrangement proved satisfactory for operation even at levels of 100 watts. The assembly room could be made gas-tight in the event of a runaway so as to contain any noxious fission products until they had cooled. The provided shielding was adequate to protect operators from any nuclear flash. Fortunately the adequacy of these measures has never been tested although criticality has been reached many thousands of times.

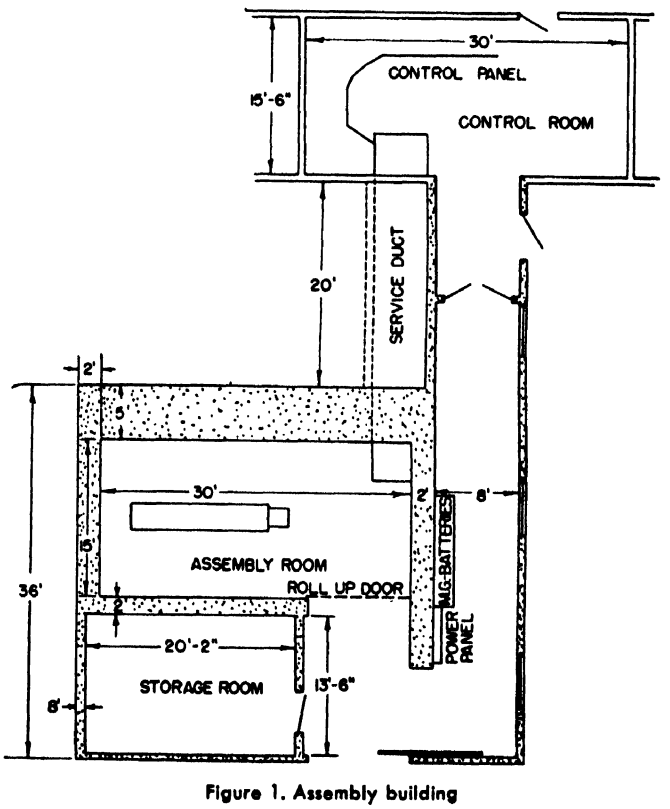

Figure 1. Assembly building

The building *in toto* consisted of: assembly room, fuel storage room, control room, and shop and laboratories.

ASSEMBLY STRUCTURE

The main features which governed the design of the assembly structure were:

1. Provision for low reactivity during manual operation to minimize hazards for personnel. Appreciable multiplication in the reactor only by remote control.
2. Provision of adequate safety and control rods for a variety of assemblies.
3. Flexibility of size and composition of core and reflector.
4. Accessibility of assembly interior for loading and insertion of probe foils.
5. A removable neutron source to provide a signal for safety and monitoring at all times.

Low reactivity during manual operations was achieved by making the assembly in two halves; one stationary, the other mounted on a mobile platform. The two halves are separated during loading and brought together only by remote control. To minimize the reflection of moderated neutrons back into the reactor when personnel enter the space between the halves, a boron loading shield was installed and loading performed through removable plugs in the shield. In the assemblies studied so far this precaution has been found unnecessary.

The reactivity of intermediate reactors is most easily decreased by removal of both fuel and moderator. Four control rods and six safety rods were located in each half of the assembly. These rods were almost identical in composition with the rest of the assembly and distributed over the core. This guarantees that removal of these rods produced about the same change in k as the fraction of the core that they comprise and that when fully inserted they have little or no effect on the assembly.

The achievement of flexibility was obtained by selection of sufficiently small piece size of the assembly materials. This was done by choosing two inches as the diameter of the rods of which the assembly is composed and by making up these rods by strings of discs that were adequately thin. The interstices between the rods posed somewhat of a problem. Experience has shown that these can be corrected for if left empty.

The flexible use of sodium was at first accomplished by use of 0.4 inch thick cans filled with sodium and sealed off, and in some cases the interstitial spaces in the tube sheet assembly were filled and sealed off. Again, experience has shown that this is unnecessary. In such mock-ups, the sodium can be replaced by suitable amounts of aluminum or magnesium where the equivalent amount is established by reactivity coefficient test.

The form of the reactor assembly (Fig. 2) was chosen to be a right hexagonal prism resting on a side parallel to its axis. It consisted of a hexagonal core within a hexagonal reflector and breeding blanket. The reactor is separated into stationary and mobile

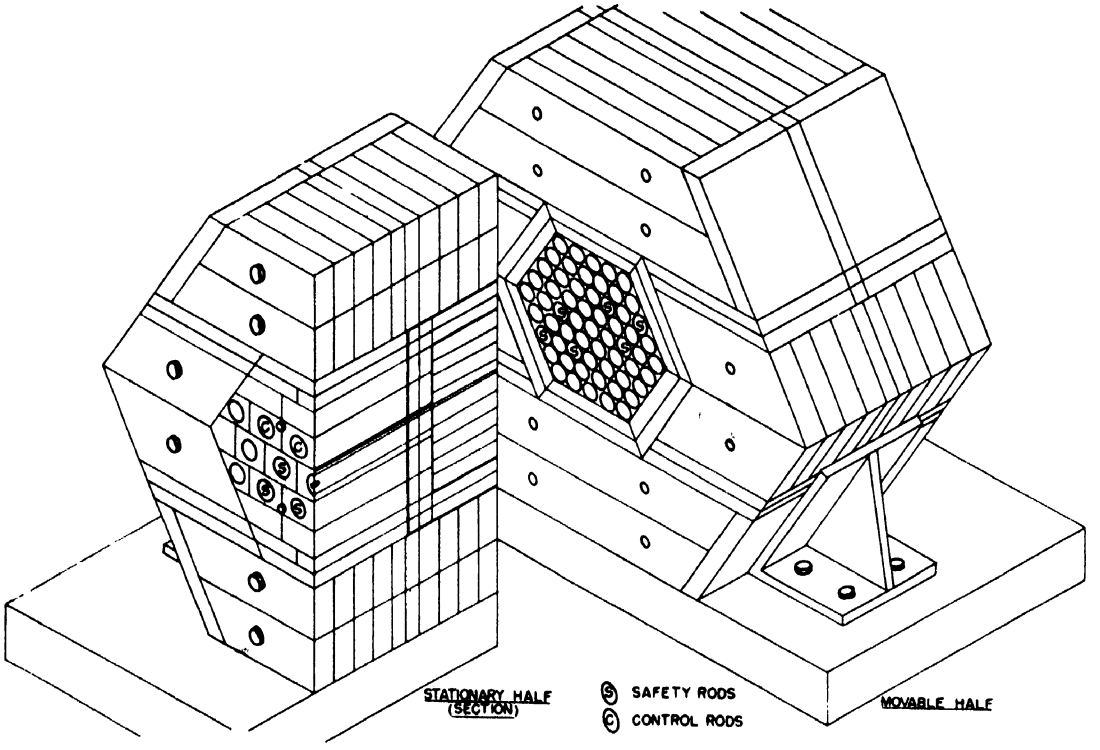

Figure 2. Core and reflector assembly

halves by a vertical plane perpendicular to the axis of the structure. The two halves when separated expose a core face in each half to permit loading. The safety and control rods passed through holes in the ends of the reflector and blanket. Figure 3 illustrates the separation feature.

A basic core structure of two similar halves forms a mechanical skeleton for other materials to be placed in the core. Each half of the core consists of an array of close-packed thin-walled tubes (Fig. 4). Both low carbon steel and aluminum have been used as materials of construction for the tubes and leaders and sides when the latter were employed. Initially three core sizes were constructed with an across flats diameter equal to the length: 40, 50 and 60 centimeters. Since that time a variety of larger sizes have been employed.

By inserting rods into the tubes, the basic core structure is filled to form the completed core. The numbers of rods required in the three examples given are 122, 182 and 254, respectively. The core rods are assembled from discs of the various component materials (see Figs. 5 and 6). Slightly smaller diameter discs also shown are used in loading the control and safety rods. Uranium discs 0.020-inch thick and beryllium discs of 0.100 inch, 0.400 inch and 0.800 inch provided a satisfactory number of combinations to mock the variety of situations desired.

The discs have holes in the center and are assembled in a V-block and bolted together by a threaded axial dural rod using special threaded beryllium end pieces so as not to distort the assembly composition at the mid-plane or end-reflector boundaries.

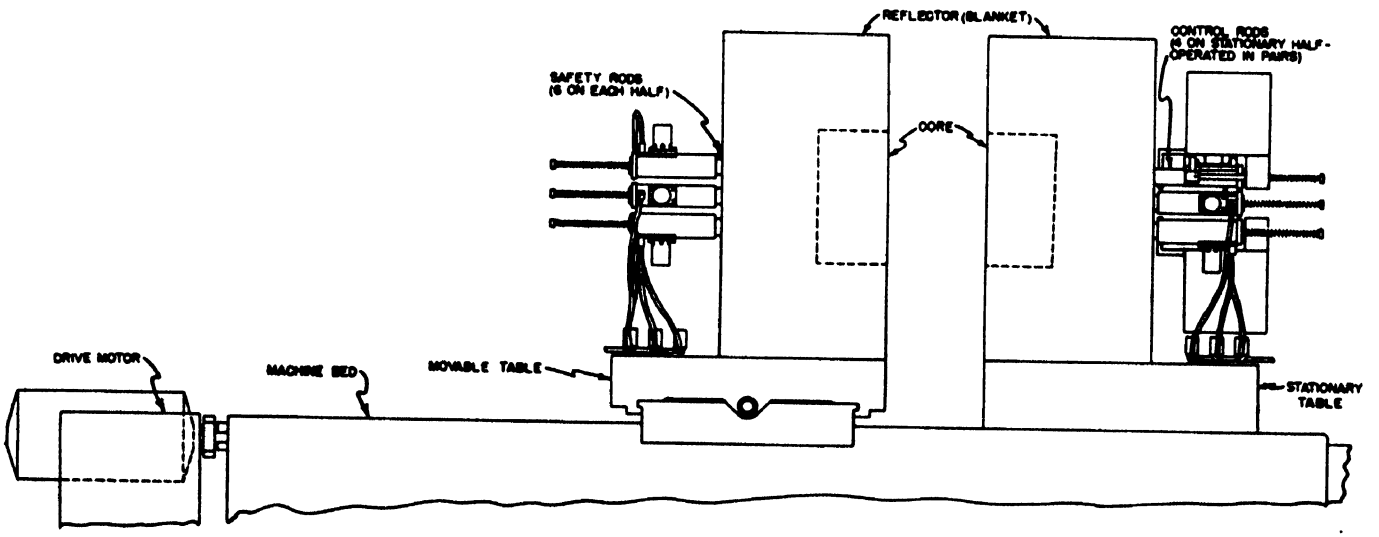

Figure 3. General assembly—PPA

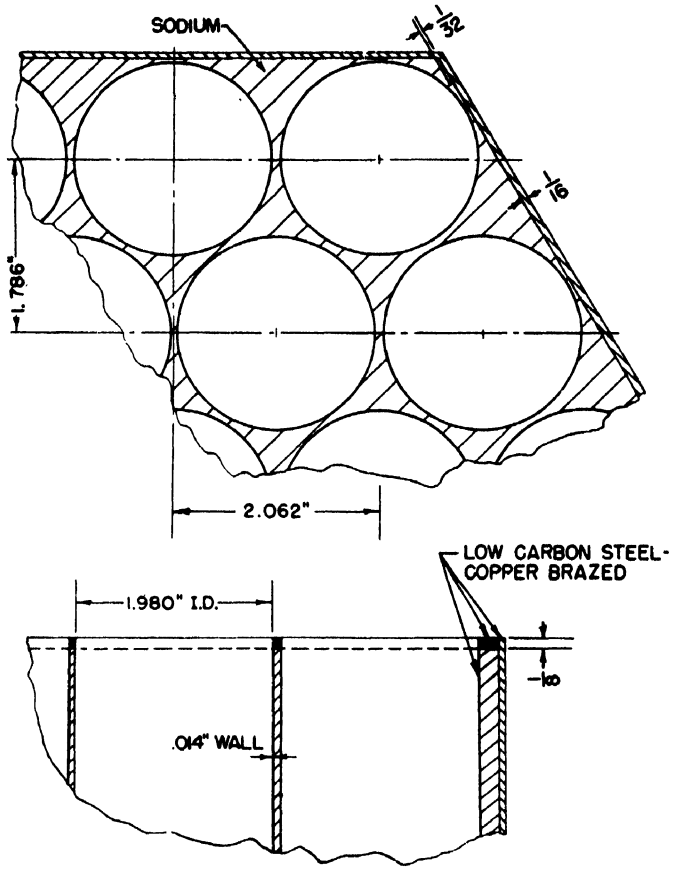

Figure 4. Critical experiment (core sections)

In many of the studies done with the first assemblies, the reflector and blanket were composed of blocks to reduce machining. However, experience showed that flexibility called for loading the reflector as rods into tubes and ultimately the blanket as well.

CONTROL

General Description of Mechanism

The two halves of the assembly were mounted on the bed and table of a horizontal boring machine (Fig. 3). To minimize friction, the machine was fitted with a forced oil pressure lubricating system to provide hydraulic film support on the ways and these were made of hardened steel. The lead screw of the machine was made twice standard size to minimize springiness. This is important because the table is designed for 25 tons, yet any binding or chatter could cause large errors in reactivity measurement and any sudden break-loose could be hazardous.

To eliminate the effects of backlash in gears and threads of lead screw, a separate screw was installed in the table for measurement purposes. It carries no load and any axial slip of the table with respect to this screw is mechanically added to rotation in determining table travel.

The safety rods are pneumatically operated against springs. Release of operating air trips safety rods and they are driven out by springs in 0.1 to 0.2 seconds.

The control rods are operated by a lead screw and dc motor drive.

Assembly Drive (Fig. 7)

Amplidyne powered two-horsepower motor assembly drive permits bed motion between 6 and 0.3 inches per minute. The bed separation may be readily adjusted for any value up to 5 feet. The table position is transmitted to the control room where it may be read to 0.001 inch. As the two halves approach, two automatic slow-downs occur to provide against the increasing sensitivity of reactivity at small separations and to avoid any accidental possibility of passing criticality at high speed. If at any time the circuits to sense excess flux level or excess rate of change of level are actuated, the halves run apart at maximum speed regardless of operations in the control room.

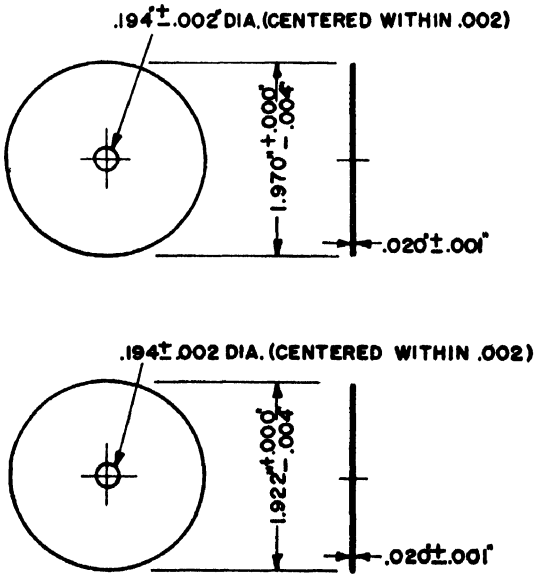

Figure 5. Uranium discs

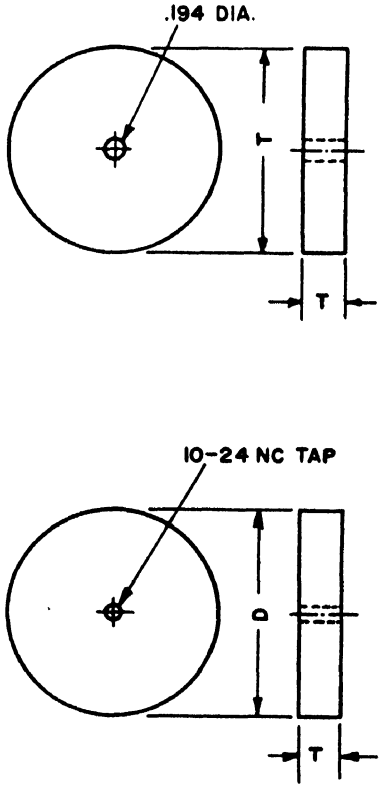

D	T
1.970	.100
	.400
	.800
1.922	.100
	.400
	.800

D	T
1.970	400
1.922	.400

Figure 6. Beryllium discs

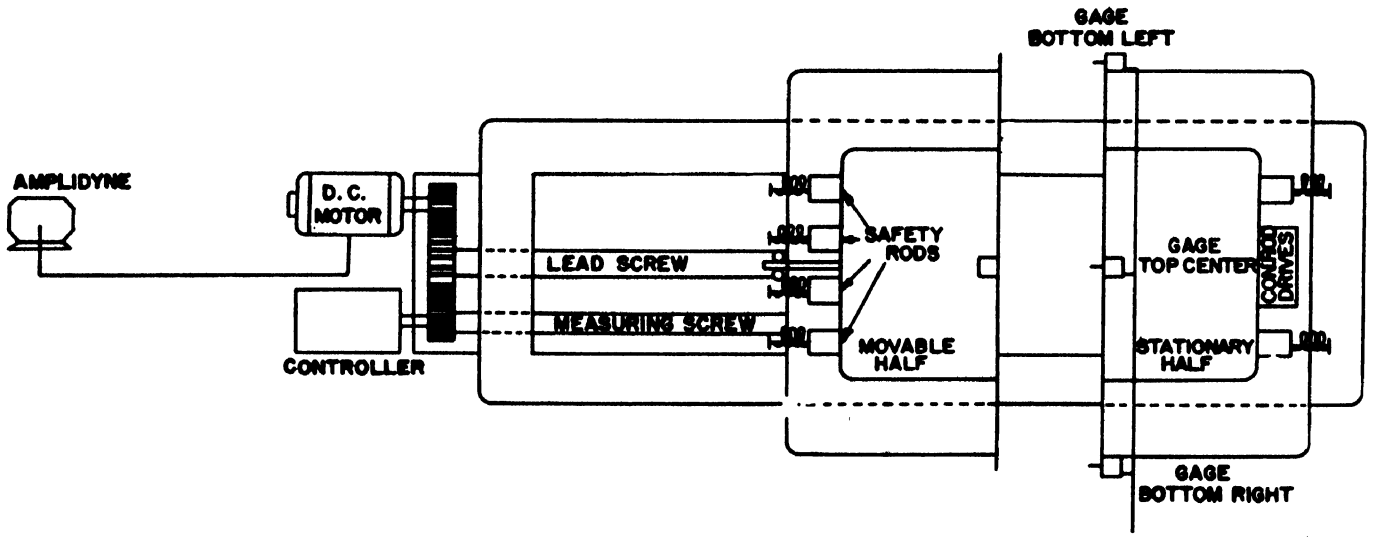

Figure 7. Schematic assembly control

Interlocks provide that the assembly will remain apart and cannot be run together except by insertion of a key. Furthermore, except for running part of the assembly (on battery power if necessary) no action will take place unless: (*a*) ac power is available; (*b*) the safety rods are cocked; (*c*) the control rods are at the position of minimum reactivity; and (*d*) all trip circuits have been reset.

When the two halves are run together reproducibility is achieved by finally pressing them together with a definite force, and the final position is checked at three points by 0.001-inch remote selsyn indication.

Safety Rods (Fig. 8)

The springs in the rods provide 5 g removal acceleration and the rods are stopped by dash pots. Solenoid valves release insertion air pressure with loss of current. Safety rod "in" or "out" position is indicated at the control console.

Control Rods

The control rods are driven in pairs by amplidyne powered dc motors. The control provides automatic rod follow-up of any position set by the operator to 0.001 inch. Continuous indication by multiple selsyns is provided at the console. Rod speed is limited for reasons of safety.

Safety Features

Scram buttons which bring the reactor to the least reactive position rapidly—safety rods are ejected, control rods run out and halves separated—are provided in various locations including the control and assembly rooms.

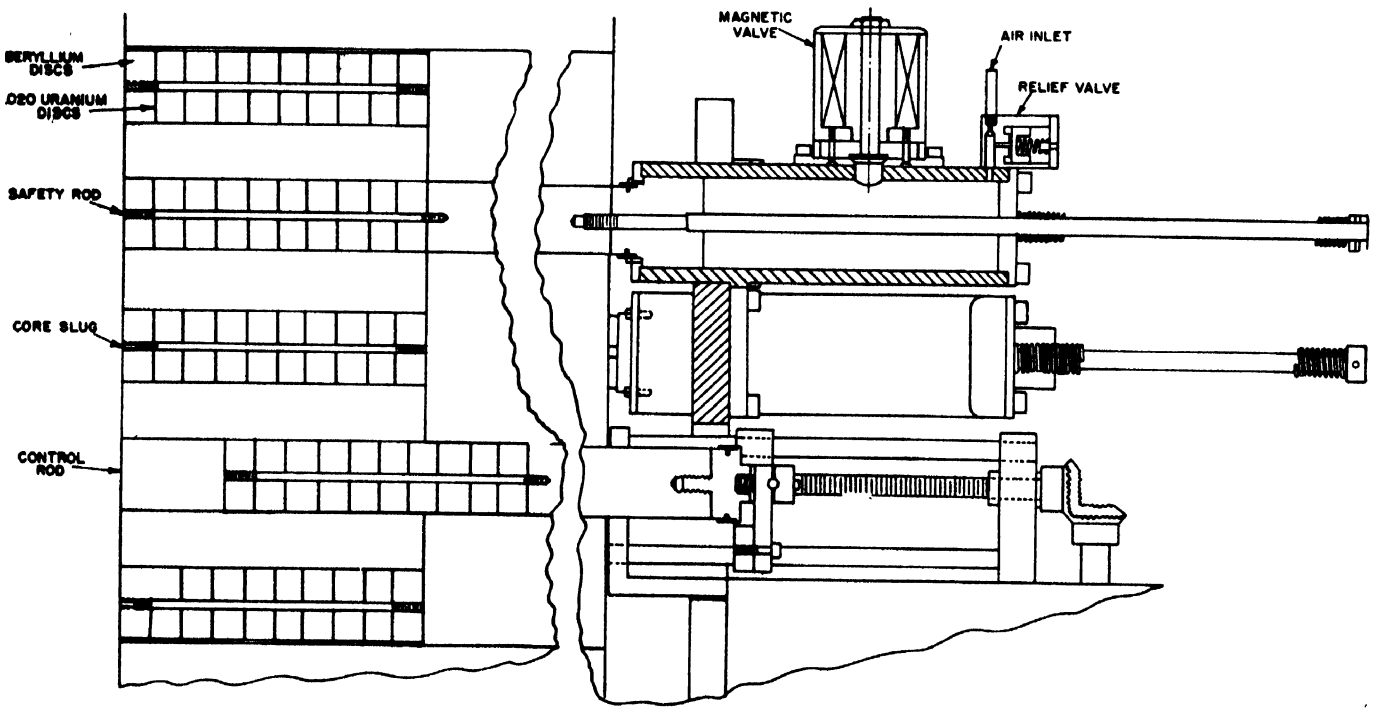

Figure 8. Safety rod, control rod, a core slug assembly

INSTRUMENTATION

Multiplication Measurements

During preliminary assembly of a reactor it is important to measure its multiplication constant as accurately as possible after each addition of fuel. Neutron detectors are used for this purpose.

To follow the multiplication rapidly over a wide range—from counting rate with source along to criticality—high counting-rate systems are required. Ion chambers filled with BF_3 and surrounded with paraffin provide the desired efficiency at low fluxes, and do not saturate readily at high fluxes. One such chamber design is shown in Fig. 9. It has cylindrical electrodes, the center electrode and four inches around the outer electrode are filled with paraffin. Enriched BF_3 is used at one atmosphere. A block diagram of associated electronic gear is shown in Fig. 10. The counting rate loss is a few per cent at 10^5 per second.

Linear and logarithmic recording of rates are provided. Speakers in the assembly and control rooms provide audible indication of counting rate.

Safety Circuits and Monitors

The safety circuits must measure intensity in 0.1 seconds to be as fast as the safety mechanisms. To permit this at low multiplication constants, a large source $\sim 10^7$ neutrons/second at the core center and a very high chamber sensitivity where current rather than individual pulses is measured are used.

A number of independent safety circuits are available:

1. A linear response based on rate of rise.
2. A linear response based on slightly exceeding the operating level.
3. A linear response based on some upper pre-set maximum level.

The second device is an arrangement for trip at or slightly above full scale reading of the output meter at the console. Thus by switching amplifier sensitivity to maintain a useful scale reading the trip point is kept reasonably close to the operating point.

The amplifiers have low drift and sufficient feedback to provide rapid response with input resistors as large as 10 inch ohms.

Loss of power automatically trips all circuits.

HANDLING OF FUEL

Storage

The quantity of highly enriched fuel used in these assemblies has occasionally been quite large, e.g., 130 kilograms. Aside from proper protection from the obvious fire and theft, adequate storage must provide protection from oxidation and inadvertent nuclear catastrophe. The first is achieved by working in a well dehumidified atmosphere.

Nuclear accident risk is minimized by storing the material in a vault on shelves in special "space preserving baskets" which permit a storage density of only 500 grams per cubic foot in a tier of shelves.

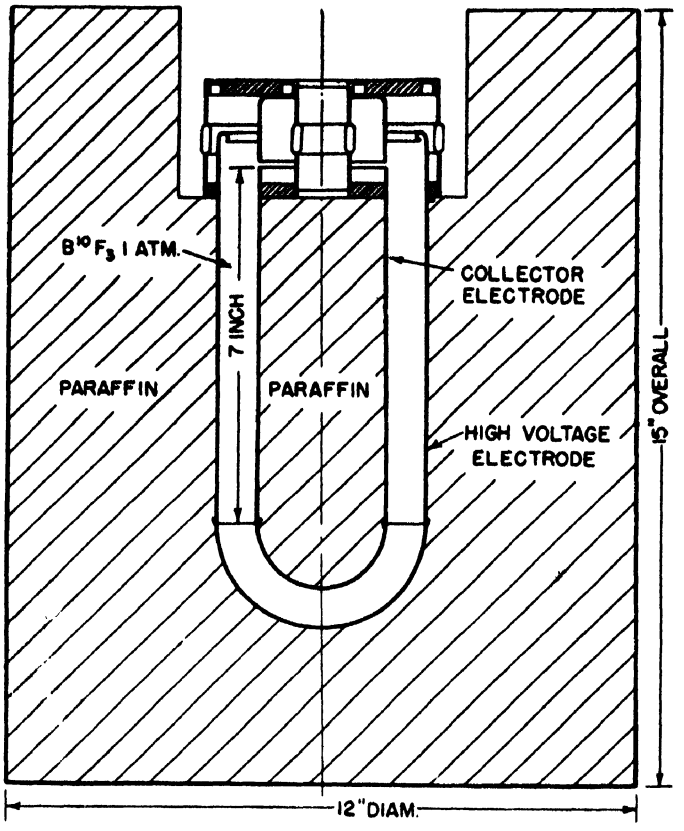

Figure 9. BF_3 Ionization chamber

These baskets are also used to store assembled fuel rods. Rods are assembled on tables in the vault and rules limit the material in use on one of these tables at any one time.

Approach to Criticality

To exclude the possibility of nuclear accident in the assembly room, the following are among the rules adopted:

1. Any assembly is studied beforehand for expected behavior and the loading procedure planned with appropriate check points.
2. The source counting rates are taken and firing level of trips checked.
3. Reciprocal multiplications are used to predict criticality as loading proceeds.
4. The safety and control rods are loaded early to be effective.
5. Whenever criticality is near, loading steps are reduced to or below the value of the control rods so that criticality can only be achieved with these rods.

Interlocks provide that the order of assembly be the following;

1. Source must be in.
2. Operators must return key to control room.
3. Safeties must be cocked one at a time.
4. With control rods out (least reactive) assembly is run full together.
5. Control rods are inserted one at a time.

THE ORNL CRITICAL ASSEMBLY FACILITY

At Oak Ridge National Laboratory a facility rather similar to the one at KAPL has been set up. For the sake of brevity the ORNL facility will be described in

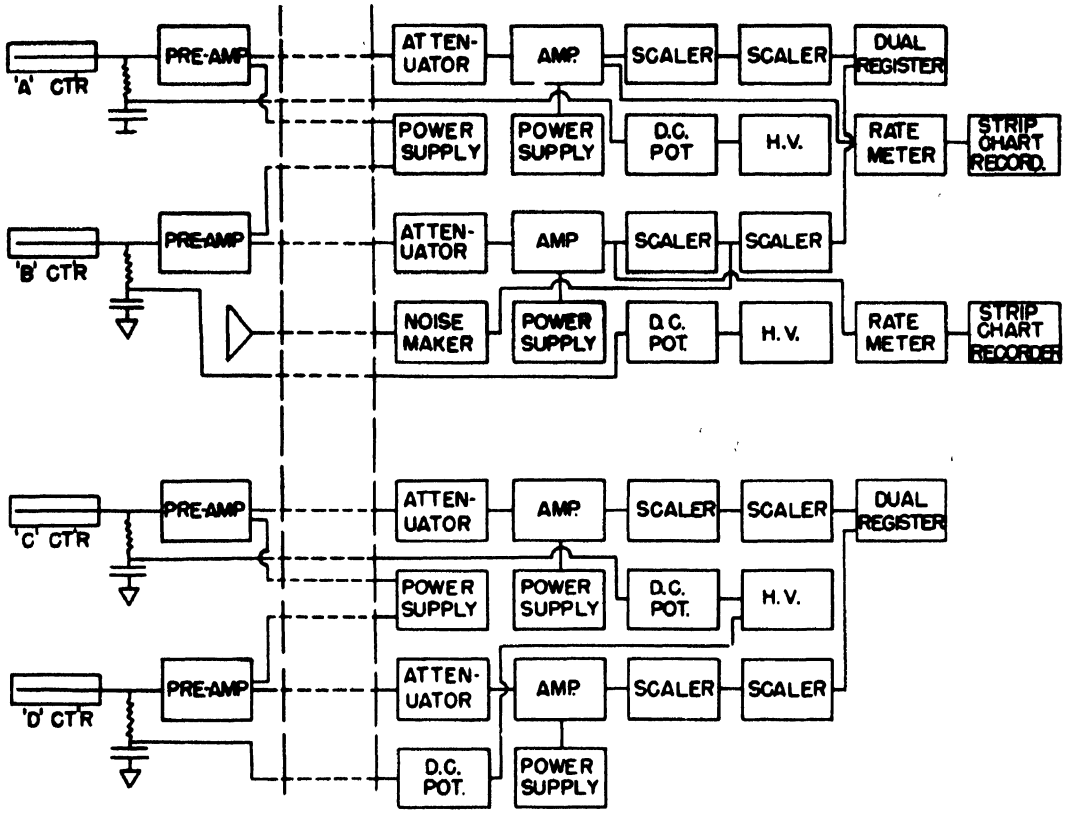

Figure 10. Counter circuits

terms of its differences from the one at KAPL. An overhead view of this assembly is shown in Fig. 11. One difference is in the "honeycomb" structure which holds the assembly components. The "cells" of the "honeycomb" at ORNL are square instead of round like those at KAPL, and consequently the component materials are fabricated into square 3-in. × 3-in. plates rather than into 2-in. circular discs.

At ORNL, the safety rods are air cocked but magnetically held. The movable table rides on V-notch wheels with those on one side track positioning instead of on forced oil floated ways. These changes result in a simpler design.

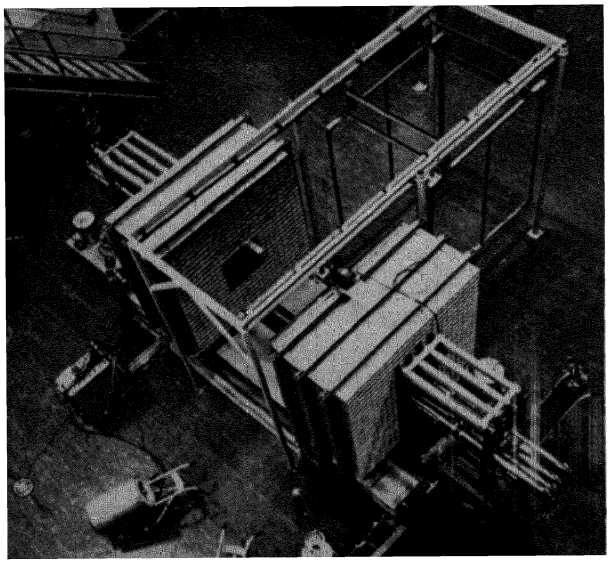

Figure 11. Oak Ridge critical assembly

TECHNIQUES AND SAMPLE RESULTS

So far the equipment and its objectives have been discussed. The remainder of the report will discuss some of the measurements that were carried out and the techniques used.

The most carefully studied assemblies were SAPL-IV and SAPL-V. They are described in Table I.

The first thing that must be done with a critical assembly to make accurate measurements is to obtain accurate calibration of control rods. The value of safety rods individually and in groups was obtained

Table I. Composition of SAPL-IV and SAPL-V

	SAPL-IV	*SAPL-V*
	Core	
U^{235}	47.54 kg	58.1 kg
Excess k	0.29 cents	0.26 cents
Be	82.73 kg	72.55 kg
Na	19.15 kg	24.2 kg
Fe	19.59 kg	18.15 kg
Al	1.9 kg	1.7 kg
Volume	85.05 liters	85.13 liters
	Reflector	
Be	143.45 kg	143.14 kg
Na	0.416 kg	—
Fe	23.5 kg	23.5 kg
Al	3.3 kg	3.3 kg
Volume	100 liters	99.9 liters
	Blanket	

A 12-inch natural uranium blanket surrounded both reflectors

by following the flux level when they are ejected rapidly. If Δk_0 is the reactivity difference between critical and prompt critical, then a rapid change in $k(\Delta k)_{rod}$ produces a change in prompt multiplication of the delayed neutron source. The counting rates at critical and after the rod ejection have the ratio

$$1 + \frac{(\Delta k)_{rod}}{\Delta k_0} \qquad (1)$$

Δk_0 is given the value of 100 cents for convenience in measurement of reactivity changes.

This measurement required very rapid rod ejection to separate the effects of prompt and delayed neutrons, and high counting rates to follow the flux with precision through the drop. A typical result is shown in Fig. 12. It was found that the effect of the various rods was linearly additive over a range of \$4.00.

To calibrate the control rods, the significance of reciprocal multiplication was calibrated in cents using the calibrated safety rods. The change in $1/M$ caused by removal or insertion of a safety rod is directly proportional to its Δk value. This proportionality was accurately verified over the same \$4.00 range.

Finally, the $\Delta(1/M)$ value of the control rods is measured over their lengths of travel and this is converted to dollars or cents by the preceding calibration.

To use an accurately calibrated set of rods, the assembly must have a high degree of reproducibility—i.e., when a change to be measured is made, it must stand out above spurious changes in geometry, etc. Because of the precision of design and manufacture, it was found that a reproducibility of 0.1 cents was easily obtained and 0.01 cents could be obtained with great care. Hence with care, total changes of one cent could be measured accurately.

Since SAPL-IV was not an exact mock-up of the reactor of interest, it was desired to extrapolate to determine the reactivity of the true reactor. This was done by measuring the reactivity value in cents per

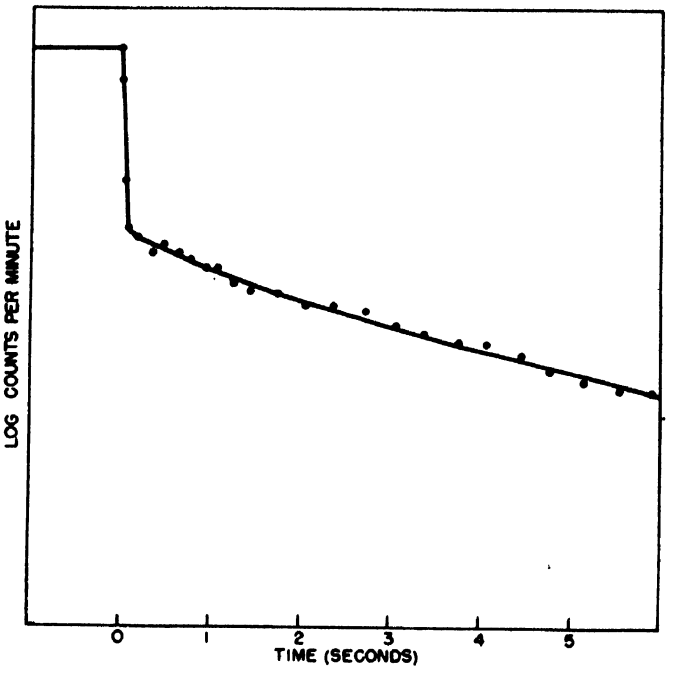

Figure 12. Rod drop

mole of reactor materials averaged over the SAPL-IV core and reflector. The reactor core volumes were not quite correct so that a transformation had to be made in which linear dimensions times density = constant. The transformed reactor had the same size as SAPL-IV. Table II illustrates the extrapolation. The result is that the contemplated reactor was 465 cents over critical.

The distribution of fission heat source was determined from the fission product, gamma activity induced in fuel discs. The fission rate corresponding to a given activity was calibrated in a known thermal flux. The resulting contour for SAPL-V is shown in Fig. 13 on the following page.

The fraction above the 0.5 ev cadmium cut-off is an index of low energy spectrum and xenon poisoning. A

Table II. Calculation of Reactivity from SAPL-IV

	Reactor	*Transformed reactor*	*SAPL-IV*	*Transformed reactor − SAPL-IV*	*Cents/mol*	*Cents*
Core						
U (mol U^{235})	224 mols	228	202	+26 mols	13.15	+342
Be	8730	8850	9060	−210	0.48	−101
Na	1375	1395	840	+555	0.284	+158
SS	1028	1042	—	+1042	0.0032	+3
Fe			492	−492	0.057	−28
Al			63	−63	0.210	−13
Volume	83.7 liters	85.5	85.5			
						+361
Reflector						
Be	15,930	16,200	16,040	+160 mols	0.236	+38
Na	451	458	9.5	+448	0.226	+102
Fe	—		404	−404	0.065	−26
Al			108	−108	0.130	−14
SS	103	105	—		0.0425	+4
Volume	93.52 liters	95.5	96.4 liters			
						+104
					Total net	465 cents

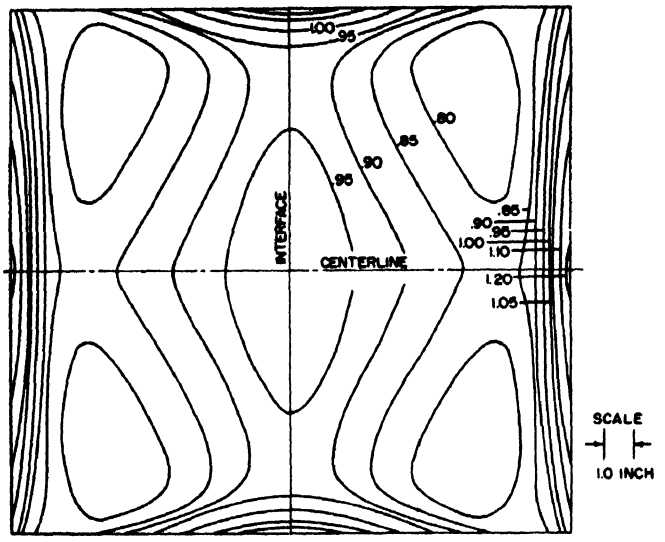

Figure 13. Contour graph of power distribution in PPA-5

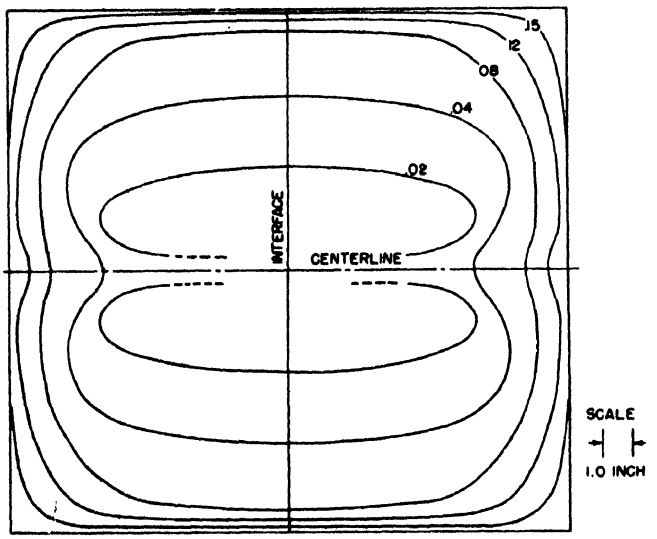

Figure 14. Contour graph of cadmium-fraction distribution in PPA-5

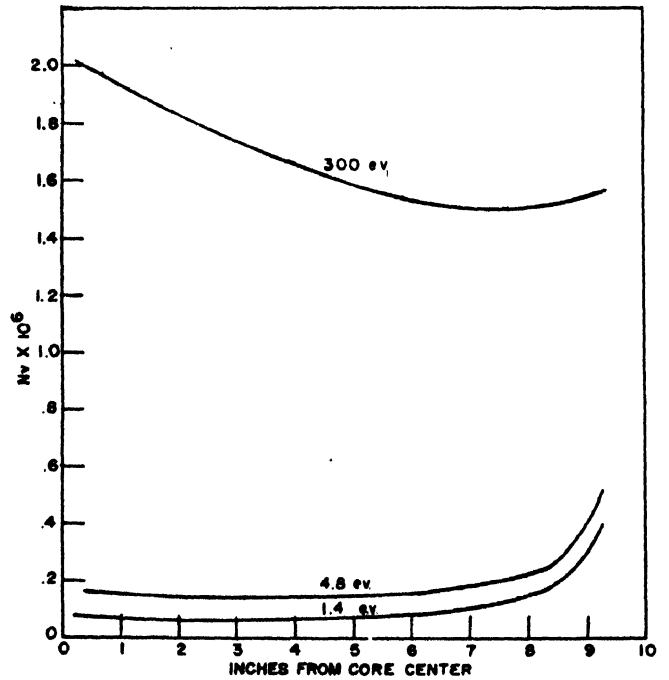

Figure 15. Epithermal neutron traverse-PPA-5

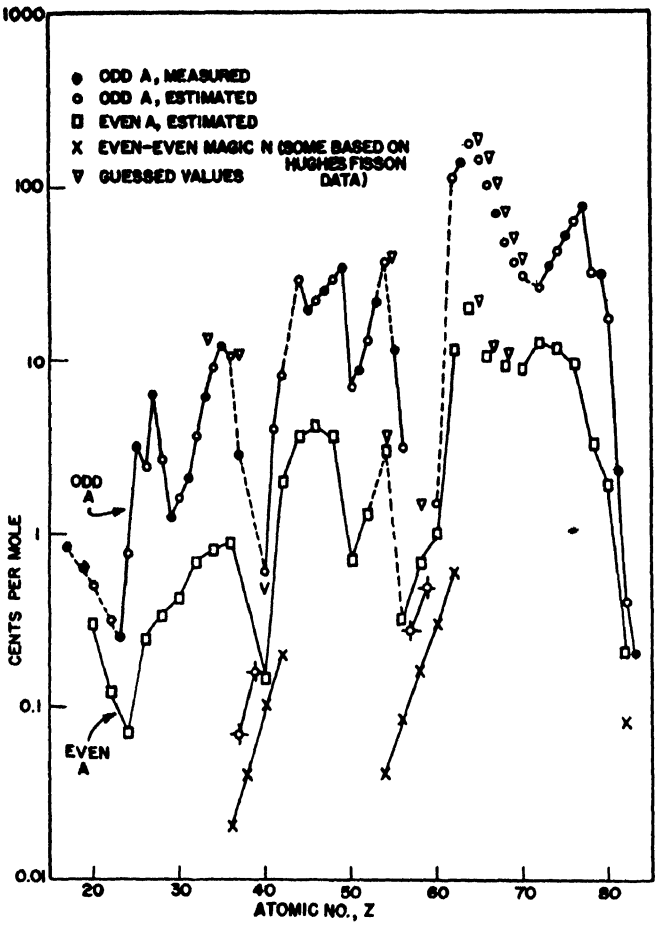

Figure 16. Reactivity changes at center of SAPL-V due to capture alone

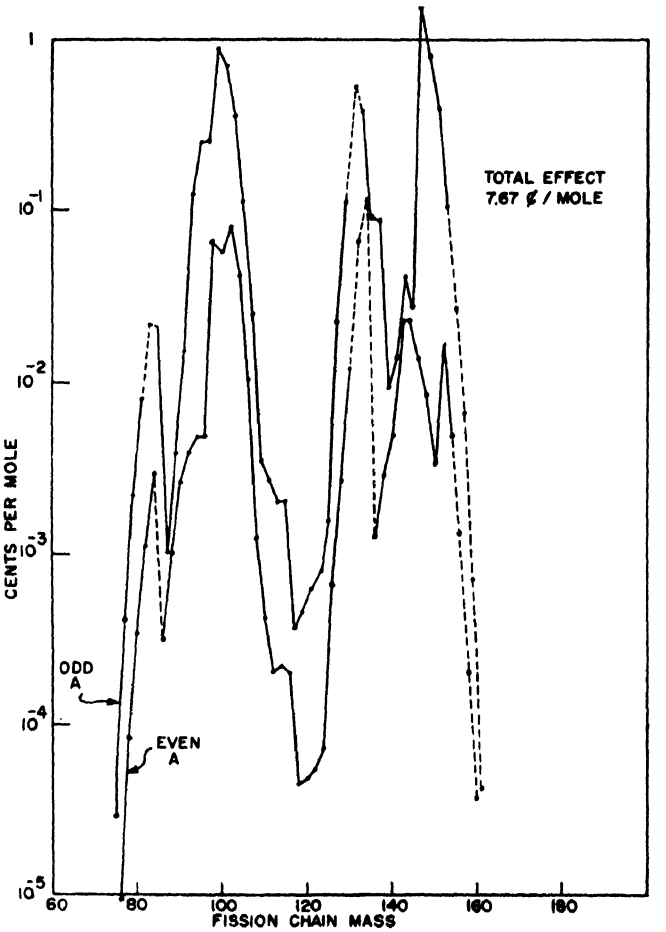

Figure 17. Estimated poisoning by fission products for SAPL-V

Table III. Reactivity Coefficients in SAPL-V

Element	*Atomic number*	*Cents/mol*	*Element*	*Atomic number*	*Cents/mol*
Hydrogen	1	+ 5.24	Molybdenum	42	− 3.15
Lithium	3	− 1.98	Ruthenium	44	− 11.0
Beryllium	4	+ 0.68	Rhodium	45	− 18.81
Boron	5	− 24.0	Palladium	46	− 7.90
Carbon	6	+ 0.347	Silver	47	− 25.2
Nitrogen	7	− 0.02	Cadmium	48	− 9.7
Oxygen	8	+ 0.287	Indium	49	− 33.8
Fluorine	9	+ 0.49	Tin	50	− 1.67
Sodium	11	+ 0.236	Antimony	51	− 8.74
Magnesium	12	+ 0.236	Tellurium	52	− 2.13
Aluminum	13	+ 0.141	Iodine	53	− 22.1
Silicon	14	+ 0.122	Cesium	55	− 11.56
Phosphorus	15	+ 0.318	Barium	56	− 0.584
Sulphur	16	− 0.1797	Cerium	58	− 0.204
Chlorine	17	− 0.750	Neodymium	60	− 0.881
Calcium	20	− 0.215	Samarium	62	−137.4
Titanium	22	− 0.046	Ytterbium	70	− 15.33
Vanadium	23	− 0.17	Tantalum	73	− 17.15
Chromium	24	− 0.043	Wolfram	74	− 8.7
Manganese	25	− 3.11	Rhenium	75	− 50.7
Iron	26	− 0.02	Osmium	76	− 18.37
Cobalt	27	− 6.33	Iridium	77	− 78.5
Nickel	28	− 0.275	Platinum	78	− 12.5
Copper	29	− 0.788	Gold	79	− 33.2
Zinc	30	− 0.375	Mercury	80	− 4.72
Germanium	32	− 0.840	Thallium	81	− 2.29
Arsenic	33	− 6.22	Lead	82	− 0.013
Selenium	34	− 1.403	Bismuth	83	− 0.0075
Bromine	35	− 12.24	Thorium	90	− 9.18
Rubidium	37	− 2.11	Uranium	92	− 8.65
Niobium	41	− 4.03	Uranium-235	92	+ 19.0

contour of activity induced through cadmium is shown in Fig. 14.

The spectrum at the low energy end was determined by the sandwich technique using indium, gold, and manganese. The sensitivity was calibrated in a known dE/E spectrum. The results are given in Fig. 15.

The absorption cross section of many elements was determined from their reactivity coefficients at the center of SAPL-V. The results are calibrated in terms of known cross sections and crudely corrected for scattering change in neutron energy, and are shown in Fig. 16 and tabulated in Table III. The data are striking in the contrasting absorption of odd and even Z isotopes and in showing the low absorption at magic numbers. This data has been used to estimate poisoning by fission products in Fig. 17.

Additional reactivity coefficient measurements with cadmium fuel sandwich inversion were used to determine the capture-to-fission ratio of both U^{235} and Pu^{239}. In such a sandwich either the cadmium surrounds the fuel or the fuel the cadmium. In either case the neutron absorption is the same. The change in reactivity observed then is due entirely to the extra fission neutrons produced when the fuel is on the outside. A thin foil reactivity coefficient on the other hand reflects the neutrons absorbed as well as those produced. By measuring the number of fissions taking place in these experiments, the relative absorption to fission ratio is determined.

With this work, we have determined the nuclear properties of the materials and from these, the nuclear reaction rates that will occur in this type of reactor, the influence of changing the amount or type of coolant or structural material, or even the core size. The effects of burn-up and thermal expansion can be estimated from these results, the conversion ratio as well. Results such as these are being used daily to solve our problems in nuclear design; the critical assembly has taken its place as a versatile and valuable tool in the atomic age.

Record of Proceedings of Session 20A

THURSDAY AFTERNOON, 18 AUGUST 1955

Chairman: Mr. G. von Dardel (Sweden)

Vice-Chairman: Mr. F. Ba Hli (Burma)

Scientific Secretaries: Messrs. M. Trocheris and F. de Hoffmann

PROGRAMME

P/659 Measurements of the resonance absorption integrals for various materials and ν_{eff} - the multiplication coefficient of resonance neutrons for fissionable isotopes.....P. E. Spivak *et al.*

P/833 Resonance capture integrals..... R. L. Macklin and H. S. Pomerance

P/427 Studies on the neutron resonance absorption of U^{238}.....V. S. Crocker

P/883 Measurements of the effective resonance integral of uranium with the pile-oscillator.....V. O. Eriksen *et al.*

P/948 Computation of the effective resonance integral.....E. F. M. van der Held

DISCUSSION

P/5 Experiments on some characteristics of the NRX reactor. Part I—Methods and prolonged fuel irradiation.....D. G. Hurst

P/6 Experiments on some characteristics of the NRX reactor. Part II—Temperature and transient poison effects.....A. G. Ward

P/835 Reactivity changes and reactivity lifetimes of fixed-fuel elements in thermal reactors.....B. I. Spinrad *et al.*

P/432 Long term reactivity changes in natural uranium reactors.....D. J. Littler

DISCUSSION

P/834 Small thermal homogeneous critical assemblies.....A. D. Callihan *et al.*

P/428 Plutonium-water critical assemblies.....C. C. Horton and J. D. McCullen

DISCUSSION

MR. KOZODAEV (USSR) presented paper P/659 as follows: In setting up a nuclear chain reaction it is very important to know the parameters directly affecting the neutron economy. These parameters include the capture and fission cross sections as well as the number of neutrons produced per neutron capture.

For the experimental determination of these parameters it is expedient to use a detector whose sensitivity is independent of the energy of the neutrons and of the angular distribution of the neutron flux at the location of the fissionable sample.

With the sample so located one can readily determine the characteristics of the material in question in any given neutron spectrum from the readings of the detector. In order that the results of measurement will not be affected by the self-shielding of the sample, it must be thin and the detecting system must detect small changes in the neutron flux.

An experiment having the above-mentioned attributes was developed in 1952 by the authors of the paper and used for measuring the resonance absorption integrals of various materials and for measuring the number of secondary neutrons (ν_{eff}) released in various materials.

A diagram of the experimental arrangement is shown in Slide 1 (Fig. 1 of P/659).

The graphite cube measuring 190 cm on a side has a cubic cavity 50 cm on a side. The sample is mounted in a special holder, in the centre of this cavity, in the path of the neutron beam. The beam enters the cavity through a boron collimator. There are 12 proportional counters, containing BF_3 (enriched in B^{10}) at a pressure of 500 mm Hg, uniformly distributed over the walls of the graphite box at a distance of 50 cm from the cavity. A measurement consists of determining the change in the total counting rate of all the counters following the introduction of the specimen to be investigated into the experimental cavity.

The size and form of the beam through the cavity is controlled by the collimating device (the diameter is less than 15 mm). Over its entire path from the entry channel to the front wall of the box, the beam is surrounded by a shield of paraffin impregnated with boron which serves to minimize the background due to scattered neutrons. The entire front wall of the box is also shielded by a layer of borated paraffin 15 cm thick.

The desired neutron spectrum was obtained by installing cadmium or boron filters of appropriate thickness in the path of the incident beam. When a thermal neutron beam was desired a graphite block 40 cm in length was inserted well into the channel. The flux

through the cadmium-filter amounted to only a few per cent of the total flux.

The pulses from all 12 counters are fed, by means of cathode followers mounted next to the counters, to the amplifying and discriminating system and thence to the scaling circuit with an over-all scaling factor of 1:16,000.

The over-all resolving power of the detecting system is comparatively high (1 μsec) which permits recording up to 10^4 pulses per second without noticeable skipping. The characteristic curve of the counting system has a slope of 2 per cent per 10 v in the operating range. The slight slope of the characteristic, the high feed-back in the amplifiers and stabilization of the power supplies of the plates and heaters of all tubes ensures stable operation of the detecting system and permits determining the number of pulses with an accuracy of 0.02–0.03 per cent.

The non-response of the detecting system to scattered neutrons in the specimen was verified by using thick samples of scattering material (graphite and bismuth). The tests showed that the effect of scattering in the specimen is less than the natural measurement error (0.03 per cent).

Photoneutron sources having different neutron energies were used to check the uniformity of the detector efficiency at different neutron energies.

It follows from the above that the change in the total number of pulses recorded by the counters per unit time when a specimen is introduced into the cavity is directly related to the change in the number of neutrons in the cavity due to absorption in the sample and to production of fission neutrons, if the sample is fissionable.

Obviously, when a sample of non-fissionable material is introduced into the cavity, the reduction in the total count will be proportional to the absorption of neutrons in the given substance, provided the specimen is sufficiently thin.

By making measurements on a substance whose resonance absorption is known (lithium) as well as on the experimental samples we can readily obtain the desired values of the resonance absorption intervals for the substances in question.

The above-mentioned requirement that self-shielding of the specimen must be absent throughout the entire neutron energy range makes it necessary to use relatively thin specimens and hence the potentialities of this method are limited primarily by the magnitude of the minimum relative effect which can be detected.

As was already noted, the measuring system used permits detecting changes in flux amounting to 0.02–0.03 per cent. It can be shown that the minimum value of the resonance absorption integral which can be measured with an accuracy of within 30 per cent is equal to not less than $\frac{1}{60}$ of the maximum neutron absorption cross section at the resonances. (In the printed text of the paper it is erroneously stated that the minimum resonance integral amounts to 0.006 of the maximum absorption cross section; the correct figure is 0.015.)

It can also be shown that the minimum value of the resonance absorption integral that can be measured with an accuracy within 30 per cent equals $\frac{1}{20}$ of the neutron scattering cross section of the given substance. Obviously in investigating a substance for which the maximum cross sections are not known, it is essential to measure the effects obtained with specimens of different thickness in order to make certain that self-shielding is absent.

To illustrate the potentialities of this method of investigating neutron resonance absorption, the measured values of the resonance integrals for a series of elements are listed in Slide 2 (Table I of P/659).

For certain elements the results obtained in the present investigation can be compared with the resonance activation integrals based on data reported by Harris, Muelhause, and Thomas and by Lichtenberger, Nobles, Monk, Kubitschek and Dancoff. Comparison shows that the values of resonance activation integrals computed on the basis of the data given by these investigators, taking into account the relative abundance of the isotopes in question, are in agreement, within the limits of experimental error, with the resonance absorption integrals measured in the present investigation.

Supplementary to the data given in Table I, I would like to mention the results of measurements of the resonance absorption integral for Pu^{240} obtained in an investigation by Erozolimski, Kutikov and Dobrynin. The measurements were made by means of the previously described set-up, using plutonium specimens containing 1.6 per cent Pu^{240}. The number of Pu^{240} atoms per cm^2 in these specimens was varied from 4×10^{18} to 10^{19}. Through comparison of the data on ν_{eff} for the Pu^{240} specimens in a cadmium-filtered neutron spectrum with the value of ν_{eff} for pure Pu^{239} in the same spectrum we can obtain the values of the resonance absorption integrals for Pu^{240} and also evaluate the self-shielding factor for the experimental samples.

The value of the resonance absorption integral for Pu^{240} obtained as a result of the investigations was $11{,}000 \pm 4000$ barns.

The same experimental set-up was used for investigating fissionable substances. In this case the quantity determined was ν_{eff}, the number of fission neutrons per neutron captured.

The effect ΔN_1, i.e., the change in the number of pulses per unit time recorded by the counters, incident to the introduction of the specimen containing a fissionable isotope may be characterized by

$$\Delta N_1 = -K_1 \cdot Q + K_2 \cdot Q \cdot \nu_{eff} \qquad (1)$$

Here Q is the number of neutrons of the primary spectrum absorbed per unit time in the specimen, K_1 is the efficiency of the counter in detecting the primary neutrons and Q_2 is the efficiency of the indicator in detecting fission neutrons.

To determine the ν_{eff} it is necessary to make another measurement, designed to obtain the value of ΔN_2 related to ν_{eff} and Q by a different expression. For this

purpose the indicating system was modified: a spherical filter consisting of a mixture of paraffin and boron and containing a window for emergence of a neutron beam, was introduced into the cavity of the box. The filter was made thick enough for the response of the detecting system to the effect of neutron absorption in the specimen to become negligibly small. Hence, in this case, the change in the counting rate ΔN_2 incident to the introduction of the specimen into the box (i.e., into the spherical filter) is given by

$$\Delta N_2 = K_3 \cdot Q \cdot \nu_{eff} \qquad (2)$$

where K_3 is the efficiency of the detecting system in detecting fission neutrons in the presence of the spherical paraffin-boron filter in the box cavity.

Denoting the ratio $\Delta N_1/\Delta N_2$ by X, we obtain

$$\nu_{eff} = \frac{K_1}{K_2} \cdot \frac{1}{\left(1 - \frac{K_3}{K_2} X\right)} \qquad (3)$$

The coefficient K_3/K_2 can readily be measured by means of a thermal neutron converter, for which one can utilize a specimen containing fissionable material; the specimen is mounted in the center of the box, in the thermal neutron beam, and shielded with cadmium on all sides except for an opening for the emergent neutron beam. The ratio of the effect due to this specimen in the presence of the spherical filter to the effect produced by the specimen in the absence of the filter is obviously equal to the desired coefficient K_3/K_2.

To determine the absolute value of ν_{eff} it would be necessary to find the absolute magnitude of the ratio of the coefficients K_1/K_2, which, incidentally, is very near to unity since the efficiency of the indicator is only very weakly dependent on the energy of the neutrons.

It is, however, sufficient to measure the relative dependence of ν_{eff} on the neutron beam spectrum and then normalize this dependence to the value of ν_{eff} for thermal neutrons. For this determination the effects are measured in the presence of different filters in the beam (gadolinium, cadmium or boron carbide in layers of different thickness) and also with a beam of thermal neutrons. In order to obtain the variation of ν_{eff} with the neutron energy one need only determine the variation of the coefficient K_1/K_2 or, in fact, simply of K_1, inasmuch as K_2 is independent of the energy of the primary neutron.

In the case of the present investigation the dependence of the coefficient K_1 on the neutron spectrum was determined in the following manner: In addition to measurements with the fissionable specimens a series of measurements was also made with a specimen of boron carbide. The change in the number of pulses recorded by the counters when the boron specimen is introduced is proportional to the coefficient K_1 and the number of neutrons absorbed in the boron specimen.

As the next step a thin LiF target was mounted in place of the specimen.

The alpha-particles and H^3 nuclei released by neutron capture in the Li^6 entered the thin mica window of the proportional counter. The design of this counter is pictured in Slide 3 (Fig. 2 of P/659). The number of counter pulses is proportional to the number of neutrons absorbed in the thin layer. Since the lithium target and the boron specimen were mounted at the same spot and since the capture cross sections of lithium and boron have the same dependence on the neutron energy, the ratio of the count with the boron specimen to the count with the lithium target is a quantity proportional to the coefficient K_1. Thus the various values of this ratio as determined with different neutron spectra gives the desired variation of the coefficient K_1. These measurements showed that given a suitable arrangement of the counters the response to the neutron spectrum behind the thickest filter used does not differ from the response to thermal neutrons by more than the experimental error ($\pm 1\%$).

Having the variation of the coefficient K_1 and the value of K_3/K_2 we can readily evaluate the variation of ν_{eff} of the fissionable material under investigation from measurements of the ratio X in different neutron spectra. Specifically, Spivak, Erozolimski, Kutikov, Dorofeev, Lavrenchik and Dobrynin carried out measurements of ν_{eff} in the epithermal primary neutron region, i.e., from 0.2 to 100 ev.

The measurements were made using the neutron beam from the PTR reactor. The energy interval of the primary neutrons was varied by means of gadolinium, cadmium and boron filters installed in the path of the neutron beam.

The results of measurements on U^{235}, U^{233} and Pu^{239} are summarized in Table I on this page.

The first column shows the material and thickness of the filters; the second, the neutron energy interval as determined by computation; the third, fourth and fifth columns show the values of ν_{eff} for U^{235}, U^{233} and

Table I

Measurement Conditions	*Effective energy interval*	U^{235}	U^{233}	Pu^{239}
Thermal neutron beam	0.025	1	1	1
The difference between the effects obtained for a 1 gm/cm² cadmium filter and a 0.08 gm/cm² gadolinium filter was utilized	0.15–0.5	1.00 ± 0.03	1.00 ± 0.02	0.90 ± 0.03
Cadmium filter 1 gm/cm²	0.4–3	0.78 ± 0.02	0.98 ± 0.02	0.88 ± 0.02
Cadmium/boron carbide filter 0.5 gm/cm²	0.6–6	0.73 ± 0.02	0.98 ± 0.02	0.89 ± 0.02
Cadmium/boron carbide filter 1 gm/cm²	2.5–25	0.74 ± 0.02	1.00 ± 0.025	0.88 ± 0.02
Cadmium/boron carbide filter 2 gm/cm²	8–130	0.72 ± 0.02	1.00 ± 0.025	

Pu^{239}, respectively, normalized to unity for the thermal neutron spectrum.

The data of Table I show that the value of ν_{eff} for U^{238} remains constant throughout the investigated range of primary neutron energies while the value of ν_{eff} for U^{235} drops off sharply at an energy of a few electron-volts and then remains constant in the 10–100 ev energy interval. In the case of Pu^{239}, ν_{eff} decreases in the 0.1–0.4 interval; with further increase of the mean energy of the primary neutron spectrum the value of ν_{eff} remains 12 per cent below the thermal spectrum value.

The above results are in good agreement with the data obtained by S. Nikitin, V. Belkin and P. Krupchitski, who investigated the energy dependence of ν_{eff} in the same neutron energy range by other methods. (A report on this investigation was presented at a recent meeting of the Physico-Mathematical Department of the Academy of Sciences of the USSR.)

The data for U^{235} and Pu^{239} are also in good agreement with the results obtained by Kanne, Stewart and White, presented at this Conference. If we deduce the corresponding variation of ν_{eff} from the variation of alpha, i.e., the radiative capture-to-fission ratio, with the neutron spectrum reported by these investigators, we can make the following comparison of results:

For the U^{235} isotope the value of ν_{eff} in the neutron spectrum bounded on the left by 30 ev (cut-off energy) amounts to 0.77 of its thermal spectrum value according to the data of Kanne, Stewart and White, while according to the data of Spivak, Erozolimski, Dorofeev, Lavrenchik, Kutikov and Dobroynin the value of ν_{eff} in the near neutron spectrum equals 0.73 of its thermal spectrum value.

For Pu^{239}, according to Kanne, Stewart and White, ν_{eff} in the interval starting with the 5 ev cut-off energy amounts to 0.86 of the thermal spectrum value while according to the data of Spivak *et al.*, the corresponding figure is 0.88 for the analogous spectrum. Lastly one should mention the results of investigations by two groups of physicists of the Brookhaven and Hanford Laboratories who employed a very elegant method for measuring the variation of ν_{eff} for a number of fissionable isotopes in the near epithermal region (to 0.1 ev). The drop in the value of ν_{eff} for Pu^{239} discovered by these groups is confirmed by the results obtained by the above-mentioned group of Soviet physicists who showed that the value of ν_{eff} for Pu^{239} amounts to approximately 0.9 of its thermal spectrum value in the energy region between the boundaries of gadolinium and cadmium absorption.

Mr. E. P. WIGNER (USA) presented paper P/833 and made the following two remarks: First, with reference to the different methods of measuring the resonance integral he said:

Two methods of measuring this quantity are described in this paper. I should add that we have just heard about a third method of measuring this same quantity.

Then with reference to the measurements of the resonance integral for iron and coppers, he pointed out that the results were in good agreement with the measurements given in the preceding paper.

Mr. F. FENNING (UK) presented paper P/427.

Mr. V. O. ERIKSEN (Norway) presented paper P/883.

Mr. M. BOGAARDT (The Netherlands) presented paper P/948.

DISCUSSION OF P/659, P/833, P/427, P/883 AND P/948

Mr. E. R. COHEN (USA): Would Mr. Wigner care to comment on the $1/v$ component of the resonance integral in formulating reactor calculations?

Mr. WIGNER (USA): Whether one should include the $1/v$ component or whether one should not is fundamentally a matter of convention. It was decided not to include the $1/v$ component because its magnitude depends on the position of the cadmium cut-off which seems to be an arbitrary matter, and therefore has little to do with the actual resonance absorption. If we had a material to shield our samples which would have a higher cut-off, the resonance integral would turn out to be smaller and, in order to avoid this ambiguity, it was decided to eliminate the $1/v$ component. Of course, this elimination is only possible if the cross section between the thermal region and the first resonance drops to a very small value, so that one can reasonably separate the thermal absorption from the resonance absorption. There is another reason for eliminating the $1/v$ component, to facilitate reactor calculations. Not only U^{238} but also the U^{235} absorption has a $1/v$ part and the two approximately compensate. Therefore, in addition to the reason which I mentioned, there is a practical reason for the elimination of the $1/v$ component.

Mr. WARD (Canada): I should like to ask Mr. Wigner whether, in the analysis of the effective resonance integral for thick uranium, any allowance has been made for the depression of the resonance neutron flux due to the presence of the sample.

Mr. WIGNER (USA): This is a point on which I wanted very much to comment and I appreciate the question. The results of the British group and the results obtained in the United States are very difficult to compare because they mean a different thing by resonance integral. Our coefficient is the amount of resonance integral in unit flux per unit logarithmic energy range. When we apply our resonance integral to calculate the absorption of a lump, we first calculate the average flux (per unit logarithmic energy range) at all parts of the lump and multiply this then with our A. This does not give an important correction for small lumps, but for large ones, it is a significant correction. We apply this separatedly and call A the absorption of the uranium in unit flux. This also makes it difficult to compare the results obtained by Mr. Crocker with results of Mr. Creutz and his collabora-

tors because Mr. Crocker's measurements automatically include the attenuation of the neutron density with the penetration of the beam into the sample. Mr. Creutz' measurements do not include that, or, rather, if we evaluate his measurements, we correct for the attenuations. There is still considerable doubt in our minds as to what the proper attenuation coefficient is; in other words, what is the diffusion length of resonance neutrons in our samples. Perhaps a comparison with Mr. Creutz' measurements will answer this question. I have heard from numerous sources that the K (inverse diffusion length) which we originally used—I think it was 0.022 times the density—is too low, which would indicate that our assumption of the width resonance band is too high. In other words, the resonance band which we assumed to extend from the lowest resonance to about 6000 or 8000 volts is actually narrower.

Mr. M. RAIEVSKY (France): I would like to ask a question in connexion with P/659. The important thing about the apparatus described is that the measurements are independent of the energy and scattering of the neutrons. The speaker indicated that measurements showed that the detecting system was independent of the scattering and mentioned an accuracy of 0.03 per cent, but the written report is not very clear on the manner in which this was determined. Actually the apparatus would be independent of the scattering if it were isotropic but as a matter of fact it can not be isotropic because there is a collimator, 10 cm in diameter, mounted at the entry of the beam and when viewed from the centre, i.e., from the point of the specimen, the collimator subtends a solid angle of 1 per cent. Consequently the neutrons scattered in the direction of the collimator are lost to the counters. One should therefore expect an effect due to scattering on the order of 1 per cent, that is, 30 times greater than the effect indicated. I would like to know what means were employed to eliminate this effect, since the written report is not explicit on this point.

My second question has to do with the effect of scattering in air along the path of the beam. The mean length of the neutron path in air is about 25 metres. The effect of scattering in air cannot be entirely negligible: It must produce divergence, i.e., enlarge the beam at the point of the target. What measures were taken to eliminate the effect of air scattering?

Mr. KOZODAEV (USSR): Let me answer the second question first.

The authors of the paper I reported on showed, by experiments with different photoneutron sources, that with a given arrangement of the counters in the graphite box, the detecting system is not sensitive to change in the neutron spectrum.

The scattering of neutrons in the air could not affect the accuracy of measurements in the given set-up.

It is difficult for me to give an accurate reply to the first question here and now. Special experiments were made to prove that the effect of scattering in the specimen is of minor importance. In Spivak's investigation, very thin specimens were used; furthermore, experiments made with thick specimens of scattering substances (graphite, bismuth) showed that neutron scattering does not affect the measurement accuracy.

Unfortunately, the paper submitted to the Conference does not contain a table describing the specimens used. However, I have some documentation indicating that the specimens were very thin and that the effect was sufficiently great to permit determination of the resonance absorption integrals with adequate accuracy. Special calculations carried out in connexion with the investigation showed that for the determination to be correct, the product of the number of atoms by the scattering cross section must be less than a certain value (0.3). This necessary condition was always observed in the experimental measurements. Accordingly, for their different specimens the investigators always selected a sufficiently low specimen thickness to ensure a low enough number of scattering atoms. For example, for measurements on hafnium, which has a large resonance absorption integral, the investigators used a quantity of material equal to about 2×10^{19} atoms/cm^2. The effect was sufficiently strong to determine the sought value with an accuracy of within about 20 per cent.

Mr. RUDIK (USSR): I would like to ask Mr. Eriksen the following question: Do you in any way take into account neutron capture in the region above the cadmium cut-off energy? Certain rough measurements indicate that the effect is appreciable and may amount to about 15 per cent of the measured value.

Mr. ERIKSEN (Norway): The effect of fast fission and resonance fission was not taken into account; no correction was made for it. I thought it was really a small effect. I cannot see how it could be 15 per cent.

Mr. D. G. HURST (Canada) presented paper P/5 and gave additional results on the changes of reactivity of the whole reactor as follows:

The course of the reactivity during the first 1000 Mw-days output of a charge of uranium was studied last year as part of an extensive experimental programme. The principal reactivity changes are expected to arise from the growth of Sm^{149}, the burn-up of U^{235} and its partial replacement by Pu^{239}, and possibly a changing light-water content due to deformation of the fuel, but this last effect we believe to be small. The net reactivity, expressed as equivalent π^2/h^2 in metres^{-2} is plotted versus total-energy output.

The points on Slide 4 show the sum of $\pi^2/(\text{Weir setting}/22\text{ cm})^2$ plus corrections for control rod position, heavy-water temperature, and xenon poison. The xenon poison was calculated with parameters to be discussed in paper P/6. Because of uncertainties in calculating critical height when the poison is changing rapidly, only cases where the xenon was not far from equilibrium are plotted and the results have not been carried back to the beginning.

The magnitude of 1 per cent of the xenon poison is indicated. Three calculated curves are shown fitted to the point at 94 Mwd. These curves have been derived

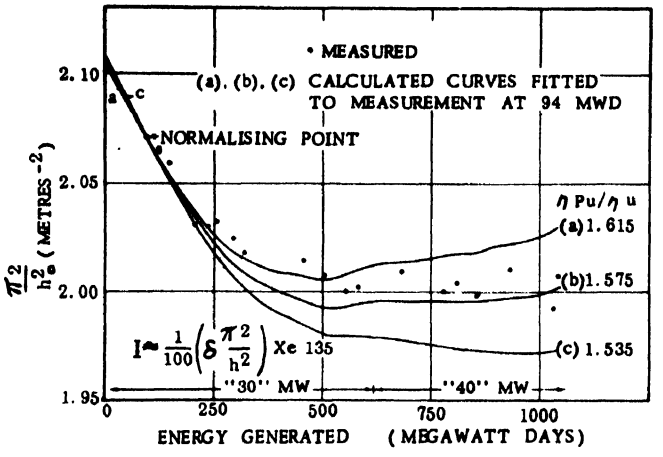

Slide 4. Reactivity vs energy output

since the text was written. The curves are all based on a 1.1 per cent yield of Sm^{149}, a conversion factor 0.8, and a plutonium cross section 1125 barns. They differ in the η assumed for Pu^{239}. For an η of natural uranium equal to 1.3 the curves (*a*), (*b*), (*c*) correspond to η (Pu) 2.10, 2.05, 2.000 for Pu^{239}.

Slide 5 shows the separate contributions from Sm^{149}, U^{235} and Pu^{239} to the calculated curves of the previous slide. The details of reactor operation have been taken into account and produce transient effects in samarium and in the three plutonium curves. In addition to its dependence on η the plutonium contribution is proportional to the product of cross section and conversion factor. A lower conversion factor than the assumed 0.8 could be compensated by a larger plutonium cross section. The initial loss is due largely to the burn-out of U^{235}, the plutonium and samarium balancing each other.

These experiments provide results for checking the consistency of a set of parameters but do not select a unique set. They are of importance to us as they have brought to light no unexpected large reactivity losses and the discrepancy between calculations and measurements appears to be in the direction of a smaller decrease of reactivity with irradiation than would be predicted from commonly used values of the parameters, a desirable result for power producing reactors where long irradiation is required.

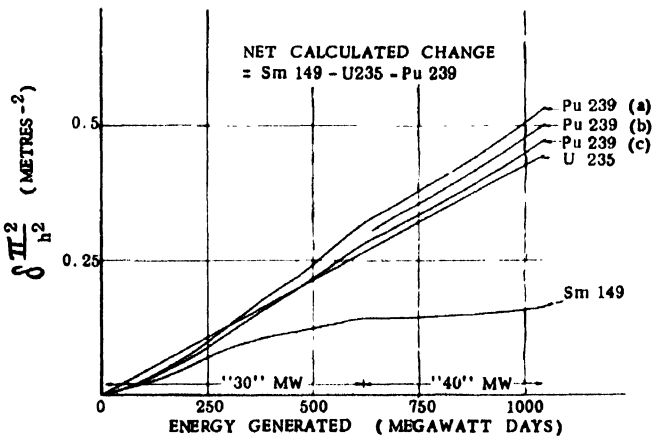

Slide 5. Components of reactivity change

Mr. A. G. WARD (Canada) presented paper P/6.

Mr. B. I. SPINRAD (USA) presented paper P/835 together with some new results as follows:

Slide 6 (Figure 10 of P/835) shows two results for a thorium U^{235} breeding system. You will notice I have not bothered about a conversion rate less than 1.1, which amounts to a breeding rate of 10 per cent, because the productivity always drops for such a breeding gain because the fission products and the U^{234} associated with breeding counterbalance the gain in productivity or reactivity which is due to the fuel that is bred. Curve 1 is for the simple burning method, returning the original productivity; curve 2 is for the time averaging, or rod-switching method. In all these systems I have calculated reactivity losses due to the build-up of Pa^{233} but I have assumed that 3 per cent of the conversion is wasted by protoactinium capture. This assumes flux in the range of 10^{14}.

Slide 7 shows the difference between the initial breeding gain and the mean breeding gain in a cycle. The main reason why productivity finally drops in these systems is accumulation of fission products. A secondary reason is that, if the thorium cross section is constant, breeding gain goes down as the U^{233} concentration increases in a breeding system, so the mean breeding gain must be less than the initial gain.

Slide 8 is a study of the recycling of plutonium back into a uranium system. Here the blue line represents the fuel efficiency of a plutonium feed-back system in terms of fissions achieved per atom of uranium loaded. The red line represents the economy that is available in concentration of uranium over an original critical system. The conditions in which this slide was pre-

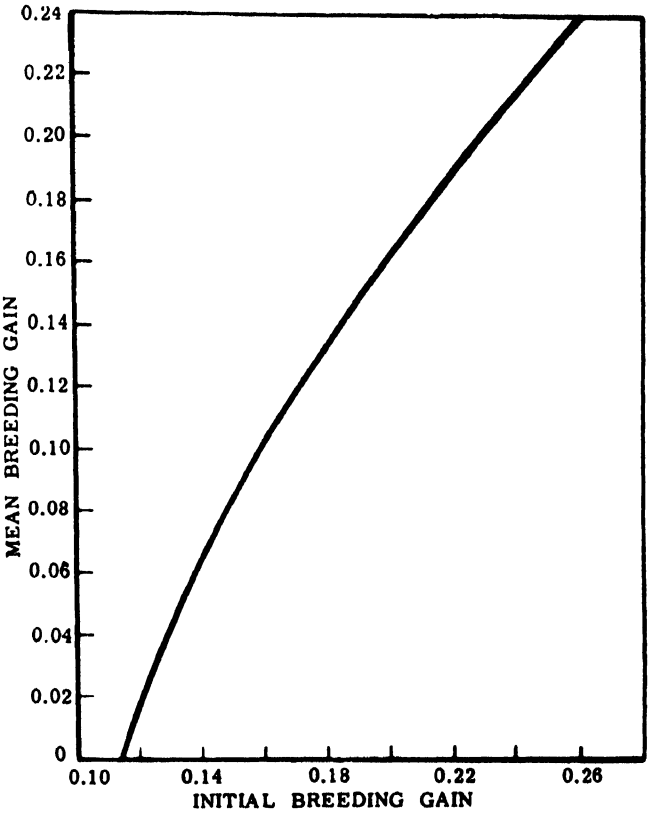

Slide 7. Decrease in breeding gain of overburned U^{233}-Th systems

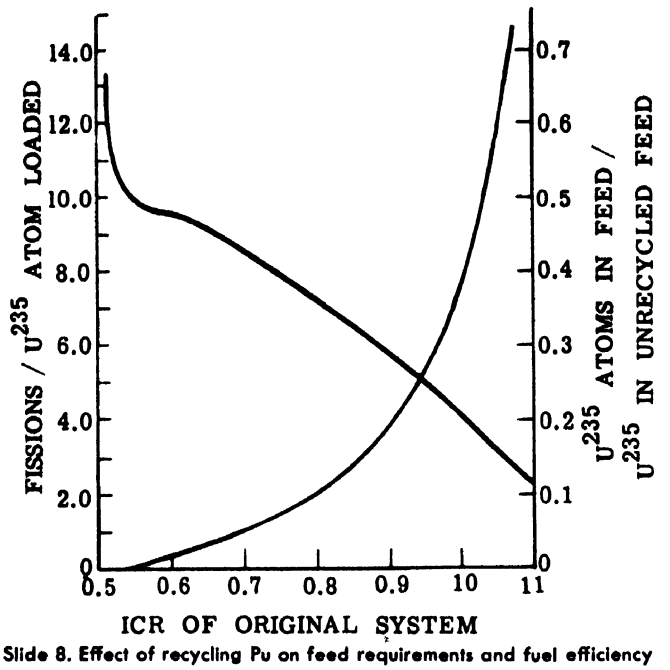

Slide 8. Effect of recycling Pu on feed requirements and fuel efficiency

pared were the following: First, the plutonium is in isotopic equilibrium up to and including Pu^{242}.

Second, as much Pu is available at the end of the run as was put in in the beginning; third, the Pu concentration is adjusted so that the fuel burn-up under the rod-switching scheme is the same as for the system, with the same ratio of U^{238} to parasitic absorption, when loaded with U^{235}-U^{238} fuel only, and operated in the same fashion. In other words, the Pu is used to hold up the reactivity of a uranium system while we burn U^{235} and all the plutonium that is formed from U^{238}. It is one way of looking at it; it is a way of making the conversion ratio stay exactly. The system of rod-switching or graded irradiation method of reactor operation is recommended.

Incremental fuel enrichment increases fuel efficiency per cycle although at the expense of conversion rate. The recycling of products also increases fuel efficiency, and is recommended when possible, when economical. Direct removal of fission products would help enormously.

Mr. D. J. Littler (UK) presented paper P/432.

Mr. A. D. Callihan (USA) presented paper P/834.

Mr. F. Fenning (UK) presented paper P/428. He made the following additional remarks which are not contained in the full text of the paper:

The experiments described in P/428 were carried out at Harwell a few years ago when about 1 kg of Pu^{239} containing 3 per cent Pu^{240} was available.

Some nitric acid was present in the solution in order to ensure that the plutonium nitrate remained in solution. This meant that the hydrogen density in the core would be somewhat lower than in the pure water reflector. In this case, with the plutonium solutions there was no need for an external source. The reason for this is, first, that some neutrons are produced by the spontaneous fission of Pu^{240}, but, as we found with some preliminary experiments, far more are produced by the (α,n) reactions on the oxygen in the water.

DISCUSSION OF P/834

Mr. B. P. Adyassevich (USSR): I should like to make a few remarks in connexion with P/834.

In the USSR, too, there was some experimental work done on small critical assemblies.

The first part of the experimental programme was devoted to determining the critical masses, the influence of different reflectors and the spectral and spatial distributions of neutrons in homogeneous-solution systems operating with thermal neutrons. The results obtained are similar to those that are given in the paper by Callihan, Morfitt and Thomas. In determining the critical mass in the range of concentrations [H]/[U] from 50 to 350 spherical flasks surrounded by spherical reflectors of different materials were filled with aqueous solutions of salts of U^{235} and Pu^{239}. Comparative tests carried out with reflectors of paraffin, graphite, iron and uranium showed that uranium reflectors are best.

The spatial distribution of fast, resonance, and thermal neutrons was determined by means of suitable detectors.

In some experiments with solution systems the power was as high as 1–2 watts.

The second part of the programme was concerned with heterogeneous systems containing appreciably larger amounts of active material. Using metal plates of U^{235} with a total weight of 15 kg and polyethylene plates, we succeeded in investigating assemblies with concentrations of U^{235} corresponding to $2.6 \leq [H]/[U] \leq 52$. Of the reflectors used in these experiments—paraffin, graphite, iron, copper, lead and uranium—uranium proved to be best once again.

In this range of concentrations the critical volume remains virtually constant.

We used the method of resonance detectors to study the neutron spectrum. Increasing the U^{235} concentration resulted in a shift of the neutron spectrum from the thermal range to energies in the 10 to 100 ev interval. The fact that the critical volume remains constant over a wide range of U^{235} concentrations indicates that ν_{eff} does not increase at energies in the 10–100 ev range. Additional experiments, in which part of the uranium-235 was replaced by Pu^{239} and U^{235}, made it possible to evaluate ν_{eff} for these isotopes as well.

It was found that for neutron energies of 10–100 ev the value of ν_{eff} for U^{235} and Pu^{239} averaged over this spectrum interval does not exceed 2.

In individual experiments in this part of the programme the power of the assembly was brought up to 50–100 watts for short intervals.

A more complete report on these experiments was made by G. N. Flerov at the July 1955 session of the Academy of Sciences of the USSR.

Mr. McKay (UK): I should like to ask Mr. Callihan whether he has any comment to make on the region of very low hydrogen-uranium or hydrogen-plutonium ratios, such as you might get in a uranium oxide slurry.

Mr. CALLIHAN (USA): Some work has been done with slurries; and insofar as they are well stirred and well mixed the critical parameters for given concentrations are about the same as those for the solutions. These were slurries of insoluble uranium salts.

Mr. MCKAY (UK): I would still be interested in slurries which contained a much higher proportion of uranium than any of the solutions which were mentioned in Mr. Callihan's paper.

Mr. CALLIHAN (USA): We have done no experiments except some work with this uranium of low enrichment where it was necessary to handle the material as a solid. There at least in comparison the behaviour was about that to be expected. One recognizes this certainly as a problem in chemical processing operations and realizes that the competitive effects of increased density and loss of moderation on settling are matters which need to be considered in chemical processing operations.

Mr. HURWITZ (USA): Because of the interest in the distribution of neutrons slowed down in water, we have been performing calculations on the spherical water-moderated and water-reflected assemblies investigated by Mr. Callihan by means of a method which avoids the approximations of the Selengut-Goertzel multigroup procedure. We calculate the core material buckling from the Fourier transform formula, $q(k^2)$, of the slowing-down density at thermal energy, as obtained by the accurate procedure discussed by Mr. Wilkins this morning.

We then calculate the reflector savings by the Volkoff approximation in which the interaction of the opposite sides of the core is neglected. This approximately, in conjunction with the Weiner-Hopf method, allows us to express the reflector savings in terms of an integral involving the Fourier transform of the slowing-down density. This integral may be evaluated numerically.

Slowing-down transform: $q(k^2)$

Buckling:

$$\frac{k_\infty q(B^2)}{1 + B^2 L_c^2} = 1$$

Reflector saving:

$$\Delta = \frac{1}{B}(\tan^{-1} BL_r + \varphi)$$

with

$$\varphi = \frac{1}{2\pi}\int_0^\infty \log\left|\frac{k+B}{k-B}\right| \frac{d\log U}{dk^2}\, 2kdk$$

$$U = \frac{(k^2 - B^2)L_c^2}{-K_\infty q(k^2) + (1 + k^2 L_c^2)}$$

	B^2	Δ	r_c
$q(k^2)$ from B_3	0.0304 cm^2	5.8 cm	12.2 cm
$q(k^2)$ from $S - G$	0.025 cm	6.5 cm	13.6 cm
Multigroup $S - G$	—	—	13.8 cm
Experiment	—	—	13.2 cm

The table above gives numerical results which were obtained for the experimental assembly with 13.2 cm critical radius by Mr. Francis. The calculations gave 0.0304 cm^{-2} for the core material buckling, B^2. The reflector savings was 5.8 cm, and the calculated critical radius was 12.2 cm. To check the consistency of the numerical work and the accuracy of the Volkoff approximation, we repeated the calculation for the slowing-down Fourier transform which is obtained by the Selengut-Goertzel approximation. The results were 0.025 cm^2 for the core material buckling, 6.5 cm for the reflector savings, and 13.6 cm for the critical radius. This latter figure is in satisfactoy agreement with the critical radius of 13.8 cm obtained by Prohammer with a direct application of the Selengut-Goertzel multigroup procedure.

These results demonstrate two things. First, the Selengut-Goertzel approximation underestimates reactivity as compared to a more accurate procedure using the same nuclear data. Secondly, the cross-section data and fission spectrum used in the calculation of the slowing-down density transform overestimate reactivity. This is consistent with the fact that these data yield too small an age. We are therefore reexamining the transport cross sections and fission spectrum data to see whether a set of data can be found which is consistent with both the integral and differential experimental results.

Session 21A

ZERO ENERGY AND EXPONENTIAL EXPERIMENTS

LIST OF PAPERS

		Page
P/600	Exponential experiments with slightly enriched uranium rods in ordinary water ..... H. Kouts *et al.*	183
P/601	Pressurized water reactor (PWR) critical experiments ..... S. Krasik and A. Radkowsky	203
P/603	The theory of uranium water lattices ..... J. Chernick	215
P/604	Physics aspects of the pressurized water reactor (PWR) ..... A. Radkowsky and S. Krasik	229
P/790	Some experiences from measurements on an exponential pile of uranium and heavy water ..... R. Persson *et al.*	239
P/791	Characteristics of the Swedish heavy water reactor ..... E. Hellstrand *et al.*	242
P/361	Study of the neutronics of two French heavy water reactors ..... J. Horowitz	256
P/605	Exponential experiments on D_2O uranium lattices ..... E. R. Cohen	268
P/920	Calculations for a heavy water and natural uranium 10 Mw reactor ..... S. Gallone and C. Salvetti	279
P/429	The experimental basis of lattice calculations ..... P. W. Mummery	282
P/607	Normal uranium, graphite-moderated reactors: a comparison of theory and experiment water cooled lattices ..... P. F. Gast	288
P/606	Uranium graphite lattices—the Brookhaven reactor ..... I. Kaplan and J. Chernick	295
P/599	Exponential experiments in graphite systems ..... D. E. Davenport	309
P/623	A heavy-water research reactor ..... A. I. Alichanov *et al.* (This paper appears in Session 9A, Vol. 2.)	317

Exponential Experiments with Slightly Enriched Uranium Rods in Ordinary Water

By H. Kouts, G. Price, K. Downes, R. Sher, and V. Walsh,* USA

EARLIER WORK

Light water was one of the first moderators considered for nuclear reactors. Early calculations, however, led to the belief that the relatively large thermal neutron absorption by hydrogen would not permit its use in obtaining a chain-reacting system with natural uranium.

By 1944, the experimental values of cross sections had changed enough to cause the use of water to be reconsidered. Calculations done by A. M. Weinberg[1] still indicated that criticality could not be reached. However, it seemed much closer than was thought true before, and uncertainties in the analysis were still large enough to allow the possibility that k_∞ would be greater than 1. An experimental program to settle the question was therefore carried out in 1944–45, at Oak Ridge.

The Oak Ridge measurements were made in exponential experiments, with natural uranium rods of diameter 1.18 in. (3.00 cm), 1.10 in. (2.794 cm), and 0.787 in. (2.00 cm). Several volume ratios of water to uranium were assembled with each rod size. Although the experiments were primarily meant to provide values of the buckling B^2, there were also measurements of migration areas and temperature coefficients of reactivity. In addition, an attempt was made to find values of the thermal utilizations of some of the lattices.

The exponential experiments were assembled in a tank which rested on a thermal column on top of the Oak Ridge graphite reactor. In each case the basic cell was an equilateral triangle, and the lattice was rectangular in cross-section. The water tank had inlet and outlet vents, for filling and emptying; these also permitted a continuous flow in and out of hot water for temperature coefficient measurements.

Calculations of the thermal utilization had led to the prediction that an annular air gap about the fuel rods would increase the maximum attainable k. Mathematically this effect is a consequence of the boundary conditions which the flux must satisfy at the fuel-moderator interface. Physically, it results from the fact that scattering material has been removed from the volume near the boundary of the fuel rods, where it would have deflected neutrons away from the uranium. Three of the exponential assemblies were made with rods having air gaps of this sort, so that the reality of the effect and its magnitude could be observed. The air gaps were obtained by sealing each uranium rod in two concentric aluminum tubes, separated by aluminum spacing elements.

The buckling of each lattice was found from indium foil measurements of the spatial thermal neutron distribution. These foils were wrapped around plastic rods, which were inserted into the assembly in the centers of lattice cells. Flux traverse measurements were made along the three principle axes of the rectangular assembly, and the observed variations in foil activities were fitted to the appropriate cosine and exponential functions. All measurements were limited to the region higher than 50 cm above the surface of the thermal column, in order that flux harmonics might be avoided. For most of the assemblies, buckling measurements were made with two or more water temperatures. Thus values of dB^2/dt were obtained, as well as B^2 at room temperature.

Table I lists the experimental values of B^2 at 25°C and the observed temperature coefficients. Figure 1

Table I. Buckling and Temperature Coefficients of Light Water Moderated, Natural Uranium Rod Lattices. From 1944–45 Experiments at Oak Ridge

Rod diameter (in.)	Air gap (in.)	Volume water / Volume uranium	Buckling B^2 ($cm^{-2} \times 10^4$) at 25°C	$\frac{dB^2}{dT}$ ($cm^{-2}/°C \times 10^6$)
1.18	None	1.14	− 5.34	
1.18	None	3.27	−42.15	+1.50
1.18	None	0.273	−67.92	−2.3
1.18	None	1.78	− 3.79	+0.20
1.18	None	1.36	− 1.98	+0.002
1.18	None	3.17	−34.95	+0.817
1.10	None	2.06	− 8.01	+0.31
1.10	None	1.57	− 3.16	+0.159
1.10	None	1.42	− 3.39	−0.034
1.10	0.45	1.92	− 0.20	−0.089
1.10	0.45	1.56	+ 0.27	
0.787	None	1.80	− 2.78	
0.787	None	1.50	− 6.60	−0.25
0.787	None	2.10	− 3.29	
0.787	0.354	2.01	0.00	+0.016

* Brookhaven National Laboratory. Prepared by H. Kouts. Including work by T. Arnette, S. Bernstein, G. Branch, F. Beyerly, E. Cashwell, C. Clifford, I. Coveyou, B. Feld, Haydn Jones, R. McCord, H. W. Newson, W. Neyer, F. V. Pruitt, R. B. Stewart, J. R. Rush, R. Scalletar, L. Slotin, L. B. Watson, A. M. Weinberg—Clinton Laboratories (Now Oak Ridge National Laboratory).

shows the buckling plotted against the water-to-uranium volume ratio for the 1.10-in. and 1.18-in. rods. These sizes would have nearly the same reactivity, and so they have been grouped together on the graph. Figure 2 shows the experimental values of B^2 for the 0.787-in. rods again plotted against the volume ratio.

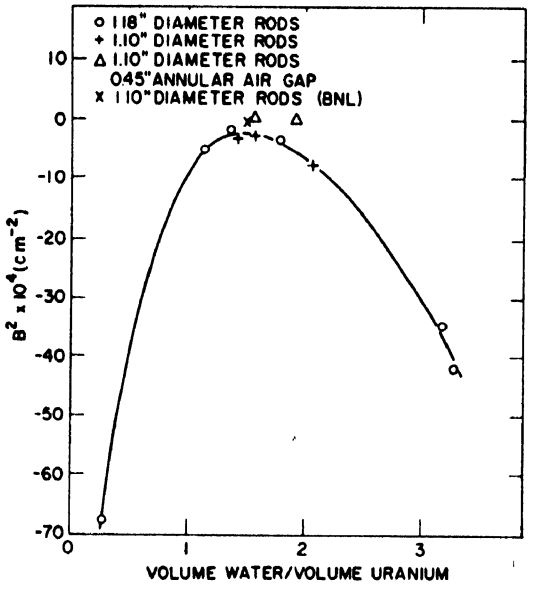

Figure 1. B^2 vs volume ratio, 1.10 inch and 1.18 inch diameter natural uranium rods in light water. From 1944–45 Oak Ridge experiments

According to Fig. 1, the maximum value of B^2 obtainable with the larger rods was about -3×10^{-4}, at a water-to-uranium volume ratio of about 1.5. From Fig. 2 it is seen that the 0.787-in. diameter rods gave also a maximum value of about -3×10^{-4} for B^2, but the peak value in this case occurred at a volume ratio of about 1.9.

The annular air gaps did indeed increase the reactivity; in fact one lattice (1.10-in. diameter rods, 0.45-in. air gap on the radius, 1.56 volume ratio) had a positive value of the buckling after an allowance had been made for absorption in the aluminum tubing and spacers.

For measurements of the age of fission neutrons in these assemblies, the uranium rods were wrapped in cadmium. A source of fission neutrons was applied, and cadmium-covered indium foils were exposed throughout the lattice. The observed activities of these foils as a function of the distance r from the source led to the evaluation of the mean neutron age from fission energies to the large indium resonance at 1.46 electron volts. The source used to find the distribution for small values of r was a small sample of enriched uranium, effectively a point. A beam of neutrons through a hole in the reactor shield produced the necessary fissions. The source used for large values of r was a plane array of Oak Ridge pile slugs, each 1.10 in. in diameter by 4.0 in. long, placed under the lattice in the tank on the thermal column. The space distribution observed with the plane source was differentiated to convert it to a point source curve, and the result was joined onto the measured point source distribution to give a single extended curve $f(r)$. The age to the indium resonance τ_{In} was then calculated from

$$\tau_{In} = \frac{1}{6}\overline{r^2} = \frac{1}{6}\frac{\int_0^\infty r^4 f(r)\,dr}{\int_0^\infty r^2 f(r)\,dr} \qquad (1)$$

A calculated correction had to be added to convert τ_{In} to τ_{th} the age to thermal. The values of τ_{th} which were obtained (Table II) are plotted in Figs. 3 and 3a against the water-to-uranium volume ratio.

The purpose of the cadmium wrapped around the fuel rods was to suppress fissions in the lattices. We now believe that such a precaution was not sufficient; the fast fission effect and the fraction of fissions in U^{235} produced above the 0.4 electron volt cadmium cutoff probably caused the measurements to be wrong. The effect of epi-cadmium fissions would have been to spread out the source supplying the neutrons measured at the indium resonance, and this in turn would have led to values of τ_{th} which were too high.

As mentioned before, the primary purpose of the exponential experiments was to show if it were possible to make a chain reacting system with natural uranium rods and light water. It appeared from the results that it might indeed be possible to do so, if suitable annular air gaps were placed about the fuel rods. However, it seemed unlikely that even tricks of this sort could provide enough excess reactivity to overcome the xenon poisoning which would exist in a high flux reactor.

It was pointed out in the final report on the Oak Ridge experiments that a very small increase in enrichment of the U^{235} content of the uranium used would make a reactor moderated with light water feasible. It was this point which later prompted the Brookhaven program of exponential experiments with light water and slightly enriched uranium rods.

BROOKHAVEN MEASUREMENTS WITH 0.750-IN. DIAMETER, 1.027% ENRICHED URANIUM RODS

The first series of Brookhaven exponential experiments was done with approximately 1.8 tons of uranium, enriched to 1.027 ±0.001% U^{235} by weight

Table II. Neutron Age from Fission to Thermal Energies. From 1944–45 Oak Ridge Experiments

Rod diameter (in.)	Air gap (in.)	Volume water / Volume uranium	τ_{th} (cm^2) at 25°C
1.18	None	1.14	54.7
1.18	None	3.27	39.9
1.18	None	0.273	131.0
1.18	None	1.78	44.0
1.18	None	1.36	51.7
1.18	None	3.17	40.1
1.10	None	2.06	44.9
1.10	None	1.57	49.2
1.10	None	1.42	51.0
1.10	0.45	1.92	94.5
1.10	0.45	1.56	112.0
0.787	None	1.80	48.4
0.787	None	1.50	51.5
0.787	None	2.10	46.5
0.787	0.354	2.01	110.0

(95.16 atoms U^{238} per atom of U^{235}). The metal was fabricated into 0.750 ±0.001-in. diameter cylindrical rods, four feet long. These were straightened to within 0.015-in. lateral deviation in the four-foot length; they were then clad with 0.030 in. of aluminum, drawn on to ensure a tight fit. Each end of the tubing was capped with an aluminum plug, to provide a water-tight containment of the uranium.

The experiments were carried out in a water tank placed over a thermal column which occupies a portion of the top of the Brookhaven pile shield. This thermal column is made of five one-foot-thick layers of graphite, each slightly wider than the one below. The stepped design prevents fast neutron leakage up the sides of the thermal column, and the well-machined surfaces of the graphite blocks which make up the structure give a void-free construction which ensures a well-moderated source of neutrons at the top surface. The cadmium ratio of this source as measured with 0.005-in. thick indium foils is better than 10^5.

The water tank is cylindrical, six feet in diameter and six feet high. Surrounding it is a crude radiation shield made of steel plates and heavy concrete.

Figure 4 shows the structure which was used to support and position the uranium rods. The top of this structure was a steel ring, inside the hole in the center of which was inserted a 1.5-in. thick aluminum disc, with holes drilled in it to space the uranium rods for the water-to-uranium volume ratio desired. A similar disc was put at the bottom of the support structure, so that the spacing between rods was maintained at both ends. The top and bottom spacing elements were separated by an aluminum cylinder, perforated so that water could get in and out freely. Since the fuel rods were suspended from the top fuel rod locating plate, the whole structure could be removed from the water tank as a unit. This feature permitted assembling the experiments remotely, and then transferring the loaded lattice by crane to the water tank.

Distilled water was used as the moderator. There were occasional spectroscopic tests of the purity, and there were frequent tests of reproducibility of the data. During a large part of the experiments the water contained large amounts of boric acid (for migration area measurements). Sheets of cadmium were inserted to suppress fissions when measurements were not being done. Because of the possibility that boron or cadmium might plate onto the fuel rods, reproducibility was sought and maintained throughout the experiment.

The radius of a loaded lattice was at most about 40 centimeters, whereas the radius of the water tank was about 90 centimeters. Thus the experiments were done with an effectively infinite water reflector. This had the effect of making the 1.8 tons of uranium equivalent to about 1.4 times the mass in an unreflected experiment.

Altogether six volume ratios of water-to-uranium were assembled. There were measurements of the buckling B^2, the migration area M^2, the fast effect and the thermal utilization f.

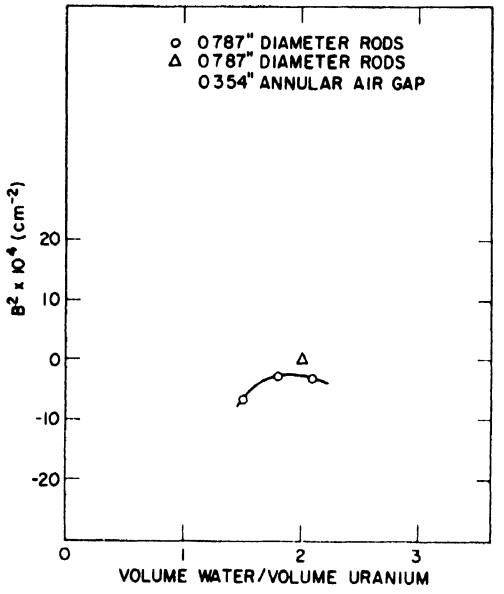

Figure 2. B^2 vs volume ratio, 0.787 inch diameter natural uranium rods in light water. From 1944–45 Oak Ridge experiments

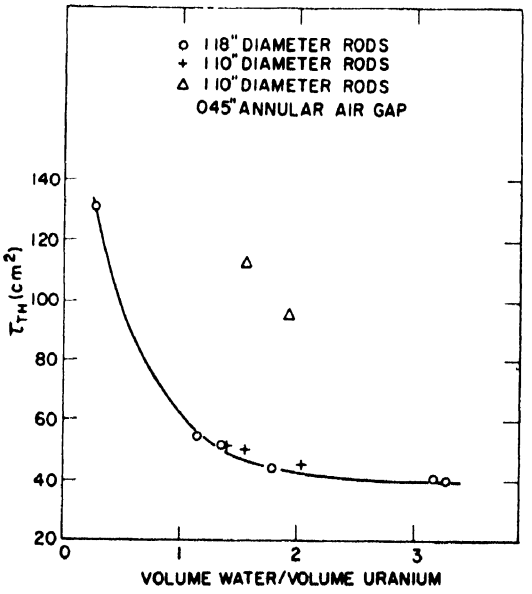

Figure 3. τ_{th} vs volume ratio, 1.10 inch and 1.18 inch diameter natural uranium rods in light water. From 1944–45 Oak Ridge experiments

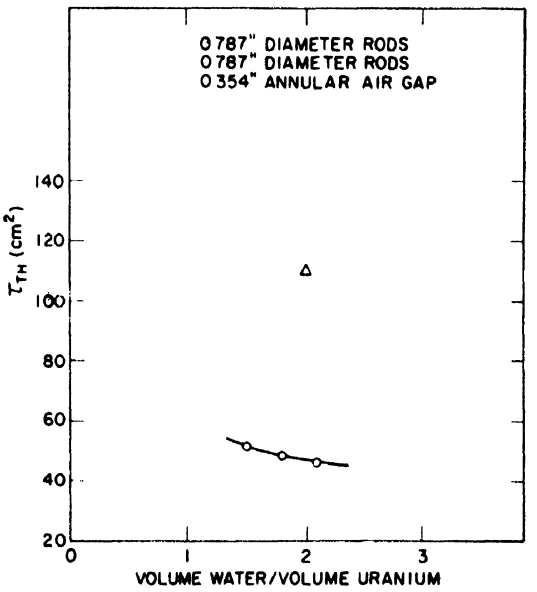

Figure 3a. τ_{th} vs volume ratio, 0.787 inch (2.00 cm) diameter natural uranium rods in light water. From 1944–45 Oak Ridge experiments

Buckling

In an exponential experiment the buckling is usually found from differentiation of the measured thermal neutron flux distribution. For a cylindrical array such as was used here, the space dependence of the flux can be written as a series of Bessel functions:

$$\varphi = \sum_{n=1}^{\infty} J_0\left(a_n \frac{r}{R+\lambda}\right) f_n(z) \qquad (2)$$

where r and z are cylindrical coordinates in the lattice, λ is the reflector savings, R is the loaded radius, and a_n are the successive roots of

$$J_0(r) = 0 \qquad (3)$$

The coefficients $f_n(z)$ have the form

$$f_n = C_n \exp\left[\left\{\left(\frac{a_n}{R+\lambda}\right)^2 - B^2\right\}^{1/2} s\right] + D_n \exp\left[-\left\{\left(\frac{a_n}{R+\lambda}\right)^2 - B^2\right\}^{1/2} s\right] \qquad (4)$$

C_n is small compared with D_n, since the first term is only important near the upper boundary of the lattice. Furthermore, the rates of decay of the harmonics ($n > 1$) are greater than those of the fundamental, and so above some value $s = z'$ the flux can be represented accurately by the fundamental alone:

$$\varphi \sim A_1 J_0\left(a_1 \frac{r}{R+\lambda}\right) f_1(z), \; z > z' \qquad (5)$$

Ordinarily, one would measure the radial and axial flux distributions in the region of validity of Equation 5. The radial distribution would be fitted to $J_0(a_1 r/r_0)$, the axial distribution would be fitted to $C_1 \exp[z/L] + D_1 \exp[-z/L]$, and the buckling would be obtained as

$$B^2 = \left(\frac{a_1}{r_0}\right)^2 - \frac{1}{L^2} \qquad (6)$$

However, the number of fuel rods used in these experiments did not permit accurate measurements of the radial flux distribution. Symmetry conditions made only five positions available for flux measurements along any one radius, and the outermost of these was so near the water reflector as to make it useless. Thus only four points were available along any one radius, and these were not enough to provide any real accuracy.

On the other hand, the axial flux distributions showed in every case the behavior of the presence of the fundamental only, above about 10 cm above the bottom of the lattice. Moreover, corrections for the effect of the top boundary (the first term of Equation 4) were small below about 70 cm from the top of the lattice. Thus there was a region of about 60 cm in z over which the flux was well represented by an exponential, and so good values of L could be determined. It was therefore decided to base evaluation of B^2 on measurements of L alone.

To determine B^2 this way, one would measure L for a wide range of rod loadings. Each such loading would be idealized as a cylinder having a radius R defined by

$$R = b\sqrt{N} \qquad (7)$$

N being the number of rods loaded, and πb^2 being the area of a single lattice cell. Least squares fits would then be made to λ and B^2 in the expression

$$L = \left\{\left(\frac{a_1}{R+\lambda}\right)^2 - B^2\right\}^{-1/2} \qquad (8)$$

Such an analysis contains an implicit assumption that λ and B^2 have the same value for all pairs of values of L and R. This method of finding B^2 had never been used before, and so there remained some doubt as to the validity of the assumption just mentioned. A conclusive test could have been provided by the performance of a few critical assemblies, but these could not be done because the amount of uranium fabricated was not sufficient. Thus the accuracy of the method was not confirmed until later, when measurements were performed with a slightly higher enrichment of fuel.

The measurements of neutron flux distributions were made with indium foils, 0.220 in. in diameter and 0.005 in. thick. These were placed in foil-holding rods inserted through the top fuel-locating plate. At first the foil rods used were thin-walled aluminum tubes, with slots punched out at 10 cm intervals. The foils were placed between aluminum covers, and then wedged in the slots. Later the aluminum tubes were replaced with solid plastic (methyl methacrylate) rods, having in them machined depressions for holding the indium foils. This kind of foil rod could be constructed much more accurately than the former, and except for a high replacement rate because of breakage, it proved much more satisfactory.

Because of the large local variation of flux, the foils had to be centered accurately in lattice cells. This was accomplished by the use of plastic spacers located at 30 cm intervals throughout the height of the assembly.

A careful analysis was made of foil-counting in-

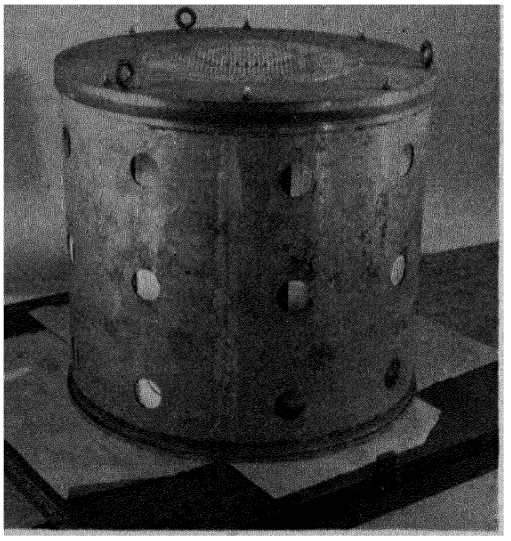

Figure 4. Brookhaven exponential experiment assembly

accuracies; these included both random and systematic errors from foil counting methods, the statistics of foil counting, the weight variations of the foils, and the uncertainties in separating foils during exposure to the neutron flux. According to this analysis, the predicted uncertainties in individual foil counts were at most about 1.5 per cent. The observed standard deviations showed slightly less error than this.

All values of the relaxation lengths were obtained from least-squares fits of exponentials to the observed axial flux variations.

Values of B^2 were found for water-to-uranium volume ratios 1.334, 1.584, 1.834, 2.334, 2.834, and 3.834. In each case the volume ratio given was that of the actual volume of water to that of uranium, the aluminum being ignored. The experimentally determined values of B^2 and λ are given in Table III, and are plotted in Figs. 5 and 6. The experimental errors included are derived from the standard deviations of the least squares fits which were made; thus they may not include some systematic errors.

Table III. Experimental Values of Buckling and Reflector Savings, 0.750-in. Diameter Rods of 1.027% Enriched Uranium in Light Water

$\frac{\text{Volume water}}{\text{Volume uranium}}$	B^2 ($cm^{-2} \times 10^4$)	λ (cm)
1.334	28.9 ± 0.5	7.71 ± 0.14
1.584	34.7 ± 0.3	7.16 ± 0.10
1.834	37.5 ± 0.8	6.94 ± 0.23
2.334	36.7 ± 0.5	6.90 ± 0.16
2.834	32.9 ± 0.2	6.94 ± 0.11
3.834	18.6 ± 0.6	6.42 ± 0.22

Figure 5 has the characteristic shape of a buckling curve for a thermal reactor. Heating these lattices would expel water, and hence decrease the water-to-uranium volume ratio. Therefore one would expect a zero temperature coefficient near the peak of the buckling curve, with a negative coefficient at lower volume ratios and a positive coefficient for higher volume ratios. For these lattices the peak is at a volume ratio of about 2, and the safe design region is below this point.

If the slowing-down and diffusion of neutrons does not take place isotropically in a reactor core, the interpretation of associated exponential experiments must be modified accordingly. The effect has been considered by G. Young and J. Wheeler; they showed that if the anisotropy is large, it is possible to draw grossly inaccurate conclusions from a simple exponential experiment.

As will be seen later, the experimental values of the migration area are nearly constant over the range of volume ratios studied, and are not very different from the value of M^2 for fission neutrons in pure water. Thus it appears that because of large inelastic scattering, uranium in water can be considered to be very nearly equivalent for neutron slowing-down to the water displaced. This feature would make the existence of anisotropy very unlikely. Nevertheless, it appeared worth-while to determine the effects of whatever non-isotropic processes do occur.

The anisotropy measurement which was performed was originally suggested by E. P. Wigner. Its principle can be illustrated by considering a subcritical lattice in the shape of a parallelepiped, with edges $l_x = l_y; l_z$. The fuel elements are assumed to be parallel to the z axis. If the thermal neutron source activating this assembly is placed at one end of the lattice (with edges l_x and l_y), the one-group critical equation is

$$k_\infty - 1 = M_\perp^2(B_x^2 + B_y^2) - M_\parallel^2 B_z^2 \qquad (9)$$

$M_\perp^2$ and $M_\parallel^2$ have physical meaning associated with the mean square distance a fission neutron travels in directions perpendicular to and parallel to the rods, respectively. B_x^2 and B_y^2 are defined by

$$B_x^2 = B_y^2 = \frac{\pi^2}{(l_x/2 + \lambda)^2} \qquad (10)$$

and

$$B_z^2 = 1/L^2 \qquad (11)$$

where L is the relaxation-length for decay of the fundamental in the z direction.

If, on the other hand, the source is placed on one of the sides of the lattice (that defined by y and z), in place of Equation 9 one would have

$$k_\infty - 1 = M_\parallel^2 b_z^2 + M_\perp^2(b_y^2 - b_x^2) \qquad (12)$$

where

$$b_z^2 = \frac{\pi^2}{(l_z/2 + \lambda)^2} \qquad (13)$$

$$b_y^2 = B_y^2 \qquad (14)$$

$$b_x^2 = 1/(L')^2 \qquad (15)$$

L' is now the relaxation length of the fundamental in the x-direction. From Equations 9 and 12,

$$M_\perp^2 M_\parallel^2 = \frac{B_z^2 + b_z^2}{B_x^2 + b_x^2} \qquad (16)$$

A "double lattice" measurement of this sort was carried out with the 1.334 volume ratio lattice, with the result

$$M_\perp^2/M_\parallel^2 = 1.039 \pm 0.028 \qquad (17)$$

Thus the anisotropy found is just outside the error limits of the experiment. It was therefore neglected.

Migration Area

The measurements of M^2 were based on its definition by the critical equation; for reasons to be discussed in connection with later measurements, this was taken to have the form

$$k_\infty = \exp[M^2 B^2] \qquad (18)$$

Since the assemblies studied were heterogeneous, k_∞ could also be expressed through the four-factor formula

$$k_\infty = \epsilon p f \eta \qquad (19)$$

Thus from equating Equations 18 and 19,

$$\epsilon p f \eta = \exp[M^2 B^2] \qquad (20)$$

Table IV. Experimental Values of Migration Areas for 1.027% Enriched, 0.750-in. Diameter Uranium Rods in Light Water

$\frac{\text{Volume water}}{\text{Volume uranium}}$	M^2 (cm^2)
1.334	28.9 ± 1.7
1.834	28 2 ± 1 2
2.834	27.4 ± 0 4
3.834	27.5 ± 1.1

The measurement consisted in dissolving boric acid in the moderator water, and measuring the effect of this neutron poison on the buckling. Aside from B^2, the only other quantity in Equation 20 which would be affected appreciably by the additional neutron absorber is f; M^2 would also be decreased to some extent through the change in diffusion length, but it can be shown that within the error of the measurements, this effect can be neglected.

Thus as successively increasing amounts of boron were added to the moderator water, the value of f and B^2 changed together so as to maintain the correctness of Equation 20. At each boron concentration, B^2 was measured by the method discussed above. Also, the boron concentrations were measured, and the thermal utilizations were calculated.† M^2 could then be determined as the slope of the straight-line plot of B^2 against $\ln f$.

The best straight-line fits of B^2 vs $\ln f$ were obtained by the method of least squares. The values of the migration area so obtained are given in Table IV, and are plotted in Fig. 7. The measurement was carried out for four of the six volume ratios studied.

A comparison of Fig. 7 with Figs. 3 and 4, results of Oak Ridge measurements of τ_{th}, shows striking differences. The Brookhaven values are smaller at all volume ratios; furthermore, they do not show the rapid increase at smaller volume ratios which was seen in the Oak Ridge measurements. Further Brookhaven experiments with smaller rods (discussed later in this paper) tend to substantiate the low values of M^2, and they are believed to be correct.

Several causes could have contributed to the high values seen in the course of the Oak Ridge experiments. One of these, mentioned earlier is that the measurements depended on complete suppression of fissions by the cadmium sheathing of the rods. Actually, the cadmium could only have eliminated fissions caused by neutrons with energies below about 0.4 electron volts, and could not have noticeably influenced neutrons with higher energies. Experiments not discussed here indicate that the fraction of fissions caused by neutrons with energies above the cadmium cut-off rises from about 0.11 at a volume ratio of 4 to about 0.38 at a volume ratio of 1. Thus the cadmium used at Oak Ridge could not have performed its function. The effect of epithermally induced fissions would have tended to smear out the neutron source, thus invalidating the experiment. As the volume ratio decreased, the per cent of disturbing epithermal fissions increased; therefore the Oak Ridge values of migration areas must be considered to be least reliable at small volume ratios, where they do indeed differ most from the Brookhaven values.

Another point which must be considered is that the quantity sought in the Oak Ridge measurements was defined by Equation 1; the quantity derived from Brookhaven measurements was defined by Equation 20. According to elementary homogeneous reactor theory, these two definitions should be equivalent, but there seems to be no good reason why they may not be somewhat different for a heterogeneous pile.

The difference between Brookhaven and Oak Ridge results is discussed also by J. Chernick, in another paper in these proceedings.[2] There both sets of measurements are considered in the light of recent calcula-

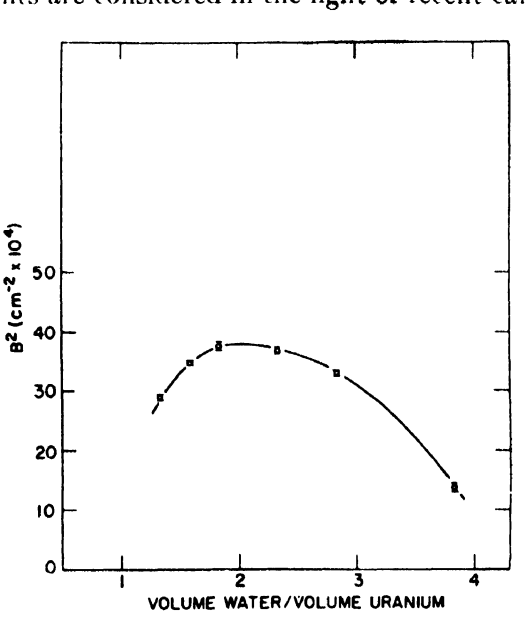

Figure 5. Experimental values of buckling for 0.750 inch diameter, 1.027% enriched uranium rods in light water

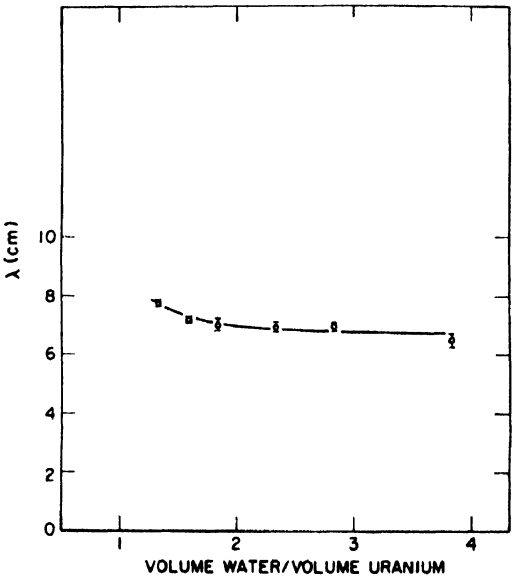

Figure 6. Experimental values of reflector savings for 0.750 inch diameter, 1.027% enriched uranium in light water

† Calculations by K. Puechl, Walter Kidde Nuclear Laboratory, using diffusion theory plus a correction for the P_3 content of the flux.

tions of the slowing down of neutrons in uranium-water lattices, and the conclusion is reached that the Brookhaven results compare reasonably well with computations using a reasonable value for the inelastic scattering cross section of uranium. The Brookhaven results also seem reasonable in the light of the most recent calculations of neutron slowing-down and diffusion in pure water.[3]

Fast Effect

Values of ϵ were measured for two of the lattices: those with the volume ratios 1.334 and 3.834. The method resembles one used by D. L. Hill at Los Alamos, in 1944.

The measurement consisted in finding the ratio of U^{238} fissions to U^{235} fissions in a typical fuel rod. The following simple analysis will show how this quantity, which we shall call F, is related to the fast effect.

ϵ is defined to be the number of neutrons slowing down past the U^{238} fission threshold, per neutron from thermal fission. Since it can be shown that the U^{235} fissions in the fast fission region are negligible, an equivalent definition is: ϵ is the number of neutrons slowing down past the U^{238} fission threshold, per neutron from U^{235} fission. Thus

$$\epsilon = (1 - n - r) + n\nu_{28}(1 - n - r) + n^2\nu_{28}^2(1 - n - r) + \cdots = \frac{(1 - n - r)}{1 - n\nu_{28}} \quad (21)$$

where n is the probability that an average fission neutron will cause fission in U^{238}, r is the probability that a fission neutron will be lost to other processes (radiative capture, fast neutron leakage, etc.) before slowing down past the U^{238} fission threshold, and ν_{28} is the average number of neutrons per U^{238} fission.‡

On the other hand, the number U^{238} fissions per neutron from thermal fission is

$$n + n^2\nu_{28} + n^3\nu_{28}^2 = \frac{n}{1 - n\nu_{28}} \quad (22)$$

and the number of thermal fissions on the same basis is of course

$$1/\nu_{25} \quad (23)$$

where ν_{25} is the number of neutrons per U^{235} fission. Thus the number of fast fissions per U^{235} fission is the ratio of Equation 22 to Equation 23; this is

$$F = \frac{n\nu_{25}}{1 - n_{28}} \quad (24)$$

(F is the quantity to be measured; it was mentioned above.)

If fast neutron leakage is neglected, one can write

$$r = \alpha n \quad (25)$$

where α is the neutron capture-to-fission ratio, averaged over the fission neutron spectrum and the U^{238} fission cross section. Then from (21), (24), and (26),

$$\epsilon - 1 = F\frac{\nu_{28} - 1 - \alpha}{\nu_{25}} \quad (26)$$

At the present time, the value of ν_{28} is somewhat uncertain. Old Los Alamos measurements by J. M. Blair and A. O. Hanson give

$$\frac{\nu_{28}}{\nu_{25}} = 0.983 \pm 0.55 \quad (27)$$

Recently there have been developments placing this result in doubt, and the experiment is being redone by J. L. Fowler at Oak Ridge and J. Terrell at Los Alamos. For the purpose of this analysis it has been assumed that

$$\nu_{28} = \nu_{25} = 2.5 \quad (28)$$

If, however, ν_{28} is noticeably different from this value, the deduced values of ϵ will be changed appreciably.

Since fast fissions in U^{238} are produced by neutrons which have nearly the energy with which they in turn were produced,

$$\alpha = \frac{\int_{E_0}^{\infty} dEN(E)\sigma_\gamma^{28}(E)}{\int_{E_0}^{\infty} dEN(E)\sigma_f^{28}(E)} \quad (29)$$

with $N(E)$ the fission neutron spectrum, σ^{28} the radiative capture cross-section, and E_0 the U^{238} fission threshold. All radiative capture below the U^{238} threshold is thus considered as part of the resonance capture.

Numerical integration of Equation 29 leads to

$$\alpha = 0.107 \quad (30)$$

Then from Equations 26, 28, and 30

$$\epsilon - 1 = 0.557F \quad (31)$$

The evaluation of ϵ rests on Equation 31, which still contains an uncertain value of ν_{28}.

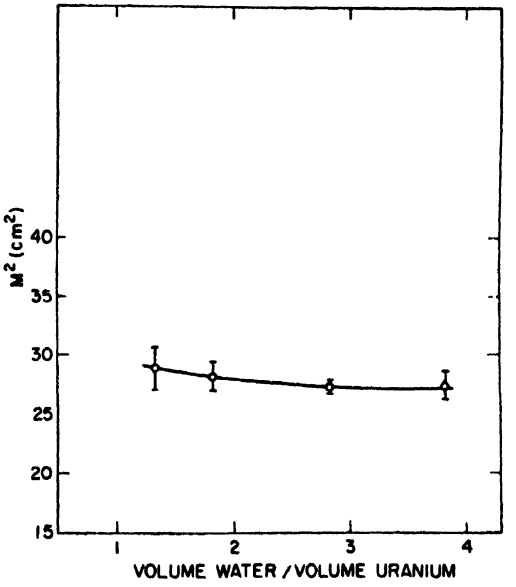

Figure 7. Experimental migration areas of lattices of 0.750 inch diameter, 1.027% enriched uranium in light water

‡ The abbreviation 28 dates back to the Manhattan Project. At that time it was customary to represent a nucleus of a fissioning species by a two-digit number, the first of which was the last digit of the atomic number and the last of which was the last digit of the atomic weight. Thus 28 is the element with atomic number 92 and atomic weight 238.

In these experiments, F was determined in the following way. A fuel rod was cut cross-wise into sections, and between these were placed sandwiches of aluminum and uranium foils. The aluminum foils served to capture fission products from the uranium, and the activities of these fission products led to a measure of the fission density in the uranium.

Two such sandwiches were used per measurement of ϵ. One consisted of three layers of 0.0007-in. thick aluminum on each side of a depleted uranium foil, this entire sandwich being compressed between two sections of the fuel rod. The depleted uranium foil contained only 7×10^{-6} parts of U^{235} per part of U^{238}. In the neutron flux of the exponential experiments, the U^{235} fission rate in the foil was less than 1% of the U^{238} fission rate; accordingly any fissions occurring in it could be attributed to U^{238} alone. The second foil sandwich was precisely the same as the first, except that the depleted uranium was replaced by an aluminum foil, 0.005 in. thick. The two sandwiches were separated by a section of uranium rod two in. long. The experimental arrangement of fuel rod and aluminum and uranium foils is shown in Fig. 8.

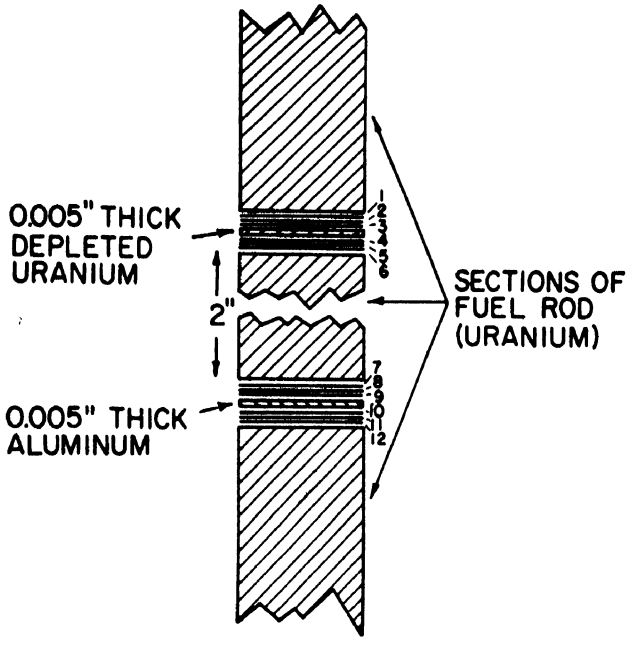

Figure 8. Schematic arrangement of fuel rod and uranium and aluminum foil used to measure fast effect

It was assumed that the fission densities in the section of fuel rod used were the same as if the uranium had not been cut and the foil sandwiches inserted. Actually, the foil sandwiches constituted a low absorption region through which thermal neutrons could stream; this effect increased the thermal fission rates locally. A simple calculation showed that this streaming could have altered the measured values of ϵ by at most about 0.01%; thus the effect was not observable.

The fuel rod used was inserted in a water-tight aluminum tube with 0.755-in. inner diameter and 0.785-in. outer diameter, and was put in the center of an exponential lattice, replacing a standard uranium rod. The entire lattice was then exposed to the neutron source for a period of about eighteen hours. At the end of this time the rod was removed, and the activities of the foils designated in Fig. 8 as 1, 3, 4, 6, 7, 9, 10, and 12 were determined with end-window β-ray counters.

In a measurement of this sort, the fission product activities of foils 1, 6, 7, and 12 are proportional to the local fission density in the fuel rod. The fission product activities of foils 3 and 4 are proportional to the fission density in the depleted uranium foil. The 0.0007-in. thick aluminum foils used here are commonly called "catcher foils." Since the range of fission products in aluminum is approximately 0.0004 in.,[5] one catcher is sufficient to stop the fission products emitted by the uranium with which it is in contact.

The activities of foils 9 and 10 give the background which must be subtracted from all other foil count rates. These decay rates are caused by the thermal activation of impurities, and by n, $2n$ and n, α reactions in the aluminum. Actually, the two foil sandwiches were not located at the same height in the lattice, and so were not exposed to the same neutron flux levels. Therefore before the background correction given by foils 9 and 10 could be applied, it had to be multiplied by the ratio of flux densities at the heights of the two sandwiches.

The determination of F from the foil-counting was carried out as follows. Catcher foils 1, 3, 4, 6, 9, and 10 were counted simultaneously, being rotated about among the counters so that each foil was counted the same number of times in each counter. At the same time, foils 7 and 12 were counted in a separate pair of counters, giving a decay curve for the fission products. This curve was used to correct the activities of the catcher foils back to the beginning of the foil-counting, called time $t = 0$. (Normally foil-counting began 30 minutes after the end of the exposure in the exponential lattice; this permitted the short-lived activity from radiative capture in the aluminum to die out.)

The backgrounds as determined from foils 9 and 10 were subtracted from the catcher foil activities, and the activities of foils 1, 3, 4, and 6 were corrected to $t = 0$ by means of the decay curve measured with foils 7 and 12. The corrected activities for each foil were then summed for all counters. Finally, these sums were added for foils 1 and 6 to obtain a quantity proportional to the fission density in the fuel rod, and were summed for foils 3 and 4 to get a number proportional to the fission density in the depleted uranium. This latter number when corrected for the slightly different atomic densities in the depleted uranium and the fuel rod was proportional to the fission density in U^{238} in the rod. Thus

$$f_{25} = C_1(R_1 - R_2) \qquad (32)$$
$$f_{28} = C_2 R_2$$

where R_1 and R_2 are respectively the final corrected decay rates for foils 1, 6, and for foils 3, 4, the latter corrected for U^{238} density. f_{25} and f_{28} are respectively the fission densities locally in the U^{235} and the U^{238} in the fuel rod. C_1 and C_2 are constants of proportionality, which would be equal except that the decay

curves of fission products from U^{238} and U^{235} are not precisely the same. Then from Equation 32,

$$\frac{f_{28}}{f_{25}} = F = K\frac{R_2}{R_1 - R_2} \tag{33}$$

with

$$K = C_2/C_1 \tag{34}$$

The quantity K depends upon the exposure time, and the period of time during which counting took place. A separate calibration experiment was necessary to determine it.

A "double" fission chamber was constructed, having the design shown in Fig. 9. The cathode of each half of the chamber had on it a carefully weighed amount of uranyl nitrate, deposited in solution and then dried. One cathode was sensitized with a sample of the depleted uranium used in the fast effect measurements; the other had natural uranium. In each case the layer of uranyl nitrate was thin compared with the path length of fission products, so that each fission on a cathode led to a count in its half of the chamber.

A sandwich of aluminum catcher foils with depleted and normal uranium foils was placed in the chamber; the arrangement of this sandwich is shown in Fig. 10.

The chamber was then exposed to a mixture of fast and thermal neutrons of approximately the same character as that observed in one of the exponential assemblies. The fission rates in the two halves of the fission chamber were recorded, and the catcher foils were afterwards removed and counted in the same way as for a fast effect measurement. The ratio of observed count rates led to the ratio of U^{235} fission rates to U^{238} fission rates in the flux used, and the catcher foil activities led to the ratio of associated decay rates.

The equivalence of the two halves of the fission chamber was tested by interchanging the cathodes.

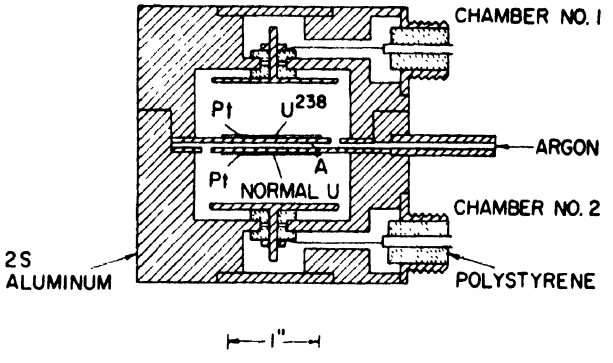

Figure 9. Fission chamber used for fast effect calibration experiment

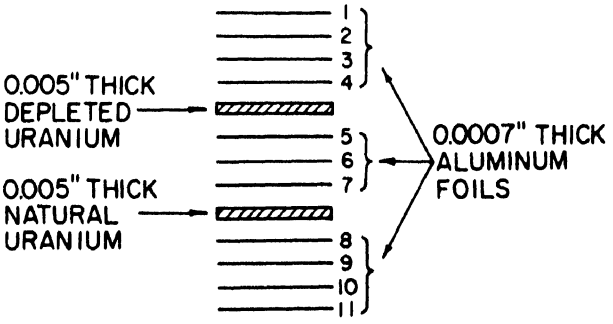

Figure 10. Schematic of uranium-aluminum sandwich used in fast-effect calibration experiment

The subsequent change in ratio of count rates was 0.3%, which was below the probable error from the counting statistics.

As a result of this calibration experiment, it was determined that for the exposure times and counters used,

$$K = 1.06 \pm 0.01 \tag{35}$$

Then from combining Equations 31, 33, 35,

$$\epsilon - 1 = 0.590\frac{R_2}{R_1 - R_2} \tag{36}$$

The values of ϵ determined in these experiments were:

$\frac{Vol.\ water}{Vol.\ uranium}$	ϵ
1.334	1.081 ± 0.005
3.834	1.051 ± 0.004

The probable error includes only counting statistics, and not the uncertainty in ν_{28}.

These values should be compared with a measurement of ϵ for a single 0.750-in. diameter uranium rod, exposed in the reflector of the Brookhaven graphite pile. There it was found that $\epsilon = 1.019 \pm 0.003$. It is apparent that the interaction fast-effect, caused by high energy neutrons from neighboring rods, is considerably greater than that of a single rod. This feature is of course directly caused by the extremely close spacing of fuel rods which the use of a light water moderator demands.

The existence of abnormally large values of ϵ in water, uranium rod lattices was predicted at an early stage in the Manhattan Project by L. Szilard.

Thermal Utilization

The values of the migration area reported earlier were obtained with calculated values of f.[2] Since there was some question about the theoretical methods used to obtain these, a direct measurement of the thermal utilization seemed useful. These measurements were also motivated, of course, by the desire to test experimentally the methods used to calculate k_∞ through the four-factor formula.

The method used was the direct one of determining the thermal neutron flux distribution in a single lattice cell, both in the fuel rod and the moderator water. The flux curves in the water and the uranium were then used to provide the respective flux averages $\bar{\varphi}_w$ and $\bar{\varphi}_u$; the thermal utilization was finally derived as

$$f = \frac{\Sigma_u{}^a\bar{\varphi}_u}{\Sigma_u{}^a\bar{\varphi}_u + \Sigma_w{}^a\bar{\varphi}_w} \tag{37}$$

with $\Sigma_u{}^a$ and $\Sigma_w{}^a$ the respective macroscopic absorption cross sections of uranium and water, averaged over a Maxwell energy distribution with the most probable velocity 2200 m/sec. The values of f obtained this way were uncertain by an amount depending on the cross-sections used, and incidentally on the mean neutron temperature. The influence of neutron temperature is however only very slight.

The flux distributions were found with foils about 1.5 millimeters in diameter and 0.25 millimeters thick,

and consisting of methyl methacrylate plastic and dysprosium oxide. The foils were punched out of a small sheet made in a hot press from a powder mixture of the two substances. Dysprosium was considered an ideal detector, because it makes cadmium difference measurements unnecessary. In fact, the cadmium ratio of a dysprosium foil in the water lattice was greater than 100.

To find the flux distribution in the uranium, it was necessary in effect to imbed the foils in a fuel rod. This was accomplished by cutting a rod in two crosswise, and machining small holes in one of the surfaces so exposed. With foils placed in these holes, the rod was then put back together and placed in the neutron flux in the exponential assembly.

The foils in the water were placed in a piece of methyl methacrylate inserted horizontally into the lattice. The two sets of detectors (in the water and in the uranium) were not placed at the same elevation. However, the difference in height was measured to within 0.1 mm and the known relaxation length for the vertical decay of the neutron flux was used to correct for the error so introduced. The undertainty produced by this correction was at most about 0.2%, and was therefore neglected.

Each foil used was counted to high statistics in each of six end-window β-ray counters. The relative activity was then obtained by summing over the observed activities (corrected for decay, etc.); thus there was no need to intercalibrate counters.

In all, six complete intracell flux traverse measurements were done; one in the 1.334, one in the 1.834, two in the 2.834, and two in the 3.834 volume ratio lattices. The experimental values of f so obtained are given in Table V; they are also plotted in Fig. 11.

Figure 11 also shows for comparison the curve of thermal utilization vs volume ratio. This theoretical curve was obtained by a diffusion theory calculation, modified for the P^3 content of the angular flux distribution. It will be observed that the theoretical curve is consistently higher than the experimental values. This feature can also be seen in terms of the actual flux distributions measured in the fuel and the moderator. The measured flux dip in the fuel was considerably greater than the calculated dip, and the measured flux rise in the moderator was considerably higher than was calculated.

Both the measurements and the calculations are still in doubt here, for reasons which will be discussed in the section on 0.600-in. diameter rods.

Table V. Experimental Values of Thermal Utilization, 0.750-in. Diameter, 1.027% Enriched Uranium Rods in Light Water

$\frac{\text{Volume water}}{\text{Volume uranium}}$	f
1.334	0.910
1.834	0.871
2.834	0.819
3.834	0.755

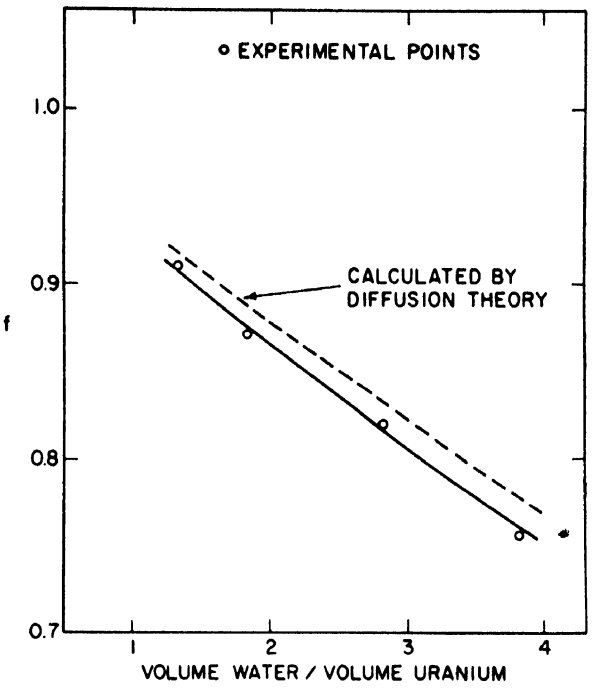

Figure 11. Thermal utilization of 0.750+ inch diameter, 1.027% enriched uranium rods in light water

Also in the section on 0.600-in. diameter rods there will be given reasons for believing that the migration area analysis using calculated values of f is in any case correct. Therefore the values of M^2 in Table IV and Fig. 7 are considered to be reliable.

BROOKHAVEN MEASUREMENTS WITH 0.600-IN. DIAMETER RODS

After the completion at Brookhaven of the exponential experiments with 0.750-in. diameter rods, just discussed, a somewhat expanded program of water moderated lattice studies was begun. This work is still under way. It involves the assembling of forty-five different lattices with all combinations of the following variables:

Rod diameter: 0.600, 0.387, 0.250 in.
Uranium enrichment: 1.299%, 1.143%, 1.027% (by weight)
$\frac{\text{Volume water}}{\text{Volume uranium}}$: 1, 1.5, 2, 3, 4

For each lattice, measurements are being made of the buckling, the migration area, the thermal utilization and the fast effect. In addition, there are some measurements of the neutron temperature and the epithermal fission fraction, and the resonance escape probability is being studied (as yet with no reliable results).

This extended program of water-uranium lattice studies has been prompted by a growing interest in the usefulness of the system for producing electrical power. In particular, the Pressurized Water Reactor under construction by the Westinghouse Atomic Power Division, to be the first large scale American nuclear power plant, is to have a design somewhat similar to that studied in the Brookhaven experiments. This fact has led to complementary programs of

experiments by the Brookhaven and Westinghouse groups, with the same fuel rods being used in turn by the two organizations at their respective sites. A discussion of the Westinghouse experiments[6] is given elsewhere in these proceedings.

Buckling

In addition to simply obtaining values of B^2, it was considered advisable to devote a fraction of the reactivity measurements to a study of the validity of the way of measuring the buckling discussed earlier. The major point in question was the assumed constancy of B^2 and λ over a wide range of numbers of fuel rods loaded. Two-group calculations by K. Puechl and a similar but more extensive study by J. Chernick indicated that the reflector savings should decrease slightly with increasing radius of core loading; this effect would cause the values of B^2 derived from the experiments to be about 3% too low.

The experimental study of the validity of the method was undertaken in four separate ways. First, the number of fuel rod loadings at which relaxation lengths were measured was increased. This permitted separate evaluations of B^2 and λ from experiments relatively near to and relatively far from critical. Thus it could be seen whether the measurement method was internally consistent in predicting the same critical masses at very different levels of reactivity. Second, a way of carrying out the more usual form of exponential experiment was found. In other words, the radial and axial buckling were found from measurements of the radial and axial flux distributions at a single high value of fuel rod loadings. One lattice (1.143% enriched, 1.5 volume ratio) was subjected to measurements of B^2 and λ by both methods. Third, a lattice whose critical mass was found by the method in question was loaded to a moderately high reactivity and the critical mass was found from an extrapolation of the observed multiplication of the spontaneous fission neutrons. Fourth, lattices measured by all these methods were taken to critical by the Westinghouse group. As a result of these four separate tests, the procedure for measuring buckling which has been discussed in connection with the 0.750-inch diameter rod lattices was shown to lead to remarkably good results.

For purposes of simplifying, the procedure discussed earlier will be called method I. To recapitulate, it consists in measuring the relaxation length L for several values of the loaded core radius R, and fitting this observed variation of L with R to a single pair of values of B^2 and λ. The procedure of finding B^2 and λ from radial and axial flux traverses will be called method II.

Method I was used to find the buckling and reflector savings of nine of the fifteen assemblies with 0.600-in. diameter rods. With each lattice, values of the vertical relaxation length were found for twenty-two different core radii. The buckling and reflector savings were determined from the top eleven and bottom eleven loadings separately, and then from all twenty-two relaxation lengths taken together.

All relaxation length measurements, except those for the 1:1 water-to-uranium volume ratio, 1.143% enrichment lattice, were made with indium foils, 0.220 in. in diameter and 0.005 in. thick. These foils were centered in a lattice cell, and oriented vertically so as to equalize the fluxes incident on opposite faces.

The foil holders were small rods of methyl methacrylate plastic, with holes milled in to contain the foils. Tight-fitting plastic plugs were inserted in the holes over the foils, keeping them secure.

The lattices with equal volumes of uranium and water were so compact that there was not enough room between fuel rods to insert the foil-holder rod. With the 1:1, 1.299% enrichment lattice, a fuel channel was therefore left empty, and the foil rod was inserted in this position. The effect of omitting the rod was then determined separately, and the actual loading was corrected to an effective one.

The same lattice with 1.143% enriched rod was treated somewhat differently. The foils used in the relaxation length measurement were exposed in a fuel rod cut into sections approximately 8 cm long. The foil diameters were the same as those of the fuel rod (0.600 in.).

Approximately 2.3 tons of each enrichment of uranium were available for these measurements, and so the experiments could be done with considerably more reactivity than was available with the 0.750-inch diameter rods. Thus in many cases the vertical relaxation length was long enough to require corrections for influence of the top boundary of the assemblies on the flux distributions.

The effect of a top boundary is to cause axial flux distributions to have the form

$$\varphi = C \sinh\left[\frac{z_0 - z}{L}\right] \tag{38}$$

where C is a constant, L is the relaxation length, and z_0 is the height at which the flux extrapolates to zero. To find L, then, one should fit the measured flux distributions to Equation 38.

Actually, end effect corrections were made as follows. z_0 was found at a high rod-loading from a least squares fit of a sinh function to a many-point axial distribution. In subsequent measurements of relaxation lengths, each saturated foil activity was multiplied by the factor

$$\frac{\exp\left[\frac{z_0 - z}{L_0}\right]}{\sinh\left[\frac{z_0 - z}{L_0}\right]} \tag{39}$$

with L_0 an approximate value of L. The corrected flux values were fitted to an exponential; this fit provided a second approximation L_1 to L. New correction factors were obtained by replacing L_0 in Equation 39 by L_1, and the calculation was recycled, the procedure being repeated until it converged. This way of correcting for end effects was considerably simpler than fitting a sinh function to each set of flux values in a relaxation length measurement.

With each of the nine lattices to which method I was applied, twenty-two values of the vertical relaxation were found at different core radii. The relaxation lengths were divided into two groups; those with the eleven largest numbers of fuel rods loaded, and those with the eleven smallest numbers of rods. These two sets of data were analyzed separately for the buckling and reflector savings, and then another determination was provided by combining all twenty-two relaxation lengths in a single calculation. The results of these analyses are shown in Tables VI and VII. A comparison of B^2 as obtained from the highest numbers and lowest numbers of fuel rods loaded shows no apparent trend of one set being higher consistently than the other. Therefore method I seems to lead to results which are at least internally consistent.

Method II was used to find the buckling and reflector savings of seven of the lattices. In these cases the assembly was loaded to a k_{eff} of about 0.97, and measurements were made of the radial and axial thermal neutron distributions. It was assumed that far enough from the source and the boundaries, the flux had the macroscopic (cell-to-cell) space variation

$$\varphi = AJ_0\left(\frac{2.4048}{R+\lambda}r\right)\sinh\left(\frac{z_0 - z}{L}\right) \qquad (40)$$

with R defined by Equation 7 and A a constant. Least squares fits of the radial flux to the Bessel function led to values of λ, and least squares fits of the axial flux to the sinh function gave values of L. B^2 was then found from

$$B^2 = \left(\frac{2.4048}{R+\lambda}\right)^2 - \frac{1}{L^2} \qquad (41)$$

Axial flux distributions were determined as discussed earlier. The radial flux distributions were obtained with indium foils placed in a fuel rod. Two such rods were used with each lattice. One was used to expose foils at successive positions on a radius, while simultaneously foils were exposed in the other rod at a fixed location. The foils in the fixed rod served as monitors, registering any changes which may have occurred in the source strength. The ratios of saturated activities of the foils in the first rod to those in the second were therefore the relative fluxes at different points on a radius.

Since it was not possible to load the fuel rods exactly in the shape of a cylinder, the flux distribution given by Equation 40 was not strictly correct. Therefore flux measurements were made along six separate radii, as shown in Fig. 12. Three of these were diagonals of the basic hexagonal pattern in the lattices; these are called the "straight" radials. The other three were not straight lines, but were formed by zig-zagging out along paths intermediate between the straight radial lines.

The three flux positions farthest from the center on each radial traverse showed the characteristic be-

Table VI. B^2 for Lattices of 0.600-in. Diameter, Slightly Enriched Uranium Rods in Light Water, as Found by Method I

Volume water / Volume uranium	U^{235} weight per cent	$B^2(cm^{-2} \times 10^4)$		
		High 11 loadings	*Low 11 loadings*	*All loadings*
1	1.299	31.08 ± 1.24	34.71 ± 1.18	32.11 ± 0.54
1.5	1.299	53.52 ± 1.25	52.31 ± 0.78	51.87 ± 0.50
2	1.299	60.88 ± 0.78	60.58 ± 1.50	61.08 ± 0.32
3	1.299	61.16 ± 0.43	58.84 ± 0.94	60.99 ± 0.26
4	1.299	49.82 ± 0.75	49.17 ± 0.69	50.28 ± 0.27
1.5	1.143	40.15 ± 0.55	40.14 ± 0.68	40.23 ± 0.30
2	1.143	47.53 ± 1.10	48.15 ± 0.63	48.22 ± 0.31
3	1.143	46.82 ± 0.81	47.52 ± 0.96	47.12 ± 0.33
4	1.143	35.97 ± 0.53	35.96 ± 0.37	36.03 ± 0.16

Table VII. Reflector Savings of Lattices of 0.600-in. Diameter, Slightly Enriched Uranium Rods in Light Water, as Found by Method I

Volume water / Volume uranium	U^{235} weight per cent	λ (cm)		
		High 11 loadings	*Low 11 loadings*	*All loadings*
1	1.299	8.13 ± 0.27	7.60 ± 0.16	7.94 ± 0.10
1.5	1.299	7.02 ± 0.32	7.38 ± 0.16	7.44 ± 0.10
2	1.299	7.08 ± 0.16	7.11 ± 0.21	7.04 ± 0.06
3	1.299	6.67 ± 0.09	6.94 ± 0.12	6.70 ± 0.05
4	1.299	6.80 ± 0.21	6.82 ± 0.12	6.64 ± 0.07
1.5	1.143	7.52 ± 0.16	7.51 ± 0.12	7.50 ± 0.08
2	1.143	7.29 ± 0.30	7.11 ± 0.12	7.10 ± 0.25
3	1.143	6.76 ± 0.25	6.66 ± 0.18	6.68 ± 0.10
4	1.143	6.46 ± 0.06	6.46 ± 0.23	6.45 ± 0.10

havior of the flux rise near the reflector. These points were therefore discarded in the analysis, and the least squares fits which led to the experimental values of the reflector savings λ were based only on the remaining portion of the flux curves.

With one lattice (1:1 volume ratio, 1.143% enriched rods) flux traverses were made along radii at two different heights in an attempt to discover if the reflector savings was independent of z. Within the experimental error of the measurement (about 0.2 cm in λ), no difference was observed.

The measured values of B^2 and λ are listed in Tables VIII and IX. The combined results of measurements of buckling and reflector savings obtained by both experimental methods are shown in Figs. 13 and 14, for the three fuel enrichments.

The buckling and reflector savings of one assembly (1.143% enriched, 1.5 volume ratio) were obtained with both methods I and II. The results agree to within their indicated probable errors.

One determination of the critical mass was made by extrapolating to infinity the multiplication of spontaneous fission neutrons. The lattice used consisted of 1.143% enriched rods with a water-to-uranium volume ratio of 2. This assembly was loaded to a moderately high neutron multiplication, with appropriate flux monitors, safety rod, and emergency shut-down equipment, and with high flux levels maintained by a Po-Be source. At the maximum loading, the source was removed. A small BF_3 counter was inserted near the central fuel rod, and the count rates were measured. Rods were then removed from the periphery, so that count rates could be measured at several smaller rod loadings.

Table VIII. Buckling of Lattices of 0.600-in. Diameter, Slightly Enriched Uranium Rods in Light Water, Measured by Method II

Volume water / Volume uranium	U^{235} by weight	B^2 ($cm^{-2} \times 10^4$)
1	1.143%	21.19 ± 0.23
1.5	1.143	39.87 ± 0.56
1	1.027	9.66 ± 0.52
1.5	1.027	29.60 ± 0.70
2	1.027	35.83 ± 0.47
3	1.027	32.93 ± 0.34
4	1.027	21.01 ± 0.29

Table IX. Reflector Savings of Lattices of 0.600-in. Diameter, Slightly Enriched Uranium Rods in Light Water, Measured by Method II

Volume water / Volume uranium	U^{235} by weight	(cm)
1	1.143%	8.15 ± 0.13
1.5	1.143	7.62 ± 0.18
1	1.027	8.68 ± 0.15
1.5	1.027	7.49 ± 0.23
2	1.027	7.14 ± 0.19
3	1.027	6.63 ± 0.18
4	1.027	6.43 ± 0.19

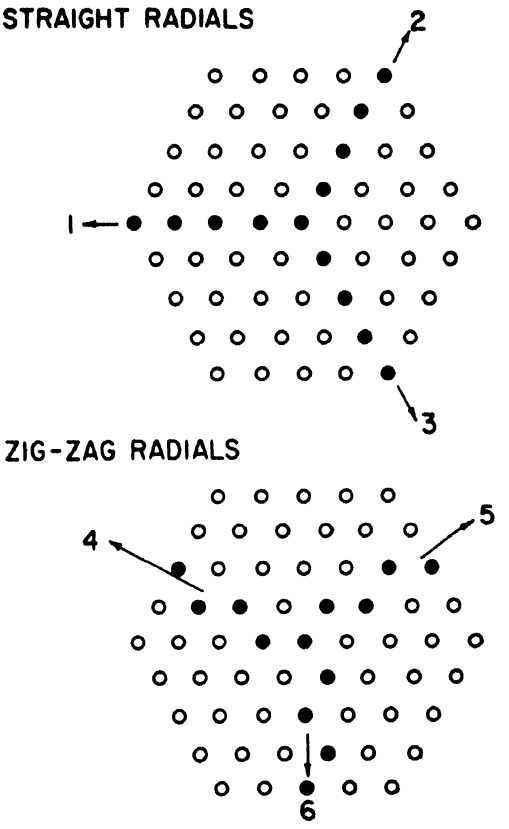

Figure 12. Lines along which radial flux distribution was measured

According to diffusion theory, the thermal neutron flux at any given point in the lattice should (sufficiently near critical) have the form

$$\varphi = \text{constant} \cdot \left\{ \left(\frac{a_0}{R+\lambda} \right)^2 - \left(\frac{a_0}{R_c+\lambda} \right)^2 \right\}^{-1} \quad (42)$$

where a_0 is the first root of the zero order Bessel function, and R_c is the critical radius. Therefore a plot of the reciprocal of the count rate against the quantity

$$\left(\frac{a_0}{R+\lambda} \right)^2 \quad (43)$$

should be a straight line, intersecting the axis at

$$\left(\frac{1}{R+\lambda} \right)^2 = \left(\frac{1}{R_c+\lambda} \right)^2 \quad (44)$$

Clearly, the solution of Equation 44 depends on the value of λ chosen. However, the measurements were done at a high enough neutron multiplication to define R_c quite well. For instance, the indicated critical mass for λ = 7.5 cm was 471 rods, while at λ = 0 cm it was 472 rods. Thus for a reasonable value of λ (the buckling measurements gave λ = 7.10 cm), the critical loading was 471 rods.

The values of B^2 and λ found in buckling measurements by method I led to a predicted critical mass of 467 rods. The difference amounts to about 0.9% in B^2, which is the same order of magnitude as the random errors in the buckling measurements.

Thus the Brookhaven measurements have been shown in three separate ways to be consistent, within their experimental errors.

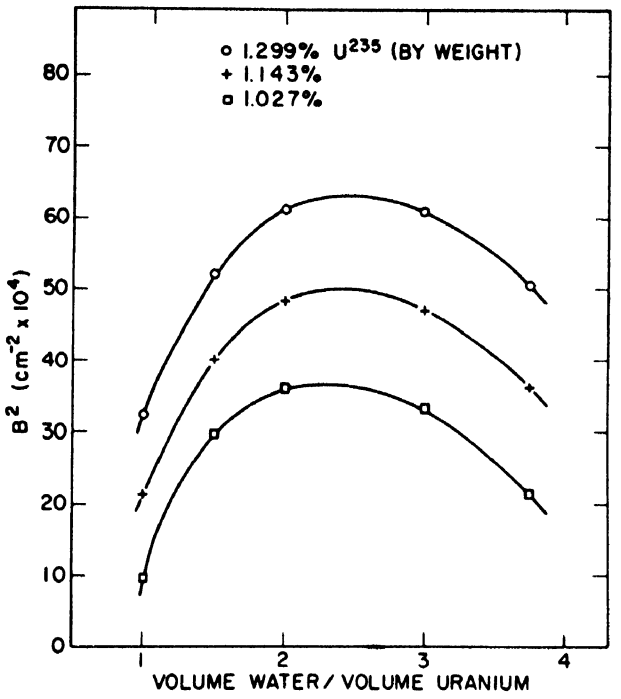

Figure 13. Experimental values of buckling, 0.600 inch diameter, slightly enriched uranium rods in light water

The Westinghouse group has taken to critical several of the lattices studied at Brookhaven.[6] The critical masses reported to date have been compared with the Brookhaven predictions in Table X. The two most accurate Brookhaven measurements of the buckling predicted critical masses which were observed within experimental error to be correct. The least accurate Brookhaven measurement predicted a critical mass which differs from the observed value a little more than the probable error.

Thus every attempt to find out how valid the Brookhaven measurements are has led to the conclusion that they are self-consistent and correct, with the cited experimental error being a good measure of the inaccuracy in predicted critical size. The probable errors in the values of B^2 and λ given in the tables were derived solely from the standard deviations from the least squares fits. Thus there seem to be no appreciable systematic errors in the experiments.

Fast Effect

The fast effect should be nearly independent of fuel enrichment in the range covered by these experiments. Therefore it was not considered necessary to find ϵ for all the lattices which were assembled. Instead, measurements were done in eight of the fifteen lattices, including all five volume ratios with the 1.299% enriched uranium and three volume ratios with the 1.143% enriched uranium. In addition, one measurement was carried out in a lattice with a water-to-uranium volume ratio of 0.1785, which was almost the smallest which could be obtained by close-packing the uranium. The fast effect for such a small volume ratio is close to that in a large solid piece of uranium.

The experimental methods discussed in connection with the 0.750-in. rod measurements were used here with no significant change. The experimental results are given in Table XI, and have been plotted as a function of the water-to-uranium volume ratio in Fig. 15. The probable errors given in Table XI are derived solely from the statistics of foil-counting, and do not include systematic errors.

R. L. Hellens, of the Westinghouse group, has pointed out that some of his calculations of the fast effect of these assemblies show that a small but appreciable correction must be applied to account for fast neutron leakage. In an assembly with a positive value of the buckling, there is a net flow outward of neutrons from each point in the core, and this feature would tend to decrease the measured value of ϵ below that calculated for an infinite lattice. Moreover, the experimental fast effect should then depend on the buckling, and hence on the fuel enrichment. The effect is not very large, and it is difficult to calculate accurately.

Unfortunately, the measurements were not accurate enough to establish the magnitude of this trend. ϵ was measured at two different fuel enrichments for three of the five volume ratios, viz: 4:1, 1.5:1, and 1:1. The latter two show a possible increase in ϵ with decreasing enrichment (hence decreasing buckling), but the observed differences are just within the experimental errors. The former shows an opposite trend—which also is zero to within experimental error. Thus no conclusions on the size of this effect could be drawn. It appears in any case to be small.

Thermal Utilization

The measurements of f which were begun with 0.750-in. diameter rods were continued with 0.600-in. rods. The method was still an experimental determina-

Table X. Comparison of Brookhaven and Westinghouse Criticality Studies with 0.600-in. Diameter Rods of 1.299% Enriched Uranium in Light Water

Volume water / Volume uranium	Critical number of rods	
	Brookhaven (predicted)	Westinghouse (observed)
1.5	486.6 ± 7.4	478
2	337.4 ± 2.9	335
3	265.6 ± 1.9	266

Table XI. Experimental Values of the Fast Effect, 0.600-in. Diameter Rods of Slightly Enriched Uranium in Light Water

Volume water / Volume uranium	% U^{235} by weight	ϵ
1	1.299	1.105 ± .002
1.5	1.299	1.072 ± .001
2	1.299	1.061 ± .001
3	1.299	1.047 ± .001
4	1.299	1.043 ± .001
1	1.143	1.109 ± .002
1.5	1.143	1.074 ± .001
4	1.143	1.042 ± .001
0.1785	1.299	1.227 ± .011

tion of the intracell flux distribution. Some of the techniques, however, were changed in the course of measurements with the smaller rods.

The greatest change was introduced in the way foils were held in position in the moderator. When the 0.750-in. rods were being studied, the foils in the water were placed in rectangular slabs of methyl methacrylate plastic, which were inserted horizontally between the fuel rods. The foil holders used with 0.600-in. rods were small triangular-symmetried pieces such as that shown in Fig. 16; these were inserted vertically into the lattices through holes in the top fuel-rod locating plate. The geometry of the new foil holders permitted the use of a much larger number of foils in the water than before, and thus led to more detailed flux plots. Figure 16 shows a typical experimental flux plot, in this case for the 1.5:1 volume ratio, 1.143% enrichment lattice.

The foil holders used with the 4:1 and 3:1 volume ratio lattices of 1.299% enriched rods were made of 0.6 millimeter thick methyl methacrylate. Those used for all other measurements consisted of a double thickness of 0.08 millimeter thick aluminum. The two groups of measurements did not seem to agree very well. Similar measurements of f were carried out by the Westinghouse group, with methyl metha-

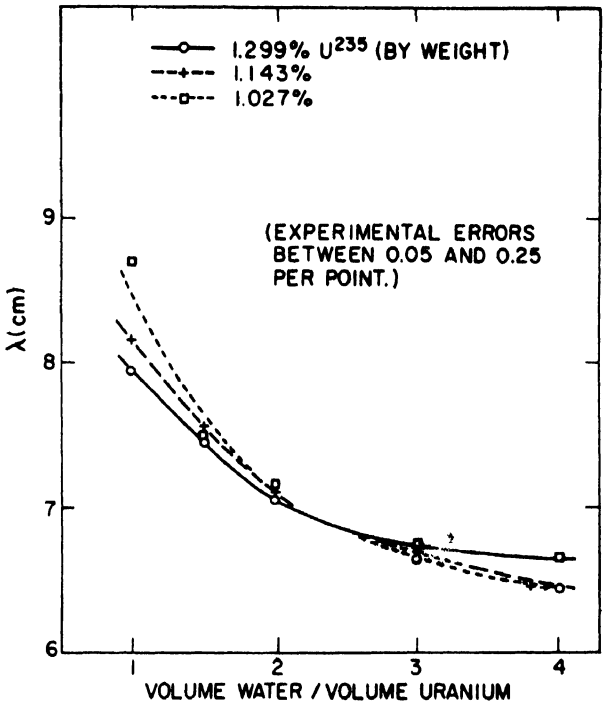

Figure 14. Reflector savings of 0.600 inch diameter, slightly enriched uranium rods in light water

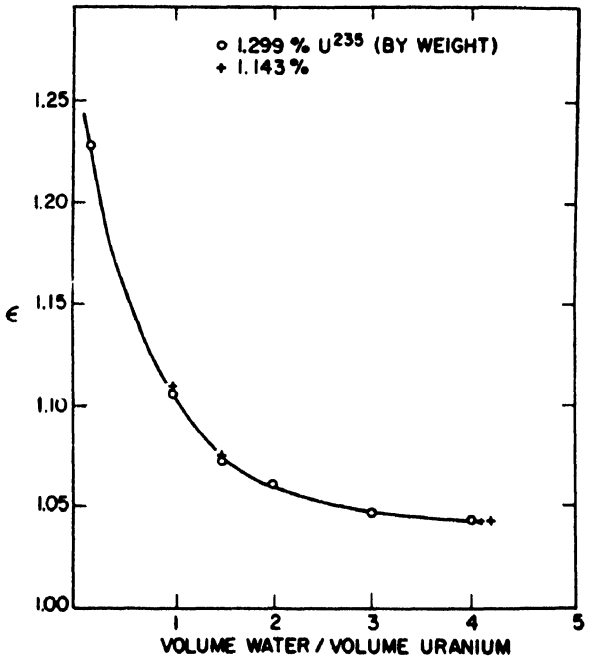

Figure 15. Experimental fast effect of 0.600 inch diameter, slightly enriched uranium rods in light water

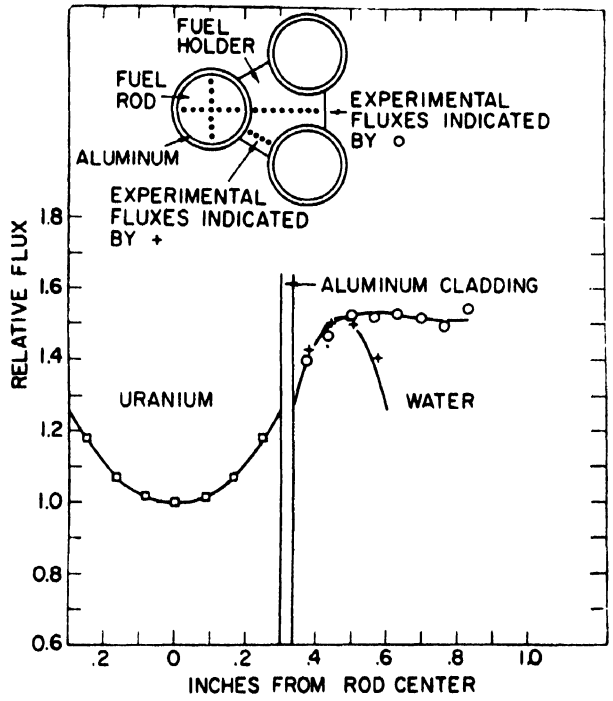

Figure 16. Experimental intracell flux traverse, 0.600 inch diameter, 1.143% enriched uranium rods in light water. Volume ratio = 1.5:1

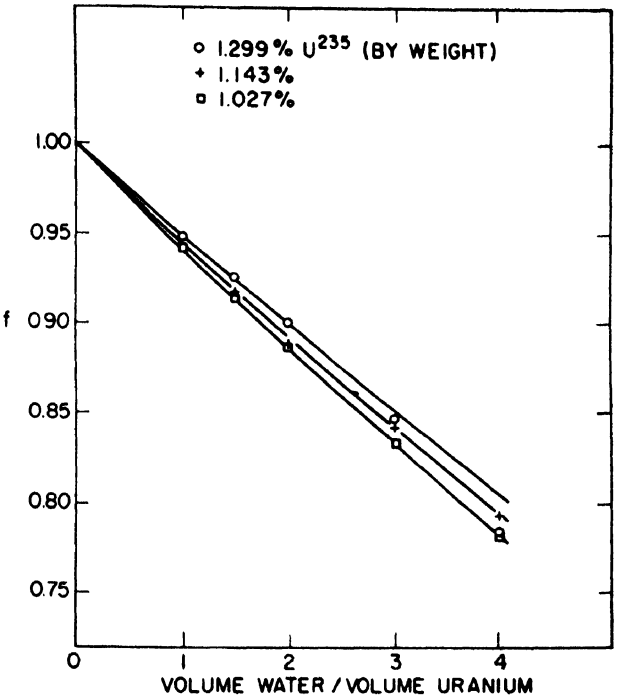

Figure 17. Measured thermal utilization, 0.600 inch diameter, slightly enriched uranium rods in light water

Table XII. Experimental Values of Thermal Utilization for Slightly Enriched Uranium Rod, Light Water Moderated Lattices

Volume water / Volume uranium	% U^{235} by weight	f (measured)	f (from smooth curves)
1	1.299	0.948	0.949
1.5	1.299	0.925	0.924
2	1.299	0.900	0.899
3	1.299	0.846	0.851
4	1.299	0.784	0.804
1	1.143	*	0.945
1.5	1.143	0.917	0.918
2	1.143	0.888	0.893
3	1.143	0.842	0.842
4	1.143	0.793	0.793
1	1.027	0.941	0.941
1.5	1.027	0.913	0.912
2	1.027	0.886	0.885
3	1.027	0.833	0.833
4	1.027	0.781	0.781

* Not measured.

crylate foil holders used throughout. There was a consistent tendency for measurements done with aluminum foil-holders to lead to larger values of f than those done with the plastic. The source of the disagreement is not certain; because of its existence, however, the measurements which are reported here must be considered as in doubt by an amount varying from about 0.01 in f at the 4:1 volume ratio to about 0.002 in f at the 1:1 volume ratio. This uncertainty probably will be resolved in the very near future.

The experimentally measured thermal utilizations for fourteen of the fifteen lattices are given in Table XII. Values of f taken from the smooth curve plots of Fig. 17 are also given. A measurement was not performed for one of the fifteen assemblies; this was the one with a 1:1 volume ratio and 1.143% enriched rods. The missing number can however be interpolated directly from the curves with very good accuracy, and this has been done.

Two points deviate markedly from the smooth curves in Fig. 17. These were the measurements made with plastic foil holders.

The implications of these experiments for the mean neutron temperature in the moderator are very interesting. The wider spaced lattices have values of f which apparently can be matched with P_3 calculations based on a mean neutron energy of 0.035 volts. The results with more closely spaced lattices (particularly the very tightly grouped 1:1 volume ratio) fit much higher neutron temperatures. The precise values of the temperature which lead to a good fit are not important, because of uncertainties in the methods of calculation. However, the trend toward higher temperature with closer rod spacings has been definitely observed.

Migration Area

The migration areas of these assemblies are of interest mostly because they are ingredients in the analysis of the neutron economy. With the buckling and the migration area known, k_∞ is also known.

In addition, measured values of M^2 can lead to information on the inelastic and scattering cross-sections of uranium, through comparison with calculated values. This course has to be followed cautiously, however; there are reasons why the measured and calculated values could differ and yet both still be right. This point will be discussed later after the results of the experiments have been presented.

Migration area measurements with the 0.600-in. diameter rods were done in two different but related ways. Briefly, these were

(1) The moderator water was poisoned with B_2O_3, and the thermal utilization and buckling were measured at several such concentrations. This was the measurement used with 0.750-in. rods also, and was discussed earlier in connection with those experiments. In the following it will be called "the poison method."

(2) Values of thermal utilization and buckling were measured as a function of fuel rod enrichment. This will be called "the enrichment method."

Theoretically, both kinds of method depend on use of the critical equation:

$$\epsilon p f \eta \mathfrak{L} = 1 \tag{45}$$

where $\mathfrak{L}$ is the fractional neutron non-leakage in a single fission cycle. According to one-group diffusion theory,

$$\mathfrak{L} = (1 + M^2B^2)^{-1} \tag{46}$$

On the other hand, the expression derived from age theory (continuous slowing-down is)

$$\mathfrak{L} = \exp[-\tau B^2](1 + L_{th}^2B^2)^{-1} \tag{47}$$

For the assemblies studied here, B^2 was at most about 6×10^{-3}, and L^2 was about 4 cm.^{2} Thus at most

$$B^2L_{th}^2 \sim 2.4 \times 10^{-2} \tag{48}$$

Therefore

$$(1 + B^2L_{th}^2)^{-1} \sim \exp[-B^2L_{th}^2]$$

$$\mathfrak{L} = \exp[-B^2\tau](1 + L_{th}^2B^2)^{-1} \sim \exp[-M^2B^2] \tag{48a}$$

At the outset, one is faced with having to choose between describing the leakage by means of Equations 46 and 48a. There are reasonable *a priori* arguments for each. Equation 48a is the limiting expression for multigroup diffusion theory; on the other hand, the thermal flux distributions arising from the slowing-down of neutrons in water can be fitted reasonably well to a one-group diffusion kernel. The latter however leads to Equation 46. Since grounds for a choice between the two non-leakage kernels were not apparent at the beginning, analysis of the experiments was done starting from both assumptions. This procedure eventually led to a choice of Equation 48a as the preferred form for the non-leakage.

The "poison method" of finding M^2 consists in adding B_2O_3 to the moderator water, and then measuring B^2 and f. The presence of the boron does not affect the values of ϵ, p, η, and M^2 very much, and so from Equations 45 and 46,

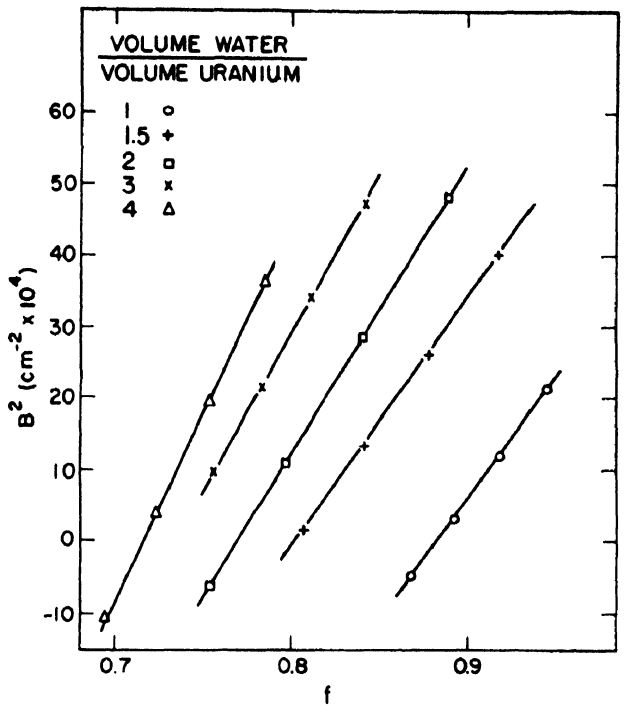

Figure 18. f vs B^2 for boron poisoned lattices of 0.600 inch diameter, 1.143% enriched uranium rods in light water

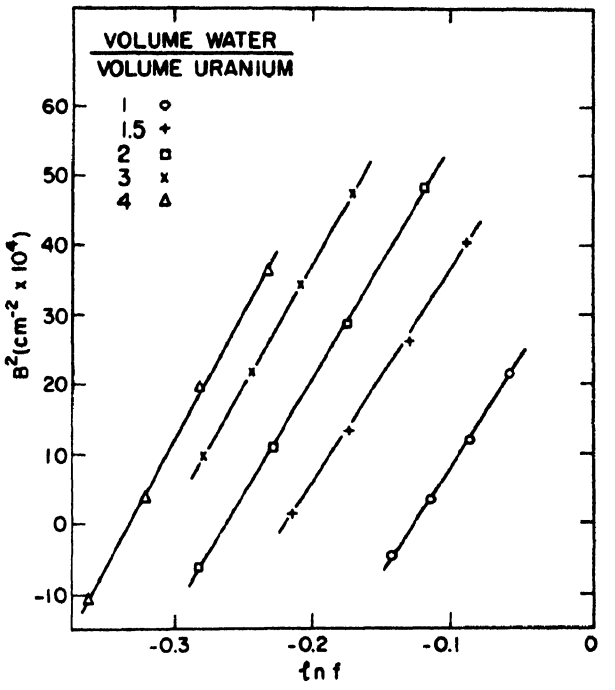

Figure 19. ln f vs B^2 for boron poisoned lattices of 0.600 inch diameter, 1.143% enriched uranium rods in light water

$$\epsilon p\eta \left[\frac{df}{d(B^2)}\right] = M^2$$

Also from Equations 45 and 46,

$$\epsilon p\eta[f]_{B^2=0} = 1$$

Therefore

$$M^2 = \frac{1}{[f]_{B^2=0}} \frac{df}{d(B^2)} \tag{49}$$

One-group theory therefore relates the measured values of f and B^2 linearly, and the migration area is the slope of the straight line divided by its intercept.

An analysis of the experiment with the age theory kernel starts from recasting Equations 45 and 48a in the form

$$\ln(\epsilon p\eta) + \ln f = M^2B^2$$

In this case it is $\ln f$ which is linearly related to B^2, and M^2 is calculated as

$$M^2 = \frac{d(\ln f)}{dB^2} \tag{50}$$

To obtain M^2 by the "enrichment method" one must first notice that η and f are simultaneously changed by varying the U^{235} content of the fuel. Including this in the analysis leads to two expressions similar to Equations 49 and 50. If one-group theory is assumed,

$$M^2 = \left[\frac{1}{(\eta f)_{B^2=0}}\right]\left[\frac{d(\eta f)}{d(B^2)}\right] \tag{51}$$

Or assuming the validity of the age-theory kernel,

$$M^2 = \frac{d(\ln \eta f)}{d(B^2)} \tag{52}$$

In the poison measurements, boron was added to the water as boric acid crystals. Care was taken to assure complete solution of the salt, the mixture being agitated for several hours with a mechanical stirrer. The boron concentrations were then found by chemical analysis. In each case at least two quantitative boron determinations were made, and these generally agreed to within better than 0.5%.

The poison method was used with 1.143% enriched rods to find the migration areas of all five of the lattices which were assembled. The thermal utilizations and bucklings were measured by the methods discussed previously. Figures 18 and 19 show the experimental results, with B^2 plotted against f and $\ln f$, respectively. Since the two variables were not necessarily measured with the same boron concentrations in every case, the points upon which the curves of Figs. 18 and 19 are based are interpolations. The curves show equally good fits of the measured points to straight lines.

The curves of Figs. 18 and 19 were subjected to least squares fitting, to provide the slopes, the intercepts, and hence the migration areas. The results of the analysis are given in Table XIII. The values of k_∞ calculated from the measured bucklings and migration areas are shown in Table XIV. It is apparent that though the sets of values of M^2 obtained using the two critical equations differ noticeably. the values of k_∞ match quite well. Thus the latter quantity may be considered as well-determined.

The measurements of f and R^2 upon which the enrichment method of determining M^2 depends have already been discussed. In carrying through the analysis with Equations 51 and 52, however, it is necessary to use calculated values of η. Consistency in the choices for the different enrichments is easily

obtained; one begins with a value of η for natural uranium, writing it as

$$\eta_{nat} = \frac{\eta_{25}}{1 + N\sigma_{28}^a/\sigma_{25}^a}$$

with η_{25} the (preassumed) value for pure U^{235}, N the atomic ratio of U^{238} to U^{235} in natural uranium, and σ_{28}, σ_{25} respectively the mean thermal cross sections of U^{238} and U^{235}. These choices of η_{nat} and η_{25} then determine a value for the ratio

$$\frac{\sigma_{28}^a}{\sigma_{25}^a}$$

and the enrichment dependence of η is obtained from the variation of N.

The best values of present cross sections give

$$\eta_{nat} = 1.327 \pm 0.015 \qquad (53)$$

The analysis of various reactor experiments has not been any more successful in fixing this number; in the literature one can find values ranging from 1.28 to 1.35. On the basis of the evidence available, the value in Equation 53 seems to be the best yet determined, and it was chosen for analyzing the migration area measurements.

The one-group migration areas obtained using Equation 51 were found from least-squares fits of (ηf) against B^2. The age-theory values obtained from the use of Equation 52 were obtained from least-squares fits of straight lines to the variation of ln (ηf) against B^2. The results are given in Table XV. The probable errors assigned are compounded from the probable errors in B^2 and f and the uncertainty in η.

Additional analyses of the poison method were made with measured values of B^2 and with values of f which were calculated by two different schemes. One set of calculated thermal utilizations was obtained from ordinary diffusion theory; another was found from P_3 calculations. The calculated values of f did not match the experimental values very well. Nevertheless, the deduced migration areas were not changed appreciably from the values obtained with the use of purely experimental data. Therefore it is concluded that uncertainties in thermal utilization measurements do not affect the migration areas which have been obtained.

Table XVI, giving the "enrichment method" values of k_∞ for the 1.143% enriched rods, can now be compared with Table XIV, which is based on migration areas obtained from the poison measurements. It is apparent that the two sets of values of k_∞ agree moderately well (except for the 4:1 lattice) if the age theory analysis is used, but seem irreconcilable if the one-group critical equation is used. This result seems to establish quite definitely that the more correct critical equation is, as obtained from Equations 45 and 48a

$$\epsilon p f \eta = \exp[M^2 B^2] \qquad (54)$$

Equation 50 is a special case of Equation 52, where η is not varied. Therefore all of the measured values of f and B^2 for the different boron poisonings and fuel rod enrichments can be analyzed at once with the latter. Best values of M^2 have been obtained in this way; the results have been listed in Table XVII, and are plotted in Fig. 20.

The reasons for the large difference between these results and those obtained at Oak Ridge has been discussed in connection with the 0.750-in. diameter rod measurements. There is also a noticeable difference between the experimental results with 0.600 and 0.750-in. rods. The migration areas with the smaller rods are larger, a feature which can readily be ascribed to the greater first-flight inelastic scattering probability when larger rods are used. Also, the migration areas of the smaller rods show a definite tendency to

Table XIII. Migration Areas of Lattices According to the Poison Method. 0.600-in. Diameter Rods of 1.143% Enriched Uranium in Light Water

Volume water / Volume uranium	M^2 (cm^2) from one-group equation	M^2 (cm^2) from age theory equation
1	33.66 ± 1.08	32.78 ± 1.08
1.5	35.55 ± 1.26	33.15 ± 0.88
2	32.19 ± 0.77	30.21 ± 0.69
3	30.91 ± 1.26	28.38 ± 1.07
4	28.75 ± 1.17	27.72 ± 1.08

Table XIV. k_∞ for 1.143% Enriched, 0.600-in. Diameter Uranium Rods in Light Water, (Values Based on Measured B^2 and on M^2 from Table XIII)

Volume water / Volume uranium	k_∞ from one-group analysis	k_∞ from age theory analysis
1	1.071 ± 0.003	1.072 ± 0.003
1.5	1.143 ± 0.005	1.142 ± 0.005
2	1.155 ± 0.005	1.157 ± 0.004
3	1.146 ± 0.007	1.143 ± 0.006
4	1.104 ± 0.005	1.105 ± 0.005

Table XV. Migration Areas of 0.600-in. Diameter Rods of Slightly Enriched Uranium in Light Water. Obtained by Enrichment Method

Volume water / Volume uranium	M^2 from one-group analysis (cm^2)	M^2 from age theory analysis (cm^2)
1	34.34 ± 1.63	32.29 ± 1.39
1.5	39.91 ± 2.09	34.59 ± 1.64
2	36.94 ± 1.43	31.57 ± 1.15
3	36.08 ± 1.22	30.62 ± 1.30
4	36.23 ± 1.28	31.91 ± 1.33

Table XVI. k_∞ for 1.143% Enriched, 0.600-in. Diameter Uranium Rods in Light Water (Values Based on Measured B^2 and on M^2 from Table XV)

Volume water / Volume uranium	k_∞ from one-group analysis	k_∞ from age theory analysis
1	1.073 ± 0.004	1.071 ± 0.003
1.5	1.161 ± 0.009	1.149 ± 0.007
2	1.178 ± 0.007	1.164 ± 0.006
3	1.170 ± 0.006	1.155 ± 0.007
4	1.131 ± 0.005	1.122 ± 0.005

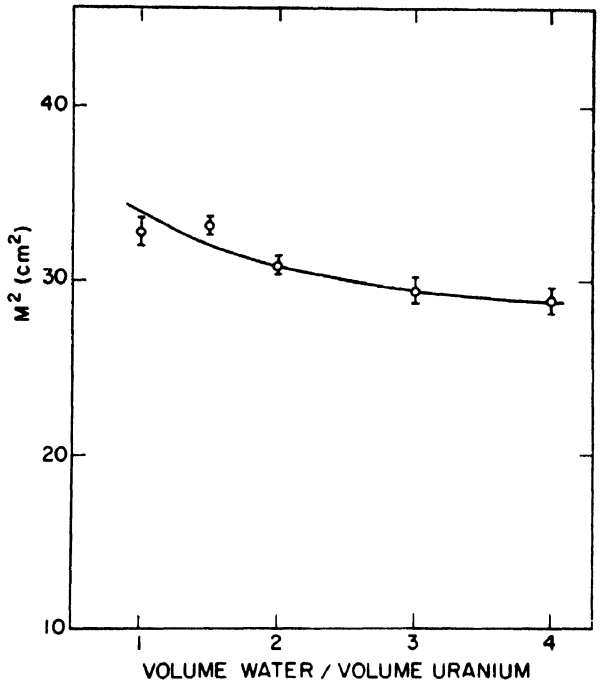

Figure 20. Best values of migration areas of fission neutrons in lattices of 0.600 inch diameter, slightly enriched uranium rods and light water

increase as the volume ratio is diminished. Such a trend seems to exist also with the 0.750-in. rod values (Table IV), but it is not outside experimental error.

As mentioned earlier, one must be careful about comparing these experimental values of M^2 with those calculated by neutron slowing-down theory. The lattices studied are strongly heterogeneous, and strictly speaking the migration areas which have been measured are defined only by the non-leakage probability (Equation 48a). It is not at all certain that these quantities are related to $\overline{r^2}$ in the same way as the migration area for homogeneous assemblies. In the past, attempts have been made to "homogenize"

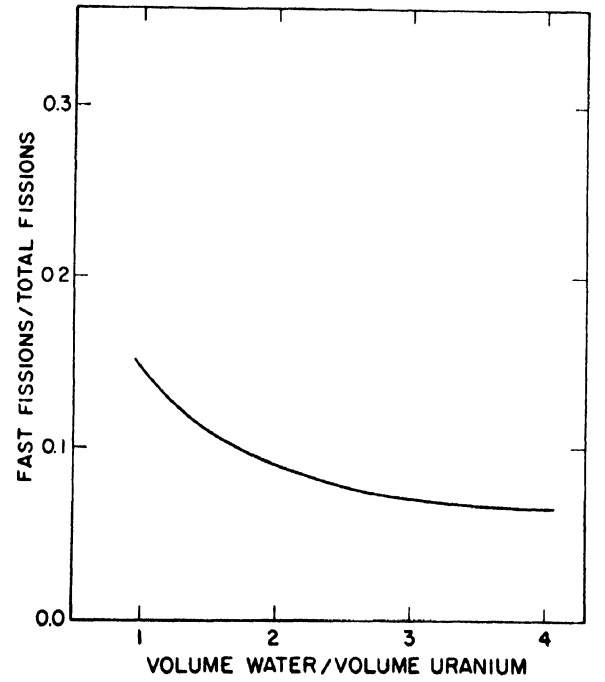

Figure 21. Experimental fast fission fraction for 0.600 inch diameter uranium rod lattices in light water

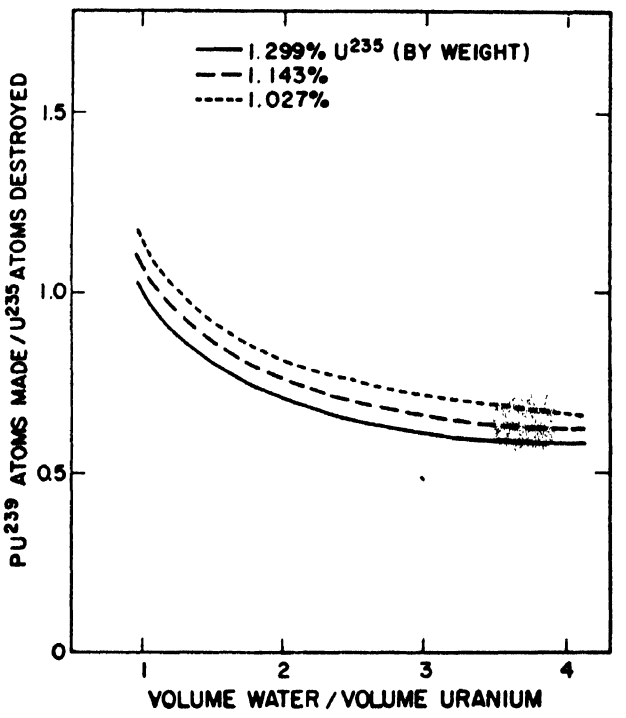

Figure 22. Conversion ratio of 0.600 inch diameter, slightly enriched uranium rod lattices in light water

heterogeneous reactor theory by defining quantities like the mean age, cross-sections, and diffusion lengths over a lattice cell, but these efforts have all depended on some simplified model of the slowing-down and diffusion processes. The most that can be said in general is that the calculated (from slowing-down theory) and measured (from leakage) values of the migration area for heterogeneous assemblies should be of the same orders of magnitude.

Neutron Temperature

The mean thermal neutron temperature of one lattice (1.143% enriched rods, 3:1 volume ratio) was found by a method resembling that used by G. B. Gavin at the Knolls Atomic Power Laboratory.[9] The experiment consisted in finding the relative effects on neutron multiplication of boron and cadmium in solution in the water moderator. The ratio of the observed danger coefficients led to the ratio of the mean cross-sections of the two poisons over the low energy neutron flux spectrum; since the two have very different cross-section curves in this energy region, a basis for estimating the neutron temperature existed.

Table XVII. Best Experimental Values of Migration Areas of Fission Neutrons in Lattices of 0.600-in. Diameter, Slightly Enriched Uranium Rods in Ordinary Water

$\frac{\text{Volume water}}{\text{Volume uranium}}$	M^2 (cm^2)
1	32.70 ± 0.77
1.5	33.05 ± 0.55
2	30.78 ± 0.44
3	29.31 ± 0.73
4	28.70 ± 0.71

The lattice was loaded to a neutron multiplication of about 500, with suitable critical assembly precautions being taken, and the count rate from spontaneous neutron multiplication was measured. A predetermined amount of boric acid solution was added to the moderator, after the equivalent volume of water had been removed, and the count rate was again measured. A measured amount of cadmium sulfate solution was then similarly added, and the count rate was recorded again.

It can be shown that the relation between the observed count rates and the small amounts of poison is

$$\frac{\frac{1}{R_2} - \frac{1}{R_1}}{\frac{1}{R_1} - \frac{1}{R_0}} = \frac{\Sigma_{Cd}}{\Sigma_B} \qquad (55)$$

where the R_i are the observed count rates in the order in which they were measured, and the Σ's are the indicated macroscopic cross-sections of the poisons in the moderator. These macroscopic cross-sections were averaged over the $1/v$ energy dependence of boron and the characteristic resonance curve of cadmium, with the Maxwell energy distribution used as a weight function. It was found that the experimental results could be matched with a neutron temperature of $304° \pm 17°$K, where the probable error contains the statistical inaccuracies of the counting and the uncertainties in the experimental cross sections of boron and cadmium. Since the water at the time of the measurement was at 297°K, the mean neutron temperature was $7° \pm 17°$ above the moderator temperature. To within experimental error, then, the low energy neutrons were in thermal equilibrium with the water.

IMPLICATIONS OF THE EXPERIMENTS

The war-time Oak Ridge experiments led to the conclusion that light water moderated natural uranium lattices could not be used as successful high flux reactor cores. They did however point up the fact that a slight increase in enrichment would make the use of a light water moderator feasible.

The Brookhaven measurements, in addition to providing experimental data on the reactivity of such slightly enriched uranium systems, have shed some interesting light on their neutron economies.

The high values of ϵ which can be obtained with the closer spaced lattices imply that a large fraction of the heat energy which would be produced in a going reactor of this type would be derived from direct burning of the U^{238}. The fast effect measurements are really determinations of the fast fission fraction; that the latter quantity is the directly measured one, and the former is only inferred. The measured fast fission fractions with 0.600-in. rods are shown in Fig. 21. Because of these large U^{238} burnouts, a power reactor of this type could be run longer periods of time before fuel replacement became necessary.

The tightly packed lattices also have a surprisingly large plutonium production rate. This can be estimated from the measured values of k_∞, ϵ, and f, and from the assumptions regarding η which were made in connection with the migration area measurements by the enrichment method. These measured and assumed components of the neutron economy permit the inferring of the resonance escape probability. These are all of the quantities necessary for estimating the plutonium production rate in the core with reasonable accuracy. The results of such an analysis are shown in Fig. 22. It is seen that for small volume ratios, the conversion ratio, defined as the number of plutonium atoms produced per atom of U^{235} destroyed, is greater than one. This feature again is a consequence of the large fast fission fraction because an appreciable amount of U^{238} is also being burned.

It should be noted that Fig. 22 shows only the conversion factor in the core. A reactor design of this type which had also a conversion blanket would produce considerably larger amounts of plutonium.

The large values of the fast effect even make thermal plutonium breeding possible, at least in principle. The experimental value of η for Pu^{239} is 2.03 ± 0.03. Normally then one would suppose that per neutron cycle in a plutonium fueled reactor only 1.03 ± 0.03 neutrons could be made available for leakage, capture in the moderator, and breeding. Actually, with an appreciable fast effect, the number of neutrons which can be used for breeding per atom of plutonium destroyed is $\eta\epsilon$, making the possibility of thermal plutonium breeding more likely.

The numbers which have been used to estimate conversion ratios apply to clean, cold reactor cores. The high temperatures in a power reactor certainly would change the nature of the curves obtained from the Brookhaven measurements, and the conversion ratios would be modified also. There would be other changes caused by fuel burnout, and small effects from fission product build-up. The long-term processes which would occur in a power reactor are complicated. Therefore trustworthy information on the effect of these high conversion and breeding rates must eventually be found from the behavior of such full scale reactor projects, particularly from the reactivity changes over long periods of time.

REFERENCES

1. Weinberg, A. M., unpublished.
2. Chernick, J., P/606, *Theory of Lattices of Slightly Enriched Uranium Rods in Water, Part I*, Volume 5, Session 21A, these Proceedings.
3. Wilkins, J., Hellens, R. L. and Zweifel, P., P/597, *Status of Experimental and Theoretical Information on Neutron Slowing Down Distribution in Hydrogenous Media*, Volume 5, Session 19A, these Proceedings.
4. Krasik, S. and Radkowsky, A., P/601, *Pressurized Water Reactor (PWR) Critical and Exponential Experiments*, Volume 5, Session 21A, these Proceedings.
5. Segre and Wiegand, Phys. Rev. *70*, 808 (1946).
6. Hellens, R. L., private communication.
7. Gavin, G. B., "A Determination of the Neutron Temperature at the Center of the Thermal Test Reactor," KAPL-1142 (22 June, 1954) (unclassified).

Pressurized Water Reactor (PWR) Critical Experiments

By S. Krasik* and A. Radkowsky,† USA

The aims of the PWR critical experiment program are (1) to provide essential reactor physics information which cannot be obtained by available calculational procedures, (2) to provide general guidance to the analytical nuclear design program and (3) to substantiate and verify the significant reactor calculations. There are two distinct parts to the critical experiment program which meet substantially different needs.

One part of the program relates specifically to the actual PWR design. The information developed in this part of the program deals primarily with reactor control, flux distributions and the temperature coefficient of reactivity. By its nature an experiment designed to provide this type of information becomes in many respects a nuclear mockup of the actual reactor design.

The principal reason for carrying on this part of the experimental program is the difficulty of the computations which would otherwise be required. This difficulty lies essentially in the magnitude of the required computations. In some measure this is due to the geometrical complexity of a light water moderated power reactor. Apart from the computational difficulty, a second reason for carrying on this part of the experimental program is the uncertainties of the available theoretical models. A third reason is the lack of sufficiently detailed cross-section information. Even if the latter two considerations could be circumvented, the limiting factor today is the magnitude of the computation. While large scale digital computation holds out considerable promise for the future, at the present time a completely analytical approach to the PWR nuclear design is not feasible.

The type of information obtained in the experimental program considered above, while essential, tends to be quite specific to the reactor design being studied. The experimental information is not easily extended even to reactors of the same type if they differ in some significant way from the reactor under study. The extensions which can be made tend to be empirical or even qualitative in character.

The other part of the experimental reactor physics program—and of equal importance to the first—aims to provide experimental information of considerably broader scope. As remarked above the nuclear mockup experiment provides little or no explanation of basic difficulties which may arise in a design and equally little guidance as to significant directions in reactor design. The second part of the experimental program, particularly when coupled with a strong theoretical program, supplies this need.

This experimental program, through the study of critical experiments of simple geometry, aims at measurements of such fundamental reactor constants as critical bucklings, migration areas, resonance escape probabilities, thermal utilizations and fast fission factors. The experiments are related to the PWR design in the use of the same reactor core materials. The range of parameter variation is deliberately broadened, however, to demonstrate the trends in the important reactor constants.

Experiments of this second type are required principally because of the deficiencies of the theoretical models and the lack of sufficiently detailed cross-section information. Computational difficulties, while they exist, are of secondary importance. In many cases this type of experimental work guides the theoretical approach by emphasizing the important physical features of the problem. The greatest value of these measurements is in the testing of the theoretical models. Once the validity of a theoretical approach has been well verified, the reactor designer has both latitude and certainty in his design studies.

Two PWR experimental critical facilities will be discussed. The PWR flexible critical facility which has recently started operations is primarily designed for mockup design studies. Simple lattice studies will be carried on in this facility as a secondary effort. The other facility, which has been in operation for some time, is designed primarily for critical experiments on simple uranium-water lattices. Because of the considerably longer operating history, the experimental data to be presented has been obtained on this facility. This work will be discussed first followed by a brief discussion of the flexible critical facility.

URANIUM-WATER LATTICE EXPERIMENTS

This series of experiments was planned several years ago when it became clear that a pressurized water reactor using a fuel element of high uranium content was an important type of nuclear power reactor. At the time Brookhaven National Laboratory had been conducting exponential experiments on uranium-water lattices. The new program was planned as an extension of the existing exponential experiment

* Westinghouse Atomic Power Division.

† Reactor Development Division, US Atomic Energy Commission. Including work by A. Radkowsky, US Atomic Energy Commission; J. R. Brown, A. Z. Kranz, S. Krasik and B. Noordhoff, Westinghouse Atomic Power Division.

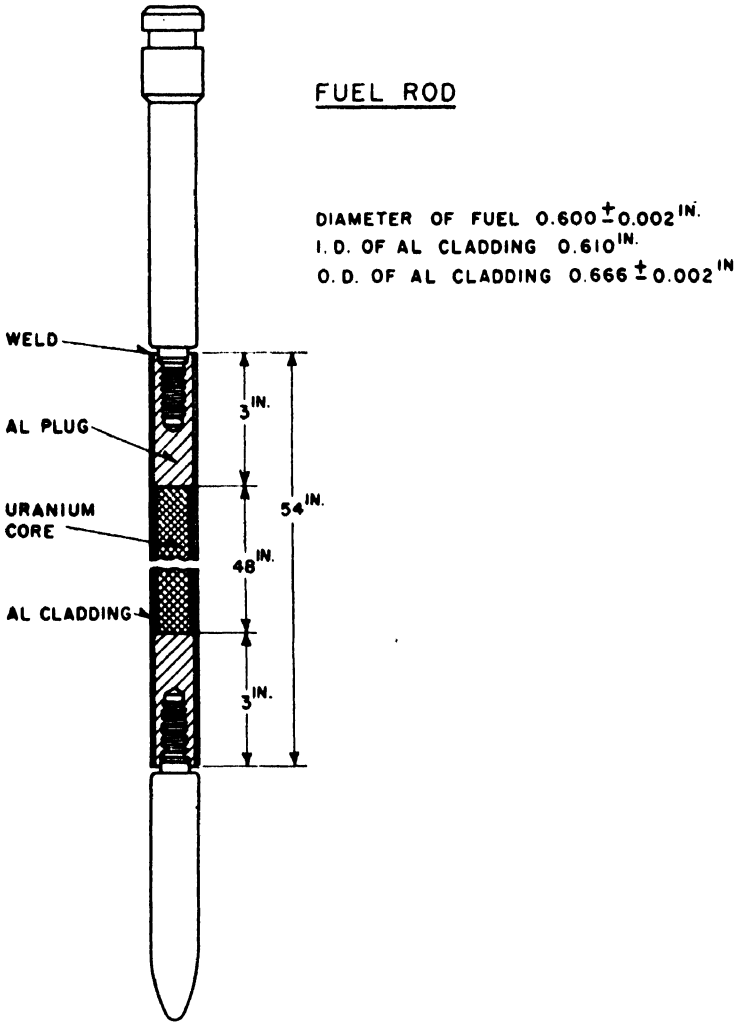

DIMENSIONS OF THE LATTICE PLATES

0.600" DIAM. URANIUM

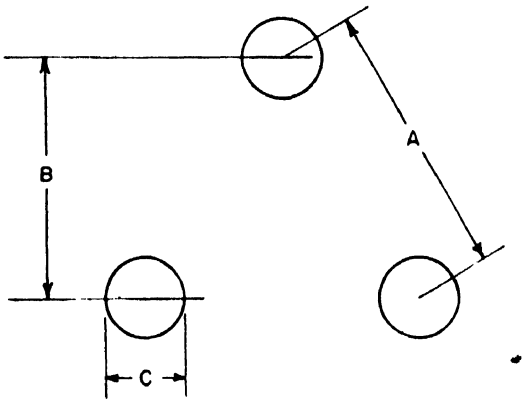

W/U VOLUME RATIO	A	B	C
1 To 1	0.856	0.741	.687
1.5 To 1	0.947	0.820	.687
2 To 1	1.030	0.892	.687
3 To 1	1.177	1.019	.687
4 To 1	1.309	1.134	.687

Figure 1

program with the addition of a critical experiment program at the Westinghouse Atomic Power Division.

Because of the specific advantages of exponential experiments for certain types of studies and the advantages of a critical experiment for others, the program was planned as a joint series of exponential and critical experiments using the same fissionable material in sequence. In an exponential experiment the bucklings of a lattice may be measured over a wide range of geometries. Poisoned water experiments with a wide range of bucklings can be measured easily. In general there is more freedom in an exponential experiment with respect to planning, execution and hazard of experiments because criticality need not be reached. On the other hand a critical experiment permits measurements of critical size and danger coefficients to be made quite precisely. Temperature coefficients of reactivity and control rod worths are easily measured with good accuracy. An advantage of the critical facility is that a sufficiently high neutron flux is available to permit a direct measurement of the resonance escape probability. A notable advantage of using two facilities is that it permitted important reactor parameters such as migration area to be measured by quite different techniques.

The experiments were originally planned using uranium metal since it was believed at the time that the reactor fuel element would be metallic. Since the emphasis of the PWR design is now on a uranium oxide fuel element, a somewhat similar type of program using oxide material has been started. It is a significant comment on the value of this type of work, however, to observe that a great deal of the information developed in the metal program is of direct value to the PWR oxide design program.

Description of the Critical Experiments

The material for the series of experiments consists of three lots of slightly enriched uranium of approximately two tons each. The nominal enrichments of the uranium are 1.3%, 1.15% and 1.0%. (The enrichments quoted are the percentages of uranium-235 isotope in the uranium metal.) The uranium in each lot is first fabricated into rods of 0.600-inch diameter. After completion of the exponential and critical experiments at this diameter, the rods are drawn to a diameter of 0.387 inch and finally to a third diameter of 0.250 inch. At the present time all planned measurements with the 0.600-inch diameter have been completed and all lots of the rods have been reduced to 0.387-inch diameter. Because of the limited information expected from critical experiments with the 1.0% material, only exponential experiments at Brookhaven National Laboratory were made with that material.

CRITICAL ASSEMBLY
1.5 To 1 W/U RATIO

1.3 % ENRICHMENT
0.600" DIAM. URANIUM
478 FUEL RODS

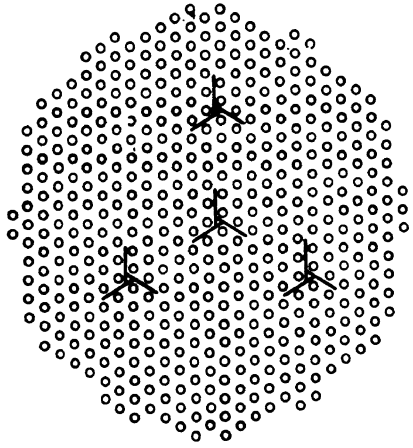

CRITICAL ASSEMBLY
2 To 1 W/U RATIO

1.3 % ENRICHMENT
0.600" DIAM. URANIUM
335 FUEL RODS

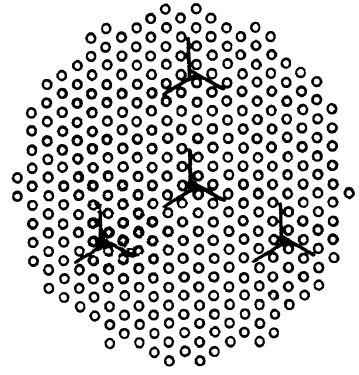

CRITICAL ASSEMBLY
3 To 1 W/U RATIO

1.3 % ENRICHMENT
0.600" DIAM. URANIUM
266 FUEL RODS

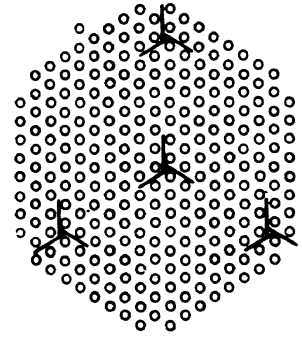

CRITICAL ASSEMBLY
2 To 1 W/U RATIO

1.15 % ENRICHMENT
0.600" DIAM. URANIUM
463 FUEL RODS

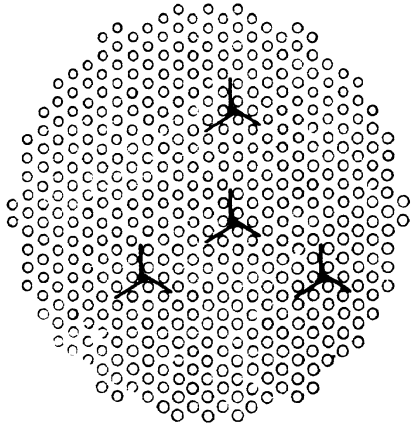

CRITICAL ASSEMBLY
3 To 1 W/U RATIO

1.15 % ENRICHMENT
0.600" DIAM. URANIUM
383 FUEL RODS

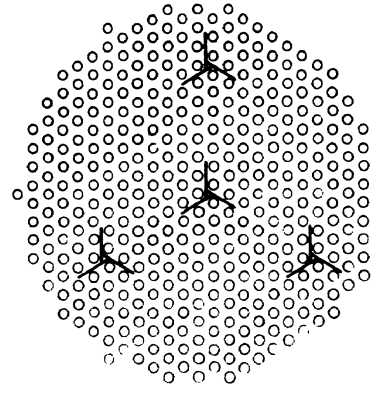

CRITICAL ASSEMBLY
3 To 1 W/U RATIO

1.3 % ENRICHMENT
0.387" DIAM URANIUM
631 FUEL RODS

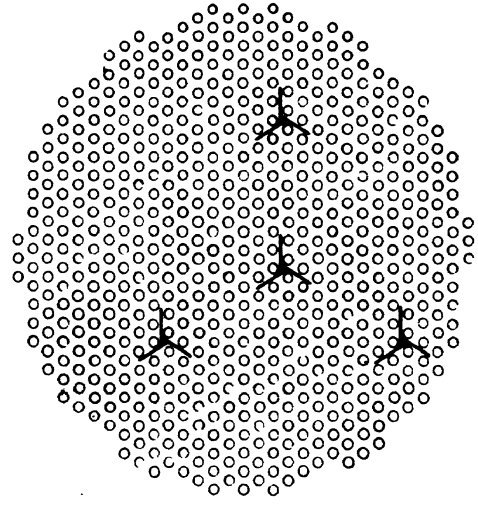

Figure 2

The rods are drawn to the specified diameter and cut to a length of 48 inches. They are then clad in thin aluminum tubes fitted with end plugs and sealed by welding. Next, suitable end pieces of aluminum are attached to the rods. The sketch on the left side of Fig. 1 shows a typical fuel rod. The inside diameter of the aluminum tubing is nominally 0.010 in. larger than the diameter of the uranium rod. The wall thickness of the aluminum is nominally 0.028 in. Thus the outside diameters of the clad rods are 0.666 in., 0.453 in. and 0.316 in. for the three uranium diameters.

The fuel rods are placed in a tank by suspending them by their top end piece in holes in a matrix support plate. The tank has a sufficiently large diameter and has sufficient water at the top and bottom of the lattice to form an essentially infinite water reflector. The matrix support plate is a two inch thick aluminum plate with holes of appropriate diameter forming a hexagonal pattern. The bottoms of the fuel rods fit into a thin aluminum guide plate which is attached to the upper support plate by aluminum rods at the periphery. Several support plates and associated guide plates are available for each rod diameter the holes being arranged to give water-to-uranium volume ratios of 1.5 to 1, 2 to 1 and 3 to 1. The sketch on the right of Fig. 1 shows the dimensions and spacing of the holes in the lattice plate for the 0.600-in. diameter rods (dimensions are in inches) and water to uranium volume ratios are given and not water to total metal ratios.

The reactor is controlled by Y-shaped control rods consisting of cadmium blades clad with stainless steel. Four rods are generally used. The space for inserting these rods is provided between the uranium rods in the lattice plate so that with the rods fully withdrawn, the uranium-water lattice is of uniform geometry throughout.

Critical Sizes

Table I gives pertinent critical information on six lattices which have been made critical. The lattice pattern at criticality is shown in Fig. 2 for each of these six cases. These diagrams show only the pattern at criticality. They are not drawn to scale. In the case of the 3/1 lattice at 1.15% enrichment, 0.600-in. diameter, 383 rods are shown on the diagram. The extra three peripheral rods give the lattice a positive period of 140 seconds. The control rod locations are shown on the diagrams. The rods were fully withdrawn from the lattice at criticality in every case.

Insofar as possible the critical lattices approximate a cylinder. In order to determine the buckling it is necessary to determine the equivalent radius of the critical lattice in some quantitative way. This was done by associating a cell area with each rod and defining the radius of the circle having the same total area as all the cells. Thus the radius of the critical core is determined from the relation

$$\pi R^2 = NA \tag{1}$$

where R is the effective radius of the core, N is the number of fuel rods, and A is the area of a unit cell. For the 0.600-in. diameter rods, for example,

$$R = 0.525X\sqrt{N} \tag{2}$$

where X is the center-to-center spacing of the rods.

The buckling values were calculated from the equation

$$B^2 = \left(\frac{2.405}{R + \lambda}\right)^2 + \left(\frac{\pi}{h + 2\lambda}\right)^2 \tag{3}$$

where λ is the reflector savings.

In the buckling values given in Table I the reflector savings which were used were those obtained by the Brookhaven exponential experiments.[1]

Migration Area by the Water Height Experiment

The migration area for neutrons in the uranium-water lattice can be determined by an interesting experiment. The lattice is adjusted to criticality at various radii (greater than the critical radius) by having the water at less than full height. The rate of change of reactivity with water height is measured at each critical height. From a series of these measurements the migration area can be deduced.

A one group theory[2] for proceeds as follows:

$$k_{eff} = k_\infty \frac{1}{1 + M^2B^2} \tag{4}$$

where k_{eff} is the effective multiplication constant of the lattice, k_∞ is the infinite medium multiplication constant and

$$\left(\frac{1}{1 + M^2B^2}\right)$$

is the non-leakage probability. M^2 is the migration area and B^2 the geometrical buckling. B^2 is given by Equation 3. It is convenient to change the notation of the reflector savings and write B^2 as follows:

$$B^2 = \left(\frac{2.405}{R + \lambda_R}\right)^2 + \left(\frac{\pi}{h + \lambda_H}\right)^2 \tag{5}$$

Table I. Critical Sizes of Uranium-Water Lattices

W/U	*Enrichment (per cent)*	*Rod diameter (inches)*	*Number rods at critical*	*Effective radius (cm)*	*Buckling (cm^{-2})*
3	1.3	0.600	266	25.60	60.8×10^{-4}
2	1.3	0.600	335	25.14	61.2×10^{-4}
1.5	1.3	0.600	478	27.61	52.4×10^{-4}
3	1.15	0.600	380	30.60	47.0×10^{-4}
2	1.15	0.600	463	29.56	48.4×10^{-4}
3	1.3	0.387	631	25.86	59.9×10^{-4}

where R is the core radius, h the core height and λ_R and λ_H the radical and the total axial reflector savings respectively. The equivalent bare height H is, by definition

$$H = h + \lambda_H$$

Further

$$\frac{\partial H}{\partial h} = 1$$

if λ_H remains constant with water height.

Now in the experiment the reactivity ρ is actually measured.

$$\rho = \frac{k_{eff} - 1}{k_{eff}} = \frac{k_\infty - 1 - M^2B^2}{k_\infty} \tag{6}$$

$$\frac{\partial \rho}{\partial h} = -\frac{M^2}{k_\infty}\frac{\partial B^2}{\partial h} = \frac{2\pi^2 M^2}{k_\infty}\frac{1}{H^3} \tag{7}$$

The manner in which the data is handled is to plot h the water height above the bottom of the core against the inverse cube root of

$$\frac{\partial \rho}{\partial h}$$

A straight line is fitted to the data by a least squares fit and

$$\frac{M^2}{k_\infty}$$

is calculated from the slope of the line. The intercept of the line gives the total axial reflector savings λ_H for the experiment.

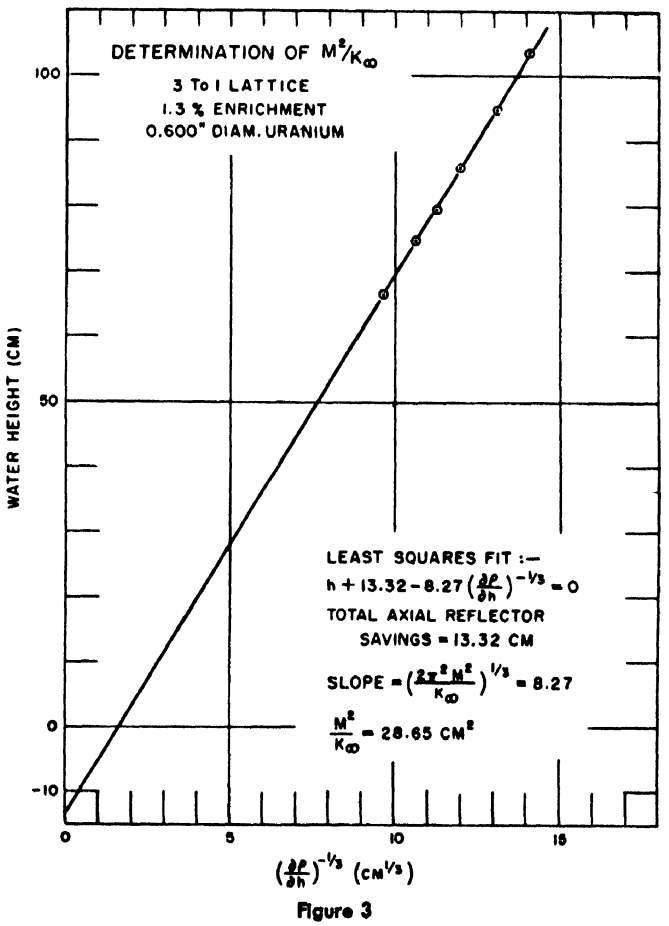

Figure 3

It should be noted that while the bottom reflector (axially) is water and aluminum, the upper reflector is a forest of exposed fuel rods. Since it is important that the reflector savings due to this forest of rods should not vary during any of the experiments, the critical water height used was never greater than 43 inches. Thus there was always a minimum of five inches of exposed fuel rods above the water. The total axial reflector savings obtained in this way will not necessarily agree with the total axial reflector savings of the lattice with a full water reflector on both top and bottom.

Figure 3 shows a typical plot of experimental data from which a determination of

$$\frac{M^2}{k_\infty}$$

can be made. The value of k_∞ can be expressed in terms of M^2 and the critical buckling of the lattice in question. From this M^2 and k_∞ can be determined by using the critical bucklings tabulated in Table I.

The values of M^2 and k_∞ determined in this way for three lattices are tabulated in Table II.

The error in these M^2 determinations, due to experimental inaccuracies, is estimated to be about ± 1.5 cm.^{2}

Another method of determining M^2 can be developed by comparing critical lattices with rods of differing enrichments at a given W/U ratio. This method depends on a rather good value for η and particularly on the value of f, the thermal utilization. The results obtained at Westinghouse by this method are still considered preliminary.

Temperature Coefficient of Reactivity

The reactivity change as a function of reactor temperature change was studied for each of the lattices. The temperature changes are accomplished by electric immersion heaters in the reflector region of the core. A circulating pump takes water from the bottom of the core tank and discharges it at nearly full water height. This discharge is directed at the fuel rods in the core. The reactor tank holds approximately 800 gallons of water when completely filled and the pump circulates 150 gallons per minute.

Table II. Migration Area Determination by Water Height Method

W/U	Enrichment (per cent)	Rod diameter (inches)	$M^2(cm^2)$	k_∞
3	1.3	0.600	35	1.21
2	1.3	0.600	37	1.23
3	1.15	0.600	34.8	1.16

The temperature is obtained from calibrated resistance thermometers placed at various points around the core and from a platinum resistance thermometer in the core. The temperature variations throughout the water are in the range of ± 0.1°C.

Two methods are used to measure the reactivity change. For small values of the temperature coefficient the reactivity change is determined by the change in period of the reactor from a positive initial period of about 100 seconds. For larger coefficients the reactivity is determined by inserting a control rod a short distance into the lattice and calibrating the rod by period measurements. The calibrated rod is used to compensate for the reactivity changes with temperature.

Figure 4 gives the temperature coefficient of reactivity as a function of temperature (both in Centigrade units) for a number of lattices. All of the coefficients shown are negative except for the 3 to 1 lattice at the lowest temperature. The estimated experimental error in the temperature coefficient is about $\pm 0.05 \times 10^{-4}$ in reactivity per degree Centigrade. No studies were made with lattices having a positive temperature coefficient of reactivity over an extended range.

Thermal Utilization

The thermal utilization, f, is defined as the number of thermal neutrons absorbed in fuel per thermal neutron absorbed in the reactor. Two methods have been used to determine the thermal utilization of the uranium-water lattices. In the first method a series of special foils are irradiated to obtain a flux traverse through a fuel rod and the adjoining water moderator.

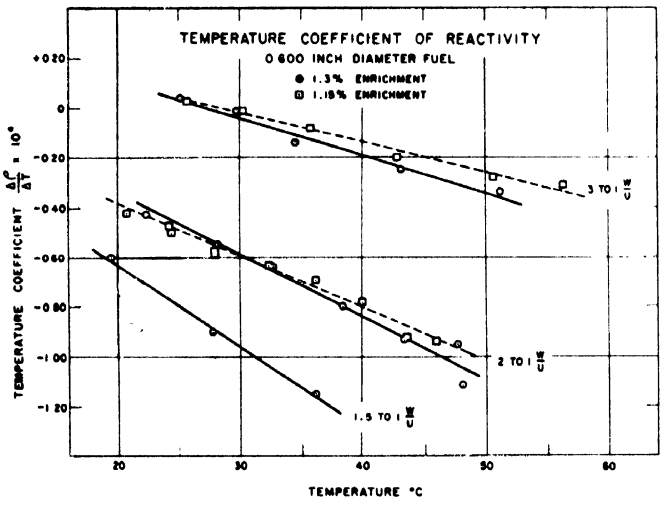

Figure 4

The thermal utilization is then calculated from this traverse. This is the method used in the Brookhaven exponential experiments.[1] In the second scheme a sector foil of uranium-235 is exposed, one piece of the foil being inside the fuel rod, the other in the moderator. The ratio of the fission product activities of the two foils permits calculation of the thermal utilization.

The sketch on the right side of Fig. 5 shows both schemes. In this diagram four adjacent fuel rods in the lattice are shown. The lower half of the diagram shows the flux traverse scheme.

In the flux traverse method one of the fuel rods is cut into two halves at the center. A special top on the cladding tube of this rod permits the tube to be opened for insertion of a foil holder between the two halves of the fuel rods. The foil holder is a disc of uranium one-eighth inch thick and of the same enrichment and diameter as the fuel of the rod being used. In the face of the uranium disc thirteen equally spaced holes are cut, 0.070 inches in diameter and approximately 0.020 inches deep.

The space between the adjacent fuel rods is fitted with a triangular shaped piece of one-fourth inch thick Lucite cut to fit the space between the fuel rods. As shown on Fig. 5 a number of holes are cut into the Lucite block to accommodate foils of the same size used in the fuel rod. The foils in the water are located to take flux traverses along two directions, one along the median plane between adjacent rods the other on the line of centers of adjacent rods.

The foils used in the experiment are made of dysprosium oxide molded in polyethylene in equal weight proportions. The foils are punched from stock 0.015 inch thick and at a diameter of 0.065 inch.

For the thermal utilization measurement the inside foil holder is loaded with the foils and placed at the center of a fuel rod. The outer holder is positioned at the center of the lattice axially, adjacent to the rod with the inner foil holder. The foils are arranged in the geometrical pattern shown in Fig. 5. The special rod and holder are located near the center of the lattice. The foils are then irradiated to activate the dysprosium. After irradiation the foils are removed and β counted for activity.

The dysprosium has a high thermal cross section with approximately a $1/v$ energy relationship over the thermal energy range up to about 1 ev. The cadmium ratio of the dysprosium used was measured in the lattice and found to be approximately 35.

In calculating the thermal utilization the flux shape is deduced from the experimental points using a diffusion theory expression for the thermal flux in a lattice cell to interpolate between experimental points. The flux is then averaged in the moderator, in the fuel and finally an average value is obtained at the cladding. The thermal utilization is then calculated using tabulated cross sections for the materials concerned and averaging over a Maxwellian distribution at room temperature.

There is a major difficulty with this technique in the tighter lattices since only a few foils can be positioned in the moderator. Further the data taking, curve fitting and analysis is fairly laborious. A simpler scheme is the sector foil arrangement. This is shown in the diagram at the top of Fig. 5.

The shaded quadrilateral shown in this diagram is composed of two triangles of symmetry of the lattice. The ratio of the shaded area inside the fuel rod to the shaded area outside the fuel rod is the same as the ratio of total fuel area to total moderator area in a lattice cell section. Two foils are used in this measurement, one inside the fuel rod, the other outside. For purposes of this discussion the foils can be considered to have the area shown shaded. The foils are an alloy of uranium-235 in aluminum approximately 0.005

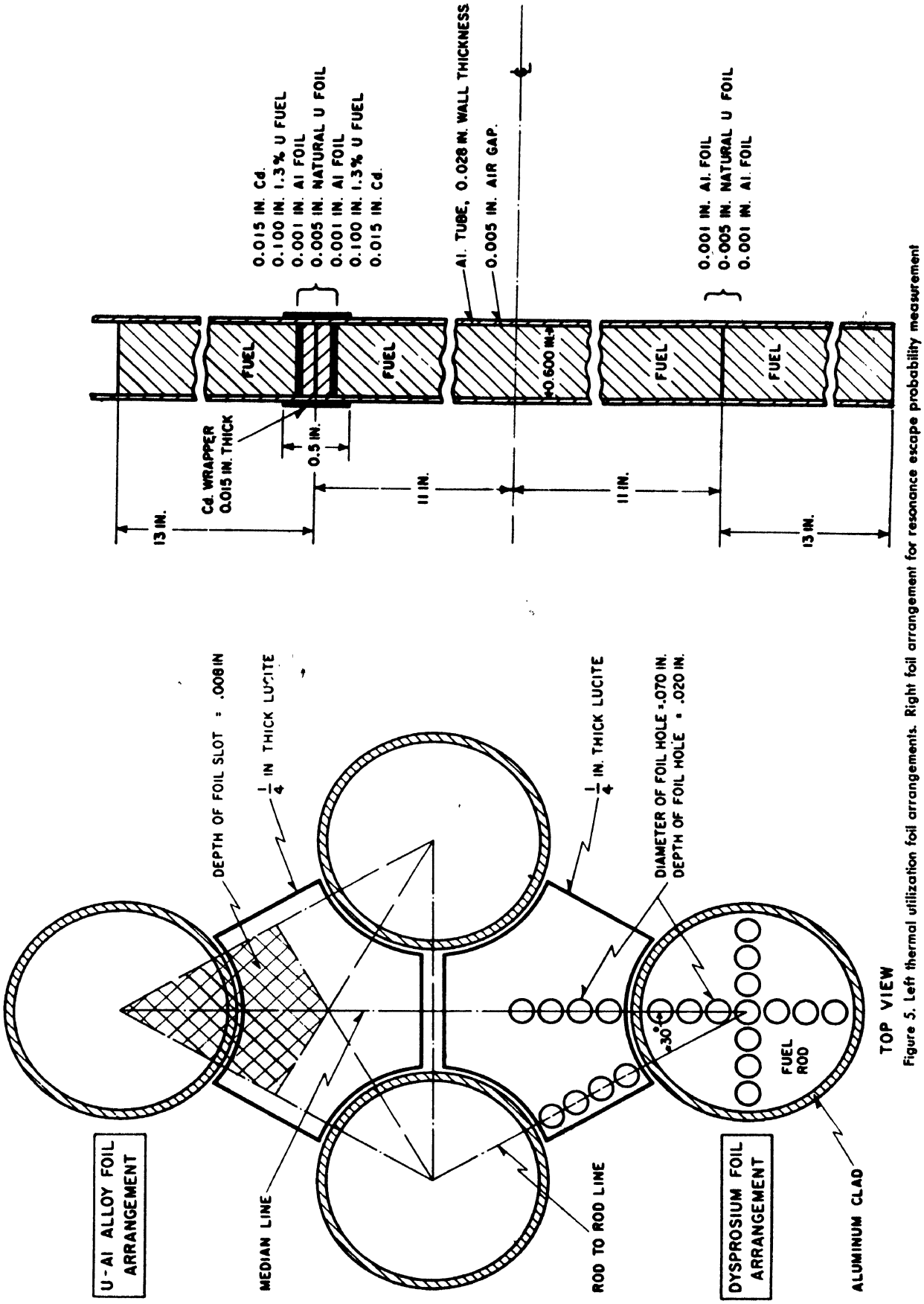

Figure 5. Left thermal utilization foil arrangements. Right foil arrangement for resonance escape probability measurement

inches thick. When the foils are irradiated the fission products formed at any point are essentially proportional to the thermal flux at that point. By counting the fission product activity of the entire foil, the thermal flux is, in effect, averaged over the area occupied by the foil. The foils were covered with 0.001-in. aluminum foil to prevent contamination from the fuel rods.

This scheme gives experimentally the ratio of the average thermal flux in the moderator to the average thermal flux in the fuel. By multiplying by the appropriately averaged cross sections, the thermal utilization may be calculated. This average was taken over a Maxwellian distribution at room temperature. As a check in one of the lattices, W/U of 3/1, 0.387-inch diameter rods, 1.3% enrichment, the cadmium ratio was measured on a sector foil in both the water and the fuel and found to be 12 in both within experimental error. The thermal utilization as determined by the sector foil method agrees within the experimental error with that calculated from the dysprosium foil activities.

Table III gives the thermal utilizations of the lattices which have been measured.

Table III. Thermal Utilization of Water-Uranium Lattices

W/U	Enrichment (per cent)	Rod diameter (inches)	Thermal utilization
3	1.3	0.600	0.849
2	1.3	0.600	0 890
1.5	1.3	0.600	0.918
1	1 3	0.600	0.949
3	1.15	0.600	0.836
2	1.15	0 600	0.881
3	1.3	0.387	0.858

It is estimated that the accuracy of the value tabulated is $\pm 0.4\%$ based on estimates of the experimental errors. The lattice having a W/U ratio of 1 was measured only by the dysprosium foil technique because the sector method had not at that time been developed. This lattice consisted of an inner zone at a W/U ratio of 1 and an outer zone at a W/U ratio of 2 since there was an insufficient number of rods to achieve criticality at a W/U ratio of 1 throughout the lattice. Because of the limited number of foils which could be located in the water in this lattice, this measurement is subject to considerably more uncertainty than the others. The last value tabulated in Table III was taken only by the sector method.

Resonance Escape Probability

This experiment determines the ratio of plutonium nuclei formed in the fuel by capture in the resonance region to that formed by capture in the thermal region. The measurement is made by exposing two uranium foils in the reactor, one covered with cadmium, the other bare. The ratio of the plutonium formation in the two foils is determined by counting techniques. The resonance escape probability is then calculated using the measured value of the thermal utilization and known cross-section information.

The probability that a neutron entering the resonance region will be captured in uranium-238 is by the definition of p,

$$(1 - p)$$

This is the number of plutonium nuclei formed by resonance capture per neutron entering the resonance region.

The number of neutrons captured as thermal neutrons in the fuel per neutron entering the resonance region is

$$pf$$

where f is the thermal utilization.

The fraction of the thermal neutrons captured in fuel which are captured in uranium-238 is defined as F.

$$F = \frac{\Sigma_{a238}}{\Sigma_{a238} + \Sigma_{a235}} \tag{8}$$

where the Σ's are the macroscopic absorption cross sections for uranium-238 and uranium-235 averaged over the thermal spectrum (assumed Maxwellian at room temperature). The number of plutonium nuclei formed by thermal capture in uranium-238 per neutron entering the resonance region is

$$pfF$$

If ρ is defined as the ratio of plutonium formed by capture in the resonance region to the plutonium formed by capture in the thermal region

$$\rho = \frac{(1 - p)}{pfF} \tag{9}$$

The experiment measures the relative activity associated with plutonium formation in a bare foil and in a cadmium covered foil. If this ratio is defined as C,

$$C = \frac{\text{Bare foil plutonium activity}}{\text{Covered foil plutonium activity}}$$

then

$$\rho = \frac{1}{C - 1} \tag{10}$$

Using this definition of C, the following expression for p is obtained:

$$p = \frac{(C - 1)}{(C - 1 + fF)} \tag{11}$$

It should be noted that this simple theory neglects the effects of neutron leakage from the reactor.

The manner in which the foils are exposed is shown in the diagram on the left side of Fig. 5. The bare foil and the cadmium covered foils are exposed in the same fuel rod. The uranium fuel in this rod is sectioned in three pieces as shown and the rod is equipped with a special top plug so that the uranium fuel may be removed for insertion of the foils. The foils in the fuel rod are irradiated simultaneously. One foil is located 11 inches above, the other 11 inches below the lateral central plane of the active lattice. For the newer ex-

periments a 3 inch spacing above and below the center plane is used. During the irradiation the special rod is located quite close to the vertical center line of the active lattice.

The foils used were, in general, natural uranium foils 0.005 inches thick and the same diameter as the fuel rod. The foils were covered on both sides by 0.001-inch aluminum foils to prevent contamination by recoil fission fragments from the fuel. In the uncovered foil these three items constituted the entire package of foils. In the cadmium covered foil two 0.100-inch thick uranium discs of the same enrichment as the fuel rod were included on both sides. This layer of fuel minimizes streaming of fast neutrons through the cadmium wrapper directly into the foil. Finally the covered foil package was completed by two 0.015-inch thick cadmium foils. The cadmium covering on the diameter is provided by a 0.5 inch high, 0.015-inch thick cadmium foil wrapped around the cladding of the fuel rod.

The plutonium production rate in the foils is determined by measuring the 2.33 day Np^{239} activity. The reaction is

$$U^{238}(n\gamma)U^{239}\xrightarrow[23\ min]{\beta,\gamma}Np^{239}\xrightarrow[2.33d]{\beta,\gamma}Pu^{239}$$

The neptunium activity was measured by measuring the γ-ray decay activity. The principal gamma ray peak of the neptunium decay spectrum occurs near 104 kev. This is attributed to plutonium X-rays resulting from internal conversion of the γ-rays associated with the neptunium decay.

The relative plutonium production in the two foils was measured by measuring the intensities of the 104 kev gamma peak. A scintillation spectrometer was used for the purpose. There is a considerable background in the foil due particularly to the fission product activity in the foil and to a lesser extent due to the 94 kev peak from the decay in natural uranium. To correct for the fission product activity, the decay of the 104 kev X-ray line produced by the γ-rays acting on the heavy elements was followed by exposing an enriched foil and counting it over a number of weeks. The natural uranium foils were counted for at least two weeks after exposure. In one case the foils were counted for twelve weeks. The long counting periods were used to analyze the decay constant of the activity being measured.

After some measurements had been made with the natural uranium foils, it became apparent that considerably less correction to the data would be required if the fission product activity in the foil were reduced. This has been done by obtaining foils of uranium which are very highly depleted in uranium-235. The data for the 0.600 inch, 1.3% rods was obtained with natural foils. Subsequent data has been taken with depleted foils.

The experimental results of the p measurement are tabulated in Table IV.

In general the experimental error in these determinations of p is estimated to be about $\pm 1\%$. The measurement at the W/U ratio of 1 was made with a dual lattice having an inner zone at a W/U ratio of 1 and an outer zone with a W/U ratio of 2. The value of p obtained for this lattice must be considered tentative until the calculated flux distributions for this lattice have been fully analyzed and evaluated.

FLEXIBLE CRITICAL EXPERIMENT

A brief description will now be given of the PWR flexible critical experiment and of the work planned for this facility. As was pointed out in the introduction, this facility is used to provide nuclear design information primarily on flux distributions, control characteristics and temperature coefficient of reactivity.

The attempt made in the design of this facility was to obtain a reactor which resembled the actual PWR design in considerable detail, at least with respect to nuclear properties. The word flexible in the description of the facility indicates a freedom of rearrangement. This is possible to a limited extent. Without rebuilding the basic fuel elements themselves, it is possible to vary the water to metal ratio in the seed and in the blanket; the basic cluster size of the reactor; the number of seed units; the geometrical disposition of the seed units; and the number, size and geometrical arrangement of the control rods. With a limited additional effort the fuel loading of the seed may be modified.

Table IV. Measurements of Resonance Escape Probability

W/U	Enrichment	Rod diameter (inches)	p
3	1.3	0.600	0.850
2	1.3	0.600	0.794
1.5	1.3	0.600	0.720
1	1.3	0.600	0.597
3	1.15	0.600	0.839
2	1.15	0.600	0.792

While the flexibility indicated is available, it is a considerable task to rebuild the entire core structure. For this reason, once a full scale core has been built up, it is unlikely that it would be changed to duplicate a minor design change in the PWR. In point of fact in making the original mockup, it is necessary to make certain compromises in duplication. Furthermore the facility is not designed to be operated at temperature much above ambient temperature. The facility then may be a good duplicate of the cold reactor but it is only a fair duplicate of the hot operating reactor.

The inevitable differences between a critical experiment and the operating reactor require an approach to interpretation of data obtained with the facility The approach adopted for the PWR is quite simple. A theoretical model must be used to convert data obtained on the critical facility to PWR operating data. The model to be used will be the same as that used for the design calculations. This model will be used first to calculate the results to be expected from the cold,

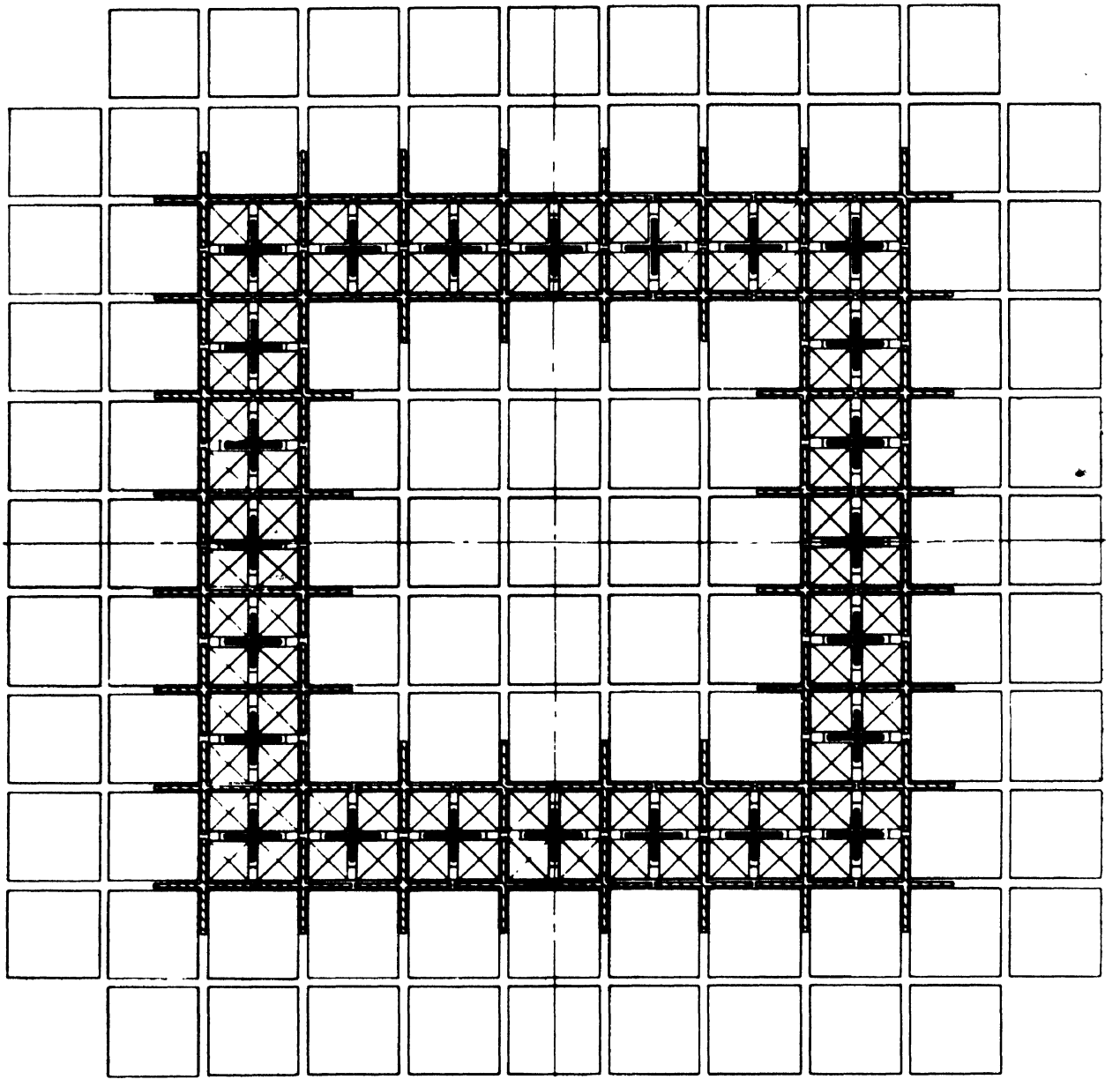

Figure 6. Reference reactor core cross section

critical experiment. Insofar as the calculated results agree with the measurements, the theoretical model can be trusted to calculate conditions in the operating reactor. The closer the experiment is to the operating reactor the more limited is the dependence on the theoretical scheme. For example, while the water in the critical experiment cannot be heated to PWR operating temperature, a moderator of reduced hydrogen density can be used. While this will not produce the same neutron distribution in energy as exists in the operating reactor, the difference between the reactor and the experiment is significantly reduced.

Description of Facility

Figure 6 is a diagram of the PWR reference core in cross section. The units with the *X*'s inscribed are the seed units, while the open squares are the positions of the blanket units. As shown, the control rods are used only in the seed region.

Figure 7 is a cross section of a seed unit and of a blanket unit. Figure 8 shows a longitudinal view of a seed unit. A longitudinal view of the blanket unit would be quite similar to the seed unit.

The seed unit shown in Fig. 8 is a subassembly and consists of 13 zirconium plates. The plates are essentially the same dimensions as the seed fuel plates in the PWR core. The fuel is added to the seed by means of extruded polyethylene tapes with the enriched U^{235} as U_3O_8 contained within the tape. The tape is sealed to the zirconium strip by a thin layer of polyethylene.

There is a limited amount of uranium oxide which may be mixed with the polyethylene and permit a good fuel tape to be extruded. The ratio which is used in the seed cluster is about 1 to 1 by volume. The tapes are extruded 1.25 in. wide and 0.030 in. thick. The tapes are cut to a length of six feet before they are attached to the zirconium, then the active core is six feet long.

The maximum amount of U^{235} which can be produced in a fuel tape is approximately 30 gm. To obtain the desired seed loading it is necessary to have two fuel tapes in one of the water channels of each seed subassembly.

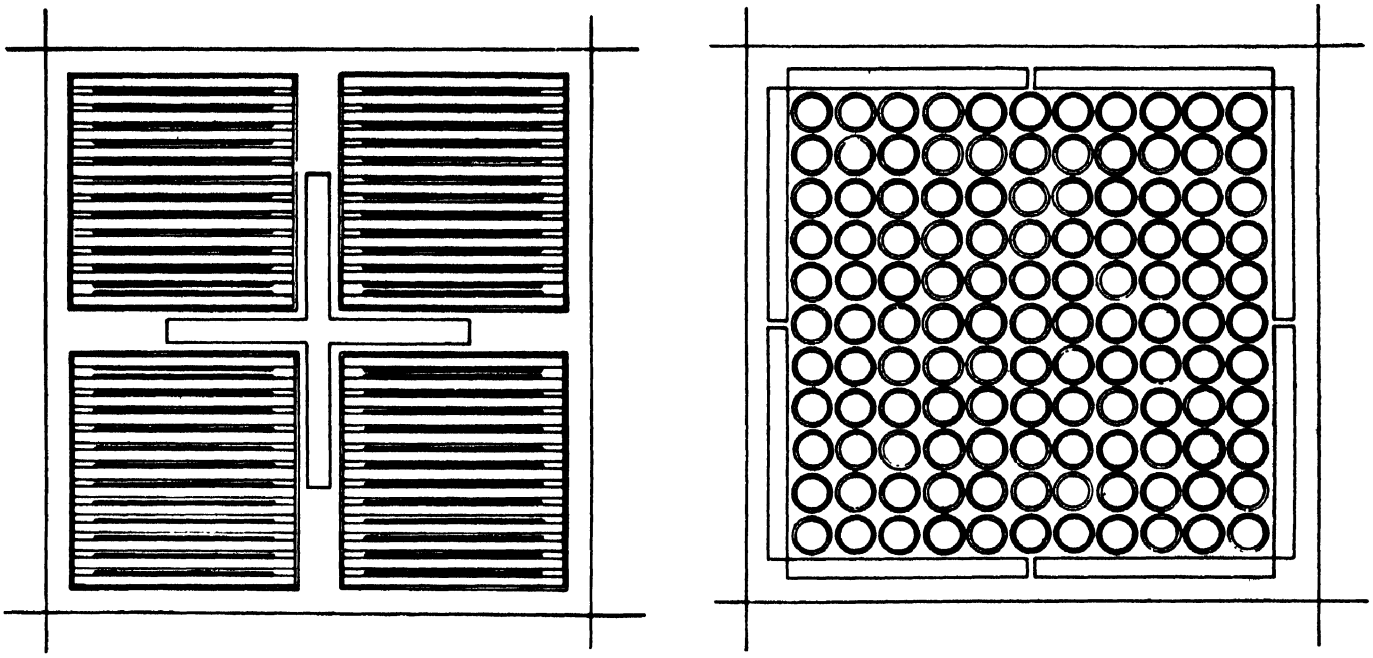

Figure 7. Seed cluster. Oxide bundle (blanket)

The polyethylene tape technique is used to provide the fuel loading of the reactor for two reasons. First, it permits the fuel loading to be changed, and second it provides an excellent reactor shutdown mechanism in the event of a reactor runaway. Should a reactor excursion take place, the fission recoil particles in the plastic both heat the plastic and release hydrogen through the formation of cross linking. The hydrogen gas expands the softened plastic causing water to be ejected from the water channels and shutting the reactor down. This shutdown occurs at a sufficiently low power to limit the damage caused by the runaway.

Clearly if this shutdown mechanism is to be operative, there must be a reasonable amount of water left in each water channel for expulsion. This limits the amount of plastic to about half the thickness of the channel. Furthermore if more plastic were used, the safety shutdown achieved by draining the water from the reactor tank would be seriously compromised by the moderation of the hydrogen in the plastic.

The seed subassemblies are held together by flexible pins fitted at intervals along the sides of the bundle. The entire subassembly is jacketed in a thin aluminum can as shown in Fig. 8 which provides a guide for the control rod channel. The top and bottom of each unit is provided with suitable end pieces for support and handling.

The blanket units are made up of tubes of aluminum filled with oxide pellets of the same size as in the PWR fuel elements. The oxide tubes are six feet in length and are held in the bundle by spacer plates located along the length of the bundle. Zirconium plates are attached to the periphery of the bundle to mock up the design of the blanket units in the PWR core. The individual units of the core are loaded into a tank which can be filled with water. The units are supported at the bottom by a heavy support plate and positioned at the top by an egg-crate structure. The control rod drives can be positioned from a flexible arrangement supported on a framework above the core tank. Cadmium-silver control rods are used. These have the appropriate thickness to mock up the effectiveness of hafnium rods.

The design of the experiment is closely related to the PWR design so that individual units of the PWR core can be interchanged with the mockup units should this be desired.

In addition to the natural uranium oxide, natural uranium bars of the same dimensions as the zirconium bars making up the seed units are available. These bars permit mockup of high uranium metal alloy for the blanket region. By using the plastic tapes, zirconium bars and uranium bars, the equivalent of a slightly enriched metal lattice can be built up.

Experimental Program

Only an indication of the planned experimental program can be given since it lies largely in the future. To the present time a few lattices have been made critical on this facility. These were equivalent to slightly en-

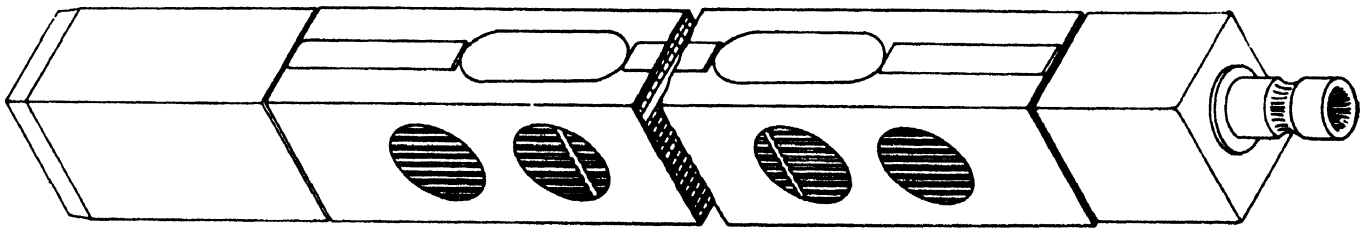

Figure 8. Seed bundle

riched uranium-zirconium alloy lattices in water. Some data has been taken with these lattices but has not yet been analyzed in detail.

The next planned experiment is a seed and blanket study. A slab seed equivalent to one side of the PWR core will be set up with a uranium blanket. Criticality and control studies will first be made with this unit. This will involve measuring the shutdown capabilities of the control rods, the reflector savings of the blanket and the equivalent distributed poison worth of the control rods. This latter experiment will be carried out either by adding boron loaded plastic tapes to the seed or by reducing the fuel loading of the seed.

The next experiments will be thermal flux traverses across the seed blanket interface region. This is important to verify the calculated one-dimensional distributions in the PWR design.

Control rod bank studies will next be carried out to permit engineering design of the control system to proceed. The neutron fluxes at the position of the pressure vessel will be measured to permit estimates of the neutron flux available for instrumentation to be made.

As this program proceeds the core will in all probability be built up to its full size. This will permit detailed thermal flux distributions to be measured. As noted above it is planned to use a moderator with reduced hydrogen density to mock up conditions similar to those in the hot reactor.

The program outlined above is an indication of the type of work planned for this type of facility. This program will extend over a period of several years, overlapping the start of the PWR plant itself.

REFERENCES

1. Kouts, H. C., P/600, *Exponential Experiments with Slightly Enriched Uranium Rods in Ordinary Water*, Volume 5, Session 21A, these Proceedings.
2. Glasstone, S. and Edlund, M. C., *The Elements of Nuclear Reactor Theory*, D. Van Nostrand Co., Inc., New York (1952).

The Theory of Uranium Water Lattices

By J. Chernick,* USA

Interest in the United States in uranium water lattices has gone through several cycles since the early days of the Manhattan Project. Consideration of water as a possible moderator with natural uranium fuel elements was of prime interest until dampened by preliminary measurements of its thermal neutron absorption cross section. Later calculations, stimulated by an improved set of cross sections and the suggestion of L. Szilard that the interaction fast effect might prove decisive in close packed lattices, indicated that a multiplication factor very close to unity could be achieved in optimum arrangements of ordinary uranium and water. A series of exponential experiments on rod lattices carried out at the Clinton Laboratories in 1944–45 showed that a multiplication factor slightly in excess of unity could indeed be obtained with an assembly of normal uranium rods in water at room temperature when the rods were surrounded by a suitable air gap. Again, the discovery of the large poisoning effect of Xe^{135} discouraged further experiments along these lines.

With the release of uranium enriched in U^{235} as a reactor fuel, water has again become competitive with weaker absorbers such as D_2O and graphite as a moderator for thermal research and power reactors. Interest in slightly enriched uranium rod lattices in water has led to an extensive and continuing program of experiments to determine the basic nuclear properties of these lattices. The program was initiated at the Brookhaven National Laboratory (BNL) in 1951 in cooperation with a group under K. Cohen then of the H. K. Ferguson Company and has continued since 1952 in collaboration with the Westinghouse Atomic Power Division (WAPD).

The theory of uranium fueled, water moderated assemblies has been advanced not only by the staff of the above laboratories, but also by members of various other laboratories. Individual contributors, too numerous to mention here, are acknowledged in the body of the present paper.

GENERAL CONSIDERATIONS

The early work on the theory of nuclear chain reactions in a lattice of uranium and moderator was outlined by E. P. Wigner[1] in 1946. Many of the problems discussed in this paper remain incompletely solved. The advantages possessed by the reactor physicist today are due mainly to improvements in computing techniques and machinery and in the knowledge of nuclear constants afforded by integral experiments and cross-section measurements. For example, Wigner's study of resonance capture[2] in uranium fueled assemblies was based on very meagre data on the low energy resonances in U^{238}. Reactor calculations were generally limited to what could be done on a hand computing machine.

On the other hand, diversification of the reactor field has brought a shift in the emphasis on many problems. Where the early work was directed toward the problem of assembling any practical system with a multiplication factor greater than unity, one of the goals today is to achieve a conversion ratio greater than unity. A knowledge of the neutron spectrum and capture to fission ratio as a function of energy is much more critical in the latter case. Similarly, economic considerations emphasize the importance of studies of long range reactivity effects and reactor control. Metallurgical, heat transfer and chemical processing limitations have brought to the fore novel and often complex reactor components and have increased the need for adequate nuclear constants and computational techniques.

Theoretical methods of treating neutron transport in normal or slightly enriched uranium lattices are generally patterned after Fermi's basic work. That is, the reactor system is assumed to be predominantly thermal and the multiplication factor for an infinite system is given by the conventional four factor formula

$$k_\infty = \eta\epsilon pf \qquad (1)$$

The multiplication factor k_{eff} for a finite system is then obtained from models of the slowing down and thermal diffusion process appropriate to the moderating system.

For water moderated reactors, and especially for close packed lattices, the older work requires considerable refinement. The increased importance of fast fission in these assemblies has already been mentioned. Accurate calculations of this effect in heterogeneous systems require a considerable effort and the results are sensitive to changes in such nuclear data as the inelastic cross-sections of U^{238} and the variation of ν and α of U^{238} as a function of energy. The older literature found no relevant difference between values of ϵ for finite and infinite systems. Where the interaction fast effect is large, this assumption is invalid. The standard formula for p is strained when extrapolated

* Brookhaven National Laboratory, Upton, New York.

to lattices where resonance capture is large. As early as 1944, Dancoff and Ginsburg showed that surface resonance capture was decreased in close packed lattices of uranium rods in water by the shielding effect of neighboring rods. Again, epithermal fission in U^{235} while negligible for widely spaced lattices of natural uranium in water becomes increasingly important when the spacing is decreased or the U^{235} enrichment is increased.

Early investigators recognized the limitations of diffusion theory in calculations of the intracell flux distribution and thermal utilization of uranium lattices. However, until large scale exponential experiments were initiated on these lattices at various AEC sites, there was no way of comparing studies of more elaborate forms of the one-velocity Boltzmann equation with experiment. Some progress has also been made on the companion problems of chemical binding in hydrogenous moderators and on the thermal neutron spectrum in homogeneous systems where the ratio of the absorption cross-section to the slowing down power of the system is not negligible.

NEUTRON TRANSPORT IN HYDROGEN MODERATED REACTORS

The complex machinery required for exact computations of neutron transport in reactor lattices and uncertainties in nuclear data have been such that until recently such calculations were not attempted. Instead, slowing down problems have generally been treated by use of a homogeneous approximation to the reactor system.

In an infinite homogeneous system, the steady state slowing down problem simplifies into an integral equation in a single variable, the neutron energy. Problems of this type have been fully discussed by Placzek[3] and Marshak.[4]

For hydrogen, or a mixture of hydrogen with elements that scatter without energy loss, an exact solution of the integral equation is obtained. When energy degradation in elastic collisions is taken into account, analytical solutions may still be obtained but only over energy intervals which decrease with the mass of the heaviest element in the mixture. Except for a light element such as deuterium such a procedure becomes very laborious and a number of more approximate methods have been devised. In the method of synthetic kernels, for example, one replaces the exact kernel of the integral equation by a soluble approximation. The formula for resonance capture p based on synthetic kernels due to Fermi and Wigner becomes

$$p = \frac{\Sigma_s(E_0)}{\Sigma(E_0)}\, e^{-\frac{1}{\xi}\int_E^{E_0}\frac{\Sigma_a}{\Sigma}\frac{dE}{E}} \qquad (2)$$

with $\Sigma = \Sigma_s + \gamma_0\Sigma_a$ and $\gamma_0 = 0$ or 1 respectively. A more accurate kernel for single elements due to Greuling and Goertzel yields $\gamma_0 = 1$ for hydrogen, and $\gamma_0 = \frac{2}{3}$ for a heavy element.

For mixtures of hydrogen and heavy elements, Goertzel[5] has suggested an exact treatment of the hydrogen kernel combined with the Fermi approximation for heavy elements. This procedure results in a pair of coupled differential equations and when applied to reactor calculations has become known as the Selengut-Goertzel method.

The most common method of treating slowing down problems with space variation is the use of multigroup equations with the neutron leakage terms approximated by diffusion theory. Refinements of the multigroup equations based on spherical harmonics methods have been investigated by G. Safanov of the Rand Corporation and by J. Fleck.[6] When the number of neutron groups or reactor regions becomes excessive for hand computation, the solution of multigroup equations is generally carried out on high speed electronic computing machines. The ORACLE at the Oak Ridge National Laboratory (ORNL), the ADVAC at the Argonne National Laboratory (ANL) and the UNIVAC at the AEC Computing Facility at New York University are examples of such machines. A two-dimensional reactor code capable of handling up to 15 neutron groups and a few thousand space points has been perfected by Stark and Roe of the Knolls Atomic Power Laboratory (KAPL) and is operated on a service basis by the AEC Computing Facility. A more flexible version of this reactor code is being prepared as a joint effort by WAPD, KAPL and the AEC Computing Facility.

A discussion of slowing down methods applicable to uranium water systems is beyond the scope of the present paper. However, the work of Feymman and Welton at Los Alamos on the "effective cross sections" or one-velocity method and its extensions[7] should be noted, as well as the work of Greuling, Garabedian and Weinberg on variational methods, that of Volkoff and LeCaine on slowing down kernels, that of Davison[8] on spherical harmonics approximations and that of Selengut[9] on slab reactors with linearly anisotropic scattering. In addition, the extremely useful multigroup reactor surveys of G. Safanov of Rand deserve mention, as does the recent work of Selengut on water moderated reactors and the use of mode methods for D_2O moderated and reflected systems by Edlund and Noderer of ORNL.

According to a result from the general theory of multiplying systems,[10] the non-leakage probability during moderation in a bare, homogeneous, near critical reactor is given by $P_\infty(B^2)/p$, where $P_\infty(B^2)/p$ is obtained as a series in the even moments of the slowing down distribution for a point source in an infinite medium. The use of diffusion theory for thermal neutrons then results in the formula

$$k_{eff} = \frac{k_\infty P_\infty(B^2)/p}{1 + L^2B^2} \qquad (3)$$

for the multiplication factor of a bare, finite reactor. This result is frequently applied to reflected reactors by assuming the equivalence of bare and reflected systems with the same fundamental flux mode.

To first order, the non-leakage probability is given by $1 - B^2\theta$, where θ is the neutron age or $\frac{1}{6}$ the

Table I. Parameters of Empirical Formula for Inelastic Scattering of Fission Spectrum Neutrons

Parameters: $\beta = 1/T$, T = nuclear temperature
$K = \sigma_i(E)/[1 - (1 + \beta E)e^{-\beta E}]$

Element	β	K
Al	1.35	0.80
Fe	1.2	1.45
Cu	2.0	1.56
Cd	2.0	2.08
W	2.5	2.75
Au	2.5	2.68
Pb	1.15	2.5
Bi	1.0	2.8

second moment of the slowing down distribution. More accurately, $P_\infty(B^2)/p$ is given by $\exp(-B^2\theta)$ for Gaussian slowing down and $(1 + \theta B^2)^{-1}$ for a one-group diffusion theory kernel. The failure of the slowing down density in water to follow either distribution satisfactorily has resulted in the use of more complicated kernels. Thus Greuling matched the early experimental results of Fermi, Anderson *et al.*, for the slowing down density in water to a convolution of three diffusion kernels.

An exact formula for the neutron age in a mixture of hydrogen and heavier elements that scatter without energy loss was first derived by Fermi. J. Ashkin of Los Alamos extended the formula to include neutron absorption. Early calculations of the age of fission neutrons to indium resonance energy in water, water-aluminum mixtures, etc., were obtained in this manner. The results for pure water compared favorably with experiment. Later calculations based on improved cross sections and the Watt formula[11] for the fission spectrum showed more neutrons slowing to thermal in the vicinity of a point fission source in water than were observed experimentally. The most recent of these calculations, by Certaine and Aronson[12] of the Nuclear Development Associates (NDA) and Hurwitz and Zweifel[13] of KAPL result in a best value of 25 cm^2 for the age to indium resonance in water.

The age of fission neutrons in mixtures of water and heavy elements is reduced by energy losses in inelastic collisions. Inelastic collisions are particularly important in the Mev energy range where the hydrogen cross-section falls off sharply.

The determination of non-elastic collision cross-sections and the resulting neutron energy losses involve difficult experiments and present data are incomplete. Where sufficient information on the level structure of the nucleus is available, such as that on Pb, inelastic scattering may be assumed to result in discrete energy losses and the gaps in the experimental results may be filled[14] with the aid of current theoretical models of the nucleus. Where many closely spaced levels are expected, as in U^{238} in the Mev energy range, an adequate fit of the experimental data is obtained by the use of the statistical formula

$$P(E,E') = CE'e^{-E'/T} \qquad (4)$$

for the distribution resulting from an inelastic collision at incident neutron energy E. According to statistical theory, the nuclear temperature is given approximately by $T = (DE)^{1/2}$, with D identified as the average spacing of low lying energy levels.

The data available on uranium in 1952 was fitted to Equation 4 by G. Speisman at BNL. He obtained a value of $D = 25$ kev from the data for 1.5 and 3 Mev neutrons. More recently J. Weil of KAPL has suggested a value of $D = 37$ kev based on current data for 14 Mev neutrons. The formula has also been applied by F. Bjorlund of the California Research and Development Company (CR and D) to a number of lighter elements, by using recent data for 1.5, 3 Mev and fission spectrum neutrons. Despite the question of applicability, Bjorlund obtains a fit of the experimental data which would appear to be adequate for most reactor calculations with $\beta = 1/T$ independent of energy over this energy range. In addition, he finds that the product K of the inelastic cross-section $\sigma_i(E)$ and the normalization factor $C = [1 - (1 + \beta E)e^{-\beta E}]^{-1}$ of the distribution (4) appears to be generally independent of energy. Bjorlund's values of β and K are listed in Table I.

The value of the average logarithmic energy loss in an inelastic collision $\xi_i(E)$ is of interest in modifications of Fermi age theory which take inelastic scattering into account. On the basis of Equation 4

$$\xi_i(E) = \frac{\gamma - 1 + \log x + e^{-x} + E_1(x)}{1 + (1 + x)e^{-x}} \qquad (5)$$

with $\gamma = 0.5772$, $x = \sqrt{E/D}$. A plot of the average logarithmic energy loss for uranium is shown in Fig. 1 for $D = 25$ kev. Such a model was first used by Soodak and Forman in 1944 to obtain the neutron age in mixtures of uranium and water. They employed the standard Fermi age formula with first and last flight corrections.

The latter corrections may require some explanation, since they do not occur in the standard Fermi age-diffusion treatment. The last flight correction is generally introduced because the root mean square distance travelled by a neutron to the position where it crosses energy E is somewhat less than the distance

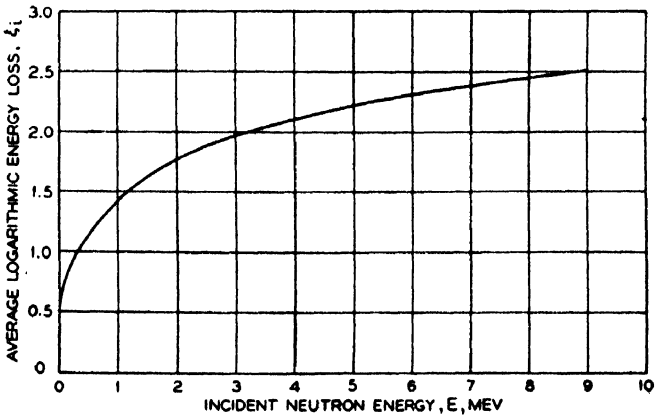

Figure 1. Av. logarithmic energy loss in inelastic collision with U vs incident neutron energy

to the position of collision at energy E. In the Fermi, Wigner and Greuling-Goertzel approximations, the difference in neutron ages is given by

$$\theta_\phi - \theta_q = \frac{1}{3}\frac{\gamma_0}{\Sigma_s(E)\Sigma_{tr}(E)} \tag{6}$$

with $\gamma_0 = 0$, 1 respectively in the Fermi and Wigner approximations.

Similarly, a first flight correction is generally applied to correct for the distance travelled by a source neutron to the position where it makes its first slowing down collision. The first flight correction is important in uranium water systems. An accurate transport theory calculation for mixtures of hydrogen and non-slowing down elements by Hurwitz and Zweifel[13] yields Equation 6 at source energy where

$$\gamma_0 = \left[1 + \frac{2}{3}\frac{\Sigma_{SH}}{\Sigma_{tr}}\right]^{-1}$$

and Σ_{SH}/Σ_{tr} is the ratio of the hydrogen cross section to the transport cross section of the mixture. The use of a first flight correction will reduce much of the error inherent in the use of simple Fermi age theory. An accurate correction to the Fermi age for mixtures of hydrogen and non-slowing down elements has been derived by Hurwitz and Zweifel[13] for the special case of energy-independent cross sections.

A comparison between the neutron leakage from an actual reactor and neutron age approximations is readily obtained for the case of a bare slab reactor. For a mono-energetic isotropic (fission) source in a homogeneous slab the probability π_0 of first flight leakage is given by

$$\pi_0 = \tfrac{1}{2}\int_0^a F(x)E_2(x/\lambda)dx \Big/ \int_0^a F(x)\,dx \tag{7}$$

where $F(x)$ is the spatial distribution of the source and a is the reactor width. For a sinusoidal distribution, $F(x) = \sin \pi(x + \delta)/a$ with δ the extrapolation length, and for $a \gg \lambda$, the total mean free path, the formula

$$\pi_0 = \frac{B^2}{2}\left(\frac{\lambda^2}{3} + \frac{\lambda\delta}{2}\right) \tag{8}$$

is obtained, with $B^2 = \pi^2/a^2$, the geometrical buckling of the reactor. In the presence of non-slowing down elements, the process cascades and, ignoring changes in the spatial distribution, the value of π_0 is increased by the ratio of the total to the slowing down cross section of the medium.

The result[8] shows the influence of the actual primary source distribution near a reactor boundary on first flight neutron losses.

Similar calculations are readily carried out for a bare lattice composed of alternating slabs of fuel and moderator. The results are again sensitive to perturbations in the fission source distribution due to the boundary, the blackness of fuel and moderator components to thermal neutrons and even the order in which the lattice components are stacked.

Since all neutron losses may be considered as first flight losses, the neutron leakage may be calculated from a knowledge of the distribution of the neutron flux in energy and space within a few mean free paths of the reactor boundaries. T. Auerbach[15] of BNL has computed the leakage factor π_0 from a bare slab of hydrogen under the simplification of constant mean free path and obtains the formula

$$\pi_0 = \frac{2}{3}\gamma^2 + \left(1 + \frac{281}{45}\gamma^2\right)(1 - e^{-\gamma^2 u}) - \frac{\gamma^2}{3}\left(1 - e^{-(\frac{1}{2} - \frac{1}{16}\gamma^2)u}\right) \tag{9}$$

For values of $u = \ln E_0/E \gg 1$ and $\gamma^2 u \ll 1$, with $\gamma^2 = B^2\lambda^2$, his result reduces to $\pi_0 = \gamma^2\theta$, with

$$\theta = \tfrac{1}{8}(1 + 3u + e^{-u/2})$$

in conformity with a second moment calculation of the neutron age.

Calculated values of the age of fission neutrons to indium resonance in water uranium mixtures show little variation if the uranium to water volume ratio, v, is less than unity. For values of $v > 1$, the calculations are sensitive to assumed values of the inelastic cross sections for U^{238}, which have undergone frequent changes in the past. For equal volumes of uranium and water, calculated ages have run about 20% higher than the value for pure water. The results of more recent calculations by R. Hellens of WAPD are given in a companion paper.[16]

For mixtures of water and other elements, Ehrlich and Deutsch of KAPL have recommended the formula

$$\theta = \theta_{H_2O}(1 + v)^2/(\rho + vx)^2 \tag{10}$$

with ρ the water density, and $x = 0.40$, 0.38, 0.59 and 0.59 for zirconium, stainless steel, beryllium and boron respectively.

A different type of slowing down problem is presented by neutrons approaching thermal equilibrium with the moderator. In the presence of an absorber, equilibrium is incomplete and the energy spectrum departs from Maxwellian. The resulting distribution for a $1/v$ absorber was obtained by Wigner and Wilkins[17] for hydrogen gas and Wilkins later extended the treatment to heavy moderators. The effects of chemical binding and crystal reflection were neglected in this work. Chemical binding effects were first considered by Teller and Metropolis for graphite lattices. The latter estimated that the standard rate of neutron energy loss due to moderator atom oscillations was reduced by a factor $F(T) \approx 1 - \sqrt{T_0/T}$, with T_0 the moderator temperature. Their results were used by P. Morrison to compute the increase in neutron temperature for uranium-graphite lattices by means of a modified Fermi age model of the slowing down process. Morrison found a sizeable increase in mean neutron temperature and noted that it depended only on the ratio of the absorption to slowing down power of the medium.

The results of Wigner and Wilkins have been used by K. Cohen, now of the Walter Kidde Laboratories, and R. Cohen of NAA to estimate the increase in mean

temperature of a Maxwellian distribution in terms of this parameter. They use formulas of the type

$$T/T_0 = 1 + C\Sigma_a(kT_0)/\overline{\xi\Sigma_s} \qquad (11)$$

with $C \approx 1.4$. More recently, R. Cohen has examined the effect of $1/v$ capture on neutron leakage at epithermal energies. Using a modification of Fermi age theory, with a reduced rate of neutron energy loss which neglects binding effects[18], he concludes that the effective neutron age is substantially decreased in D_2O moderated reactors in spite of the increased number of collisions required for thermalization. For further details, attention is invited to a paper by E. R. Cohen[19].

The Wigner-Wilkins model for a $1/v$ absorber has been extended to include rotational effects in D_2O molecules by Brown and St. John of the DuPont Savannah River Laboratory. They have computed the resulting energy spectrum as a function of the absorption strength of a homogeneous D_2O moderated medium.

Slowing down in water has recently been investigated by von Dardel.[18] Binding effects in water moderated systems were examined in 1950 by A. Radkowsky, now of the Naval Reactors Branch of the AEC (NRB). He concluded that the water molecules were free of rotational and vibrational effects over the important range of thermal energies and used the Born approximation to obtain the effective mass of the bound protons. He writes

$$\left(\frac{2A}{A+1}\right)^2 = \frac{\sigma_s(A)}{\sigma_s(A=1)} \qquad (12)$$

to obtain the effective mass A of hydrogen in water from experimental scattering cross-section data. Radkowsky used these results under the assumption of isotropic scattering in the center of mass system to compute values of the diffusion coefficient and the diffusion length of thermal neutrons in water. A comparison of the latter calculations with experimental data for water at various temperatures is given in Fig. 2, with the theoretical curve representing averages over a Maxwellian distribution of velocities. Danzker, Garabedian and Henry of WAPD have shown that the values of L^2 are raised when averaged over a Wigner-Wilkins distribution.

In summary, some progress has been made on the complex problems of neutron moderation in the region approaching thermal equilibrium. In a lattice, the problem is further complicated by the separation of the absorbing and moderating components. Thus the results for homogeneous systems are directly applicable only when the dimensions of both fuel and moderator elements are small compared to a mean free path.

In a lattice, the diffusion length for thermal neutrons may be defined by the equation

$$f_{eff} = \frac{f_\infty}{1 + L^2B^2} \qquad (13)$$

in keeping with Fermi's model of the neutron cycle. The first calculation of this type was that of Plass[20] who obtained f_{eff} for a cubic lattice by means of diffusion theory. More recently A. M. Weinberg has solved the same problem for an infinitely long slab lattice of rectangular cross section. To first order, their results agree with the formula

$$L^2 = (1 - f)L_1^2 + fL_0^2 \qquad (14)$$

where L_0, L_1 are the diffusion lengths for fuel and moderator respectively. The second term is relatively unimportant for graphite or D_2O moderated lattices. The homogeneous formula $L^2 = \bar{D}/\bar{\Sigma}_a$ is sometimes used to obtain L^2 for a lattice by use of flux weighted cross sections with disadvantage factors derived from lattice experiments.

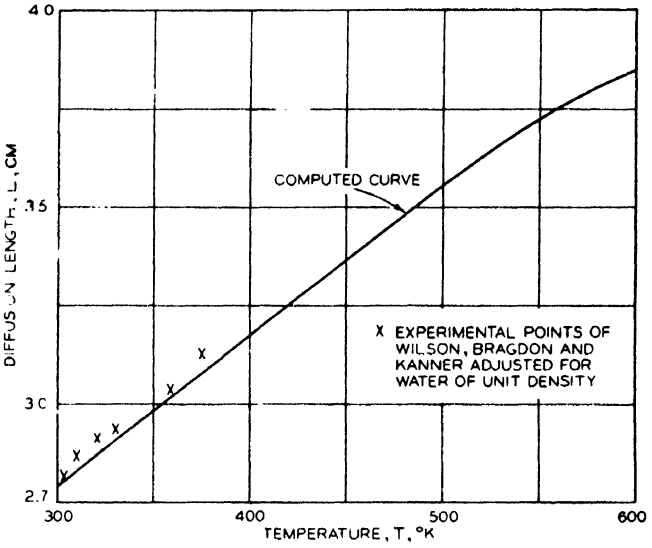

Figure 2. Diffusion length of neutrons in H_2O vs temperature

The adequacy of simple formulas such as Equation 14 in more complex situations requires further investigation. Thus the formula breaks down for the case of a bare slab lattice of finite length and infinite transverse dimensions, for an arbitrary thermal source distribution, if the fuel elements are black to thermal neutrons. In this case, the use of Equation 14 can result in large errors, since the actual thermal leakage is zero if the lattice is arranged with fuel elements at its boundaries.

FAST FISSION

Fission induced by neutrons with energies greater than the fission threshold of U^{238} or Th^{232} is called fast fission. For U^{238} this threshold may conveniently be taken at 1 Mev. In Fermi's model of the neutron cycle all fissions are either fast or thermal. On this basis ϵ (Equation 1) is defined for uranium fueled reactors as the number of neutrons slowing down past 1 Mev per neutron produced by thermal fission.

The importance of fast fission of U^{238} to the first generation of nuclear reactors was that it made possible a slim margin of neutron production over neutron losses. Its importance today is that it permits a substantial increase in the conversion ratio of power reactors and breeders.

Table II. Fast Fission Factor ϵ in Homogeneous U^{238}-H_2O Assemblies

V_{H_2O}/V_U	ϵ	ϵ^*	ϵ
0	1.227	1.227	1.170
1	1.093	1.098	1.081
2	1.060	1.065	1.055
3	1.044	1.048	1.042
4	1.035	1.038	1.034

Corrections for more accurate treatment of energy losses in uranium collisions

V_{H_2O}/V_U	*Standard* ϵ	*Corrected for inelastic collisions*	*Corrected for isotropic elastic collisions*
0	1.2274	1.2345	1.2216
1	1.0925	1.0932	1.0918

* Values given in last column are based on a current compilation. Other values are based on older cross sections with $\bar{\sigma}_i = 2.0$. The asterisk indicates values uncorrected for energy losses in oxygen collisions.

In a lattice, unmoderated source neutrons cause fast fission both in the fuel element of origin and in neighboring fuel elements. Early lattices were so widely spaced, that the latter effect was negligible. The value of ϵ for unmoderated neutrons will be called the interaction fast fission factor.

In addition, fast fission may result from neutrons which have suffered multiple collisions with the moderator. The backscattering effect is small in widely spaced lattices even for a relatively poor moderator such as graphite, while the effect is important in closely packed lattices with water as the moderator.

We shall discuss first the recent methods developed to calculate ϵ for homogeneous systems since they yield both a lower bound and a fair approximation to the uranium-water lattices in actual use.

The idea of using some form of the slowing down integral equation for a homogeneous mixture to obtain an estimate of ϵ is a natural one and appears to have occurred independently to several investigators. Thus D. Kurath of ANL reported its use in a survey of the multiplication factor of slab lattices of natural uranium and water. F. H. Clark of KAPL treated the same equation with neglect of energy losses in oxygen collisions and the method has since been extended by J. Weil and H. Hurwitz at KAPL. At BNL, an exact integral equation was set up to obtain the number of neutrons slowing down past the fission threshold of U^{238} as a function of neutron energy, and solved by a rapidly convergent iterative procedure. At WAPD, R. Hellens developed a successive neutron generation treatment of the same problem. The methods perfected at BNL, KAPL and WAPD are essentially exact within our present knowledge of cross sections, the neutron yield and energy distribution in fission and the energy distribution of scattered neutrons.

The iterative method used at BNL was motivated by the fact that neutron collisions in uranium water mixtures result in either very weak or very strong energy degradation. In an infinite, homogeneous system, ϵ is a function only of source energy. Thus one can define $\epsilon(E)$ as the fast fission factor for any neutron starting a new flight at energy E, with $\epsilon(E) = 1$, for $E < 1$ Mev. For a fission spectrum $N(E)$, the fast fission factor is given by

$$\bar{\epsilon} = \int_0^\infty \epsilon(E)N(E)\,dE \tag{15}$$

If p_f, p_c, p_e, p_i are the respective probabilities of fission, capture, elastic and inelastic collisions with the fuel at energy E, and similarly if p_O, p_H are the oxygen and hydrogen collision probabilities, then $\Sigma p = 1$ and

$$\epsilon = p_i\bar{\epsilon}_i + p_e\bar{\epsilon}_e + p_O\bar{\epsilon}_O + p_H\bar{\epsilon}_H + \nu_{28}p_f\bar{\epsilon} \tag{16}$$

with the bars representing averages over the energy degraded neutrons. Differences in the fission spectrum with incident neutron energy, $(n,2n)$ reactions etc., are neglected in this treatment.

Equation 16 is still a complicated integral equation, since, for example

$$\bar{\epsilon}_O = \frac{1}{E(1-\alpha)}\int_{\alpha E}^{E} \epsilon(E')\,dE'$$

with $\alpha = (15/17)^2$ for oxygen.

A series of calculations at BNL have shown, however, that elastic collisions with the fuel may be adequately treated as involving no energy loss, and inelastic collisions as resulting in energy degradation below the fission threshold. Thus $\bar{\epsilon}_i = 1$, $\bar{\epsilon}_e = \epsilon$. Similarly, neglect of energy losses in oxygen collisions result in an error of at most ½% in ϵ (Table II). For $\bar{\epsilon}_O = \epsilon$, $\bar{\epsilon}_H = 1$, the first approximation to $\bar{\epsilon}$ is given by

$$\bar{\epsilon}^{(0)} = \frac{1 - \int_0^\infty \frac{p_f(1+\sigma_c/\sigma_f)}{1-(p_e+p_O)}N(E)\,dE}{1 - \int_0^\infty \frac{\nu_{28}p_f}{1-(p_e+p_O)}N(E)\,dE} \tag{17}$$

This simple approximation underestimates ϵ, since the effect of overstating energy losses in hydrogen collisions is more important than the effect of understating energy losses in oxygen collisions. However, more accurate values are readily obtained by iteration through Equations 16 and 15.

An alternate method presently in use at KAPL for treating this problem consists in writing the flux equation in terms of the lethargy u in the form

$$\phi(u)\sum_t(u) = S(u) + \int_0^u M(u,u')\phi(u')\,du \tag{18}$$

where $M(u,u')$ is the kernel describing the energy degradation process. For sufficiently small lethargy intervals, the solution of Equation 18 is written as

$$\phi_i\sum_{t_i} = S_i + \sum_{j<i} M_{ji}\phi_j \tag{19}$$

where M_{ji}, the transition probability between groups j and i, is calculated from the usual formulas for energy losses following elastic and inelastic scattering. Inte-

gration of the flux over the U^{238} fission cross-section yields the fast fissions produced by the thermal fission source and cascading the process yields the ratio of total fast fissions to thermal fissions.

These methods may, of course, be used to follow the neutron cycle to lower energies than 1 Mev. In particular, they are suited to the investigation of resonance capture in the continuum region of U^{238}.

The BNL results for ϵ as a function of water to uranium volume ratio are presented in Table II. The effect of simplifying assumptions for the neutron energy degradation is also shown. The first set of values is based on older cross-sections which yield an average value of 2.03 b for the inelastic cross-section of U^{238}. The last column corresponds to a current compilation. A constant value of $\nu(28) = 2.5$ is assumed. Recent experimental results by R. Taschek and theoretical calculations by R. B. Leachman at Los Alamos on the variation of $\nu(28)$ with energy would tend to raise the values of ϵ, particularly at low water to uranium volume ratios. On the other hand, capture to fission ratios for U^{238} in current use are considerably smaller than older Los Alamos data and yield an average value of $\alpha(28) = 0.10$ over the energy range from 1 to 10 Mev, when weighted with the Watt spectrum. Any increase in capture cross-sections would tend to decrease ϵ. Calculations of ϵ have also been carried out by J. Weil of KAPL and by R. Hellens and D. Schiff of WAPD using comparable cross sections and the results are in general agreement with those obtained at BNL.

THE INTERACTION FAST EFFECT

The first general study of fast fission in uranium lattices is that of Castle, Ibser, Sacher and Weinberg[21] in 1943. They reduced the problem to the essentially geometrical problem of determining the first flight collision probability in a fuel lump, and obtained formulas for spherical, slab and cylindrical fuel elements. An error in their formulation for hollow cylinders was corrected by Guggenheim and Pryce.[22] The general theory has since been improved in several respects. Thus, although their treatment neglects radiative capture above the fission threshold, it has since become customary to take this effect into account. Secondly, their definition of the first flight collision probability has been extended to include first collisions in all fuel elements. The corresponding geometrical problem for a lattice of rods is complex and has been investigated by A. Radkowsky of NRB and by Chernick and Mozer of BNL. In addition, studies of interaction effects for slab lattices have been carried out both at BNL and at KAPL. Finally, we have shown that the general theory can be extended to account accurately for the variation of neutron cross-sections with energy. In order to do this it is necessary to retain some of the less vulnerable assumptions of CP-644.[21] The first assumption, which we have shown to be quite adequate for homogeneous systems, regards energy degradation in uranium collisions on an all or none basis. The second assumption is that the fast neutrons are uniformly distributed over the fuel elements after their first collision. In this case, if we write P_∞, P_0 for the first flight interaction collision probability for primary and uniform sources respectively, one obtains the formula

$$F = \frac{\nu(25)\int_0^\infty \frac{P_\infty p_f}{1 - P_0 p_e} N(E)\,dE}{1 - \int_0^\infty \frac{\nu(28) P_0 p_f}{1 - P_0 p_e} N(E)\,dE} \tag{20}$$

for F, the ratio of fast to thermal fissions, with $p_f(E) = \sigma_f/\sigma_t$ for U^{238}, $p_f + p_c + p_e + p_i = 1$, and $N(E)$ the fission neutron spectrum. Similarly,

$$\epsilon_{int} = \left[1 - \int_0^\infty \frac{P_\infty p_f (1 + \sigma_c/\sigma_f)}{1 - P_0 p_e} N(E)\,dE\right] \times \frac{\left[1 - \int_0^\infty \frac{\nu(28)(P_0 - P_\infty) p_f}{1 - P_0 p_e} N(E)\,dE\right]}{1 - \int_0^\infty \frac{\nu(28) P_0 p_f}{1 - P_0 p_e} N(E)\,dE} \tag{21}$$

The second factor in the numerator vanishes if the distribution of primary sources is uniform. In the latter case, one obtains the relationship familiar from one velocity models,

$$\epsilon - 1 = \frac{F}{\nu(25)} [\bar{\nu}(28) - 1 - \bar{\alpha}(28)] \tag{22}$$

with the bars representing weighted averages over the fission spectrum.

The ratio F of fast to thermal fissions in an isolated uranium rod has been determined experimentally by S. Untermyer of ANL and by Kouts, Price *et al.* at BNL. Their results are compared in Fig. 3 with values obtained from Equation 20. Corrections for the non-uniform distribution of thermal fission sources, and for backscattering from the moderator (graphite) are not included. Values of $\nu(25) = \nu(28) = 2.5$ are assumed. The results show the sensitivity of the theoretical curve to the recent increase in inelastic cross sections at and above 1.5 Mev, and the need for additional experiments on thicker uranium rods.

For slab lattices, the first flight collision probability P_∞ is most easily derived by making use of the periodicity of the lattice. In order to avoid unwarranted generality, we consider only isotropic, symmetric sources confined to the fuel elements. The source neutrons are then uniformly scattered in directions $\mu = \cos\theta$, where θ is the angle between the neutron direction and the normal to the plane of symmetry. Let $J(\mu)\,d\mu$ be the neutron current crossing a fuel moderator interface (say) from the left in the direction μ. In crossing to the next such interface, the current is depleted by a factor $\exp -[(a_0/\lambda_0\mu) + (a_1/\lambda_1\mu)]$ where a_i/λ_i, $i = 0,1$ are the widths of the component slabs in mean free paths, and the current is increased by the contribution from source neutrons. The periodicity condition is

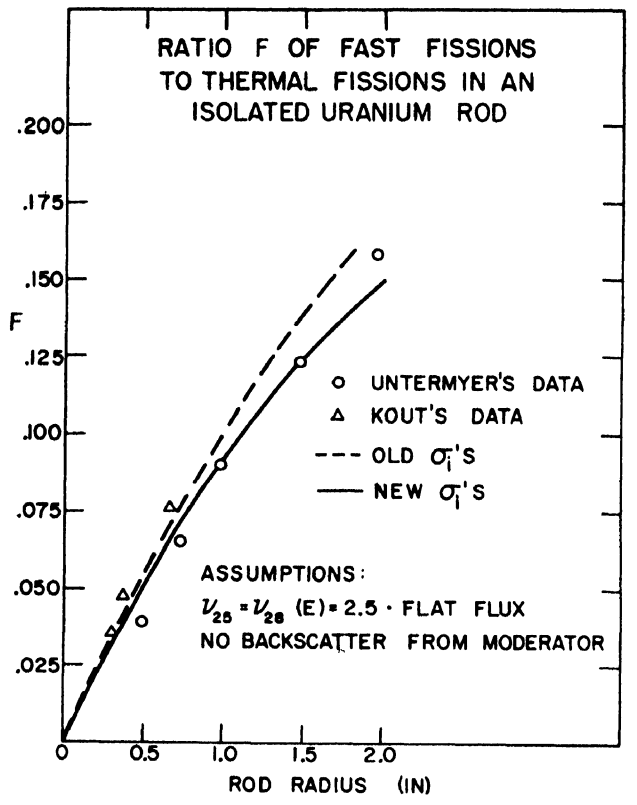

Figure 3. Ratio F of fast fissions to thermal fissions in an isolated uranium rod

$$J(\mu)\exp-[(a_0/\lambda_0\mu)+(a_1/\lambda_1\mu)]+\int_0^{a_0}\frac{S(x)}{2}\exp[-(a_0-x)/\lambda_0\mu]\,dx=J(\mu)\quad(23)$$

which yields $J(\mu)$ for an arbitrary source distribution.

The number of moderator collisions is given by $Q(\mu)=[J(\mu)-J(\mu)e^{-a_1/\lambda_1\mu}]$ and hence

$$Q(\mu)=\frac{1-e^{-a_1/\lambda_1\mu}}{1-e^{-[(a_0/\lambda_0\mu)+(a_1/\lambda_1\mu)]}}\int_0^{a_0}\frac{S(x)}{2}e^{-(a_0-x)/\lambda_0\mu}\,dx\quad(24)$$

Since the source is symmetric, an equal number of collisions occur with neutrons entering the moderator from the right. Integrating over all directions yields the first flight collision probability for the moderator and its complement P_∞,

$$P_\infty=1-\int_0^1\frac{1-e^{-a_1/\lambda_1}\,d\mu}{1-e^{-[(a_0/\lambda_0\mu)+(a_1/\lambda_1\mu)]}}\times\int_0^{a_0}S(x)e^{-(a_0-x)/\lambda_0\mu}\,dx\quad(25)$$

In particular, for a uniform source $S=1/a_0$, and

$$P_0=1-\int_0^1\frac{\lambda_0\mu}{a_0}\frac{(1-e^{-a_0/\lambda_0\mu})(1-e^{-a_1/\lambda_1\mu})}{(1-e^{-[(a_0/\lambda_0\mu)+(a_1/\lambda_1\mu)]})}\,d\mu\quad(26)$$

The formula for P_∞ for $a_1=\infty$ and a diffusion theory source is derived by an alternate method in CP-644.[21] Equation 26 has been discussed by F. H. Clark of KAPL who showed that P_0 increases monotonely when the components of the lattice are uniformly expanded in size. When the primary sources are confined to the fuel elements, stronger statements can be proved. Thus, for a uniform source P_0 is greater than the corresponding value for homogeneous systems regardless of the direction of the source neutrons. On the other hand, if the thermal fission sources are confined to the moderator, P_∞ is smaller, and the overall value of ϵ for a lattice may well be smaller, than that of the corresponding homogeneous case.

Periodicity conditions may be used to determine the current of unmoderated neutrons in more complicated lattices. Thus if the unit cell in a lattice of rods of arbitrary shape is a rectangle with sides a, b, the lattice is periodic with respect to any block of m by n cells. At azimuthal angles ϕ such that $\tan\phi=nb/ma$, the neutron current is again periodic.

Although references to earlier work on the interaction fast effect in uranium rod lattices exist, the first published investigation appears to be that of A. Radkowsky in 1950 who discussed computational techniques for uranium water lattices on a one-velocity basis. Radkowsky's work has since been extended at BNL and at the Walter Kidde Laboratories.

At BNL, we have relied principally on mesh methods of determining first flight collision probabilities in hexagonal rod lattices with some checks afforded by analytical formulae. Complexities arising from the spatial variation of the thermal fission sources, the presence of fuel cladding and the shielding effect of intervening fuel elements limits the usefulness of analytical approaches to the problem. On the other hand, if the fuel elements are divided into a suitable mesh all of these effects are readily included and the contribution of each ring of neighboring elements may be obtained from an accurate scale drawing of the lattice. This detailed breakdown is useful if the value of ϵ for a finite assembly is desired.

The probability that a neutron starting a new flight in a small volume element V_i will suffer its first collision in volume element V_j is given by

$$P_{ij}(E)=\frac{K_{i_1}(d_{ij}')V_j}{2\pi\lambda d_{ij}}\quad(27)$$

where λ is the mean free path in uranium, d_{ij} is the actual distance between volume centers and d_{ij}' is the distance in mean free paths. The function $K_{i_1}(x)$ has been adequately tabulated.[28] Summing P_{ij} over j and use of a thermal flux weighted average over the fuel element yields P_∞.

Curves of P_0 versus energy calculated by B. Mozer of BNL for typical slab and rod lattices are shown in Figs. 4 and 5. F. H. Clark of KAPL has suggested that results for slab lattices could be applied to rod lattices with the same moderator to fuel volume ratios and with equal surface to volume ratios for the fuel elements. The graphs show that the approximation is fairly close for hexagonal lattices. An interesting lattice that has not been thoroughly investigated is one consisting of square rods in a rectangular array. In the limit such a lattice goes over into a slab lattice

and Clark's conjecture fails since there is a discontinuous change in the fuel surface to volume ratio.

The effect of preferential forward scattering in uranium may be investigated in the following manner. In the extreme case where the elastic scattering is taken as completely forward (straight ahead approximation), a heavy scatterer acts as a void, since it has no effect either on energy degradation or in changing the neutron direction. In this case, its elastic scattering cross section may be neglected. A comparison of this model with that of isotropic scattering carried out by B. Mozer of BNL by means of Equation 26 indicates that the effect of anisotropic scattering in uranium is small for the lattices of interest. For homogeneous systems, the effect of anisotropy disappears altogether. Anisotropic scattering may be expected to be more important in widely spaced lattices with thick fuel elements, where the interaction of neighboring elements is small. For the same reason, the effect of the dip in the thermal flux distribution in a fuel element is more important in an isolated fuel element than in a closely packed lattice.

BACKSCATTERING EFFECTS

While fast fission caused by backscattering of neutrons from the moderator is important in closely packed water uranium lattices, relatively little attention has been paid to this problem. In some studies, its effect was completely disregarded. At BNL, the results for homogeneous systems were corrected by use of the difference in interaction effects between the lattice and the corresponding homogeneous system. A similar method of correcting for heterogeneity has been adopted at KAPL. While this method accounts for the gross effect, further investigation appeared desirable, since the additional fast fissions caused by a first collision source in the moderator of a lattice might prove smaller than that produced in a homogeneous system. To anticipate somewhat, the results of more elaborate investigations at BNL have shown that the above method of correction is fairly accurate. The difference in various methods of obtaining the correction for heterogeneity is shown in Table III. The correction for 0.75-in. rods in a hexagonal lattice runs from about 0.010 to 0.014 as the water to uranium volume ratio increases from 1 to 4.

Of the possible methods of treating backscattering effects from the moderator, one of the simplest is that of one group diffusion theory with a first collision source in the moderator. Diffusion theory would appear to be adequate for this purpose for uranium-graphite lattices. Its applicability to water-uranium lattices is under investigation at BNL.

For uranium-water lattices, a further extension of the method of Castle, Ibser, *et al.*[21] suggests itself. If the fast neutrons are assumed to be uniformly distributed over the moderator, as is approximately the case if the moderator dimensions are not large compared to a mean free path, then integral equations in the energy variable similar to Equation 16 can be set up to obtain the fast effect in terms of first flight collision probabilities. These equations may be solved

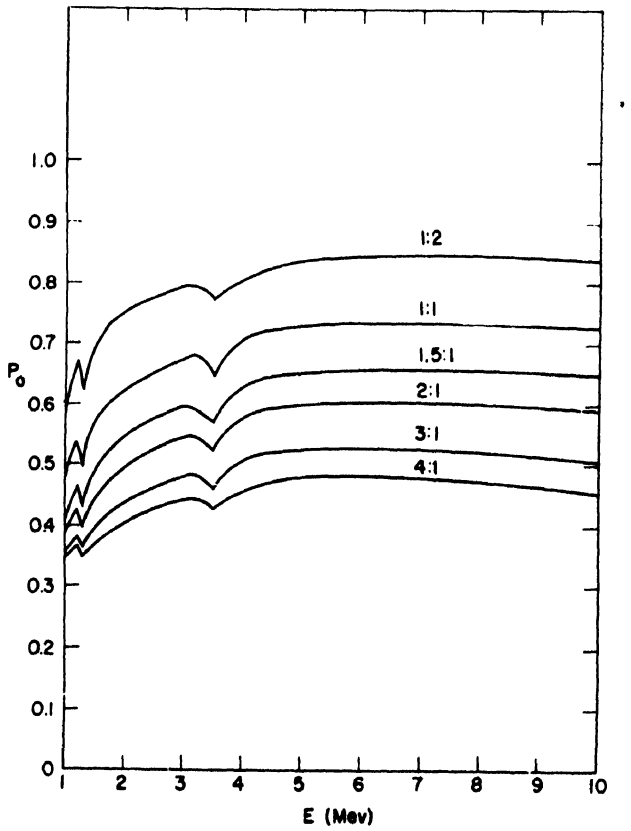

Figure 4. The probability P_0 of first collision in fuel versus neutron energy for a uniform source in the fuel (uranium-water slab lattices with 0.375 in. fuel slabs at various moderator to fuel volume ratios)

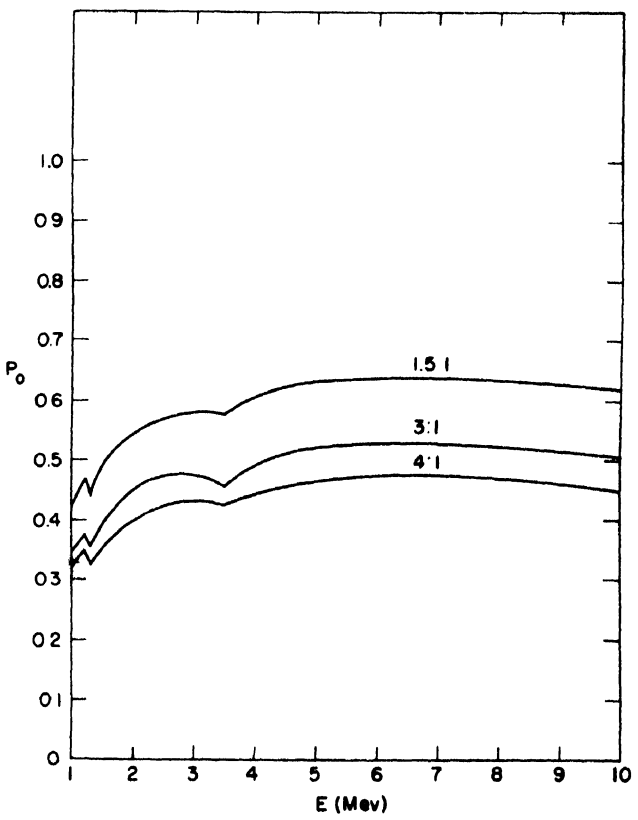

Figure 5. The probability P_0 of first collision in fuel versus neutron energy for a uniform source in the fuel. (Hexagonal uranium-water lattice with 0.75 in. dia. rods at moderator to fuel volume ratios of 1.5, 3 and 4 to 1)

Table III. Corrections to the Fast Fission Factor for Heterogeneity

V_{H_2O}/V_U	Standard ϵ_{int}	0.75-in. rods in hexagonal lattice $\Delta\epsilon$	0.375-in. slabs $\Delta\epsilon$	ϵ^*_{int}	0.375-in. slabs $\Delta\epsilon$
0	1.227	0	0	1.227	0
1	1.066	0.011	0.012	1.081	0.009
2	1.039	0.013	0.014	1.050	0.011
3	1.028	0.014	0.015	1.037	0.012
4	1.022	0.015	0.016	1.029	0.014

V_{H_2O}/V_U	Standard ϵ^*	0.375-in. slabs $\Delta\epsilon$	0.30-in. slabs $\Delta\epsilon$
0	1.227	0	0
1	1.098	0.011	0.010
2	1.065	0.011	0.010
3	1.048	0.012	0.011
4	1.038	0.014	0.012

* Homogeneous values of ϵ and the difference $\Delta\epsilon$ with results for corresponding heterogeneous cases are tabulated. ϵ_{int} is the interaction fast effect. The asterisk indicates values uncorrected for energy losses in oxygen collisions.

by iteration, or if energy losses in oxygen collisions are neglected, the problem reduces to a first order differential equation which can be solved by numerical quadrature.

We forego the detailed treatment of these equations, since a similar set will be discussed in the section on resonance capture. Some of the BNL results for slab lattices are shown in Table III. Graphs of first flight collision probabilities for a uniform source in water are shown in Fig. 6. The peaks in the curves are due to oxygen resonances.

Further work on fast fission in uranium water lattices is in progress at KAPL under J. Weil and at WAPD under R. Hellens. D. Schiff of WAPD has discussed the solution of the problem by a method which we again defer to the section on resonance capture. Schiff has used this method to obtain ϵ for homogeneous systems on a Univac.

RESONANCE CAPTURE

The early investigations of Wigner[2] and Dancoff indicated that resonance capture in lumps of uranium could be separated into volume and surface absorption terms. The first experiments on resonance capture on uranium in bulk were those of Creutz, Jupnik and Snyder. This work has only recently been published.[24] Later experiments by A. Mitchell, Hughes and Goldstein, C. Muelhouse, Risser and Arfken, and S. Untermyer have borne out this division of resonance capture. They led to minor variations on the following formula for the effective resonance integral

$$I_r = \int (\sigma_a)_{eff} \frac{dE}{E} = (9 + 25.5S/M) \text{ barns} \quad (28)$$

where S/M is the ratio of surface to mass of the fuel element. For thin rods, Untermyer has suggested the modification

$$I_r = 9.23\left(1 + \frac{2.50}{(M/S) + 0.10}\right) \quad (28a)$$

which yields the conventional value of 240 b at infinite dilution.

The value of p for uranium lattices is obtained almost universally from a formula of the type

$$p = e^{-1/T} \quad (29)$$

with $T = E - 1 + FV_{mod}(\xi\Sigma_s)_{mod}/V_u I_r$ where again following Wigner's suggestion, the fuel disadvantage factor F and excess absorption $E - 1$ of the moderator are obtained by use of diffusion theory. The fuel disadvantage factor F is sometimes used to modify only the volume absorption term. For uranium water lattices, B. I. Spinrad of ANL has recommended adding a further term to T, viz., $\xi/\Delta u$ where Δu is an estimate of the lethargy band over which line resonance absorption takes place. The argument here is that neutrons can jump the entire resonance band in collisions with hydrogen. Wigner suggested, and Dancoff proved, that surface resonance capture in close packed uranium water lattices is significantly decreased by the shielding effects of adjacent fuel elements. The correction to the surface term in Equation 28 is of the order of 20% for some of the BNL experimental lattice arrangements. Finally the magnitude of the volume term in Equation 28 has been under attack on the basis that a lower value of about 7.5 b would presumably be in better agreement with some integral

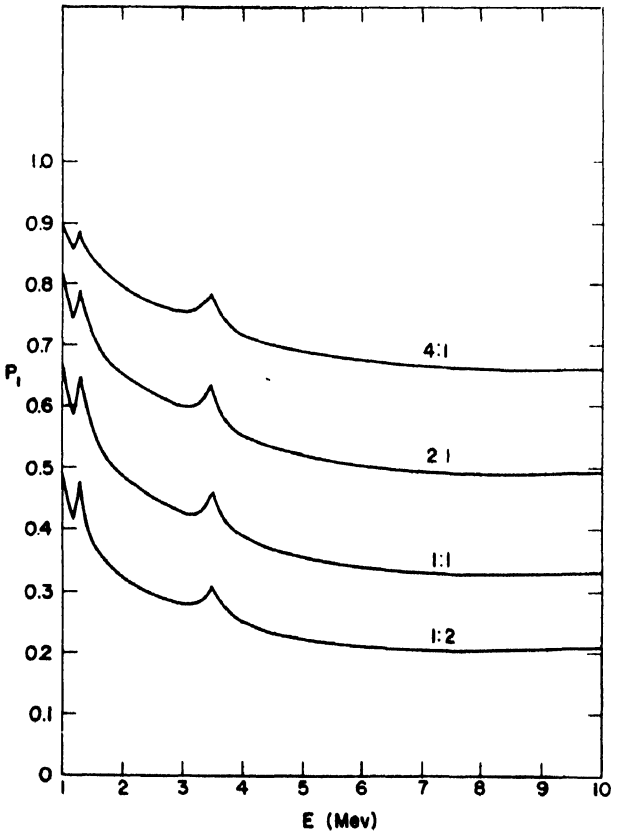

Figure 6. The probability P_1 of first collision in moderator versus neutron energy for a uniform source in the moderator. (Uranium-water slab lattices with 0.375 in. fuel slabs at various moderator to fuel volume ratios)

Table IV. Values of p for Single Resonances in a Lattice of Uranium Rods in Water*

Energy (ev)	σ_0 (kb)	Γ (mv)	Γ_n/Γ	$T_0 = 300°K$ p	$T_0 = 370°K$ p
6.70	23	25	0.060	0.96072 ± 0.0012	0.95841
20.9	32	34	0.26	0.98562 ± 0.00037	0.98487
37.0	40	58	0.57	0.98898 ± 0.00032	0.98835
66.5	19	48	0.48	0.99566 ± 0.00014	0.99538
81.6	2.2	27	0.07	0.99798 ± 0.00007	0.99778
104	18	86	0.71	0.99629 ± 0.00024	0.99604
118	12	52	0.52	0.99783 ± 0.00008	
195	11.7	210	0.88	0.99812 ± 0.00027	

* The lattice consists of a hexagonal array of rods of 0.6-in. dia. surrounded by a 0.033-in. gap. Distance between rod centers is 1.0925 in.

experiments, and that the $1/v$ contribution of thermal capture above the cadmium cutoff had not been subtracted in some experiments. All of these corrections would tend to increase p. On the other hand, it is difficult to avoid shielding effects in experiments designed to determine the effective resonance integral of uranium. Such a possibility is suggested by the fact that a value of 276 ± 12 barns (personal communication from J. Harvey of BNL) is obtained for the resonance integral of uranium at infinite dilution, by adding up the contributions of the individual resonances.

The rapid improvement in the knowledge of resonance parameters for uranium brought about by recent fast chopper experiments has precipitated a search for more rigorous computational techniques. At WAPD, D. Schiff has for some time been experimenting with a multigroup method of obtaining p for hexagonal uranium water lattices by means of a large digital computer such as the Univac. He uses a three dimensional mesh with the neutrons restricted to paths parallel to the principal axes of the lattice. Schiff has tested the method on homogeneous systems and has published results for fast and epithermal fission factors as well as resonance capture for a mixture of equal volumes of uranium and water. The chief restriction of the method is the limited number of directions in which the neutron can travel.

A Monte Carlo approach to the same problem has been undertaken by R. D. Richtmyer.[25] Most of Richtmyer's runs on the Univac have to date been of an exploratory nature treating single resonances with a dE/E spectrum for neutrons above the resonance. Information on the extent of flux recovery between resonances is not yet available. In addition to values of p for single resonances, some information on the spatial distribution of the absorptions within a fuel rod has been obtained and differential effects due to temperature changes have been investigated. A run with 10,000 case histories is found to take about two and one-half hours of Univac time. Richtmyer's results on low level resonance capture in a hexagonal uranium water lattice are shown in Table IV.

How far one can go with an analytical approach to the problem of resonance capture is not yet clear. An analytical study has been carried out by T. A. Welton of ORNL, a transform method is under investigation at Harwell by J. H. Tait and at BNL, N. Corngold is exploring rigorous methods of obtaining p for slabs and homogeneous systems. Monte Carlo results should prove extremely valuable in testing new approaches to the subject. Thus Richtmyer's results already indicate that slowing down by elements other than hydrogen is of minor importance in the resonance region. As we show next, the problem of resonance capture in a lattice moderated only by hydrogen reduces to that of determining first flight collision probabilities within the resonance. We use the methods discussed in the section on fast fission for this purpose.

Consider a reactor system consisting of separated fuel and moderator regions. We designate these regions by subscripts 0 and 1 and take the moderator to be hydrogen. Let $F_i(E)$ be the collision density in region i. Let $P_i(E)$ be the probability that a neutron scattered into an energy interval dE in region i will suffer its first collision in region i. Let $p_{s0} = \Sigma_{s0}/(\Sigma_{s0} + \Sigma_{a0})$ be the scattering probability in the fuel. We ignore absorption by the moderator and the contribution of source neutrons to the line resonance range. Then

$$F_0 = (1 - P_1)\int_E^{E_0} \frac{F_1(E')\,dE'}{E'} + \frac{P_0}{1-\alpha_0}\int_E^{E/\alpha_0} p_{s0}\frac{F_0(E')\,dE'}{E'} \tag{30a}$$

$$F_1 = P_1\int_E^{E_0} F_1(E')\frac{dE'}{E'} + \frac{1-P_0}{1-\alpha_0}\int_E^{E/\alpha_0} p_{s0}\frac{F_0(E')\,dE'}{E'} \tag{30b}$$

For uranium, $\alpha_0 \approx 1$. In the limiting case where only hydrogen moderation is considered, we let $\alpha_0 \to 1$ and obtain

$$F_0 = \frac{1-P_1}{1-P_0p_{s0}}\int_E^{E_0}\frac{F_1(E')\,dE'}{E'} \tag{31a}$$

$$F_1 = \frac{P_1 + p_{s0}(1-P_0-P_1)}{1-P_0p_{s0}}\int_E^{E_0}\frac{F_1(E')\,dE'}{E'} \tag{31b}$$

The formula for p is given by

$$p = E\int_E^{E_0}\frac{F_1(E')\,dE'}{E'} \tag{32}$$

Now Equation 31b reduces under differentiation to a first order differential equation and may be solved in the usual manner. The formula obtained for p is

$$p(E) = \exp\left[-\int_E^{E_0} \frac{(1-p_{s0})(1-P_1)}{1-P_0p_{s0}} \frac{dE'}{E'}\right] \quad (33)$$

For a series of non-overlapping resonances, p is then a multiplicative function, $p = \pi p_n$, where p_n is the resonance escape factor for the n^{th} resonance. If uranium is regarded as a pure absorber ($p_{s0} = 0$), or if the fuel elements are sufficiently thick ($P_0 = 1$), it may be seen that the value of p depends only on the first flight collision probability for the moderator. For thick moderator elements, $P_1 \rightarrow 1$ and $p \rightarrow 1$. The homogeneous approximation is obtained by taking $P_0 = (\Sigma_{a0} + \Sigma_{s0})/\Sigma_t$, $P_1 = \Sigma_1/\Sigma_t$ in which case

$$p = \exp\left[-\int_E^{E_0} \frac{\Sigma_{a0}}{\Sigma_t - \Sigma_{s0}} \frac{dE'}{E'}\right] \quad (33a)$$

The treatment can be generalized to account for energy degradation in oxygen and uranium collisions by the methods discussed in the last section. For non-overlapping resonances, and an assumed dE/E distribution above each resonance, the integral Equations 30 again reduce to differential equations. The chief problem is the validity of approximations to the spatial and angular distribution of the resonance neutrons required to compute first flight collision probabilities. At KAPL, G. M. Roe[26] assumes a uniform, isotropic distribution of resonance neutrons in the moderator in order to estimate their transmission through lumps of uranium. Richtmyer's work is generally based on a uniform spatial distribution of neutrons scattered into the resonance in the moderator from higher energies. Neutrons slowed into the resonance in the fuel appear to have a small effect on p. Further results on the effect of scattering collisions with small energy losses within the resonance in perturbing the spatial distribution need to be obtained before the separation of the energy and spatial problems of resonance capture, suggested here, can be implemented.

The extensive tables required to compute Doppler broadened resonances are now available. The first of these tables[27] was prepared as a joint effort by BNL and the AEC Computing Facility at NYU. The tables have since been further extended by the Computing Facility in collaboration with WAPD.

THERMAL UTILIZATION

The initiation of large scale studies of D_2O-uranium lattices at NAA and similar studies of H_2O-uranium lattices at BNL provided the incentive to go beyond diffusion theory in the determination of the thermal flux distribution within a lattice cell. The solution of the one-velocity Boltzmann equation by spherical harmonics expansions had been considered in earlier work by G. Placzek,[8] C. F. Mark[28] and others. The extension of their work to a lattice of cylindrical rods has been investigated by R. R. Haefner at ANL, by members of the Walter Kidde Laboratories and by J. Fleck at BNL. These investigations are all based on a one-velocity model with a uniform distribution of source neutrons in the moderator. The geometry is simplified into one of radial symmetry, and the P_3 spherical harmonics solution is used in order to reduce the scope of the work. The most rigorous of these formulas is that of Fleck, who accounts for the finiteness of the moderator and for its neutron absorption and anisotropic scattering properties. One-velocity parameters are obtained by integration over the transport equation, generally by assuming a Maxwellian distribution of velocities. In the case of H_2O, the effective mass of the moderator is determined by the method introduced by A. Radkowsky, which we have discussed. Fleck's formulation has been used for a Univac survey of the intracell flux distributions for the BNL experimental lattices. The method has been extended to multiregion lattices at KAPL by J. Weil who is presently engaged in coding the method for routine calculations on their digital computers.

Other methods of solving the one-velocity Boltzmann equation have been suggested. Thus Feurzeig and Spinrad[29] have developed an IBM procedure for the direct solution of the one-velocity Boltzmann equation for spheres and cylinders. A similar method had been developed earlier for spheres by R. D. Richtmyer and J. Von Neumann and adapted for use on the Los Alamos Maniac. At Hanford, G. W. Stuart and R. W. Woodruff have been perfecting a successive neutron generation approach to the problem. A Serber-Wilson treatment has been studied by A. Henry of WAPD. For isotropic scattering, the Boltzmann equation reduces to the integral equation

$$\vec{n(r)} = \int[(1+f)\vec{n(r')} + \vec{S(r')}]K(\vec{r},\vec{r'})\, d(\vec{r'}) \quad (34)$$

and J. Chernick has suggested the use of the formula

$$n(r_i) = \sum_{j=1}^{N} P_{i,j}[(1+f)n(r_j) + S(r_j)] \quad (35)$$

which simplifies the problem into the solution of a set of N linear equations; for slab lattices, a geometrical argument yields

$$P_{i,i\pm k} = \frac{1}{2\delta}\{E_3[(k-1)\delta] - 2E_3(k\delta) + E_3[(k+1)\delta]\}$$
$$P_{i,i} = (\delta + E_3(\delta) - \tfrac{1}{2})/\delta \quad (36)$$

with

$$E_n(\delta) = \int_0^1 e^{-\delta/\mu}\mu^{n-2}\, d\mu$$

for a mesh of width δ. For many problems, good accuracy is obtained with relatively large mesh widths.

H. B. Keller of the AEC Computing Facility has suggested the use of an interpolation formula in Equation 34 to obtain the coefficients P_{ij}. A similar method has been used by J. Fleck on the multivelocity Boltzmann equation.[6]

Integral equations for anisotropic scatterers have been considered by B. Carlson[30] and others at Los

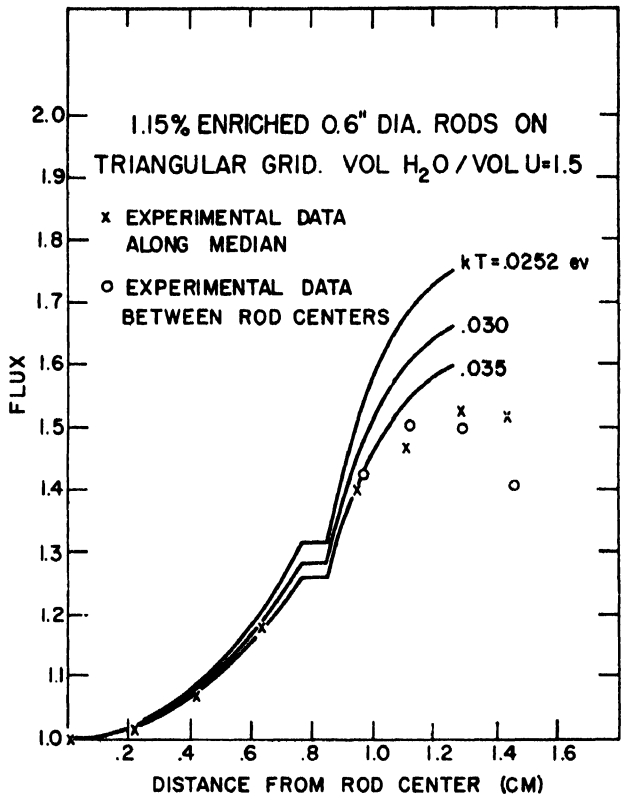

Figure 7. Flux distribution in U-H_2O lattice

Alamos. Frankel and Nelson[31] have reviewed the Los Alamos methods of treating displacement integral equations.

Spherical harmonic calculations of intracell flux distributions show a much larger flux depression within the fuel elements than does diffusion theory, and are in general agreement with experimental data. Thus Haefner's P_3 calculations for a widely spaced D_2O-uranium rod lattice fit the NAA experiments at a neutron temperature close to that of room temperature. The experimental flux distributions for H_2O-slightly enriched uranium lattices obtained at BNL and WAPD have been compared with the results of Univac runs and show good agreement with the wider lattices at a value of $kT \approx 0.025$ ev. At water to uranium volume ratios less than 3:1, however, the neutron temperature (averaged for an assumed Maxwellian distribution of velocities) must be increased to account for the increased flattening shown in the experimental data for the flux distributions in the moderator. The effective kT values to be used are still somewhat in doubt since BNL and WAPD experimental data for the flux peak in the moderator differ by about 10%.

A comparison of BNL experimental results with P_3 calculations is shown in Fig. 7 at a water to uranium volume ratio of 1.5. The U^{235} enrichment is 1.15%, but the flattening of the experimental flux curves in the moderator appears to depend less on increases in U^{235} content than on the tightness of the lattice. These results indicate that the degree of heterogeneity of the lattice is important in determining its effective neutron temperature.

The validity of P_3 and P_5 calculations for closely packed slab lattices is being investigated at BNL by a comparison with solutions based on Equation 35. The effect of cylindricalization of the moderator in a hexagonal lattice has been studied at BNL by B. Mozer and S. Oleksa by use of diffusion theory for the exact geometry. Relaxation calculations gave an accurate fit of the azimuthal variation of the experimental data in the moderator.

EPITHERMAL FISSION IN U^{235}

Although slightly enriched uranium water lattices are predominantly thermal, neutron absorptions in the U^{235} resonances above 0.3 ev become important even for natural uranium when the uranium volume approaches equality with that of water. The basic Equations 1 and 3 for the neutron cycle must then be modified to account for U^{235} resonance capture and fission. Whether k increases or decreases as a result of resonance absorptions in U^{235} depends on the value of η for these resonances.

In 1949, E. P. Wigner suggested[32] that the variation of the capture to fission ratio of U^{235} with energy could be obtained at intermediate energies from a study of the statistical distributions of the fission and neutron widths determined experimentally at low energies. The absence of adequate experimental data prevented the immediate application of Wigner's theory. By 1954, however, considerable data on the low level resonance parameters for U^{235} has been accumulated. S. Oleksa of BNL has analyzed the available data on the basis of several different distributions. The variation of $\alpha(25)$ with energy on the basis of an exponential distribution for both Γ_f and Γ_n is shown in Fig. 8 along with experimental data obtained in KAPL integral experiments. Oleksa found that the variation of $\alpha(25)$ is a slow one no matter which of several distributions is assumed to hold for the fission and scattering widths. The different distributions used gave values of α that did not differ markedly and were in general agreement with the results of the KAPL integral experiments.

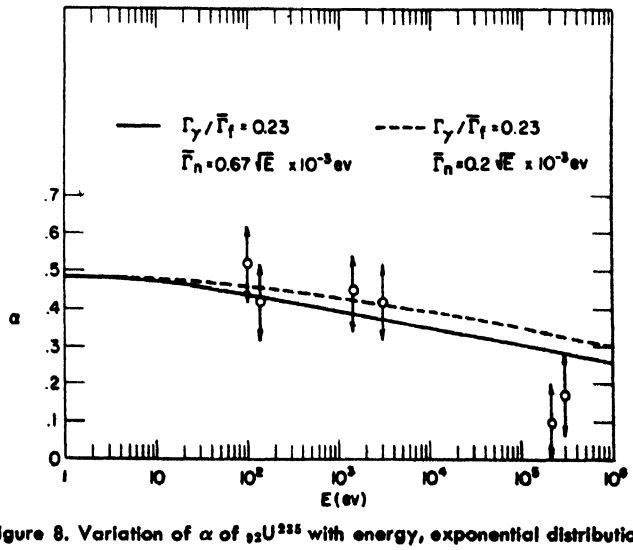

Figure 8. Variation of α of $_{92}U^{235}$ with energy, exponential distribution

Any variation of $\alpha(25)$ with energy in the thermal energy range contributes importantly to the nuclear temperature coefficient of a thermal reactor. The variation of α with temperature indicated by a KAPL analysis of the neutron spectrometer data available in 1951 disagreed with an estimate of its approximate constancy obtained from a BNL analysis of the temperature coefficients of graphite-normal uranium lattices. Recent accurate measurements of $\alpha(25)$ at BNL have shown that the variation of α with energy is much smaller than was indicated by the older spectrometer data.

REFERENCES

1. Wigner, E. P., *Theoretical Physics in the Metallurgical Laboratory of Chicago*, Journal of App. Phys., 857–863 (1946).
2. Wigner, E. P., *Resonance Absorption of Neutrons by Spheres*, CP-4 (1946).
3. Placzek, G., *On the Theory of Slowing Down of Neutrons in Heavy Substances*, Phys. Rev. *69*, 426–438 (1946).
4. Marshak, R. E., *Theory of the Slowing Down of Neutrons by Elastic Collision with Atomic Nuclei*, Rev. Mod. Phys., *19*, 185–238 (1947).
5. Goertzel, G., *Criticality of Hydrogen Moderated Reactors*, TAB-53 (1950).
6. Fleck, J. A., *The Energy Dependent Boltzmann Equation Applied to Criticality Calculations for Bare Graphite-Moderated Reactors*, BNL-298 (1954).
7. Davison, B., *Extension of Feynmann's Method for Determining Neutron Energy Spectrum and Spatial Distribution to the Case of Anisotropic Scattering*, A.E.R.E. T/R 590 (1950).
8. Davison, B., *A New Method for Calculating the Critical Radius of Systems Containing Hydrogen and Fissile Material*, A.E.R.E. T/R 826 (1952).
9. Selengut, D. S., *Conditions for Criticality in Certain Types of Nuclear Reactors*, AECD-3024 (1950).
10. Glasstone, S. and Edlund, M. C., *The Elements of Nuclear Reactor Theory*, Ch. 12, Van Nostrand Co., New York (1952).
11. Watt, B. E., *Energy Spectrum of Neutrons from Thermal Fission of U^{235}*, Phys. Rev. *87*, 1037–1041 (1952).
12. Certaine, J. and Aronson, R., *Distribution of Fission Neutrons in Water at the Indium Resonance Energy*, NDA-15C-40 (1954).
13. Hurwitz, H., Jr. and Zweifel, P. F., *Slowing Down of Neutrons by Hydrogenous Moderators*, KAPL-1269 (1955).
14. Oleksa, S., *The Inelastic Scattering Cross-Section of Lead*, BNL-273 (1953).
15. Auerbach, T., *Neutron Leakage from Hydrogen Moderated Systems*, (unpublished).
16. Krasik, S., P/601, *Critical Experiments and Physics Aspects of PWR*, Volume 5, Session 21A, these Proceedings.
17. Wigner, E. P. and Wilkins, J. E., Jr., *Effect of the Temperature of the Moderator on the Velocity Distribution of Neutrons with Numerical Calculations for H as Moderator*, AECD-2275 (1944).
18. von Dardel, G. F., *A Study of the Interaction of Neutrons with Moderating Materials*, Phys. Rev. *94*, 1272–1283 (1954).
19. Cohen, E. R., P/611, *Survey of Neutron Thermalization*, Volume 5, Session 23A, these Proceedings.
20. Plass, G. N., *The Diffusion Length and the Utilization of Thermal Neutrons in a Heterogeneous Pile*, AECD-3214 (1943).
21. Castle, H., Ibser, H., Sacher, G. and Weinberg, A. M., *The Effect of Fast Fission on k*, CP-644 (1943).
22. Guggenheim, E. A. and Pryce, M. H. L., *Fast Fission in Tubes*, MT-199 (1945).
23. Goldstein, M., *A Table of the Function $K_1(x)$*, LAMS-728 (1948); see also Bickley, W. G. and Naylor, J., Phil. Mag., *20*, 343–7 (1935).
24. Creutz, E., Jupnik, H., Snyder, T. and Wigner, E. P., *Review of the Measurements of Resonance Absorption by Uranium in Bulk*, Journ. Appl. Phys., 255–279 (1955).
25. Richtmyer, R. D., *Monte Carlo Study of Resonance Escape in Hexagonal Reactor Lattices*, NYO-6479 (1955).
26. Roe, G. M., *The Absorption of Neutrons by a Resonance Absorber*, KAPL-1241 (1954).
27. Sailor, V. L., Rose, M. E., Miranker, W., Leak, P. and Rabinowitz, G., *A Table of the Integral*

$$\Psi(x,t) = \frac{1}{2\sqrt{\pi t}} \int_{-\infty}^{\infty} \frac{e^{-(x-y)^2/4t}\, dy}{1+y^2}$$

BNL-257 (1953).
28. Mark, C. F., *The Spherical Harmonics Method*, CRT-340 (1947).
29. Feurzeig, W. and Spinrad, B. I., *Numerical Solution of Transport Theory Problems for Spheres and Cylinders*, ANL-5049 (1953).
30. Carlson, B., *Neutron-Diffusion Theory*, AECD-2835 (1949).
31. Frankel, S. and Nelson, E., *Methods of Treatment of Displacement Integral Equations*, AECD-3497 (1953).
32. Wigner, E. P., *On the Variation of η with Energy in the 100–10,000 ev Region*, BNL-25 (1949).

Physics Aspects of the Pressurized Water Reactor (PWR)

By A. Radkowsky* and S. Krasik,† USA

The reactor of the PWR plant is, conceptually, a small, highly enriched core acting as a source of neutrons surrounded by a subcritical lattice of natural uranium and light water. This type of reactor has become known as a "seed and blanket" arrangement, the term "seed" referring to the highly enriched core while the term "blanket" is applied to the natural uranium and water lattice. In such an arrangement the criticality of the assembly is largely governed by the seed. Neutrons leaking from the seed are multiplied by fissions occurring in the blanket so that from the beginning of core life a substantial fraction of the total power is produced in the natural uranium blanket. It is an important objective in the design of this type of reactor to maximize the fraction of the total energy delivered by the blanket over the reactor lifetime.

The seed and blanket reactor has a number of advantages over a reactor of uniform enrichment some of which are of particular importance in a reactor development program. These are discussed below.

1. There are several advantages associated with the fuel loading of the reactor. First, the fissionable material investment is lower because the fuel is concentrated in a region of high statistical weight insofar as reactivity is concerned. Secondly the relatively high rate of plutonium production in the blanket region immediately adjacent to the seed tends to maintain the reactivity lifetime for high burnup of the fuel.

2. There are several important advantages associated with the fact that the reactivity is largely governed by the seed. First, the seed is a small, highly enriched core which can be designed to have a substantial negative temperature coefficient of reactivity. This property of the reactor is important for the safety of the reactor and for simplification of the control system. The negative temperature coefficient of reactivity can be achieved without compromising the design of the natural uranium-water lattice for maximum reactivity. Secondly, the neutron flux decay in the reactor after shutdown is characteristic of a highly enriched reactor. In a slightly enriched core with a relatively high fast effect ($\sim$1.06 to 1.10) the increased yield of delayed neutrons from fission of U^{238} maintains the power at a significantly higher level immediately after shutdown.[1] This fact is of importance in ensuring safety of the reactor in the event of loss of coolant flow. A third advantage is that the control can be limited to the seed region.

3. The seed and blanket arrangement provides a high degree of flexibility in design and operation. The reactor is designed in small sections all of which are individually removable and alike dimensionally. Thus seed and blanket units can be replaced, interchanged, or rearranged during any stage of the operating life of the reactor. A further advantage of practical importance is that reactors of varying properties can be designed using uranium at two standard enrichments, i.e., natural uranium and highly enriched uranium.

The principal disadvantage of the seed and blanket design is the relatively poor flux distribution. Because the natural uranium-water lattice is subcritical, the neutron flux distribution tends to fall off exponentially away from the seed. Thus the blanket region tends to be somewhat larger in size for a given power output. This is partially offset by the shielding advantages of the blanket which permit reduced gamma shields inside the pressure vessel. The fact that the power density is highest in the seed is offset principally by the properties of the material used for the seed. These permit a design having a high power density because they can be fabricated and used in shapes having excellent heat transfer properties.

The design of a seed and blanket reactor presents some challenging physics problems. One is the calculation of the neutron distribution in energy in the vicinity of the seed-blanket interface. Another is the question of long term reactivity changes in view of the large spatial variation in plutonium production in the blanket. Still another is the determination of power distributions with various seed arrangements. Extensive experimental and theoretical study will be required to solve these problems. As yet only a start has been made toward their solution.

GENERAL PROPERTIES OF THE SEED AND BLANKET DESIGN

A considerable insight into the physics design of the reactor can be gained by considering the division of the total reactor power between the seed and the blanket. In Appendix B an expression is derived for the ratio of blanket power to seed power. An approximation is also given which is adequate for this part of the discussion.

* Reactor Development Division, US Atomic Energy Commission. Including work by A. Radkowsky, US Atomic Energy Commission; M. J. Galper, R. L. Hellens and S. Krasik, Westinghouse Atomic Power Division.

† Westinghouse Atomic Power Division.

$$\frac{\text{Blanket power}}{\text{Seed power}} = \left[\frac{k^b \epsilon}{1 - k^b}\right]\left[\frac{k^s - 1}{k^s}\right] \quad (1)$$

In this expression k^b is the multiplication constant of the blanket region and k^s the multiplication constant of the seed region. ϵ is the fast fission factor in the blanket.

For purposes of orientation in considering Equation 1 it may be noted that in a practical reactor of this type k^s can have any desired value from 1.0 up to about 1.9. On the other hand k^b is always less than unity and may range from 0.75 to about 0.9 for a practical design. Within these stated ranges, Equation 1 shows that the fraction of the power produced in the blanket increases both with increasing k^b and increasing k^s. The gain as k^b approaches unity is particularly significant. While the blanket power increases with increasing k^s, the rate of gain is markedly less for values of k^s in excess of about 1.6.

There are then two aims in the design of a reactor of this type. The first is a seed of high reactivity with a high leakage of excess neutrons into the blanket. The second is a blanket which uses these neutrons as effectively as possible by having a high multiplication constant.

In addition to the requirement of high leakage from the seed, there is the additional requirement of maintaining the seed at criticality despite its high reactivity. The criticality and leakage requirements can be met simultaneously by designing the seed to have a high geometrical buckling. For this reason it is necessary that at least one characteristic dimension of the seed region be relatively small.

The high buckling requirement for the seed may, in a practical reactor, conflict with the heat transfer requirements. Suppose, for example, the seed is a tall, right circular cylinder surrounded by a cylindrical blanket. The seed volume for a given height of reactor is fixed by the buckling requirement. Heat transfer considerations will then determine the maximum reactor power.

It is possible, however, to separate the high buckling requirements of the seed from the heat transfer requirements. One method of effecting this separation is to distribute the seed volume determined by heat transfer requirements into several seeds separated by blanket material, each seed having the appropriate buckling. A somewhat different approach has been selected for the PWR. The seed is formed in the shape of an annular cylinder whose radial location is adjusted to provide the appropriate volume for heat transfer considerations. The radial thickness of the annulus, which essentially determines the buckling, is adjusted for appropriate neutron leakage properties.

The actual choice of annular thickness is a compromise between seed fuel loading and the fraction of the total reactor power produced in the blanket. There is a minimum annular thickness for criticality determined by the maximum available k^s. For limiting values of k^s in the neighborhood of 1.9, the total seed loading required rises sharply as the annular thickness is reduced to the lower limit. On the other hand, as shown by Equation 1, the fraction of power produced in the blanket also rises.

There are several reasons, however, why a high fuel loading is undesirable. First and most obvious, a substantial tieup of fuel in inventory is costly. Second, as the fuel loading of the seed rises, an increasingly serious thermal peak develops in the blanket region immediately adjacent to the seed. Not only is this flux peak undesirable because of thermal stress considerations, but it results in a back current of thermal neutrons into the seed. This reduces the fraction of power produced in the blanket below that given by Equation 1. (This effect on the power ratio is shown in the equations derived in Appendix B.) A further consequence of a high thermal absorption in the seed is the expected reduction in control rod effectiveness. Finally, the considerable degree of uncertainty in the reflector savings presented to the seed by the blanket over the operating life of the reactor is an important consideration. A design in which small variations in reflector savings will cause the seed to vary from a condition of low excess reactivity to one of high excess reactivity is not desirable.

For these reasons but principally because the expected gain in blanket power with high reactivity is not fully realized, the compromise choice for the annulus width is about 15 cm which is associated with a k^s around 1.6.

The choice of fuel element and arrangement in the reactor must take into account material, thermal, hydraulic and mechanical considerations as well as physics considerations. The blanket fuel element choice of zirconium-clad uranium oxide is based on meeting materials requirements of radiation stability and corrosion resistance as well as physics requirement of good neutron economy. The choice of hydrogen to uranium ratio in the blanket must take into account thermal and hydraulic considerations as well as the physics requirement of a high multiplication constant. The choice which was made, a hydrogen to uranium atomic ratio of approximately 5 in the cold reactor, provides close to the maximum reactivity in the hot reactor. The oxide fuel element diameter of approximately 0.4 inch is determined by central temperature conditions in the fuel element. The thickness of zirconium cladding on the fuel element is determined by fission product containment requirements and mechanical design considerations. The amount and disposition of zirconium used for structural purposes is determined by mechanical considerations.

The fuel element in the seed is principally zirconium since the highly enriched uranium represents only a small fraction of the volume. The choice of fuel element shape and channel thickness is based primarily on mechanical, thermal and hydraulic considerations. The resulting metal to water ratio of 1.25 is quite satisfactory from a physics point of view, however. This ratio permits a reasonable fuel loading and is appropriate for a good negative temperature coefficient of reactivity.

The outer reflector of the PWR is water. Since the leakage of neutrons from the blanket is relatively low, the reflector properties are not particularly significant to the reactor design.

CALCULATIONAL METHODS AND RESULTS

All of the physics calculations made for PWR design purposes have used few-group diffusion theory.[2] In the major fraction of the work to date two group diffusion theory has been used. Certain of the calculations of group constants, however, have been multigroup in nature using the order of fifty groups.

The chief reason for going beyond a single energy group in reactor studies of this type is to take into account the varying spatial distributions of the neutron energy groups. It is presently believed that a four group description is the minimum which will permit an adequate calculation of PWR properties. The division of groups in such a scheme is as follows:

1. A high energy group comprising all neutrons with energies above the effective fast fission threshold in uranium-238.
2. A slowing down group starting at the lower limit of the high energy group and extending down in energy to the region of resolved resonances in uranium-238.
3. A resonance energy group covering the uranium-238 resolved resonances.
4. A thermal energy group starting at the lower limit of the resonance group and covering the entire thermal distribution.

No design calculations have as yet been made using the full four-group approach. At the present time group constants are being calculated for this model.

A three-group approach has been used for certain studies, particularly those associated with the spatial dependence of plutonium production. In this model the high energy group and the slowing down group of the four-group model are combined into a single group. The most serious error made in using this model is the calculation of the true fast fission in the blanket.

The three-group formulation as well as a two-and-one-half group formulation and a two-group formulation are given in Appendix A.

The calculation of group constants for the design studies was carried out, in general, by the usual integrations and averaging of mono-energetic cross sections.[2] Two of the group constants deserve particular mention, however. Calculations of the slowing down distributions were made as described in another paper.[3] The resonance escape probability was calculated according to the method given by Wigner.[2] In the cases of certain parameters such as the migration area, resonance escape probability, fast effect and thermal utilization, experimental results[4,5] were used to substantiate, insofar as possible, the methods used for calculation.

The calculations of the reactors themselves were carried out using both digital and analog computers. The digital computations for the most part used the UNIVAC. A one-dimensional, multi-region code was developed for this purpose. Both two-group and three-group codes were used, with the principal emphasis placed on the two-group work. A resistive analog computer especially designed to solve the two-group equations was also used; the principal advantage of this computer was the adjustability of the reactor constants at each lattice point. This flexibility permitted studies to be made in which the isotopic depletion and buildup could be varied from point to point. The one-dimensional computers and codes have available between twenty and thirty lattice points. In some cases these points can be non-uniformly distributed. No multi-dimensional analysis of the PWR has yet been made.

An extensive survey program has been developed using the one-dimensional multi-region codes. The purpose of this study was not only to complete design studies but to explore the effects of various parameter changes. A number of the problems calculated are, therefore, not actual design problems but are illustrative of trends. A few of the survey results will be presented to indicate the nature of the study and the type of results obtained.

Figure 1 is a radial plot of thermal and fast flux distributions for a cylindrical annular seed with a cylindrical inner and outer blanket. The seed thickness is 17 cm; the inner radius of the seed is located at 43 cm and the overall radius of the reactor is 93 cm. The flux plots are shown for the reactor in its hot condition with three values of seed loading. The lowest fuel loading 28.9 kg of uranium-235 is approximately the loading for hot, clean criticality. The two higher loadings of 38.6 kg and 64.6 kg are adjusted for criticality in the calculation by assuming a uniformly distributed thermal poison cross section in the seed. These flux maps show the outward leakage of fast neutrons from the seed, the inward leakage of thermal neutrons into the seed and the effect of the thermal absorption of the seed on the thermal flux peak near the seed-blanket interface. While the presence of the distributed thermal absorber for criticality exaggerates the effect, the size of the thermal flux peak is chiefly associated with the fuel loading of the seed and its thermal absorption properties.

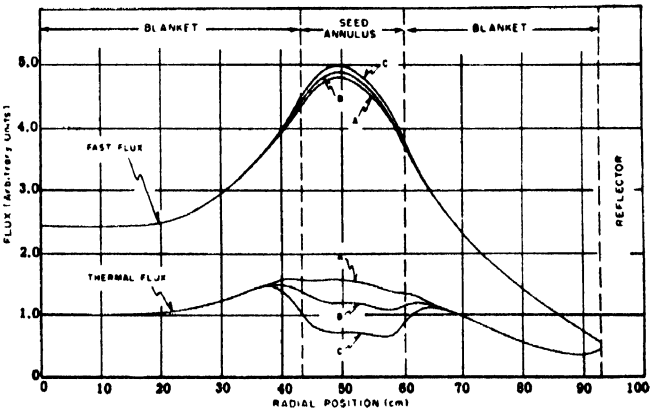

Figure 1. Effect of seed loading on flux shapes. Seed loading: A = 28.9 kg, B = 38.6 kg, C = 64.6 kg

Figure 2 illustrates the effect of annular thickness of the seed on the required fuel loading and the fraction of the total power produced in the blanket. A series of reactors similar to the reactor of Fig. 1 were calculated with varying annular thickness; the inner radius of the annulus was held fixed at 43 cm and the radial thickness of the outer blanket was held fixed at 50 cm. The plot of seed loading shown is that required for hot, clean criticality. The division of power between seed and blanket was calculated from the flux plots including the fast effect in the blanket. Since this series of reactors has varying heat transfer properties, Fig. 2 does not represent a design study but illustrates the trend of seed loading and blanket power with seed thickness. (The blanket properties of the reactors shown in Figs. 1 and 2 are somewhat different accounting for the difference in the loading figures.)

Figure 3 illustrates the effect of seed loading on the fraction of the total power produced in the blanket. A series of reactors with cylindrical annular seeds were calculated for five values of annular thickness. The reactor geometry was the same as that described for the reactor of Fig. 2. Flux distributions for a number of fuel loadings were calculated as in Fig. 1 and the blanket power fraction calculated for each fuel loading. The envelope curve in Fig. 3 represents the hot, clean reactor. This illustrates the increase in blanket power fraction with increase in seed loading as the annular thickness is varied. This curve is essentially a cross plot of the two curves of Fig. 2. The straight lines moving off downward to the right illustrate, for each annular thickness, the loss in blanket power with increased seed loading. This effect results from the increased thermal flux peak in the blanket with increasing thermal absorption of the seed.

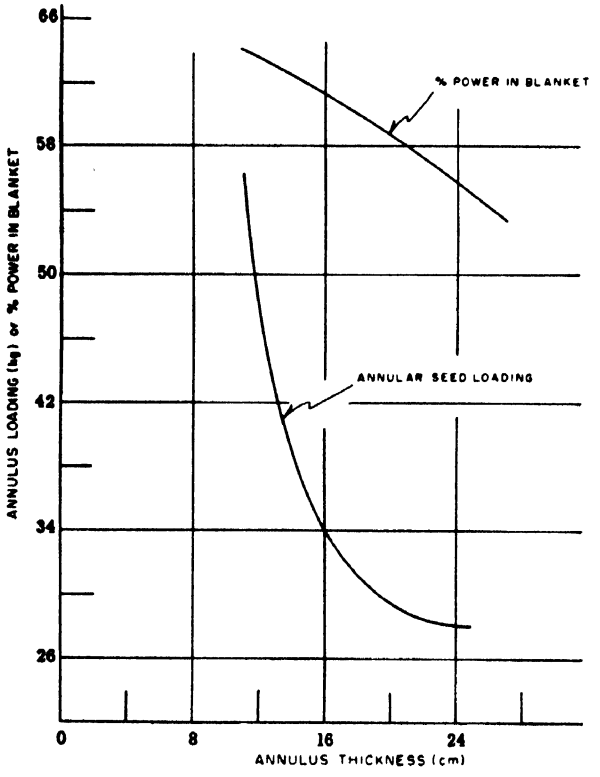

Figure 2. Survey study. Loading and blanket power vs annular thickness; outer blanket thickness constant; hot, clean criticality

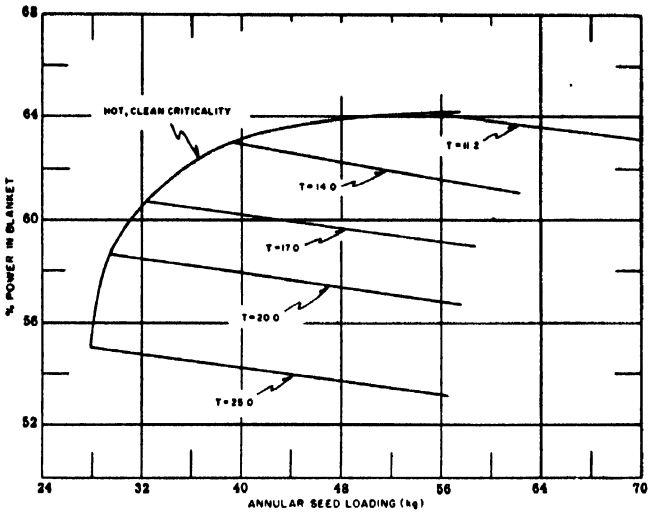

Figure 3. Effect of seed loading on blanket power. T = thickness of annulus (cm)

REACTOR CONTROL

There are two problems associated with control of the PWR reactor. One problem is to provide the gross reactivity control required for shutdown, fuel depletion, fission product poisoning, etc. The other problem is to ensure the stability of the reactor under operating conditions. Since one important aspect of gross reactivity control is related to reactor stability and in particular to the temperature coefficient of reactivity, this will be discussed first.

Extensive studies have shown that a substantial negative temperature coefficient of reactivity is an extremely important factor in providing overall plant stability and ensuring safety of the reactor in the event of certain types of accidents. Figure 4 illustrates the point with respect to plant stability.

In the transient response study shown in Fig. 4 a reactor plant having a temperature coefficient of reactivity of -3×10^{-4} in reactivity per degree Fahrenheit is initially operating at full load with full coolant flow in the reactor. The transient is induced by a step change in steam throttle operating from 100% of full flow to 20% of full flow. No external reactor control is operative. The behavior of the plant for approximately 100 seconds following the load decrease is shown by the graphs. The reactor, through the influence of the negative temperature coefficient of reactivity, drops smoothly in output power to meet the new load demand. While the plant conditions used for this calculation are somewhat different from those of the PWR plant, the effectiveness of the negative temperature coefficient in minimizing reactor transient control requirements is clearly shown.

The calculation given in Fig. 4 was made on a reactor plant dynamic simulator. This is an analog computer of the differential analyzer type in which the equations governing the kinetic behavior of the plant components are simulated by electric circuits and electro-mechanical devices. Approximately forty

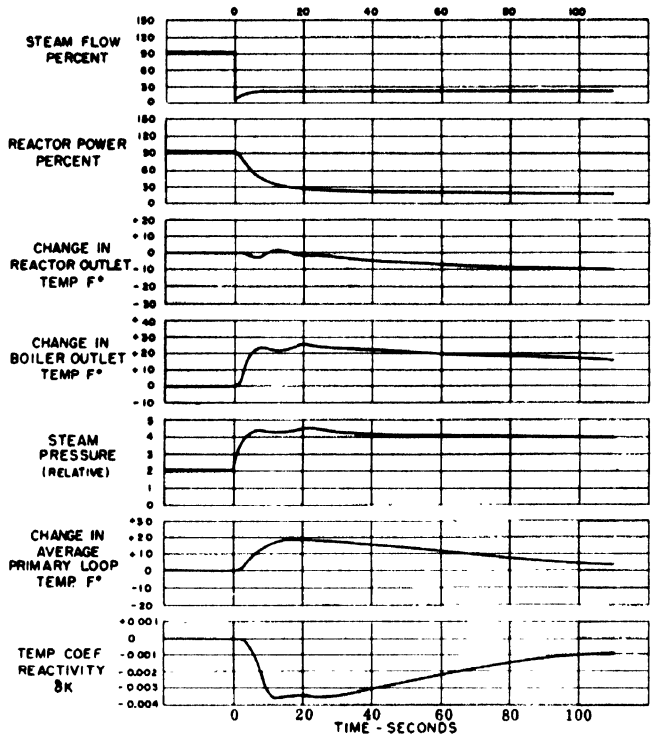

Figure 4. Transient plant response to step change in steam throttle opening. Initial opening, 100% steam flow; final opening, 20% steam flow; temperature coefficient, $-3(10^{-4})$ $\delta K/°F$; coolant flow, 100%

coupled equations were used in the calculation shown.

Simulator studies of accident conditions such as loss of coolant flow or inadvertent addition of reactivity, particularly during reactor startup, have shown the importance of the negative temperature coefficient in protection of the reactor.

For the reasons discussed above, the PWR has been designed to have a substantial negative temperature coefficient at operating temperature. In general, the temperature coefficient has been computed by criticality calculations at two distinct temperatures rather than by evaluation of derivatives. In such calculations the reactor constants are determined at each of the temperatures. At one temperature criticality is achieved by adjusting an appropriate parameter such as the seed loading. At the other temperature criticality with the previously calculated loading is determined by assuming ν, the number of neutrons emitted per fission, to be a variable. The reactivity change is taken as

$$\frac{\nu - \nu_0}{\nu_0}$$

where ν_0 is the true physical value of ν. The temperature coefficient is determined by dividing by the temperature difference between the two conditions.

Studies of this type have shown that the overall temperature coefficient of the PWR is dependent primarily on the properties of the seed and is essentially independent of the temperature coefficient of the blanket. The value of the temperature coefficient is, however, dependent on the condition of the reactor, particularly the position of the control rods. It is expected that the temperature coefficient of the PWR will range between -2×10^{-4} and -4×10^{-4} in reactivity per degree Fahrenheit at operating temperature.

The preceding discussion indicates that while a negative temperature coefficient of reactivity is highly desirable its cost in terms of gross reactivity control is substantial. Even taking into account the decrease in temperature coefficient with reduced temperature, a reactivity change of the order of 10% will be required in the PWR to cover the temperature range between ambient temperature and plant operating temperature.

The gross reactivity control requirements of the PWR will be met principally through the use of neutron absorbing control rods. A burnable poison will probably be used in addition to minimize the reactivity excursion due to fuel depletion. As presently designed 24 cruciform shaped control rods will be used, one for each structural unit of the seed. The rods will be used only in the seed region; each will be located in a cruciform shaped channel. The rod shape is chosen to provide a maximum of control rod surface with a minimum volume of channel.

The control rod material will probably be hafnium since it combines excellent material properties with high effectiveness. The strong resonances of hafnium in the epi-cadmium energy region enhance the effectiveness of the rod by adding to the thermal neutron absorption some epithermal neutron absorption. Another possible material for the control rods is steel alloyed with B^{10}.

Reactivity control for the PWR is required for the following specific purposes: (1) cold shutdown margin; (2) cold to hot reactivity change; (3) equilibrium xenon and samarium poison; (4) operational margin for transient load conditions; and (5) fuel depletion and stable fission product poison buildup.

The cold shutdown margin is required for safe handling of the reactor. In general a shutdown margin of 5% in reactivity would be considered adequate; it is necessary, however, to provide additional margin to handle certain casualty conditions such as a control rod stuck in the withdrawn position.

The cold to hot reactivity swing has been discussed above in connection with the temperature coefficient of reactivity. This item is the largest single reactivity control requirement for the PWR.

The remaining control items, (3), (4) and (5) above will be discussed jointly. The hot, clean critical loading of the PWR reference seed design is presently estimated as 32 kg of uranium-235. The extra fuel loading required for equilibrium xenon and samarium poison is estimated to be 6 kg. The present lifetime specification of the first PWR seed requires a reactivity lifetime of 3000 full power hours with full power equilibrium xenon and samarium override at the end of life. Assuming that the initial division of power between seed and blanket obtains for the first 3000 hours of operation, 14 kg of fuel is specified for a depletion allowance. The total of 52 kg of uranium-235 is the nominal loading of the first PWR seed.

It is planned to compensate for most of the reac-

tivity change associated with fuel depletion by incorporating a burnable poison in the seed. This is a small quantity of natural boron which will deplete with the fuel in such a manner as to minimize the reactivity change due to fuel depletion. A separate paper on the theory and application of burnable poisons will be published by one of us (A.R.) in the near future. The exact manner in which the burnable poison will be used in the PWR will depend on the reactivity changes associated with the plutonium buildup in the blanket layer immediately adjacent to the seed. This problem has not yet been analyzed. If a burnable poison is used, the total fuel loading of the seed will be increased slightly to compensate for the unburned poison residue at the end of the seed life.

In addition to the reactivity margin for equilibrium xenon and samarium, some margin is required to handle the xenon transient following a sharp reduction in reactor power. The margin to be provided is as yet uncertain pending a detailed analysis of the reactivity excursion associated with the seed depletion and the plutonium buildup in the blanket. Even under severe reactivity transient conditions, the hot to cold reactivity margin is available for startup of the reactor at reduced temperature.

It is the present plan to withdraw the control rods individually but to maintain them in registry as a bank. Because the reactivity requirement to be handled by the control rods at operating temperature is relatively small, it is expected that the control rod bank will be well withdrawn during power operation.

The control studies which have been made to the present have been quite limited in scope. It is planned to carry out the bulk of the initial studies experimentally using the PWR flexible critical experiment.[5]

The use of rod type reactor control results in certain distortions of the neutron flux pattern which must be taken into account in making the thermal analysis of the reactor. The partial insertion of the rod bank during reactor power operation results in a modification of the axial flux distribution. It is changed from a half-cosine to a compressed half-cosine with an exponential-like tail in the region occupied by the rods. Calculations of these distributions have not yet been completed. An estimated allowance has been provided, however, in the preliminary heat transfer design.

A further allowance in the heat transfer design must be made for the thermal flux peak which develops in the control rod channels when the rods are withdrawn. The control rod channel, which is filled with water, develops a thermal flux peak for two reasons. First, the water is more effective than the remainder of the seed as a moderator. Second, the absorption of thermal neutrons is considerably smaller in the water than in the fuel elements. The thermal flux peak in the water channel propagates into the adjacent fuel plates resulting in a local hot spot. This effect could be alleviated in part by adding zirconium extensions to the control rods. Pending a multidimensional analysis of the power distribution in the reactor, no plans have yet been made to add these extensions. Filler strips of zirconium are planned, however, around the boundaries of the seed structural units to limit thermal flux peaking due to inter-cluster water channels.

LONG TERM REACTIVITY CHANGES

The question of long term reactivity gains in the PWR is of great importance since the behavior of the reactor from this point of view will determine its reactivity lifetime. The problem is not well understood for several reasons. First, there is a lack of detailed information on the cross section of various isotopes particularly in the thermal and epithermal region. Second, the calculation of the neutron distribution in energy at various positions in the reactor is very difficult. The problem is here outlined to the extent that it is presently understood.

The production of plutonium in the blanket is markedly different in the region immediately adjacent to the seed than in the remainder of the blanket. In the interface region the neutron fluxes are undergoing spatial transitions due to the difference in nuclear properties of the two regions. Near the interface the flux distribution is characterized by a high leakage of fast neutrons out of the seed. Away from the interface the fast to slow flux ratio takes on the asymptotic value characteristic of the blanket material and the geometry. There is an additional transition at the outer boundary of the blanket near the reflector.

The nature of the isotopic buildup will first be discussed for the asymptotic region. Calculations have been carried out for the isotopic changes in natural uranium as a function of flux-time (thermal flux) using as the thermal spectrum a Maxwellian distribution at PWR operating temperature and best available cross-section data. Since the production of plutonium by

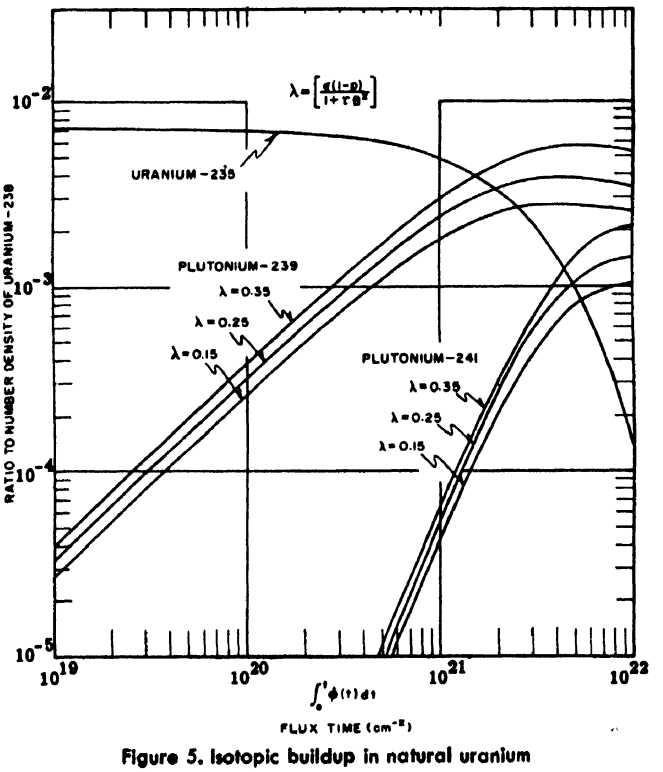

Figure 5. Isotopic buildup in natural uranium

resonance capture involves the fast flux, other parameters, namely, the fast fission factor, the fast neutron leakage and the resonance escape probability must enter the calculation. These effects may be taken into account by introducing the parameter

$$\lambda = \left[\frac{\epsilon(1-p)}{(1+\tau B^2)}\right]$$

where the fast effect is represented by ϵ, the nonleakage probability by

$$\frac{1}{(1+\tau B^2)}$$

and the resonance capture by $(1-p)$. Calculations were made for values of λ of 0.15, 0.25 and 0.35.

Figure 5 shows the depletion of uranium-235 and the calculated buildup of the Pu^{239} and Pu^{241} densities. Figure 6 shows the calculated values of η, the number of neutrons emitted in fission per thermal neutron absorbed in fuel as a function of flux time for $\lambda = 0.35$ and $\lambda = 0.15$. The value of λ characteristic of the PWR blanket is approximately 0.35.

The conversion ratio to be expected in the asymptotic region of the blanket, i.e., the number of plutonium atoms formed per uranium-235 atom destroyed, may be estimated as follows:

1. The ratio of conversion due to thermal capture is

$$\frac{N^{238}\sigma_a{}^{238}}{N^{235}\sigma_a{}^{235}}$$

where the N's are the number densities of the respective uranium isotopes and the σ's are the thermal absorption cross sections. This ratio for the blanket is 0.59.

2. For each thermal neutron absorbed in U^{235}, η^{235} neutrons are produced. These are enhanced by the factor ϵ due to fast fission. Due to (outward) leakage of fast neutrons only the fraction

$$\left(\frac{1}{1+\tau B^2}\right)$$

are available for resonance capture. The fraction

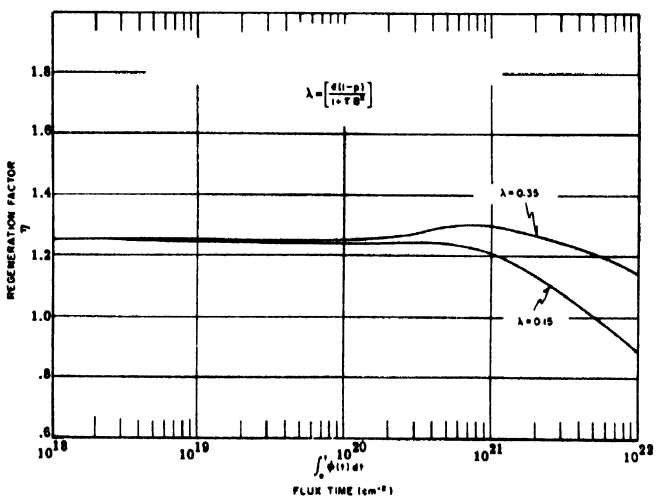

Figure 6. Change in η with flux time for natural uranium

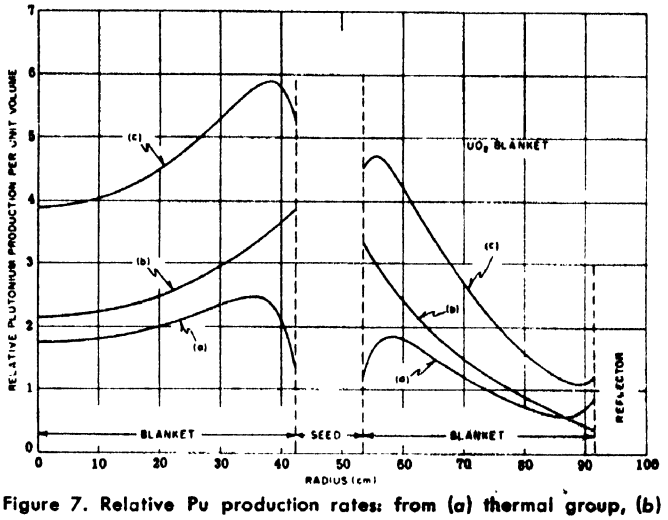

Figure 7. Relative Pu production rates: from (a) thermal group, (b) epithermal group, (c) total (a) + (b). UO_2 blanket

$(1-p)$ are captured leading to the conversion ratio associated with resonance capture

$$\frac{\eta^{235}\epsilon(1-p)}{(1+\tau B^2)}$$

This ratio for the blanket is 0.73; in calculating this ratio account is taken of the net inward leakage of fast neutrons to the asymptotic region of the blanket by using a negative value for B^2. The age used is that from fission to the uranium-238 resonance.

There is an additional contribution to the conversion ratio of about 0.02 associated with fast parasitic capture.

The sum of these contributions is 1.34. This is the estimated conversion rate of U^{235} to Pu^{239} in the asymptotic region of the blanket at the start of reactor life.

An estimate of the effect of fast leakage from the seed on the conversion ratio in the interface region has been made by the use of three-group calculations. The results of a typical calculation are shown in Figs. 7 and 8. (It should be noted that this reactor is not the PWR reference design.) Figure 7 shows the relative plutonium production in the blanket due to thermal capture and resonance capture. Figure 8

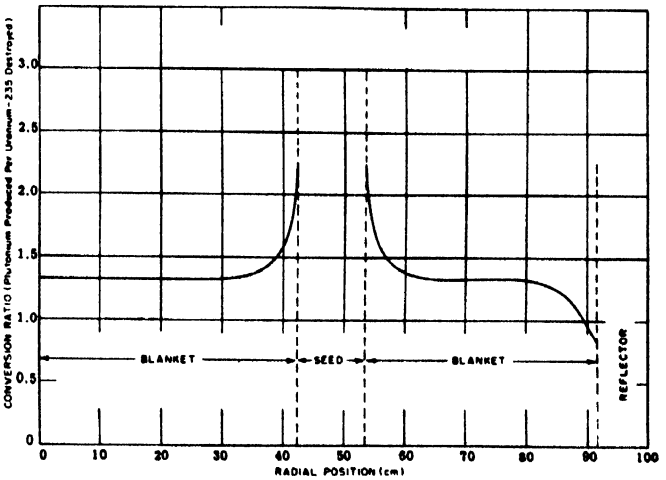

Figure 8. Local conversion ratio in UO_2 blanket

shows the local conversion ratio in the blanket, i.e., the number of Pu^{239} nuclei formed per unit volume per uranium-235 nucleus destroyed in that volume. It is noteworthy that the conversion ratio for the particular geometry studied reaches a maximum of about 2.25 at the seed-blanket interface. Over a substantial part of the blanket the local conversion ratio is the 1.34 value quoted above. The ratio falls sharply at the blanket-reflector interface because of epithermal neutron leakage out of the blanket into the reflector.

The overall conversion ratio of the example calculated, seed and blanket combined, is 0.79 at the start of core life. While the number of fissile nuclei in the reactor is decreasing with life, the new fissile nuclei are being formed most rapidly in a region of considerable importance insofar as reactivity is concerned. This coupled with the high fission cross section of plutonium holds considerable promise for an extended reactivity lifetime. Thus, while the lifetime problem of the PWR has not yet been calculated in detail, there appears to be good reason for optimism at least with respect to reactivity.

REFERENCES

1. Sun, K. H., Charpie, R. A., Pecjak, F. A. and Jennings, B., *Delayed Neutrons from U^{238} and Th^{232} Fission*, Physical Review *79*, p. 3 (1950).
2. Glasstone, S. and Edlund, M. C., *The Elements of Nuclear Reactor Theory*, D. Van Nostrand Co., Inc., New York (1952).
3. Wilkins, J. E., Hellens, R. L., and Zweifel, P., P/597, *Status of Experimental and Theoretical Information on Neutron Slowing Down Distributions in Hydrogenous Media*, Volume 5, Session 19A, these Proceedings.
4. Kouts, H. C., P/600, *Exponential Experiments with Slightly Enriched Uranium Rods in Ordinary Water*, Volume 5, Session 21A, these Proceedings.
5. Krasik, S. and Radkowsky, A., P/601, *Pressurized Water Reactor (PWR) Critical Experiments*, Volume 5, Session 21A, these Proceedings.

APPENDIX A: FORMULATION OF THE GROUP EQUATIONS

The three group equations which are used are:

$$-D_f\nabla^2\phi_f + \Sigma_f\,\phi_f = \frac{k}{p}\,\Sigma_s\phi_s \qquad \text{(A-1)}$$

$$-D_r\nabla^2\phi_r + \frac{\Sigma_r}{p}\,\phi_r = \Sigma_f\phi_f \qquad \text{(A-2)}$$

$$-D_s\nabla^2\phi_s + \Sigma_s\,\phi_s = \Sigma_r\phi_r \qquad \text{(A-3)}$$

In these equations ϕ is the neutron flux, D is the diffusion constant, p the resonance escape probability, k the multiplication constant and the Σ's denote macroscopic cross sections. The subscripts f, r and s refer to the fast, resonance and slow energy groups respectively. Σ_f and Σ_r are slowing down cross sections; Σ_f is related to the age τ_f from the fast group to the resonance group by the definition

$$\Sigma_f = \frac{D_f}{\tau_f}$$

and correspondingly

$$\Sigma_r = \frac{D_r}{\tau_r}$$

where τ_r is the age from the resonance group to the thermal group.

Equation A-1 differs from some standard formulations in that the source term is written

$$\frac{k}{p}\,\Sigma_s\phi_s$$

Clearly if k is defined by the conventional four-factor formula

$$k = f\eta\epsilon p$$

the number of source neutrons per thermal neutron absorbed is

$$\frac{k}{p} = f\eta\epsilon$$

where f is the thermal utilization, η is the number of fission neutrons produced per thermal neutron absorbed in fuel and ϵ is the fast fission factor.

In Equation A-2 the total absorption of neutrons in the resonance group can be written as

$$(\Sigma_r + \Sigma_{ra})\phi_r$$

where Σ_r has its previously defined significance and Σ_{ra} is a true absorption cross section in the resonance group. If p is defined in the most natural way as

$$p = \frac{\Sigma_r}{\Sigma_r + \Sigma_{ra}}$$

then

$$(\Sigma_r + \Sigma_{ra})\,\phi_r = \frac{\Sigma_r}{p}\,\phi_r$$

Another formulation of the few group equations is called the two-and-one-half group model. This model is derived from the three-group model, Equations A-1, A-2 and A-3 by making the physical assumption that there is no diffusion in the resonance group, i.e., $\nabla^2\phi_r = 0$. Substitution leads to the equations

$$-D_f\nabla^2\phi_f + \Sigma_f\,\phi_f = \frac{k}{p}\,\Sigma_s\phi_s \qquad \text{(A-4)}$$

$$-D_s\nabla^2\phi_s + \Sigma_s\,\phi_s = p\Sigma_s\phi_f \qquad \text{(A-5)}$$

This set of equations is used for two-group design studies.

The two-group model which was used for the survey studies is given by the following equations

$$-D_f\nabla^2\phi_f + \frac{1}{p}\,\Sigma_f\phi_f = \frac{k}{p}\,\Sigma_s\phi_s \qquad \text{(A-6)}$$

$$-D_s\nabla^2\phi_s + \Sigma_s\phi_s = \Sigma_f\phi_f \qquad \text{(A-7)}$$

These equations differ from the usual two-group equations in the source term and in the form of the fast absorption term. By comparison with the three-group equations above, it can be seen that Equation A-6 contains the physical assumption that the resonance absorption is proportional to the fast flux.

APPENDIX B: DIVISION OF POWER BETWEEN SEED AND BLANKET

1. Power Produced by Thermal Neutron Fission

The discussion will be based on the two-group formulation Equations A-6 and A-7 of Appendix A. It is assumed that the seed and blanket arrangement is the usual one in which the seed is completely surrounded by blanket material. Only the blanket has an outer surface.

Equation A-7 is multiplied by $1/p$ and added to Equation A-6. The result is

$$-\left[D_f\nabla^2\phi_f + \frac{D_s}{p}\nabla^2\phi_s\right] = \frac{(k-1)}{p}\Sigma_s\phi_s \quad \text{(B-1)}$$

Equation B-1 is first applied to the seed region. In the seed region p is unity. The multiplication constant in the seed region will be denoted by k^s. Equation B-1 is integrated over the volume of the seed region and the volume integral of the Laplacian converted to a surface integral. The result is

$$-\int_{S_{SB}}[D_f\nabla\phi_f + D_s\nabla\phi_s]\cdot\underline{n}\,dS = (k^s-1)\int_{V_s}\Sigma_s\phi_s\,dV \quad \text{(B-2)}$$

where S_{SB} indicates the seed-blanket interface surface, V_s the volume of the seed and $\underline{n}$ is taken as the surface normal to S_{SB}.

In applying Equation B-1 to the blanket, k^b will be used to denote the multiplication constant of the blanket. No designation need be given to p or ϵ since these differ from unity only in the blanket. Carrying out the integration as before, the result is

$$-\int_{S_{BO}}\left[D_f\nabla\phi_f + \frac{D_s}{p}\nabla\phi_s\right]\cdot\underline{n}\,dS - \int_{S_{BS}}\left[D_f\nabla\phi_f + \frac{D_s}{p}\nabla\phi_s\right]\cdot\underline{n}\,dS = \frac{(k^b-1)}{p}\int_{V_B}\Sigma_s\phi_s\,dV \quad \text{(B-3)}$$

In this equation S_{BO} indicates the outer surface of the blanket, S_{BS} the blanket-seed interface surface, V_B the volume of the blanket and $\underline{n}$ the surface normal.

The next step in the derivation is to define certain reactivity loss terms.

The term δk_{fo} is defined by the equation

$$-D_f\int_{S_{BO}}\nabla\phi_f\cdot\underline{n}\,dS = (\delta k_{fo})\frac{1}{p}\int_{V_B}\Sigma_s\phi_s\,dV \quad \text{(B-4)}$$

The term δk_{fo} may be considered to be the loss in blanket reactivity due to fast neutron leakage from the outer surface of the blanket into the reflector.

In a similar way the term δk_{so} is defined. This may be considered to be the loss in blanket reactivity due to slow neutron leakage from the outer surface of the blanket into the reflector.

$$-D_s\int_{S_{BO}}\nabla\phi_s\cdot\underline{n}\,dS = \delta k_{so}\int_{V_B}\Sigma_s\phi_s\,dV \quad \text{(B-5)}$$

Finally the term δk_{ss} is defined. This also represents an effective reactivity loss, in this case associated with thermal neutron leakage from the blanket into the seed.

$$-D_s(1-p)\int_{S_{BS}}\nabla\phi_s\cdot\underline{n}\,dS = \delta k_{ss}\int_{V_B}\Sigma_s\phi_s\,dV \quad \text{(B-6)}$$

With these definitions Equation B-3 may be written as:

$$-\int_{S_{BS}}(D_f\nabla\phi_f + D_s\nabla\phi_s)\cdot\underline{n}\,dS = \frac{(k^b-1-\delta k_{fo}-\delta k_{so}-\delta k_{ss})}{p}\int_{V_B}\Sigma_s\phi_s\,dV \quad \text{(B-7)}$$

Equations B-2 and B-7 are now added. Because of the current continuity conditions the terms $D_f\nabla\phi_f$ and $D_s\nabla\phi_s$ are equal on the two sides of the boundary. The normals in the integrals are opposite in direction, however, so that the integrals cancel. The result of the addition is

$$(k^s-1)\int_{V_s}\Sigma_s\phi_s\,dV = \frac{(1-k^b+\delta k_{fo}+\delta k_{so}+\delta k_{ss})}{p}\int_{V_B}\Sigma_s\phi_s\,dV \quad \text{(B-8)}$$

If Σ_f^* is the effective macroscopic cross section for U^{235} fission in the blanket, Σ_s in the blanket is related to Σ_f^* by the Equation

$$\Sigma_s = \frac{\nu\Sigma_f^*}{f\eta} = \frac{\nu p\epsilon}{k^b}\Sigma_f^* \quad \text{(B-9)}$$

Σ_f^* for the seed region is related to Σ_s for the seed region by the equation

$$\Sigma_s = \frac{\nu}{k^s}\Sigma_f^* \quad \text{(B-10)}$$

Now if P_B is defined as the power produced in the blanket by thermal fission of U^{235} and P_S is the corresponding quantity for the seed,

$$P_B = \int_{V_B}\Sigma_f^*\phi_s\,dV = \frac{k^b}{\nu p\epsilon}\int_{V_B}\Sigma_s\phi_s\,dV \quad \text{(B-11)}$$

and

$$P_S = \int_{V_s}\Sigma_f^*\phi\,dV = \frac{k^s}{\nu}\int_{V_s}\Sigma_s\phi_s\,dV \quad \text{(B-12)}$$

Using these definitions in Equation B-8 gives

$$\frac{P_B}{P_S} = \left(\frac{k^s-1}{k^s}\right)\left[\frac{k^b}{1-k^b+\delta k_{fo}+\delta k_{so}+\delta k_{ss}}\right]\frac{1}{\epsilon} \quad \text{(B-13)}$$

2. Enhancement of the Blanket Power by the Fast Effect

The ratio of fast to thermal fissions may be expressed in terms of the fast fission factor ϵ.

The conventional definition of ϵ states that $(\epsilon - 1)$ represents the increase in the number of neutrons entering the slowing down region due to fast fission. Now for each neutron produced by fast fission $1/\eta'$ neutrons are absorbed where η' is defined as the number of fission neutrons produced per fast neutron absorbed. Accordingly

$$\left[\frac{\text{Number of neutrons produced by fast fission}}{\text{Number of neutrons produced by thermal fission}}\right] \times \left(1 - \frac{1}{\eta'}\right) = (\epsilon - 1) \quad \text{(B-14)}$$

If the number of neutrons produced per fission is taken to be the same for both slow and fast fission,

$$\frac{\text{Rate of fast fissions}}{\text{Rate of slow fissions}} = \left(\frac{\eta'}{\eta' - 1}\right)(\epsilon - 1) \quad \text{(B-15)}$$

Since η' is approximately 2, this ratio is approximately $2(\epsilon - 1)$.

Thus the blanket power taking fast fissions into account exceeds P_B by the fraction:

$$2(\epsilon - 1)$$

Denoting the total blanket power by P_B^*

$$P_B^* = P_B[1 + 2(\epsilon - 1)] \cong [1 + (\epsilon - 1)]^2 = \epsilon^2 \quad \text{(B-16)}$$

since $(\epsilon - 1) \ll 1$.

Introducing this into Equation B-13

$$\frac{P_B^*}{P_S} = \left(\frac{k^s - 1}{k^s}\right)\left[\frac{k^b}{1 - k^b + \delta k_{fo} + \delta k_{so} + \delta k_{ss}}\right]\epsilon \quad \text{(B-17)}$$

A simplified expression for the power ratio can be obtained. If all leakage of neutrons out of the outer boundary of the blanket is neglected, δk_{fo} and δk_{so} vanish. If the leakage of thermal neutrons from the blanket back into the seed is neglected, δk_{ss} vanishes. With these assumptions

$$\frac{P_B^*}{P_S} = \left[\frac{k^s - 1}{k^s}\right]\left[\frac{k^b}{1 - k^b}\right]\epsilon \quad \text{(B-18)}$$

3. Enhancement of the Blanket Power by Fast Neutron Leakage from the Seed

The leakage of neutrons, whose energy is above the U^{238} fission threshold, from the seed into the blanket enhances the blanket power. This effect can be calculated in detail by a four-group treatment. This has not yet been done. A very rough estimate indicates that this effect may add 2% to the percentage of power produced in the blanket.

Some Experiences from Measurements on an Exponential Pile of Uranium and Heavy Water

By R. Persson, M. Bustraan,* and E. Blomsjö,† Sweden

In Sweden we have, in co-operation with the Dutch-Norwegian organization, JENER, performed some exponential experiments with rods of natural uranium in heavy water.

Our experimental arrangement was built with particular attention to flexibility and a rapid determination of the material buckling.

We have used a cylindrical tank, 3.0 m high and 1.0 m in diameter. This diameter was chosen primarily because of a shortage of uranium but also in order to have an exponential decay in the axial direction without too large corrections for the harmonics and for the end effect. The neutron source, about 1.5 curie RaBe, is placed 0.5 m above the bottom. The tank wall is of 10 mm aluminium and is covered with boron plastic, 3–4 mm thick. The plastic (polyethylene) contains about 0.3 gm boron carbide per cm^2. Its advantages in comparison to cadmium will be mentioned below.

The flexibility is attained by suspending each uranium rod from a roller which may be moved along a slotted beam. The distance between the beams is continuously variable. The rollers and the beams can be moved from the outside (see Fig. 1). The whole arrangement is covered by a sheet of plexiglass which makes ocular inspection possible. By uncovering relatively small holes on either side of a diameter perpendicular to the beams we can put in or take out rods without emptying the tank.

In order to obtain the results as fast as possible, we use BF_3 proportional counters instead of foils. The neutron distribution in the axial direction is measured by two long horizontal detectors, each about 36 cm in effective length, placed in line and approximately symmetric about the axis. The distance between the detectors is fixed by a spacer. The advantages of this detecting arrangement are:

1. A high counting rate. It is even so that the uncertainty (1 μsec) in the dead time limits the source strength and the pressure of the BF_3 gas. Measuring time for one lattice is about four hours to give the relaxation length with an accuracy of the order of a few per mille.

2. A small asymmetry of the detector assembly to the axis is unimportant (1 cm leads to a change of less than 0.5 per thousand in the counting rate).

3. The influence of harmonics is greatly reduced (in the ideal case the first and second harmonics are completely eliminated).

4. Integration over several cells. The method is rather insensitive to any crookedness of the rods. In the first measurements we placed the detectors in horizontal channels, 2.5 cm in diameter and 20 cm apart in the vertical direction. The effect of the channels on the relaxation length can be determined experimentally and amounts to a few tenths of a per cent; it is dependent on the lattice parameters. In some measurements each uranium rod consists of several slugs placed in an aluminium tube and each slug has a small hole in one end (helium hole), about 10 mm deep and 6 mm in diameter. These holes slightly disturb the neutron flux in the neighbourhood, so that there is a periodic variation superimposed on the exponential decay. In order to avoid this difficulty we now use continuously movable detectors in the vertical direction, which allow us to perform measurements at heights differing by the length of the slugs.

The radial distribution is determined by the geometry, which means that we have to find the extrapolated radius. The change in extrapolation length when there is a 10 mm aluminium wall covered with boron plastic will be determined in a separate experiment, using a method developed by G. von Dardel.[1] The decay of thermal neutrons in a small geometry is measured as a function of the geometrical buckling. There will be a change of the time constant if we place an aluminium ring covered with boron plastic around a cylindrical container with thin aluminium walls which is filled to a certain height with heavy water. From this change we can calculate the change in extrapolated radius with good accuracy, probably better than ± 0.5 mm. The extrapolation length for thermal neutrons in D_2O is about 1.8 cm and with the given boundary we assume 2.2 ± 0.2 cm (preliminarily) from the inner surface of the tank. Then the extrapolated radius should be 52.2 ± 0.2 cm. The transport mean free path increases, however, with energy in the low-energy region and we may expect that the extrapolated radius we want to use for the radial buckling is somewhat larger than the value valid for thermal neutrons. Therefore the radial distribution has to be measured.

One of the difficulties encountered in these experiments is the effect of the helium holes already mentioned. Another disturbance is the backscattering of

* On leave from JENER, Kjeller, Norway.
† Aktiebolaget Atomenergi, Department of Physics, Stockholm, Sweden.

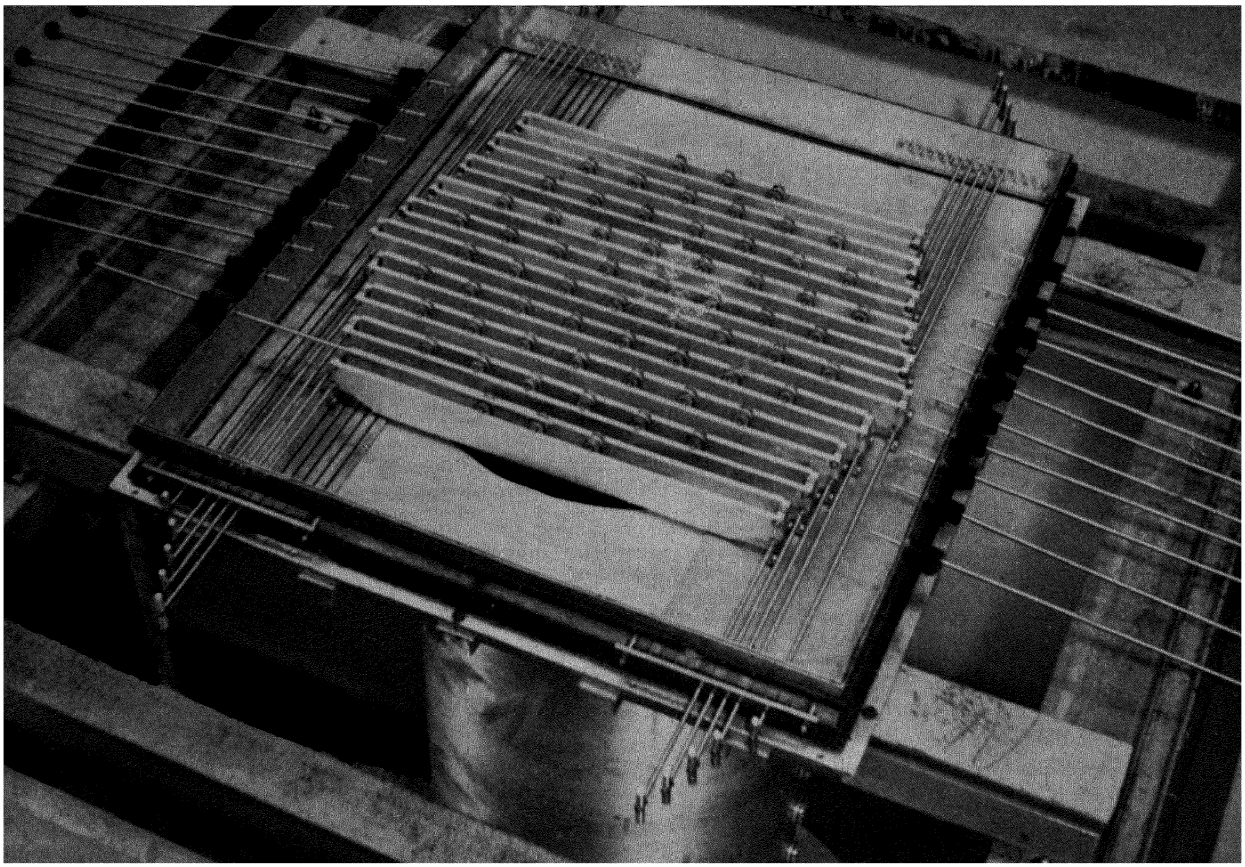

Figure 1. The mechanical construction for rearranging lattices

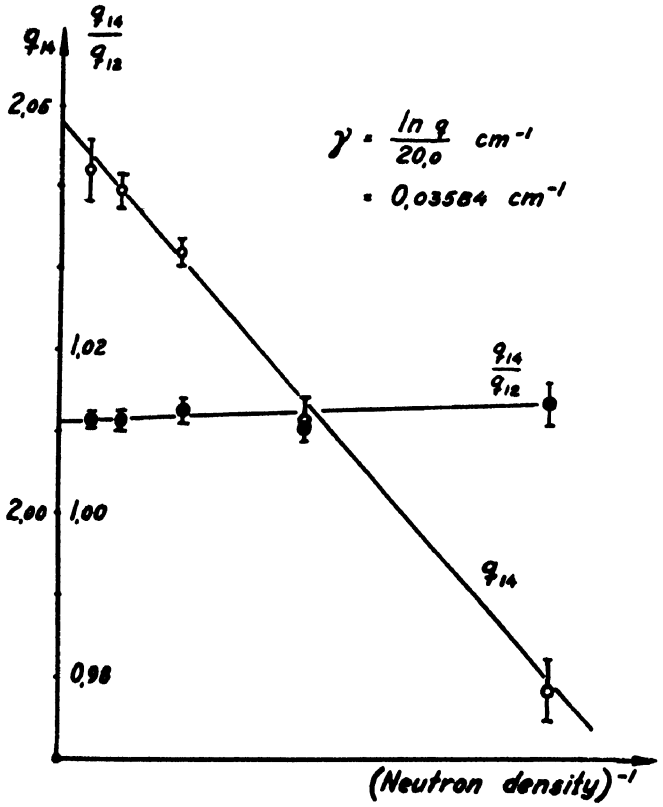

Figure 2. The ratio (q) of the intensity in one channel to that in the next channel above versus the inverse of the neutron density. The ratio of q's for two different lattices is also shown

fast neutrons by the surroundings. The area used for the experiments is only 4.5 m wide, and there are iron beams and other material around the top and the bottom of the tank which scatter some of the fast neutrons that leak out. By using boron plastic instead of cadmium this effect is decreased by a factor of about two.

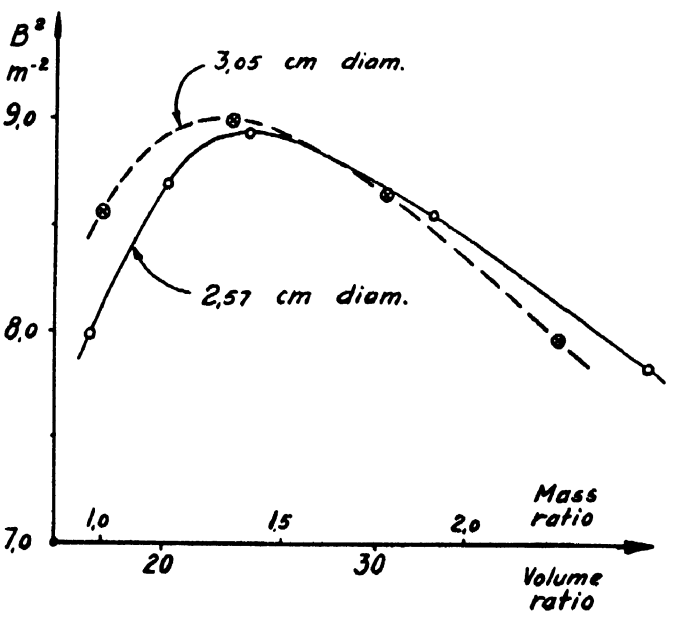

Figure 3. Preliminary results of the material buckling for two different rod diameters as a function of the volume and mass ratios. The thickness of the aluminum canning is in both cases 5 per cent of the rod diameter

This extra background varies slowly along the axis, and we can therefore find the correct value of the relaxation length by extrapolation, as shown in Fig. 2. The increase in the extrapolated radius when boron plastic is used instead of cadmium seems to be less than 1 mm.

Owing to transition effects it is not possible to measure closer to the bottom of the lattice than 20–30 cm. Bent rods can also lead to an incorrect relaxation length. The long detectors integrate over several cells, however, so that this effect is very small if the rods are not bent too much. The dead time of the detecting system has been about 10 μsec, but is now changed to 1 μsec leading to a maximum dead time correction of 3–5 per cent.

Some preliminary results are given in Fig. 3.

REFERENCE

1. Dardel, G. von and Sjöstrand, N. G., *Diffusion Parameters of Thermal Neutrons in Water*, Phys. Rev. *96*, 1245–1249, (1954).

Characteristics of the Swedish Heavy Water Reactor

By E. Hellstrand, G. Jonsson, K-E. Larsson, B. Pershagen, and R. Persson,* Sweden

Part I. Transfer Functions and Neutron Life Time, by Eric Hellstrand

The Swedish natural uranium heavy water reactor is of the CP-3 type. It has been described elsewhere.[1] It is designed for a power level of about 300 kw. During the first period of operation various characteristics were determined. Four of the experiments are reported here.

STUDIES OF THE TRANSFER FUNCTIONS WITH A ROTATING CADMIUM SHUTTER

A periodic modulation of the reactivity of the pile has been achieved by rotating an eccentrically mounted cadmium disc in and out of a fixed cadmium box in the central channel. For small perturbations the theory for a bare reactor gives the following relations for the phase and amplitude of the modulation in the neutron density caused by a variation in the reactivity.[2,3]

$$\tan \varphi = - \frac{\omega \left(l + \sum_j \frac{\beta_j \tau_j}{1 + \omega^2 \tau_j^2} \right)}{\sum_j \frac{\beta_j \omega^2 \tau_j^2}{1 + \omega^2 \tau_j^2}} \qquad (1)$$

$$A^2 \sim \frac{1}{\left(\sum_j \frac{\beta_j \omega^2 \tau_j^2}{1 + \omega^2 \tau_j^2} \right)^2 + \omega^2 \left(l + \sum_j \frac{\beta_j \tau_j}{1 + \omega^2 \tau_j^2} \right)^2} \qquad (2)$$

where $\omega = 2\pi/T$ frequency of modulation, β_j = fraction of fission neutrons (including photo neutrons) in the jth group of delayed or photo neutrons, $= \tau_j$ life time of the jth group,

$$l = \frac{3L^2}{\lambda_t v} \cdot \frac{1}{1 + L^2 B^2}$$

effective mean life of thernal neutrons in the multiplying medium, L is the diffusion length and λ_t the transport mean free path for thermal neutrons in the multiplying medium.

The frequency was varied between 21 and 6×10^{-3} sec^{-1} and the pile power used was 1.5 watt.

The method used to determine φ and a quantity proportional to A is the same as that used by Gilbert and Fergusson.[2] The signal from a BF_3 chamber situated in the graphite is amplified by a backed-off dc amplifier, the output of which is connected to the end contacts of a sine-cosine potentiometer. Either of the moving contacts of the potentiometer may be connected to the input of a velodyne integrator where the incoming signal is integrated with the aid of a motor generator. As the potentiometer is mounted on the same shaft as the disc, the input to the integrator will be the product of the amplified signal $F(t)$ and sin $(\omega t + \phi)$ or cos $(\omega t + \phi)$, ϕ being the sum of the phase angle φ and the fixed angle between the disc and one of the moving contacts of the potentiometer.

When integration is over a whole number of periods, the results on the integrator can be written as

$$N_1 = K \sin \phi$$

$$N_2 = K \cos \phi$$

Hence $\tan \phi = N_1/N_2$, from which we get ϕ, and $K = (N_1^2 + N_2^2)^{1/2}$ where K is a quantity proportional to the amplitude A.

RESULTS

The theoretical curves of the phase angle φ and the relative amplitude K as a function of the period of revolution $T(T = 2\pi/\omega)$ are given in Figs. 1 and 2, together with the experimental points. For the theoretical curves the values used for the delayed neutrons are those given by Hughes *et al.*,[4] and for the photo neutrons those of Johns and Sargent.[5]

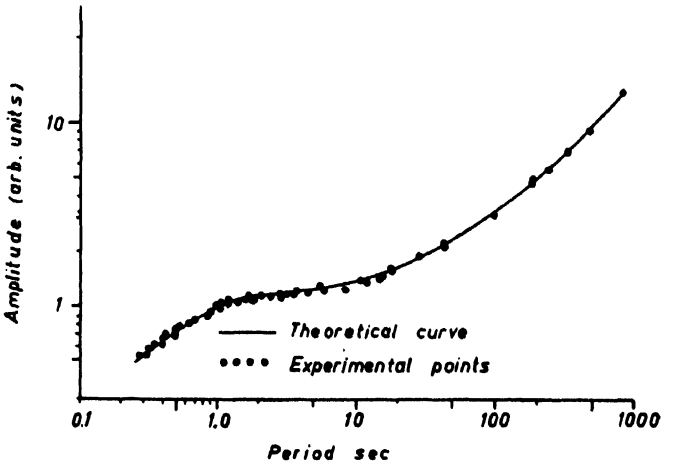

Figure 1. Amplitude response versus period of modulation

* Aktiebolaget Atomenergi, Department of Physics, Stockholm, Sweden.

Before plotting the experimental phase values a correction was made for the distortion caused by various delay times such as the time for the ion collection in the BF_3 chamber and the effective time constant of the input circuit of the amplifier. The magnitude of the correction can be represented by the quantity

$$\Delta\varphi = \arctan \omega\tau'$$

where τ' is of the order of 10 msec.

In order to determine τ' and l Equation 1 may be rewritten in the following way

$$|\tan \varphi| = \frac{l}{\beta} \cdot \frac{1 + \epsilon_1}{1 - \epsilon_2} \cdot \omega$$

where

$$\epsilon_1 = \frac{1}{l} \sum_j \frac{\beta_j \tau_j}{1 + \omega^2 \tau_j^2} \qquad \epsilon_2 = \frac{1}{\beta} \sum_j \frac{\beta_j}{1 + \omega^2 \tau_j^2}$$

Thus $\tan \varphi$ should lie on a straight line when plotted as a function of $[(1 + \epsilon_1)/(1 + \epsilon_2)] \cdot \omega$. The constant τ' therefore has to be so chosen that a plot of the corrected experimental values of $\tan \varphi$ versus $[(1 + \epsilon_1)/(1 + \epsilon_2)] \cdot \omega$ is a straight line through the origin. If only points from the highest frequency region are used, ϵ_1 and ϵ_2 are small compared to unity and small errors in the used values of l and the β_j's and τ_j's therefore become unimportant. The slope of the line gives l/β and thus l.

The values of τ' and l obtained in this way are ($\beta = 0.79 \times 10^{-2}$)

$$\tau' = 10.0 \pm 0.8 \text{ msec}$$

$$l = 0.70 \pm 0.03 \text{ msec}$$

RESPONSE OF THE REACTOR TO A STEP CHANGE IN REACTIVITY

Immediately after a sudden change in the reactivity of a pile the concentration of delayed neutron emitters may to a first approximation be considered constant. The delayed neutrons then represent a constant source of thermal neutrons the strength of which with the usual notations will be

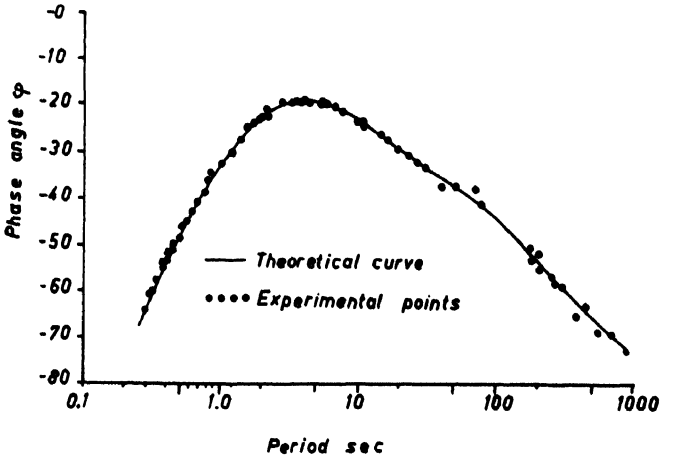

Figure 2. Phase-shift response versus period of modulation

$$\rho \cdot e^{-B^2\tau} \cdot \sum_j \lambda_j c_{j0} = \beta \cdot k \cdot e^{-B^2\tau} \cdot \sum_a \cdot n_0 \cdot v$$

where n_0 is the neutron density and the c_{j0}'s are the concentrations of delayed neutron precursors before the reactivity change. By choosing the value 0.79×10^{-2} for β, the contribution from the photoneutrons is also allowed for. The only change in the neutron density then comes from the change in the number of prompt neutrons, and the time behaviour of the fundamental space mode of the neutron density will be described by the following relation

$$\frac{1}{k_{eff}} \frac{dn(t)}{dt} = \frac{\rho - \beta}{l} \cdot n(t) + \frac{\beta}{l} \cdot n_0 \qquad (3)$$

If the change in the reactivity is a true step function, i.e., $\rho(t) = 0$ for $t < 0$, $\rho(t) = \rho_0$ for $t > 0$, integration of Equation 3 yields ($k_{eff} \approx 1$).

$$\frac{n(t)}{n_0} = 1 + \frac{\rho_0}{\beta - \rho_0} \left(1 - e^{-\frac{\beta - \rho_0}{l} t}\right) \qquad (4)$$

Thus if ρ_0 is known and $n(t)/n_0$ is measured, l can be deduced from Equation 4.

In the case under consideration the reactivity change was produced by rapidly pulling out a cadmium absorber from the center of the reactor. $\rho(t)$ was thus not a true step function but the change was rapid enough to allow the use of Equation 4 to determine l, since the absorber traversed the first meter in 60 msec and most of the reactivity change occurred in less than half this time.

ρ_0 could in principle be deduced from the asymptotic value of n/n_0 but the value so obtained would be rather uncertain in our case. ρ_0 was therefore determined instead from the pile period.

In Equation 3 it was assumed that the contribution to $n(t)$ from the delayed neutrons was constant. In a more rigorous treatment, however, the increase in the number of delayed neutrons should also be taken into account. This can be done in an approximate way by assuming that the increase in the $c_j(t)$'s is caused only by the increase in the number of prompt neutrons, i.e., that $c_j(t)$ follows the relation

$$\frac{dc_j(t)}{dt} = \frac{\beta_j k}{p} \cdot \sum_a \cdot n(t) \cdot v - \lambda_j c_j(t)$$

with $n(t)$ from Equation 4. The equation above can then be directly integrated and the experimental values corrected accordingly.

The neutron density was measured with a BF_3 chamber and the amplified pulses from the chamber were fed to a scaler, the output of which was connected to a 20-channel time analyser.[6] The channel width normally used was 49.2 msec and the pile power was about 2 watts.

Results

In Fig. 3 a curve is shown which was obtained from 25 consecutive runs with the chamber at the tank wall. In order not to obscure the figure, only the curve

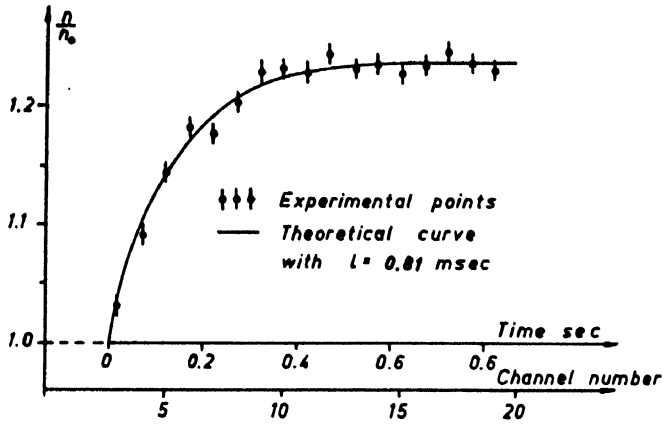

Figure 3. n/n_0 versus time with the detector at the tank wall

corrected for the increase in the delayed neutrons is given. The curve has been normalized to give the correct value of $(n/n_0)_{asym}$. This normalization does not change the time constant of the curve and thus does not influence the determination of l.

From the corrected experimental results l has been determined by a least-square fit to the theoretical curve. The results of the different measurements are summarized in Table I.

Table I

Detector position	*Run*	l *msec*	$\pm \Delta l$ *msec*
In the tank	1	0.62	0.12
	2	0.70	0.09
	3	0.64	0.10
At the tank wall	4	0.81	0.09
	5	0.80	0.10
In the graphite	6	0.92	0.18
	7	0.80	0.20

The weighted mean value is

$$l = 0.74 \pm 0.05 \text{ msec}$$

The value thus agrees fairly well with the value found with the rotating cadmium shutter. The weighted mean value from the two measurements is

$$l = 0.71 \pm 0.03 \text{ msec}$$

REFERENCES

1. Eklund, S., *The Swedish Reactor*, J. Nuclear Energy, Vol. *1:* 93–100, (1954).
2. Gilbert, G. W. and Fergusson, G. J., *An Investigation of the Delayed Neutrons from Fission*, CRP-377 (1948).
3. Harrer, J. M., Boyar, R. E. and Krucoff, D., *Transfer Functions of Argonne CP-2 Reactor*, Nucleonics *10*, No. 8: 32–36, (1952).
4. Hughes, D. J., Dabbs, J., Cahn, A. and Hall, D., *Delayed Neutrons from Fission of* U^{235}, Phys. Rev. *73:* 111–124, (1948).
5. Johns, M. W. and Sargent, B. W., *Photo Neutrons in a Heavy Water Reactor*, CRP-416, (1949).
6. Dardel, G. v., *A Multichannel Time-Analyser for Precision Work*, Appl. Sci. Res. Section B, Vol. *3:* 209–229, (1953).

Part II. Reactivity Equivalence of Control Variables, by G. Jonsson

Normally, the reactivity of the reactor can be changed by one of the following three variables: the heavy water level, the position of the control plates and that of the safety rods. The effect on the reactivity of the two safety rods is comparatively high, and they are used only to start up and shut down the reactor while the two control plates can be moved continuously when running the reactor, and their position is easily read off with good accuracy on a dial at the control desk. The placing of the safety rods ($S1$ and $S2$) and the control plates ($R1$ and $R2$) is shown in Fig. 1.

A reactivity calibration of the control plates is necessary for the analysis of the behaviour of the power control system. The calibration of the safety rods will show whether the safety conditions are satisfied in all possible states of the reactor. For example, one must know whether the reactor can be made subcritical even at the highest D_2O level. As one safety rod may be regarded as a reserve for the other, it is the individual effect of each rod that is most interesting, and it seems reasonable to measure that effect directly against the D_2O level.

GENERAL

The control rods were calibrated by measuring the time constant of the power rise in the supercritical reactor. The excess reactivity was calculated from the Nordheim formula:

$$\delta k = \kappa \left(l + \sum_i \frac{\beta_i}{\kappa + \lambda_i} \right) \qquad (1)$$

where $1/\kappa$ is the time constant mentioned. A subcritical method was used for the safety rod calibration.

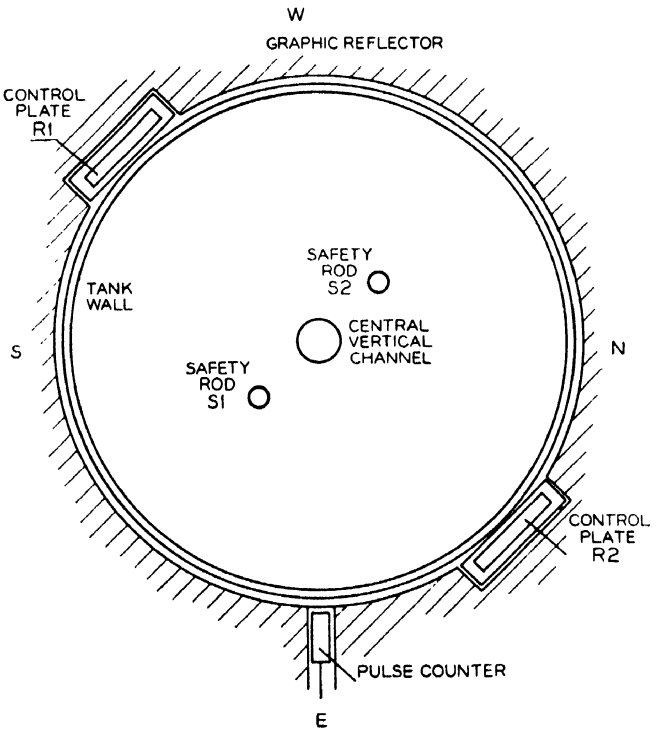

Figure 1

That method has been described by Jacrot, Netter and Raievski.[1]

The following symbols are introduced: N = counting rate, measured with a BF_3 counter in the reactor, H = the extrapolated height of the reactor defined by the heavy water level, R = the extrapolated radius. Index c means the values at criticality.

In the subcritical case one has a relation

$$N = \frac{A}{1 - k} \tag{2}$$

where A is a constant, only dependent on the strength of the neutron source in the reactor and the sensitivity and location of the counter. Further,

$$1 - k = K \frac{H_c^2 - H^2}{H^2} \tag{3}$$

K is a constant, dependent on H_c:

$$K = \frac{k_\infty - 1}{k_\infty} \cdot \frac{1}{1 + \left(\frac{2.41 \cdot H_c}{\pi \cdot R_c}\right)^2} \tag{4}$$

$R = R_c = 111$ cm (k_∞ has not yet been determined with the accuracy required here).

From Equations 2 and 3 one gets

$$\frac{1}{N} = \frac{K}{A} \cdot H_c^2 \left(\frac{1}{H^2} - \frac{1}{H_c^2}\right) \tag{5}$$

The reactivity of a subcritical reactor can be determined in the following way. One introduces a known change in reactivity Δk_0, and N is measured before and after that change (N_1 and N_2, respectively). If

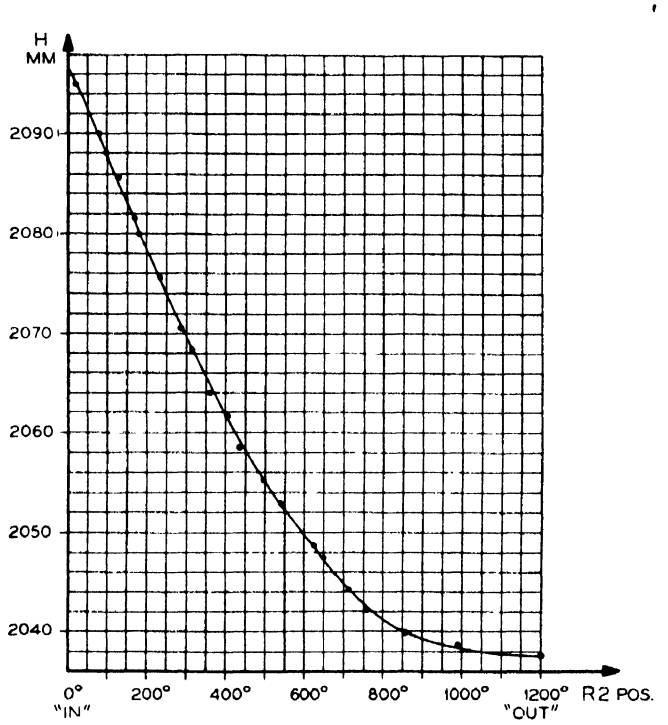

Figure 2. Calibration of control plate R2 against D_2O level. R1 position = 577°

Δk_0 is defined to be positive for a decrease in reactivity, Equation 2 gives

$$1 - k = \Delta k_0 \cdot \frac{N_2}{N_1 - N_2} \tag{6}$$

The reactivity equivalence of a neutron absorbing body can thus be measured by first making the reactor critical without the absorber. It is then introduced, and the reactivity equivalence (Δk) is determined from Equation 6. Δk_0 may be represented by a previously calibrated and smaller absorber. However, the change may also be achieved by variation of the heavy water level. Then it is necessary to know the water level coefficient of the reactivity, which is defined

$$\alpha = \frac{dk}{dH}$$

Suppose that the critical level H_c' has been observed for the unloaded reactor. With the absorber put in, one can measure a series of values N with different water levels. If the $1/N$ values are plotted against $1/H^2$, a straight line should be obtained, according to Equation 5. An extrapolation to $1/N = 0$ gives the new critical level, H_c''. If the water level coefficient (α_0) has been measured with the level H_0, one gets from Equations 3 and 4 the following formula for the reactivity equivalence of the absorber:

$$\Delta k = \frac{\alpha_0 H_0 \left[1 + \left(0.766 \cdot \frac{H_0}{R_c}\right)^2\right]}{2\left[1 + \left(0.766 \cdot \frac{H_c''}{R_c}\right)^2\right]} \cdot \frac{(H'')^2 - (H_c')^2}{(H_c')^2} \tag{7}$$

MEASUREMENTS

During the critical and supercritical measurements the power level was about 1 watt, and the over-all temperature 22°C. A calibration of the two control plates was made against the D_2O level by means of the automatic power control. Figures 2 and 3 show the curves obtained. It was also shown, that there is a slight coupling between the two plates, which is seen on Fig. 3.

With the plate $R2$ at a constant position of 10 degrees, a series of measurements were made on the period of the supercritical reactor. The supercritical state was caused by drawing out the plate $R1$ a certain distance from the critical position. By means of Fig. 3 that distance was translated into the corresponding H value. The δk values were obtained from the Nordheim formula, Equation 1, where the numerical values for the delayed neutron groups were derived from a report by Lipkin (Hughes' values).[2] The slope of the lines $\delta k = f(1/H^2)$ in Fig. 4 (obtained at two slightly different water levels) gives a value on the coefficient α at $H_0 = 2087$ mm:

$$\alpha_0 = (7.0 \pm 0.1) \times 10^{-5} \text{ mm}^{-1}$$

The probable errors in the values used for the delayed neutron groups have not been considered in the

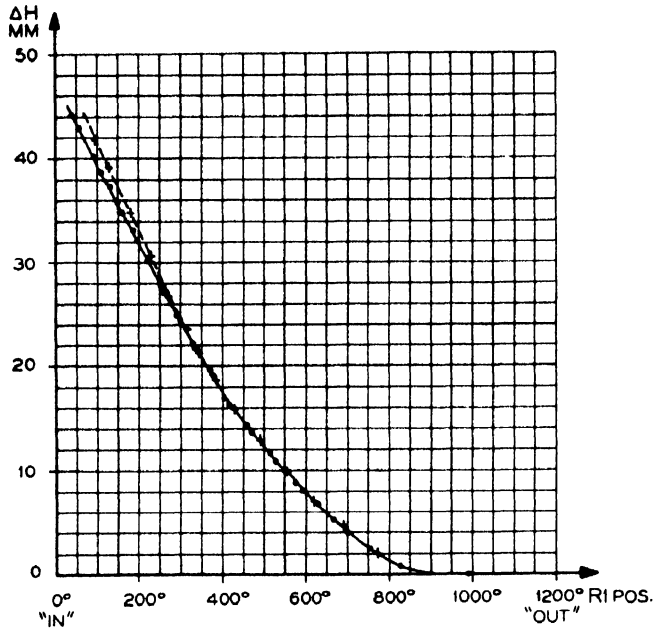

Figure 3. Calibration of control plate R1 against D_2O level. R2 position = 1200° and 350° (full curve) and 10° (dotted curve)

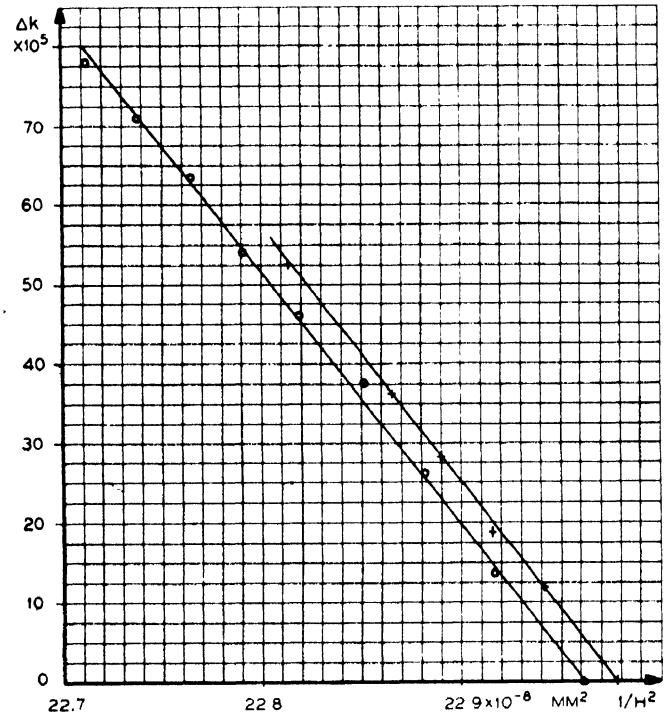

Figure 4. Results from the supercritical measurements

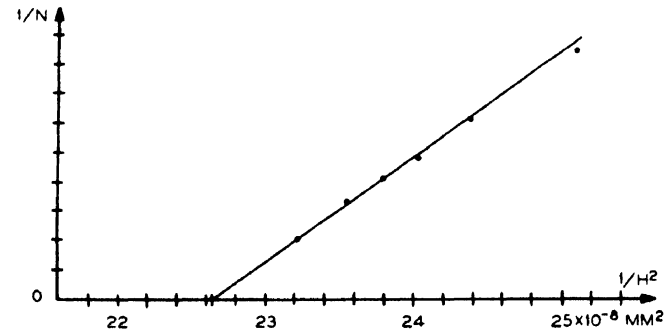

Figure 5. Estimation of the critical D_2O level with the loading R1 + R2

limits of error for α_0. One can now calculate the total effect of the two plates from Equation 7, where H' and H'' are obtained from Figs. 2 and 3.

$$\Delta k_{R1+R2} = 762 \times 10^{-5}$$

The reactivity equivalence of the safety rods were determined from subcritical measurements. A RaBe source was placed in the central vertical channel of the reactor at the point, where the maximum flux had been measured previously. A calibration of $S1$ was made against the water level as described before, but first the method was checked with the reactor loaded with $R1 + R2$. Figure 5 shows, that Equation 5 applies, and a comparison with the result from above shows that the error in H_c, obtained at the extrapolation in Fig. 5, where the last point was measured 25 mm below H_c, is about 2 mm.

The critical level for the unloaded reactor (with the control plates out) was $H_c' = 1999$ mm. With $S1$ dropped the measured values are shown in Fig. 6, from which is obtained the new critical level $H_c'' = 2255 \pm 2$ mm.

Insertion in Equation 7 gives the reactivity equivalence

$$\Delta k_{S1} = 1.77\%$$

The relative error is about 3.5%. From the slopes of the curves in Figs. 5 and 6 one gets the relative values of the constant K. One finds, that the ratio between K_{2255} and K_{2099} is 0.96, while the theoretical value from Equation 4 is 0.91. The difference is not too large, and it gives an idea about how the constant A varies, due to the fact that the neutron flux distribution must have been changed with the water level

$S2$ and $S1 + S2$ can be calibrated at a constant water level by using Equation 6, where the reactivity change Δk_0 is achieved by means of the two control plates. Using the above value $\Delta k_{R1+R2} = 762 \times 10^{-5}$ the result was $\Delta k_{S1} = 1.39\%$, $\Delta k_{S2} = 1.36\%$, $\Delta k_{S1+S2} = 2.34\%$.

Apparently the values are too small. The reason is that Δk_{R1+R2} has another value than that determined above when the neutron flux distribution is disturbed

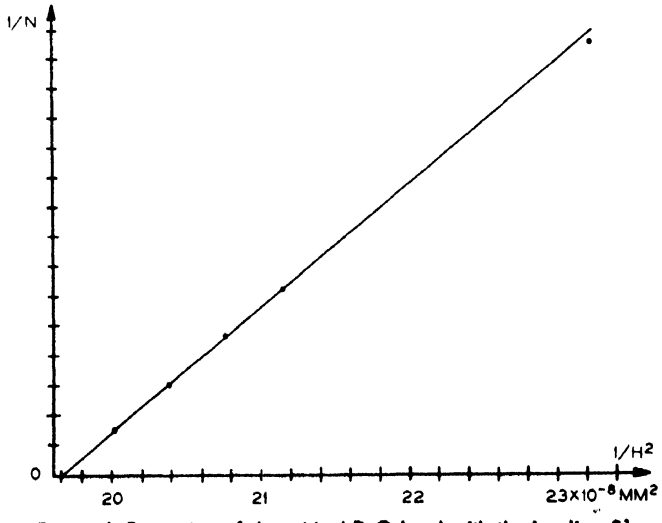

Figure 6. Estimation of the critical D_2O level with the loading S1

by the safety rods. The most probable effect is, that, regarding the geometry in Fig. 1, the flux near the control plates will increase as $S1$ or $S2$ is dropped, and it will increase still more with the loading $S1 + S2$. Thus a higher value should be used for Δk_{R1+R2}. But for reasons of symmetry this value must be about the same with $S1$ dropped as for $S2$ dropped.

The last conclusion gives a method to determine Δk_{S2}. From the value Δk_{S1} measured against water level one can get a value Δk_0, which is then used in Equation 6 for Δk_{S2}. This is $\Delta k_0 = 1.06\%$, hence

$$\Delta k_{S2} = 1.72\%$$

The relative error is about 5%. With the same Δk_0 value one gets $\Delta k_{S1+S2} = 3.1\%$, but the real value must be greater, for the reasons mentioned above. However, it is impossible to determine it more closely from the measurements. The coupling between $S1$ and $S2$ might even be of the same nature as for the control plates, i.e., $\Delta k_{S1+S2} > \Delta k_{S1} + \Delta k_{S2} = 3.5\%$.

COMPARISON OF THE RESULTS

Δk for the safety rods and α were also measured by Mr. N. G. Sjöstrand by means of a pulsed neutron source in the subcritical reactor. A description of this method will be given by him in a separate paper about subcritical measurements. Only the results are given here.

	Percentage of reactivity equivalence	
	Above	*Sjöstrand (prel. values)*
Safety rod $S1$	1.77 ± 0.06	1.7 ± 0.2
Safety rod $S2$	1.72 ± 0.09	1.7 ± 0.2
$S1 + S2$	3.1	3.2 ± 0.3
1 mm of D_2O	0.0070 ± 0.0001	0.0070

A few words might be added about the reliability of the safety system. When it is actuated, not only the safety rods but also the control plates are automatically forced to their "in" position. If now, as mentioned in the introduction, one of the rods is allowed to be out of action, it must be possible to shut down with only $S1 + R1 + R2$, which represent together a reactivity equivalence of about 2.9%. That means, that the highest permitted D_2O level should be at $H = 2480$ mm. However, it is impossible to get that level, because a "brim off-flow" is placed in the tank at $H = 2400$ mm.

REFERENCES

1. Netter, F. and Raievski, V., *Etude du facteur de multiplication dans la pile de Saclay*, Rapport C.E.A. No. 215 (1953).
2. Lipkin, H., *Liaison de la reactivité de la pile ZOE modifiée avec la constante de temps d'une montée en puissance.* Note C.E.A. No. 49 (1954).

Part III. Measurement of Neutron Distributions and Absolute Determination of the Power Level of the Swedish Heavy Water Reactor, by Karl-Erik Larsson

A simple way of testing the approximations used in diffusion theory is to measure the neutron distributions in a reactor. For a cylindrical reactor without the disturbing influence of experimental channels it is sufficient to measure the height distribution axially and the radial distribution in a central section to determine the extrapolated dimensions of the reactor. An analysis of the distribution curves also gives a value of the buckling. If the relative neutron distribution measurements over the whole of the reactor system are combined with an absolute measurement of the neutron flux at one point, preferably in the centre, the establishment of an absolute power scale is possible.

MEASUREMENTS OF THE NEUTRON DISTRIBUTIONS

Method

The measurement of a neutron flux within a solid structure such as a reactor is always a difficult task, because the detecting device will disturb the distribution. Moreover the construction prevents the measurement being made at arbitrary positions within the reactor. The only admittance to the interior of the system is by way of the uranium rods and the channels which traverse the construction. As measurements in the existing rather wide channels may be expected to give distributions which would lead to erroneous values of the extrapolated dimensions of the reactor, an arrangement was made whereby a series of measurements could be made in an aluminium tube put into the heavy water instead of the uranium rods. This aluminium tube was of the same dimensions as a fuel rod. As the reactor contains 126 uranium bars this substitution of a rod by an aluminium tube imposes a rather small disturbance of the flux. The neutron distributions were consequently measured in the vertical direction in the wide central channel, in six positions corresponding to uranium rods at 14.7, 29.4, 44.1, 58.8, 73.5, and 88.2 cm from the axis of the reactor and in a vertical channel passing through the reflector graphite at a distance of 122 cm from the axis (see Fig. 1). The uranium rods were so chosen, that there were no channels passing in their immediate neighbourhood. In the horizontal direction the distributions were studied in a channel (no. 6N) extending through the concrete shield, and the graphite up to the reactor tank. The axis of this channel crosses the vertical axis of the reactor at 42 cm above the maximum of the vertical distribution. The neutron distribution was also measured in a horizontal channel (No. 10) tangent to the reactor tank at a height corresponding to the maximum of the vertical distribution. Measurements in these channels are sufficient to give complete vertical and radial distribution curves.

A simple and reliable method for determining the distribution in a channel is to irradiate a copper band, and subsequently measure the 12.9 hour activity in-

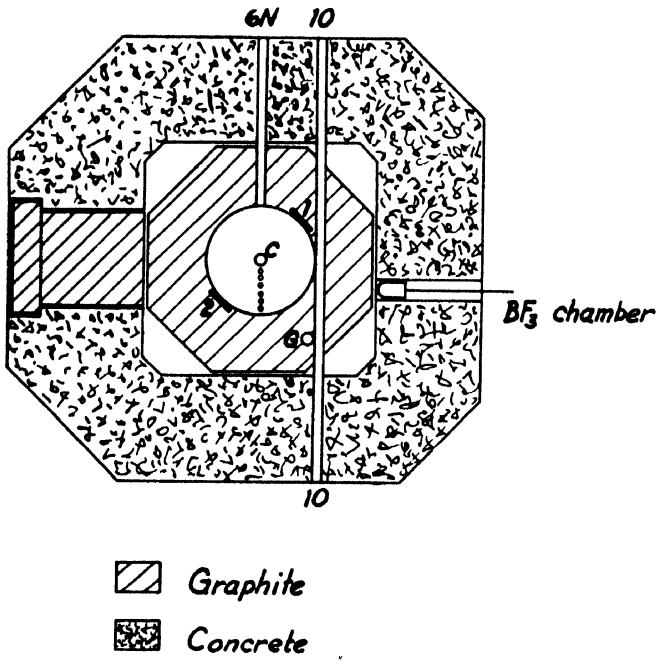

Figure 1. Horizontal section through the reactor with the channels used in the experiment. 10 and 6N are horizontal channels. C is the central channel through the reactor tank and below it a row of six uranium rods. G is the vertical channel through the graphite. 1 and 2 are the control plates

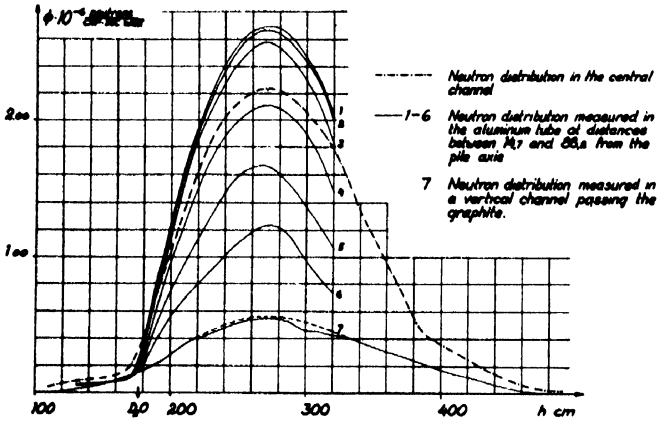

Figure 2. Experimental height distributions

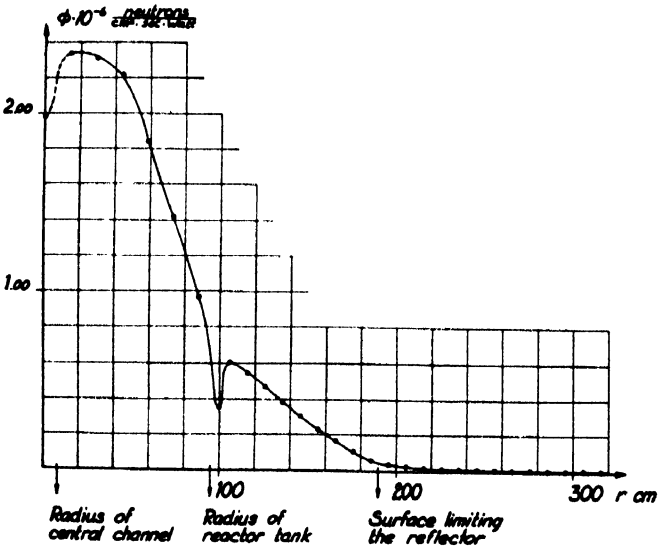

Figure 3. Radial neutron distribution in a plane 35 cm above the maximum flux

duced in Cu^{63}, the activity induced in Cu^{65} with a period of 4.3 minutes being negligible after a few hours. For this experiment copper bands of dimensions $0.1 \times 20 \times 4000$ mm were used, the β-activity being measured at intervals of 10 cm under an end window GM counter screened by 3 cm of lead. The slit limiting the area to be measured was of dimensions 10×19 mm. The γ-radiation from the remaining parts of the band was found to give a negligible background in the counter. The bands were activated at power levels between 1 and 40 watts for one hour. The constancy of the thickness of the bands was checked by weighing and confirmed by the smoothness of the distribution curves obtained.

Results

The results of the measurements in the eight vertical channels are given in Fig. 2. The flux in these as well as the following curves is given on an absolute scale according to measurements to be described in the next section. A preliminary examination of the curves shows as expected that the distribution in the central channel ($\phi = 153$ mm) is somewhat broader than those along the aluminium tube ($\phi = 31$ mm) successively substituted for the uranium rods. As regards the distribution in the graphite channel the disturbing effect of four different horizontal channels in its immediate neighbourhood is clearly discernible. A complete radial distribution is given in Fig. 3. Three features dominate the appearance of this curve: the depression caused by the central channel—amounting to 19%, the depression at the boundary of the reactor core caused by the aluminium walls of thickness 3.5 mm and the air gap of thickness 22 mm, and finally the increase of the thermal flux at the inner boundary of the reflector graphite, due to the increased slowing down of fast neutrons escaping from the core.

According to simple diffusion theory the neutron distributions in the reactor may be represented by an expression $\phi = A \cos(\pi h/H) \cdot (J_0(\alpha r) + BY_0(\alpha r))$, where H is the extrapolated height and α and B are constants, which may be determined from the distributions found. For an undisturbed reactor without channels the form of the radial solution is $J_0(\beta r)$, where $\beta = 2.405/R$, R being the extrapolated radius. The buckling for such a reactor is determined by

$$B^2 = \left(\frac{\pi}{H}\right)^2 + \left(\frac{2.405}{R}\right)^2$$

An analysis of the experimental data shows that it is possible to fit a function $\cos \pi h/H$ to the part of the height distributions corresponding to the uranium rods, as shown in Fig. 4. The value of the extrapolated height obtained from the measurement in the central channel is $H = 210$ cm, and from the measurements in the narrow aluminium tube inserted in place of a uranium rod $H = 205$ cm. Also, the heavy water level was 10 cm above the critical level so that

$H_0 = 195$ cm as measured in the aluminium tube
$H_0 = 200$ cm as measured in the central channel

These values may be somewhat too low, as the function $\cos \pi h/H$ does not reproduce the real distribution at the lower ends of the uranium rods. This is probably due to the bottom reflector, and is evident in the result of the measurement in the central channel. Accordingly the final result is given as

$$H_0 = 195\{^{+15}_{-6}\ \text{cm}$$

The lower curve of Fig. 4 shows the fit between the experimental distribution found in the vertical channel in the graphite and the analytic function found for the central channel. The deviations at heights corresponding to the upper and lower water levels are to be expected, since the distributions in the graphite will be broadened. In the radial direction a function $f(r) = J_0(0.02227r) + 0.1651Y_0(0.02227r)$ fits the experimental points rather well, as is shown in Fig. 5. The extrapolated radius is obtained from $f(r) = 0$ which gives

$$R_0 = 115 \pm 1\ \text{cm}$$

These two values of H_0 and R_0 give for the geometric buckling

$$B_g^2 = \left(\frac{\pi}{195}\right)^2 + \left(\frac{2.405}{115}\right)^2 = (7.0 \pm 0.4) \times 10^{-4}\ \text{cm}^{-2}$$

The extrapolation length (d) from the wall of the central channel is according to diffusion theory determined by $[f(r)/f'(r)]_{r=a}$, which gives

$$d = 70\ \text{cm}$$

The theoretically calculated values of all these constants using two-group theory are: $H_0 = 200$ cm, $R_0 = 114.5$ cm, $B_g^2 = 6.9 \times 10^{-4}\ \text{cm}^{-2}$, and $d = 79$ cm, so that the agreement seems reasonably good.

The above value of the buckling does not take the effect of the channels into consideration. If the analytical distribution functions found are substituted into the diffusion equation $\Delta\phi + B^2\phi = 0$ the value of the buckling becomes

$$B^2 = \left(\frac{\pi}{195}\right)^2 + (0.02227)^2 = (7.6 \pm 0.4) \times 10^{-4}\ \text{cm}^{-2}$$

which value may be said to be corrected for the influence of the central channel (and partly for the influence of the others) running through the reactor core.

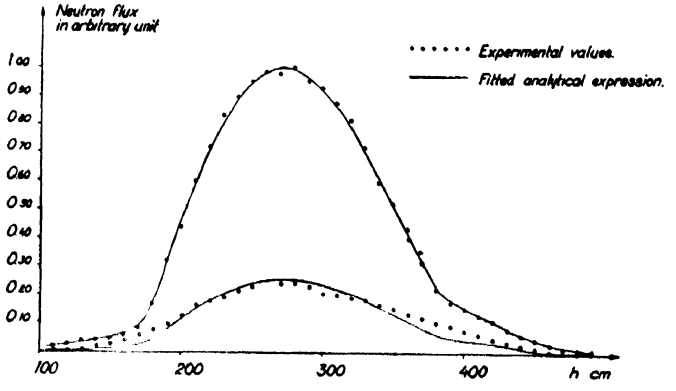

Figure 4. The fit of a theoretical curve to the experimental height distribution

ABSOLUTE DETERMINATION OF THE POWER

The absolute determination of the power level of the reactor may be divided into three steps: (*a*) calculation of the ratio of the neutron flux at the centre of the reactor, ϕ_0, to the power P; (*b*) an absolute determination of ϕ_0; (*c*) the establishment of a relative scale for the control instrument, which is calibrated absolutely by the methods outlined above.

Calculation of ϕ_0/P

A calculation of ϕ_0/P may be made in several different ways, of which two will be considered here. One of the methods is based on the measurement of the total thermal neutron source strength (Q neutrons/sec) of the reactor. If this quantity is known the corresponding power P is evidently given by

$$P = \frac{Q}{p \cdot \nu \cdot F} \qquad (1)$$

where p = resonance escape probability, ν = number of fast neutrons per fission, and F = number of fissions/watt-sec.

Of these quantities p may be calculated rather accurately; ν and F are given from other experiments. The problem is then to measure the thermal neutron source strength Q. If τ is the mean lifetime of thermal neutrons in the total reactor system and $\rho(r,h)$ is the thermal neutron density as a function of radius and height of the reactor, Q is given by

$$Q = \frac{1}{\tau}\oint \rho(r,h)\, dV \qquad (2)$$

where the integration extends over the whole of the reactor system. From the measurements of the neutron distributions in the reactor it follows that

$$\rho(r,h) = \frac{\phi_0(1+K)}{v(T)} f(r) \cdot \varphi(h) \qquad (3)$$

where $\phi_0(1+K)$ = central thermal neutron flux corrected for depression caused by the central channel, $f(r)$ and $\varphi(h)$ = radial and height neutron distribution functions in the reactor, and $v(T)$ = neutron velocity as a function of neutron temperature T.

A combination of Equations 1, 2 and 3 finally gives

$$\frac{\phi_0}{P} = \frac{\tau \cdot v(T) \cdot p \cdot \nu \cdot F}{(1+K)2\pi \cdot \int_0^{\infty} f(r) r\, dr \cdot \int_{-\infty}^{+\infty} \varphi(h)\, dh} \qquad (4)$$

From other measurements, $\tau = 0.73 \pm 0.03$ msec, $\nu = 2.5$ neutrons/fission, $F = 3.1 \times 10^{10}$ fissions/watt-sec, and the calculated value of p is 0.905. The neutron distribution measurements described above give $1 + K = 1.19$, $\int f(r) r\, dr = 4370$ and $\int \varphi(h)\, dh = 160$. These figures then give for the required ratio

$$\frac{\phi_0}{P} = 9.05 v(T)\ \text{neutrons/cm}^2 \cdot \text{sec} \cdot \text{watt} \qquad (5)$$

Another way of calculating ϕ_0/P involves calculation of the number of fissions/sec in a central uranium

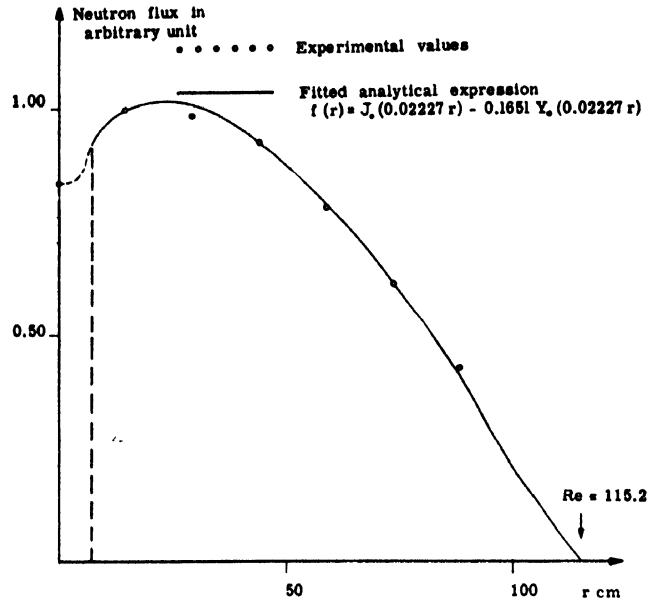

Figure 5. The fit of a theoretical curve to the experimental radial distribution

rod and then summation over all the rods using the known neutron distribution curves. Consider thus a uranium rod in the central channel of the reactor. The undisturbed flux at height h may be $\phi_0 \cos \pi h/H$. The number of fissions in a volume element Sdh of this rod, with the cross sectional area S, is:

$$\frac{\epsilon\nu - 1}{\nu - 1} \cdot S\, dh \cdot N_u \sigma_f \cdot \frac{\bar{\rho}}{\rho_M} \phi_0 \cos \frac{\pi h}{H} \qquad (6)$$

where $(\epsilon\nu - 1)/(\nu - 1)$ is the fractional increase in the number of fissions caused by fast fission ($\epsilon = 1.03$ = fast fission factor), N_u is the number of uranium nuclei per cm^3, σ_f is the fission cross section in barns, $\bar{\rho}$ is the average neutron density in the uranium and ρ_M the undisturbed density without the uranium rod. The total number of fissions in the reactor is obtained by integration over the length of a rod and summing over all the rods

$$\frac{\epsilon\nu - 1}{\nu - 1} \cdot \phi_0(1 + K) \cdot S \cdot N_u \cdot \sigma_f \cdot \sum_i \frac{\bar{\rho}}{\rho_M} f(r_i) \times \int_{h_{1i}}^{h_{2i}} \cos \frac{\pi h}{H}\, dh \qquad (7)$$

As the number of fissions per watt-sec is F the ratio ϕ_0/P becomes

$$\frac{\phi_0}{P} = \frac{F}{\frac{\epsilon\nu - 1}{\nu - 1} \cdot S \cdot N_u \cdot \sigma_f \cdot \frac{\bar{\rho}}{\rho_M} \times 1 \Big/ \sum_i f(r_i) \int_{h_{1i}}^{h_{2i}} \cos \frac{\pi h}{H}\, dh \cdot (1 + K)} \qquad (8)$$

where $\bar{\rho}/\rho_M$ is assumed independent of position. With $\sum_i$ calculated from the known distributions and $= 1.228 \times 10^4$, $S = \pi \cdot 1.45^2$ cm^2, $\sigma_f = 4.18$ barns at $v = 2.2 \times 10^5$ cm/sec, $N_u = 4.73 \times 10^{22}$ atoms/cm^3, and $\bar{\rho}/\rho_M = \frac{3}{5}$ according to a theoretical calculation the ratio becomes

$$\frac{\phi_0}{P} = 10.5\, v(T) \text{ neutrons/cm}^2 \cdot \text{sec} \cdot \text{watt} \qquad (9)$$

The two expressions, Equations 5 and 9, differ by 16%, which is not unexpected in view of the great number of sources of error involved in Equations 4 and particularly 8. Concerning the neutron temperature in a reactor, there are a great number of independent measurements made under different experimental conditions. It seems justifiable to assume a neutron temperature 100°C above that of the moderator. If $T = 393°K$, the velocity $v(T) = 2.55 \times 10^5$ cm/sec and Equations 5 and 9 give respectively

$$\frac{\phi_0}{P} = 2.31 \times 10^6 \text{ neutrons/cm}^2 \cdot \text{sec} \cdot \text{watt} \qquad (5')$$

$$\text{and } \frac{\phi_0}{P} = 2.68 \times 10^6 \text{ neutrons/cm}^2 \cdot \text{sec} \cdot \text{watt} \qquad (9')$$

A closer examination of the sources of error reveals that the uncertainty of the results in Equations 5′ and 9′ is ±20%. Thus the two expressions agree within the limits of error.

The Measurement of ϕ_0 and the Calibration of the Control Instrument

The absolute determination of the thermal neutron flux in the centre was made by activating gold foils and measuring the absolute disintegration rate, using the coincidence technique. As the resonance flux in the centre is rather high, cadmium difference measurements must be made. The cadmium ratio found in the centre was 3.07. The absolute value of the flux ϕ_0 was calculated assuming a neutron temperature of 393°K. The measured values of ϕ_0 were proportional to the power levels, as given by the control BF_3 ionization chambers, within 2%. The absolute value of the flux given in the distribution curves discussed above is based upon these measurements of ϕ_0.

The last link in the chain of measurements determining the power level consists in the calibration of the control instruments according to the power values found. The relative power level of the reactor is given

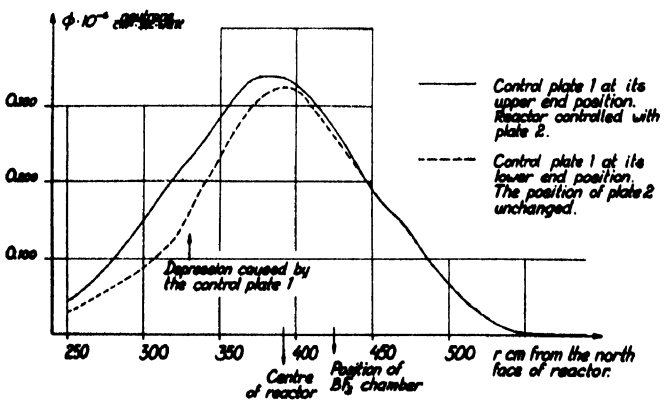

Figure 6. Neutron distributions in channel No. 10 measured at constant power level

by a current measuring BF_3 chamber placed in a channel passing through the concrete shield at a height corresponding to the maximum of the height distribution curve (see Fig. 1). This chamber is movable in its channel between two positions corresponding to a variation of the neutron flux by a factor of 10. By correlating the current value in one end position to the measured power the energy scale is fixed. An important question in this connection is whether the form of the flux distribution in this channel is dependent on the position of the control plate (No. 1 in Fig. 1). To investigate this the following experiment was made:

At a certain power level a copper band was activated in a channel 10 passing between the tank and the BF_3 chamber (Fig. 1), a gold foil being simultaneously activated in the centre of the reactor. The control plate 1 was completely withdrawn during this activation, the reactor power being adjusted by control plate 2. With the position of control plate 2 unchanged the amount of heavy water was then increased so much that the control plate 1 had to be brought into the position of maximum absorption in order to maintain the power level, as determined by the current in the BF_3 chamber unchanged. With this configuration the shadowing effect of control plate 1 at the chamber site must have reached its maximum. A copper band and a gold foil were then activated at the same positions as before. The activity of the gold foil was found to be constant within 2% and independent of the change of the control plate position. The neutron distribution in channel 10 for the two cases are given in Fig. 6. As will be seen from these curves the neutron flux on the same side of the maximum as the chamber position is practically unchanged by this change of control plate position, while the flux on the other side is deeply depressed. The conclusion drawn from this experiment is that the position chosen for the chamber is appropriate for the description of the reactor's real power level.

Part IVA. The Influence of the Experimental Channels on the Reactivity. Theoretical Part, by B. Pershagen

The Swedish reactor, which is a natural uranium-heavy water reactor of the CP-3 type, has a vertical central channel, two vertical eccentric channels for the safety rods and five horizontal experimental channels passing through the reactor core. The channels cause local depressions in the neutron density, which is equivalent to a loss of reactivity. Originally, the effect of the channels was estimated by means of ordinary diffusion theory. In this way the effect is underestimated as was evident from direct measurements with the critical reactor on the central and one of the horizontal channels. A more accurate calculation must take into account the deviations from the ordinary diffusion theory which appear near the surface of a channel.

THE LINEAR EXTRAPOLATION LENGTH

We consider a cylindrical channel with radius a in a uniform scattering and capturing medium occupying a volume V. It is known that if the dimensions of V are large compared to the mean free path in V, then the neutron density distribution in V can be determined by means of the diffusion approximation provided that the boundary conditions at the surface of the channel are known. In order to characterize the effect of the channel it is convenient to introduce the linear extrapolation length, which for cylindrical symmetry is defined by

$$\lambda = \frac{\rho(a,z)}{\left.\dfrac{\partial\rho(r,z)}{\partial r}\right|_{r=a}} \tag{2.1}$$

where z is the co-ordinate parallel to the channel axis and $\rho(r,z)$ is the diffusion approximation to the neutron density. λ must be determined by the transport theory.

Since, in the interesting case of large V, the influence on the neutron density near the surface of the channel due to other boundaries is small, it is sufficient to consider the idealized case of a single channel in an infinite medium, where in the absence of the channel, the neutron density is independent of r. On the other hand it is necessary to take into account the variation of the neutron density along the axis of the channel since a hollow channel allows free passage of neutrons and therefore the neutron density at the points of the surface of the channel will depend on the neutron density at all points of the channel.

Calculations of λ have been done by Davisson.[1,2] He considered a cylindrical channel in an infinite scattering medium with a periodic neutron density distribution along the axis of the channel. Putting

$$\rho(r,z) = \psi(r)e^{i\alpha z} \tag{2.2}$$

where α^2 is a measure of the curvature ("buckling") of the axial neutron density distribution, we get from Equation 2.1

$$\lambda = \frac{\psi(a)}{\psi'(a)} \tag{2.3}$$

In so far as the radius of the channel is concerned, Davisson considered two cases: (a) the channel radius is comparable to the mean free path and (b) the channel radius is comparable to π/a, i.e., the thickness of the layer in which the neutron density is positive, and the channel radius large compared to the mean free path. In case (a) Davisson obtains

$$\lambda = \frac{l}{\alpha^2 a(a+l)} + \frac{3\pi}{8}\frac{1}{\alpha}\frac{al}{(a+l)^2} + 0\{(\log \alpha a)^4\} \tag{2.4}$$

where l is the mean free path in the scattering medium.

In case (b) Davisson also considered the effect of an absorbing wall of the channel. Characterizing the absorption in the wall by $C = \Sigma l$, where Σ is the macro-

scopic absorption cross section of the wall material and t the wall thickness, he obtains for small αa and C

$$\frac{\lambda}{l} = \frac{1 - \frac{3}{8}(\alpha a)^2 - \frac{3}{2}C + 0[(\alpha a)^4 \log \alpha a] + 0(C^2)}{(\alpha a)^2 - \frac{3\pi}{8}(\alpha a)^3 + 3C + 0(\alpha a)^4 + 0(C^2 \log C)} \tag{2.5}$$

For a channel with an absorbing wall where the radius is comparable to the mean free path, it can be seen from Equations 2.4 and 2.5 that if $\alpha a \ll 1$ and $C \ll 1$, λ is approximately given by

$$\lambda = \frac{l}{(\alpha a)^2 \frac{a+l}{a} + 3C - \frac{3\pi}{8}(\alpha a)^3} \tag{2.6}$$

THE EFFECT OF CHANNELS PARALLEL TO THE AXIS OF THE REACTOR

Central Channel

We consider a cylindrical reactor with a channel along the axis of the reactor and use two-group theory. The extrapolation lengths at the surface of the channel are different for the fast and slow groups, since the mean free paths are different and since fast neutrons are not absorbed appreciably by the channel wall. Using suffix 1 for the fast and 2 for the slow group we obtain from Equation 2.6

$$\lambda_1 = \frac{l_1}{(\alpha a)^2 \frac{a+l_1}{a} - \frac{3\pi}{8}(\alpha a)^3} \tag{3.1}$$

and

$$\lambda_2 = \frac{l_2}{(\alpha a)^2 \frac{a+l_2}{a} + 3C - \frac{3\pi}{8}(\alpha a)^3} \tag{3.2}$$

Since the influence of reflectors on the neutron density distribution near the channel is negligible, we can replace the actual, reflected reactor with a bare reactor (the "extrapolated" reactor), having the same buckling as the actual reactor. If B_0^2 is the buckling for the reactor in the absence of the channel, then the buckling B^2 which is required for the reactor with the channel will be larger. The loss of reactivity due to the channel, $\Delta k/k_0$, where k_0 is the multiplication factor for the reactor without the channel, may be determined from the two-group critical equation.

$$k_0 = (1 + L_1^2 B_0^2)(1 + L_2^2 B_0^2) \tag{3.3}$$

where L_1 is the slowing-down length and L_2 the diffusion length. For small changes of the buckling, $\Delta B^2 = B^2 - B_0^2 \ll B_0^2$, we obtain from 3.3, using the fact that $L_1^2 \approx L_2^2$

$$\frac{\Delta k}{k_0} \propto \frac{M^2 \Delta B^2}{1 + \frac{1}{2}M^2 B_0^2} \tag{3.4}$$

where $M^2 = L_1^2 + L_2^2$ is the migration area.

The buckling for the reactor without the channel can be written as

$$B_0^2 = \alpha_0^2 + \beta_0^2 \tag{3.5}$$

with $\alpha_0 = \pi/H$ and $\beta_0 = 2.405/R$, where H and R are the extrapolated height and radius of the reactor. The introduction of the channel parallel to the axis of the reactor does not appreciably change the axial buckling. Therefore

$$B^2 = \alpha_0^2 + \beta^2 \tag{3.6}$$

and

$$\Delta B^2 \approx 2\beta_0 \Delta\beta \tag{3.7}$$

It can be shown that solving the two-group equations with the appropriate boundary conditions gives the following characteristic equation for determining β

$$\frac{J_0(\beta R)}{Y_0(\beta R)} = \frac{J_0(\beta a) + \beta\lambda J_1(\beta a)}{Y_0(\beta a) + \beta\lambda Y_1(\beta a)} \; (= q) \tag{3.8}$$

where J and Y are Bessel functions of the first and second kinds, respectively, and λ is an average extrapolation length, defined by

$$\frac{M^2}{\lambda} = \frac{L_1^2}{\lambda_1} + \frac{L_2^2}{\lambda_2} \tag{3.9}$$

The numerical evaluation of β from 3.8 can be simplified, since the change in the buckling due to the channel is small. Putting $\beta = \beta_0 + \Delta\beta$, where $\Delta\beta \ll \beta_0$ and $\beta_0 R = 2.405$, we obtain in the first approximation, using the fact that the R.H.S. of 3.8 is a slowly varying function of β

$$\Delta\beta = -\frac{Y_0(2.405)}{2.405 J_1(2.405)} \beta_0 \cdot q_0 = -0.4084\beta_0 q_0 \tag{3.10}$$

where

$$q_0 = \frac{J_0(\beta_0 a) + \beta_0\lambda J_1(\beta_0 a)}{Y_0(\beta_0 a) + \beta_0\lambda Y_1(\beta_0 a)} \tag{3.11}$$

Combining Equations 3.10, 3.7 and 3.4 we finally obtain for the reactivity change

$$\frac{\Delta k}{k_0} \approx -0.8168 \frac{M^2 \beta_0^2 q_0}{1 + \frac{1}{2}M^2 B_0^2} \tag{3.12}$$

Eccentric Channel

The foregoing treatment can be generalized to the case of an eccentric channel. We find for a channel with a relatively small radius, located not too eccentrically

$$\Delta\beta \approx -\frac{0.4084\beta_0 q_0 J_0^2(\beta_0 r_c)}{1 - 2q_0 \sum_{m=1}^{\infty} \frac{Y_m(\beta_0 R)}{J_m(\beta_0 R)} J_m^2(\beta_0 r_c)} \tag{3.13}$$

where r_c is the distance between the axis of the reactor and the axis of the channel.

THE EFFECT OF CHANNELS PERPENDICULAR TO THE AXIS OF THE REACTOR

For geometrical reasons it is difficult to treat a channel perpendicular to the axis by the method which was used in the preceding section. Since, however, the depression of the neutron density due to a channel with a relatively small radius and with a not too strongly absorbing wall is small, one may use perturbation theory to estimate the effect of the channel on the

Table 1

Channel	Radius, cm	Wall thickness, cm	Distance from axis, cm	Distance from upper extrapol. boundary, cm
Central, vertical	8.1	0.4		
Two channels for safety rods, vertical	4.0	0.5	30.2	
"8" and "9," horizontal	3.75	0.5	31.4	84.1
"12" and "13," horizontal	3.75	0.5	31.4	142.4
"20," horizontal	4.0	0.45	18.8	102.6

criticality of the reactor. The channel may be interpreted as an absorber of neutrons with a fictitious absorption cross section that can be determined from the extrapolation length.

The effect of an absorber in different parts of a reactor can be estimated by means of the statistical weight theorem,[3] according to which the change of the buckling may be written as

$$\Delta B^2 \approx \frac{3\Sigma}{l} \frac{\iiint_{absorber} \phi_0^2(r,z)\, dV}{\iiint_{reactor} \phi_0^2(r,z)\, dV} \qquad (4.1)$$

where Σ is the macroscopic absorption cross section of the absorber, l the transport mean free path in the reactor and $\phi_0(r,z)$ the neutron flux in the absence of the absorber.

The fictitious absorption cross section of a channel is related to the extrapolation length at the surface of the channel by the formula

$$\lambda = \frac{l}{3\Sigma t} \qquad (4.2)$$

where t is the wall thickness.

For the extrapolated reactor the neutron flux in the absence of the channel can be written as

$$\phi_0(r,z) = AJ_0(\beta_0 r) \sin(\alpha_0 z) \qquad (4.3)$$

Inserting Equations 4.3 and 4.2 in 4.1 and integrating we obtain for a channel parallel to the reactor axis

$$\Delta B^2 \approx \frac{2}{R^2 J_1^2(\beta_0 R)} \frac{a}{\lambda} J_0^2(\beta_0 r_c) \qquad (4.4)$$

or since $\beta_0 R = 2.405$

$$\Delta B^2 \approx 1.284 \frac{a}{\lambda} \beta_0^2 J_0^2(\beta_0 r_c) \qquad (4.5)$$

For a channel perpendicular to the reactor axis with the length $2c$ located at a distance b from the axis and z_c from the upper extrapolated boundary of the reactor we obtain in a similar manner

Table 2

Channel	Reactivity reduction (%)			
	Total		Absorption in Al wall	
	Calc.	Exp.	Calc.	Exp.
Central	0.904	0.88	0.201	0.20
Ch. for safety rod	0.245	—	0.126	—
"8"	0.177	0.18	0.115	0.12
"12"	0.143	—	0.093	—
"20"	0.250	—	0.151	—

$$\Delta B^2 \approx 1.634 \alpha_0 I(b,c,\beta_0) \frac{a}{\lambda} \beta_0^2 \sin^2(\alpha_0 z_c) \qquad (4.6)$$

where $$I(b,c,\beta_0) = \int_0^c J_0^2\left[\beta_0 \sqrt{b^2 + x^2}\right] dx \qquad (4.7)$$

For the calculation of λ from 2.6 for a channel perpendicular to the reactor axis, the neutron density distribution along the axis of the channel may be approximated by a cosine distribution.

NUMERICAL RESULTS AND COMPARISON WITH EXPERIMENTS

The dimensions and positions of the six experimental channels and the two channels for the safety rods in $R1$ are shown in Table 1.

In the numerical calculations the following values were used: $\alpha_0 = 0.0150$ cm^{-1}, $\beta_0 = 0.0210$ cm^{-1}, $L_1^2 = 113.4$ cm^2, $L_2^2 = 109.1$ cm^2, $l_1 = 3.25$ cm, $l_2 = 2.44$ cm and $\Sigma_{wall} = 0.0115$ cm^{-1} (aluminium). The results are shown in Table 2. The effect of absorption in the channel walls can be calculated separately by putting $C = 0$ in 3.2. The results are compared with experiments in the next section.

The total loss of reactivity due to the channels is 2.28%. In view of the approximate nature of the calculations and the uncertainty in the measurements the agreement between theory and experiment is surprisingly good.

The effect of channels on the given lattice is twofold: (*a*) the absorption of neutrons in the channel walls decreases the thermal utilization and (*b*) the holes in the moderator increase the migration length and therefore the leakage of neutrons from the reactor. The total increase in M^2 due to the channels is about 8.6%.

REFERENCES

1. Davisson, B., *Linear Extrapolation Length of the Neutron Density at the Surface of a Large Hollow Cylindrical Shaft*, CRT-419, Chalk River (1949).
2. Davisson, B., *Influence of a Cylindrical Channel on a Periodic Neutron Density Distribution*, AERE T/R 738, Harwell (1951).
3. Rennie, C. A., *Lecture Notes on Pile Theory*, AERE R/L 5, p. 21, Harwell (1952).

Part IVB: The Influence of the Experimental Channels on the Reactivity. Experimental Part, by R. Persson

The dimensions and positions of those experimental channels, which penetrate the reactor core, are shown in Table 1 of the preceding section. The influence of the central vertical channel and of channel No. 8 on the reactivity was investigated experimentally, by placing cylindrical aluminium containers with and without heavy water in the channels. Graphite cylinders and a uranium rod were also introduced in the central vertical channel. From the calibrating curves of the control plates, and by using the reactivity coefficient 7.0×10^{-5}/mm change of the heavy water level, we obtain the different effects expressed in reactivity.

THE CENTRAL VERTICAL CHANNEL

A cylindrical aluminium container (137 mm od, 125 mm id and in the following called Al I) was filled with D_2O to about the same level as the water in the tank. Around this container it was possible to place an aluminium tube (147 mm od, 139 mm id, and in the following called Al II). The channel itself consists of an aluminium tube with 162 mm od and 154 mm id.

Experiment No.	Material introduced				Change of D_2O level (mm)
	Al I	Al II	D_2O	U	
1	x	—	—	—	+37.0
2	x	x	—	—	+62.6
3	x	x	—	x	+38.3
4	x	x	x	x	+ 3.5
5	x	x	x	—	+29.3
6	x	—	x	—	− 3.9
7	x	—	x	—	− 3.2
8	x	x	x	—	+30.1

(*a*) The difference between Exp. No. 2 and Exp. No. 1 gives 25.6 mm. The influence of the channel walls is then $25.6 \times (4 \times 158)/4 \times 143) = 28.3$ mm change in the D_2O level.

(*b*) From Exp. No. 5–8 we can calculate the influence of the hole in the moderator. The water in the container gives the following change of D_2O level:

$$-3.6 - 33.3 \frac{6 \times 131}{4 \times 143} = 49.4 \text{ mm}$$

According to investigations with graphite (see below) this figure might roughly be multiplied by the ratio of the diameter of the hole to that of the introduced water cylinder. We thus obtain

$$49.4 \times {}^{16}\!/_{25} = 64 \text{ mm change of } D_2O \text{ level}$$

The flux depression caused by the hole in the moderator can be found approximately from the difference in the influence of Al II with and without heavy water in Al I. Because the influence on the reactivity is proportional to the square of the flux we obtain

$$1 - \sqrt{25.6/33.3} = 0.12$$

that is, a flux depression of about 12%. But the heavy water in Al I does not fill up the whole channel and the depression caused by the hole in the moderator may be somewhat larger.

(*c*) According to No. 4 and 5 the influence of putting in a uranium rod corresponds to −25.8 mm change of D_2O level.

(*d*) By placing graphite cylinders (diameter 100 mm or 147 mm) below the heavy water container we could study the influence of the hole in the bottom reflector (diameter 300 mm)

Graphite cylinder	*Change of D_2O level*
Diameter 100 mm	−0.8 ± 0.1 mm
Diameter 147 mm	−1.7 ± 0.1 mm

From this we conclude that the hole in the reflector means a change of +7 mm in D_2O level.

(*e*) Graphite cylinders of different lengths (1.0, 0.5 and 0.25 m) and different diameters (100 and 147 mm) were introduced in the channel. The measurements gave the results shown in Fig. 1.

THE HORIZONTAL CHANNEL "8"

(*a*) By taking away the protective aluminium tube (60 mm od, 56 mm id) we obtained −5.8 mm change of D_2O level. The tube in the tank (75 mm od, 69 mm id)

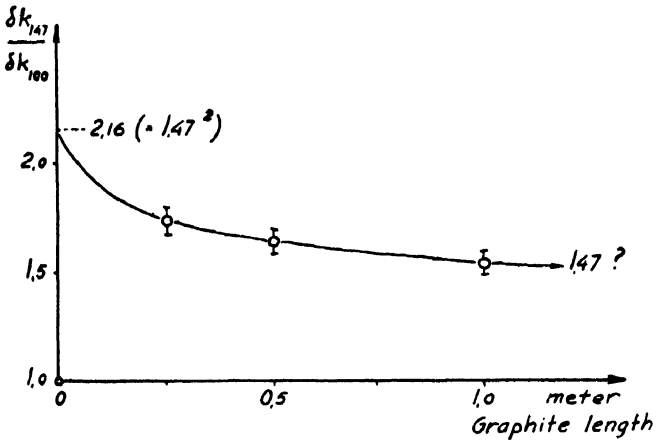

Figure 1. The ratio of the reactivity changes with graphite pieces of diameter 147 mm and 100 mm respectively, placed in the central channel

corresponds thus to $5.8 \times (72.3/58.2) = 10.8$ mm and the total influence is 16.6 mm change of D_2O level.

(*b*) An aluminium container (50 mm od, 47 mm id) filled with D_2O gave a change of −1.2 mm. The diameter of the hole in the moderator is 75 mm and the influence of this hole is thus about

$$\left(5.8 \frac{48.5 \times 1.5}{58.2} + 1.2\right) \frac{75}{47}$$

= 7.7 mm change of D_2O level

(*c*) The hole in the graphite reflector corresponds to a change of about 1 mm.

SUMMARY

If the change of the D_2O level is transformed to change of reactivity we obtain what we have to pay in reactivity for the channels:

Material	*Vertical channel* *Per cent*	*Channel "8"* *Per cent*
Al	0.20	0.12
D_2O	0.45	0.05
U	0.18	—
Graphite	0.05	0.01
	0.88%	0.18%

A comparison of experimental results and theoretical calculations is in Table II of the preceding section.

Study of the Neutronics of Two French Heavy Water Reactors

By J. Horowitz,* France

The two French reactors—the Châtillon reactor, called ZOE, and the Saclay reactor, which will be designated as P2 in this paper—have been the object of detailed neutronic studies, the principles of which are discussed in this paper. These studies were, in the main, carried out under the authority of the Reactor Development Department, under the direction of Professor J. Yvon, chief of the department. The physicists who carried out the various experiments are mentioned in the text. Unless indicated otherwise, they belong to this department. The theoretical part of the work was performed by A. Amouyal, P. Benoist, G. Besset, J. Bussac, J. Horowitz, C. Mercier, V. Raievski, P. Tanguy, and M. Trocheris of the Mathematical Physics Division.

MACROSCOPIC DISTRIBUTION OF THE NEUTRON FLUX IN P2 AND ZOE: COMPARISON BETWEEN THE LAPLACIANS OF THE LATTICES

The measurements of the macroscopic neutron distribution in P2 and ZOE, the determination of the Laplacian, and a comparative computation of the two lattices have yielded valuable information.

On the Saclay reactor, which has the unique peculiarity of being gas cooled, although it is a heavy-water reactor, there is reason to hope that we will show the loss in reactivity brought about by the gas piping. The effect of these cavities on neutron leakage is amplified for a reactor of this type, where the high flux gradient favors neutron transport.

On the other hand, the lattice of the Châtillon reactor has a very large pitch, and thick uranium rods. This gives rise to certain effects, which will be analyzed below.

The known characteristics of the two reactors are given in Table I.

The central cell of ZOE may be provided with an experimental axial channel, but, in the absence of an indication to the contrary, we shall consider the cases in which the uranium rods are in their normal positions.

Experimental Results. Measurement of Neutron Distribution

P2

Neutron distribution was determined by G. Vendryes, who measured the activation of copper foils, applied to six uranium rods located in the same axial half-plane. A seventh foil was set in the empty central channel. The shim plates were raised, and the seven foils were then irradiated simultaneously by several exponential increases in reactivity obtained by withdrawing the safety rod.

The various curves obtained, after the corrections, are well represented by the same law

$$\cos\left(\pi \frac{Z}{H_e}\right)$$

with $H_e = 224 \pm 3$ cm.

The extrapolation length above the free surface of the heavy water, which is defined as the distance between this level and the plane where the extrapolated value of the cosine curve becomes zero, is rather poorly defined graphically, but seems to be several centimeters. The experimental curve is different from the cosine law in the vicinity of the free surface, and then remains essentially constant above it (6 to 8 per cent of maximum density). From this value, and if the angular distribution of the neutrons were that given by Milne's problem, we could derive an extrapolation distance of approximately 6 cm. This figure appears to be large, but is accounted for by the fact that some neutrons are reflected, either by the pipe blocks of the pile, or by the vertical graphite extension of the lateral reflector. The graphite would equal 3 cm of additional heavy water, according to an estimate of J. Bernot, who measured the effect of the shim plates on the reactivity when they are placed in front of this particular part of the reflector.

The neutron distribution in the radial direction is obtained by comparing homologous points on the various measuring foils. The experimental results then consist of seven points, six of which are shown on Fig. 1; the seventh, which corresponds to the central cell, which contains no uranium, is at a point 1.52 times the curve which goes through the other points.

Most experimental points are located on the curve given by a Bessel function: $J_0\left(j \frac{r}{R_e}\right)$ with $j = 2.405$, first root of function J_0, and $R_e = 132 \pm 2$ cm.

Nevertheless, the distribution observed shows a considerable rise close to the periphery of the core, in the vicinity of the reflector, which affects the last two points of the measurement (see Fig. 1).

ZOE

In 1953, A. Ertaud and R. Beauge carried out similar measurements on the Châtillon reactor, follow-

Original Language: French.

* Chief of the Division of Mathematical Physics, C.E.A.

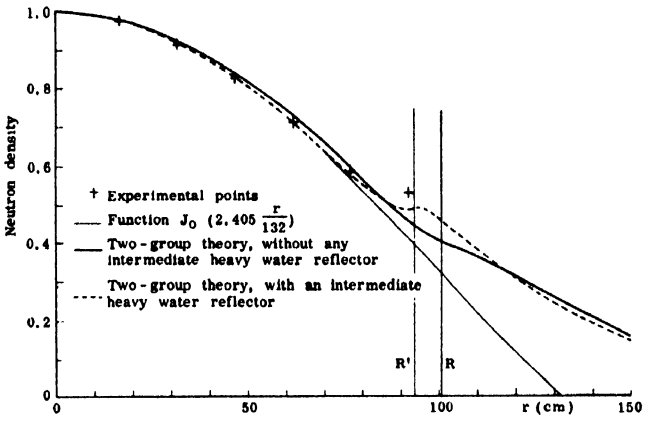

Figure 1. Radial distribution in P2

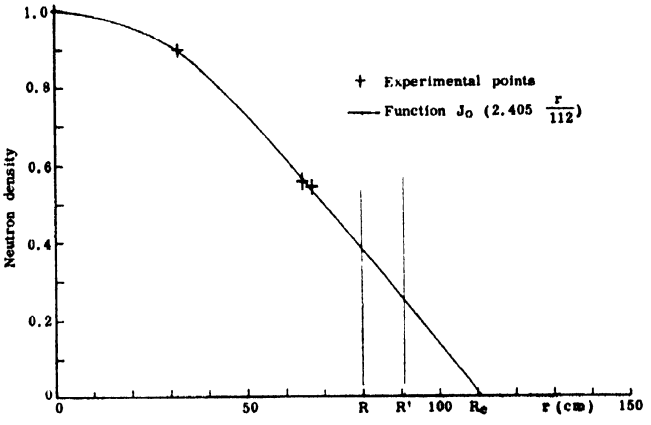

Figure 2. Radial distribution in ZOE

ing its modifications, and before it resumed operation at a substantial power level. The longitudinal neutron distribution is properly given by a sine law, using as the value for the extrapolated height $R_e = 172 \pm 3$ cm.

As in the case of P2, the extrapolation distance, in the upper part of the reactor, is hard to evaluate; it does seem to be of the same order of magnitude.

Unfortunately, the radial measurements bear only on 4 rods, none of which is really close to the vessel (see Fig. 2). Therefore, the only figure which can be given with any good accuracy is the radius R_e, of the equivalent unreflected reactor, $R_e = 112 \pm 5$ cm.

The extrapolation distances which were justified for the two reactors, permit one to compute a value for the Laplacian, which we will term "experimental":

$$\kappa^2 = \frac{\pi^2}{H_e^2} + \frac{j^2}{R_e^2} = (5.3 \pm 0.15) \times 10^{-4}\ \text{cm}^{-2} \quad \text{for P2}$$

and $(7.9 \pm 0.4) \times 10^{-4}\ \text{cm}^{-2}$ for ZOE

Before these values are compared with those given by computation of the cell Laplacian, it will be necessary however, to correct the results for P2, since 3 uranium rods are lacking at the center of its lattice; this is equivalent to a variation of approximately 12 cm in the critical level, and, thus, the Laplacian of a complete P2 lattice would be:

$$(5.5 \pm 0.15) \times 10^{-4}\ \text{cm}^{-2}$$

Computation of the Neutron Flux Distribution with Two-Group Theory

A theoretical interpretation of the distributions actually observed (P. Benoist and J. Bussac), in particular those of the density increase noted in the vicinity of the reflector, revealed the following points:

(*a*) The "one-group theory" is plainly inadequate, and gives very different results (10% in the Laplacian) from the two-group theory, for heavy water reactors having dimensions close to those under study.

(*b*) When endeavoring to allow for both the lower reflector and the lateral reflector, it is not possible, in the two-group theory, to write out accurately or rigorously the expression for the flux in the core in the form of a product of functions of axial and radial coordinates. This is similar to what happens in the one-group theory in the expression for the flux found in a cylindrical reflected reactor, for instance. Nevertheless, J. Yvon[1] showed that it was possible, without any appreciable error, to treat this problem approximately by leaving out the perturbations due to the "corners."

Here, again, we are led to use a method of successive approximations which leaves out the effect of the "corners" in the multiplying cylinder; the radial problem will be solved by considering the case of a reactor having no vertical reflector, but an estimated extrapolated height H_e; the axial computation which must determine H_e will use the value, found in the first computation, of extrapolated radius R_e.

(*c*) The Laplacian, as computed by the two-group theory, depends directly on the radius taken for the critical cylinder. It would seem unduly optimistic to use the actual radius, R, of the vessel which contains the heavy water in the calculations. It seems preferable to use in the computation, the radius of a cylinder which has the same surface area as the sum of the surface areas of the actual cells. This gives us a radius $R' < R$. In order not to neglect the excess of heavy water, the region between R' and R has been interpreted as a third region, which is treated as a heavy

Table I

Item		*P2*	*ZOE*
Radius of the uranium rods (cm)	a	1.3	1.825
Thickness of aluminum cladding (cm)		0.1	0.1
Thickness of intermediate cladding (Al) (cm)		0.1	—
Thickness of outside plunger (Al) (cm)		0.15	—
Inside radius of moderator (cm)	c	3	1.925
Cell radius (cm)	b	7.93	9.765
Total number of cells	N	139	67
Central cells (no uranium rods)		3	0
Radius of cylinder equivalent to the sum of the cells $R' = b\sqrt{N}$ (cm)		93.5	80
Radius of the vessel (cm)	R	100.5	91
Thickness of the vessel walls (Al) (cm)		0.3	0.3
Thickness of the bottom of the vessel (Al) (cm)		0.6	0.6
Estimated diffusion length of the graphite used as a reflector (cm)		50	45
Critical height (length of submerged rods) (cm)		180	141
Heavy water thickness under the uranium rods (cm)		5.4	1

water reflector. Vertically, the same procedure has been followed in order to allow for the heavy water located below the uranium rods. The somewhat tiresome computations carried out from these hypotheses, give the following results:

	P2	ZOE
R_e	132.6 cm	114.3 cm
H_e	221.4 cm	175.7 cm
κ^2	5.3×10^{-4} cm^2	7.6×10^{-4} cm^2

The agreement with experiment is excellent for P2, but not so good in the case of ZOE, although still within the limit of experimental errors. The interpretation considered here thus allows, it would seem, to take proper account of the effect of the excess heavy water in the vessel on multiplying cells, and the two-group theory is completely satisfactory.

(*d*) Finally, taking the intermediate heavy-water reflector into consideration makes it possible to achieve a larger increase in the radial flux curve, in the vicinity of the vessel, even though the increase observed is still inadequately explained (see Fig. 1). Local effects may be the cause of this phenomenon.

Table II summarizes the methods and results.

Note: the heights H and H' allow for an extrapolation distance of 6 cm for both reactors.

It is convenient to know the radius R_m, a value between R' and R, which would give the same result in the two-group theory using two regions, rather than the complete 3-region computation:

	P2	ZOE
R'	93.5	80
R_m	95.7	82.9
R	100.5	91

Comparison of the Multiplication Constant of the ZOE and P2 Lattices

With two critical reactors and the knowledge of their Laplacians, it was interesting to compute the multiplication factor of each lattice, starting from the same model, in order to show the differential effects which we mentioned at the beginning. For this purpose the formulae do not have to be too exact in that they may contain similar errors for both reactors. On the other hand, any factor which is unique for one of the reactors must be treated with the utmost care.

Table II. Summary

Type of theory	1 group	2 groups	2 groups
Number of media	2	2	3
Radial computation:			
From 0 to R', region	multiplying	multiplying	multiplying
From R' to R region	multiplying	multiplying	D_2O
From R to ∞ region	C	C	C
Axial computation			
From 0 to H', region	multiplying	multiplying	multiplying
From H' to H region	multiplying	multiplying	D_2O
From H to ∞ region	C	C	C
P2			
Radial computation R_e =	128.6	137.8	132.6
Axial computation H_e =	215.9	225.1	221.4
Laplacian in m^{-2}	5.6	5.0	5.3
ZOE			
Radial computation R_e =	115.6	122.7	114.3
Axial computation H_e =	170.1	177.6	175.7
Laplacian in m^{-2}	7.7	7.0	7.6

It is convenient to present this study as a computation of the value of the parameter η which makes each reactor critical[2]

$$\eta = \frac{(1 + L^2\kappa^2)(1 + L_s^2\kappa^2)}{\epsilon p f}$$

The formulae used are classical. However let us note:

(*a*) In order to allow, in the computation of f, for the depression of the neutron flux in the annular air space of P2, we have used an approximate formula which correlates the fluxes on either side of the gas mass $(c - a')$

$$n(c) - n(a') = -2N_m J(a'), \quad N_m = 1 - \frac{2\varphi_0}{\pi} - \frac{\sin 2\varphi_0}{\pi}$$

$$\varphi_0 = \arcsin \frac{a'}{c}$$

(*b*) The average capture cross section which comes into the computation of L^2 was obtained by weighting the cross section of each medium by the mean fluxes and corresponding volumes.

(*c*) Finally, in order to allow for the increase in the neutron path due to the presence of the cooling channels, an attempt was made at computing L^2 and L_s^2, either by the elementary[2] or by the Behrens,[3] theory.

We note that some anisotropy appears in this latter theory and that L^2 and L_s^2 no longer are scalar quantities. Thus the thermal leakage $(L^2\kappa^2)$ shall be written henceforth as

$$\frac{\pi^2}{H_e^2} L_t^2 + \frac{j^2}{R_e^2} L_r^2$$

As regards the numerical constants used, let us note in particular the value $\kappa_0 = 1$ of the parameter which represents the reciprocal of the diffusion length in uranium, according to the elementary diffusion theory and the value of the "age" of thermal neutrons in heavy water, which is not known with accuracy. This uncertainty loses its importance in view of the fact that we are merely trying to draw a comparison between the two reactors. We took:

$$\tau = 120 - 23P \text{ cm}^2$$

A table of the values obtained for the computation of the two lattices is given below. The results for the parameter η are

		P2		ZOE	
Laplacian ($10^4\kappa^2$)		5.5	±0.15	7.9	±0.4
η: Theory	Elementary	1.313	±0.005	1.299	±0.010
	Behrens	1.327	±0.005	1.299	±0.010

Despite the inaccuracy in the Laplacian operator of ZOE in particular, it would seem that in the computation above, the multiplication factor of ZOE was overestimated with respect to that of P2. A more detailed study of the differences between the two reactors brings to light a certain number of corrections that are needed, all of which tend to compensate for the differences.

Corrections Having To Do with the Presence of Gas Tubes in P2

The approximate formula used in the computation of f allows, in principle, for the variation of density on either side of the air annulus, but not for the increase in density in the moderator cell. Now, elementary diffusion theory is very inadequate for this purpose, and this accounts for corrections in f, and in L^2, which may vary from one reactor to the next.

The use of Behrens' formula, for the computation of L^2 and L_e^2, underestimates the effect of the voids surrounding the uranium rods caused by the cooling channels. This is due to the fact that this formula was drawn up for the case of voids uniformly distributed in a constant flux, with a constant probability that all the neutrons penetrate the voids. However, the inevitable creation and the very probable disappearance of a neutron in the uranium rod require additional crossings of the void by the neutrons, and thus an increase in the correction which has to be applied to the diffusion and moderation lengths. This factor, which may be as much as 20 to 30 per cent of the Behrens' correction, and which should work to the detriment of P2 is just about compensated for by the "finite reactor" correction, which is large for a reactor of small dimensions, such as P2. The Behrens' correction term would indeed apply to a sine law distribution of the neutron flux, and must be reduced, in order to allow for the perturbation created by the proximity of the ends of the reactor.

Corrections Having To Do with the Greater Dimensions of the ZOE Cells

The substantial difference in the radii of the cells in ZOE (9.765 cm) and P2 (7.93 cm) accounts for further corrections which must be incorporated into the original computation.

The additional factor ϵ, due to the fast fissions created in a rod by the neutrons produced in another rod, is reduced when the distance between the rods increases.

The Wigner-Weinberg correction[2] is of dubious value, and its elimination would be unfavorable to the larger cells, thus to ZOE.

On the other hand, the conventional formula for p is only an approximate one, and would give a value $p = 1$, for an infinite cell radius, which is certainly incorrect. At a resonance energy the distribution of the neutrons being slowed down is not exactly uniform in the cells, but does show a maximum in the vicinity of the rods. This maximum increases for an increase in the $b/\sqrt{\tau'}$ ratio, for the neutrons cannot escape from the rods much farther than the square root of the age, τ, of the resonance neutrons. The correction to be applied to p is proportional, on the one hand, to the departure from uniformity of the flux (a function of the radius of the cell), and on the other hand, to the capture in the rod (a function of the radius a). Thus, the customary formula is unduly optimistic in its assumption, and for two reasons, the correction needed is larger for ZOE than for P2. This effect is probably substantial: the difference from the classical formula can be computed, for the case of a cell of infinite radius, by using the expression (C. Mercier):

$$1 - p_\infty = \frac{a^2}{4\tau'} \cdot \frac{\int_{eff} \sum_{\infty} \frac{dE}{E}}{\Sigma_{1\infty}' \xi}$$

Instead of the value 0 we thus find, for $(1 - p)$, in the case of a rod having the same cell radius as ZOE:

$$1 - p_\infty = 0.0191$$

and, in the case of P2

$$1 - p_\infty = 0.0130$$

While the elementary theory underestimates the mean value of the flux in the moderator, this discrepancy increases as the cells get larger. The balance sheet of the neutron leakage is plainly optimistic for the two reactors, but, here again, more so for ZOE than for P2.

Conclusion

The various effects enumerated, which are all unfavorable for a reactor having a relatively large cell radius (ZOE) make it possible to interpret the difference observed between the computed reactivities of the two reactors, as was shown by a coarse estimate on the orders of magnitude of these effects. We hope that systematic exponential experiments will make it possible to determine quantitatively the effects due to the interaction of the rods, in particular those having to do with ϵ and L^2.

DISTRIBUTION OF THE THERMAL NEUTRON FLUX INSIDE THE CELL

In order to improve on the computation method, a study of the distribution of the thermal neutrons in a cell was initiated. Preliminary measurements using the autoradiograph technique have already been the subject of publications.[4] The measurements were continued by P. Zaleski, using a new design which gives a better detector arrangement, with a reduction of the air layer which surrounds the detector as it enters the uranium, and which affords the possibility of changing the uranium rod diameters under study.

The detectors used were manganese films prepared under vacuum, each less than one micron thick. In order to obtain exclusively the thermal neutron distribution simultaneous exposure was made of two detectors, one without a filter, and the other one surrounded by cadmium.

The cell under study can be idealized in the following manner: the cylindrical uranium rods of radius a, clad in an aluminum tube having a mean radius c, with the tube closed on one end.

In order to carry out the measurements, this sample was placed in the hole ordinarily occupied by the central rod of the Châtillon reactor thereby producing a cell made up of U-Al-air-Al-D_2O. The height of the cell is 150 cm. The study of the flux distribution is

Table III

	ZOE	P2	
$10^4\kappa^2$	7.9 ± 0.4	5.5 ± 0.15	
	1.0384	1.0286	
p	0.9177	0.9148	
	0.9805	0.9470	
		*	†
L_r^2	141	150	159
L_z^2	141	150	169
L_{ar}^2	117	147	153
L_{az}^2	117	147	159
$10^4\kappa_r^2 = \frac{j^2}{R_e^2}$	4.6 ± 0.4	3.3 ± 0.1	
$10^4\kappa_r^2 = \frac{\pi^2}{H_e^2}$	3.3 ± 0.1	2.2 ± 0.1	
$k_\infty = (1 + L_r^2\kappa_r^2 + L_z^2\kappa_z^2)(1 + L_{ar}^2\kappa_r^2 + L_{az}^2\kappa_z^2)$	1.214 ± 0.010	1.170 ± 0.005	1.183 ± 0.005
$\eta = \frac{k_\infty}{\epsilon p f}$	1.299 ± 0.010	1.313 ± 0.005	1.327 ± 0.005

* L^2 and L_a^2 computed by the elementary method † L^2 and L_a^2 computed from the Behrens formulae

carried out along a direction perpendicular to the axis of the cell.

The arrangement described above makes it possible to cause a to vary (5 values), which entails a variation of a' (with the thickness of the aluminum remaining constant and equal to 1 mm), as well as $c - a'$, the thickness of the air layer (c remaining constant and equal to 3.4 cm).

Various studies and experiments are under way, in order to observe the effects of changing other geometric parameters so as to introduce other material and to obtain a distribution of the neutron flux at energies other than thermal.

The results achieved up to this day are summed up in Table IV.

Table IV

a (cm)	$c - a'$ (cm)	N_M	N_{exp}	κ (cm^{-1})
0.5	2.8	0.76	0.86 ± 0.15	1.34 ± 0.15
0.75	2.55	0.68	0.85 ± 0.08	1.18 ± 0.07
1	2.3	0.60	0.80 ± 0.07	1.05 ± 0.05
1.5	1.8	0.43	0.46 ± 0.05	0.97 ± 0.04
1.75	1.55	0.33	0.44 ± 0.05	0.95 ± 0.03

Let $n(r)$ be the neutron flux at a distance r from the axis and $\bar{n}$ the mean flux in uranium. According to the elementary theory $n(r)$, is, in the uranium, of the form $n(r) = AI_0(\kappa_0 r)$. Retaining this analytical form, it is possible to adjust the Laplacian operator κ_0 so as to obtain for the ratio $n(a)/\bar{n}$ (which enters into the computation of the thermal utilization factor) a value which allies with experimental findings. κ_0 then will be determined by the relationship:

$$\left(\frac{n(a)}{\bar{n}}\right)_{exp} = \frac{\kappa_0 A I_0(\kappa_0 a)}{2I_1(\kappa_0 a)}$$

Table IV shows that the values of κ_0 obtained in this fashion vary a great deal with a. Figure 3 shows the experimental curves, $n(r)$ and the relevant $AI_0(\kappa_0 r)$ curves, which normally correspond to condition $n(a) = AI_0(\kappa_0 a)$.

Calculations were carried out using the spherical-harmonics method for a graphite cell, without any aluminum. The radius a of the uranium rod was kept constant and equal to 1.3 cm. The thickness $(c - a)$ of the air layer was made to vary between 0 and 2.2 cm. The values of κ_0 obtained with the P_5 approximation do not vary much with c; in fact they remain close to 1, which is in good agreement with the value derived above by interpolating between the results obtained for $a = 1$ and $a = 1.5$ cm.

The curves in Fig. 4 give, for the various possible cases, the distribution of thermal neutrons in uranium, aluminum and air. A notable variation of the flux in air can be observed; this effect is given by the quantity:

$$N = -\frac{n(c) - n(a')}{aJ(a')}$$

where $J(a')$ is the magnitude of the current at point a'. The elementary theory leads to $N = 0$.

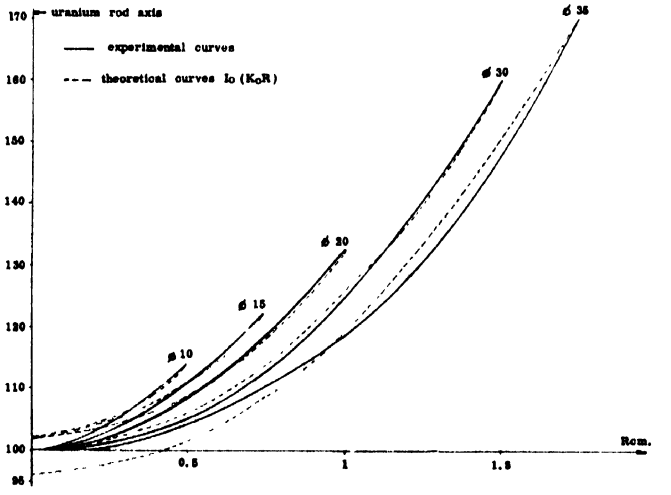

Figure 3

It is of interest to compare the experimental values in Table IV with the quantities N_M, given by an approximate formula developed by C. Mercier:

$$N_M = 1 - \frac{2\varphi_0}{\pi} - \frac{\sin 2\varphi_0}{\pi}$$

where

$$\sin \varphi_0 = \frac{a'}{c}$$

In order to prove this formula, it is necessary to make a hypothesis concerning phase density $D(r, \theta, \varphi)$ at the boundary of the cladding for the neutrons which pass into the air. Indeed, allowing for the straight-line propagation of the neutrons in the gas, it is possible to write rigorously the following formula:

$$J(a) = 2v \int_0^{\pi} \sin^2 \theta \, d\theta \left[\int_0^{\pi/2} D(a, \theta, \varphi) \cos \varphi \, d\varphi + \frac{c}{a} \int_{\pi - \varphi_0}^{\pi} D(c, \theta, \varphi) \cos \varphi \, d\varphi \right]$$

It is then assumed that the angular dependence of the neutrons which emerge from the uranium and moderator is well represented by the first two spherical harmonics:

$$D(r, \theta, \varphi) = \frac{1}{4\pi} \left[n(r) + 3 \frac{J(r)}{v} \sin \theta \cos \varphi \right]$$

By putting this expression into the accurate formula, the indicated result is achieved. In fact, this result is more general, and only presupposes that

$$D(r, \theta, \varphi) = \frac{1}{4\pi} \left[n(r) + \frac{3J(r)}{v} f(\theta) \cos \varphi \right]$$

$f(\theta)$ is an arbitrary function, except that it must fulfill the formulae which relate density and current, i.e.,

$$\int_0^{\pi} \sin^2 \theta f(\theta) \, d\theta = 1$$

Comparison of the values N_{exp} and N_M shows adequate agreement, but the values computed are systematically too low. However, the computation of this same quantity, when made with the P_5 method for the values of the radii indicated above, gives values which are clearly distinct, particularly for the small cladding thicknesses. This matter is still under study.

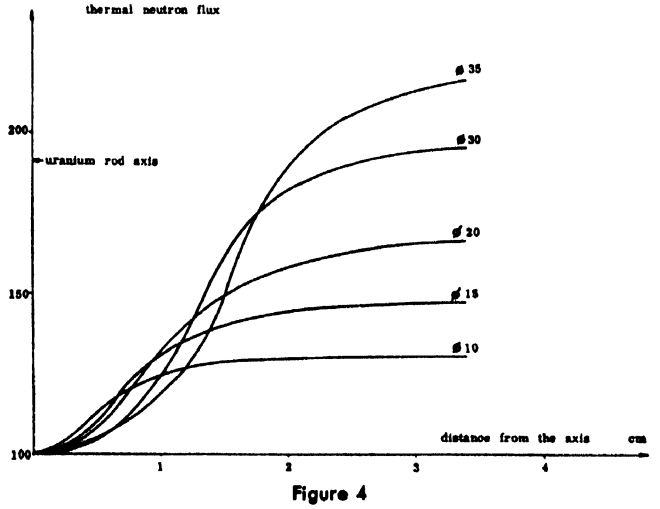

Figure 4

VARIATION OF THE REACTIVITY WITH HEAVY-WATER LEVEL

When the pile is critical for a given height of heavy water H_c, an increase δH_c in the water level brings about a δK_e increase in reactivity. The knowledge of quantity $\delta k_e/\delta H_c$ is of great practical importance. Many effects which modify the reactivity (xenon effect, temperature, etc.) are indeed compensated for and detected by a variation of the moderator level. On the other hand, it is of interest to compare the measured values of $\delta k_e/\delta H_c$ with the theoretical findings.

Experimental Determination

A measurement of $\delta k_e/\delta H_c$ was carried out on the Châtillon reactor by A. Ertaud and R. Beauge, and on the Saclay reactor by J. Bernot and V. Raievski, by the classical method using the formula of Nordheim for a heavy-water reactor. This formula, which correlates the excess of reactivity with the reactor period, has been verified experimentally by V. Raievski for the Saclay reactor (see below). The results are summarized in Table V.

Comparison with Theory

The simplest method of computation is obtained by replacing the complete reactor by an unreflected one of radius R_e (extrapolated radius) and height H_e. It can be used within the framework of a one-group or two-group theory, or of the age-velocity theory. In the two-group theory we may write

$$\kappa^2 = \frac{\pi^2}{H_e^2} + \frac{2.405^2}{R_e^2}$$

and

$$\frac{\delta k_e}{\delta H_e} = \frac{2}{H_e} K$$

$$\kappa = \frac{\pi^2}{H_e^2} \left\{ \frac{L^2}{1 + L^2\kappa^2} + \frac{L_s^2}{1 + L_s^2\kappa^2} \right\}$$

$$\simeq \frac{\pi^2}{H_e^2} M^2 \frac{1 + 2\frac{L^2 L_s^2}{M^2} \kappa^2}{1 + M^2\kappa^2}$$

The results obtained by the application of the above formulae give the relative variation with the heavy-water level which is in good agreement with the experimental results obtained for the Saclay reactor (supposing $\delta H_c = \delta H_e$), but it is found that the value of M^2 which should be taken in this case is $M^2 = 412 \text{ cm}^2 \pm 30 \text{ cm}^2$, a value substantially too large.

It is necessary, therefore, to allow for the presence of the reflector. A computation with the two-group theory was made by P. Tanguy, allowing separately for the vertical and the lateral reflectors.

For the one-group theory computation, in which the formulae are easy to handle, the corrections due to

Table V

	Châtillon reactor	Saclay reactor			
Heavy-water height H_c (mm)	1410	1800	1870	1899	2149
Extrapolated height H_e (mm)	1720	2240 ± 30			
$\frac{\delta k_e}{\delta H_c}$ (10^{-5}/mm)	9.6	6.6 ± 0.3	5.8 ± 0.3	5.7 ± 0.3	4.2 ± 0.3

the interaction of the reflectors and to the presence of a heavy-water blanket between the multiplying region and the vessel can be estimated.

In a computation of this type, the change δk_∞ which has to be made in the multiplication factor k_∞ of the pile has to be applied in such a way that it remains critical once the level is changed by an amount δH_c. For an unreflected reactor, the variation of reactivity δk_e is equal to the ratio $\delta k_\infty / k_\infty$. This no longer applies rigorously to a reactor with a reflector.[5] There is a correction factor, due to the fact that the neutron flux of a divergent chain reaction is no longer proportional to the critical flux, when the reactor is reflected.

Nevertheless, the presence of delayed neutrons considerably increases the period of the reactor for a given excess reactivity, and the correction factor becomes negligible for the value of δk_e which we will consider here.

Finally, we obtain a relationship of the form:

$$\frac{\delta k_e}{\delta H_c} = \frac{2}{H_e} K(1 + \epsilon)$$

in which ϵ is a factor giving the correction due to the reflector, which does not depend much on the values ascribed to the constants L^2, L_s^2, etc. in the multiplying region and which is equal to 0.17 for the Saclay reactor and 0.18 for the Châtillon reactor. In the latter case, an important part of the ϵ effect, about a quarter, is due to the presence of the heavy-water blanket.

Evaluation of Migration Area M^2

By taking the experimental values of $\delta k_e / \delta H_c$ it becomes possible to compute the value of coefficient K at a given level for each reactor. By going back to the equation for κ, it will be seen that it is possible to derive an approximate value of M^2 from it, if one assumes that L^2 and L_s^2 are close to each other, which is the case for both the two reactors.

For the Saclay reactor, one must allow for an anisotropic effect due to the cooling channels; that is one must discriminate between a diffusion length and a moderation length which are different along the axis of the reactor and along the direction perpendicular to it. One can write:

$$L_s^2 = L_r^2(1 + \gamma \times 10^{-2})$$

$$L_{ss}^2 = L_{sr}^2(1 + \gamma \times 10^{-2})$$

γ (expressed in per cent) represents anisotropy.

The following results are obtained:

Châtillon reactor

$$M^2 \simeq 230 \text{ cm}^2$$

Saclay reactor

$$M_s^2 = (352 - \gamma) \pm 25 \text{ cm}^2$$

EXPERIMENTAL VERIFICATION OF THE NORDHEIM FORMULA

The Nordheim formula makes it possible to establish the correlation between excess reactivity $(k_e - 1)$ and the period τ of the reactor. This relation can be written in the following form:

$$k_e - 1 = \frac{\bar{\theta}}{\tau} + k_e \sum_i \frac{P_i \beta_i \tau_i}{\tau + \tau_i}$$

$\bar{\theta}$ is the mean duration of a cycle, namely the mean lifetime of the neutrons in the reactor, allowing for the presence of the reflector. τ_i, β_i and P_i, respectively, are the lifetime, the abundance and the geometric factor which correspond to the delayed neutrons of species i. For the photoneutrons, β_i is defined in the case of a source of U^{235} in an infinite heavy-water medium; P_i is the probability that the γ-rays have of being absorbed by heavy water. For P_i, a value is taken of 0.25. For the delayed fission neutrons, there is no geometry effect and $P_i = 1$. The values of Hughes, Dabbs, Cahn and Hall[6] were adopted for the delayed fission neutrons, and the values of Johns M. W. and Sargent B. W.[7] for the photoneutrons.

It should be noted that the multiplication of prompt neutrons emitted from fast fission, a phenomenon which does not involve the delayed neutrons, whose energy is less than the fast fission threshold, suggests that a value be taken for β_i differing from the experimental figure. The correction factor was computed for the Saclay reactor by J. Bussac and V. Raievski, and found to be equal to +2.3 per cent.

Finally, for those periods which can be readily measured experimentally, from a few seconds to 10,000 seconds, the term $\bar{\theta}/\tau$ is negligible.

The purpose of the two experiments which we shall describe is to test the validity of this formula as an absolute standard of reactivity measurement.

In both cases, we have to compare the value of the excess reactivity, as computed from the Nordheim formula by measuring a rising period, with the direct measurement of the excess reactivity. The first experiment is less accurate since the influence of the short-period delayed neutrons cannot be considered a small correction. The second, on the contrary—namely the modulation—is very accurate, for its determination requires only a knowledge of the total fraction, β, of delayed neutrons.

Table VI

Initial position	*20 cm*	*15 cm*	*10 cm*
τ (seconds)	13.75 (±2%)	24.00 (±2%)	49.76 (±1%)
δk_e (Nordheim) (10^{-5})	265 (±1%)	200 (±1%)	130 (±1%)
$A_{0\ exp}$	2.11 ± 0.06	1.93 ± 0.05	1.60 ± 0.05
$A_{0\ theo}$	2.093 ± 0.004	1.82 ± 0.005	1.537 ± 0.005

Transient Conditions (J. Bernot and V. Raievski)

A sudden unknown increase δk_e is made in the reactivity of the reactor. The variation of the flux as a function of time is recorded during the first seconds which follow the gain in reactivity. The measurement of the rising period, τ, gives, according to the Nordheim formula, the value of δk_e. Knowing δk_e, the instantaneous flux variation can be computed, allowing for the influence of the delayed neutrons, and this value can be compared with the experimental figure. More accurately, the flux increases, as a function of time, according to

$$Y = \frac{\phi}{\phi_0} = A_0 e^{\frac{t}{\tau}} + \sum_i A_1 e^{-\lambda_i t}$$

From an experimental measurement of Y, we can derive

$$A_0 = \frac{Y e^{-\frac{t}{\tau}}}{\epsilon(t)}$$

in which $\epsilon(t)$ is a function which does not depend strongly on δk_e, but does depend on the values, chosen for the β_i and τ_i ascribed to the short-period delayed neutrons. It follows that the experimental values of A_0 are not too accurate since the corrections made necessary by the delayed neutrons and represented by function $\epsilon(t)$, are not small.

Experimental Arrangement

At the center of the reactor, we set up two concentric cadmium cylinders. The outside cylinder, which is fixed, is 21 cm in length. It completely covers the inside cylinder, which is movable and 20 cm long in its lower position, and is constantly restrained by a powerful spring. Three stops afford the possibility of keeping the cylinder 25, 15, or 10 cm withdrawn. For each of these positions, the reactor is stabilized to a power of a few watts, so that its reactivity is all but nonexistent. The inside cylinder is then released. It reaches its lower position in approximately fifty milliseconds. A two-spot oscillograph which is photographed with a camera using a film moving at a constant speed receives on its screen the impulses from a 1000 cycle/sec generator used to measure time, an impulse which gives the zero time at which the cylinder reaches its low position and an impulse for every 100 counts, as measured by a counter placed beside the reactor vessel.

ϕ_0 can be determined with accuracy from a sufficiently prolonged initial count. A second counter, placed in the reflector, makes it possible to measure the period of the divergent exponential and thus to determine δk_e (Nordheim).

The results are summed up in Table VI, which shows good agreement between the experimental results and the computation.

Reactivity Modulation (V. Raievski)

This method was designed to measure the average lifetime, $\bar{\theta}$, of the neutrons in the reactor. It also provides a means of measuring the reactivity. The value obtained depends only on the total fraction, β, of delayed neutrons, and the values β_i and τ_i ascribed to the various delayed neutron groups which enter into the results only in the form of rather small correction factors.

The reactivity of the reactor is varied periodically by inserting, into the axial channel, a cadmium cylinder with a periodically varying surface. By using the subcritical method, it is possible to measure the amplitude of the variation of the reactivity with respect to a reference standard which is equal to the value of the effect of a given heavy-water variation with respect to a known critical level by making use of the Nordheim formula.

On the other hand, a measurement is made of the amplitude and phase of the modulation of the neutron flux as a function of the modulation frequency. At time t, let the reactivity value be $\delta k_e e^{i\omega t}$. The fundamental solution of the kinetic equations gives for the density modulation:

$$\frac{\delta n}{n} = \delta k \frac{1 - i\omega \sum_i \frac{\beta_i \tau_i}{1 + i\omega\tau_i}}{i\omega\left(\bar{\theta} + \sum_i \frac{\beta_i \tau_i}{1 + i\omega\tau_i}\right)}$$

If we write:

$$\epsilon_1 = \frac{1}{\bar{\theta}} \sum_i \frac{\beta_i \tau_i}{1 + \omega^2 \tau_1^2};$$

$$\epsilon_2 = \frac{1}{\beta} \sum_i \frac{\beta_i}{1 + \omega^2 \tau_1^2};$$

$$z = \frac{1}{(1 - \epsilon_2)^2} \left| \frac{n}{\delta n} \right|^2$$

$$\eta = \omega^2 \left(\frac{1 + \epsilon_1}{1 - \epsilon_2} \right)^2$$

At sufficiently high frequencies ϵ_1 and ϵ_2 are only small corrective terms. We can then write

$$z = \frac{\beta^2}{\delta k^2} + \frac{(\bar{\theta})^2}{\delta k^2}\eta$$

By measuring z as a function of η, it is possible, knowing β, to determine $\bar{\theta}$ and δk.

Experimental Arrangement

An aluminum cylinder is covered with two cadmium bands having an opening of 90 degrees, diametrically opposed. The cylinder rotates inside another fixed cylinder of identical design. The device is placed in the axial channel of the reactor. Computations show that the modulation of the reactivity as a function of rotation angle φ is given by the relationship

$$\Delta k = \Delta k_0 \frac{2}{\pi}\left\{\frac{\pi + 2\varphi}{4} - 1 + \sqrt{2}\cos\frac{\varphi}{2}\right\}$$

which has been checked exactly by subcritical experiments.

The modulation of the density is measured with a parallel-plate ionization chamber covered with B_4C and a dc amplifier which has total negative feedback. The band transmitted by the detection system is measured by modulating the flux of neutrons received by the chamber with the help of a cadmium filter. For an electric field of more than 1000 v/cm in the chamber, the transmitted band extends to 100 cycles/sec. The signal is demodulated by a contact ring which rotates synchronously with the cylinder. The angle of the brushes makes it possible to select the phase of the signal. In order to eliminate the effect of reactor drift and amplifier drift, both half cycles are demodulated. The contribution of various harmonics to the measured signal does not exceed 1.5% of the value of the fundamental.

Experimental Results

The subcritical method, using Nordheim's formula, gives

$$\delta k = 44 \times 10^{-5} \pm 2.5 \times 10^{-5}$$

The modulation method, for frequencies varying from 0.15 to 25 cycles/sec gives

$$\frac{dk}{\beta} = 0.058 \pm 0.001$$

from which one obtains, by taking $\beta = 800 \times 10^{-5}$ (including the photoneutrons):

$$\delta k = 46.5 \times 10^{-5} \pm 1 \times 10^{-5}$$

These results are in good agreement.

AVERAGE LIFE OF THE NEUTRONS IN A REACTOR

In a thermal reactor, the average lifetime of the neutrons, $\bar{\theta}$, is defined as being the average time needed for prompt neutrons issuing from a thermal fission to bring about a new thermal fission. This is the same value $\bar{\theta}$ which comes into Nordheim's formula, but, for the usual rising period measurements it appears only as a correction term. The accurate measurement of $\bar{\theta}$ is none the less a very interesting one from the theoretical standpoint.

The measurement was carried out for ZOE and P2 by V. Raievski. The experiment has already been described above. As shown earlier the measurement of z as a function of η makes it possible to determine $(\bar{\theta})^2/\beta^2$. Knowing β, one can then determine $\bar{\theta}$.

ZOE

$$\frac{\bar{\theta}}{\delta k} = 2.62 \pm 0.06$$

$$\frac{\delta k}{\beta} = 0.045 \pm 0.001$$

By taking $\beta = 800 \times 10^{-5}$, one can obtain

$$\bar{\theta} = (0.95 \pm 0.03) \times 10^{-3} \text{ sec}$$

$$\delta k = (36 \pm 1) \times 10^{-5}$$

P2

$$\frac{\bar{\theta}}{\delta k} = 2.15 \pm 0.04$$

$$\frac{\delta k}{\beta} = 0.058 \pm 0.001$$

By taking $\beta = 800 \times 10^{-5}$, one gets:

$$\bar{\theta} = (1.00 \pm 0.02) \times 10^{-3} \text{ sec}$$

$$\delta k = (46.5 \pm 1) \times 10^{-5}$$

The interpretation of this experiment presupposes that, except in the vicinity of the absorber, the distribution of the modulated flux is proportional to that of the stationary flux. This hypothesis appears to be borne out by the fact that, within the limit of experimental errors, the relationship between z and η is truly linear, up to a frequency of 25 cycles/sec. For high frequencies, there is departure from the linear law. In this realm, the phenomena are best described by the propagation of neutron waves. For the phase of $\delta n/n$, this propagation effect already begins to be at frequencies as low as 10 cycles/sec.

Conversely, in the region of very small frequencies (less than 0.15 cycles/sec), the factors which depend on β_i and τ_i ascribed to the various species of delayed neutrons are no longer correction terms, and would bring in additional errors if the determination of $\bar{\theta}$ were made in this range of frequencies.

The experimental values given above are clearly higher than the average life computed for an unreflected reactor equivalent to ZOE and P2. One finds indeed, by using a two group theory that $\bar{\theta} = 0.71 \times 10^{-3}$ sec for ZOE and $\bar{\theta} = 0.76 \times 10^{-3}$ sec for P2. The difference is due to the presence of the reflector, which can be allowed for by computations similar to those mentioned earlier. These computations give a correction on the order of 30 per cent, which is in good agreement with the experience.

NEUTRON SPECTRUM OF THE SACLAY REACTOR

The neutron spectrum from the vessel of the Saclay reactor was studied using a time-of-flight spectrome-

ter by M. Galula, B. Jacrot and F. Netter, of the Nuclear Physics Department.

The detector used is a proportional counter which operates on enriched boron fluoride. Its efficiency as a function of the time of flight is $1 - e^{-400t}$ (t in seconds per meter).

The curve in Fig. 5 shows the neutron density as a function of energy, E, for constant channel width, as measured for the neutron-beam emerging from the reactor vessel in a direction normal to the wall.

$$\Delta n = \frac{dn}{dt}\Delta t$$

$$= \frac{dn}{\Delta\lambda}\Delta\lambda$$

where $\Delta\lambda$ represents the constant channel width, in wavelengths. This curve is obtained from experimental counting rates by correcting them for the departure from a $1/v$ law of the efficiency of the counter; and the air transmission from the vessel.

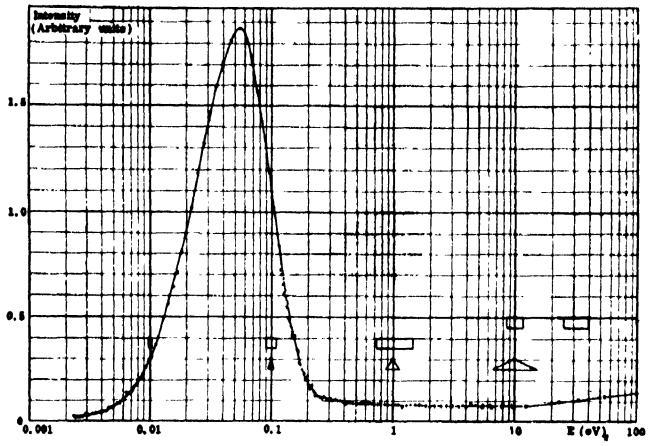

Figure 5. Neutron spectrum coming out of the vessel

Between 0.5 and at least 10 ev, the spectrum is represented by a horizontal line, which, in the coordinates chosen, gives the dE/E distribution law characteristic of the asymptotic energy distribution of the neutron flux during the slowing-down process.

In the thermal region, the spectrum is nearly Maxwellian, about the equilibrium temperature of 323°K. This is obtained from a comparison of the experimental spectrum corrected for air transmission with a spectrum computed from Maxwell's law (Fig. 6). This temperature, 323°K, is very closely identical to that of the heavy water in the moderator.

The characteristic parameter, for each Maxwell curve, is the time of flight for neutrons at the equilibrium temperature. Among the curves tried out, which correspond to various values of this parameter, that which gives the best agreement corresponds to an equilibrium temperature of 323 ± 15°K. The error is due in part to the errors inherent in the computation, (5 degrees approximately); the rest comes from uncertainties in the calibration of time and energy.

It will be noted that, on the curve shown in Fig. 5, the abscissa of the maximum is 0.056 ev, namely twice the energy kT which corresponds to the equilibrium temperature.

EFFECTS OF TEMPERATURE ON REACTIVITY

It is advisable to look separately into the effects, on reactivity, of the temperature of the uranium and moderator, the temperature effect of the moderator being greater in the case of the heavy water-reactor.

Temperature Effect of the Uranium

This was measured by V. Raievski in the case of P2, by using the following methods. Progressively increasing the level of the heavy water gave the reactor an excess reactivity which was a linear function of time, $k_1 = at$. The power P of the reactor increased, as well as maximum temperature T of the uranium, bringing about a loss of reactivity due to the temperature effect $\delta k_2 = -(T - T_0)$. The initial temperature and power were $T_0 = 18°C$, $P_0 = 200$ kw. The reactor rapidly reached a condition which was characterized by a linear variation of T with time: $T = (a/\beta)t +$ constant. From the measurement of a/β, one derives, for the temperature coefficient of uranium in P2, the value:

$$\beta = (1.25 \pm 0.25) \times 10^{-5}/°C$$

During this experiment, which lasted five minutes, the temperature T increased from 18°C to 78°C, the power from 200 kw to 500 kw.

In the case of ZOE, the measurement was made by R. Beauge, by giving the reactor a sudden increase in reactivity δk. In this case, the power of the reactor first increases, then decreases. At the maximum, the temperature effect exactly compensates δk. By measuring the temperature increase of the uranium and heavy water, and by allowing for the temperature effect of D_2O (which is a correction), we obtain, for the temperature coefficient of uranium:

$$\beta = (1.08 \pm 0.15 \times 10^{-5}/°C)$$

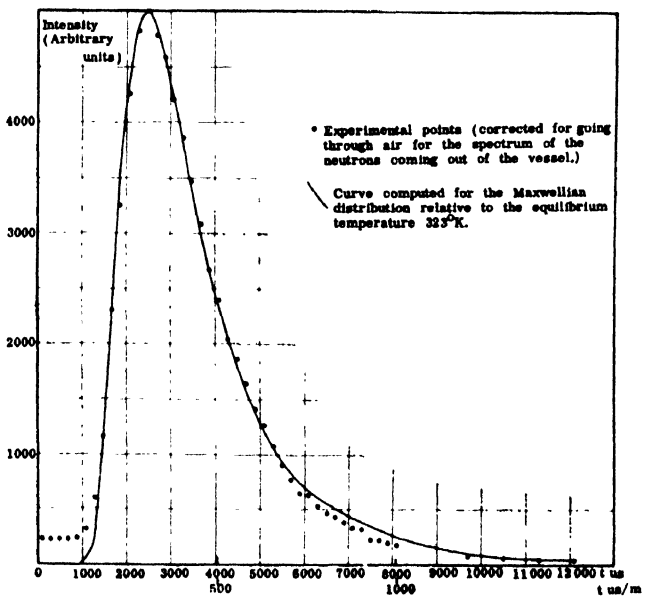

Figure 6. Maxwellian spectrum representative of the experimental spectrum of the neutrons coming out of the vessel

The uranium temperature is measured at the hottest point.

These two determinations of β (which are not too accurate) serve principally to give us a correction term for the measurement of the temperature coefficient of heavy water.

Temperature Effect in Heavy Water

This was measured for P2, by V. Raievski, by increasing the temperature of the lattice by circulating carbon dioxide heated by the compression of the blowers. The power was maintained constant at 800 w, the loss in reactivity due to the temperature effect was constantly compensated for and measured, by an increase in the level of the heavy water. Following deduction of the temperature effect of the uranium, we obtain for a variation of reactivity δk due to temperature variation, δT, of heavy water ($17° < T < 41°$):

$$10^5 \frac{\delta k}{\delta T} = -(11.7 \pm 0.6) - (0.35 \pm 0.04)(T - 11.3)$$

It is apparent in this formula that the temperature $T_0 = 11.3°C$ corresponds to the maximum of density of heavy water and that the variation of $\delta k/\delta T$ with T must be ascribed to the non-linear variation of the density of heavy water with the temperature. On the right-hand side of the expression, the first term would thus represent the effect of the increase of the neutron temperature on the reactivity, while the second term would show the effect of the variation of the moderator density.

For ZOE, the measurement was carried out by A. Ertaud and R. Beauge in the following manner. The reactor was operated for one night at 100 kw, in which case the heavy water had attained a temperature of 45°C.

The reactor was then shut down to cool off, and the temperature of the heavy water allowed to decrease from 45 to 10 degrees. Measurements were made at regular intervals, of the reactivity of the reactor, noting the temperature.

After correcting for the uranium effects, the results obtained were:

$$10^5 \frac{\delta k}{\delta T} = -(14.2 \pm 1) - (0.33 \pm 0.06)(T - 11.3)$$

The temperature coefficient is the result of many effects. A computation was made (C. Mercier) allowing for the following factors: (*a*) the variation in density of heavy water with temperature; (*b*) the variation of the transport cross section of heavy water (the experimental curves of σ_{sc} suggest the value $(1/\sigma)(d\sigma/dT) \simeq -45 \times 10^{-5}$; and (*c*) the temperature variation of the various capture cross sections all of which were assumed to follow $1/v$ laws, except for U^{235}. For U^{235} the fission cross section measured at Saclay was used, and it was supposed that the effective radiative capture cross section was in a constant ratio to the fission cross section.

If it can be further assumed that the quantity ν for uranium is independent of the energy, the variation of η for natural uranium is given by

$$\frac{1}{\eta}\frac{d\eta}{dT} \simeq -7 \times 10^{-5}$$

Finally, the temperature of the thermal neutron distribution always has been made equal to that of the moderator.

The results obtained are:

$$\text{P2:} \quad 10^5 \frac{dK}{dT} = -18 - 0.23(T - 11.3)$$

$$\text{ZOE:} \quad 10^5 \frac{dk}{dT} = -16 - 0.21(T - 11.3)$$

Thus one obtains the order of magnitude of the coefficients measured. There still remains a significant difference which may arise from a lack of knowledge of the relevant physical quantities, from the inaccuracy of the computation, or from neglecting other significant effects.

XENON EFFECT

Experimental Determination

Poisoning by Xe^{135} has been the object of measurements carried out on P2 by J. Bernot. These measurements were spread over a week. The power of the reactor was about 800 kw, and was kept constant by varying the heavy water level. The temperature of the heavy water was some 37°C. From the excess reactivity δk, supplied by increasing the level of the water, we derive a reactivity variation δk due to the xenon effect making allowance for the temperature effects δk_0 and δk_1 of uranium and heavy water.

At equilibrium, for an average flux of $\phi = (0.95 \pm 0.13)10^{12}$ cm^{-2} sec^{-1}, the value found for δk was $10^5 \delta k = -470 \pm 35$.

Comparison with the Theory

If the neutron flux were uniform and equal to ϕ_0 the relative variations $\delta k_\infty/k_\infty$ and $\delta f/f$ of the infinite multiplication coefficient and the thermal utilization would be given by the expression

$$\frac{\delta k_\infty}{k_\infty} = \frac{\delta f}{f} = -\frac{\sigma_{Xe}\gamma\Phi_0}{\lambda + \sigma_{Xe}\Phi_0}\frac{\sigma_f}{\sigma_U}$$

in which σ_{Xe} = the absorption cross section of Xe^{135} for a reactor spectrum, λ = the disintegration constant of $Xe^{135} = 2.1 \times 10^{-5}$ sec^{-1}, γ = the fission yield in $Xe^{135} = 6.2$ per cent, and σ_f/σ_U = the ratio of the fission and absorption cross sections of natural uranium in a reactor spectrum = 0.544.

By allowing for a slight modification of the thermal neutron leakage we would have, for the case of a uniform flux, a reactivity change of $\delta k_0 = 0.93\ \delta k_\infty/k_\infty$.

Since the flux is not uniform, δk is different from δk_0. The non-uniformity correction given in the case of P2 for the flux under consideration is $\delta k = 1.38\delta k_0$.

By taking $\sigma_{X_e} = 3.5 \times 10^6$ barns, we have $10^5\delta k = -580 \pm 70$.

It should be noted that $\sigma_{X_e} = 3.5 \times 10^6$ barns[8] is the thermal cross section and not a cross section averaged over a Maxwellian spectrum. The measurement made by J. Bernot seems to indicate that the mean cross section, for a temperature of neutrons of the order of 37°C, is lower by approximately 20 per cent, than the published value. An older measurement, made by V. Raievski gave the same conclusion.

MISCELLANEOUS STUDIES ON THE SHIM PLATES AND CONTROL RODS

Calibration of the Shim Plates

The shim plates were first calibrated at a subcritical level by comparing the effect of the plate to that of the heavy-water level which, in turn, was measured by the period method. These measurements made it possible to draw curves giving the effect, on reactivity, of a given plate or sheet, as a function of its position. We felt it was necessary to measure this effect also at a high power, namely at the highest possible water level. The application of the method mentioned above would have required, in this case, in order to keep the reactor subcritical, that large quantities of absorbing material be introduced. This would modify the flux considerably, and the effect measured would not be that due to the plate at the same water level, but, rather at a high power and in the absence of absorbing material. In order to avoid these drawbacks a new method was designed by V. Raievski. In this method, we initiate low amplitude oscillations of the plate (1.7 cm) at a low frequency ($\sim$ 0.2 cycles/sec) and observe the amplitude modulation of the flux which results from it. This gives the effect on reactivity of a small displacement of the plate by direct reading, with an accuracy greater than that offered by the older method. The measurements carried out showed, in particular that the effect of the plate at a given position depends markedly on the water level. In connection with the control-rod problem, the effect of strong absorbers placed in the central channel of ZOE on its reactivity have been systematically studied by A. Ertaud and R. Beauge.

The measurements carried out with cadmium tubes (length equal to the height of heavy water = 150 cm; diameter: 10; 20; 28 and 45 mm; thickness: 7 mm) were compared with the results of computations made using the two-group theory where, for the thermal group, the extrapolation length formula given by Davison and Kushneriuk[9] was used. An agreement was found between the theory and the experiment.

Cadmium rods of various lengths (from $L = 10$ cm to $L = 150$ cm) and various shapes have been compared. We considered circular cylinders of diameter Φ, varying from $\Phi = 10$ mm to $\Phi = 50$ mm, plates having a thickness of 0.7 mm and a width, l, varying from $l = 10$ mm to $l = 50$ mm, and cross-shaped cylinders using two cross-shaped sections the arms of which had respective lengths of $a = 30$ mm and $a = 45$ mm.

In particular we were able to conclude from these experiments that, for lengths greater than 30 cm (where the end effects are small), the effect of rods of the same length on the reactivity depends only on their apparent diameter $\bar{D}$. More accurately, one considers the section of the rod and its apparent diameter $D(\bar{\Omega})$ for a direction $\bar{\Omega}$. $\bar{D}$ is the average of $D(\bar{\Omega})$ for all directions parallel to the plane of the selected cross section. In the case of cross-shaped, circular cylinders and of plates, $\bar{D}$ is respectively equal to

$$\varphi, \quad \frac{2a\sqrt{2}}{\pi} \text{ and } \frac{2L}{\pi}$$

This law also has been obtained by V. Raievski, who used a device built for the modulation experiments described earlier. By computing the reactivity variation as a function of the angle φ of the two cylindrical sectors according to the method described above, one obtains a reproduction of the experimental results to within a few per cent.

Other absorbing materials (B_4C, B_2O_3, LiCl powders) have been compared with cadmium. Let us mention, among the results obtained, that an aluminum tube having an internal diameter of Φ(15 mm $< \Phi <$ 40 mm) filled with B_4C powder (density $\sim$ 1.2) has an effect which is greater by some 13 per cent than that of a cadmium rod of the same diameter. Replacing the aluminum tube with a cadmium tube increases the effect only very slightly.

REFERENCES

1. Yvon, J., J. Phys. Rad. *12*, 5, p. 573 (1951).
2. Guggenheim, E. A. and Pryce, M. H. L., Nucleonics, *11*, 2, p. 50 (1953).
3. Behrens, Proc. Phys. Soc., *62*, 358A, p. 607 (1949).
4. Ertaud, A. and Zaledio, P., J. Phys. Rad. *14*, 191, (1953) and *15*, 75A (1954).
5. Rumsey, V. H., Can. J. Phys., *32*, 435.
6. Hughes, D. J., Dobbs, J., Cahn, A. and Hall, D., Phys. Rev., *73*, 11, (1948).
7. Johns, M. W. and Sargent, B. W., CRP-1116.
8. Nucleonics *10*, 5, p. 64.
9. Davison, B. and Kushneriuk, A., MT-214.

Exponential Experiments on D_2O-Uranium Lattices

By E. Richard Cohen,* USA

A program to investigate the basic physics of lattices of uranium metal rods in a heavy-water moderator has been carried out at North American Aviation, Inc. and, to a smaller extent, at Argonne National Laboratory over the last five years. The basic experimental programs have been limited to the consideration of rods of uranium from 0.75 inch to 2.00 inch in diameter. The lattice spacings were chosen to give ratios of moderator volume to uranium volume from 15 to 200. In all cases the lattice was a square array. Experiments at the two laboratories were coordinated and the design of facilities was planned so that inter-comparisons between laboratories could be made.

EXPERIMENTAL FACILITIES

The exponential experiments at Argonne and North American Aviation were both performed in an experimental tank driven by a thermal neutron flux coming from a graphite thermal column upon which the tank rested. The lattices to be tested were assembled in the tank and the tank was then filled with the D_2O moderator. In all cases the experiments were conducted in such a way that the test region would never become a self-sustaining reactor. If there was any doubt about this, measurements could be made as a function of moderator level in the tank to be sure that criticality would not be reached. (In a true exponential experiment—when the neutron density follows the exponential law $e^{-\nu s}$—criticality can not be attained at any moderator level.)

The experimental tank at Argonne was fabricated by forming and welding aluminum sheet, 0.25 inch thick, into a cylinder 5 feet in diameter and 6 feet high. The bottom of the tank was a standard dished end, 0.25-inch thick, welded to the side wall. The walls were reinforced by four 0.5-inch × 2.0-inch rings welded to the outer surface and spaced at one-foot intervals. Measurements of the tank, made after it was in final position, indicated that the internal diameter was constant to ±0.062 inch. The tank was closed at the top with a flat 1.0-inch thick aluminum cover plate which was bolted to the upper tank flange. A gas tight seal was insured by a ⅜-inch × ⅜-inch neoprene gasket. Access to the interior of the tank, for inserting and removing foils, was provided by a channel 3½-inch wide cut in the cover plate along a diameter. This channel was sealed with an aluminum cover plate and neoprene gaskets. Eight small secondary openings in the channel cover allowed additional access. These had individual gasketed aluminum cover plates which were held down with wing bolts.

The dimensions of the tank at North American Aviation were the same except for a flat rather than a dished bottom. The stiffening rings were omitted and minor modifications were incorporated into the design of the access openings in the top cover plate. The undersides of the top cover plate and of all hatches, as well as the outside surface of the experimental tank, were covered with a 0.030-inch thick cadmium sheet and a thin protective aluminum sheet.

At Argonne National Laboratory the experimental tank was mounted upon an extension of the CP-2 reactor thermal column which was carried upward to a point 2 feet above the top of the upper shield. The top of the upper shield thus became the floor of the exponential experiment room. The D_2O storage tank was placed on the main floor of the reactor building so that there was a difference of approximately 25 feet in the level of the two tanks. The storage tank was connected to the experimental tank by a two-inch stainless steel pipe line for draining and filling. After the system had been repeatedly flushed with dry helium, approximately 7000 pounds of D_2O were added. The height of the D_2O in the experimental tank was determined by observing the meniscus level in a sight glass 42 inches high on the outside of the tank. As a safety precaution, a lead pan 15 feet in diameter and 1 foot deep was placed at floor level in order to contain the D_2O in case of a leak and prevent it from flooding the reactor graphite.

The physical arrangement at North American Aviation was similar to that at Argonne; the main difference was in the neutron source. In the early part of the program five PoBe sources with a total neutron yield of 10^9 neutrons/second were used. These sources were placed 24 inches below the bottom of the experimental tank in a cylindrical graphite pedestal five feet in diameter and three feet high. The sources were arranged in a cross-shaped pattern with one source on the axis of the pedestal and the other four symmetrically positioned at a distance of approximately 17 inches from the pedestal axis. The central source was selected to be approximately 5 per cent stronger

* North American Aviation, Inc., Nuclear Engineering & Manufacturing, Los Angeles, California. Including work by A. H. Barnes, R. R. Haefner, B. Hamermesh, N. L. Krisberg, C. O. Muehlhause, B. I. Spinrad, Argonne National Laboratory; A. T. Biehl, E. R. Cohen, F. B. Estabrook, S. W. Kash, R. A. Laubenstein, D. H. Martin, D. C. Woods, North American Aviation, Inc.

than each of the four peripheral sources. In this way it was possible to remove several of the harmonics in the neutron distribution and obtain a flux which would provide a zero-order Bessel function distribution of neutrons at the bottom of the experimental tank. For "shutdown" the sources could be withdrawn from the graphite pedestal into individual cadmium-covered, borated-paraffin-filled boxes which were adjacent to the pedestal.

Because of the decay of the Po these sources had to be replaced after several months when the neutron levels in the experimental tank had decreased to values which were too low for accurate counting. The need for higher flux levels in order to investigate lattices with low multiplication could not be met with radioactive sources. Therefore, instead of continuing with the PoBe sources, a low-power homogeneous solution reactor (water boiler) was constructed to serve specifically as a neutron source for the exponential experiments.[1] From this source, operating at a level of only a few watts, it was then possible to obtain fluxes of the order of one hundred times larger than could be obtained with the PoBe sources. A general view of the water boiler and experimental tank is shown in Fig. 1. The concrete shielding blocks have been removed to show the water boiler tank. The water boiler core is imbedded in a five-foot diameter, six-foot high graphite pedestal which serves as reflector and thermal column. There is a minimum of 3 feet of graphite between the reactor core and the bottom of the experimental tank, which sits directly above the graphite pedestal. The dark bands around the tank are steel straps holding the cadmium sheet in position. The scaffolding on top of the shielding blocks is a working platform from which foil holders and fuel rods can be loaded into the tank.

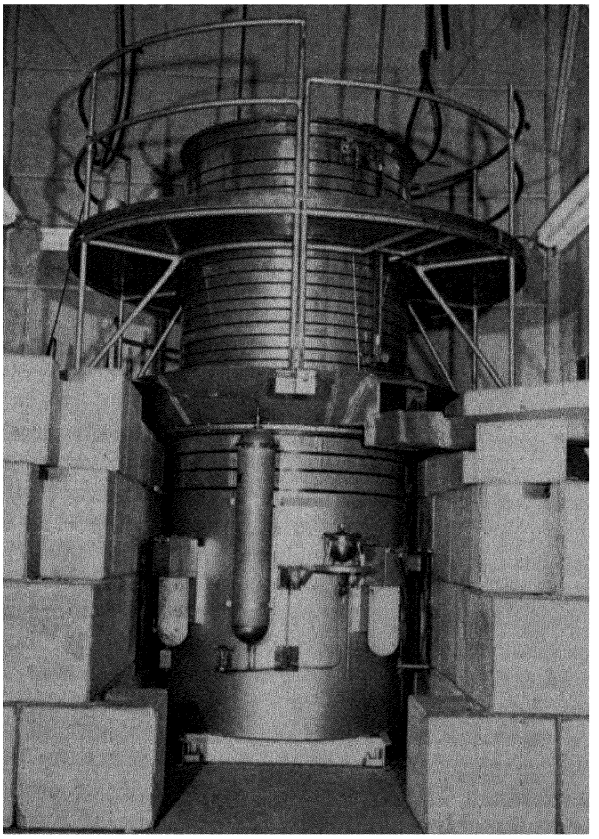

Figure 1. Water boiler neutron source and exponential tank assembly

NEUTRON DETECTION EQUIPMENT

For most purposes indium-foil detectors were used to explore the neutron density in the multiplying medium. Indium foils 1 cm × 1 cm and weighing 100 mg were used by the North American Aviation group while somewhat smaller circular foils were used at Argonne. Each foil was placed in a cadmium or aluminum shell, or "box," 0.05 cm thick. The cadmium boxes were thick enough to be practically opaque to thermal neutrons; the aluminum boxes were transparent to neutrons and were used as foil supports and to facilitate interchange between the cadmium-covered and "bare" foil positions. For measurements inside the uranium and for detailed flux maps in the moderator small gold foils proved to be more useful. It was possible to punch these foils to a size of 0.2 × 1.0 cm and 0.012 cm and still maintain reproducible weight to within 0.5 per cent as measured by neutron activation in a standard flux. Each foil was counted for 10,000 counts or a maximum of 29 minutes on three different Geiger counters using standard scaling and counting circuits.

In comparing the activity among the foils no calibration in a standard neutron flux was made. This was justified experimentally since no difference in activity was found, within statistical counting accuracy, when different foils were exposed in the same neutron flux. However, care was taken to select sets of foils having the same area and the same weight. Several sets, each consisting of twenty-five matched foils, were prepared.

In measurements of over-all lattice "buckling" two light aluminum foil holders were used. One holder, for vertical traverses through the lattice, had slots every 5 centimeters. This was supported inside a thin-walled aluminum tube 3.5-cm diameter which in turn was held in position on the axis of the tank by two aluminum grids. The horizontal foil holder had slots at positions corresponding to the centers of the lattice cells and to positions midway between these centers. There was a different horizontal foil holder for each different lattice spacing so that foils could be positioned at the center of the lattice cells or at points half way between these centers. The horizontal foil holder was supported at each end by a vertical aluminum rod just inside the tank wall, and its vertical position could be adjusted by means of pins which passed through these supports.

MEASUREMENT AT NORTH AMERICAN AVIATION

The purpose of the exponential experiment is the measurement of B^2, the "buckling" of the neutron distribution. In the exponential tank the gross neutron distribution can be approximated by the form

$$\phi(r,z) = AJ_0(\mu r) \sinh \nu(h - z) \qquad B^2 = \mu^2 - \nu^2 \quad (1)$$

where h is the effective height of the exponential tank and $(2.4048)/\mu$ is its effective radius. Neither of these quantities can be determined directly from the geometry of the tank, however, because of the impossibility of defining experimentally a boundary which is black to neutrons of all energies. The effective height and effective radius must therefore be determined by fitting the observed neutron distribution to the assumed analytic form. Hence measurements of the neutron density along the axis of the tank and along a radius will permit one to calculate B^2. There are, of course, several complications involved in the measurement. The major effects are the periodic structure of the medium which requires that measurements be made at equivalent points in each lattice cell, transient effects due to the boundary between the thermal column and the active lattice, and the existence of distributed extraneous sources which do not follow the form of Equation 1. These sources arise from photoneutron production in the heavy water, direct fast neutrons from the neutron source, or fast neutron back-scatter from the walls of the laboratory. The following outline of experimental procedures will indicate the corrections required.

On most lattices four types of exposures are made for each lattice: (1) bare foil axial exposures, (2) half-cadmium axial exposures, i.e., alternate foils were cadmium covered, the others were bare, (3) bare radial exposures, and (4) cadmium-covered radial exposures.

Saturated activities for each foil were calculated in the usual way from counter readings and the known exposure time, wait time, count time, counter dead time and background counting rate. All activities on a single run were counted on three to six counters; since absolute values of flux were not required, data from each counter was handled separately and laborious cross normalization was thereby avoided.

To obtain the thermal neutron activity at a given point it is necessary to subtract the epithermal activity from the total bare foil activity. Let A_B and A_{cd} represent the saturated activities for bare and cadmium-covered foils, then the thermal neutron activity is given by

$$A = A_B - CA_{cd} \tag{2}$$

where the constant C depends upon the thickness of the indium foil and the cadmium cover. For 100 mg/cm^2 foils and 0.05-cm cadmium, $C = 1.07$.[2] Accordingly the ratio of thermal to epithermal activity is given by

$$R = A_{th}/1.07A_{cd} \tag{3.1}$$

and

$$A_{th} = \frac{R}{R+1} A_B \tag{3.2}$$

Normally two separate measurements are required to determine A_{th}. However, counter sensitivity normalizations are avoided by exposing bare and cadmium-covered foils at the same time and counting on the same counters. Data from each counter is plotted and the value of R is read from the graphs. The average value of R from the several counters is then used to compute A_{th}.

The thermal neutron flux along the axis of the tank requires the fitting of three parameters A, ν, and h, of which ν is of primary interest. Initially the fitting was done analytically by least squares, but adequate accuracy is obtainable graphically if approximate values of A, ν, and h are assumed and the deviations from the approximate function are plotted. Thus, instead of plotting ϕ directly one considers

$$y(z) = \frac{\phi - A_0 \sinh \nu_0(h_0 - z)}{A_0 \cosh \nu_0(h_0 - z)}$$

$$\approx \frac{\delta A}{A_0} \tanh \nu_0(h_0 - z) + (h_0 - z)\,\delta\nu + \nu_0\,\delta h \tag{4}$$

where

$$A = A_0 + \delta A, \quad \nu = \nu_0 + \delta\nu, \quad \text{and} \quad h \doteq h_0 + \delta h$$

At large values of z, $\tanh \nu_0(h_0 - z) \approx \nu_0(h_0 - z)$, while at small values of z, $\tanh \nu_0(h_0 - z) \approx 1$. Thus, from the slope of $y(z)$ in these two regions and from the value of $y(0)$, the three corrections can be determined. If necessary, the process is repeated with the corrected first approximations.

Along the radius the thermal and epithermal flux distributions have the form

$$\phi_{th} = A_{th} J_0(\mu_{th} r)$$

$$\phi_{cd} = A_{cd} J_0(\mu_{cd} r) \tag{5}$$

The two radial bucklings μ_{th} and μ_{cd} will generally differ at the most by a few per cent and hence if the observed bare-foil activities are forced to fit a function of this form, the observed value of μ must be corrected in order to give μ_{th}

$$\mu_{th} = \frac{(R+1)\mu - \mu_{cd}}{R} \tag{6}$$

The values of μ and μ_{cd} are determined graphically in a manner similar to that used for the axial fitting. With approximate values A_0 and μ_0, let $\mu = \mu_0(1 + \delta)$ and plot the function

$$y(r) = \frac{\phi}{A_0 J_0(\mu_0 r)} \approx \frac{A}{A_0} - \delta \frac{\mu_0 r J_1(\mu_0 r)}{J_0(\mu_0 r)} \tag{7}$$

The correction factor δ can be read directly as the slope of a straight line if the independent variable $\mu_0 r J_1(\mu_0 r)/J_0(\mu_0 r)$ is used instead of r. Since μ is determined primarily the diameter of the tank, it varies only slightly from lattice to lattice. Hence a single value of μ_0 will serve for all lattices and suitable "Bessel-function graph paper" can be prepared beforehand. The average value of μ_{th} was determined from exposures made at three different heights in the experimental tank.

Some correction is still required to account for the disturbance of the flux by the foil holders and the foils themselves. The horizontal foil holder introduces an azimuthal asymmetry into the flux distribution but its effect on μ and ν is only second order. The situation

is different with the axial foil holder, which is located in the center of the tank at the maximum of the neutron flux and has more absorption per unit length. It can be considered as a line sink which depresses the neutron flux near the axis. Without the vertical foil assembly in the tank the flux is

$$\phi_1 = AJ_0(\mu_1 r) \sinh \nu_1(h - z) \qquad (8.1)$$

and with the vertical foil holder assembly in position the flux can be represented by

$$\phi = C[J_0(\mu r) + \alpha N_0(\mu r)] \sinh \nu(h - z) \qquad (8.2)$$

The buckling B^2 is given either by $\mu_1^2 - \nu_1^2$ or by $\mu^2 - \nu^2$; whereas the experimentally measured quantities are μ_1 and ν. If it is assumed that the extrapolated radius of the tank is unchanged by the addition of the foil holder one finds that the corrected value of the radial buckling is given by

$$\mu = \mu_1[1 + 0.409\alpha] \qquad \alpha = \frac{S}{4D} \qquad (9)$$

where S is the absorption cross section per unit length of the foil holder, and D is the diffusion coefficient of heavy water.

BUCKLINGS OF D_2O-URANIUM LATTICES

The series of D_2O-uranium lattice studies at North American Aviation consists of 35 lattices using uranium with three different enrichment values. These are referred to as "depleted," "natural," and "enriched." The composition and density of the metal for each of these enrichments is given in Table I.

Table I

Fuel	*Density, gm/cm³*	*Atomic fraction U^{235}*	*Macroscopic absorption cross section (Maxwell average)*
Depleted	18.80	4.962×10^{-3}	0.2557 cm^{-1}
Natural	18.88	7.205×10^{-3}	0.3200
Enriched	18.83	9.124×10^{-3}	0.3763

The fuel rods were assembled by loading individual 4-inch slugs into an aluminum tube. The tube was commercially pure with a wall thickness of 0.1 cm. The rods were positioned in the lattice by two aluminum grid plates, the lower grid plate was 1 inch above the bottom of the tank, the upper grid plate was 60 inches above the bottom. Thus an experimental region 150 cm high was provided within which to make measurements. Usually measurements were confined to a 100-cm region beginning at about 30 cm from the bottom of the tank in order to avoid the transients near the boundaries. Figure 2 shows a typical lattice in position in the experimental tank.

The summary of the measurements is given in Table II. For three of the enriched lattices the total buckling is larger than the radial buckling in a 5-foot tank. This would have made ν^2 negative and would have converted the hyperbolic axial distribution into a trigonometric function. Besides violating the conditions of the exponential experiment this would produce a region which would be capable of becoming self-sustaining. These lattices were therefore measured in a 4-foot diameter tank. The moderator to uranium ratios indicated in the table have been computed from the dimensions of the cell; because of the impossibility of filling a cylindrical region with a square lattice, these ratios are not the same as would be computed from the total number of rods and the dimensions of the tank. In most lattices therefore there is a small amount of excess moderator which can be considered as a thin "reflecting" region surrounding the active lattice. It is as a result of this reflector that the thermal and epithermal fluxes can have different radial bucklings, but since the radial bucklings are actually measured for each individual lattice the resultant total buckling cannot be in

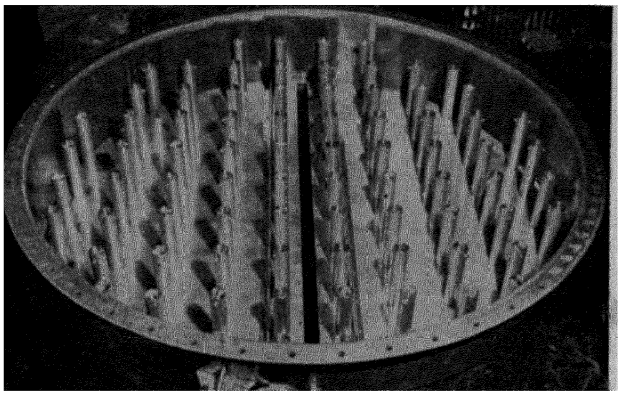

Figure 2. Lattice in position in experimental tank. The heavy water has not yet been added. The aluminum plate is the upper positioning grid which maintains the lattice spacing. The slot in the plate is for the insertion of foils.

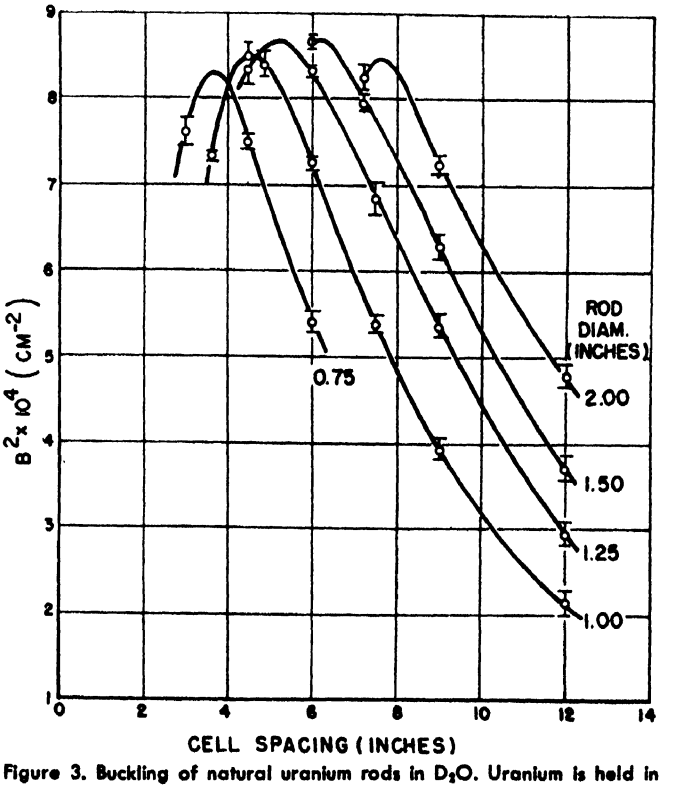

Figure 3. Buckling of natural uranium rods in D_2O. Uranium is held in 0.1 cm wall aluminum tubes

serious error from this cause. Figure 3 shows the buckling of natural uranium rods as a function of rod size and cell spacing for natural uranium. Figure 4 shows similar curves for the depleted and enriched material and includes also the curves for natural uranium of the same rod sizes for comparison.

INTERPRETATION

In order to understand the physics of heterogeneous systems more must be known about the lattice than just the buckling. For this reason extensive additional measurements were also made on each lattice. These measurements can best be discussed in terms of the bearing which each has on the theory of lattice calculations.

Disadvantage Factors

The neutron distribution in the uranium rod and in the D_2O moderator was explored for each lattice. It is well known that diffusion theory is unable to give an adequate description of the neutron flux in a uranium rod, which is not only highly absorbing but also only a few mean free paths in diameter; hence the experimental disadvantage factors must be used

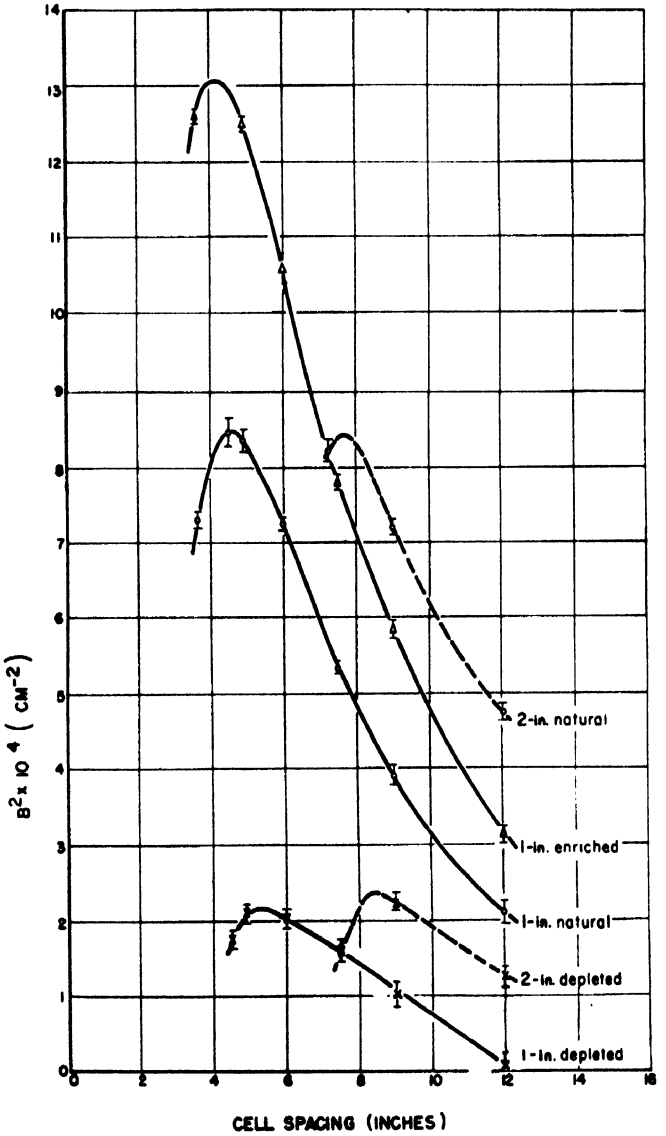

Figure 4. Buckling of depleted and enriched lattices

in calculations of the thermal utilization and the thermal diffusion length.

The thermal utilization factor, f, was calculated from the expression

$$\frac{1-f}{f} = \frac{\Sigma_{al}V_{al}}{\Sigma_u V_u}F + \frac{\Sigma_m V_m}{\Sigma_u V_u}FF_m \qquad (10)$$

where V is volume fraction and Σ is the macroscopic absorption cross section properly averaged over a Maxwellian distribution at the appropriate neutron temperature. The subscripts refer in an obvious way to uranium, aluminum and moderator. In all of the lattices the fuel was clad in aluminum 0.1-cm thick. The disadvantage factor F is the ratio of the thermal neutron flux averaged over the surface of the fuel rod to the thermal flux averaged over the total volume of the uranium. More appropriately, F may be defined directly as the ratio of the average thermal neutron flux in the aluminum cladding to the average thermal flux in the uranium. F_m is similarly defined as the ratio of average thermal flux in the moderator to the average thermal flux in the aluminum. The factor F_m is experimentally a more convenient quantity than the excess absorption, E-1, given by Glasstone and Edlund.[3] The excess absorption is useful because it depends only upon the properties of the moderator and is independent of the properties of the fuel and cladding material. The relationship between F_m and E may be easily derived.

Thermal Utilization

The applicability of an exponential experiment to heterogeneous lattices assumes that it is possible to define equivalent homogeneous parameters for the system, and that the variation of the gross neutron distribution does not affect the determination of these parameters. It is assumed that the neutron density can be expressed as a product of two factors, one depending on the gross behavior ignoring the cell structure, the other defining the variation of neutron density in the cell and which is the same in each cell independent of its position in the lattice. This is an assumption similar to that which is used for the description of wave functions in crystals. In an exponential experiment however, the large radial neutron currents near the side of the experimental tank could vitiate this approximation. To investigate this effect a series of measurements were made in a square lattice cell near the edge of a 4-foot diameter tank. The lattice consisted of 1-inch enriched-uranium rods on a 4.9-inch spacing. The neutron density contours which were measured in this cell are shown in Fig. 5.

If the assumption of factorization is valid, dividing each observed flux value by the over-all Bessel-function flux distribution should give a result which is appropriate for a cell in an infinite medium and from which the radial current has disappeared. This procedure has, in fact, always been followed in the analysis of data near the tank center, where it is a small correction. In the peripheral cell analysis, the Bessel-function correction effectively removes the large radial

Table II. Summary of D_2O-Uranium Lattices (North American Aviation)

Enrichment (at. %)	*Rod diameter (inches)*	*Cell side (inches)*	*Number of rods in tank*	$\frac{V_m}{V_u}$	B^2† (m^{-2})	F	FF_m	R
0.4962	1.00	4.50	120	24.82	1.76	1.162	1.537	5.5
		4.90	120	29.64	2.10		1.563	6.3
		7.50	52	71.02	1.60		1.633	16.4
		12.00	16	183.7	0.105		1.792	44.5
	2.00	7.25	52	15.71	1.61	1.420	2.427	5.7
		9.00	32	24.80	2.25		2.594	8.9
		12.00	16	44.94	1.2		2.796	19.4
0.7205	0.75	3.00	285	19.35	7.60	1.133	1.406	3.0
		4.50	120	45.09	7.48		1.474	7.0
		6.00	80	81.13	5.40		1.508	11.1
	1.00	3.625	208	15.69	7.31	1.190	1.520	2.7
		4.50	120	24.82	8.47		1.578	4.5
		4.90	120	29.64	8.36		1.598	5.7
		6.00	80	45.03	7.25		1.657	8.4
		7.50	52	71.02	5.36		1.718	12.7
		9.00	32	102.8	3.92		1.789	21.0
		12.00	16	183.7	2.11		1.901	39.3
	1.25	4.50	120	15.47	8.32	1.290	1.809	3.0
		6.00	80	28.39	8.30		1.918	6.3
		7.50	52	44.99	6 84		1.976	9.8
		9.00	32	65.29	5.35		2.064	14.2
		12.00	16	117.0	2.92		2.237	25.7
	1.50	6.00	81	19.36	8.65	1.356	2.139	4.4
		7.25	52	28.79	7.94		2.221	6.9
		9.00	32	44.97	6.29		2.341	11.1
		12.00	16	80.81	3.69		2.527	22.0
	2.00	7.25	52	15.71	8.23	1.502	2.560	4.7
		9.00	32	24.80	7.22		2.806	8.0
		12.00	16	44.94	4.76		3.174	16.1
0 9124	1.00	3.625	124*	15.69	12.6	1.238	1.721	2.6
		4.90	68*	29.64	12.5		1.829	4.9
		6.00	52*	45.03	10.6		1.924	7.1
		7.50	52	71.02	7.81		1.968	11.2
		9.00	32	102.8	5.85		2.009	16.0
		12.00	16	183.7	3.13		2.131	33.0

* Measurements made in 4-foot tank.

† Buckling values are as measured and uncorrected for the presence of the 0.1-cm wall aluminum fuel tubes. D_2O absorption cross section $\Sigma_a = (1.05 + 0.09) \times 10^{-4}$ cm^{-1} corresponds to hydrogen-deuterium ratio H/D = 0.0024.

current; the corrected flux pattern shown in Fig. 6 appears only slightly distorted from what might have been expected for an infinite lattice.

Disadvantage factors for the peripheral cell were obtained by mechanically integrating the flux over the rod and the moderator portion of the cell. Table III compares the peripheral lattice cell disadvantage factor measurements with the corresponding values for a central lattice cell; the peripheral cell values are considered accurate to ±2 per cent, the central cell values to ±1 per cent. The agreement between the two sets of values is quite good; in fact, the values of FF_m, the quantity most significantly affecting the thermal utilization, differ by only about 0.5 per cent.

We conclude that the usual assumption of f constant over the lattice is, indeed, valid, and that the multiplying media of an exponential experiment can be suitably averaged and treated as homogeneous.

Table III. Disadvantage Factor Measurements*

	Central cell with Bessel correction	*Peripheral cell*	
		With Bessel correction	*Without Bessel correction*
F	1.245	1.209	1.217
F_m	1.469	1.505	1.490
FF_m	1.829	1.820	1.813

* F_m is the moderator disadvantage factor, the ratio of the average neutron flux in the moderator to the average neutron flux at the surface of the uranium rod.

Anisotropy of Neutron Diffusion

The possibility of anisotropy confusing the interpretation of exponential experiments has been pointed out by B. I. Spinrad of Argonne National Laboratory and by others. The one-group diffusion equation can be written

$$\nabla D \nabla \phi + (k - 1)\Sigma_a \phi = 0 \qquad (11)$$

where ϕ is the neutron flux, k the multiplication constant and Σ_a the macroscopic absorption cross section. In an anisotropic medium the diffusion coefficient may not be a scalar but a dyad with different values along the three principal axes of the medium. In a rod lattice it is therefore possible that the diffusion coefficient perpendicular to the rods may not be the same as the diffusion coefficient parallel to the

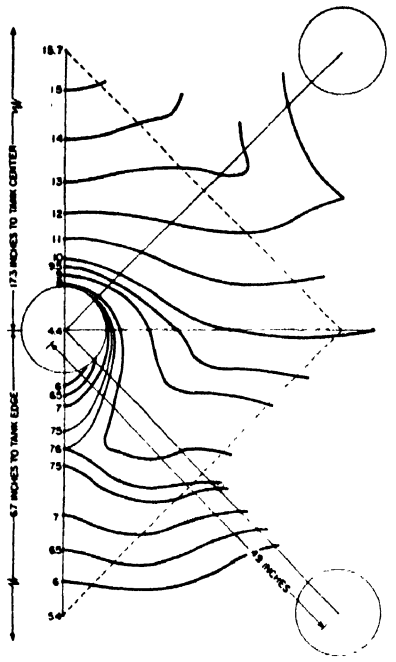

Figure 5. Experimental neutron density contours in a lattice cell with large transverse neutron current. One inch diameter rod on 4.9 inch square cell spacing. Neutron density varies by a factor of three across the cell

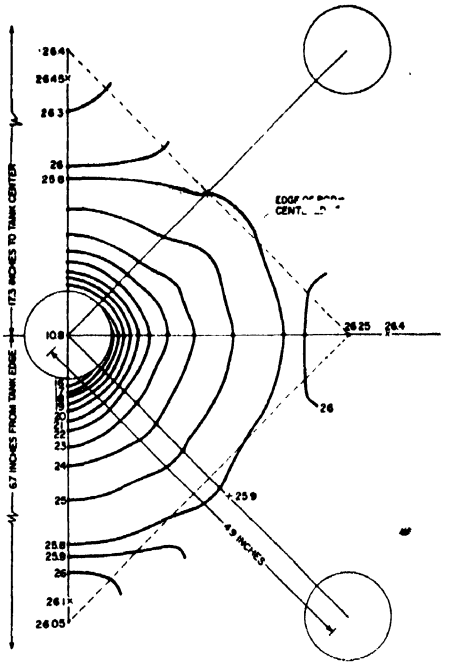

Figure 6. Neutron density of Fig. 5 corrected by dividing each observed neutron density by a zero order Bessel function of the distance from the center of the tank. The radial current has been almost completely removed, the remaining asymmetry is less than 10 per cent

rods. In such a case one cannot unambiguously define a lattice buckling B^2 but one has instead

$$D_r\mu^2 - D_s\nu^2 = (k-1)\Sigma_a \qquad (12)$$

corresponding to the neutron distribution of Equation 1.

If measurements of μ^2 and ν^2 are made in two different geometries it is possible to determine $\rho = D_s/D_r$. Neutron distributions in three different lattices were measured in four-foot and five-foot diameter tanks. The results are indicated in Table IV. Lattice A is 1-inch uranium rods in a 4.9-inch square spacing; lattice B is the same rods in a 6.0-inch square spacing; and lattice C is 1-inch enriched uranium (0.912 atom per cent U^{235}) in 7.5-inch spacing.

The results are not conclusive and no correction has been made to the data listed in Table II for the three enriched lattices which were measured in the small tank.

Direct Measurement of Effective Absorption Cross Section

The ratio, R, of thermal foil activity to epithermal foil activity defined in Equation 3 depends upon the thermal and epithermal neutron densities and upon the ratio of the thermal absorption cross section of indium to its resonance integral.

$$R = \frac{\int_0^{E_c} \sigma_{in}(v)N(v)v\,dv}{\int_{E_c}^{\infty} \sigma_{in}\frac{q}{\xi\Sigma_s}\frac{dE}{E}} \qquad (13)$$

where $N(v)$ is the neutron density, q the slowing-down density and $\xi\Sigma_s$ the mean slowing-down power of the medium. The energy limit E_c is the cadmium cut-off energy, $E_c = 0.35$ ev. If one assumes that the thermal flux can be approximated adequately by a Maxwellian distribution corresponding to 20°C, and that the indium thermal neutron absorption cross section can be approximated by $\sigma(v) = \sigma_{in}{}^0(v_0/v)^{0.75}$ where $\sigma_{in}{}^0$ is the absorption cross section for monoenergetic neutrons with velocity $v_0 = 2200$ m/sec, and that the indium resonance cross section is sufficiently sharp that all of the other terms in the integral in the denominator can be removed from under the integral sign, one obtains

$$R = \frac{1.013N_{th}v_0\xi\Sigma_s}{q_{th}}\frac{\sigma_{in}{}^0}{\left(\int \sigma_{in}\frac{dE}{E}\right)_{eff}} \qquad (14)$$

Table IV. Measurement of Anisotropy

Lattice	4-foot diameter tank		5-foot diameter tank		ρ
	μ, m^{-1}	ν, m^{-1}	μ, m^{-1}	ν, m^{-1}	
A	3.86 ± 0.01	2.51 ± 0.04	3.10 ± 0.01	1.122 ± 0.02	1.06 ± 0.05
B	3.86 ± 0.01	2.74 ± 0.03	3.10 ± 0.01	1.546 ± 0.02	1.03 ± 0.03
C	3.86 ± 0.01	2.64 ± 0.03	3.10 ± 0.01	1.341 ± 0.01	1.02 ± 0.03

The conservation of neutron requires that the slowing down density must equal the total rate of absorption and leakage of neutrons. Hence $q = N_{th}v_0(\bar{\Sigma}_a + B^2D)$ where the bar indicates the spatial average. Equation 14 then becomes

$$\Sigma_a = \frac{1.013\overline{\xi\Sigma_s}}{R} \frac{\sigma_{in}^0}{\left(\int \sigma_{in} \frac{dE}{E}\right)_{eff}} + B^2D \quad (14.1)$$

Thus this expression allows one to calculate the mean macroscopic absorption cross section from the activity ratio. Since B^2D is of the order of 20 per cent of $\bar{\Sigma}_a$, high accuracy in the knowledge of D or of B^2 is not required. If D is accurately known (and it is the average value over the lattice which is needed), it is also possible to obtain an accurate value of $L^2 = D/\bar{\Sigma}_a$. On the other hand, if the calculated values of the other parameter can be relied upon, the activity ratios provide a measurement of the indium resonance integral. On the basis of the lattices of Table II the result is

$$\frac{\left(\int \sigma_{in} \frac{dE}{E}\right)_{eff}}{\sigma_{in}^0} = 3.68 \pm 0.13 \quad (15)$$

This is the effective value, including the self-shielding effect of the indium foils which are not thin to resonance neutrons. Measurements of this shielding effect have been made at North American Aviation, Inc. and give a factor of 3.9 for a foil 95 mg/cm² thick. Other laboratories[4] have reported 3.88 for 92 mg/cm² and 3.66 for 88 mg/cm². Thus the thin foil resonance integral ratio becomes 14.3 ± 0.5. This may be compared with the value 13.9 which is computed directly from cross-section data.

Direct Measurement of Age

If the moderator of a lattice is poisoned by the addition of boron it is possible to determine the Fermi age of fission neutrons from the change in the buckling. The assumption is made that only the leakage and thermal absorption properties of the lattice are changed by the addition of the poison. Hence η, ϵ, p, and τ will remain unaltered and only L^2, f, and B^2 are changed. This assumption is valid if the additional poison is insufficient to alter the neutron spectrum. With these conditions one can write

$$(\bar{\nu}^2 - \nu^2)\tau = \ln\left[\frac{1 + \bar{B}^2\bar{L}^2 f}{1 + B^2L^2 \bar{f}}\right] \quad (16)$$

where the barred values refer to the poisoned lattice. The accuracy of the calculation depends primarily on the accuracy with which the change in buckling can be measured and the accuracy with which the average absorption cross section of the lattice is known. Because of the inter-relatedness of the constants in Equation 16 it is highly pessimistic to evaluate errors from a naive consideration of that equation.

Data were taken on a natural uranium, 1-inch diameter rod lattice on a 4.9-inch square cell spacing and with the moderator poisoned with approximately 150 mg of B_2O_3 per liter. The comparison between this lattice and the corresponding unpoisoned lattice is shown in Table V. The measured age is

$$\tau = 107 \pm 5 \text{ cm}^2 \quad (17)$$

Table V. Determination of Neutron Age

Lattice parameter	*Unpoisoned D_2O*	*Poisoned D_2O*
ν	1.122 ± 0.040	3.386 ± 0.014 m^{-1}
B^2	8.36 ± 0.15	−1.85 ± 0.12 m^{-2}
F	1.19 ± 0.01	1.20 ± 0.01
FF_m	1.60 ± 0.01	1.69 ± 0.01
f	0.978 ± 0.002	0.778 ± 0.006
L^2	125 ± 3	106 ± 3 cm^2
τ	107 ± 5 cm^2	

The age for this lattice computed to indium resonance is 102 ± 5 cm². This would then imply that the effective age from indium to thermal is 5 ± 7 cm² in agreement with the value of approximately 6 cm² from the analysis by Cohen[5] on the epithermal moderation of neutrons. The excellent agreement is certainly fortuitous, as is indicated by the magnitude of the assigned errors. Furthermore, the error in Equation 17 includes only random error with no allowance for systematic error or shortcomings in the theory.

Direct Measurement of Thermal Diffusion Length

The activity ratio, R, has often been used as a means of measuring the thermal diffusion length of a reactor. It has been shown above that this measurement more accurately provides a means of determining only $\bar{\Sigma}_a/\overline{\xi\Sigma}_s$ and that, in order to evaluate L^2, it is also necessary to know the slowing-down cross section $\overline{\xi\Sigma}_s$ and the thermal diffusion coefficient D. It is possible to measure the diffusion coefficient quite accurately by the boron-poison method[6] but there does not appear to be a good independent method for the evaluation of $\overline{\xi\Sigma}_s$ available at the present time. One ought then to use the activity ratio for a determination of the slowing-down cross section and seek elsewhere for a method to determine the thermal diffusion length or the absorption cross section, $\bar{\Sigma}_a$.

If thermal neutrons are allowed to diffuse into a region in which there is no multiplication, the neutron density will still have the form of Equation 1 and the measured buckling will be $B^2 = -1/L^2$ where L is the thermal diffusion length. A lattice was therefore assembled from rods of PbCd alloy. The rods were composed of 4-inch long, 0.998-inch diameter slugs loaded into the 1.00-inch internal diameter, 0.040-inch wall aluminum tubes that had been used for the uranium-lattice experiments. The slugs were made by extrusion of an alloy containing approximately 0.15 per cent cadmium and 2.5 per cent antimony by weight in commercially pure lead. All of the slugs were prepared from a single melt in 11 separate extrusions. A representative sample of each extrusion was analyzed for cadmium content by chemical[7] and mass spectrographic methods. The cadmium content was determined to be 0.153 ± 0.003 per cent and the

density of the alloy was 11.35 gm/cm³. The Maxwellian averaged cross sections for absorption and scattering were calculated to be 0.270 ± 0.025 cm^{-1} and 0.360 ± 0.033 cm^{-1} respectively. The absorption cross section was also measured directly by the pile-oscillator method[8] at Argonne National Laboratory and found to be 0.267 ± 0.005 cm^{-1}.

Four non-multiplying lattices were investigated. The lead-cadmium alloy rods were spaced in square arrays 4.9, 6.0, 9.0, and 12.0 inches between centers. The results are summarized in Table VI; the errors listed are the limits of uncertainty.

Epithermal neutrons in the tank will produce a distortion of the measured neutron flux distribution. A correction therefore had to be applied to the measured activities to correct for that component of the thermal flux which arose from the moderation of epithermal neutrons and hence had a distribution characteristic of the epithermal neutron distribution rather than the thermal distribution. Because of the uncertainties in the details of this correction, its effect was minimized by restricting the measurements to activity ratios (Equation 3) greater than 200.

The errors assigned to the calculated value of L^2 are based on the accuracy of the measured disadvantage factors and the accuracy with which the cross sections are known. The calculations were based on the measured absorption cross section of the lead-cadmium alloy, which, it was felt, was more accurate and more directly applicable than the value based on nuclear cross sections and alloy composition. The absorption cross section for D_2O was taken[6] to be $(1.05 \pm 0.09) \times 10^{-4}$ cm^{-1} and the scattering cross section 0.402 ± 0.006 cm^{-1}. For the aluminum cladding the assumed values were $\Sigma_a = 0.0115$ cm^{-1} and $\Sigma_s = 0.0920$ cm^{-1}.

The agreement between the calculated and measured values of L^2 is excellent. It may, therefore, be concluded that the conventional methods for computing the thermal diffusion length in heterogeneous lattices in terms of the absorption cross sections weighted by the neutron flux is adequate if the correct disadvantage factors are used. Since diffusion theory does not give correct disadvantage factors for geometries of interest in reactor design, it is necessary to use experimentally determined disadvantage factors.

COMPARISON WITH OTHER DATA

Experimental Measurements at Argonne National Laboratory

A lattice of 1-inch diameter rods in a square array with a cell spacing of 4.9 inches between centers of adjacent rods was investigated. The uranium was formed as rods and hence there was no need for aluminum jacketing and the rods were left bare. Before the bare rods were exposed to D_2O they were washed successively with trichlorobenzene, dilute nitric acid and distilled water, and were then thoroughly dried.

The average value of μ from three measurements was found to be 3.092 ± 0.003 m^{-1} corresponding to an effective tank radius of 77.96 ± 0.6 cm. The axial foil holders used at Argonne had negligible absorption so that no correction was required to the observed axial traverse. The presence of the central foil detector is the reason for the higher radial buckling quoted for the same size tank in Table II. The axial relaxation constant was found to be 0.853 ± 0.003 m^{-1}, from which the buckling is determined to be $B^2 = 8.79 \pm 0.02$ m^{-2}. The value given in Table II for the same geometry but with the rods clad in 0.1 cm aluminum is 8.36 ± 0.14. The additional aluminum in the lattice should decrease the buckling by an amount given by the formula

$$\delta B^2 = \frac{-\delta \bar{\Sigma}_a}{\bar{\Sigma}_a [L^2 + k\tau \exp(-B^2\tau)]} \qquad (18)$$

where $\bar{\Sigma}_a$ is the flux-averaged absorption cross section of the lattice, k is the infinite multiplication constant, τ is the Fermi age, and L^2 the thermal diffusion length. From this expression it may be deduced that an aluminum tube in the Argonne experimental measurement would have lowered the measured buckling by 0.44 m^{-2} which yields $B^2 = 8.35 \pm 0.02$ m^{-2} to compare with the value listed in Table II.

In connection with the exponential experiments, calculations were performed using the P-3 spherical harmonic approximation to the transport equation in cylindrical coordinates.[9] Numerical results were obtained for a 1-inch diameter natural uranium rod surrounded by D_2O. The calculation indicates a flux depression at the center of the rod which is twice as large as the value predicted by first order diffusion theory, in agreement with the experimental result.

The thermal flux in a 1-inch fuel rod was measured using small circular foils, 0.16-cm diameter, of copper, indium, dysprosium or uranium as the neutron detector. These foils were held in a uranium foil holder which fitted closely into a slot in the uranium rod. Several different measurements were made, only a few of the foil positions being occupied in any single exposure in order to minimize the flux depression interaction of the foils. The average of many determinations may be expressed by the formula[10]

$$\phi(r) = 1 + 0.134r^2 + 0.067r^4 \ (r \text{ in cm}) \qquad (19)$$

The flux at the surface of the uranium is 1.278 times the value at the center and the disadvantage factor (the ratio of surface flux to the average flux) is $F = 1.192$.

In comparison with this, measurements at Chalk River and at Hanford[11] give smaller values. Chalk River measurements were made in ZEEP—the Zero Energy Experimental Pile. These results indicate lower disadvantage factors than measured by North American although for a 1.5-inch diameter rod the data was obtained using fuel rods which had been exchanged between the laboratories. The measurements at Hanford were made in a graphite moderated assembly but since the scattering mean free path in graphite is not greatly different from the scattering mean free path in heavy water the results should not

Table VI. Measurement of Thermal Diffusion Length

	Lattice spacing (inches)			
	4.9	*6.0*	*9.0*	*12.0*
ν, m^{-1}	8.80 ± 0.08	7.39 ± 0.07	5.40 ± 0.05	4.54 ± 0.04
μ, m^{-1}	3.10 ± 0.01	3.10 ± 0.01	3.10 ± 0.01	3.10 ± 0.01
L^2 (exp), cm^2	147 ± 3	222 ± 4	512 ± 14	909 ± 27
F	1.15 ± 0.01	1.13 ± 0.01	1.13 ± 0.01	1.15 ± 0.01
FF_m	1.56 ± 0.02	1.61 ± 0.02	1.73 ± 0.02	1.80 ± 0.02
L^2 (calc), cm^2	143 ± 5	221 ± 8	516 ± 19	906 ± 33

Table VII. Anisotropy Comparison of Chalk River and California Measurements (1.50-inch diameter, natural uranium rods)

v_m/v_u	*Experiment*	μ^2, m^{-1}	ν^2, $^{-1}$	ρ^*
26.2	ZEEP	3.61 ± 0.04	−4.32 ± 0.04	1.050 ± 0.011
	NAA	9.61 ± 0.03	1.39 ± 0.04	
33.0	ZEEP	3.50 ± 0.02	−3.73 ± 0.02	1.053 ± 0.007
	NAA	9.61 ± 0.03	2.13 ± 0.01	

* No correction has been made for the difference in purity of the heavy water. This would *increase* ρ by 0.014.

differ appreciably (on the basis of first order diffusion theory there would be no difference at all). The disadvantage factor measured at Hanford, should agree with the Argonne measurement made in CP-2 which is also graphite moderated. However, the value 1.19 for a rod diameter of 1.84 inches is significantly lower than the value 1.25 ± 0.02 which would be inferred from an interpolation of the data at North American and is in disagreement with the Argonne measurement of 1.192 for a smaller rod.

Comparison with Chalk River Data

The measurements of the buckling of a 1-inch diameter, natural uranium rod on a 4.9-inch square lattice spacing (moderator to uranium ratio = 29.6) at Argonne National Laboratory and at North American Aviation are in excellent agreement. However, measurements of lattice bucklings in critical experiments at Chalk River, Canada, give lower values by approximately 3.5 per cent. The reason for this difference was sought in terms of the purity of the materials. Isotopic analyses of the heavy water from the United States and Canadian laboratories were carried out at Chalk River; the United States heavy water had a purity of 99.76 per cent by weight D_2O, Canadian heavy water had a purity of 99.81 per cent. A correction for this difference increases the discrepancy by approximately 1 per cent in B^2 for the lattices which were compared.

The uranium used in both experiments was compared by the danger coefficient method at North American Aviation, Inc. and the Canadian uranium was found to be slightly less reactive than the United States samples. This difference amounted to an absorption impurity equivalent to 0.7×10^{-6} by weight of boron, and is too small by a factor of 5 or 6 to explain the discrepancy in the buckling measurements.

The effect of anisotropic diffusion, which has previously been mentioned, might also be of importance here. The Canadian measurements of B^2 made use of ZEEP, the Zero Energy Experimental Pile, and were critical experiments rather than exponential experiments. The comparison is shown in Table VII where the NAA data are for a fictitious lattice interpolated from the data of Table II. The anisotropy factor is much larger than those given in Table V for measurements in different geometries but with the same techniques applied to both measurements; nor is it in agreement with direct anisotropy measurements of the same lattice in two different geometries in ZEEP, listed in Table VIII.

It would therefore appear that no identifiable cause has yet been isolated by either laboratory to explain the discrepancy. It may be that several individual sources are combining to produce this difference or that some systematic error exists in one or both of the experimental facilities or in the analysis and reduction of the data.

Table VIII. ZEEP Anisotropy Measurement

Experiment	μ^2, m^{-1}	ν^2	κ^2	ρ
I	6.401 ± 0.050	−1.804 ± 0.013	8.20 ± 0.05	0.989 ± 0.033
II	3.698 ± 0.077	−4.537 ± 0.034	8.23 ± 0.08	

REFERENCES

1. Remley, M. E., Science 119: 21 (1954).
2. Kundstadter, J. W., Phys. Rev. 78: 484 (1950).
3. Glasstone, S. and Edlund, M. C., *Nuclear Reactor Theory*, van Nostrand, New York, p. 270 (1952).
4. Sargent, B. W. and Duckworth, J. C. (unpublished).
5. Cohen, E. R., Conference on Nuclear Engineering, University of California, Los Angeles, p B-47 (1950).
6. Kash, S. W. and Woods, D. C., Phys. Rev. 90: 564 (1953).
7. Silverman, L. and Trego, K., Analyst 77: 143 (1952).
8. Muehlhause, C. Private Communication.
9. Haefner, R. R. and Spinrad, B. I. (unpublished).
10. Muehlhause, C. (unpublished).
11. Davenport, D. E. (unpublished).

Calculations for a Heavy Water and Natural Uranium 10 Mw Reactor

By Sergio Gallone and Carlo Salvetti,* Italy

In Italy nuclear research is organized and financed by the Comitato Nazionale per le Ricerche Nucleari (CNRN, National Committee for Nuclear Research). The activity in the field of nuclear energy is assigned to the "Laboratori CISE," Milano which works for the National Committee on a contract basis.

In 1953 the National Committee decided to assign to the CISE Laboratories the study of a heavy water and natural uranium reactor of 10 Mw power.

The reasons for this decision were the following:

The CNRN wanted a reactor with a flux of the order of 10^{13}n/cm^2/sec for the study of radiation effects, the production of highly active radioisotopes and experiments in neutron physics. In addition some plutonium extraction was planned and it was also foreseen that heat extraction experiments on high temperature testing rods were to be made.

These requirements could obviously be fulfilled with a heavy water reactor of the above-mentioned type, without using enriched fuel, which, of course, was not available at that time.

Moreover CISE Laboratories had already some experience both in heavy water and metallic uranium production methods; a plant for metallic uranium production (about 5 tons/year) was then under construction and is now completed.

NEUTRON CALCULATIONS

A heterogenous heavy-water natural uranium reactor of 10 Mw power has therefore been studied; the reactor which is heavy-water cooled, is cylindrical with side and bottom graphite reflector.

The materials are assumed to have the following characteristics:

Fuel: metallic uranium, density 18.8 gm/cm^3.

Moderator: heavy water with 100 cm diffusion length.

Reflector: graphite with 45 cm diffusion length.

Let us consider a reactivity Δk defined by the following formula:

$$1 + \Delta k = \frac{k_\infty e^{-\tau B^2}}{1 + L^2(1-f)B^2} \qquad (1)$$

where: k_∞ is the reproduction factor for a lattice containing only U and D_2O; τ and L are the Fermi age of fission neutrons and the thermal diffusion length in heavy water respectively; f is the thermal utilization factor in the U + D_2O lattice; and B is the geometrical buckling which is entirely determined if the volume V of the core is given together with the geometry and physical properties of the reflector.

It is to be noted that the effects of structural materials, poisons, depletion, temperature, etc. have not been included in the right-hand side of Equation 1. Thus $1 + \Delta k$ represents the effective multiplication factor which the reactor with the specified volume (or geometrical buckling) would have in the absence of structural materials, poisoning, depletion, temperature effects, etc. These effects are intended to be estimated apart and included in a reactivity loss $\overline{\Delta k}$. The difference $\delta k = \Delta k - \overline{\Delta k}$ gives the reactivity which permits radioisotopes production or introduction of any other absorbing material; control devices must

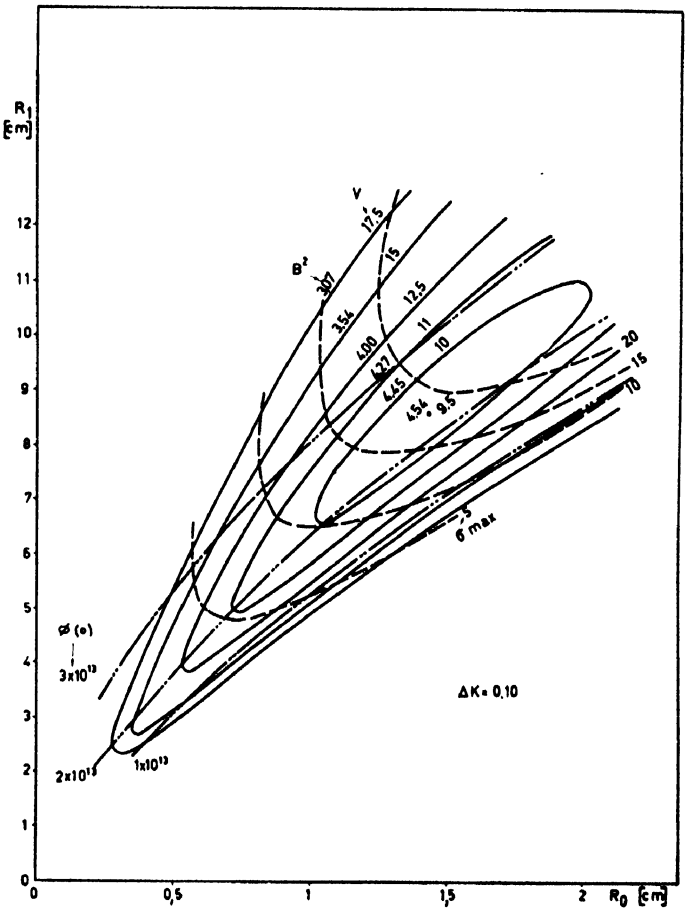

Figure 1

* Università di Milano e Laboratori CISE.

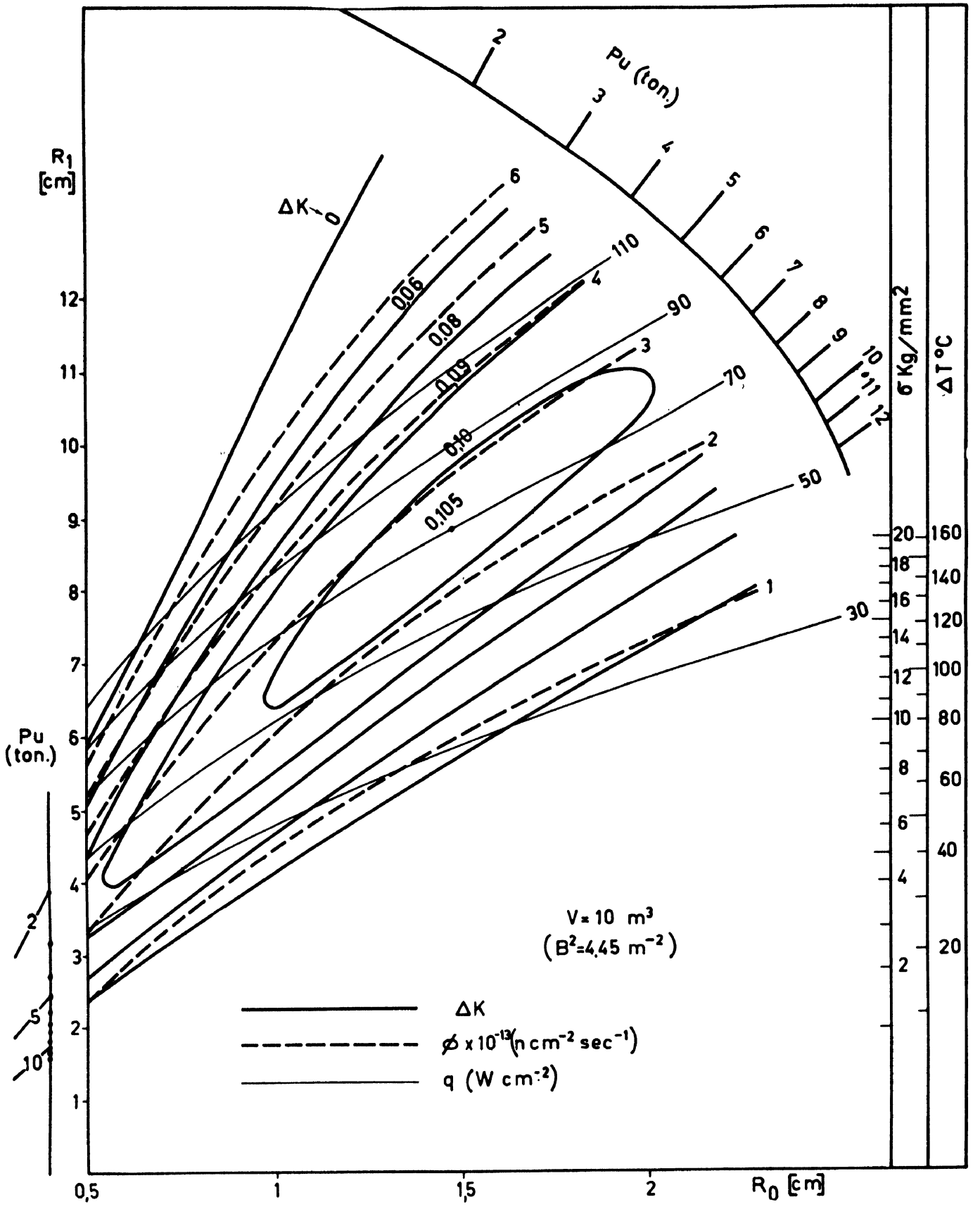
Pu (ton.)
R1 [cm]
ΔK
0
0,06
0,08
0,09
0,10
0,105
110
90
70
50
30
6
5
4
3
2
1
V = 10 m³
(B² = 4,45 m⁻²)
ΔK
ø x 10⁻¹³ (n cm⁻² sec⁻¹)
q (W cm⁻²)
σ Kg/mm²
ΔT °C
R0 [cm]
0,5
1
1,5
2

Figure 2

in any case complete the compensation of δk in order to insure criticality in steady-state conditions. We are not however mainly concerned with this last problem.

In order to obtain some elements for the choice of a "convenient" lattice for a given core volume, i.e., for a given quantity of heavy water, the following two problems have been solved: (*a*) finding the volume V of the core as a function of lattice parameters for a given reactivity Δk, and conversely (b) finding the reactivity Δk as a function of lattice parameters for a given volume V of the core.

These calculations have been performed using the approximate formula:

$$1 + \Delta k = \frac{k_\infty}{1 + (k_\infty - 1)\frac{B^2}{B_0^2}} \qquad (2)$$

where B_0^2 is the material buckling of the U plus D_2O lattice.

The results of these calculations are illustrated in Figs. 1 and 2.

Figure 1 shows the contours of constant core volume for a fixed reactivity $\Delta k = 0.1$ as a function of rod radius R_0 and equivalent cell radius R_1.

Lines of equal maximum neutron flux are also indicated on the figure.

Figure 2 shows the contours of constant Δk for a fixed core volume $V = 10$ m^3 and lines of constant maximum neutron flux. Lines of constant uranium weight (in metric tons) are obtained by connecting, with straight lines, corresponding points of the two tonnage (P_U) scales.

The connection between geometrical buckling B and core volume V is obtained, in the one-group approximation, by applying the well-known Yvon method, for infinite reflector thickness and an aluminum tank 0.8 cm thick.

THERMAL AND MECHANICAL CONDITIONS OF FUEL ELEMENTS DURING OPERATION

The thermal and mechanical conditions of the central fuel elements have been calculated: i.e., the temperature drop ΔT(°C) between axis and rod surface, the maximum thermomechanical stress σ (kg/mm^2) in uranium metal due to the temperature gradient, and the maximum heat flow q (w/cm^2) at the rod surface.

These results have been plotted together with those of the neutron calculations on the same diagrams. In this way, for a fixed core volume (Fig. 2) at the reactivity Δk, the thermal neutron flux ϕ, the temperature drop ΔT, the mechanical stress σ and the heat flow q are given as a function of lattice parameters. These diagrams give the thermal and mechanical conditions in which a fuel element works while operating at full power; the technology requirements, which have to be fulfilled in the manufacture of fuel elements, are thus determined.

CONCLUSIONS

The present calculations have been made in order to give first approximation data for the choice of an actual reactor and have in fact been used for this purpose. A set of exponential experiments has, of course, also been planned.

The Experimental Basis of Lattice Calculations

By Peter W. Mummery,* UK

The calculation of criticality data for thermal nuclear reactors is an approximate procedure because the necessary nuclear data cannot be measured sufficiently accurately. Furthermore, the methods of calculation are often approximate in themselves so that the calculation of a large number of possible systems can be quickly carried out. It is necessary therefore to carry out integral experiments, including determinations of the critical sizes of some proposed reactors, and to correlate these results with the calculations.

This correlation becomes most important when fuels other than natural uranium are available, because the emphasis on reactor design is then to produce the best design for a particular purpose rather than just a reactor which can be made critical.

Throughout this analysis standard two-group theory is used with the critical equation.

$$\eta\epsilon pf = (1 + K^2L^2)(1 + K^2L_S^2)$$

RELATIVE IMPORTANCE OF PARAMETERS USED IN LATTICE CALCULATIONS

The material buckling or Laplacian K^2 of a particular lattice determines the critical size of a reactor using that lattice. For a given fuel element and coolant design the dependence on the various data of the moderator to uranium volume ratio for maximum K^2, i.e., V^0, is examined. Table I gives typical results for graphite and heavy-water moderated lattices fuelled with natural uranium.

These results show that the dependence on β, A and $\eta\epsilon$ is similar for the two moderators but the dependence on L_{sm}^2, α and γ is quite different. This is reasonable as can be seen from the following arguments.

β characterises the moderator absorption and diffusion area and, in the vicinity of V^0, moderator absorption and thermal neutron leakage in a graphite reactor are respectively similar to thermal neutron leakage and moderator absorption in a heavy water reactor.

A characterises the uranium resonance absorption which is similar for both moderators in the vicinity of V^0.

L_{sm}^2 characterises the fast neutron leakage which is greater in the heavy water reactor.

α characterises the moderator absorption which is greater in the graphite reactor.

γ characterises the thermal neutron leakage which is greater in the heavy water reactor.

It is seen that A and $\eta\epsilon$ are the two most important items in this analysis. Furthermore $\eta\epsilon$ is the most important factor in determining the value of K^2 at $V = V^0$. Unfortunately these two factors are the most difficult to measure directly to the required accuracy. It is necessary, therefore, to deduce these quantities from suitable series of exponential or critical experiments.

METHOD OF CORRELATION OF EXPERIMENTS WITH CALCULATION

The method of correlation is therefore as follows:

1. Measure the Laplacian or buckling as a function of lattice pitch for various fuel element shapes and coolants.
2. Calculate the thermal utilisation using measured cross sections and densities and fine-structure distributions.
3. Calculate the slowing-down area using the measured slowing-down area in the moderator and calculating the small effect of other materials present. For gas coolants and for natural water slightly enriched reactors these effects may be large and experimental determinations are necessary.
4. Calculate the diffusion area in the reactor from the measured diffusion area in the moderator and the data used in calculating the thermal utilisation.
5. Calculate the small effect of the variation in η with lattice pitch, due to the neutron spectrum changing; and the small effect of the variation in ϵ with lattice pitch due to neutrons from one fuel element causing U^{238} fissions in neighbouring elements.

Table I

X'	$\frac{dV^0/V^0}{dx/x}$	
	Graphite	*Heavy Water*
L_{sm}^2	+0.05	+0.15
$\alpha = N_m\sigma_m$	−0.25	−0.04
$\beta = \frac{1}{N_u\sigma_u}\frac{(\bar{\phi}_m)}{(\bar{q}_u)_{th}}$	−0.3	−0.2
$\gamma = \frac{1_{tm}}{3}$	−0.05	−0.15
$A = \frac{N_u\left(\int \sigma_u \frac{dE}{E}\right)_{eff}}{N_m\sigma_{sm}\xi_m}\frac{(\bar{\tau}_u)}{(\bar{q}_m)_{res}}$	+0.7	+0.7
$\eta\epsilon$	−1.4	−2.2

* Atomic Energy Research Establishment, Harwell.

6. For each combination of fuel element and coolant deduce those values of $\eta_0\epsilon_0$ and the uranium resonance integral $(\int\sigma_u\, dE/E)_{eff}$ which will fit the observed values of K^2. η_0 and ϵ_0 refer to a pure Maxwellian spectrum and an isolated fuel element respectively.

7. The dependence of fast fission factor and effective resonance integral on the fuel element shape and on the coolant can then be determined.

8. These deductions can be compared with the difficult direct measurements of neutron yield and effective resonance integral.

EXPERIMENTAL DETERMINATION OF LAPLACIANS OR BUCKLING

The majority of the determinations of K^2 were carried out by means of exponential experiments. These covered three lattice pitches for each of the following fuel elements, 1.20-inches diameter, 1.00-inches diameter and a tube, 1.64-inches outside diameter, 1.30-inches inside diameter. This tube contained nearly the same mass of uranium per unit length as did the 1.00 solid rod. In addition, one experiment was carried out with a 1.36-inch diameter element and a critical experiment was carried out with BEPO which contains 0.90-inch diameter elements.

Complete details of the lattices used in these experiments are given in Appendix I but in all cases the air channel around the fuel element was small so that the effect of this on the migration area was small. Experiments were carried out with one lattice and also with BEPO to determine the asymmetry in the migration area due to the presence of the air channels. In the first case this was determined by comparing the results of two exponential experiments in which the exponential form of the neutron flux was the first parallel to the direction of the fuel elements and then perpendicular to it. In the case of BEPO it was determined by comparing the results of an exponential and a critical experiment. The results were 1.00 ± 0.02 and 1.08 ± 0.04 respectively for the cases of a 1.60-inch and a 2.10-inch diameter air channel respectively.

The exponential experiments were carried out with an approximate cube of lattice containing about two hundred lattice positions and measurements were confined to a region in which the indium-cadmium ratio was constant. Ten grammes of radium were used to form a radium-alpha-beryllium neutron source.

The purity of the materials used was compared with standards by pile oscillator experiments in the GLEEP.

EXPERIMENTAL DETERMINATION OF FINE-STRUCTURE DISTRIBUTIONS

Measurements of thermal neutron fine structure distributions were carried out in small assemblies which replaced the GLEEP thermal column. The assemblies contained a minimum of 36 lattice positions. A measurement of fine-structure distribution at the centre of this assembly has been shown to give the same result as a measurement at the centre of a much larger assembly.

The measurements have in the main been made with 0.020-inch diameter manganese wires but the results have been checked in the uranium using the uranium as a detector. In this case gamma rays of energy greater than 411 kev were observed as a measure of the fission distribution and after a correction had been made for the U^{238} fission contribution the results agreed well with the manganese distributions.

CORRELATION OF FINE-STRUCTURE DISTRIBUTIONS WITH CALCULATIONS

The principle adopted in this correlation is to predict the experimental results by using diffusion theory formulae with adjusted "constants." A number of spherical harmonic calculations have been carried out in order to investigate the inadequacy of diffusion theory.

In the simple case of a lattice containing only fuel elements and moderator the quantity required in a calculation of thermal utilisation is the ratio of mean flux in the moderator to mean flux in the uranium. For convenience in calculation this is split into two parts G, the ratio of maximum to average flux in the uranium and S, the ratio of average to minimum flux in the moderator. Then, in cylindrical geometry,

$$G = \left[\frac{K_u^2g^2 - K_u^2a^2}{2K_ua}\right] \times \left[\frac{I_1(K_ug)K_0(K_ua) + K_1(K_ug)I_0(K_ua)}{I_1(K_ug)K_1(K_ua) - K_1(K_ug)I_1(K_ua)}\right]$$

and so depends only on the dimensions of the fuel element and K_u, the inverse diffusion length in the element

$$S = 1 + \frac{l_uK_u^2(a^2 - g^2)X}{l_gK_g^2G(b^2 - c^2)}$$

where

$$1 + X = \left[\frac{K_g^2b^2 - K_g^2c^2}{2K_gc}\right] \times \left[\frac{I_1(K_gb)K_0(K_gc) + K_1(K_gb)I_0(K_gc)}{I_1(K_gb)K_1(K_gc) - K_1(K_gb)I_1(K_gc)}\right]$$

For a moderator which has a small absorption cross section we obtain by expansion:

$$S = 1 + \frac{l_uK_u^2(a^2 - g^2)}{2l_gG(y^2 - 1)} \left\{\left[\frac{y^4}{y^2 - 1} + \frac{K_g^2c^2(y^6 + 2y^4 - y^2)}{8(y^2 - 1)}\right] \ln y - \frac{3}{4}y^2 + \frac{1}{4} - \frac{K_g^2c^2}{48}(8y^4 - y^2 - 1)\right\}$$

where $y = b/c$.

In the case of graphite the terms containing K_g contribute only an amount of the order of 0.1%–0.2% to S in the region of interest. Therefore, we see that the terms K_u and $l_uK_u^2/l_g$ determine the fine-structure distributions, according to diffusion theory.

In practice, of course, the lattice cell is not cylindrical. For the case of a cylindrical fuel element in a square lattice cell the angular fine-structure distribution has been obtained by diffusion theory.[1] The appropriate corrections can then be applied to the observations in order to compare them with the cylindrical cell formulae.

In fact from the experimental distributions we obtain

$$K_u = 0.89 \text{ cm}^{-1}$$

and

$$\frac{l_u K_u^2}{l_g} = 0.36 \text{ cm}^{-2}$$

for uranium of density 18.9 gm per cm^3 and graphite of density 1.60 gm per cm^3.

These values are to be compared with calculated values

$$K_u = 0.85 \text{ cm}^{-1}$$

and

$$\frac{l_u K_u^2}{l_g} = 0.37 \text{ cm}^{-2}$$

using the nuclear data for uranium referred to in the paper by Egelstaff *et al.* and tabulated in Appendix II, and the formulae

$$K_u^2 = 3\Sigma_a(\Sigma_a + \Sigma_s)$$

$$l_u K_u^2 = 3\Sigma_a$$

This agreement is fortuitous since other measurements confirm the tendency for K_u to vary with fuel element diameter and $l_u K_u^2/l_g$ with air channel diameter.

The P_3 spherical harmonic approximation, using the method described in the paper by Tait, gives values for G and S which are greater than those of diffusion theory and greater than those observed. Agreement can be obtained by suitably adjusting the nuclear data used.

CALCULATION OF THERMAL UTILISATION

The calculation of thermal utilisation requires a knowledge of the appropriate cross sections in addition to the physical details of the lattice and the fine-structure distributions. For this purpose the uranium cross-section data referred to in the paper by Egelstaff *et al.* has been used. The aluminium and graphite cross sections have been determined in the GLEEP pile oscillator by comparison with standards using a boron cross section of 783 barns at 2200 m/sec. The data used are tabulated in Appendix II. The absolute cross section of the graphite standard has been determined by correlating a series of diffusion length measurements with the GLEEP comparisons of absorption cross section.

The calculation of the cross sections to be used has taken account of the neutron spectrum in the pile by assuming it to be represented by a Maxwellian distribution with a $1/E$ tail. The figures used have been provided by J. S. Storey who has assumed that the Maxwellian distribution is valid to an energy of $4.3kT$. This cut-off point and the proportion of the $1/E$ contribution, λ, has been determined by an analysis of the neutron spectrum in BEPO.

Values of λ for other lattices have been computed from the formula

$$\lambda = \frac{CN_u\sigma_u V_u}{N_m\sigma_{sm}\xi_m V_m} \frac{(1 + K^2L^2)}{(f_u)}$$

where f_u is the fraction of neutrons captured in the uranium.

The constant C normalises the calculated value to the observation in BEPO[2] and the variation in λ across the lattice cell is obtained by assuming that it is inversely proportional to the thermal fine-structure flux. This formula gives good agreement with the changes observed in indium-cadmium ratio measurements when the lattice construction is changed.

The effect of the small air channels on the fine-structure flux distribution has been taken into account by a factor R which is the ratio of minimum flux in the graphite to maximum flux in the graphite. This factor has been evaluated from diffusion theory[3] and is approximately

$$R = 1 + \frac{l_u K_u^2 a}{3G}(1 - g^2/a^2)(1 - a/c)$$

The formula for S for no air channels is then modified by replacing G by GR. The ratio average flux in moderator to average flux in uranium is then given by GRS.

CALCULATION OF SLOWING DOWN AND DIFFUSION AREAS

The slowing down area in a lattice containing uranium and graphite has been taken to be

$$L_s^2 = (353 - 85P)\frac{(1 + a^2 - g^2)}{(b^2 - c^2)}$$

for a graphite density of 1.65 gm per cm^3. This assumes that the air channels can be allowed for separately by a correction to the graphite density. The slowing down of neutrons by elastic collisions in the uranium is neglected and for simplicity it has been assumed that the effective mean free path during slowing down is the same in the uranium and graphite. The small amount of aluminium is regarded as air.

The diffusion area in the lattice has been calculated by diffusion theory assuming that the cross sections used are weighted by the fine-structure flux distributions. For a graphite density of 1.65 gm per cm^3, the measured diffusion areas in graphite fit the formula, $L_m^2 = 1.10/\sigma G$ m^2 for graphite of cross section σ_G mb

Table II

Uranium diameter, in.	$\eta_{0.60}$	$(\int \sigma_u dE/E)_{eff}$	η_0
1.20	2.006 ± 0.010	7.6 ± 0.3	1.943 ± 0.010
1.00	1.989 ± 0.007	7.7 ± 0.3	1.935 ± 0.007
1.64 od 1.30 id	1.970 ± 0.006	9.8$_5$ ± 0.3	1.936 ± 0.006

measured at 2200 m/sec.

DETERMINATION OF THE YIELD OF NEUTRONS, $\eta_0\epsilon_0$, AND THE EFFECTIVE URANIUM RESONANCE INTEGRAL $(\int\sigma_u dE/E)_{eff}$

The critical equation is

$$\eta\epsilon pf = (1 + K^2L^2)(1 + K^2L_s^2)$$

and K^2, L^2, L_s^2 and f are known. The thermal utilisation f refers to the thermally fissile material, i.e., U^{235} in this analysis.

Now

$$\eta = \eta_0(1 + \delta\eta)$$
$$\epsilon = \epsilon_0(1 + \delta\epsilon)$$

where $\delta\eta$ allows for the neutron spectrum departing from a Maxwellian and $\delta\epsilon$ allows for the U^{238} fissions in fuel elements adjacent to the source element. η_0 then refers to a Maxwellian distribution and ϵ_0 to a single fuel element. $\delta\eta$ is calculated from the neutron cross-section data and $\delta\epsilon$ is obtained by assuming that the lattice outside the source fuel element can be considered to be a homogeneous mixture.

Therefore, we now have

$$\eta_0\epsilon_0 p = \frac{(1 + K^2L^2)(1 + K^2L_s^2)}{(1 + \delta\eta)f(1 + \delta\epsilon)}$$

which is known.

It is now assumed that p can be expressed by:

$$p = \exp - \left[\frac{N_u V_u (\int\sigma_u\, dE/E)_{eff}}{N_m\sigma_{sm}\xi_m V_m}\right]$$

The use of resonance neutron fine structure distributions does not appreciably alter the results of the analysis and as it is a rather doubtful refinement it is neglected. The equation can then be written as

$$\ln(\eta_0\epsilon_0) = \ln\left[\frac{(1 + K^2L^2)(1 + K^2L_s^2)}{(1 + \delta\eta)f(1 + \delta\epsilon)}\right] + \frac{N_u V_u (\int\sigma_u\, dE/E)_{eff}}{N_m\sigma_{sm}\xi_m V_m}$$

Graphs of the first quantity on the right-hand side of this equation vs the second are given in Fig. 1 for the three fuel element shapes used in the series of exponential experiments. It is seen that the fit to the assumed functional form is good The values of $\eta_0\epsilon_0$ and $(\int\sigma_u\, dE/E)$ are given in Table II.

The errors result only from the error on K^2.

Figure 2 shows $(\int\sigma_u\, dE/E)_{eff}$ as a function of the surface to mass ratio of the fuel element and if

$$(\int\sigma_u\, dE/E)_{eff} = A + BS/M$$
$$A = 5.0 \pm 0.5 \text{ barns}$$
$$B = 35 \mp 5 \text{ cm}^2 \text{ per gm}$$

For the case of tubes the outer surface only has been used in calculating S/M.

The values of η_0 quoted in the last column of Table II are deduced from $\eta_0\epsilon_0$ by calculating η_0 according to the known standard method using declassified data.

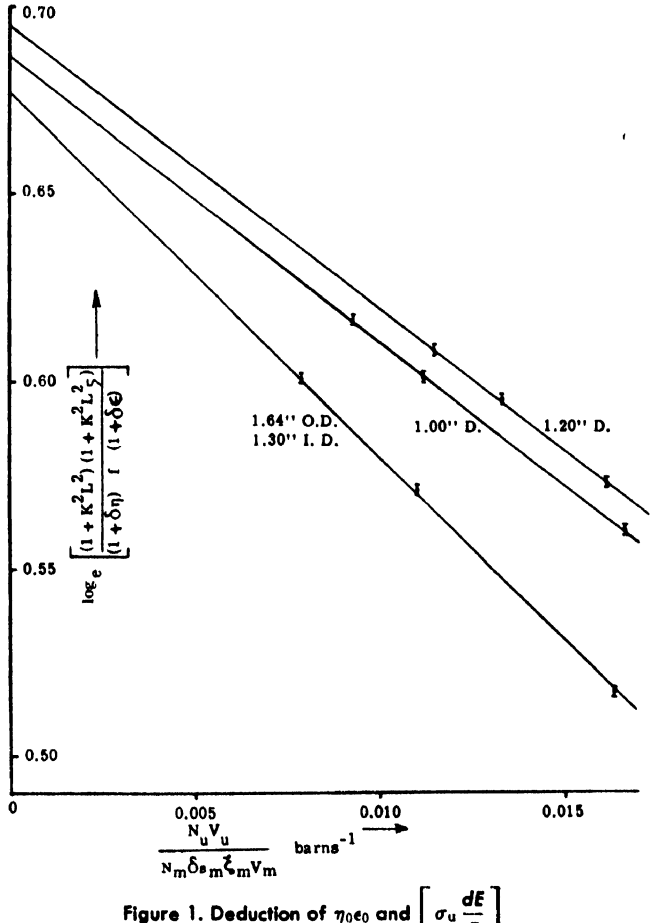

Figure 1. Deduction of $\eta_0\epsilon_0$ and $\left[\sigma_u \frac{dE}{E}\right]_{eff}$

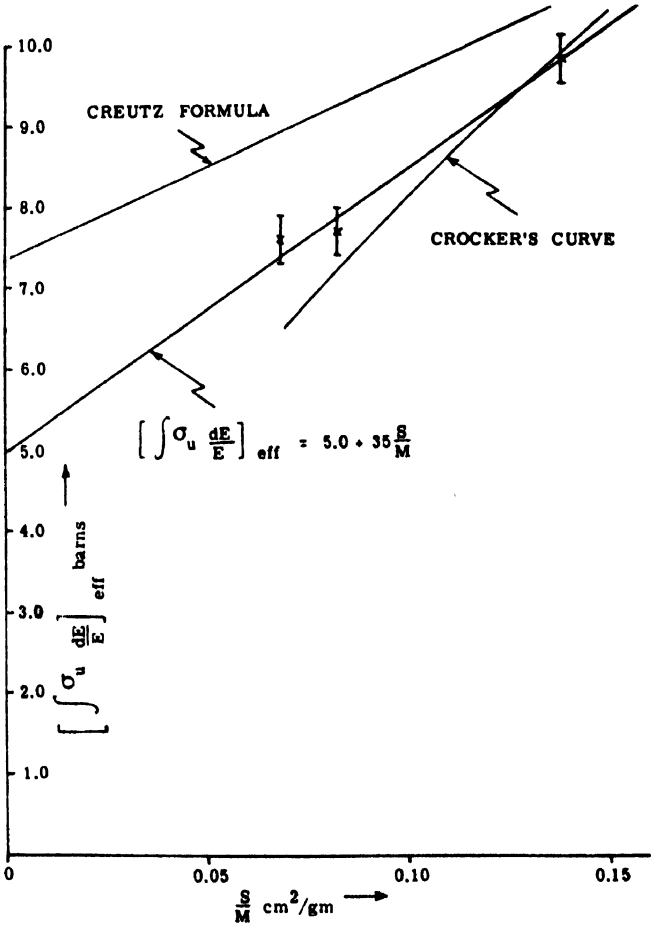

Figure 2. Deduction of surface to mass formula

Table III

Uranium diameter, in.	*Lattice pitch, in.*	η_0
1.36	8.91	1.934
1.20	8.91	1.937
	8.25	1.937
	7.56	1.936
1.00	8.25	1.939
	7.56	1.938
	6.30	1.942
1.90 (BEPO)	7.25	1.941
1.64 od 1.30 id	8.91	1.937
	7.56	1.938
	6.30	1.936

The values of η_0 for all the experiments have been deduced by using the formula for the effective uranium resonance integral deduced above. These are tabulated in Table III.

There is a total variation in η_0 of 0.4% only showing that the formulae adopted are in excellent agreement with the experimental results.

COMPARISON WITH DIRECT MEASUREMENTS

An attempt has been made in a paper by Crocker to relate self-indication measurements of the epi-cadmium absorption of a beam of neutrons in uranium with the effective uranium resonance integrals in a reactor. Creutz *et al.*[4] have published results obtained by determining the U^{239} activity in irradiated uranium spheres. The agreement between these measurements and the analysis considered in this paper is reasonably good bearing in mind the errors involved.

The value for η_0 deduced from these experiments, 1,94, is to be compared with 2.19 ± 0.14 deduced from the data quoted in papers by Egelstaff, Raffle and Sanders. However, pile-oscillator measurements suggest that a value of 2.05 is more appropriate. The error on 1.94 is difficult to estimate since there may be a systematic error in the method of calculation assumed. It is likely that the value is not in error by more than a few per cent and it is, therefore, of equal value to that deduced from direct measurements of absorption and fission cross sections and of the neutron yield per fission.

CONCLUSIONS

It is concluded that integral measurements can be successfully correlated with simple lattice calculations and that the values of neutron yield and effective uranium resonance integral deduced have errors comparable with values deduced by other techniques. The value of η deduced for U^{235} appears to be rather lower than that deduced in other ways.

Use of a method of calculation which has been correlated with experiment will give accurate predictions of neutron fates in reactors.

ACKNOWLEDGEMENT

The author wishes to thank the many people who have helped to produce the experimental results, formulae and computations referred to in this paper.

Appendix I: Experimental Determinations of Laplacian K^2

Uranium diameter, in.	*Lattice pitch, in.*	*Coolant channel diameter, in.*	*Aluminium sheath thickness, in.*	*Graphite cross section at 2200 m/sec, mb*	*Graphite density, gm/cm³*	K^2, m^{-2}
1.36	8.91	1.91	0.11	4.65	1.62	0.90
1.20	8.91	1.91	0.04	4.65	1.62	0.97
	8.25	1.60	0.04	4.86	1.61	1.04
	7.56	1.75	0.04	4.93	1.62	1.03
1.00	8.25	1.60	0.10	4.86	1.61	0.56
	7.56	1.75	0.04	4.93	1.62	0.86
	6.30	1.88	0.10	4.65	1.62	0.96
0.90 (BEPO)	7.25	2.10	0.03	4.90	1.63	0.83
1.64od 1.30id	8.91	1.91	—	4.65	1.62	0.67
	7.56	1.75	—	4.93	1.62	0.80
	6.30	1.88	—	4.65	1.62	0.55

Appendix II: Cross-Section Data

All values are quoted at 2200 m/sec.

σ_{235}^a	721	barns
σ_{235}^f	638	barns
σ_{238}^a	2.77	barns
σ_{AC}^a	0.217	barns (standard)
σ_G^a	4.72	millibarns (standard)

REFERENCES

1. Newmarch, D. A., *The Diffusion Theory of Fine Structure in Thermal Neutron Reactor Assemblies Consisting of Cylindrical Fuel Elements Set in a Square Lattice Array.* AERE RP/R 1704.
2. Taylor, B. T., *Measurement of the Neutron Spectrum at the Centre of the Harwell Pile.* AERE N/R 1005.
3. Newmarch, D. A., *A Modification to the Diffusion Theory of the Thermal Fine Structure in a Reactor to Account for the Effect of Air Channels.* AERE RP/R 1447.
4. Creutz, E., *et al., Review of Measurements of the Resonance Absorption of Neutrons in Uranium in Bulk.* Journal of Applied Physics *26*, p. 257 (1955).

Normal Uranium, Graphite-Moderated Reactors: a Comparison of Theory and Experiment—Water Cooled Lattices

By Paul F. Gast,* USA

A large amount of data is now available giving the bucklings measured in exponential experiments on a variety of water cooled, graphite moderated lattices. Analysis of this data in terms of theory has just begun and the subject is presently in a rather chaotic state. Initial attempts to fit the data by the classical, four-factor formula for the multiplication constant have not been completely successful even for a restricted selection of measurements from all the available data. Shortcomings in the classical formula are readily apparent and ways to improve the treatment are presently known but have not yet been applied because of calculational complexity. The methods are adapted for high speed computer use and some computations are now in progress.

Success in developing a satisfactory lattice theory will be dependent upon reducing the number of adjustable parameters through independent measurement of such quantities as f and p. A test reactor which will provide sufficient neutron flux to facilitate such measurements is now under construction and will soon be in operation.

With the application of methods now known, and the accumulation of additional experimental data it can be expected a satisfactory theory of graphite uranium lattices will be developed.

COMPARISON OF LATTICE THEORY AND EXPERIMENT

Davenport[1] has presented the results of exponential experiments on graphite moderated lattices. A large fraction of this data was obtained with lattices designed for light water cooling of the uranium. Data were obtained both with and without the water present in the annular space surrounding the uranium. In what follows, the measurements with water present will be designated "wet," those without water as "dry."

For the initial attack on the problem of theoretical interpretation of the large amount of data available, measurements made with a single size of natural uranium fuel element were selected. This selection of a single fuel element diameter reduced the complexity of the initial approach to the problem by eliminating variations in ϵ and η, and also by holding constant the effective resonance absorption cross section of the uranium.

The fuel element of 1.36-inch diameter was selected for the study since there was more data available for this diameter from the exponential experiments and because this data could be supplemented by additional information obtained from actual reactor operation for one of the lattices. Measurements from a set of six lattice spacings were available with this fuel element ranging from $6\frac{3}{16}$ to $10\frac{3}{8}$ inches. Both wet and dry values of the buckling had been determined for each spacing.

Analysis of the data for this restricted set of instances was attempted by the classical formula for the buckling

$$B^2 = \frac{fp\eta\epsilon - 1}{L^2 + fp\eta\epsilon\tau} \qquad (1)$$

This equation can be rewritten, using the constancy of $\eta\epsilon$ for the cases considered, in the form:

$$\ln \frac{1 + B^2L^2}{f(1 - B^2\tau)} - \ln p = \text{const} = \ln \eta\epsilon \qquad (2)$$

The values of f were calculated from the formulas of Rumsey and Volkoff. These formulas are an extension to include the effect of the water annulus, of those presented by Guggenheim and Pryce[2] and others.[3] Since the formulas are not available in an unclassified report they have been reproduced in Appendix I.

Values of L^2 and of τ were obtained from the usual formulas which also are given in Appendix I.

The values of the measured bucklings are then used to calculate the first term in Equation 2 for each lattice. The value of $\ln p$ is then given by an expression of the form:

$$\ln p = \frac{-N_u V_u \sigma_{eff}(1 + \delta)}{Z + N_u V_u \sigma_{eff}(Y - \delta)} \qquad (3)$$

This formula, due to Rumsey and Volkoff is also discussed in Appendix I where the meanings of the symbols Z, Y, and δ are given. These quantities can be calculated from the dimensions and cross sections of the various lattice components. In addition: N_u is

* Hanford Atomic Products Operation, General Electric Company. Including work done by E. D. Clayton, D. J. Donahue, W. B. Farrand, C. R. Richey, G. W. Stuart, and R. W. Woodruff.

Table I. Values of Effective Resonance Cross Section

Lattices paired	*Dry values*	*Wet values*
6 3/16–7	1.67 barns	1.65 barns
6 3/16–7 1/2	1.69	1.71
6 3/16–8	1.69	1.65
6 3/16–8 3/8	1.69	1.66
6 3/16–10 3/8	1.57*	1.54*
7–7 1/2	1.75*	1.84*
7–8	1.71	1.66
7–8 3/8	1.72	1.67
7–10 3/8	1.52*	1.48*
7 1/2–8	1.66	1.44*
7 1/2–8 3/8	1.70	1.54*
7 1/2–10 3/8	1.45*	1.36*
8–8 3/8	1.76*	1.70
8–10 3/8	1.67	1.34*
8 3/8–10 3/8	1.88*	1.24*
Average excluding stars	1.69	1.67
Average including stars	1.68*	1.57*
Range	1.45–1.88	1.24–1.84

the atomic density of uranium, V_u is the volume of uranium, and σ_{eff} is the effective resonance absorption cross section of the uranium rod, commonly given by $A(1 + \mu S/M)$, where S/M is the surface to mass ratio of the rod and A and μ are constants.

A value of σ_{eff} may be obtained from Equation 2 for any pair of lattice measurements. Such values were computed from each pair of wet measurements and from each pair of dry measurements. The results are given in Table I. If the process described above gave a complete interpretation of the data the values of σ_{eff} obtained would be expected to lie close to a mean value. Actually only half of the results are so grouped, the remaining ones showing wide deviations. The broad deviants are starred in the Table. The values obtained for $\eta\epsilon$, 1.346 in the dry lattice and 1.349 in the wet lattice, are consistent with a calculated η of 1.30 and an ϵ of 1.033. The calculated values of the buckling are not particularly sensitive to the σ_{eff} for resonance capture as is shown by Fig. 1 where the curves calculated with the average values show good agreement with the measured bucklings in all cases except those of the 10 3/8-inch lattice. The lack of agreement for this latter case represents a serious unexplained discrepancy.

When the values of σ_{eff} were used with the expression $\sigma_{eff} = A(1 + \mu S/M)$ values of A were obtained of 8.12 barns for dry lattices and 8.00 barns for wet lattices. The value of μ was taken as the usually accepted one of 2.5.

Table II. Comparison of Values of f and p for 8 3/8-inch Lattice

	Wet	*Dry*
f calculated in above analysis	0.867	0.896
f measured	0.876	0.903
p calculated in above	0.899	0.888
p measured	0.867	.....
fp calculated above	0.779	.....
fp measured	0.759	.....

The neutron density in the exponential piles is not great enough to make direct measurements of f and p feasible for all cases. However, for the 8 3/8-inch lattice f has been determined by foil activations and p has been determined from the production of plutonium achieved in reactor operation. The results are tabulated in Tables I and II. The difference between the last two numbers in Table II amounts to 2.6% in k, a serious discrepancy in the design of large reactors.

It has long been recognized that the thermal neutron distribution throughout a lattice cell is given inadequately by diffusion theory. The calculation of the disadvantage factor in the uranium rod is especially inaccurate and the inner boundary conditions for the neutron density in the graphite are also in need of improvement. In the calculations reported here a measured disadvantage factor for the uranium was used.

Some improved results have been obtained in the calculation of the neutron density by the use of the spherical harmonics expansion of the neutron flux. These calculations, carried out by R. R. Haefner and by J. W. Weil broke off the expansion after the P_3 term. This procedure probably gives an adequate representation of the neutron flux in such moderators as

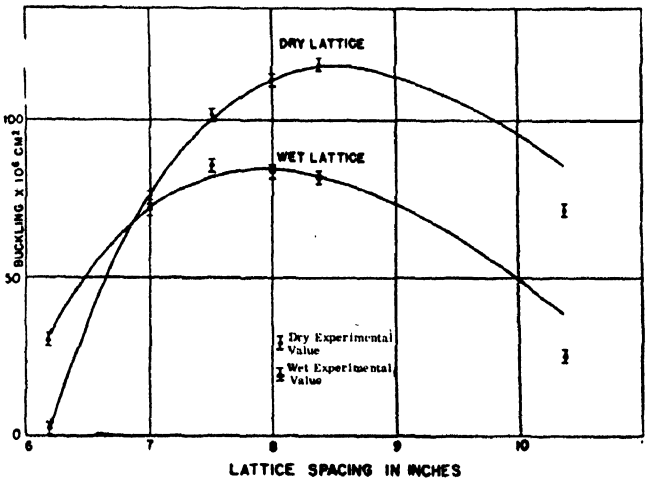

Figure 1. Theoretical buckling curves

graphite and heavy water but there is some question about the adequacy in a strongly absorbing material such as uranium.

In a material of high atomic weight the neutron density can be obtained as a power series in Σ_s/Σ_t which will converge more rapidly the stronger the absorption as compared to the scattering. This expansion is obtained from the integral form of the transport approximation to the Boltzmann equation (isotropic scattering in the laboratory system).

$$\vec{\phi}(\vec{r}) = \vec{S}(\vec{r}) + \int_u \frac{\Sigma_s \vec{\phi}(\vec{r}) e^{-\Sigma_t |\vec{r}-\vec{r}'|}}{4\pi |\vec{r} - \vec{r}|^2} d\vec{r}' \qquad (4)$$

The source term S in this particular case represents those neutrons, entering the uranium from outside, which have not yet made their first collision in the uranium. The solution of the equation was obtained

by G. W. Stuart and R. W. Woodruff by the Neumann-Liouville procedure of successive substitutions, namely writing:

$$K(r,r') = \frac{e^{-\Sigma|\vec{r}-\vec{r}'|}}{4\pi|\vec{r}-\vec{r}'|^2}$$

$$\phi(\vec{r}) = S(\vec{r}) + \sum_s \int_u K(r,r')S(\vec{r}')\,d\vec{r}' \qquad (5)$$

$$+ \sum_s^2 \iint_u K(r'',r')K(r',r)S(\vec{r}'')\,d\vec{r}''\,d\vec{r}' + \cdots$$

where the integrals are each carried out over the volume of the uranium. The terms in the series of Equation 5 have physical meaning. The first term is the density of uncollided neutrons; the second term those neutrons which have suffered a scattering collision in the uranium; the third term those which have suffered two scattering collisions, and so on. For this reason the method has been named the "Method of Successive Generations." The integrals are adaptable for computation on high speed, digital computers. For their first computations, Stuart and Woodruff have taken the directional distribution of the neutron flux entering the rod as independent of angle. It is expected that the results may later be extended to include other entering distributions, for example, the spherical harmonics. The results can be made more general by measuring the rod radii in units of mean free path and locations within the rod in fractions of the radius. In Fig. 2 we show results for the first three

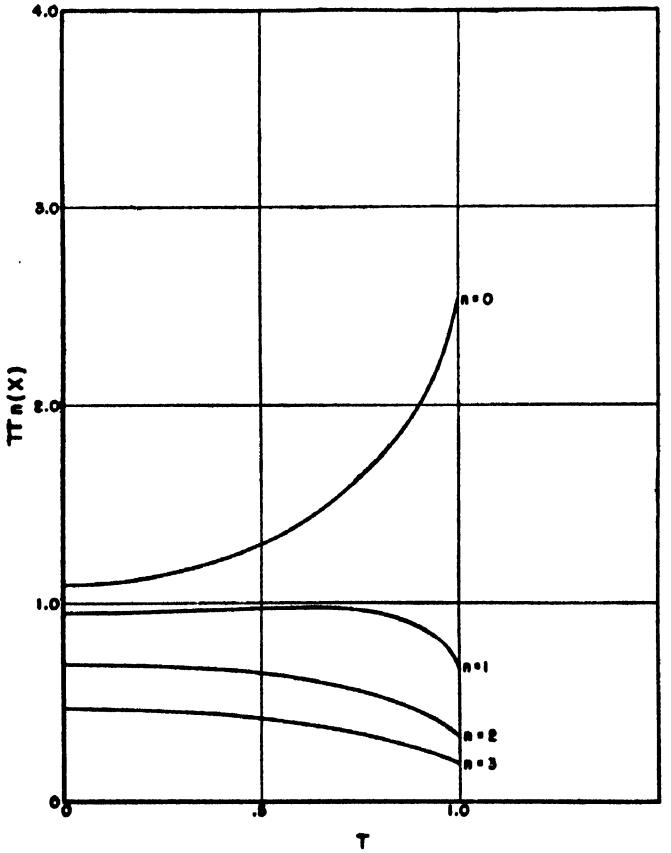

Figure 2. $\pi n(X)$ vs T for $X = 1.00$

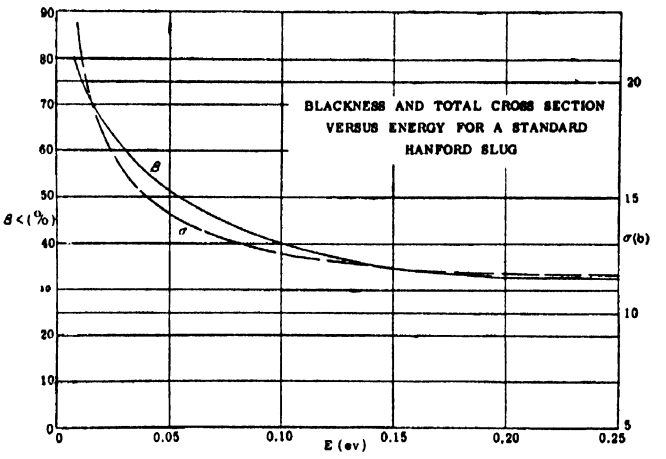

Figure 3. Blackness and total cross section versus energy for a standard Hanford slug

generations for a rod of radius equal to the mean free path. The entering flux is given by the $n = 0$ curve. Further machine calculations are now in progress to extend the method.

Some preliminary results of interest have already been obtained. In uranium it is reasonable to assume that thermal neutrons are scattered without energy change and that each entering neutron therefore retains its entering energy until it either escapes from the rod or is captured. Consequently it has been possible to compute the blackness, i.e., fraction of the entering neutrons absorbed, as a function of energy for any rod diameter. The results for one diameter are shown in Fig. 3. These results can then be applied to a determination of the hardening of the neutron energy spectrum produced by the slug. As an example, Fig. 4 shows that if the spectrum incident upon the rod is Maxwellian, then the exit spectrum is well represented by a Maxwellian distribution of higher temperature. In the particular example shown, the incident temperature is 293°K on a rod of 1.36-inch diameter and the exit spectrum temperature is 73°K higher.

While these results are all of interest, there is a long road yet to travel to achieve a satisfactory solution of the thermal neutron problem. The greatest difficulty remaining is probably in the treatment of the water annulus. A transport approximation may not be valid for scattering from water molecules and higher spherical harmonics may be required. The angular, differential scattering cross sections of neutrons on water molecular are largely unknown in the thermal energy range.

In lattices of the type under consideration, about 5% of the fissions of U^{235} are produced by neutrons of energy above 0.5 ev. The bulk of these fissions are due to the $1/v$ portion of the cross section but 10%, or 0.5% of the total, arise from resonance peaks. It has been customary in the past to regard all events arising from the $1/v$ portions of cross sections as accounted for in the thermal neutron calculations of f and η. Only the excess absorption, above that arising from the $1/v$ portions has been treated in the resonance capture formula.

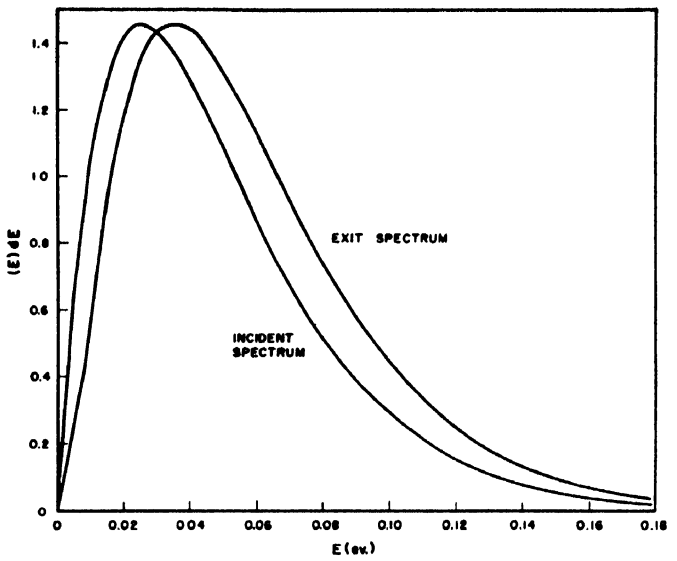

Figure 4. Incident and exit flux spectra of a nominal Hanford uranium slug

This method of treatment encounters difficulties in studies of the effects associated with the temperature of the moderator. The distribution in energy of those neutrons which have been "thermalized" is strongly affected by a change in moderator temperature. Any such change makes an important contribution to the temperature coefficient of reactivity because of the non-$1/v$ nature of most of the important cross sections. On the other hand, the slowing down distribution is unaffected by changes in moderator temperature apart from any effects which result from density changes. These difficulties are particularly prominent in cases where the fuel elements contain significant amounts of Pu^{239} with its resonance peak at 0.3 ev. In this case the temperature coefficient is increased and also the amount of higher isotopes of plutonium formed depends significantly upon the moderator temperature.

It is proposed that all processes occurring during slowing down be properly treated as such and that only thermalized neutrons be considered in the calculation of f and η. As a first step in this direction, the classical four-factor formula would be modified to include "resonance" fission. The multiplication factor would be given by:

$$k = \frac{\eta_{th}\epsilon f p}{1 - (1 - p)\eta_R \epsilon} \qquad (6)$$

in which η_{th} and η_R are the neutrons produced per neutron captured in uranium at thermal energies and resonance energies respectively and the value of p should be computed for the total absorptive processes in the resonance energy range. The buckling would be given by the usual formula in which the age would now be given by

$$\tau = \tau_{th} + \frac{(1 - p)\eta_R \epsilon}{\eta_{th}\epsilon f p}\tau_R \qquad (7)$$

in which τ_{th} is the age of thermal neutrons and τ_R is the mean age of neutrons undergoing resonance capture.

The method of successive generations is well suited for the computation of p, η_R and τ_R when uranium metal fuel elements are used since scattering without energy loss can reasonably be assumed in the fuel element. Starting initially with a $1/E$ spectrum in the moderator an iterative procedure can be used to determine the total absorptions in the fuel and the final energy spectrum. The results for dry lattices would then be as reliable as the cross-section curves permitted. The treatment of the water annulus would create some additional problems in wet lattices.

EXPERIMENTAL REACTOR

The carrying through of any such program of development of the theory as suggested above would be greatly aided by reliable measurements of f, p, ϵ, and other parameters in a variety of lattices. To carry out such measurements on a routine basis requires higher neutron levels than are available in exponential piles.

A special type of experimental reactor to facilitate these measurements is under construction and will soon be in operation. In addition to these measurements the reactor is expected to provide a means of measuring changes in buckling, as compared to a standard lattice, with high precision and to be useful in determination of temperature coefficients of reactivity. Figure 5 is a drawing showing the principal features. Of interest here is the large central cavity into which a section of test lattice may be placed. The reactor is made critical by a ring of highly enriched fuel elements surrounding the cavity and by similar elements in the rear wall of the reactor and in the movable front wall. The front wall is here shown retracted from the face to allow the loading of a test section in the cavity. The fuel elements in the front and rear walls are movable with respect to the moderator for the purpose of leveling the neutron density distribution within the cavity.

The operating control rods consist of alternating sections of cadmium and a highly enriched uranium alloy. In its most absorptive position the rod is positioned so that the uranium alloy sections are covered by cadmium sleeves. A short motion of the rod serves to withdraw the uranium from the sleeves replacing it

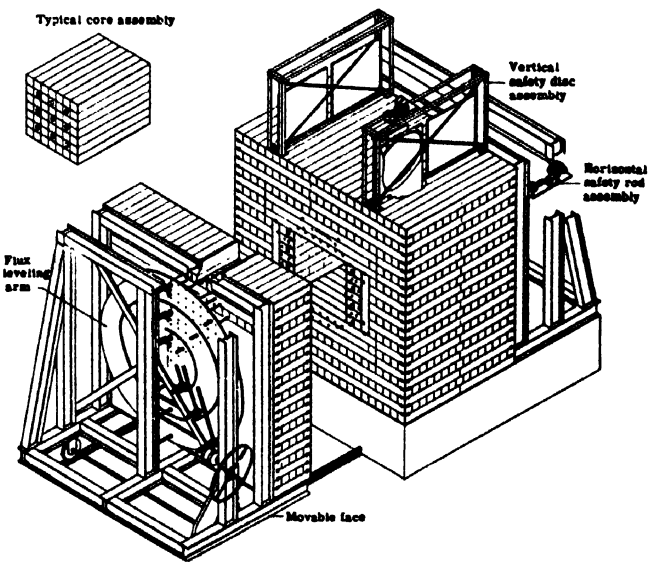

Figure 5. Physical constants testing reactor assembly

with the next adjoining cadmium section. In this condition the rod emits one fast neutron, on the average, for each neutron absorbed and is therefore essentially non-absorbing. The advantages of this construction are two-fold. The absorptive power of the rod can be changed without changing its position in the reactor; this allows control with minimum distortion of the neutron distribution. By judicious use of several rods it will be possible to maintain a symmetrical neutron distribution in the test lattice. The short distance which the rod must travel to go from the non-absorptive to the fully absorptive condition quickly in an emergency. The rods are spring loaded and can be put in the fully absorptive condition in ¼ second.

Additional safety is provided by four absorbing disks (cadmium-in-steel sandwich) which drop in slots, and finally, by melting of the fuel elements which are tubular and go to a more self shielding configuration upon melting.

TRANSLATION OF RESULTS TO ACTUAL REACTORS

The exponential experiments are carried out in graphite stacks which are solid except for the holes for the insertion of the tubes carrying the uranium and cooling water. In contrast, the actual reactor will be pierced with several groups of holes, for entry of control rods, for entry of safety rods, to allow a slow circulation of the atmosphere in which the pile is contained, and to allow for the exposure of experimental equipment and materials in the pile. Also the density and chemical purity of the graphite and uranium in the actual pile may be different from that of the materials used in the experiments. The atmosphere in which the pile is contained is not air, the atmosphere in which the experiments are performed. In some cases the amount of cooling water is different in the actual pile as compared with experiment. Corrections must be made for all of these differences to determine the reactivity status of any reactor design.

The effects of changes in purity and of density can be computed by the use of the appropriate formulas from Appendix I. In the case of large holes, such as those provided for control rods, neutron streaming must be taken into account, making the density correction somewhat more elaborate. The correction for cooling water changes is usually done empirically by interpolation or extrapolation from exponential experiment results.

The importance of the corrections is indicated by the following example. The exponential experiment buckling for an 8⅜-inch lattice using a 1.36-inch diameter uranium fuel element with no water is 118×10^{-6} cm^{-2}. Bucklings determined from the critical size of actual piles using this same basic lattice range from 84×10^{-6} cm^{-2} to 98×10^{-6} cm^{-2}. For a wet lattice of the same dimensions the exponential experiment gives 80×10^{-6} while actual pile loads had values ranging from 54 to 69×10^{-6}.

The various effects which were mentioned above account for the greater part of the observed differences. In some cases, there are, however, residual differences of the order of 5×10^{-6} cm^{-2} which are unexplained.

CONCLUSION

At present no completely satisfactory theory of heterogeneous, graphite, uranium lattices exists. Proper treatment of the thermal neutrons will require development of methods for treating the effect of the water annulus and for dealing with the actual energy spectrum and the non-$1/v$ cross sections. Such methods are foreshadowed in present work, but their development and application is a matter for the future. Treatment of neutron reactions in the resonance energy range will require inclusion of fission reactions along with the presently treated capture reactions and a more accurate treatment of both.

Additional direct experimental measurements of such quantities as f and p are desirable in order to reduce the number of adjustable parameters at the disposal of the theoretician.

A vigorous program along these lines may be expected to produce a satisfactory theory which will treat not only room temperature lattices but give acceptable values for temperature coefficients of reactivity and for the reactivity changes occurring with exposure of the fuel.

REFERENCES

1. Davenport, D., P/599 *Exponential Experiments in Graphite Lattices*, Volume 5, Session 21A, these Proceedings.
2. Guggenheim, E. A. and Pryce, H. L., *A Quantitative Study of Uranium-Graphite Lattices.*
3. Glasstone, S. and Edlund, M. C., *The Elements of Nuclear Reactor Theory*, Chapter IX, Van Nostrand, New York, London (1952) or
Weinberg, A. M., in *The Science and Engineering of Nuclear Power*, Clark Goodman, Ed., Vol. II, Chapter 6, Addison-Wesley, Cambridge (1949).

APPENDIX I: THERMAL UTILIZATION

The equation for thermal utilization as derived by V. H. Rumsey and G. M. Volkoff is

$$f_u = f_0(1 + \delta)$$

where

$$\frac{1}{f_0} - 1 = R_{al} + R_w + R_g + S_w + S_g + B_{w2} + B_{wg}$$

(the subscripts w, al, g, u, and $w2$ denote water, aluminum, graphite, uranium, and aluminum process tube, respectively)

$$\delta = \frac{q_w V_w}{q_g V_g}\left[X + \frac{1}{2}\kappa w^2 t_w^2 \frac{N_g \sigma_g V_g}{N_w \sigma_w V_w}\right]\left(1 + \frac{q_w V_w}{q_g V_g}\right)$$

The relative absorption terms R_i are defined as

$$R_i = \frac{N_i \sigma_i V_i}{N_u \sigma_u V_u} G_0$$

where G_0 is the disadvantage factor of the uranium,

$$G_0 = \frac{\kappa_u r_u}{2} \frac{I_0(\kappa_u r_u)}{I_1(\kappa_u r_u)}$$

κ_u is the effective inverse diffusion length of the metal and r_u is the radius of the uranium. B_{ij} denotes the "blocking" term in the j^{th} medium due to the neutron density across the i^{th} medium,

$$B_{w2} = \kappa_w^2 t_w^2 \frac{N_{al}\sigma_{al}V_2}{N_w\sigma_w V_w}$$

and

$$B_{wg} = \kappa^2 w^2 t_w^2 \left[\frac{N_g\sigma_g V_g}{N_w\sigma_w V_w} + R_g\left(\frac{1}{2} + \frac{N_{al}\sigma_{al}(V_{cap} + V_{can})}{N_w\sigma_w V_w}\right)\right]$$

κ_w is the inverse diffusion length of water, t_w is the water annulus thickness, V_2 is the volume of the aluminum in the process tube, and $V_{cap} + V_{can}$ is the volume of the aluminum in the slug can and the slug end cap. The "self blocking" terms S_w and S_g are defined as:

$$S_w = \tfrac{1}{2}\kappa_w^2 t_w^2$$

and

$$S_g = X[1 + R_{al} + R_w + B_{w2} + S_w]$$

where X is the disadvantage factor of the moderator,

$$1 + X = \frac{\kappa_g^2(r_2^2 - r_1^2)}{2\kappa_g r_1}\frac{I_1(\kappa_g r_2)K_0(\kappa_g r_1) + K_1(\kappa_g r_2)I_0(\kappa_g r_1)}{I_1(\kappa_g r_2)K_1(\kappa_g r_1) - K_1(\kappa_g r_2)I_1(\kappa_g r_1)}$$

κ_g is the inverse diffusion length in the moderator, r_1 is the inside radius of the graphite and r_2 is the effective outside radius of the graphite. q_w and q_g denote the rate of production of thermal neutrons per unit volume per second for water and graphite, respectively. The q_w/q_g is taken to be the ratio of the slowing down power of water to graphite, $q_w/q_g = 20$.

The thermal utilization of graphite, aluminum, and water can be calculated from the following equations:

$$f_g = f_g' - \frac{f_g'}{1 - f_0}(f_u - f_0)$$

$$f_{al} = f_{al}' - \frac{f_{al}'}{1 - f_0}(f_u - f_0)$$

and

$$f_w = f_w' - \frac{f_w'}{1 - f_0}(f_u - f_0)$$

where

$$f_g' = (R_m + B_{wm} + S_m)f_0$$

$$f_{al}' = (R_1 + R_2 + B_{w2})f_0$$

and

$$f_w' = (S_w + R_w)f_0$$

Lattice Diffusion Length

The lattice diffusion length is determined from the expression:

$$L_t^2 = \sum_i L_i^2 f_i$$

where L_i is the diffusion length for component i and f_i the corresponding utilization for this component. The above equation is the result of weighting the transport mean free path as to flux and volume and the absorption cross section in the same manner.

Fermi Age

For a graphite-uranium lattice the Fermi age is determined by the equation:

$$\tau_{dry} = [364(1 - P_1) + 231P_1]\left[1 + \frac{V_w + V_u + V_{al}}{V_g}\right]^2\left[\frac{1.6}{\rho}\right]^2$$

where ρ denotes the graphite density and

$$P_i = \left(\frac{P + P'}{2}\right)\frac{\sigma_i}{\sigma}$$

P and P' are the probabilities of collision inside the uranium lump for thermal and fast source distributions, respectively, σ_i and σ are the cross sections for inelastic scattering and total cross section for fission neutrons. The Fermi age for the wet lattice is determined from the expression:

$$\frac{V_{total}}{\tau_{wet}} = \frac{V_u + V_g + V_{al}}{\tau_{dry}} + \frac{V_{water}}{\tau_{water}}$$

where $\tau_{water} = 33$ cm^2.

Resonance Escape Probability

The equation for resonance escape probability can be expressed

$$P = \exp\left(\frac{-f_r}{1 - f_r}\right)$$

where f_r is the utilization of the fuel material for resonance neutrons. Therefore f_r has the same form as the thermal utilization expression

$$f_r = f_0(1 + \delta)$$

where

$$\frac{1}{f_0} - 1 = R_1 + R_2 + R_w + B_{w2} + S_w + R_m + B_{wm} + S_m$$

Substituting in the expressions for the various terms and gathering terms

$$\frac{1}{f_0} - 1 = \frac{G_0}{N_u V_u \sigma_{eff}}\left\{N_g\sigma_g V_g\left[1 + \kappa_w^2 t_w^2\left(\frac{1}{2} + \frac{N_{al}\sigma_{al}(V_{cap} + V_{can})}{N_w\sigma_w V_w}\right)\right] + (1 + X)(N_{al}\sigma_{al}V_{al} + N_w\sigma_w V_w)\right\} + \kappa_w^2 t_w^2\left\{\frac{1}{N_w\sigma_w V_w} \times [(X + 1)N_{al}\sigma_{al}V_2 + N_g\sigma_g V_g] + (X + 1)\frac{1}{2}\right\} + X$$

Letting

$$Z = G_0 \left\{ N_g \sigma_g V_g \left[1 + \kappa_w^2 t_w^2 \left(\frac{1}{2} + \frac{N_{al}\sigma_{al}(V_{cap} + V_{can})}{N_w \sigma_w V_w} \right) \right] + (X+1)(N_{al}\sigma_{al}V_{al} + N_w \sigma_w V_w) \right\}$$

and

$$Y = \kappa_w^2 t_w^2 \left\{ \frac{1}{N_w \sigma_w V_w} [(X+1) N_{al}\sigma_{al} V_2 + N_g \sigma_g V_g] + \frac{1}{2}(X+1) \right\} + X$$

results in

$$\frac{1}{f_0} - 1 = \frac{Z}{N_u V_u \sigma_{eff}} + Y$$

Now since

$$f_r = f_0(1 + \delta)$$

then

$$\frac{1}{f_r} - 1 = \frac{Z + N_u V_u + \sigma_{eff}(Y - \delta)}{N_u V_u \sigma_{eff}(1 + \delta)}$$

and

$$\ln P = \frac{-N_u V_u \sigma_{eff}(1 + \delta)}{Z + N_u V_u \sigma_{eff}(Y - \delta)}$$

Uranium Graphite Lattices—The Brookhaven Reactor

By I. Kaplan and J. Chernick,* USA

The design and operation of the Brookhaven reactor offered an opportunity for a critical comparison of an important aspect of reactor theory and practice. Although this study is limited to the case of a relatively primitive type of pile—a thermal, natural uranium, graphite-moderated, air-cooled pile—it can serve as a means of examining one of the successful recipes which has been developed for reactor design. The semi-empirical theory of reactor design must be distinguished from the more rigorous mathematical methods which are available for the treatment of many problems in neutron transport. Methods involving the Boltzmann equation have been applied successfully to such problems as the slowing down of neutrons by elastic collisions with atomic nuclei, but it has not yet been possible to use them widely in practical pile design. Here it has usually been necessary to use approximations which are known to be unsatisfactory, and to "adjust" the values of certain constants in the approximate formulas so as to make the theoretical results agree with those of exponential or critical experiments. Although the limitations of this procedure are recognized, the field of reactor physics has not yet reached the stage at which design calculations can be made safely without recourse to semi-empirical recipes.

The first object of this report is to describe the nuclear design calculations used for the Brookhaven reactor. The results of these calculations will be compared with experimental results obtained during subcritical operation of the reactor, during the initial period of critical operation, and in later measurements of certain reactor parameters. The discussion will include the multiplication factor, the migration area, the critical buckling and critical size, the effect of the central transverse gap, the excess reactivity needed, the temperature coefficient of the reactivity, and the xenon poisoning.

DESCRIPTION OF THE REACTOR AND GENERAL DESIGN CONSIDERATIONS

The Brookhaven reactor was designed as a research tool to meet the needs of many institutions in the northeastern part of the United States. A large number of groups was expected to use the facilities of the Brookhaven National Laboratory, and this meant that the reactor must be capable of supporting a large research program. The reactor had to be large enough, therefore, to accommodate many experiments at the same time and to be capable of continuous and reliable operation so as to avoid interruption of research. These considerations led to the choice of a thermal, normal uranium, graphite-moderated, air-cooled pile, the over-all design of which was settled in June 1947.

The Brookhaven pile consists of a 25-foot cube of graphite penetrated by a square array of 1369 channels (37 on a side) capable of containing uranium. The channels have a circular, cross-section area of 36 cm^2 and are spaced on 8-inch centers. The graphite cube is built in two equal parts separated by a central, transverse air gap. The gap permits the coolant air to enter each channel at its center so that hot air leaves from each end of the channel. The incoming cold air strikes the metal which generates heat at the greatest rate and cools the graphite at the center of the structure. The metal assemblies contain uranium slugs 1.1 inch in diameter (1.4 cm in radius) and 4.0 inches long; thirty-three of these slugs are contained in a finned-aluminum cartridge 11 feet long, and each loaded channel contains two cartridges, one on each side of the central gap.

The pile was designed to have enough excess reactivity to allow sustained operation at a maximum flux of 5×10^{12} neutrons per cm^2 per sec. To attain this neutron flux, the maximum temperature at the uranium-aluminum interface was expected to be 350°C, and the temperature of the exit air was expected to be about 200°C. An air flow rate of 270,000 cubic feet per minute was needed with a pressure drop across the graphite of 55 inches of water (103 mm Hg). Under these conditions, the pile was expected to operate at a rate of 25 to 28 megawatts, depending on the metal loading.

In a general way, the design of the Brookhaven pile is based on that of the Oak Ridge graphite pile, with modifications caused by the desire for a higher neutron flux. To attain the higher flux, the uranium slugs are loaded into the long, finned-aluminum containers mentioned above, and the air channels surrounding the cartridges are increased in area over that of the Oak Ridge pile. The most important departure from the Oak Ridge design is the use of the central transverse gap into which the cooling air is introduced. The gap offers the advantage that the cold air is brought into the center of the pile and traverses only half of it; the power needed to pump the air is then only about one-third as great as would be needed if the air were to travel from one end of the pile to the other. Each of

* Brookhaven National Laboratory, Upton, New York.

these three methods for increasing the efficiency of heat removal decreases the neutron economy of the pile. The fins make it necessary to use more aluminum than was used at Oak Ridge, while the greater channel area and the central gap increase the neutron leakage. The over-all design of the pile, therefore, required a careful balance between increased engineering efficiency and losses in neutron economy. In the case of the central gap, great pains were taken with the calculations, both because of the novelty of the problem and the delicacy of the balance.

An additional design problem arose because insufficient information about the purity of the graphite was available during the design period. The functional properties of the graphite were actually determined experimentally after the design of the pile had been settled. It was found, after careful sampling and testing, that the graphite to be used in the core of the reactor was significantly better than was assumed in the design calculations. The calculations were then repeated with the actual graphite parameters to get a more realistic estimate of how the pile would behave. Although this procedure led to considerable extra work, it provided a valuable lesson in some of the practical problems of reactor design.

For the reader's convenience, a brief outline of the nuclear design procedure will now be given; the details will be discussed in the following sections of the report. The value of the multiplication factor was first computed for an infinite, heterogeneous lattice at room temperature and without fission product poisoning; the slowing-down and diffusion areas were then calculated under the same conditions and without taking into account the effect of the central gap. The results led directly to the critical buckling and critical size of a bare, cold, unpoisoned pile without a central gap. The calculations were made for different values of the radius of the uranium rod, for different distances between rod channels, and for different values of the area of the rod channel. On the basis of these calculations, and with proper regard for the requirements of heat removal, a choice could be made of the three main lattice parameters: the rod radius, the lattice spacing, and the channel area. The effect of the amount of aluminum in the fuel container was then found as a function of the ratio of aluminum volume to uranium volume. The value of this ratio was fixed by making a suitable compromise between metallurgical and heat-removal requirements on the one hand and the increase in critical size on the other hand. The effect of the central gap on the critical size was found as a function of the gap width, and the excess reactivity which could be obtained was computed as a function of pile size for different values of the gap width. The excess reactivity needed to meet the requirements set on the pile were found by estimating the effect of increased temperature on the reactivity, the effect of fission product poisoning, and the reactivity needed for experimental purposes. These estimates indicated that an excess reactivity (δk) between 0.020 and 0.025 would be needed. The early calculation of excess reactivity as a function of pile size showed that this amount of reactivity could be supplied by a cubic pile 25 feet on a side and with a gap 7 centimeters wide. This gap width was satisfactory from the viewpoint of heat removal and was chosen as the design value. As mentioned above, the early calculations were uncertain because of the incomplete information about the properties of the graphite. The choice of a 25-foot pile was, therefore, a somewhat pessimistic one. The effect of the more favorable graphite properties was to decrease the metal loading and allow a thicker graphite reflector than was considered feasible at first.

THE CALCULATION OF THE MULTIPLICATION FACTOR

The methods used for the calculation of the multiplication factor and other reactor quantities were developed, for the most part, during the years 1941–1944 during the early work on chain-reacting piles. Much of this material is now available [1–4] so that the basic theory will not be discussed; the emphasis will be on showing how the theory is used.

The multiplication factor for an infinite, natural-uranium, graphite pile can be written in the familiar form:

$$k = \eta \epsilon p f \tag{1}$$

where η is the number of neutrons produced for each thermal neutron absorbed in uranium; ϵ, the fast fission factor, is the total number of neutrons which reach the resonance energy region of the fuel per neutron produced by thermal fission; p, the resonance escape probability, is the fraction of neutrons which escape resonance capture and become thermal neutrons; f, the thermal utilization, is the fraction of all thermal neutrons produced which are absorbed in the uranium.

The quantity η is given by

$$\eta = \frac{\sigma_f(U^{235})N(U^{235})\nu_t(U^{235})}{\sigma_a(U^{235})N(U^{235}) + \sigma_a(U^{238})N(U^{238})} \tag{2}$$

where ν_t is the average number of neutrons produced per thermal fission; σ_f is the fission cross section; σ_a is the (total) absorption cross section; N is the number of atoms per unit volume. Thus, η depends only on the nuclear properties and abundance ratios of U^{235} and U^{238} and can, in principle, be calculated from available information. In practice, however, it is customary to use an "adjusted" value of η obtained from exponential experiments on particular lattices. The value used in the calculations for the Brookhaven reactor was

$$\eta = 1.315 \pm 0.004 \tag{3}$$

which was obtained as a result of exponential experiments done between 1941 and 1944.

The fast fission factor ϵ is given by the formula:

$$\epsilon = 1 + \frac{\left(\nu_t - 1 - \frac{\sigma_c}{\sigma_f}\right)\frac{\sigma_f}{\sigma_c} P}{1 - \frac{\nu_f \sigma_f + \sigma_{el}}{\sigma} P'} \tag{4}$$

where σ_f, σ_{el} and σ_c are the average cross sections of natural uranium for fission, elastic scattering, and capture, respectively, for fission neutrons, and σ is the total cross section; ν_t, ν_f are the average numbers of neutrons per thermal and per fast fission, respectively; P is the probability that a fast neutron from the primary thermal fission will make a collision with a uranium nucleus in the rod; P' is the probability that a later-generation fast neutron will make a collision before escaping from the rod.

The following values of the nuclear quantities were used in the calculations: $\sigma_f = 0.29$ barns, $\sigma_{el} = 1.5$ b, $\sigma_c = 0.04$ b, $\sigma = 4.3$ b, $\nu_t = \nu_f = 2.55$. The quantities P and P' can be taken equal without introducing any significant error. They are functions of only two parameters: $N\sigma r$ and $\kappa_0/\sigma N$, where N is the number of uranium atoms per cm^3, r is the radius of the cylindrical fuel element, and κ_0 is the reciprocal of the diffusion length of thermal neutrons in uranium. For uranium of density 18.9 gm/cm^3, $N = 0.0478 \times 10^{24}$ so that $N\sigma = 0.206$; $\kappa_0 = 0.65$. Values of P and ϵ for uranium cylinders are given in Table I. The values of P and ϵ can be plotted conveniently as functions of the rod radius, and the resulting curves can be used for interpolation.

The thermal utilization factor f was calculated from the formula given by simple diffusion theory:

$$\frac{1}{f} = F(\kappa_0 r_0)\left\{\frac{N_1\sigma_{a_1}V_1}{N_0\sigma_{a_0}V_0} + \frac{N_a\sigma_{a_2}V_2}{N_0\sigma_{a_0}V_0}\right\} + E(\kappa_c r_g, \kappa_c r_c) \quad (5)$$

where V_0, V_1, V_2 are the volumes (in cm^3) of uranium, graphite and aluminum, respectively, in the unit cell; N_0, N_1, N_2 are the numbers of atoms per cm^3, of uranium, graphite and aluminum, respectively; r_0 is the radius (in cm) of the uranium rod; r_g is the inner radius of the moderator in the unit cell; r_c is the equivalent radius of the lattice cell, i.e., the value of the radius of the assumed spherical cell which gives the same moderator volume as in the actual unit cell; b is the equivalent thickness of the moderator: $b = r_c - r_g$; κ_0 is, as before, the reciprocal of the diffusion length of thermal neutrons in uranium; κ_c is the reciprocal of the diffusion length of thermal neutrons in graphite.

Table I. Values of the Fast Fission Factor for Uranium Rods as a Function of Rod Radius

Radius (cm)	*P*	*Fast fission factor (ε)*
0	0.000	1.000
0.5	0.118	1.012
0.75	0.167	1.017
1.00	0.212	1.023
1.25	0.252	1.028
1.50	0.289	1.032
1.75	0.323	1.037
2.0	0.355	1.042
3.0	0.459	1.057
4.0	0.539	1.071
5.0	0.600	1.083

The function $F(\kappa_0 r_0)$, which is called the "disadvantage factor," is the ratio of the thermal neutron density at the surface of the uranium rod to the average thermal neutron density in the rod. For a cylindrical rod:

$$F(\kappa_0 r_0) = \frac{\kappa_0 r_0}{2}\frac{I_0(\kappa_0 r_0)}{I_1(\kappa_0 r_0)} \quad (6)$$

The function $E(\kappa_c r_g, \kappa_c r_c)$ enters because the neutron density in the moderator is not uniform, and is greater than it is in the uranium. This gives rise to the so-called "excess neutron absorption in the moderator" which is measured by the quantity $(E - 1)$. The function E is given by the expression:

$$E(\kappa_c r_g, \kappa_c r_c) = \frac{(\kappa_c r_c)^2 - (\kappa_c r_g)^2}{2\kappa_c r_g} \times \left\{\frac{I_0(\kappa_c r_g)K_1(\kappa_c r_c) + I_1(\kappa_c r_c)K_0(\kappa_c r_g)}{I_1(\kappa_c r_c)K_1(\kappa_c r_g) - I_1(\kappa_c r_g)K_1(\kappa_c r_c)}\right\} \quad (7)$$

where I_0, I_1 are modified Bessel functions of the first kind; K_0, K_1 are modified Bessel functions of the second kind.

The values of the cross sections in Equation 5 are usually taken to be those which correspond to the most probable value of the neutron velocity in a Maxwellian distribution at room temperature. Strictly, integrals of $nv\sigma$ over the Maxwellian flux distribution should be used. Since, however, the absorption cross sections involved depart only slightly, if at all, from $1/v$-dependence, and since they enter as ratios, it is customary to assume that the thermal neutrons are monoenergetic with a speed of 2200 m/sec, and to use the corresponding values of the cross sections except when some "adjustment" is necessary.

It is known that Equation 5 is incorrect because simple diffusion theory does not apply strictly to the type of lattice considered. The use of more advanced methods, e.g., spherical-harmonic expansions, to obtain more accurate expressions for f introduces considerable mathematical complexity. Hence, in order to compensate for the shortcomings of the diffusion theory, while preserving its mathematical convenience, Equation 5 has been used with an "adjusted" value of the ratio $\sigma_{a_1}/\sigma_{a_0}$. In the experiments which led to the value $\eta = 1.315$, agreement between theory and experiment was achieved by taking $\sigma_{a_1}/\sigma_{a_0} = 0.78 \times 10^{-3}$. The values (at the time of those experiments) of the cross sections were $\sigma_{a_1} = 0.0047$ b and $\sigma_{a_0} = 7.3 \pm 0.2$ b, so that $\sigma_{a_1}/\sigma_{a_0} = 0.64 \times 10^{-3}$ would be the "unadjusted" value of the ratio. The use of the "adjusted" value of the ratio decreases f by about 1.5%; this is about the amount by which simple diffusion theory overestimates thermal utilization.

In the original design calculations, it was assumed that two kinds of graphite would be available, designated by the code names AGOT and AGHT. The AGOT graphite was a superior variety to be used for the uranium-containing core of the pile insofar as practical, while the AGHT graphite, of lower quality, was to be used for the reflector. During the period of

Table II. Properties of the Graphite Used in the Brookhaven Reactor

Property	AGOT (original design)	AGOT (average experimental)	AGHT (original design)	AGHT (experimental)
Density (ρ_1)	1.62 gm/cm³	1.69 gm/cm³	1.60 gm/cm³	1.61–1.65 gm/cm³
Diffusion Length (L_1)	50.16 cm	49.3 cm	47.6 cm	48.0 cm
κ_1 ($= 1/I_1$)	0.0199_4 cm^{-1}	0.0203_3 cm^{-1}	0.021 cm^{-1}	0.0208 cm^{-1}
σ_{a_1}	0.0049 b	0.0047_8 b	0.0057 b	0.0056 b

detailed engineering design and construction, an extensive program of measurements of the thermal neutron-diffusion length and the density was carried out; the results are shown in Table II, together with the original design values.

In addition to the values of the graphite parameters, the following values were used for other constants: uranium: $\sigma_{a_0} = 7.1$ b; $\kappa_0 = 0.649$ cm^{-1}; $\rho_0 = 18.9$ gm/cm³; aluminum: $\sigma_{a_2} = 0.23$ b; $\rho_2 = 2.70$ gm/cm³. The resonance escape probability p was calculated from the formula:

$$p = \exp\left[-\left(\frac{1}{f_r} - 1\right)^{-1}\right] \tag{8}$$

where f_r is the "resonance utilization"

$$\frac{1}{f_r} = F(\kappa_0 r_0)\left\{\frac{(N_1\sigma_{a_1})_r}{(N_0\sigma_{a_0})_r}\right\} + E(\kappa_1 r_0, \kappa_1 r_c) \tag{9}$$

In Equation 9, the constants are those appropriate to the resonance region; the following values were used: graphite: for $\rho_1 = 1.60$ gm/cm³, $(N_1\sigma_{a_1})_r = 0.0108$ cm^{-1}, and $\kappa_1 = 0.1075$ cm^{-1}; uranium:

$$\sigma_{a_0} = \frac{\int \sigma_{eff}\frac{dE}{E}}{\ln E/E_0} = \frac{9.25\left(1 + \frac{8}{3}\frac{S}{M}\right)}{\ln E/E_0}$$

$$\ln E/E_0 = 5.6;\ (\kappa_0)_r = 0.0222 \text{ cm}^{-1}$$

The above values result from combined theoretical and experimental work;[5–8] their use is linked to the particular value of η chosen, and to the adjustment of the formula for the thermal utilization. The method shown for the calculation of ϵ, f and p, together with the value $\eta = 1.315$ form a "recipe" for the calculation of k. Although this recipe does not include recent theoretical and experimental information and is, therefore, not up-to-date, it can be used successfully for the design of natural-uranium, graphite-moderated, air-cooled reactors.

Calculations made for the Oak Ridge pile, as well as preliminary calculations for the Brookhaven pile indicated that a rod diameter of one inch together with a lattice spacing of 8 inches would result in a value of k in the neighborhood of the maximum. Preliminary calculations of critical size and heat transfer requirements showed that a channel area in the neighborhood of 36 cm² would be satisfactory, as would a value of 0.2 for the aluminum-uranium volume ratio. Further calculations were then made by fixing the channel area at 36 cm² and the aluminum-uranium ratio at 0.2 and varying the rod radius and the lattice spacing. Only two values of the lattice spacing were used in the final calculations, namely 8 inches and 8⅜ inches, because these spacings could be obtained with the graphite pieces available without wasting too much graphite. The value of the rod radius was varied from 1.0 cm to 1.7 cm. The results are shown in Tables III and IV. The value of the thermal utilization of the moderator, f_{mod}, given by

$$f_{mod} = 1 - f\left[1 + \frac{N_2\sigma_{a_2}V_2}{N_0\sigma_{a_0}V_0}F(\kappa_0 r_0)\right] \tag{10}$$

is also listed, along with that of $f_{al} = 1 - f - f_{mod}$. The ratio of the volume of graphite to that of uranium is also listed:

$$\frac{V_1}{V_0} = \frac{r_1^2 - r_0^2}{r_0^2} \tag{11}$$

In these calculations, the original design values of the graphite parameters were used.

It must be pointed out that the fourth decimal figure in the numbers listed in Tables III and IV is

Table III. The Multiplication Factor as a Function of Rod Radius or Graphite-Uranium Volume Ratio

Lattice dimension = 8 in., aluminum-uranium volume ratio = 0.2, channel area = 36 cm²

Rod radius r_0 (cm)	Graphite-uranium volume ratio (V_2/V_0)	η	ϵ	f	p	k	f_{mod}	f_{al}
1.0	119.97	1.315	1.0224	0.8399	0.9287	1.0487	0.1529	0.0072
1.1	99.15	1.315	1.0243	0.8596	0.9168	1.0615	0.1330	0.0074
1.2	83.31	1.315	1.0261	0.8754	0.9044	1.0683	0.1169	0.0077
1.3	70.99	1.315	1.0280	0.8881	0.8915	1.0703	0.1040	0.0079
1.4	61.21	1.315	1.0299	0.8984	0.8783	1.0686	0.0935	0.0081
1.5	53.32	1.315	1.0316	0.9069	0.8647	1.0638	0.0849	0.0082
1.6	46.86	1.315	1.0333	0.9138	0.8507	1.0563	0.0778	0.0084
1.7	41.51	1.315	1.0350	0.9198	0.8368	1.0476	0.0716	0.0086

certainly not significant; in fact, even the third figure should not be taken seriously. The fourth decimal was carried only for the sake of consistency, and the results were rounded off in later calculations either of the critical size or the excess reactivity. Under the conditions of the calculations, the multiplication factor has a rather flat maximum for values of the rod radius between 1.2 cm and 1.4 cm in the case of the 8-inch lattice; for the 8¾ inch lattice, the maximum is for rod radii between 1.3 cm and 1.5 cm.

The final choice of the rod radius and lattice spacing was not made on the basis of the multiplication factor alone. The rod radius eventually chosen was 1.40 cm which led, with a lattice spacing of 8 inches, to a critical size for the pile in the neighborhood of the minimum value, as will be seen later. It also turned out that this value of the rod radius was convenient for reasons connected with the manufacture and availability of uranium rods.

The effect on the multiplication factor of varying the channel area is shown in Table V; it is evident that, with the methods used, the effect is very small. The effect on k of the variation of the aluminum-uranium volume ratio is shown in Table VI.

The calculations discussed so far were made on the basis of the original design values of the graphite parameters. The chief differences between these values and those found in the sigma-pile experiments were an increase in density from 1.62 gm/cm³ to 1.69 gm/cm³, or 4.14 per cent, and a decrease of 2.3 per cent in the thermal absorption cross section per atom. The increase in the density is the more important change; it causes a decrease in f because of increased neutron absorption by the moderator, and an

Table IV. The Multiplication Factor as a Function of Rod Radius or Graphite-Uranium Volume Ratio

Lattice dimension = 8¾ in., aluminum-uranium volume ratio = 0.2, channel area = 36 cm²

Rod radius r_0 (cm)	Graphite-uranium volume ratio (V_2/V_0)	η	ϵ	f	p	k	f_{mod}	f_{al}
1.0	132.58	1.315	1.0224	0.8256	0.9354	1.0383	0.1673	0.0071
1.1	109.57	1.315	1.0243	0.8469	0.9247	1.0548	0.1458	0.0073
1.2	92.07	1.315	1.0261	0.8637	0.9135	1.0646	0.1287	0.0076
1.3	78.45	1.315	1.0280	0.8774	0.9108	1.0696	0.1148	0.0078
1.4	67.64	1.315	1.0299	0.8885	0.8897	1.0706	0.1035	0.0080
1.5	58.93	1.315	1.0316	0.8976	0.8774	1.0684	0.0942	0.0082
1.6	51.79	1.315	1.0333	0.9053	0.8647	1.0637	0.0864	0.0083
1.7	45.38	1.315	1.0350	1.9117	0.8521	1.0573	0.0798	0.0085

Table V. The Multiplication Factor as a Function of Channel Area

Lattice dimension = 8 in., rod radius = 1.40 cm, aluminum-uranium volume ratio = 0.2

Channel area (cm²)	Radius of channel, r_0 (cm)	ϵ	η	f	p	k
20.25	2.538	1.0299	1.315	0.8908	0.8885	1.0684
24.50	2.738	1.0299	1.315	0.8922	0.8844	1.0687
27.14	2.938	1.0299	1.315	0.8941	0.8828	1.0690
30.91	3.138	1.0299	1.315	0.8956	0.8812	1.0690
36.00	3.385	1.0299	1.315	0.8978	0.8792	1.0690
41.60	3.638	1.0299	1.315	0.9001	0.8769	1.0690
53.73	4.138	1.0299	1.315	0.9049	0.8721	1.0688
67.57	4.638	1.0299	1.315	0.9091	0.8666	1.0670

Table VI. The Multiplication Factor as a Function of the Aluminum-Uranium Volume Ratio

Lattice dimension = 8 in., rod radius = 1.40 cm, channel area = 36 cm²

Aluminum-uranium volume ratio (V_2/V_0)	f	f_{al}	f_{mod}	k	$-\delta k_{al}$
0.	0.9057	0.0	0.0943	1.0773	0.0
0.10	0.9020	0.0041	0.0939	1.0729	0.0044
0.15	0.9003	0.0061	0.0936	1.0709	0.0064
0.20	0.8984	0.0081	0.0935	1.0686	0.0087
0.25	0.8966	0.0101	0.0933	1.0665	0.0108
0.30	0.8949	0.0120	0.0931	1.0645	0.0128
0.35	0.8930	0.0140	0.0930	1.0622	0.0151
0.40	0.8913	0.0160	0.0927	1.0602	0.0171
0.45	0.8894	0.0179	0.0927	1.0579	0.0194
0.50	0.8875	0.0199	0.0926	1.0557	0.0216

increase in p because of the improved moderating properties of the graphite. The decrease in σ_{a_1} tends to increase the value of f. The recalculated values for the case of the rod radius of 1.40 cm, lattice spacing of 8 inches, channel area of 36 cm^2 and aluminum-uranium volume ratio of 0.2, are: $\epsilon = 1.0299$ (unchanged), $\eta = 1.315$ (unchanged), $f = 0.8964$, $p = 0.8843$, $k = 1.0735$. The value of k was increased from 1.0686 to 1.0735, or by 0.46 per cent. This increase is significant because it corresponds to an increase of 7.1 per cent in the value of $k - 1$. The recalculated values of f_{mod} and f_{al} are 0.0956 and 0.0080, respectively.

EXPERIMENTAL RESULTS RELATED TO THE MULTIPLICATION CONSTANT

It has so far not been possible to measure k directly. Measurements of ϵ and f have recently been made and these can be compared with the calculated values; successful direct measurements of η and p have not yet been made. Experimental values of k can be obtained indirectly, from measured value of the critical buckling and the migration area. The critical buckling can be determined with good precision from the actual critical size of the pile. The migration area, however, is difficult to measure experimentally; it can, in principle, be obtained from the results of period measurements made at different metal loadings in the neighborhood of criticality. The results of these measurements will be discussed later.

Experimental values of ϵ and f have been obtained for the Brookhaven pile. The details of the methods used are given in the report: "Exponential Experiments with Slightly Enriched Uranium Rods in Ordinary Water," by H. Kouts, G. Price, K. Downes, R. Sher and V. Walsh.* The methods will, therefore, not be discussed here, and only the results will be given. Values obtained for ϵ for uranium rods of different diameter are listed in Table VII. Some of the values are for uranium slightly enriched in U^{235} but this should not have any significant effect on the fast fission effect. The error in the experimental values is estimated to be ± 0.004. The results indicate that at the smaller rod radii the theoretical values agree reasonably well with the experimental values; at the larger radii, the theoretical values seem to be somewhat smaller than the experimental values. It is not yet clear, however, because of the uncertainties in both the experimental and theoretical values, that the discrepancy is a real one. Further experiments are to be made with larger rods to try to settle this question. In the case of the Brookhaven rods, with a radius of 1.40 cm, the agreement between theory and experiment is quite good; the theoretical value, together with its (unknown) uncertainty, probably falls within the limits of the experimental value.

The thermal utilization was determined experimentally by measuring the thermal, neutron-flux distribution in a cell of the Brookhaven pile. The activation of dysprosium-oxide foils was measured as a function of position in a cell, both in the uranium and in the graphite. The value of f was then obtained by using the averaged values of the flux in the uranium rod, in the aluminum and in the graphite together with the appropriate values of the absorption cross sections. The values of f obtained were:

	Experimental value of f	*Theoretical value of*
1.40 cm rod	0.890	0.896
1.72 cm rod	0.920	0.918

The agreement is excellent, much better in fact than can at present be accounted for on theoretical grounds.

The Calculation of the Critical Size and the Excess Reactivity

The critical size can be calculated on the basis of either a modified one-velocity model or the age-theory model if the slowing-down and thermal-diffusion areas are known in addition to the multiplication factor. The slowing-down area was calculated from the following formulas:

$$\theta_\perp = [364(1 - P) + 231P]\left[1 + 2\frac{V_0}{V_1}\right]\left[\frac{1.6}{\rho_1}\right]^2\left[1 + \left(2 + \frac{a}{\lambda_f}\right)\phi\right] \tag{12}$$

$$\theta_\parallel = [364(1 - P) + 231P]\left[1 + 2\frac{V_0}{V_1}\right]\left[\frac{1.6}{\rho_1}\right]^2\left[1 + \left(2 + 2\frac{a}{\lambda_f}\right)\phi\right]$$

the meaning of which will be discussed briefly. The number 364 cm^2 is the result of measurements of the age of fission neutrons in graphite of density 1.6 gm/cm^3. The age to indium-resonance energy has been measured[9] as 311 cm^2 and the computed age from indium resonance to thermal energy is 53 cm^2. The quantity P represents the probability that a fast neutron makes an inelastic collision inside a uranium rod; it has been calculated to be 0.15 for a rod 1.40 cm in radius. The first quantity in brackets on the right side of Equation 12 gives, therefore, the effect of inelastic scattering in uranium on the age of the fission neutrons. The second factor in brackets gives the effect of elastic scattering in uranium. The third factor simply corrects for the difference between the density of the Brookhaven graphite and that of the graphite on which the age measurements were made. The last factor is a correction needed because of the air channels;[10] ϕ is the fraction of void space in a unit cell, a is the equivalent radius of the void space, and λ_f is an average mean free path of the neutrons in the absence of channels and was taken equal to 3.5 cm for graphite of density 1.6 gm/cm^3. Two formulas are needed, one for the slowing-down area perpendicular to the direction of the air channels, and one parallel to the air channels. The channels are large enough so that the resulting anisotropy is significant. The diffusion area was calculated from Equations 10, 11 and 12:

* See Session 21A, this volume.

$$L_\perp^2 = f_{mod}L_1^2[1 + (2 + a/\lambda_t)\phi]$$
$$L_\parallel^2 = f_{mod}L_1^2\left[1 + \left(2 + \frac{2a}{\lambda_t}\right)\phi\right] \quad (13)$$

In Equation 13, L_1 is the diffusion length of thermal neutrons in graphite and λ_t is the corresponding mean free path, taken as 2.71 cm for graphite of density 1.6 gm/cm³.

The perpendicular and parallel migration areas are usually defined by the relations:

$$M_\perp^2 = \theta_\perp + L_\perp^2; \qquad M_\parallel^2 = \theta_\parallel + L_\parallel^2 \quad (14)$$

A somewhat better approximation to the results of age theory is given by taking:

$$M_\perp^2 = k\theta_\perp + L_\perp^2; \qquad M_\parallel^2 = k\theta_\parallel + L_\parallel^2 \quad (15)$$

There are also two critical bucklings:

$$B_\perp^2 = \frac{k-1}{M_\perp^2}; \qquad B_\parallel^2 = \frac{k-1}{M_\parallel^2} \quad (16)$$

An average value of the buckling of a cubical pile can be defined by the expression

$$\overline{B^2} = \tfrac{2}{3}B_\perp^2 + \tfrac{1}{3}B_\parallel^2 \quad (17)$$

and a reasonably good approximation to the critical size of a bare cubical pile is then given by

$$L_c = [3\pi^2/\overline{B^2}]^{1/2} \quad (18)$$

For a bare cylinder of height H, the critical radius R_c may be obtained from the formula:

$$k - 1 = \frac{(2.405)^2 M_\perp^2}{R_c^2} + \frac{\pi^2}{H^2}M_\parallel^2 \quad (19)$$

with $M_\perp^2$ and $M_\parallel^2$ given either by Equations 14 or 15. The analogous formula for a cylinder is:

$$k\frac{\exp\left\{-\left[\frac{\pi^2}{H^2}\theta_\parallel + \frac{(2.405)^2}{R_c^2}\theta_\perp\right]\right\}}{1 + \frac{\pi^2}{H^2}L_\parallel^2 + \frac{(2.405)^2}{R_c^2}L_\perp^2} = 1 \quad (20)$$

In the early design calculations which involved the variation of several lattice parameters, it was most convenient to use the simple one-group approximation; in later, more precise calculations, the age theory Equation 20 was used.

The results of a typical set of calculations of the critical size of a bare cubical reactor are shown in Table VIII. The values of the lattice parameters and constants used were those of Table III. The actual value of $L_\perp^2$ used was 2800 cm² to take into account experimental results which indicated that the neutron temperature in graphite is about 80°C higher than the graphite temperature. The simple one-group model was used in these calculations. As in the case of the multiplication factor, more digits have been carried than are justified in order to insure consistency in rounding off the numbers. The calculated critical size has a rather flat minimum in the neighborhood of a rod radius of 1.4 cm. The results are shown graphically in Fig. 1 where they are compared with the results for the 8⅜ inch lattice spacing. The choice of the combination of a 1.40-cm rod radius and an 8-inch lattice spacing is evidently satisfactory. The critical buckling is plotted in Fig. 2 which shows the effect of the anisotropy due to the air channels. The effect of channel area on the critical size is shown in Fig. 3 for the same lattice parameters and the effect of aluminum-uranium volume ratio is shown in Fig. 4.

The final design values of the migration area, buckling and critical size, based on the actual properties of the graphite were:

$$\theta_\perp = 385.5\ \text{cm}^2,\ \theta_\parallel = 406.8\ \text{cm}^2;$$
$$L_\perp^2 = 316.1\ \text{cm}^2,\ L_\parallel^2 = 336\ \text{cm}^2$$

$M_\perp^2 = 702$ cm², $M_\parallel^2 = 740$ cm² for $M^2 = \theta + L^2$

$M_\perp^2 = 730$ cm², $M_\parallel^2 = 770$ cm² for $M^2 = k\theta + L^2$

$B_\perp^2 = 104.8 \times 10^{-6}$ cm^{-2}, $B_\parallel^2 = 99.3 \times 10^{-6}$ cm^{-2} (21)

from Equation 16 with $M^2 = \theta + L^2$.

$B_\perp^2 = 100.7 \times 10^{-6}$ cm^{-2}, $B_\parallel^2 = 95.5 \times 10^{-6}$ cm^{-2} (22)

from Equation 16 with $M^2 = k\theta + L^2$.

If the expressions of Equation 21 are used for the buckling, the critical size of a bare cubical pile comes out 17.6 feet, according to Equation 18; if Equation 22 is used, the result is 17.9 feet.

In all of the calculations considered so far, the effect of the central gap has been neglected. The presence of the gap allows neutrons to leak out of the pile more easily, or to move more easily from

Table VII. Experimental and Theoretical Values of the Fast Fission Factor in Uranium Rods in a Uranium-Graphite Lattice

Rod diameter (inches)	*Rod radius (cm)*	*Percentage U^{235} by weight*	*Location of rod in pile*	*Experimental value of ε*	*Theoretical value of ε*
0.387	0.476	1.0	reflector	1.012 ± 0.004	1.012
0.600	0.762	1.0	reflector	1.020	1.017
0.750	0.953	1.0	reflector	1.027	1.022
0.750	0.953	1.0	fuel channel	1.022	1.022
1.10	1.40	0.7	reflector	1.035	1.030
1.10	1.40	0.7	fuel channel	1.034	1.030
1.345	1.72	0.7	reflector	1.043	1.035
1.345	1.72	0.7	fuel channel	1.046	1.035

Table VIII. Critical Length of a Bare Cubical Pile as a Function of Rod Radius
Lattice dimension = 8 in., channel area = 36 cm² aluminum-uranium volume ratio = 0.2

Rod radius, r_0 (cm)	Average slowing-down area, $\bar{\theta}$ (cm²)	Average thermal-diffusion area, $\bar{L}^2$ (cm²)	Average migration area $\bar{M}^2$ (cm²)	Average critical buckling $\bar{B}^2$ (cm^{-2} × 10^6)	Critical length (ft)
1.0	430.17	515.01	945.18	51.58	24.9
1.1	428.94	446.51	875.45	70.32	21.3
1.2	427.57	391.25	818.83	83.49	19.5
1.3	426.13	346.83	772.96	91.02	18.7
1.4	424.58	310.61	735.19	93.37	18.5
1.5	422.94	280.56	703.50	90.75	18.7
1.6	421.20	256.20	677.40	83.16	19.6
1.7	419.37	234.83	654.20	72.80	20.9

regions of greater neutron density to regions of smaller neutron density. Work on the theory of the effect of a central gap has recently been summarized[13] and will not be discussed here. It has been shown that one effect is to change the buckling in the direction perpendicular to the plane of the gap by the amount

$$\delta(\epsilon^2) = \epsilon^2 - \epsilon_0^2 = [\delta(\epsilon^2)]_{quadratic} + [\delta(\epsilon^2)]_{linear} \quad (23)$$

where ϵ_0^2 is the buckling for zero gap width, and ϵ is obtained from the Equation

$$-\epsilon \cot \frac{\epsilon L}{2} = \frac{3}{2\lambda}\left[\frac{1 - \gamma h K_1(\gamma h)}{1 + (1 + \gamma h)e^{-\gamma h}}\right] \quad (24)$$

The linear contribution is given by

$$[\delta(\epsilon^2)]_{linear} = \frac{8h\epsilon_0^2}{L} e^{-\gamma h} \quad (25)$$

In Equations 24 and 25, γ^2 is the component of the buckling parallel to the plane of the gap; γ^2 is assumed to be unaffected by the gap, i.e., $\gamma = \gamma_0^2 = 2\pi^2/L^2$, for a cubical reactor of side L; h is the gap width, and λ is the neutron mean free path in the reactor.

The increase in critical size can be obtained from the buckling; it can also be found from the convenient approximation:

$$\delta L = -\frac{3h^2}{2\lambda} \ln \frac{\gamma h}{2} + 4he^{-\gamma h} \quad (26)$$

The effect of the gap was first calculated for the bare cubical pile with the following characteristics: lattice spacing = 8 in., rod radius = 1.4 cm, channel area = 36 cm², aluminum-uranium volume ratio = 0.2, average critical buckling = 93.4 × 10^{-6} cm^{-2}, critical size = 18.5 ft. The results for different values of the gap width are shown in Table IX. The increase in the critical buckling which would be needed to keep the critical size of the cubical pile unchanged is indicated in the form B^2/B_0^2, where B_0^2 represents the average critical buckling in the absence of a gap and B^2 is the value where there is a gap. The critical size, i.e., the length which the critical pile must have if the buckling is unchanged, is also shown. It is evident that the critical size increases significantly with gap width: the increase is 1 ft at a gap width of 6 cm and 2 ft at a gap width of 10 cm. A gap width of 7 cm was actually chosen because it allowed reasonably economical pumping of air without making the increase in pile size too large.

The effect of the gap varies somewhat with the size of the pile, as is shown in Table X. The buckling for criticality at a given gap width decreases as the pile size increases. This effect, together with the fact that the neutron economy turned out to be more favorable than was expected in the original design, made it possible to use an 8-cm gap instead of the original 7-cm gap. The pile was actually built in such a way that the gap width could be changed slightly by moving one-half of the pile and, during the initial period of pile operation, the gap was increased to 8 cm.

The critical size discussed so far has been that of a bare, cubical pile operating at room temperature and

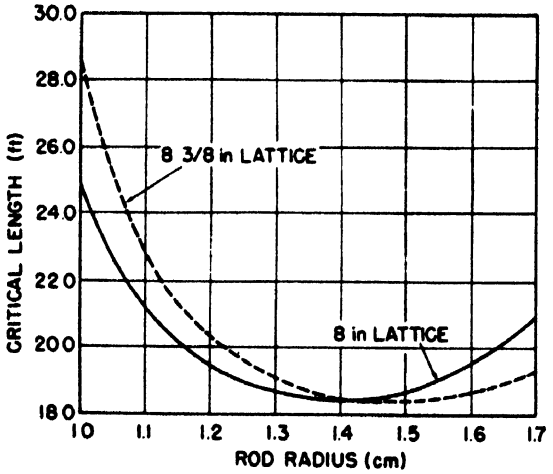

Figure 1. Critical size of a bare cubic pile as a function of rod radius

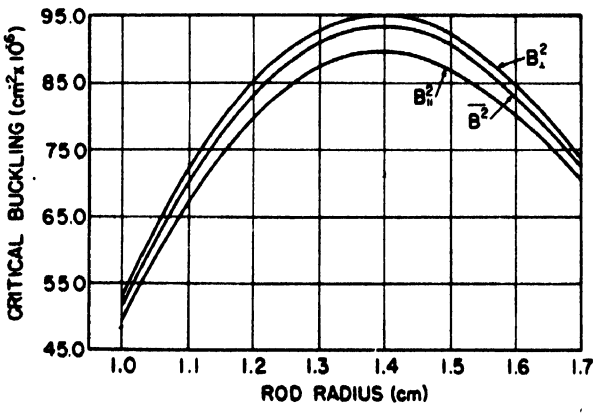

Figure 2. Critical buckling of a bare cubic pile as a function of rod radius

zero power. Although the analysis of such a pile permits the choice of some of the important parameters in the design, it does not allow the final determination of the pile size and the actual metal loading. It is necessary to calculate the amount of excess reactivity needed to overcome the effect of the negative temperature coefficient of the reactivity, and to make up for the loss of reactivity caused by fission product poisoning. To these must be added an estimate of the excess reactivity needed to take care of experimental research, isotope production and special needs which might arise during the operation of the pile. Preliminary calculations showed that the total excess reactivity needed would be close to 0.023, i.e., the size and metal loading of the pile would have to be large enough so that the cold, unpoisoned pile will have a multiplication factor close to 1.023.

The excess reactivity k_{ex} as first calculated, for a bare cubical pile of side L, from the formula:

$$k_{ex} = k \frac{\exp\left\{-\frac{\overline{B^2}}{\overline{B_0^2}}\frac{3\pi^2}{\overline{L^2}}\bar{\theta}\right\}}{1+\frac{\overline{B^2}}{\overline{B_0^2}}\frac{3\pi^2}{\overline{L^2}}} - 1 \qquad (27)$$

where the bars represent average values defined as described earlier. The calculations were made for the design values of the various lattice parameters and for the original graphite parameters. The excess reactivity available is shown in Table XI as a function of gap width and pile size. The blank spaces indicate either a very small, or a negative, value of the excess reactivity; in the latter case, of course, a pile of the size and gap width indicated would be subcritical. The results show that, with the original design values of the graphite parameters, the desired excess reactivity could be obtained with a gap width of 7 cm and a pile size of 25 ft. This combination was more desirable on the basis of both nuclear and engineering requirements than other combinations which could also lead to the desired excess reactivity; it was, therefore, chosen.

The fact that the graphite properties turned out to be better than was expected means that the excess reactivity for a given pile size is greater than the value just obtained. The effect is shown in Table XII. The calculations were made for a gap width of 7 cm, for different pile sizes, and for two different estimates of the gap effect. The value $B^2/B_0^2 = 1.134$ was obtained from Table IX; the value 1.146 was an earlier value obtained by using an approximate form for the quadratic effect instead of Equation 24. With the measured values of the graphite parameters, the desired excess reactivity should be obtained with a cubical pile with an effective length of 23 feet.

Table IX. Effect of Gap Width on the Critical Buckling and Critical Size of a Bare Cubical Pile

Gap width (h, cm)	Quadratic effect on critical buckling ($\overline{B^2}/\overline{B_0^2}$)	Total effect on critical buckling ($\overline{B^2}/\overline{B_0^2}$)	Critical size of bare cubical pile (L_c ft)
0	1.000	1.000	18.5
1	1.004	1.009	18.6
2	1.012	1.022	18.7
3	1.025	1.038	18.9
4	1.041	1.059	19.1
5	1.059	1.081	19.2
6	1.079	1.106	19.5
7	1.102	1.134	19.7
8	1.125	1.160	20.0
9	1.150	1.188	20.2
10	1.175	1.218	20.5
11	1.201	1.249	20.8
12	1.227	1.278	21.1

Table X. Effect of Gap Width on the Critical Buckling of Piles of Different Sizes

Gap width, h (cm)	Relative critical buckling (rigorous quadratic effect plus linear effect) for pile size (ft)				
	18.5	22	23	24	25
5	1.081	1.075	1.070	1.070	1.065
6	1.106	1.098	1.093	1.091	1.086
7	1.134	1.121	1.116	1.114	1.109
8	1.160	1.149	1.143	1.137	1.136

The calculations discussed so far showed how a set of design parameters was arrived at which would meet the requirements set on the Brookhaven reactor. We can now complete the detailed calculation of the critical size of the pile and the metal loading, both for the cold, zero-power pile and for the pile under actual operating conditions. Before these calculations could be made, however, it was necessary to fix the length of the metal cartridges. In the original design calculations, the total length of the fuel elements was taken to be 23 feet, i.e., 2 cartridges each 11.5-ft long. This choice allowed for one foot of graphite reflector at each end of the fuel channel. After the graphite properties became known, the question of cartridge length was reconsidered together with the problem of heat removal. Computations were made on the possibility of "bowing" the metal loading, i.e., of using cartridges of different length in different parts of the pile, the shortest at the center of the pile, the others gradually increasing in length toward the outer parts of the pile. The power needed to remove the pile heat was calculated for various arrangements and compared with that needed for cartridges of a single length. The problems of making cartridges of different lengths

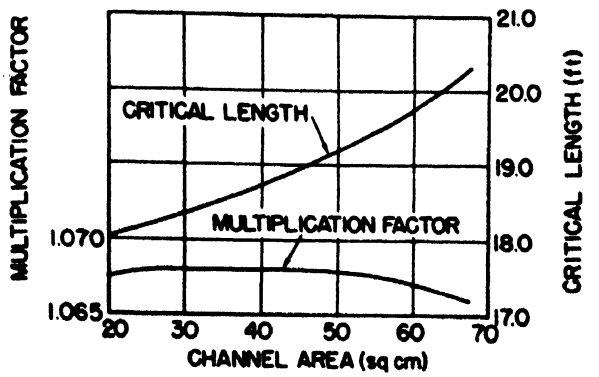

Figure 3. Multiplication factor and critical size of a bare cubic pile as functions of channel area

Table XI. Excess Reactivity as a Function of Pile Size for Different Values of the Gap Width

Pile size (ft)	Gap width (cm)							
	0	5	6	7	8	9	10	12
18	.....	.....	.....	.....	.....	.....	.....	.....
19	0.0020	.....	.....	.....	.....	.....	.....	.....
20	0.0083	0.0033	0.0017	.....	.....	.....	.....	.....
21	0.0137	0.0091	0.0076	0.0060	0.0042	0.0023	.....	.....
22	0.0184	0.0142	0.0128	0.0113	0.0097	0.0079	0.0061	0.0021
23	0.0225	0.0186	0.0174	0.0160	0.0145	0.0129	0.0112	0.0075
24	0.0261	0.0226	0.0214	0.0201	0.0188	0.0173	0.0157	0.0123
25	0.0294	0.0261	0.0250	0.0238	0.0225	0.0212	0.0197	0.0166

were considered, as well as those connected with the leak detection system. It was decided that a reasonable solution of all the problems involved in the particular case of a pile to be used as a tool for research was to use cartridges of uniform length, and the length was chosen as 11 ft per cartridge. It was also decided to load the metal so that the loaded core of the pile approximates a cylinder, because this kind of loading requires less uranium than does a cubical loading.

It was also necessary to investigate at considerable length the effect of the graphite around the loaded core of the pile which, because of its effect as a neutron reflector, helps decrease the uranium needed for criticality. A careful analysis which we made of the initial operation of the Oak Ridge pile showed that the experimental results were consistent with a reflector saving of 60 cm. This value was also obtained from the two-group theory of the reflector effect for a uranium-graphite pile with a graphite reflector for which the thermal neutron diffusion length is about 50 cm. For such a system, the reflector saving is given, to a good approximation, by the very simple expression:

$$\delta = 1.2L_1 \tanh \frac{T}{L_1} \qquad (28)$$

where T is the thickness of the reflector, and L_1 is the thermal neutron diffusion length in the reflector; δ is the decrease in the critical dimension, caused by the presence of the reflector, e.g., for a spherical or cylindrical system, δ is the decrease in the radius of the metal-bearing core.

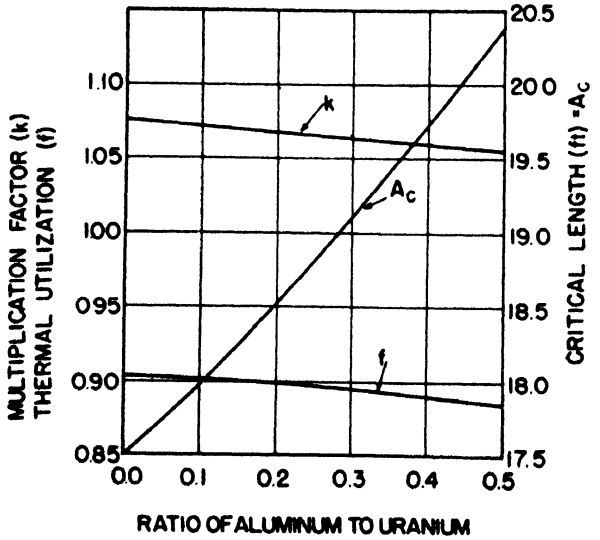

Figure 4. Thermal utilization, multiplication factor and critical size as functions of aluminum-uranium volume ratio

We can now calculate the critical size, number of channels and amount of uranium for the cylindrical loading surrounded by a reflector. The effective reflector thickness may be obtained by replacing the 25 ft × 25 ft cross section of the pile by a circular cross section 14.1 ft in radius. The difference between the radii of the loaded cylinder and the pseudo-cylindrical pile is assumed to be a reasonably good approximation to the reflector thickness. The total length of the loaded cylinder is 670.6 cm (22 ft) plus the total reflector saving, 86 cm or 756.6 cm. The number of loaded channels n is obtained from the simple geometrical relationship

$$n = 7.069r^2 \qquad (29)$$

where r is the radius of the loaded core in feet. The weight of 22 feet of uranium slugs was 76.86 kg and the weight of uranium for a given loading is, in metric tons: $W = 0.5433r^2$.

The critical size R for the cylinder corresponding to a given excess reactivity is obtained from the relationship:

$$k_{ex} = k \frac{\exp\left\{-\frac{\overline{B^2}}{\overline{B_0^2}}\left(\frac{\pi^2}{H^2}\theta_\parallel + \frac{(2.405)^2}{R^2}\theta_\perp\right)\right\}}{1 + \frac{\overline{B^2}}{\overline{B_0^2}}\left(\frac{\pi^2}{H^2}L_\parallel^2 + \frac{(2.405)^2}{R^2}L_\perp^2\right)} - 1 \qquad (30)$$

Table XII. Excess Reactivity as a Function of Pile Size for a Gap Width of 7 cm

Length of the side of a cubical pile (ft)	Excess reactivity		
	Actual graphite		Design graphite
	$B^2/B_0^2 = 1.134$	$B^2/B_0^2 = 1.146$	$B^2/B_0^2 = 1.146$
18	−0.0082	−0.0089	−0.013
19	0.000	−0.0009	−0.006
20	0.0067	0.0060	0.000
21	0.0127	0.0121	0.060
22	0.0181	0.0174	0.0113
23	0.0226	0.0222	0.0160
24	0.0267	0.0262	0.0201
25	0.0302	0.0298	0.0238

where R is the effective radius, equal to the sum of the loading radius and the reflector saving: $R = r + \delta$. For convenience, the final values of the important pile parameters are summarized: $k = 1.0735$; $\epsilon = 1.0299$; $f = 0.8964$; $f_{mod} = 0.0956$; $p = 0.8843$; $\theta_\perp = 385.5$ cm^2; $\theta_\parallel = 406.8$ cm^2; $L_\perp^2 = 316.1$ cm^2; and $L_\parallel^2 = 333.6$ cm^2 and the corresponding values of M^2 and B^2 are given in Equations 21 and 22 and the lines preceding these equations. The theoretical value of the ratio B^2/B_0^2 used was 1.134 for a 7 cm gap.

The results of the calculations are shown in Table XIII. The cold, zero-power pile should become chain reacting at a uranium loading of 386 channels, and the required value of the excess reactivity should be reached in the neighborhood of 750 channels. With the original design values of the graphite properties, the corresponding numbers of channels would have been 475 and about 1200. The marked disparity between the original design loading for full operation and the final calculated loading, a difference of about 450 channels worth of uranium, is due largely to the fact that the better graphite properties permit a smaller metal loading. This increases the reflector saving which, in turn, reduces the metal requirement still further. The effect illustrates, in a dramatic way, the very great importance of the graphite properties—thermal neutron absorption and density—in the design of a uranium-graphite pile.

EXPERIMENTAL RESULTS OBTAINED WITH THE SUBCRITICAL BROOKHAVEN REACTOR

During the construction of the Brookhaven reactor, circumstances were such that for a two-month interval, in January and February 1950, the graphite structure was available for experimental work. The extent of the program was limited, however, by the requirement that the reactor be kept well below criticality. The upper limit on the amount of uranium that could be loaded was set to correspond to a value of 0.99 for the effective multiplication factor, i.e., $k_{eff} \leq 0.99$. This limit was set by the condition that there be no danger of contaminating the graphite structure with radioactivity.

Subcritical measurements were made at eight different loadings, from 100 channels ($k_{eff} = 0.90$) to 301 channels ($k_{eff} = 0.99$). The work included studies such as flux distribution measurements, exponential experiments, and transient response measurements. The results obtained were used to determine the critical radius and buckling, to evaluate the effects of the gap and cooling channels, and to find certain other lattices constants for which experimental and theoretical results could be compared. Because of space limitation, only the results of the measurements can be given; the details will be published elsewhere.

Table XIII. Critical Size, Critical Loading and Excess Reactivity of the Brookhaven Reactor

Effective radius (cm)	Effective radius (ft)	Loading radius (ft)	Number of loaded channels	Weight of uranium (metric tons)	Excess reactivity
285	9.35	7.39	386	29.67	0.000
305	10.0	8.06	460	35.29	0.0071
335	11.0	9.12	588	45.19	0.0158
366	12.0	10.32	754	57.86	0.0223
381	12.5	10.90	840	64.55	0.0251

The critical radius of the pile was determined in an experiment in which the flux at the center of the pile was measured in a series of metal loadings—with 100, 145, 177, 221, 241, 253, 277 and 301 loaded channels. Theoretical analysis showed that in a pile with a gap, we may write (except for small corrections)

$$\frac{1}{(nv)_{max}} = A\left[\frac{1}{R^2} - \frac{1}{R_c^2}\right] \qquad (31)$$

where R is the effective radius of the pile at some loading, and R_c is the effective radius at criticality. In practise, the reciprocal of the thermal neutron counting rate at the position of maximum flux was plotted as a function of $1/R^2$. The position of maximum flux, in a pile with a central gap, is not at the center of the pile; there are two maxima, each at the radical center of the pile, but situated some distance from the axial center, the distance depending on the loading. In the sub-critical experiments, this distance varied from 2½ to 4 feet. Measurements of the radial neutron flux distribution at the different loadings showed that the reflector saving was 61.0 ± 1.4 cm, in good agreement with the prediction of the two-group theory and our interpretation of the Oak Ridge critical experiment. The results of the criticality experiment are shown in Table XIV. When $1/S_{max}$, where S_{max} is the maximum counting rate, was plotted against $1/R^2$, the result was a straight line in accord with Equation 31; extrapolation to $1/S_{max} = 0$ gave $R_c = 285.4$ cm. When the small corrections to Equation 31 due to the gap effect were taken into account the result was $R_c = 286.1$ cm, or a loading radius of 225.1 cm, equivalent to 385 loaded channels. This result agrees almost exactly with the predicted value of 386 loading channels. This remarkable agreement must be considered partly fortuitous, however, for several reasons. First, it was known that the effect of the gap is overestimated by Equations 23, 24, and 25, so that the prediction of 386 channels should be high. Second, the uncertainties in the calculation of k, M^2 and, therefore, in B^2 and R_c should tend to make the experimental and theoretical values of R_c disagree somewhat.

The critical buckling parallel to the direction of the channels, and with the gap effect neglected, can be expressed in the form:

$$B_\parallel^2 = \frac{k-1}{M_\parallel^2} = \frac{(2.405)^2}{R_c^2}\frac{M_\perp^2}{M_\parallel^2} + \frac{\pi^2}{H^2} \qquad (32)$$

This equation gives a relationship between $B_\parallel^2$, R_c^2 and the ratio of the migration areas; the last ratio enters because of the anisotropy due to the cooling channels. If the theoretical value of the ratio $M_\perp^2/M_\parallel^2$ is used, a value of $B_\parallel^2$ can be obtained; the calculated value of the ratio was 0.942. With the known values

Table XIV. Critical Size of the Brookhaven Reactor from Subcritical Measurements

Number of loaded channels	Effective radius of loading (cm)	Maximum counting rate		Effective multiplication factor (k_{eff})
		S_{max}	S_{max} (including gap corrections)	
100				0.9018
145	199.01	343	357	0.9363
177	213.48	473	491	0.9524
221	231.39	745	752	0.9684
241	238.93	913	916	0.9741
253	243.31	1043	1053	0.9771
277	251.76	1381	1386	0.9831
301	259.86	1900	1900	0.9873
Critical (extrapolated)	286.1			1.0000

of the various parameters, and with the value of R_c obtained from the experiment, it was found that $B_\parallel^2 = (92.4 \pm 0.7) \times 10^{-6}$ cm^{-2}. The prediction on the basis of one-group diffusion theory was 99.3×10^{-6} cm^{-2}; the approximation to age theory (Equation 22) gave 95.5×10^{-6} cm^{-2}. The experimental result was, therefore, closer to the value predicted by the approximation to age theory.

A value of the critical buckling parallel to the direction of the channels was also obtained from an exponential experiment at a loading of 100 channels in a square array; the result was $B_\parallel^2 = (95.7 \pm 3.5) \times 10^{-6}$ cm^{-2}. Although this result seems to agree better with the predicted values than that obtained from the "critical experiment," the uncertainty in the result was considerably greater.

The effect of the gap on the geometrical buckling of the reactor can be computed from experimental flux distributions. Both the axial and the radial thermal-flux distribution were determined by foil-activation measurements. The flux distributions were then fitted analytically and the geometrical buckling was determined from the distribution. The buckling in the absence of the gap was measured by fitting the portion of the flux curve for points far from the gap; in this region, the effect of the gap is no longer felt and the flux curve could be fitted with the usual kind of distribution function. The result found was that for both the axial and radial components of the geometrical buckling $B^2/B_0^2 = 1.105$, compared with the value of 1.134 used in the calculations of the critical size and excess reactivity.

The results of the exponential experiments can be combined with results of the "critical" experiment to give a value of the ratio of axial to radial migration areas. The result obtained was $M_\parallel^2/M_\perp^2 = 1.095 \pm 0.036$ as compared with the theoretical value of 1.06; the agreement is, again, reasonably good.

In addition to the reactor quantities discussed above, estimates of the thermal utilization in the moderator and in the uranium could be made from the results of cadmium-ratio measurements. The cadmium ratio is the ratio of the saturated activity induced in an indium foil to the saturated activity when the foil is covered with cadmium. The relation between f_{mod} and the measured cadmium ratio can be obtained by considering the absorption and production of neutrons in a lattice cell. If nv is the thermal flux averaged over the graphite of a lattice cell, then, to a good approximation,

$$f_{mod} = \frac{\lambda_{tr}}{3(1+\phi)L_1^2}\frac{nv}{q} \qquad (33)$$

Values of nv and q can be obtained from indium-foil activities with the aid of conversion factors measured in a standard sigma-pile (large graphite block with one or more calibrated neutron sources). The factor $(1+\phi)$ enters because the presence of air holes increases the lifetime of thermal neutrons.

The following conversion factors were obtained experimentally:

$$q \text{ (In res)} = 0.00164 S_{cd}$$

$$nv = 0.0942 S_{th} = 0.0942 S_{al}\left(1 - \frac{1.11}{C.R.}\right)$$

where S_{cd} and S_{al} are the saturated indium activities with and without cadmium; $C.R.$ is the cadmium ratio S_{al}/S_{cd}, and the factor 1.11 was obtained from a set of sigma-pile measurements with cadmium-foil covers of varying thickness;[14] the measured cadmium ratio in the Brookhaven pile is 6.10. When these values, together with the appropriate values 2.57, 49.2 and 1.072 for λ_{tr}, L, and $(1+\phi)$, respectively, are inserted into Equation 33, the result is: $f_{mod} = 0.0945$. The agreement with the calculated value (0.0956) is better than expected since the uncertainty in the experimental value was estimated to be about 10%; the agreement was, however, gratifying.

EXPERIMENTAL RESULTS OBTAINED DURING THE INITIAL OPERATION OF THE CRITICAL BROOKHAVEN REACTOR

Some of the experiments done with the subcritical pile were repeated in the final approach to criticality and in the critical reactor. The actual critical loading radius was 226.43 cm, corresponding to a critical loading of 390.1 channels, as found by the extrapolation of subcritical foil measurements in the usual kind of criticality determination. The critical radius was also determined from measurements of the reactor period corresponding to different values of the excess reactivity at loadings of 393, 397, 401, 405 and 409 channels. When the excess reactivity was plotted against $1/R^2$ and extrapolated to zero excess reactivity, the critical loading was found to be 226.28 cm. The actual critical loading was, therefore, 4 channels greater than that predicted from the experiments discussed in the last section. About half of this difference was caused by the difference in temperature between February and August; the rest has not been explained.

The effect of the gap on the buckling was determined at loadings of 301, 349, 387, 409, and 419 channels. The geometrical buckling parallel to the direction of the channels can be written:

$$B_{\parallel}^2 \text{ (no gap)} = \frac{(2.405)^2}{R^2}\left(\frac{M_{\perp}^2}{M_{\parallel}}\right) + \left(\frac{\pi}{2l}\right)^2 \quad (34)$$

where l is the effective half-length of the pile, and

$$B_{\parallel}^2 \text{ (gap)} = \frac{(2.405)^2}{R^2}\left(\frac{M_{\perp}^2}{M_{\parallel}}\right) + \beta^2 \quad (35)$$

where β^2 is obtained from the flux distribution in the neighborhood of the gap. With the observed values of l, R and β, and with the theoretical value 0.942 for $M_{\perp}^2/M_{\parallel}^2$, the values of B^2/B_0^2 for the effect of the 7-cm gap were found to be 1.111, 1.113, 1.100, 1.103, and 1.139 at the five loadings indicated, respectively; the average value was 1.107. When the gap width was changed to 8 cm, at 419 channels, the value was increased to 1.139.

An estimate of the migration area was also obtained from the measurements of the reactor period. In the neighborhood of criticality, the excess reactivity can be written in the form:

$$k_{ex} = 1.11(2.405)^2 M_{\perp}^2 \left[\frac{1}{R^2} - \frac{1}{R_c^2}\right] \quad (36)$$

when the gap width is 7 cm. The value of the excess reactivity is obtained from the period by using the usual inhour formula[15]

ih of reactivity =

$$\frac{54}{T} + \frac{2013}{T+0.62} + \frac{204}{T+2.19} + \frac{535}{T+6.5} + \frac{2036}{T+31.7} + \frac{787}{T+80.3} \quad (37)$$

where T is the pile period in seconds. The slope of the graph of k_{ex} against $1/R^2$ yields a value of $M_{\perp}^2$. The value found was $M_{\perp}^2 = 680 \pm 20$ cm^2 as compared with the theoretical value of 730 cm^2. The agreement was not as good as was expected. There were some difficulties with instruments during the course of these experiments, and further experiments were done; unfortunately, these have never been analyzed and this question has not been settled. In connection with this problem of the migration area, however, we analyzed similar experiments made during the initial operation of the Oak Ridge reactor. The analysis gave a value of $M^2 = 728$ cm^2 as compared with a theoretical value of 737 cm^2. Thus the agreement for the Oak Ridge reactor was better than that for the Brookhaven reactor, and it seems likely that the Brookhaven experiments were at fault.

A value of k was obtained from the known values of the critical buckling parallel to the direction of the channels, the ratio of the migration areas, and the value of M^2. The result was $k = 1.068$ as compared with the theoretical value of 1.074; the discrepancy was evidently due to the low value of M^2 obtained from the period measurements.

In the course of the design work, a good deal of theoretical work was done on the temperature coefficient of the reactivity, and measurements of the temperature effects were made during the initial operation of the reactor. The variation of the effective multiplication factor may be written:

$$\frac{\partial k_{eff}}{\partial T} = \frac{\partial k}{\partial T} - B^2 \frac{\partial M^2}{\partial T} \quad (38)$$

with

$$B^2 = \frac{k - k_{eff}}{M^2} \quad (39)$$

Since temperature coefficients are usually measured in a pile near its critical loading and close to room temperature, B^2 is very close to B_c^2. We also have:

$$\frac{1}{k}\frac{\partial k}{\partial T} = \frac{1}{\eta}\frac{\partial \eta}{\partial T} + \frac{1}{\epsilon}\frac{\partial \epsilon}{\partial T} + \frac{1}{f}\frac{\partial f}{\partial T} + \frac{1}{p}\frac{\partial p}{\partial T} \quad (40)$$

Equation 39 may be rewritten:

$$\frac{\delta k_{eff}}{k} = \frac{\delta \eta}{\eta} + \frac{\delta \epsilon}{\epsilon} + \frac{\delta f}{f} + \frac{\delta p}{p} + (k-1)\frac{\delta M^2}{M^2} \quad (41)$$

Each of the factors which contributes to the temperature coefficient can be studied separately, theoretically or experimentally. The details of the treatment cannot be given because of space limitations. The contributions predicted for the Brookhaven pile were:

$$\frac{1}{\eta}\frac{\partial \eta}{\partial T} = -7.4 \times 10^{-5}/°\text{C (from cross-section data)}$$

$$= -4.8 \times 10^{-5}/°\text{C (from experimental data)}$$

$$\frac{1}{f}\frac{\partial f}{\partial T} = 2.6 \times 10^{-5}/°\text{C}$$

$$\frac{1}{p}\frac{\partial p}{\partial T} = -1 \times 10^{-5}/°\text{C to } -2 \times 10^{-5}/°\text{C}$$

(from theory and experimental data)

$$B^2\frac{\partial M^2}{\partial T} = 3.8 \times 10^{-5}/°\text{C}$$

$$\frac{1}{\epsilon}\frac{\partial \epsilon}{\partial T} = 0$$

With these values, the theoretical temperature coefficient (reduced to vacuum) of the Brookhaven pile for a uniform rise in temperature in both the uranium and the graphite should lie between -7×10^{-5}/°C and -10.5×10^{-5}/°C. Of this amount, the contribution of the resonance escape probability is an effect due only to a change in the uranium temperature; the other contributions arise from changes in the neutron temperature which depends, in turn, directly on the moderator temperature. Hence, the metal coefficient should be between -1×10^{-5}/°C and -2×10^{-5}/°C, while the graphite coefficient could lie, according to the theoretical predictions, between -5×10^{-5}/°C and -9.5×10^{-5}/°C.

When measurements of the temperature coefficients are made, the effect of the air (nitrogen) in the pile must be taken into account, since a change in temperature causes a change in the partial pressure of

nitrogen in the pile and, therefore, in the number of neutrons absorbed in the nitrogen. This effect can be interpreted in terms of the "barometric coefficient of the reactivity". This quantity was measured in several experiments and the best value obtained was -0.35 ± 0.03 inh/mm Hg or -0.91×10^{-5}/°C, in reactivity. The metal and graphite coefficients as measured were:

Graphite coefficient (in air):
$$(-1.82 \pm 0.26) \times 10^{-5}/°C$$
Metal coefficient (in air):
$$(-1.95 \pm 0.13) \times 10^{-5}/°C$$

The experimental graphite coefficient, reduced to vacuum, was -4.1×10^{-5}/°C. This result is somewhat lower than the lower limit of the predicted value. Nevertheless, in view of the many uncertainties in the calculations, the result is not unsatisfactory. The measured value of the metal coefficient agreed with the upper limit of the expected value.

In the course of the design work, it was also necessary to estimate the effect of fission product poisoning on the reactor. This was done on the basis of the theory of the effect and experimental information obtained from the operation of the Oak Ridge pile. Two problems were considered: the first is the magnitude of the equilibrium poisoning effect of Xe^{135}; the second is that of the poison transients involved in the start-up and shut-down operations which contribute to the control problem.

The equilibrium xenon-poison effect was computed by calculating the effect on the thermal utilization. The formula for $1/f$ (Equation 5) has an additional term

$$H_x = \frac{N_x \sigma_{a_x} V_x}{N_0 \sigma_{a_0} V_0} \tag{42}$$

where the subscript x refers to xenon-135. The equilibrium value of H_x is

$$H_x = y\sigma_{a_x} \frac{\sigma_f}{\sigma_{a_0}} \frac{nv}{(\lambda_x + nv\sigma_{a_x})} \tag{43}$$

where y is the fission yield of Xe^{135}, σ_{a_x} is the absorption cross section of Xe^{135}, λ_x the disintegration constant of Xe^{135}, nv is the flux, σ_f is the averaged fission cross section per atom of ordinary uranium, and σ_{a_0} is the absorption cross section of uranium. Equations 42 and 43 are valid at a point of the pile, so that the value of H must be weighted with the square of the flux and averaged over the metal-containing portion of the pile. The effect of the xenon was calculated with the following values of needed quantities:

$y = 0.063$, $\sigma_{a_x} = 2.9 \times 10^6 b$, $\lambda_x = 2.1 \times 10^{-5}$ sec^{-1}

average flux/maximum flux = 0.434, metal loading = 700 channels = 53.9 metric tons,

$\sigma_f(U) = 3.9$ b, $\sigma_{a_0} = 7.2$ b

For operation at 25 megawatts, the loss in reactivity was found to be $\delta k = -0.0074$.

The xenon effect was measured experimentally, but only in low power runs. The measured effect was used to compute a value of the product $y\sigma_{a_x}$; the result obtained was 16.5×10^4 b, somewhat lower than the value 18×10^4 b used in the calculations. The latter value was obtained from experiment with the Oak Ridge reactor; in view of the uncertainties in both measurements, the agreement is not bad.

The equilibrium xenon effect as calculated, namely $\delta k = -0.0074$, together with a calculated temperature effect of about $\delta k = -0.008$ gave a total excess reactivity requirement of $\delta k = 0.015$ to 0.016. It was also decided to allow about 0.0075 for experimental purposes, giving the estimated total agreement of about 0.023 in excess reactivity.

Finally, calculations of the xenon transients, especially the increase in the poisoning effect after a shutdown from continued high-power operation, showed that this increase would be sufficiently small so that the problem of xenon over-ride would be unimportant.

REFERENCES

1. Wigner, E. P., *Theoretical Physics in the Metallurgical Laboratory at Chicago*, J. Appl. Phys. *18*, 857 (1946).
2. Glasstone, S. and Edlund, M. C., *The Elements of Nuclear Reactor Theory*, New York: D. Van Nostrand and Co., Inc. (1952).
3. Guggenheim, E. A. and Pryce, M. H. L., *Uranium-Graphite Lattices*, Nucleonics *11*, 50 (*February* 1953).
4. *The Reactor Handbook*, Vol. 1: Physics. United States Atomic Energy Commission.
5. Creutz, E., Jupnik, H., Snyder, T. and Wigner, E. P., *Review of the Measurements of the Resonance Absorption of Neutrons by Uranium in Bulk*, J. Appl. Phys. *26*, 257 (1955).
6. Wigner, E. P., Creutz, E., Jupnik, H. and Snyder, T., *Resonance Absorption of Neutrons by Spheres*, J. Appl. Phys. *26*, 260 (1955).
7. Creutz, E., Jupnik, H., Snyder, T. and Wigner, E. P., *Effect of Geometry on Resonance Absorption of Neutrons by Uranium*, J. Appl. Phys. *26*, 271 (1955).
8. Creutz, E., Jupnik, H. and Wigner, E. P., *Effect of Temperature on Total Resonance Absorption of Neutrons by Spheres of Uranium Oxide*, J. Appl. Phys. *26*, 276 (1955).
9. Hill, J. E., Roberts, L. D., and McGammon, G., *Slowing Down of Fission Neutrons in Graphite*, Atomic Energy Commission Document, AECD-3390.
10. Behrens, D. J., *The Effect of Holes in a Reacting Material on the Passage of Neutrons*, Proc. Phys. Soc. (London) *62A*, 607 (1949).
11. Plass, G. N., *The Thermal Neutron Diffusion Length in a Heterogeneous Pile*, J. Appl. Phys. *23*, 621 (1952).
12. Friedman, F. L., *Elementary Pile Theory*, in The Science and Engineering of Nuclear Power, Vol. I, ed. by C. Goodman, Cambridge: Addison-Wesley (1947).
13. Chernick, J. and Kaplan, I., *The Nuclear Reactor with a Transverse Air Gap*, J. Nuclear Energy, in press.
14. Kunstadter, J., *A Correction to be Applied to the Activity of Neutron-Activated, Cadmium-Covered Indium Foils*, Phys. Rev. *78*, 484 (1950).
15. Hughes, D. J., Dabbs, J., Cahn, A. and Hall, D., *Delayed Neutrons from Fission of U-235*, Phys. Rev. *73*, 111 (1948).

Exponential Experiments in Graphite Systems

By D. E. Davenport,* USA

The first exponential experiments in the United States with graphite-uranium systems were begun in 1941.[1–6] This series of measurements had as its single-minded objective the discovery of the lattice which would most likely permit construction of a chain-reacting pile for plutonium production. More than fifty lattices were measured in a period of three years. Most of the measurements were made under the handicaps of a shortage of time and materials. The Hanford lattice was chosen on the basis of these measurements. These experiments are now mostly of historic importance because of their limited nature and necessarily complex experimental arrangements.

When additional reactor construction was undertaken at Hanford, a new series of exponential measurements was begun, since the state of pile theory still precluded calculation of improved reactor designs. These exponential experiments were directed toward two main objectives: (1) finding a better water-cooled graphite lattice for plutonium production in view of the increase in quality of available materials and the changing definition of the "optimum" lattice, and (2) providing improved knowledge of lattice theory, both for its own sake and to permit more accurate lattice calculations for future reactor designs. To date, these measurements have included nearly 100 exponential experiments using natural uranium.

In order to aid the design of sodium-cooled graphite power reactors, a new series of exponential experiments was started in the North American Aircraft laboratories in Downey, California, in 1954. The measurements have included natural and enriched uranium rods arranged singly and in clusters in the graphite matrix. Since the measurements have just been initiated, there is only a small quantity of data yet available.

EARLY EXPONENTIAL EXPERIMENTS (1941–1944)

One of the principal objectives of the original exponential experiments was to find the graphite-to-uranium ratio (C/U) which would give the reactor lattice the maximum buckling. Since the buckling is inversely related to the size of the reactor necessary to produce a chain reaction, the lattice with the largest buckling would be most likely to produce a chain-reacting pile for a given pile size. When the values of the bucklings are combined with the C/U ratios, the pile requiring the minimum amount of uranium for a critical reactor can also be calculated. It was recognized that the buckling did not depend on the C/U ratio alone but also on the size of the uranium lumps and their state of purity. Separate measurements were made of these effects.

Additional exponential experiments were made on single lattices to determine the effect on the buckling of water, aluminum, air, and other impurities in the lattice as well as the lattice temperature. Because of their limited nature, these measurements will not be presented here.

A summary of the results of those buckling measurements which were directed toward finding the buckling as a function of C/U is given graphically in Fig. 1. The measurements fall into three main groups.

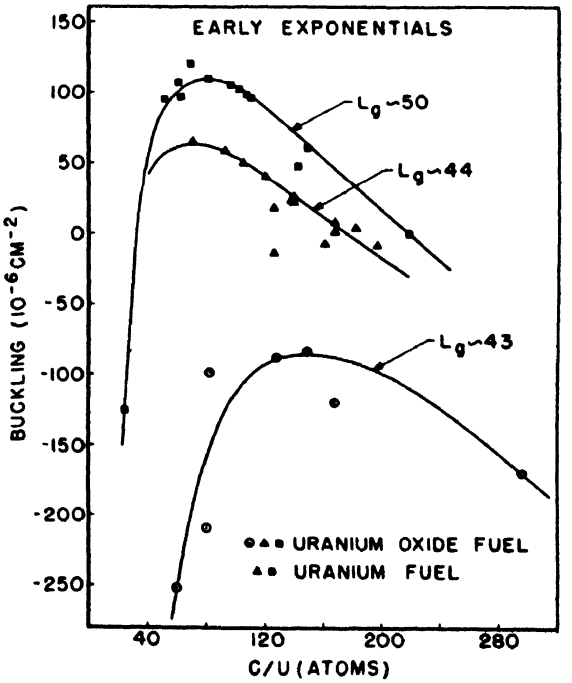

Figure 1. Buckling vs C/U for the early exponential experiments (1941–1944). The data in the lowest curve was obtained with low-purity U_3O_8 and graphite with a diffusion length, l_g, of 43 cm. The data in the upper two curves were obtained with uranium oxide and uranium metal of improved purity

* Hanford Atomic Products Operation, General Electric Co. Including work by H. L. Anderson, the Metallurgical Laboratory, the Manhattan Project; E. D. Cashwell, R. F. Christy, D. K. Froman, D. B. Hall, P. Morrison, K. Way, G. Weil, A. M. Weinberg, M. D. Whitaker and W. H. Zinn, the Metallurgical Laboratory; E. Z. Block, E. D. Clayton, D. E. Davenport, W. B. Farrand, J. H. Hall, E. E. Jones, R. C. Lloyd, G. L. Lynn, G. N. Plass, D. C. Pound and C. R. Richey, Hanford; F. B. Estabrook, S. W. Kash and R. A. Laubenstein, North American Aviation Inc.; and the late E. Fermi.

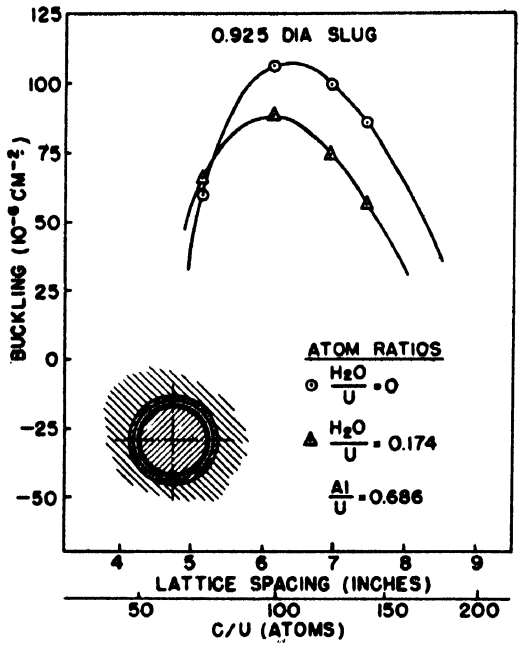

Figure 2a. A plot of the measured buckling vs lattice spacing and C/U atom ratio for the 0.925-inch-diameter slug and the 1.36-inch-diameter slug. The inset in Fig. 2a shows the geometry of the fuel rod assembly for all of the externally-cooled, solid rods. Figure 2a: experimental bucklings vs lattice spacing for 0.925" diameter slug with small water annulus

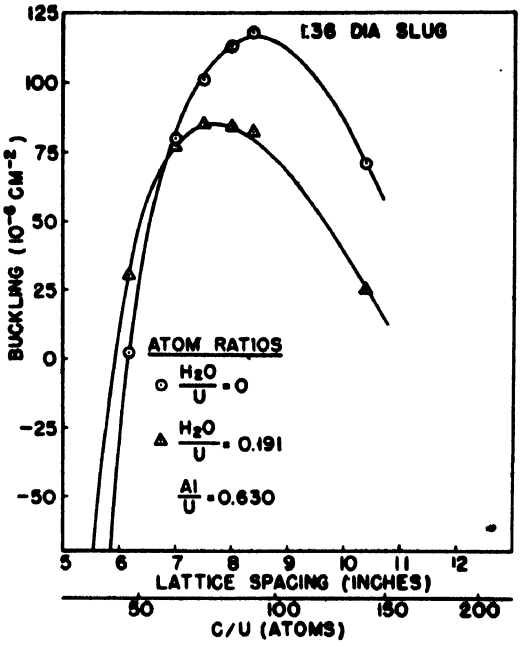

Figure 2b. Experimental bucklings vs lattice spacing for 1.36" diameter slug with 0.193 cm H_2O annulus

The lowest curve contains the first few measurements made with rather impure U_3O_8. The diffusion length of the graphite, L_g, was about 43 cm. The scatter of the data resulted largely from differences in U_3O_8 lump size used and extraneous materials in the lattices.

The middle curve contains data measured with both uranium oxide and uranium metal. The oxide and metal were of much better purity than in the lower curve, but the graphite purity was only slightly improved. Again, the wide variation in surface-to-mass ratio (S/M) of the fuel used causes scatter of the points. The two full triangles which fall below the curve were obtained with uranium of lower quality than the remainder of the points on the curve.

The upper curve gives the final measurements with improved graphite ($L_g \sim 50$). In this case about half of the metal measurements were made with cylindrical rods instead of cubes or spheres. The two measurements with oxide fuel elements fall on the curve through the metal points if the lower point is corrected for the low graphite density used in that measurement (1.5 gm/cm^3 instead of 1.6 gm/cm^3).

THE HANFORD EXPONENTIAL EXPERIMENTS

In the Hanford exponential experiments, the lattice buckling has been measured as a function of fuel-rod diameter, lattice spacing, and water-annulus thickness for solid, cylindrical fuel rods of natural uranium. A few measurements have been included using hollow, internally-cooled, cylindrical fuel rods.

The exponential piles were approximately eight-foot cubes resting on a twenty-inch graphite base, which contained Ra-Be neutron sources. The uranium rods were canned in aluminum tubes and assembled in aluminum process tubes as shown in the inset in Fig. 2a. The effective width of the pile was determined by horizontal neutron-flux traverses taken at two or three heights in the pile. It was found that, for all piles measured, the effective width was $2 \pm \frac{1}{4}$ inches larger than the geometric width, i.e., the extrapolation distance was $1 \pm \frac{1}{8}$ inches. Scattering of fast neutrons back through the cadmium shields (which covered all pile faces) is believed to account for the fact that this extrapolation distance is about $\frac{1}{4}$ inch larger than the theoretical value.

The relaxation measurements were made with both indium foils and BF_3 proportional counters with a reproducibility of $\pm 2 \times 10^{-6}$ cm^{-2} for the solid-slug lattices. In the case of the hollow-slug lattices, the reproducibility was more nearly $\pm 4 \times 10^{-6}$ cm^{-2}.

Lattices Using Solid Natural-Uranium Fuel Rods

The measurements of lattices using solid, natural-uranium fuel rods included three rod diameters: 0.925 inch, 1.175 inches and 1.36 inches. A summary of the water-to-uranium ratios (molecules to atoms) and the lattice spacing associated with each fuel rod size is given in Table I.

Since the buckling was measured for each case with and without the water in the cooling annulus (wet

Table I. Summary of Solid Rod Lattices Measured

Rod diameter (inches)	H_2O/U (atoms)	Lattice spacing (inches)							
		5 3/16	6 3/16	7	7 1/2	8	8 3/8	10 3/8	12 3/8
0.925	0.17	X	X	X	X				
	0.30		X		X				
	0.79	X	X	X	X				
1.175	0.18		X		X				
1.36	0.19	X	X	X	X	X	X	X	
	0.30		X		X				X

Table II. Description of Material in Solid Slug Exponential Experiments

For slug diameter (in inches)	*0.925*			*1.175*	*1.36*		*1.66*
	Case I	*Case II*	*Case III*		*Case I*	*Case II*	
URANIUM:							
Volume of U/cm of length (cm^3/cm)	4.34	4.34	4.34	7.00	9.37	9.37	13.96
Slug length (cm)	19.43	19.43	19.43	19.43	10.27	10.27	10.16
Slug radius (cm)	1.175	1.175	1.175	1.49	1.727	1.727	2.11
Slug density (solid in gm/cm^3)	18 91	18.91	18.91	18.90	18.75	18.75	18.75
Slug density (equivalent in gm/cm^3)	17.98	17.98	17.98	18.09	17.14	17.14	18.75
ALUMINUM:							
Volume of process tube/cm of length (cm^3/cm)	1.36	0.87	1.75	1.75	2.31	0.97	no tube
Outside radius of Al process tube (cm)	1.55	1.59	1.91	1.91	2.20	2.20	no tube
Effective inside radius of tube (cm)	1.40	1.50	1.75	1.75	2.02	2.13	no tube
Volume of can/cm of length (cm^3/cm)	0.68	0.68	0.68	0.87	1.14	1.14	0.97
Outside radius of Al can (cm)	1.27	1.27	1.27	1.59	1.83	1.83	2.20
Inside radius of Al can (cm)	1.18	1.18	1.18	1.50	1.74	1.74	2.13
Thickness of double-end cap, or Al spacer between slugs (cm)	1.02	1.02	1.02	1.02	0.94	0.94	no end cap
Total volume of Al/cm of length (cm^3/cm)	2.25	1.76	2.64	2.93	4.25	2.91	0.97
WATER:							
Volume of water/cm of length (cm^3/cm)	1.03	1.80	4.66	1.73	2.33	3.68	no water
Water annulus thickness (cm)	0.123	0.208	0.490	0.16	0.193	0.296	no water
Radius of hole in graphite (cm)	1.567	1.922	1.922	1.922	2.215	2.215	2.215

and dry), the number of measurements involved is twice the indicated number of lattices. A detailed description of the amount of materials and geometry of the components of each of the lattices is given in Tables II and III.

In Fig. 2 the buckling measurements are plotted against lattice spacing (and C/U atom ratio) for the 1.36-inch-diameter fuel rod (slug) and the 0.925-inch diameter fuel rod. The measurements are for the smallest water annulus investigated in each case. For the 1.36-inch-diameter slug the measurements in the 5 3/16-inch lattice are not shown, since they would require a scale reduction (the wet lattice buckling was -114×10^{-6} cm^{-2}, and the dry lattice buckling was -225×10^{-6} cm^{-2}).

It is to be noted that for the larger lattice spacings (overmoderated lattices) the buckling of the dry lattice is larger than the buckling of the wet lattice. As the lattice spacing is reduced, the buckling curves approach each other and cross, so that for small lattice spacings the wet lattice has a higher buckling than the dry lattice. This general observation is important to pile design from the safety standpoint. If one is to minimize the probability and extent of a reactor disaster involving loss of cooling water, the reactor lattice should be chosen to the left of the intersection of the dry- and wet-buckling curves ("crossover point"). In this way the lattice will be "fail-safe" with regard to loss of water.

The "fail-safe" characteristic depends on the fact that the loss of moderator (water) from the undermoderated lattices decreases the resonance escape probability more than the loss of poison and scattering medium around the slug increases the thermal utiliza-

Table III. Description of Material in Solid Slug Exponential Experiments

Ratios of Al, H_2O, and C atoms to U atoms per cell*

Slug diameter	*H_2O/U*	*Al/U*	*Lattice spacing (inches)*	*C/U*
0.925	0.174	0.686	5 3/16	69.9
			6 3/16	100.7
			7	129.0
			7 1/2	148.7
	0.305	0.537	5 3/16	68.2
			6 3/16	99.0
			7	127.4
			7 1/2	147.1
	0.790	0.805	5 3/16	68.2
			6 3/16	99.0
			7	127.4
			7 1/2	147.1
1.175	0.180	0.551	6 3/16	61.0
			7 1/2	90.6
1.36	0.191	0.630	5 3/16	32.4
			6 3/16	47.3
			7	61.1
			7 1/2	70.7
			8	80.9
			8 3/8	89.4
			10 3/8	139.0
			12 3/8	198.8
	0.302	0.431	6 3/16	47.3
			7 1/2	70.7
			12 3/8	198.8
1.66	no water	0.088	6 3/16	29.0
			7 1/2	43.4
			12 3/8	122.0
			15	179.2

* The quality of the graphite used in these experiments is such that the diffusion length at density 1.6 gm/cm^3 is 54.4. Densities of graphite range from 1.647 gm/cm^3 to 1.658 gm/cm^3.

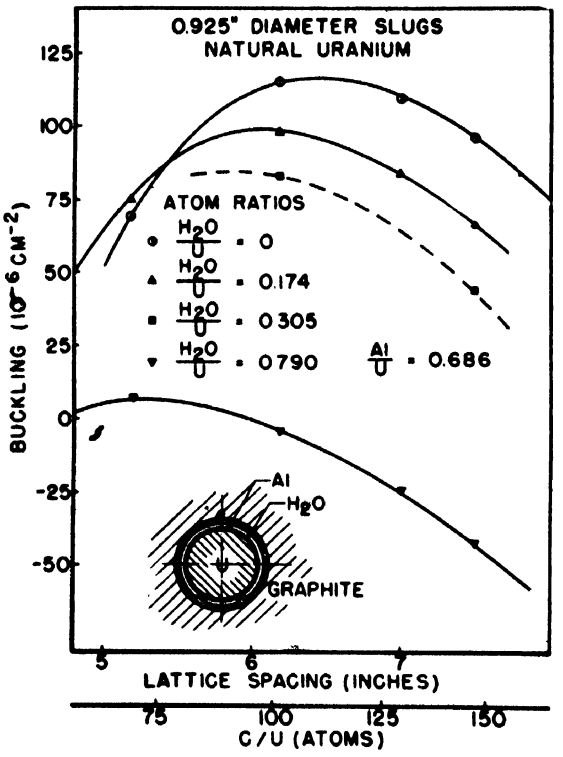

Figure 3a. Buckling vs lattice spacing for different water-annulus thicknesses. All data have been corrected to the same amount of aluminum for each slug size

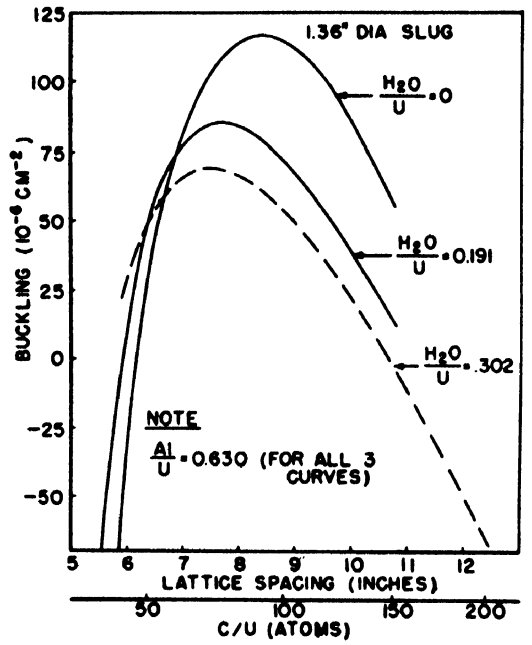

Figure 3b. Buckling vs lattice spacing comparison for a 1.36" diameter slug in two different annuli-data corrected to the same Al/U ratio

tion. In the case of the larger lattice spacings, the moderating effect of the water becomes progressively less important until, for overmoderated attices, the loss of water becomes essentially the loss of poison. This "fail-safe" region does not exist for coolants which are not at the same time moderators.

The exact value of the lattice spacing at the "crossover point" depends upon the amount of water being considered. Figure 3 shows the effect of using thicker water annuli for the 0.925-inch- and 1.36-inch-diameter fuel rod lattices. In the case of the larger water annuli the measurements have been corrected to the same amount of aluminum as was used for the smaller annuli, so that the same dry-lattice buckling curve serves as the reference for all wet-lattice buckling curves.

Although the 0.925-inch-diameter slug data is incomplete for smaller lattices, it is seen that the "crossover point" shifts to smaller lattices as the amount of water in the lattice is increased. The "crossover point" appears to shift from a 5.3-inch-lattice spacing for the 0.925-inch slug with a H_2O/U atom ratio of 0.17 to about 4.6-inch-lattice spacing for a H_2O/U atom ratio of 0.79. In the case of the 1.36-inch-diameter slug, a 50% increase in the amount of water changes the "crossover point" from a 6.9-inch-lattice spacing to a 6.7-inch-lattice spacing.

Only two lattice spacings and a single water annulus have been measured using the 1.175-inch slug. Since the measurements fell on either side of the "crossover point," its value was estimated in Fig. 4a by fitting the points with curves of the same shape as observed for the other two slug sizes.

The effect of slug size on the location of the "crossover point" and the buckling at the "crossover point" can be seen in Fig. 4b for one H_2O/U atom ratio. Since the H_2O/U and Al/U atom ratio chosen for comparison was close to an actual measurement condition for all three slug sizes, corrections to measured values were small.

As the slug diameter increases, the C/U atom ratio at the "crossover point" is seen to decrease. This may be explained by the fact that as the slug diameter increases, both the disadvantage factor of the slug and the thickness of the water annulus increase. Both of these effects increase the relative poison effect of the

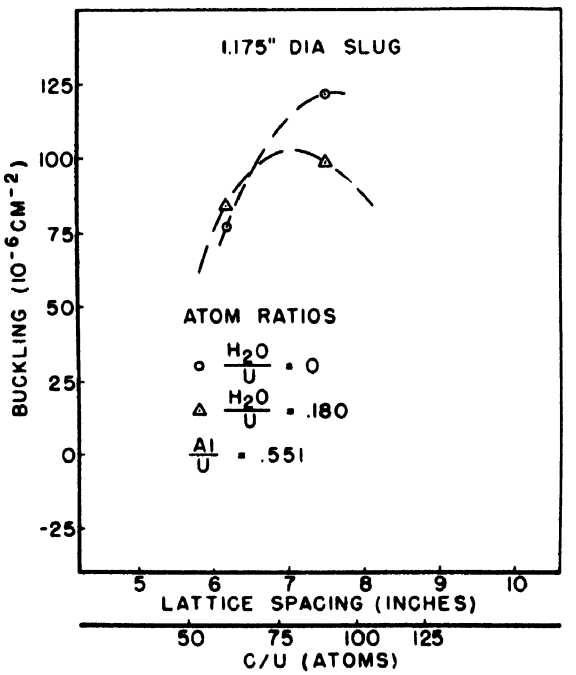

Figure 4a. Plot of the buckling vs the lattice spacing and C/U atom ratio for the 1.175-inch slug. The curves were drawn in from the curve shapes of the 0.925-inch and 1.36-inch-diameter slug measurements

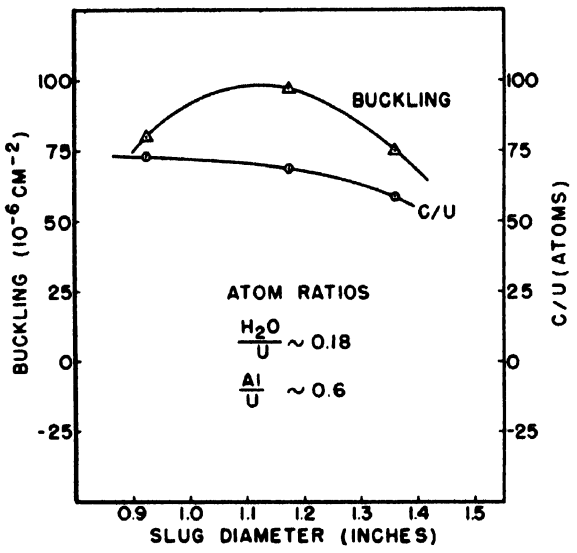

Figure 4b. Plot of the "crossover-point" buckling and C/U atom ratio vs the slug diameter in inches. Lattice values at the intersection of the wet and dry buckling curves

water, and, therefore, require a greater change in resonance escape probability to overcome the effect. This implies lattices with lower C/U ratios. The maximum in the "crossover-point" buckling results from the fact that the maximum in the 1.175-inch-diameter slug buckling curve is greater than for the other two slug diameters. This peaking of the buckling value at some slug size might be expected from general considerations of the effective resonance-energy cross section of U^{238} and the slug disadvantage factor as functions of slug size. As the slug size increases, the effective resonance-energy cross section of U^{238} decreases, raising the bucklings, especially for small C/U ratios. However, as the slug size increases the slug disadvantage factor increases, which reduces the thermal utilization and thus reduces the bucklings, especially for the larger C/U ratios. The net result of these two effects is a maximum in the buckling vs slug-size curve.

Internally-Cooled Slugs

Internally-cooled slugs would seem to have several advantages from the neutron economy standpoint over externally-cooled slugs:

1. The thermal utilization would be increased by the absence of the blocking effect of the water on the outside of the slug. The moderator on the inside of the slug should increase the average neutron flux in the uranium and decrease the average flux in the water.
2. The resonance escape probability would decrease because of the added interior surface and the slight increase in the exterior surface necessary to provide for the same amount of uranium.
3. The lattice diffusion length would decrease. This may be partly offset by a gain in the Fermi age due to decreased probability of inelastic scattering with water on the interior of the slug.

The main disadvantage would seem to be the loss in fast effect when the slug size is effectively reduced by placing the water in an internal cooling annulus. This effect is largest when the above gains are also greatest, i.e., for large diameter slugs.

To get a measure of the total effect of these advantages and disadvantages, buckling measurements were made on a series of lattice spacings for two in-

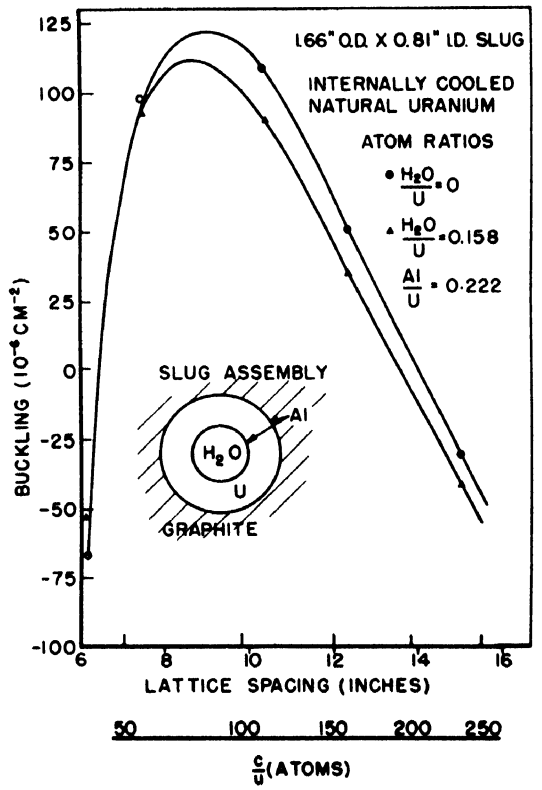

Figure 5a. Buckling of internally-cooled slugs plotted vs lattice spacing and C/U atom ratio for two different water channel diameters

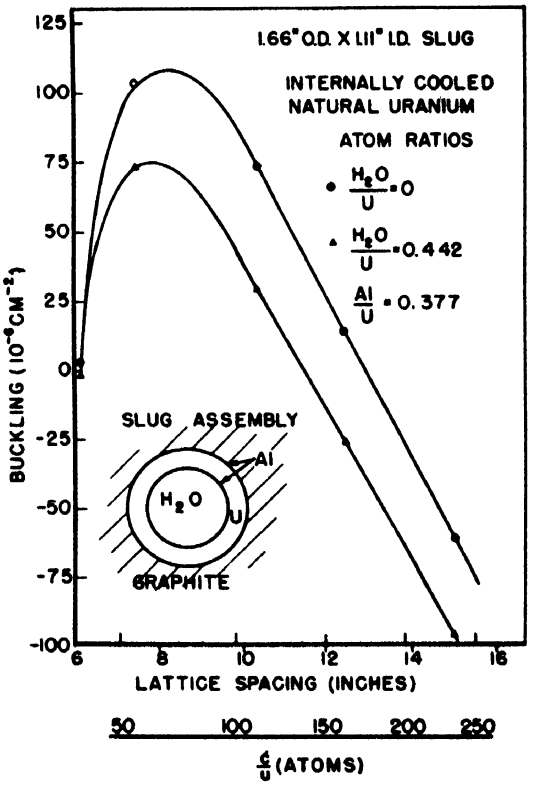

Figure 5b. In each case the buckling for the lattice is plotted for measurements made with and without water in the central channel

ternally-cooled fuel rod assemblies. The slug geometries were 1.66-inch od × 0.81-inch id and 1.66-inch od × 1.11-inch id, with the water placed in the core of the slug as in Fig. 5. The 0.81-inch id slug had about the same H_2O/U ratio as the smallest H_2O/U ratio used with the three solid-slug sizes.

The results of the measurements with and without water in the cooling channel are given in Fig. 5. The general curve shapes are similar to those for externally-cooled slugs. However, the wet- and dry-lattice-buckling curves are generally closer together. In the undermoderated lattices, the wet- and dry-lattice bucklings are almost the same over the range of measured lattice spacings. In the overmoderated lattices the wet- and dry-lattice bucklings differ by less than half the amount observed for the same H_2O/U ratio with externally-cooled slugs. The intersection of the wet- and dry-lattice buckling curves is at smaller C/U ratio (40–50) than in the solid-slug cases. This results from the fact that the removal of water no longer increases the resonance capture but, rather, decreases it, thus raising the dry bucklings relative to the wet bucklings.

From these measurements one must conclude that any reactivity gain obtained from an increase in thermal utilization by using internally-cooled slugs is offset by decreases in the resonance escape probability and the fast effect. Intracell traverses of the thermal neutron flux should help evaluate the thermal utilization increase. Theoretical calculations indicate that changes in resonance escape probability are not very large (~1% for the 1.66-inch od × 0.81-inch id compared with a solid 1.45-inch-diameter slug).

The Effect of Coring a Slug

One may obtain a measure of the effect of coring a slug by combining the dry-lattice bucklings of the two hollow slugs with those of the 1.66-inch solid slug. The

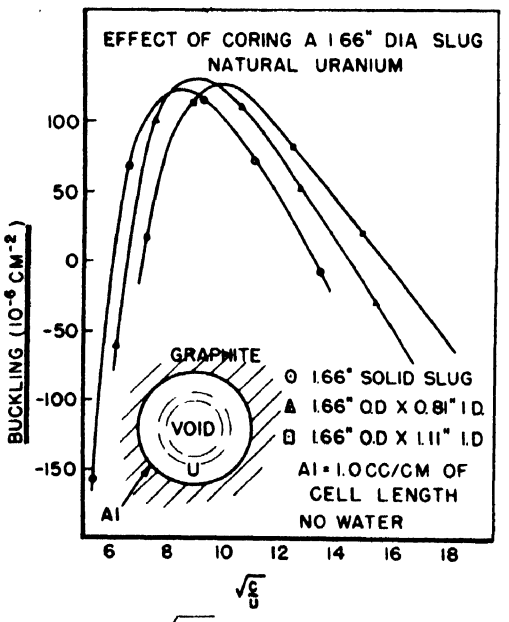

Figure 6a. Buckling vs $\sqrt{C/U}$ (atom ratio) for three fuel elements having the same outer diameter (1.66 inches) but different inner diameters (ID = 0, 0.8 inch, and 1.11 inches)

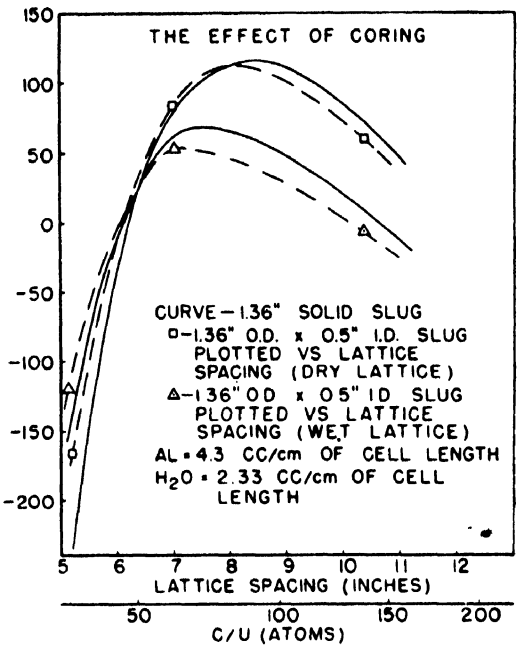

Figure 6b. Comparison of buckling vs lattice spacing for a solid slug (full line) and a cored slug (dotted line) with the same external water annulus

effect of the internal aluminum liner must be subtracted from the hollow-slug lattices before comparison. Figure 6a is a graph of the corrected data plotted against $\sqrt{C/U}$.

The relative height of the maxima of the curves is not too significant since there were not enough points to determine them accurately. The curve shapes are generally as one would anticipate, the buckling of the undermoderated lattices increasing as the hole size was increased (and C/U increased); for the overmoderated lattice the situation is just reversed.

One measurement was made of the effect of coring on externally-cooled slugs. A ½-inch core was removed from the 1.36-inch-diameter slug and the ends of the hole plugged with aluminum to prevent water from entering the core. Measurements were then made of the dry- and wet-lattice bucklings for the 5 3/16-inch, 7-inch, and 10⅜-inch lattice spacings. The results are compared with the solid-slug measurements in Fig. 6b. For the cored slugs, the bucklings are increased for the small lattice spacings and decreased for the large lattice spacings. The coring effectively moves the intersection of the wet- and dry-buckling curve to the left.

U^{235} LOADED LATTICES

In order to obtain a simple lattice which would lend itself better to theoretical interpretation, measurements were taken in lattices which used essentially pure U^{235} as fuel. With U^{235} fuel elements the problems associated with both fast-effect and resonance-escape probability of U^{238} are eliminated.

The three lattices measured used U^{235}-aluminum alloy pieces which had the same canned diameter as the 1.36-inch-diameter natural uranium (1.44 inches.) They were measured in the same process tube assembly giving a water volume of 2.33 cm³/cm cell length.

Because of the very high bucklings of these lattices the measurements were carried out in four-foot-square piles. In the case of the wet 4¾₁₆-inch lattice the measurements were made as an approach to critical which, with the experimental facilities available, limited the precision to $\pm 100 \times 10^{-6}$ cm^{-2}. The results of the measurements are shown in Fig. 7, where the triangles are the bucklings of the wet lattices and the circles are the bucklings of the dry lattices.

A point of interest in this measurement is the fact that the wet lattice has a higher buckling than the dry lattices just as for natural uranium, though the curve shapes are rather different. In the case of natural uranium the intersection of the buckling curves is caused by the rapidly decreasing resonance-escape probability for the dry lattices. In the case of the U^{235} lattice the higher value of the buckling for the wet lattice arises principally because of the reduced migration area. In these high k lattices fast leakage is very important so the increase in Fermi age on losing water overcomes the effect of poison removal in the smaller lattices.

NORTH AMERICAN AVIATION INC. EXPERIMENTS

The North American Aviation Inc. (NAA) exponential experiments were carried out in piles approximately 4 feet square and 5 feet high. The thermal column of a small homogeneous reactor, the Water Boiler Neutron Source, served as the pile base. The small pile size limited buckling measurement precision to approximately $\pm 12 \times 10^{-6}$ cm^{-2}.

Effect of Enrichment in a Single-Rod Lattice

A measurement of the effect of enrichment on buckling has been made with a 1-inch-diameter fuel rod in a 9½-inch lattice spacing. The enrichments used were 0.49 (depleted), 0.71 (natural), and 0.90 weight % of U^{235}.

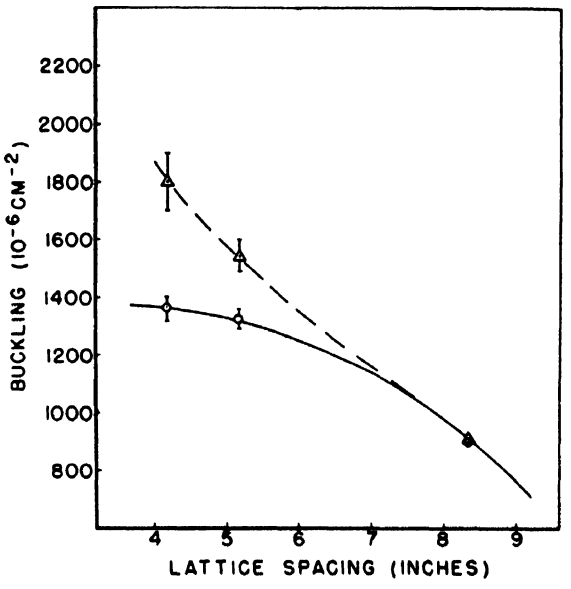

Figure 7. Buckling vs lattice spacing for lattices loaded with U^{235}-aluminum-alloy slugs. The triangles, were lattices with 2.33 cc of H_2O/cm cell length. Circles were lattices with no water in the cooling annulus

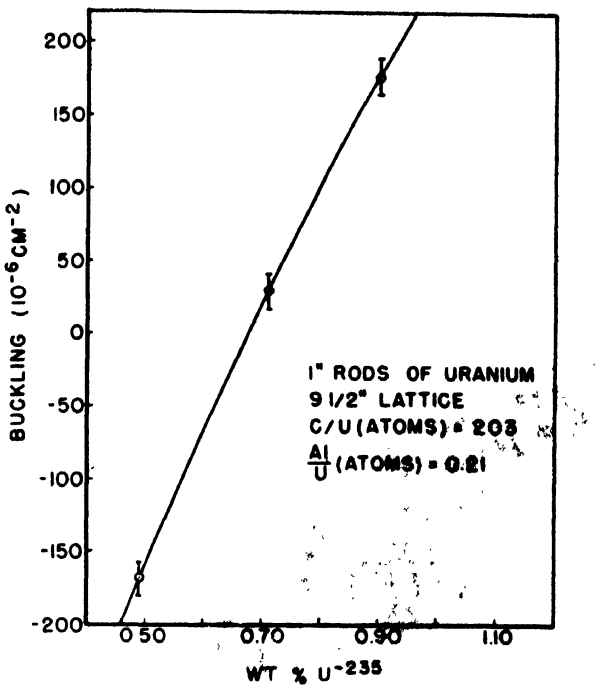

Figure 8. Effect of enrichment. Buckling vs weight per cent of U^{235} in the fuel rod

The results of the measurements are plotted in Fig. 8.

The change in buckling with enrichment agrees quite well with that calculated from cross-section changes and estimates of slug disadvantage factor changes.

Cluster Lattices

Measurements have been completed on five lattices using cluster-type fuel elements with aluminum being used to "mock-up" the sodium coolant. The measurements included three lattices with 7-rod clusters of ¾-inch natural uranium rods and two lattices with 4-rod clusters of 1-inch enriched (0.90 weight % U^{235}) uranium rods. Since the two types of clusters contain almost the same weight of uranium and aluminum per unit length, the preliminary results of the measurements have been plotted together in Fig. 9a.

A comparison of the curve shape for the 7-rod cluster with single-rod measurements may be seen in Fig. 9b. The dry-lattice Hanford measurements have all been corrected to no aluminum in the lattice. If the 7-rod cluster measurements are corrected to no aluminum in the lattice, the maximum will rise approximately to the single rod maxima. The curve shape, however, appears to be appreciably flatter. The reason for this is not apparent.

CONCLUSIONS

Four general conclusions concerning water-cooled graphite-uranium lattices can be drawn from these exponential experiments:

1. The maximum in the buckling vs C/U atom-ratio curve for a given natural uranium fuel assembly occurs at a value of C/U between 50 and 100. The smaller the slug diameter and the thinner the water annulus, the larger the value of C/U at which the maximum occurs.

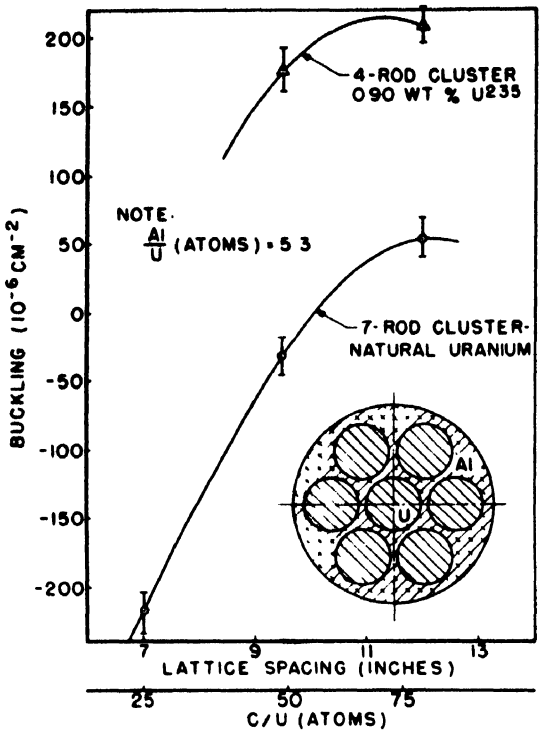

Figure 9a. Plot of buckling vs lattice spacing for 7-rod clusters of natural uranium and 4-rod clusters of enriched uranium

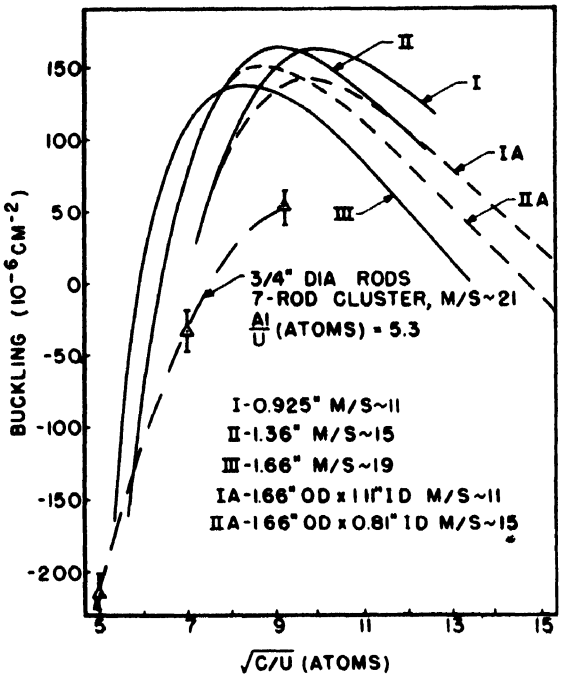

Figure 9b. Plot of buckling vs $\sqrt{C/U}$ for all dry, natural uranium lattices. The mass-to-surface-area ratio (M/S) in g/cm² has been indicated for each slug geometry

2. Lattices with externally-cooled slugs exhibit a "fail-safe" behavior on loss of water if the C/U ratio is somewhat smaller than at the maximum buckling for that fuel assembly. In these undermoderated lattices, the large decrease in the resonance escape probability accompanying the loss of water lowers the lattice buckling.

3. Internally-cooled slugs provide only small reactivity gains over externally-cooled slugs for rod diameters of less than 1.5 inches.

4. U^{235}-loaded lattices exhibit a "fail-safe" behavior on loss of water from undermoderated lattices because of the increase in the migration area accompanying the loss of water.

REFERENCES

1. Anderson, H. L., Feld, B., Fermi, E., Weil, G. and Zinn, W., *Neutron Reproduction in a Lattice of Uranium Oxide and Graphite-Exponential Experiment*, C-20 (26 March, 1942).
2. Fermi, E., *Preliminary Report on the Exponential Experiment at Columbia University*, C-26 (March, April 1942).
3. Allison, S. K., *The Fourth Intermediate Pile at Chicago*, C-102, (no date).
4. Fermi, E., Christy, R. F. and Weinberg, A. M., *Effect of Temperature Changes on the Reproduction Factor*, C-254 (September 1952).
5. Fermi, E., Snell, A. H., Manley, S. H., Zinn, W. H., Wilson, V. C., Wigner, E. P. and Mitchell, A. C. G., *Physics Research Report for Month Ending 15 October 1942*, CP-297.
6. Christy, R. F., Froman, D. K., Hall, D. B., Hall, J. H., Plass, G. N. and Weinberg, A. M., *Intermediate Piles Nos. 30, 31A, 31B, and 32*, CP-575 (13 April 1943).

Record of Proceedings of Session 21A

FRIDAY MORNING, 18 AUGUST, 1955

Chairman: Mr. O. Gamba (Argentina)
Vice-Chairman: Mr. A. G. Ward (Canada)
Scientific Secretaries: Messrs. M. Trocheris and F. de Hoffmann

PROGRAMME

P/600	Exponential experiments with slightly enriched uranium rods in ordinary water	H. Kouts *et al.*
P/601	Pressurized water reactor (PWR) critical experiments	S. Krasik and A. Radkowsky
	DISCUSSION	
P/790	Some experiences from measurements on an exponential pile of uranium and heavy water	R. Persson *et al.*
P/791	Characteristics of the Swedish heavy water reactor	E. Hellstrand *et al.*
P/361	Study of the neutronics of two French heavy water reactors	J. Horowitz
P/605	Exponential experiments on D_2O uranium lattices	E. R. Cohen
P/623	A heavy-water research reactor	A. I. Alichanov *et al.*
	DISCUSSION	
P/429	The experimental basis of lattice calculations	P. W. Mummery
P/607	Normal uranium, graphite-moderated reactors: a comparison of theory and experiment water cooled lattices	P. F. Gast
P/606	Uranium graphite lattices—the Brookhaven reactor	I. Kaplan and J. Chernick
	DISCUSSION	

Mr. I. KAPLAN (USA) presented paper P/600.

Mr. S. KRASIK (USA) presented paper P/601 and made the two following remarks.

1. As regards the values found for the migration areas (Table II of P/601): It may be observed that the values of the migration area obtained are somewhat higher than those obtained from the exponential experiments described in the preceding paper. We would point out that this measurement depends on a reactivity measurement which in turn in a critical experiment is associated with a period through the inhour equation. There have been data reported to this Conference on neutron periods and yields as well as other effects which have not yet been fully taken into account in analyzing these experimental results. For this reason no great significance should be attached to the apparent discrepancy in migration areas.

2. As regards the "seed and blanket" arrangement in the PWR flexible critical experiment: The seed region of the reactor is designed to leak neutrons effectively into the blanket region. A principal reason for going to a design of this type is the reduction on fuel loading which can be achieved. Furthermore, in operation the plutonium is formed preferentially adjacent to the seed because of the leakage of fast neutrons from the seed. This results in a longer reactivity lifetime because of the favorable location of the preferential formation.

Mr. Krasik further called the attention of the reader to paper P/604 by A. Radkowsky and S. Krasik, which discusses the physics of PWR.

DISCUSSION OF P/600 AND P/601

Mr. BARKOV (USSR): In P/601, presented by Mr. Krasik, it was shown how the migration area is determined from the variation of the reactivity of the assembly. The calculations were based on the one-group model. It can readily be shown that if we take for K_{eff} the expression obtained from the age theory the migration area computed on the basis of the measurements will be smaller by a factor $e^{-M^2B^2}$ than in the case when the one-group equation is used.

It will be seen that the results will depend on which equation is used in the analysis. The results of the determinations of M^2 given in papers P/600 and P/601 differ by about 20 per cent precisely because different relationships of K_{eff} with M^2 were employed. In P/600 the second equation was used, whereas in P/601 the first was used. In the light of this difference the procedures employed in the USSR for determining the slowing-down lengths appear to be more dependable. I shall describe these procedures briefly.

K. N. Mukhin and L. M. Barkov, working with uranium-water lattices and using the indium-detector method, measured the spatial distribution of the slowed-down neutrons from a point source of U^{235} fission neutrons.

A triangular uranium lattice, assembled of cylindrical blocks about 4 cm in diameter, was built in a large water tank measuring 100 × 100 × 140 cm. To suppress multiplication in the assembly due to slowed-down neutrons the uranium blocks were clad with cadmium 0.6 mm thick. As analysis of the system shows, multiplication by thermal and epithermal neutrons—neutrons having energies up to approximately 2 ev—is suppressed by the large amount of cadmium.

The fission neutron source was a U^{235} target which was bombarded by thermal neutrons brought into the centre of the lattice by means of a small-diameter tube. The PTR reactor was used as the source of thermal neutrons.

The indium detector permitted determining the spatial distribution of slowed-down neutrons to a distance of 60–70 cm from the source.

The experimental results indicate the absence of anisotropy in the distribution of slowed-down resonance neutrons, both radially and in height.

Furthermore, values of τ for the three investigated lattices were found by means of the equation: $\tau = (1/6)\overline{r^2}$.

The same investigators also found that in pure water, τ for resonance neutrons equals 30 ± 1.5 cm^2. For the most tightly packed lattice, as the measurements of G. A. Stoliarov, V. P. Katkov, L. V. Komissarov and Iu. V. Nikol'ski have shown, the fast-neutron multiplication factor reaches a value of 1.15. However, in determining τ, the fast-multiplication factor was not taken into account.

The results of tests aimed at determining τ and the fast multiplication factor in uranium-water lattices are in agreement with the results of theoretical calculations, as has been reported by S. M. Feinberg at the July session of the Academy of Sciences of the USSR.

The results of experimental determination of the migration area and consequently of τ carried out by Krasik and Radkowsky for close-packed lattices are also in satisfactory agreement with these theoretical calculations.

Mr. SHAPIRO (USSR): I would like to make a few remarks in connection with the highly interesting and valuable paper presented by Mr. Kaplan.

The effect of an air space around the uranium blocks on neutron multiplication was examined in the paper presented by Mr. Kouts. This effect has been studied in the Soviet Union by I. M. Frank and his associates. The effect of an air gap around the blocks on the parameter B^2 and on the thermal utilization in subcritical uranium-graphite assemblies was measured. It was found that the increase of B^2 and f in the presence of an air gap is about 1.5 times smaller than predicted by diffusion theory. We ascribe this difference to the inadequacy of the one-velocity diffusion theory for thermal neutrons.

We also investigated another method of increasing the thermal neutron utilization in a heterogeneous system. It is based on non-uniform heating of the moderator in the elementary cells. The moderator layer adjacent to the uranium block is kept cooler than the peripheral layer. The layer near the block has a temperature T_1, the layer away from the block has a temperature of T_2; T_2 is higher than T_1. This leads to cooling of the neutrons diffusing into the block. With a given neutron flux the density of the neutrons in the uranium increases due to the decrease of their velocity and this leads to an increase in the thermal utilization. In principle the thermal utilization can even exceed the value proper to a homogeneous mixture of uranium with a moderator. The increase of B^2 and thermal utilization was discovered in experiments with an uranium-graphite assembly, designed to permit heating part of the graphite in each cell by means of an electric current. In assemblies with water cooling in which the temperature of the moderator is higher than the water temperature, neutrons migrating into the uranium block are cooled by a water layer. This leads to an appreciable increase in thermal utilization, f, when the system is heated. This also was discovered in the experimental investigations.

Mr. Kouts' paper gives data on the temperature of thermal neutrons in a heterogeneous uranium-water system. Our measurements indicate that for the same mean lifetime of the thermal neutrons their temperature in a heterogeneous medium is lower than in a homogeneous medium. Here we have what is called diffusion cooling, i.e., cooling of the neutron gas at the expense of greater leakage of neutrons having a higher velocity. It becomes manifest when the absorption coefficient of the block varies more slowly with the energy than is called for by the $1/v$ law.

The last remark relates to the paper by Kaplan and Chernick, which will be presented later. I want to mention, however, that we measured the temperature effect of K_∞, h, f and p. The results for the temperature effect of the quantities h and p are in good agreement with the experimental data cited in the paper by Kaplan and Chernick.

In conclusion I want to point out that all the questions I have touched upon here are discussed in detail in the reports comprised in the Proceedings of the July 1955 session of the Academy of Sciences of the USSR.

Mr. MUMMERY (UK): As time is short I will make two comments only, based on our experience with water lattices.

First of all, in addition to doing exponential experiments we have carried out an approach to critical type experiments with quite interesting results. If one carries out the usual method of plotting these results—that is, to divide the number of rods loaded in the system by the counting rate obtained in a counter placed inside the system—and plots this against the number of rods in the system, one does in effect get a very good straight line from a very small number of rods. In fact, in one particular case we had a line straight all the way from 16 to about 300 rods where we were subcritical by only one per cent.

The second comment refers to the remarks in the first papers on the determination of migration area by using uranium of different enrichments. We have

also done this, and I just wanted to make it quite clear that I think the factor which is important is not the value of η as such but the ratio of the 238 cross section to the 235 cross section. This is to be compared with the boron poison method where the important factor is the ratio of the boron cross section to the U^{235} cross section.

Mr. LEWIS (Canada): Mine is a simple question directed to Mr. Kaplan concerning the statement that the results accord with the reasonable value of the inelastic scattering cross section of uranium. Is the same value satisfactory for the heavy-water lattice experiments present in paper P/605?

Mr. KAPLAN (USA): I am sorry, I do not know the answer to that, but I think we could get together with Mr. Cohen after the meeting and straighten it out.

Mr. COHEN (USA): I should like to make some comments on this point. I am not sure we can get very much out of the comparison. All our measurements have assumed the usual formula for the fast factor, and we have not investigated at all the details of the inelastic scattering in uranium. The fast effects that we have in our heavy-water lattices are all of the order of two or three per cent, and in this range there is really not enough discrimination to determine any details of the inelastic scattering.

Mr. R. PERSSON (Sweden) presented paper P/790 as follows:

Our experience in exponential pile experiments is rather limited because we began our measurements about six months ago and for only part of this time has heavy water been available for the experiments. So you must not expect extensive results—only some material for the discussion.

Slide 1 (Fig. 1 of P/790) shows the arrangement which was designed to give high flexibility. On this slide we have a view of the upper part of the tank. The rods are suspended by aluminum wires hanging over rollers running along the slotted beams. Both the rollers and the beams are adjustable from outside by means of bars, as you can see from the slide. The whole assembly is covered by a perspex cover, and through several small holes in this cover it is possible to take out or put in uranium rods without emptying the tank. The diameter of the tank is only 1 m. The primary reason was that we were, and are, short of uranium. The tank wall is 1 cm thick and is covered with plastic (polyethylene) containing boron carbide. In comparison with cadmium this plastic reduces the number of fast neutrons scattered back from the surroundings by a factor of about 2.

Slide 2 gives us a view of the tank from below. On the tank wall there are flanges for horizontal channels penetrating the tank. To begin with we have placed the detectors in these channels.

The neutron distribution in the axial direction is measured by two proportional boron trifluoride counters, about 36 cm in effective length. The counters are placed in line and approximately symmetrically about the axis. The distance between the detectors is

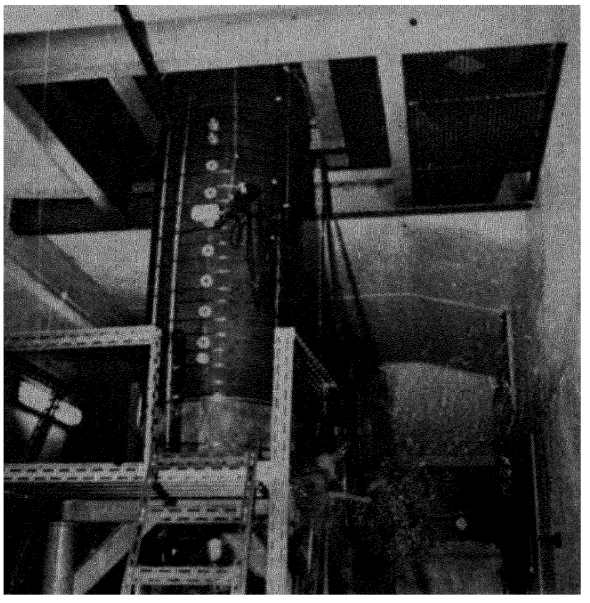

Slide 2

fixed by a spacer: We think that this detecting arrangement has several advantages. Firstly, the counting rate is high; secondly, a small asymmetry of the detector assembly relative to the axis is unimportant; thirdly, the influence of harmonics is greatly reduced; and fourthly, integration over several cells means that the method is rather insensitive to small differences between cells and the straightness of the rods.

As mentioned before, to begin with we placed the detectors in the horizontal channels. Now we use an arrangement so that the counters are movable continuously in the vertical direction. Instead of measuring in fixed positions we are now planning to have the detector assembly moving with a constant speed of about 10–20 cm/hr. By using a time analyser we can integrate over constant time intervals.

Slide 3 (Fig. 2 of P/790) shows how the exponential decay constant γ is determined from the experimental values. After corrections for dead time, spontaneous fission background and the end effect, we plot the ratio q of intensity in one position of the detector to the intensity in the next position above against the inverse of the neutron density. If we had a real exponential, the result would be a horizontal line, but we get the points on a nearly straight line with a certain slope depending on the background of scattered neutrons. We estimate the decay constant by extrapolation to infinite intensity. To compare different lattices, we take ratios of the different q's and extrapolate in the same way, but in this case the accuracy is better.

We assume that the radial part of the buckling is determined by the geometry. The change of the extrapolation caused by the aluminum wall and the boron-filled plastic is to be determined in a separate experiment using a pulsed method. By this method the change of buckling is translated into a change of the time decay of thermal neutrons in a small geometry. Mr. Sjöstrand will give more information, if you wish, about this.

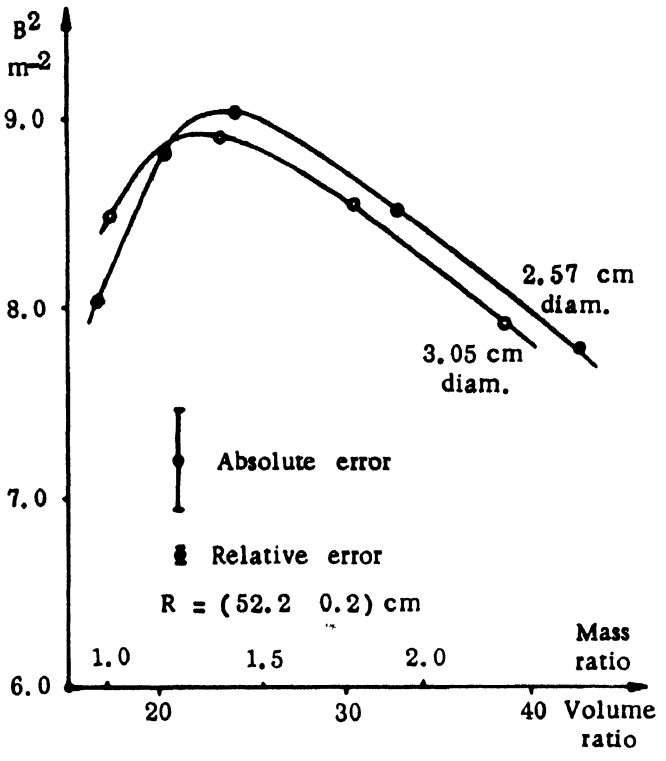

Slide 4

Assuming the transport mean free path to be 2.5 cm in D_2O, we estimate an extrapolation length of (2.2 ± 0.2) cm, which means an extrapolated radius of (52.2 ± 0.2) cm.

In Slide 4 some preliminary results on the material buckling are given. These results differ somewhat from those given in the text because the two curves were not compared the first time—we were in a hurry to get on with the work. A comparison with values reported from Canada and the United States shows that our values are rather high. This discrepancy may be caused by some systematic error because the results of the Canadian experiments using a critical assembly also differ from those obtained by North American Aviation.

I hope that Mr. Cohen will excuse me if I use some of his results.

If you compare the flux of the thermal and fast neutrons, you will have different radial buckling because the extrapolation length is different for the two groups and this difference will be more important for a smaller diameter of a tank.

I think the quantity we want to find is the μ in the basic function, not the buckling of the whole solution. If we write the expression of the buckling for the thermal neutrons and assume that the correct buckling has a somewhat larger extrapolated radius, you will see that the experimental value of the buckling is a straight line, if the buckling is plotted as a function of $1/R^2$.

I have made a comparison with the values from North American Aviation. They have used two different tank diameters, 5 feet and 4 feet, and we have used 1 metre. It seems that the values from Chalk River are the most accurate.

Mr. E. HELLSTRAND (Sweden) presented paper P/791.

Mr. J. HOROWITZ (France) presented paper P/361.

Mr. E. R. COHEN (USA) presented paper P/605.

Mr. VLADIMIRSKI (USSR) presented paper P/623 as follows:* My communication is a continuation of the report on the heavy-water reactor. The construction of the reactor was described at Session 9A. The reactor was designed to permit of changing the positions of the neutron rods rather rapidly; this made it possible to investigate the critical volume with different lattices.

The critical volume was measured with different arrangements of the natural uranium rods in the reactor.

All critical experiments were carried out with the heavy-water temperature at 20–23°. We determined the heavy-water level in the reactor at which the assembly becomes critical with the control rods fully retracted. In addition, the neutron density distribution radially and in height was determined for the different arrangements of the rods. The neutron density measurements were made at a reactor power of about 100 watts. The density measurements were made with dysprosium and gold detectors as well as by measuring the reactivity.

The experimental density distribution in height was fitted to a sine curve by the method of least squares while the radial distribution was approximated by the sum of Bessel and Neuman functions. The experimental value of the buckling was determined from the data. The results of measurements of the critical volume were processed so as to obtain an independent experimental value of the buckling. The calculation procedure has been described in the papers by Galanin presented at this Conference.

The buckling values determined from the density distribution measurements and computed from the critical volume were compared with theoretical values calculated on the basis of the nuclear constants of the reactor materials. The following values which are based on 1950 data were used for these constants.

$$\eta = 1.33; \qquad \epsilon = 1 + 0.017\rho$$

$$-\ln\varphi = \frac{5.6\rho^{3/2}(1 + 0.2\rho^{1/2})}{a^2 - 0.94S_U - 0.96S_{Al}}$$

$$\tau = \frac{139}{1 - 0.54\dfrac{S_U}{a^2} - 1.6\dfrac{S_{Al}}{a^2}}$$

For uranium, $\sigma_a = 7.1$, $\sigma_s = 9.0$; for D_2O, $\sigma_a = 10^{-3}$; for aluminum, $\sigma_a = 0.28$.

The numerical values of the coefficients in the formula for neutron resonance absorption, where not given in the written paper, are taken from the report by Burgov, presented at the July session of the Academy of Sciences of the USSR in Moscow.

* Complete paper P/623 appears in Session 9A, Vol. 2, these Proceedings.

Table I

Diameter of uranium rods, cm	2.8	2.8	2.8	2 2	2.2	2.2
Thickness of aluminum cladding, cm	0.1	0.1	0.1	0.1	0.1	0.1
Mesh of square lattice, cm	11.5	13.8	16.26	9	12.7	6.3
Number of rods	120	120	86	272	107	292
Critical level of reactor, cm	131	120	148	118.5	174.5	181.6
Length of uranium rods, cm	160	160	160	162.5	162.5	162.5
Critical volume of heavy water, including water-jacket around reactor bottom and sides, m^3	3.09	2.78	3.52	2.764	4.175	4 104
Volume of core, m^3	2 02	2.64	3.28	2.52	2.86	Part of volume taken up by lattice 7 cm

The results of the critical measurements are listed in Table I on this page. The uranium rods used in the test were 2.8 and 2.2 cm in diameter. Critical experiments with six different lattice spacings were carried out with each size of rod. The end results of these six critical tests are summarized in Table II on this page. Comparison of the value of the buckling obtained by the different methods shows satisfactory agreement of the experimental data with the computed values over a rather wide range of lattice parameters. The value of the buckling is in fairly close agreement with the data reported by Mr. Cohen. A comparison of the computed and experimental values of the critical size showed that the error in the computation values of the multiplication factor does not exceed 1 per cent and, what is more important, enhanced the reliability of all our theoretical deductions.

The errors inherent in the experimental measurements and theoretical calculations were so great that we were unable to improve appreciably on the accuracy of the reactor material constants as measured earlier.

We could only establish that increasing the value of the resonance absorption by ten per cent with a simultaneous increase in the number of secondary neutrons would lead to better agreement of the results. This can be seen in this table from the relatively high theoretical values of the buckling for the most closely packed lattices.

The complex of physical constants characterizing a reactor cannot be determined uniquely from the experimentally derived values of the critical size and the buckling corresponding to different lattice arrangements. Through appropriate selection of the 1950 physical constants, we succeeded in obtaining satisfactory agreement of the experimental and theoretical results. However, in view of later measurements of the number of fission neutrons and neutron cross sections, as well as independent measurements of resonance capture in uranium, made by Égiazarov, it became apparent that certain of the physical constants were in reality different from the values accepted in 1950. In connection with this, early in 1955, A. P. Rudik carried out a new analysis for a lattice. The calculation procedure was identical with that described in the paper by A. D. Galanin.

Table III shows the values of the physical constants assumed in 1950 and 1955. The cross sections are for the thermal region and are normalized to the standard value of 750 barns for boron. The 1955 cross section values are in agreement with the latest published data.

In accordance with the latter data the values of the thermal and fast neutron multiplication factors have been changed to some extent. It was also necessary to change the value of τ, the square of the slowing-down length in heavy water. This was necessary because in 1955 τ was computed on the basis of cross sections below the junction point of the Maxwell and Fermi neutron spectra, whereas, in 1950, τ was computed for thermal neutrons. Otherwise the same characteristics of heavy water and of the graphite reflectors were assumed in the 1955 and 1950 calculations.

Some change was also made in the manner of taking into account the capture and multiplication of neutrons in the process of slowing down. Thus, in 1950, it was assumed that ν_{eff} is independent of the energy and

Table II

Mesh of square lattice, cm	11.5	13.8	16.26	9	12.7	6.3
Laplacian measured by density distribution, m^{-2}	6 1 ±0 5	—	6.8 ±0.3	8.0 ±0.5	—	—
Laplacian calculated from the critical size by the effective boundary conditions method, m^{-2}	7.9	7.6	6.5	7.9	7.0	3.3
Laplacian calculated from the critical size by numerical solution of the cylinder problem, m^{-2}	—	—	—	8.0 ±0.1	7.4 ±0.15	
Laplacian calculated from the values of the constants, m^{-2}	8.3 ±0.5	7.6 ±0.4	6.7 ±0.4	8.4 ±0.6	7.4 ±0.4	4.0 ±0.9
Multiplication factor calculated from the constants	1.214	1.244	1.258	1.195	1.241	1.071

Table III

	σ_s	σ_a	l_{cu}	σ_{Al}	ν	η	$(\epsilon - 1) \times 10^2$	τ
1950	2.53	640	3	0.28	2.065	1.33	1.7ρ	140
1955	2.8	690	2.74	0.238	2.11	1.34	2.35ρ	120

$k = 1.183$ $\quad -\ln\varphi = \dfrac{5.6}{S_{D_2O}}[\rho^{3/2} + 0.55\rho^2]$

$\varphi = 0.875$ $\quad -\ln\varphi = \dfrac{7.3}{S_{D_2O}}[\rho^{3/2} + 0.2\rho^2]$

$-\ln\varphi = 0.133$ $\quad -\ln\varphi = \dfrac{5.6}{S_{D_2O}}[\rho^{3/2} + 0.2\rho^2]$

$-\ln\varphi = 0.102$ $\quad \varphi = 0.903$

that the capture cross section σ_a follows the $1/v$ law. The 1955 analysis was based on the latest experimental data of Nikitin *et al.* on the energy dependence of σ_a and ν_{eff}.

The multiplication factor corresponding to the experimentally determined critical volume was found to be $k = 1.183$. Using selected values of the physical constants, i.e., $\eta = 1.34$ and $\epsilon = 1.026$ and the experimental cross-section data for determining τ, we found that the resonance absorption $\psi = 0.133$.

This is somewhat higher than the value for the resonance absorption given by the formula derived from the experimental data of N. A. Burgov.

Analysis of the critical experiments, using the selected values of the physical constants and assuming that the resonance absorption is comprised of a blocked and an unblocked component, leads to the following equations for ψ:

$$-\ln\varphi = \psi = \frac{5.6}{S_{D_2O}}(\rho^{3/2} + 0.55\rho^2)$$

or

$$-\ln\varphi = \psi = \frac{7.3}{S_{D_2O}}(\rho^{3/2} + 0.2\rho^2)$$

It is impossible to choose between these two equations on the basis of the analysis of only one lattice.

DISCUSSION OF P/790, P/791, P/361, P/605 AND P/623

Mr. V. Raievski (France): I would like to make a few remarks on the difficulties encountered in investigating a reactor by the pulse method. In general it is noted that the higher harmonics fall off rapidly and become negligible and only the fundamental mode need be observed. This is a valid conclusion but is not a sufficient condition.

When the cadmium is introduced, the neutron density has a distribution which in harmonics may be described by

$$\vec{n(r)} = \Sigma a_k \vec{\varphi_k(r)}$$

where $\vec{\varphi_k(r)}$ are the proper functions for a non-perturbed reactor of the same volume.

In the first instance following the withdrawal of the cadmium these harmonics decrease with their natural period T_k towards a low but not zero value, depending on the sources of slowed-down neutrons. These sources may be regarded as constant if the period of observation is shorter than the period of the slowed-down neutrons. These sources have the same distribution as the initial density and comprise a number of higher harmonics.

The fundamental harmonic increases according to the law indicated by Mr. Hellstrand:

$$c(t) = 1 + \frac{\rho_0}{\beta - \rho_0}\left(1 - e^{\frac{\beta - \rho_0}{\ell} t}\right)$$

and approaches the asymptotic value

$$\frac{C_{asy}}{C_0} = \frac{\beta}{\beta - \rho_0}$$

(The observation time is assumed to be much shorter than the periods of the slowed-down neutrons.)

It follows that the density does not vary in accordance with the simple law but rather according to a more complex law which may be written as

$$\frac{n(t)}{n_0} = A\vec{C(r)} + \vec{B(r,t)}$$

where

$$\vec{A(r)} = \frac{a_0\vec{\varphi_0(r)}}{\Sigma a_k \vec{\varphi_k(r)}}$$

is the relative importance of the fundamental harmonic in the initial distribution and depends on the position of observation.

$\vec{B(r,t)}$ is a function of the time and the position which tends rapidly (in a time much shorter than the period P_0 of the fundamental harmonic) towards a value $\vec{B_0(r)}$, dependent on the position.

Slide 5 shows the variation of the fundamental mode and of the first harmonic; the latter may be added or subtracted from the fundamental mode, according to the position of the counter.

I have purposely exaggerated, in my paper, the contribution of the harmonic in order to show that the

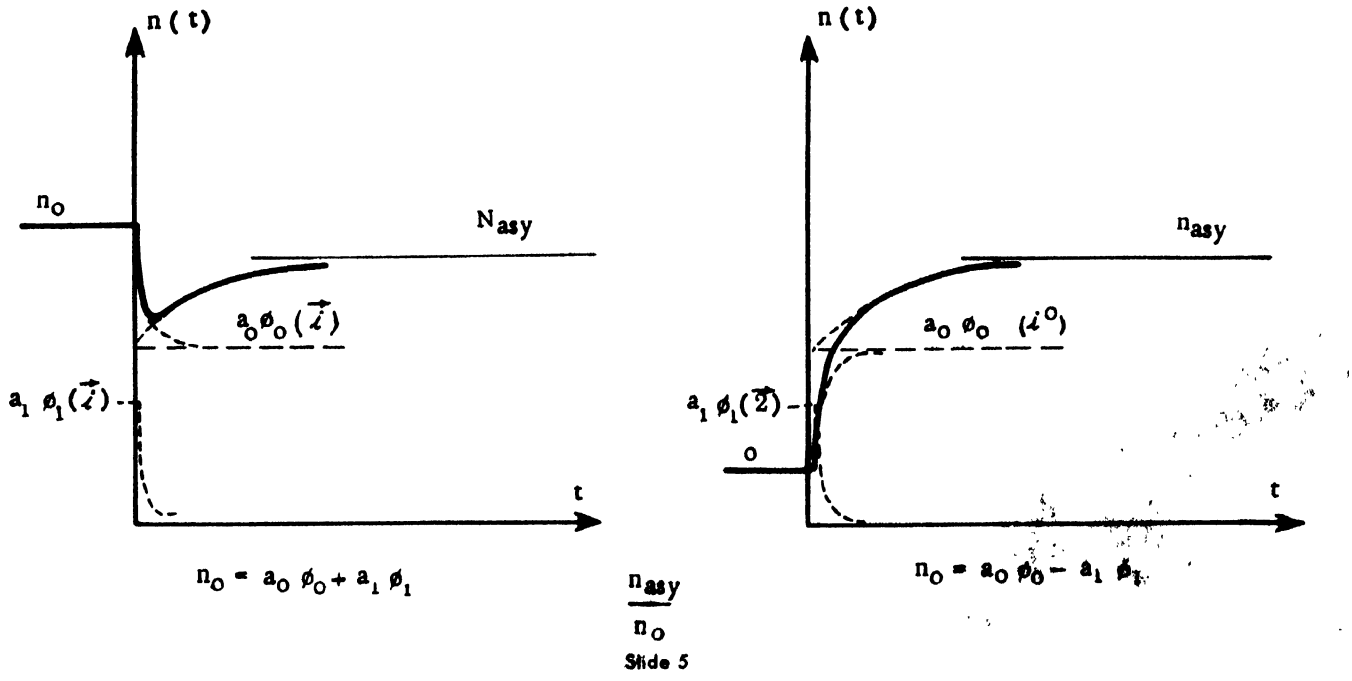

Slide 5

ratio n_{asy}/n_0, which permits determining the reactivity ρ_0, depends on the position of the counter.

Such is not the case in Mr. Hellstrand's report since he normalized the curves to obtain a ratio λ for the density equal to that of the fundamental harmonic which, assuming $B = 0$, permits eliminating the coefficient A. This normalization requires a prior measurement of the reactivity ρ_0 of the cadmium obtained through observation of the period of divergence of the reactor. Analysis of the normalized curve so obtained gives the value l of the mean life of the neutrons, but this value depends on the measurement of ρ_0, that is, on the periods and abundances of slowed down neutrons.

This difficulty does not exist in the case of modulation; here the ratio of the higher harmonics to the fundamental increases with the frequency. By continuous variation of the frequency one can determine the frequency at which the harmonic modes become troublesome; in this way one can obtain, the desired data without divergence and independent of the periods and relative abundances of the slowed down neutrons. The ratio n_{asy}/n_0 depends on the position.

Mr. SPINRAD (USA): I would like to ask Mr. Vladimirski to comment further on the origins of his data for the age of neutrons in heavy water, since the older numbers mentioned are in quite large disagreement with the numbers we have used for some time.

Mr. VLADIMIRSKI (USSR): An appropriate correction for the increase in the slowing-down time in the range of low energies, connected with the chemical bond of neutrons, was introduced into the neutron cross-section values. Subsequently our conclusion regarding the increase in the slowing-down time (or Fermi time) was not validated. Moreover, in our new figures we use the Fermi time for the slowing down to the boundary of the neutron spectra, whereas formerly we used the Fermi time for the center of the Maxwellian spectrum.

Mr. COHEN (USA): I would like to check with Mr. Persson whether the uranium rod lattices that were presented included aluminum cladding or whether they were bar uranium. If the 1-mm cladding that we had on our uranium rods were removed, this would have increased the maximum buckling from 8.6 to 9 reciprocal square meters, which would bring it into agreement with your data.

Mr. PERSSON (Sweden): The aluminium cladding was included in the results. We have even thicker aluminium cladding than you have. I think the discrepancy is larger than shown in the figure.

Mr. MUMMERY (UK) presented paper P/429 as follows:

The calculation of criticality data for thermal neutron reactors is essentially an approximate procedure because the basic nuclear data cannot be measured sufficiently accurately. Furthermore, the methods of calculation which are often used are in themselves approximate so as to enable large numbers of calculations to be carried out quickly. It is therefore necessary to carry out integral experiments, including determinations of the critical sizes of some proposed reactors and correlate results with calculations.

I think that one of the particular cases when this correlation is important is when we are thinking of using fuels other than natural uranium and when perhaps the emphasis on reactor design is to produce the best design for a particular purpose rather than just to get a reactor which can be made critical.

In 1951 we had completed a number of exponential experiments and found that the results were not consistent with the methods of calculation we had been using. This paper which I am reading to you today outlines the basic method we produced at that time in order to correlate a variety of experiments with a simple type of calculation.

Throughout this analysis I am using the standard two-group theory with the critical equation

$$\eta\epsilon pf = (1 + K^2L^2)(1 + K^2L_s^2)$$

The material buckling or the Laplacian of a particular lattice will determine the critical size of a reactor using that lattice, and for a given element in fuel and design, I was interested to determine the dependence on the various data used, of the moderator to uranium volume ratio for maximum K^2.

If we say that this moderator to uranium volume ratio which leads to a maximum value of K^2 is V^0, then we can determine how this value V^0 depends upon the accuracy of the parameter x. The values for typical graphite and heavy-water natural-uranium systems are tabulated in the paper.

For example, the effect of the slowing-down area of the moderator in determining this parameter V^0 is much more marked for heavy water than for graphite. This of course is a natural consequence of the greater leakage associated with natural uranium heavy-water systems. However, when we look at some of the parameters we find that there is not that difference.

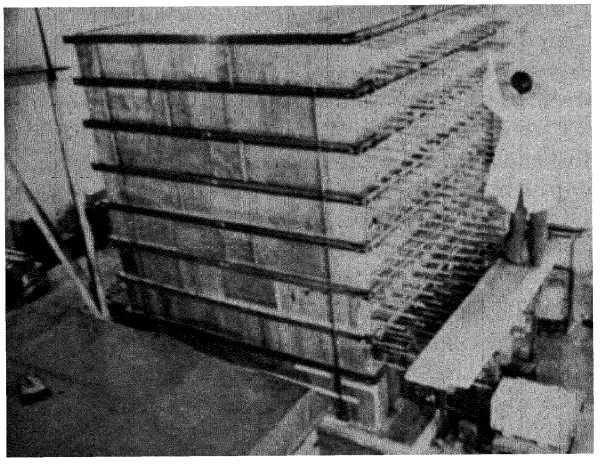

Slide 6

Beta (β) for instance, is a parameter which is related to the absorption cross section of the uranium and the ratio of the thermal flux in the moderator to thermal flux in the uranium. There is not much change either in parameter A which is basically determined by the effective resonance integral of the uranium used relative to the slowing-down properties of the moderator. However, the other parameters are quite different. For instance, gamma (γ), which is dependent on the transport mean free path in the media, is different in the two cases.

This again arises because γ is the parameter which determines the thermal neutron leakage. Alpha (α) varies very considerably also because α is proportional to the absorption cross section of the moderator which is much greater in the graphite systems than in the heavy systems we have considered here.

I think that the table points out three things. First of all, that some parameters have a different importance for different systems and therefore by measurements on the different systems we can examine that importance. Secondly, that the two most important parameters, however, do not vary appreciably from one system to another. These two parameters are $\eta\epsilon$ the product of which is slightly larger in the heavy-water system because K is larger. The other one is A which is proportional to the effective uranium resonance integral.

Therefore, I conclude that these factors, $\eta\epsilon$ and A are the most important ones that we should attempt to deduce. The method of correlation of experiment with calculation is outlined in the following way:

First of all, we want to measure K^2. Secondly we want to measure the thermal utilization, which is dependent upon cross sections and upon the fine-structure flux distribution. We want to calculate or to measure the slowing down area in the lattice. In the case of lattices containing primarily moderator, we assume this can be calculated from a measurement in the moderator alone. In other lattices we have to make special measurements, as, for instance, have been outlined this morning with the water systems. We also want to calculate L^2 which, by conventional techniques, can be obtained from the diffusion area in the moderator plus a knowledge of fine structure flux distributions. From what Mr. Cohen has said this morning, we have seen that this is in fact practicable.

We see from the factors here that we are now left with $\eta\epsilon$ and p as unknowns. However, I want to introduce two small further computed corrections. First of all, there will be a small effect upon ϵ due to the presence of neighbouring rods. This is the type of feature which is so important in a light-water-moderated reactor. Nevertheless, there is a very small effect present in a number of other reactors. Therefore, I would write, $\epsilon = \epsilon_0(1 + \delta\epsilon)$ where $\delta\epsilon$ is a correction factor which is calculated.

η itself may have a dependence on neutron spectrum and some data on this were presented in earlier papers to this Conference. Therefore, I have written eta (η) which in this notation is for the fissile material as $\eta = \eta_0(1 + \delta\eta)$ where η_0 is the value in a pure thermal Maxwellian spectrum and $\delta\eta$ represents a spectrum correction.

I would now like to say a little about the experimental determinations.

The majority of the determinations of buckling have been carried out in exponential experiments. Slide 6 shows one of the very early exponential experiments and just gives an idea of the scale of the experiment with which we have been working.

This earlier discussion has shown us that we wish to carry out experiments in which the moderator to uranium ratio is varied for a given design of fuel element and coolant, and we therefore obtained a set of graphite bricks which could be arranged into a variety of lattice arrangements for this type of work.

Slide 7 shows one arrangement of the bricks. This unit here is the fundamental building block, and four of these close together will form a cylindrical fuel element channel. This cylindrical fuel element channel can be filled in with further tubes of graphite—one tube of graphite there, and several tubes of graphite as

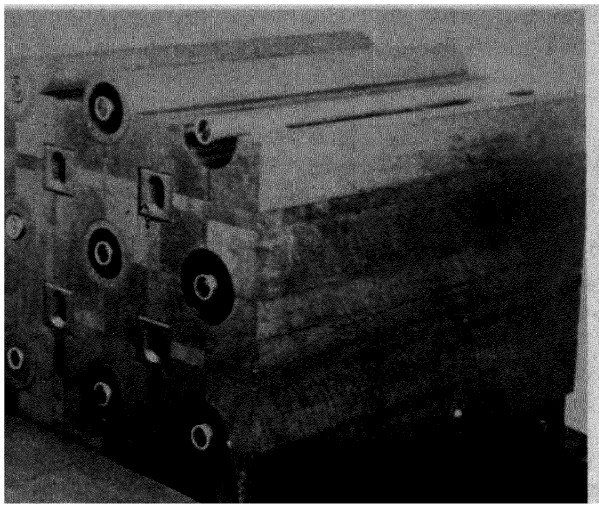

Slide 7

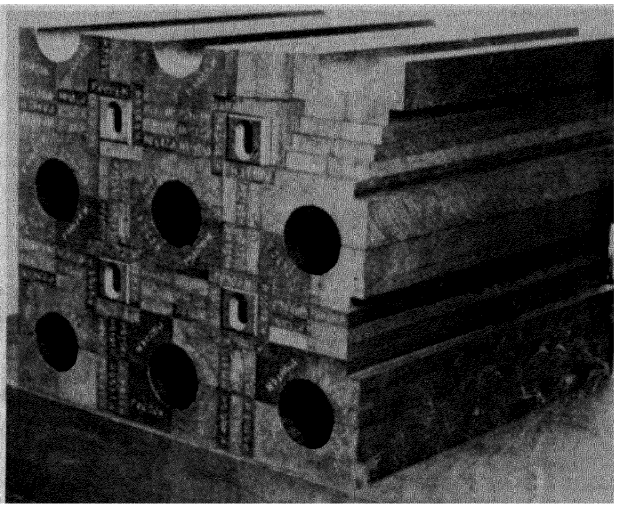

Slide 8

in this case. Furthermore, in order to increase the lattice spacing, we have small slabs of graphite which fit between these main blocks and so expand the lattice pitch. The other units here are the moveable graphite blocks in which we make our foil measurements.

Slide 8 shows the structure built up into one of the larger lattice pictures, and one can see that it is a rather complicated structure.

The measurements which I wish to report in this paper consist of a set of natural uranium fuel elements —one set, 3.05 cm in diameter; one set, 2.54 cm in diameter, and the third set which were tubes, 4.16 cm outside diameter and 3.30 cm inside diameter. The interesting thing about the tube is that it contained approximately the same mass of uranium per unit length as did one of the solid cylindrical rods.

In addition, I am reporting an experiment with a larger diameter rod and also a critical experiment with BEPO, which had a smaller diameter rod.

One of the things which we have done in all our experiments has been to look for these migration area anisotropies which have been discussed in earlier papers; and in the graphite experiments, where we have only a very small air channel around the uranium, we cannot find any anisotropy. We have made a measurement which consists of doing two exponential experiments under different geometrical conditions and obtained a result of unity for the ratio of the two migration areas to an accuracy of two per cent. However, in the case of the pile BEPO, which has a channel diameter of just over 5 cm, we observed a value for this anisotropy factor of 1.08 plus or minus four per cent.

As I have indicated earlier, we wish to carry out fine-structure flux distribution measurements in order to analyse our experimental buckling results. In the type of exponential experiment which I have described, we do not have sufficient neutron flux available to make these measurements, so we make them in small assemblies located in the GLEEP thermal column. Slide 9 gives a picture of the situation. This hole in the GLEEP pile is where the thermal column has been unstacked. We have a railway system here, supported on concrete blocks, which carried one of these assemblies containing approximately 36 lattice positions. There is a removable portion in the middle in which the fine-structure determinations are carried out.

Slide 10 shows a closer view of the assembly which has been used. In general, we have used manganese wires for making these determinations, but we have checked our results by comparison with uranium-foil detectors.

I should like also to follow up Mr. Cohen's comment on the fine structure as a function of position in the lattice. We have also carried out a similar type of measurement and, to within an accuracy of about two per cent, we believe that the neutron flux distribution

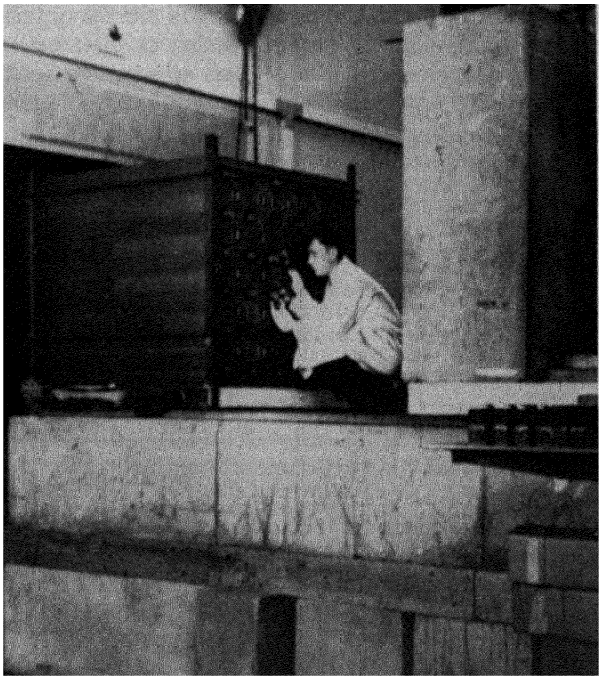

Slide 9

is truly the product of macroscopic flux and microscopic flux for an infinite system.

I wish now to talk about the correlation of our fine-structure distribution measurements with calculations. In this connection it is easier if we can use empirical formulae.

$$\left(\frac{\bar{\phi}_m}{\bar{\phi}_u}\right)_{th} = GRS$$

where G = max/avg in uranium; R = min in moderator/max in uranium; and S = avg/min in moderator.

$$G = \left[\frac{K_u^2 g^2 - K_u^2 a^2}{2K_u a}\right] \left[\frac{I_1(K_u g)K_0(K_u a) + K_1(K_u g)I_0(K_u a)}{I_1(K_u g)K_1(K_u a) - K_1(K_u g)I_1(K_u a)}\right]$$

$$R = 1 + \frac{l_u K_u^2 a}{3G}\left(1 - \frac{g^2}{a^2}\right)\left(1 - \frac{a}{c}\right)$$

$$S = 1 + \frac{l_u K_u^2 (a^2 - g^2)}{2l_0 G(y^2 - 1)}\left[\left(\frac{y^4}{y^2 - 1} + \frac{K_0^2 c^2 (y^6 + 2y^4 - y^2)}{8(y^2 - 1)}\right) \ln y - \frac{3}{4} y^2 + \frac{1}{4} - \frac{K_0^2 c^2 (8y^4 - y^2 - 1)}{48}\right]$$

where $y = b/c$.

We see from these equations that the rates of the moderator flux to the uranium flux has been split into three factors: G, which is characteristic of uranium; R, which is characteristic of any air channel which is present, and S, which is characteristic of the moderator. These expressions are, I am sure, quite well-known to everybody. g and a refer to the inside and outside diameters of the fuel element. R gives the rise in flux going across the air channel and is a simple diffusion theory expression. S is an expansion of the usual expression to show the effect of absorption in the moderator. That is, only in two terms, do we have a factor depending on absorption in the moderator. In fact, for the lattice as we have studied it, this correction can almost be neglected.

Let us tabulate the results of fitting experimental results to these expressions.

	Experimental	*Calculated*
K_u	0.89 cm^{-1}	0.85 cm^{-1}
$l_u^2 K_u^2 / l_0$	0.36 cm^{-2}	0.37 cm^{-2}

Natural uranium density is taken as 18.9 gm/cm³; graphite density as 1.60 gm/cm³, and the calculations assume $lK^2 = 3\Sigma_a$ and $K^2 = 3\Sigma_a(\Sigma_a + \Sigma_s)$.

We see that the experimental value to fit these results is K_u = 0.89 cm. The experimental value of the second quantity is 0.36. The calculations, in fact, are basically P_1 approximation. However, this agreement is rather fortuitous because other measurements confirm that, in this simple treatment, both K_u and the second quantity do vary with other details of the lattice structure. In doing this type of work with the fine-structure distributions, we have been very much aware that we are trying to fit very simple formulae, and so we have carried out a number of spherical harmonic calculations. Some of these will be reported by Mr. Tait at a meeting tomorrow.

One other feature which we have examined has been the departure from cylindrical asymmetry of the lattice cells that are used in practice, and a report has been produced on that.

Having obtained the fine-structure distributions, if we make use of the best cross-section data available, we now have calculated thermal utilization.

We are now left with calculating slowing-down areas and diffusion areas. To calculate the slowing-down area, we have adopted the following relation for the slowing-down area in a graphite reactor containing one rod emitting neutrons:

$$L_s^2 = 353 - 85P \text{ cm}^2$$

where P is the probability of collision of fission neutrons in the source rod:

$$L_m^2 = (1.10/\sigma_0) \text{ m}^2$$

σ_0 is measured at 2200 m/sec on the UK scale and the graphite density is 1.65 gm/cm.³

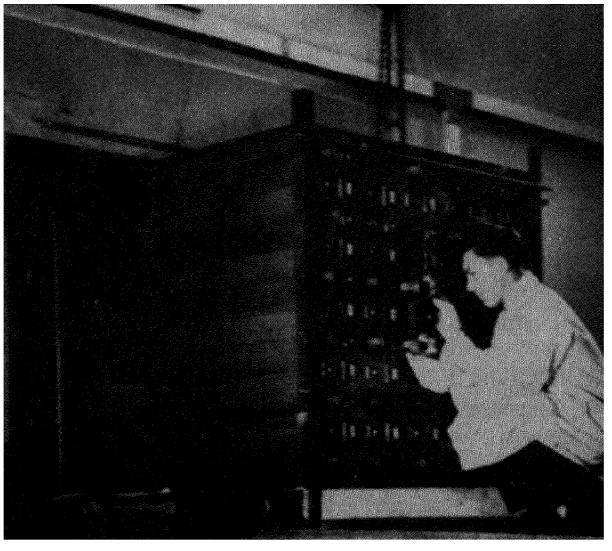

Slide 10

The factor P allows for the degradation of the energy spectrum of the neutrons emitted from the rod. In calculating the effect in a lattice, we apply two corrections. One is for the effect of any small air channels which may be present, and we apply a simple density correction here. Secondly, we have to apply a correction for the presence of the other uranium bars. It has been conventional to do this on the assumption that the slowing down of neutrons in the other uranium bars can be neglected, but that the effective mean free path is the same as that in graphite.

Diffusion areas in the moderator I shall not discuss in detail, but we have made a considerable number of measurements of diffusion areas in which the purity of the graphite has also been compared against stand-

ard samples by pile-oscillator techniques. This results in a relation of the kind shown above, where the quantity σ_g is the graphite cross section measured at 2200 metres per second, on our own scale, and the graphite density is 1.65 gm/cm³. If we all believe that we can make diffusion length measurements equally well, then this relation enables us to compare our cross-section scales.

We now have calculated L^2, L_s^2, f, and have observed K^2. If we now make these small corrections to η and ϵ to allow, in this case, for the departure of the spectrum for a Maxwellian and, also in this case, for the presence of other rods, we can write our expression in this form, where this quantity here is the one which we wish to determine.

$$\eta\epsilon pf = (1 + K^2L^2)(1 + K^2L_s^2)$$

$$\eta_0\epsilon_0 p = \frac{(1 + K^2L^2)(1 + K^2L_s^2)}{(1 + \delta\eta)f(1 + \delta\epsilon)}$$

$$p = \exp\left[\frac{-N_u V_u(\int\sigma_u\, dE/E)_{eff}}{N_m\sigma_m\xi_m V_m}\right]$$

$$\log(\eta_0\epsilon_0) = \ln\left[\frac{(1 + K^2L^2)(1 + K^2L_s^2)}{(1 + \delta\eta)f(1 + \delta\epsilon)}\right] + \frac{N_u V_u(\int\sigma_u\, dE/E)_{eff}}{N_m\sigma_m\xi_m V_m}$$

If now we assume some model for calculating the resonance escape probability, then we can in fact take $\log_e$ of both sides of these expressions and obtain the last one. This means that if we plot this quantity here against this quantity, in which we have said we know all the factors, we can obtain both the effective uranium resonance integral, and $\eta_0\epsilon_0$ which is characteristic of the fuel.

I should say perhaps that the formula for p is only one formula which can be used. We have used others in which the conventional allowance has been made for the fine structure of resonance neutrons, but this has made very little difference to our results.

The experimental results obtained from the larger diameter rod, the next diameter rod, and the tube, are plotted in Slide 11 (Fig. 1 of P/429). The intercept determines the value of $\eta_0\epsilon_0$ and the slope of the lines determines the effective uranium resonance integral.

Also shown in P/429 are the results of our experiments for the two rods and the tube, the values of the effective uranium resonance integral, values of $\eta_0\epsilon_0$ from which by making use of the standard ϵ_0 calculations, we get values of η_0 which are in very good agreement with each other.

Slide 12 (Fig. 2 of P/429) shows the plot of the effective uranium resonance integral as a function of surface-to-mass ratio of the fuel. The three experimental points appear here and the comparison is with Mr. Crocker's curve which you saw yesterday and the old Creutz formula. The best straight line gives a value of 5 barns plus 35 times the surface-to-mass ratio in cm²/gm for the effective resonance integral.

To show the discrepancies in the value of eta deduced from this type of analysis, we can compare 1.94 obtained by analysis for η of U^{235} in a Maxwell spectrum at room temperature with values deduced from other techniques: pile oscillator, 2.05; and basic nuclear data, 2.19. It is difficult, of course, to say how accurate any one of those figures will be, and I am very much aware that deduction of a quantity like this by integral experiments depends on the models one has assumed. However, I believe that this value is unlikely to be in error by more than a few per cent, perhaps five, and is therefore not very consistent with some of the other values which have been quoted. The 2.05, for instance, I believe has an error of perhaps two or three per cent, and the 2.19 certainly has an error of more than five per cent.

I conclude, therefore, by saying that one can correlate integral measurements of this kind with simple lattice calculations. However, the values of resonance integral deduced and the value of η deduced are at some variance with other experiments.

Mr. P. F. GAST (USA) presented paper P/607.

Mr. I. KAPLAN (USA) presented paper P/606.

DISCUSSION OF P/429, P/607, AND P/606

Mr. MARTELLY (France): In connection with measurements of the anisotropy of the Laplacian, I should like to describe the method which we have used in Saclay.

If the relation between the quantities

$$\frac{1}{\rho}\left(\frac{d^2\rho}{dx^2} + \frac{d^2\rho}{dy^2}\right) \quad \text{and} \quad \frac{1}{\rho}\left(\frac{d^2\rho}{dz^2}\right)$$

(the channels being oriented along the z-axis) is represented graphically, the general differential equation yields a straight line which is not parallel to the second bisectrix of the coordinate axes but the slope of which gives the anisotropy (Slide 13). The case of an exponential experiment is represented by the point E.

The case of the critical pile is represented by the point C, dividing the segment formed by the points of

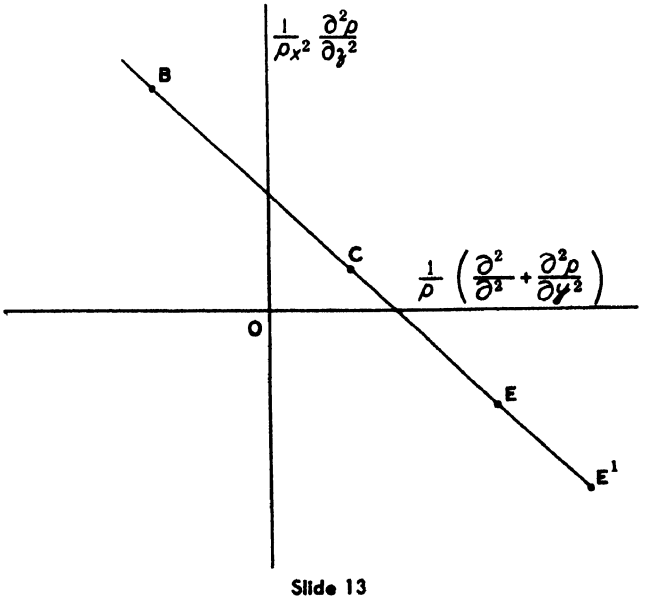

Slide 13

intersection with the axes into two parts in the ratio two-thirds/one-third.

The method of measuring the anisotropy, described by two earlier speakers, consists of varying the dimensions of the cylinder which gives the representative straight line by extrapolation of the segment determined by two rather close points: E and E'.

We used another method which consisted of determining a point B in another region by irradiating the experimental medium by a cylindrical source, for which the density of the emitted neutrons can be represented by the Bessel function I_0 in the radial direction and by sine functions along the z-axis.

Under these conditions there is an appreciable increase in the accuracy of determining the angular coefficient of the representative straight line; at the same time the Laplacian of the actual reactor can be reliably determined by interpolation.

The accuracy we have thus attained in determining the coefficient $1 - \alpha$ (α being the quantity, in the neighborhood of unity, giving the ratio of the two principal—longitudinal and transverse—Laplacians) is of the order of 0.6%. Thus, we found

$$(1 - \alpha) = 0.013 \pm 0.006$$

while calculation according to the theory of Behrens (which comprises a number of approximations) results in a value of 0.017.

Session 22A

ZERO ENERGY EXPERIMENTS ON FAST REACTORS AND REACTOR KINETICS

LIST OF PAPERS

			Page
P/404	Experimental studies on fast neutron reactors at A.E.R.E.	J. E. R. Holmes *et al.*	331
P/598	The fast exponential experiment	F. C. Beyer *et al.*	342
P/609	A survey of the theoretical and experimental aspects of fast reactor physics	D. Okrent *et al.*	347
P/775	Stability conditions in the non-linear dynamics of heterogeneous reactors	H. J. Lipkin and R. Thieberger	364
P/934	The influence of the temperature coefficient on the transfer function of a heavy water reactor	J. Pelser	367
P/334	The dynamic problems of power reactors and analogue computers	P. Braffort	369
P/610	Kinetics of stationary reactor systems	T. A. Welton	377
P/612	Experimental checks of control rod theory	P. F. Gast	389
P/434	Neutron flux instrumentation systems for reactor safety and control	R. J. Cox *et al.*	393

Experimental Studies on Fast Neutron Reactors at A.E.R.E.

By J. E. R. Holmes, D. D. McVicar, H. Rose, R. D. Smith, and L. R. Shepherd, UK

ZEPHYR

A small experimental fast reactor, Zephyr, consisting essentially of a plutonium core surrounded by a natural uranium envelope, has been in operation at Harwell since February, 1954. Zephyr has already been described in a published paper[1] so that it is sufficient merely to summarize the main points of its construction in this present paper.

The general arrangement of the reactor is shown schematically in Fig. 1; and a horizontal section through the reactor is shown in Fig. 2.

The core forms a right cylinder, approximately 15 centimetres in length and diameter, the plutonium being in the form of nickel canned rods which are mounted vertically in equilateral array in a suitable matrix. A solid uranium matrix and one of air spaced thin steel tubes have been employed in the core assemblies investigated so far. The envelope of the reactor consists of about 8 tonnes of 1-in. diameter natural uranium rod arranged in the form of a right cylinder symmetrically situated around the core. Sections of the envelope may be moved to uncover the core. Instruments and samples may be introduced into either the core or the envelope in any region by removing plutonium or uranium rods or displacing them to other available channels. It has been found that this has no detectable effect on the neutron distribution in the system.

Control of the system is achieved by movement of sections of the uranium envelope in the vicinity of the core. These moving sections consist of; (*a*) a shut-off-block, a large cylinder of uranium immediately below the core which may be ejected pneumatically to reduce reactivity by more than 2%, and, (*b*) the control rods (6 in number), which are 2.5 centimetre diameter uranium rods that move in channels parallel to the axis of the core, each governing about 0.01% in reactivity per centimetre of movement. The maximum rate of increase of reactivity which may be achieved by movement of the control rods is $2 \times 10^{-3}\%$ per second.

The power level and excess period trips operate to drop out the control rods and eject the shut-off-block, if certain levels are exceeded. As an ultimate safety device, each plutonium fuel element is provided with a fusible link at its centre. This link separates at a certain temperature with the result that the lower part of the element drops off leaving a gap at the centre and thereby causing a drop in reactivity.

Power level is measured by means of pulse operated fission chambers,[2,3] which monitor the neutron fluxes at fixed regions near to the core. The amplified pulses are fed, alternatively, into linear or logarithmic rate-meters and the time derivative of the logarithmic meter is displayed in a period or reactivity meter. The normal operating (fission) power of the reactor is 2 watts, corresponding to a flux of 8×10^8 neutrons/cm^2/sec at the centre of the core. This power is less than 10% of the heat developed by the natural radioactivity of the plutonium. No cooling is required at such low powers.

ZEUS

A second low-power fast reactor has been constructed at Harwell and should be in operation before the end of the year. This reactor, ZEUS, is actually a full scale, uncooled version of the reactor which is to be built at Dounreay. Zeus has been built for the purpose of studying the neutron characteristics, critical conditions and control calibrations of the projected power reactor.

The core of Zeus is an assembly of vertical tubes containing pellets of highly enriched uranium (40–50% U^{235}) mixed with natural uranium pellets, the mixture ratio being variable. The degree of enrichment chosen for the Dounreay reactor will be based upon the outcome of Zeus experiments with different degrees of enrichment. An envelope of natural uranium surrounds the core of Zeus and this is also in the form of vertically mounted rods.

Zeus is controlled by the movement of groups of fuel elements near the boundary of the core. Power level is monitored by fission chambers in the same manner as that adopted in Zephyr. Since the maximum operating power is only 100 watts, no coolant is required.

Apart from the main purpose of supplying data required for the Dounreay reactor, Zeus will provide us with a useful facility for studying fast systems in which the fuel is diluted with source material. The manner in which the neutron energy spectrum is modified by dilution and the resulting changes in the properties of fast systems is one of the main considerations of our Zero-energy programme. Zephyr has provided us with data on highly concentrated plutonium cores; Zeus will take us about half-way down the scale of U^{235}/U^{238} mixtures, while the envelopes of both Zeus and Zephyr provide data on a very dilute U^{235}/U^{238} mixture (viz. natural uranium).

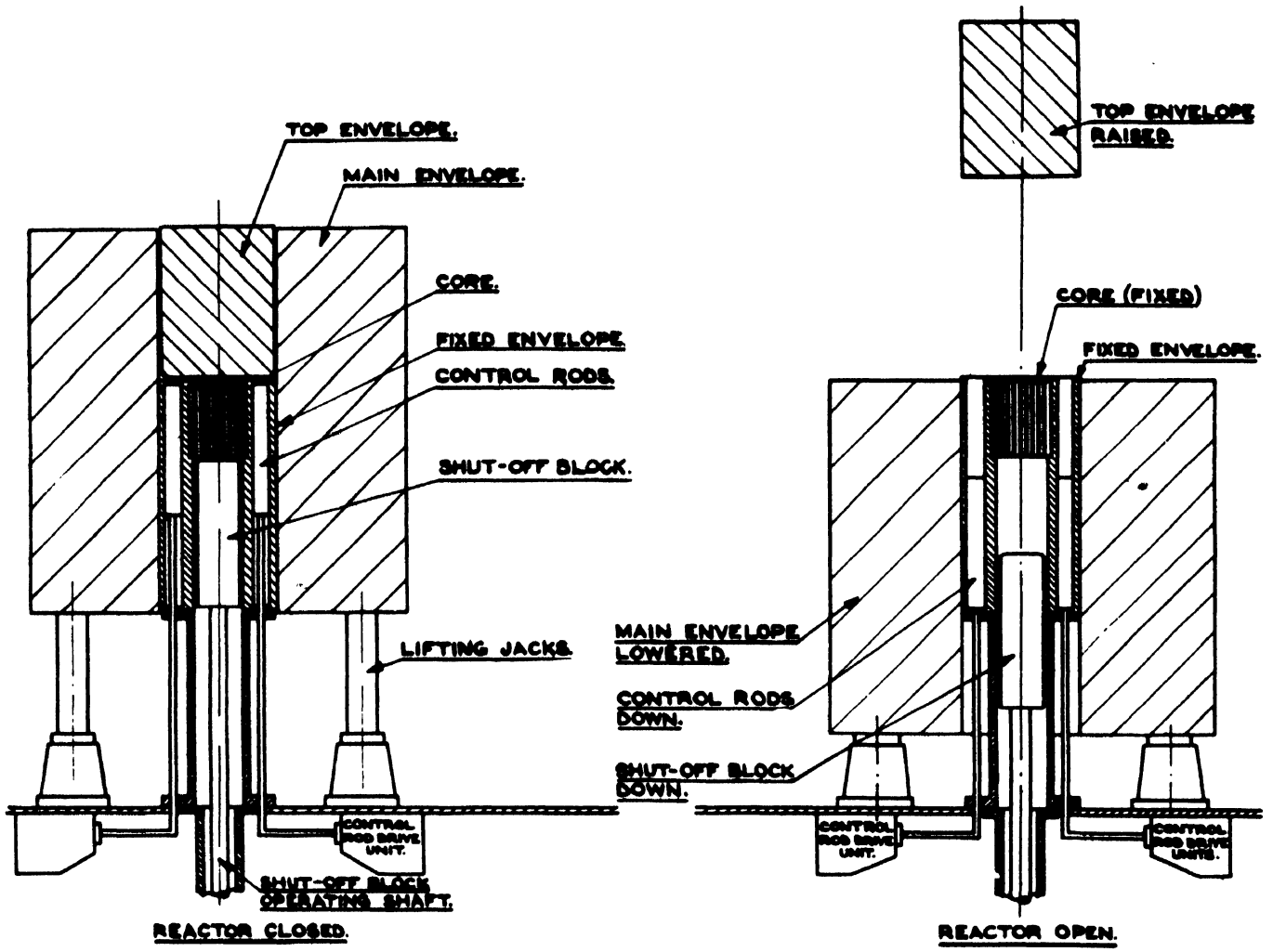

Figure 1. Schematic diagram of Zephyr showing operating and loading positions

THE PURPOSE OF ZEPHYR

Zephyr was built for the purpose of studying the neutron physics of a plutonium/uranium fast reactor. We wished to check theoretical procedures, to examine, for example, the limitations of a one group theory and to determine the feasibility of measuring the neutron transport properties of materials by methods analogous to the so-called danger coefficient measurements which may be carried out in thermal reactors. A knowledge of neutron energy spectra was required and the extent to which this affected the characteristics of the system. Above all we wished to check the neutron economy and to determine the breeding properties of a plutonium/uranium fast reactor. The experiments carried out on Zephyr, have been determined by considerations of these objectives.

A comprehensive study of fast reactors could be extended over several years and the results which we have obtained, so far, represent only the beginning of a fairly long programme. Most of the work reported here refers to the first core assembly, in which the plutonium rods were mounted in a uranium matrix so that the core dilution was 49% by volume of Pu^{239} to 33% by volume of U^{238} with 10% by volume of nickel in the loaded region. It is clear from these measurements, that we shall need to cover a fairly wide range of core constitutions before we can claim to have a comprehensive quantitative knowledge of the nuclear processes which take place. In the meantime much useful data has been obtained and a brief survey of this will be given here.

REACTIVITY CALIBRATION

Many of the experiments on Zephyr depend upon a knowledge of the reactivity changes resulting from given movements of the control rod. An immediate task on each new assembly, therefore, is to calibrate the control rods, in terms of reactivity changes and to intercalibrate the effects of the control rods and shut-off-block, so that we know how much the reactivity is reduced in a shut down as compared with, say, one centimetre of control rod movement. This intercomparison actually constitutes a part of the critical assembly procedure.[1]

The simplest forms of reactivity calibration is calibration in terms of the delayed neutron fraction. Thus if $\Delta\rho$ is the change in reactivity produced by a given control rod movement it is relatively easy to determine by observations on the reactor kinetics the ratio $\Delta\rho/\Sigma\beta_i$ (where $\Sigma\beta_i$ is the sum of the delayed neutron groups expressed as a fraction of the total neutrons emitted in fission). Since this has already been covered

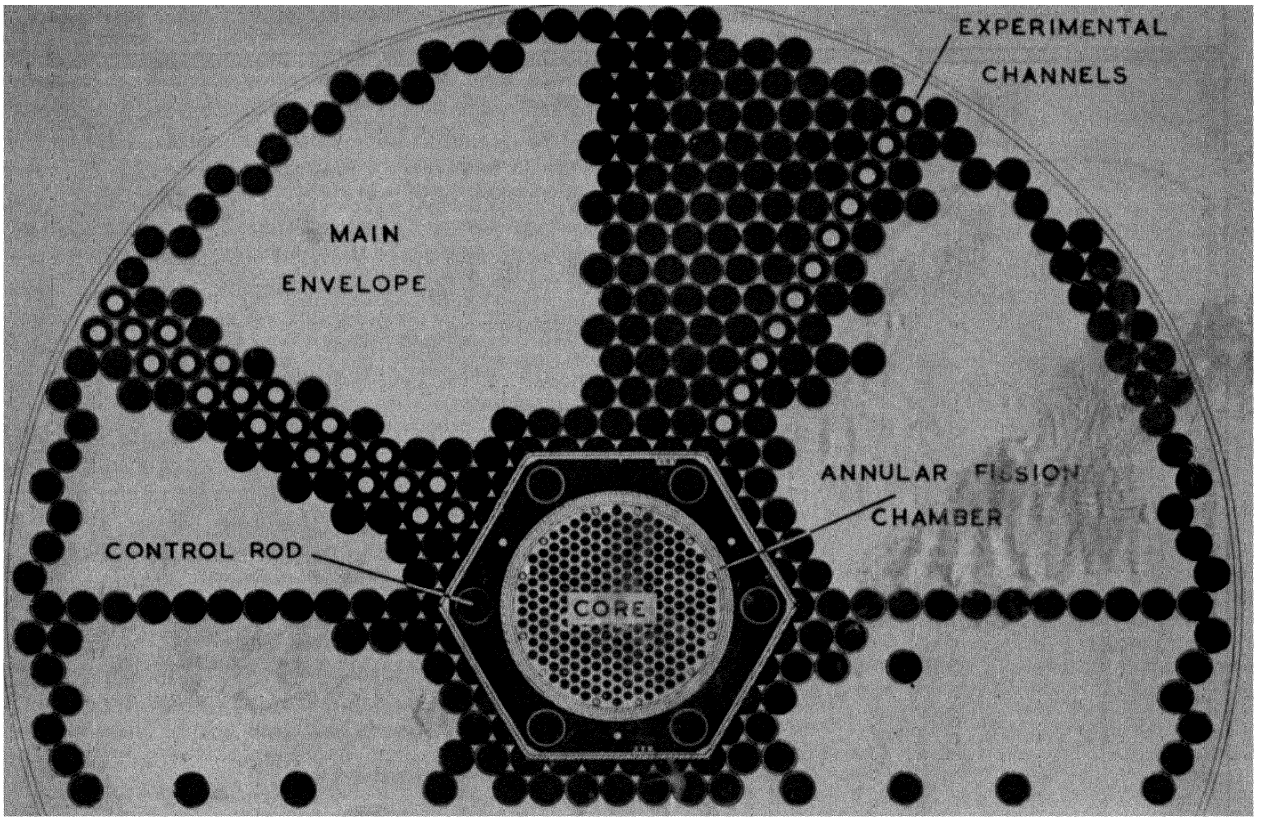

Figure 2. Horizontal section through core and envelope of the reactor

in a published paper[1] it is not necessary to repeat in detail here.

In principle it is a simple matter to convert the calibration in terms of the delayed neutron fraction into an absolute calibration, since the $\Sigma\beta_i$ is a quantity which may be measured in a straightforward experiment. The procedure is complicated, however, by the fact that, in Zephyr, fission occurs in three isotopes namely Pu^{239}, U^{238} and U^{235} and $\Sigma\beta_i$ has to be calculated for an average type of fission taking into account the difference in the spatial distribution of the three types of fission. Also, delayed neutrons differ from prompt neutrons in their energy and, consequently, in their effectiveness in sustaining the chain reaction. As a result of this last factor, the effective value of $\Sigma\beta_i$ in the reactor is very difficult to estimate and is expected to differ from the true value by several per cent.

An alternative method of calibration involves the observation of the change in control rod setting which must be made to compensate for the reactivity change obtained, when a small sample of fissile material, e.g., Pu^{239}, is introduced into the centre of the core. The basis for this method is described under "Perturbation Measurements" below. The actual reactivity change depends upon the quantity $(\nu - 1)\sigma_f - \sigma_c$ of the sample (where σ_f and σ_c are respectively the fission and non-fission capture cross sections of the isotope and ν is the number of neutrons per fission) and it may be calculated, if we know the neutron production rate and flux distribution throughout the reactor and also the ν, σ_f and σ_c of the sample.

NEUTRON DISTRIBUTION

It is desirable to make measurements on the total neutron flux with a detector having a response which is independent of the neutron energy. In practice, the nearest approach to such a detector is obtained by measuring the fission rate of Pu^{239}. The variation of the Pu^{239} fission cross section over the important energy range is small and adequate corrections can be made on the basis of relatively inaccurate neutron energy spectra.

In order to investigate the flux distribution and the breeding characteristics of the system measurements have been made on the variation of the fission rates of Pu^{239}, Pu^{240}, U^{235} and natural uranium throughout the reactor. The measurements of the fission rate of any particular material have been made relative to the rate at the centre of the core of the reactor where the values of the fission cross sections have been determined.

The general behaviour of the neutron spectrum as the neutrons diffuse outwards from the core through the envelope has been investigated by extending the fission rate measurements to other fissionable materials where the fission cross section varies with neutron energy. Materials with a fission threshold are of particular value in this respect and measurements have been made with Np^{237} (threshold 0.2 Mev), U^{238} (threshold 0.9 Mev) and Th^{232} (threshold 1.2 Mev).

The fission chambers used for these experiments are principally of two sizes: the smaller chambers have an

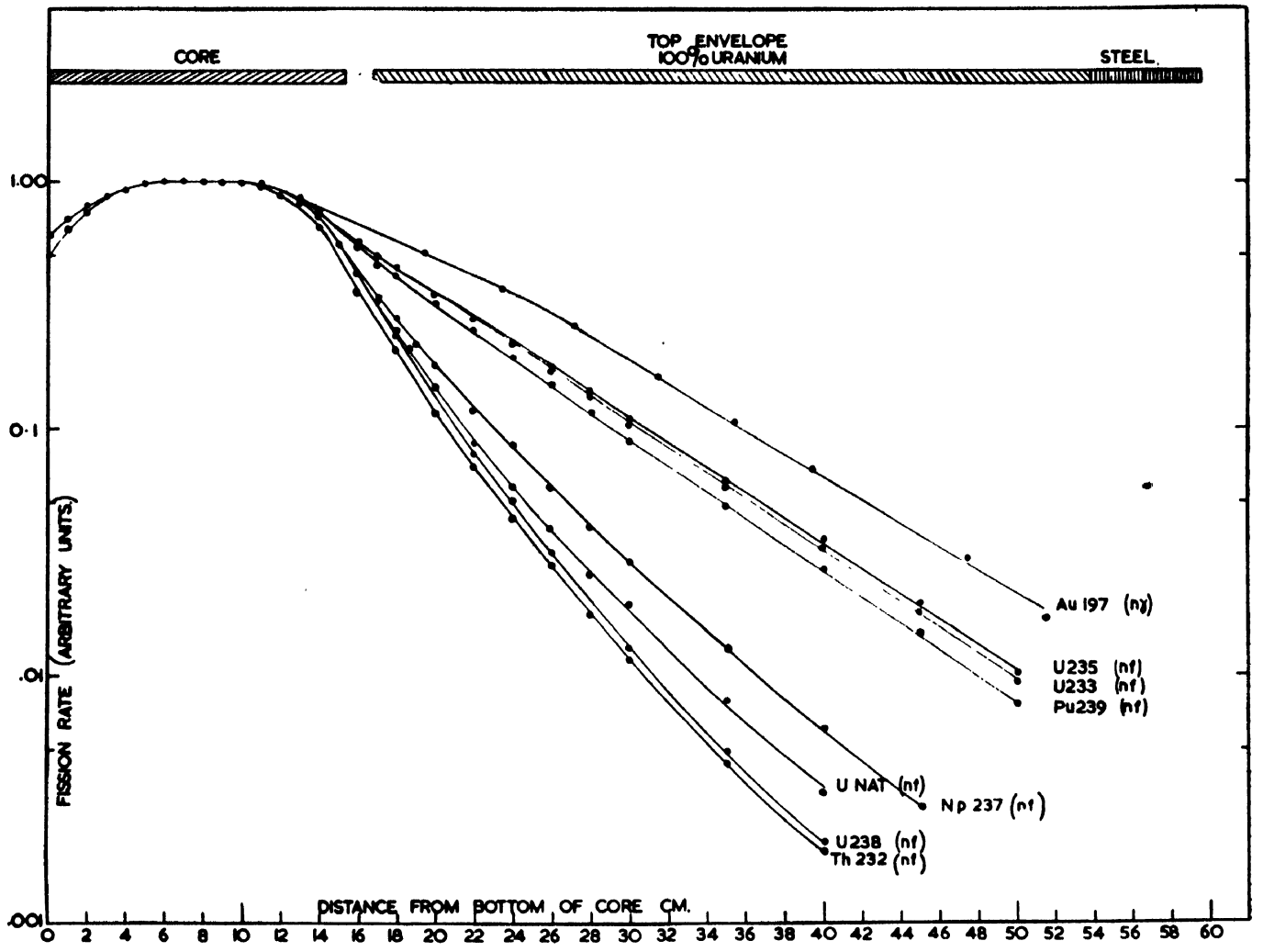

Figure 3. Variation of fission rates through core and top envelope relative to centre of core

external diameter of ¼-in. and an active length of 2 cm whilst the corresponding dimensions of the larger chambers are ½-in. and 5 cm. These chambers were specially constructed by R. Aves and are described elsewhere.[2,3] Measurements in the core were made with the ¼-in. diameter chambers which were inserted through a channel in the solid uranium hexagon above the core. Ten such channels are available and they line up with fuel element channels in the core matrix along a radius from the centre channel outwards. If the fuel element is removed from the core, fission chambers may be placed at any point from the bottom of the core matrix upwards, and it is possible to follow the fission rate in a chamber as it is moved vertically upwards from the bottom of the core through the centre and out through the solid portion of the uranium envelope. However, because this type of chamber contains only a very small amount of fissionable material (~½ mg) it is not practicable to make measurements in the outer regions of the envelope with these chambers and most of the measurements in the envelope were made with the larger type of chamber. The latter were inserted into the ½-in. diameter channels which are available in the main envelope (Fig. 2).

The results of these measurements along a vertical axis through the centre of the core are shown in Fig. 3 and also in Fig. 4, where they are presented as the variation of the relative cross sections. All curves are normalised to unity at the centre of the core. Also shown are measurements on the radiative capture rate in Au^{197} obtained by R. M. Absalom and Miss M. U. Lea during a series of activation measurements.

Measurements at a distance of less than six cm from the outside of the envelope become difficult because of

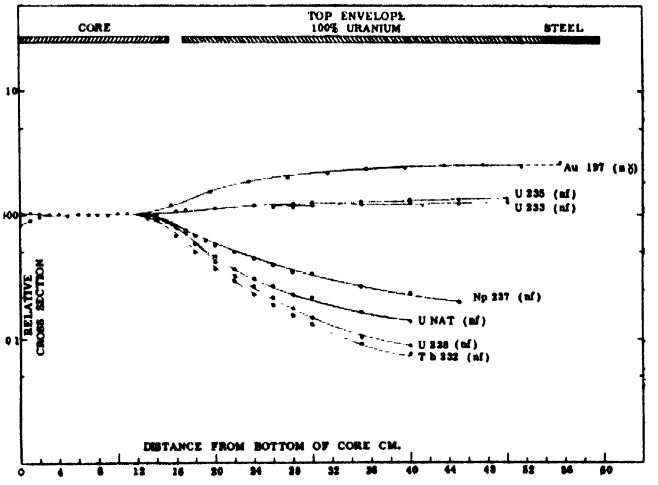

Figure 4. Variation of cross sections through core and top envelope relative to centre of core

the penetration of thermal and low energy neutrons scattered back from the concrete shielding wall of the reactor.

Fission cross sections have been measured at the centre of the core relative to the fission cross section for Pu^{239} by using chambers containing a known amount of fissionable material. In the case of thermally fissile materials the effective mass present has been determined by measurements in a known thermal flux. Alternatively, the effective mass has been deduced from the alpha-particle emission rate in the chamber. Unfortunately, the geometry of the small chambers is, of necessity, far from ideal for this latter type of measurement and the accuracy is low. Table I gives the ratio of the fission cross sections for a variety of materials to the fission cross section of Pu^{239} as measured at the centre of the core.

In the relatively concentrated Zephyr cores, Pu^{240} behaves as a fairly good fuel, which is of interest since it implies that the Pu^{240} content of highly degraded plutonium, from thermal reactors having a high burn-up, is of some value in fast systems. Also, the conversion of Pu^{239} into Pu^{240}, admittedly a small factor in a fast reactor, is by no means a complete loss.

A survey has been made of the Pu^{239} fission rates at different radii in the core and from these measurements flux contours on a vertical section of the core have been drawn and are shown in Fig. 5.

There is a general tendency for the shape of the contours to conform to the shape of the core; however, once clear of the core the contours quickly approach spherical symmetry. The slight depression along the central plane is due to the fusible links in the plutonium elements, which reduce the amount of Pu^{239}, over the inner 1.5 cm by about 25%.

In the uranium envelope the neutron flux distribution rapidly assumes an almost spherical distribution with a form:

$$\phi \propto r^{-1} \sinh [(r_0 - r)/L]$$

where r_0 is an extrapolated radius of the envelope. The diffusion length L is about 12 cm.

NEUTRON ENERGY SPECTRA

A knowledge of the neutron energy spectrum in the core and its variations as the neutrons diffuse through the envelope is important for the interpretation of many aspects of the behaviour of the system.

Table I. Ratios of Fission Cross Sections at the Centre of the Core

Material	$\frac{\sigma(n,f)}{\sigma(n,f)_{Pu^{239}}}$
Pu^{240}	0.6 ± 0.15
Np^{237}	0.42 ± 0.08
U^{238}	0.098 ± 0.006
U^{nat}	0.104 ± 0.006
U^{235}	0.78 ± 0.05
U^{233}	1.26 ± 0.07
Th^{232}	0.026 ± 0.004

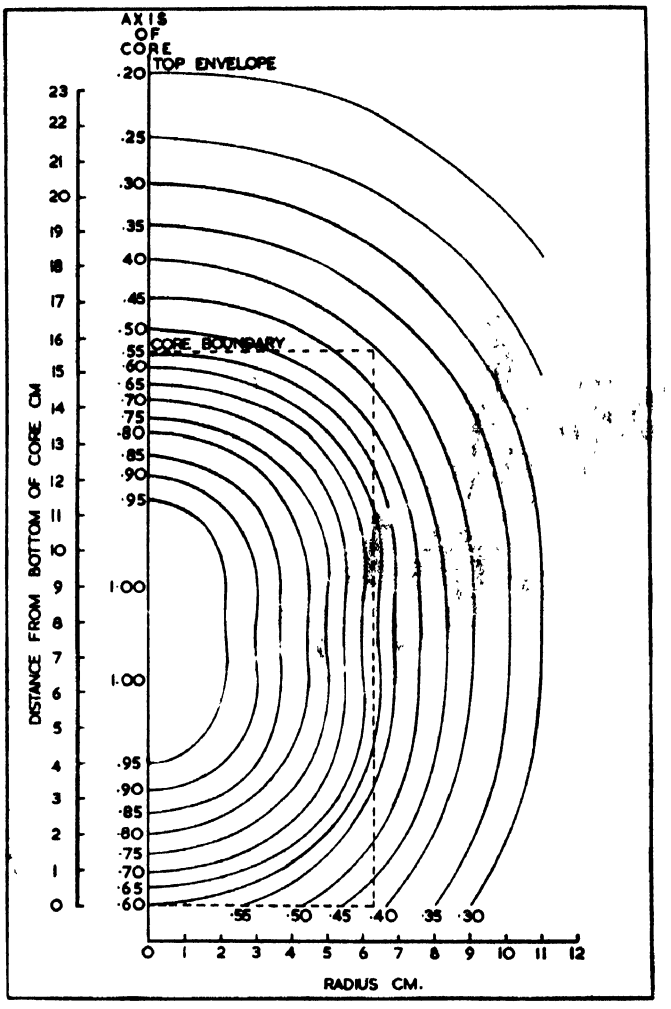

Figure 5. Distribution of neutron flux in a vertical section through the core centre

Investigation of the energy distribution of the neutron fluxes in different regions of Zephyr have been made by, (*a*) direct methods, using proportional counter neutron spectrometers and recoil proton measurements in photographic plates, and, (*b*), indirect methods involving measurements with energy sensitive detectors. Because of the large size of the spectrometers, the indirect method only, has been used in deriving a core spectrum, but in the envelope, where space is not so restricted, measurements of both types have been carried out.

Direct neutron spectroscopy inside a diffusing medium, where the energy distribution is continuous over a wide range, is not an easy matter. Above 2 Mev, the measurement of recoil proton tracks in photographic plates is reliable but extremely tedious. Pulse analysis in a hydrogen filled, recoil-proton, proportional counter, is superior to the photographic plate method and can be pushed to a lower energy limit, namely 0.3 Mev. Wall effects with the higher energy recoils are the most serious limitation in this case and even with a high-pressure filling and a heavy stopping gas (e.g., krypton) the chamber has to be made inconveniently large. Some investigations of the spectra in the uranium envelope of Zephyr have been made using the recoil proton counter and this work has been augmented by photographic plate studies.

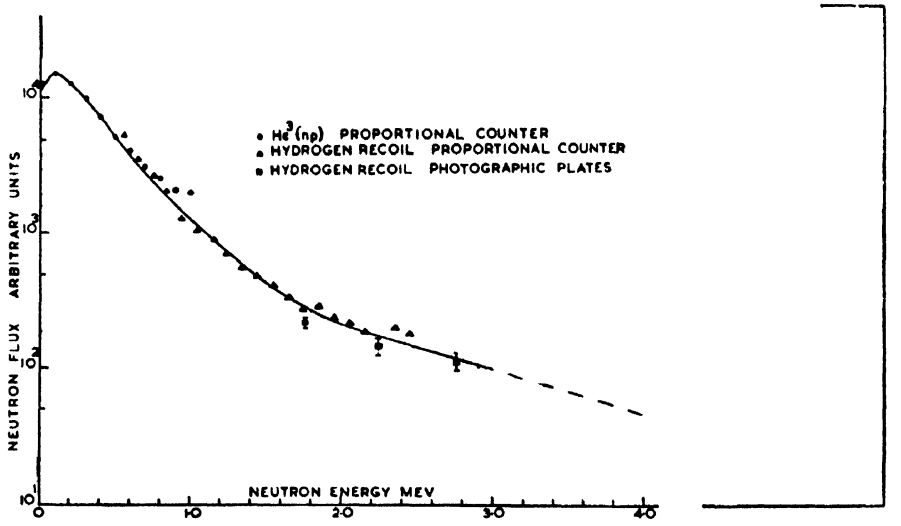

Figure 6. Neutron spectrum in envelope of Zephyr: radius of 28 cm from centre of core

A He^3-proportional counter, developed by R. Batchelor and R. Aves[4] has also been used in Zephyr, in order to extend the measurements down to about 50 kev. The results are rather difficult to analyse in continuous spectra containing a high proportion of neutrons above 1 Mev, because He^3 recoils give pulses which may be confused with the $He^3(n,p)H^3$ pulses. However, in the highly degraded spectrum of the outer envelope region, the method is quite effective.

Direct measurements of the spectrum have been made at three positions in the envelope. Figure 6 shows the composite spectrum measured at a radius of 28 cm from the centre of the core, i.e., about half-way out through the main envelope.

Cross sections deduced from this spectrum show satisfactory agreement with the values measured either with fission chambers or by activation measurements e.g., for the $Au^{197}(n,\gamma)$ reaction the measured cross section is 0.40 ± 0.04 barns whilst that deduced from the spectrum is 0.42 ± 0.04 barns.

The energy sensitive detectors fall into two main classes, namely, those sensitive only to neutrons above certain threshold energies, i.e., U^{238} and Np^{237} fission and the $Al^{27}(n,p)Mg^{27}$ and $S^{32}(n,p)P^{32}$ reactions, and detectors sensitive preferentially towards low energy neutrons, i.e., (n,γ) activation detectors, such as gold. A comparison of reaction rates in these various detectors, and in an energy-insensitive detector such as a Pu^{239} fission chamber, gives a very good picture of the distribution in energy of the neutron flux at a point of measurement.

The results obtained from this type of measurement can be seen in Fig. 4 which shows the variation of the cross sections relative to the centre of the core. Over the greater part of the core the cross sections vary little showing that an equilibrium spectrum exists in the core. The measured cross sections indicate that the average neutron energy in this core spectrum is approximately 1.5 Mev compared with 2.0 Mev for a fission spectrum. The core spectrum is, therefore, only slightly degraded from a fission spectrum. The radiative capture cross section of Au^{197} at the centre of the core is 0.18 ± 0.02 barns compared with 0.12 barns measured in a fission spectrum by D. J. Hughes;[5] this reaction captures preferentially the lower energy neutrons in the spectrum.

As soon as the core boundary is reached degradation becomes apparent from the increase of the $Au^{197}(n,\gamma)$ cross section; since it is known that the cross section for this reaction increases at lower neutron energies. More markedly still, the cross sections for the threshold reactions $Np^{237}(n,f)$, $U^{238}(n,f)$ and $Th^{232}(n,f)$ all show a rapid decrease; the latter two reactions have a higher threshold and show a greater change in cross sections than the fission of Np^{237}. It will be noticed that the higher the threshold the more rapid the change in cross section just outside the core boundary.

Beyond 10 cm from the core boundary the degradation of the spectrum becomes less rapid and a new equilibrium spectrum is approached in the outer regions of the envelope where the relative cross sections tend to be constant. The ratios of the cross sections for the equilibrium spectrum in the envelope to the values for the core equilibrium spectrum show that these two spectra differ considerably. This ratio is given below for several of the reactions which have been studied.

$Au^{197}(n,\gamma)$	2.6
$U^{235}(n,f)$	1.3
$Np^{237}(n,f)$	0.17
$U^{nat}(n,f)$	0.11
$U^{238}(n,f)$	0.05

The average energy in the envelope equilibrium spectrum is about 0.3 Mev whilst the most probable energy is in the region of 0.1 Mev. There is, therefore, a large change in the spectrum between the core and the outer regions of the envelope. As a result of this, many of the important nuclear parameters can varies widely depending on the position in the reactor.

The investigations have shown that the shape of the spectrum above 2 Mev remains substantially the same

as for a fission spectrum throughout the reactor, although the proportion above 2 Mev changes by a factor of about 20 between the two extremes. This suggests that the inelastic scattering cross section of natural uranium remains approximately constant above 2 Mev and that the scattered neutron loses a large part of its energy in the collision.

It is reasonable to suppose that in any mixture of U^{238} and fissile material there will be an equilibrium spectrum depending on the concentration of fissile material. In Zephyr the constitution ranges from a relatively concentrated core, containing Pu^{239} and U^{238} in the atomic ratio of approximately 5 to 4, to the natural uranium of the envelope.

High power fast reactors may have cores in which Pu^{239} or U^{235} are well diluted in U^{238}. The neutron energy distributions found in such cores must lie between those of the core and envelope of Zephyr.

BREEDING OF FISSILE MATERIAL

The total relative fission rates of Pu^{239}, U^{238} and U^{235} in the reactor have been evaluated by numerical integrations of the fission chamber measurements. The results are shown in Table II and are normalised to give a total of 100 fissions in the system. (The figures are accurate to about 5%.)

These results reveal an interesting state of affairs, namely that, of all the fissions occurring in the system, about one third occurs in the envelope and one quarter of the total fissions are in U^{238}. This latter fact has an important bearing on the breeding characteristics of the system, for not only does it signify a useful addition to the neutrons available for breeding, but also it represents a direct consumption of U^{238}, which is the ultimate purpose of breeding.

A neutron balance sheet can be drawn up by combining the fission rate measurement with activation measurements on the radiative capture of U^{238}.

The cross section for the reaction $U^{238}(n,\gamma)U^{239}$ has been determined by R. M. Absalom, M.U. Lea and T. B. Ryves in a variety of positions in the reactor. The method involves irradiation of a uranium oxide sample, followed by solution of the sample in nitric acid, the removal of fission products by solvent extraction, β counting of a liquid sample over a period of several half-lives and subsequent gravimetric analysis of the sample to determine the uranium content. Since the half-life of U^{239} is only 23 minutes the precounting procedure must be carried out very quickly.

An integration of these measurements over the reactor shows that for each 100 fissions in the system 168 ± 17 neutrons are captured in U^{238} to produce Pu^{239}. An estimate of the leakage shows that for this number of fissions about 30 neutrons escape from the outside of the envelope.

Table II. Distribution of Fissions in the Reactor

	Pu^{239}	U^{235}	U^{238}	Total
Core	63.5	0.3	4.3	68.1
Envelope	0	10.0	21.9	31.9
Total	63.5	10.3	26.2	100.0

The loss of Pu^{239} and U^{235} by radiative capture cannot be determined by direct activation measurements in a low power reactor like Zephyr because the amounts of Pu^{240} and U^{236} so formed lie below the limit of detection. It is evident however, from a variety of indirect data that these effects are relatively unimportant, and it is difficult to establish a neutron balance if the ratio of capture to fission is assumed to be much greater than 0.1. In any case, in Zephyr Pu^{240} is a fairly favourable fuel and the conversion of a Pu^{239} atom into a Pu^{240} atom is far from being a complete loss.

The good breeding characteristics of the system are clearly demonstrated by the results. If we define the breeding ratio as the ratio of U^{239} generated in the U^{238} to the sum of the consumption of Pu^{239} and U^{235}, then we obtain a value of 2.1 ± 0.2.

The two main factors contributing to this favourable result are the low ratio of radiative capture to fission in the fissile materials. (Pu^{239} and U^{235}) and, no less, the considerable contribution made by U^{238} fission. It is interesting to speculate on the effect of core dilution on these factors. One would suppose that a fission neutron released in a mass of pure U^{238} would have a greater probability of producing a fast fission in the U^{238} than would a neutron released in a mixture of U^{238} and some other isotopes. Thus, dilution of the core of a fast reactor with U^{238}, rather than separation of all the latter in the envelope should be beneficial to the fast fission process. In other words, the fast fission factor in Zephyr may be somewhat lower than that in a reactor with a dilute core. On the other hand degradation of the neutron spectrum in the core will favour the radiative capture process forming Pu^{240} and furthermore make the latter a poorer fuel. Dilution of a core by materials other than U^{238} is likely to have an adverse effect on all the factors and, if it is unavoidable, a material with low inelastic scattering cross section would be preferable. Provided that strong inelastic scattering diluents are avoided then any fast Pu^{239}/U^{238} system should have a breeding factor substantially greater than unity.

PERTURBATION STUDIES

According to a simple one group transport theory, the effect on reactivity of introducing a small sample of material of volume δV into a vacant space at some point $(\underline{r})$ in a reactor is given by:[6]

$$\Delta\rho = \frac{[\beta - g(\underline{r})\alpha][\phi(\underline{r})]^2\,\delta V}{\int p(\underline{r}')\phi(\underline{r}')\,dV}$$

where $\phi(\underline{r}')$ and $p(\underline{r}')$ represent the neutron flux and neutron production rate at (r'), the integral being taken over all regions of the reactor in which fission occurs; α and β are the conventional parameters of the one group theory (referring to the sample) and $g(\underline{r})$ is the value at $(\underline{r})$ of the so-called perturbation factor.

The integral in the denominator is easily determined from fission chamber measurements provided that ν is

known for all the isotopes contributing fissions. α and β may be replaced by the more conventional nuclear constants if it is so desired, for, in the general case,

$$\beta - g(r)\alpha = N[(\nu - g(\underline{r}))\sigma_f + (1 - g(\underline{r}))\sigma_{str} - g(r)\sigma_c]$$

where σ_{str} is the scattering (elastic + inelastic) component of the transport cross section, i.e.

$$\sigma_{str} = \sigma_{in} + 2\pi \int_0^\pi \sigma_e(\theta)(1 - \cos\theta)\sin\theta\, d\theta$$

σ_{in} being the inelastic scattering cross section and $\sigma_e(\theta)$ the differential elastic scattering cross section per unit solid angle measured in the laboratory space.

In the diffusion theory approximation $g(r)$ is determined by the expression

$$1 - g(\underline{r}) = 3[j(\underline{r})/\phi(r)]^2$$

where $j(\underline{r})$ is the neutron current at $\underline{r}$. This expression may be used to calculate $g(r)$ in any particular region. It will be seen that the contribution of scattering to the reactivity change varies with the square of the neutron current while fission and non-fissile capture are mainly sensitive to the square of the neutron flux.

This simple one-group theory has formed the basis of the perturbation measurements reported here. If measurements are made at two points having known and differing values of $g(\underline{r})$, then it is possible to determine the two parameters α and β of the sample material, or the corresponding cross sections. The positions chosen in Zephyr corresponded to a region of zero neutron current ($g(\underline{r}) = 1$) and a region near the core boundary where the neutron current was fairly large. In the former position the reactivity change is determined by $(\nu - 1)\sigma_f - \sigma_c$ (or just σ_c for non-fissile materials) and from the measurement of the change this quantity can be determined.

The investigations carried out in Zephyr have covered about 70 natural elements and, more recently, several separated isotopes. Most of the elements were tested in the form of small cylinders (5.6 mm in diameter by 20 mm in length) which were moved into and out of empty channels in the core. It was thought that neutron scattering along the channels might cause spurious effects, but observations indicated that the creation of a void in a channel filled with a given material was, within experimental limits, exactly equivalent to placing a corresponding volume of that material at the same point in an empty channel. Those materials which could not be obtained as solid cylinders were examined as powders or liquids in small containers made from magnesium or aluminium foil, the effects of these containers being determined separately. Gaseous elements, such as oxygen, were examined as compounds. A few materials were tested in the form of long rods which passed into the core, through channels in the top envelope section. These rods were moved in 1 cm steps through the core. The outer end of the rod was, in every instance, so far from the core that its movement had no effect, and therefore the observed reactivity change for each step was identical to that which would be obtained if a 1 cm cylinder had been introduced or removed from the given region.

Reactivity changes were determined by control rod balance rather than by the period of oscillator methods. The limit of measurement was about 5×10^{-7} in reactivity. Limitations set by the pulse counting method of power level measurement made it appear unlikely that a greater sensitivity could be obtained by an oscillator method.

The effects of sample materials in the core of Zephyr are well illustrated by Figs. 7a and 7b, which show the reactivity changes obtained per centimeter movement of a copper rod in a central channel (No. 1) and in a channel just inside the core boundary (No. 241). Within the confines of the core these curves conform to the simple one group theory outlined above and the behaviour of the copper can be explained in terms of two parameters α and β or alternatively σ_{str} and σ_c. At the core boundary the simple diffusion theory relationship fails, an effect partly attributable to the rapid change in neutron energy spectrum and partly due to the fact that such a theory is not accurate at boundaries. However, within the core, the reactivity change may be attributed to a capture effect which is negative and varies approximately with the square of the neutron flux (actually it varies as $g(\underline{r})\phi^2(\underline{r})$ but $g(\underline{r})$ only shows $\sim$10% variation from unity) and to a scattering effect which varies with the square of the neutron current. The capture effect is a maximum at the core centre, while the "pure" scattering effect is zero at the centre and, to all intents and purposes, over the finite region occupied by the experimental samples when placed at the mid point channel (No. 1). It was observed that the change in reactivity produced by the presence of the copper is positive over the greater part of the core and only negative over a relatively small central region. This was true of all the natural elements in different degrees and, of all the materials examined, only highly enriched B^{10} showed a uni-

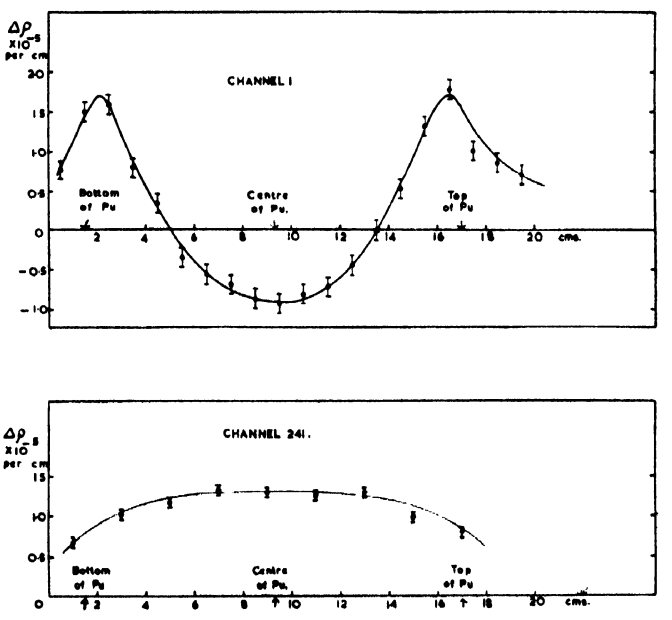

Figure 7. Reactivity changes produced by a copper rod in the core

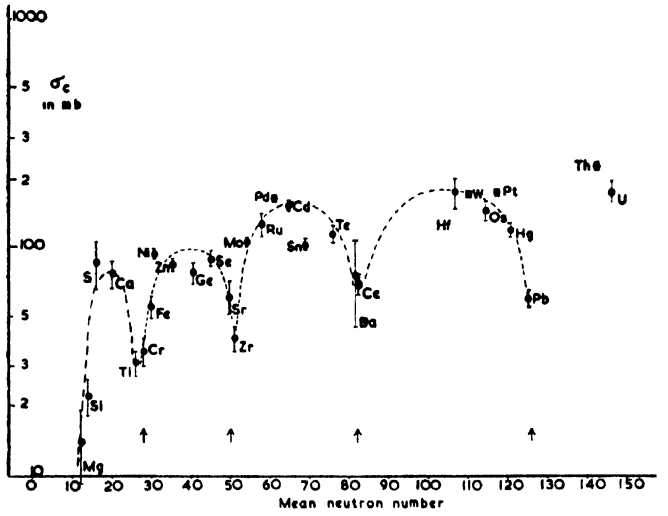

Figure 8. Effective capture cross sections in Zephyr: even Z elements

versal negative effect (Li^6 should also do so, but was not studied).

A small sample of Pu^{239} was used as the standard in all the measurements, the reactivity change produced by introducing this sample into the core centre being used, both as a basis for the control rod calibration and also, by direct comparison, to give the value of $\beta - g(r)\alpha$ for other samples. Measurements were made in two standard positions, namely, at the mid region of the central channel (where $g(r) = 1$) and at the mid region of a boundary channel (No. 241).

The central channel measurement gave $\beta - \alpha$ (i.e., $-\sigma_c$ for the non-fissionable samples). The resulting values of σ_c are plotted in Figs. 8 and 9. Several interesting points come out of these results.

In the first place it is evident that the σ_c obtained in the perturbation experiments are higher than the true values. Table III shows comparative values of σ_c by the perturbation and activation methods for certain cases where only a single isotope is involved.

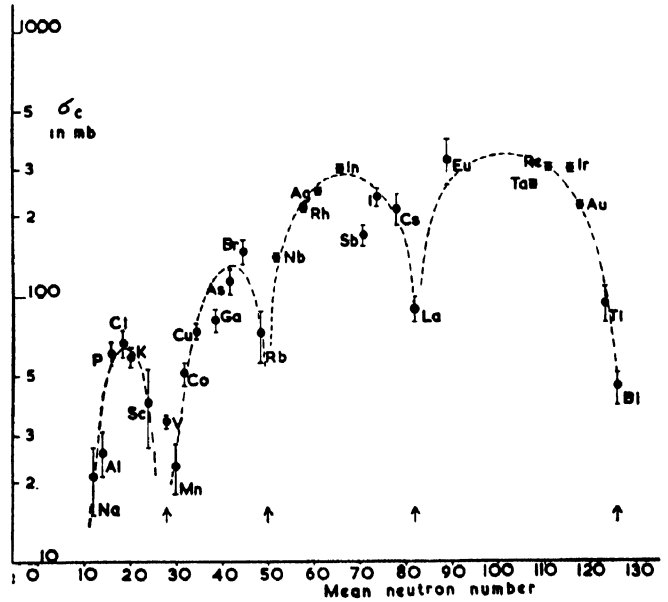

Figure 9. Effective capture cross sections in Zephyr: odd Z elements

Table III

Isotopes	σ_c *mb*	σ_{act} *mb*
Na^{23}	21 ± 6	0.53 ± 0.04
Al^{27}	26 ± 5	3.0 ± 0.2
V^{51}	29 ± 8	4.0 ± 0.4
Mn^{55}	34 ± 2	5.3 ± 0.5
As^{75}	114 ± 12	78 ± 7
I^{127}	238 ± 20	158 ± 16
Ta^{181}	265 ± 5	228 ± 25
Au^{197}	220 ± 5	183 ± 8

Our interpretation of these differences is based upon the fact that the nuclear properties of the core (and reflector for that matter) depend upon neutron energy and so, if a neutron undergoes inelastic scattering in the sample, then the relative probabilities that it will produce fission, radiative capture, or that it will escape from the system, are thereby changed. In other words the effectiveness of the neutron in sustaining the chain reaction has been altered. It requires a fall in effectiveness of only a few per cent to explain the results which are observed.

The effective capture cross section of the perturbation measurements is thus compounded from the true radiative capture cross section and a function of the inelastic scattering properties of the species in question, with the latter effect predominating in the lighter nuclei, and the former in the heavier isotopes.

Further interesting features are revealed by an examination of the plots of effective capture cross sections of the elements examined against their mean neutron numbers. These plots show marked drops in the σ_c in the regions of the so-called magic numbers while the peak regions in between these magic numbers are much higher in the case of odd Z nuclei than for even Z species, particularly for the heavier elements. It should be noted, of course, that the odd Z nuclei also have an odd total number of nucleons while the even Z elements have more nuclei with even numbers of nucleons than odd numbers. The effect, therefore, may be associated with the total number of nucleons rather than the Z number. Separated isotopes are being examined with a view to settling this point.

The peak values of the σ_c even in the case of the odd Z elements are small in comparison with the fission cross sections of the nuclear fuels, a fact which is of importance in the neutron economy of fast reactors. It is quite evident, for example, that radiative capture in fission products can have only an insignificant effect even with very high degrees of fuel burn up.

Transport cross sections have been obtained by combining the results of measurements made in channels 1 and 241. Figure 10 shows the relative values of transport cross sections for a large number of elements. The ordinates correspond to values in barns, if the value of $1 - g(r)$ in channel 241 is taken as 0.10. The best calculation using modified one-group diffusion theory suggested a value of $1 - g(r) = 0.13$ in this core while averaging published σ_{str},[7,8,9,10] over the Zephyr core spectrum for C, Fe, W and Pb and

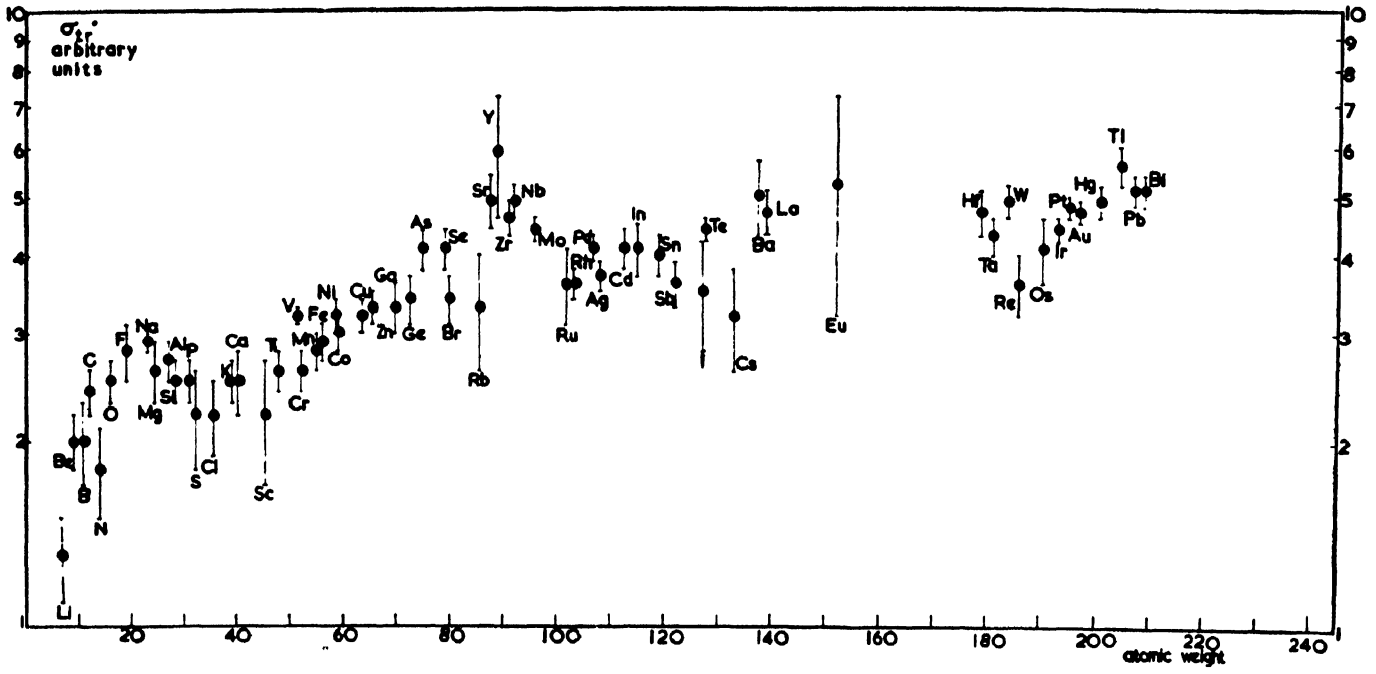

Figure 10. Effective transport cross sections in Zephyr

using these materials as standards gave values of $1 - g(\underline{r})$ ranging from 0.10 to 0.13. It must be emphasized that no great accuracy can be claimed either in the theoretical or experimental derivation of $g(\underline{r})$, but, at least, there appears to be some measure of agreement.

Comparisons of the quantity $x = (\nu - 1)\sigma_f - \sigma_c$ for the various fissile materials have been made by the perturbation method. The quantity is positive, of course, for Pu^{239}, U^{235} and U^{233} and, in the Zephyr core spectrum, it is also positive for U^{238}. Th^{232}, on the other hand, has a negative value of x. Since x for Pu^{239} has been used as a basis for calibrating reactivities and also for deriving the σ_c and σ_{str} above, it is appropriate to use this as a standard for comparison with the other fissile materials. Thus we find:

$$x^{U^{235}}/x^{Pu^{239}} = 0.51$$

$$x^{U^{233}}/x^{Pu^{239}} = 0.91$$

$$x^{U^{238}}/x^{Pu^{239}} = 0.034$$

$$x^{Th^{232}}/x^{Pu^{239}} = -0.046$$

In a more dilute core we should expect $x^{U^{238}}$ to become negative.

REMARKS UPON CONTROL OF REACTIVITY

The perturbation experiments in Zephyr demonstrate the fact, that except in a small region near the centre of the core the effect of scattering predominates over absorption in all non-fissile materials with the exception of certain separated isotopes, viz: B^{10} and Li^6. The situation would be more favourable to absorption in a large dilute core, but even so it can be said that absorbing control rods, unless they are constructed from the mentioned separated isotopes, will be ineffective in fast reactors.

Two alternatives remain, namely: (*a*) to move fuel into and out of the core, and (*b*) to move scattering material.

In the second case the maximum effect is obtained by moving the material in the region of maximum neutron current which is usually near the core boundary. If a fairly linear response is required for a large movement, then this movement should take place as nearly as possible, over a surface of constant current —generally, more or less, this is also a constant flux surface. If, on the other hand, a large response is required for a small movement, it is better to move a fairly large section of material in the direction of the neutron current. The control rods of Zephyr act primarily as scatterers and move roughly at right angles to the neutron current. The Zephyr shut-off-block on the other hand moves along the line of the current.

The scattering method is not very good if the reactor core is large, because the volume of scattering material, which must be moved, becomes excessive. For this reason the control of Zeus is based on fuel movement.

REFERENCES

1. Holmes, McVicar, Rose, Shepherd, Smith, R. D. and Smith, A. M., "Operational Features of Zephyr," *J. Nuclear Energy*, Vol. I, pp. 47–52 (1954).
2. Aves, Barnes and MacKenzie, "Fission Chambers for Neutron Detector," *J. Nuclear Energy*, Vol. I, pp. 110–116 (1954).
3. Holmes, McVicar, Shepherd and Smith, R. D., "Electrical Characteristics of Fission Chambers," *J. Nuclear Energy*, Vol. I, pp. 117–123 (1954).
4. Batchelor and Aves, "Helium-3 Fast Neutron Spectrometer," A.E.R.E. N/R 1499.
5. Hughes, "Pile Neutron Research," Addison Wesley, Cambridge, Mass., pp. 110, 111 (1953).

6. Fuchs, "Perturbation Theory in Neutron Multiplication Problems," *Proc. Phys. Soc.* A. Vol. 62 (December 1949).
7. Willard, Bair and Kington, "Elastic Scattering Angular Distributions of Fast Neutrons on Light Nuclei," *Phys. Rev.* Vol. 98, p. 669 (1955).
8. Walt, M. and Beyster, R. J., "Interaction of 4.1 Mev Neutrons with Nuclei," *Phys. Rev.* Vol. 98, p. 677 (1955).
9. Barshall, Battat, Bright, Graves, Jorgensen and Manley, "Measurement of Transport and Inelastic Scattering Cross Sections for Fast Neutrons," *Phys. Rev.* Vol. 72, p. 881 (1955).
10. Walt and Barschall, "Scattering of 1 Mev Neutrons by Intermediate and Heavy Elements," *Phys. Rev.* Vol. 93, p. 1062 (1954).

The Fast Exponential Experiment

By F. C. Beyer, R. H. Bryan, H. H. Hummel, D. H. Lennox, F. H. Martens, W. A. Reardon, N. Rosenzweig, A. B. Smith, and B. I. Spinrad,* USA

The fast exponential experiment was designed to obtain fundamental information about the physics of dilute fast reactors in the range of compositions contemplated for such systems as set by such engineering considerations as heat transfer, structural support and coolant flow. The exponential experiment was chosen for this purpose because it combines a low investment of fuel with a high degree of safety.

The measurements have so far yielded accurate values for the bucklings of systems with various mixtures of fuel and diluent material, and with isotopic ratios of U^{238} and U^{235} in the range 3:1 to 7:1. In addition, reflector savings of Pb, Fe, U, and Al have been measured, and an indication of the various energy spectra has been obtained by measuring the U^{235}-U^{238} fission ratio. The behavior of equilibrium neutrons in natural uranium has also been investigated.

ENRICHED EXPONENTIAL EXPERIMENTS

The source of neutrons for the Fast Exponential Experiment was a light water moderated, enriched uranium reactor of rectangular geometry. A lead and water reflection shield reduced the leakage from the rear and sides. Located on the front leakage face was a converter plate, or "pedestal," of natural uranium, 8 in. thick, which reduced the interaction between the source core and the exponential assembly. It also produced an energy spectrum of neutrons which matched the equilibrium spectrum of a fast assembly more closely than the leakage spectrum of the thermal core.

The exponential assembly itself consisted of a rectangular stack of iron cans, 3 in. by 3 in. by 24 in., filled with the appropriate mixture of the two isotopes of uranium and diluent materials in the form of plates 3 in. by 24 in. by ca 0.075 in., and made up of 25% enriched uranium, natural uranium, and aluminum, stacked in a uniform fashion into the cans. Al of reduced bulk density was chosen to simulate Na. The volume occupied by Al could be replaced by Na to check the validity of the Al substitution. The volume fraction of the various constituents of the assemblies are listed in Table I, along with the results obtained to date.

The assembly rests upon a bottom reflector, 12 in. thick, which serves to eliminate the effect of neutrons scattered from the floor and also permits reflector savings data to be obtained. The whole assembly rests on a traveling cart, which is withdrawn from the source when a new loading is made. The cart then is moved at slow speed towards the source until contact is made. In this way, new assemblies could be loaded without the danger of reaching criticality in a fast system; in case of doubt, observation of the reactivity of the source core during the motion of the cart could be used to detect an approach to criticality in the assembly. These components are shown diagrammatically in Fig. 1. Figure 2 is a photograph of the facility.

In the assemblies, channels of 1¼ in. by ¼ in. cross section are provided through which detectors can be moved to obtain neutron flux distributions. In most cases, these flux traverses were made using miniature fission chambers with external dimensions of 0.2 in. by 1 in. by 1 in.

Within the assembly, in a region of the core where only the fundamental mode is present, the spatial and energy variations of the flux are separable. The spatial dependence obeys the source-free asymptotic equation

$$\nabla^2\phi + \kappa^2\phi = 0 \tag{1}$$

where κ^2 is the buckling and ϕ the neutron flux.

For the boundary conditions of the experiment, the spatial distribution of the fundamental mode is expressed as

$$\phi = X(x)Y(y)Z(z) \tag{2}$$

where:

$$X = A_1(e^{-\kappa_x x} + \gamma e^{\kappa_x x}) \tag{3}$$

$$Y = A_2 \cos \kappa_y(y - y_0) \tag{4}$$

$$Z = A_3 \cos \kappa_z(z - z_0) \tag{5}$$

$$\kappa_y^2 + \kappa_z^2 - \kappa_x^2 = \kappa^2 \tag{6}$$

Our convention is to label the exponential direction as x, the vertical direction as z, and the remaining direction as y. Measurement of the flux direction along the three axes of the assembly in a region of the core where the fundamental mode is present enables a determination of κ_x, κ_y, κ_z, and κ. Because the reflector introduces spectral perturbations, the fundamental mode of the core is present only in a region far from the reflector. However, the equilibrium flux itself, which is attained far from the neutron source, is separable throughout

* Argonne National Laboratory.

Table I. Fast Exponential Experimental Results and Comparison with Theoretical Predictions

A. Compositions*

System designation	$U^{238}:U^{235}$ atom ratio	Vol % U	Vol % Fe	Vol % Al	Vol % void
1	3.13	35.11	10.36	14.76	39.77
2a	5.00	34.59	10.36	0	55.05
2b	5.00	34.59	10.36	14.76	40.29
2c	5.00	34.59	10.36	29.52	25.53
3	6.82	34.33	10.36	14.76	40.55

B. Results

System designation	1		2a		2b		2c		3	
	Expt	Theo	Expt	Theo	Expt	Theo	Expt	Theo	Expt	Theo
Root buckling, κ (cm^{-1})	0.0538 ±0.0018	0.0600	0.0379	0.0423	0.0411 ±0.0005	0.0462	0.0455	0.0501	0.0323 ±0.0004	0.0364
Reflector savings, S, (cm)										
U	21.8	18.4			27.6	18.8			27.8	18.3
Fe	26.0	19.3	No measurement		29.9	22.6	No measurement		29.4	24.5
Al	—	17.0			28.0	20.1			29.2	22.3
Pb	26.9	18.4			34.0(?)	22.8			32.5	26.1
$U^{235}:U^{238}$ fission ratio per atom	20.3	16.6	24.0	20.2	26.0	21.9	28.0	23.6	34.0	26.5

* Excluding Al separators used for providing detector channels.

core and reflector in the x, y, and z directions. The equilibrium distribution has a spectrum which depends only on z.

For each experimental flux plot obtained, a least squares fit to a cosine or exponential curve was made using the Argonne electronic digital computer (AVIDAC). At least one plot was obtained for each of four different chambers (loaded, respectively, with U^{235}, U^{238}, Np^{237}, and Pu^{240}) in each of the three directions. The fittings were made only over those regions in which the spectrum, as measured by the chambers of varying spectral response, was constant to within 1% in detector ratio.

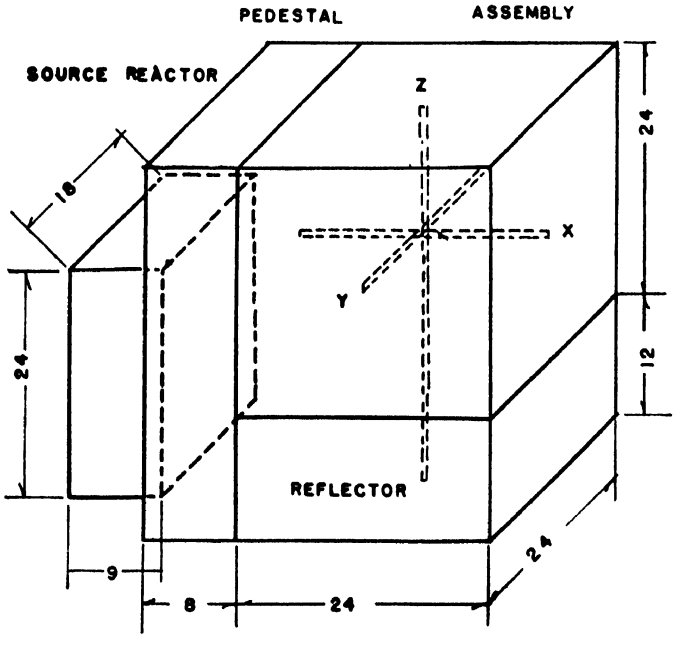

Figure 1. Diagrammatic sketch of fast exponential experiment

The statistical weight of each curve is considered to be the reciprocal mean square of the residuals. The weighted mean value of κ from all curves in each direction from the same core composition is then found; finally the buckling is deduced from these weighted means.

$U^{235}:U^{238}$ fission ratios were obtained by comparing the counting rates of a natural uranium chamber and an enriched uranium chamber in the center of the assembly. The relative efficiencies of the chambers were calibrated by exposure to a thermal neutron flux in which only the U^{235} underwent fission. Corrections were made for the relative amounts of each isotope in the chambers. An independent calibration was also obtained by measuring the ratio of chamber response in a fission spectrum. Using thermal calibration, they gave a fission ratio/atom of 5.0 ± 0.5, which is to be compared with the accepted value of 4.2.[3] Since the chambers cannot be shielded against epi-cadmium neutrons reflected from surrounding objects (the floor, etc.), some of this discrepancy may be explained by experimental circumstances.

A knowledge of the position of the maximum in the neutron distribution in the z direction together with the z curvature (κ_z) enables a calculation of the extrapolated end point of the cosine function located in the reflector. The distance of this end point from the core-reflector interface is defined as the reflector savings for the material and assembly. Each individual z distribution may be used to obtain a value of the reflector savings. An alternative procedure employed the average value of κ and κ_y and individual x (expo-

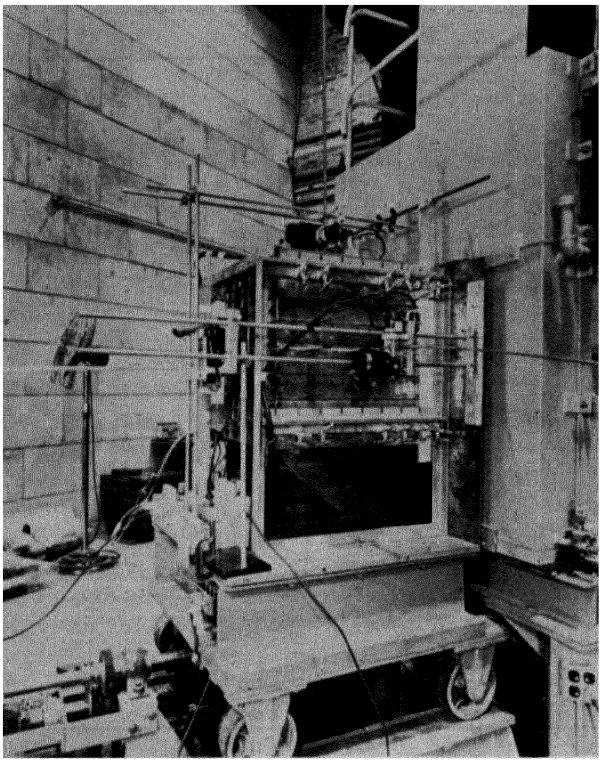

Figure 2. Fast exponential experiment

nential) distributions to obtain the associated z distribution and reflector savings. In the latter method, variations in reflector savings from distribution to distribution depend largely on the precision of exponential, rather than the κ_z measurement.

The experimental values of κ, for reflector savings, and for U^{235}:U^{238} fission ratios/atom are summarized and compared with theoretical values in Table I. Theoretical values for κ listed in Table I were obtained by normal mode transport theory calculations employing twenty energy groups and carried out by fission source iteration. Although transport theory was used, the deviations from diffusion theory were unimportant in all cases. Reflector savings given in Table I were calculated by nine-group diffusion theory on the UNIVAC (operated by the Computing Facility at New York University) using a code prepared by J. Cook and M. Butler of Argonne National Laboratory. This is a one-dimensional calculation in slab geometry, the buckling transverse to the direction of the reflector being determined as an eigen-value.

Cross sections used in the reflector savings calculations are listed in Table II. The transport cross section, σ_{tr}, is defined as $\sigma_{tot} - \int_{-1}^{1} \mu\sigma_{sc}\, d\mu$, where μ is the cosine of the scattering angle, σ_{sc} is the scattering cross section, and σ_{tot} is the total cross section. Lower energy transport cross sections for U^{235} and U^{238} listed in Table II are in reasonable agreement with angular distribution data at 0.5 and 1.0 Mev obtained at the Los Alamos Scientific Laboratory (LASL) by Allen, Taschek, and Walton. Properties of Al, Fe, and Pb were based on what literature data were available at the time.[6-11] The transport cross sections of Al and Fe below 1 Mev used in buckling calculations do not differ enough from those inferred from data of A. Langsdorf and R. Lane[12] to affect the buckling appreciably. Transport cross sections of Fe and Al in the lower energy groups of Table II are weighted according to $(1/\sigma_s)^2$ for these pure materials, corresponding to constant slowing-down density in the reflector.

Cross sections used to predict κ were averaged in a method appropriate to the core, and the transport cross sections were about 4% above what would be obtained from the listed cross sections. The complete listing of the 20-group constants requires too much bulk to reproduce here, and does not shed enough additional light on the fundamental assumptions to warrant additional discussion.

The effect on core buckling of variation of parameters was studied. It was found that on changing the spectrum in inelastic scattering for uranium from $E^{1/2}e^{-E}\,dE$ to dE, the value for κ for assembly 1* increases about 1%, while the change to $E\,dE$ decreases κ by about 2%; for assembly 3 there is no change in κ. An increase in the low energy capture cross section of U^{235}, compensated by a decrease at high energy such as to make the average value over the Experimental Breeder Reactor core spectrum[2] constant, caused the κ for assembly 1 to be decreased by 2-3%; the κ of assembly 3 was decreased by 4% for an $E\,dE$ inelastic spectrum, and 6% for the other two spectra. A change of inelastic threshold of uranium from 0.2 to 0.4 Mev reduced κ by 1% or less. Older values of the U^{235} fission cross-sections which are 10–15% higher in the region around 100–200 kev (these are the numbers listed in Table II, for which corrections have been made in obtaining results of Table I), gave κ values greater by 4% for assembly 1 and 6% for assembly 3 than did presently accepted constants. The theoretical values of κ of Table I are the best present values taking these variations into account.

Elastic moderation was taken into account by using group-removal cross sections based on the scattering part of the group-average transport cross sections. Elastic energy degradation was found to have a minor effect on the energy spectrum, the main perturbations being local in energy and associated with scattering resonances in Al and Fe.

It is seen from the data of Table I that values of κ as measured in the experiments are about 10% below those calculated. The calculated value for assembly 1 is in reasonable accord with what would be expected from an extrapolation of experimental results on other systems obtained by H. Paxton and co-workers at Los Alamos. There are indications that complete spectral equilibrium is not attained in the exponential experiment, which is possible because the criteria used for determining equilibrium are insensitive to changes in the spectrum below about 700 kev. Hence, a more detailed study of approach to equilibrium is now being undertaken experimentally.

* The assemblies to which reference is made are those listed in Table I.

Table II. Cross Sections* for Calculations of Reflector Savings

$\nu = 2.51$

Fission spectrum: $e^{-E} \sinh \sqrt{2E}$

Group j	Mev	U^{235} σ_f	U^{235} σ_c†	U^{235} $3\sigma_{tr}$	U^{238} σ_c	U^{238} $3\sigma_{tr}$	U^{238} σ_f[a]	Fe $3\sigma_{tr}$	Al $3\sigma_{tr}$	Pb $3\sigma_{tr}$
1	1.400–∞	1.25	0.07	13.92[5]	0.05	13.88[5]	0.532	5.97	4.92	10.5
2	0.700–1.400	1.20	0.13	15.48	0.103	15.30	0.018	5.70	7.92	11.7
3	0.400–0.700	1.23	0.16	17.79	0.144	17.73		5.85	11.40	12.0
4	0.200–0.400	1.50	0.28	22.23	0.180	22.11		8.70	9.30	18.9
5	0.100–0.200	1.83	0.70	28.77	0.237	28.53		9.30	8.70	26.4
6	0.050–0.100	2.20	1.00	35.10	0.300	33.30		11.13	7.38	30.0
7	0.025–0.050	2.60	1.30	40.68	0.420	38.16		5.76	4.23	31.5
8	0.010–0.025	3.30	1.65	43.11	0.530	42.78		4.23	3.93	33.0
9	0.000–0.010	5.00	2.50	67.50	1.000	40.80		19.50	4.08	33.0

Group j	U^{235} σ_{in}	U^{238} σ_{in}	Fe σ_{in} $(1 \to j)$	Fe σ_{in} $(2 \to j)$	Al σ_{in} $(1 \to j)$	Al σ_{in} $(2 \to j)$	Pb σ_{in} $(1 \to j)$	Pb σ_{in} $(2 \to j)$
1	1.40[5]	2.10[4]						
2	0.75	0.96	0.45		0.29		0.4	
3	0.36	0.47	0.15	0.13	0.11	0.02	0.2	0.1
4	0.13	0.17	0.07	0.09		0.08	0.1	0.1
5			0.03	0.04		0.03		0.1
6			0.02	0.02		0.01		
7			0.01	0.01				
8				0.01				

* σ_f = fission cross section.
σ_c = radiative capture cross section.
σ_{tr} = transport cross section.
σ_{in} = inelastic cross section.

† These values are the rapidly varying ones discussed in the text. The values used for the "best" κ estimates have a nearly instant capture/fission ratio of 0.14 below Group 1.

It is similarly observed that there is a systematic difference between calculated and measured reflector savings, which may be due to the same cause, or may be due to incorrect choices of transport and inelastic scattering cross sections used in the calculations.

Effects of diluent materials on core buckling are obviously minor.

EQUILIBRIUM NEUTRONS IN NATURAL URANIUM

The fast assembly and pedestal were replaced by a cube of natural uranium, 24 in. on a side (see Fig. 3), in order to study the equilibrium distribution of neutrons in this material. The uranium was a dense stack of 2 in. by 3 in. by 6 in. bricks. By the same methods as previously described, the diffusion length L, defined as $1/i\kappa$, is found to be 10.0 ± 0.2 cm. This compares with an earlier value of 9.6 cm obtained at LASL. If the diffusion length is calculated using cross sections consistent with those used for enriched buckling calculations except for the indicated changes in inelastic scattering threshold and inelastic spectrum of U^{238}, the values listed in Table III are found.

It should be borne in mind that uncertainties in the capture and transport cross sections of U^{238} make inferences about inelastic scattering properties based on the diffusion length alone rather unreliable.

Calculated values for the ratio of U^{235}/U^{238} fissions per atom are also given in Table III. These numbers

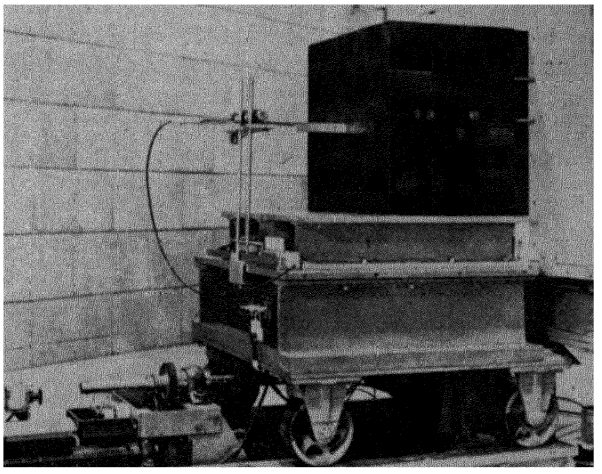

Figure 3. Natural uranium stack in place

Table III. Calculated Properties of an Infinite Block of Natural Uranium

Inelastic scattering threshold, Mev	Inelastic spectrum	L, cm	U^{235}/U^{238} fission ratio per atom
0.2	$E^{1/2}e^{-E}\,dE$	8.80	225
0.2	dE	8.60	216
0.2	$E\,dE$	9.30	221
0.4	$E^{1/2}e^{-E}\,dE$	9.76	242

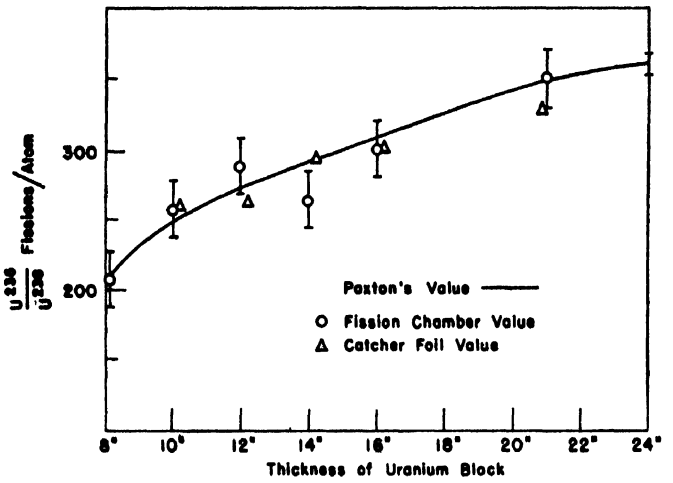

Figure 4. U^{235}/U^{238} fission ratio in natural uranium vs block thickness

are basically in excellent agreement with a value of 220 obtained by H. Paxton, *et al.* of LASL, in a cylinder 15 in. in diameter and about 26 in. high, by radiochemical techniques (counting of Mo^{99}). The value measured by the authors is 363 ± 40, using both miniature fission chambers, intercalibrated in a thermal neutron flux, and a "catcher foil" technique, in which fission fragments from the surface of a foil are caught in an Al foil, which is then counted. Values close to 220 were obtained by a limited number of radiochemical analyses, and there is the possibility of a fundamental disagreement between radiochemical and other techniques.

The difference in the two results may also be explained if equilibrium is not attained in the smaller assembly. To test this, the fission ratio was measured for blocks, the height and length of which were retained at 24 in., while the thickness was varied from 10 in. to 24 in. From Fig. 4 it may be seen that equilibrium is not achieved in any assembly smaller than a 24 in. cube, if indeed it is achieved there.

An inelastic removal cross section for U^{238} from the 1.4–∞ Mev group of about 3 barns would be needed to agree with the higher ratio values, both in the natural uranium and in the enriched assemblies. However, a series of exponential experiments in uranium at enrichments extending up to 9%, performed by H. Paxton, *et al.*, and analyzed by G. Hansen, yielded U^{235}/U^{238} fission ratios consistent with calculations using a cross section of 2 barns. These ratios were again obtained radiochemically.

REFERENCES

1. Glasstone, S. and Edlund, Milton C., *Elements of Nuclear Reactor Theory*, D. Van Nostrand Co., New York (1952).
2. Huddleston, C. and Eggler, C., private communication.
3. Based on work of Leachman, R., Los Alamos Scientific Laboratory.
4. Based on work of Beyster and Carter, Los Alamos Scientific Laboratory, interpreted by Hansen, G. As pointed out by Bethe, H., their work also suggests an inelastic spectrum from group 1 similar to $E^{1/2}e^{-E}dE$.
5. Based on work of Hansen, G. of Los Alamos Scientific Laboratory, using results of Jurney, E. and Zabel, C. and of Paxton, H. and co-workers, all of Los Alamos Scientific Laboratory.
6. Kiehn, R. and Goodman, C., *Neutron Inelastic Scattering*, Phys. Rev. *95:* 989 (1954).
7. Endt, P. M. and Kluyver, J., *Energy Levels of Light Nuclei (Z = 11 to Z = 20)*, Rev. Mod. Phys. *26:* 95 (1954).
8. Whitehead, W. and Snowdon, S., *Angular Distribution of Neutrons Scattered from Al, Fe and Pb*, Phys. Rev. *92:* 114 (1953).
9. Barschall, H., *Scattering of 1-Mev Neutrons by Intermediate and Heavy Elements*, Phys. Rev. *93:* 1062 (1954).
10. Jurney, E., *Inelastic Collision and Transport Cross Sections for Some Light Elements*, LA-1339 (1951).
11. Neutron Cross Section Advisory Group, *Neutron Cross Sections*, AECU-2040 and Supplements (1952).
12. Langsdorf, A., and Lane, R., *Angular Distribution of Scattering of Moderate Energy Neutrons*, Bull. Am. Phy. Soc. *30*, 3 (28 April, 1955).

A Survey of the Theoretical and Experimental Aspects of Fast Reactor Physics

By D. Okrent, R. Avery, and H. H. Hummel,* USA

Fundamental differences exist between the physics of fast power reactors and that of their thermal counterpart. While the calculation and measurement of the various performance criteria remain important problems, the fast reactor has markedly different attributes. A new set of theoretical and experimental techniques are employed, and the chief physics design problems have changed appreciably.

The neutron energy spectrum bears no resemblance to the $1/E$ high-energy tail of the thermal reactor. Even though elastic moderation may not be negligible, inelastic scattering has become the major mode of energy degradation and, also, all absorptions occur at high energies. Further, since the relative amounts of absorption and energy degradation will change considerably, there will be a wide variance among the spectra found in the early experiments with small amounts of fissionable material, in the moderate sized development reactors and in the ultimate large-scale fast power reactors. Since there is a rapid change of transport and other cross sections with energy, one can make a strong argument for the use of a multigroup treatment for parameter type studies, for design of specific reactors, and for analyses of experiments. There is also a strong incentive for obtaining as detailed spectral information as is possible from available experiments.

The type of neutron energy spectrum to be expected over the range of fast power reactors is illustrated in Fig. 1. The curve labeled EBR-1 describes the average neutron energy spectrum in the core of a one-megawatt reactor, using a highly enriched uranium fuel, stainless steel cladding and NaK (eutectic sodium-potassium alloy) coolant.[1] The core has a volume of about six liters and is surrounded by a natural uranium blanket. The curve labeled EBR-II describes the anticipated spectrum for a reactor of about sixty megawatts, using a medium-enriched uranium fuel (~50%), steel cladding and sodium coolant.[2] The core now has a volume of about fifty liters and again is surrounded by a natural uranium blanket. The curve labeled PBR applies to a possible full-scale, fast power breeder reactor, which might be fueled with a moderately enriched uranium fuel (15 to 20%) or a plutonium-U^{238} mixture. Again the cladding is presumed to be steel and the coolant to be sodium. Such a reactor might have a core volume of 800 liters and generate 600 or more megawatts of heat. In all three of the reactors the coolant occupies approximately half the volume of the core. For comparison with these three calculated curves the fission spectrum has also been plotted in Fig. 1 (the dashed line). All curves have been normalized to a total area of unity. All are expected to have the shape of the fission spectrum at high energies.

Perhaps the most interesting aspect of the comparison lies in the relatively small displacement of the flux peak over the wide span of reactors considered. However, the amounts of higher energy neutron flux relative to the peak differ considerably. If one computes the median point for fissions in U^{235} for these spectra (the energy below which half the total fissions in U^{235} would occur), one finds a distinct difference. These median points are noted on the curves of Fig. 1 by the vertical arrows.

As shown in Fig. 2, fission cross sections for the primary fuels in the fast region lie between one and two barns, compared to the many hundreds of barns at thermal energies. A high capture cross-section ma-

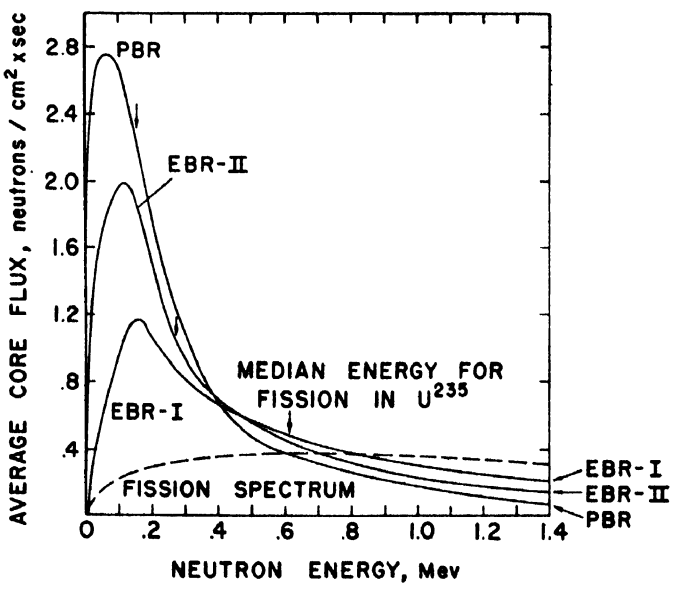

Figure 1. Comparison of neutron energy spectra of small (EBR-I), intermediate (EBR-II) and large (PBR) fast power-breeder reactors

* Argonne National Laboratory. Including work primarily by R. Avery, H. H. Hummel, and D. Okrent, Argonne National Laboratory; B. Carlson, G. Hansen, and H. C. Paxton, Los Alamos Scientific Laboratory.

terial like U^{238} has values between 0.1 and 0.3 barn in the region of major interest. A high total cross-section material like uranium has values between 7 and 13 barns over this region compared to a much higher number for water at thermal energies.

As a consequence, the characteristics of fast reactors are much different. A relatively small, light water, thermal reactor like the Experimental Boiling Reactor No. 1,[3] having a core volume of 92 liters, has a critical mass of approximately 3.6 kilograms of U^{235}. A fast power reactor of the same core volume would have a critical mass more than fifty times greater. This huge value makes high power densities a prerequisite for a fast power reactor. It also means that initial physics experiments will generally be done on very small systems, where the critical mass will fall in the range of available fissionable material. Such a system might have core dimensions equivalent to only a few mean free paths.

CALCULATION METHODS

As will be shown in the following, diffusion theory is fairly accurate in predicting both flux distribution and critical mass for the larger assemblies of primary design interest. Because of this and in view of its ready applicability to various geometries, this method has been used for design work thus far. Multigroup problems are solved numerically[4–7] on computing machines, using the fission-source iteration technique. For analysis of concentrated integral experiments, more sophisticated methods are required, some of which are discussed below.

The first of these methods to be mentioned is that of numerical integration of the integral Boltzmann equation, carried out in spherical geometry by B. Carlson. This is a straightforward procedure in which the assembly is divided into spherical shells, over each of which the flux is assumed constant. It becomes prohibitively complicated unless transport cross sections (see Appendix for definitions) in all regions for a given group are identical and unless the transport approximation is made. This is a semi-empirical recipe in which scattering is assumed isotropic and the total cross section is replaced by the transport cross section. This method is referred to in the following as "integral theory." No data on the accuracy of the method as a function of shell thickness are available.

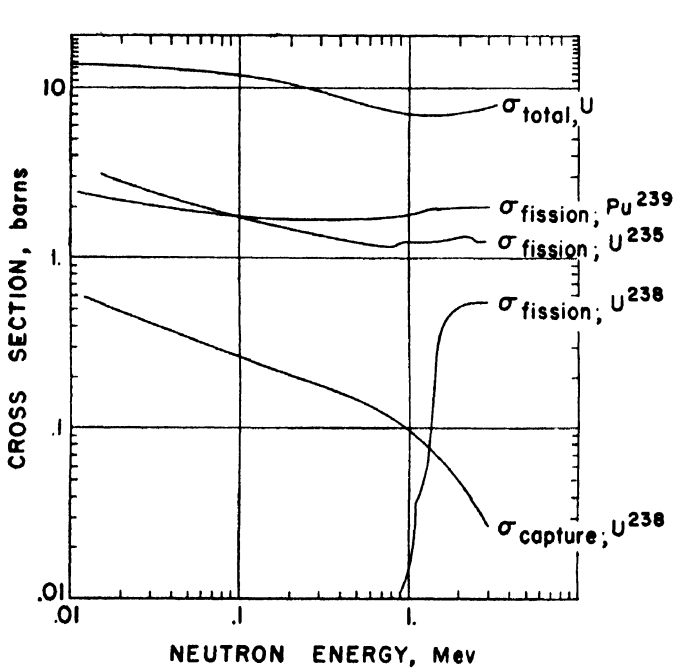

Figure 2. Cross sections for U^{235}, U^{238} and Pu^{239} as a function of energy

Second to be mentioned is the multigroup Serber-Wilson method. The problem of extending asymptotic diffusion theory to the multigroup case has been discussed by B. Davison.[8] The difficulty of having an insufficient number of asymptotic roots to satisfy the boundary conditions was circumvented by B. Carlson by a technique of triangularization of the matrices, the eigenvalues of which provide the desired roots. Carlson found that the accuracy of this method for determination of the critical radius is about the same as for a one-velocity calculation. However, the fluxes compared unfavorably with integral theory.

Another way that the problem of insufficient asymptotic solutions can be dealt with is to use the fission-source iteration technique. In this case only asymptotic solutions for single groups are required. The case of a spherical core with a finite spherical reflector has been treated.[9] The calculation is done analytically; reiteration is accomplished by fitting the fission source in the core and that in the reflector each with a single harmonic.

Last to be discussed is the S_n method of B. Carlson.[10] In this the integro-differential Boltzmann equation is integrated over angle by assuming the angular dependence of the flux to be linear in each of n intervals. One is led for each group to $n + 1$ ordinary differential equations which are integrated numerically in sequence to obtain $n + 1$ functions describing the flux at $n + 1$ angles. Boundary conditions in going from one region to another are obtained simply by requiring continuity of these functions. Either spherical, cylindrical or plane geometry can be used. Anisotropic scattering and time dependence can be included. The technique is thus comparable to the spherical harmonics methods in generality of application, but is much easier to use. The multigroup spherical harmonics method itself has not been programmed for computing machines because of its complexity.

Carlson compared the critical radii obtained by the S_4 method, the Serber-Wilson method and the extrapolated end-point method[11,12] for a variety of small assemblies, using one velocity group. The extrapolated end-point method is known to be very accurate and was used as a standard. In general, for reflected spheres, the error of the S_4 method in determining the radius ranged between -0.7 and -1.1%, while the error of the Serber-Wilson method ranged between -1.4 and -2.2%. The accuracy of the S_n method was improved by a factor of 2 on going from the S_4 to the S_6 approximation. Even S_2 was found to be much better than diffusion theory. Of particular interest is that the flux shape was already well defined in the S_4

approximation.

The S_n method had been programmed by Carlson in spherical geometry for the IBM Type 701 calculator in a multigroup form and hence was available for a detailed comparison with diffusion theory. A number of calculations were made, using both three and ten groups, over a wide range of reactor sizes, with some variance in composition. In each calculation the radius of the core was varied until criticality was obtained. The transport approximation was used in these calculations.

The ratio of critical radii for the two methods (diffusion theory to S_4) is plotted as a function of the critical radius by the S_4 method in Fig. 3. We see that for a reactor like EBR-I, having a core radius of roughly 10 cm, diffusion theory predicts a radius 9% too high. For a reactor like EBR-II, with a radius of about 25 cm, however, the error is down to 2 or 2.5%. For a large-scale reactor, diffusion theory and the S_4 method agree on critical radius.

Calculations were also made by the multigroup Serber-Wilson method[9] for some of the reactors used in deriving Fig. 3. It was found that over the range of core radii up to 22 cm, the error in critical radius relative to the S_4 method was -0.5 to -1.0%.

Of course, in an engineering design or in the analysis of experiment, not only the critical mass but also the spatial variation of flux is of considerable interest. Hence, detailed comparisons of the fluxes predicted by the three methods have been made in the multigroup case. In the following are presented results for three power reactors. Reactor I resembles EBR-I, Reactor II is similar to EBR-II, and Reactor III represents a large-scale power reactor. The problem specifications are given in Table I. Three energy groups were used, as follows:

Group	*Energy range, Mev*
1	∞–1.4
2	1.4–0.4
3	0.4–0

Fluxes computed by the S_4 method for the three

Table I. Problem Data for Three-Group Comparison Calculations

	σ_{tr}, cm^{-1}	*To*	*From transfer cross section, cm^{-1}* *1*	*2*	*3*
Reactor I					
Core:	0.140293	1	0.105563	0.037600	0.051444
Critical radius by the	0.175530	2	0.058735	0.153807	0.031342
S_4 method = 10.96 cm	0.284164	3	0.017926	0.020085	0.249021
Reflector:	0.138177	1	0.085857	0.000661	0.000396
R = 48.37 cm	0.172943	2	0.053424	0.153431	0.000242
	0.284164	3	0.016607	0.016572	0.278893
Reactor II					
Core:	0.108744	1	0.075832	0.012521	0.016966
Critical radius by the	0.142448	2	0.040047	0.127197	0.103336
S_4 method = 21.62 cm	0.222568	3	0.012357	0.013720	0.209136
Reflector:	0.170934	1	0.104158	0.000946	0.000568
R = 61.80 cm	0.207081	2	0.070350	0.181536	0.000346
	0.354240	3	0.021838	0.021390	0.346748
Reactor III					
Core:	0.107109	1	0 071826	0.004981	0.004685
Critical radius	0.141092	2	0.038873	0.127229	0.002851
= 48.86 cm	0.220507	3	0.012051	0.012761	0.215100
Reflectors:	0.170934	1	0.104158	0.000946	0.000568
R = 87.10 cm	0.207081	2	0.070350	0.181536	0.000346
	0.354240	3	0.021838	0.021390	0.346748

Table II. Energy Spectra at Center of Core*

Group	*Reactor I*			*Reactor II*			*Reactor III*	
	S_4	*D.T.*	*S.W.*	S_4	*D.T.*	*S.W.*	S_4	*D.T.*
1	0.958	0.921	0.965	0.636	0.621	0.640	0.308	0.306
2	1.249	1.227	1.241	1.190	1.169	1.194	0.901	0.896
3	0.793	0.852	0.794	1.174	1.210	1.166	1.791	1.798

* S_4 indicates the S_4 method, *D.T.* indicates the diffusion theory, *S.W.* indicates the Serber-Wilson method.

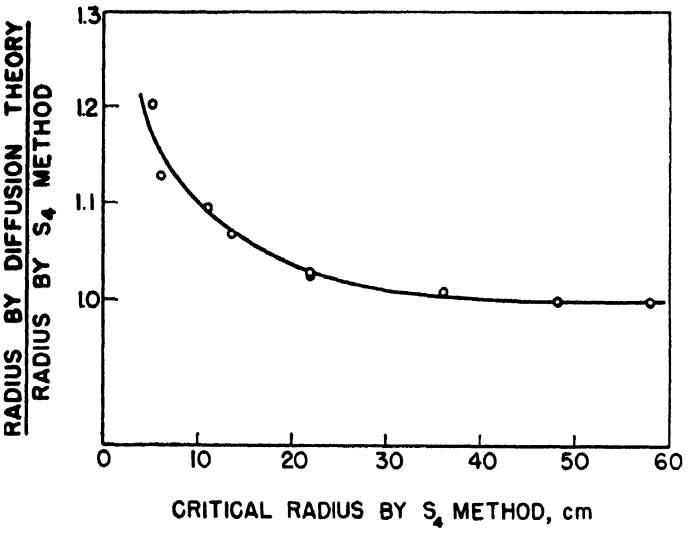

Figure 3. The ratio of critical radii (diffusion theory to S_4) as a function of S_4 critical radius

reactors are shown in Figs. 4, 5 and 6. In Tables II and III are listed the errors in fluxes obtained by diffusion theory and Serber-Wilson relative to S_4. In Table II are tabulated group fluxes at the center of the reactor, normalized in each case to a total flux of three. In Table III are listed the errors in the flux shape, group by group. In each group for all methods, the flux has been normalized to unity at the center, and deviations then computed.

For these three examples the largest error for diffusion theory in the energy spectrum at the center of the core is 7%. This occurred for Reactor I, much better agreement being obtained for the larger reactors. The error in energy spectrum at the center by the Serber-Wilson method is less than 1% in all cases.

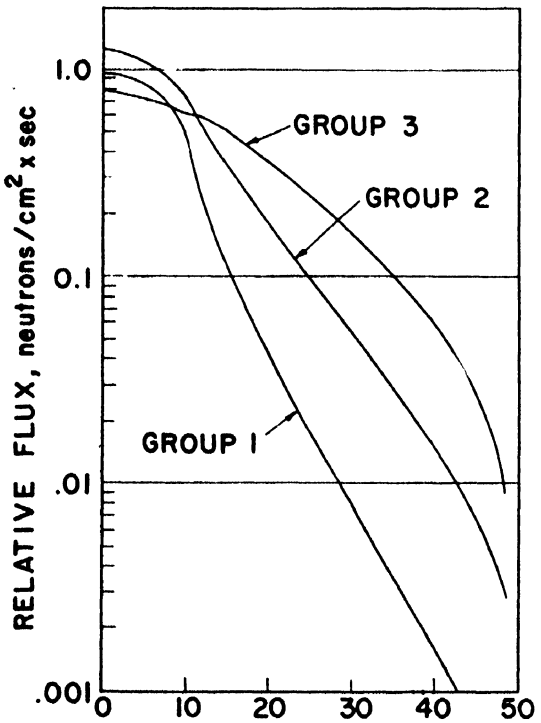

Figure 4. Three-group flux for reactor I by S_4 method: (core radius is 10.96 cm; reflector radius is 48.37 cm)

An examination of group fluxes as a function of radius shows that diffusion theory fluxes are considerably larger in the reflector for Reactor I, while agreement becomes fairly good for Reactor III. It is noted that in assemblies smaller than Reactor I, this ratio of fluxes has approached two in the reflector.

The Serber-Wilson fluxes exhibit the characteristic discontinuity at the core-reflector interface. Away from the boundary they are closer to S_4 than to diffusion theory. However, for group 1, the flux in the reflector is not very satisfactory, apparently because of the impossibility of adequately representing this flux with asymptotic solutions. Deviation of the Serber-Wilson flux from S_4 for more concentrated assemblies is similar to that for Reactor I. The flux discontinuity at the interface for group 1 ranges up to a factor of 2.5.

Since these three methods have been programmed for different computing machines, only a rough comparison of relative computing times is possible. The following table gives some estimates for the three-group problems.

Method	*Machine*			
	IBM CPC	*UNIVAC*	*AVIDAC*	*IBM 701*
Diffusion theory	20 hr	10 min		1.5 min*
Serber-Wilson	10 hr		50 min	10 min*
S_4				15–30 min

* Estimated.

The time required for the Serber-Wilson method on the AVIDAC (Argonne's electronic digital computer) is based on five iterations at 10 minutes each. For three-group diffusion theory, using a step function first-source guess for the various regions, a total of about ten iterations at one minute each is usually sufficient to bring convergence on flux shape and criticality. A brief outline of the multigroup diffusion theory method is presented in the Appendix. This calculation has been programmed[13] for the UNIVAC in three one-dimensional geometries: spherical, cylindrical (axially bare) and slab (radially bare). Up to twenty groups can be used on the program, but something between six and ten seems quite adequate to describe a fast spectrum.

The staff at Knolls Atomic Power Laboratory (KAPL) have recently programmed the two-dimensional diffusion theory problem for the UNIVAC. The machine time required per problem is considerably greater, of course. A two-group problem, employing 600 mesh points, requires 30–60 minutes for a single iteration on fission source. However, since machines presently under construction are expected to be more than ten times faster than the UNIVAC, it should become quite feasible to carry out two-dimensional diffusion theory and one-dimensional S_n problems on a routine basis.

The Serber-Wilson method does not appear to offer sufficient advantage over S_n in either computing time

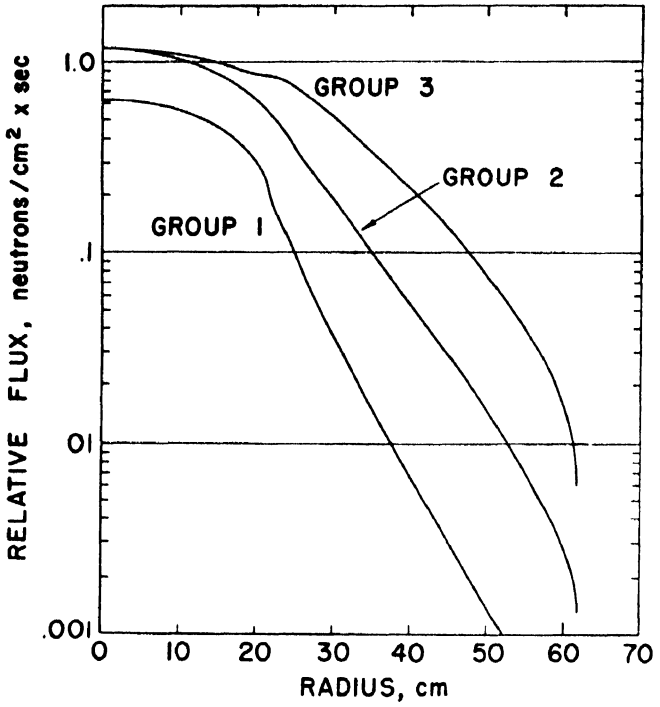

Figure 5. Three-group flux for reactor II by S_4 method: (core radius is 21.62 cm; reflector radius is 61.80 cm)

or ease of coding to offset its relative inflexibility and poorer accuracy for fluxes. It has not proved possible to use it at all for assemblies larger than Reactor II because certain exponential integrals could not be evaluated for the resulting ranges of arguments. Its one advantage is its possible use with computing machines of limited storage capacity. The AVIDAC has only a 512-word memory, including space for orders.

It is possible to make significant progress in fast-reactor design studies without high-speed computing equipment. Most of the major design characteristics evolving from early one- and two-group calculations have withstood comparison with those based on multi-group calculations surprisingly well.

In addition, there is a valuable multigroup technique which can be readily performed in a few hours with the aid of only a desk computer. Specifically, the flux behavior in an unreflected fast system can be characterized rather well by use of a single spatial mode. (This would be rigorous if the extrapolation distance were energy independent.) One can therefore find the neutron energy spectrum and material buckling (B^2) of such a system by space-independent calculations. One limits the more general equations in the Appendix by assuming

$$\nabla^2\phi_j(r) = -B^2\phi_j(r) \qquad (1)$$

and

$$\phi_j(r) = \phi_j F(r) \qquad (2)$$

for all j, resulting in a set of N algebraic equations. Here N is the total number of groups and $\phi_j(r)$ is the total flux in group j at the general spatial coordinate position r. These can now be solved by assigning an arbitrary fission source, making a first guess on buckling, and iterating on the latter until the calculated fluxes produce the assigned fission source within the desired accuracy.

The value of this method is not limited to bare cores. For a reflected fast reactor of simple geometry and of intermediate or large size, the flux in most of the core is characterized by the fundamental mode and the true average core spectrum is similar to that predicted by analysis of the equivalent bare core. Thus one can obtain core spectra in this manner for use in assigning cross sections for one- or two-group multi-dimensional calculations.

For analyses of small, bare, fast critical assemblies, one replaces the diffusion theory fundamental mode solution by the corresponding asymptotic solution of the Boltzmann equation; that is, the diffusion theory group leakage term,

$$\frac{B^2}{3\Sigma_{tr,j}}$$

Table III. Flux Relative to S_4 Flux*

r, cm	Group 1 S.W.	Group 1 D.T.	Group 2 S.W.	Group 2 D.T.	Group 3 S.W.	Group 3 D.T.
Reactor I						
0	1.00	1.00	1.00	1.00	1.00	1.00
5	1.00	1.00	1.00	1.00	1.00	1.01
10	1.12	1.00	1.03	1.03	1.00	1.10
10.96	1.38	1.13	1.07	1.11	0.97	1.10
10.96	0.62	1.13	0.90	1.11	1.03	1.10
13	0.74	1.34	0.93	1.18	1.00	1.11
15	0.88	1.42	0.94	1.23	1.00	1.14
20	1.00	1.50	0.98	1.30	1.00	1.20
25	1.03	1.52	1.00	1.34	1.03	1.23
30	1.18	1.52	1.00	1.39	1.07	1.30
35	1.27	1.52	1.05	1.42	1.08	1.30
40	1.33	1.66	1.07	1.39	1.08	1.30
45	1.41	1 63	1.00	1.32	1.08	1.32
Reactor II						
0	1.00	1.00	1.00	1.00	1.00	1.00
10	1.00	1.00	1.00	1.00	1.00	1.00
20	1.12	1.00	1.00	1.01	0.98	1.06
21.62	1.35	1.08	1.04	1.09	0.95	1.06
21.62	0.70	1.08	0.95	1.09	1.05	1.06
25	0.85	1.25	0.95	1.11	1.02	1.08
30	0.95	1 22	0.95	1.15	1.04	1.09
35	1.00	1.18	0.98	1.23	1.04	1.12
40	1.09	1 21	1.00	1.25	1.09	1.17
45	1.23	1.35	1.04	1.25	1.12	1.23
50	1.40	1.54	1.09	1.27	1.18	1.27
Reactor III						
0		1.00		1.00		1.00
20		1.00		1.00		1.00
40		1.00		1.00		1.00
48.8		1.05		1.03		1.03
52		1.15		1.09		1.03
60		1.04		1.09		1.03
70		1.06		1.14		1.05
80		1.17		1.09		1.06

* *S.W.* indicates the Serber-Wilson method, *D.T.* indicates diffusion theory, S_4 indicates the S_4 method. All group fluxes are normalized to unity at $r = 0$.

is replaced by

$$\frac{B}{\tan^{-1}\left(\frac{B}{\Sigma_{tr,j}}\right)} - \Sigma_{tr,j}$$

where $\Sigma_{tr,j}$ is the macroscopic transport cross section for group j. This gives the spectrum and flux shape near the center of such an assembly quite well.

THE CROSS-SECTION PICTURE

This discussion of errors of one or two per cent in various methods of calculation is perhaps misleading. Our knowledge of methods of calculation, at least for simple geometries, unfortunately goes far beyond our knowledge of the microscopic cross sections required to compute actual designs or to predict experiments. In brief, our present state of information is the following. The fission cross sections of the primary heavy isotopes (U^{235}, U^{238}, Pu^{239}) are fairly well known. Total cross sections as a function of energy are well measured. Some data is available on the angular distribution of scattering in the important energy range. The technique is well developed and such data is rapidly accumulating. Important strides are being made in measurements of inelastic scattering, but the data available, particularly on the outgoing spectrum, is still only fragmentary. There are data on the capture cross sections of the activating isotopes, but data on the non-activating isotopes are essentially non-existent.

The fission curves of Fig. 2 are believed to be quite accurate (~5%) above 0.5 Mev. Below 0.5 Mev, however, considerable uncertainty exists, perhaps of the order of 20%. This is due primarily to the difficulty of measuring the incident flux absolutely at the lower energies,[14] so that an accurate, absolute measurement for one isotope can be made. Precise relative fission measurements for the remaining isotopes are essentially a straightforward matter, but some work, particularly below 0.5 Mev, is still required. Unfortunately, the lower energy region is where most fissions occur in the larger fast power reactors.

The capture cross section for U^{238} presented in Fig. 2 is of uncertain accuracy. These are fairly old measurements and the data miss the curve by as much as twenty per cent.

There have been essentially no direct monochromatic measurements of alpha ($\alpha = \sigma_{capture}/\sigma_{fission}$) for the primary fuels in this energy range. One attempt is currently being made, using the method of spherical shells, by R. L. Macklin of Oak Ridge National Laboratory. Since his detector is energy sensitive, he has restricted his measurements to the region between five and fifty kilovolts, where inelastic scattering should not interfere. Another approach is being planned at the Los Alamos Scientific Laboratory, using a large liquid scintillator.

Some measurements of alpha have been made by KAPL[15] in the intermediate energy range (a few kilovolts), but relatively few of the neutrons in a fast power reactor are expected to reach this low energy.

A limited set of alpha measurements has been made in EBR-I. By long-term, high power irradiation of samples originally depleted in the isotope resulting from capture, it is possible to generate enough of the secondary isotope that a mass spectrographic measurement[16] can be made. Then, if the fissions in the sample can be determined,[17] a measurement of alpha in the particular neutron energy spectrum present at this position has been accomplished.

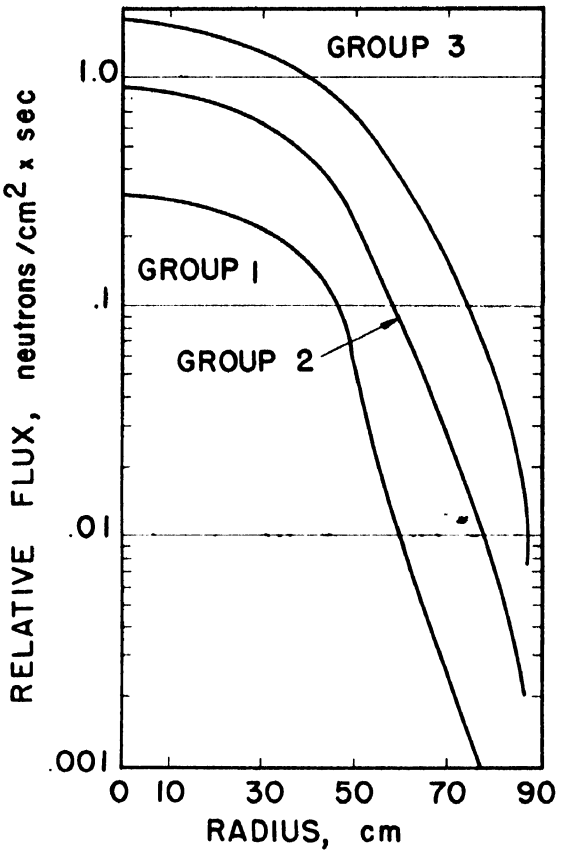

Figure 6. Three-group flux for reactor III by S_4 method: (core radius is 48.86 cm; reflector radius is 87.10 cm)

EBR-I consists of a highly enriched core with a natural uranium blanket, the latter being surrounded by a graphite reflector. Thus, the neutron energy spectrum varies widely through the reactor from almost fission spectrum to near thermal.

A summary of the alpha data for EBR-I is given in Fig. 7. Values for alpha of U^{235} are available in the core and for Pu^{239} in the blanket. These have been plotted as a function of radial position in the reactor. Also plotted are four curves intended to outline approximately the spectrum which has been calculated for various positions in the reactor. The vertical scale on the right gives the "lethargy" (natural logarithm of $10/E$ in Mev), and at each radial position these lines give the energies below which 10, 20, 50 and 80 per cent, respectively, of the fissions in a sample of U^{235} would occur. For orientation purposes, a few energies are marked on the lethargy scale.

Direct measurements have been and are being made on the spectrum at various positions. Accessibility problems and the inadequacy of existing techniques at lower energies make a completely experimental determination impossible. A new and more

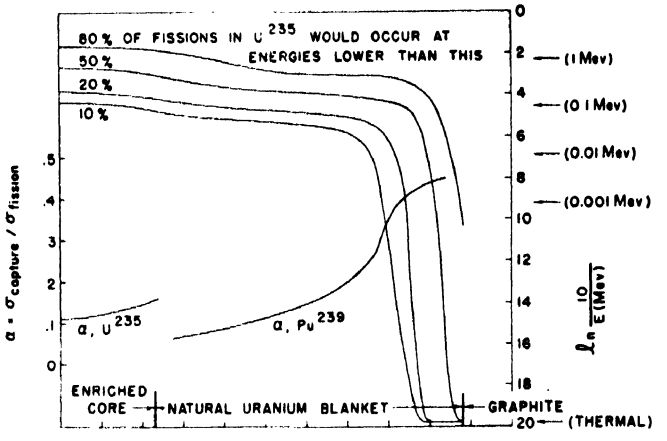

Figure 7. Variation of alpha and neutron energy spectrum in EBR-I

extensive set of irradiations is also in progress and should provide more precise measurements of alpha. In the previous experiment the determination of the fissions in plutonium was perhaps the most uncertain quantity, since radiochemical methods could not be applied.

The existing measurements do supply reassurance as to the likely value for alpha in a large-scale, plutonium-fueled, fast reactor. The spectrum of such is expected to match approximately that found at a radial position of about 25–28 cm in EBR-I, a smaller radius than that at which the sharp rise in alpha occurs. The data on U^{235} are currently limited to neutron energies considerably higher, however, so that the performance of a large reactor fueled with U^{235} remains in doubt.

The total cross section for uranium is given in Fig. 2; the other fissionable isotopes have almost identical cross sections in this energy region. The total cross sections for most materials have been measured[18] and limited data are available on angular distributions.[19] Extensive new measurements[20,21] are being made on elastic scattering, however, and relatively precise information should soon be available for reactor calculations.

Until very recently, there have been few accurate, direct measurements of inelastic scattering cross sections for materials of interest at energies of interest. Some spherical shell measurements[22] have been the primary source of useful data. It is noted that for an experiment similar to that of reference 22, Carter and Beyster have obtained values for a U^{238} shell of 2.0 barns, using a U^{238} fission detector, and 1.0 barn, using a Np^{237} fission detector. For a U^{235} shell the result with a U^{238} detector was 1.5 barns.

The tempo of measurement[20,23,24] has been increasing in this field, however, so that soon educated guesses, based on nuclear theory, will no longer be the major source for describing the energy degradation in fast reactors. It is to be hoped that an accurate measurement of where in energy the neutrons go upon inelastic scattering will be achieved soon. This is of particular interest for the major contributor to energy degradation, U^{238}. Its cross section just above threshold energies is of considerable interest, since it appreciably affects the neutron energy spectra of the larger, fast power reactors.

Capture cross sections for the structural materials, the fission products and other elements of possible interest remain largely unknown and difficult to measure. Most of the important isotopes do not activate, so that different methods are required. In principle, the method used to measure alpha in EBR could be used. In practice, the available flux, the attainable separation of isotopes and the relatively low capture cross sections make the measurement marginal. An irradiation is in progress on K^{39} and also on some Pu^{240}, prepared by extracting plutonium from curium following the alpha decay of Cm^{244}.

It is to be hoped that other approaches, using attenuation in spherical shells or capture gamma rays, will provide new data. Fortunately, there are theoretical and experimental signs of regular behavior in this energy range and most of the materials considered for structure or coolant in fast reactors appear to be rather innocuous. The measurements in a fission spectrum,[25,26] plus recent studies on level spacing and radiation widths by the staff of Brookhaven National Laboratory,[27,28] provide one with a rough insight into the variation of capture cross sections from isotope to isotope.

PERFORMANCE ESTIMATES

In the development program at Argonne National Laboratory for future fast power breeder reactors, attention has been largely focused on two separate reactors: PBR (Power Breeder Reactor) and EBR-II (Experimental Breeder Reactor II).

To illustrate the general nuclear characteristics of fast reactors and the considerations that are important in their design and evaluation as power breeder reactors, we give some results of specific calculations on these two reactors as well as more general parametric surveys.

The method of calculation used was one-dimensional, multigroup diffusion theory. In view of the cross-section uncertainties, the results are at best only qualitatively correct in indicating trends and approximate magnitudes.

The full scale reactor and the prototype are assumed to have the same composition except for fuel enrichment. A very useful parametric study thus results from calculating several reactors of this composition, with the enrichment a parameter varying over the entire range of interest. Table IV lists the steady state properties of spherical assemblies with four different Pu^{239} enrichments and two U^{235} enrichments. These include PBR and EBR-II with both types of fuel, and in addition a Pu^{239} assembly more concentrated than EBR-II and one intermediate in enrichment between PBR and EBR-II. The energy breakdown of the ten energy groups used in the calculations is included in the table. In all of these assemblies the following values were used:

	Pu^{239}	U^{235}	U^{238}	Fe	Na
Core volume fractions	← 0.32 altogether →			0.14	0.54
Blanket volume fractions	0	0	0.7	0.1	0.2

Blanket thickness—45 cm (including extrapolation distance)

The normalization corresponds to one fission neutron born in the core.

It is noted that the median fission energies of Table IV are considerably higher than those quoted for similar assemblies in Fig. 2, primarily because U^{238} fissions are included. These occur only at high energies, of course, raising the median point.

The fissions in U^{238} provide a bonus to breeding ratio, since a net gain in neutrons available for breeding results from this process without destruction of the primary fissionable isotope.

The fast fission bonus is determined primarily by what the fission neutrons see in their first collisions. If all the collisions above the U^{238} fission threshold are with U^{238} atoms, then the fast fission bonus is at a maximum. In general, however, the neutron may be degraded below the fission threshold by collisions with atoms other than U^{238}. The probability of this is determined essentially by the composition. The problem is complicated by the fact that neutrons may escape from the core at energies above the U^{238} fission threshold. For the assemblies we have been considering, the blanket has a higher density of U^{238} atoms than the core, and hence a higher probability for U^{238} fission by fast neutrons present. Thus, while for the small concentrated assemblies the fast fission bonus in the core is small, the increased fast leakage into the blanket just about compensates for this. In practice one finds that the fast fission bonus is relatively independent of core dilution for this type of assembly. This conclusion, of course, does not hold if one dilutes with a material other than U^{238}.

With the assumptions made on capture cross sections, the parasitic losses in the structural material are not very important.

The breeding gains, as calculated, are very encouraging. Aside from possible errors in cross sections, they will be reduced in actual operation by fission product captures and possibly by the control mechanism. The calculated critical masses will increase in

Table IV. Survey of Steady-state Properties of Reflected Spherical Assemblies of EBR II-PBR Composition with Various Enrichments

	Concentrated Pu^{239} fuel		*EBR-II Pu^{239} fuel*		*EBR-II U^{235} fuel*		*Intermediate Pu^{239} fuel*		*PBR Pu^{239} fuel*		*PBR U^{235} fuel*	
Core volume (liters)	12.5		50		50		200		800		800	
Core radius (cm)	14.4		22.85		22.85		36.28		57.59		57.59	
Ratio fuel atoms to U^{238} atoms	1.76		0.403		1.01		0.177		0.103		0.174	
Critical mass of fuel (kg)	43.1		82.7		150		178		446		712	
Flux integral for: *Group Energy interval (Mev)*	*Core*	*Blanket*	*Core*	*Blanket*	*Core*	*Blanket*	*Core*	*Blanket*	*Core*	*Blanket*	*Core*	*Blanket*
1 2.23–∞	2.60	2.55	3.58	1.78	3.45	1.71	4.40	1.11	4.99	0.62	4.89	0.61
2 1.35–2.23	2.32	2.91	3.45	2.11	3.34	2.04	4.51	1.36	5.31	0.77	5.23	0.77
3 0.498–1.35	5.33	13.42	9.43	10.72	8.94	10.19	14.33	7.51	18.84	4.55	18.40	4.48
4 0.183–0.498	4.11	20.29	8.59	17.34	8.04	16.37	15.25	13.51	22.72	8.54	22.09	8.37
5 0.0674–0.183	3.09	31.03	7.26	27.63	5.95	25.15	14.55	22.23	24.14	15.37	21.84	14.61
6 0.0248–0.0674	0.95	11.00	2.41	9.86	1.71	8.81	5.18	8.03	9.08	5.63	7.59	5.26
7 0.00912–0.0248	0.34	4.03	0.94	3.65	0.57	3.21	2.20	3.02	4.09	2.16	3.13	1.97
8 0.00335–0.00912	0.097	1.38	0.32	1.29	0.15	1.09	0.88	1.11	1.81	0.83	1.21	0.73
9 0.00123–0.00335	0.028	0.39	0.12	0.38	0.040	0.31	0.41	0.36	0.99	0.30	0.54	0.24
10 0–0.00123	0.005	0.094	0.031	0.099	0.005	0.072	0.15	0.11	0.46	0.11	0.16	0.067
Pu^{239} fissions	0.334	0	0.315	0	0	0	0.293	0	0.279	0	0	0
Pu^{239} captures	0.0399	0	0.0431	0	0	0	0.0463	0	0.0491	0	0	0
U^{235} fissions	0	0	0	0	0.372	0	0	0	0	0	0.328	0
U^{235} captures	0	0	0	0	0.0748	0	0	0	0	0	0.0758	0
U^{238} fissions	0.0128	0.102	0.0387	0.0740	0.0276	0.0711	0.0607	0.0476	0.0764	0.0271	0.0718	0.0268
U^{238} captures	0.0144	0.684	0.0662	0.604	0.0402	0.547	0.157	0.483	0.280	0.333	0.231	0.313
Na + Fe captures	0.0017	0.0054	0.0033	0.0044	0.0029	0.0042	0.0056	0.0036	0.0085	0.0024	0.0097	0.0023
Internal breeding ratio	0.039		0.187		0.090		0.464		0.855		0.571	
Total breeding ratio	1.87		1.89		1.31		1.89		1.87		1.35	
Ratio of fuel captures to fuel fissions	0.120		0.138		0.201		0.158		0.176		0.231	
Ratio of U^{238} fissions to fuel fissions	0.345		0.362		0.265		0.370		0.371		0.300	
Escape from blanket	0.075		0.052		0.048		0.032		0.017		0.017	
Median fission energy for all core fissions (Mev)	0.59		0.49		—		0.41		0.36		—	
Ratio of maximum to average core power	1.27		1.40		1.36		1.61		1.87		1.84	
Buckling (cm^{-2})	0.01190		0.00656		—		0.00346		0.00173		—	
Reflector savings (cm)	14.4		16.0		—		17.1		17.9		—	

practice, first because the fission cross sections used herein are slightly higher than currently accepted, secondly because no allowance has been made for over-riding long term reactivity losses, and thirdly because of the geometrical idealization of the calculation. A practical design will probably be cylindrical, will have a moderate density blanket section next to the core for heat transfer reasons, will have low density regions near the core in order to get the sodium in and out, etc.

The high maximum-to-average power ratio in the core is of considerable concern, particularly that portion in a direction transverse to the coolant flow. For the large reactors, this transverse maximum-to-average power ratio is about 1.6. A possible method of flattening this transverse power is to vary the concentration of plutonium across the core. By reducing the concentration at the center, where the flux is high, and raising it at the edge, a marked reduction in this ratio can be achieved, with only a small increase in critical mass. For example, in the large reactor, the transverse maximum-to-average power ratio can be reduced to a value of 1.1, with an increase in critical mass of only ten per cent, if one varies the core enrichment in steps, using five concentric annuli.

The actual reactivity losses due to high power operation will be a complicated function of unloading schedules. To obtain an estimate of the magnitude of such effects, the long term changes were determined between the initial clean reactor and conditions after a two per cent average burnup by fission of the combined total atoms of U^{238} and Pu^{239} in the core. The reactivity effects associated with such a burnup are presented in Table V, in units of $\delta k/k$.

Table V. Long Term Reactivity Effects in Units of $\delta k/k$ for PBR and EBR-II, Resulting from Two Per Cent Burnup of Core Alloy (U^{238} and Pu^{239})

	PBR	*EBR-II*
Net Pu^{239} removed from core	−0.0186	−0.0328
Pu^{239} added to blanket	0.0098	0.0084
Fission product formation	−0.0104	−0.0018
Total of all effects	−0.0192	−0.0262

One can also express the results in terms of the extra loading of fuel needed to compensate for the net, long-term reactivity loss. In both PBR and EBR-II, $\delta k/k \sim \frac{1}{2}\delta M/M$, where $\delta M/M$ represents a fraction of the critical mass uniformly distributed over the core. Thus, for both reactors, four to five per cent would have to be added to the critical mass if the reactor operation envisaged were that used for the calculation.

The effect of this accrual of fission products on breeding gain should be small. It is estimated that the parasitic capture rate at the end of this buildup would reduce the breeding gain by 0.04 in PBR and by 0.01 in EBR-II.

The control system would have to handle these losses in reactivity, as well as those due to heating, the normal shutdown requirements, and a possible Doppler effect.[29]

For PBR, the reactivity change associated with a uniform expansion is given by $(\delta k/k)/(\delta V/V) \sim -0.3$. In going from cold to hot operation the volume might increase by 1 to 2 per cent, yielding a reactivity loss of ~0.3 to 0.6 per cent. For EBR-II, $(\delta k/k)/(\delta V/V) \sim -0.5$ yielding a reactivity loss of ~0.5 to 1 per cent.

In PBR, the effect of Na density on reactivity is given by $(\delta k/k)/(\delta \rho/\rho)_{Na} \sim 0.02$ and in EBR-II by $(\delta k/k)/(\delta \rho/\rho)_{Na} \sim 0.05$. The Na density will decrease by 10 or 15 per cent in going from cold to hot, giving a reactivity loss of ~0.2 per cent in PBR and ~0.5 per cent in EBR-II.

The possible methods of control include interchange of fuel with U^{238}, insertion of poison (B^{10}), and the use of various reflectors between core and blanket. The thermal reactor concept of a "black" control rod has no place in fast reactors. One of the strongest poisons, B^{10}, has a capture cross section of only two barns at 100 kilovolts, so that large amounts would be required.

To obtain, say, a reactivity decrease of one per cent in PBR, one would have to interchange 7 kg of U^{238} with an equal volume of B^{10} (density 2.5 grams per cm^3) at the center of the core. At the core-blanket interface, ten times as much material would be needed for the same reactivity. For the same amount of U^{238}, a U^{238}-Pu^{239} interchange is about twice as effective as a U^{238}-B^{10} interchange with, of course, a reversal in sign. The relative worth between the center of the core and the core-blanket interface is also approximately ten for the U^{238}-Pu^{239} interchange in PBR. All of the above estimates were made in cylindrical geometry, the changes being made uniformly along the axial direction.

For the smaller reactors, reflector control appears feasible. For EBR-II, it is calculated that a nine-cm thick steel or high density uranium reflector would lose about 12% $\delta k/k$ upon substitution of the sodium coolant in its place; this is for a cylindrical reflector completely surrounding the reactor except at the ends. For PBR, however, this number is cut by a factor of eight or more for the same thickness reflector. This is due to the reduced importance of neutron leakage to the reactivity of the larger reactor. Further, the use of a reflector made of steel or some other non-fertile material introduces large masses of a possibly strong parasite. If its capture cross section is presently unknown, it may prove to be considerably higher than anticipated, resulting in a significant loss in breeding ratio. Also, a non-fertile reflector next to the core would reduce the fission of U^{238}.

The neutron lifetime, l, of these reactors can be calculated readily, employing the relation

$$l = (\delta k/k)/C \qquad (3)$$

where $\delta k/k$ is the loss of reactivity associated with the uniform insertion of a $1/v$-absorber with macroscopic capture cross section C/v. The results of such a calculation for the four plutonium-fueled assemblies of Table IV are plotted in Fig. 8 as a function of plu-

Table VI. Parametric Survey of Core Com

Assembly number	1	2	3	4	5	6	7	8	9	10	11	12
Core radius (cm)	20	20	20	20	20	20	20	20	20	50	50	50
Volume fraction Na	0.8	0.8	0.8	0.5	0.5	0.5	0.2	0.2	0.2	0.8	0.8	0.8
Volume U^{235} / Volume U^{238} + Volume Fe	1	0.5	0	1	0.5	0	1	0.5	0	1	0.5	0
Critical mass Pu^{239} (kg)	154.7	157.3	160.3	149.1	151.0	153.7	155.6	153.7	150.6	413.8	413.9	420.8
												Flux Integral
Group Energy interval (Mev)												
1 2.23–∞	5.23	5.48	5.76	3.37	3.78	4.30	2.47	2.85	3.37	7.70	8.52	9.51
2 1.35–2.23	5.70	5.86	6.02	4.11	4.43	4.81	3.15	3.49	3.93	9.29	9.96	10.72
3 0.498–1.35	11.03	11.52	12.04	8.53	9 71	11.21	6.79	8.11	10.03	19.17	21.46	24.26
4 0.183–0.498	10.13	10.70	11.31	9.36	11.42	14.57	8.14	11.04	16.98	20.39	24.07	29.15
5 0.0674–0.183	11.14	10.82	10.46	13.33	12.77	11.72	14.10	13.80	12.53	25.47	25.01	24.02
6 0.0248–0.0674	3.68	3.70	3.68	3.83	4.24	4.37	3.47	4.48	4.95	9.94	10.41	11.46
7 0.–0.0248	1.77	1.89	1.98	1.28	1.76	2.29	0.814	1.48	2.51	7.46	9.24	11.04
U^{238} core fissions / Fuel fissions	0 099	0.049	0	0.281	0.140	0	0.388	0.193	0	0.245	0.122	0
U^{238} blanket fissions / Fuel fissions	0.307	0.305	0.304	0.215	0.215	0.214	0.157	0.157	0.160	0.142	0.142	0.144

tonium concentration in the core. The calculated lifetime is 0.8×10^{-7} sec for EBR-II and 1.7×10^{-7} sec for PBR.

To determine the influence of the blanket, the lifetimes were also evaluated for the equivalent bare core as a function of enrichment and are shown in Fig. 8, curve (*b*).

The effect of the blanket on the lifetime decreases with increasing core size. This result is reasonable physically, since for the larger core size a smaller fraction of the neutrons causing fissions have spent part of their lifetime diffusing in the blanket.

The very short neutron lifetimes will result, of course, in extremely short reactor periods even for reactivities only slightly above prompt critical. In the design therefore, one must try to insure, insofar as possible, against the reactor becoming prompt supercritical. One must also try to guarantee that there is a very rapidly acting negative temperature coefficient to shut down the reactor in the event of prompt supercriticality. Expansion of the fuel seems the most likely mechanism.

To provide some estimate of the effects of quite large departures from the reference design of PBR, a series of twenty-seven assemblies of varying core composition and size were calculated. The problem parameters and results are given in Table VI.

The calculations, using seven energy groups, were all made in cylindrical geometry. The same equivalent bare height (121.44 cm) was used in all problems, and for critical mass purposes it was assumed that the axial reflector savings was 2 by 15 cm. The blanket composition was 0.7 U^{238}, 0.1 Fe and 0.2 Na and the blanket thickness was 60 cm. Core radii of 20, 50 and 80 cm were investigated and for each radius, Na volume fractions of 0.8, 0.5 and 0.2 were considered. For each of the resulting assemblies, it was assumed that the diluent for the Pu^{239} fuel was either all U^{238},

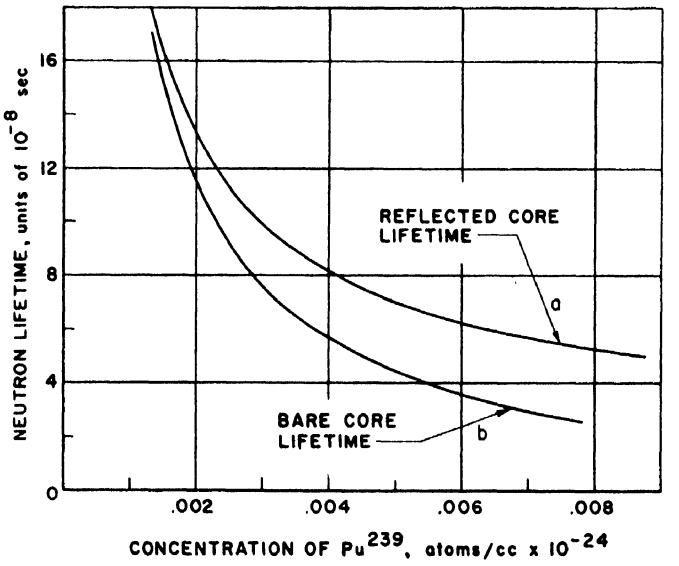

Figure 8. Neutron lifetime vs concentration of Pu^{239} atoms: (a) with reflected core, (b) for equivalent bare core

half U^{238} and half Fe, or all Fe. The amount of fuel was determined by criticality.

The flux normalization is on the basis of one fission neutron born in the core. The group-energy breakdown used in these calculations is given in Table VI on pages 356 and 357.

The results are perhaps of most value in providing some insight into the change of neutron energy spectrum with core composition. They also provide information on the relative effects on critical mass of Na, Fe and U^{238}, uniformly distributed over the core, for each core size.

This is not an all inclusive list, of course. Oxide fuel elements are another possibility, for example. Cores of this type would contain less U^{238}, and have considerably more moderating action. The net effect on the neutron energy distribution, compared to the

position of Reflected Cylindrical Assemblies

13	14	15	16	17	18	19	20	21	22	23	24	25	26	27
50	50	50	50	50	50	80	80	80	80	80	80	80	80	80
0.5	0.5	0.5	0.2	0.2	0.2	0.8	0.8	0.8	0.5	0.5	0.5	0.2	0.2	0.2
1	0.5	0	1	0.5	0	1	0.5	0	1	0.5	0	1	0.5	0
485.9	452.5	396.5	596.0	530.6	405.7	817.3	792.7	772.7	1067.6	951.4	743.8	1381.0	1207.8	800.9
for Core														
4.12	4.82	5.81	2.80	3.33	4.14	8.42	9.47	10.82	4.28	5.06	6.21	2.86	3.42	4.31
5.39	6.06	6.97	3.76	4.30	5.08	10.45	11.38	12.52	5.67	6.47	7.56	3.86	4.45	5.34
11.84	14.50	18.69	8.42	10.69	14.63	22.06	25.37	29.75	12.61	15.81	21.06	8.72	11.20	15.79
14.75	21.03	36.09	11.10	17.31	37.75	24.60	30.51	39.86	16.15	24.15	46.08	11.69	18.73	45.53
26.72	27.88	28.55	24.29	26.53	28.92	32.62	32.89	32.66	31.16	33.95	37.75	26.84	30.08	35.98
8.58	11.24	13.80	6.30	10 14	15.21	13 50	14.70	15 44	10.33	14.51	19.87	7 06	11.95	20.65
3.47	6.84	14.59	1.53	4.28	15.17	11.82	16.22	22.16	4.39	9.91	28 14	1.76	5.34	26.34
0.431	0.216	0	0.511	0.256	0	0.294	0.148	0	0.469	0.236	0	0 538	0.268	0
0.081	0.080	0.082	0.051	0.050	0.054	0.082	0.082	0.082	0.048	0.041	0.043	0.031	0.036	0.027

typical PBR design, would be roughly as follows. Above 0.5 Mev about the same per cent of neutrons would exist, but the lower end of the spectrum would shift downwards in energy. The median energy for the fission in U^{235} in the spectrum moves from about 0.155 Mev in the metal-fueled PBR to about 0.095 Mev in an oxide-fueled assembly of the same size.

The critical mass would be reduced by 15 to 20% for the oxide case, partly because of the rise in fission cross section with lowering of neutron energy and partly because of the removal of some U^{238}. For these large reactors, the uniform removal of some U^{238} from the core adds reactivity, for its capture cross section has become paramount.

EXPERIMENTAL RESULTS AND THEIR COMPARISON WITH THEORY

The major experimental results available are on fairly small U^{235} systems. The health hazards of plutonium-handling, the large critical mass of big assemblies, and the relative safety and ease of the smaller U^{235} experiments have combined to make these the primary source of data. A number of small uranium assemblies in simple geometry have been examined by H. Paxton, *et al.*, and are reported in Table VII. For the reflected experiments, the reflector was normally dense natural uranium in all cases, infinitely thick insofar as critical mass was concerned.

A limited number of these assemblies have been calculated by G. Hansen, using six-groups in the S_4 approximation, with rather good success in predicting critical radius. Multigroup diffusion theory has been applied fairly extensively, using six and ten groups, with some variation in the more uncertain cross sections. The fairly consistent result has been that diffusion theory predicts too large a critical radius for these systems, and the variance from experiment

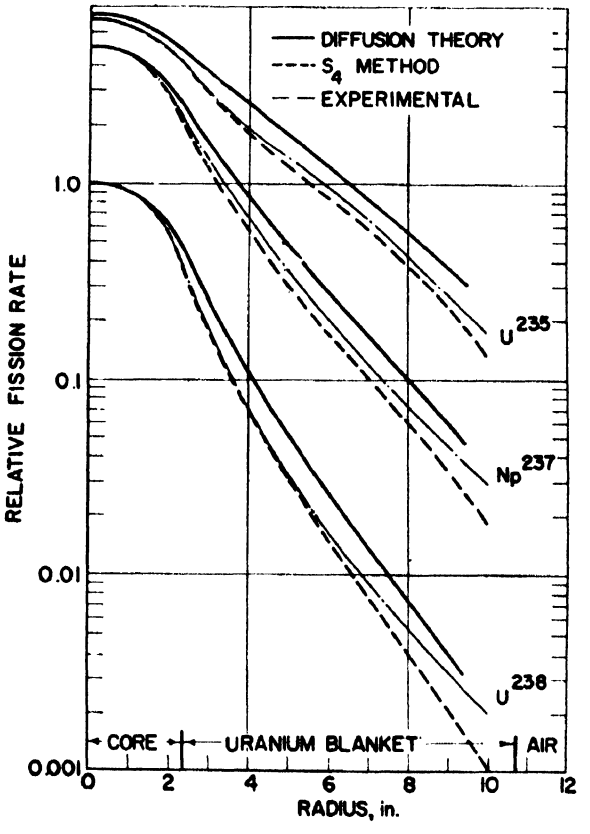

Figure 9. A comparison of experimental relative fission curves with the predictions of S_4 and diffusion theory for the Topsy reactor

bears a close resemblance to the variance of diffusion theory from the S_4 method given in Fig. 3.

Calculated power distributions and neutron energy spectra agree fairly well with experiment, where available. In Fig. 9 is plotted a comparison of experiment with the S_n method and diffusion theory for assembly No. 5 of Table VII, the so-called "Topsy" reactor. The comparison is made on the basis of the relative

Table VII. Experimental Values of Critical Mass

A. Bare Assemblies

Assembly number	Geometry	Atoms U^{235} / Atoms U	Critical mass U^{235} (kg)	Void fraction
1	Sphere	~0.9	49	—
2	Cylinder (R = 13 cm)	0.54	87	—
3	Cylinder (R = 13 cm)	0.38	100	—
4	Cylinder (R = 14.5 cm)	0.29	123	—

B. Assemblies with Thick Natural Uranium Reflectors

Assembly number	Geometry	Atoms U^{235} / Atoms U	Critical mass U^{235} (kg)	Void fraction
5	Sphere	~0.9	16	0
6	Sphere	~0.9	20	0.15
7	Sphere	~0.9	25	0.3
8	Sphere	~0.9	37	0.5
9	Sphere	0.80	18	0
10	Sphere	0.68	21	0
11	Sphere	0.47	27	0
12	Cylinder (R = 19.3 cm) (contains by volume fraction) U 0.30, Fe 0.14, Al 0.54	0.54	93	0.02

fission rates for three heavy isotopes. The experimental results and both calculations have been arbitrarily normalized to a value of unity at the center for fission in U^{238}. The calculations in Fig. 9 were based on six-group cross sections, prepared by Hansen without relying on any information drawn from other critical assemblies. He concluded that agreement between the S_4 method and the detector measurements is comparable to the agreement among different measurements.

The agreement is very good in this example, even for diffusion theory, which missed the critical radius considerably. The S_4 calculation was within 1% of critical radius, while diffusion theory predicted a k_{eff} of only 0.89 for a reactor having the experimentally critical mass (k_{eff} = 1 at critical).

The results of Fig. 9 demonstrate the tendency for the diffusion theory flux to lie above the S_4 flux in the reflector or blanket, particularly for the smaller assemblies. Also illustrated is the failure of diffusion theory flux to bend sharply down at the core-reflector interface, as does S_4. Angular distributions available from the S_4 calculations show that the basic criterion of the validity of diffusion theory is strongly violated in this region; that is, $\overline{\mu^2}$ (the square of the neutron direction cosine, averaged over angular distribution) over most of the core is close to one-third, the value it must have at the center because of spherical geometry. As the core-reflector interface is approached, $\overline{\mu^2}$ rises very sharply, particularly in the highest energy group, and then falls off out in the reflector. Diffusion theory, on the other hand, requires a zero spatial derivative of this quantity to be applicable, rigorously.

Hansen and Carlson have also obtained rather good agreement with experiments on a bare, enriched uranium sphere, assembly No. 1 of Table VII, the so-called "Godiva" reactor. Both the S_4 method and integral theory gave good results. Hansen also performed a spherical harmonics analysis on the reactor. Using a three-group treatment in the P_3 approximation he obtained a critical radius 1% greater than integral theory gave with the same cross sections. Integral theory, in turn, predicted a critical radius about 1½% greater than experiment. Despite this 2½% deviation of the P_3 calculation from the experimentally critical radius, the calculation did give excellent agreement with measured fission rate distributions for U^{235} and U^{238}, as can be seen in Fig. 10. In particular, it predicted accurately the slight hardening of the spectrum between core center and boundary, a fact which was experimentally confirmed by the increase in the ratio $\sigma_f U^{238}/\sigma_f U^{235}$. The deficiencies of the P_3 approximation seem to be most marked for values of the flux near the sphere surface, although this may be related to small deviations of the experimental assembly from a perfectly spherical, bare sphere.

It is perhaps worth mentioning that some success in fitting both critical mass and flux distributions in small assemblies by diffusion theory has been attained by artificially raising the transport cross sections above fact in the higher energy groups.

A comparison of experiment and a diffusion theory calculation for an early core-loading in EBR-I is given in Fig. 11. Theory and experiment have been normalized to a value of unity at the center for fission in U^{235}. This is an engineering reactor and its considerable asymmetries render it difficult to analyze. This particular ten-group calculation was made in spherical geometry, setting the core radius so that the core volume was correct, but other radii at the values which would be truly correct in cylindrical geometry. The fluxes generally lie well above experiment in the blanket. If a cylindrical calculation is made, using an equivalent bare core height axially, the flux falls much closer to experiment in the inner blanket regions. In the outer blanket regions, however, this approximation allows too much end leakage and the flux falls below experiment. By using a total of twenty groups, with an emphasis on lower energies, excellent agreement with the shape of the U^{235} fission curve near the graphite has been obtained. The very sharp rise in U^{238} capture near the graphite has not been duplicated by calculation thus far. Presumably, a more detailed description of the resonance processes is required.

The experimental curves of Figs. 9 and 11 illustrate a particularly useful way of obtaining spectral information. It would be extremely desirable to measure the neutron energy spectrum in detail as a function of energy at various interesting positions in each experimental assembly. Unfortunately the means developed to date are all extremely tedious. Nuclear track plates have been used for the region above five hundred kilovolts, while the cloud chamber has been relatively successful between 100 and 500 kilovolts.[1,80] This still leaves the lowest energy region uncovered. Furthermore, the high flux requirements of the cloud

chamber, shielding problems, and the difficulties of taking out a truly representative beam combine to make such measurements very special rather than routine.

Until the advent of some simple direct means of measuring spectrum, other spectral indices are desirable. Such are obtained by measuring relative fission rates for isotopes having different energy thresholds, by comparing these with the primary fuel, and by comparing them with other isotopes activated by fast neutrons. Considerable use has been made in the past of fission in Np^{237} and U^{238}. Also, neutron capture in gold and the $P(n,p)S$ reaction have been used. The cross sections for these elements and several others which may make useful detectors are given in Fig. 12. The variation of these spectral indices with reactor size is illustrated in Table VIII. The reaction ratios for the various isotopes relative to fission in U^{238} have been calculated for the three spectra depicted in Fig. 1.

Detector ratio measurements are not without difficulties. Although the spatial distribution of the reaction of any single isotope in an assembly is relatively easy to obtain, and is of some interest, the measurements become considerably more valuable when they are normalized relative to one another. This usually requires foils of known weight or isotopic composition, and conceivably a knowledge of thermal cross sections or fission product yields. A possible normalization of considerable interest is one made relative to the same reaction ratio in a fission spectrum flux. Such a measurement lends itself to analysis. Further, if accurate, absolute ratio measurements in a fission spectrum were available, a different means of normalization would be provided.

A limited set of measurements have been made by Paxton, *et al.*, at the centers of bare uranium assemblies of differing enrichments. The results are presented in Table IX. Where available, an estimate of reproducibility is given, but these do not include any possible systematic errors. Not all the assemblies were critical, of course, since some considerable enrichment above natural is required for a block of uranium to sustain a chain reaction. The lower enrichment assemblies were in the form of exponential columns, sitting on top of a source reactor. For all assemblies the ratio $\sigma_f U^{235}/\sigma_f U^{238}$ was measured, while various other ratios were also measured at the high enrichments. For the enrichment range between four and nine per cent, heterogeneous effects are believed to have made the reported values about ten per cent higher than the true average.

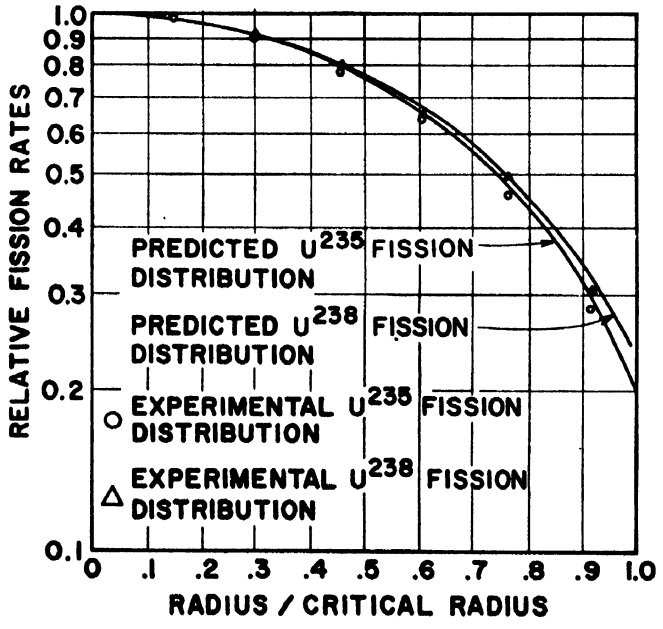

Figure 10. A comparison of experiment and a multigroup spherical harmonics calculation for Godiva (both fission rates are arbitrarily normalized to unity at the core center)

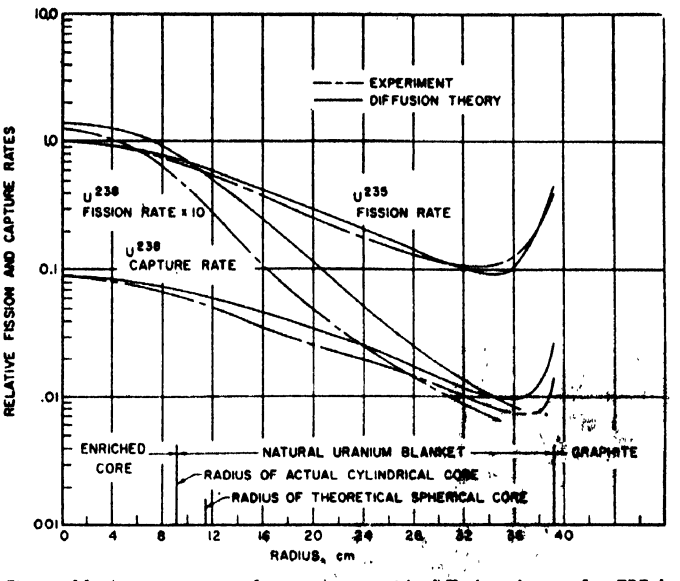

Figure 11. A comparison of experiment with diffusion theory for EBR-I

By and large, these results are fairly consistent with the measurements of Carter and Beyster. However, there is major experimental disagreement between the results of Table IX for natural uranium and that given in reference 31. In general, the fast exponential results reported therein for more dilute uranium systems have not agreed well with theoretical predictions made using cross sections which fit results in the smaller critical assemblies. It is true that the smaller assemblies are relatively insensitive to cross sections in the neighborhood of neutron energies of 100–200 kilovolts. It is not clear, however, that there is enough leeway in these parameters to allow such a discrepancy.

An attempt has been made to derive information on the detailed inelastic scattering properties of U^{235} and U^{238} by fitting the other ratios listed in Table IX. Thus far these efforts have met with failure. Truly precise data, together with very accurate microscopic reaction cross sections for the detectors, are needed for a good chance of success.

A detailed measurement of the spectrum at the center of the core of EBR-I[1] has been made, and it is compared with the results of a ten-group diffusion theory calculation in Fig. 13. The theoretical results are presented in the form of a block diagram, and the curves have been normalized to include the same total area over the energy range of the graph. The group-

Table VIII. Calculated Reaction Ratios for Core Spectra of EBR-I, EBR-II and PBR

	EBR-I	*EBR-II*	*PBR*
σ_f U^{238} (barns)	0.157	0.091	0.051
σ_f Pu^{239}/σ_f U^{238}	11.9	20.0	35.4
σ_f U^{235}/σ_f U^{238}	8.7	16.2	32.1
σ_c U^{238}/σ_f U^{238}	0.84	1.87	3.92
σ_f Np^{237}/σ_f U^{238}	5.0	5.7	6.9
σ_f U^{234}/σ_f U^{238}	5.3	6.1	7.3
σ_c Au/σ_f U^{238}	1.6	3.9	8.6
$\sigma_{n,n'}$ In/σ_f U^{238}	0.69	0.71	0.74
$\sigma_{n,\alpha}$ B/σ_f U^{238}	0.91	2.2	4.8
$\sigma_{n,p}$ P/σ_f U^{238}	0.07	0.07	0.07

energy structure used in the calculation had been picked to study low energy effects, and another choice might have been more appropriate for this comparison. The group-energy structure and the particular cross sections used for removal from a group by inelastic scattering are listed in Table X for U^{235}, U^{238} and Fe. The energy degradation by inelastic scattering was assumed to follow the equation

$$\sigma(E_0 \rightarrow E) = \text{Const. } E\sigma_c(E)e^{-E/T} \qquad (4)$$

where $\sigma_c(E)$ is proportional to the cross section for formation of the compound nucleus and was taken to be

$$\sigma_c(E) = 1, \qquad E \geq E'$$
$$= \sqrt{\frac{E'}{E}}, \qquad E \leq E' \qquad (5)$$

It was assumed that $T = 1$ Mev and $E' = 0.5$ Mev.

Surprisingly good agreement has been obtained with measurements of prompt neutron lifetime for the bare uranium assemblies of Table VII. In Fig. 14 a comparison with theory is made for the four available experimental values. These calculations were made by multigroup diffusion theory, using the $1/v$ absorber method discussed in the section on performance estimates; multigroup perturbation theory gives comparable results. It must be noted that the particular set of cross sections employed in this set of calculations used somewhat higher inelastic group removal values for U^{235} than those of Table X. This resulted in a lower average energy for the spectrum; a value of $\sigma_f U^{235}/\sigma_f U^{238}$ for Godiva of 6.9 is predicted by these cross sections, compared to the experimental value of 6.0–6.3. If the inelastic cross sections are adjusted to fit the spectral indices, the good agreement on lifetime breaks down, differences of 10–20 per cent appearing for Godiva.

Table X. Inelastic Removal Cross Sections (Barns) Used in Calculation of EBR-I Spectrum

Group no.	*Energy band*	σ_{in} U^{235}	σ_{in} U^{238}	σ_{in} *Fe*
1	∞–1.35 Mev	1.6	2	0.7
2	1.35–0.50	1.2	1	0.3
3	0.50–0.30	0.6	0.6	—
4	0.30–0.18	0.3	0.3	—
5	0.18–0.11	—	—	—
6	0.11–0.067	—	—	—
7	0.067–0.025	—	—	—
8	0.025–0.009	—	—	—
9	0.009–0.0034	—	—	—
10	0.0034–0	—	—	—

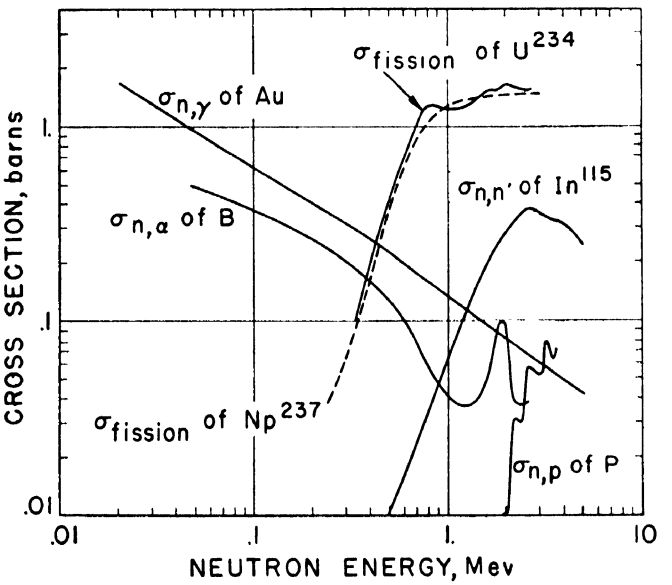

Figure 12. Reaction cross sections for several spectrum-measuring detectors

A distinct difference between thermal and fast critical assemblies appears when one considers the possibilities of determining capture cross sections by oscillator or static reactivity measurements. Inelastic scattering may have a greater reactivity effect than capture for many materials. For small assemblies, elastic scattering will become paramount in nonfissionable materials as one moves radially outward.

Table IX. Spectral Measurements in a Series of Bare Uranium Assemblies

Reaction ratio	*Enrichment of uranium in U^{235}*							
	~0.9	*0.54*	*0.38*	*0.092*	*0.065*	*0.051*	*0.043*	*0.0072*
σ_f, U^{235}/σ_f, U^{238}	6.2–6.5	8.7–9.6	10–11	30–32	40	48–51	57	200–215
σ_f, Pu^{239}/σ_f, U^{238}	9–9.6	12–14.5	—	—	—	—	—	—
σ_f Np^{237}/σ_f, U^{238}	4.5–4.8	5.3	—	—	—	—	—	—
σ_f, U^{234}/σ_f, U^{238}	5.2	—	—	—	—	—	—	—
σ_c, Au/σ_f, U^{238}	0.57–0.63	—	—	—	—	—	—	—
σ_c, U^{238}/σ_f, U^{238}	0.5	0.67–0.87	—	—	—	—	—	—

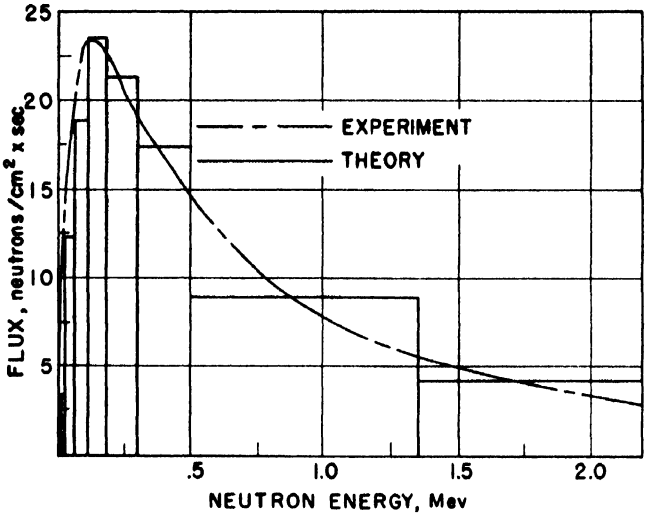

Figure 13. Comparison of measured neutron energy spectrum at center of EBR-I with ten-group diffusion theory calculation

Typical experimental results in a highly enriched, bare uranium assembly (Godiva) are given in Figs. 15 and 16. Similar results for the Topsy assembly are given in Figs. 17 and 18.

The results for the fissionable materials lend themselves to analysis, and Hansen has matched the measurements in Godiva for U^{235} and natural uranium quite well. In Fig. 19 is presented a comparison of experiment with perturbation theory wherein recourse to the diffusion approximation was not used. The three group fluxes of his P_3 solution to the assembly were employed, and second order effects were allowed for. The partial reactivity contributions associated with various effects for the case of natural uranium are given in Fig. 20.

In Figs. 15–20 the ordinate is given in arbitrary units or in units of "cents" per gram atomic weight, where a cent is defined as $\frac{1}{100}$ of the reactivity difference between delayed and prompt critical.

Considerably more difficulty is met in trying to predict accurately the reactivity effects of the nonfissionable materials. One can, however, find an element of regularity in the experimental results. A systematic difference between the reactivity effects for even and odd elements in intermediate reactors has previously been noted.[32] In the experiments at intermediate neutron energies considerably greater capture cross sections were noted for elements having odd atomic weights (A) (i.e., odd protons, Z, and even neutrons, N, or vice versa) than for elements in the same vicinity of the periodic table but having an even atomic weight (even Z, even N). A similar effect has been observed in the Godiva and Topsy assemblies, particularly for the heavier isotopes. Also a strong association with "magic numbers" has been observed. In Fig. 21 are plotted the reactivity effects at the center of Godiva for a series of odd A-odd Z elements. Maxima appear in the neighborhood of Z = 20, 50, and 80 or 82, and of N = 20, 50, 82 and 126.

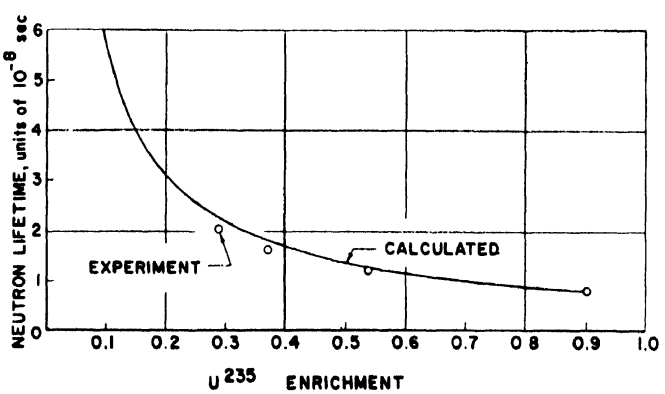

Figure 14. Prompt neutron lifetime of bare uranium assemblies vs U^{235} enrichment

APPENDIX: UNIVAC SOLUTION OF ONE-DIMENSIONAL DIFFUSION EQUATIONS

The computational approach taken for the numerical solution of a multiregion, multigroup diffusion theory problem is that of iteration on fission source distribution. Let us take the system to be described by the following set of simultaneous equations, the set for each region having appropriate constants.

$$D_j\nabla^2\phi_j(r) - (\Sigma_{c,j} + \Sigma_{f,j} + \Sigma_{in,j} + \Sigma_{mod,j})\phi_j(r) + \sum_{l=1}^{j-1}\sum_{in,l}\rightarrow_j\phi_l(r) + \sum_{m=1}^{j-1}\left[\sum_{mod\ m}\rightarrow_j\phi_m(r)\right] + \gamma_j S(r) = 0 \qquad (6)$$

where

$$S(r) = \sum_{k=1}^{N}\nu_k\sum_{f,k}\phi_k(r) \qquad (7)$$

and D_j = diffusion coefficient for group j = $(\frac{1}{3})\Sigma_{tr,j}$, $\phi_j(r)$ = total flux in group j at general spatial coordinate position, r, $\Sigma_{c,j}$ = macroscopic capture cross section, $\Sigma_{f,j}$ = macroscopic fission cross section,

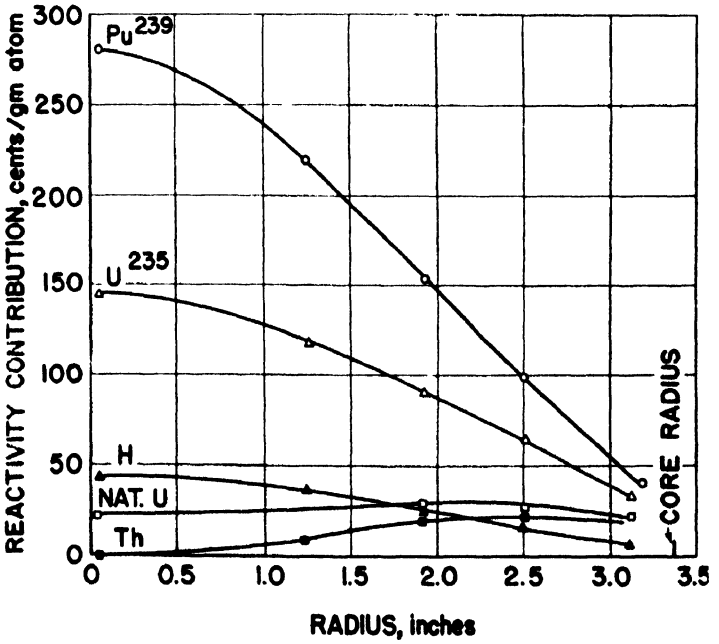

Figure 15. Reactivity contribution values for fissionable materials (and hydrogen) in Godiva

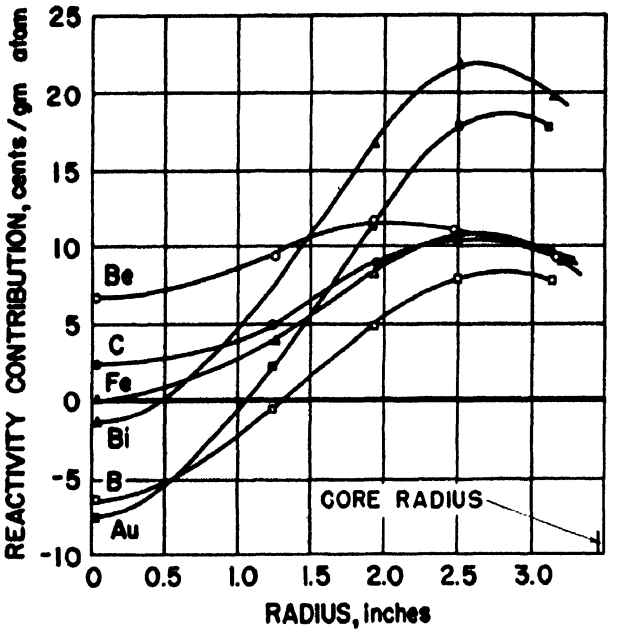

Figure 16. Reactivity contribution values for representative non-fissionable elements in Godiva

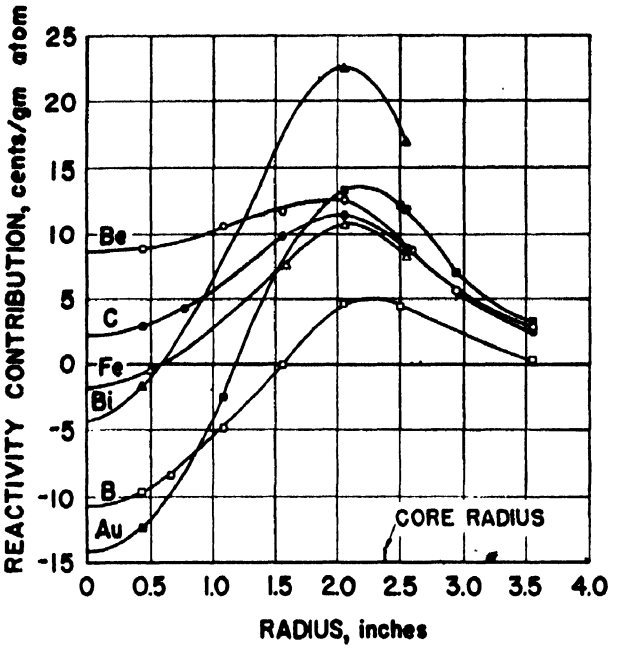

Figure 18. Reactivity contribution values for representative non-fissionable elements in Topsy

$\Sigma_{in,j}$ = macroscopic cross section for scattering inelastically out of group j, $\Sigma_{mod,j}$ = macroscopic cross section for scattering elastically (moderation) out of group j, γ_j = fraction of fission neutrons born in group j, ν_k = total neutrons born per fission in group k, $\Sigma_{in,1\to j}$ = macroscopic cross section for scattering inelastically from group 1 into group j, $\Sigma_{mod,m\to j}$ = macroscopic cross section for moderation from group m into group j, and N = total number of groups, where highest energy group is $j = 1$.

We also have

$$\Sigma_{tr,j} = \Sigma_{tot,j} - \bar{\mu}_j \Sigma_{el,j} \qquad (8)$$

where for group j, Σ_{tot} = total cross section, Σ_{el} = elastic scattering cross section, and $\bar{\mu}$ = average cosine of the scattering angle.

If a spatial distribution of the fission source of arbitrary magnitude, $S(r)$, is assumed, it is possible to solve for the flux in group 1, then in group 2, 3 . . . N, successively. The spatial distribution of fission source produced by these fluxes is then calculated and compared with the guess for convergence in shape and magnitude. Convergence on shape is attained by successive iteration. If the initially chosen reactor is not critical, convergence on magnitude is obtained by a change in dimensions or composition. About three composition changes are sufficient.

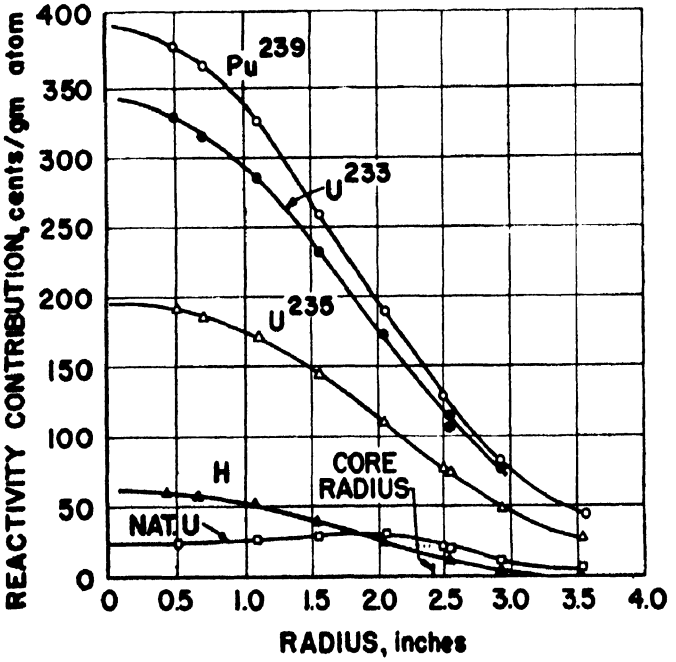

Figure 17. Reactivity contribution values for fissionable materials (and hydrogen) in Topsy

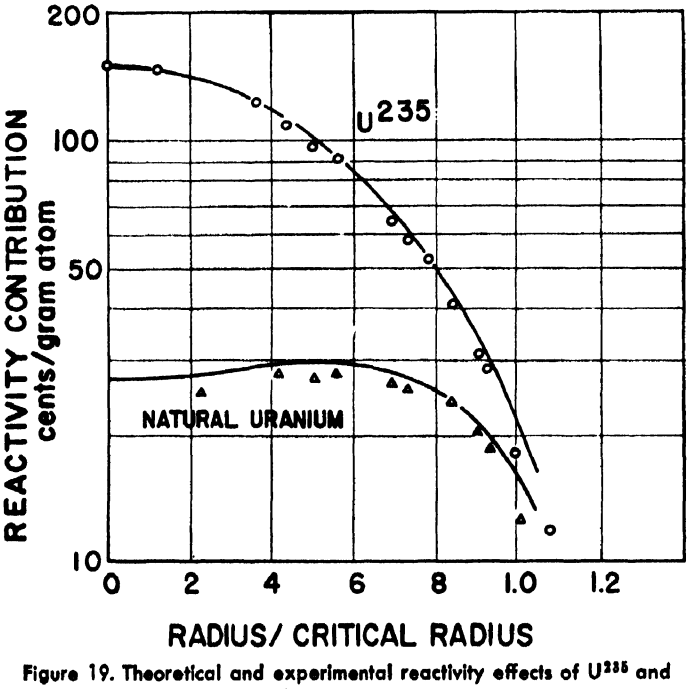

Figure 19. Theoretical and experimental reactivity effects of U^{235} and natural uranium in Godiva: (the full lines represent theory; the points are experimental)

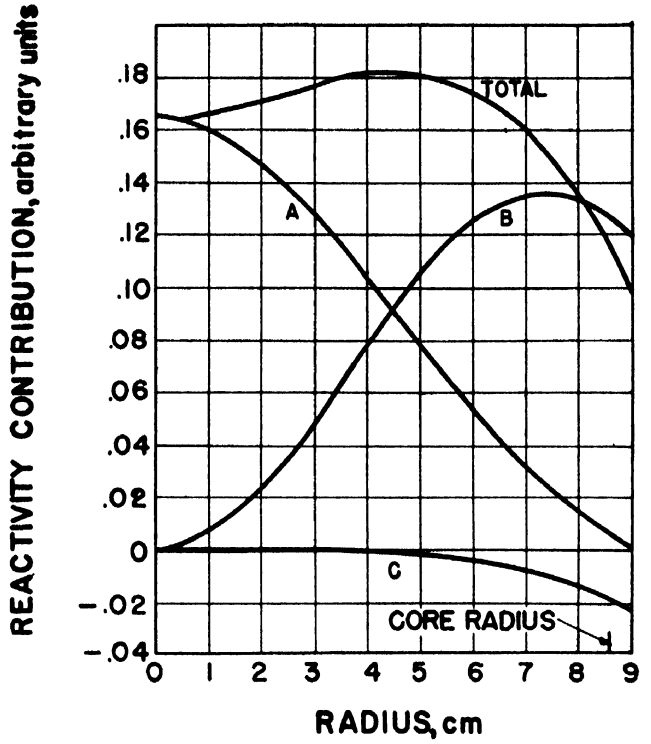

Figure 20. Partial reactivity contributions in Godiva for natural uranium which are associated with: (A) capture, fission and inelastic scattering; (B) transport scattering; and (C) second order effects

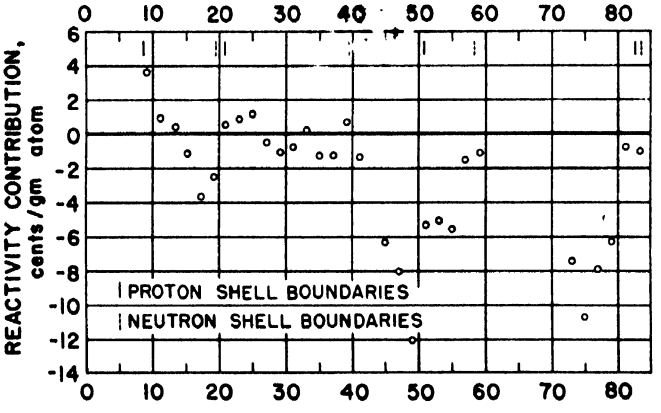

Figure 21. Reactivity contribution values at center of Godiva for odd-even elements (odd number of protons, odd atomic weight)

REFERENCES

1. Lichtenberger, H. V., Thalgott, F. W., Kato, W. Y. and Novick, M., P/813, "Operating Experience and Experimental Results Obtained from a NaK-Cooled Fast Reactor," Volume III, Session 14.A, these Proceedings.
2. Barnes, A. H., Koch, L. J., Monson, H. O. and Smith, F. A., P/501, "The Engineering Design of a Prototype Fast Neutron Reactor Power Plant," Volume 3, Session 14A, these Proceedings.
3. Dietrich, J. R., Lichtenberger, H. V. and Zinn, W. H., P/481, "Experimental Determinations of the Self-Regulation and Safety of Operating Water-Moderated Reactors," Volume 13, Session 6.3, these Proceedings.
4. Ehrlich, R., and Hurwitz, H. Jr., *Multigroup Methods for Neutron Diffusion Problems*, Nucleonics *12, 2:* 23 (1954).
5. Roe, G. M., *Adaptation of Multigroup Methods to Cylindrical Geometries*, KAPL-950 (1954).
6. Habetler, G. J., *General One-Dimensional Multigroup*, KAPL-1182 (1954).
7. Weinberg, A. M., *Current Status of Nuclear Reactor Theory*, Am. J. Phys. *20:* 401 (1952).
8. Davison, B., *Transport Theory of Neutrons*, LT-18 (1947).
9. Hummel, H. H., McDowell, R., Rosenzweig, N. and Satkus, D., *AVIDAC Setup for Multigroup Serber-Wilson Calculations*, ANL-5440 (to be published).
10. Carlson, B., *Solution of the Transport Equation by S_n Approximations*, LA-1891 (1955).
11. Frankel, S., and Nelson, E., *Methods of Treatment of Displacement Integral Equations*, LADC-79 (1953).
12. Frankel, S., and Goldberg, S., *The Mathematical Development of the End-Point Method*, LADC-76 (1945).
13. Butler, M. K. and Cook, J. M., *UNIVAC Programs for the Solution of One-Dimensional Multigroup Reactor Equations*, ANL-5437 (to be published).
14. Diven, B. C., P/594. "Techniques for Measurement of Fast Neutron Flux," Volume 4, Session 17A, these Proceedings.
15. Kanne, W. R., P/595, "A[illegible] in the Intermediate Energy Range," Volume 4, Session 18A, these Proceedings.
16. Inghram, M. G., Hess, D. C., Hayden, R. J. and Stevens, C. M., P/596, "Mass Spectrometric Methods for Determination of Nuclear Constants," Volume 4, Session 16A, these Proceedings.
17. Crouthamel, C. E., and Turk, E., P/721, "Determination of Nuclear Constants by Chemical Methods," Volume 7, Session 8B.1, these Proceedings.
18. AEC Neutron Cross Section Advisory Group, *Neutron Cross Sections*, AECU-2040 (1952).
19. Walt, M., and Barschall, H. H., *Scattering of 1-Mev Neutrons by Intermediate and Heavy Elements*, Phys. Rev. *93:* 1062 (1954).
20. Walt, M., P/588, "Angular Distributions and Non-Elastic Neutron Scattering," Volume 2, Session 6A, these Proceedings.
21. Taschek, R. F., P/573, "Elastic, Non-Elastic and Transport Neutron Cross Sections," Volume 4, Session 15A, these Proceedings.
22. Carter, R. E., and Beyster, J. R., *Inelastic Collision Cross Sections for Fission Spectrum Neutrons*, Phys. Rev. *90:* 389 (1953).
23. Day, R. B., P/581, "Gamma-Rays from Inelastic Neutron Scattering," Volume 2, Session 6.A, these Proceedings.
24. Cranberg, L., P/577, "Time of Flight Techniques Applied to Fast Neutron Measurements," Volume 4, Session 14A, these Proceedings.
25. Hughes, D. J., Spatz, W. D. B. and Goldstein, N., *Capture Cross Sections for Fast Neutrons*, Phys. Rev., *75:* 1781 (1949).
26. Hughes, D. J., Garth, R. C. and Levin, J. S., *Fast Neutron Cross Sections and Nuclear Level Density*, Phys. Rev., *91:* 1423 (1953).
27. Hughes, D. J., *Neutron Widths of Nuclear Energy Levels*, Bull. Am. Phys. Soc. *30:* 22 (1955).
28. Harvey, J. A., *Level Spacings of Heavy Nuclei*, Bull. Am. Phys. Soc. *30:* 23 (1955).
29. Goertzel, G., P/613, "Doppler Effect in Intermediate and Fast Reactors," Volume 5, Session 23A, these Proceedings.
30. Rosen, L., P/582, "Techniques for Measurement of Neutron Cross Sections and Energy Spectra for Sources which are Continuous in Energy and Time," Volume 4, Session 15A, these Proceedings.
31. Beyer, F. C., Hummel, H. H., Lennox, D. H., Martens, F. H., Reardon, W. A., Rosenzweig, N., Smith, A. B. and Spinrad, B. I., P/598, "The Fast Exponential Experiment," Volume 5, Session 22A, these Proceedings.
32. Hurwitz, H., Jr., Knolls Atomic Power Laboratory, Personal Communication.

Stability Conditions in the Non-Linear Dynamics of Heterogeneous Reactors

By Harry J. Lipkin*† and R. Thieberger,† Israel

The coupling between the temperature and the reactivity of a nuclear reactor causes the reactor-kinetics equations to become non-linear. Ergen and Weinberg[1] have developed a mechanical-analog method for determining stability conditions for a homogeneous reactor in certain specific cases of reactor cooling. A sufficient condition for reactor stability is that energy be either conserved or dissipated in the mechanical analog, i.e., that there exists a positive definite function of the reactor variables whose time derivative can be shown to be negative definite. This function is referred to as the Hamiltonian, because of the mechanical analogy.

The Hamiltonian method has been extended to the case of a heterogeneous reactor consisting of two media, such as uranium and heavy water, where heat is produced in one medium and extracted from the second.[2] The temperatures of the two media are in general quite different, depending upon the heat transfer between them, and both temperatures are coupled to the reactivity with different coefficients. By methods similar to those of Ergen and Weinberg, it is possible to set up a mechanical analog and a Hamiltonian for this case, thus obtaining a two body problem. The following conclusions result from this treatment: the important constant characterizing each medium is a *thermal* coefficient of reactivity, rather than the temperature coefficient normally used. This thermal coefficient is defined as the change in reactivity per unit of heat added, rather than per degree of temperature rise. If the thermal coefficients of the two media are equal, the dynamic equations reduce to the homogeneous case. If they are unequal, the stability of the reactor is improved if heat is produced in the medium having the higher coefficient. Because of the very large heat capacity of water which drastically reduces the thermal reactivity coefficient, the stability condition is met in reactors which use light or heavy water as a moderator and coolant. The kinetic transients are, therefore, damped very much more strongly than in the case of a homogeneous reactor.

The method can be extended further to the case of n media, each coupled to the reactivity with a different coefficient. If the heat produced is distributed between the media in a constant proportion, and if the power extracted and the rate of heat transfer between media are linear functions of the various temperatures, the kinetic equations can be reduced to a form similar to that obtained for a homogeneous reactor with Newton's law of cooling. In the general case, the temperature variables appear as a vector in an n-dimensional vector space, and the coefficients of reactivity and heat transfer as matrix operators in this space. A Hamiltonian function can be obtained which is a quadratic form whose coefficients are functions of the reactor constants. The positive definiteness of this form is a sufficient condition for reactor stability.

The effect of delayed neutrons can also be considered approximately by this method for the case where the kinetic transients are slow compared to the delayed neutron periods. If the delayed neutron equations are expanded in a power series in the delayed neutron periods and only the first two terms are kept, a Hamiltonian can easily be found. The result shows additional damping, and the stability condition is again expressed by the positive definiteness of a quadratic form whose coefficients are functions of the reactor constants, including in this case the delayed neutron constants.

THE HAMILTONIAN FOR A HETEROGENEOUS REACTOR CONTAINING TWO MEDIA

For a heterogeneous reactor containing two media, such as uranium and heavy water, the basic kinetic equations can be written:

$$(d/dt)(\log P) = -(\alpha_U T_U/\tau + \alpha_D T_D/\tau) \quad (1a)$$

$$\mu_U(dT_U/dt) + \mu_D(dT_D/dt) = P - P_e \quad (1b)$$

These equations express the multiplication of neutrons and the conservation of energy. The subscripts U and D refer respectively to uranium and heavy water. P is the reactor power, P_e the power extracted from the reactor, τ the average neutron generation lifetime, and T, α, and μ are respectively the temperature, the temperature reactivity coefficient, and the heat capacity of the medium indicated by the subscript. The zero points for the two temperatures are taken as the temperatures in an equilibrium state in which the reactor is just critical. Delayed neutrons are neglected.

It is convenient to introduce as new variables the temperature difference between the uranium and the

* Stagiaire at the Commissariat à l'Energie Atomique, Fort de Châtillon, Fontenay aux Roses, Seine, France, at the time this work was begun. The hospitality and assistance of the C.E.A. is gratefully acknowledged. See reference 2.

† The Weizmann Institute of Science, Rehovoth and Israel Atomic Energy Commission, Tel-Aviv.

heavy water and the total heat contained in the reactor:

$$T = T_U - T_D \tag{2a}$$

$$Q = \mu_U T_U + \mu_D T_D \tag{2b}$$

The coefficients appropriate for use with these variables are

$$\beta_T = [(\alpha_U/\mu_U) - (\alpha_D/\mu_D)]\mu_D/(\mu_U + \mu_D) \tag{3a}$$

$$\beta_Q = (\alpha_U + \alpha_D)/(\mu_U + \mu_D) \tag{3b}$$

These are thermal reactivity coefficients, β_T being proportional to the difference between the uranium and heavy water coefficients and β_Q being an average thermal coefficient for the two media. In the new variables, the fundamental Equations 1 become

$$(d/dt)(\log P) = -(\beta_T \mu_U T/\tau + \beta_Q Q/\tau) \tag{4a}$$

$$dQ/dt = P - P_e \tag{4b}$$

If the thermal coefficients for the two media are equal, β_T vanishes, and Equations 4a and 4b become independent of T and reduce to those for the case of a homogeneous reactor. If β_T does not vanish, Equations 4a and 4b are not sufficient to determine the dynamics of the reactor. A relation describing the heat transfer must be added. Assuming that the rate of heat flow between the uranium and the heavy water is proportional to the temperature difference between them, this relation can be expressed in the form

$$dT/dt + T/t_0 = (P - P_e)/\mu_U \tag{5}$$

where t_0 is the relaxation time characterizing the heat transfer and is

$$t_0 = \mu_U \mu_D/[k(\mu_U + \mu_D)]$$

k being the ratio of power transferred between the media to the temperature difference T.

For the case where the power extracted is a constant $P_e = P_0$, the Hamiltonian is obtained immediately by multiplying Equation 4a by $P - P_0$ and substituting Equations 4b and 5:

$$dH/dt = (d/dt)(P - P_0 \log P + \beta_T \mu_U T^2/2\tau + \beta_Q Q^2/2\tau) = -\beta_T \mu_U T^2/t_0 \tag{6}$$

Equation 6 differs from the corresponding expression obtained by Ergen and Weinberg for a homogeneous reactor only in the two terms involving T. In the homogeneous case oscillations of constant amplitude are obtained; here the oscillations are either damped or unstable, depending upon the sign of β_T. A sufficient condition for stability is that β_T be non-negative; i.e., that the thermal reactivity coefficient of the uranium be greater than or equal to that of the heavy water.

EXTENSION TO THE CASE OF N MEDIA

Consider a reactor consisting of n media where the power extracted and the heat transfer between media are linear functions of the temperatures and the heat produced is distributed between the media in a constant proportion. A system of equations of the following form is obtained:

$$(d/dt)(\log P) = -\sum_k \alpha_k T_k/\tau \tag{7a}$$

$$\sum_j a_{kj} dT_j/dt + b_{kj} T_j = c_k P + d_k \tag{7b}$$

where T_k and α_k are the temperature and the reactivity coefficient of the k^{th} medium, the sums go from 1 to n, and there are n equations of the form of Equation 7b. The coefficients a_{kj}, b_{kj}, c_k and d_k depend upon the heat capacities, the heat transfer constants and the system of cooling. Equations 7a and 7b have exactly the same form as the equations for a homogeneous reactor with the power extracted a linear function of the temperature (Newton's law of cooling), except that T_k is a vector in an n-dimensional vector space and the various coefficients are matrix operators in this space.

The Hamiltonian of the system is easily obtained after a transformation to "normal coordinates." This is a generalization of the transformation of Equation 2 for the two-medium case to the variables T and Q, and is an inhomogeneous linear transformation of the variables T_k to new variables T_k, such that Equation 7b can be written with diagonal matrices replacing a_{kj} and b_{kj}, with the coefficients c_k replaced by unity, and with all the d_k replaced by the same constant P_0, while Equation 7a retains the same form. After the transformation the Equations 7a and 7b become

$$(d/dt)(\log P) = -\sum_k \sigma_k T_k'/\tau \tag{8a}$$

$$dT_k'/dt + T_k'/t_k = P - P_0 \tag{8b}$$

where σ_k and t_k are the new coefficients. Equations 8a and 8b are similar in form to Equations 4a and 5, and the Hamiltonian is again obtained by multiplying Equation 8a by $P - P_0$ and substituting the Equations 8b to obtain:

$$dH/dt = (d/dt)\left(P - P_0 \log P + \sum_k \sigma_k T_k'^2/2\tau\right) = -\sum_k \sigma_k T_k'^2/t_k \tag{9}$$

A sufficient condition for the stability of the reactor is thus that all the quantities σ_k and t_k be positive.

DELAYED NEUTRONS

If delayed neutrons are considered, a correction term must be added to the neutron multiplication Equations 1a, 4a, 7a and 8a, to indicate that a change in the number of delayed neutron emitters present in the reactor represents a sink or source of neutrons. This can be done by replacing $d/dt(\log P)$ in these equations by $(1/P)(d/dt)\left(P - \sum_i C_i\right)$ where C_i is the density of the i^{th} delayed neutron group, expressed in units of power in the same way that P represents the neutron density. Equation 8a thus becomes:

$$(1/P)(d/dt)\left(P + \sum_i C_i\right) = -\sum_k \sigma_k T_k'/\tau \tag{10a}$$

where the sum on i is over all delayed neutron groups and the sum on k is over the n media. The C_i satisfy the usual equations expressing the production and decay of delayed neutron emitters:

$$dC_i/dt = (\beta_i P/\tau)\left(1 - \sum_k \sigma_k T_k'\right) - C_i/\tau_i \quad (10b)$$

The solution of Equations 10a and 10b is quite complicated, but the Hamiltonian method can be applied approximately for the case where the change in power is slow compared to the delayed neutron periods τ_i, i.e.

$$d(\log P)/d(t/\tau_i) \ll 1 \quad (11)$$

For this case the reactivity is small compared to unity, and the term containing the sum of T_k' in Equation 10b can be neglected. Then by successive differentiation of Equation 10b, C_i can be expressed as a series in powers of τ_i, each term multiplying a higher derivative of P:

$$C_i = (\beta_i\tau_i/\tau)(P - \tau_i dP/dt + \tau_i^2 d^2P/dt^2 + \cdots) \quad (12)$$

Because of the assumption in Equation 11 the successive terms in Equation 12 decrease rapidly, and an approximate result can be obtained by introducing the first two terms of Equation 12 into Equation 10a to obtain

$$(1/P)(d/dt)\left(P + \sum_i \beta_i\tau_i P/\tau\right) - \left(\sum_i \beta_i\tau_i^2/\tau P\right)(d^2P/dt^2) = -\sum_k \sigma_k T_k'/\tau \quad (13a)$$

which can be written

$$(1/P)(dP/dt) - \left(\sum_i \beta_i\tau_i^2/\bar{\tau}\right)(1/P)(d^2P/dt^2) = -\sum_k \sigma_k T_k'/\bar{\tau} \quad (13b)$$

where the average neutron lifetime $\bar{\tau}$ is defined as

$$\bar{\tau} = \tau + \sum_i \beta_i\tau_i \quad (13c)$$

The Hamiltonian is obtained as before by multiplying Equation 13b by $P - P_0$. After a slight rearrangement of terms the result is obtained:

$$dH/dt = (d/dt)\left[P - P_0 \log P - \left(\sum_i \beta_i\tau_i^2/\bar{\tau}\right)(d/dt)(P - P_0 \log P) + \sum_k \sigma_k T_k'^2/2\bar{\tau}\right] = -\sum_k \sigma_k T_k'/t_k - \left(\sum_i \beta_i\tau_i^2/\bar{\tau}\right) P_0[(d/dt)(\log P)]^2 \quad (14)$$

The effect of the delayed neutrons is thus to increase the stability of the reactor, as is shown by the additional damping term on the right-hand side of Equation 14.

REFERENCES

1. Ergen, W. K. and Weinberg, A. M., "Some Aspects of Non-Linear Reactor Dynamics," Physica XX, 413 (1954).
2. Lipkin, H. J., "A Study of the Non-Linear Kinetics of the Châtillon Reactor," Journal of Nuclear Energy, *1*, 203 (1955).

The Influence of the Temperature Coefficient on the Transfer Function of a Heavy Water Reactor

By J. Pelser,* The Netherlands

A nuclear reactor can be considered as a system in which an input signal, the excess reactivity, which is a function of time causes an output signal, the reactor power, P, to vary as a function of time. The relation between input and output can be given by the equations:

$$\frac{dP}{dt} = \frac{\delta k}{l^*} P - \frac{\beta}{l^*} P + \sum \psi \lambda_i C_i \qquad (1)$$

$$\frac{dC_i}{dt} = \frac{P\beta_i}{\psi l^*} - \lambda_i C_i \qquad (2)$$

in which the constants[1]

i	λ_i	β_i
1	14	25×10^{-5}
2	1.61	85×10^{-5}
3	0.456	241×10^{-5}
4	0.154	213×10^{-5}
5	0.0315	166×10^{-5}
6	0.0125	25×10^{-5}

are due to the delayed emitted neutrons[2] and

i	λ_i	β_i
7	0.277	20×10^{-5}
8	0.0169	6×10^{-5}

are due to photoneutron generation in the heavy water. In case the variations with time in the output signal are small compared with the signal itself, the Equations 1 and 2 can be linearized and a transfer function $G(s)$ can be defined as the ratio between the Laplace transforms of the output and the input signal when the initial conditions are taken as zero.

In case of a sinusoidal input signal with an angular frequency ω, the ratio between output and input signal becomes

$$G(j\omega) = \frac{\prod_{i=1}^{i=\delta} (j\omega + \lambda_i)}{l^* j\omega \prod_{i=1} (j\omega + \alpha_i)} \qquad (4)$$

Since the reactivity of the reactor depends on the temperature of it, there is a feed-back from the output to the input as shown in Fig. 1.

The transfer function of the feed-back loop $H(s)$ will in general be a complicated function since it depends on the cooling system in which delays in pipelines, heat-exchangers, etc., appear.

In order to draw a simplified picture we will however, assume the presence of only a time constant so that:

$$H(s) = \frac{K}{1 + TS} \qquad (5)$$

Because this feed-back is internal the reactor always behaves like a system with a transfer function

$$G'(s) = \frac{G(s)}{1 + G(s)H(s)} \qquad (6)$$

It is now possible to compute $G(s)$ in case of a simplified reactor.

In this case[3] $l^* = 1.25 \times 10^{-3}$ sec

Then:

$$G(s) = \frac{800(s + 14)(s + 1.61)(s + 0.456)(s + 0.277)(s + 0.154)(s + 0.0315)(s + 0.0169)(s + 0.0125)}{s(s^8 + 22.81s^7 + 136.0s^6 + 217.7s^5 + 110.7s^4 + 21.74s^3 + 1.524s^2 + 336.4 \times 10^{-1}s + 228 \times 10^{-6})}$$

This transfer function has a form as:

$$G(s) = \frac{\prod_{i=1}^{i=\delta} (s + \lambda_i)}{l^* s \prod_{i=1}^{i=\delta} (s + \alpha_i)} \qquad (3)$$

The time constant T is found to be 4800 sec

$$T = \frac{W}{C}$$

$$K = \frac{\alpha \cdot P}{C}$$

$$= 4 \times 10^{-5} P$$

where W = heat capacity = 30,000 kw-sec/°C, C = cooling rate = 6.25 kw/°C, α = temperature coeffi-

* Joint Establishment for Nuclear Energy Research, Kjeller, near Lillestrøm, Norway.

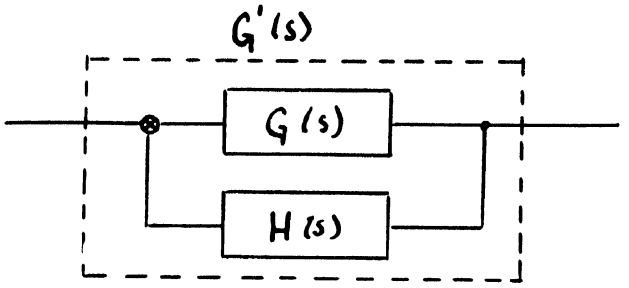

Figure 1

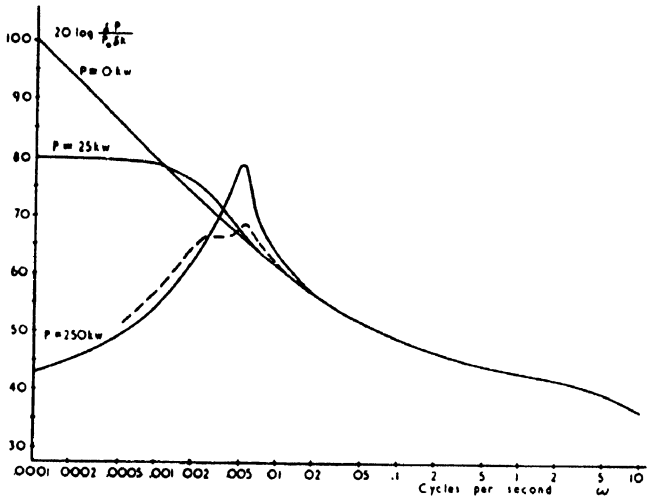

Figure 2. Magnitude of transfer function of JEEP reactor: full line, computed; dotted line, measured at a power level of 250 kw

cient = 25×10^{-5}/°C, and P = reactor power in kw. The magnitude of the transfer function $G'(j\omega)$ is given in Fig. 2 for power levels of 25 and 250 kw.

In order to verify the computed function a series of measurements were made. It was found impracticable to apply a sinusoidal input signal because of the long periods. Therefore a step function change in reactivity

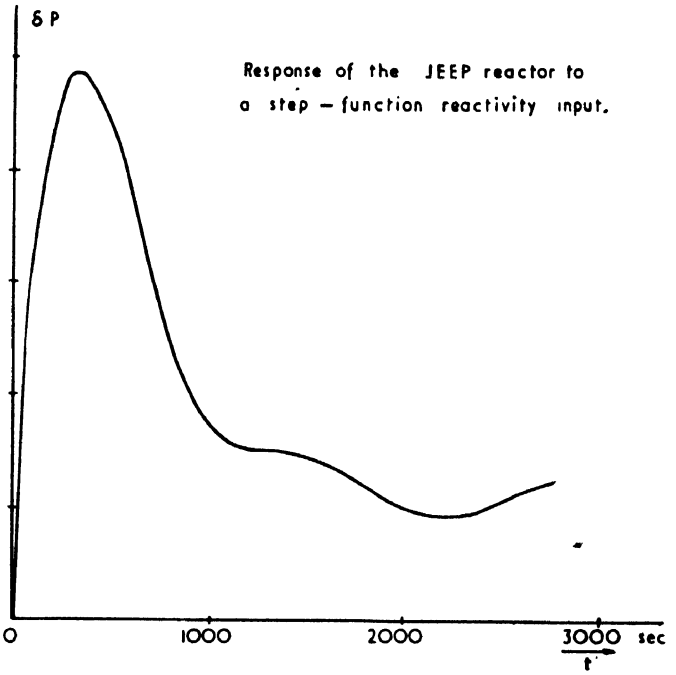

Figure 3. Response of the JEEP reactor to a step-function reactivity input

was given as input signal and the response of the power output of the reactor was recorded (Fig. 3 shows a typical example). The transfer function was derived by differentiation of these curves and taking the Fourier transform. The result is shown as the dotted line in Fig. 2.

REFERENCES

1. Hughes, D. J., Dabbs, J., Cahn, A. and Hall, D., *Delayed Neutrons from Fission of U^{235}*, Phys. Rev. 73: 111 (1948).
2. Johns, M. W. and Sargent, B. W., *Photoneutrons in a heavy water pile*, Can. J. Phys. 32: 136 (1954).
3. Measurements by the author (to be published).

The Dynamic Problems of Power Reactors and Analogue Computers

By Paul Braffort,* France

The design of complex devices, such as nuclear reactors, particle accelerators, etc., needed for the development of nuclear physics and techniques, calls for extensive mathematical work. The need to solve a number of differential equations, to carry out partial integrations, taking account of their non-linearity, the complex geometry of the boundary conditions, etc., makes it necessary that large departments be set up to do computation work. As is the case in many other fields, these departments, in an ever growing number of cases, are backed up by electronic computers which are more adaptable and work faster than the human operators.

Digital computers are particularly useful for the accurate determination of the parameters on which steady state operation of the reactor depends, in particular when the "Laplacian" is computed for the complicated geometries encountered in reactors. The analogue method was also used for the resolution of some diffusion problems, with the help of the relaxation technique but, at the present time, the partial differential equations cannot be conveniently handled by the analogue computers.[1,2]

Thus, it is in the field of kinetics that analogue computers are, most helpful at the present time. Kinetics is understood to include all the phenomena having to do with the changes, as functions of time, of power, temperature (of uranium, moderator coolant, secondary circuit), etc.

What must be done is to solve systems of non-linear differential equations, which cannot be treated by mathematical analysis. The parameters which appear in the equations depend on the peculiarities of the reactors which they describe. By varying these parameters, one can rapidly draw a network of curves from which the optimal operating conditions for the reactor are derived, such as the control rod speed, automatic control and thermal exchange parameters.

It is in dealing with problems of this type that the analogue computers show their superiority, since they actually operate as scale models. They can show, by direct reading, the value of the physical factors simulated, the variations of which can be followed as a function of time. Obviously, the precision achieved is not so great as in the digital computers but is quite adequate for the engineer. The analogue machine has the advantage that the engineer can easily vary the parameters of the system under study.

Naturally, the use of the analogue computer is particularly effective where servomechanisms are involved, for instance, in resolving problems having to do with the automatic control of nuclear reactors. Efficiency is complemented by safety, for it would be dangerous to try out directly a badly designed automatic control device on a full scale reactor.[3]

Control is the field in which we expect to bring in the greatest number of original results as regards the applications of the analogue computer method to reactor problems, but it struck us as being worth while to describe our work on reactor kinetics and dynamics in some detail. There are various papers bearing on the subject in the literature. However, these refer either to devices which have been built specially to solve the kinetic equations system of the reactor, or to commercial analogue computers, on which the relevant problem was solved.

One original aspect of our work was that we carried it out on a commercial type computer (Djinn analogue computer, made by the Derveaux Laboratories) equipped with an interconnection panel designed according to our specifications by M. J. Girerd in order to make it possible to insert readily the equations of the type we had to solve. This enabled us to complete very easily a duplicate wiring set-up having a similar structure. In particular, we were able to show, on one and the same panel, both the kinetic equations and the equations of poisoning by fission products.

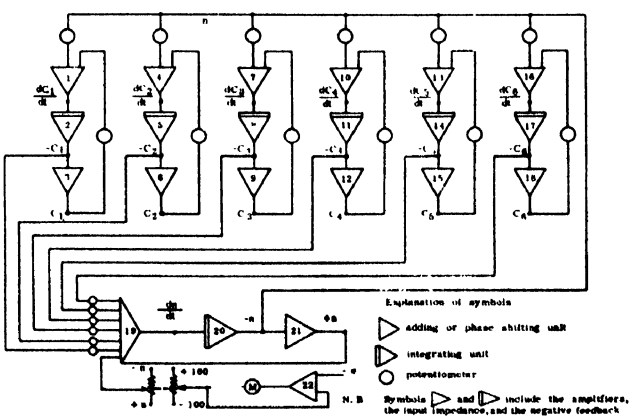

Figure 1. Block diagram of the kinetic equations for a reactor

Original language: French.

* Engineer at the Electrical Construction Department of the C.E.A.

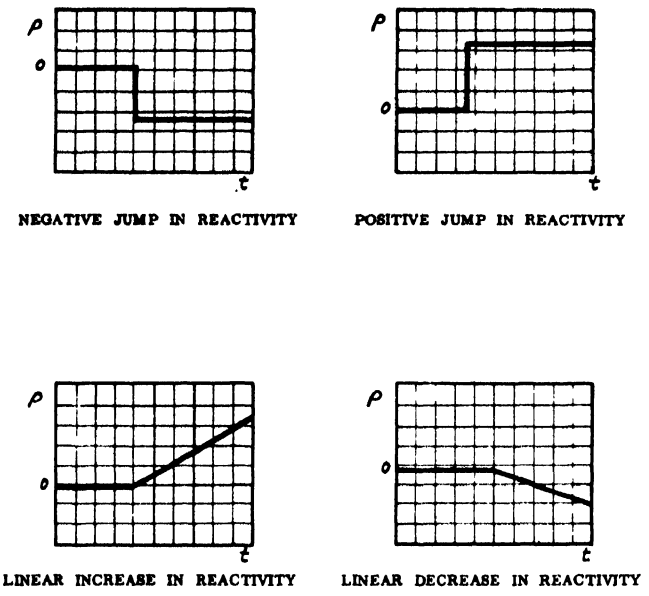

Figure 2. Types of reactivity changes

Finally, our computer has a "memory," which makes it possible to break up the computation while recording the values of the various functions which appear in the chain of operations. Thus, we can determine the functions, values, put them back into the calculation, and then, derive the precision of the machine. This check was made several times and showed the precision obtained to be better than 1%, which is of the same order of magnitude as the precision of the resistors and capacitors. We can thus state that the computation was not significantly affected by the drift of the amplifiers used in the machine.

KINETIC PROBLEMS

The reader is familiar with the set of equations which describes the kinetic behavior of a reactor.

$$\frac{dn}{dt} = \frac{\rho - \beta}{\tau} n + \sum_i \lambda_i C_i$$

$$\frac{dC_i}{dt} = \frac{\beta_i}{\tau} n - \lambda_i C_i$$

in which n is the fission power at a given point, and C_i the concentration of the i^{th} delayed neutron emitter. If ρ is a function of time, this system no longer is linear, and mathematical analysis no longer can be of any help, except for very special cases.

The analogue computing circuit consists of a linear part made up only of function amplifiers, integrators, phase shifters, summation devices, and a multiplier, which gives the product ρn.

Some of the papers refer to the use of a digital multiplier. We felt it would be adequate, taking account of the narrow band-pass required by the necessary functions, to use a servo as a multiplier. This gives, using the conventional principles of analogue computer design, the over-all schematic shown in Fig. 1. It will be seen that each equation involving C_i requires three amplifiers. A slightly different circuit would make it possible to use only one amplifier for each equation containing C_i, but it would then be impossible to measure

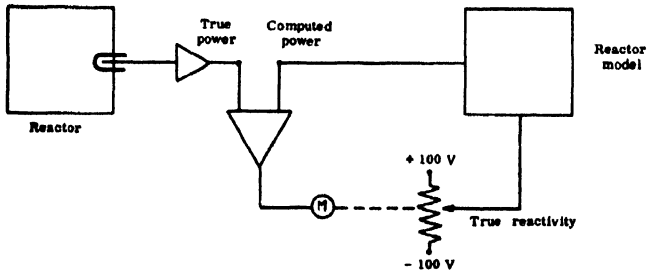

Figure 3. Schematic of a measuring circuit for true reactivity

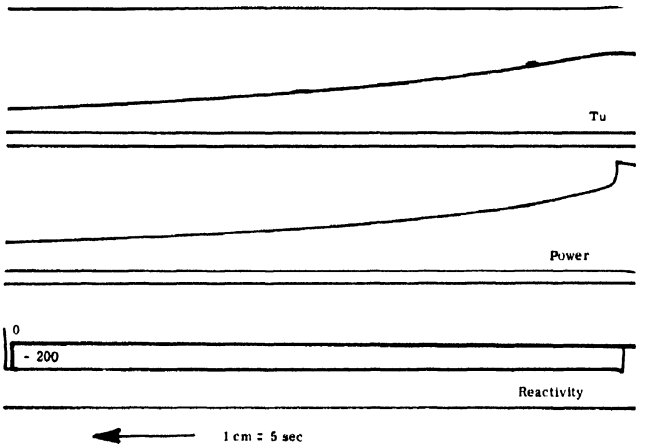

Figure 4a. Negative drop in reactivity .2% (200 per 10^5)

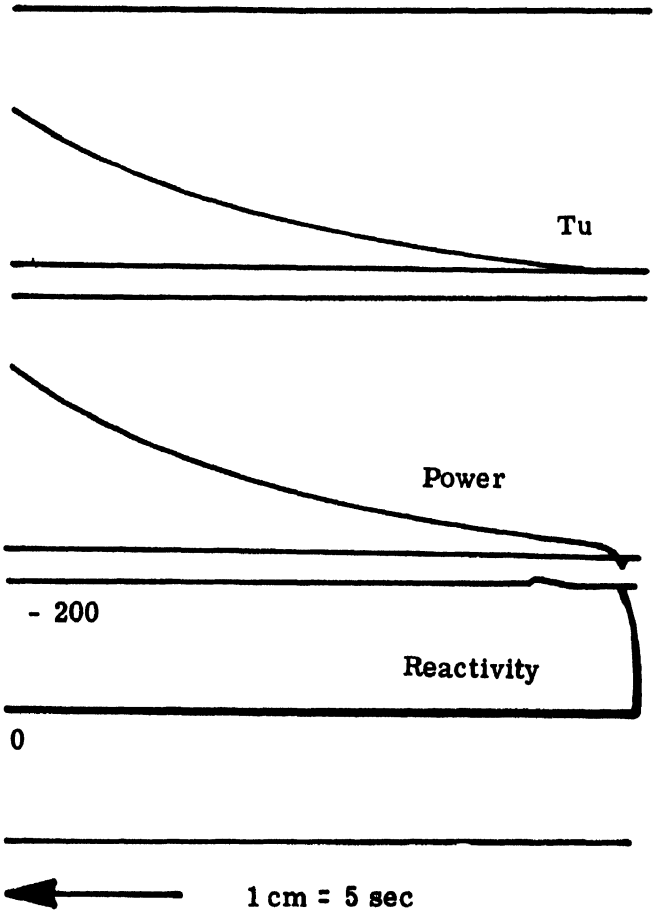

Figure 4b. Positive jump in reactivity 0.2% (200 per 10^5)

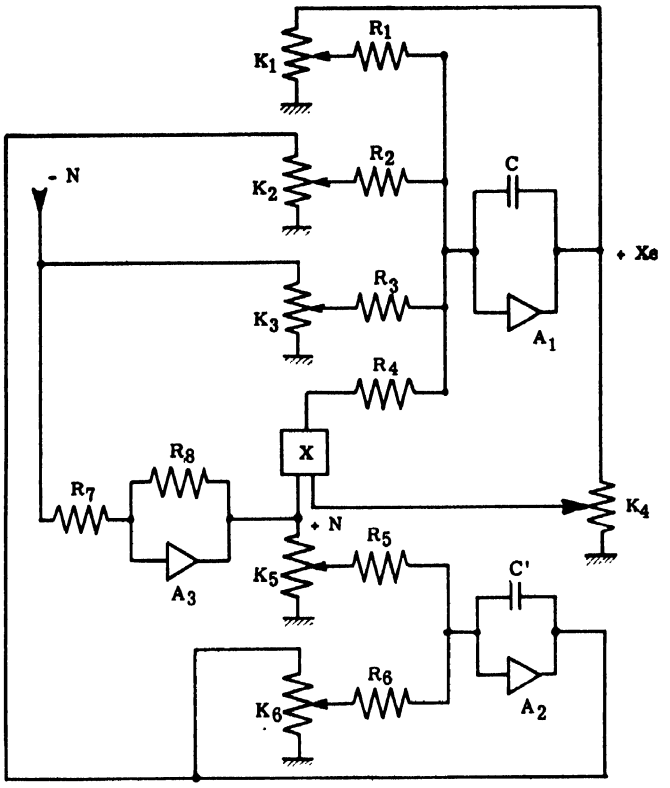

Figure 5. Poisoning; block diagram

derivatives dC_i/dt (which, in this system, are to be found at the output end of the summation amplifiers 1, 6, 11, 16, 21, 26). It would then no longer be possible carefully to check on the accuracy of the computations.

In the system so represented, we set a function ρ of various forms: positive and negative jumps, linear increases and decreases, etc. Fig. 2. On the other hand, in order to keep track of variations in reactor power following a lengthy shutdown, computations were made by changing the time scale according to second-minute and second-hour homothetic ratios. Allowance has been made for the photoneutrons which appear in the heavy water moderated reactors.

Figure 3 shows a typical set of curves obtained in this fashion.

The high precision obtained in solving the kinetic equations for a reactor with the help of the analogue computer, a precision which is close to that with which the power is actually measured in an operating reactor, warrants the following suggestion:

Instead of measuring the reactivity of the reactor, or rather its period, by synthesizing (with some electrical device), the expression $(dn/dt)/n$, which is the logarithmic derivative of the power, and thus not strictly equal to ρ/τ,[5] one can set in the true power as the controlling magnitude in a servo which, in turn, controls the potentiometer which defines ρ in an analogue circuit for the kinetic equations of the reactor. This setup gives a solution $n(t)$ which is compared with the true power, thus defining an error signal for the servo. If the latter is sufficiently rapid and accurate, the position of the slave potentiometer will, at each moment, permit a determination of the real value of the reactivity (Fig. 4).

DYNAMIC PROBLEMS

It has been assumed, up until now, that the reactivity could be varied only because of the motion of the adjusting rods, but some physical phenomena which take place in the reactor cause spontaneous reactivity variations, which have to be allowed for in complete computations.

The accumulation of the fission products in the reactor is a source of "poisoning." The reactivity is decreased by reason of the large thermal neutron capture cross section of some of these products.

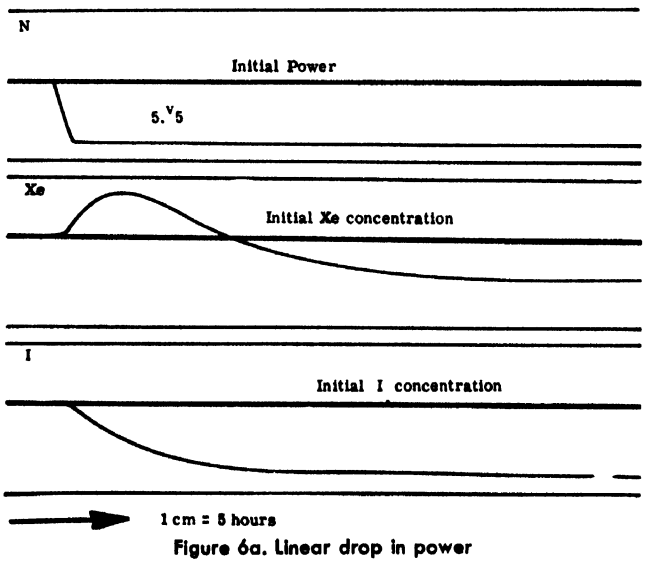

Figure 6a. Linear drop in power

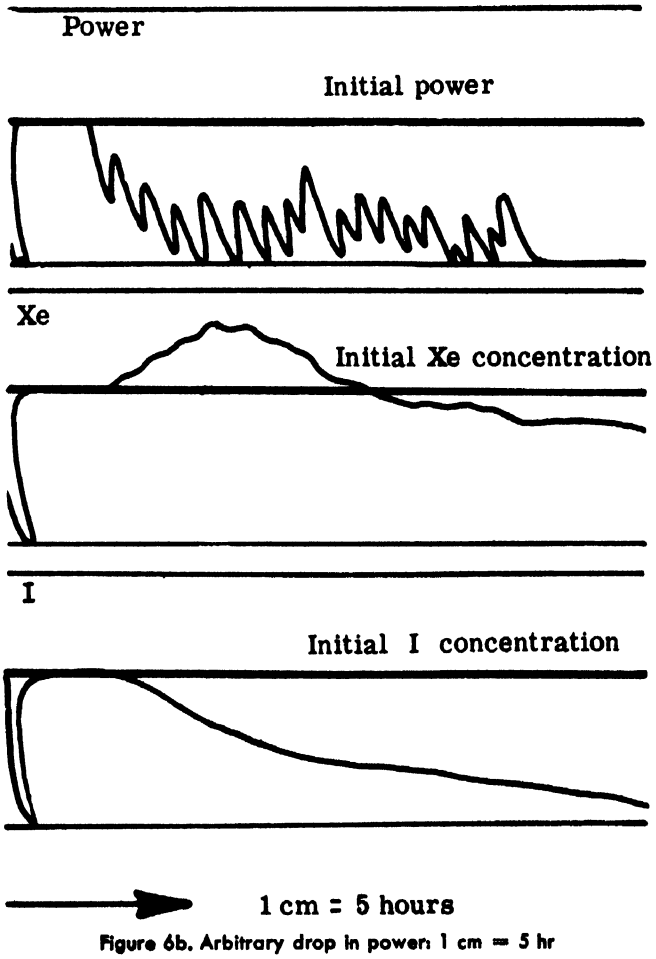

Figure 6b. Arbitrary drop in power: 1 cm = 5 hr

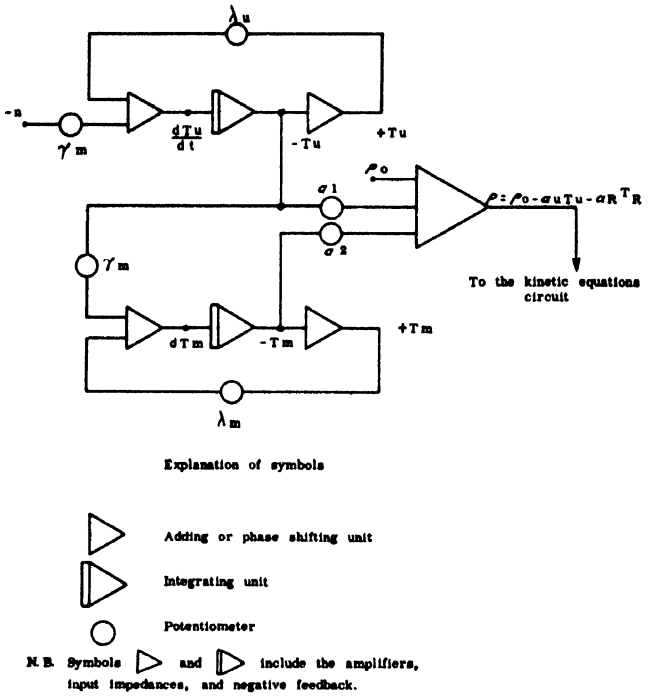

Figure 7. Block diagram for temperature effect

The fission products are produced, for example according to the following scheme

$$U \rightarrow \begin{cases} Xe \\ Te \rightarrow I \rightarrow Xe \end{cases} \text{Xe poisoning}$$

$$U \rightarrow \begin{cases} Pm \rightarrow Sm \\ Nd \rightarrow Pm \rightarrow Sm \end{cases} \text{Sm poisoning}$$

In this paper, we only consider the effects caused by xenon. Te is left out, since its average life is 2 minutes, while I is 6.7 hr. The system equations will thus be:[6]

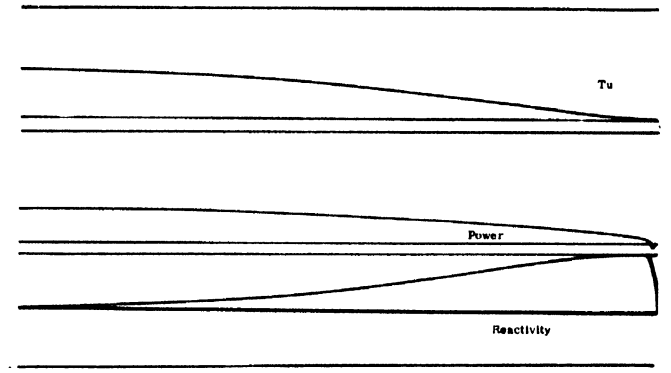

Figure 8. Effect of uranium temperature on reactivity after 200 per 10^5 positive jump

$$\frac{dI}{dt} = A_I n - \lambda_I I$$

$$\frac{dX}{dt} = A_x n + \lambda_I I - \lambda_x X - KnX$$

in which I and X are the concentrations of iodine and xenon atoms, n the power of the reactor, and λ_I and λ_X the disintegration constants of I and Xe. The analogue circuit is shown on Fig. 5.

The problem to be solved, by using this setup, is the following: Is it possible to reduce the power of the reactor according to a definite schedule, in order to minimize the additional reduction in reactivity caused by the accumulation of xenon?

It is known that, for a sudden drop in power, the xenon concentration increases by a large amount controlled by the neutron flux which corresponded to the initial equilibrium.

The typical results of various tests are presented in the recordings shown on Fig. 6. It will be seen that,

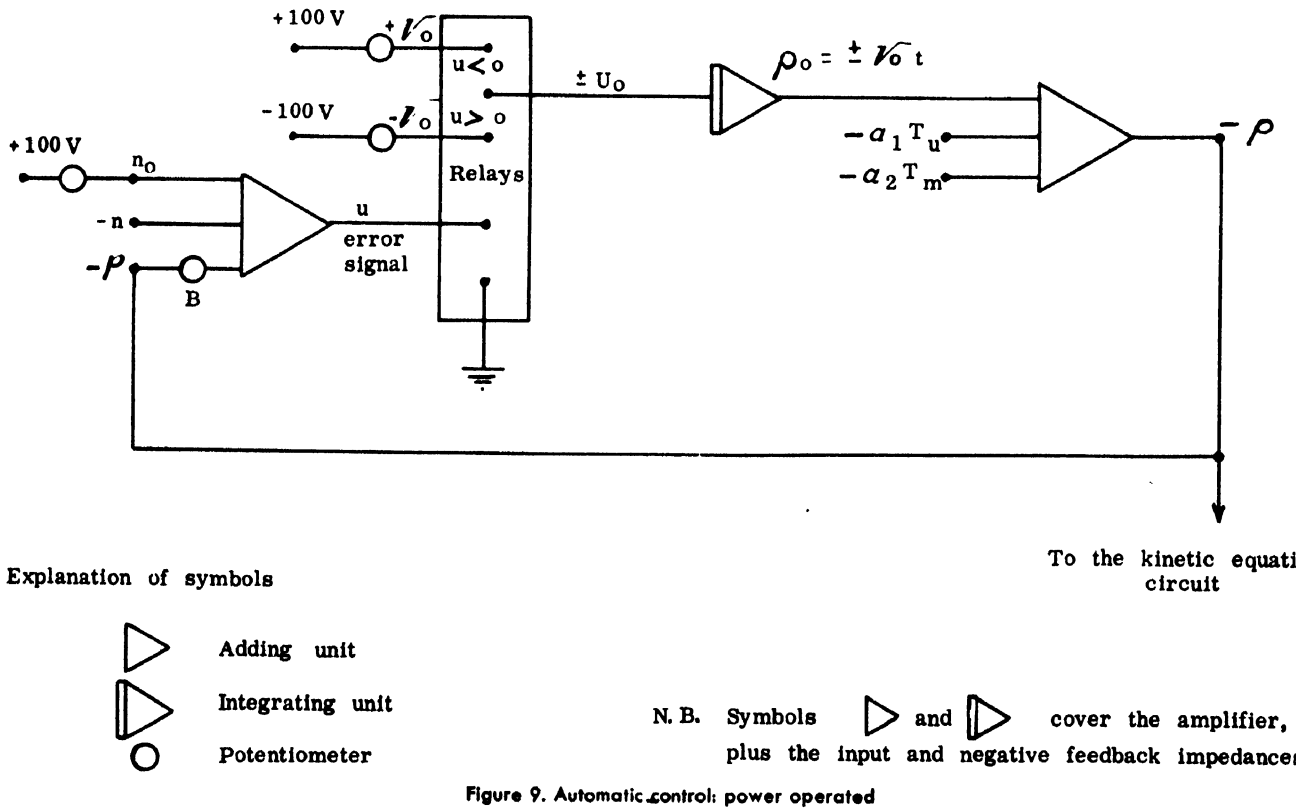

Figure 9. Automatic control: power operated

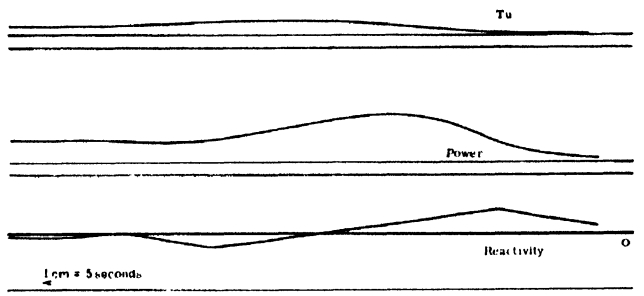

Figure 10a. Automatic control for the case of $B = 0$: rod speed, 10 per 10^5/sec

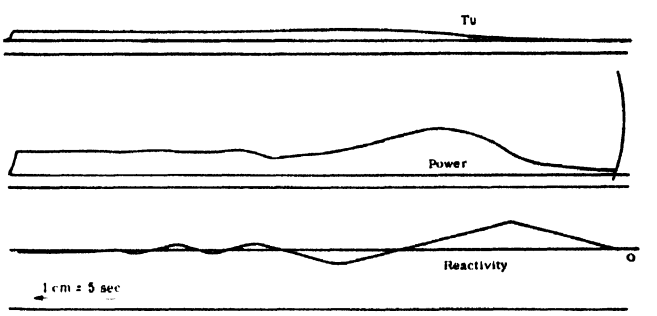

Figure 10b. Automatic control for the case of $B = 0$: rod speed, 20 per 10^5/sec

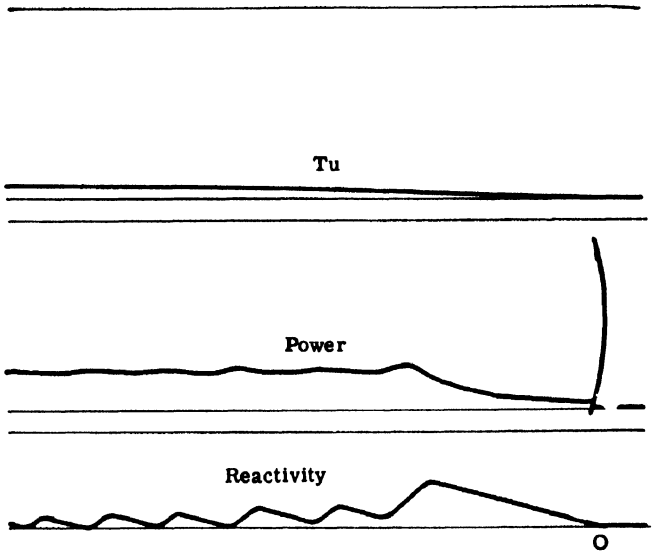

Figure 10c. Automatic control for the case of $B = 0$: speed of ascent of rods, 20 per 10^5/sec; speed of descent of rods, 75 per 10^5/sec

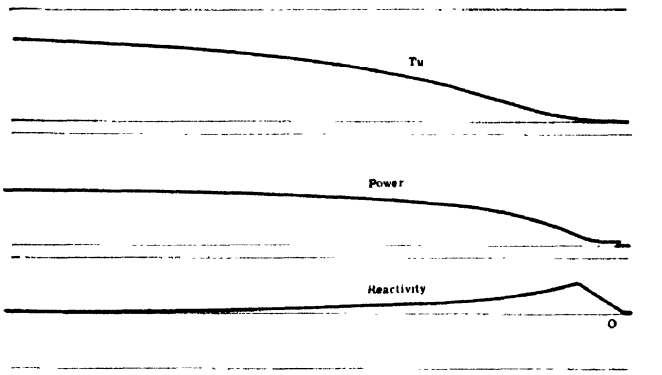

Figure 10d. Automatic control for the case of $B = 1$: speed of rods, 50 per 10^5/sec

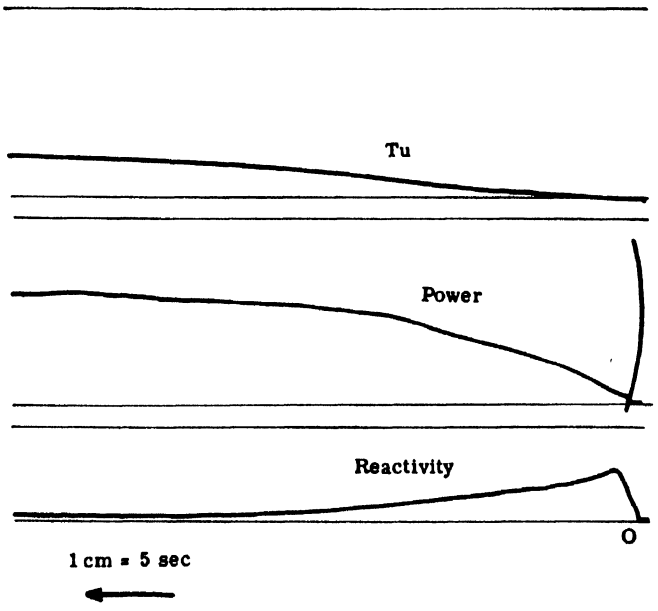

Figure 10e. Automatic control for the case of $B = 1$: speed of rods, 100 per 10^5/sec

due to the orders of magnitude of λ_I and λ_X, it is impossible to reduce appreciably the "hump" in the xenon concentration curve, unless inacceptably slow power decreases have to be countenanced.

The temperature effect, as is well known, is a consequence of the variation in reactivity due to the changes in the cross sections applicable to the various phenomena which form a part of the chain reaction.

If it is deemed desirable not to consider partial differential equations, coincidence has to be established between some mean temperatures, particularly fuel, moderator, coolant and exchanger temperatures.

We used equations of the following type:

$$\rho = \rho_0 - \alpha_1 T_u - \alpha_L T_M$$

$$\frac{dT_u}{dr} = \gamma_1 n - \lambda_V T_u$$

$$\frac{dT_M}{dr} = \gamma_2 T_u - \lambda_M T_M$$

in which T_u and T_M are the temperatures of the uranium and moderator respectively, and λ_u and λ_M the time constants of the relevant heat exchange phenomena. The schematic of the relevant analogue circuit is shown on Fig. 7.

We drew the curves corresponding to various values

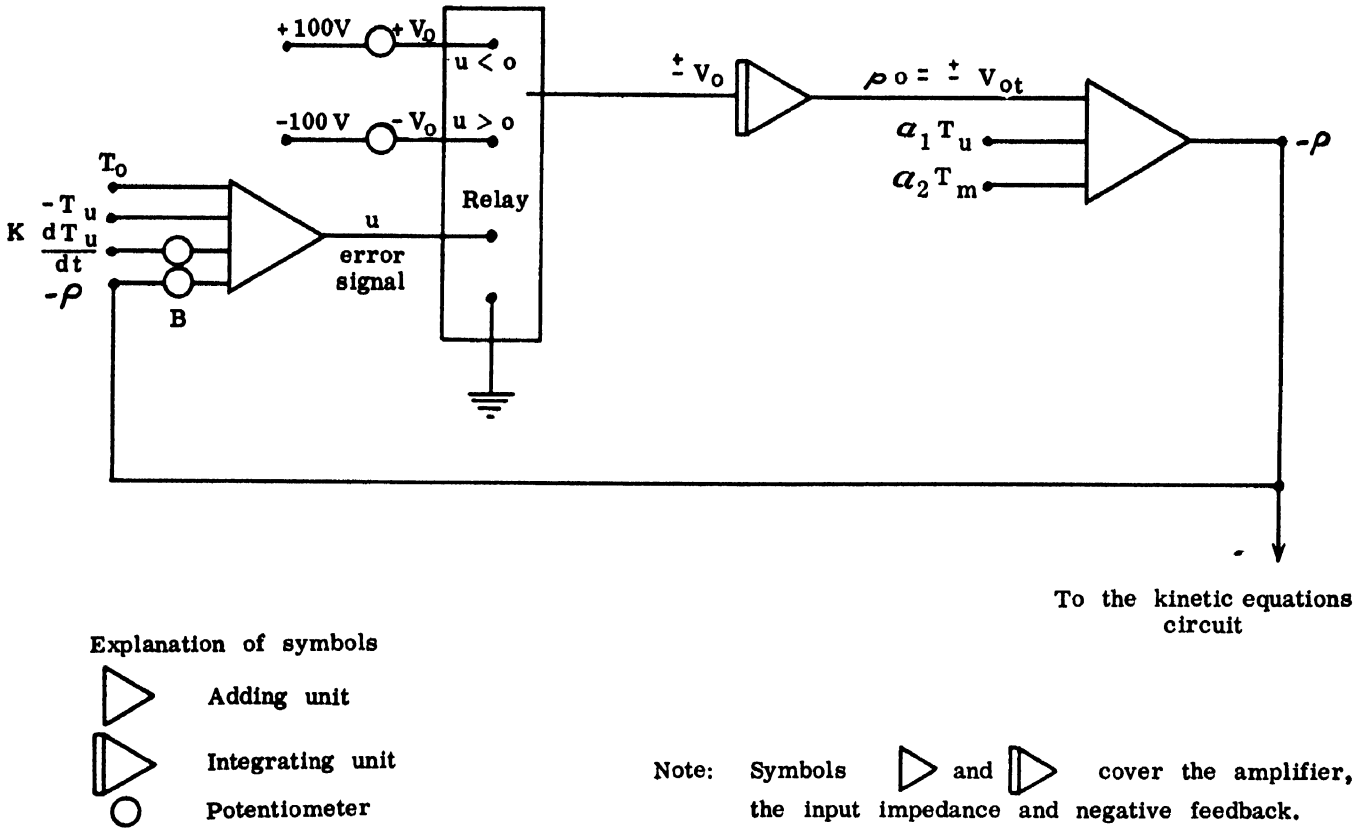

Figure 11. Automatic control temperature operated

of the coefficients, by varying, in particular: α_1 between 0 and 3 parts per 10^5 per degree of uranium temperature, α_2 between 0 and 30 parts per 10^5 per degree of uranium temperature; and λ_u between 0.010 and 0.030.

It will be noted, in particular, that, for the rapidly changing phenomena which are of interest to us, the variations in the moderator temperature are negligible (Fig. 8).

CONTROL PROBLEMS

In controlling a nuclear reactor it is necessary to cause the control rods to move in a certain manner, in other words, to impress a certain form on the curve $\rho(t)$, the reactivity as a function of time. Since we are dealing with events which take place within a few minutes' time, we can leave out the effects of xenon and samarium but, on the other hand, we must allow for the temperature effect.

The analogue circuit thus will be made up of: the kinetic network, the temperature network, and a special network, which simulates the control pattern.

The "all or nothing" type of control is particularly worth while: in other words, the control rods go up or down at a constant speed, according to the algebraic sign of an error signal. This type of control, which has been described in the literature, is used in the Saclay reactor in a special form (Aubergine).[7]

Even as was done for this reactor, a correction signal proportional to the reactivity will be inserted. This total signal, as computed by a summation-type amplifier, controls a three position relay. According to the position it occupies, on one side or the other, this relay gives a positive or negative constant voltage (which can be set to any one of a number of absolute values) which is used as the input for an integrating amplifier. The latter delivers a voltage which increases or decreases according to a predetermined linear function: this is the signal which corresponds to the ascent or descent of the control rods, and it is passed on to the kinetic circuit described above. Taken as a whole, the circuit is that shown on Fig. 9.

In order to simulate a control system devoid of a reactivity correcting signal, coefficient B is zeroed in the formula of the error signal

$$s = A(n_{required} - n_{obtained}) - B\rho$$

For the purposes of analogue wiring, this means that a

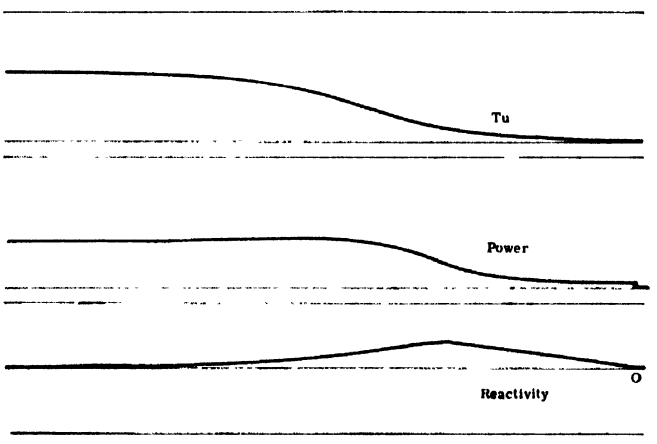

Figure 12. Automatic piloting, uranium temperature controlled: rod speed, 10 per 10^5/sec; $B = 1_0$

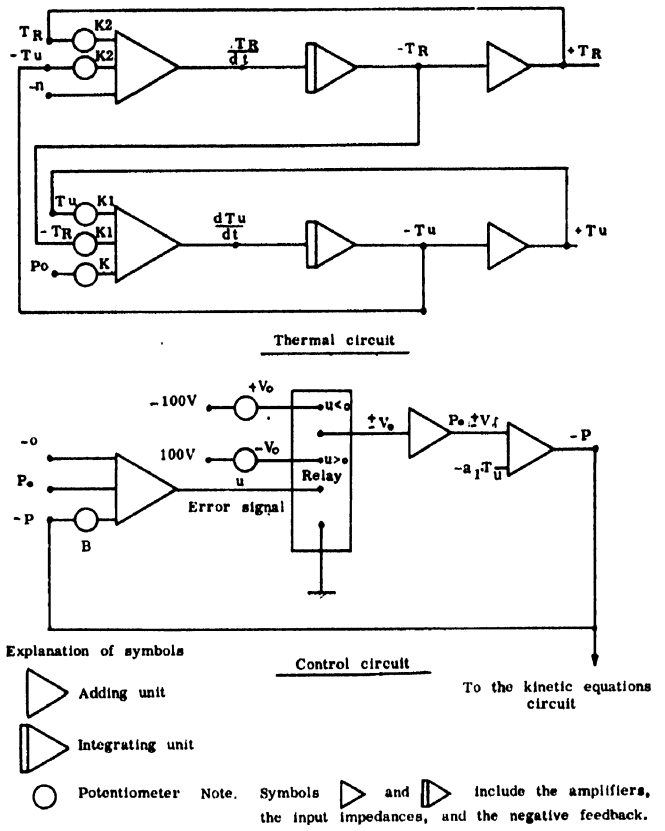

Figure 13. Automatic control of a nuclear power plant

potentiometer is placed at position O. By varying the position of the sliding contact of this potentiometer, the influence of the respective rates of the ($n_{required} - n_{obtained}$) and ρ signals on the behavior of the automatic control device considered can be investigated.

Other potentiometers make it possible to include the temperature effect coefficient, the speeds of ascent and descent of the control rods, etc.

Thus, it is possible to vary all these parameters in order to obtain a family of curves, some of which are reproduced on Fig. 10.

A number of important indications are drawn from the curves, among which we will mention the following:

1. In the absence of a reactivity correcting signal $B \neq 0$, there is some overshooting of the power, which may be large if the power itself is large.

2. This can be reduced if the speed of descent of the rods is larger than their speed of ascent. Nevertheless, undesirable fluctuations of the power will persist.

3. For $B \neq 0$, as shown here, we achieve control without any power overshooting, as was expected from theoretical and experimental work, on the Saclay reactor.[7]

4. Coefficient A and the speed of ascent of the control rods must be such as to satisfy:[7]

$$\left(\frac{A}{B}\right)^2 < \frac{\left(\frac{d\rho}{dt}\right)_{max}}{P_{max}^2}$$

if one wishes to be again in the area of critical operation of the automatic control device. This point was recently confirmed by experiments carried out at Saclay.[8]

5. The temperature effect does not alter the behavior of the control device, as long as the speed of the rod adjustment is adequate.

6. It is not impossible, in principle, to use very high rates of speed for the control rods as long as B is not zeroed, since the absolute magnitude of the reactivity necessarily remains limited.

We also designed analogue circuits which simulated automatic control by the temperature, rather than the power, and even by the demand of a postulated network load. The schematics of these designs are shown in Figs. 11 and 13. Typical curves are shown in Figs. 12 and 14.

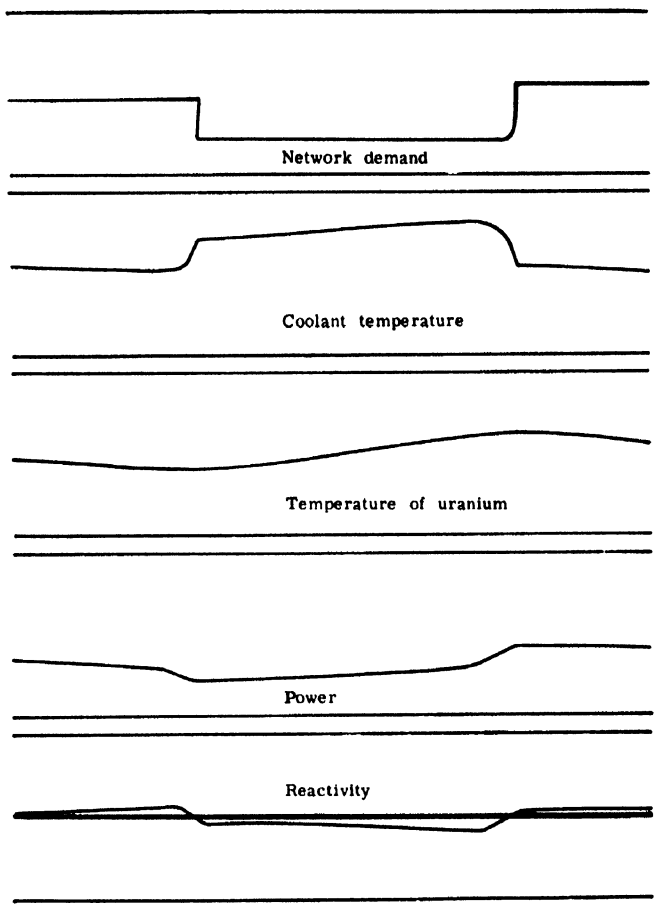

Figure 14. Automatic control by network demand

We shall merely outline the value of these studies, which are being pursued actively, in particular with respect to the thermo-transistor setups, which already enable us to stress the essential role of the reactivity correcting signal on the speed and accuracy of the controlling system.

The analogue circuits render precious services in the study of problems of kinetics, more specifically of cybernetics, having to do with nuclear reactors. Their use will doubtless develop rapidly, not only in the laboratories and servo research divisions, but also as a part of the control consoles of the reactors themselves.

REFERENCES

1. Sorka, W. W., *Analog methods in computation and simulation*, McGraw-Hill Co. (1954).
   Weill, J., *Les machines analogiques: le simulateur de pile* (complementary thesis), Paris (1953).
2. Howe, H. M. and Haneman, U. S. Jr., Proc. I.R.E. 41, p. 1487.
   Wade, E. J. and his group, *Electrica simulator*, U.S.P. 2,569,646 (2 October 1951).
   Fierro, D., Schneider, H. and Spooner, R. B., Nucleonics, p. 16 (April 1953).
   Spooner, R. B., Nucleonics, p. 36 (April 1954).
   Kron, G., *Electric circuit models of thermonuclear reactor*, Trans. Amer. Inst. Elect. Engrs., 73, part. I, p. 259–265 (1954).
3. Braffort, P., *La simulation dans les problèmes de pilotage automatique* (Bulletin d'Information Scientifique et Technique du C.E.A. 1st year, No. 3, p. 1).
4. Bell and Strauss, A.E.C.D. 2764.
   Pagels, W., A.E.C.D. 2764.
   Hurst, D. G., Electr. Eng., 70, p. 476.
   Trimmer, T.I.D., 5031, p. 311.
   O'Meara, F. E. and Fishbeck, K. H., Proc. of the 1953 Conference on Nuclear Energy, D-29°.
   Braffort, P. and Carteron, J., C.E.A. paper being prepared.
   Stone, J. J. and Mann, E. R., O.R.N.L. 1632 (20 April 1954).
   Burnup, T. E., A.E.R.E. RE/R 1486 (August 1954).
   Collies, D. M., Meeks, L. A. and Palmer, J. P., O.R.N.L. 1572 (September 1954).
   Wilson, I. and Burnup, T. E., A.E.R.E. RE/R 1485 (September 1954).
5. Weill, J., Onde Electrique, No. 321, p. 692 (1953).
   Weill, J., J. Phys. et Rad., 14, p. 46 (1953).
6. O'Meara, F. E., J. Appl. Physics, 29, p. 1200 (1953).
   Caillet, C. and Carpentier, J., C.E.A. paper being prepared.
7. Bonnaure, P., Braffort, P., Pelchowitch, J. and Weill, J., J. of Nuclear Energy, I, p. 24 (1954).
   Weill, J., P/335, "Complete Automatic Control System for Operating Nuclear Reactors," Volume 3, Session 12A, these Proceedings.
   Weill, J., Personal communication.
   Girerd, J., Personal communication.

Kinetics of Stationary Reactor Systems

By T. A. Welton,* USA

I. INTRODUCTION

The study of the time behavior of nuclear reactors has received much attention for two reasons. There was, on the one hand, the war-time incentive to obtain the most violent possible explosion from a temporarily super-critical assembly of the fissionable material, and, on the other hand, the following drive to devise reactors which were as safe as possible in their operation. These two lines of attack at first had little in common, not so much because of the divergence in aim, but because of the vast physical difference between the bomb-type system and the large, sluggish, thermal reactor. In recent years, however, the increasing demand for compact, enriched, and incompletely thermal reactors with high power density, has attached a much increased importance to the understanding of the time behavior of reactors other than bombs.

The questions of interest divide rather naturally into two general classes. The first type of question always refers to an accident of some sort. It may be imagined that a structural failure in the reactor causes the reactivity to rise rapidly. An operational error or an electronic failure may cause a similar difficulty. The typical question is that of predicting the consequences of any specified accident, so that suitable precautions can be taken. The prototype calculation is, of course, that of the energy yield of a bomb system when a planned structural change is executed.

The second type of question involves essentially the problem of stability, in which a small deviation from a steady operating condition is imagined. The question is then whether or not a return to the steady condition occurs without damage to the reactor.

The typical calculation is then similar in content to the conventional stability calculation for a servomechanism.

The two types of question shade into each other, the distinction being essentially one of emphasis. The first type emphasizes the magnitude and specific character of the initiating accident, the concomitant reactor behavior depending sensitively on these details. The second type emphasizes the steady behavior of the reactor, the accidental departure from equilibrium being unimportant in detail. This accident may not even be a mechanical or human failure, but rather an essentially statistical feature of normal reactor operation, such as turbulence.

It is the second type of question which will be discussed in this paper. For this purpose, it will be convenient to introduce some definitions. A *reactor system* will be defined as consisting of a chain-reacting region with attached heat-removal and reactivity-control mechanisms. A *stationary* reactor system will be defined as a reactor system whose equations of motion are unaltered by translating the origin of the time variable. In the nomenclature of non-linear differential equations, the word stationary would be equivalent to the term *autonomous*. A stationary reactor system is therefore one in which all operations occur automatically, in response to previous actions of the system rather than to the wishes of a human operator or some externally-sequenced controlling mechanism.

An *equilibrium* of a stationary reactor system is some combination of values for the variables of the system which allows all variables to remain constant in time.

An equilibrium is *stable* or *unstable* according to whether a small departure from equilibrium results or does not result in a return to equilibrium.

A reactor system may have more than one equilibrium for a given setting of the controls, although this is quite unusual. In some cases it is useful to distinguish between *linear* and *non-linear* stability. Linear stability implies that the disturbing accident is arbitrarily small, while non-linear stability implies an accident which is sufficiently large for non-linear effects to become important, although no *direct* damage from the large magnitude of the accident is assumed. Non-linear stability implies linear stability and linear instability implies non-linear instability. Linear stability can be associated with either non-linear stability or instability and non-linear instability similarly permits no conclusion on linear stability.

The basic problem of the field to be discussed is the discovery of a necessary and sufficient condition, in convenient form, for the non-linear stability of a general stationary reactor system. This ideal is yet to be achieved, inasmuch as the only method now available for attacking the general problem is that of detailed numerical integration of the equations of motion. This unfortunately cannot be claimed to be convenient, and is actually usually unfeasible for economic reasons. This paper will describe a number of partially successful attacks on the general problem, each of

* Oak Ridge National Laboratory. Including work by J. Chernick and J. A. Fleck, Jr., Brookhaven National Laboratory; W. K. Ergen, G. T. Trammell, A. M. Weinberg, and T. A. Welton, Oak Ridge National Laboratory.

which is useful in suitably specialized circumstances, and all of which are presumably useful in gaining the insight necessary for further progress.

Section II of this paper contains a deduction of the equations of motion for a stationary reactor system, to serve as a basis for the work to be described. Also included is a description of the various simple systems which have been studied.

Section III contains a treatment of the linear stability problem, together with some illustrative examples.

Section IV contains a treatment of the principal effects of compressibility.

Section V contains a treatment of non-linear stability.

The author is indebted to other workers for making their results available to him. These include, in addition to those listed on the title page, J. Franklin and H. B. Keller of the Institute of Mathematical Sciences of New York University. Informal discussions with H. Hurwitz of Knolls Atomic Power Laboratory and J. M. Stein of Westinghouse Atomic Power Division have also helped to shape the author's approach to the subject.

Finally, apologies are in order for the selection of material. This article is not intended as a simple compendium of existing knowledge on the subject of reactor kinetics. Rather, material has been chosen to make possible an orderly presentation of one fairly unified point of view, which necessarily reflects a considerable amount of the author's own background. Some work has been taken badly out of context for the purposes at hand; in a presentation from some other equally valid viewpoint, the distortions inherent in the present work would be exchanged for others.

II. GENERAL FORMULATION

The kinetic equations for reactor systems have been presented in nearly as many forms as there are authors. The writer has found the following formulation convenient; no more than this can be claimed. It is perhaps wise first to place the equations on a sound footing physically by explicitly stating the idealizations which will here be used. All of these idealizations are made in order to allow writing the reactor equations in terms of the past history of a discrete (and finite) set of reactor variables. The required physical assumptions can be detailed as follows:

(*a*) The spatial distribution of fissions does not depend (except for magnitude) on the other variables of the system.

(*b*) The spatial distribution of velocities of flowing coolant, moderator, and fuel is essentially independent of the variables of the system.

(*c*) The reactor system is prevented from interacting with its surroundings.

Provision (*a*) allows the use of the concept of effective reactivity, with all fissions distributed as the "fundamental mode" of the system. Thus the fission history of the reactor is completely specified by giving the reactor power as a function of time, together with a fixed spatial distribution function for the fissions. It is implied that all changes in reactor configuration due to control rod motion, fluid expansion and similar factors are to be treated as small perturbations, affecting in an important way only the effective reactivity, which is the average number of fissions arising directly from a single fission. Within the author's experience, this condition is universally satisfied to adequate accuracy.

Provision (*b*) allows the specification of the temperature and density state of the fluid components of the reactor system in terms of inlet and outlet temperatures as functions of time. Specifically ruled out, for example, is the possibility of a gross change in the flow pattern induced by differential viscosity changes arising from differential heating. There is no reason in principle why such effects should not be included, but they seem in general to have small importance and in most cases to add unduly to the difficulty of treatment. It should be emphasized that those small motions of expansion by the liquid system which are required for reactivity change are usually to be included as small perturbations on the main motion; unimportant in their effects on heat removal but vital for their effects on reactivity.

Provision (*c*) is the one which renders the reactor system stationary and is therefore important in principle. It is, however, difficult to define completely and resort must be made to examples. Suppose a steady volume flow of constant temperature cooling water is supplied to the heat exchanger of a reactor system and that the heated water is exhausted without possibility of return. The reactor system, including the heat exchanger, but not the water supply, is then said to be isolated from its surroundings because, although the surroundings carry away heat, they do not carry any time-dependent information into the reactor system. In general, it is this non-introduction of time-dependent information which is involved in provision (*c*). For this purpose, the boundaries of the reactor system must be suitably enlarged to include all important sources of feed-back. Too large a reactor system increases the difficulty of calculation, while too small a system will ignore important sources of instability. A compromise must be made in every system, and often should be made differently for calculation of different phenomena in the same system. General rules are extremely difficult to give, while experience and sound intuition are of the greatest assistance. A number of illustrations will appear in the course of this paper.

The general equations of motion for a reactor system can now be deduced, subject to provisions (*a*), (*b*), and (*c*). For the moment, ignore delayed neutrons and let:

$P(t)$ = reactor fission power at time t

$F(t,\tau)$ = number of fissions produced at time t per unit range of τ by a fission occurring at time $t - \tau$.

A simple integral equation can then be written for the power

$$P(t) = \int_0^\infty d\tau F(t,\tau)P(t-\tau) \tag{1}$$

Note that the function $F(t,\tau)$ would be independent of t if the reactivity of the system did not change with time. Although Equation 1 is required for a completely general treatment, a considerable simplification can be made in all cases of interest by assuming that P does not change by a large fraction of itself during the time required for F to drop a small fraction of its peak value. Assume:

$$P(t-\tau) = P(t) - \tau\dot{P}(t) \tag{2}$$

neglecting higher terms in the Taylor expansion. Substitution of Equation 2 in Equation 1 yields

$$P(t) = P(t)\int_0^\infty d\tau F(t,\tau) - \dot{P}(t)\int_0^\infty d\tau F(t,\tau)\tau$$

$$\text{or} \quad P(t) = \frac{\int_0^\infty d\tau F(t,\tau) - 1}{\int_0^\infty d\tau F(t,\tau)\tau} P(t) \tag{3}$$

It is consistent with the condition that validates Equation 2 to assume that each fission produces in the next generation a number of fissions which differs only slightly from unity. Accordingly, let

$$\int_0^\infty d\tau F(t,\tau) = 1 + k(t) \tag{4}$$

and define

$$\bar{\tau} = \int_0^\infty d\tau F(t,\tau)\tau \tag{5}$$

The quantity $k(t)$ will be termed the excess prompt reactivity and $\bar{\tau}$ will be called the prompt generation time.

It should be noted that $\bar{\tau}$ depends only slightly on time, since $k(t)$ is to be small compared with unity, and this dependence will be systematically ignored.

The fundamental Equation 1 now appears in a simplified approximate form

$$\dot{P}(t) = \frac{1}{\bar{\tau}} k(t)P(t) \tag{6}$$

which has become a standard starting point in treatments of reactor kinetics. It must be emphasized that it is not a general equation. It is possible to find reactor models for which it is exact, but in general two assumptions must be invoked for its validity:

$$|k(t)| \ll 1 \tag{7a}$$

$$\left|\frac{\dot{k}}{k}\right| \ll \frac{1}{\bar{\tau}} \tag{7b}$$

Condition 7a guarantees the consistency of the Taylor expansion of $P(t)$, as well as the consistency of the assumption that $\bar{\tau}$ is independent of time. Condition 7b is required in order that the instantaneous reactivity be well defined. If k contains higher frequencies than $1/\bar{\tau}$, then Equation 6 becomes only qualitatively meaningful, since the detailed averaging out of these high frequencies by the differential Equation 6 and the integral Equation 1 may be quite different, unless $F(t,\tau)$ has exactly the exponential form required to validate Equation 6.

It is now necessary to modify the equation to take into account the effect of a time-dependent neutron source. Let $S(t)$ be the neutron source strength present in the reactor in the fundamental mode. For convenience, the specification of source strength will be as the reactor power which would be present if no reproduction occurred, so that all fissions are those produced (in the fundamental mode) directly by absorption of *source* neutrons. With this definition, Equation 6 must be replaced by

$$\dot{P}(t) = \frac{1}{\bar{\tau}} k(t)P(t) + \frac{1}{\bar{\tau}} S(t) \tag{8}$$

To verify that this form is correct, assume k and S independent of time, take k negative and $P = 0$ (source multiplication problem), so that

$$P = \frac{S}{-k} \tag{9}$$

This result also follows from the definition of k and S. If one fission results directly in $1 + k$ fissions, then the total number of fissions resulting from a single source fission is

$$1 + (1+k) + (1+k)^2 + \cdots = \frac{1}{1-(1+k)} \tag{10}$$

and the total power resulting from source strength S is given by Equation 9.

In normal operation of any reactor running at a macroscopically important power density, the important neutron source is that supplied by the delayed-neutron emitting fission fragments. In practice then, $S(t)$ will be given in terms of a linear integral operation on the past history of the reactor power. It is convenient to write

$$S(t) = \beta\int_0^\infty d\tau D(\tau)P(t-\tau) \tag{11}$$

where β will be called the effective fraction of delayed neutrons and $D(\tau)$ is a delay distribution function which satisfies

$$\int_0^\infty d\tau D(\tau) = 1 \tag{12}$$

The original provision (b) suffices to insure that D will be a function of the delay time only, and not of the absolute time. It must be remembered, however, that $D(\tau)$ alters its form as the flow of fuel (if any) is altered, and the parameter β likewise alters its value with the fuel flow conditions. Only in a fixed fuel reactor will β and $D(\tau)$ be related directly to the periods and yields of the conventional delayed neutron periods.

The reactor power equation will then be written

$$\dot{P}(t) = \frac{1}{\bar{\tau}} k(t)P(t) + \frac{\beta}{\bar{\tau}}\int_0^\infty d\tau D(\tau)P(t-\tau) \tag{13}$$

The excess prompt reactivity can be conveniently rewritten:

$$k(t) = \delta(t) - \beta - \phi(t) \tag{14}$$

where $\delta(t)$ is the reactivity which is under direct external control (control rods, for example) and $\phi(t)$ is the negative reactivity contribution arising from the reactor power (thermal expansion, for example). The combination $\delta - \phi$ is the excess delayed reactivity, and if δ is held constant, the equilibrium of the reactor system will occur when the power becomes such as to make $\phi = \delta$. A time variation for δ violates the original provision (*c*), but it will be convenient to retain this generality for the time being.

Provision (*c*) guarantees that $\phi(t)$ shall be given by an integral operation on the reactor power, invariant under time displacement. Provision (*b*) makes it likely that this integral operation will be linear, and in fact all reactor systems which have been studied, to the author's knowledge, actually have this property. This linear property requires, for example, that heat transfer coefficients be independent of temperature difference over the range of interest. Throughout the remainder of this treatment, then, a simple general form for ϕ will be used

$$\phi(t) = \int_0^\infty d\tau G(\tau) P(t - \tau) \tag{15}$$

The quantity $G(\tau)$ obviously is the negative reactivity contribution at time τ arising from unit fission energy released in the reactor at time zero, and might properly be called the energy coefficient of negative reactivity. If P and ϕ are held constant

$$\phi = P \int_0^\infty d\tau G(\tau) \tag{16}$$

so that $\int_0^\infty d\tau G(\tau)$ is properly called the power coefficient of negative reactivity. If δ is held fixed, the equilibrium of the reactor system is attained at a power such that ϕ by Equation 16 becomes equal to δ. The quantity $G(\tau)$ is not necessarily positive, but

$$\int_0^\infty d\tau G(\tau)$$

will be positive for any reasonable system. Exceptions can be found by exercise of sufficient ingenuity, but the resulting systems do not appear very promising from the viewpoint of safety.

An expression for ϕ will be useful in what follows. Differentiation of Equation 15 yields

$$\dot{\phi}(t) = \int_0^\infty d\tau G(\tau) \frac{\partial}{\partial t} P(t - \tau) = -\int_0^\infty d\tau G(\tau) \frac{\partial}{\partial \tau} P(t - \tau) \tag{17}$$

and integration by parts then leads to

$$\dot{\phi}(t) = G(0)P(t) + \int_0^\infty d\tau \dot{G}(\tau) P(t - \tau)$$

$$\dot{\phi}(t) = G(0)\left\{P(t) - \int_0^\infty d\tau K(\tau) P(t - \tau)\right\} \tag{18}$$

where the new kernel $K(\tau)$ is given by

$$K(\tau) = -\frac{1}{G(0)} \dot{G}(\tau) \tag{19}$$

and therefore satisfies

$$\int_0^\infty d\tau K(\tau) = 1 \tag{20}$$

The quantity $G(0)$ is the *instantaneous* negative reactivity effect from unit fission energy. For much of what is to follow, $G(0)$ will be taken as a positive (non-zero) quantity. This is generally a valid assumption, but the nature of the approximation will require some examination. Any truly instantaneous reactivity effect must arise *directly* from the heating of the fuel. Such effects (Doppler effect, change of thermal base in a homogeneous reactor) exist, but they may be quite unimportant in comparison with effects which require a finite time for establishment, such as thermal expansion, for which $G(0)$ would vanish. It is extremely unusual for $G(0)$ to be negative, and this case will not be considered.

It is very convenient to define a dimensionless logarithmic power variable by

$$P = P_0 e^Q \tag{21}$$

where

$$P_0 \int_0^\infty d\tau G(\tau) = \delta$$

The constant P_0 is, of course, just the equilibrium power. Equations 13, 14, and 21 yield

$$\dot{Q} = \frac{1}{\bar{\tau}}(\delta - \beta - \phi) + \frac{\beta}{\bar{\tau}} e^{-Q(t)} \int_0^\infty d\tau D(\tau) e^{Q(t-\tau)} \tag{22}$$

If then the assumption of positive $G(0)$ is made, Equation 22 can be differentiated and combined with Equation 18 to give

$$\ddot{Q} = \frac{\dot{\delta}}{\bar{\tau}} - \frac{G(0)P_0}{\bar{\tau}}\left[e^{Q(t)} - \int_0^\infty d\tau K(\tau) e^{Q(t-\tau)}\right] + \frac{\beta}{\bar{\tau}} \frac{d}{dt}\left[e^{-Q(t)} \int_0^\infty d\tau D(\tau) e^{Q(t-\tau)}\right] \tag{23}$$

It is convenient to define a new constant

$$\Omega^2 = \frac{G(0)P_0}{\bar{\tau}} \tag{24}$$

This quantity has the dimensions of a squared reciprocal time, and will appear as the square of a circular frequency, of fundamental importance for the kinetics of a reactor system. By making use of the property (Equation 20) of $K(\tau)$, Equation 23 can be rewritten as

$$\ddot{Q} + \Omega^2(e^Q - 1) = \frac{\dot{\delta}}{\bar{\tau}} + \Omega^2 \int_0^\infty d\tau K(\tau)[e^{Q(t-\tau)} - 1] + \frac{\beta}{\bar{\tau}} \frac{d}{dt}\left[e^{-Q} \int_0^\infty d\tau D(\tau) e^{Q(t-\tau)}\right] \tag{25}$$

This equation displays the variable Q as the coordinate of a one-dimensional, non-linear oscillator. The

externally applied force is $\dot{\delta}/\bar{\tau}$, while the other two terms on the right of Equation 25 are hysteresis effects which, under suitable conditions, will lead to damping. It will be a large part of the task of this paper to deduce as generally as possible the conditions on $K(\tau)$ and $D(\tau)$ under which this damping will occur.

At this point it will be useful to name and describe briefly the simple special cases of reactor systems which have been studied by various authors. The simpler cases mainly serve to build up a collection of fairly useful mathematical techniques, and, in fact, no detailed stability calculations of the type under consideration have been performed for a reactor system with any realistic degree of complication.

Case *A* is the so-called constant power extraction-no delayed neutron system. In it β is set equal to zero and, strictly, the heat removal is idealized by the assumption that a definite, constant amount of heat, P_0, is extracted per unit time. As stated, ϕ for case *A* cannot be written in the standard form of Equation 18. Equation 22 becomes

$$\dot{Q} = \frac{1}{\bar{\tau}}(\delta - \phi) \tag{26}$$

and Equation 18 must be replaced by

$$\phi(t) = G(0)\{P(t) - P_0\} \tag{27}$$

so that ϕ remains constant when the reactor power exactly balances the heat extraction. The notation $G(0)$ is retained with unchanged meaning, although $G(\tau)$ is no longer a defined quantity. Combination of Equations 26, 27, 21, and 24 yields

$$\ddot{Q} + \Omega^2(e^Q - 1) = \frac{\dot{\delta}}{\bar{\tau}} \tag{28}$$

which is actually equivalent to Equation 25, with $K(\tau)$ set equal to zero, in addition to β.

This equation has been treated by a variety of methods. The method chosen for use in this discussion makes full use of the analogy to elementary particle mechanics. It is adequate for the purpose at hand and has the advantage of familiarity to the physicist, who is probably the most common worker in the field of reactor kinetics. Other methods, based on the standard treatment of non-linear, second order, autonomous systems have found considerable favor. In general, the author has found that although these methods, familiar to the mathematician, make possible elegant treatments of the simpler systems, they do not seem capable of easy generalization to the complicated systems which are of real interest.

The motion represented by Equation 28, with $\dot{\delta} = 0$, is a simple conservative, periodic motion. There exists an energy constant

$$E = \tfrac{1}{2}\dot{Q}^2 + \Omega^2(e^Q - Q) \tag{29}$$

with a potential energy which is positive everywhere, and which increases monotomically to infinity as $|Q|$ becomes infinite; $Q = 0$ being the point of minimum potential energy.

Under these conditions, specification of the value of E determines *two* turning points and the motion is strictly periodic. Note that for small amplitudes, Equation 28 becomes

$$\ddot{Q} + \Omega^2 Q = 0 \tag{30}$$

which makes explicit the role played by the constant Ω^2 as a squared frequency. It will be seen that this oscillation never appears in such simple form in actual systems because of the delayed neutron effects, but its theoretical importance will be apparent. Note also that $G(0)$ must be positive, as has been assumed, in order to achieve stability. This requirement corresponds to the elementary statement that a negative temperature coefficient of reactivity leads to stable reactor operation.

Detailed properties of the solutions of Equation 28 ($\dot{\delta} = 0$) have been given by many authors. These properties are largely unnecessary for the matters at hand, but the interested reader should refer to Ergen and Weinberg[1] for a treatment based essentially on the mechanical analogy here used.

Case *B* is the reactor system with constant heat-removal and constant delayed neutron source. This is the simplest system which is sufficiently realistic to allow conclusions about real reactor systems, inasmuch as the delayed neutron source plays an absolutely controlling role in reactor kinetics. The formal description of this case again sets $K(\tau) = 0$, but replaces the actual $D(\tau)$ by a function which dies very slowly compared with the characteristic time Ω^{-1}. This has the result that

$$\int_0^\infty d\tau D(\tau)P(t - \tau) = P_0 \tag{31}$$

very closely, if the system is stable. If the system is *not* stable, such a simple averaging may be incorrect and a proof of instability with this model should therefore not be regarded as conclusive. As to the validity of this model for actual reactor systems, it should be remarked that Ω^{-1} becomes fairly small compared with a mean delay period for many present-day reactors at high power densities.

The complete equation of motion for Q in case *B* is

$$\ddot{Q} + \Omega^2(e^Q - 1) = \frac{\beta}{\bar{\tau}}\frac{d}{dt}e^{-Q} = -\frac{\beta}{\bar{\tau}}\dot{Q}e^{-Q} \tag{32}$$

This equation will be discussed in a later section.

Case *C* is the simplest example of a reactor system with non-zero $K(\tau)$. It will be called a reactor with complete mixing and no delayed neutron source. The name refers to a fluid fuel reactor in which fuel is injected at a fixed temperature into a reacting region. The flow is taken to be so random in character that the fluid filling the reactor has a temperature which is uniform over the reactor. Although such a random flow is inefficient hydraulically, some approximation to this situation is present in many reactors.

This case is specified by $\beta = 0$ and by a simple expression for $K(\tau)$, which can be derived as follows. Let C be the heat capacity of the reactor, and let λ be

the fraction of the reactor fluid which enters and exits per second. Let the inlet fluid temperature be zero, the reactor (and outlet) temperature be T, and the decrease in reactivity per unit rise of reactor temperature be α. A simple heat balance equation can be written by equating the rate of increase of heat energy content of the reactor to the difference between fission energy input and output in the form of heated fluid:

$$C\dot{T} = P - \lambda CT$$

or

$$\alpha\dot{T} + \lambda\alpha T = \frac{\alpha}{C}P$$

or

$$\dot{\phi} + \lambda\phi = \frac{\alpha}{C}P \tag{33}$$

This equation can be integrated immediately to yield

$$\phi(t) = \frac{\alpha}{C}\int_0^\infty d\tau e^{-\lambda\tau}P(t-\tau) \tag{34}$$

from which is obtained

$$G(\tau) = \frac{\alpha}{C}e^{-\lambda\tau}$$

$$G(0) = \frac{\alpha}{C}$$

$$K(\tau) = -\frac{\dot{G}(\tau)}{G(0)} = \lambda e^{-\lambda\tau} \tag{35}$$

The complete equation of motion for case C is then

$$\ddot{Q} + \Omega^2(e^Q - 1) = \Omega^2\lambda\int_0^\infty d\tau e^{-\lambda\tau}[e^{Q(t-\tau)} - 1] \tag{36}$$

Case C has been studied at some length by J. Chernick[3] under a different name and with application to an entirely different reactor situation. The form of Equation 33 allows application to what is usually called the case of Newton's law of cooling, in which heated fuel loses heat to coolant at a rate proportional to the temperature difference between fuel and coolant. Case C, since it can be described by two coupled first-order equations, is susceptible to treatment by the conventional methods of non-linear, dissipative mechanics. Proceeding in this way, Chernick[3] has proved the stability of the system described by Equation 36. A treatment in terms of the methods to be described will be given in a later section.

Case D is another idealized circulating fuel reactor, the so-called slug-flow case with constant power density and constant importance for reactivity effects of fuel density changes. Delayed neutrons are again neglected. It is assumed that all fuel entering the reactor spends exactly the same time, θ, within the reacting region, that the fuel enters at fixed temperature zero, that the temperature contribution to reactivity is determined by the volume average of the temperature, and that the fuel heats while it is in the reactor at a rate independent of position, but proportional to the reactor power.

The equations are deduced as follows. Let C be the total heat capacity of the fluid in the reactor, introduced at assumed inlet temperature zero. Let $T(t,s)$ be the temperature of fluid at time t which has been present in the reacting region for time s. A simple integral relation can then be written between T and P:

$$CT(t,s) = \int_0^s d\tau P(t-\tau) \tag{37}$$

A simple consequence is that if P and T are constant, the outlet temperature $T(\theta)$ becomes

$$T(\theta) = \frac{\theta}{C}P \tag{38}$$

This is clearly a correct relation, coinciding exactly in this case of no time dependence with the relation deduced from Equation 33 for the case of no time dependence

$$T = \frac{1}{\lambda c}P \tag{39}$$

The parameters $1/\lambda$ and θ play the role of mean residence times for fluid particles within the reacting region of the cases C and D, respectively.

The other assumptions for case D can now be invoked to write

$$\phi(t) = \frac{\alpha}{\theta}\int_0^\infty dsT(t,s) \tag{40}$$

where α has the same significance as in case C. Combination of Equations 37 and 40 yields

$$\phi(t) = \frac{\alpha}{C\theta}\int_0^\infty ds\int_0^s d\tau P(t-\tau)$$

or

$$\begin{aligned}\phi(t) &= \frac{\alpha}{C\theta}\int_0^\theta d\tau P(t-\tau)\int_\tau^\theta ds \\ &= \frac{\alpha}{C}\int_0^\theta d\tau P(t-\tau)\left(1-\frac{\tau}{\theta}\right) \\ &= \frac{\alpha}{C}\int_0^\infty d\tau 1(\theta-\tau)\left(1-\frac{\tau}{\theta}\right)P(t-\tau)\end{aligned} \tag{41}$$

where $1(\theta-\tau)$ is the unit step function, vanishing for $\tau > \theta$. From Equation 41

$$G(\tau) = \frac{\alpha}{C}1(\theta-\tau)\left(1-\frac{\tau}{\theta}\right)$$

$$G(0) = \frac{\alpha}{C}$$

$$-\dot{G}(\tau) = \frac{\alpha}{C\theta}1(\theta-\tau)$$

$$K(\tau) = -\frac{\dot{G}(\tau)}{G(0)} = \frac{1}{\theta}1(\theta-\tau) \tag{42}$$

The complete equation of motion becomes

$$\ddot{Q} + \Omega^2(e^Q - 1) = \frac{\Omega^2}{\theta}\int_0^\theta d\tau[e^{Q(t-\tau)} - 1] \tag{43}$$

This equation has been derived and studied in some detail by Ergen,[1] who has shown that with the excep-

tion of special values for θ, the system of Equation 43 is damped. The equation is too idealized for an actual reactor, but is interesting as the simplest example studied containing an integral operator which is not reducible to a differential operation.

It is not profitable at this point to describe more specialized models, inasmuch as the methods developed to treat these simple cases are capable of great generality.

III. LINEARIZED TREATMENT

As in all stability analyses, the most pressing problem is to be able to guarantee the linear stability of a reactor system. This guarantee can be made unequivocally by the use of simple methods, and all engineering experience strongly suggests that such a guarantee is not only a necessary, but usually a sufficient condition for successful operation. Such methods as exist for the discussion of non-linear stability are easily suggested by the linear treatment, and one important stability problem—that of the effect of compressibility—can be treated completely within the linear framework.

Consider the basic Equation 25 under the assumption that only terms linear in Q are to be retained:

$$\ddot{Q} + \Omega^2 Q = \frac{\dot{\delta}}{\bar{\tau}} + \Omega^2 \int_0^\infty d\tau K(\tau) Q(t-\tau) + \frac{\beta}{\bar{\tau}} \frac{d}{dt}\left[-Q(t) + \int_0^\infty d\tau D(\tau) Q(t-\tau)\right] \quad (44)$$

The stability of this system is often investigated by the use of Nyquist's theorem, but for the further purposes of this paper a more convenient procedure is to use the mechanical analogy previously outlined. Multiply Equation 44 by $\dot{Q}$, and call $\dot{\delta}/\bar{\tau}$, which is the applied force, f. The result can be written

$$f\dot{Q} = \frac{d}{dt}\left[\frac{1}{2}\dot{Q}^2 + \frac{1}{2}\Omega^2 Q^2\right] - \Omega^2 \int_0^\infty d\tau K(\tau) Q(t-\tau)\dot{Q}(t) + \frac{\beta}{\bar{\tau}}\left[\dot{Q}^2(t) - \int_0^\infty d\tau D(\tau)\dot{Q}(t-\tau)\dot{Q}(t)\right] \quad (45)$$

Ergen[1] and Ergen and Weinberg[2] have made extensive use of a stability criterion which can be stated as follows:

If a periodic motion of the system is induced by application of a suitable force f (control-rod motion), then if positive work is always done on the system by f, averaged over a cycle, the free motion ($f = 0$) would damp.

This condition is plausible, but must be used with caution as these authors observe. First, if the criterion is to be used in the non-linear case, the positive sign of the rate of working must be demonstrated for *all* possible wave forms. This difficulty is obviated in the linearized case, where the only possible natural periodic wave form is a sinusoid. The second difficulty is that the transition from positive rate of working to damping is an intuitive one, albeit extremely plausible. This objection can be removed by the simple observation that if instability is to be possible, then for some choice of the parameters $\beta/\bar{\tau}$ and Ω^2, the stability must be neutral, with the solution a truly periodic sinusoid. At this point of neutral stability, the rate of working will exactly vanish, so that for instability to be possible, the rate of working must vanish at some point in the parameter space.

Now assume a sinusoidal variation for Q

$$\begin{aligned} Q(t) &= q \sin \omega t \\ \dot{Q}(t) &= \omega q \cos \omega t \\ Q(t-\tau) &= q \cos \omega\tau \sin \omega t - q \sin \omega\tau \cos \omega t \\ \dot{Q}(t-\tau) &= \omega q \cos \omega\tau \cos \omega t + \omega q \sin \omega\tau \sin \omega t \end{aligned} \quad (46)$$

and average Equation 45 over a cycle:

$$\begin{aligned} \langle f\dot{Q}\rangle &= +\frac{\Omega^2 q^2}{2}\int_0^\infty d\tau K(\tau)\omega \sin \omega\tau \\ &\quad + \frac{\beta\omega^2 q^2}{2\bar{\tau}}\left[1 - \int_0^\infty d\tau D(\tau)\cos \omega\tau\right] \\ &= \frac{\Omega^2\omega^2 q^2}{2}\int_0^\infty d\tau K(\tau)\frac{\sin \omega\tau}{\omega} + \frac{\beta\omega^2 q^2}{2\bar{\tau}} \\ &\quad \int_0^\infty d\tau D(\tau)(1 - \cos \omega\tau) \end{aligned} \quad (47)$$

It is clear that $\langle f\dot{Q}\rangle$ is necessarily positive if

$$\int_0^\infty d\tau K(\tau)\frac{\sin \omega\tau}{\omega} \geq 0 \quad (48)$$

$$\int_0^\infty d\tau D(\tau)(1 - \cos \omega\tau) \geq 0 \quad (49)$$

Physically $D(\tau)$ must be non-negative and $(1 - \cos \omega\tau)$ is likewise non-negative, so that Equation 49 is automatically satisfied. It is then said that the delayed neutrons *always* lead to damping in the linearized case. Ergen[1] has shown that this holds true even in the non-linear case, and his proof will be reproduced in Section V. A sufficient condition for linear stability is therefore that Equation 48 be satisfied for all ω. This condition leads to what will be termed *unconditional* linear stability, since stability is independent of the values of the parameters. It has been shown by the author[4] that Equation 48 also implies unconditional non-linear stability and this proof will also be presented in Section V. Ergen and Weinberg[2] originally deduced the criterion of Equation 48 for linear stability by straightforward application of Nyquist's theorem.

Conditional linear stability is obtained when $\langle f\dot{Q}\rangle$ is positive for all ω for the *actual* values of the parameters, but some choice of parameters would lead to instability. In general, the requirement of conditional linear stability is a suitable basis for reactor design, although some suspicion exists that it may not be *absolutely* safe. Such a strong guarantee can be had by requiring unconditional non-linear stability, but this may place too great a burden on other aspects of the design.

It will be useful to consider the various simple cases described in Section II from the point of view of the linear treatment.

Case A has $K(\tau) = 0$ and $\beta = 0$ and therefore possesses only neutral stability, as is obvious from the simple equation of motion (Equation 30).

Case B has $K(\tau) = 0$ and $D(\tau) = \lim_{\lambda \to 0} \lambda e^{-\lambda \tau}$. The equilibrium is stable since $D(\tau)$ is non-negative. This case can often be used to give general assurance as to the stability of a reactor system, in spite of its obvious crudity. The linearized equation of motion is

$$\ddot{Q} + \frac{\beta}{\bar{\tau}} \dot{Q} + \Omega^2 Q = 0 \tag{44}$$

with a simple "viscous" damping term. It is important to note that for most interesting reactors

$$\frac{\beta}{\bar{\tau}} > 2\Omega \tag{45}$$

so that the motion is overdamped. With reasonable overdamping, it is unlikely that possible complicated effects in $K(\tau)$ can cause serious danger of conditional instability.

Case C is described by $\beta = 0$, $K(\tau) = \lambda e^{-\lambda \tau}$. It is unconditionally stable since

$$\int_0^\infty d\tau K(\tau) \frac{\sin \omega\tau}{\omega} = \frac{\lambda}{\lambda^2 + \omega^2} > 0 \tag{46}$$

Case D is described by $\beta = 0$, $K(\tau) = (1/\theta)1(\theta - \tau)$. It is in general conditionally stable, although at worst its stability is neutral. The crucial quantity is

$$\int_0^\infty d\tau K(\tau) \frac{\sin \omega\tau}{\omega} = \frac{1}{\omega\theta} \int_0^\infty d\tau \sin \omega\tau = \frac{1 - \cos \omega\theta}{\omega^2 \theta} \geq 0 \tag{47}$$

The possible zeros of the expression ($\omega = 2\pi n/\theta$) correspond to possible conditions of neutral stability. These have been simply explained by Ergen,[1] as arising from a coincidence between the fluid transit time and some multiple of the period $2\pi/\Omega$ possessed by the system of case A. This coincidence allows the requirement of constant heat removal to be satisfied. The system would, of course, become unconditionally stable if β were taken non-zero, and, as Ergen has pointed out, any dispersion of possible residence times will have the same effect.

At this point it is in order to discuss some of the physical conditions under which stability becomes conditional. First, following Ergen,[1] consider the generalization of case D to a system in which there are many transit times, power density variation both over a given fluid path and between various fluid paths, and variations of effectiveness of temperature changes. Let $\rho(\theta)\, d\theta$ be the probability that a fluid particle entering the reactor have residence time in the range $d\theta$. Let $T(t,s,\theta)$ be the temperature of a fluid particle at time t, which entered at time $t - s$ and will leave at $t - s + \theta$. Let $f(s,\theta)P(t)$ be the rate of heating at time t of a fluid particle with location specified by s and θ, and let $g(s,\theta)$ be the reactivity increase produced by unit temperature rise of all the reactor fluid, if its effectiveness were that appropriate to the point (s,θ).

A simple argument yields

$$\phi(t) = \frac{1}{\bar{\theta}} \int_0^\infty d\theta \rho(\theta) \int_0^\theta ds\, g(s,\theta)\, T(t,s,\theta) \tag{47}$$

where $\bar{\theta} = \int_0^\infty \theta\, d\theta \rho(\theta)$.

If the temperature of a given fluid element is calculated by tracing its energy input since entrance at zero temperature, there is obtained

$$T(t,s,\theta) = \int_0^s d\tau f(s - \tau,\theta) P(t - \tau) \tag{48}$$

Combination of Equations 47 and 48, with several reversals of integration order, yields for $G(\tau)$:

$$G(\tau) = \frac{1}{\bar{\theta}} \int_\tau^\infty d\theta \rho(\theta) \int_\tau^\theta ds\, g(s,\theta) f(s - \tau,\theta)$$

$$G(0) = \frac{1}{\bar{\theta}} \int_0^\infty d\theta \rho(\theta) \int_0^\theta ds\, g(s,\theta) f(s,\theta) \tag{49}$$

It is convenient to define $f(s,\theta)$ and $g(s,\theta)$ to be zero outside the reactor ($\theta > s > 0$), in which case $K(\tau)$ can be found by differentiation of $G(\tau)$.

$$K(\tau) = -\frac{G(\tau)}{G(0)} = -\frac{\int_\tau^\infty d\theta \rho(\theta) \int_\tau^\theta ds f(s - \tau,\theta) \dfrac{\partial g(s,\theta)}{\partial s}}{\int_0^\infty d\theta \rho(\theta) \int_0^\theta ds f(s,\theta) g(s,\theta)} \tag{50}$$

As a check, f and g can be taken constant to reduce to the cases C and D:

$$f(s,\theta) = g(s,\theta) = l(s)\, l(\theta - s)$$

$$\frac{\partial g}{\partial s} = \delta(s) l(\theta - s) - l(s)\, \delta(\theta - s) \tag{51}$$

Evaluation of Equation 50, taking the s integration to extend slightly beyond $s = \theta$, yields

$$K(\tau) = \frac{\int_\tau^\infty d\theta \rho(\theta)}{\int_0^\infty \theta\, d\theta \rho(\theta)} \tag{52}$$

Letting $\bar{\theta}$, the mean residence time, replace the symbol $1/\lambda$ in case C and θ in case D, $\rho(\theta)$ becomes for the two cases

$$\text{Case } C: \quad \rho(\theta) = \frac{1}{\bar{\theta}} e^{-\theta/\bar{\theta}}$$

$$\text{Case } D: \quad \rho(\theta) = \delta(\theta - \bar{\theta}) \tag{53}$$

These yield:

$$\text{Case } C: \quad K(\tau) = \frac{1}{\bar{\theta}} e^{-\theta/\bar{\theta}} \tag{54}$$

Case D: $$K(\tau) = \frac{1}{\bar{\theta}} 1(\bar{\theta} - \tau)$$

which agree with the previous results.

Ergen[1] points out that the result in Equation 52 is unchanged if f and g are taken to vary arbitrarily with θ, providing the s-dependence, Equation 51, is retained. With this generality, the essential stability parameter can be evaluated:

$$\begin{aligned}\int_0^\infty d\tau K(\tau) \frac{\sin \omega\tau}{\omega} &= \frac{1}{\omega\bar{\theta}} \int_0^\infty d\tau \sin \omega\tau \int_\tau^\infty d\theta \rho(\theta) \\ &= \frac{1}{\omega\bar{\theta}} \int_0^\infty d\theta \rho(\theta) \int_0^\theta d\tau \sin \omega\tau \\ &= \frac{1}{\omega^2\bar{\theta}} \int_0^\infty d\theta \rho(\theta)(1 - \cos \omega\theta) \geq 0 \end{aligned} \quad (55)$$

It is clear that real instability is impossible, although as Ergen[1] points out, it is possible to obtain neutral stability by a pathological choice for $\rho(\theta)$.

Instability or conditional stability can clearly arise only if f and g vary with s as well as θ. This variation necessarily occurs in any real reactor but, to the author's knowledge, the effect has never been carefully evaluated for an actual reactor and shown to outweigh the stabilizing delayed neutron effect.

It should also be mentioned that a rather different approach to the problem of stability in circulating-fuel reactors has been initiated by Fleck.[5] His approach essentially avoids the formulation in terms of time delay operations by writing partial differential equations for such quantities as $T(t,s,\theta)$. No strong advantage is yet apparent for such an approach.

Another source of instability lies in the propagation of information on reactor outlet temperature around the external heat removal loop and back to the reactor inlet. The resulting time delay, which can be completely incorporated by careful calculation of $K(\tau)$, can easily be in such a range as to be quite dangerous to stability. Such effects do not generally seem to be important, however, because the heat exchanger attenuates the dangerous information sufficiently, causing the reactor inlet fluid to assume a temperature very close to a constant value. Each such situation should be evaluated on its own merits.

Finally there may be some concern as to the effect on $D(\tau)$ produced by circulation of fuel. It has, of course, been shown that no tendency toward instability can ever be produced by the delayed neutrons, but the stabilizing tendence can be weakened both by the reduction in β and the change in shape of $D(\tau)$ attendant on circulation. If a system is conditionally stable, then these alterations in delayed neutron damping must be carefully calculated. A number of authors have given procedures for this calculation, a convenient reference being to two articles by Fleck.[6,7]

IV. COMPRESSIBILITY EFFECTS

It seems appropriate to discuss at this point the question originally treated by Trammell,[8] of the effect of reactor compressibility on stability. This question was explicitly ignored in setting up the general formalism of Section II, but it can in some circumstances become important. Assume a reactor in which the power-produced reactivity decrease does not arise directly from temperature change, but rather from variations in reactor density. Let

$$\phi(t) = \int dx\, g(x)\, \rho(x,t) \quad (56)$$

where $\rho(x,t)$ is the excess of density above equilibrium as a function of time and position in the reactor, $g(x)$ is the effectiveness function, and the integral is extended over the reactor.

It is convenient to assume constant heat removal. This will be seen to have no essential effect on the phenomena of interest. The excess density ρ satisfies the acoustical wave equation, which can be given a simple form on the assumptions that only a single medium participates in the motion and that wave propagation is much more rapid than fluid flow

$$\ddot{\rho} - c^2\nabla^2\rho = -c^2 \frac{d\rho}{dT} \nabla^2 T \quad (57)$$

Here c is the speed of sound in the medium, $d\rho/dT$ is the change in density with temperature at constant pressure, and T is the excess temperature at a given point in the reactor. The temperature can in turn be given in terms of reactor power by

$$T(x,t) = f(x)[P(t) - P_0] = P_0 f(x)(e^Q - 1) \quad (58)$$

where $f(x)$ involves heat capacity and power distribution. This relation assumes instantaneous heat transfer from fuel to fluid.

Finally, it is necessary to write ρ in terms of normal modes:

$$\rho(x,t) = \sum_n \rho_n(t)\, u_n(x) \quad (59)$$

The normal coordinates ρ_n satisfy

$$\begin{aligned}\dddot{\rho}_n + \mu_n\ddot{\rho}_n + \omega_n^2\dot{\rho}_n \\ = -c^2 P_0 \frac{d\rho}{dT} (e^Q - 1) \int dx\, u_n(x) \nabla^2 f(x)\end{aligned} \quad (60)$$

where ω_n is the natural frequency of the n^{th} mode, and μ_n is an assumed friction coefficient. The functions u_n are assumed orthonormal, and satisfy

$$\nabla^2 u_n + \frac{\omega_n^2}{c^2} u_n = 0 \quad (61)$$

so that Equation 60, by integration by parts and linearization, becomes

$$\dddot{\rho}_n + \mu_n\ddot{\rho}_n + \omega_n^2\dot{\rho}_n = \omega_n^2 P_0 \frac{d\rho}{dT} Q(f,u_n) \quad (62)$$

where $(f,u_n) \equiv \int dx f(x)\, u_n(x)$.

The reactivity contribution must also be written in terms of normal coordinates

$$\phi(t) = \sum_n \rho_n(t)(g,u_n) \tag{63}$$

The reactor power equation must be written in linearized form

$$\dot{Q} + \frac{\beta}{\bar{\tau}} Q = -\frac{1}{\bar{\tau}} \phi \tag{64}$$

In order to obtain Equation 64, $D(\tau)$ is specified as for case B.

If it is now assumed that the system has time dependence $e^{i\omega t}$, Equations 62, 63, and 64 can be combined to obtain

$$(\omega_n^2 - \omega^2 + i\mu_n\omega)\rho_n = \frac{P_0}{\bar{\tau}} \frac{d\rho}{dT} \frac{\omega_n^2(f,u_n)}{\omega^2\left(1 - \frac{i\beta}{\omega\bar{\tau}}\right)} \sum_{n'} (g,u_{n'})\rho_{n'} \tag{65}$$

A further simple manipulation yields the secular equation

$$\frac{P_0}{\bar{\tau}} \frac{d\rho}{dT} \frac{1}{\omega^2\left(1 - \frac{i\beta}{\omega\bar{\tau}}\right)} \sum_n \frac{\omega_n^2(f,u_n)(g,u_n)}{\omega_n^2 - \omega^2 + i\mu_n\omega} = 1 \tag{66}$$

There will be a root of Equation 66 in the neighborhood of each ω_n. Trammell has shown that there is also a root which approximates to Ω, if Ω is much smaller than the lowest ω_n. A convenient approximate expression for this root is obtained by remembering that, using completeness,

$$\sum_n (f,u_n)(g,u_n) = (f,g) \tag{67}$$

and using the approximation

$$\frac{\omega_n^2}{\omega_n^2 - \omega^2 + i\mu_n\omega} \simeq 1 \tag{68}$$

These assumptions give rise to

$$-\omega^2 + \frac{\beta}{\bar{\tau}} i\omega + \Omega^2 = 0 \tag{69}$$

where Ω^2, given by

$$\Omega^2 = \frac{P_0}{\bar{\tau}} \frac{d\rho}{dT} (f,g) \tag{70}$$

is clearly identical with the characteristic squared frequency previously introduced. The Equation 69 for ω is identical with that which would be obtained for the simple case B in the linearized approximation. Trammell has shown that in addition to the usual delayed neutron damping, improvement of the approximation of Equation 68 will lead to a *tendency* toward instability depending on the friction coefficients μ_n. Normally, if the roots of Equation 69 are much less than the lowest ω_n, the delayed neutron damping will far outweigh the frictional anti-damping. To obtain an estimate of this effect, assume that only the $n = 0$ mode contributes appreciably. This is in simple cases an excellent approximation and leads to

$$-\omega^2 + \frac{i\beta}{\bar{\tau}} \omega + \frac{\Omega^2}{1 - \frac{\omega^2}{\omega_0^2} + \frac{i\mu_0\omega}{\omega_0^2}} = 0 \tag{71}$$

If the last term is expanded, assuming ω/ω_0 small, there results

$$-\omega^2\left(1 - \frac{\Omega^2}{\omega_0^2}\right) + i\omega\left(\frac{\beta}{\bar{\tau}} - \frac{\Omega^2}{\omega_0^2}\mu_0\right) + \Omega^2 = 0 \tag{72}$$

This exhibits explicitly the frictional anti-damping tendency, as well as a shift of frequency. It is clear the formulation of Section II, neglecting compressibility effects, actually makes the approximation (good in all reactor systems encountered by the author) that $\Omega^2 \ll \omega_0^2$.

A more serious effect of compressibility has also been pointed out by Trammell. Each acoustical frequency ω_n is slightly altered by the coupling with the nuclear energy production. During the course of an acoustical vibration, the reactor material is compressed. This increases the reactivity and the power, governed by the prompt multiplication of the delayed neutron source, increases with a phase lag. The increased power causes an expansion of the reactor material which reinforces the vibration. The resulting tendency toward increase of amplitude *may* overcome the frictional damping, in which case the amplitude increases to be controlled only by the entry of nonlinear frictional effects.

To make the argument more precise, assume that ω lies close to ω_0 so that only the $n = 0$ term in the sum is important. The resulting equation is

$$\omega_0^2 - \omega^2 + i\mu_0\omega = \frac{\Omega^2\omega_0^2}{\omega^2\left(1 - \frac{i\beta}{\omega\bar{\tau}}\right)} \tag{73}$$

A simple iteration procedure yields an approximate solution

$$\omega^2 = \omega_0^2 + i\mu_0\omega - \frac{\Omega^2\omega_0^2}{\omega^2} \frac{1 + i\beta/\omega\bar{\tau}}{1 + \frac{\beta^2}{\omega^2\bar{\tau}^2}}$$

$$\omega \simeq \omega_0$$

$$\omega \simeq \omega_0 + \frac{i\mu_0}{2} - \frac{\Omega^2/2\omega_0}{1 + \frac{\beta^2}{\omega_0^2\bar{\tau}^2}} - \frac{\Omega^2/2\omega_0^2}{1 + \frac{\beta^2}{\omega_0^2\bar{\tau}^2}} \frac{i\beta}{\bar{\tau}} \tag{74}$$

The result in Equation 74 displays the effect of nuclear power generation on the natural frequency (third term) and on the damping (fourth term). It then appears that the combination of delayed neutrons and compressibility can give rise to a serious mechanical instability if

$$\frac{\Omega^2}{\omega_0^2 + \beta^2/\bar{\tau}^2} \frac{\beta}{\bar{\tau}} > \mu_0 \tag{75}$$

a condition first derived by Trammell. This nuclear anti-damping of acoustical vibrations seems only to be of importance for the lowest frequency normal mode. This is ordinarily a motion of the type encountered in a Helmholtz resonator, with the reactor proper supplying the elasticity and the fluid in the external piping acting as inertia. Any reactor system *may* encounter the inequality in Equation 75, but the most serious offenders are the liquid fuel, liquid moderator, or homogeneous reactors, especially those containing high temperature water. This tends to give a large expansion coefficient, large Ω^2 (for given power density) and small τ. The expression in Equation 75 does not strictly hold for the liquid moderator-fixed fuel reactor since fission energy was assumed to give an *instantaneous* temperature rise, but the appropriate thermal relaxation effect can easily be inserted.

V. CRITERIA FOR UNCONDITIONAL NON-LINEAR STABILITY

Although it is doubtful whether the contents of this section has great practical value, save from the standpoint of reassurance, there is considerable theoretical interest in general theorems or non-linear phenomena.

It has been shown by Ergen[1] that delayed neutrons always give damping. The argument is rather easily made by a modification of the energetic argument which was used in the linear case. Using the notation of the general Equation 25 and the linearized energy Equation 45, the general problem with delayed neutrons by $K(\tau) = 0$ can be written as

$$\dot{Q} = \frac{\delta}{\bar{\tau}} - \frac{1}{\bar{\tau}}\phi + \frac{\beta}{\bar{\tau}}\int_0^\infty d\tau D(\tau)[e^{Q(t-\tau)}e^{-Q(t)} - 1] \qquad (76)$$

$$\phi = G(0)P_0(e^Q - 1)$$

The mechanical analogy can be carried through by writing $P = (1/\bar{\tau})\phi$, so that Equation 76 becomes

$$\dot{Q} = P + \frac{\beta}{\bar{\tau}}\int_0^\infty d\tau D(\tau)[e^{Q(t-\tau)}e^{-Q(t)} - 1] + \frac{\delta}{\bar{\tau}}$$

$$\dot{P} = -\Omega^2(e^Q - 1) \qquad (77)$$

Transposition and multiplication of one equation by the other yields

$$\dot{P}\frac{\delta}{\bar{\tau}} = \frac{d}{dt}\left[\frac{1}{2}P^2 + \Omega^2(e^Q - Q)\right]$$

$$+ \Omega^2\frac{\beta}{\bar{\tau}}\int_0^\infty d\tau D(\tau)[e^{Q(t-\tau)} - e^{Q(t)} - e^{Q(t-\tau)}e^{-Q(t)} + 1] \qquad (78)$$

As previously, assume that δ is such as to induce a periodic motion of Q. If instability is to be possible, there must be some non-zero value of $\beta/\bar{\tau}$ which allows neutral stability. For this value of $\beta/\bar{\tau}$ and the correct frequency and wave form, δ must vanish. Therefore, unless $\langle \dot{P}\delta/\bar{\tau} \rangle$ vanishes for some non-zero $\beta/\bar{\tau}$, the system is unconditionally stable. Taking averages over a period

$$\left\langle \dot{P}\frac{\delta}{\bar{\tau}} \right\rangle = \Omega^2\frac{\beta}{\bar{\tau}}\int_0^\infty d\tau D(\tau)$$
$$[1 - \langle e^{Q(t-\tau)}e^{-Q(t)}\rangle + \langle e^{Q(t-\tau)}\rangle - \langle e^{Q(t)}\rangle] \qquad (79)$$

The last two terms in the square brackets cancel since each involves an average over the same set of values. Ergen uses the theorem that if a_i and b_i are two sets of positive numbers, then $\sum_i$ takes on its smallest value if $a_1 > a_2 > a_3 >$, and $b_1 < b_2 < b_3 \cdots$. The symbol $\langle\ \rangle$ signifies $(\omega/2\pi)\int_0^{2\pi/\omega} dt$, which is the limit of a sum. The above result can be rewritten

$$\left\langle \dot{P}\frac{\delta}{\bar{\tau}} \right\rangle = \Omega^2\frac{\beta}{\bar{\tau}}\int_0^\infty d\tau D(\tau)$$
$$[\langle e^{Q(t)}e^{-Q(t)}\rangle - \langle e^{Q(t-\tau)}e^{-Q(t)}\rangle] \qquad (80)$$

If the sequence $e^{Q(t)}$ is identified with the sequence a_i and the sequence $e^{-Q(t)}$ with the sequence b_i, the first average is seen to have a minimal value. In the second average, $e^{Q(t-\tau)}$ is to be identified with a rearrangement of the sequence, a_i and that average then has a non-minimal value. Since $D(\tau)$ is always positive,

$$-\left\langle \dot{P}\frac{\delta}{\bar{\tau}} \right\rangle < 0 \qquad (81)$$

and unconditional non-linear stability follows.

Ergen[1] has used a similar technique to demonstrate unconditional non-linear stability for case *D*. While the proof is there quite elegant, he has been unable to give a complete treatment for the case of general $K(\tau)$. The author,[4] however, has given a proof that the condition on $K(\tau)$ for non-linear stability is identical with that derived in the linear case.

Take $\beta = 0$, so that the equation of motion becomes

$$\ddot{Q} + \Omega^2(e^Q - 1) = \Omega^2\int_0^\infty d\tau K(\tau)[e^{Q(t-\tau)} - 1] \qquad (82)$$

It will be shown that this equation corresponds to the motion of a complicated, conservative mechanical system.

Consider the following Lagrange function:

$$L = \frac{1}{2}\left[\dot{Q} + \int_0^\infty d\omega q(\omega)\right]^2 - \Omega^2 e^Q$$
$$+ \frac{1}{2}\int_0^\infty \frac{d\omega}{\omega\kappa(\omega)}[\dot{q}^2(\omega) - \omega^2 q^2(\omega)] \qquad (83)$$

with $\kappa(\omega) = \frac{2}{\pi}\int_0^\infty d\tau K(\tau)\sin\omega\tau$.

The equations of motion are

$$\ddot{Q} + \Omega^2 e^Q = -\int_0^\infty d\omega\,\dot{q}(\omega)$$

$$\frac{1}{\omega\kappa(\omega)}[\ddot{q}(\omega) + \omega^2 q(\omega)] = \dot{Q} + \int_0^\infty d\omega' q(\omega') \qquad (84)$$

In the second equation, take a time derivative and substitute from the first equation:

$$\left(\frac{d^2}{dt^2}+\omega^2\right)q(\omega) = \omega\kappa(\omega)\left[\ddot{Q}+\int_0^\infty d\omega'\dot{q}(\omega')\right]$$
$$= -\omega\kappa(\omega)\Omega^2 e^Q \qquad (85)$$

This equation can be solved for $q(\omega)$ in terms of the past history of Q by

$$\dot{q}(\omega,t) = -\Omega^2\kappa(\omega)\int_0^\infty d\tau \sin\omega\tau e^{Q(t-\tau)} \qquad (86)$$

When Equation 86 is inserted in the first Equation 84, and the integration order reversed, there results

$$\ddot{Q}+\Omega^2 e^Q = \Omega^2\int_0^\infty d\tau\int_0^\infty d\omega\,\kappa(\omega)\sin\omega\tau e^{Q(t-\tau)} \qquad (87)$$

which is just the required equation if one remembers

$$K(\tau) = \int_0^\infty d\omega\,\kappa(\omega)\sin\omega\tau \quad \text{and} \quad \int_0^\infty d\tau\,\kappa(\tau) = 1 \qquad (88)$$

In this formulation $q(\omega)$ plays the role of a "field" with a continuum of natural frequencies. Any motion of Q must excite motion of $q(\omega)$ and if this excitation *absorbs* energy from the Q-motion, Q must decrease to zero. Unfortunately, although there exists an energy constant for the system, q-motion *may* possess *negative* energy and its excitation will then *increase* the energy of Q-motion.

If canonical variables are introduced in conventional fashion, the Hamiltonian can be found:

$$H = \frac{1}{2}\left[P-\int_0^\infty d\omega\,q(\omega)\right]^2+\Omega^2 e^Q+\frac{1}{2}\int_0^\infty \omega\,d\omega\,\kappa(\omega)$$
$$\times\left[p^2(\omega)+\frac{q^2(\omega)}{\kappa^2(\omega)}\right]-\frac{1}{2}\left[\int_0^\infty d\omega\,q(\omega)\right]^2 \qquad (89)$$

The author[4] has shown that the last term can be ignored in deducing stability. If $\omega\kappa(\omega)$ is positive, the remainder is necessarily positive and becomes larger as either the Q-motion or the q-motion is excited. Therefore the system possesses unconditional non-linear stability if

$$\int_0^\infty d\tau\,\kappa(\tau)\frac{\sin\omega\tau}{\omega} > 0 \qquad (90)$$

agreeing with the previous linear result.

If this condition is not satisfied, build-up of Q-motion may take place by simultaneous increase of q-motion. It is indeed surprising that such a general theorem can be proven in the non-linear case.

REFERENCES

1. Ergen, W. K., *Kinetics of the Circulating Fuel Nuclear Reactor*, Journal of Applied Physics 25: 702-11 (1954).
2. Ergen, W. K. and Weinberg, A. M., *Some Aspects of Non-Linear Reactor Dynamics*, Physica 20: 413-26 (1954).
3. Chernick, J., *The Dependence of Reactor Kinetics on Temperature*, Brookhaven National Laboratory Report, BNL-173 (T-30) (1951).
4. Welton, T. A., *A Stability Criterion for Reactor Systems*, Oak Ridge National Laboratory Report, ORNL 1894 (1955).
5. Fleck, J. A., Jr., Private communication and forthcoming Brookhaven National Laboratory Report.
6. Fleck, J. A., Jr., *Kinetics of Circulating Reactors at Low Power*, Nucleonics 12: 52-55 (1954).
7. Fleck, J. A., Jr., *Theory of Low Power Kinetics of Circulating Fuel Reactors with Several Groups of Delayed Neutrons*, Brookhaven National Laboratory Report, BNL-334 (T-57) (1955).
8. Trammell, G. T., *Undamped Vibrations in Reactors*, Oak Ridge National Laboratory Report, ORNL 1893 (1955).

Experimental Checks of Control Rod Theory

By Paul F. Gast,* USA

In the course of development of nuclear reactors many measurements have been made of the effectiveness of control rods in changing the multiplication factor. The great bulk of these measurements have been made on control rods whose effectiveness could not be calculated accurately from basic principles because of complicated geometry or for other reasons. Only rarely have measurements been obtained in situations susceptible of accurate theoretical treatment. Murray and Niestlie[1] have described the analysis of one such set of measurements made in a small, enriched, hydrogen moderated reactor. The purpose of this present paper is to analyze similar measurements made in a large, graphite moderated reactor using natural uranium. In this latter situation the treatment of the fast neutrons is subject to less question than in hydrogen moderated reactors and inaccuracies in their treatment have less influence on the results of a rod calculation. The large size of the reactor also eliminates any serious question in the use of an equivalent bare reactor model in the calculations.

The experiments here analyzed were carried out primarily for the purpose of establishing data for the operation of a reactor and comparison with theory was a secondary consideration. The situation with respect to geometry is therefore not ideal. However, a method has been developed for obtaining an accurate approximation to the solutions of the appropriate differential equation in the geometry of the experiments. The method may have applications to similar problems elsewhere and it will therefore be described in some detail. One such application is described at the end of the paper.

The agreement shown between theory and experiment in the instances reported here leaves something to be desired. Since the reactor physics of the situation is supposedly well understood and the application of the theory has been carried out with sufficient accuracy, the lack of excellent agreement is not understood. Opportunities to do experiments of this type are infrequent and it is urged that further information be obtained at every opportunity.

DESCRIPTION OF THE EXPERIMENTS

A pile was constructed which consisted of a lattice of canned, cylindrical uranium rods in a graphite moderator. The rods were arranged in a square lattice array in the graphite. The loaded core was in the form of a rectangular parallelepiped and was surrounded by a thick reflector consisting of the graphite matrix into which no uranium had been loaded. The experiments were part of the program for initial loading of a reactor and a limited time could be devoted to them.

The pile is treated throughout this paper as being an unreflected one having the dimensions obtained by adding the reflector savings to the core dimensions. In the horizontal plane the effective dimensions are 630 cm by 915 cm. The height of the pile was increased by loading uranium until it became critical with no control rods inserted. One of the controls to be measured was then inserted along the vertical center line and the height of the loading was increased until the pile again became just critical.

The distribution in neutron intensity in the vertical direction is given by $\cos(\pi z/H)$ in all cases, with H varying from case to case. The contribution to the buckling, $-\nabla^2\phi/\phi$, arising from this source is then $(\pi/H)^2$. Since the material buckling of the lattice, $B^2 = (k-1)/(L^2+k\tau)$, is constant, a decrease in $(\pi/H)^2$ occasioned by adding to the pile height after insertion of a control must be just equal to the increase in buckling in the horizontal directions produced by the insertion of the control.

A vertical hole of square cross section, 9.5 cm on a side, existed along the vertical center of the pile. The increase in critical height, as compared to an empty hole, was determined for three cases: the hole filled with small balls of boron steel; the hole filled with small balls of ordinary carbon steel; and a cylindrical, boron steel rod of 6.67 cm diameter suspended in the hole. The boron content of the balls and the rod was sufficient to make them black to thermal neutrons. The results are summarized in Table I.

APPLICATION OF THEORY

The various methods of computing the effect of control rods have been summarized by Murray and

Table I. Measurements of Rod Effectiveness

Rod	*Horizontal buckling*	*Increase in buckling**
None	36.7×10^{-6} cm^{-2}	0 cm^{-2}
Steel balls	42.5	5.8×10^{-6}
Cylindrical rod	42.7	6.0
Boron steel balls	44.8	8.1

* The uncertainty in the buckling increase values is estimated to be $\pm 0.3 \times 19^{-6}$ cm^{-2}.

* Hanford Atomic Products Operation. Including work by G. C. Fullmer, P. F. Gast, and C. L. Miller, Hanford.

Niestlie[1] including a bibliography of previous work. The application of the methods to piles of rectangular cross section is not straightforward and a description of the method used may be of interest.

Consider first a pile of square cross section with a cylindrical control rod located along its center line, as shown in Fig. 1. In regions far from the rod, the neutron density will be given by:

$$\phi = \sum_n A_{4n} Z_{4n}(Br) \cos 4n\theta$$

where

$$Z_{4n} = J_{4n} + C_{4n} Y_{4n}$$

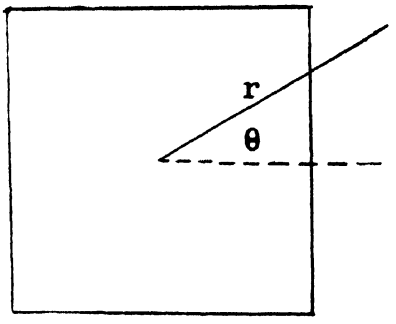

Figure 1

J and Y being Bessel functions of the first and second kind respectively. The A's and C's are constants to be determined by the conditions that $\phi = 0$ on the square boundary and by the appropriate boundary conditions at the control rod. For rods that are considered here, whose dimensions are small compared to the pile dimensions, the C_{4n} are negligible for all n except $n = 0$. It will also be shown that an acceptable fit to the boundary may be obtained by dropping all terms higher than $n = 1$. The equation then becomes

$$\phi = A_0 J_0 + A_0 C_0 Y_0 + A_4 J_4 \cos 4\theta$$

The constants contain an arbitrary scale factor which may be removed in a number of ways. We choose, for later convenience, to write:

$$\phi = Y_0(Br) + C_0 J_0(Br) + A_4 J_4(Br) \cos 4\theta \quad (1)$$

where the constants now have altered meanings from the previous equation. For fitting on the boundary of a square of side W we chose the points:

$$\theta = \pi/8 \qquad r = W/2 \cos(\pi/8)$$

and

$$\theta = \pi/4 \qquad r = W/\sqrt{2}$$

This gives:

$$C_0 = -\frac{Y_0(BW/2 \cos \pi/8)}{J_0(BW/2 \cos \pi/8)} \quad (2)$$

and:

$$A_4 = \frac{Y_0(BW/\sqrt{2})}{J_4(BW/\sqrt{2})} - \frac{Y_0(BW/2 \cos(\pi/8)) J_0(BW/\sqrt{2})}{J_0(BW/2 \cos(\pi/8)) J_4(BW/\sqrt{2})} \quad (3)$$

In the limiting case of no rod, this fitting method leads to the requirement

$$B = \frac{2 \times 2.4048 \times \cos \pi/8}{W} = \frac{4.4435}{W}$$

as compared with a true value of

$$B = \frac{\sqrt{2}\pi}{W} = \frac{4.4429}{W}$$

Table II gives the deviation of the line $\phi = 0$ from the side of the square for the case of no rod and the case of a rod somewhat stronger than any of present interest. Equation 1 is a satisfactory approximation.

Table II. Deviation of Line $\phi = 0$ from the Boundary of the Square of Side Unity

Distance along side from center line	*Deviation ($\phi = 0$) − boundary*
No rod	
0.000 (center line)	-2×10^{-4}
0 100	-2×10^{-4}
0 207 (fitting point)	0
0 300	$+1 \times 10^{-4}$
0 400	$+3 \times 10^{-4}$
0 500 (corner, fitting point)	0
Strong rod, $\Delta B^2 = 16.5 \times 10^{-6}$ cm^{-2}	
0.000 (center line)	-1.0×10^{-2}
0.100	-0.5×10^{-2}
0.207 (fitting point)	0
0.300	$+1.2 \times 10^{-2}$
0.400	$+2.0 \times 10^{-2}$
0.500 (corner, fitting point)	0

In fitting the boundary conditions at the control rod, the zero order and fourth order terms may be considered separately. We make the assumption that, in all cases, the fast neutrons are scattered, without energy loss, by the material of the control. This leads to the condition that the slope of the fast neutron density vanish at the surface of the hole of radius a in which the control operates. The second requirement is that the thermal neutron density distribution at the surface of the hole extrapolate to zero at $r = r_{eff}$ determined by the particular control used. These assumptions lead to an equation which is a modification of Murray's result:

$$\frac{Y_0(BW/2 \cos \pi/8)}{J_0(BW/2 \cos \pi/8)} = Y_0(Br_{eff}) - \frac{k\tau}{L^2} \frac{BY_1(Ba)}{bK_1(ba)} K_0(br_{eff}) \quad (4)$$

in which L^2 is the square of the thermal diffusion length, τ is the Fermi age to thermal energies, k is the multiplication constant, and

$$b = \sqrt{\frac{1}{L^2} + \frac{1}{k\tau}}$$

The equation may be regarded as a relation between B and r_{eff} for a given W and a.

The constant C_4 may be determined from the same type of equation:

$$J_4(Br_{eff}) = C_4\left[Y_4(Br_{eff}) - \frac{k\tau}{L^2}\frac{Y_4'(Ba)}{K_4'(ba)}K_4(br_{eff})\right] \tag{5}$$

where $Y_4' = dY_4/dr$ etc. However, C_4 is numerically negligible as previously indicated.

We obtain an approximate solution for a rectangle by replacing in the solution for a square $r = \sqrt{x^2 + y^2}$ by $r = \sqrt{x^2 + c^2y^2}$ where c is the ratio of width to length of the rectangle. This transforms the square into a rectangle and the circular control into an elliptical one. The boundary conditions are fit to the same accuracy as in the square. The resulting function $\psi(B_s\sqrt{x^2 + c^2y^2})$ is no longer an eigenfunction of the equation

$$\nabla^2\psi + B^2\psi = 0 \tag{6}$$

We can, however, determine an upper limit for B^2 from the expression

$$B_{approx}^2 = \frac{\int\psi(-\nabla^2\psi)\,dA}{\int\psi^2\,dA} \tag{7}$$

where the integral is taken over the area of the rectangle.[2] The integrals can be evaluated by straightforward but tedious calculation to give

$$B_{approx}^2 = \frac{1 + c^2}{2}B_s^2 \tag{8}$$

where B_s^2 designates the buckling obtained in the square.

That the approximation is a good one is indicated by the following facts. First, with no control rod present, B_{approx}^2 becomes the true value $(\pi/W)^2 + (\pi/L)^2$ where W is the width of the rectangle and L its length. Secondly, the buckling of an ellipse was calculated by this method and compared with exact values. The error was 0.46 per cent where the ratio of the axes was 1.5, and 1.4 per cent at a ratio of 2.0. The error rises to 17 per cent for an infinite ratio. In the rectangle of interest here, the ratio of length to width is 1.45. Figure 2 shows a comparison between the neutron density calculated by the approximation used here and the actual measured density. The measurements were made along a line passing 66.7 cm from the rod, the only location for which measurements are available. The density was not quite symmetric about the center line and the measured points for both sides of the pile are plotted. The asymmetry accounts for most of the scatter, with the mean of the two values lying close to the calculated curve in all cases. The example shown is for the case of the carbon steel ball control but equally satisfactory agreement would be obtained in other cases.

To complete the treatment of the problem it is necessary to relate the elliptical rods of our calculation to the actual rods on which the experiments were performed. We will do this by determining the equivalence between elliptical and circular rods and in the following section we will discuss the representation of our actual rods by circular ones. For the fast neutron boundary conditions equivalent areas will best represent the loss of moderation so that

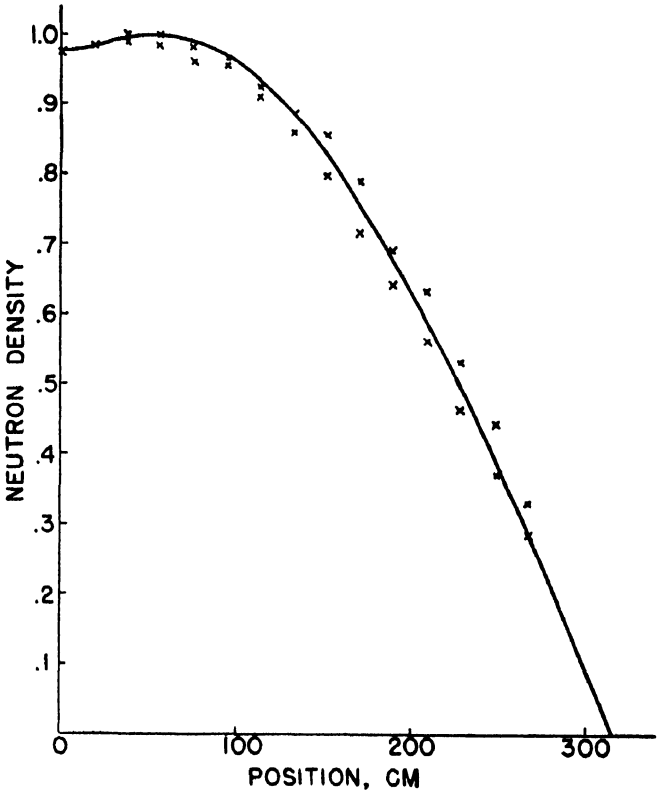

Figure 2. Neutron density with steel balls in control slot

$$a^2 = \frac{c}{\pi}(\text{area of hole})$$

This a is the semi-minor axis of the ellipse and also will be the a used in Equation 4. For the thermal neutron boundary conditions we make the assumption that the density near the control rod can be represented to good approximation by the solution of the Laplace equation $\nabla^2\psi = 0$. This assumption is reasonable for small rods in large piles which consequently have small buckling. By comparison of the electrostatic potential distribution around elliptic and circular cylinders we obtain the result that the semi-minor axis, or r_{eff} in Equation 4 is given by:

$$r_{eff} = \frac{2c}{\sqrt{1 - c^2}}e^{-\alpha}R_{eff} \tag{9}$$

where $\alpha = \tanh^{-1} c$ and R_{eff} is the effective radius of the actual control rod.

A curve of increase in B^2 over the case of no control, versus the R_{eff} of the rod was calculated by the methods outlined and is shown in Fig. 3.

CALCULATION OF EFFECTIVE RADIUS

The boundary condition for thermal neutrons at the surface of a control rod is specified by giving a quantity:

$$d = \phi\Big/\frac{d\phi}{dr}$$

which holds at the surface. The calculation of the quantity d has been developed by Kushneriuk and McKay[3] and by Davison and Kushneriuk.[4] By assuming, reasonably, that in the vicinity of the rod ϕ

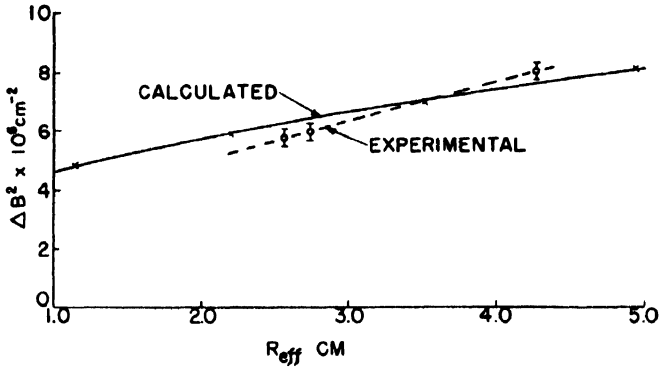

Figure. 3 Buckling changes produced by rods

is of the form $\log r/R_{eff}$ an expression for the effective radius may be obtained:

$$R_{eff} = R_0 \exp(-d/R_0) \qquad (10)$$

in which R_0 is the actual radius.

In the case of the boron steel balls the square, black absorber is replaced by a circular black absorber of equal perimeter. If the side of the square is s then:

$$R_{eff} = \frac{2s}{\pi} \exp(-d\pi/2s) \qquad (11)$$

where d may be obtained from the appropriate curve in either of the references 3 or 4.

For the case of the cylindrical black rod in the hole, we again replace the square by a circle of equal perimeter and obtain d from CRT-566[3] for the case of a black rod surrounded by a gap.

For the case of the steel balls, reference to CRT-566 reveals that the boundary conditions for this type of material are essentially those of simple diffusion theory. We therefore treat the problem by diffusion theory and obtain

$$d(R_0) = \frac{D_G}{D_{st}} \frac{I_0(\nu R_0)}{\nu I_1(\nu R_0)} \qquad (12)$$

where D_G is the diffusion coefficient in graphite, D_{st} is the diffusion coefficient in the stack of steel balls, and ν is the inverse diffusion length in the stack of balls.

In this case, where the material is not strongly absorbing, we replace the square by a circle of equal area to maintain the amount of absorber constant.

In Fig. 3 we have plotted the measured values of ΔB^2 against the calculated effective radii for comparison with the calculated curve.

DISCUSSION OF THE RESULTS

The fit of the measured points to the calculated curve in Fig. 3 is not as good as might be hoped for. If taken at face value, the measured points would indicate a steeper increase in ΔB^2 with increasing R_{eff}. This greater slope is difficult to understand. Adjustments in the values of L^2 and τ used in the calculation and changes in the fast neutron boundary conditions shift the calculated curve up or down with only slight change of slope over the region of interest. Other methods of approximation, for example replacing the rectangular boundary by a circle, also produce little change in the slope. On the whole, the calculated curve here presented, based on the best known values of L^2 and τ and the most reasonable boundary conditions, gives the best fit to all three points.

Opportunities to do experiments of this type arise infrequently and it is hoped that others will take every opportunity to extend the experimental information available in this field.

FURTHER APPLICATIONS OF THE APPROXIMATION METHOD

In the design of large reactors it is sometimes required that a group of control rods be used. These rods are often arrayed in a regular square, triangular, or hexagonal pattern and, when inserted, occupy a central region of the reactor. Calculation of the effectiveness of the entire pattern by the methods used for a few rods would be prohibitively complex.

It is possible, following the method originally developed by J. A. Wheeler, to regard the action of each rod as equivalent to a poisoning of the area which it occupies in the pattern. The general calculation of the amount of poisoning, or the reduction in buckling which is produced by each rod is beyond the scope of this paper. A simple example will suffice to illustrate the method for our purposes. In the event that it is desired to reduce the effective buckling to zero in the region penetrated by the rod pattern, then the boundary condition will be zero slope for the neutron density on the periphery of the region assigned to each rod. The left-hand side of Equation 4 will then be replaced by the derivatives of the Bessel functions, becoming:

$$J_1(BR)/J_1(BR)$$

in which R is the radius of a circle of area equal to the area assigned to each rod in the pattern. For a given spacing between rods, given R, the modified equation gives the required r_{eff} to achieve zero buckling; or conversely, for a given control rod design, the required spacing may be achieved.

It often occurs in design problems of this type that the area occupied by the rod pattern may reasonably be approximated by an ellipse with the ratio of its axes the same as the length to width ratio of the rectangular face of the pile which the rods enter. The problem may then be solved by a modification of the methods outlined above for a single rod in a rectangle. The results achieved vary in accuracy from mere aids to estimation up to accurate calculation depending upon how well the postulated ellipse represents the actual rod pattern boundary. In a recent calculation of this sort at Hanford the effectiveness of a pattern of 21 rods was given to within 8% of the measured value.

REFERENCES

1. Murray, R. L. and J. W. Niestlie, *Nucleonics 13*, No. 2, 18 (1955).
2. See, for example: Pauling, L. and E. B. Wilson, "Introduction to Quantum Mechanics," pp. 180–181, McGraw-Hill, New York and London (1935).
3. Kushneriuk, S. A. and C. McKay, Report CRT-566, Chalk River, Ontario (July 1954).
4. Davison, B. and S. A. Kushneriuk, Report MT-214 (1946).

Neutron Flux Instrumentation Systems for Reactor Safety and Control

By R. J. Cox, A. B. Gillespie, and W. Abson,* UK

INTRODUCTION—INSTRUMENTATION REQUIREMENTS

As the heat generated by a nuclear reactor is due to the fission of atoms by neutron bombardment it is natural that instruments capable of measuring neutron flux should play an important role in control instrumentation systems. Some types of experimental reactors can be controlled perfectly satisfactorily without any other form of measuring equipment. With power producing nuclear reactors they are almost indispensable during the start-up process but once the temperature rise is significant they can be relegated to a secondary role.

When the neutron multiplication constant K of a reactor is changed to a value less than unity, the neutron flux falls exponentially to a level determined by the neutron sources in the reactor. With a graphite moderated natural uranium reactor the U^{238} spontaneously emits neutrons, 100 tonnes of uranium giving a sub-critical neutron power of about a milliwatt. If the operating power is a few hundred megawatts this corresponds to less than 10^{-11} of the full power. With a heavy water reactor, neutrons are produced by a reaction between fission product gamma radiations and deuterium. The sub-critical power due to this so called photo-neutron process is about 10^{-4} of full power one hour after shut-down, falling to about 10^{-6} after several days. Thus the range of neutron flux between sub-critical and full power varies considerably between different types of reactor.

When a reactor is sub-critical it is extremely difficult to predict by how much the control elements must be moved in order to bring the reactor to critical (i.e., $K = 1.0$). If the K of a graphite-moderated natural uranium reactor is set to 1.001 the power rises exponentially and increases by a factor of ten in 145 seconds, but if the K is set to 1.01 the power will increase by a factor of ten in less than one second. If the control elements move fast it is conceivable that the power could be increasing at this fast rate while the power is very low. The power could then reach levels high enough to damage the reactor before the shut-down devices could work. Hence it is important that both the neutron flux and its rate of growth should be measured at all powers from sub-critical to full power. It is convenient during the start-up phase to use reactor period meters which display the neutron flux level on a logarithmically calibrated scale and also indicate the rate of growth or decay on a meter calibrated in reactor period (time for the neutron flux to change by a factor of e).

Measuring the sub-critical neutron flux presents some problems due to the presence of gamma rays that interfere with the neutron flux measurement. Surrounding the neutron detector with four inches of lead reduces the gamma flux by more than 100 times but reduces the neutron flux by only 1½ times. It is frequently worthwhile to insert neutron sources into the reactor to increase the sub-critical neutron flux level. In Britain antimony-beryllium sources are used. These have a half-life of about 60 days and are activated while the reactor is running. A subcritical neutron power of 10^{-7} of the full power can be obtained in a natural uranium graphite reactor for a loss in K of a few times 10^{-5}. Where the bulk of these sources is inconvenient radium-beryllium sources are used, a few curies of Ra producing a sub-critical power of about 10^{-2} watts. Mean-current ionisation chambers plus dc amplifiers are used wherever possible because of their simplicity and the wide range of fluxes that can be covered in one equipment. But where the neutron to gamma ratio is very low, pulse counting equipment must be used.

In an experimental reactor the neutron flux is the quantity of primary interest. The operating level is usually recorded by a multirange dc amplifier. Shifts in flux level are shown by a recorder which displays the difference between the actual and demanded values. The safety rods are dropped when the neutron flux exceeds a pre-determined level measured by a number of "shut-down" amplifiers.

In a power producing reactor the primary interest is the total rate of heat generation. The neutron flux level does not measure this directly for a number of reasons, the most important of which is the heat generated by fission products. If a reactor is shut-down from full power, the heat produced by neutrons will fall to very low levels but the fission products will continue to produce heat equal to a few per cent of full power and will decay only slowly. Thus the reactor

* United Kingdom Atomic Energy Authority, Atomic Energy Research Establishment, Harwell, Berks.

must continue to be cooled even when sub-critical. When running near full power, the power output will lag behind the neutron flux indication because of the fission product time lag and also because of the thermal time-constant of the system. The neutron flux measurement while not providing a direct measure of the rate of heat generation provides an indication of changes in power level that will be apparent as changes in temperature conditions somewhat later. In power producing reactors running at high temperatures, the temperature coefficient of reactivity acts as a powerful stabilising influence. Therefore, the movement of control elements is not so critical as during the start-up phase but the control of coolant conditions becomes more important. For this reason emergency shut-down devices measuring neutron flux cannot be used set to a fixed level. A neutron flux that might be safe at full coolant flow might be dangerous under conditions of lower coolant flow. The "trip setting" must be adjusted to take account of the coolant conditions at all times.

IONISATION CHAMBERS AND DC MEASURING EQUIPMENT

Ionisation chambers with boron coated electrodes or filled with boron trifluoride gas, similar to the design shown in Fig. 1, have been in use for several years in British reactors.[1] The same basic design, with variations in the electrode coating and/or gas filling can be used for the various measurements required for reactor control, e.g., high-level power indication and the operation of shut-down circuits and also for the measurement of power level and reactor period over considerable ranges of neutron flux during start-up.

Ion Chamber Design and Characteristics

The type RC/1 chamber shown in Fig. 1 is 3½ in. diameter and 9 in. long, excluding the terminals. The main body of the chamber and the electrodes are made of aluminium (99.8% purity); the lead-through terminals are sealed by thin lead washers (*A*) held in compression against quartz insulators (*B*) by means of a high tensile steel bolt (*C*).

Boron trifluoride fillings have been used in this type of chamber, but better saturation characteristics are obtained with chambers having boron lined electrodes and filled with a gas such as argon, methane or hydrogen. The effects of ion recombination in these gases is less than in BF_3 and the boron coating can be restricted so that intense ionisation occurs only where there is a well defined collecting field between the electrodes. Hydrogen has the further advantage of having the lowest stopping power for electrons relative to its stopping power for alpha particles and lithium nuclei; hydrogen filled ion chambers therefore have a lower gamma radiation sensitivity, for a given neutron sensitivity, than chambers filled with a gas of higher atomic number. With the electrode spacing used (6 mm), a hydrogen pressure of 150 cm of Hg gives a sensitivity approaching the maximum possible

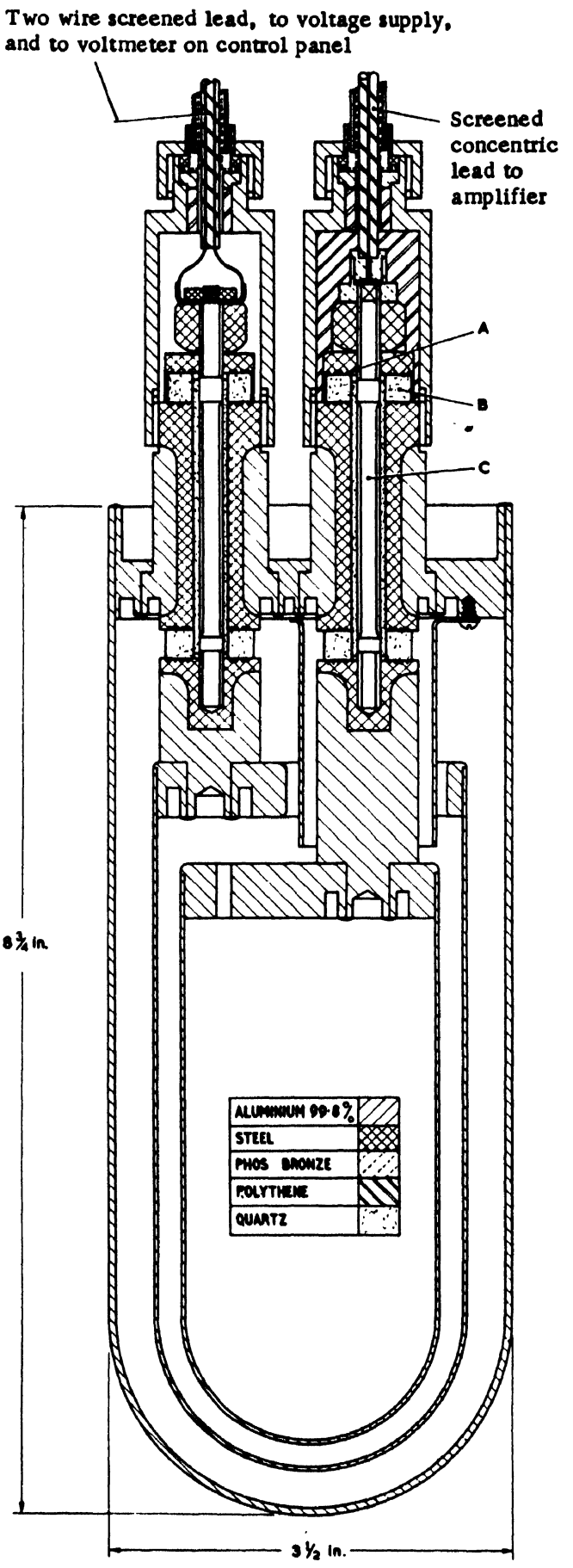

Figure 1. Type RC/1 ionization chamber

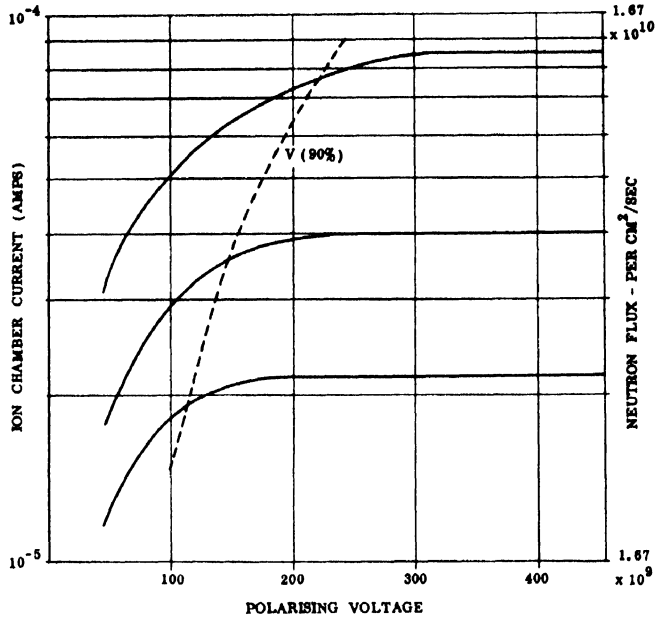

Figure 2. Saturation characteristics of type RC/1 ion chamber: electrodes coated with 1 mg/cm² of natural boron over area of 500 cms²; hydrogen gas pressure 150 cms of Hg

with boron coated electrodes and Fig. 2 shows typical saturation characteristics for this pressure. It is necessary to operate the ion chamber on the flat part of the saturation characteristic at a point well removed from the knee of the curve. This is particularly important for high level power control applications and it is usual to employ a polarising voltage supply at least three times that required to give 90% ion collection ($V_{90\%}$). Batteries are often used as a simple and reliable form of supply free from short period fluctuations and it is convenient in this case to limit the maximum voltage to some 300-400 volts; the ion chambers must therefore give 90% collection with 100 volts polarising potential at the highest flux level at which they are required to operate. The flux level for a given value of $V_{90\%}$ can be increased by reducing the pressure of the hydrogen filling, although this leads to a reduction in the neutron sensitivity. Table I gives some results obtained with an RC/1 type chamber for hydrogen pressures between 150 and 15 cm of Hg. A further improvement in saturation characteristics for a given neutron flux is obtained if only the negative electrode is coated.

The lower limit of flux level at which an ionisation chamber can be used will depend on the relative response to neutrons and gamma radiation. Figure 3 shows the neutron and gamma radiation sensitivities for an RC/1 chamber, with a natural boron coating, at different hydrogen pressures. The best neutron to gamma discrimination is obtained at the lower hydrogen pressures and the ratio is further improved by the use of an electrode coating somewhat highly enriched in boron-10.

Thus with an enriched boron coating and a hydrogen pressure of 15 cm of Hg, a gamma radiation dose-rate of 1 r/hr would give a current of 6×10^{-13} amp, equivalent to a slow neutron flux of about 100 neutrons/cm²/sec.

A further limitation to the use of dc ionisation chambers for sub-critical neutron flux measurements or for measurements over a large range of neutron levels, is the effect of residual induced activity in the materials of the chamber itself. Figure 4 shows the time decay of current due to residual activity in an RC/1 chamber with a natural boron coating on both electrodes and a hydrogen gas pressure of 150 cm of Hg. The measurements were taken on a chamber after operation in a flux of 3×10^{10} n/cm²/sec for a period of about ten weeks. The residual activity current during the first twenty minutes following removal from the neutron flux is due mainly to the 2.3/min half-life Al^{28} isotope. The longer-lived activities are due to

Table I. Hydrogen Pressure versus Flux at which $V_{90\%}$ = 100 Volts, for RC/1 Chamber with Both Electrodes Coated with 1 mg/cm² of Natural Boron, Total Coated Area = 500 cm²

Hydrogen pressure (cm of Hg)	*Neutron flux (n/cm²/sec)*	*Saturation current (amp)*
150	3×10^{9}	1.8×10^{-5}
75	8×10^{9}	3.2×10^{-5}
45	2×10^{10}	7.0×10^{-5}
15	1×10^{11}	1.4×10^{-4}

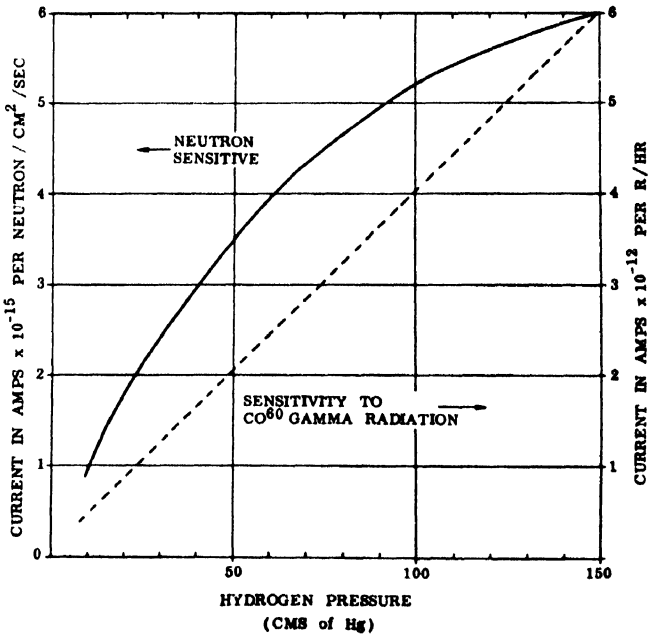

Figure 3. Neutron and gamma radiation sensitivity of type RC/1 ion chamber vs pressure of hydrogen filling: electrodes coated with 1 mg/cm²; thickness of natural boron over area of 500 cm²,

impurities in the aluminium electrodes and to silicon, manganese and iron in the materials of the sealed lead-through terminals. For many applications the comparatively high residual current due to Al during the first twenty minutes after a shut-down is not important. At thirty minutes after shut-down the chamber can be used at a neutron flux level approximately 1.0×10^{-6} times the level at which it has been previously used. By using an "enriched" coating and

a lower hydrogen pressure (15 cm of Hg) this figure may be reduced to about 1.0×10^{-7}.

Dc Measuring Equipment

Different arrangements of electronic measuring instruments are used with the ionization chambers to perform specific functions. The standard arrangements used in UK reactors are described below.

Multi-Range Linear Channel

The function of this arrangement is to provide a reliable and reasonably accurate measure of the neutron flux over the range covered by the detector. This is the simplest and most frequently used measuring channel and a block schematic is given in Fig. 5. The wide range is achieved by switching the measuring resistor of the fedback dc amplifier usually in factors of 3 or 10. If an electrometer valve type of dc amplifier is used, a full-scale output voltage of some 10 volts is required to render the zero drift of the amplifier negligible. This involves the use of measuring resistors ranging from 10^5 to 10^{12} ohms to cover a current range of 10^{-4} down to 10^{-12} amp. Wire-wound resistors can be used on the two highest current ranges permitting an overall accuracy of 1% or better. On the lower current ranges high value composition resistors must

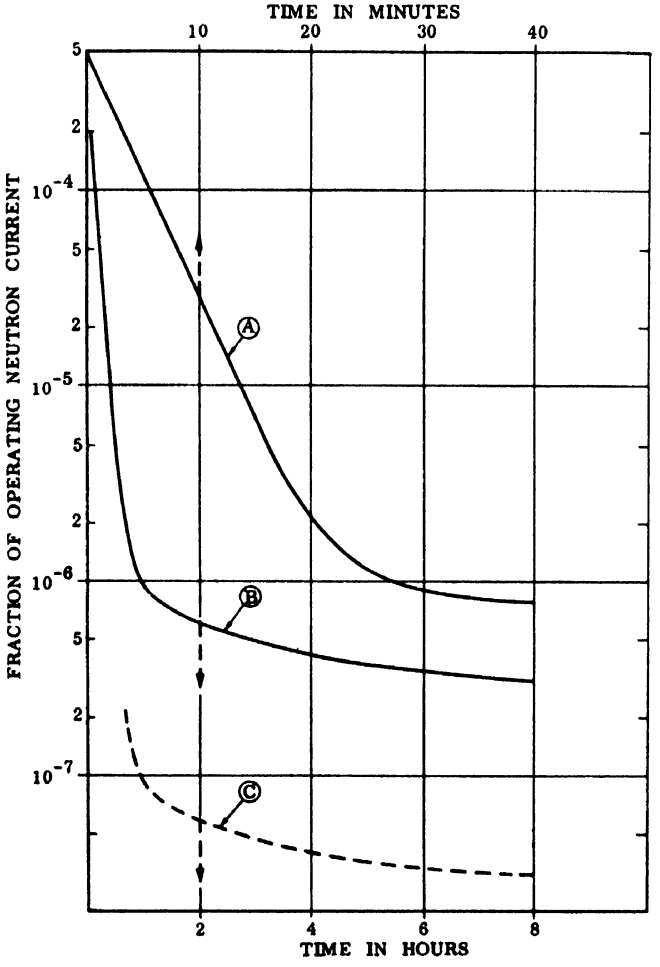

Figure 4. Residual activity current in type RC/1 ion chamber following removal of neutron flux: curves (A) and (B), electrodes coated with natural boron, (500 cms²) hydrogen pressure 150 cm of Hg; curve (C) estimated result for hydrogen pressure, 15 cm of Hg and enriched boron coating

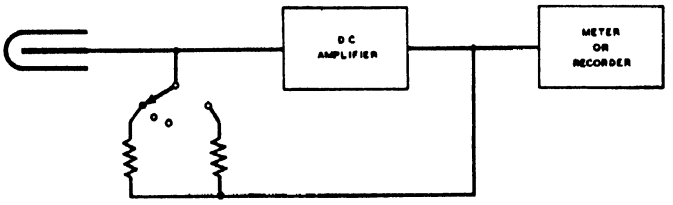

Figure 5. Multi-range linear channel

be used and here the long term accuracy cannot be relied on to better than a few per cent. This is acceptable however, because the lower current ranges are only required during start-up or shut-down and high accuracy is relatively unimportant.

Alternatively by using a high impedance chopper amplifier full-scale voltages in the region of 10 mv are possible and this allows all the measuring resistors to be scaled down by a factor of 10^3. Up to the present high impedance choppers have been used in multi-range channels for the measurement of currents above 10^{-10} amp. Recent developments indicate that it might be possible to reduce this lower limit, and as the chopper amplifier is no more complex than the electrometer valve type, it is likely to supersede the latter in this particular type of flux measuring channel.

Logarithmic Channel

Here the instrumentation is intended to provide an output voltage which is proportional to the logarithm of the input ionisation chamber current over as wide a range as possible. Further, by differentiating the output of the logarithmic amplifier, a voltage inversely proportional to reactor period can be obtained. A logarithmic characteristic may be produced by operating a thermionic diode in the retarding field region. Under this condition the voltage across the diode varies as the logarithm of the current through the diode. A multi-electrode valve may also be used to provide a logarithmic characteristic, and a block schematic of a typical logarithmic channel using an electrometer pentode is shown in Fig. 6. The first dc amplifier maintains the anode current of the pentode constant by varying the screen grid potential to accommodate changes in grid potential. The screen grid potential varies as the logarithm of the input current, and the stability of the circuit to variations in heater supply is better than that of the single diode.

Using an ME.1400 (CV.432) at 200 μa of anode current the logarithmic characteristic extends over six decades from 5×10^{-11} to 5×10^{-5} amp. Alternatively the electrometer pentode ME.1403 (CV.2348) at an anode current of 10 μa will operate satisfactorily from 10^{-13} to 10^{-7} amp. It is hoped to develop a special valve for this circuit which will extend the range to at least eight decades. Amplifiers using the ME.1400 with simple heater stabilisation have exhibited long term drifts much less than 10% of the scale reading.

The rest of the logarithmic channel is conventional. This comprises a fed-back differentiating circuit feeding an output to the period meter, followed by a

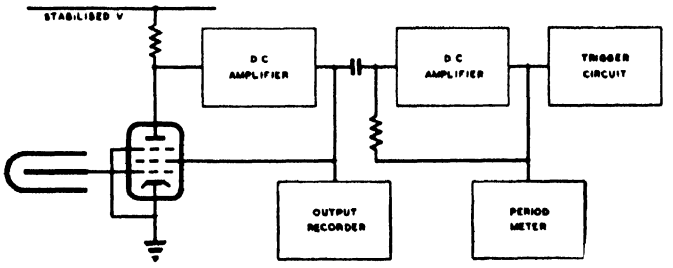

Figure 6. Logarithmic channel

trigger circuit which can be arranged to shut the reactor down should the period fall below a pre-set safe minimum.

Backed-Off Channel

The instruments in this channel are designed to provide an accurate error signal proportional to the difference between the demanded and actual operating levels. This signal may be displayed at the control desk to enable an operator to hold the reactor power level steady, or alternatively the error signal may be included in the control rod servo system to provide automatic control of the reactor.

The accurate error indication of this channel is usually only required over the top two decades of reactor power. Since accuracy is of prime importance in this channel wire wound measuring resistors must be used. Since the amplifier is also likely to be included in the control rod servo system it is wise to design it to have as high a bandwidth i.e., as short a time-constant, as possible. These requirements are best met by an electrometer valve type of dc amplifier in conjunction with a chopper amplifier providing continuous and automatic zero correction. A block schematic of such an arrangement is given in Fig. 7.

The demanded operating level is fixed by the value of the measuring resistor which in a practical system would probably comprise a series of switched values. The full-scale voltage across the measuring resistor is 100 mv and the complete channel has an accuracy not worse than 0.1%.

Shut-Down Channel

The function of this arrangement is to provide a reliable indication and switching action which can be used to shut the reactor down automatically should the flux reach a dangerous level. The emphasis here is on reliability and to a lesser extent accuracy combined with instrumental design to give the highest possible degree of "failure to safety."

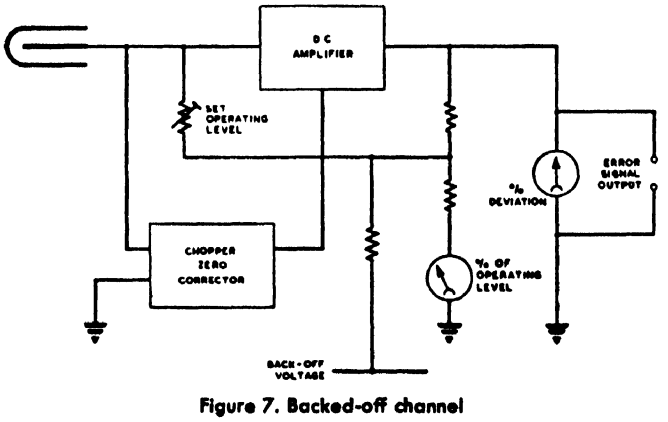

Figure 7. Backed-off channel

Figure 8 gives the block schematic of an ac shut-down system which has been designed to satisfy the above requirements. The chopped input to the ac amplifier keeps this fully loaded until the voltage across the ion chamber load resistor just equals the tripping value. When this happens the output of the ac amplifier falls to zero, and allows the polarised relay to de-energise. Should the ionization chamber voltage exceed the tripping value the phase sensitive rectifier prevents the relay being re-operated. The ac amplifier must be operated from a dc heater supply to guard against possible heater to cathode short-circuits in the amplifier valves.

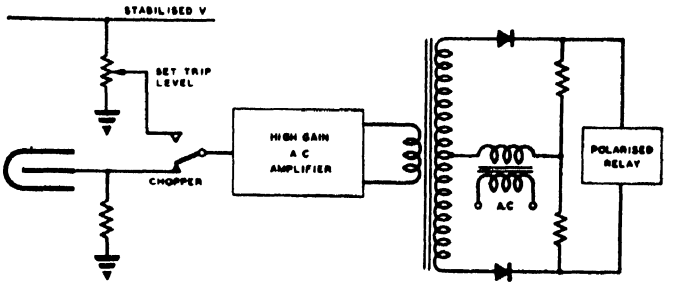

Figure 8. Ac shut down channel

An alternative dc system which also possesses a high degree of "failure to safety" is given in Fig. 9. This comprises a conventional fed-back dc amplifier having energised relays A and B in the long-tailed pair anodes. The circuit is designed so that both relays remain energised throughout its linear operating regime. The triggering level is reached when diode D_1 "catches" the output valve cathode at earth. Thereafter the feed-back disappears causing the long-tailed pair circuit to go rapidly out of balance and de-energising relay A. Diode D_2 will cause similar trigger action in the opposite direction. To guard against either diode going open-circuit, each heater is wired in series with one valve in the dc amplifier.

PULSE COUNTING SYSTEMS

The deciding factor governing the use of mean-current ionisation chambers at sub-critical power levels is the ratio of neutron to gamma radiation intensities at the ion chamber position. Residual activity effects in the chamber itself can be controlled by removing a low level control chamber to a position of reduced neutron flux when the reactor is running at full power, but it is still necessary to ensure that the ratio of neutron flux to gamma radiation dose-rate is less than 100 (neutrons/cm^2/sec per r/hr) if a chamber of the type RC/1 design is to be used at a sub-critical level. It is possible to overcome this limitation to some extent by the use of a "compensated" chamber and experimental chambers have been described[1] in which the effective gamma sensitivity is reduced by a factor of about 100. In some applications, however, it may be

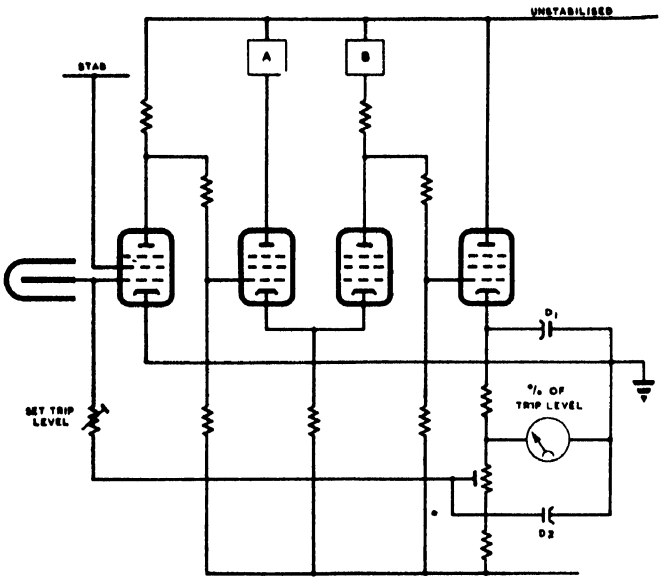

Figure 9. Dc shut-down channel

necessary to measure low level neutron fluxes in the presence of very high gamma radiation backgrounds, and here pulse counting equipment with amplitude discrimination must be used. It is desirable to cover as large a range of counting rates as possible and fission chambers used as electron collection pulse counters have advantages over BF_3 counters in this respect because of their shorter collection time.

Fission Counter and Pulse Counting Channel

A simple coaxial cylinder design of fission counter developed for use in reactor instrumentation applications is shown in Fig. 10. The cathode is coated over an area of 140 cm^2 with a 1 mg/cm^2 layer of U_3O_8 highly enriched in the U^{235} isotope and the sensitivity is then about 0.05 counts/sec per neutron/cm^2/sec. Tank argon is used as the gas filling at a pressure of 4.5 atmospheres and the collection time with an anode voltage of 500 volts is of the order of 0.1 microseconds.

A block schematic of a comprehensive pulse counting channel is given in Fig. 11. The fission counter feeds a high gain pulse amplifier having differentiating and integrating time-constants both equal to 0.08 microseconds. From the amplifier output the pulses are fed to an amplitude discriminator and thence to an eight decade scaler. Multiple outputs of scales and unscaled pulses are subsequently used to operate a linear and a logarithmic rate-meter, the latter unit in turn feeding a reactor period meter. The discriminator and scaler unit has a resolving time of 0.25 μsec except on every fifth pulse when it is 0.3 μsec. These figures apply only if the amplifier pulse width at the discriminator level is 0.15 μsec or less. For a pulse width greater than 0.15 μsec the resolving time figures are increased by the same amount. Both ratemeters are calibrated up to 10^6 counts/second.

Figure 12 gives typical bias curves for such a pulse counting channel. It will be seen that the effect of a gamma radiation dose-rate of 3×10^4 r/hr is negligible. The complete channel can be used up to counting

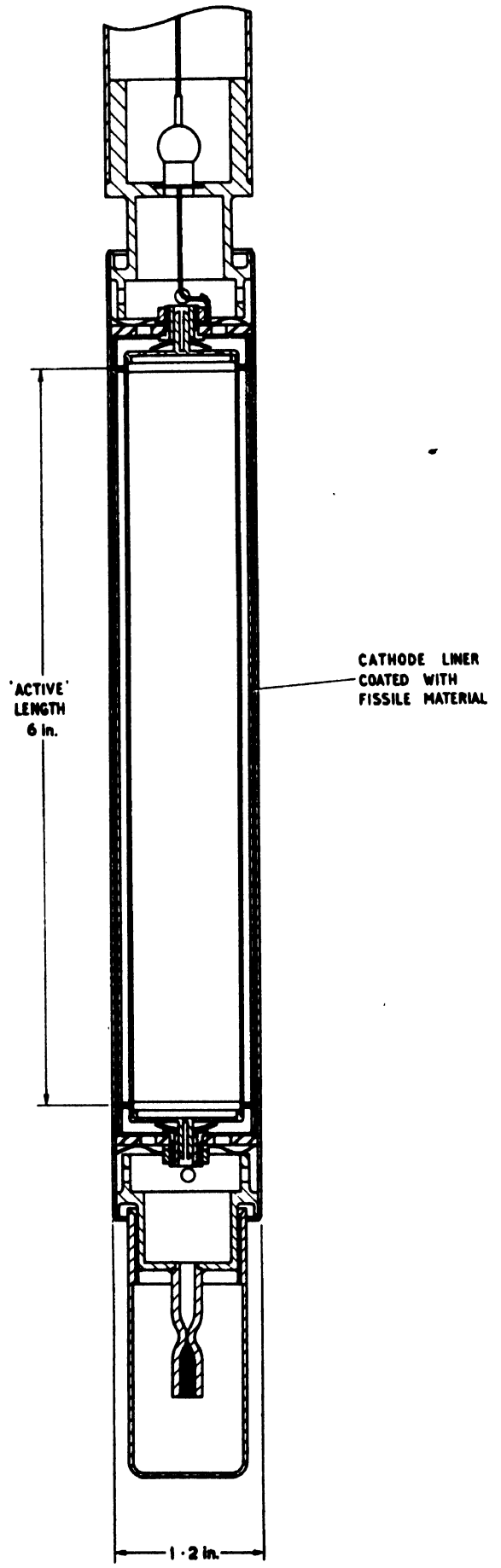

Figure 10. Fission counter: cathode coated with U^{235} oxide (1 mg/cm^2) over area of 140 cm^2; sensitivity to thermal neutrons ~0.05 cps per r/cm^2/sec

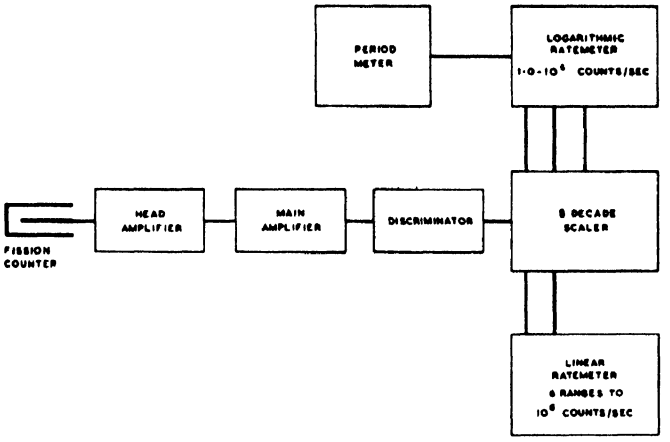

Figure 11. Pulse counting channel

rates of 3×10^5 counts/sec before counting losses affect the linearity significantly.

RELIABILITY AND SAFETY

Instruments used on nuclear reactors are designed to be as reliable as possible. But they should also be designed so that if the instruments themselves fail then their failure should be immediately apparent. For example, the chopper stabilised dc amplifier described in the section on the backed-off channel has been designed such that, should the stabilising unit fail, the deviation meter will be driven immediately to full-scale in either direction and this event used to sound a warning or initiate corrective action.

Instruments which are intended to shut-down the reactor are designed as far as possible to "fail safe," i.e., a failure of the equipment itself would cause the reactor to shut-down. This makes the reactor safer but also prone to accidental shut-down. These devices are, therefore, usually grouped in threes, so that two must operate for the same unsafe condition in order to shut-down the reactor but a single one operating will merely sound a warning.

When a reactor is sub-critical, the neutron flux is so low that most of the neutron flux measuring instruments will not be giving significant indications, and it is desirable to have a routine system of testing as a part of the reactor "pre-start up check," to see that they are in an operating condition. With dc amplifier systems this is done by feeding to the input a current equal to normal operating conditions and checking that the meter reading is within the required accuracy. With pulse counting equipment, a pulse generator of known repetition frequency is used to feed simulated fission counter pulses to the amplifier input, and the output indications of the counting rate meter are checked.

With mean-current ionisation chamber systems, a failure in the polarising potential supply, or in the connections to the chamber, could lead to a dangerous situation. For example, during maintenance while the reactor is sub-critical the connecting lead can, by mischance or mistake, become disconnected. At low powers the instrument channel might appear to be in a satisfactory operating condition as the contact potential between the electrodes may be sufficient to saturate the chamber. This potential would however be quite inadequate at high powers. The danger can be guarded against by providing two leads to the polarising electrode, one connected to the potential supply and a separate potential measuring lead back to the control room. A voltmeter or simple form of electronic relay gives an indication that both leads are intact and that the potential is adequate.

CONCLUSIONS

Ionisation chambers and dc measuring equipment can be used for the measurement and control of reactor power level from the subcritical state provided that the neutron/gamma radiation levels of the order of 100 (n/cm²/sec per r/hr) can be achieved at the ion chamber positions. This is feasible in large thermal reactors by the appropriate use of neutron sources and lead shielding. A range of six to seven decades in neutron flux level can be measured in a single instrumentation channel. Larger ranges, e.g., 10 decades, might be covered by the use of two such channels with an overlap of two or three decades. Alternatively, pulse type fission counters might be used for measurement over the lower ranges, if the neutron to gamma ratio is too low for satisfactory discrimination with a dc ionisation chamber measurement.

Direct-current ionisation chamber systems provide a satisfactory and stable method of indicating short period changes in high power level operation and can be used for the operation of shut-down controls, pro-

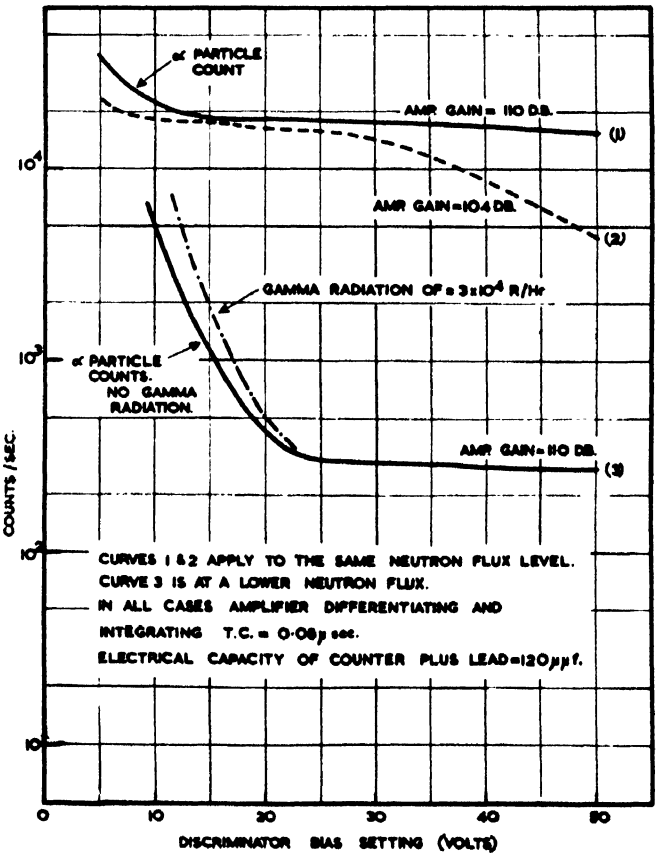

Figure 12. Fission counter discriminator bias curves

vided that the neutron flux 'trip' level is adjusted to take account of coolant conditions.

ACKNOWLEDGEMENTS

The authors wish to acknowledge the contributions of Mr. F. Wade and Mr. P. G. Salmon, of A.E.R.E., to the development of the ion chamber and fission chamber described.

REFERENCE

1. Jaques, T. A. J., Bollinger, H. A. and Wade, F., *Neutron Detectors for Reactor Instrumentation*, Proc. I.E.E. *100*, Part I, pp. 110–116 (1953).

Record of Proceedings of Session 22A

FRIDAY AFTERNOON, 18 AUGUST 1955

Chairman: Mr. S. Eklund (Sweden)
Vice-Chairman: Mr. M. Ristic (Yugoslavia)
Scientific Secretaries: Messrs. F. de Hoffmann and J. Leite Lopes

PROGRAMME

22A.1. Zero Energy Experiments (concluded)

P/404	Experimental studies on fast neutron reactors at A.E.R.E. ..... J. E. R. Holmes *et al.*
P/598	The fast exponential experiment ..... F. C. Beyer *et al.*
P/609	A survey of the theoretical and experimental aspects of fast reactor physics ..... D. Okrent *et al.*
	DISCUSSION

22A.2. Reactor Kinetics

P/775	Stability conditions in the non-linear dynamics of heterogeneous reactors ..... H. J. Lipkin and R. Thieberger
P/934	The influence of the temperature coefficient on the transfer function of a heavy water reactor ..... J. Pelser
P/334	The dynamic problems of power reactors and analogue computers ..... P. Braffort
P/610	Kinetics of stationary reactor systems ..... T. A. Welton
	DISCUSSION

Mr. L. R. SHEPHERD (UK) presented paper P/404.

Mr. B. I. SPINRAD (USA) presented paper P/598.

Mr. D. C. OKRENT (USA) presented paper P/609.

DISCUSSION OF P/404, 598, AND 609

Mr. KAZACHKOVSKY (USSR): I have the following question. To which constitution of the core, the dilute or the concentrated, do the following figures mentioned in the paper relate: the conversion factor; the ratio of the fission rate in the core to that in the blanket; and the activation measurement of σ.

Mr. SHEPHERD (UK): I have not fully understood the question, but the core dilution in which these measurements were made—the ones that I showed—were 40 atoms of U^{238} to 50 of plutonium.

Mr. KAZACHKOVSKY (USSR): I would like to clarify my question. It is stated in the paper that measurements were made both with a dilute core and with a concentrated core. The paper then goes on to give certain data: the conversion factor and the ratio of the fission rate in the core to that in the envelope. To which variation do these data refer? To the original, dilute condition, when the core contained U^{238}, or to the second, concentrated condition, when the core contained only Pu^{239}?

Mr. SHEPHERD (UK): They refer to the diluted system, but the difference was not very great.

Mr. KAZACHKOVSKY (USSR): Another question for Mr. Shepherd. How much neutron leakage was there from the reflector of the reactor?

Mr. SHEPHERD (UK): We only have an estimate of this. The estimate which we have is 30 ± 15 per hundred fissions. It is a very rough figure, but you see we have a concrete wall around our reactor which makes it very difficult to calculate accurately what the leakage is.

Mr. KAZACHKOVSKY (USSR): A final question for Mr. Shepherd. Was there an appreciable difference between the shapes of the curves of fission distribution, as determined by the various threshold detectors, for U^{238}, Pu^{240} and Np^{237}?

Mr. SHEPHERD (UK): I am not quite sure whether I know what difference you want. There is an appreciable difference between the response curve, of say Np^{237}, and that for U^{238}. The Np^{237} fission rate, as one goes into the blanket, falls off less rapidly than U^{238}. There was furthermore a noticeable difference between the values in the core with the diluted system and the concentrated.

Mr. KAZACHKOVSKY (USSR): It seems to me that reaction cross-sections, assumed in paper P/598 to be equal to $\sigma_f + \sigma_c + \sigma_{in}$, do not tally with the data given in Walt's paper, P/588. Thus, for U^{238}, in the case of Group 2, the cross section is seen to be $1.20 + 0.13 + 0.75 = 2.08$, as against 2.55 obtained by Walt. For

Group 3, we have: $1.23 + 0.16 + 0.36 = 1.75$, as against 2.65 according to Walt. A similar position obtains for U^{238}.

Is there not here some supplementary explanation? Or perhaps I have not quite correctly understood the data given in paper P/598?

Mr. SPINRAD (USA): I believe you are right if you take the cross section for group transfer as being the inelastic cross section. The point is that the group transfer cross section for which fast neutrons are lost from one group into lower energy groups must, of course, fall within the inelastic cross section because some of the inelastic events—and an appreciable fraction even—are due to a neutron still being found in the group in which it originated.

Mr. H. J. LIPKIN (Israel) presented paper P/775.

Mr. J. PELSER (The Netherlands) presented paper P/934.

Mr. P. BRAFFORT (France) presented paper P/334.

Mr. T. A. WELTON (USA) presented paper P/610.

Session 23 A

REACTOR THEORY

LIST OF PAPERS

		Page
P/611	A survey of neutron thermalization theory ..... E. R. Cohen	405
P/433	The calculation of the fine structure of the thermal neutron flux in a pile, by the spherical harmonics method ..... J. H. Tait	417
P/608	Comparison of theory and experiment for intermediate assemblies ..... H. Hurwitz, Jr. and R. Ehrlich	423
P/430	A method for calculating the critical mass of an intermediate reactor ..... M. E. Mandl and J. Howlett	433
P/665	Calculations for heterogeneous reactors with a small number of blocks ..... G. A. Bat	437
P/937	The Fermi age treatment for a homogeneous reactor with reflector ..... H. H. Woldringh	440
P/916	Matrix formulation of the two-group diffusion theory for a multiple reflector spherical reactor ..... P. Schmid	444
P/647	Absorption and multiplication of the moderating neutrons in the two-group theory ..... A. D. Galanin	448
P/664	Application of the method of effective boundary conditions for calculating the critical dimensions of reactors ..... A. D. Galanin	451
P/431	Upper and lower bounds for critical size according to one-group diffusion theory ..... R. T. Ackroyd	454
P/663	Critical size of heterogeneous reactor with small number of rods ..... A. D. Galanin	462
P/649	The theory of resonance absorption in heterogeneous systems ..... I. I. Gurevich and I. Y. Pomeranchouk	466
P/613	An estimation of Doppler effect in intermediate and fast neutron reactors ..... G. Goertzel	472
P/666	The thermal coefficient in a heterogeneous reactor ..... A. D. Galanin	477
P/669	Heterogeneous methods for calculating reactors. Survey of results and comparison with experiment ..... S. M. Feinberg	484
P/1003	Natural uranium-beryllium and natural uranium oxides-metallic beryllium lattices computation of cylindric reactors ..... O. Gamba *et al.*	501
P/656	Equation for the importance of neutrons, reactor kinetics and the theory of perturbation ..... L. N. Ussachoff	503
P/668	The thermal reactor regulators' efficiency ..... A. D. Galanin	511
P/796	The cylindrically symmetrical solution of Milne's problem usin gspherical harmonic analysis ..... L. Trlifaj	515
P/655	Solution of the generalized Milne problem ..... G. A. Bat and D. F. Zaretsky	519
P/667	Effective boundary conditions for "grey" bodies ..... D. F. Zaretsky	525

A Survey of Neutron Thermalization Theory

By E. Richard Cohen,* USA

In elementary reactor theory thermal neutrons are often represented as a monoenergetic group, and the absorption and scattering cross sections of the medium are properly averaged to give the correct interaction rates assuming that the neutrons have a Maxwellian distribution of velocities which can be characterized by the temperature T_0 of the moderating medium. This obviously can not be an exact description since absorption removes neutrons from the medium and thereby disturbs the equilibrium. However if the absorption cross section has the usual inverse dependence on velocity, absorption, per se, is not primarily responsible for the non-equilibrium. In such a case the probability per unit time for absorption is independent of the neutron velocity or of the thermal motion of the moderator. Under these circumstances it is easy to show that if the neutron distribution were initially an equilibrium distribution it would remain so, merely being depleted in amplitude by the absorption. Also if the source of neutrons is a pulse at time $t = 0$, the effect of absorption is to deplete the neutron density uniformly, without otherwise altering the neutron spectrum. If λ is the constant capture probability for neutrons per unit time and $N(v,t)$ is the neutron velocity distribution at time t after a pulse source, $N(v,t)e^{\lambda t}$ will be the solution of the problem without absorption. Hence $N(v,t)$ will asymptotically approach an equilibrium distribution as $t \to \infty$.

The steady-state neutron distribution in the presence of absorption is therefore complicated not by absorption itself but by the fact that the neutron source does not produce an equilibrium distribution and the neutrons are absorbed before this neutron distribution is established. The neutron distribution in the presence of absorption therefore depends on the specification of the source of neutrons.

GENERAL FORMULATION

In a reactor the neutrons are produced with energies which are large with respect to the energy of thermal motion of the moderator, kT_0. In this case the neutrons slow down into the thermal region, and in the initial stages of this process the thermal motion of the moderator can be neglected. The slowing down of fast neutrons has been treated by Placzek[1] and by Marshak.[2] Both of these authors consider only the slowing down process in a stationary moderator and their work will not be discussed in any detail here. As long as the neutron source energies are sufficiently high an equilibrium slowing down distribution will be established before the effects of the thermal motion of the moderator become important. If this restriction is satisfied the details of the source distribution are unimportant and the specification of the source can be replaced by a condition on the asymptotic neutron distribution for large velocities, which can in turn be determined from the asymptotic behavior of the slowing down in a stationary moderator.

The description of the kinetic behavior of a mixture of two gases is complicated by the non-linearity of the Boltzmann equation. Thus a completely general discussion of the diffusion of neutrons into a medium with which they exchange energy is a problem not easily treated. It is however possible to linearize the equation if we are dealing with neutron densities to be expected in reactors. A thermal neutron flux of 10^{13} n/cm^2-sec corresponds to a density of less than 10^8 n/cm^3 or to an equivalent gas pressure of approximately 10^{-12} atmospheres. Interactions between a neutron and a moderator atom are therefore infrequent compared with molecular collisions in a gas, or the frequencies of vibration of a crystal lattice. The moderator can therefore validly be assumed to be unaffected by the neutrons, and neutron-neutron collisions are completely negligible.

We can then write

$$\frac{\partial N(\vec{r},\vec{v},t)}{\partial t} + \vec{v}\cdot\nabla N(\vec{r},\vec{v},t) = S(\vec{r},\vec{v},t) - \gamma(\vec{r},\vec{v},t)N(\vec{r},\vec{v},t) + \int \{G_s(\vec{r},\vec{v}'\to\vec{v},t)N(\vec{r},\vec{v}',t) - G_s(\vec{r},\vec{v}\to\vec{v}',t)N(\vec{r},\vec{v},t)\}\,d^3v' \quad (1)$$

where $N(\vec{r},\vec{v},t)$ is the number of neutrons per unit volume of coordinate-velocity six-space; $G_s(\vec{r},\vec{v}\to\vec{v}',t)$ is the scattering rate per neutron from velocity $\vec{v}$ to

* North American Aviation, Inc., Nuclear Engineering and Manufacturing, Los Angeles, California. Including work by H. Hurwitz, Jr., Knolls Atomic Power Laboratory; E. P. Wigner and J. E. Wilkins, Jr., Metallurgical Laboratory; E. R. Cohen, North American Aviation, Inc.; D. H. Brown and D. S. St. John, Savannah River Laboratory; R. R. Bate, R. R. Coveyou and R. K. Osborn, Oak Ridge National Laboratory.

velocity $\vec{v}'$ and $\gamma(\vec{r},v,t)$ is the absorption rate per neutron at velocity $\vec{v}$. In addition to the indicated variables, G_s and γ also depend on the various dynamic variables of the moderator, to the extent that the absorption and scattering processes are functions of these variables, but do not depend on the neutron density. In the region of neutron velocities of interest here, there is no inelastic nuclear scattering, but inelastic molecular scattering or inelastic interactions of the neutrons with a crystal lattice are important.

As usual with the equations of kinetic theory, the completely general Equation 1 has been treated only in general terms. The time dependent equation has been considered in an approximate manner by von Dardel,[3] but extensive numerical calculations have been done only for the steady state, space independent problem. In this case Equation 1 can be rewritten as

$$\int G_s(v' \to v)N(v')\,dv' + S(v) = \{V(v) + \gamma(v)\}N(v) \quad (2)$$

where $V(v) = \int G_s(v \to v')\,dv'$

Monatomic Gaseous Moderator

In the case of a monatomic gaseous moderator, the calculation of $G_s(v \to v')$ is classical. We assume that the gas has a velocity distribution given by

$$M(v_2)\,dv_2 = \frac{4}{\sqrt{\pi}}\left(\frac{m}{2kT}\right)^{3/2} v_2^2 e^{-\frac{mv_2^2}{2kT}}\,dv_2 \quad (3)$$

Then

$$G_s(v \to v')\,dv' = \tfrac{1}{2}\int_0^\infty \int_{-1}^1 v_r\sigma_s(v_r)M(v_2)P(v \to v';v_2)\,d\mu\,dv_2\,dv' \quad (4)$$

where $v_r = [v^2 + v_2^2 - 2vv_2\mu]^{1/2}$ is the relative velocity of the two colliding nuclei and

$$P(v \to v';v_2)\,dv' = 0 \qquad v' < v_m$$
$$= \frac{2v'\,dv'}{v_M^2 - v_m^2} \qquad v_m < v' < v_M$$
$$= 0 \qquad v_M < v'$$

The two velocities v_m and v_M are the minimum and maximum velocities attainable by a neutron of velocity v colliding with a moderator atom of mass m (relative to the neutron mass as unity) and velocity v_2 with the angle $\cos^{-1}\mu$ between the initial velocities of moderator and neutron in the laboratory system,

$$v_m = V_c - mv_r/(m+1)$$
$$v_M = V_c + mv_r/(m+1)$$

and $V_c = [v^2 + 2mvv_2\mu + m^2v_2^2]^{1/2}/(m+1)$

is the velocity of the center of mass. The value of $\sigma_s(v_r)$ will depend of course on the particular gas being considered. Brown and St. John[4] consider the scattering cross section to be expressible as a sum of terms of the form

$$\sigma_i e^{-\alpha_i v^2}$$

since this form is amenable to calculation and has sufficient generality to fit many moderators. In particular, both the hydrogen and deuterium cross sections can be fitted by the two-term expression

$$\sigma_s(v) = \sigma_0 + \sigma_1 e^{-\alpha v^2} \quad (5)$$

The actual calculation is tedious but straightforward; it is complicated by the necessity to evaluate the double integral over a region whose boundaries are intersecting hyperbolas and straight lines and which depend upon whether $v < v'$ or $v > v'$. The result is

$$G_s(v' \to v) = \Sigma\sigma_i G(v',v;\alpha_i)$$

where

$$G(v',v;\alpha_i) = \frac{(m+1)^2}{4m}\frac{\tau_i^3}{\lambda_i}\frac{v}{v'}\left\{\exp[-\alpha_i\tau_i^2v'^2][\operatorname{erf}(\beta\theta_i v - \beta\zeta_i v') \pm \operatorname{erf}(\beta\theta_i v + \beta\zeta_i v')] + \exp\left[\frac{\beta^2}{m}(v'^2 - \lambda_i v^2)\right][\operatorname{erf}(\beta\theta_i v' - \beta\zeta_i v) \mp \operatorname{erf}(\beta\theta_i v' + \beta\zeta_i v)]\right\} \quad (6)$$

where the upper signs refer to $v < v'$ and the lower signs refer to $v > v'$

$$\tau_i^2 = \frac{m\beta^2}{m\beta^2 + \alpha_i}$$
$$\theta_i = \frac{m+1}{2\tau_i\sqrt{m}}$$
$$\zeta_i = \tau_i\sqrt{m} - \theta_i$$
$$\lambda_i = 1 + m(1 - \tau_i^2)$$
$$\operatorname{erf}(x) = \frac{2}{\sqrt{\pi}}\int_0^x e^{-u^2}\,du$$
$$\beta^2 = \frac{1}{2kT}$$

The function $V(v)$ may be found by integrating $G_s(v \to v')$, but it is much easier to go back to Equation 4 and perform the integration over v' first; then, since

$$\int P(v \to v';v_2)\,dv' = 1$$

we have

$$V(v) = \tfrac{1}{2}\int_0^\infty \int_{-1}^1 v_r\sigma_s(v_r)M(v_2)\,d\mu\,dv_2 = \sum_i \sigma_i W_i(v)$$

where

$$W_i(v) = \tau_i^3\left[\left(\tau_i^2 v + \frac{1}{2m\beta^2 v}\right)\operatorname{erf}(\sqrt{m}\,\beta\tau_i v)\exp[-\alpha\tau_i^2v^2] + \frac{\tau_i}{\beta\sqrt{\pi m}}e^{-m\beta^2v^2}\right] \quad (7)$$

Molecular Gases and Liquids

In the region of neutron energies below 1 ev the neutron does not collide with individual atoms but rather with the molecule as a whole. If the energy is

high enough the vibrational states of the molecule can be excited by the collision; in the region of major interest for the thermalization of neutrons however, only the rational states of the atom can be excited. For H_2O vibrational states can be excited only above 0.20 ev while rotational states can be excited above 0.006 ev. In describing the collisions of a neutron with a water molecule it will therefore be adequate to consider only the rotational states of the molecule. Sachs and Teller[5] have shown that the hydrogen atom in a molecule can be described in terms of an equivalent free mass-point whose mass is a tensor. Such a description is physically plausible. If the neutron collides with the hydrogen atom in a direction perpendicular to the plane of the water molecule the hydrogen atom will be effectively free and its effective mass is 1; if the neutron strikes the hydrogen in the line joining the atom to the center of gravity of the molecule the system recoils as a whole and the effective mass is 18. For the incident neutron in the direction perpendicular to these two directions the effective mass has some intermediate value. If I_x, I_y, I_z are the principal moments of inertia of the molecule, $\vec{r}$ is the position of the hydrogen atom with respect to the center of mass, and M_0 is the mass of the molecule, the effective mass tensor is

$$(M^{-1})_{ii} = \frac{r_j^2}{I_k} + \frac{r_k^2}{I_j} + \frac{1}{M_0} \quad (M^{-1})_{ij} = -\frac{r_i r_j}{I_k} \quad (i \neq j)$$

In order to apply the theory of a monatomic gas to molecular gases (and, in a poorer approximation, to liquids) one can define the effective mass of the molecule, m^*, given by the trace of the inverse mass tensor,

$$\frac{1}{m^*} = \frac{1}{3}\left[\frac{r_x^2 + r_y^2}{I_z} + \frac{r_y^2 + r_z^2}{I_x} + \frac{r_z^2 + r_x^2}{I_y}\right] + \frac{1}{M_0} \quad (8)$$

Brown and St. John have used the results of Sachs' and Teller's analysis in a calculation of the neutron distribution in D_2O which will be further discussed below. For that molecule the effective mass tensor has principal components (2, 3.517, 20). Thus, the effective mass of the deuterium atom in the D_2O molecule is 3.596 mass units. The effective mass of the oxygen is 17.607 and it is a valid first approximation to consider oxygen as an infinitely heavy atom and neglect any energy transfer in collisions between it and a neutron. This is not as good an approximation as the equivalent assumption for H_2O, both because of the difference in mass and because of the much larger hydrogen scattering cross section which makes the scattering in light water predominantly hydrogen collisions.

Crystalline Moderators

For a crystalline moderator such as graphite or beryllium it is necessary to consider the detailed structure of the crystal lattice. The theory of neutrons scattered by crystalline lattices has been discussed by various authors. Finkelstein[6] has discussed the model of an Einstein oscillator, Weinstock[7] and Cassels[8] have each considered a Debye crystal but restricted themselves to single phonon transfers. D. A. Kleinman[9] has considered the inelastic scattering of neutron by a crystal lattice and has found an approximate expression for the differential inelastic scattering cross section.

Brockhouse and Hurst[10] have investigated the problem experimentally and show that for scatterers heavier than aluminum it is approximately valid to treat the scatterer as a free gas. This can be seen from the following simple argument. The kinetic energy of the equivalent oscillators in the crystal will be $\frac{1}{2}kT$. The energy transferred in a collision will therefore have a distribution with a spread in energy of approximately

$$\left(\sqrt{E} + \sqrt{\frac{Tk}{2m}}\right)^2 - \left(\sqrt{E} - \sqrt{\frac{kT}{2m}}\right)^2 = \sqrt{\frac{8kTE}{m}}$$

If this energy is large compared to $k\Theta$, where Θ is the Einstein temperature of the oscillator, there will be several values of n for which the probability of transferring an energy equal to $nk\Theta$ will be important and these probabilities will form a histogram approximation to the energy loss distribution in an equivalent Maxwell gas. This approximation will be better as the number of states involved increases. Hence the criterion for the validity of replacing an Einstein crystal by a free gas is

$$E/kT \gg (m/8)(\Theta/T)^2 \quad (9)$$

The same criterion can be applied to a Debye oscillator; in this case the approximation to a free gas should be somewhat better since there is a continuum of oscillators. The detailed calculation of the energy loss to an Einstein oscillator has been carried out by Pope[11] and by Placzek.[5]

We can conclude that, in general, the approximation of a free gas tends to be better for heavier elements where the Einstein or Debye temperature is low and breaks down for crystals in which the Einstein temperature, and hence the lever spacing, is large. Unfortunately, graphite is in this latter class, since $k\Theta \approx 0.15$ ev. For graphite and beryllium it may be necessary either to carry out a detailed quantum mechanical analysis of the scattering process or to determine experimentally the differential inelastic scattering cross section for slow neutrons as function of neutron energy and angle of scattering.

SLOWING DOWN IN HYDROGEN

The equation which has been obtained for the neutron density can not be handled analytically in the general case, and recourse must be had to numerical methods. There are, however, a few special cases in which an analytic attack is possible. These cases shall now be mentioned. All of them are restricted to a scattering cross section which is independent of velocity.

One can consider a hypothetical monatomic hydrogen moderator for which the scattering cross section is independent of velocity.[12] The notation can also be simplified by introducing the variable $x = \beta v$,

$x' = \beta v'$ which is equivalent to measuring all velocities in terms of the most probable neutron velocity, $v_0 = \sqrt{kT/2}$. For $m = 1$, and $\alpha_i = 0$ the scattering function $G_s(v' \to v)$ is greatly simplified, and we have (in terms of the variables x, x' and with $\sigma_s = 1$)

$$G_s(x' \to x) = 2\frac{x}{x'}\operatorname{erf}(x) \qquad x < x'$$

$$= 2\frac{x}{x'}\exp(x'^2 - x^2)\operatorname{erf}(x) \qquad x' < x \quad (10)$$

and $$V(x) = \frac{2x^2+1}{2x}\operatorname{erf}(x) + \frac{e^{-x^2}}{\sqrt{\pi}}$$

The kernel $G_s(x' \to x)$ is not symmetric, but it is possible to find a transformation which will symmetrize it. This follows from the principle of detailed balancing and the fact that the Maxwell distribution is an equilibrium distribution; hence

$$M(x)G_s(x \to x') = M(x')G_s(x' \to x)$$

and therefore

$$S(x,x') = \sqrt{M(x)}\,G_s(x \to x')\frac{1}{\sqrt{M(x')}} = S(x',x) \quad (11)$$

and for scattering in hydrogen one obtains the symmetric kernel

$$S(x,x') = 2\exp\{-\tfrac{1}{2}(x'^2 - x^2)\}\operatorname{erf}(x) \qquad x < x'$$

$$= 2\exp\{-\tfrac{1}{2}(x^2 - x'^2)\}\operatorname{erf}(x') \qquad x' < x \quad (12)$$

Equation 2 now becomes (neglecting the source term)

$$\int_0^\infty S(x,x')\nu(x')\,dx' = [V(x) + \beta\gamma]\nu(x)$$

$$e^{-\frac{1}{2}x^2}\int_0^x e^{\frac{1}{2}u^2}\operatorname{erf}(u)\nu(u)\,du + e^{\frac{1}{2}x^2}\operatorname{erf}(x)\int_x^\infty e^{-\frac{1}{2}u^2}\nu(u)\,du = \tfrac{1}{2}[V(x) + \beta\gamma]\nu(x) \quad (13)$$

where $\nu(x) = N(x)/\sqrt{M(x)}$.

The function $S(x,x')$ of Equation 12 has the form of a Green's function of an ordinary second-order differential equation, and hence the integral operator of Equation 14 is the inverse of a second-order differential operator. In order to convert Equation 13 into a differential equation one must find a linear operator of the form

$$L(x) = \frac{d}{dx}p(x)\frac{d}{dx} + r(x) \quad (14)$$

which will give zero when it operates upon either $e^{-\frac{1}{2}x^2}$ or $\operatorname{erf}(x)e^{\frac{1}{2}x^2}$. These conditions give

$$\frac{1}{p(x)} = e^{-x^2} + \sqrt{\pi}\,x\operatorname{erf}(x) \quad (15.1)$$

and $$r(x) = p(x)[p(x)e^{-x^2} - x^2] \quad (15.2)$$

When one operates on Equation 13 with the operator $L(x)$ the integral equation is then converted into the differential equation

$$\frac{d}{dx}\left[p(x)\frac{d}{dx}(V + \beta\gamma)\nu(x)\right] + \left[r(x)(V + \beta\gamma) + \frac{4}{\sqrt{\pi}}\right]\nu(x) = 0 \quad (16)$$

This second-order homogeneous linear differential equation can be reduced to a Riccati equation by the substitutions

$$\mu(x) = [V(x) + \beta\gamma]\nu(x) \qquad y(x) = p(x)\mu'(x)/\mu(x) \quad (17)$$

which convert Equation 16 into

$$py' = -y^2 - p\left\{r(x) + \frac{4}{\sqrt{\pi}}[V(x) + \beta\gamma]^{-1}\right\} \quad (18)$$

The boundary condition on this equation is determined from the condition that $N(x)$ is normalized such that $N''(0) = 2$. This leads to the conditions $\mu(0) = 0$, $\mu'(0) = \beta\gamma$ and hence

$$\lim_{x\to 0}\left\{y(x) - \frac{1}{x}\right\} = 0$$

and $\mu(x)$ can therefore be computed from

$$\mu(x) = \beta\gamma x\exp\int_0^x\left\{\frac{y(u)}{p(u)} - \frac{1}{u}\right\}du \quad (19)$$

The solution of Equation 18 can be obtained in a series of ascending odd powers of x beginning with x^{-1} and the integral in Equation 19 computed numerically. The series for $y(x)$ was carried to $x = \frac{1}{2}$; beyond that point it was more convenient to continue by numerical integration. Wigner and Wilkins carried out this calculation for values of $1/4\sqrt{\pi}\,\beta\gamma = 0.1$, 0.2 and 1.0 and their results are shown in Fig. 1.

We know from the theory of slowing down in a stationary moderator that the asymptotic neutron distribution for large x is given by

$$N(x)\,dx = \frac{Cx\,dx}{(x + \beta\gamma)^3} \quad (20)$$

The constant C is determined by the conservation of neutrons. The slowing down density can most easily be determined by the condition that the total number of neutrons absorbed at velocities below x is equal to the slowing down density at x. Therefore the slowing down density $q(x)$ is given by

$$q(x) = \beta\gamma\int_0^x N(u)\,du \approx \tfrac{1}{2}x^2N(x) \qquad \text{for large } x$$

Since the integral is convergent for $x \to \infty$ we therefore have

$$C = 2\beta\gamma\int_0^\infty N(x)\,dx$$

The deviations from the familiar dv/v^2 law for the slowing down spectrum thus arise at high energies not from the thermal motion of the moderator (which

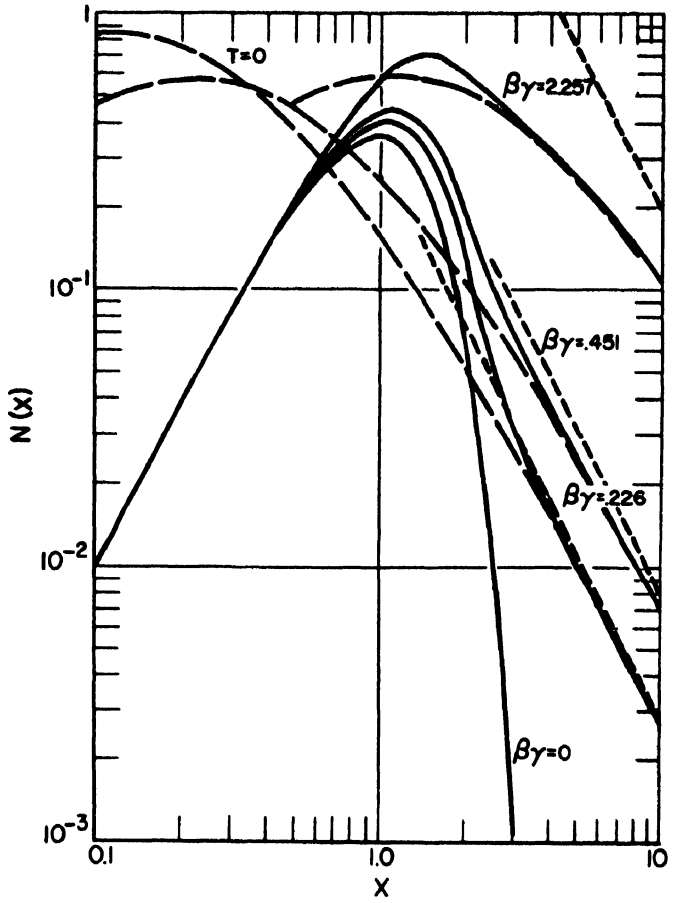

Figure 1. Neutron distribution in hydrogeneous moderator. The scattering cross section is assumed constant and the absorption cross section assumed to vary inversely as the relative neutron velocity $\beta\gamma$ is the ratio of the probability of absorption to the probability for scattering at velocity $x = 1$. Short dashed lines represent asymptotic distribution $N(x) = C/x^2$; long dashed lines represent the neutron distribution for a moderator at $T = 0$

would tend to increase the density) but from absorption (which decreases it). The comparison should therefore be made not with the dv/v^2 law but with Equation 20 which is correct in the limit as the temperature of the moderator goes to zero. The neutron distribution in hydrogen for a moderator at $T = 0$ is also shown in Fig. 1 for comparison with the distribution at finite temperature calculated by Wigner and Wilkins.

SLOWING DOWN IN A HEAVY MODERATOR

J. E. Wilkins[13] has also investigated the behavior of Equation 2 in the limit of very heavy moderators ($m \gg 1$). It is possible in this case to transform the integral equation into a second-order differential Equation which is accurate to order $1/m$ and which appears to be exact in the limit as the mass of the moderating atoms becomes large.

The symmetrized kernel for scattering with constant cross section is (cf Equation 12)

$$S(x,y) = \theta^2[e^{\frac{1}{2}(x^2-y^2)}\{\operatorname{erf}(\theta x - \zeta y) \pm \operatorname{erf}(\theta x + \zeta y)\} + e^{\frac{1}{2}(y^2-x^2)}\{\operatorname{erf}(\theta y - \zeta x) \mp \operatorname{erf}(\theta y + \zeta x\}] \quad (21)$$

where $2\sqrt{m}\,\theta = m + 1$, $2\sqrt{m}\,\zeta = m - 1$, and the upper sign refers to $x < y$, the lower sign to $x > y$.

In the limit of large m, Wilkins has shown that

$$\int_0^\infty S(x,y)\nu(y)\,dy = x\nu(x) + \frac{1}{2m}[(4 - x^2)x\nu(x) + \nu'(x) + x\nu''(x)] + \cdots \quad (22)$$

where $\nu(x) = N(x)/\sqrt{M(x)}$. Therefore since one also has

$$V(x) = \left(x + \frac{1}{2mx}\right)\operatorname{erf}(\sqrt{m}x) + \frac{e^{-mx^2}}{\sqrt{\pi m}} \approx x + \frac{1}{2mx} + 0\left(\frac{1}{m}\right) \quad (23)$$

the integral equation becomes

$$x\nu'' + \nu' + \left(4x - x^3 - \frac{1}{x} - 2m\beta\gamma\right)\nu = 0 \quad (24)$$

which, if we reintroduce $N(x) = xe^{-\frac{1}{2}x^2}\nu(x)$, is equivalent to

$$xN'' + (2x^2 - 1)N' + (4x - 2m\beta\gamma)N = 0 \quad (25)$$

This equation has also been derived by H. Hurwitz[14] in a manner which has somewhat more physical insight. Hurwitz starts with an equation for the neutron flux as a function of energy rather than with the neutron density. He writes

$$[\sigma_s(E) + \sigma_a(E)]\phi'E) = \int \phi(E')\sigma_s(E' \to E)\,dE' \quad (26)$$

where $\phi(E)\,dE = (2kT)^{\frac{3}{2}}N(x)x^2\,dx$ is the neutron flux and $E = kTx^2$ is the neutron energy. The scattering and absorption cross sections are the actually observed cross sections in the laboratory frame. We now express the flux in terms of the deviation from the Maxwellian distribution which would exist if there were no absorption. We therefore define

$$\phi(E) = \phi_0(E)\psi(E) = Ee^{-E/kT}\psi(E)$$

Then Equation 26 can be written

$$[\sigma_s(E) + \sigma_a(E)]\psi(E) = \int \psi(E')\phi_0(E')\sigma_s(E' \to E)\frac{1}{\phi_0(E)}\,dE' = \int \sigma_s(E \to E')\psi(E')\,dE' \quad (26.1)$$

where the last step follows from the principle of detailed balancing and the fact that the Maxwellian is the equilibrium distribution. The function $\psi(E')$ is now expanded in a Taylor series and we obtain a differential equation for $\psi(E)$ in terms of the moments of the energy transfer.

$$[\sigma_s(E) + \sigma_a(E)]\psi(E) = \psi(E)\int\sigma_s(E \to E')\,dE' + \psi'(E)\int\sigma_s(E \to E')(E' - E)\,dE' + \tfrac{1}{2}\psi''(E)\int\sigma_s(E \to E')(E' - E)^2\,dE' + \cdots \quad (26.2)$$

The moments can be evaluated for any moderator if the differential energy transfer cross section $\sigma_s(E \to E')$ is known. For a heavy moderator (the zero moment is correct for any moderator) one has

$$\int \sigma_s(E \to E')\, dE' = \sigma_s(E)$$

$$\int \sigma_s(E \to E')(E - E')\, dE' \approx \frac{2}{m}(2kT - E)\sigma_s(E)$$

$$\int \sigma_s(E \to E')(E - E')^2\, dE' \approx \frac{4}{m} kTE\sigma_s(E) \qquad (27)$$

Therefore if terms of order smaller than $1/m$ are neglected the integral equation can be converted into the second-order differential equation

$$EkT\psi'' + (2kT - E)\psi' - \frac{m\sigma_a(E)}{2\sigma_s(E)}\psi = 0 \qquad (28)$$

which is the equivalent of Equation 25, with $x\sigma_a(E) = \beta\gamma\sigma_s(E)$; we have only to express $\psi(E)$ in terms of $N(x)$ and transform the independent variable from E to x.

The convergence of the moment expansion in Equation 26.2 can be investigated most easily if the known physical behavior of ψ is introduced. For small values of $E(E < 2kT)$, ψ is approximately unity and the series solution of Equation 28 will converge within some radius of convergence. For $E \gg kT$, $\psi \sim E^{-2}e^{E/kT}$ and $\psi'' \sim (kT)^{-2}\psi$. The mean square energy transfer is $4kTE/m$ and hence the expansion is asymptotically convergent if

$$\frac{4kTE}{m}\psi'' \ll \psi \qquad (29)$$

and this condition implies that $E \ll (m/4)kT$ and hence in the limit of large m, Equation 27 should converge for all value of E. Wilkins developed Equation 25 with the restriction that $mx^2 \gg 4$; on the other hand Hurwitz' solution appears to be valid with only the restriction that $x^2 \ll m/4$ Thus Equation 25, or its equivalent, Equation 28, is valid for the entire range of x for sufficiently large m.

The series solution for $N(x)$ can most easily be obtained by writing $N(x) = \mu(x)x^2e^{-x^2}$ so that $\mu(x)$ is the deviation from the Maxwellian distribution. A straightforward calculation leads to

$$\mu(x) = \sum a_n x^n \qquad a_0 = 1 \qquad a_1 = \frac{\Delta}{3} \qquad \Delta \equiv 2m\beta\gamma$$

$$a_n = \frac{1}{n(n+2)}[\Delta a_{n-1} + 2(n-2)a_{n-2}] \qquad (30)$$

Although this series is convergent for all x, the convergence is slow for $x \gg 1$ and it is more convenient from a calculational standpoint to find an asymptotic expansion for large x. This will also allow a comparison with other known solutions. The series for large x is as follows:

$$N(x) \approx \frac{C}{x^2}\left[1 - \frac{\Delta}{2x} + \frac{\Delta^2 + 16}{8x^2} - \frac{\Delta^3 + 76\Delta}{48x^3} + \frac{\Delta^4 + 220\Delta^2 + 2304}{384x^4} - \cdots\right] \qquad (31)$$

In each term the leading power in Δ is just the term corresponding to the expansion of $e^{-\Delta/2x}$. This is equivalent to the usual "resonance escape" probability

$$\exp\left\{-\int \frac{2\sigma_a}{\xi\sigma_s}\frac{dv}{v}\right\}$$

for an absorption cross section which varies inversely with velocity. The asymptotic solution can therefore be written as

$$N(x) \sim \frac{Ce^{-\Delta/2x}}{x^2 - 2} \qquad (32)$$

The slowing down density $q(x)$ may be found by integrating Equation 25. We obtain

$$q(x) = \beta\gamma\int_0^x N(x')\, dx' = \frac{1}{m}\left[(x^2 - 1)N + \frac{1}{2}xN'\right] \qquad (33)$$

The asymptotic form for the slowing down density in a stationary moderator is

$$q(x) = \tfrac{1}{2}\xi x^2 N(x)$$

so that, using the approximate solution of Equation 32 we can define an effective value of ξ, the mean logarithmic energy loss, as

$$\xi = \frac{2}{m}\left[1 - \frac{2}{x^2} + \frac{\Delta}{4x^3} - \cdots\right] \qquad (34)$$

The slowing down power is therefore decreased by the finite temperature of the moderator and increased by the presence of absorption. In a stationary moderator $\xi = 2/m$ for large m and the mean energy loss per collision is $(2/m)E$; at a finite temperature of the moderator there is a transfer of energy from moderator to neutron so that the mean energy loss is reduced to $(2/m)(E - 2kT)$; thus Equation 34 properly reflects the results of Equation 27.

NUMERICAL METHODS

For moderators of intermediate mass, or for which the cross sections are not simple analytic expressions, recourse must be made to numerical methods of solution. There are two different approaches which have been used. One method involves the iteration of the integral equation; the other, which has a more direct physical appeal, involves following the history of individual neutrons from collision to collision.

Iteration

Brown and St. John at the Savannah River Laboratory[4] and Niestlie and Berman[15] have utilized high-speed electronic digital computers (IBM 701) to carry out a numerical integration of Equation 2. In order to adapt the problem to a digital computer it is necessary to terminate the scattering integral at some finite value. If this value v^* is large enough so that $G_s(v \to v') \approx 0$ for $v' > v > v^*$, the neutron density $N(v)$, $(v > v^*)$ will be adequately given by the solution for the slowing down of neutrons in a stationary moderator. Hence Equation 2 is modified to

$$S^*(v) + \int_0^{v^*} G_s(v' \to v)N(v')\,dv' = [V(v) + \gamma]N(v) \quad (2.1)$$

where

$$S^*(v) = S(v) + \int_{v^*}^{\infty} G_s(v' \to v)N(v')\,dv'$$

For $v' > v^*$ it is then sufficiently accurate to take

$$G_s(v' \to v)\,dv = 0 \qquad v < \alpha v'$$

$$= \frac{2\sigma_s(v')v\,dv}{(1-\alpha^2)v'^2} \qquad \alpha v' < v < v'$$

$$= 0 \qquad v' < v$$

and

$$\alpha = (m-1)/(m+1) \quad (35)$$

Furthermore, in this region $N(v)$ is adequately given by $A/\sigma_s(v)v^2$ and hence in the absence of any true sources below v^* we have

$$S^*(v) = \frac{Av}{1-\alpha^2}\left[\frac{1}{v^{*2}} - \frac{\alpha^2}{v^2}\right] \qquad \alpha v^* \le v \le v^*$$

$$= 0 \qquad v \le \alpha v^* \quad (36)$$

Equation 2.1 is now converted into a form suitable for numerical calculation by replacing the integral by a sum. This gives

$$N_i = \frac{S_i + \sum_{j=1} G_{ij}\,\Delta v_j N_j}{V_i + \gamma} \qquad i = 1, 2, 3, \cdots \quad (37)$$

If one defines the matrix K_{ij} by

$$K_{00} = 1 \qquad K_{0j} = 0$$

$$K_{i0} = \frac{S_i}{V_i + \gamma} \qquad K_{ij} = \frac{G_{ij}\,\Delta v_j}{V_i + \gamma} \quad (38)$$

and normalizes the system by defining $N_0 = 1$, Equation 2.1 is thereby replaced by a linear matrix equation $N = KN$ which is solved by standard machine iteration.

Brown and St. John have applied this formulation to the slowing down of neutrons in heavy water using the equations quoted in an earlier section for the scattering kernel with velocity-dependent cross sections. The most difficult part of the calculation is the initial determination of G_{ij}. Once these have been determined the K_{ij} may be found for various values of absorption; but temperature and absorption can not be related to a single parameter because of the velocity dependence of the scattering cross section. The deuterium scattering cross section was fitted with the constants (see Equation 5) $\sigma_0 = 3.3$ barns, $\sigma_1 = 1.6$ barns, $\alpha_1 = 2.88$ ev/amu, $m = 3.6$ amu, and the moderator temperature was taken to be $kT = 0.025$ ev. The results are shown in Fig. 2 for values of γ equal to 0.046, 0.064, 0.1 and 0.2. These correspond respectively to macroscopic absorption cross sections Σ_a (cm^{-1}) = 0.0121, 0.0169, 0.0264, 0.0528. All of the curves are normalized arbitrarily to the same number of neutrons at the energy $E = 0.005$ ev. Curve A gives the pure Maxwellian distribution. The other curves give the computed neutron spectra for various values of the absorption parameter, γ.

Monte Carlo Calculation

A quite different numerical approach has been followed at Oak Ridge National Laboratory by R. K. Osborn, R. R. Bate and R.R. Coveyou. This method consists of calculating the detailed behavior of a representative neutron as it loses or gains energy in successive collisions until it is absorbed. Several thousand neutron "histories" are assembled in this way and from them the neutron density is determined. The calculation was directly designed to take full advantage of the unique capacity of the ORACLE for performing an enormous number of simple operations in a short time.

A neutron at a preassigned source speed is considered to be released into the moderating medium. Since the cross sections are known, the probabilities of absorption and capture are determined. A selection is made from a table of random numbers (which is stored in the machine and actually computed by it) to determine whether the collision is an absorption or a scattering. If the event is an absorption that fact is recorded and a new neutron is introduced at the source speed. If the event is a scattering a decision must be made regarding the speed of the target nucleus and the angle of approach between neutron and target. Having made this selection it is then a simple matter, on the assumption of isotropic scattering in the center-of-mass system to select a new speed for the neutron. This new neutron now repeats the same sequence until it is finally absorbed, thus terminating a history.

A closer scrutiny indicates, however, that a Monte Carlo calculation of the slowing down process cannot

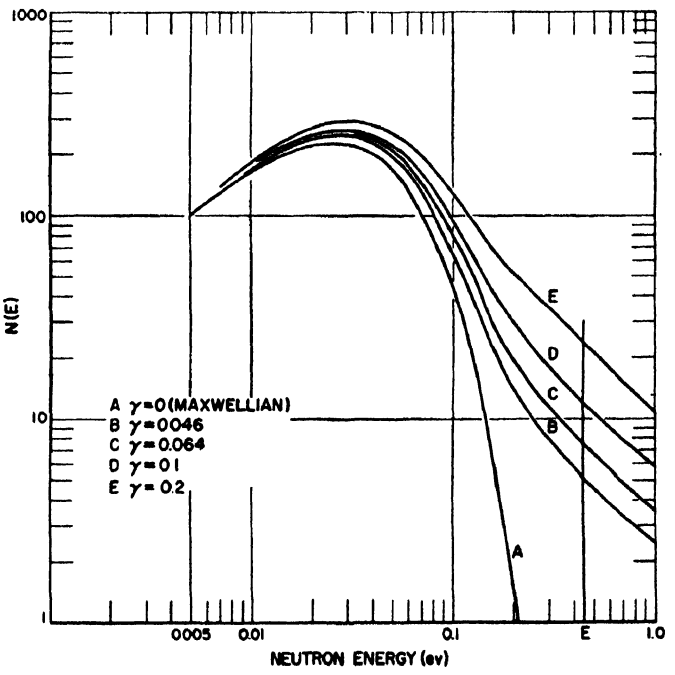

Figure 2. Neutron density in heavy water. Absorption cross section assumed 1/v; scattering cross section fitted to experimental data solution of integral equation by numerical iteration

proceed quite so directly as indicated. In the first place the probability of scattering is $\sigma_s V(v)$ and it is undesirable to compute $V(v)$ at each stage of the process. At the expense of some indirectness in the method this calculation can in fact be avoided. A more complicating consideration arises in connection with the choice of the parameters characterizing a scattering subsequent to the decision that the event is indeed a scattering. This choice must be an appropriate selection from the speed and angle distribution of the targets as seen by the neutron. The technique whereby these complications were circumvented was suggested by H. Kahn of the Rand Corporation.

The reaction rate for a neutron of velocity $\vec{v}$ with an atom of velocity $\vec{v}_2$ and with $\vec{v} \cdot \vec{v}_2 = \mu v v_2$ is written

$$R(v,v_2;\mu) = \frac{v_r \sigma_s}{v + v_2} [vM(v_2) + v_2 M(v_2)] + \sigma_a(v_r) v_r M(v_2) \quad (39)$$

where $M(v_2)$ is the Maxwellian distribution of moderator velocities. Three numbers are now defined by

$$P_1 = \sigma_a(v)v/N$$
$$P_2 = \sigma_s v/N$$
$$P_3 = \sigma_s v_m/N \quad (40)$$

where $N = \sigma_a(v)v + \sigma_s v + \sigma_s v_m$ and v_m is the mean moderator velocity. A random number η is now selected from the interval (0, 1) to determine if the neutron is absorbed or scattered. If η is less than P_1 the neutron is absorbed, if it lies between P_1 and $P_1 + P_2$ a velocity for the moderator atom v_2 is chosen from the distribution $M(v)$; if $\eta > P_1 + P_2$, v_2 is chosen from the distribution $vM(v)$. A selection is also made of the value of μ, and the relative velocity between neutron and moderator is computed. A decision based on the value of another randomly selected number from the interval (0, 1) accepts the scattering with a probability equal to $v_r/(v + v_2)$. If the scattering is accepted the energy of the scattered neutron is determined and the calculation proceeds to follow this neutron. If the scattering is rejected the entire collision is cancelled and a new decision is made, including the determination as to whether the collision is an absorption or a scattering. Thus a posteriori selection properly corrects for the fact that the scattering probability depends on the relative velocity of neutron and target, computed after collision.

The results of a calculation are obtained from the machine in the form of a histogram of the number of scattering events and the number of absorptions which occur in each of a set of intervals into which the range of the velocity variable has been subdivided. A single calculation consisted of as many histories as might be required to provide a total of at least 65,000 scattering events. The time for a calculation was of the order of four hours. The energy range from 0 to $1024 \cdot \frac{3}{2}kT$ was divided equally in the velocity interval into 512 parts. This corresponds at room temperature to $\Delta v = 169$ m/sec.

Two cases were calculated which duplicate Wigner and Wilkins' calculation for hydrogen. The comparison of the results are shown in Fig. 3. The solid lines are the same curves as in Fig. 1; the points represent the results of the machine calculation on the ORACLE.

A useful measure of flux distribution is provided by the concept of the neutron effective temperature. This was defined as the temperature determined by a least-squares fit of a Maxwell-Boltzmann distribution to the computed flux in the region $0 \leq E \leq 3 \cdot 6kT$. No significance is to be attached to the choice of the upper limit, except that it serves to exclude the $1/v^2$ portion of the neutron density spectrum. The ratio of effective neutron temperature T_n to the actual moderator temperature T_0, for all of the cases calculated was fit by the equation

$$T_n = T_0 \left[1 + 0.91 \frac{m\sigma_0}{\sigma_s}\right] \quad (41)$$

where σ_0 is the absorption cross section for monoenergetic neutrons at energy kT_0. This relation was found to hold for moderators from $m = 1$ up to $m = 25$ and for $m\,\sigma_0/\sigma_s$ from 0 to 0.5, to within 5 per cent. The calculated temperature for those cases which have been examined is given in Table I. The quantity K which appears in the table is the ratio of the ab-

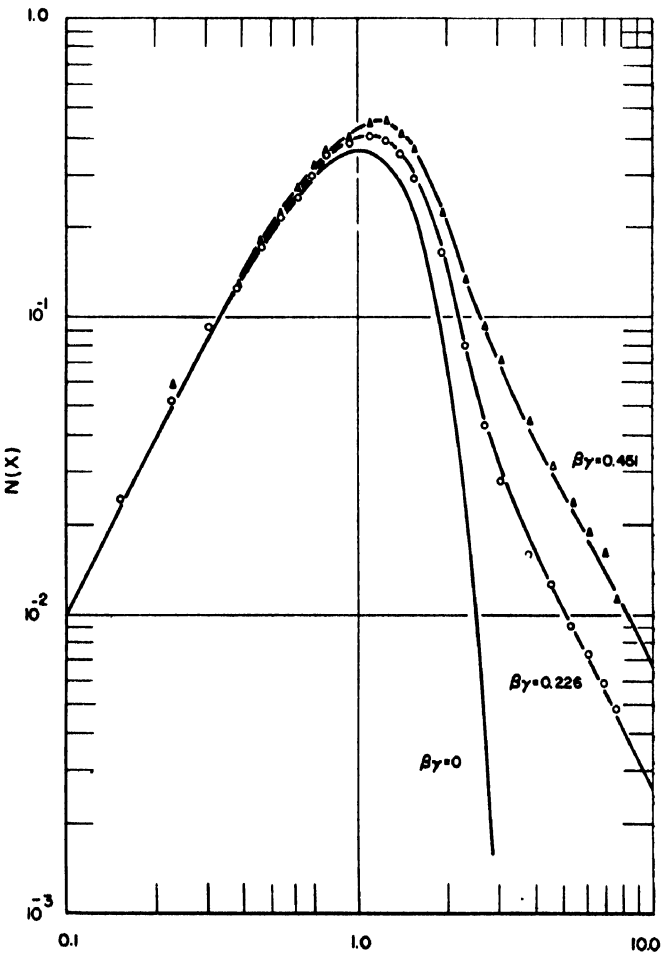

Figure 3. Monte Carlo calculation of neutron density in hydrogen. The results of the calculation are given by the points. The solid lines are the analytic solution of Fig 1; the only adjustment is the absolute normalization

sorption cross section at $E = \frac{3}{2}kT$ to the (constant) scattering cross section; hence $K = \sqrt{\frac{3}{2}}\,(\sigma_0/\sigma)_s$.

NEUTRON TEMPERATURE IN A HEAVY MODERATOR

It is possible to take the results of these analyses of neutron slowing down and apply them to the calculation of neutron age and neutron temperature. Using Equations 33.1 and 34 we can write the slowing down density in terms of the neutron density

$$q(v) = \frac{\sigma_s}{m}(v^2 - 2v_0^2)N(v) \tag{42}$$

where $v_0 = \sqrt{2kT_0}$ is the characteristic neutron velocity corresponding to the temperature T_0 of the moderator. Although this equation is an approximation which is valid only in the limit $v^2 \gg v_0^2$, we shall assume that it can be used with adequate accuracy down to neutron velocities which actually approach thermal values. We shall then assume that the neutron velocity spectrum can be represented by a Maxwellian distribution with a neutron temperature T_n in the range $0 < v < yv_n$ and by a slowing down distribution in the range $yv_n < v$. Hence we write

$$N(v)\,dv = \frac{4v^2}{\sqrt{\pi}\,v_n^3} e^{-v^2/v_n^2}\,dv \qquad 0 < v < yv_n \tag{43.1}$$

and

$$v_0\sigma_0 N(v) = \frac{dq}{dv} \qquad yv_n < v \tag{43.2}$$

where $v_0\sigma_0$ is the constant absorption probability per unit time, $v_0\sigma_0 = \gamma\sigma_s$. Equation 43.2 is a statement of the conservation of neutrons and states that the slowing down density is reduced, as neutron energy decreases, by the absorption of neutrons. Combining this with Equation 42 the solution for $q(v)$ is

$$q(v) = \left(\frac{v - \sqrt{2}\,v_0}{v + \sqrt{2}\,v_0}\right)^{\epsilon} \qquad \epsilon = m\beta\gamma/2\sqrt{2} \tag{44}$$

The neutron density then follows directly from Equation 42

$$N(v) = \frac{m}{\sigma_s v_n^2}\left(\frac{v}{v_n} - \sqrt{2t}\right)^{\epsilon-1}\left(\frac{v}{v_n} + \sqrt{2t}\right)^{-(\epsilon+1)} \tag{45}$$

where $t = v_0^2/v_n^2$ is the ratio of moderator temperature to neutron temperature. (If one sets $t = 0$ these equations reduce to the elementary form which neglects the effects of moderator motion.)

We must now impose on the solution the conditions of conservation and continuity at the transition point $v = yv_n$. Thus the neutron density from Equation 45 must give the same value for $N(v)$ as Equation 43.1. Furthermore the slowing down density $q(yv_n)$ must be equal to the absorption rate in the thermal region. This leads to the two equations for $q(yv_n)$ as a function of y. From the continuity of neutron density we have

$$q(yv_n) = \frac{4}{\sqrt{\pi}}\frac{\sigma_s v_n}{m} y^2(y^2 - 2t)e^{-y^2} \tag{46.1}$$

and from the conservation of neutrons we obtain

$$q(yv_n) = \frac{\gamma\sigma_s}{\sqrt{t}}\left[\operatorname{erf}(y) - \frac{2y}{\sqrt{\pi}}e^{-y^2}\right] \tag{46.2}$$

These two expressions must be equal, and therefore

$$m\beta\gamma = \frac{4y^2(y^2 - 2t)e^{-y^2}}{\sqrt{\pi t}\left[\operatorname{erf}(y) - \frac{2y}{\sqrt{\pi}}e^{-y^2}\right]} \tag{47}$$

The parameter t, which relates the neutron temperature to the moderator temperature is still to be fixed. It is of course possible to choose $t = 1$, but one can also attempt to fit the distribution calculated by Equations 43.1 and 45 to the Wilkins distribution, Equation 30. A convenient method for making this fitting is to equate moments. The kth moment of the neutron velocity distribution is defined as

$$M_k = \int_0^\infty v^k N(v)\,dv$$

Since the neutron density varies as v^2 for $v \ll v_n$ and as v^{-2} for $v \gg v_n$ it is apparent that the moments are finite only in the open interval $-3 < k < 1$. It is therefore impossible to define a mean velocity or a mean energy for this distribution, but a characteristic energy can be defined in terms of the negative moments. We shall define

$$\bar{E} = \frac{\int_0^\infty N(v)\,dv}{\int \frac{1}{v^2}N(v)\,dv} \tag{48}$$

For the Wilkins distribution the integration may be carried out easily to first order in Δ if one replaces Equation 30 by the recursion formulas

$$a_0 = 1, \qquad a_1 = \frac{1}{3}\Delta, \qquad a_n = \frac{2(n-2)}{n(n+2)}a_{n-2} \tag{30.1}$$

The result is

$$\bar{E} = \frac{1}{2}v_0^2\left[1 + \frac{\Delta}{\sqrt{\pi}} + \cdots\right] \tag{48.1}$$

For the approximate distribution we have, using Equation 43.1 and Equation 45 in the appropriate velocity ranges,

$$\bar{E} = \frac{\frac{1}{2}v_0^2\left[\operatorname{erf}(y) - \frac{2y}{\sqrt{\pi}}e^{-y^2}\right]}{p_{th}\left[(t + J)\operatorname{erf}(y) - \frac{2}{\sqrt{\pi}}Je^{-y^2}\right]} \tag{48.2}$$

where

$$J \approx \frac{\epsilon}{16}\left[\ln\frac{1}{s} - \frac{2\sqrt{2t}\,y}{(y - \sqrt{2t})^2}\right],$$

$$p_{th} = \left(\frac{y - \sqrt{2t}}{y + \sqrt{2t}}\right)^{\epsilon} = s^{\epsilon}$$

p_{th} is the probability that a neutron will reach thermal

energies. When we equate Equations 48.1 and 48.2 we obtain an equation which implicitly relates t and y; this must now be combined with Equation 47, another implicit relationship, in order to determine t. It is found that in the region $0 < m\sigma_0/\sigma_s < 0.5$ the result may be expressed by the approximate linear relationship

$$T_n = T_0\left[1 + 0.60\,\frac{m\sigma_0}{\sigma_s}\right] \tag{49}$$

The analytic solution of Equations 47, 48.1 and 48.2 indicates however, for very small values of $m\sigma_0/\sigma_s$, that the relationship should be

$$T_n = T_0\left[1 + \frac{2m\sigma_0}{\sqrt{\pi}\,\sigma_s} + 0(\epsilon^2 \ln \epsilon)\right] \tag{49.1}$$

It is not certain whether a more accurate calculation would verify Equation 49 or Equation 49.1. The results obtained by Osborn, Bate and Coveyou (Table I) lie midway between these two expressions, but they have not yet extensively explored the region $m \gg 1$ where the present theory is valid. For hydrogen moderation, where the mean logarithmic energy loss in the slowing down region is $\xi = 1$ the coefficient might be expected to be larger than for heavy elements where $\xi = 2/m$.

NEUTRON AGE[10]

One may also apply this approximate formulation to an evaluation of the age of neutrons in an absorbing moderator. The usual Fermi age theory expresses the migration area as an integral over the slowing down region plus the migration area of thermal neutrons. The integral (the Fermi Age) is usually written with a lower limit equal to kT_0. It is obvious that this limit can not be correct. The correct lower limit should be deducible from a consistent model which relates absorption to slowing down.

If one considers the one-dimensional problem of the neutron distribution from a plane source, the migration area may be directly related to the second spatial moment. The equation for the slowing down and diffusion of neutrons from a plane source in the Fermi Age approximation is

$$Dv\,\frac{d^2N(v,z)}{dz^2} - \sigma_0 v_0 N(v,z) + \frac{\partial q(v,z)}{\partial v} + \delta(z)\delta(v - v_1) = 0 \tag{50}$$

where v_1 is the velocity of the source. This equation is assumed to hold in the slowing down region; below the transition velocity yv_n the thermal neutron density is given by

$$D\,\frac{d^2f(z)}{dz^2}\,\phi_1(y) - \sigma_0 v_0 \phi_0(y) f(z) + q(yv_n,z) = 0 \tag{51}$$

where

$$\phi_0(y) = \frac{4}{\sqrt{\pi}} \int_0^{yv_n} \frac{v^2}{{v_n}^3}\, e^{-v^2/{v_n}^2}\, dv$$

$$\phi_1(y) = \frac{4}{\sqrt{\pi}} \int_0^{yv_n} \frac{v^3}{{v_n}^3}\, e^{-v^2/{v_n}^2}\, dv$$

We now take the Fourier transform of Equations 50 and 51 and obtain

$$-D\omega^2 v Q(v,\omega) - \sigma_0 v_0 Q(v,\omega) + \frac{1}{m}\sigma_s(v^2 - 2{v_0}^2)\left\{\frac{\partial Q}{\partial v} + \frac{1}{\sqrt{2\pi}}\,\delta(v - v_1)\right\} = 0 \tag{52}$$

$$-D\omega^2 F(\omega)\phi_1(y) - \sigma_0 v_0 F(\omega)\phi_0(y) + Q(yv_n,\omega) = 0 \tag{53}$$

The treatment is now similar to that in the previous section; the conditions of continuity provides a relationship between y and $m\beta\gamma$. This relationship also includes a dependence on t and ω. The details will not be repeated here.

From $F(\omega)$ one obtains the thermal neutron density by inverting the Fourier transform; if all that is required, however, is the second moment of the distribution, it can be obtained by considering the power series expansion of $F(\omega)$ in powers of ω^2, and we find

$$M^2 = -\left.\frac{d \ln F(\omega)}{d(\omega^2)}\right|_{\omega^2 = 0} \tag{54}$$

The migration area may therefore be found quite readily. The result is

$$M^2 = \frac{mD}{2\sigma_s} \ln \frac{{v_1}^2}{y^2{v_n}^2 - 2{v_0}^2} + L^2\,\frac{\phi_1}{\phi_0} \tag{55}$$

where $L^2 = 2D/\sqrt{\pi t}\,\sigma_0$ is the thermal diffusion length. It is interesting to point out that the second term is just the ratio of the diffusion coefficient to the absorption coefficient, each averaged over the thermal component of the neutron spectrum. If we define the effective migration energy E_m as the lower limit of an equivalent age integral for migration we have

$$M^2 = \frac{mD}{2\sigma_s} \ln \frac{{v_1}^2}{2E_m} + L^2 \tag{56}$$

Table I. Effective Neutron Temperatures*

m	K	$m\sigma_0/\sigma_s$	T_n/T_0
1	0.18	0.221	1.24
	0.36	0.441	1.42
2	2^{-5}	0.076	1.09
	2^{-7}	0.0194	1.02
9	2^{-5}	0.344	1.28
12	2^{-5}	0.478	1.35
	2^{-8}	0.576	1.04
	2^{-10}	0.0143	1.00
16	2^{-5}	0.612	1.55
19	2^{-5}	0.727	1.58
25	2^{-5}	0.957	1.81

* Osborn, R. K., Bate, R. R., and Coveyou, R. R., (unpublished).

where $E_m = kT_n(y^2 - 2t)$

$$\times \exp\left\{\frac{1 - \frac{2}{\sqrt{\pi}}y + y^2 - e^{y^2}[1 - \operatorname{erf}(y)]}{y^2(y^2 - 2t)}\right\}$$

The migration area of thermal neutrons is an important quantity, but in the model of a thermal reactor which assumes that all absorption (other than that which occurs in definite sharp resonances) is in the thermal group, it is more appropriate to define an "age to absorption." The important distinction here is that the quantity of prime interest is the mean square distance which a neutron travels between production and absorption, rather than the mean square distance of a thermal neutron from the source. Since the probability for absorption per unit time is independent of the neutron velocity, the density of absorption is proportional to the total neutron density rather than the thermal component of the neutron density.

The absorption density is given by

$$A(\omega) = \frac{1}{\sqrt{2\pi}}\int_{-\infty}^{\infty} e^{i\omega z}\int_0^{v_1} N(v,z)\sigma_0 v_0\, dv\, dz$$

$$= \sigma_0 v_0 F(\omega)\phi_0(y) + m\beta\gamma\int_{yv_n}^{v_1}\left[\frac{v^2 - 2v_0}{v_1^2}\right]^{\delta}\left[\frac{v - \sqrt{2v_0}}{v + \sqrt{2v_0}}\right]^{\epsilon}\frac{dv}{v^2 - 2v_0} \quad (57)$$

where $\delta = mD\omega^2/2\sigma_s$. From this we find that $A(0) = 1$, and that

$$-\left.\frac{d \ln A(\omega)}{d(\omega)^2}\right|_{\omega=0} = \frac{mD}{2\sigma_s}\left[\ln\frac{v_1^2}{y^2v_n^2 - 2v_0^2} + (1 - p_{th})\ln\frac{y^2 - 2t}{2t} + p_{th}\frac{e^{y^2} - 1 - y^2}{y^2y^2 - 2t)} + \epsilon\int_s^1 u^{\epsilon-1}\ln\frac{(1+u)^2}{4u}\,du\right] \quad (58)$$

In a manner which is completely analogous to the calculation of the energy E_m for the lower limit of the "age" of thermal neutrons we can also define an energy E_{eff} which is the effective lower limit of the Fermi "age to absorption."

The results of these calculations are presented in Fig. 4. Two calculations are presented for each migration area; one corresponds to the temperature of the neutrons equal to the temperature of the moderator ($t = 1$), the other corresponds to Equation 49. Unfortunately, measured values of the effective temperature of thermal neutrons appear to depend on the method of measurement. B. T. Taylor,[17] using a crystal spectrometer, measured no temperature increase above the moderator temperature in the Harwell reactor. G. B. Gavin[18] using foil techniques found no increase in the Thermal Test Reactor. On the other hand, Zinn[19] analyzed the neutron beam from the Argonne Reactor with a crystal spectrometer and found a temperature increase of approximately 90°C, and Branch[20] measured an increase of 140°C in the Oak Ridge Graphite Reactor. Other measurements, equally discordant, appear in the literature.[21]

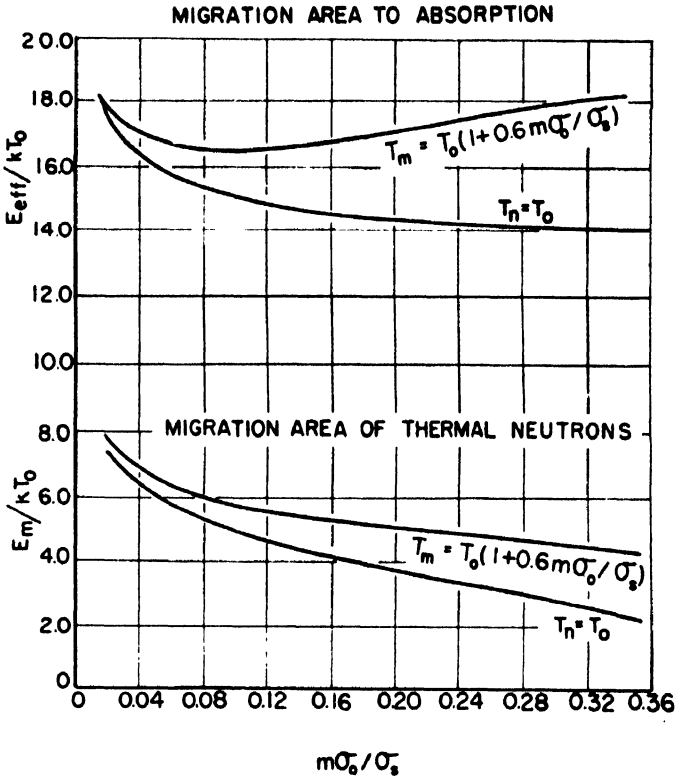

Figure 4. Effective lower limit of Fermi age integral; E_{eff} should be used in calculations which neglect epithermal absorption to give correct migration area from source point to absorption: E_m gives correct migration area of thermal component of neutron density. See page 414, Equation 56

The values of E_m and E_{eff} do not depend on the assumptions made with regard to the neutron temperature, nor do they depend strongly on the value of $m\sigma_0/\sigma_s$. In the interval $0.01 < m\sigma_0/\sigma_s < 0.5$ it would be an adequate approximation to write $E_m = 4kT_0$ and $E_{eff} = 16kT_0$. (However, both energies become logarithmically infinite as the absorption approaches zero.) In a reactor calculation in which no absorptions are assumed except in the thermal group it is therefore appropriate to terminate the Fermi age integral at any energy equal to $16kT_0$. This correction to the age may be important in heavy-water moderated reactors.

A measurement of neutron age in D_2O-uranium exponential experiments appears to confirm this effect.[22]

REFERENCES

1. Placzek, G., Phys. Rev. 69: 423 (1946).
2. Marshak, R. E., Rev. Mod. Phys. 19: 185 (1947).
3. von Dardel, G. F., Transactions Royal Institute Technology, Stockholm, No. 75 (1954).
4. Brown, H. D. and St. John, D. S. (Unpublished).
5. Sachs, R. G. and Teller, E. Phys. Rev. 60:18, (1941). See also A. Messiah, Phys. Rev. 84: 204, (1951) and Placzek, G. Phys. Rev., 86: 377 (1952).
6. Finkelstein, R. J., Phys. Rev. 72: 907 (1947).
7. Weinstock, R., Phys. Rev. 65: 1 (1944).
8. Cassels, J. M., Proc. Roy. Soc. (London) A208, 527 (1951).
9. Kleinman, D. A., Thesis, Brown University (1951).
10. Brockhouse, B. N. and D. G. Hurst, Phys. Rev. 88: 542 (1952).

11. Pope, N. K., Can. J. Phys. 30: 597 (1952).
12. Wigner, E. P. and Wilkins, J. E. Jr., AECD 2275 (1948).
13. Wilkins, J. E., Jr. Unpublished.
14. Hurwitz, H., Jr. (Private Communication).
15. Niestlie, J. W. and Berman, A. J. Bull. Am. Phys. Soc. 30 No. 3, Abstract B12 (1955).
16. Cohen, E. R., Proceedings 1955 Conference on Nuclear Engineering, B-47 (1955).
17. Taylor, B. T., AERE-NR-1005 (1952).
18. Gavin, G. B., KAPL-1142 (1954).
19. Zinn, W. H., Phys. Rev. 71: 752 (1947).
20. Branch, G. M., MDDC 747 (1946).
21. Hughes, D. J., Pile Neutron Research, Addison Wesley (1953).
22. Cohen, E. R., P/605 "Exponential Experiments in Uranium-D_2O Lattices," Volume 5, Session 21A, these Proceedings.

The Calculation of the Fine Structure of the Thermal Neutron Flux in a Pile, by the Spherical Harmonics Method

By J. H. Tait, UK

This paper describes the calculation of the fine structure of the thermal neutron flux in a pile by the spherical harmonics method. In a pile one is interested in the neutron distribution in a particular lattice cell, and also in the variation of the average of this distribution from cell to cell. Except at points near to boundaries, the average varies slowly, and in general it can be calculated quite accurately using the diffusion approximation. However, the calculation of the fine structure necessitates the use of more complicated methods, because the neutron distribution is changing appreciably over a distance of one neutron free path.

The neutron distribution in a lattice cell has been calculated by several methods. W. Feurzeig and B. I. Spinrad[1] have considered the solution of a two-region cell problem using a numerical iterative procedure. The flux is estimated at a discrete number of points, and this is then improved by repeated integrations of the Boltzmann equation. The numerical examples given in their paper dealt with the fine structure in a heavy water pile. The fine structure has also been calculated by the Serber Wilson method.[2] However, in applying this method to the present problem one is not assured necessarily of the same accuracy as in a critical size calculation.

The calculation of the fine structure by the spherical harmonics method has also been reported by Kash[3] for the case of spherical geometry. He calculated the neutron distribution in a 2-inch natural uranium sphere immersed in a D_2O medium, using the P_3 and P_5 spherical harmonics approximations. He found very little difference in the two distributions.

FORMULATION OF THE PROBLEM

The following assumptions are made in the calculation.

(*a*) The cell of the pile is replaced by a cylindrical one, leaving the same cross sectional area. This assumption has been investigated by Newmarch[4] and Clark. Using the diffusion approximation they calculated the thermal utilisation factor for a cylindrical rod in a square cell, and in a cylindrical cell having the same cross sectional area. For cases where the spacing of the rods was very close, i.e., of the order of twice the diameter of the rod, the difference was of the order of 0.1%.

(*b*) The cell is infinitely long. This assumption is reasonable for points not too near the ends of a cell.

(*c*) The neutron distribution is repetitive from cell to cell, i.e., there is no net neutron current across the lattice cell boundary.

(*d*) The slowing down of fast neutrons to thermal is replaced by a uniform production of thermals in the moderator. This assumption is justified provided that the cell size is smaller than the slowing down length.

(*e*) The scattering in the moderator is assumed to be isotropic in the laboratory system. The theory could easily be generalised for the case of anisotropic scattering.

THE SPHERICAL HARMONICS METHOD IN CYLINDRICAL GEOMETRY

A general treatment of the spherical harmonics method, applicable in principle to any geometry has been given by J. C. Mark.[5] An alternative treatment has been given by B. Davison,[6] and this is more economical in algebraic manipulation.

For the case of isotropic scattering the one-velocity Boltzmann transport equation is as follows, for a source free medium

$$\Omega \cdot \text{grad}\ \Psi(r,\Omega) + \frac{\Psi(r,\Omega)}{l} = \frac{c}{4\pi l}\iint \Psi(r,\Omega')\, d\Omega' \quad (1)$$

where Ω is a unit vector describing the direction of motion of the neutron, r is the position vector, l is the neutron mean free path and c the number of secondaries per collision. Ψ is the angular distribution of neutron flux.

For systems with right circular symmetry and infinite length, Ψ is a function of one space coordinate, the distance r of the point r from the axis of the cylinder and of two angular coordinates. The following angular coordinates are chosen, η the projection of Ω upon the axis of the cylinder and ω the angle between the projection of Ω on a plane perpendicular to the axis of the cylinder and r (see Fig. 1). With the variables, r, η, and ω Boltzmann's equation now becomes

$$\cos\omega(1-\eta^2)^{\frac{1}{2}} \cdot \frac{\partial\Psi}{\partial r} - \frac{\sin\omega(1-\eta^2)^{\frac{1}{2}}}{r}\frac{\partial\Psi}{\partial\omega} + \frac{\Psi(r,\eta,\omega)}{l} = \frac{c}{4\pi l}\Psi_0(r) \quad (2)$$

where $\Psi_0 = \int\int \Psi \cdot d\Omega'$ is the flux. Due to the symmetries of the problem $\Psi(r,\eta,\omega)$ is an even function of

η and ω. Therefore, $\Psi(r,\Omega)$ can be expanded in spherical harmonics, as follows

$$\Psi(r,\Omega) = \frac{1}{4\pi}\left\{\Psi_{00}(r) + 3\cdot\cos\omega\cdot P_1^1(\eta)\Psi_{11}(r) + 5\left[P_2(\eta)\Psi_{02}(r) + \frac{1}{12}P_{22}^2(\eta)\cos\omega\Psi_{22}(r)\right] + 7\left[\frac{1}{6}P_3^1(\eta)\cdot\cos\omega\Psi_{13}(r) + \frac{1}{360}P_3^3(\eta)\cdot\cos 3\omega\cdot\Psi_{33}(r)\right]\right\} \quad (3)$$

To obtain the equations for the Ψ_{nm}, Equation 3 is multiplied by $P_n^m(\eta)\cdot\cos m\omega$ and integrated with respect to η over the range $-1 \leq \eta \leq 1$, and ω over the range $0 \leq \omega \leq 2\pi$. One obtains the set of equations,

$$\begin{aligned}&\dot{\Psi}_{m+1,n+1}(r) - \dot{\Psi}_{m+1,n-1}(r) \\ &+ (n+m)(n+m-1)\dot{\Psi}_{m-1,n-1}(r) \\ &- (n-m+2)(n-m+1)\dot{\Psi}_{m-1,n+1}(r) \\ &+ \frac{(m+1)}{r}\{\Psi_{m+1,n+1}(r) - \Psi_{m+1,n+1}(r)\} \\ &- \frac{(m-1)}{r}\{(n+m)(n+m-1)\cdot\Psi_{m-1,n-1}(r) \\ &- (n-m+2)(n-m+1)\Psi_{m+1,n+1}(r)\} \\ &= -\frac{2(2n+1)}{l}\Psi_{nm}(r) + \frac{2(2n+1)c}{l}\Psi_{00}(r)\cdot\delta_{0n} \quad (4)\end{aligned}$$

In the P_{2N+1} spherical harmonics approximation, the equations with $n = 0, \ldots 2N+1$, and $m = 0, \ldots n$, [$m + n$ even] are written out. In all these are $(N+2)\times(N+1)$ equations. In the last $(N+1)$ equations the moments $\Psi_{m,2N+2}(r)$ are neglected, resulting in $(N+2)(N+1)$ differential equations for the remaining $(N+2)(N+1)$ moments.

By elimination it can be shown that the neutron flux $\Psi_{00}(r)$ satisfies the equation

$$\prod_{i=1}^{N+1}\left(\nabla^2 - \frac{\gamma_i^2}{l^2}\right)\Psi_{00}(r) = 0$$

The γ_i depend on the order of the approximation and on the value of the parameter c, but not on the geometry. The expressions for the various moments Ψ_{nm} in the P_3 approximation are given in Appendix A.

THE DETERMINATION OF THE FINE STRUCTURE WHEN NO AIR GAP IS PRESENT

With the assumption of a uniform distribution of sources in the moderator, Boltzmann's equation in that region has a source term $S/4\pi$.

A particular solution of this equation is $\Psi_{00}(r) = Sl/(1-c)$ and all other moments zero. To this particular solution, the general solution in the P_{2N+1} approximation must be added. When $c = 1$ the solution simplifies even further.

In the uranium rod the solution is finite at $r = 0$; therefore the expressions for the moments do not contain the Bessel functions of the second kind.

For example, in the P_3 approximation, there are nine constants to determine, three for the solution in the rod and six for the solution in the moderator. These nine constants are determined from the boundary conditions. At the boundary between the rod and the moderator, the angular distribution of neutron flux must be continuous. In the P_3 approximation this means that the six moments are continuous, providing six of the equations for the determination of the nine constants.

Now the neutron distribution is repetitive as one proceeds from cell to cell. Then if Ω^* is the direction of the reflection of Ω with respect to the cell boundary, the following condition is applicable

$$\Psi(r,\Omega) = \Psi(r,\Omega^*)$$

In cylindrical geometry this reduces to

$$\Psi(b,\eta,\omega) = \Psi(b,\eta,\pi-\omega)$$

where b is the outer radius of the cell.

On inspection of the series of Equation 3, this condition means that

$$\Psi_{11}(b) = 0$$
$$\Psi_{13}(b) = 0$$
$$\Psi_{33}(b) = 0$$

This then provides a further three equations and with the six other equations enables us to determine the nine constants.

In a typical example, the thermal utilisation factor was calculated as follows,

Diffusion theory	0.907
Spherical harmonics P_3 approx.	0.8930
Spherical harmonics P_5 approx.	0.888

THE DETERMINATION OF THE FLUX WHEN AN AIR GAP IS PRESENT

We have first to determine the six equations which replace those obtained by equating moments at the boundary $r = a$, in the case of no air gap.

Consider now the form that Boltzmann's equation takes for points in the air gap, where one can assume that the mean free path is infinite. Equation 2 now takes the simple form

$$\cos\omega\frac{\partial\Psi}{\partial r} - \frac{1}{r}\sin\omega\frac{\partial\Psi}{\partial\omega} = 0 \quad (5)$$

Multiply this equation by $P_1^1(\eta)$ and integrate over ω and η; then the following equation is obtained for $\Psi_{11}(r)$

$$\dot{\Psi}_{11}(r) + \frac{1}{r}\Psi_{11}(r) = 0$$

i.e.,

$$\Psi_{11}(r) = \frac{A}{r}$$

Therefore,

$$a_1\Psi_{11}(a_1) = a_2\Psi_{11}(a_2) \quad (6)$$

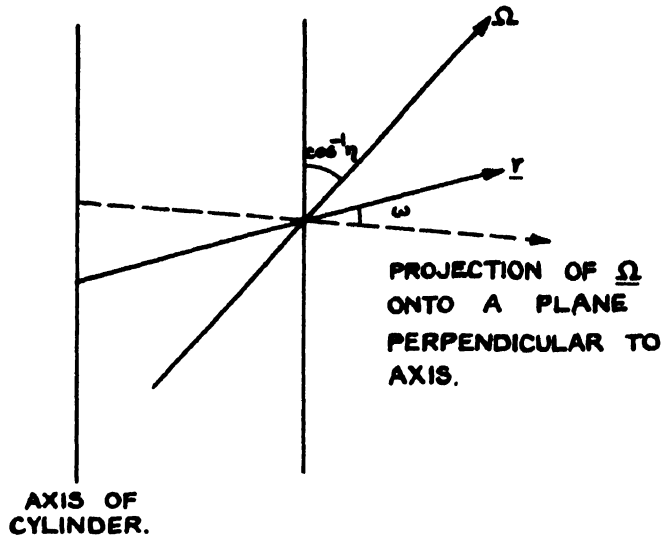

Figure 1

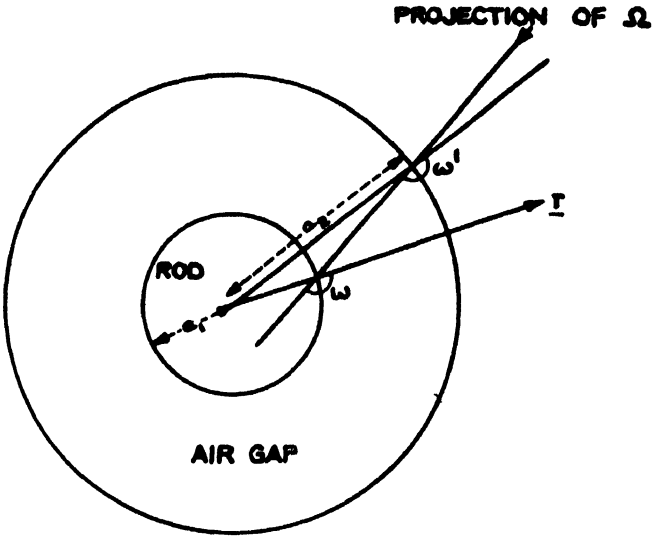

Figure 2

where a_1 and a_2 are the inner and outer radii of the air gap.

Similarly if Equation 5 be multiplied by $P_3^1(\eta)$ and integrated over ω and η, it can be shown that

$$\Psi_{13}(r) = \frac{B}{r} \tag{7}$$

i.e., $$a_1\Psi_{13}(a_1) = a_2\Psi_{13}(a_2)$$

If Equation 5 be multiplied by $P_3^3(\eta)\cos 3\omega/\cos\omega$ and integrated then it can be shown that

$$\Psi_{33}(r) = \frac{1}{r^3}\left\{\frac{1}{2}r^2[2\cdot 4A - 4B] + D\right\}$$

from which formula it can be deduced that

$$a_1^3\{\Psi_{33}(a_1) - 12\Psi_{11}(a_1) + 2\Psi_{13}(a_1)\} = a_2^3\{\Psi_{33}(a_2) - 12\Psi_{11}(a_2) + 2\Psi_{13}(a_2)\} \tag{8}$$

Equations 6, 7 and 8 must be three of the six equations relating the angular distribution of the neutron flux on the inside of the air gap to that on the outside of the air gap.

Since this only gives three equations an alternative approach is necessary. Consider now the effect of the solution inside on the solution outside the air gap and the effect of the solution outside the air gap on the solution inside.

Suppose that the solution outside the air gap is known and one wishes to determine the solution inside the air gap.

Let Ω be some fixed direction in space, a_1 is a point on the inner surface of the air gap, and a_2 is that point on its outer surface, from which a neutron traveling in the direction of Ω should start in order to pass through a_1.

Then,

$$\Psi(\Omega,a_1) = \Psi(\Omega,a_2) \tag{9}$$

or $$\Psi(\eta,\omega,a_1) = \Psi(\eta',\omega',a_2)$$

η, ω are the angular coordinates of the direction Ω at the point a_1 and η', ω' those of Ω at the point a_2.

Now η is the projection of Ω on the axis of the cylinder, and therefore $\eta = \eta'$. As ω is the angle between the projection of Ω on a plane perpendicular to the axis of the cylinder and r, for the purpose of determining a relation between ω' and ω the cross sectional diagram as shown in Fig. 2 will suffice.

From the diagram it can be seen that,

$$\frac{a_2}{\sin\omega} = \frac{a_1}{\sin\omega'}$$

i.e., $$\omega' = \sin^{-1}\left(\frac{a_1\sin\omega}{a_2}\right)$$

For neutrons entering the rod, i.e., for $\pi/2 \leq \omega \leq \pi$, Equation 9 becomes,

$$\Psi(\eta,\omega,a_1) = \Psi\left(\eta, \sin^{-1}\left[\frac{a_1\sin\omega}{a_2}\right]a_2\right) \tag{10}$$

This is the first condition.

Consider now the effects of the air gap and the rod inside it upon the conditions outside the air gap.

That is, one wishes to determine

$$\Psi(\omega,\eta,a_2) \quad \text{for} \quad 0 \leq \omega \leq \pi/2 \quad \text{and} \quad -1 \leq \eta \leq +1$$

If $\omega' > \sin^{-1}(a_1/a_2)$ then a neutron starting out from a point on the outer face of the air gap will miss the rod inside.

Therefore, for $\pi/2 \geq \omega' \geq \sin^{-1}(a_1/a_2)$

$$\Psi(\pi - \omega',\eta,a_2) = \Psi(\omega',\eta,a_2) \tag{11}$$

For $\sin^{-1}(a_1/a_2) \geq \omega' \geq 0$, neutrons entering the inner face of the moderator come from the rod inside the air gap, giving the condition

$$\Psi(\omega',\eta,a_2) = \Psi\left(\sin^{-1}\left[\frac{a_2}{a_1}\sin\omega'\right], \eta, a_1\right) \tag{12}$$

We have to replace the conditions of Equations 10, 11 and 12 by six equations relating the coefficients A_1, B_1, etc.

The six equations are divided equally between Equation 10 on the one hand and Equations 11 and 12 on the other.

To do this Equation 10 is multiplied by the spherical harmonics $P_n^m(\eta)\cos m\omega$ and integrated over all η and ω between $\pi/2$ and π. Similarly Equations 11 and 12 are multiplied by $P_n^m(\eta)\cos m\omega$ and integrated over all η and the relevant ranges of ω, the results being added so as to give finally the integration of ω over the range 0 to $\pi/2$. There are six spherical harmonics P_n^m, so that if one had used all of them, twelve equations would be obtained. Thus one has to use only half of the spherical harmonics. The only two consistent approaches would be to use the odd or the even harmonics only. On the grounds of previous experience it is known that the former leads to a better approximation, and this approach was actually used.

The six equations obtained are given in Appendix B. From these six complicated equations it is possible to obtain the three simple relations, Equations 6, 7 and 8.

In practice, three of the equations given in Appendix B are used together with Equations 6, 7, 8 and the three obtained from the boundary condition at the outer surface of the cell.

The neutron distribution has been calculated in a cell having the following dimensions: $a_1 = 1.27$ cm, $a_2 = 3.49$, $b = 11.29$. The values of the constants in the uranium were: $c_u = 0.533$ and $l_u = 1.383$. In the graphite, $c_c = 0.999$ and $l_c = 2.462$.

The neutron distributions obtained using diffusion theory and the P_3 approximation are shown in Fig. 3. The curves are normalised to have the same average flux in the rod.

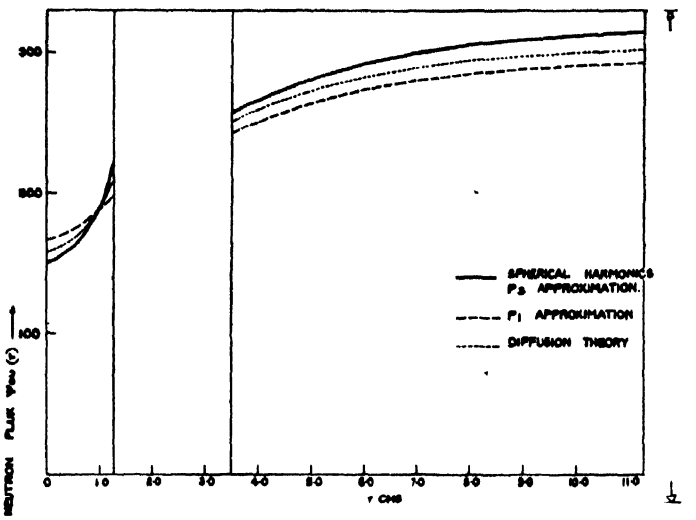

Figure 3. Neutron distribution in a cell with an air gap calculated by diffusion theory and spherical harmonics P_1 and P_3 approximations

APPROXIMATION TO THE CORRECT APPLICATION OF THE SPHERICAL HARMONICS METHOD

It is rather a cumbersome procedure to solve nine equations for every set of cell dimensions. There is, however, an approximation by which one can reduce the number of equations.

The formulae for the various moments in the P_3 approximation contain two and sometimes three terms [see formulae in Appendix A]. One term, i.e., $A_1I_0(\gamma_1 r) + B_1K_0(\gamma_1 r)$ in $\Psi_{00}(r)$ corresponds to the diffusion approximation, while the other terms take into account any divergences from the diffusion theory at points near to a boundary.

The formulae for the transient terms in the moderator are given as the sum of a Bessel function of the first kind I and one of the second kind K. The first is an increasing and the second a decreasing function for increasing argument. If the radius of the cell is several moderator mean free paths, this is true in a graphite moderated pile; then at the centre of the moderator in a cell the transient term should be small, and it therefore follows that at the inner boundary the K function predominates over the I function and at the outer boundary the reverse is the case. Now, at the outer boundary, one can expect that the transient effects are small, and one therefore makes the approximation of neglecting the I term in the formulae for the transients.

This results in neglecting in the P_3 approximation two of the constants, and also one of the equations simplifies to a simple relation between two of the constants. Having neglected two of the constants, two of the conditions at the outer boundary of the moderator have to be neglected; one naturally retains the current condition $\Psi_{11}(b) = 0$ and ignores the other two.

The value of f obtained by the simplified procedure is practically the same as that obtained when the complete set of nine equations are solved.

APPENDIX A

The formulae for the various moments in the P_3 approximation are as follows.

$$\Psi_{00}(r) = \sum_{i=1}^{2} \{A_iI_0(\gamma_i x) + B_iK_0(\gamma_i x)\}$$

$$\Psi_{11}(r) = \sum_{i=1}^{2} G_1(\gamma_i)\{A_iI_1(\gamma_i x) - B_iK_1(\gamma_i x)\}$$

$$\Psi_{02}(r) = -\tfrac{1}{2}\sum_{i=1}^{2} G_2(\gamma_i)\{A_iI_0(\gamma_i x) + B_iK_0(\gamma_i x)\} + MI_0(\beta x) + NK_0(\beta x)$$

$$\Psi_{22}(r) = 3\sum_{i=1}^{2} G_2(\gamma_i)\{A_iI_2(\gamma_i x) + B_iK_2(\gamma_i x)\} + 2MI_2(\beta x) + 2NK_2(\beta x)$$

$$\Psi_{13}(r) = -\tfrac{3}{2}\sum_{i=1}^{2} G_3(\gamma_i)\{A_iI_1(\gamma_i x) - B_iK_1(\gamma_i x)\} - \frac{5}{\beta}\{MI_1(\beta x) - NK_1(\beta x)\}$$

$$\Psi_{33}(r) = 15\sum_{i=1}^{2} G_3(\gamma_i)\{A_iI_3(\gamma_i x) - B_iK_3(\gamma_i x)\} - \frac{30}{\beta}\{MI_3(\beta x) - NK_3(\beta x)\}$$

where

$$x = r/l$$

$$\beta = \sqrt{7}$$

$$G_1(\gamma) = -\frac{a}{\gamma}$$

$$G_2(\gamma) = \frac{1}{\gamma^2}\left\{-\frac{1}{2}\gamma^2 + \frac{3a}{2}\right\}$$

$$G_3(\gamma) = \frac{1}{\gamma^2}\left\{\frac{(5+4a)}{6}\gamma^2 - \frac{5a}{2}\right\}$$

$$a = 1 - c$$

γ_1^2 and γ_2^2 are the roots of the equation,

$$\frac{3}{8}x^2 - \left(\frac{35+55a}{24}\right)x + \frac{35a}{8} = 0$$

APPENDIX B

The equations connecting the various moments across the air gap, in the P_3 approximation are as follows.

$$-\pi\Psi_{00}(a) + 2\pi\Psi_{11}(a) + \frac{5\pi}{8}\Psi_{02}(a) - \frac{5\pi}{16}\Psi_{22}(a) = -\pi\Psi_{00}(c) + 4\left(\frac{c}{a}\right)\left[\sin^{-1}\left(\frac{a}{c}\right) + \left(\frac{a}{c}\right)\sqrt{1-a^2/c^2}\right]\Psi_{11}(c) + \frac{5\pi}{8}\Psi_{02}(c) + \frac{5\pi}{16}\left(\frac{2a^2}{c^2} - 3\right)\Psi_{22}(c) + \frac{28}{45}(1-a^2/c^2)^{3/2}\Psi_{33}(c)$$

$$-3\pi\Psi_{00}(a) - \frac{105\pi}{4}\Psi_{02}(a) + \frac{5\pi}{8}\Psi_{22}(a) + 16\pi\Psi_{13}(a) = -3\pi\Psi_{00}(c) - \frac{105\pi}{4}\Psi_{02}(c) + \frac{5\pi}{8}\left(\frac{3c^2-2a^2}{c_2}\right)\Psi_{22}(c) + 32\left(\frac{c}{a}\right)\left[\sin^{-1}\left(\frac{a}{c}\right) + \left(\frac{a}{c}\right)\sqrt{1-a^2/c^2}\right]\Psi_{13}(c) - \frac{32}{15}(1-a^2/c^2)^{3/2}\Psi_{33}(c)$$

$$15\pi\Psi_{00}(a) - \frac{75\pi}{4}\Psi_{22}(a) - \frac{225\pi}{8}\Psi_{22}(a) + 8\pi\Psi_{33}(a) = 15\pi\Psi_{00}(c) + 192\left(\frac{c}{a}\right)(1-c^2/a^2)\left[\sin^{-1}\left(\frac{a}{c}\right) - \left(\frac{a}{c}\right)\sqrt{1-a^2/c^2}\right]\Psi_{11}(c) - \frac{75\pi}{4}\Psi_{02}(c) + \frac{375\pi}{8}\left(\frac{1}{3} - \frac{14a^2}{15c^2}\right)\Psi_{22}(c) - \left(\frac{32c}{a}\right)(1-c^2/a^2)\left[\sin^{-1}\left(\frac{a}{c}\right) - \left(\frac{a}{c}\right)\sqrt{1-a^2/c^2}\right]\Psi_{13}(c) - 32\left\{\sqrt{1-a^2/c^2}\left[-\frac{5a^2}{3c^2} + \frac{2}{3} + \frac{c^2}{2a^2}\right] - \frac{\sin^{-1}\left(\frac{a}{c}\right)}{2a^3/c^3}\right\}\Psi_{33}(c)$$

$$\pi\Psi_{00}(c) + 4\left[\frac{\pi c}{a} - \frac{c}{a}\sin^{-1}\left(\frac{a}{c}\right) - \sqrt{1-a^2/c^2}\right]\Psi_{11}(c) - \frac{5\pi}{8}\Psi_{02}(c) + \frac{15\pi}{16}\left[1 - \frac{2a^2}{3c^2}\right]\Psi_{22}(c) - \frac{28}{45}(1-a^2/c^2)^{3/2}\Psi_{33}(c) = \pi\Psi_{00}(a) + 2\pi\Psi_{11}(a) - \frac{5\pi}{8}\Psi_{02}(a) + \frac{5\pi}{16}\Psi_{22}(a)$$

$$3\pi\Psi_{00}(c) + \frac{105\pi}{4}\Psi_{02}(c) - \frac{15\pi}{8}\left(1 - \frac{2a^2}{3c^2}\right)\Psi_{22}(c) + \frac{32}{15}\left(1 - \frac{a^2}{c^2}\right)^{3/2}\Psi_{33}(c) + 32\left[\frac{\pi c}{a} - \frac{c}{a}\sin^{-1}\frac{a}{c} - \sqrt{1-a^2/c^2}\right]\Psi_{13}(c) = 3\pi\Psi_{00}(a) + \frac{105\pi}{4}\Psi_{02}(a) - \frac{5\pi}{8}\Psi_{22}(a) + 16\pi\Psi_{13}(a)$$

$$45\pi\left[\frac{4a^2}{3c^2} - 1\right]\Psi_{00}(c) - 384(1-a^2/c^2)^{3/2}\Psi_{11}(c) + \frac{225\pi}{4}\left(\frac{4a^2}{3c^2} - 1\right)\Psi_{02}(c) + \frac{375\pi}{8}\left[1 - \frac{2a^2}{c^2} + \frac{8a^4}{5c^4}\right]\Psi_{22}(c) + 64(1-a^2/c^2)^{3/2}\Psi_{13}(c) + 16\left[\pi\frac{c}{a} - \frac{c}{a}\sin^{-1}\left(\frac{a}{c}\right)\right.$$

$$+\frac{1}{3}\left(1-\frac{a^2}{c^2}\right)^{1/2}\left\{16\frac{a^2}{c^2}\left(1-\frac{a^2}{c^2}\right)-3\right\}\Psi_{33}(c)$$

$$=-45\pi\left[\frac{4a^2}{3c^2}-1\right]\Psi_{00}(a)+96\pi(1-a^2/c^2)\Psi_{11}(a)$$

$$-\frac{225\pi}{4}\left(1-\frac{4a^2}{3c^2}\right)\Psi_{02}(a)$$

$$+\frac{375\pi}{8}\left\{\frac{1}{3}\left(1-\frac{c^2}{a^2}\right)\left(3-\frac{4a^2}{c^2}\right)+\frac{c^2}{a^2}-2\right.$$

$$\left.+\frac{8a^2}{5c^2}\right\}\Psi_{22}(a)-\pi\left(1-\frac{a^2}{c^2}\right)\Psi_{13}(a)+\frac{\pi a^2}{2c^2}\Psi_{33}(a)$$

REFERENCES

1. Feurzeig, W. and Spinrad, B. I., *Numerical Solution of Transport Theory Problems for Spheres and Cylinders.* Argonne National Laboratory (1953).
2. Bunemann, O., Private Communication.
3. Kash, S. W., *P_3 and P_5 Approximation Spherical Harmonic Calculations for Natural Uranium Spheres in D_2O.* North American Aviation Memorandum 553 (1952).
4. Clark, A. C. and Newmarch, D. A., *The Diffusion Theory of Fine Structure in Thermal Neutron Reactor Assemblies Consisting of Cylindrical Fuel Elements set in a square lattice array.* Harwell Report RP/R. 1704 (1955).
5. Mark, C., *The Spherical Harmonic Method 1.* Canadian Report CRT-340 (1947).
6. Davison, B., *Some Remarks on Applications of the Spherical Harmonics Method in the Case of Complex Geometries.* Harwell Report T/R.700 (1951).

Comparison of Theory and Experiment for Intermediate Assemblies

By H. Hurwitz, Jr. and R. Ehrlich,* USA

Early measurements of the thermal neutron cross sections of plutonium made it evident that the prospects of a plutonium breeding cycle utilizing thermal-neutron reactors were poor. As a result there was interest in exploring the possibilities of intermediate power breeder reactors. A program of critical experimentation was accordingly undertaken for the purpose of studying the properties of assemblies in which the majority of the fissions are caused by neutrons of intermediate energy. Although as an outcome of this and related programs it was learned that intermediate energy plutonium breeders are not feasible, a great deal of interesting information was obtained which is relevant to other types of power reactors.

The experimental program, which is described in another paper by T. M. Snyder, was accompanied by an extensive program of reactor calculations.[1] The nature of these calculations and the comparison of the results with experimental measurements will be described in this paper.

CALCULATIONAL METHODS

The major part of the theoretical analysis of the experiments to be discussed was based on the Fermi age-diffusion differential equation which is a good approximation to the Boltzmann equation if the neutron mean free path is small compared to the dimensions of the assembly and the fractional energy loss of the neutron per collision is small.† In the applications to be discussed here the core radius is of the order of ten times the neutron mean free path, and, since the moderator is beryllium, the average logarithmic energy loss per collision is only 0.206.

The age-diffusion equation also involves the assumption that the various regions of the core are homogeneous. Since the fissionable material in the assemblies to be discussed was present in the form of foils of thickness of approximately one gram of U^{235} per square centimeter, the approximation is not entirely justified. In particular, for neutrons having energies near the peak of a U^{235} resonance, the probability of absorption in one traversal of a U^{235} disk is not small compared to unity. Accordingly, it is necessary to employ in the calculations an effective uranium cross section which corrects for the effects of spatial self-shielding. This effective cross section also must correct for the effect of energy self-shielding which exists even in a homogeneous medium when the absorption cross section varies strongly in an energy region of order of the neutron energy loss per collision. The procedure used in obtaining a slowly varying effective absorption cross section for use in the age-diffusion equation is similar to that employed in Doppler effect temperature coefficient calculations.[2]

The age-diffusion equation may be written in the form:

$$-\nabla \frac{1}{3\sigma_{tr}} \nabla nv + \sigma_a nv = -\frac{\partial q}{\partial u} + S(r,u); \qquad q = \xi \sigma_s nv \tag{1a}$$

where nv is the neutron flux per unit range of logarithmic energy u. The logarithmic energy variable, u, is defined as $\ln (E_0/E)$ where E is the neutron energy and E_0 is a conveniently chosen base energy (usually 10^7 ev). The slowing-down density‡ is q, and ξ is the average logarithmic energy loss per elastic scattering collision. All cross sections are macroscopic, i.e., the sum, over the various elements which are present in a particular region, of the atomic cross section times the atomic density. The absorption cross section, σ_a, includes radiative capture, fission, and inelastic scattering cross sections. The scattering cross section is σ_s and the transport cross section is $\sigma_a + \sigma_s(1 - \overline{\cos\theta})$ where $\overline{\cos\theta}$ is the average of the cosine of the scattering angle (in the laboratory system). The source term $S(r,u)$ represents neutrons liberated in fissions ($S_f(r,u)$) and neutrons produced at u by inelastic scattering from a higher energy ($S_{in}(r,u)$). The fission contribution may be written down as follows:

* Including work by E. L. Zimmerman and associates, Oak Ridge National Laboratory; and H. Hurwitz, Jr., R. Ehrlich, and associates, Knolls Atomic Power Laboratory.

† The age-diffusion approximation breaks down at large distances from a source of fast neutrons, but this effect, though important in shielding calculations, is not important for criticality calculations.

‡ If the absorption cross section is not small compared to the scattering cross section but the ratio of capture to scattering varies slowly with energy, the agreement between the Boltzmann and age-diffusion equations may be improved by writing the slowing-down density in the form $(\xi\sigma_s + \gamma\sigma_a)nv$ where γ is a constant (see Reference 3, page 168). If the simpler form $\xi\sigma_s$ is used for the slowing-down density, the corrections to the age-diffusion equation may be incorporated into the self-shielding factor which multiplies the absorption cross section.

$$S_f(r,u) = \nu\left[\int_{-\infty}^{u_T} nv\sigma_f\,du' + nv_T\sigma_{f_T}\right]\chi(u)$$

where ν is the number of neutrons emitted per fission and $\chi(u)$ is the fission spectrum normalized so that $\int\chi(u)\,du = 1$. Here nv_T and σ_{f_T} are the thermal neutron flux and fission cross section respectively.

The inelastic scattering contribution may be written

$$S_{in}(r,u) = \int_{-\infty}^{u} nv\sigma_{in}(u')\chi(u' \rightarrow u)\,du'$$

The fraction of neutrons scattered inelastically at energy u' that are degraded to energy u is $\chi(u' \rightarrow u)$, normalized such that

$$\int_{-\infty}^{\infty}\chi(u' \rightarrow u)\,du = 1$$

It is customary to calculate the thermal neutron flux nv_T by means of a one-velocity diffusion equation:

$$-\nabla\frac{1}{3\sigma_{tr_T}}\nabla nv_T + \sigma_{a_T}nv_T = q_T \qquad (1b)$$

The cross sections σ_{a_T} and σ_{tr_T} are generally obtained by averaging over a Maxwellian spectrum in the appropriate way.[5] The source term, q_T, is the slowing-down density evaluated at an energy just above the thermal energy. This treatment of the thermal neutrons clearly does not give an accurate picture of the neutron flux in the thermal region. When detailed information is needed about this region of the spectrum, one must employ methods which take into account the effects of the thermal motion and chemical binding of the moderator atoms.[4]

Although Equations 1a and 1b represent a substantial simplification of the Boltzmann equation, it is still not possible to solve the equations analytically except in certain special cases. Accordingly, it has been necessary to resort to numerical methods. The approach has been greatly facilitated by the availability of high-speed digital computing machines.

The numerical procedures for solving Equations 1a and 1b usually involve assuming a spatial dependence for the fission distribution and then integrating Equation 1a, starting at high energy and working towards low energy. After the neutron flux has been obtained as a function of u and r, the resulting fission distribution can be calculated and compared with the assumed distribution. If the calculated distribution of fissions has approximately the same spatial dependence as the assumed distribution, the ratio of the number of fissions in the calculated distribution to those in the assumed distribution gives a good value of the reactivity (i.e., the ratio of the average number of neutrons emitted per fission to the number ν_c, which would have to be emitted to produce a steady-state chain reaction in the assembly). If the calculated distribution does not agree well with the assumed distribution, a second iteration may be required. Since in most of the assemblies of interest the neutron migration distance is comparable to the core dimension, the calculated fission distribution does not depend sensitively on assumed distribution; a few iterations suffice.

A straightforward procedure for numerically integrating Equation 1a is to use the flux and source at an initial value of u to calculate $\partial q/\partial u$, from which the flux at a slightly larger value of u is found. This "explicit" integration scheme has the disadvantage of being unstable unless the interval in u is of the same order of magnitude as the square of the linear dimension of the spatial intervals. Hence, if a fine spatial mesh is desired, an inconveniently large number of intervals in u may be required.

This stability difficulty may be avoided by "implicit" integration schemes in which expressions for $\partial q/\partial u$ are employed which involve the spatial dependence of the flux at the new value of u. In these schemes, the partial differential equation in u and r is replaced by a finite set of coupled spatial differential equations. These spatial differential equations may be solved either by analytic or numerical methods, with no restriction on the size of the spatial interval. Hence if only crude results are needed it is possible to employ a comparatively small number of energy intervals, or neutron groups, and still obtain qualitatively correct answers.

Procedures for obtaining the multi-group equations from the age-diffusion equation have been previously described.[6] The equation for the flux, NV_i, in the ith group may in general be written in the form:

$$-\nabla D_i\nabla NV_i + \Sigma_{a_i}NV_i = q_{i-1}^0 - q_i^0 + \int_i s\,du \qquad (2)$$

where

$$D_i = \frac{\left(\frac{1}{3\xi\sigma_s\sigma_{tr}}\right)_{iav}}{\left(\frac{1}{\xi\sigma_s}\right)_{iav}}$$

$$NV_i = U_i\left(\frac{1}{\xi\sigma_s}\right)_{iav}(q)_{iav} \qquad (3)$$

$$\Sigma_{a_i} = \frac{\left(\frac{\sigma_a}{\xi\sigma_s}\right)_{iav}}{\left(\frac{1}{\xi\sigma_s}\right)_{iav}}$$

Here q_i^0 is the slowing-down density evaluated at the low energy (high u) limit of the group. The value of q_{i-1}^0, the slowing-down density at the low energy limit of the next higher group, is equal to q_i^I, the slowing-down density at the high energy limit of the ith group. The averages indicated in Equation 3 are with respect to u, and the interval of u corresponding to the ith group is u_i. To complete the set of equations in Equations 1 and 2 it is necessary to postulate a relationship between $(q)_{iav}$ and q_i^0 and q_i^I of the form

$$(q)_{iav} = \omega_1 q_i^I + \omega_2 q_i^0 \qquad (4)$$

Several schemes for choosing ω_1 and ω_2 have been used in practice. In one scheme (known as scheme A), which is particularly useful when a small number of groups is employed, ω_1 is set equal to zero, and ω_2 is estimated for each group and region of the assembly with the aim of making the spatial average of $(\omega_2 q)$

approximately equal to the average of the spatial averages of q^0 and q^1. (If a poor choice is made for ω_2 the group may be recalculated with a better choice.) In scheme B, ω_1 and ω_2 are set equal to ½. This eliminates the trial and error feature of scheme A, but may introduce oscillations in the flux as a function of u when there is a rapid variation of flux with position.[5] A third scheme, which is equivalent to assuming a linear variation of nv in the group (rather than of q as in Scheme B) corresponds to the choice

$$\omega_1 = \left(\frac{1}{\xi\sigma_s}\right)^1 \Big/ \left(\frac{2}{\xi\sigma_s}\right)_{av}$$
$$\omega_2 = \left(\frac{1}{\xi\sigma_s}\right)^0 \Big/ \left(\frac{2}{\xi\sigma_s}\right)_{av} \qquad (5)$$

In this scheme nv^0 and nv^1 [(i.e., $q^0/\xi\sigma_s)^0$ and $q^1/(\xi\sigma_s)^1$ as well as nv] are continuous at interfaces. This tends to reduce the oscillations at interfaces between highly dissimilar regions introduced in scheme B.

When appreciable quantities of hydrogen are present in the assembly, the age-diffusion equation may be improved to take into account the finite magnitude of the neutron energy loss in a collision with a proton nucleus (but not the correlation between energy loss and angle of scattering).[6] In this approximation a function $\eta(r,u)$ may be defined which represents the hydrogen slowing-down density, i.e., the number of neutrons scattered by hydrogen per unit time and volume from an energy above $E = E_0e^{-u}$ to a lower energy. This function obeys the equation

$$\frac{d\eta}{du} = -\eta + nv\sigma_H \qquad (6)$$

where σ_H is the hydrogen scattering cross section.

In the multi-group formalism, this equation is converted to a difference equation in the variable u with increments in u corresponding to the group widths, and integrated simultaneously with the flux equation. The hydrogen slowing-down density provides, in effect, an additional source of neutrons in each group arising from hydrogen collisions in higher energy groups. (When this procedure is used, the hydrogen scattering cross section is treated as an absorption cross section in the flux equations and $\int \eta\, du$ represents a neutron source.)

Since the multi-group equations constitute a finite set of coupled linear differential equations, they may in principle be solved analytically. Nevertheless, even when the spatial fission distribution has been assumed, it is most convenient to solve the equations numerically by means of spatial difference equations. In one dimensional problems (e.g. in spherical geometry or cylindrical geometry with a sinusoidal axial flux variation) the Laplacian operator is represented by a three-point difference formula.[5,7] It is possible to formulate the difference equation in such a manner that the neutron conservation laws implied by the age-diffusion equation are rigorously fulfilled by the difference equations. This provides automatic checks on the accuracy of the numerical work and facilitates the preparation of neutron balance tables of the type illustrated in reference 5.

In the one dimensional cases, continued fraction methods are available for solving the spatial difference equations for each group.[5] These methods avoid loss of significant figures in the numerical work which might otherwise occur when the neutron migration length in the group is small compared to the dimensions of the assembly.

The development of high-speed digital computing machines has made it feasible to extend the multi-group formulation to two dimensional problems.[8] The Laplacian operator is then represented by a five-point difference formula. The most practical procedure for solving the two-dimensional difference equations is to employ iteration, or relaxation, methods. It might seem at first glance that the use of the simplest iteration techniques in the spatial variables in conjunction with an implicit difference equation scheme in the energy variable would have no advantage over an explicit integration with respect to the energy variable since in either case the number of intervals in u required to cover a range Δu is of the order $\Delta u/(\Delta x)^2$ (Δx is the linear dimension of the spatial mesh). There is, however, an advantage in the multi-group procedure if improved iteration techniques are employed. For example, the use of the extrapolated Liebman procedure[9] reduces the number of iterations per group to the order of magnitude $\sqrt{\Delta u/\Delta x}$, and methods which converge still more rapidly have been suggested.

In addition to providing detailed information about the dependence of neutron flux on position and energy, the multi-group technique can be used to obtain equally detailed information about the function adjoint to the neutron flux. This adjoint function, when properly normalized, is equal to the iterated fission probability $F(r,u)$ i.e., the average number of fissions produced per generation an infinite number of generations after a neutron of logarithmic energy u has been introduced at the point r into a just-critical assembly. The multi-group equations for the adjoint function are derived from the equations adjoint to Equations 1a and 1b by a procedure entirely analogous to that used in obtaining the multi-group equations for the flux.[5] The source term in the adjoint equations has the spatial distribution of $F_H(r)$ which is the average of $F(r,u)$ over the fission spectrum. It has the energy dependence of $\sigma_f(u)$ and so is most important in the lower energy groups. In the numerical solution of the

Table I. SAPL PPA-5 Composition

Constituent	Vol %	Core atomic ratio	Reflector	
			vol %	atomic ratio
U^{235}	3.57	1.00	—	—
Fe	4.35	2.18	4.91	0.0439
Be	47.06	33.8	78.03	1.00
Na	28.37	4.26	—	—
Al	0.72	0.26	1.26	0.0080
Void	15.74	—	15.80	—

Table II. Core Cross Sections

Group	Range in $u = \ln 10^7/E$	$\frac{1}{\xi\sigma_s}$ (cm)	$\frac{1}{3\xi\sigma_s\sigma_{tr}}$ (cm^2)	$\frac{\sigma_a}{\xi\sigma_s}$	$\frac{\sigma_f}{\xi\sigma_s}$
1	0–0.5	78.1	416	.615	.172
2	0.5–1.0	52.1	224	.410	.115
3	1–2	41.5	136	.236	.0913
4	2–3	22.7	36.8	.0564	.0521
5	3–6	17.2	18.4	.0670	.0555
6	6–10.5	14.8	13.0	.220	.158
7	10.5–12	13.6	10.4	.491	.352
8	12–15	13.1	9.32	.756	.520
9	15–16	13.1	10.3	.407	.312
10	16–16.8	13.1	9.72	.761	.662
11	16.8–19.8	13.1	8.25	2.14	1.76
12	Thermal	—	0.47[f]	0.30[e]	0.25[e]

	$\frac{\sigma_{in}Fe}{\xi\sigma_u}$	$\frac{\sigma_{in}U}{\xi\sigma_u}$	χ_f
1	.29[a]	.139[c]	.0244
2	.19[a]	.093[c]	.1190
3	.0995[b]	.037[d]	.4049
4	—	—	3058
5	—	—	.1459

[a] Distributed 0.4 in group 3; and 0.6 in group 4.
[b] Distributed in group 4.
[c] Distributed 0.1 in group 3; 0.2 in group 4; and 0.7 in group 5.
[d] Distributed 0.2 in group 4; and 0.8 in group 5.
[e] In cm^{-1} with $\xi\sigma_s = 1$.
[f] In cm with $\xi\sigma_s = 1$.

Table III. Reflector Cross Sections

Energy group	Range in $u = \ln 10^7/E$	$\frac{1}{\xi\sigma_s}$ (cm)	$\frac{1}{3\xi\sigma_s\sigma_{tr}}$ (cm^2)	$\frac{\sigma_a}{\xi\sigma_s}$
1	0–0.5	53.2	280	.00112
2	0.5–1.0	35.4	120	.00074
3	1–2	27.2	70.0	.00057
4	2–3	15.1	19.3	.00032
5	3–6	10.9	8 76	.00023
6	6–10.5	9.40	6.40	.00031
7	10.5–12	8.61	5.20	.0015
8	12–15	8.26	4.75	.0039
9	15–16	8.21	4.66	.0098
10	16–16.8	8.21	4.66	.0153
11	16.8–19.8	8.17	4.60	.0440
12	Thermal	—	$\frac{1}{3\sigma_{tr}} = 0.561$ cm	$\sigma_a = .011\ cm^{-1}$

adjoint equations, the spatial dependence of $F_H(r)$ is assumed, and the adjoint multi-group equations are solved for the various groups in succession, starting with the lowest energy group and working upwards. If necessary, the calculation is repeated with an improved assumption for $F_H(r)$ to make the calculated shape of $F_H(r)$ agree with the assumed shape. The value of ν_σ calculated from the adjoint equations must in principle agree with that calculated from the flux equation, so that a comparison of the two values gives a test of the numerical accuracy of the calculations.

COMPARISON OF THEORY AND EXPERIMENT

The most detailed comparisons of theory and experiment for intermediate-energy beryllium moderated assemblies have been made for a reflected assembly known as SAPL PPA-5, investigated at the Knolls Atomic Power Laboratory, and for two unreflected assemblies, known as CA-1 and CA-18, at Oak Ridge National Laboratory. The physical construction and composition of SAPL PPA-5 is described in detail by T. Snyder.[1] The SAPL PPA-5 had a highly enriched U^{235} beryllium-moderated core with a beryllium reflector and a uranium blanket. The coolant was simulated by solid sodium in thin cylindrical steel cans. The composition and dimensions of an equivalent spherical model having the same core-plus-reflector volume as the actual assembly are given in Table I. The core radius is 27.6 cm, the outer reflector radius is 35.5 cm, and the outer blanket radius is 67 cm. A radial increment, Δr, of 1.97 cm was used for the integrations. The energy groups and the macroscopic group average cross section used in the multi-group calculations (Scheme *A*) for the core,

Table IV. Assumed Blanket Cross Sections

Energy group	Range in $u = \ln 10^7/E$	σ_c^{238} (cm^{-1})	σ_f^{238} (cm^{-1})	σ_{in} (cm^{-1})	σ_f^{235} (cm^{-1})	σ_a (cm^{-1})	$\frac{1}{3\sigma_{tr}}$ (cm)
1	0–0.5	.0006	.0369	0.08[a]	.000442	0.118	1.80
2	0.5–1.0	.0006	.0293	0.08[a]	.000442	.110	1.72
3	1–2	.0024	.0203	0.07[b]	.000442	.0932	1.70
4	2–3	.0050	—	0.0473[c]	.000463	.0528	1.41
5	3–6	.0104	—	—	.000578	.0111	.881
6	6–10.5	.0224	—	—	.00227	.0255	.575
7	10.5–12	.026	—	—	.0074	.0346	.59
8	12–15	.035	—	—	.0125	.0519	.66
9	15–16	.040	—	—	.0085	.0502	.70
10	16–16.8	.045	—	—	.021	.0702	.70
11	16.8–19.8	.089	—	—	.0892	.194	.557
12	Thermal	—	—	—	.185	.341	.652

[a] Distributed 0.15 in group 3; 0.35 in group 4; and 0.5 in group 5.
[b] Distributed 0.3 in group 4; and 0.7 in group 5.
[c] Distributed 1.0 in group 5.

reflector and blanket are given previously in Tables II, III, and IV.

These calculations were performed at the time of the experimental work on SAPL PPA-5. Since then better cross section measurements have resulted in improvements in cross section data which are not taken into account in these calculations. At high energies (above 500 kev) a rough correction for the anisotropic scattering in beryllium was made. This correction consisted of a reduction in σ_{tr} and ξ reaching 30 per cent at 10 Mev as compared to the value of these quantities which would be obtained assuming isotropic scattering in the center-of-mass system. The uranium absorption cross sections were reduced by a self-shielding factor calculated as a function of energy by G. M. Roe for the 0.020-inch uranium disks used in the critical assembly.

With this data, the calculated ν_c for the assembly is 2.41 from the flux calculation and 2.43 from the adjoint calculation. In the spherical model used for this calculation, the core and reflector radii were chosen to give core and reflector volumes corresponding closely to those of the actual hexagonal assembly. The spherical model overestimates the reactivity of the actual hexagonal assembly by about 5 to 10 per cent. Thus, if the calculation had been performed with the correct geometry, the value of ν_c would presumably agree with the correct value, 2.48, to within 5 per cent.

The calculated and measured power (fission) distributions for SAPL PPA-5 are compared in Fig. 1. Several different experimental traverses in the hexagonal core are given. Allowing for the difference in traverse lengths because the assembly was a hexagonal prism, it is seen that the shapes of the experimental and theoretical curves are in qualitative agreement. A more detailed comparison of the experimental and theoretical power distributions would clearly require multi-group calculations in two spatial dimensions. Computing facilities for performing such calculations were not available at the time the SAPL PPA-5 studies were in progress.

The fuel statistical weights (i.e., reactivity coefficient in cents per mole of U^{235} in the core for SAPL

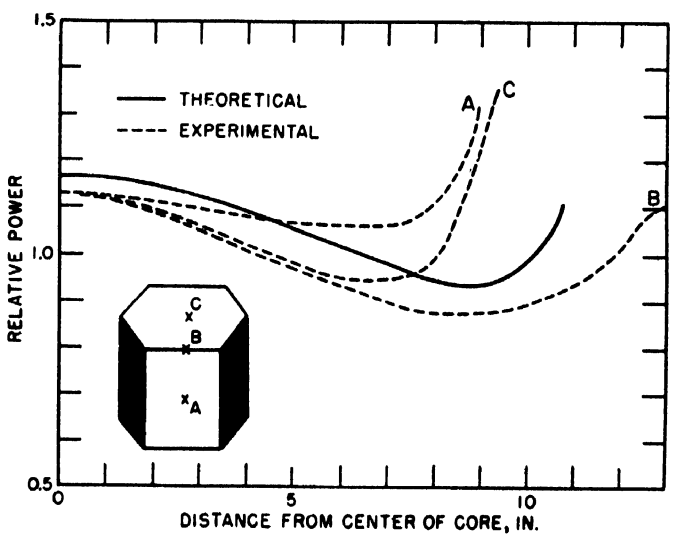

Figure 1. Power distribution in the PPA-5 core; traverses are from center of core to designated points on interface

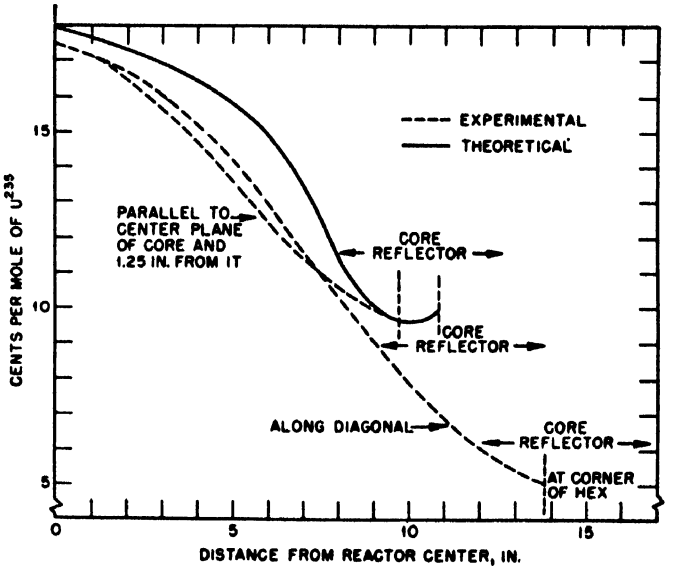

Figure 2. Statistical weight of the fuel vs the core position for PPA-5

Table V. Iterated Fission Probabilities in SAPL PPA-5[a]

	Theoretical		*Experiment*	
	Core center	*Core edge*	*Core center*	*Core edge*
F_L, .002-in. Au foil	1.02×10^4	0.51×10^4	1.04×10^4	0.75×10^4
F_L, .025-in. Au foil	0.98×10^4	0.49×10^4	0.97×10^4	0.69×10^4
νF_H	1.62×10^4	0.83×10^4	1.63×10^4	1.07×10^4

[a] All quantities are in cent units. The experimental results at the core edge appear too high because the measurements actually are an average over a disk extending 2 in. into the core.

PPA-5 as given by theory and experiment are compared in Fig. 2. This calculation involves the adjoint functions, m, normalized to the iterated fission probability $F(r,u)$ by the relation

$$F(r,u) = \frac{m\int\int n\nu\sigma_f \, du \, d\,vol}{\int\int(\nu n\nu\sigma_f \int \chi m \, du) \, du \, d\,vol}$$

The statistical weight of the fuel is given by

cents per mole

$$= \frac{100P(r)[\nu F_H(r) - (F_{Lf}(r) + \bar{\alpha}(r)F_{L\alpha}(r))]}{0.0087N_U}$$

where $P(r)$ = normalized power distribution

N_U = number of moles of U^{235} in the core

ν = number of neutrons per fission

$F_H(r)$ = fission-spectrum average of $F(r,u)$

$F_{Lf}(r)$ = average of $F(r,u)$ for neutrons producing fissions in U^{235}

$F_{L\alpha}(r)$ = average of $F(r,u)$ for neutrons absorbed by radiative capture in U^{235}

$\bar{\alpha}(r)$ = average value of σ_c/σ_f in the neutron spectrum at point r

\$1 = 0.0087 in k = reactivity difference between prompt and delayed critical.

The dollar value was computed using the measured delayed-neutron spectrum,[13] the calculated F values, and the equation

$$\$ = d\frac{\int \chi_d(u)R(u) \, du}{\int \chi(u)R(u) \, du}$$

where $d(= 0.00755)$ is the delayed fraction, χ_d is the delayed-neutron fission spectrum, and

$$R(u) = \int_{core} d\,vol\left[F(r,u)\int \nu n\nu\sigma_f(r,u) \, du\right]$$

Experimental measurements of νF_H and of F_L for gold foils were made in SAPL PPA-5 by H. B. Stewart.[12] A comparison of theoretical and measured values is given in Table V.

The adjoint functions are also useful for calculating the generation time, τ of the reactor from the relation

$$\tau = \nu\int\int Fn \, du \, d\,vol$$

The generation time, τ, is defined to be the product of the amount by which the prompt reactivity differs from unity with the reactor period which would exist in the absence of delayed neutrons. (The "prompt reactivity" is the reactivity which would exist in the absence of delayed neutrons.) The generation time is equal to the average time taken by a fission neutron produced in one generation to cause a fission in the next generation. In performing the time average, the fissions which are produced are weighted by the value of F_H at the point where they occur. The neutron density, n, is normalized to one fission neutron emitted per unit time in the whole reactor. For PPA-5, τ is 4 μsec.

Figures 3 and 4 show the distribution of flux as a function of u for 1-watt reactor operation in SAPL PPA-5. Figure 3 shows the distribution at the center of the reactor. Experimental points measured with manganese, gold, and indium detectors are included. In addition, a low energy curve obtained by age theory.

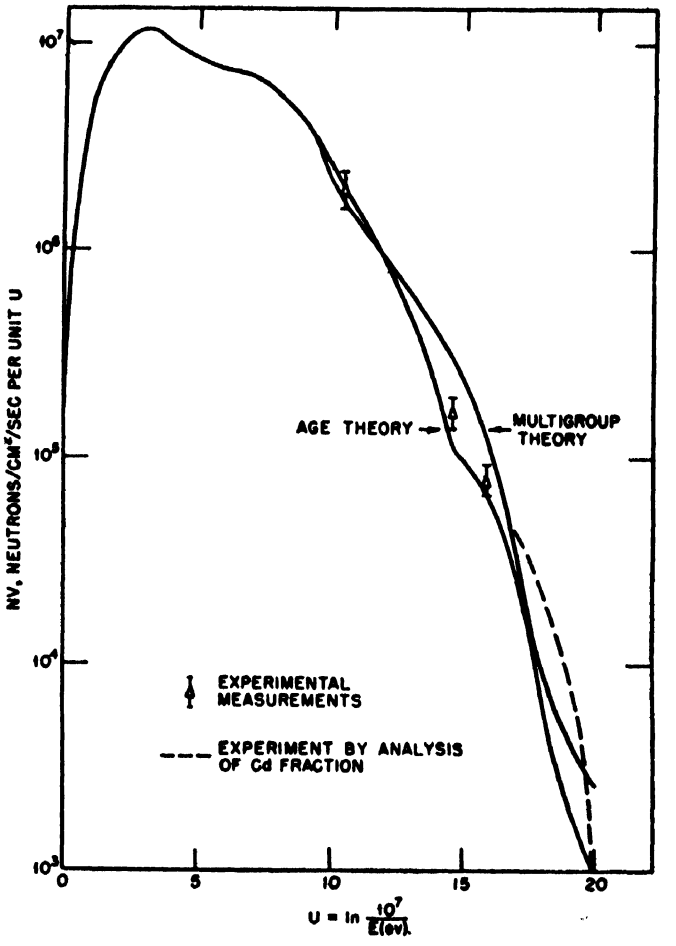

Figure 3. Neutron flux per watt vs u at the center of the PPA-5 core

using the buckling given by the multi-group solution, is included. The groups used in the calculation were somewhat wide at energies below that corresponding to $u = 10.5$; therefore the rapid energy attenuation of the flux is given only approximately by the multi-group procedure. However, the age-theory results, corresponding to a much larger number of narrow groups, agree with experimental results very well down to an energy of 1 ev. The experimental values are believed to be high in the energy region below 1 ev due to the channeling of slow neutrons from the reflector to the center of the core in the voids between the matrix tubes. This effect may also explain the fact that the experimental value of the fraction of fissions produced by neutrons below the cadmium cut-off at the core center is 0.02 instead of 0.01 as predicted by theory. Figure 4 shows the flux distribution at the core-reflector interface. Since the experimental results are an average over 2-in. diameter disks in the last row (ring 6) of core rods, two theoretical curves are given in Fig. 4, one at the interface and one 1.55 in. in from the interface.

A group of interesting experiments was performed in SAPL PPA-5 in order to investigate the resonance structure of the U^{235} cross sections. These experiments included measurements of the fission distribution throughout stacks of U^{235} disks, the dependence of U^{235} reactivity coefficient on disk thickness, and the change of reactivity with temperature of the uranium due to Doppler broadening of the U^{235} resonances. In the U^{235} disk-stacking experiment, measurements were made of the fission distribution in stacks of two up to eight 0.020-in. thick U^{235} disks located in ring 2 (core center) and ring 6 (core edge). The observed fission distribution throughout the stacks was roughly parabolic. At the ring 2 location the ratio of fissions per unit volume at the edge of the stack to fissions per unit volume at the center of the stack ranged from 1.11 for a stack of two disks to 1.23 for a stack of eight disks. In the lower neutron spectrum in ring 6, the corresponding numbers are 1.30 and 1.63. An analysis of these results by G. M. Roe showed that they are consistent with a ratio of 0.1 between the natural U^{235} resonance widths and resonance spacings. This early analysis has not been extended to take into account the recent conclusions concerning the statistical distributions[12] of spacings and resonance parameters in U^{235} but it appears that the predictions covering the disk stacking experiments will not be substantially modified by the latest information.

The measurement of the variation of the U^{235} reactivity coefficient with disk thickness, and of the Doppler effect reactivity temperature coefficient give information on the fluctuations of capture to fission ratio (alpha) from resonance to resonance.[2,12] If alpha were constant for the various resonances, a decrease in self-shielding (resulting from a decrease in the U^{235} thickness) or a broadening of the resonances by an increase in U^{235} temperature would increase reactivity. Since the observed fluctuations in alpha are due to fluctuations in fission widths,[2,12] the resonances with high alpha are comparatively narrow and hence strongly

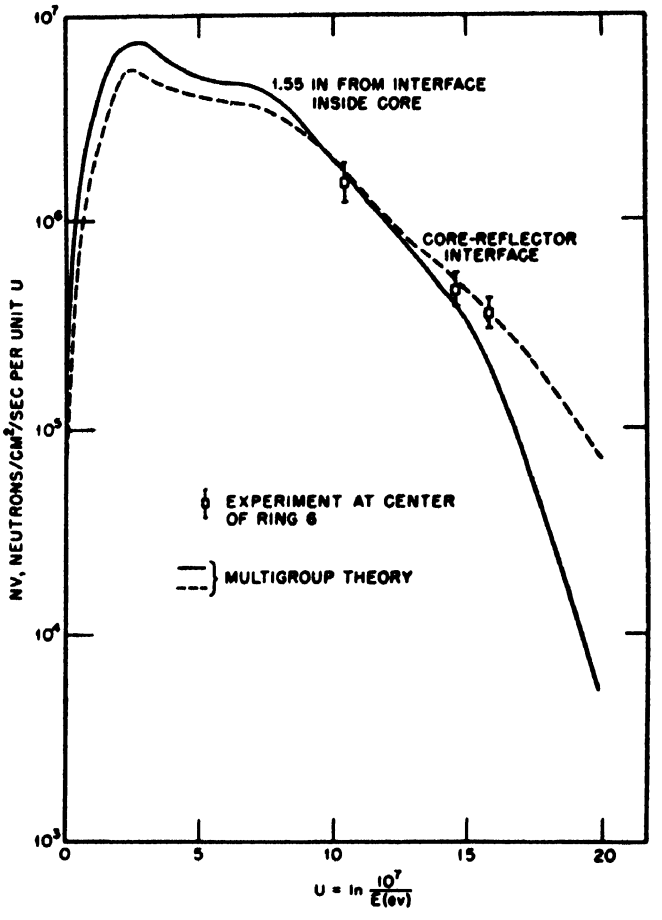

Figure 4. Neutron flux per watt vs u at the edge of the PPA-5 core

effected by self-shielding. Thus, a reduction in self-shielding tends to increase U^{235} captures more than U^{235} fissions so that it is possible for the net reactivity change with self-shielding to be opposite to that which would exist in the case of constant alpha. The sign of the change in reactivity due to a reduction in self-shielding is not necessarily the same for Doppler temperature coefficient experiments and for experiments in which the U^{235} thickness is varied, since in the latter case the influence of the low energy part of the neutron spectrum is relatively more important. In the experiments performed in SAPL PPA-5 it was found that the U^{235} reactivity coefficient per mole is slightly greater for 0.040 inch disks than 0.020 inch disks near the center of the core (ring 2), but near the edge of the core (ring 6) the reverse is true. This indicates that the reduction in the average capture to fission ratio with increasing thickness is the predominant effect in the comparatively high neutron spectrum in ring 2.

The calculation of the Doppler temperature coefficient of reactivity is difficult because of the near cancellation of positive and negative effects. On the basis of information available at the time of the SAPL PPA-5 studies, it was estimated that the Doppler effect would contribute a reactivity change of the order of one third of a per cent if the U^{235} temperature were doubled. The sign of the effect could not be reliably predicted.

Table VI. Composition of the PPA-11

Constituent	Core		Reflector Volume %	Inner blanket Volume %
	Relative mols	Volume %		
U^{235}	1	10.56	—	4.04
U^{238}	—	—	—	55.81
Be	1.74	7.10	65.56	4.71
Na	2.03	40.00	13.86	16.18
Fe	4.74	28.00	8.55	10.58
Al	0.77	6.42	6.50	6.58
Void	—	7.37	5.53	5.60

The experiments were equally difficult because of the smallness of the Doppler effect. An oscillation technique was employed in which the temperature of a small quantity of U^{235} in the assembly was alternately raised and lowered. The concurrent oscillation in power level did not exceed the background noise level in the experiment, which indicated that the magnitude of the Doppler temperature coefficient in SAPL PPA-5 was not larger than indicated by the theoretical studies. Similar Doppler coefficient measurements with improved techniques which are now available can provide a valuable integral test of the present U^{235} resonance data.

After the studies on the intermediate assembly SAPL PPA-5 were concluded, the investigations were extended to assemblies with higher neutron spectra. One of these assemblies, known as SAPL PPA-11, was constructed for the purpose of investigating the properties of a fast reactor in which the fissionable material in the core is diluted by the structural material and coolant which would be required in a practical fast power reactor. The core of this assembly contained only a small amount of beryllium, but in order to keep the critical mass within reasonable limits a thin beryllium reflector was provided. Although this reflector degraded the neutron spectrum near the edges of the core, the spectrum near the center of the core was typical of that in a high power fast reactor. As in SAPL PPA-5 the coolant was simulated by solid sodium in steel cans. The reflector was surrounded by a region rich in U^{238} which simulated the breeding blanket of a plutonium-producing fast reactor. The composition of SAPL PPA-11 is given in Table VI. The assembly was critical with 123.7 kg of U^{235} contained in a core structure consisting of 43.4 cm-long rods filling the first five rings of a 9-ring hexagonal matrix having 2 inch cross-flats unit cells. The core was surrounded by 1½ rings of beryllium reflector rods (about 7 cm thick) and 2½ rings of inner blanket rods (about 11 cm thick). The beryllium end reflector was 9.7 cm thick and the end blanket was 7.7 cm thick. Outside the 9-ring matrix, there was an additional blanket of about 30 cm natural-uranium (26,000 kg). For the purpose of calculation, this reactor was simulated by a spherical core of 24-cm radius containing 114 kg of U^{235} surrounded by 8-cm-thick shells of reflector and inner blanket. The natural-uranium blanket was omitted since the IBM machines which were used to perform the calculation were programmed to handle no more than three spatial regions. This does not appreciably affect the over-all criticality. The calculation gave $k = 1.003$. Allowing 10 per cent in mass for the difference between spherical and hexagonal geometries, a calculated mass for the SAPL PPA-11 of 124 kg is obtained, in good agreement with experiment.

At Oak Ridge two unreflected critical assemblies (approximately cubic in geometry) were constructed specifically for the purpose of allowing a straightforward comparison of theory and experiment.[1] The assemblies (known as Ca-1 and Ca-18) were built in an aluminum matrix and used beryllium as moderator and highly enriched uranium as fuel. The uranium was in the form of 0.01 inch thick, 2.860 inch diameter disks interspersed between beryllium disks. The assembly composition is described in Table VII. The reactivity for these assemblies was calculated by the multi-group procedure[13] using cross sections which are more accurate than those available when the SAPL PPA-5 calculations were performed. The results are given in Table VIII.

In the calculations summarized in Table VIII the buckling (i.e., $-\nabla^2 nv/nv$) was assumed to vary with energy in such a manner that the neutron flux at a given energy extrapolates to zero at a distance of $0.7\lambda_{tr}$ beyond the core boundary, where λ_{tr} is the transport mean free path at the particular energy. The effect of U^{235} self shielding, which in Method II was calculated on the assumption of isotropic flux, is greater in CA-18 than CA-1 since the competition of structure and moderator absorption with fission is stronger in the

Table VII. Description of Oak Ridge National Laboratory Assemblies

	CA-1	CA-18
Dimensions	21.0 × 21.0 × 23.2 in.	24.0 × 28.4 × 24.1 in.
Spacing of 0.010-in. fuel disks	1 in.	4 in.
U^{235} loading	18.08 kg	7.65 kg
Observed reactivity	1.0054	1.0020
Be:U^{235} atomic ratio	390	1560
Volume fractions:		
Aluminum	0.0610	0.0611
Beryllium	0.9060	0.9128
Uranium	0.0064	0.0016
Stainless Steel	0.0004	0.0003
Void	0.0262	0.0242

former case. The improved self-shielding factor calculations employed in Method IV take into account the slightly higher neutron flux in the direction normal to the foils. This correction increases the calculated reactivity by about one third of a per cent for CA-1 and by two per cent for CA-18. The anisotropy of the beryllium scattering assumed in Method III and IV makes the calculated age to thermal energy in beryllium agree with the measured age of 98 cm.[2] It corresponds to a reduction of the product $\xi\sigma_{tr}$ for fission spectrum neutrons by a factor 0.76 as compared with the value which would be calculated from the measured total cross section of beryllium assuming isotropic scattering in the center of mass system. Experimental measurements of the anisotropy in beryllium scattering[14] would suggest a larger correction for this effect, which would further reduce the calculated reactivity. It would be possible to adopt a slightly larger correction for anisotropic scattering and still obtain the correct neutron age by including the effects of inelastic scattering by beryllium. However, because of the high inelastic scattering threshold of beryllium, the effect of inelastic scattering on neutron age and reactivity should be comparatively unimportant.[15]

Two other effects which should be considered are the (n,α) and $(n,2n)$ reactions in beryllium. The (n,α) cross section is accurately known.[16] The effect of this reaction is to decrease the reactivity by about 3 per cent. The $(n,2n)$ cross section is not well known. This reaction has a higher threshold than the (n,α) reaction (1.85 Mev as compared to 0.71 Mev) but its cross section is probably higher than that of the (n,α) reaction above the threshold. It is commonly assumed that the increase in reactivity due to the $(n,2n)$ reaction roughly compensates the decrease from the (n,α) reaction so that the magnitude of the net effect of the two reactions on reactivity is only of the order of 1 per cent.

A final possible source of error in the reactivity calculations is the error arising from the use of the age-diffusion equation. A detailed investigation of this point has not been made, although an analysis of the type employed in light water reactor studies[6] is feasible. In the absence of detailed calculations it is believed that the combined effect of possible errors in the buckling, due to the use of incorrect extrapolation distances as a function of energy, and the error inherent in age-diffusion theory when the buckling and energy loss per collision are moderately large, is only a few per cent in reactivity.

The various possible sources of uncertainty discussed here are large enough to explain the differences between the reactivity calculated by Method IV, Table VIII for CA-1 and CA-18 (0.963 and 0.973 respectively) and the observed reactivities (1.005 and 1.002 respectively). It is worth noting that the calculation of the fraction of fissions caused by neutrons below the cadmium cut-off is not subject to uncertainties relating to high energy neutron leakage which are important in the reactivity calculations. This fraction has the calculated values 0.46 and 0.80 in CA-1 and CA-18 respectively compared to experimental values of 0.46 ± 0.1 for CA-1 and 0.87 ± 0.03 for CA-18. The lower observed spectrum in CA-18 as compared to the calculated spectrum has not been explained in detail, but may be related to the fairly large spacing between the fuel disks in this assembly.

Table VIII. Summary of Multigroup Results for k_{eff} ($= \nu/\nu_c$)

Method	CA-1 k_{eff}	CA-18 k_{eff}
I[a]	1.0215	1.0550
II[b]	1.0102	0.9839
III[c]	0.9290	0.9153
IV[d]	0.9632	0.9734

[a] 32 energy groups, variable buckling, isotropic beryllium scattering in center of mass system.

[b] Same as I except U^{235} self shielded for isotropic flux.[3]

[c] Same as II except nonisotropic scattering in beryllium at high energy is included by reducing $\xi\sigma_s\sigma_{tr}$ to 76.2 per cent of its isotropic value for fission spectrum energy neutrons.

[d] Same as III except that neutron leakage is corrected for reflection by the external aluminum and self shielding for P_1 incident flux.

CONCLUSION

It is seen from the above discussion that the multigroup calculations based on the Fermi age-diffusion equation give descriptions of the properties of beryllium moderated assemblies with neutron spectra ranging from that of CA-18, in which 85 per cent of the fissions are due to sub-cadmium neutrons, to that of SAPL PPA-11, in which 50 per cent of the fission are caused by neutrons above 125 kev. The theory not only provides good values of reactivity but also predicts the detailed features of neutron flux and adjoint function variation with position and energy. It may be anticipated that the correlation between theory and experiment will become still better as improved experimental information on the beryllium cross sections at high energy and the U^{235} resonance structure is utilized in the calculations. The multi-group technique, particularly when used in conjunction with high speed digital computing machines which can conveniently handle problems in more than one space dimension, is therefore an increasingly valuable tool for use in the design and analysis of nuclear reactors.

REFERENCES

1. Snyder, T. M., P/602 *The Critical Assembly—A Nuclear Design Tool*, Volume 5, Session 21A these Proceedings.
2. Goertzel, G., P/613 *An Estimation of Doppler Effect in Intermediate and Fast Neutron Reactors*, Volume 5, Session 23A, these Proceedings. Roe, G. M., *The Absorption of Neutrons in Doppler Broadened Resonances*, Knolls Atomic Power Laboratory Report, KAPL-1241, (Unpublished), (1954).
3. Glasstone, S. and Edlund, M. C., *The Elements of Nuclear Reactor Theory*, 49–50, D. Van Nostrand Co., Inc., New York (1952).
4. Cohen, E. R., P/611 *Survey of Neutron Thermalization Theories*, Volume 5, Session 23A these Proceedings.
5. Ehrlich, R. and Hurwitz, H. Jr., *Multigroup Methods for Neutron Diffusion Problems*, Nucleonics, Vol. 12, No. 2, 23–30, (1954).

6. Wilkins, J. E., Hellens, R. L. and Zweifel, P. F. P/597 *Status of Experimental and Theoretical Information on Neutron Slowing Down Distribution in Hydrogenous Media*, Volume 5. Callihan, A. D. and Morfitt, J., P/834 *Small Thermal Homogeneous Critical Assemblies*, Volume 5, Session 20A these Proceedings. Mandl, M. E., *Multigroup Theory with an Application to Inelastic Scattering in Uranium*, Harwell report A.E.R.E. T/R 1500 (1954).
7. Habetler, G. J., *General One-Space-Dimensional Multigroup*, Knolls Atomic Power Laboratory Report KAPL-1182, (1954) (Unpublished); Coveyou, R. R., private communications.
8. Roe, G. M., *Adaptation of Multigroup Methods to Cylindrical Geometries*, Knolls Atomic Power Laboratory Report KAPL-950 (Unpublished) (1954). Wachspress, E. L., *Iterative Methods for Solving Elliptic-Type Differential Equations with Application to Two-Space-Dimension Multigroup Analysis*, Knolls Atomic Power Laboratory Report KAPL-1333, (Unpublished) (1955).
9. Forsythe, G. F., *Tentative Classification of Methods and Bibliography on Solving Systems of Linear Equations*, National Bureau of Standards Applied Mathematics Series 29, US Government Printing Office, Washington, D. C. (1953). Sheldon, J. W., private communication.
10. Watt, B. E., *Energy Spectrum from Thermal Fission of* U^{235}, Phys. Rev. *87*, 1037–41 (1952).
11. Hughes, Dabbs, Cahn, and Hall, *Delayed Neutrons from Fission of* U^{235}, Phys. Rev. *73*, 111-24 (1948).
12. Kanne, Stewart and White, P/595 *Capture-to-Fission Ratio of Pu-239 and U-235 for Intermediate Energy Neutrons*, Volume 4, Session 18A these Proceedings. Bethe, H. A., P/585 *The Critical Analysis of Neutron Resonances in Fissile Materials*, Volume 4, Session 18A these Proceedings.
13. The Oak Ridge National Laboratory critical calculations were done by: Mooneyham, A. O., Safanov, G. M., Holmes, D. K. and Mills, C. B.
14. Willard, Bair and Kington, *Elastic Scattering Angular Distributions of Fast Neutrons on Light Nuclei*, Physical Review *98*, 669–673, (1955). Meier, R., Ricamo, R., *Winkelverteilung gestreuter Neutronen an Beryllium*, Helvetica Physica Acta, *26*, 430–31 (1953). Barschall, H. H. *et al.*, *Measurement of Transport and Inelastic Cross Sections for Fast Neutrons: II Experimental Results*, Physical Review, *72*, 881–8 (1947). Jurney, E. T., *Inelastic Collision and Transport Cross Sections for Some Light Elements*, Los Alamos report LA-1339 (Unpublished) (1951).
15. Grace, Beghian, Preston and Halban, *The Inelastic Scattering of Fast Neutrons*, Physical Review *82*, 969 (1951). Beyster, Henkel, and Nobles, *Inelastic Collision Cross Sections at 1.0-, 4.0-, and 4.5-Mev Neutron Energies*, Physical Review *97*, 563 (1955).
16. Allen, Burcham and Wilkinson, *Resonance Phenomena in the Interaction of Fast Neutrons with Beryllium and Aluminum*, Proc. Roy. Soc. (London) *A192*, 114 (1947).

A Method for Calculating the Critical Mass of an Intermediate Reactor

By M. E. Mandl and J. Howlett,* UK

An intermediate reactor is one in which the great majority of the fissions are caused by neutrons whose energies are well below fission but well above thermal energy, that is, roughly in the range 1 to 1000 ev; this state of affairs can be achieved by suitably moderating the fissile material. Any calculation of the critical size of such a reactor must, to be at all realistic, take into account the variation of the cross sections with energy, since these suffer great changes in the intermediate-energy region. This complicates the mathematics of any analytical approach very considerably; the case of a bare sphere can be treated fairly simply,[1] but when a reflector is added the analysis becomes very involved and the computation to which it leads exceedingly intricate. The need to avoid this tedious work led to the development of the simple direct method of computation described here; a related method has been developed independently by Ehrlich and Hurwitz.[2] These direct methods still require a large amount of numerical work, but this is of a simple and highly repetitive form, very well suited for programming for an automatic digital machine; they do avoid the elaborate analysis: our experience has been that to carry through a piece of complicated algebra and guarantee that there are no mistakes is by no means a trivial undertaking.

THE DIFFERENTIAL EQUATIONS

The problem considered is the calculation of the critical size of a spherical reactor consisting of a homogeneous fissile core surrounded by a non-fissile reflector. So long as the moderator is any element heavier than hydrogen or deuterium the age-theory approximation to the neutron transport equation can be used with adequate accuracy. The argument given by Davison[1] is roughly as follows. The cross sections vary smoothly down to energies of the order of 10 ev so that the total mean free path of the neutrons does not change greatly from one collision interval to another and age-theory can be used with confidence. Below this energy the cross sections do vary rapidly, but the number of collisions made in the lower energy range is so small a fraction of the total number that no serious error can result from the use of the inaccurate approximation.

* United Kingdom Atomic Energy Authority, Atomic Energy Research Establishment, Harwell, England.

If $\psi(E,r)$ is the collision density at the point r in some system, that is the number of collisions per unit volume (and unit time) at r made by neutrons whose energy before the collision was E, then the age-theory approximation gives for the steady-state distribution:

$$-l\lambda\nabla^2\psi + \xi\frac{\partial\psi}{\partial u} + s\psi = q(r)\delta(u) \qquad (1)$$

where $u = \ln E_0/E$ (the "lethargy" corresponding to energy E, E_0 being the fission energy), ξ is the mean increase in u per collision, l the total mean free path, $\lambda = \frac{1}{3}(1 - \overline{\cos\phi})$ where ϕ is the angle of scattering, s is the probability of absorption at a collision and $q(r)$ a source term of fission neutrons. l, λ, s, ξ are functions of energy (i.e., of u) which are derived from measurements and have no simple analytical forms.

For a spherically symmetrical system we have only the single radial co-ordinate r; taking the radii of core and reflector as a, b, respectively and putting $\chi = r\psi$ Equation 1 becomes:

For the core $\quad 0 \le r \le a, \qquad u > 0$

$$-l\lambda\frac{\partial^2\chi}{\partial r^2} + \xi\frac{\partial\chi}{\partial u} + s\chi = 0 \qquad (2a)$$

For the reflector $\quad a \le r \le b, \qquad u > 0$

$$-l_1\lambda_1\frac{\partial^2\chi_1}{\partial r^2} + \xi_1\frac{\partial\chi_1}{\partial u} + s_1\chi_1 = 0 \qquad (2b)$$

(the suffix 1 referring to quantities in the reflector). The initial condition (i.e., at $u = 0$) is found as follows: If we integrate Equation 1 over a small range $(-\epsilon,\epsilon)$ in u within which l, λ, etc. may be regarded as constant, we get

$$-l\lambda\nabla^2\int_{-\epsilon}^{+\epsilon}\psi(u,r)\,du + \xi[\psi(\epsilon,r) - \psi(-\epsilon,r)] + s\int_{-\epsilon}^{\epsilon}\psi(u,r)\,du = q(r)$$

Physically, ψ must be finite always; so if $\epsilon \to 0$, $\int_{-\epsilon}^{\epsilon}\psi\,du \to 0$ also. Then since $\psi \equiv 0$ for $u < 0$, we have at $u = 0$:

$$\left.\begin{aligned} \xi\psi(0,r) &= q(r) \\ \text{i.e.,}\quad \xi\chi(0,r) &= rq(r) \\ \xi_1\chi_1(0,r) &= 0 \end{aligned}\right\} \qquad (3a)$$

The boundary conditions are:

at $r = 0$ ψ finite, $s_0\chi(u,0) = 0$, $u > 0$ (3b)

at $r = b$ $\chi_1(u,b) = 0$, $u \geq 0$ (3c)

at $r = a$ the neutron flux and current are continuous, giving the relations

$$l\chi(u,a) = l_1\chi_1(u,a)$$

$$l\lambda\left[\frac{\partial\chi}{\partial r} - \frac{\chi}{r}\right]_{r=a} = l_1\lambda_1\left[\frac{\partial\chi_1}{\partial r} - \frac{\chi_1}{r}\right]_{r=a} \quad (3d)$$

the condition $\chi_1 = 0$ at $r = b$ means that we are taking this point as the extrapolated boundary, so we must allow for the extrapolation length when interpreting any results.

METHOD OF SOLUTION

Suppose that the equations of the last section have been solved, given an initial distribution $q(r)$ of fission neutrons and values for the radii a,b; the distribution of the next generation of fission neutrons resulting from the capture of this initial set is $\int\eta fs(\chi/r)\,du$ where η is the mean number produced per capture, f is the probability that a neutron captured is captured in a fissile nucleus and the range of integration is from fission to thermal energy, that is from $u = 0$ to about $u = 18$. If the system is just critical it will just reproduce itself and the integral will be $q(r)$; thus the condition for criticality is

$$\int\eta fs\chi\,du = rq(r) \quad (4)$$

and the core radius (assuming a fixed thickness of reflector) must be chosen so that this is satisfied. The equation, however, involves the source-function $q(r)$ and this has to be found also. The method adopted is as follows.

A trial value is taken for the core radius a and a trial function $q_0(r)$; the equations are integrated numerically by the method given in the next section and the integral in Equation 4 constructed as a numerical function of r, say $q_1(r)$. If $q_1(r)/q_0(r)$ is, to the accuracy of the calculation, independent of r this part of the process is stopped; if not it is repeated, starting with $q_1(r)$ instead of $q_0(r)$ and leading to a third function $q_2(r)$, and so on. It was found that this iteration converged quickly; usually three integrations gave a $q(r)$ such that

$$\int\eta fs\chi\,du = m(a)rq(r) \quad (5)$$

where $m(a)$ is a number depending only upon a, and is evidently the multiplication rate per generation for the system with that core radius. If now the whole process is repeated for a set of values of a a table of $m(a)$ will be built up, in which we can interpolate to find the radius for which the multiplication rate is unity, thus satisfying condition expressed in Equation 4.

INTEGRATION OF THE EQUATIONS

The method used for integrating the partial differential equations was the standard one of replacing the differential coefficients by finite-difference approximations and so reducing the problem to the solution of a set of algebraic recurrence relations. Since the equations are themselves only an approximate representation of the physical process it was considered sufficient to use the simplest possible finite-difference formulae in order to simplify the computing routine.

We take intervals

$$\delta u = \alpha \quad \text{and}$$

$$\delta r = \beta \quad \text{in the core}$$

$$= \beta_1 \quad \text{in the reflector}$$

with $a = n\beta$ $b - a = n_1\beta_1$

and write

$$u_j = j\alpha, \qquad r_k = k\beta \text{ (core)} = a + k\beta_1 \text{ (reflector)}$$

$$\chi_{jk} = \chi(u_j,r_k)$$

We use the approximations

$$\left(\frac{\partial\chi}{\partial u}\right)_{j,k} = \frac{1}{\alpha}[\chi_{j+1,k} - \chi_{j,k}]$$

$$\left(\frac{\partial^2\chi}{\partial r^2}\right)_{j,k} = \frac{1}{\beta^2}[\chi_{j,k+1} - 2\chi_{jk} + \chi_{j,k-1}] \quad (6)$$

Then for all $j > 0$ Equation 2 becomes, for $0 \leq r \leq a$,

$$\chi_{j+1,k} = \frac{\alpha}{\beta^2}\cdot\frac{l\lambda}{\xi}\left[\chi_{j,k+1} - \left(2 - \frac{\beta^2}{\alpha}\frac{\xi - \alpha s}{l\lambda}\right)\chi_{j,k} + \chi_{j,k-1}\right] \quad (7)$$

with a corresponding equation for the reflector.

This holds for $k = 1, 2, \ldots n-1$; for $k = 0$, $\chi = 0$ always; similarly for $k = n_1$, $\chi_1 = 0$.

Thus the values of $\chi_{j,k}(k = 0, 1, 2 \ldots n)$ determine the values $\chi_{j+1,k}(k = 0, 1, 2 \ldots n-1)$ and the values $\chi_{1j,k}(k = 0, 1 \ldots n)$ determine $\chi_{1j+1,k}$ $(k = 1, 2, 3 \ldots n)$; that is, the relation advances the solution one step in u except for the boundary point $r = a$.

To complete the stepping-ahead process we write as approximations to the derivatives at this point

$$\left(\frac{\partial\chi}{\partial r}\right)_{j+1,n} = \frac{1}{\beta}[\chi_{j+1,n} - \chi_{j+1,n-1}]$$

$$\left(\frac{\partial\chi_1}{\partial r}\right)_{j+1,0} = \frac{1}{\beta_1}[\chi_{1,j+1,1} - \chi_{1j+1,0}] \quad (8)$$

Substituting these into the conditions expressed in Equation 3*d* we get two linear equations for the required values $\chi_{j+1,n}; \chi_{1j+1,0}$ in terms of known quantities.

The values for $j = 0$ being given by the initial condition, the solution can be computed in steps of u as far as is required.

The process is stable in the sense that the solution of the recurrence relations converges to the true solution of the partial differential equations as the intervals δu, δr are reduced to zero, provided that these interval lengths satisfy a certain inequality.[3]

For the simple diffusion equation $\partial y/\partial \epsilon = \partial^2 y/\partial x^2$, $0 \leq \kappa \leq a$, with y given at the boundaries $x = 0$ and a, the condition is

$$\frac{\delta t}{(\delta \kappa)^2} \leq \frac{1}{2}$$

Our equations are essentially of the form $\partial y/\partial t = f(t)(\partial^2 y/\partial \kappa^2) - g(t)y$, for which, with the same boundary conditions and with f and g replaced by the constant values f_j, g_j in the neighbourhood of $t = t_j = j\,\delta t$, we find the condition for

$$f_j \frac{\delta t}{(\delta \kappa)^2} - \frac{1}{4} g_j\,\delta t \leq \frac{1}{2}$$

Thus a crude but sufficient condition is:

$$\frac{\delta t}{(\delta \kappa)^2} < \frac{1}{2\ \mathrm{Max}\, f(t)}$$

In the actual computation the question was settled empirically; a reasonable subdivision of the space range having been decided—usually $\beta = a/10$, $\beta_1 = (b - a)/8$—the most suitable interval for u was found by making a few exploratory integrations with trial values, using the above result as a guide. It should be borne in mind that the stability will be affected by the finite-difference approximations used not only in the equations themselves but also in the conditions at the interface $r = a$; it was found, for example, that the use of more accurate approximations to the derivatives at $r = a$ than the crude first differences of Equation 8 upset the stability and called for a smaller interval in u.

Some further points should be mentioned. The first is that while it should be possible to make a theoretical estimate of the truncation errors of the process (i.e., the error due to the ignoring of the higher-order differences) a much simpler course is to compare two or more integrations made independently with different intervals. We repeated our integrations with α, β reduced to $\alpha/4$, $\beta/2$ respectively, so as to preserve the ratio α/β^2, taking this far enough to assure us that the wider interval was giving sufficient accuracy.

The second is that the mathematical problem as stated has a singularity at $u = 0$, because the initial distribution $q(r)$ does not satisfy the conditions at $r = a$. An approximate analytical solution could be found in this region—taking the cross sections as constant and using, for example, the Laplace transform technique—but the singularity is only a mild one and general experience with parabolic equations would suggest that the effect of ignoring it would be small and confined to the first few steps in u. This was tested by making several short experimental integrations differing only in the values given to the initial distribution $q(r)$ at $r = a$; it was found that these solutions became identical, to the accuracy required, after a few steps had been completed. Since the quantity of interest is not so much the solution itself as a weighted integral over a wide range for u, small errors near to $u = 0$ are of only minor importance.

The third is that the question of stability can be avoided, at the cost of computational complication, by using a central-difference formula for the derivative with respect to u. If we write:

$$\frac{1}{\alpha}[\chi_{j+1,k} - \chi_{j,k}] = \left(\frac{\partial \chi}{\partial u}\right)_{j+\frac{1}{2},k} + 0(\alpha^2)$$

$$= \frac{1}{2}\left[\left(\frac{\partial \chi}{\partial u}\right)_{j+1,k} + \left(\frac{\partial \chi}{\partial u}\right)_{j,k}\right] + 0(\alpha^2)$$

and then use the partial differential equation and the approximation to $\partial^2 \chi/\partial r^2$ to express the last member in terms of $\chi_{j,k}$, etc., we have a linear relation connecting the three values $\chi_{j+1,k+1}$, $\chi_{j+1,k}$ and $\chi_{j+1,k+1}$ with the three values $\chi_{j,k+1}$, $\chi_{j,k}$ and $\chi_{j,k-1}$. Thus the integration from $u = j\alpha$ to $u = (j + 1)\alpha$ now requires the solution of a set of simultaneous linear equations; this requires a more elaborate computing routine than the simple process described above but is stable for all

Table I. Results of Integration

Notation: $F_n(r)$ = input for nth solution of partial differential equation.

$I_n(r) = \int \eta f s \frac{\chi}{r} du$

$R_n(r) = I_n(r)/F_n(r)$

	A. Input				*B. Integral*				*C. Ratios*			
r	F_1	F_2	F_3	F_4	I_1	I_2	I_3	I_4	R_1	R_2	R_3	R_4
0	0	0	0	0	0	0	0	0	0	0	0	0
5	0.545	0.545	0.545	0.545	0.244	0.156	0.131	0.130	0.448	0.287	0.241	0.239
10	1.049	1.396	1.071	1.040	0.465	0.307	0.251	0.254	0.443	0.220	0.234	0.244
15	1.473	1.978	1.537	1.520	0.658	0.441	0.366	0.364	0.447	0.223	0.238	0.240
20	1.786	2.442	1.923	1.899	0.814	0.551	0.458	0.455	0.456	0.226	0.238	0.240
25	1.965	2.743	2.206	2.181	0.924	0.632	0.526	0.523	0.470	0.231	0.238	0.240
30	1.995	2.912	2.378	2.359	0.971	0.682	0.569	0.566	0.487	0.235	0.239	0.240
35	1.875	2.903	2.453	2.438	0.985	0.703	0.588	0.586	0.526	0.242	0.240	0.240
40	1.613	2.886	2.458	2.452	0.962	0.704	0.591	0.590	0.597	0.244	0.241	0.241
45	1.230	3.024	2.512	2.527	1.045	0.720	0.609	0.608	0.851	0.238	0.243	0.241
50	0.753	3.302	3.108	3.372	1.401	0.891	0.813	0.813	1.860	0.278	0.262	0.241

values of α and β,[3] and may therefore permit the use of a wider interval α in u.

The above account makes it clear that the process involves quite a large amount of numerical work; but this is all of very simple form indeed, and is highly repetitive. While it would be tedious to do this by hand, it is particularly well adapted to solution with an automatic digital computer, and several solutions were computed with the small and slow relay (Dekatron storage) machine at Harwell.

AN EXAMPLE

The rate of convergence of the process is shown by the following example, which refers to a spherical core composed of a mixture of U^{235}, Be and Na, surrounded by a non-capturing reflector; the core and reflector radii are 50 and 70 cm respectively. The initial guess for the distribution $q(r)$ was taken from the Serber-Wilson approximation,

$$q_0(r) = \frac{1}{r}\sin\frac{\pi r}{a_0} \qquad 0 \leq r \leq a$$
$$= 0 \qquad r > a$$

where a_0 is the critical radius of a bare sphere of the same composition: actually it would have been adequate to take $q_0(r)$ as constant over $0 \leq r \leq a$.

The scale of u was chosen so that the range of integration was from 0 (fission energy) to about 40 (thermal); with an interval $\delta r = 5$ in the core, stability is ensured for the whole range by taking $\delta u = 0.2$, giving 200 steps of integration. Table I shows how the distribution has converged after four integrations.

REFERENCES

1. Davison, B., A.E.R.E. Report T/R, 528.
2. Ehrlich, R. and Hurwitz, H., Nucleonics *12*, 23 (February 1954).
3. O'Brien G. G., Hyman, M. A. and Kaplan, S., J. Math. Phys. *29*, 223 (January 1951).

Calculations for Heterogeneous Reactors with a Small Number of Blocks

By G. A. Bat, USSR

Reactors with a small number of rods of varied "blackness" are examined. For thermal neutrons in the moderator, the diffusion equation is used. The properties of the rods are described by the relation between the current and neutron density at their surface. A solution is given for thin cylindrical rods in an infinite moderator. The results of the calculations are compared with experimental data.

I

Physical calculations of nuclear reactors, including determination of critical size and neutron density distribution, as well as estimation of the control rods action, are usually made for a homogeneous model. For this purpose, the real medium in which the chain reaction occurs, the lattice of uranium rods in the moderator, is replaced by an "equivalent" homogeneous medium. It is assumed that this medium has, at every point, the same multiplication parameters which the infinitely extended lattice used in the reactor scheme possesses as a whole.

The homogenization method yields quite satisfactory results for calculating reactors with a regular lattice containing tens or hundreds of cells. When, however, the lattice is irregular (as, for example, when some of the uranium rods are replaced by rods with other properties), this method can give only a rough estimate of changes in the critical parameter. For more accurate calculations and to obtain a detailed description of the neutron density distribution, real and not averaged, the actual characteristics of the medium should be used. Known calculation methods which take into account lattice heterogeneity have later been applied to reactors with a small number of different rods irregularly placed in an infinite moderator.

The calculation is based on the diffusion equation for the density $\vec{n}(\vec{r})$ of thermal neutrons in the moderator

$$\Delta \vec{n}(\vec{r}) - \frac{\vec{n}(\vec{r})}{L^2} + \frac{\vec{q}(\vec{r})}{D} = 0 \qquad (1)$$

Here L is the diffusion length, D the diffusion coefficient, $\vec{q}(\vec{r})$ the density of thermal neutron sources.

The expression for the source density has the form:

$$\vec{q}(\vec{r}) = \sum_{i,k,l} \nu_{i,k,l} j_{i,k,l} G(E_T^f | \vec{r} - \vec{r}_{i,k,l}|) - \psi_{i,k,l} G(E_{T_1}^r | \vec{r} - \vec{r}_{i,k,l}| \qquad (2)$$

$$\psi_{i,k,l} = \sum_{m,n,p} \nu_{m,n,p} j_{m,n,p} A_{m,n,p} G(E_r^f | \vec{r}_{i,k,l} - \vec{r}_{m,n,p}|) \qquad (3)$$

where ν is the number of fast neutrons produced in the rod from the capture of one thermal neutron; j the thermal neutron current incident on the rod; $G(E_t^p | \vec{r} - \vec{r}|_{i,k,l})$ the density of generation of neutrons with energy at point $\vec{r}$ from source E_t at point $\vec{r}_{i,k,l}$ with initial neutron energy E^p (the indices T, r, f correspond to thermal neutron energy, resonance neutron energy, the fission spectrum neutrons); $A_{m,n,p} G(E_r^f | \vec{r}_{m,n,p} - \vec{r}_{i,k,l}|)$ is the probability of absorption by the rod m, n, p of the resonance neutrons emitted with energy E^f by the rod i, k, l.

Equations 2 and 3 are accurate when the resonance capture of the slowing down neutrons is due only to one level at energy E_r. But, as we know, the resonance absorption of neutrons by U^{238} consists of two effects:

1. In the energy region from 6 to ~100 ev, absorption which is caused by separate strong resonance levels, depends strongly on the size and shape of the rods.

2. At higher energies (up to ~1 Mev) absorption is caused by many small, partially overlapping, resonance levels, and depends mainly on the uranium concentration in the moderator.

In the small reactors we are considering here, the first effect ("blockaded" absorption) is usually appreciably larger than the second. This greatly restricts the region of energies important in resonance capture. Special calculations show that the choice of E_r affects the results only slightly. Therefore, Equations 2 and 3 may be regarded as sufficiently accurate.

It is convenient to describe the boundary conditions for Equation 1 in the form of relationships between the current and density of the neutrons at the surface S of the rods:

$$\vec{r} \frac{\partial \ln \vec{n}(\vec{r})}{\partial \vec{r}}\Big|_{S_{i,k,l}} = \frac{\gamma}{2\pi D} \qquad (4)$$

Original language: Russian.

Consider a lattice of infinitely extended cylindrical rods. Let their radii $r_{i,k}^0$ be small compared with the spacing between their axes. In calculating the neutron density far from the rod we may consider the rod as a linear source, so as to take into account that the radius $r_{i,k}^0$ is finite in the boundary conditions, and to neglect the azimuthal asymmetry of the neutron current at the surface of the rod.

In the age approximation, the source function G is written:

$$G(E_l^p|\vec{r} - \vec{r}_{i,k}|) = \frac{\exp\{-|\vec{r} - \vec{r}_{i,k}|^2/4\tau_l^p\}}{4\pi\tau_l^p} \quad (5)$$

where τ is the neutron age

$$\tau_T^f = \tau_r^f + \tau_T^r \quad (6)$$

After some simple computations, we find the solution, for Equation 1 which vanishes at $\vec{r} \to \infty$:

$$n(\vec{r}) = -\sum_{i,k}(j_{i,k}/2\pi D)k_0\left(\left|\frac{\vec{r} - \vec{r}_{i,k}}{L}\right|\right)$$

$$+ 2(\alpha_T^f)^2\sum_{i,k}\nu_{i,k}(j_{i,k}/2\pi D)\Phi\left(\alpha_T^f\left|\frac{\vec{r} - \vec{r}_{i,k}}{L}\right|\right)$$

$$- 2(\alpha_T^r)^2\sum_{l,k}\Phi\left(\alpha_T^r\left|\frac{\vec{r} - \vec{r}_{i,k}}{L}\right|\right)\sum_{m,n}\nu_{m,n}(j_{m,n}/2\pi D)$$

$$\times (A_{m,n}/4\pi\tau_r^f)\exp\left\{-\frac{|\vec{r}_{i,k} - \vec{r}_{m,n}|^2}{4\tau_r^f}\right\} \quad (7)$$

where

$$\Phi(\alpha,\chi) = k_0(\chi)\int_0^\chi yI_0(y)e^{-\alpha^2y^2}\,dy + I_0(\chi)\int_\chi^\infty yk_0(y)e^{-\alpha^2y^2}\,dy \quad (8)$$

$\alpha^2 = L^2/4\tau$; $k_0(\chi)$, $I_0(\chi)$. I_0 and k_0 are zero-order, modified Bessel functions of the first and second kinds, respectively. The function $\Phi(\alpha,\chi)$ for the three values α is given in Fig. 1. Applying the boundary conditions

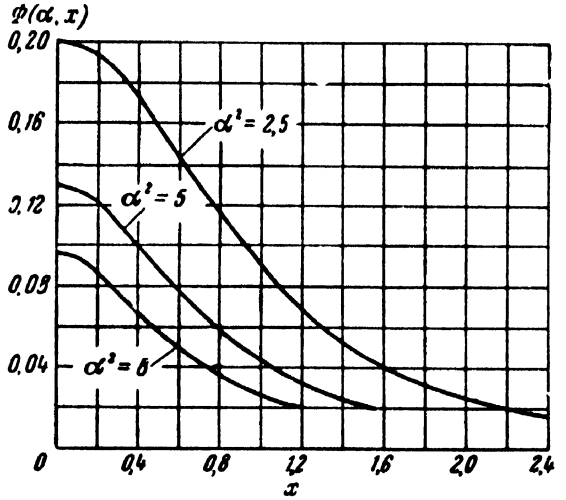

Figure 1. Function $\Phi(\alpha,\chi)$ where $\alpha^2 = 2.5, 5, 8$

at the rod surface, we obtain the following system of linear homogeneous equations:

$$0 = n_{a,b} + \sum_{i,k}'(\gamma_{i,k}/2\pi D)n_{i,k}k_0(|\vec{r}_{a,b} - \vec{r}_{i,k}|/L)$$

$$- 2(\alpha_T^f)^2\sum_{i,k}'\nu_{i,k}(\gamma_{i,k}/2\pi D)n_{i,k}\Phi(\alpha_T^f|\vec{r}_{a,b} - \vec{r}_{i,k}|/L)$$

$$+ 2(\alpha_T^r)^2\sum_{i,k}'\Phi(\alpha_T^r|\vec{r}_{a,b} - \vec{r}_{i,k}|/L\sum_{m,n}'\nu_{m,n}(\gamma_{m,n}/2\pi D)$$

$$\times (A_{m,n}/4\pi\tau_r^f)n_{m,n}\exp\{-|\vec{r}_{i,k} - \vec{r}_{m,n}|^2/4\tau_r^f\} \quad (9)$$

The accent at the sum symbol denotes that when the indices in the differences $(\vec{r}_{a,b} - \vec{r}_{i,k})$ coincide, respective functions are computed at the surface of rods a, b.

The vanishing of the determinant of Equation 9 is the critical condition. Any of the characteristics (ν, $\gamma/2\pi D$, A) of the rod may be taken as a critical parameter. The number of equations in the system (Equations 9) depends on the symmetry of the problem. If it is possible to separate a group of rods situated in equivalent conditions, then the number of equations is equal to the number of such groups.

Our results are valid for rods of infinite extent. Systems with rods of finite length are, strictly speaking, difficult to calculate. However, the fact that the rods are finite can be taken into account approximately by artificially introducing a cosine curve distribution of neutron density along the height. All the relationships derived above are valid if we make the replacements

$$1^2/L^2 \to 1/L^{*2} = 1/L^2 + \pi^2/H_z^2$$

$$\nu \to \nu^* \simeq \nu\exp\{-\pi^2\tau_T^f/H_z^2\} \quad (10)$$

where $H_z = H + 2\delta$; H is the rod length; δ is the reflector savings.

II

The critical condition for the heterogeneous reactor contains seven parameters (ν, L, $2\pi D/\gamma$, A, τ_T^f, τ_r^f, δ) which characterize the neutron properties of the rods and moderator. If the theory were accurate, then upon building from the same materials seven reactors of varied form we could determine all these parameters. Thus, a technically simple experiment would have enabled us to get results which are usually obtained by much more laborious procedures. But owing to the inaccuracy of the simplifications adopted in the theory, the latter itself needs to be verified experimentally. By comparing the results of the calculations and experiments it will be possible to find the inaccuracies of the theory and estimate the errors in its application. This method of calculating heterogeneous reactors was experimentally verified in 1951.

Three critical systems depicted schematically in Fig. 2 were built in a large (practically infinite) graphite prism. Since there are fewer reactors than the number of quantities used in the calculation, values

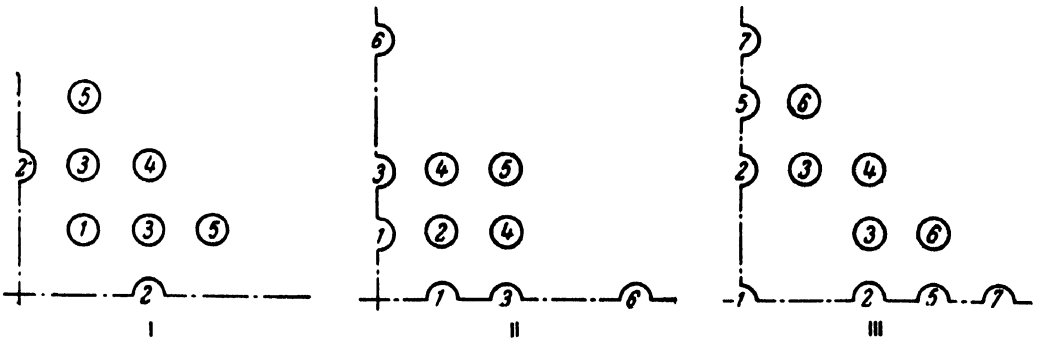

Figure 2. Geometrical characteristic of experimental reactor: rod radius: 3.2 cm; lattice spacing: 20 cm; Scheme I—rod length: 450 cm, number of rods: 28; Scheme II—rod length: 450 cm, number of rods: 28; Scheme III—rod length: 345 cm, number of rods: 33. Rod radius 3.2 cm; lattice spacing 20 cm

for four of the parameters must be selected in advance.

(*a*) The reflector savings σ can be evaluated by the usual group treatments. The height of all the piles under consideration is much larger than their "diameter." Therefore, the error in the quantity $\delta = 40$ cm leads to a relatively small error in computing ν.

Thus, if $\Delta\delta = 10$ cm, then $\Delta\nu_\delta \sim 0.005$

(*b*) A similar or even smaller error may be introduced by incorrectly choosing the position of the resonance level. Calculations show that any choice, within a reasonable range of the energy E_r (and, therefore, $\tau_T{}^r$) leads to ν changing by no more than 0.005. In our case $E_r \simeq 15$ ev; $\tau_T{}^r = 100$ cm^2; $\Delta\nu_E \sim 0.005$.

(*c*) The results of the calculations are influenced in a somewhat larger degree by the value of the resonance absorption parameter A. A has been determined from a semiempirical formula and assumed to be equal to (40 ± 4) cm^2. The inaccuracy in A is readily taken into account. Indeed, in the infinite 20-cm-spaced lattice, the resonance absorption

$$1 - \exp\left(-\frac{40 \pm 4}{20^2}\right) \simeq 0.1 \pm 0.01$$

corresponds to $A = (40 \pm 4)$ cm^2. In the reactors under consideration the moderator area per rod is, on the average, larger than in the infinite 20-cm-spaced lattice. The error in ν, therefore, is estimated to be $\Delta\nu_A \sim 0.01$.

(*d*) The inaccuracy in the adopted value $\tau_T{}^l$ of the neutron age appreciably influences ν. Assuming in accordance with our experimental data that in the systems under consideration $\tau_T{}^l = (390 \pm 10)$ cm^2, we should expect an error in ν of the order of 0.015.

Thus, the upper limit of the error in ν, introduced by the uncertainty of the parameters δ, E_r, A, $\tau_T{}^l$ leads to $\Delta\nu = \Delta\nu_\delta + \Delta\nu_E + \Delta\nu_A + \Delta\nu_r \leq 0.035$. It may be assumed that the real error will not exceed $\Delta\nu = 0.02$, and is close to the error in the direct measurement of ν. Direct measurements were carried out by B. G. Yerozolimsky, by the method of danger coefficients. They yielded $\nu = 1.647 \pm 0.017$. For practical calculations it appears convenient to regard as an eigenvalue, to assume the values of the other parameters, and, by varying L^2 and $2\pi R/\gamma$, to make the values of all three schemes under consideration coincide with the experimental value ν. When such coincidence (within the error range) was achieved, the calculations were terminated. The results of one series of the calculations are given in Table I, where η_i is thermal neutron density at the surface of the rods of group i.

The calculations show that there is no complete correlation between the schemes in which the calculated and experimental η_i and the calculated and experimental ν coincide. This suggests that the applied method of calculation is not perfect. Indeed, in the reactors under consideration the radii of the rods are rather large and the current asymmetry at their surface may be substantial. It will be noted that the diffusion length L and the blackness characteristic of the rod $2\pi D/\gamma$ in the infinite lattice depend on the temperature of the neutron gas. In the reactors under consideration, the temperature of the neutrons differs in different regions, an effect which is practically incalculable.

The values $L = 52$ cm, $2\pi D/\gamma = 3.3$, used in Table I, refer to different temperatures of the neutron gas. By increasing L and decreasing $2\pi D/\gamma$ it is possible to reduce these parameters to an equal temperature without impairing the agreement between the calculated and experimental ν.

Table I. $L = 52$ cm; $2\pi D/\gamma = 3.3$

Scheme		ν	η_1	η_2	η_3	η_4	η_5	η_6	η_7	η_{mean}
I	Experim.	1.647 ± 0.017	1	0.96	0.84	0.80	0.79			0.86
	Calculat.	1.63 ± 0.02	1	0.89	0.80	0.78	0.75			0.82
II	Experim.	1.647 ± 0.017	1	1.10	0.97	0.93	0.89	0.73		0.85
	Calculat.	1.61 ± 0.02	1	1.10	0.98	0.93	0.87	0.74		0.85
III	Experim.	1.647 ± 0.017	1	0.70	0.66	0.59	0.54	0.51	0.49	0.59
	Calculat.	1.64 ± 0.02	1	0.70	0.67	0.63	0.56	0.53	0.51	0.61

The Fermi Age Treatment for a Homogeneous Reactor with Reflector

By H. H. Woldringh,* The Netherlands

INTRODUCTION

For a homogeneous reactor with reflector the slowing-down (Fermi age) equation can be written down for the core and for the reflector respectively. At the interface the requirements of continuity of the flux per unit lethargy, $\varphi(u)$, and of $D\,\partial\varphi/\partial n$ must be fulfilled.

This is a special case of an inhomogeneous medium, for which we give a derivation of the slowing-down equation. With an appropriate boundary condition this equation determines a complete set of orthogonal functions, in which the slowing down can be calculated.

It is assumed that the scattering cross section for the epithermal neutrons is independent of energy. Generally the epithermal region has to be divided into subregions for each of which the scattering cross section may be assumed to be constant.

In the thermal diffusion equation we expand the thermal flux in a set of orthogonal functions, which fulfil the interface requirements of the thermal flux. This equation finally yields a homogeneous set of equations. Then the vanishing of the determinant of the coefficients is the critical equation.

A fictitious boundary is taken in the reflector just far enough from the core so that practically all neutrons are thermal. Then the epithermal neutrons can be assumed to obey these same boundary conditions as the thermal neutrons. Closer to the core the numerical calculation will be less elaborate.

We expect that the method, in comparison with the group-diffusion method, will have advantages, especially for small reactors.

SYMBOLS USED

u	lethargy, $u = \ln E_0/E$,
E	energy, E_0 initial energy of the source neutrons,
$\vec{r}$	space vector,
r	radial coordinate of a spherical reactor,
R_1	$r = R_1$ represents the interface between core and reflector,
R_2	$r = R_2$ represents the extrapolated outside boundary of the reflector,
R	$r = R$ represents a fictitious boundary in the reflector,
$\vec{\varphi}_{th}(\vec{r})$	thermal neutron flux,
$\vec{\varphi}(u,\vec{r})$	neutron flux per unit lethargy,
$\vec{q}(u,\vec{r})$	slowing down density,
$\vec{q}_{th}(\vec{r})$	$= q(u_{th},\vec{r})$ thermal slowing down density,
D_{th}	thermal diffusion coefficient,
D	epithermal diffusion coefficient,
Σ_a	thermal absorption cross section per cm^3,
Σ_s	epithermal scattering cross section per cm^3,
ξ	average lethargy increment per collision,
Σ_f	thermal fission cross section per cm^3,
ν	number of fission neutrons per fission,
τ	Fermi age,
B_n^2, μ_n^2, γ_m^2	eigenvalues,
v_n, w_m	eigenfunctions,
K_1, K_2	constants defined by (26),
L_2	diffusion length in the reflector,
medium 1	the core
medium 2	the reflector,
a_n	coefficients in the expansion, Equation 30.

FERMI AGE TREATMENT FOR A BARE HOMOGENEOUS REACTOR

The thermal diffusion equation is Equation 1 and, assuming that no absorption occurs in the epithermal energy region, slowing down is given by Equation 2:

$$q_{th} = \Sigma_a \varphi_{th} - D_{th}\,\Delta\varphi_{th} \tag{1}$$

$$\xi\Sigma_s \frac{\partial q}{\partial u} = D\,\Delta q \tag{2}$$

where $\vec{\varphi}_{th}(\vec{r})$ is the thermal neutron flux, $\vec{q}(u,\vec{r})$ is the slowing down density, and $q_{th} = \vec{q}(u_{th},\vec{r})$.

The source strength of fission neutrons is related to the thermal neutron flux:

$$\text{for } u = 0, \qquad q = \nu\Sigma_f \varphi_{th} \tag{3}$$

The boundary condition is:

$$\varphi_{th} = 0, \qquad q = 0 \text{ at the extrapolated boundary} \tag{4}$$

A set of orthogonal functions $v_n(r)$ is determined by:

$$\Delta v_n + B_n^2 v_n = 0 \tag{5}$$

with $v_n = 0$ at the extrapolated boundary.

* F.O.M.—KEMA Reactor Development Team, Research Laboratory of the N.V. KEMA, Arnhem, The Netherlands.

The critical equation now gives the first eigenfunction of the thermal neutron flux.

Equation 2 gives:

$$q = e^{-\tau B_0^2} v_0 \quad \text{with} \quad \tau = \int_0^u \frac{D}{\xi \Sigma_s} du \text{ (Fermi age)} \qquad (6)$$

With φ_{th} proportional to v_0 and with Equation 6, Equation 1 becomes:

$$\nu \Sigma_f e^{-\tau_{th} B_0^2} = \Sigma_a + D_{th} B_0^2 \qquad (7)$$

the critical equation of a bare homogeneous reactor.

THE DERIVATION OF THE SLOWING-DOWN EQUATION FOR AN INHOMOGENEOUS MEDIUM

The slowing-down equation has been derived for a homogeneous medium with the continuous slowing down model.[1,2] In an inhomogeneous medium, however, we cannot represent the slowing down by a single continuous relation between neutron energy and age.

For an inhomogeneous medium we consider the neutron flux per unit lethargy and especially the function:

$$\varphi_m(\vec{u,r}) = e^{-\gamma_m^2 u} w_m(\vec{r}) \qquad (8)$$

and we derive the steady-state condition for the neutrons in a lethargy element du and a volume element dv. Now the quantities Σ_s, ξ and D may be functions of position; it is assumed that they are independent of energy and that no absorption occurs in the epithermal energy region.

The number of neutrons scattered into the lethargy element du per second in a medium of mass number greater than unity is given by:†

$$du\, dv\, e^{-u} \int_{u + \ln \alpha}^{u} \Sigma_s e^{-\gamma_m^2 u'} w_m \frac{e^{u'}}{1 - \alpha} du' \qquad (9)$$

For small γ_m^2, such as occurs in reactors, Equation 9 becomes:

$$du\, dv\, \Sigma_s w_m e^{-\gamma_m^2 u}(1 + \gamma_m^2 \xi) \qquad (10)$$

with

$$\xi = 1 + \frac{\alpha}{1 - \alpha} \ln \alpha$$

The number of neutrons scattered out of the element du per second is:

$$du\, dv\, \Sigma_s \varphi_m \qquad (11)$$

The number of neutrons in the lethargy element du, which leak out of the volume element dv by diffusion is given by:

$$-du\, dv \text{ div } (D \text{ grad } \varphi_m) \qquad (12)$$

In the steady state the difference in the numbers given by Expressions 10 and 11 is equal to the number given by Equation 12:

$$\Sigma_s \xi \gamma_m^2 \varphi_m = -\text{ div } (D \text{ grad } \varphi_m) \qquad (13)$$

This equation with the boundary condition $\varphi_m = 0$ determines a complete set of orthogonal functions $w_m(\vec{r})$.[3]

With $\varphi = \sum_m b_m \varphi_m$ we get the slowing-down equation for an inhomogeneous medium:

$$\xi \Sigma_s \frac{\partial \varphi}{\partial u} = \text{div } (D \text{ grad } \varphi) \qquad (14)$$

While in the Fermi age equation, Equation 2 for a homogeneous medium, $q(\vec{u,r})$ may be the variable; now for an inhomogeneous medium $\varphi(\vec{u,r})$ must be the variable.

In the derivation we have to assume that $(1/\Sigma_s)|\text{grad } D|/D \ll 1$, and the same for ξ and Σ_s. Still we apply the equation for a system of core and reflector and we assume the quantities D, ξ and Σ_s change discontinuously at the interface. A correction should be made in a same way as for the outside boundary with the extrapolation distance.

THE EQUATIONS FOR A HOMOGENEOUS SPHERICAL REACTOR WITH REFLECTOR AND THE METHOD OF SOLVING THE EQUATIONS

The equations for an inhomogeneous medium are:

$$q_{th} = \Sigma_a \varphi_{th} - \text{div } (D_{th} \text{ grad } \varphi_{th}) \qquad (15)$$

$$\xi \Sigma_s \frac{\partial \varphi}{\partial u} = \text{div } (D \text{ grad } \varphi) \qquad (16)$$

$$\text{for } u = 0, \quad q = \nu \Sigma_f \varphi_{th} \qquad (17)$$

The relation between slowing down density and neutron flux per unit lethargy is given by:

$$q = \xi \Sigma_s \varphi \qquad (18)$$

Now the quantities Σ_a, D_{th}, ξ, Σ_s, D and Σ_f may be functions of position. Again two assumptions are made: independence on energy of the scattering cross section, and absence of absorption for the epithermal neutrons.

We now consider a homogeneous spherical reactor with reflector consisting of one layer. Then the quantities just mentioned are constant in the core and in the reflector respectively, and change discontinuously at the interface.

A fictitious boundary ($r = R$) is taken in the reflector at such a distance from the core that practically all neutrons are thermal.

Outside this boundary we may write $q_{th} = 0$; Equation 15 then becomes:

$$r > R: \Sigma_a \varphi_{th} - \text{div } (D_{th} \text{ grad } \varphi_{th}) = 0 \qquad (19)$$

With a solution of Equation 19, which vanishes at the extrapolated outside boundary of the reflector, and with the requirements of continuity for φ_{th} and $D\, d\varphi_{th}/dr$ one finds the boundary condition for φ_{th} at $r = R$ to be of the following form:

$$\left(\frac{d}{dr} + \sigma\right) \varphi_{th} = 0 \quad \text{at} \quad r = R \qquad (20)$$

with

$$\sigma = (1/R) + (1/L_2) \coth (R_2 - R)/L_2 \qquad (21)$$

† The number of neutrons scattered into an element dE is given by Glasstone, Edlund,[1] Chapter VI, §6,53.

where L_2 is the diffusion length in the reflector and $r = R_2$ the extrapolated outside boundary of the reflector.

The thermal neutron flux, φ_{th}, will be expanded below in a complete set of orthogonal functions $v_n(r)$ determined by:

$$\text{div } (D_{th} \text{ grad } v_n) + \mu_n^2 v_n = 0 \qquad (22)$$

with the boundary condition of Equation 20 for $v_n(r)$.[3]

Because there are practically no epithermal neutrons outside the boundary $r = R$ one may assume for the epithermal neutrons here the same boundary condition as that for the thermal neutrons:

$$\left(\frac{\partial}{\partial r} + \sigma\right)\varphi = 0 \qquad \text{at} \qquad r = R \qquad (23)$$

With the function $\varphi_m(u,r) = e^{-\gamma_m^2 u} w_m(r)$ Equation 16 becomes:

$$\text{div } (D \text{ grad } w_m) + \xi\Sigma_s \gamma_m^2 w_m = 0 \qquad (24)$$

This equation with the boundary condition of Equation 23 for $w_m(r)$ determines a second complete set of homogeneous functions.[3]

The slowing down can now be calculated in this second set of functions; we can derive then a relation between the thermal flux, which gives the source distribution of fission neutrons according to Equation 17 and the thermal slowing down density.

We finally solve the thermal diffusion equation by expanding the terms in the first set of functions. This will give an infinite homogeneous set of equations in the expansion coefficients of the thermal neutron flux. The vanishing of the determinant of the coefficients of this set of equations may be regarded as the critical equation.

DETERMINATION OF THE SETS OF ORTHOGONAL FUNCTIONS

The differential equation (Equation 24) can be written in the core and in the reflector respectively as follows:

$$\text{div grad } w_m + K_{1,2}^2 \gamma_m^2 w_m = 0, \qquad (25)$$

with $K_1^2 = \left(\frac{\xi\Sigma_s}{D}\right)_1$ constant in core (medium 1)

$$K_2^2 = \left(\frac{\xi\Sigma_s}{D}\right)_2 \text{ constant in reflector (medium 2)} \qquad (26)$$

The general solutions in core and in reflector respectively are:

in the core $\qquad w_m = a_m' \frac{\sin K_1 \gamma_m r}{r}$

in the reflector

$$w_m = b_m' \frac{\sin K_2 \gamma_m r}{r} + c_m' \frac{\cos K_2 \gamma_m r}{r} \qquad (27)$$

At the interface $r = R_1$ between core and reflector the requirements of continuity for w_m and $D\, dw_m/dr$ must be fulfilled. These two requirements and the boundary condition of Equation 22 at $r = R$ are three homogeneous equations in a_m', b_m', c_m'.

The vanishing of the determinant of the coefficients of this set of equations gives the values γ_m. For each γ_m the ratios of a_m', b_m', c_m' can be determined.

Then the absolute values follow from the normalization condition:

$$\int_0^R \xi\Sigma_s w_m^2 r^2 \, dr = 1 \qquad (28)$$

The coefficients of the expansion of an arbitrary function $\psi(r)$ in this set of functions are:

$$\psi = \sum_m g_m w_m, \qquad g_m = \int_0^R \psi \xi\Sigma_s w_m r^2 \, dr \qquad (29)$$

In the same way the other set of eigenfunctions can be determined.

DETERMINATION OF THE CRITICAL EQUATION

We set

$$\varphi_{th} = \sum_n a_n v_n \qquad (30)$$

We represent the quantities $\xi\Sigma_s$, Σ_a and $\nu\Sigma_f$ by a step function:

$$\begin{aligned} h(r,R_1) &= 1 \quad \text{for} \quad 0 \leqq r < R_1 \\ &= 0 \quad \text{for} \quad R_1 < r \leqq R \end{aligned} \qquad (31)$$

$$\begin{aligned} \xi\Sigma_s &= \xi_2\Sigma_{s2} + (\xi_1\Sigma_{s1} - \xi_2\Sigma_{s2})h(r,R_1) \\ \Sigma_a &= \Sigma_{a2} + (\Sigma_{a1} - \Sigma_{a2})h(r,R_1) \\ \nu\Sigma_f &= \nu_1\Sigma_{f1}h(r,R_1) \end{aligned} \qquad (32)$$

Then we make the following expansions:

$$h(r,R_1)v_n = \sum_m h_{nm} w_m \qquad (33)$$

$$w_m = \sum_k c_{mk} v_k \qquad (34)$$

$$h(r,R_1)v_k = \sum_s h_{ks} v_s \qquad (35)$$

Equations 17 and 18 give:

$$\text{for } u = 0, \qquad \varphi(0,r) = \frac{\nu\Sigma_f}{\xi\Sigma_s}\varphi_{th} \qquad (36)$$

We have to expand this expression in the set of functions w_m in order to calculate the slowing down:

$$\text{with } \varphi(0,r) = \sum_m b_m w_m \qquad (37)$$

where the coefficients b_m are related to the coefficients a_n via the expansion of Equation 33, we get:

$$\varphi(u_{th},r) = \sum_m b_m e^{-\gamma_m^2 u_{th}} w_m \qquad (38)$$

Using Equation 18 again and the expansions of Equations 34 and 35 we get:

$$q_{th} = \nu_1 \Sigma_{f1} \sum_n \sum_k a_n f_{nk} v_k \quad (39)$$

with

$$f_{nk} = \frac{\xi_2 \Sigma_{s2}}{\xi_1 \Sigma_{s1}} \sum_m h_{nm} e^{-\gamma_m^2 u_{th}} c_{mk} + \frac{\xi_1 \Sigma_{1s} - \xi_2 \Sigma_{s2}}{\xi_1 \Sigma_{s1}} \sum_m \sum_s h_{nm} e^{-\gamma_m^2 u_{th}} c_{ms} h_{sk} \quad (40)$$

The thermal diffusion equation, Equation 15 now becomes, using Equation 22 for the last term:

$$\sum_n a_n \left[\nu_1 \Sigma_{f1} \sum_k f_{nk} v_k - \Sigma_{a2} v_n - (\Sigma_{a1} - \Sigma_{a2}) \sum_k h_{nk} v_k - \mu_n^2 v_n \right] = 0 \quad (41)$$

or for $n = 1, 2, \ldots$:

$$a_n[\nu_1 \Sigma_{f1} f_{nn} - \Sigma_{a2} - (\Sigma_{a1} - \Sigma_{a2}) h_{nn} - \mu_n^2] + \sum_{k=n} a_k[\nu_1 \Sigma_{f1} f_{kn} - (\Sigma_{a1} - \Sigma_{a2}) h_{kn}] = 0 \quad (42)$$

The determinant of this homogeneous set of equations in the coefficients a_n set equal to zero may be regarded as the critical equation. The first positive root of this equation gives the critical condition of the reactor.

For a large reactor only a few terms in the expansions are needed. For a small reactor this number depends strongly on the properties of the media.

SOME GENERALIZATIONS

Generally the scattering cross section is dependent on energy. Thus we have to divide the epithermal energy region into subregions, such that for each of them we may assume the scattering cross section to be constant. The slowing down density of neutrons coming from one region, which is calculated in the orthogonal set of functions of that region, has to be expanded in the set of functions of the next region in order to calculate the slowing down in that region. In the group-diffusion method the scattering cross section may depend on the energy within a group; more groups are taken in order to get a greater accuracy. In our treatment we get a greater accuracy by taking more terms in the expansions.

The resonance absorption of neutrons in the fuel may be taken into account by considering the absorption as a negative neutron source at the resonance energy.

If there are two different layers of the reflector inside the fictitious boundary ($r = R$) then a homogeneous set of five equations (instead of three with one layer) determines the sets of orthogonal functions.

ACKNOWLEDGEMENT

I am much indebted to Prof. dr A. van Wijngaarden of The Mathematical Centre at Amsterdam for a valuable remark.

REFERENCES

(1) Glasstone, S. and Edlund, M. C., *The Elements of Nuclear Reactor Theory*, D. Van Nostrand Company, Inc., New York (1952).

(2) Wallace, P. R., *Neutron Distributions in Elementary Diffusion Theory—I*, Nucleonics 5, No. 2, 30 (1949).

(3) Courant, R. and Hilbert, D., *Methoden der Mathematischen Physik I;* Springer, Berlin (1931).

Matrix Formulation of the Two-Group Diffusion Theory for a Multiple Reflector Spherical Reactor

By P. Schmid, Switzerland

Only spherically symmetrical reactors are considered in the present paper, because the treatment of the space part of the diffusion equation is then a one-dimensional problem. At the same time the results obtained from their calculation can be adapted to cylindrical or rectangular reactors having optimum dimensions and the same core volume.

Two-group diffusion theory was chosen because the mathematical formalism is typical of multigroup treatments but still can be handled without complicated calculating machines or analogue computers.[1] On the other hand, one-group diffusion theory is too rough an approximation for consistent computations about reflected reactors whereas multigroup theories can only be successfully applied in countries where a lot is known of classified data from many reactors or exponential experiments.

Finally the choice of matrix formalisms should be justified. When solving simultaneously second-order differential equations in several adjacent regions of the independent variable, taking into account all the boundary conditions, the explicit solutions are generally terrible expressions. In terms of a matrix formalism, however, the results are given in a symbolic form only. When calculated numerically, the terms can be condensed after each step. Much time will then be saved and many sources of error can be eliminated by adopting these techniques. As a matter of fact, the necessary formalisms have been developed independently by X-ray specialists, theoretical physicists and electrical engineers.[2] They can be found in standard textbooks and applied to neutron diffusion problems. The author would like to point out this fact so as to prevent nuclear engineers from doing the same again, ignoring the wonderful work of their colleagues.

STEADY-STATE DIFFUSION IN SPHERICAL-SHELL-SHAPED MEDIA WITH CONSTANT DIFFUSION PARAMETERS

Using the well-known two-group diffusion approximation,[3] the fast and thermal neutron fluxes in multiplying ($k \neq 0$) or non-multiplying ($k = 0$) media are given by the differential equations

$$\text{div } D_f \text{ grad } \varphi_f(\rho) - \Sigma_f \varphi_f(\rho) + \frac{k}{p} \Sigma_{th} \varphi_{th}(\rho) = 0 \quad (1)$$

$$\text{div } D_{th} \text{ grad } \varphi_{th}(\rho) - \Sigma_{th} \varphi_{th}(\rho) + p \Sigma_f \varphi_f(\rho) = 0 \quad (2)$$

where φ = neutron flux, f, th = subscripts for fast and thermal group, respectively; D = diffusion constant for the flux = $\frac{1}{3}$ transp. m.f.p., Σ = macroscopic absorption cross section, k = multiplication factor of the chain reaction, p = resonance escape probability, and ρ = radius as independent variable.

If the diffusion parameters are constant within the considered shell, it is convenient to introduce the following abbreviations:

$$K_f^2 \equiv \Sigma_f / D_f \quad (3)$$

$$K_{th}^2 \equiv \Sigma_{th} / D_{th} \quad (4)$$

$$C_f^2 \equiv \Sigma_{th} / pD_f \equiv K_{th}^2 \cdot D_{th} / pD_f \quad (5)$$

$$C_{th}^2 \equiv p\Sigma_f / D_{th} \equiv K_f^2 \cdot pD_f / D_{th} \quad (6)$$

$$\psi(\rho) \equiv \rho \cdot \varphi(\rho) \quad (7)$$

Assuming spherical symmetry, Equations 1 and 2 reduce to

$$\psi_f''(\rho) - K_f^2 \psi_f(\rho) + kC_f^2 \psi_{th}(\rho) = 0 \quad (8)$$

$$\psi_{th}''(\rho) - K_{th}^2 \psi_{th}(\rho) + C_{th}^2 \psi_f(\rho) = 0 \quad (9)$$

Let the inner and outer radius of the shell be designated by r and R, respectively. If the column vector[4]

$$v(\rho) = \{\psi_f(\rho) \psi_f'(\rho) \psi_{th}(\rho) \psi_{th}'(\rho)\}$$

is known at $\rho = r$ it must be uniquely determined for all radii between r and R, because the system of Equations 8 and 9 allows only four arbitrary constants. Since those equations are linear there must exist a linear vector function (tensor), called the "transfer matrix" $T(R;r)$, which relates $v(R)$ to $v(r)$:

$$v(R) = T(R;r) v(r) \quad (10)$$

In order to determine the elements of T a very thin spherical shell with radii ρ_0 and $\rho_0 + \delta\rho$ shall be considered. As $v(\rho_0 + \delta\rho)$ cannot deviate very much from $v(\rho_0)$ for a very small $\delta\rho$, $T(\rho_0 + \delta\rho; \rho_0)$ can be written as a perturbed unit tensor E of order 4:

$$v(\rho_0 + \delta\rho) = [E + M(\rho_0 + \delta\rho; \rho_0)\delta\rho] v(\rho_0) \quad (11)$$

Therefore

$$\lim_{\delta\rho \to 0} \frac{v(\rho_0 + \delta\rho) - v(\rho_0)}{\delta\rho} \equiv v'(\rho_0) = M(\rho_0;\rho_0) v(\rho_0) \quad (12)$$

Using Equations 8 and 9, the elements of $M(\rho_0;\rho_0)$

are obtained. The explicit form of Equation 12 is then

$$\begin{pmatrix}\psi_f'(\rho_0)\\ \psi_f''(\rho_0)\\ \psi_{th}'(\rho_0)\\ \psi_{th}''(\rho_0)\end{pmatrix} = \left(\begin{array}{cc:cc} 0 & 1 & 0 & 0\\ K_f^2 & 0 & -kC_f^2 & 0\\ \hdashline 0 & 0 & 0 & 1\\ -C_{th}^2 & 0 & K_{th}^2 & 0\end{array}\right)\begin{pmatrix}\psi_f(\rho_0)\\ \psi_f'(\rho_0)\\ \psi_{th}(\rho_0)\\ \psi_{th}'(\rho_0)\end{pmatrix} \tag{13}$$

Since the diffusion parameters K^2 and C^2 are independent of ρ, $M(\rho;\rho) = M$ is constant in the region $r \leq \rho \leq R$. As H. Klepp pointed out (private communication), M should be called the "albedo tensor," corresponding to the well known scalar albedo.

If $\delta\rho \equiv d/n$ where $d \equiv R - r$, Equation 11 leads now to the recurrence relation

$$v(r + (\nu + 1)\,\delta\rho) = [E + M\,\delta\rho]v(r + \nu\,\delta\rho); \qquad (\nu = 0,1, \cdots, n-1) \tag{14}$$

Therefore

$$v(R) = \left[\lim_{n\to\infty}\left(E + M\cdot\frac{d}{n}\right)^n\right] v(r) \tag{15}$$

Remembering the well known relation

$$\lim_{m\to\infty}\left(1 + \frac{x}{m}\right)^m = e^x \tag{16}$$

Equation 15 can be written as[5]

$$v(R) = e^{Md}v(r) \equiv T(d)v(r) \tag{17}$$

Here the exponential of a square matrix X means another matrix Y of the same order which is defined by the expansion

$$Y \equiv E + X + \frac{1}{2!}X^2 + \frac{1}{3!}X^3 + \frac{1}{4!}X^4 + \cdots \tag{18}$$

It can be shown that this series always converges.[6]

The evaluation of exp (Md) can best be performed in a transformed vector space. First M (cf. Equation 13) shall be represented as a partitioned matrix consisting of the four minors A, B, C, D:

$$M \equiv \begin{pmatrix}A & B\\ C & D\end{pmatrix} \tag{19}$$

A square matrix S of the same order as M must now be obtained in order to get a transformed matrix $\bar{M}$:

$$\bar{M} \equiv SMS^{-1} = \begin{pmatrix}\bar{A} & 0\\ 0 & \bar{D}\end{pmatrix} \tag{20}$$

with vanishing minors $\bar{B}$, $\bar{C}$. The exponential of $\bar{M}d$ will be calculated and then transformed back to the original vector space in order to get

$$T(d) \equiv e^{Md} \equiv S^{-1}e^{\bar{M}d}S \tag{21}$$

It is found that S and its inverse S^{-1} must have the form

$$S^{\pm 1} = \alpha\begin{pmatrix}E & \pm\beta E\\ \mp\gamma E & E\end{pmatrix} \tag{22}$$

where

$$\alpha^2 \equiv (1 + \beta\gamma)^{-1} \tag{23}$$

E are unit minors of order 2, and β, γ are real numbers which must be determined so that Equation 20 is fulfilled. Assuming Equation 22, M transforms to

$$\bar{M} = \alpha^2 \begin{pmatrix}A + \gamma B + \beta C + \beta\gamma D; & -\beta A + B - \beta^2 C + \beta D\\ -\gamma A - \gamma^2 B + C + \gamma D; & \beta\gamma A - \gamma B - \beta C + D\end{pmatrix} \tag{24}$$

This gives the following conditions for β and γ:

$$C_{th}^2\beta^2 - (K_f^2 - K_{th}^2)\beta - kC_f^2 \equiv 0 \tag{25}$$

$$kC_f^2\gamma^2 - (K_f^2 - K_{th}^2)\gamma - C_{th}^2 \equiv 0 \tag{26}$$

For nonmultiplying media ($k = 0$) this means that

$$\alpha^2 = 1; \qquad \beta = 0; \qquad \gamma = C_{th}^2/(K_{th}^2 - K_f^2) \tag{27}$$

and therefore, according to Equation 24,

$$\bar{A} = A; \qquad \bar{D} = D \tag{28}$$

For multiplying media ($k \neq 0$) the corresponding solutions are (for α^2 cf. Equation 23):

$$\beta = (\Delta^2 + K_f^2 - K_{th}^2)/2C_{th}^2; \qquad \gamma = (\Delta^2 + K_f^2 - K_{th}^2)/2kC_f^2 \tag{29}$$

where

$$\Delta^2 \equiv +\sqrt{(K_f^2 + K_{th}^2)^2 + 4(k-1)K_f^2K_{th}^2} \tag{30}$$

or

$$\Delta^2 \cong K_f^2 + K_{th}^2 + 2(k-1)K_f^2K_{th}^2/(K_f^2 + K_{th}^2); \qquad (k - 1 \ll 1) \tag{31}$$

Then, according to Equation 24,

$$\bar{A} = \begin{pmatrix}0 & 1\\ -\bar{K}_f^2 & 0\end{pmatrix} \tag{32}$$

$$\bar{D} = \begin{pmatrix}0 & 1\\ \bar{K}_{th}^2 & 0\end{pmatrix} \tag{33}$$

with

$$\bar{K}_f^2 \equiv \alpha^2\Delta^2 - K_{th}^2 > 0 \tag{34}$$

$$\bar{K}_{th}^2 \equiv \alpha^2\Delta^2 + K_f^2 > 0 \tag{35}$$

Considering the fact that

$$[\bar{M}d]^\nu = \begin{pmatrix}\bar{A}^\nu d^\nu & 0\\ 0 & \bar{D}^\nu d^\nu\end{pmatrix} \tag{36}$$

and remembering Equation 18, it can be shown that

$$e^{\bar{M}d} = \begin{pmatrix}e^{\bar{A}d} & 0\\ 0 & e^{\bar{D}d}\end{pmatrix} \tag{37}$$

For the minors A, D, $\bar{D}$ relations like

$$A^{2\nu} = K_f^{2\nu}\cdot E \tag{38}$$

are valid, so that the following series expansions are obtained:

$$e^{Ad} = \begin{pmatrix}1 + \frac{1}{2!}K_f^2d^2 + \frac{1}{4!}K_f^4d^4 + \cdots; & \\ K_f^2d + \frac{1}{3!}K_f^4d^3 + \frac{1}{5!}K_f^6d^5 + \cdots; & \end{pmatrix}$$

$$\begin{pmatrix} d + \frac{1}{3!}K_f^2 d^3 + \frac{1}{5!}K_f^4 d^5 + \cdots \\ 1 + \frac{1}{2!}K_f^2 d^2 + \frac{1}{4!}K_f^4 d^4 + \cdots \end{pmatrix} \quad (39)$$

which actually is

$$e^{Ad} = \begin{pmatrix} \cosh K_f d; & \frac{1}{K_f}\sinh K_f d \\ K_f \sinh K_f d; & \cosh K_f d \end{pmatrix} \quad (40)$$

Similar relations hold for exp (Dd) and exp $(\bar{D}d)$. Only for exp $(\bar{A}d)$ in multiplying media the corresponding matrix is

$$e^{\bar{A}d} = \begin{pmatrix} \cos \bar{K}_f d; & \frac{1}{\bar{K}_f}\sin \bar{K}_f d \\ -\bar{K}_f \sin \bar{K}_f d; & \cos \bar{K}_f d \end{pmatrix} \quad (41)$$

Using these expressions for the minors of $\bar{M}$, the back transformation, according to Equation 21, gives

$$T(d) = \begin{pmatrix} e^{\bar{D}d}; & 0 \\ 0 & ; & e^{\bar{A}d} \end{pmatrix} - \alpha^2 \begin{pmatrix} e^{\bar{D}d} - e^{\bar{A}d}; & \beta(e^{\bar{D}d} - e^{\bar{A}d}) \\ \gamma(e^{\bar{D}d} - e^{\bar{A}d}); & -(e^{\bar{D}d} - e^{\bar{A}d}) \end{pmatrix} \quad (42)$$

which for non-multiplying media reduces to

$$T(d) = \begin{pmatrix} e^{Ad}; & 0 \\ \gamma(e^{Ad} - e^{Dd}); & e^{Dd} \end{pmatrix} \quad (43)$$

For thick shells

$$\left(\frac{\bar{K}_f}{\bar{K}_{th}} e^{\bar{K}_{th}d} \gg 1\right)$$

Equation 42 is approximated by

$$T(d) \cong \begin{pmatrix} (1-\alpha^2)e^{\bar{D}d}; & -\alpha^2\beta e^{\bar{D}d} \\ -\alpha^2\gamma e^{\bar{D}d}; & \alpha^2 \cdot e^{\bar{D}d} \end{pmatrix}$$

$$e^{\bar{D}d} \cong \frac{e^{\bar{K}_{th}d}}{2}\begin{pmatrix} 1; & 1/\bar{K}_{th} \\ \bar{K}_{th}; & 1 \end{pmatrix} \quad (44)$$

ADAPTION OF BOUNDARY VALUES BETWEEN MEDIA WITH DIFFERENT DIFFUSION CONSTANTS

Assume the following conventions:

The boundary values of all functions depending on the radius are designated by small and capital letters, corresponding to the inner and outer face, respectively. For interior points the argument ρ is given in parenthesis. The flux is designated by φ, Φ and $\varphi(\rho)$.

The central sphere and all the shells are numbered continuously, using roman and arabic figures for multiplying and nonmultiplying media, respectively. μ and ν denote any two successive shells, whereas n is used for the last (outside) shell. These numbers are applied as first subscripts.

According to the well known boundary conditions (continuity of flux and net current density) the relations

$$\Phi_\mu = \varphi_\nu; \qquad D_\mu \Phi_\mu' = D_\nu \varphi_\nu' \quad (45)$$

must hold for both fast and thermal neutrons at the interface between the two media μ and ν. Remembering Equation 7, it is found that

$$\begin{pmatrix} \psi_\nu \\ \psi_\nu' \end{pmatrix} = \begin{pmatrix} r_\nu & 0 \\ 1 & r_\nu/D_\nu \end{pmatrix}\begin{pmatrix} r_\nu & 0 \\ 1 & r_\nu/D_\mu \end{pmatrix}^{-1}\begin{pmatrix} \Psi_\mu \\ \Psi_\mu' \end{pmatrix} \quad (46)$$

Therefore an "adaption matrix" U shall be defined as

$$U\left(\frac{D_\mu}{D_\nu}\right) \equiv \begin{pmatrix} 1 & ; & 0 & ; & 0 & ; & 0 \\ \frac{1}{r_\nu}\left(1 - \frac{D_{\mu f}}{D_{\nu f}}\right); & & \frac{D_{\mu f}}{D_{\nu f}}; & & 0 & ; & 0 \\ 0 & ; & 0 & ; & 1 & ; & 0 \\ 0 & ; & 0 & ; & \frac{1}{r_\nu}\left(1 - \frac{D_{\mu th}}{D_{\nu th}}\right); & & \frac{D_{\mu th}}{D_{\nu th}} \end{pmatrix} \equiv U^{-1}\left(\frac{D_\nu}{D_\mu}\right) \quad (47)$$

This relates v_ν to V_μ according to

$$v_\nu = U(D_\mu/D_\nu) \cdot V_\mu \quad (48)$$

CRITICALITY CONDITION AND FLUX DISTRIBUTIONS

Consider a reactor composed of a central sphere and an arbitrary number of concentric shells, each consisting of a medium with constant diffusion parameters. The vector V_n (at the outer face of the whole system) is then related to the vector v_1 (at the centre) by a product of transfer matrices T and adaption matrices U. For a special system numbered by 1, II, III, 4 for instance this relation is

$$V_4 = T_4(d_4)U\left(\frac{D_{III}}{D_4}\right)T_{III}(d_{III})U\left(\frac{D_{II}}{D_{III}}\right)T_{II}(d_{II})U\left(\frac{D_I}{D_{II}}\right)T_I(d_I)\cdot v_1 \quad (49)$$

From the boundary conditions $\Phi_{nf} = \Phi_{nth} = 0$ and $\varphi_{1f}' = \varphi_{1th}' = 0$ it follows that

$$\begin{pmatrix} 0 \\ \Psi_{nf}' \\ 0 \\ \Psi_{nth}' \end{pmatrix} = W \begin{pmatrix} 0 \\ \varphi_{1f} \\ 0 \\ \varphi_{1th} \end{pmatrix} \quad (50)$$

where W is the product of all matrices in Equation 49. Equation 50 contains the criticality condition, Equation 52, and the ratio of the fast and thermal fluxes at the centre, Equation 53. Explicit relations are:

$$\begin{aligned} w_{12}\varphi_{1f} + w_{14}\varphi_{1th} &= 0 \\ w_{32}\varphi_{1f} + w_{34}\varphi_{1th} &= 0 \end{aligned} \quad (51)$$

Therefore

$$w_{12}w_{34} - w_{32}w_{14} = 0 \quad (52)$$

and

$$\varphi_{1th}/\varphi_{1f} = -w_{12}/w_{14} \quad (53)$$

φ_{1f} can be arbitrarily chosen, because the power level is a free parameter.

If the criticality condition, Equation 52, is not fulfilled, any diffusion parameters or dimensions must be changed. It is assumed that Wigner's[3] perturbation

theory, (p. 372–83), due to its flexibility and elegance, will be a helpful means for this purpose.

Starting with the known value of v_1, all amplitudes and their derivatives can be determined by successive multiplication with the transfer and adaption matrices, as shown for instance in Equation 49. If the values in the interior of the shells must be known, the transfer matrices can be split up into parts, preferably corresponding to equal thicknesses.

ACKNOWLEDGEMENTS

The author would like to express his gratitude to his colleagues Mr. F. Alder, Mr. V. O. Eriksen and Mr. R. Meier for helpful discussions.

REFERENCES

1. Spooner, R. B., *Using a Reactor Simulator for Design Analysis*, Nucleonics *12*, Nr. 4: 36–9 (1954).
2. Brillouin, L., *Wave Propagation in Periodic Structures*, McGraw-Hill Co., Inc., New York (1946).
3. Glasstone, S. and Edlund, M. C., *The Elements of Nuclear Reactor Theory*, D. Van Nostrand Co., Inc., New York (1952).
4. Aitken, A. C. *Determinants and Matrices*, Oliver and Boyd, Edinburgh (1946).
5. Wigner, E., *Gruppentheorie und ihre Anwendung auf die Quantenmechanik der Atomspektren*, Fr. Vieweg & Sohn, Braunschweig (1931).
6. Courant, R. and Hilbert, D., *Methoden der Mathematischen Physik I*, Julius Springer, Berlin (1931).

Absorption and Multiplication of the Moderating Neutrons in the Two-Group Theory

By A. D. Galanin, USSR

In a thermal reactor, a certain percentage of neutrons are captured in the slowing-down process, and nuclear fission occurs. Consider that the number of such neutrons is small and their capture takes place mainly at energies below the first resonance level of uranium-238. Also assume, at the beginning, that the fission and capture cross section in this energy range obeys the $1/v$ law. One may readily go over to a more general instance of deviations from the $1/v$ law; but then, the formula becomes less obvious (this subject is discussed in the last part of this paper).

EQUATION FOR THE CASE OF ONE MEDIUM

If neutron capture in the slowing-down process is small, then the following diffusion equation is applicable

$$\Delta n - \alpha(\tau)n - \frac{n}{L^2} = \frac{\partial n}{\partial \tau} \tag{1}$$

where $L = L(\tau)$ is diffusion length for neutrons of age τ, and $\alpha(\tau)$ differs from zero only at energy near the uranium-238 resonance maxima. Assuming the $1/v$ law to be valid and that the transport mean free path does not depend on the energy, we obtain

$$\frac{1}{L^2} = \frac{1}{L_T^2}\sqrt{\frac{E_T}{E}} \tag{2}$$

where T denotes values pertaining to the thermal region.

Introducing the new function

$$n(\mathbf{r},\tau) = \tilde{n}(\mathbf{r},\tau)e^{\chi(\tau)} \tag{3}$$

where

$$\chi(\tau) = -\int_\tau^{\tau_T}\left[\alpha(\tau) + \frac{1}{L^2(\tau)}\right]d\tau \tag{4}$$

we obtain instead of Equation 1

$$\Delta\tilde{n} = \frac{\partial \tilde{n}}{\partial \tau} \tag{5}$$

If Equation 2 occurs then

$$\int_\tau^{\tau_T}\frac{d\tau}{L^2} = \epsilon\left(1 - \sqrt{\frac{E_T}{E}}\right) \tag{6}$$

where

$$\epsilon = \frac{2\overline{(d\tau/dy)}}{L_T^2}$$

assuming

$$\overline{\frac{d\tau}{dy}} = \frac{\overline{l_s l_t}}{3\xi}; \qquad y = \ln\frac{E_0}{E} \tag{7}$$

and the bar denotes the averaging over the energy region where the neutron capture takes place.

The initial condition for the function $n(\mathbf{r},\tau)$ has the form

$$n(\mathbf{r},0) = \frac{\eta\theta}{T_0}N + \int_0^{\tau_T}\eta\theta\frac{n(\tau)}{L^2}d\tau \tag{8}$$

where T_0 is the thermal neutrons lifetime, N the thermal neutrons density, θ the thermal utilization factor, η the number of fast neutrons produced in the capture of one thermal neutron of uranium.

Upon transforming Equation 3, considering Equation 2, and assuming that the neutron capture occurs mainly below the first resonance level of uranium-238, we obtain

$$\tilde{n}(0) = \frac{ke^{-\epsilon}N}{T_0} + k\int_{e^{-\epsilon}}^1 \tilde{n}(z)\,dz \tag{9}$$

where $k = \eta\theta\varphi$ is the multiplication factor, $\varphi = e^{-\int\alpha(\tau)d\tau}$ the resonance escape probability, and the variable of integration z is connected with the energy as

$$z = e^{-\epsilon\sqrt{\frac{E_T}{E}}}$$

Substituting once again

$$\tilde{n} = \frac{1}{T_0}\tilde{\tilde{n}} \tag{10}$$

and further omitting the sign $\approx$, we obtain the following system of equations for determining the critical size and the neutron density distribution

$$\Delta N - \frac{N}{L_T^2} = -\frac{n(\tau_T)}{L_T^2}, \qquad \Delta n = \frac{\partial n}{\partial \tau};$$
$$n(0) = ke^{-\epsilon}N + k\int_{e^{-\epsilon}}^1 n(z)\,dz \tag{11}$$

The two-group treatment, as we know, consists in the use of the approximate formula:

$$\frac{\partial n}{\partial \tau} = -\frac{n(0) - n(\tau_T)}{\tau_T}$$

Since neutron absorption in the slowing-down process

Original language: Russian.

takes place mainly at low energies, the initial condition should be written:

$$n(0) = ke^{-\epsilon}N + k(1 - e^{-\epsilon})n(\tau_T)$$

Thus we obtain further

$$n \equiv n(\tau_T); \qquad \tau \equiv \tau_T$$

$$\Delta N - \frac{N}{L^2} = -\frac{n}{L^2}$$

$$\Delta n - \frac{n}{\tau}[1 - k(1 - e^{-\epsilon})] = -\frac{ke^{-\epsilon}N}{\tau} \quad (12)$$

If we introduce the effective τ and k:

$$\tau_{eff} = \frac{\tau}{1 - k(1 - e^{-\epsilon})}; \qquad k_{eff} = \frac{ke^{-\epsilon}}{1 - k(1 - e^{-\epsilon})} \quad (13)$$

then the equations take the form of the usual two-group equations:

$$\Delta N - \frac{N}{L^2} = -\frac{n}{L^2}$$

$$\Delta n - \frac{n}{\tau_{eff}} = -\frac{k_{eff}N}{\tau_{eff}} \quad (14)$$

Thus, neutron capture and multiplication in the slowing-down process are fully taken into account by the introduction, according to Equation 13, of the effective k and τ into the two-group theory.

Substituting k_{eff} and τ_{eff} in the approximate formula

$$\alpha^2 = \frac{k_{eff} - 1}{L^2 + \tau_{eff}}$$

we obtain

$$\alpha^2 = \frac{k - 1}{L_{eff}^2 + \tau}$$

where

$$L_{eff}^2 = L^2[1 - k(1 - e^{-\epsilon})] < L^2$$

We have thus derived the physically evident result that consideration of the neutron capture in the slowing-down process is reduced to a decrease of the migration area.

EQUATION FOR TWO MEDIA

Examine a reactor with a reflector. The following boundary conditions are observed at the boundary of the reflector:

For thermal neutrons (subscript 1 pertains to the active zone, 2 to the reflector; the prime denotes the derivative in the direction of the normal to the boundary):

$$N_1 = N_2; \qquad N_1' = p_{12}N_2'; \qquad p_{12} = \frac{D_2}{D_1} \quad (15)$$

For the slowing-down neutrons (n coincides with the function n in Equation 1)

$$n_1(\tau_1) = b_{12}n_2(\tau_2)$$
$$n_1'(\tau_1) = c_{12}n_2'(\tau_2) \quad (16)$$

where τ_1 and τ_2 correspond to the same energy, and b_{12}, c_{12} are equal

$$b_{12} = \frac{l_{s2}}{l_{s1}}\frac{\xi_1}{\xi_2}$$

$$c_{12} = \frac{l_{s2}l_{t2}}{l_{s1}l_{t1}}\frac{\xi_1}{\xi_2} \quad (17)$$

Here l_s is the scattering mean free path, l_t the transport mean free path, ξ the mean logarithmic energy loss. The quantities b_{12}, c_{12}, are generally energy functions. Substituting Equations 3 and 10 we obtain the following equation (again omitting the signs $\approx$ and T in L_T^2)

$$\Delta N_1 - \frac{N_1}{L_1^2} = -\frac{n_1(\tau_{1T})}{L_1^2}; \qquad \Delta N_2 - \frac{N_2}{L_2^2} = -\frac{n_2(\tau_{1T})}{L_1^2 p_{12}}$$

$$\Delta n_1 = \frac{\partial n_1}{\partial \tau_1}; \qquad \Delta n_2 = \frac{\partial n_2}{\partial \tau_2} \quad (18)$$

Their boundary conditions are:

$$n_1(\tau_1) = b_{12}^* n_2(\tau_1); \qquad n_2'(\tau_1) = c_{12}^* n_2'(\tau_1) \quad (19)$$

where

$$b_{12}^* = \frac{l_{s2}}{l_{s1}}\frac{\xi_1}{\xi_2}e^{-\chi_1(F)+\chi_2(E)}$$

$$c_{12}^* = \frac{l_{s2}l_{t2}}{l_{s1}l_{t1}}\frac{\xi_1}{\xi_2}e^{-\chi_1(E)+\chi_2(E)} \quad (20)$$

The two-group treatment may be applied to the system of Equations 18 with the boundary conditions of Equation 19 in those cases when (excepting the usual conditions of the two-group treatment applicability) the coefficients b_{12}^* and c_{12}^* (see Equation 20) do not depend strongly on energy. In this case it is well to consider that for the functions $n_1(\tau_1)$, $n_2(\tau_2)$ in the boundary conditions Equation 19 the coefficients b_{12}^*, c_{12}^* are taken not for the thermal energy, but have been averaged according to the scale τ. Thus, we have a system of two-group equations

$$\Delta N_1 - \frac{N^1}{L_1^2} = -\frac{n_1}{L_1^2}; \qquad \Delta N_2 - \frac{N_2}{L_2^2} = -\frac{n_2}{L^2 p_{12}}$$

$$\Delta n_1 - \frac{n_1}{\tau_{eff\,1}} = -\frac{k_{eff}}{\tau_{eff\,1}}N_1; \qquad \Delta n_2 - \frac{n_2}{\tau_2} = 0 \quad (21)$$

$$n_1 = \bar{b}_{12}^* n_2$$
$$n_1' = \bar{c}_{12}^* n_2' \quad (22)$$

Since averaging the coefficients in the boundary conditions is approximate, certain simplifications are possible.

Upon substitution

$$\bar{b}_{12}^* n_2 \longrightarrow n_2$$

the boundary conditions of Equation 22 will be similar to Equation 15

$$n_1 = n_2; \qquad n_2' = s_{12}n_2' \quad (23)$$

Replacing in $s_{12} = \bar{c}_{12}^* \bar{b}_{12}^*$ the average product by the product of the averages (using the weak dependence of all quantities contained in b and c upon energy) we have:

$$s_{12} = \frac{\bar{l}_{t2}}{\bar{l}_{t1}} \tag{24}$$

where $\bar{l}_t$ is the transport mean free path value averaged according to scale τ.

Equations 21 will become

$$\Delta N_1 - \frac{N_1}{L_1^2} = -\frac{n_1}{L_1^2}; \quad \Delta N_2 - \frac{N_2}{L_2^2} = -\frac{Bn_2}{p_{12}L_1^2} \tag{25}$$

$$\Delta n_1 - \frac{n_1}{\tau_{eff\,1}} = -\frac{k_{eff}N_1}{\tau_{eff\,1}}; \quad \Delta n_2 - \frac{n_2}{\tau_2} = 0$$

where $B = (\bar{b}_{12}^*)^{-1}$. Again using the slow dependence of all the quantities contained in b_{12}^* on the energy, we may describe B by a more convenient formula for practical purposes.

$$B = \frac{\tau_1}{\tau_2} s_{12} \frac{\overline{e^{-\chi_2(E)}}}{\overline{e^{-\chi_1(E)}}} \tag{26}$$

If there is no resonance absorption in the reflector, then approximately (the mean value in Equation 26 is taken by the energy logarithm):

$$\overline{e^{-\chi_2(E)}} \cong e^{-\epsilon_2}(1 + 0.1\epsilon_2) \tag{27}$$

Assuming that resonance absorption in uranium-238 occurs mainly at 7 ev, then the same averaging for the active zone yields ($\epsilon_1 \ll 1$):

$$\overline{e^{-\chi_1(E)}} \cong e^{-\epsilon_1}[0.36 + 0.64\varphi + \epsilon_1(0.01 + 0.1\varphi)] \tag{27'}$$

CONSIDERATION OF THE DEVIATION FROM THE 1/v LAW

We continue to consider that the capture in the slowing down process is small, as otherwise the two-group treatment is not applicable. If we abandon the assumption that the $1/v$ law is valid for the fission and capture, then, as is readily seen, Equation 13 changes as follows:

$$k_{eff} = \frac{ke^{-\epsilon}}{1 - k(1 - e^{-\epsilon})\,\delta}$$

$$\tau_{eff} = \frac{\tau}{1 - k(1 - e^{-\epsilon})\,\delta} \tag{28}$$

where

$$\epsilon = \int_0^{\tau_T} \frac{d\tau}{L^2(\tau)} \quad \text{and} \quad \delta = \frac{\overline{(\eta\theta)}}{(\eta\theta)_T} \tag{29}$$

The bar denotes the averaging of $\eta\theta$ over the energy region where the neutron absorption takes place:

$$\overline{\eta\theta} = \int_0^{\tau_T} \eta(\tau)0(\tau)e^{-\int_0^{\tau} \frac{d\tau'}{L^2(\tau')}} \frac{d\tau}{L^2(\tau)}$$

In this case one may consider not only the deviation of the fission and capture cross section from the $1/v$ law, but also the dependence upon energy of the lamp effect in thermal absorption [in $\theta(\tau)$] and the transport mean free path l_t in $L^2(\tau)$. The integrals can be computed only numerically. Equations 27 and 27′ do not change, but ϵ should be computed by Equation 29.

Application of the Method of Effective Boundary Conditions for Calculating the Critical Dimensions of Reactors

By A. D. Galanin, USSR

When the size of a reactor greatly exceeds the neutron moderation length $\sqrt{\tau}$, the density distribution of the thermal neutrons $N(r)$ in the homogeneous multiplying medium may be described by the one-group equation

$$\Delta N(r) + \alpha^2 N(r) = 0 \qquad (1)$$

where the "Laplacian" α^2 equals

$$\alpha^2 = \frac{k-1}{L^2 + k\tau} \qquad (1')$$

k is the multiplication factor, L the reactor diffusion length.

Equation 1 is most readily obtained when the thermal neutron density equation is written thus:

$$\Delta N(r) - \frac{N(r)}{L^2} + \frac{k}{L^2}\int W(r,r')N(r')\,dr' = 0 \qquad (2)$$

where $W(r,r')$ is the probability that the fast neutron produced at point r' in the capture of the thermal neutron will slow down to thermal energy at point r. Density $N(r)$ substantially differs within the range of the order of the system's dimensions, whereas $W(r,r')$ differs within the range of the order $\sqrt{\tau}$. Therefore, $N(r)$ the integral in Equation 2 may be regarded as a slow changing function and may be expanded into the powers $|r - r'|$:

$$N(r') = N(r) + \sum_{i=1}^{3}(x_i' - x_i)\frac{\partial N}{\partial x_i} + \frac{1}{2}\sum_{i,k=1}^{3}(x_i' - x_i)(x_k' - x_k)\frac{\partial^2 N}{\partial x_i \partial x_k}$$

Upon substitution of this expansion in Equation 2, and integration, we obtain Equation 1 if we define

$$\tau = \tfrac{1}{6}\overline{r^2} = \tfrac{1}{2}\overline{x^2} = \tfrac{1}{2}\int W(r,r')(x' - x)^2\,dr$$

and consider that

$$\int W(r,r')\,dr' = 1$$

The deviation from Equation 1, as may be seen from the above, will be substantial only near the boundary between the multiplying medium and the reflector. It is therefore worth while to examine separately the layer whose thickness is of the order of $\sqrt{\tau}$ near the boundary between the multiplying medium and the reflector, and from this examination to establish a certain effective boundary condition so that Equation 1, together with this boundary condition, would yield the correct values of the critical size and correct distribution of neutron density for the systems in question. Since the thickness of the layer is considerably smaller than the dimensions of the multiplying medium, the boundary condition may be deduced by examining neutron density distribution for the case of a plane boundary, using the two-group theory.*

Thus, the problem may be formulated as follows: by the two-group treatment we solve the problem of the neutron density distribution near the boundary between the infinite multiplying medium (with the multiplication factor $k = 1$, and the other properties the same as in the real system) and the reflector, and obtain the boundary condition

$$\lambda = -\left(\frac{1}{N}\frac{\partial N}{\partial x}\right)_{x=0} \qquad (3)$$

where N is the neutron density in the multiplying medium far from the boundary $x = 0$. Then the thermal neutron density distribution in the reactor and the critical size will be found by solving Equation 1 with the boundary condition

$$\lambda = -\frac{1}{N}\frac{\partial N}{\partial \nu} \qquad (3')$$

where ν is the normal to the multiplying medium surface.

Let us compute λ for plane geometry by the two-group treatment. Assuming that the infinite multiplying medium extends from $x < 0$, and the reflector from $x > 0$, the two-group equation is written thus:

In the multiplying medium

$$\Delta N_1 - \frac{N_1}{L_1^2} = -\frac{n_1}{L_1^2}, \qquad \Delta n_1 - \frac{n_1}{\tau_1} = -\frac{kN_1}{\tau_1} \qquad (4)$$

In the reflector

$$\Delta N_2 - \frac{N_2}{L_2^2} = -\frac{n_2}{L_1^2}\frac{B}{p}, \qquad \Delta n_2 - \frac{n_2}{\tau_2} = 0 \qquad (5)$$

Original language: Russian.

* In the present case of large systems, the two-group treatment does not introduce any appreciable errors and is quite justified.

where N and n are respectively the densities of the slow and fast neutrons; L_1^2, L_2^2 are the squares of the diffusion lengths; τ_1, τ_2 are the squares of the slowing down lengths; $p = D_2/D_1$ is the ratio of the thermal neutron diffusion coefficients. In Equation 5

$$B = \frac{l_{s_1}}{l_{s_2}} \cdot \frac{\xi_2}{\xi_1} \tag{6}$$

where l_s is the scattering mean free path averaged by the energy logarithm, and ξ is a similarly averaged mean logarithm energy loss. Equations 4 and 5 should be supplemented by boundary conditions: on the boundary of the multiplying medium and the reflector

$$\begin{aligned} N_1 &= N_2, & n_1 &= n_2 \\ N_1' &= pN_2' - tN_1, & n_1' &= sn_2' \end{aligned} \tag{7}$$

($s = \bar{l}_{t_2}/\bar{l}_{t_1}$ is the ratio of the averaged transport mean free paths); and on the boundary of the reflector, or more precisely on its extrapolated boundary, at $x = \Delta$:

$$N_2 = n_2 = 0 \tag{8}$$

The boundary conditions of Equation 7 take into account that a thin absorbing wall may be placed between the multiplying medium and the reflector. Its influence is considered by introducing t

$$t = \frac{3d}{\bar{l}_{t_1} l_{co}}$$

where d is the thickness of the wall, and l_{co} is the neutron capture mean free path in it.

The solutions of Equations 5 and 6 in the present case have the forms:

$$N_1 = 1 - \lambda x + be^{\beta x}$$

$$N_2 = A_1 e^{-\frac{x}{L_1}} + B_{1\gamma_1} e^{-\frac{x}{\sqrt{\tau_1}}} + A_2 e^{\frac{x}{L_1}} + B_{2\gamma_1} e^{\frac{x}{\sqrt{\tau_1}}}$$

$$n_1 = 1 - \lambda x - b_{\gamma_2} e^{\beta x}, \quad n_2 = B_1 e^{-\frac{x}{\sqrt{\tau_1}}} + B_2 e^{\frac{x}{\sqrt{\tau_1}}} \tag{9}$$

Here

$$\beta_2 = \frac{1}{L_1^2} + \frac{1}{\tau_1} \tag{10}$$

$$\gamma_2 = \beta^2 L_1^2 - 1, \qquad \gamma_3 = \frac{BL_2^2}{pL_1^2}\left(1 - \frac{l_2^2}{\tau_2}\right)^{-1} \tag{11}$$

and A_1, B_1, A_2, B_2, λ, l are the coefficients to be deduced from the boundary conditions of Equations 7 and 8. It is clear that λ introduced in Equation 9 coincides with λ obtained from Equation 3 as the functions N satisfies asymptotically, at $x < 0$ and $|x| \ll 1/\beta$, Equation 1 with $k = 1$ and

$$\lambda = -\frac{1}{N}\frac{\partial N}{\partial x}$$

From Equation 7, 8 and 9 one can readily obtain:

$$\lambda = s\mu' - \gamma_2(\beta + s\mu')b \tag{12}$$

where

$$b = \frac{-p\zeta' - p\gamma_3(\mu' - \zeta') + s\mu' - t}{\beta(1 + \gamma_2) + p\zeta' + \gamma_2 s\mu' - p\gamma_2\gamma_3(\mu' - \zeta') + t} \tag{13}$$

$$\zeta' = \zeta \coth \zeta\Delta, \qquad \mu' = \mu' \coth \mu\Delta,$$

$$\mu = \frac{1}{\sqrt{\tau}}, \qquad \zeta = \frac{1}{L_2} \tag{14}$$

Upon deriving the expression for λ it may be substituted in the boundary conditions for Equation 1 which will have the form:

(1) In the case of plane geometry:

$$\lambda = -\frac{1}{N}\frac{\partial N}{\partial z} \tag{15}$$

(2) In the case of spherical geometry:

$$\lambda = -\left(\frac{1}{N}\frac{\partial (rN)}{\partial r}\right)_{r=R} \tag{16}$$

where R is the sphere radius.

(3) In the case of cylindrical geometry:

$$\lambda = -\left(\frac{1}{N\sqrt{r}}\frac{\partial (\sqrt{r}N)}{\partial r}\right)_{r=R} \tag{17}$$

where R is the cylinder radius.

In the case of spherical and cylindrical geometry, the use of the functions $rN(r)$ and $\sqrt{r}\,N(r)$ instead of $N(r)$ permits approximate allowance for the surface curve. The use of Equations 15, 16 and 17 leads to the following equations for determining the critical size:

(1) Slab reactor of thickness $2H$ with the same reflectors on its bases:

$$\alpha \tan \alpha H = \lambda \tag{18}$$

(2) Spherical reactor with radius R

$$\alpha \cot \alpha R = -\lambda \tag{19}$$

(3) Cylindrical reactor with radius R

$$\frac{\alpha J_1(\alpha R)}{J_0(\alpha R)} = \lambda + \frac{1}{2R} \tag{20}$$

where J_0 and J_1 are zero and first order Bessel functions.

Of particularly great interest is the use of the effective boundary conditions method in examining problems of the critical size of a cylindrical reactor surrounded by a reflector on all sides. In this case an analytical solution of the problem is rather difficult, as one cannot separate the variables, whereas the effective boundary conditions method yields quick results.

In the first approximation one may consider that the boundary condition on the cylinder side surface does not depend on density distribution along the height, and vice versa. From Equations 18, 20 we have†

† If the properties of the reflector on the cylinder bases differ, then Equation 22 should be replaced by

$$\tan \alpha_s H = -\frac{(\lambda_{1s} + \lambda_{2s})\alpha_s}{\lambda_{1s}\lambda_{2s} - \alpha_s^2}$$

where λ_{1s} and λ_{2s} are the boundary conditions on two bases.

$$\frac{\alpha_z J_1(\alpha_z R)}{J_0(\alpha_z R)} = \lambda_r + \frac{1}{2R} \tag{21}$$

$$\alpha_z \tan \alpha_z H = \lambda_z, \qquad \alpha_r^2 + \alpha_z^2 = \alpha^2 \tag{22}$$

In these equations λ_r and λ_z are given (they are determined by the properties of the reflector on the side surface and bases, and are computed by Equation 12); α^2 is also given. Thus, Equations 21 and 22 are a system of three equations containing the four unknown quantities R, H, α_z, α_r. From them, one may obtain R as a function of H.

The solution of the problem by this method may be appreciably more accurate if one considers the dependence of the side surface boundary conditions on neutron density distribution along the height (that is, on α_z), and vice versa: For this purpose, instead of the semi-infinite multiplying medium, considered in deducing Equations 12, 13 and 14, we shall examine the slab, which is infinite in the direction perpendicular to the boundary (axis X), but limited on one of the directions lying in the dividing plane (axis Z). Then, over sufficiently large distances from the boundary along axis $X(|x| \gg 1/\beta)$ and over the entire region along the axis (with exception of a small part adjoining the boundary along axis Z) the neutron density dependence on Z may be regarded proportional to $\cos \alpha_z z$. One can readily see that as a result of the action of the Laplace operator on N and n in the left-hand side of Equations 4 and 5, $\Delta = \Delta_x + \Delta_z$ will be replaced by $\Delta_x + \alpha_z^2$. Consequently, the solution of the problem of determining λ_r is reduced to the one we have already discussed, and Equations 12–14 will be applicable if the following change is made in them:

$$\zeta \to \sqrt{\zeta^2 + \alpha_z^2}; \qquad \mu \to \sqrt{\mu^2 + \alpha_z^2}; \qquad \beta \to \sqrt{\beta^2 + \alpha_z^2} \tag{23}$$

The quantity λ_r computed by Equations 12–14 and 23 thus becomes a function of α_z. Substituting it in Equation 21 one may with the given R obtain α_r as a function of α_z. On the other hand, by similar argumentation, one may determine λ_z as a function of α_r and using Equation 22, deduce α_z as a function of α_r with H given. In plane α_r, α_z plot two functions $\alpha_r = \alpha_r(\alpha_z)$ and $\alpha_z = \alpha_z(\alpha_r)$ and determine the point of their intersection. This point will yield definite values of α_r, α_z and of $\alpha^2 = \alpha_r^2 + \alpha_z^2$. Thereby the system with the given R and H will be critical if its Laplacian α^2 deduced from Equation 1'‡ coincides with the one derived from the above examination. If this result is not obtained, then R or H should be changed and the above process should be repeated until the required value of the Laplacian is obtained.

The error of the effective boundary conditions method may be found by comparing its results with those of the exact solutions of the two-group equations. Such solutions may be obtained, for example, for a cylindrical reactor without a reflector on its bases. A comparison shows that in this case when $\alpha_r \sim 0.025$ and $\sqrt{\tau} \sim 10$, the error is about 5 to 10 per cent in α_r; and when $\alpha_r \sim 0.015$ about 2 per cent in α_r.

The accuracy of the effective boundary conditions method for the problem of the critical size of a cylinder reactor surrounded by a reflector on all sides may be evaluated by a comparison with the exact computation by the numerical solution of the two-group equations. This comparison shows that the effective boundary conditions method yields quite satisfactory accuracy also for this problem even in the case of relatively small reactors ($\alpha \sim 0.025$).

‡ For greater, accuracy, α^2 is best to be computed not by Equation 1' but by the transcendental equation $1 + \alpha^2 L^2 = ke^{-\alpha^2 \tau}$.

Upper and Lower Bounds for Critical Size According to One-Group Diffusion Theory

By R. T. Ackroyd,* UK

In the preliminary stages of the design of reactors and chemical plants approximate calculations have to be made for the critical size, before embarking on a detailed design, requiring more refined calculations. For many of these approximate calculations the use of one or two group diffusion theory is appropriate on physical grounds. However, although the differential equations and boundary conditions of diffusion theory are simple, there are only a few shapes of fissile core for which exact and simple formulae for critical size are available. For fissile cores bounded by co-ordinate surfaces of an orthogonal co-ordinate system solutions can be obtained, but usually they are not suitable for numerical work. The simplest way out of this difficulty is to set up equations for the critical size on physical grounds, but one is then faced with the difficulty of estimating the errors made in this approach.

In this note a simple method of calculating upper and lower bounds for critical size is discussed. It is based on a variational principle, and so the simple upper and lower bounds can be improved, if required. In principle the method is to obtain upper and lower bounds for the critical Laplacian of a fissile core, and then to turn these bounds into upper and lower bounds for critical size. As a simple illustration of the method upper and lower bounds are given for the critical Laplacian of bare and reflected cylinders of elliptical cross section; and for the bare cylinder these bounds are turned into bounds for the critical dimensions. In the examples the cylinders are assumed to be infinitely long to keep the discussion brief, but to emphasize the fact that the methods used apply to three-dimensional systems, a process is outlined for obtaining lower bounds for the critical Laplacian of a finite circular cylinder, which is reflected on all sides.

THEORY

Upper Bound for Critical Laplacian

Consider the fissile region V_1 and the reflecting region V_2 of Fig. 1. Let λ^2 be the critical Laplacian for V_1, and let $-\mu^2$ be the Laplacian of V_2. If ϕ_1 and ϕ_2 are guesses for the fluxes ψ_1 and ψ_2 in the regions V_1 and V_2 respectively then

$$\lambda^2 \leq \frac{\int_{V_1} D_1(\nabla\phi_1)^2\,dV + \int_{V_2} D_2[(\nabla\phi_2)^2 + \mu^2\phi_2^2]\,dV}{\int_{V_1} D_1\phi_1^2\,dV} \tag{1}$$

where D_1 and D_2 are the diffusion coefficients respectively for V_1 and V_2. In general the functions ϕ_1 and ϕ_2 need only satisfy the boundary conditions

$$\left.\begin{array}{l}(a)\ \phi_1 \text{ and } \phi_2 \text{ are continuous across the interface } S \text{ of regions } V_1 \text{ and } V_2 \\ (b)\ \phi_2 \text{ vanishes on } S_2 \text{ the extrapolated boundary of } V_2\end{array}\right\} \tag{2}$$

In particular if the perfect guess

$$\left.\begin{array}{l}\phi_1 = \psi_1 \\ \phi_2 = \psi_2\end{array}\right\} \tag{3}$$

is made, then the equality sign is attained in Equation 1. Formula 1 is a potentially useful one as with appropriate choices of ϕ_1 and ϕ_2 the critical Laplacian λ^2 can be approximated to from above as near as desired. Furthermore the guesses for the fluxes need not satisfy the boundary condition

$$D_1\left(\frac{\partial\phi_1}{\partial n}\right)_{S_1} = D_2\left(\frac{\partial\phi_2}{\partial n}\right)_{S_1} \tag{4}$$

where n is a normal to the surface S_1. The boundary condition (Equation 4) is satisfied by the perfect guess (Equation 3). Thus in obtaining an upper bound for the critical Laplacian from Formula 1, there is one boundary condition less to contend with than when the exact value of the critical Laplacian is sought by the standard method of finding solutions of the differ-

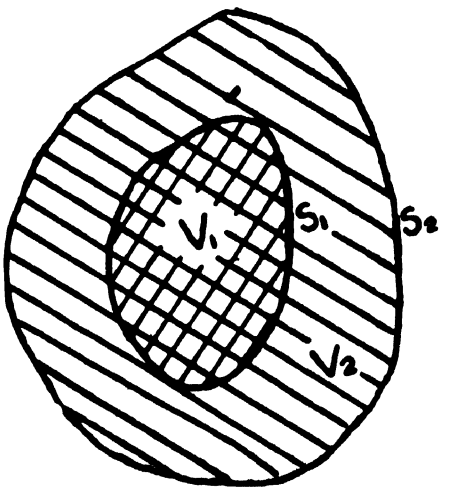

Figure 1. Reflected reactor of arbitrary shape

* U.K.A.E.A., Risley.

ential equations of one group diffusion theory which satisfy the boundary conditions of type (2), and the boundary condition of type (4).

Lower Bound for the Critical Laplacian

Two simple methods of constructing lower bounds for the critical Laplacian are given. The first method is a geometrical one and is based on the intuitive idea that the more symmetrical a fissile body of constant volume is made, the smaller its critical Laplacian becomes. The geometrical process which is considered here for making bodies more symmetrical is called Steiner Symmetrization.[1]

Steiner Symmetrization

Consider, for example, the body of Fig. 2a and the plane of Fig. 2b. The body is symmetrized with respect to the plane (the plane of symmetrization) in the following way. Let NM be the length of the intercept that the body makes with a perpendicular to the plane from a point P in the plane. At P erect perpendiculars PQ and PR each of length $NM/2$. The surface generated by Q and R, as P moves over the plane of symmetrization, defines the body Fig. 2b. This body is said to be the symmetrized form of the body Fig. 2a with respect to the given plane. The example given illustrates the theorem that symmetrization of a body leaves the volume of the body unchanged, but reduces the surface area. One therefore expects that symmetrization of a fissile body should reduce its critical Laplacian. For the special cases of (*a*) bare systems, and (*b*) reflected systems for which the diffusion coefficients of the core and reflector are equal, simple proofs can be given. For bare systems the proof is an extension to three-dimensions of the proof, due to Pólya,[1] for the gravest frequency of a membrane with clamped edges. If λ^2 is the critical Laplacian for the core of the fissile system F, (e.g. that of Fig. 2a), then the critical Laplacian for the core of the symmetrized form of F, viz F^*, (e.g. the body Fig. 2b), satisfies the inequality

$$\lambda^{*2} \leq \lambda^2 \tag{5}$$

To illustrate the use of Steiner symmetrization in obtaining a lower bound for the critical Laplacian consider the following example. In Fig. 3a a bare, hemispherical lump of fissile material is shown. If a plane parallel to the base of the hemisphere is taken to be the plane of symmetrization, then the hemisphere is transformed into an oblate spheroid Fig. 3b, for which the critical Laplacian can be calculated by the standard analytical method. If λ_{os}^2 and λ_{hs}^2 denote respectively the critical Laplacians for the oblate spheroid and the hemisphere then

$$\lambda_{hs}^2 \geq \lambda_{os}^2$$

If the result for the critical Laplacian of the oblate spheroid is not available, a lower bound for λ_{hs}^2 can be got by symmetrizing the oblate spheroid into a sphere. Since symmetrization does not change volume, the radius of the sphere is, $\alpha/\sqrt[3]{2}$, if α is the radius of the

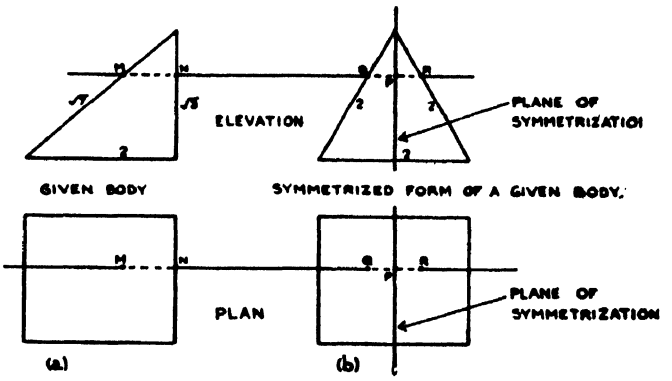

Figure 2. Example of Steiner symmetrization

hemisphere. A lower bound for the critical Laplacian λ_{hs}^2 is therefore

$$(\sqrt[3]{2} \cdot \pi/\alpha)^2 \leq \lambda_{hs}^2 \tag{6}$$

As repeated Steiner symmetrization of a body (of finite dimensions) makes its shape more and more symmetrical, ultimately the given body is transformed into a sphere by sufficient symmetrizations. Thus for bodies of given volume, the critical Laplacian according to one group diffusion theory is least for a sphere. This means critical mass is least for a sphere.

Auxiliary Systems

Although a direct application of the Formula 1 gives only an upper bound for the critical Laplacian of the fissile core of a reflected system, the formula can be used to find a lower bound for the critical Laplacian. A very simple way of achieving this is to make use of auxiliary systems. Such systems are chosen (if possible) to be similar in many respects to the given system, but they differ from the given system in that the critical Laplacians of the auxiliary systems can be calculated exactly by simple means.

To illustrate the method consider the given system Fig. 4 to be a circular cylinder of finite length with an infinite reflector. Three auxiliary systems are shown in Fig. 5. If λ^2 is the critical Laplacian of the given system, and λ_1^2, λ_2^2, λ_3^2 are the critical Laplacians for the auxiliary systems I, II, and III respectively, then

$$\lambda^2 \geq \frac{l\lambda_1^2 + m\lambda_2^2 + n\lambda_3^2}{1 + m + n} \tag{7}$$

where l, m and n are positive numbers.

The method of auxiliary systems can be useful when the lower bound given by Steiner symmetrization is

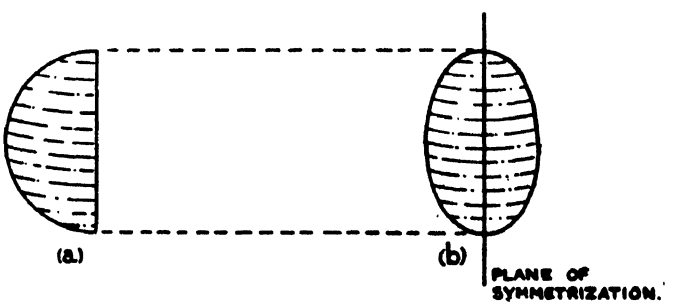

Figure 3. Symmetrization of a hemisphere with respect to a plane parallel to the base

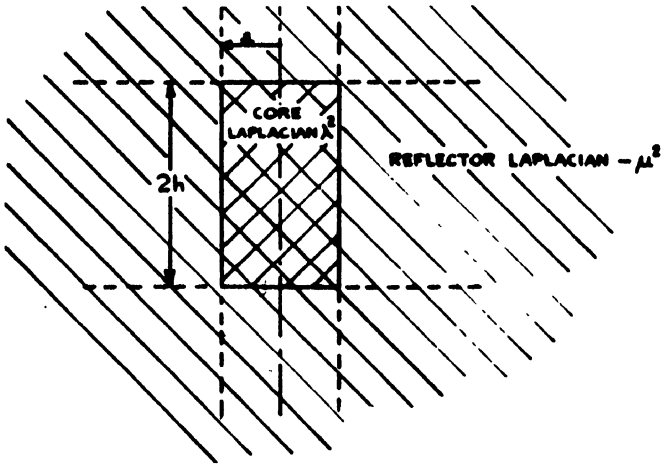

Figure 4. Circular cylinder of finite length with an infinite reflector

poor, e.g., when the length of a fully reflected cylinder is more than two or three diameters of the cylinder.

EXAMPLES

To illustrate the usefulness of two of the methods discussed in the preceding section, consider a fissile cylinder of elliptical cross-section. For simplicity the treatment is restricted to infinitely long cylinders.

Upper and lower bounds for the critical Laplacians of bare and reflected cylinders are obtained. The procedure for changing the upper and lower bounds for the critical Laplacian into upper and lower bounds for the critical dimensions is illustrated in the case of a bare cylinder. Charts are given for determining upper and lower bounds for the critical Laplacians of bare and reflected cylinders. A chart is also given for obtaining upper and lower bounds for the minor axis of a bare elliptical cylinder when one knows the major axis.

Bare Elliptical Cylinder

To obtain an upper bound for the critical Laplacian of a bare elliptical cylinder consider the bare circular cylinder of radius r_0 in Fig. 6a. If λ_c^2 is the critical Laplacian for the circular cylinder, and ψ the flux, then

$$\lambda_c^2 = \int_v \left\{\left(\frac{\partial\psi}{\partial x}\right)^2 + \left(\frac{\partial\psi}{\partial y}\right)^2\right\} \partial x\, \partial y \Big/ \int_v \psi^2\, \partial x\, \partial y \quad (8)$$

Now consider a bare cylinder of elliptical cross-section with semi-axes αr_0 and βr_0, as shown in Fig. 6b.

Put

$$\left.\begin{aligned} \xi &= \alpha_x \\ \eta &= \beta_y \end{aligned}\right\} \quad (9)$$

and define a function ϕ over the elliptical cross-section V' by

$$\phi(\xi,\eta) = \psi(x,y) \quad (10)$$

If ϕ is regarded as a guess for the flux in an elliptical cylinder, then Equation 1 gives for λ_e^2, the critical Laplacian of the elliptical cylinder

$$\lambda_e^2 \leq \int_{v'} \left\{\left(\frac{\partial\phi}{\partial\xi}\right)^2 + \left(\frac{\partial\phi}{\partial\eta}\right)^2\right\} d\xi\, d\eta \Big/ \int_{v'} \phi^2\, d\xi\, d\eta \quad (11)$$

Expressing the right-hand side of Equation 11 in terms of ψ gives

$$\lambda_e^2 \leq \frac{\dfrac{\alpha^2+\beta^2}{2\alpha^2\beta^2}\displaystyle\int_v \left\{\left(\frac{\partial\psi}{\partial x}\right)^2 + \left(\frac{\partial\psi}{\partial y}\right)^2\right\} dx\, dy}{\displaystyle\int_v \psi^2\, dx\, dy} = \frac{\alpha^2+\beta^2}{2\alpha^2\beta^2}\lambda_c^2$$

Since $\lambda_c = 2.405/r_0$, and the semi-axes of the ellipse are $a = \alpha r_0$ and $b = \beta r_0$, an upper bound for the critical Laplacian of an infinitely long, bare elliptical cylinder is

$$\lambda_e^2 \leq \frac{2.405^2}{2}\,\frac{a^2+b^2}{a^2b^2} \quad (12)$$

A lower bound for the critical Laplacian of a bare elliptical cylinder can be obtained by symmetrizing the elliptical cylinder of Fig. 6b with respect to the axial plane

$$\eta = \sqrt{\frac{\alpha}{\beta}}\,\xi \quad (13)$$

to give the circular cylinder of Fig. 6c. If λ_e^2 is the

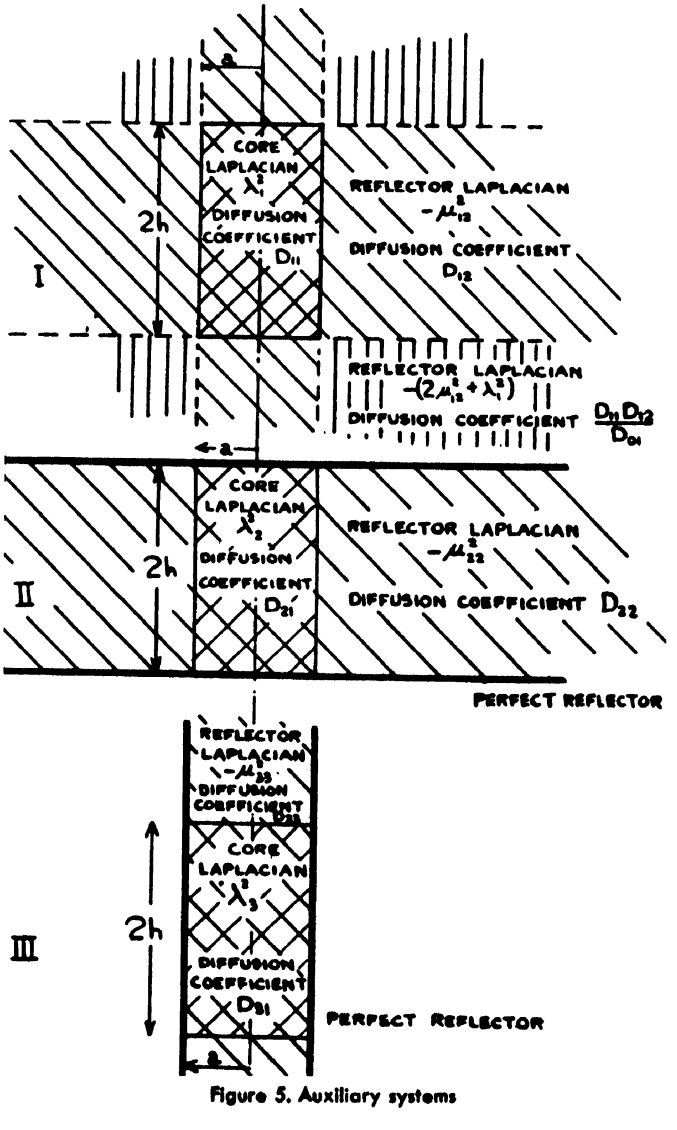

Figure 5. Auxiliary systems

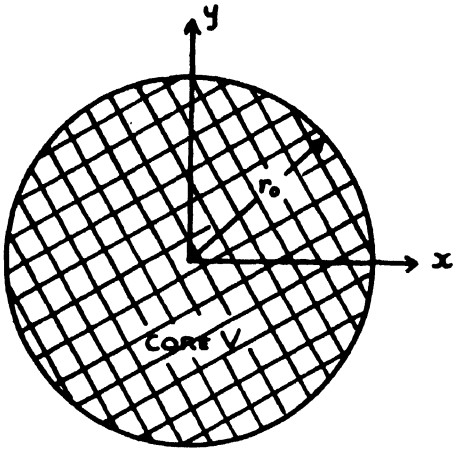

Figure 6a. Bare circular cylinder

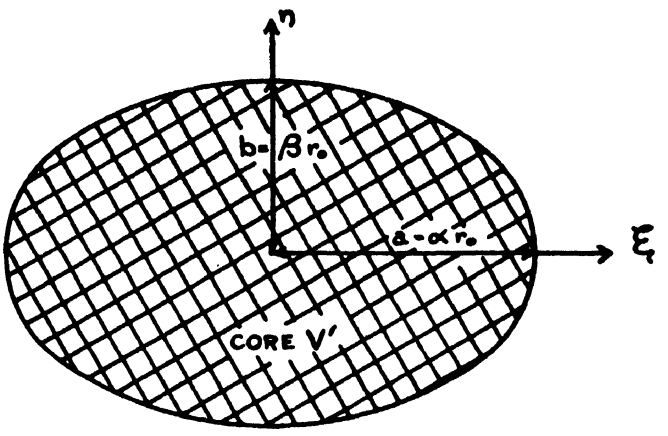

Figure 6b. Bare elliptical cylinder

critical Laplacian of the circular cylinder Fig. 6c; then

$$\lambda_s^2 \leq \lambda_c^2 \tag{14}$$

as Steiner symmetrization reduces the critical Laplacian. Since volume is unchanged by symmetrization $\lambda_s = 2.405/\sqrt{ab}$, and so a lower bare elliptical cylinder is

$$\lambda_e^2 \geq \frac{2.405^2}{ab} \tag{15}$$

When a and b are equal, the equality signs hold in Equations 12 and 15, and the upper and lower bounds for λ_e^2 coincide. If the ratio $b/a \ll 1$ for example, the difference between the upper and lower bounds can be a large fraction of the lower bound. For slender elliptical cross-sections the lower bound (Equation 15) is inferior to the following lower bound. The critical Laplacian of the elliptical cylinder is greater than that of a rectangular prism of sides $2a$ and $2b$. A lower bound for the critical Laplacian λ_e^2 of the elliptical cylinder is given by

$$\lambda_e^2 \geq \frac{\pi^2}{2}\frac{a^2+b^2}{2a^2b^2} \tag{16}$$

Chart for Upper and Lower Bounds for the Critical Laplacian

For bare elliptical cylinders with semi-axes a and b upper and lower bounds for the critical Laplacian are given by Equations 12, 15 and 16. If λ_u^2 is an upper bound, and λ_l^2 and λ_m^2 are lower bounds then

$$\lambda_u^2 = \frac{2.405^2}{2}\left(\frac{1}{a^2}+\frac{1}{b^2}\right)$$

$$\lambda_l^2 = \frac{2.405^2}{ab} \tag{17}$$

$$\lambda_m^2 = \frac{\pi^2}{4}\left(\frac{1}{a^2}+\frac{1}{b^2}\right)$$

Let A and B be respectively the reciprocals of a and b, then the contours of

$$K^2 = A^2 + B^2 \tag{18}$$

and

$$K^2 = AB \tag{19}$$

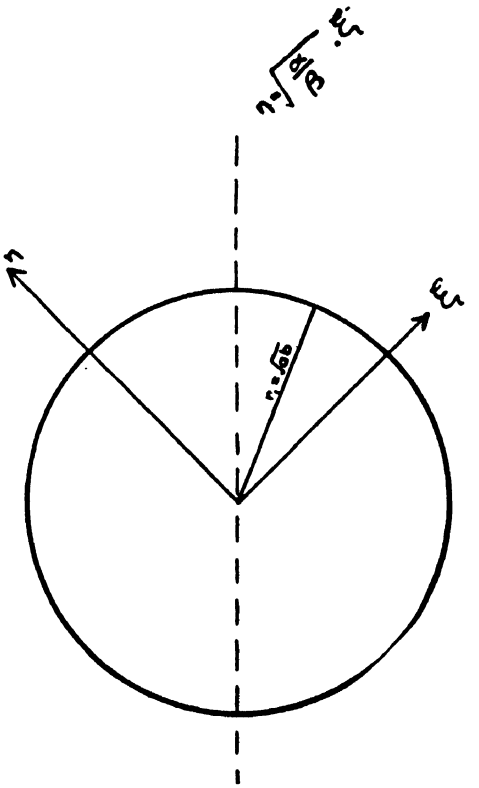

Figure 6c

are respectively circles and rectangular hyperbolae, if A and B are regarded as cartesian co-ordinates. A chart showing the contours of Equations 18 and 19 is given in Fig. 7. The larger K is the further the contours are from the origin. If a point ($A = 1/a$, $B = 1/b$) lies on the same side of the contour

$$K_1^2 = A^2 + B^2 \tag{20}$$

as the origin, then an upper bound for the critical Laplacian λ_e^2 is

$$\lambda_u^2 = \frac{2.405^2}{2} K_1^2 \tag{21}$$

Furthermore if the contour

$$K_2^2 = AB \tag{22}$$

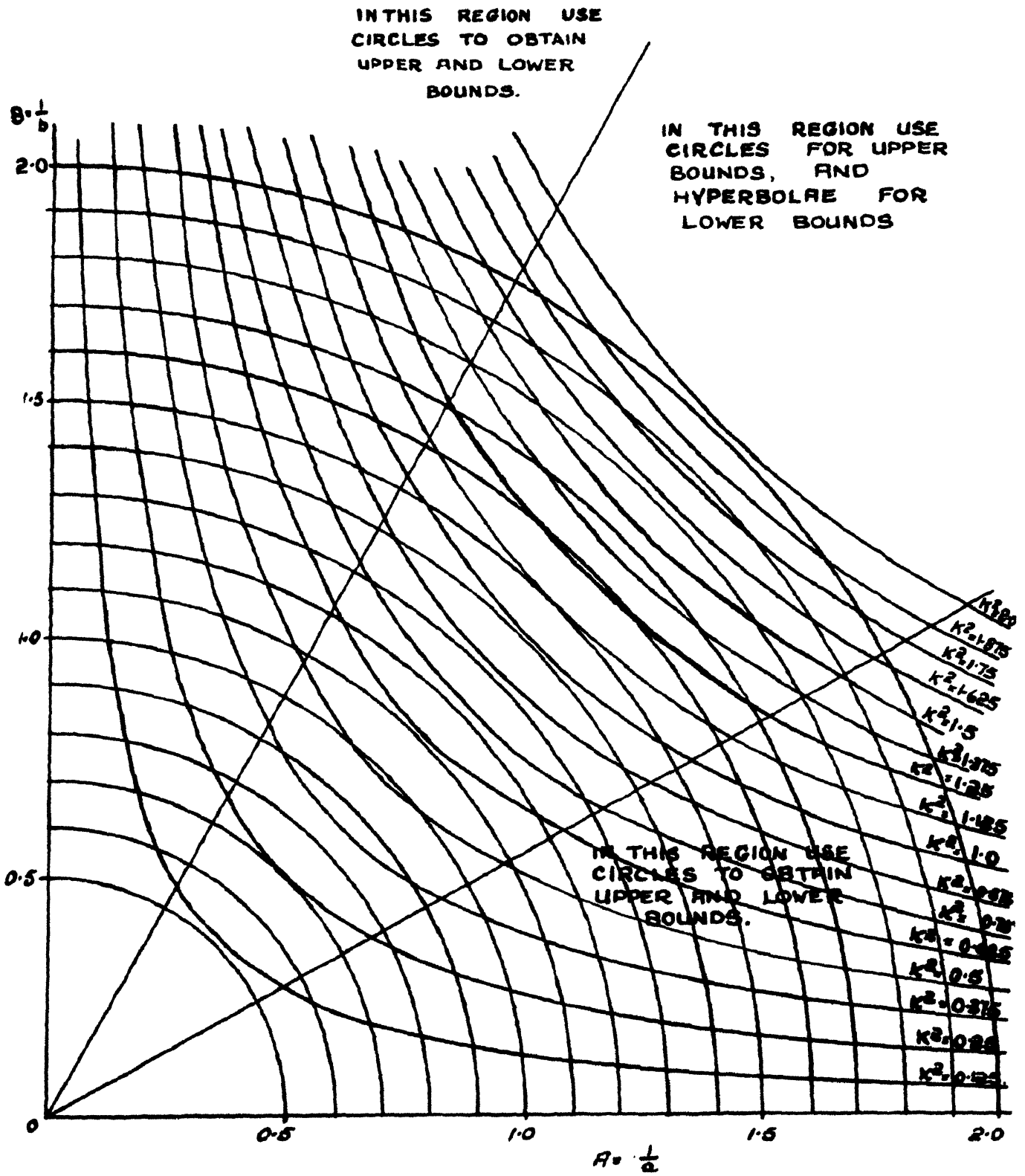

Figure 7. Chart for determining upper and lower bounds for the critical Laplacian of a bare elliptical cylinder with semi-axes a and b

is nearer to the origin than the point (A,B), a lower bound for the critical Laplacian λ_1^2 is

$$\lambda_1^2 = 2.405^2 K_2^2 \qquad (23)$$

Again if the contour

$$K_3^2 = A^2 + B^2 \qquad (24)$$

is nearer the origin than the point (A,B), then a lower bound for the critical Laplacian is

$$\lambda_m^2 = \frac{\pi^2}{4} K_3^2 \qquad (25)$$

In two parts of the (A,B) plane the lower bound λ_m^2 is greater than the lower bound λ_1^2, but for that

part of the (A,B) plane lying near the line $A = B$, the lower bound λ_1^2 is greater than the lower bound λ_m^2. The latter region lies between, and is bounded by the pair of straight lines

$$\frac{\pi^2}{4}(A^2 + B^2) = 2.405^2 AB \qquad (26)$$

Example:

The semi-axes of the ellipse are $a = 2$ and $b = \frac{3}{4}$, i.e., $A = 0.5$ and $B = 0.75$. The point ($A = 0.5$, $B = 0.75$) lies in the region of the chart where circles are used to obtain upper bounds, and hyperbolae should be used for lower bounds. This point lies on the circle of radius 0.9, and on the hyperbola for $K^2 = 0.375$. Thus

$$K_1^2 = 0.9^2 \quad \text{and} \quad K_2^2 = 0.375$$

Hence by Equations 21 and 23

$$\lambda_u^2 = 2.34 \quad \text{and} \quad \lambda_l^2 = 2.17$$

The estimated value of λ_e^2 is taken to be the arithmetic averages of the bounds; i.e. $\lambda_e^2 = 2.25$, with a maximum error of $\pm 3.75\%$. If the lower bound had been determined from the circular contours and Equation 25 then the result would have been $\lambda_e^2 = 2.17$ with a maximum error of $\pm 7.7\%$.

Chart for Critical Dimensions

Previously the size of the fissile core has been assumed to be given, and then upper and lower bounds for the critical Laplacian have been determined. Sometimes, however, the Laplacian for the core is given, i.e., the core is of a known composition, and then one has to determine upper and lower bounds for the critical dimensions. Charts can be constructed for giving by inspection upper and lower bounds for the critical dimensions of both bare and reflected cylinders. To illustrate the method of constructing such charts consider a bare cylinder. A similar but more complicated construction can be used for the chart for reflected cylinders.

Let the major axis a and the Laplacian of the bare elliptical cylinder be given, then the minor axis b can be estimated as follows: Put

$$u = \frac{2.405}{a\lambda_e}, \qquad v = \frac{2.405}{b\lambda_e} \qquad (27)$$

Then the inequalities of Equations 12, 15 and 16 become

$$uv \leq 1$$

$$u^2 + v^2 \geq 2 \qquad (28)$$

$$u^2 + v^2 \leq \frac{2.405^2 \times 4}{\pi^2}$$

If (u,v) are taken to be Cartesian co-ordinates, then the inequalities imply that the point (u,v) in Fig. 8 lies under the rectangular hyperbola $uv = 1$, and between the circles of radii $\sqrt{2}$ and $(2/\pi) \times 2.405$. These curves are shown in broken outline. The curve shown in continuous outline is for reading off b given a. The value of b obtained by inspection is the arithmetic average of the upper and lower bounds for b, which are given by the curves in broken outline. The maximum percentage error in the value of b (plus or minus) is shown inset for ratios of b/a from zero to unity. The spades indicate points of the chart for which the corresponding critical dimensions are known exactly.

Reflected Elliptical Cylinder

In obtaining upper and lower bounds for the critical Laplacian of a reflected elliptical cylinder, the reflector is assumed to be infinite, and for simplicity the diffusion coefficients of the core and reflector are taken to be the same. The following procedure for calculating an upper bound for the critical Laplacian of an elliptical cylinder with semi-axes αr_0 and βr_0 can be justified by an argument similar to that outlined in section 3.1 for bare elliptical cylinders.

The first step of the procedure is the calculation of the critical Laplacian λ_0^2 of a circular cylinder of radius r_0, which is surrounded by a reflector for which the Laplacian is $-2\alpha^2\beta^2\mu^2/(\alpha^2 + \beta^2)$, where $-\mu^2$ is

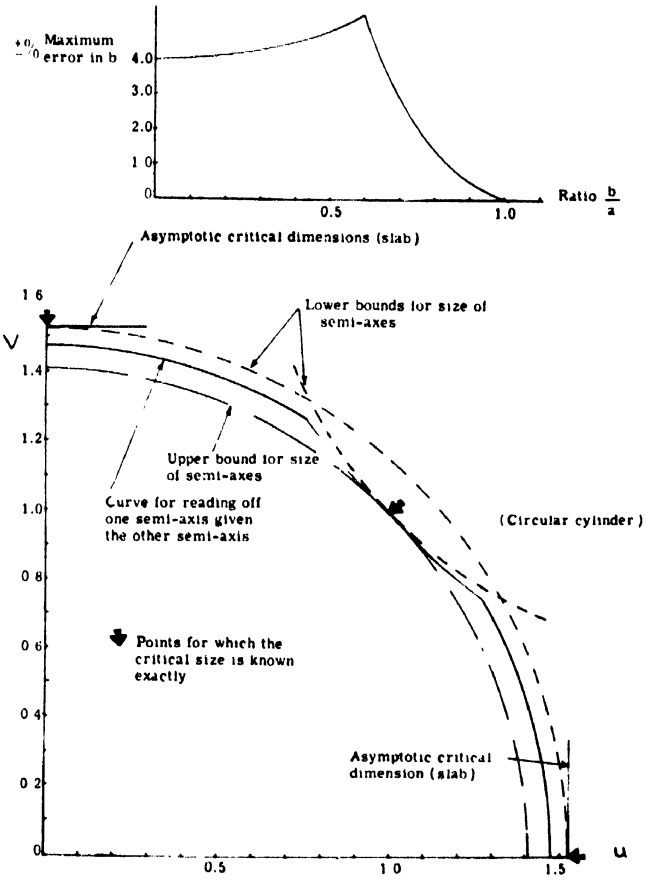

Figure 8. Chart for critical size of bare elliptical cylinder semi-axes of elliptical cross section a, b, critical Laplacian λ_e^2, $u = 2.405/a\lambda_e$, $v = 2.405/b\lambda_e$

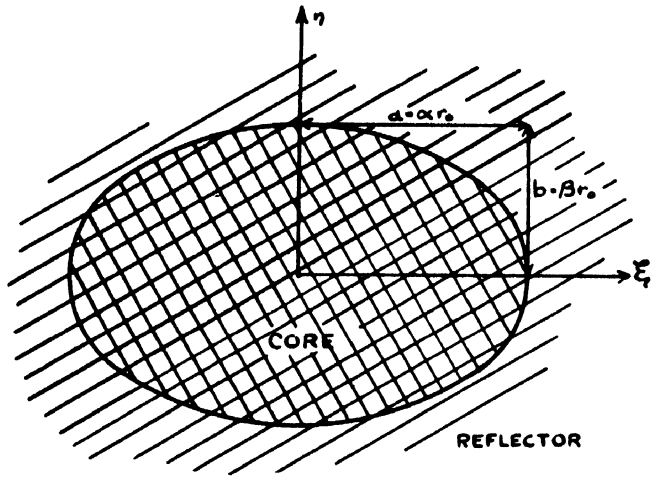

Figure 9a. Reflected elliptical cylinder

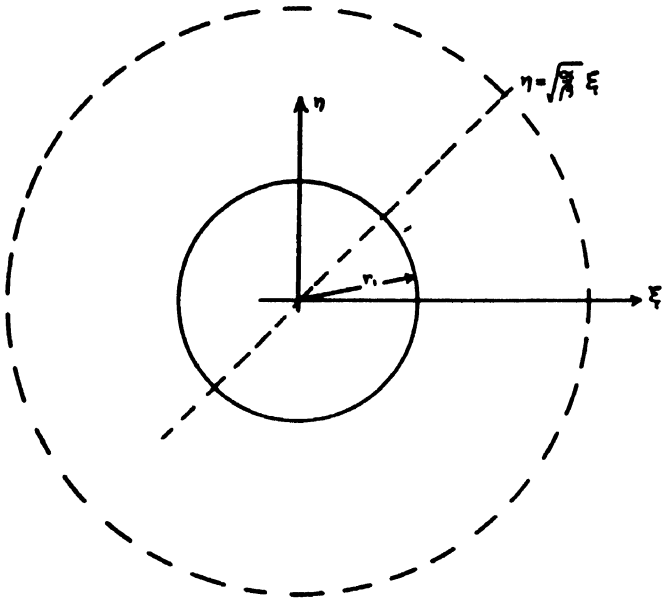

Figure 9b

the Laplacian for the reflector of the elliptical cylinder. An upper bound for the critical Laplacian of the elliptical cylinder is then given by

$$\lambda_e^2 \leq \lambda_0^2(\alpha^2 + \beta^2)/2\alpha^2\beta^2 \tag{29}$$

A lower bound for the critical Laplacian of the reflected elliptical cylinder Fig. 9a is given by the critical Laplacian of the reflected circular cylinder of Fig. 9b. The latter system is obtained from the former by symmetrizing Fig. 9a with respect to the line (13) to give Fig. 9b, and keeping the Laplacian of the reflector $-\mu^2$, and the diffusion coefficient for the core and reflector unchanged. The critical Laplacian of the system Fig. 9b is less than that of the given system Fig. 9a, as Steiner symmetrization can be shown to reduce the critical Laplacian. The radius of the core in Fig. 9b is

$$r_1 = \sqrt{\alpha\beta}\, r_0 \tag{30}$$

Since $-\mu^2$ is the Laplacian for the reflector of the system Fig. 9b, the critical Laplacian λ_e^2 of this system can be calculated from the well known formula

$$\lambda_e J_1(\lambda_e r_1)K_0(\mu r_1) - \mu J_0(\lambda_e r_1)K_1(\mu r_1) = 0 \tag{31}$$

If λ_e^2 denotes the critical Laplacian for the given system Fig. 9a, then

$$\lambda_e \leq \lambda_e \tag{32}$$

An upper bound λ_u^2 for the critical Laplacian λ_e^2 is given by Equation 29 as

$$\lambda_u^2 = \lambda_c^2 \frac{\alpha^2 + \beta^2}{2\alpha^2\beta^2} \tag{33}$$

where λ_c^2 is the critical Laplacian for a circular cylinder, for which the Laplacian of the reflector is $-2\alpha^2\beta^2\mu^2/(\alpha^2 + \beta^2)$. Thus the upper bound λ_u^2 is given in terms of the semi-axes a and b by

$$\lambda_u J_1\left(\lambda_u \sqrt{\frac{2a^2b^2}{a^2+b^2}}\right) K_0\left(\mu \sqrt{\frac{2a^2b^2}{a^2+b^2}}\right) - \mu J_0\left(\lambda_u \sqrt{\frac{2a^2b^2}{a^2+b^2}}\right) K_1\left(\mu \sqrt{\frac{2a^2b^2}{a^2+b^2}}\right) = 0 \tag{34}$$

i.e., λ_u^2 is the critical Laplacian for a circular cylinder of radius

$$\sqrt{\frac{2a^2b^2}{a^2+b^2}}$$

having a reflector of Laplacian $-\mu^2$, and which is infinite in extent.

A lower bound λ_1^2 for the critical Laplacian λ_e^2 is given by Equations 31 and 32 as

$$\lambda_1 = \lambda_e \tag{35}$$

Thus for an infinite reflector the lower bound is given by

$$\lambda_1 J_1(\lambda_1 \sqrt{ab})K_0(\mu \sqrt{ab}) - \mu J_0(\lambda_1 \sqrt{ab})K_1(\mu \sqrt{ab}) = 0 \tag{36}$$

where $-\mu^2$ is the Laplacian of the reflector of the given elliptical cylinder. Thus λ_1^2 is the critical Laplacian for a circular cylinder of radius $\sqrt{ab}$, which is reflected by material of the same composition as the reflector of the elliptical cylinder.

Chart for Upper and Lower Bounds for the Critical Laplacian

If the substitutions

$$\begin{aligned} A' &= 1/\mu a \\ B' &= 1/\mu b \\ K_u &= \frac{\lambda_u}{\mu} \\ K_1 &= \frac{\lambda_1}{\mu} \end{aligned} \tag{37}$$

are made in Equations 34 and 36, and

$$\begin{aligned} A'B' &= \gamma^2 \\ A'^2 + B'^2 &= 2\gamma^2 \end{aligned} \tag{38}$$

then K_u and K_1 satisfy.

$$KJ_1(K/\gamma)K_0(1/\gamma) - J_0(K/\gamma)K_1(1/\gamma) = 0 \tag{39}$$

If A' and B' are plotted as rectangular co-ordinates, and γ is regarded as a parameter then Equation 38 describes families of rectangular hyperbolae and circles. Instead of using γ as a parameter, K as determined by Equation 39 may be used.

In the chart of Fig. 10 the contours for

$$A'B' = \gamma^2(K)$$

and

$$A' + B^{2\prime} = 2\gamma^2(K)$$

are plotted for a range of values of K. Suppose the semi-axes a and b of an elliptical cylinder, and the Laplacian $-\mu^2$ of the reflector are given, then A' and B' are known. If the point (A', B') lies within a circle of radius K_1, then an upper bound for the critical Laplacian λ_e^2 is

$$\lambda_u^2 = \mu^2 K_1^2 \qquad (40)$$

If the point (A', B') is on the opposite side of the rectangular hyperbola

$$A'B' = \gamma^2(K_2)$$

to the origin, then a lower bound for the critical Laplacian λ_e^2 is

$$\lambda_l^2 = \mu^2 K_2^2 \qquad (41)$$

Figure 10 can be used therefore to obtain upper and lower bounds by inspection. However, when the ratio of the minor axis to the major axis is small, the lower bound given by the hyperbolic contours is not a good approximation to the actual Laplacian. For slender ellipses a better lower bound than that given by Equation 41 can be obtained by taking the critical Laplacian of an infinite slab as the lower bound. If $b \ll a$, the thickness of the slab is taken to be b. This lower bound can be read off the chart from the contours which are parallel to the A' and B' axes.

Example:

$$a = 40 \qquad \mu = 0.05$$

b	*% error in Laplacian*
40	0
33.3	±0.6
28.6	±1.75
25	±4.3
20	±8.1

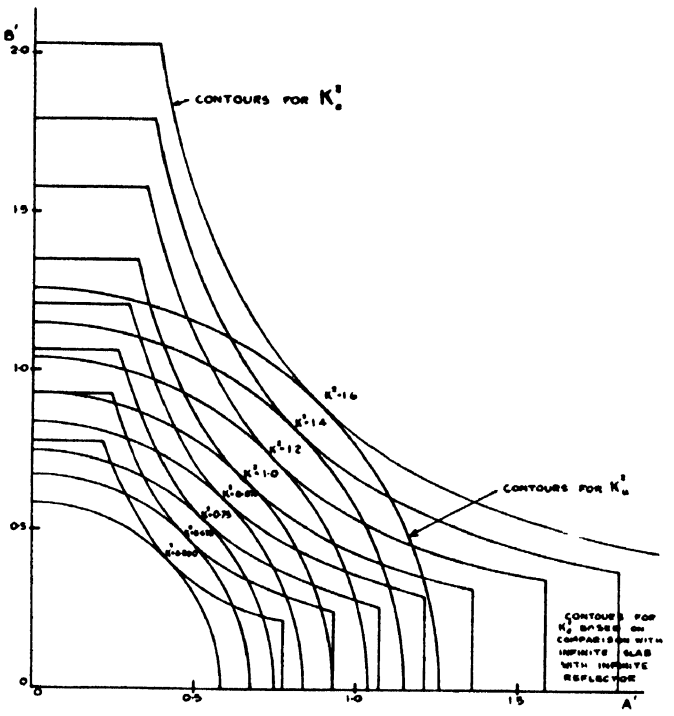

Figure 10. Upper and lower bounds for critical Laplacian of a reflected cylinder of elliptical cross section

DISCUSSION

For many purposes the simple methods of obtaining upper and lower bounds (for either the critical Laplacian or the critical dimensions) which have been illustrated above are sufficient. If required, the bounds can be improved through the use of the direct methods of the calculus of variations. For example the upper bound for the critical Laplacian of a bare fissile body can be improved to any desired degree of accuracy by the Rayleigh-Ritz approximation procedure.

A detailed treatment of the topics raised in this paper will be published shortly by the author and his colleagues. This is planned to include systematic approximation procedures, approximate solutions for the flux, and some extensions to two-group theory.

REFERENCE

1. Pólya, G., Quarterly Journal of Applied Mathematics, vol. 6 pp 267–277. (1948).

Critical Size of Heterogeneous Reactor with Small Number of Rods

By A. D. Galanin, USSR

If a reactor contains a small number of multiplying rods, its critical size cannot generally be computed by the homogeneous reactor theory. It is therefore interesting to examine the error of the homogeneous reactor treatment by comparing on a simple model its results with those of a more accurate theory.

"CYLINDRICAL" REACTOR WITH INFINITE REFLECTOR

Consider reactor multiplying rods having the form of infinitely long cylinders with radius ρ and situated in the joints of a square lattice, spaced a. The reflector is assumed to be infinite, and its scattering and slowing down properties the same as the moderator in the reactor. If the multiplying rods are devoid of resonance absorption, then the equation for determining the critical size is[1]

$$q_0 N(\boldsymbol{k}) = \sum_{\boldsymbol{k}'} H(\boldsymbol{k} - \boldsymbol{k}') N(\boldsymbol{k}') \tag{1}$$

where

$$q_0 = \frac{2\pi D}{\gamma} \frac{a^2 - \pi\rho^2}{2\pi L^2}$$

D is the diffusion coefficient, L the diffusion length in the moderator, γ the uranium rod thermal constant, $\boldsymbol{k}$, $\boldsymbol{k}'$ the rod numbers, and $N(\boldsymbol{k})$ the thermal neutron density on the rod surface.

The kernel $H(\boldsymbol{k} - \boldsymbol{k}')$ has the form

$$H(\boldsymbol{k}) = \frac{a^2}{2\pi L^2}\left[e^{\tau/L^2}\eta \int_{\tau/L^2}^{\infty} e^{-\left(z + \frac{k^2a^2}{4Iz}\right)} \frac{dz}{2z} - K_0\left(\frac{ak}{L}\right)\right] \tag{2}$$

which when $\tau/L^2 \ll 1$ may be written

$$H(\boldsymbol{k}) = \frac{a^2}{2\pi L^2}\left[(e^{\tau/L^2}\eta - 1)K_0\left(\frac{ak}{L}\right) - e^{\tau/L^2}\eta F(\boldsymbol{k})\right] \tag{3}$$

where

$$F(\boldsymbol{k}) = -\frac{1}{2}\left(1 + \frac{k^2a^2}{4L^2}\right) Ei\left(-\frac{a^2k^2}{4\tau}\right) - \frac{\tau}{2L^2} e^{-\frac{k^2a^2}{4\tau}} \tag{3'}$$

Equation 1 is a system of homogeneous linear equations for the values $N(\boldsymbol{k})$. By making the determinant of this system equal to zero we obtain an equation from which we may deduce the value of η (or any other quantity) under which the reactor will be critical.

The derived value of η corresponds to the infinite lattice multiplying factor determined by the formula[1] $k = \eta(1 + q)$. The multiplying factor thus obtained will further be denoted k_{het}. On the other hand, the corresponding homogeneous equation can be solved by the two-group approximation treatment, calculating diffusion length by the formulae following from the theory of thermal neutron absorption in the lattice:[1]

$$L_p^2 = L^2 \frac{q}{1 + q}; \qquad q = q_0 + q_1$$

$$q_1 = \frac{a^2}{4\pi L^2}\left(\ln \frac{a^2}{\pi\rho^2} + \frac{\pi\rho^2}{a^2} - 1.48\right) \tag{4}$$

The critical radius is determined by the number of rods as follows (n denoting the number of rods):

$$R = \sqrt{\frac{na^2}{\pi}} \tag{5}$$

The multiplication factor derived from the critical condition with the given radius will be called k_{II}. The multiplication factor can also be computed from

$$(1 + \alpha^2 L_p^2)e^{\alpha^2\tau} = k \tag{6}$$

where α^2 is determined by the two-group equations, i.e.,

$$\alpha^2 = -\frac{1}{2}\left(\frac{1}{L_p^2} + \frac{1}{\tau}\right) + \sqrt{\frac{1}{4}\left(\frac{1}{L_p^2} + \frac{1}{\tau}\right) + \frac{k_{II} - 1}{L_p^2\tau}} \tag{7}$$

The multiplication factor obtained from Equations 6 and 7 will be denoted k_{hom}.

Comparative calculations by the heterogeneous and homogeneous treatments have been carried out for two variants of constants:

I. $a = \sqrt{\tau} = 1$; $L^2 = 49$;
$q_0 = 0.015$; $\rho = 0.1$, $q_1 = 0.0033$

II. $a = \sqrt{\tau} = 1$; $L^2 = 8$;
$q_0 = 0.0811$; $\rho = 0.1$, $q_1 = 0.020$

The results of the calculations are given in Table I. The error of the two-group treatment and reactor homogenization, characterized by $(k_{het} - k_{II})/(k - 1)$, decreases with the increasing size of the reactor. The

Original language: Russian.

error is appreciably reduced if k_{hom} is computed instead of k_{II}. The remaining error is due to the inaccuracy of the two-group theory at the reactor boundary and the deviation of the reactor's form from a cylinder. Homogenization is much poorer in variant II than in variant I.

Let us examine now a reactor with small resonance absorption. Assuming that the resonance absorption is located at τ equal to $\tau_r \cong \frac{3}{4}\tau$, Equation 1 becomes

$$q_0 N(k) = \sum_{k'} H(k - k')N(k') - \psi \sum_{k'} H_\psi(k,k')N(k') \tag{8}$$

where ψ is resonance absorption probability, and

$$H_\psi(k,k') = \eta \frac{a^2}{4\pi\tau_r} e^{\tau_1/L^2} \frac{a^2}{2\pi L^2} \sum_{k''} e^{-\frac{a^2(k'-k'')^2}{4\tau_r}} \times \left[K_0\left(\frac{a|k - k''|}{L}\right) - F_1(k - k'') \right] \tag{8'}$$

and with F_1 differing from F (see Equation 3') by the substitution of τ by $\tau_1 = \tau - \tau_r$. In variant I it was assumed that $\psi = 0.1$; in variant II $\psi = 0.13$. The results are given in Table II. This table indicates that the inaccuracy of the homogeneous theory for resonance absorption (as, for example, the rod effect of the reactor as a whole on the resonance absorption) is partially compensated by other errors of the homogeneous theory. For variant I, this compensation is, accidentally, complete.

The above data characterize the scope of the error of the homogeneous treatment when used for calculating the critical size of a reactor with a small number of rods. With the multiplication factor given, the homogeneous theory yields smaller critical sizes.

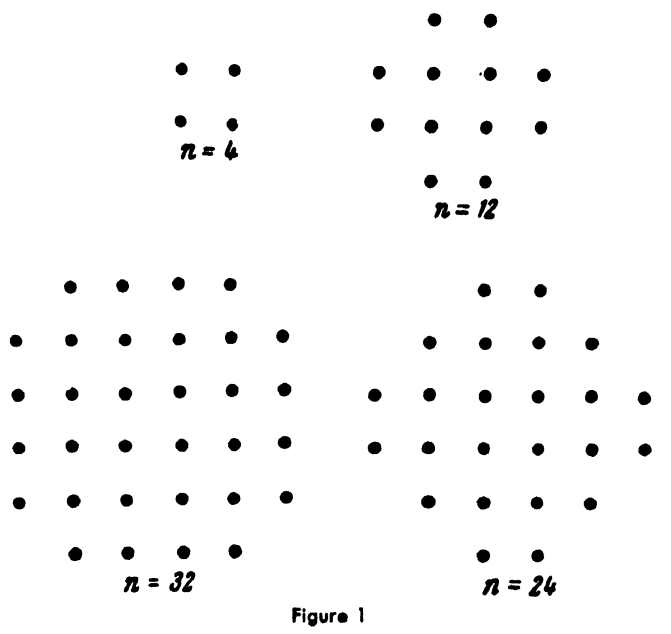

Figure 1

SLAB REACTOR WITH ABSORBING RODS

Another model for calculation was a slab reactor with ten rows of multiplying and three rows of absorbing rods, the latter situated in the center of the cells and spaced twice as wide apart as the former. The reflector possessed the same properties as the moderator in the reactor, and had finite thickness Δ. In the other two directions, the dimensions of the reactor were infinite. The arrangement of the rods is shown in Fig. 2.

Equation 1 should first be summated in one direc-

Table I

Number of blocks	Reactor radius in a units	k_{II}	k_{hom}	k_{het}	$\frac{k_{het} - k_{II}}{k - 1}$, %	$\frac{k_{het} - k_{hom}}{k - 1}$, %
			Variant I			
4	1.128	2.113	2.310	2.290	13.7	−1.5
12	1.954	1.480	1.514	1.532	9.8	+3.4
24	2.764	1.289	1.301	1.311	7.1	+3.2
32	3.192	1.234	1.242	1.250	6.4	+3.2
			Variant II			
4	1.128	2.414	2.859	2.969	28	+5.6
12	1.954	1.631	1.714	1.808	21.9	+11.1
24	2.764	1.383	1.413	1.470	18.5	+12
32	3.192	1.311	1.332	1.374	16.8	+11.2

Table II

Number of rods	*Variant I*			*Variant II*		
	k_{hom}	k_{het}	$\frac{k_{het} - k_{hom}}{k - 1}$ %	k_{hom}	k_{het}	$\frac{k_{het} - k_{hom}}{k - 1}$ %
12	1.471	1.470	−0.2	1.670	1.730	8.2
32	1.220	1.220	0.2	1.310	1.342	9.4

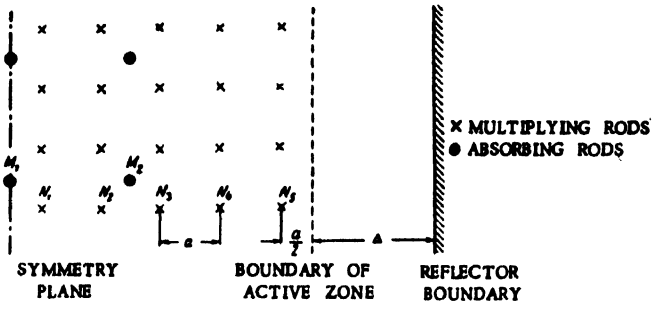

Figure 2

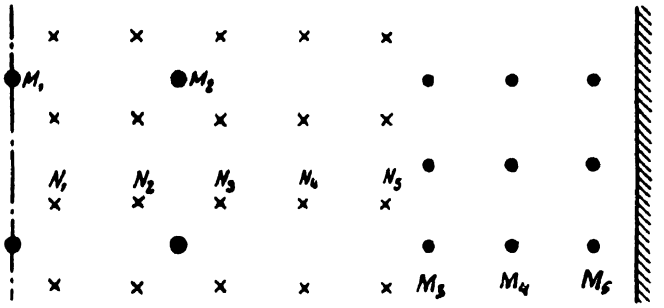

Figure 3

tion. This can be done by the methods given.[1] We then obtain

$$q_0 N(k) = \eta \sum_{k'} N(k') H_1(k - k') - \sum_{k'} N(k') H_2(k - k') - \sum_{l} \zeta_l M(l) H_3(k - l)$$

$$q_0 M(l) = \eta \sum_{k'} N(k') H_1(l - k) - \sum_{k'} N(k') H_2(l - k') - \sum_{l'} \zeta_{l'} M(l') H_3(l - l') \quad (9)$$

where $N(k)$, $M(l)$ are the thermal neutron densities on the surface of multiplying rod number k and absorbing rod number l; ζ_l is the ratio of the thermal constant of absorbing rod number l to the thermal constant of the multiplying rods. The kernels have the following form (without taking into account resonance absorption) for the infinite reflector

$$H_1(k - k') = \frac{a}{2\sqrt{\pi L}} e^{\tau/L} \int_{\tau/L^2}^{\infty} \frac{dz}{\sqrt{z}} e^{-z - \frac{a^2(k-k')^2}{4L^2 z}}$$

$$H_2(k - k') = \frac{a}{2L}\left[e^{-\frac{a}{L}|k-k'} + \frac{a}{\pi L} \ln \frac{a}{2\pi\rho}\,\delta_{kk'}\right]$$

$$H_3(l - l') = \frac{a}{4L}\left[e^{-\frac{a}{L}|l-l'|} + \frac{2a}{\pi L} \ln \frac{a}{\pi\rho'}\,\delta_{ll'}\right]$$

$$H_2(k' - l) = \frac{a}{2L}\left[e^{-\frac{a}{L}|k'-l|} + \frac{a}{\pi L}\,\tilde{\delta}_{k'l}\left\{\pi|k - l| - \frac{1}{2}\ln 4\left(\frac{1}{2} + \mathrm{sh}^2\pi(k' - l)\right)\right\}\right]$$

$$H_3(k - l) = \frac{a}{4L}\left[e^{-\frac{a}{L}|k-l|} + \frac{a}{\pi L}\,\tilde{\delta}_{kl}\left\{\frac{\pi}{2} - \ln 4\left(\frac{1}{2} + \mathrm{sh}^2\frac{\pi}{4}\right)\right\}\right] \quad (10)$$

where $\tilde{\delta}_{kl}$ and $\tilde{\delta}_{k'l}$ are unity for the nearest rods and zero in the remaining cases; ρ and ρ' are radii of the multiplying and absorbing rods (in these calculations it has been assumed that $\rho = \rho' = a/10$).

If the reflector is finite, then the terms originating from the reflected sources should be added to the kernels. If, however, the reflector is sufficiently thick (it was assumed that $\Delta = 3a$) they may be discarded. In the other kernels, the terms containing $\tilde{\delta}_{kl}$, $\tilde{\delta}_{k'l}$ need not be changed, and the exponents should be replaced as follows:

$$e^{-\frac{|x-x'|}{L}} - \frac{\mathrm{ch}\,\frac{x+x'}{L}}{\mathrm{sh}\,\frac{2d}{L}} + e^{-\frac{2d}{L}}\,\frac{\mathrm{ch}\,\frac{x-x'}{L}}{\mathrm{sh}\,\frac{2d}{L}} \quad (11)$$

for which we found a solution, which vanishes at the reflector boundary, for the one-dimensional diffusion equation with a source at a certain point. Equations 9 were solved on the assumption that $\zeta_1 = \zeta_2$, $N_1 = N_2$. The density distribution on the rods N and M, and the value of η which gives the solution of Equation 9 were deduced. For comparison with the homogeneous theory, the reactor should be divided into two parts: with and without absorption rods. In the zone with the absorption rods, k and L_p^2 can be determined by the double lattice formulae.[1] It is further required in this zone that $k = 1$, which gives the connection between η and ζ. The second equation for η and ζ yields the critical condition. The results of the calculation are given in Table III (with $a = 1$; $\sqrt{\tau} = 1.36$; $L = 82.5$; $q_0 = 0.024$; $\zeta = 2.76$). Notice that: (1) η fairly coincides in both calculations; (2) there is an appreciable maximum of density on the fourth and fifth rods; (3) this maximum is somewhat greater in the homogeneous case.

It may be assumed that there will be less agreement between the heterogeneous and homogeneous calculations if the gradients of neutron density in the reactor are large. To verify this, a reactor with an absorber in the reflector was calculated (Fig. 3). To obtain a stronger gradient it was assumed that $\zeta_3 =$

Table III

	η	N_1	N_2	N_3	N_4	N_5	M_1	M_2
Het.	1.562	1	1	1.014	1.095	1.082	0.765	0.768
Hom.	1.560	1	1.01	1.042	1.15	1.106	—	—

Table IV

	k	N_1	N_2	N_3	N_4	N_5	M_2	M_4	M_5
Het.	1.608	1	0.953	0.868	0.778	0.547	0.203	0.081	0.013
Hom.	1.593	1	0.963	0.895	0.816	0.579	0.230	0.091	0.028

$\zeta_4 = \zeta_5 = 4$ ($\zeta_1 = \zeta_2 = 2$). The results of the calculation are given in Table IV. The divergence in the multiplication factors is appreciably greater than in Table III, though it is still not large (here k in the homogeneous case is k_{II} in the sense determined in the first section). Also neutron density on the edge of the reactor is higher in the homogeneous than in the heterogeneous calculation.

The preceding calculations show that the homogeneous treatment may without much error be applied for computing critical size and neutron density distribution even when the reactor consists of a relatively small number of multiplying lumps and contains regions greatly differing in their neutron properties.

REFERENCE

1. Galanin, A. D., P/666, The Thermal Coefficient in a Heterogeneous Reactor, this Session, these Proceedings.

The Theory of Resonance Absorption in Heterogeneous Systems

By I. I. Gurevich and I. Y. Pomeranchouk, USSR

SMALL LUMPS*

Resonance absorption in systems comprising a mixture of uranium and moderator can be decreased if the neutron absorbing substance (uranium) is not uniformly distributed and is concentrated in small lumps separated by the moderator.

One can readily perceive why the use of lump systems leads to the decrement of resonance absorption.

In a homogeneous mixture of the capturing substance and moderator, the neutrons, upon slowing down to resonance energies, continue to move in the medium with a uniform content of the capturing substance, and therefore are absorbed with great probability by the latter's nuclei. In the lump system, with sufficiently large distances between the lumps, the neutron will escape from the dangerous resonance absorption zone before reaching the surface of one of the lumps. Besides this, in the heterogeneous system the interior layers of the lump are screened by the exterior ones, owing to which not all the uranium atoms take part in the resonance absorption.

Both these effects essentially decrease resonance absorption in heterogeneous systems (compared with homogeneous systems of equal concentration) if

$$\begin{aligned} L = \bar{l}\omega > \lambda_s \\ \bar{l} > \lambda_c(E_0) \end{aligned} \tag{1}$$

where $\bar{l}$ is the neutron mean path in the lump; L is the neutron mean path in the moderator cell (ω is the moderator-to-uranium volume ratio); λ_s is the neutron scattering mean free path in the moderator; and $\lambda_c(E_0)$ is the absorption mean free path of the resonance neutron in uranium.

Examine the "small" lumps for which the average size of lump $\bar{l}$ is smaller than the scattering mean free path of the neutrons in the moderator and the uranium. Let $\omega \gg 1$. The condition $\bar{l} < \lambda_s$ allows one to neglect the effect of perturbation of the resonance-neutron flux near the lump; the same condition for uranium allows one to consider the neutron moving in the lump in a straight line.

It can be shown that in the case of $\bar{l} > \lambda_s$ the resonance-neutron field is little disturbed if the neutron energy loss per collision is greater than the width of the resonance absorption danger zone:

$$\Delta E \ll E_0(1 - \epsilon)$$

$$\lambda_c(E_0 \pm \Delta E) \sim \bar{l}; \qquad \epsilon = \left(\frac{M - m}{M + m}\right)^2 \tag{1'}$$

For "small" lumps, resonance escape probability in the slowing down process (φ) can be computed by the kinetic theory of gases, where the lumps themselves serve as "molecules."

The neutron mean free path in relation to collision with lumps is equal to:

$$L = \frac{1}{c\Sigma} = \bar{l}\omega \tag{2}$$

where c is the number of lumps per unit of volume; and Σ is the lump's mean geometric cross section (for spherical lumps $\Sigma = \pi R^2$).†

Determine the mean free path of a neutron of energy E with respect to its capture by the lumps:

$$\Lambda_c = \frac{L}{\zeta(E)} \tag{3}$$

where $\zeta(E)$ is the "neutron-sticking-to-the lump" probability equal to

$$\zeta(E) = \int (1 - e^{-l/\lambda_c(E)}) f(l)\, dl \tag{4}$$

$f(l)$ is the distribution function of the neutron path in the lump. If $\bar{l}/\lambda_c(E) \ll 1$ then

$$\zeta(E) \simeq \int \frac{l}{\lambda_c(E)} f(l)\, dl = \frac{\bar{l}}{\lambda_c(E)} \tag{4'}$$

The relative probability of the neutron being captured by the lump can be represented by

$$W(E) = \frac{\frac{1}{\Lambda_c}}{\frac{1}{\Lambda_c} + \frac{1}{\lambda_s}} = \frac{\zeta(E)}{\zeta(E) + \frac{L}{\lambda_s}} \tag{5}$$

If the resonance absorption $(1 - \varphi)$ is small, then, as is well known,

$$-\ln \varphi = \frac{1}{\xi} \int W(E) \frac{dE}{E} \tag{6}$$

where ξ is the average logarithmic energy loss in the moderator.

Original language: Russian.

* The theory of resonance absorption in small uranium lumps was developed by the authors in 1943.

† $\Sigma = V/\bar{l} = S/4$, where V is the lump volume, S its surface, $\bar{l} = 4V/S$.

Notice that if the resonance-neutron field can be regarded as unperturbed and the resonance absorption is small then the relation between the values φ and W is the same for the heterogeneous and homogeneous cases. Absorption probability in the homogeneous case[1] is

$$W(E) = \frac{1}{1 + \omega \dfrac{\lambda_c(E)}{\lambda_s}} \tag{7}$$

It will be seen that in the case of very small lumps Equation 5 for $W(E)$ yields a homogeneous result for φ. If $\bar{l} \ll l_0 = \lambda_s/\omega$, then $L \ll \lambda_s$ and in the expression

$$-\ln \varphi = \frac{1}{\xi} \int \frac{\zeta}{\zeta + \dfrac{L}{\lambda_s}} \frac{dE}{E}$$

an essential part will be played by $\zeta(E) \sim L/\lambda_s \ll 1$. We may, therefore, take Equation 4′ for $\zeta(E)$. Then

$$-\ln \varphi = \frac{1}{\xi} \int \frac{\dfrac{\bar{l}}{\lambda_c}}{\dfrac{\bar{l}}{\lambda_c} + \dfrac{L}{\lambda_s}} \frac{dE}{E} = \frac{1}{\xi} \int \frac{1}{1 + \omega \dfrac{\lambda_c(E)}{\lambda_s}} \frac{dE}{E}$$

$$= \frac{1}{\xi} \int \frac{W_0(E)\, dE}{E} = (-\ln \varphi_0)$$

It is interesting to note that the transition to homogeneity takes place for lumps of size $\bar{l} \sim l_0 = \lambda_s/\omega$ for which the self-screening effect may still be strongly expressed ($\bar{l} < \lambda_s/\omega$ but with $\lambda_s/\omega \gg \lambda_c$).

Examine the second limiting case, which is particularly interesting, that of sufficiently large lumps:

$$\bar{l} \gg \lambda_s/\omega; \qquad L = \omega \bar{l} \gg \lambda_s$$

Then in the expression for

$$-\ln \varphi = \frac{1}{\xi} \int \frac{\zeta(E)}{\zeta(E) + \dfrac{L}{\lambda_s}} \frac{dE}{E}$$

we may neglect $\zeta(E) \leq 1$ in the denominator, as compared with the large quantity L/λ_s. Thus, the lump systems are described by the formula

$$-\ln \varphi = \frac{1}{\xi} \int \frac{\lambda_s}{L} \zeta(E) \frac{dE}{E} \tag{8}$$

Substituting in Equation 8 the expression of Equation 4 for $\zeta(E)$ we obtain:

$$-\ln \varphi = \frac{1}{\xi} \frac{\lambda_s}{L} \int_{(l)} I(l) f(l)\, dl \tag{9}$$

where

$$I(l) = \int_{(E)} (1 - e^{-l/\lambda_c(E)}) \frac{dE}{E} \tag{10}$$

Examine now two groups of uranium-238 levels: the first (lower) consists of several strong non-overlapping levels for which the resonance capture cross section is great, and, consequently,

$$\frac{\bar{l}}{\lambda_{c0}} \gg 1 \tag{11}$$

where $\lambda_{c0} = \lambda_c(E_0)$ is the resonance absorption length.

The second group consists of high levels (there may be many of them and they may overlap) for which the resonance cross sections are not great, so that for them

$$\frac{\bar{l}}{\lambda_{c0}} \ll 1 \tag{12}$$

For the energy region corresponding to the second group of levels, the integrand in Equation 10 may be replaced by the first term of the expansion, that is, it may be written:

$$I(l) = I_1(l) + I_2(l)$$

$$= \int_{(E)} (1 - e^{-l/\lambda_c(E)}) \frac{dE}{E} + \int \frac{l}{\lambda_c(E)} \frac{dE}{E} \tag{13}$$

Assuming that the levels of the first group do not overlap, the first integral (I_1) will be represented as the sum of integrals each evaluated for a separate level. Using the Breit-Wigner formula for each of the first-group levels,‡

$$\lambda_{ci}(E) \simeq \lambda_{ci}^0 (1 + x^2)$$

$$x = \frac{E - E_0}{\dfrac{\Gamma_i}{2}} \tag{14}$$

and so far neglecting the Doppler width, write down the expression for $I_1(l)$ in the following form

$$I_1(l) = \frac{1}{2} \sum_{(i)} \frac{\Gamma_i}{E_{0i}} \int (1 - e^{-l/\lambda_{0i}(1+x^2)})\, dx \tag{15}$$

In Equation 15 a substantial contribution is made by the region $|x| \gg 1$, $[(l/\lambda_{c0})(1 + x^2) \sim 1]$, and therefore it is approximately equal to:

$$I_1(l) \simeq \frac{1}{2} \sum_{(i)} \frac{\Gamma_i}{E_{0i}} \int (1 - e^{-l/\lambda_{0i}x^2})\, dx$$

$$= \sum_{(i)} \frac{\Gamma_i}{E_{0i}} \sqrt{\pi} \sqrt{\frac{l}{\lambda_{0i}}} \tag{16}$$

Inserting Equation 16 in 13 and Equation 13 in 9 we obtain the final expression for φ:

$$-\ln \varphi = \frac{\lambda_s}{\xi L} \left[\sqrt{\pi N} \sqrt{l} \sum_{(i)} \frac{\sqrt{\sigma_{0i} I_i^2}}{E_{0i}} + N\bar{l} \int_{(E)} \sigma(E) \frac{dE}{E} \right] \tag{17}$$

where N is the number of uranium-238 nuclei in 1 cm³ of the uranium lump.

‡ The factor $\sqrt{E_{0i}/E}$ is supposed to be unity within the range of the resonance capture effective zone i-level.

Formula 17 is a general one and is applicable to lumps of any geometrical form.

The first term of this formula represents blockaded absorption proportional to

$$\frac{\overline{\sqrt{l}}}{L} \simeq \frac{1}{\omega \sqrt{\bar{l}}}$$

With given uranium concentration in the moderator, blockaded absorption changes as $l^{-1/2}$. For low levels where the neutron width is smaller than the radiative, $\sigma_{0i} \sim E^{-1/2}$ and, consequently, in this region the blockaded resonance absorption of one level is proportional to $E_0^{-3/4}$.

The second term of Equation 17 is non-blockaded absorption proportional to $\bar{l}/L = 1/\omega$, i.e., independent in the given concentration of the lump size.

For very small lumps (which, however, are of no practical interest) φ may be computed by the general Formulae 6, 5, and 4. This yields a continuous transition from the homogeneous φ to the value given by Equation 17.

As an example, consider an infinite periodic lattice composed of long cylindrical uranium rods. In this case

$$\bar{l} = \frac{4V}{S} = \frac{4 \cdot \frac{\pi d^2}{4} \cdot h}{\pi d \cdot h} = d$$

$$L = \omega \bar{l} = \frac{\left(a^2 - \frac{\pi d^2}{4}\right) \cdot h}{\frac{\pi d^2}{4} \cdot h} \cdot d = \frac{4}{\pi d}\left(a^2 - \frac{\pi d^2}{4}\right)$$

$$\overline{\sqrt{l}} = 0.975 \sqrt{\bar{l}} \simeq \sqrt{\bar{l}} = \sqrt{d} \qquad (18)$$

In Equations 18 V, S, and h are the volume, surface, and height of the uranium lump respectively; a is the square lattice spacing.

Inserting Equation 18 in Equation 17 we obtain

$$-\ln \varphi = \frac{\lambda_s}{\xi} \cdot \frac{\alpha \cdot d^{3/2} + \beta a^2}{a^2 - \frac{\pi d^2}{4}} \qquad (19)$$

where

$$\alpha = \frac{\pi}{4} 0.975 \sqrt{\pi N} \sum \frac{\sqrt{\sigma_{0i} I_i^2}}{E_{0i}}$$

and

$$\beta = \frac{\pi}{4} N \int_{(E)} \sigma(E) \frac{dE}{E} \qquad (19')$$

are constants determined by the uranium-238 levels.

It is seen from Equation 19 that neutron resonance absorption in a lattice of cylindrical uranium rods is represented as the sum of the blockaded ($\sim d^{3/2}$) and non-blockaded ($\sim d^2$) absorptions.

The break-up of the uranium-238 levels into two groups (blockaded and non-blockaded) corresponding to both terms of Equation 17 is in fact determined by the size of the rods. Equation 17 may therefore be regarded only as an interpolation for the not-too-wide range of the rod diameters.

CONSIDERATION OF DOPPLER BROADENING

The Doppler broadening leads to increased resonance absorption ($1 - \varphi$) and to its dependence on the uranium temperature. It exerts no influence on the non-blockaded part of the resonance absorption given by the second term of Equation 17. This circumstance is associated with the fact that for each level

$$\int \sigma(E) \frac{dE}{E} \simeq \frac{1}{E_0} \int \sigma(E)\, dE$$

A level's area $\int \sigma(E)\, dE$ is always equal to $(\pi/2)\sigma_0\Gamma$ and does not depend on the Doppler width Δ.

For estimates the Doppler broadening formula is used, from the kinetic theory of gases, thus neglecting the specific effects for solids.

$$\sigma(\eta,E) = \sigma_0 \psi(\eta,x)$$

$$\psi = \frac{\eta}{2\sqrt{\pi}} \int_{-\infty}^{\infty} \frac{e^{-\frac{1}{4}\eta^2(x-y)^2}}{1+y^2}\, dy$$

$$x = \frac{E - E_0}{\frac{\Gamma}{2}}$$

$$\eta = \frac{\Gamma}{\Delta}$$

$$\Delta = \sqrt{\frac{F_{0k} T}{A}} \qquad (20)$$

Further estimates will be made for one level with $\Delta > \Gamma$.

It is known that the remote wings of the absorption bands at $\eta^2 x \gg 1$ are properly described by the Breit-Wigner dispersion formula. With $\eta^2 x \ll 1$ we have

$$\psi(\eta,x) \simeq \frac{\sqrt{\pi}}{2} \eta e^{-\frac{1}{4}\eta^2 x^2} \qquad (21)$$

Thus, for one level

$$-\ln \varphi_i' = \frac{\lambda_s}{\xi L} \int f(l) \int (1 - e^{-lN\sigma_{0i}\psi_i}) \frac{dE}{E}\, dl \qquad (22)$$

Notice that the Doppler effect must not affect resonance capture conditioned by the first levels of the blockaded group. For the lower levels where λ_{c0} is very small, this is associated with the fact that when $\bar{l}/\lambda_{c0} \gg 1$ almost all neutrons with $\Delta E = E - E_0 \gg \Delta^2/\Gamma$ are depleted in the neutron spectrum incident on the lump. The absorption contour, therefore, is practically that given by the Breit-Wigner formula. The Doppler effect may play an essential part only for relatively high levels of blockaded groups, i.e., for levels directly adjacent to the non-blockaded group.

In accordance with the above remarks, separate the blockaded resonance capture into two components:

the first consisting of the absorption connected with the lower uranium-238 resonance levels and described by an expression similar to the first term of Equation 17; the second consisting of the absorption conditioned by the intermediate energy levels with the Doppler resonance contour form.

For a rough estimation of the second component use the limiting expression for $\psi(\eta,x)$ applicable in the case when the resonance contour has a purely Doppler form.

Introducing the concept of blockaded resonance capture effective width on one level (ΔE_{eff}) by the relationship

$$\frac{\bar{l}}{\lambda_c\left(E_0 \pm \frac{\Delta E_{eff}}{2}\right)} \simeq 1 \tag{23}$$

and inserting in Equation 23 first Equation 14 and then Equation 21 we obtain

$$\Delta E_{eff}^{(r)} = \Gamma \sqrt{N\sigma_0 \bar{l}}$$

for the resonance contour described by the Breit-Wigner formula, and

$$\Delta E_{eff}^{(D)} = 2\Delta \sqrt{\ln\left(\frac{\sqrt{\pi}}{2} \cdot \frac{\Gamma}{\Delta} N\sigma_0 \bar{l}\right)}$$

for the purely Doppler contour.

It is seen from Equation 17 that the expression for the blockaded resonance capture, except for the factor of the order of unity, can be represented in the form

$$-\ln \varphi_{bl} \simeq \frac{\lambda_s}{\xi L} \sum_{(i)} \frac{(\Delta E_{eff})}{E_{0i}} \tag{24}$$

Owing to this, in the rough approximation, the formula for resonance capture considering the Doppler effect can be written thus:

$$-\ln \varphi = \frac{1}{\xi}\frac{\lambda_s}{L}\left[\sqrt{\pi N}\sqrt{l}\sum_{(i)}\frac{\sqrt{\sigma_{0i}}I_i^2}{E_{0i}} + 2\sum_{(k)}\frac{\Delta_k}{E_{0k}}\sqrt{\ln\left(\frac{\sqrt{\pi}}{2}\cdot\frac{\Gamma_k}{\Delta}N\sigma_0\bar{l}\right)} + N\bar{l}\int_E \sigma\frac{dE}{E}\right] \tag{25}$$

In Equation 25 the first term describes the blockaded resonance absorption at the lowest levels. Here, the Doppler effect has practically no influence on resonance capture. The second term gives blockaded absorption in the region of the levels characterized by the Doppler resonance contour form. And the third term represents nonblockaded resonance capture at high levels for which the contour form is not essential.

Resonance absorption dependence on temperature evidently is determined by the second term of Equation 25. Considering that $\Delta = \sqrt{E_{0k}T/A}$ and neglecting the weak logarithmic dependence of $\sqrt{\ln \alpha\bar{l}}$, the expression for resonance capture per level in the Doppler region can be represented as follows:

$$-\ln \varphi_{bl}^{(I)} \sim \frac{1}{L}\cdot\frac{\Delta E_{eff}}{E_0} \sim \frac{1}{\bar{l}}\sqrt{\frac{T}{E_0}} \tag{26}$$

Thus, in the Doppler region, resonance absorption per one level is roughly proportional to the uranium temperature square root ($\sqrt{T}$) and inversely proportional to the energy level square root.

Lump resonance capture, considering the Doppler effect, was qualitatively examined by F. L. Shapiro.

He found that the absorption integral

$$\Pi(l) = \int_{(E)} (1 - e^{-lN\sigma_0\psi(\eta,x)})\, dx$$

which determines φ,

$$-\ln \varphi = \frac{\lambda_s \Gamma_i}{2\xi L E_{0i}} \int_{(l)} \Pi(l) f(l)\, dl$$

is equal to

$$\Pi(l) = \pi\sigma_0 lN \sum_{k=0}^{\infty} (-1)^k \left(\frac{\sqrt{\pi}}{2}\right)^k \frac{(\sigma_0 lN\eta)^k}{(k+1)!\sqrt{k+1}} e^{\frac{k\eta^2}{4}} \times \left[1 - \Phi\left(\frac{1}{2}\eta\sqrt{\frac{k}{k+1}}\right)\right]^{(k+1)}$$

$$\Phi(x) = \frac{2}{\sqrt{\pi}}\int_0^x e^{-t^2}\, dt \tag{27}$$

In very strong absorptions ($\sigma_0 lN\eta^2 > 5$):

$$\Pi(l) = 2\sqrt{\pi}\sqrt{\sigma_0 lN}\left(1 + \frac{3}{2}\cdot\frac{1}{\sigma_0 lN\eta^2}\right) \tag{28}$$

In the intermediate region where absorption is associated with the Doppler effect:

$$\Pi(l) = \frac{4}{\eta}\sqrt{\ln\left(\frac{\sqrt{\pi}}{4}N l\sigma_0\eta\right)}\left[1 + \frac{0.29}{\ln\left(\frac{\sqrt{\pi}}{2}N l\sigma_0\eta\right)} - \frac{0.14}{\left[\ln\left(\frac{\sqrt{\pi}}{2}N l\sigma_0\eta\right)\right]^2}\right] + \sqrt{\ln\left(\frac{\sqrt{\pi}}{2}N l\sigma_0\eta\right)} \tag{29}$$

Equation 28 was derived for the intermediate energy interval ($10 < N\sigma_0 l\eta < (4/\eta)\sqrt{\ln N\sigma_0 l\eta}$), in which absorption is mainly determined by the Doppler contour form. In the region where Equation 29 is applicable, the principal part is played by the expression's first term which is proportional to the second term of the approximate formula, Equation 25.

As already observed in the first part of this paper, the expressions deduced for φ show a general dependence of φ on uranium concentration in the lattice and on the size of the lumps. Lack of experimental data on the precise structure of all uranium-238 absorption bands requires determination of φ by macroscopic experiment.

LARGE LUMPS

The theory of resonance absorption in large lumps was developed by A. D. Galanin. He examined the limiting case: resonance absorption by lumps with dimensions greatly exceeding the scattering mean free path in them ($\rho = d/2 \gg \lambda_s^U$) ($\rho$ is the radius of the cylindrical rod).

As before, consider that the width of the energy zone in which the effective neutron absorption by the lump occurs is much smaller than the energy change in collision with the moderator atom.

Blockaded resonance absorption by one isolated level will be examined here.

Break up the lump absorption into two parts: $\ln \varphi^{(1)}$ the absorption by the central part of the line (where the capture length is much less than the scattering length, i.e., ($\lambda_c \ll \lambda_s^U$); and $\ln \varphi^{(2)}$, the absorption by the wings of the line ($\lambda_c \sim \lambda_s^U$). In the first case, the lump surface can be considered to be a plane, since the neutron absorption in this energy region takes place in a thin layer, and, consequently, the lump surface curvature is not essential here. In the second case, when the capture mean free path in the lump, λ_c, is of the order of scattering mean free path λ_s^U, a diffusion approximation will be used. The condition $\rho \gg \lambda_s^U$ allows one to obtain continuous transition from one case to the other.

In the first case, resonance absorption has the form of Equation 8

$$-\ln \varphi^{(1)} = \frac{\pi\rho}{2a^2} \cdot \frac{\lambda_s}{\xi E_0} \int \zeta(E)\, dE \qquad (30)$$

where $\zeta(E)$ is represented by the plane "sticking" probability and L is replaced by $2a^2/\pi\rho (a \gg \rho)$. This sticking probability, computed elsewhere[2] by the exact solution of the kinetic equation, is equal to

$$\zeta = 2(1-\sigma)^{1/2} \int_0^1 S e^{SF(S)}\, dS \qquad (31)$$

where

$$\sigma = \frac{\lambda_c}{\lambda_c + \lambda_s^U} \qquad (32)$$

and

$$F(S) = -\frac{1}{\pi} \int_0^{\pi/2} \frac{1+\tan^2 y}{1+S^2\tan^2 y} \ln\left(1 - \frac{\sigma y}{\tan y}\right) dy \qquad (33)$$

In this case $\lambda_c \ll \lambda_s^U$ and $\sigma \ll 1$. Then, as follows from Equation 33 $F(S) \ll 1$ and $e^{SF(S)}$ in the integrand in Equation 31 may be expanded in the series:

$$e^{SF(S)} = 1 + SF(S) \qquad (34)$$

Substituting Equations 34 and 33 in Equation 31, and integrating over S we obtain

$$\zeta = (1-\sigma)^{1/2}\left[1 - \frac{2}{\pi}\int_0^{\pi/2} (1+\cot^2 y)\left(1 - \frac{y}{\tan y}\right)\ln\left(1 - \frac{\sigma y}{\tan y}\right) dy\right] \qquad (35)$$

For convenience of further calculations introduce the variable z

$$z = \sqrt{\frac{\lambda_{c0}}{\lambda_s^U}} \cdot x = \sqrt{\frac{\sigma}{1-\sigma}}\sqrt{1 - \frac{1}{1+x^2}}$$

$$x = \frac{E - E_0}{\frac{\Gamma}{2}}$$

and write Equation 30 as follows

$$-\ln \varphi^{(1)} = \frac{\sqrt{3}}{4a^2} \cdot \frac{\rho}{\lambda_s^U} \cdot A \int_0^z \zeta(z)\, dz;$$

$$A = \frac{2\pi\Gamma}{\xi E_0}\sqrt{\frac{(\lambda_s^U)^3}{3\lambda_{c0}}} \cdot \lambda_s \qquad (36)$$

Where $\tilde{z}$ is the matching point for $z > \tilde{z}$, the diffusion approximation is valid.

The values $\zeta(z)$, calculated by Equation 35, are given in Table 1. It has been taken into account that in the region where $\zeta(z)$ begins to deviate noticeably from unity, one may consider $x \gg 1$, so that ζ will be a function only of z and will not depend on x.

Table 1

z	0	$\frac{1}{\sqrt{2}}$	1	$\sqrt{2}$	$\sqrt{3}$
$\zeta(z)$	1	0.905	0.0832	0.731	0.661

Choose the value of matching point $\tilde{z}$ proceeding from the conditions $3\lambda_s^U = \lambda_c$, which corresponds to $\tilde{z} = \sqrt{3}$. From the data in Table 1 we find

$$\int_0^{\sqrt{3}} \zeta(z)\, dz = 1.54$$

In computing the second part of the resonance absorption, use the diffusion equation with the Bothe correction. Denoting neutron density inside the rod by $n(r)$ we can write $\varphi^{(2)}$ as follows:

$$-\ln \varphi^{(2)} = \frac{2\pi}{a^2} \cdot \frac{\lambda_s}{\xi V_0 E_0} \int dE \int_0^\rho \frac{n'r)}{T}\, r\, dr \qquad (37)$$

where T is the neutron lifetime inside the rod. As follows from the diffusion equation, neutron density with normalization ($n(\rho) = 1$) equals

$$n(r) = \frac{I_0\left(\frac{r}{L_U}\right)}{I_0\left(\frac{\rho}{L_U}\right)} \qquad (38)$$

where L_U is the diffusion length in the rod

$$L_U^2 = TD = \tfrac{1}{3}\lambda\lambda_c, \qquad \lambda^{-1} = (\lambda_s^U)^{-1} + \lambda_c^{-1}$$

Substituting Equation 38 in Equation 37, and integrating over r, we obtain

$$-\ln \varphi^{(2)} = \frac{2\pi}{3a^2}\rho\frac{\lambda_s}{\xi E_0}\int \frac{\lambda}{L_U}\frac{I_1\left(\frac{\rho}{L_U}\right)}{I_0\left(\frac{\rho}{L_U}\right)}dE$$

or upon transition to the variable z and introduction of the notations of Equation 36:

$$-\ln \varphi^{(2)} = \frac{\rho}{\lambda_s^U}\cdot A\cdot J \tag{39}$$

$$J = \int_z^\infty \frac{dz}{\sqrt{1+z^2}}\frac{I_1\left(\sqrt{3}\cdot\frac{\rho}{\lambda_s^U}\cdot\frac{\sqrt{1+z^2}}{z^2}\right)}{I_0\left(\sqrt{3}\cdot\frac{\rho}{\lambda_s^U}\cdot\frac{\sqrt{1+z^2}}{z^2}\right)} \tag{40}$$

With $\rho/\lambda_s^U \gg 1$ the integral J increases logarithmically with the increase of ρ/λ_s^U;

$$J = \text{const} + \ln\frac{\rho}{\lambda_s^U} \tag{40'}$$

(The value of φ^1 depends, of course, on the value of $\tilde{z}$.)

Therefore with $\rho/\lambda_s^U \gg 1$, with logarithmic precision

$$-\ln \varphi^2 = A\cdot\frac{\rho}{\lambda_s^U a^2}\ln\frac{\rho}{\lambda_s^U} \tag{41}$$

Since φ^1 contains no terms with the logarithm (ρ/λ_s^U), total resonance absorption coincides with Equation 41 with the same precision.

For practical purposes, when $\ln(\rho/\lambda_s^U)$ is not so large, it is desirable to have the constant in Equation 40'. The numerical computation, the results of which are given in Table 2, shows that the constant approaches zero, so that complete resonance absorption, which is the sum of Equations 36 and 39, may with satisfactory accuracy be written:

$$-\ln\varphi = \frac{A}{a^2}\cdot\frac{\rho}{\lambda_s^U}(0.67+J) \approx \frac{A}{a^2}\cdot\frac{\rho}{\lambda_s^U}\left(0.7+\ln\frac{\rho}{\lambda_s^U}\right) \tag{42}$$

It can be verified that the constant, 0.7, obtained in Equation 42 really does not depend much on the choice of the value of matching point. (Thus, for example, if we take $\lambda_c = 2\lambda_s^U$ instead of $\lambda_c = 3\lambda_s^U$, the value of the constant will differ from the previous one only by 10 per cent.)

We thus know the resonance absorption in two limiting cases: $0 \ll \lambda_s^U$ (small lumps) and $\rho \gg \lambda_s^U$ (large lumps). The expressions obtained may be interpolated over the region $\rho \sim \lambda_s^U$. For this purpose write down the ratio P of resonance absorption by large lumps $-\ln\varphi(\sigma)$, given by Equation 42, to the resonance absorption by small lumps $-\ln\varphi^{(M)}$, as follows (see Equation 19):

$$-\ln\varphi^{(M)} = 1.05A\left(\frac{\rho}{\lambda_s^U}\right)^{3/4} \tag{43}$$

We have

$$P = \left(\frac{\rho}{\lambda_s^U}\right)^{-1/2}\cdot(0.64+0.95J) \tag{44}$$

where $\rho/\lambda_s^U \ll 1$ P is unity. On the other hand, at the boundary where the theory of large lumps is applicable $P = 1.08$ when $\rho/\lambda_s^U = 1$, and slowly decreases with further increasing of ρ/λ_s^U. This suggests that the theory of resonance absorption in small lumps can be used up to the values of $\rho/\lambda_s^U \sim 1$, and the true value of resonance absorption $-\ln\varphi$ will be less than the value given by the small lump theory.

Equations 39 and 40 allow us to check the basic assumption of Equation 1' that the width of the energy zone in which the effective absorption takes place is small compared with the value of the energy change per collision with the moderator atom. It is seen from Equation 40 that the principal contribution to the integral is made by the values of z for which

$$\sqrt{3}\cdot\frac{\rho}{\lambda_s^U}\cdot\frac{\sqrt{1+z^2}}{z^2} \sim 1$$

or, since it is assumed that $\rho/\lambda_s^U \gg 1$,

$$\sqrt{3}\cdot\frac{\rho}{\lambda_s^U} \sim z$$

Hence, passing from z to the energy, we find that the width of the energy band ΔE in which the resonance absorption occurs is of the order of

$$\Delta E \sim \frac{\rho}{L_0}\cdot\frac{\Gamma}{2}; \qquad L_0 = \sqrt{\frac{1}{3}\lambda_{c0}\lambda_s^U}$$

Consequently, the following condition must be valid

$$\frac{\rho}{L_0}\cdot\frac{1}{2} \ll (1-\epsilon)E_0 \tag{45}$$

where ϵ is the fraction of energy lost by the neutron in collision with the moderator atom:

$$\epsilon = \left(\frac{M-m}{M+m}\right)^2$$

For numerical estimations we take $E_0/\Gamma = 300$ and the absorption cross section in the center of the line $\sigma = 2.5\times10^4$ barns, so that $L_0 = 2.7\times10^{-2}$ cm. Then, from Equation 45 we get that in the case of a heavy-water moderator $(1-\epsilon = 1/9)$, for example, $\rho \ll 15$ cm, and in the case of a graphite moderator $(1-\epsilon = 0.285)$, $\rho \ll 5$ cm.

Table 2

ρ/λ_s^U	1	3	5
J	0.475	1.12	1.60

REFERENCES

1. Zeldovich, Y. B. and Khariton, Y. B., Zhur. Eksp. Theoret. Fiz (Journal of Experimental Theoretical Physics) *10*, 1, 29 (1940).
2. Halpern, O., Zueneburg, R. and Clark, O., Phys. Rev. *53*, 173 (1938).

An Estimation of Doppler Effect in Intermediate and Fast Neutron Reactors

By G. Goertzel,* USA

The temperature coefficient of reactivity of a nuclear reactor is of interest in the study of the dynamic behavior of the reactor. It is of special interest when considering the possible accidents. One source of such a temperature coefficient of reactivity arises from the Doppler effect in the uranium resonances.

Thus, at the resonance energies the cross section is unusually high. This high cross section causes a reduction in neutron flux, so that, for a given energy integral of cross section, the number of events is less than the number which would occur if the resonances were smoothed out. This decrease in effectiveness of cross section when it occurs in the form of resonances is known as the self-shielding of the resonances. The ratio of effective cross section to actual cross section is known as the self-shielding factor. The self-shielding factor is unity for cross sections which show no resonances and decreases as the resonance becomes higher or narrower.

Because of the thermal agitation of the uranium nuclei in a reactor, the relative energy of neutron and nucleus occupies a range of values centered at the energy of the neutron in the laboratory coordinate system. This spread in energy values has the effect of lowering the heights of the resonances and at the same time spreading them out, keeping the integrated cross section invariant. Hence, the thermal motion of the nuclei reduces the self-shielding and increases the self-shielding factor. The larger the temperature, the larger the self-shielding factor and consequently the larger the number of reactions that occur.

In effect, resonance cross sections increase with temperature. Thus, the fissions in U^{235} will be increased with increasing temperature, leading to a positive temperature coefficient of reactivity. This positive coefficient is in part balanced by the negative coefficient of reactivity arising from the increased absorptions in the U^{235}. In fact, in intermediate reactors the temperature coefficient of reactivity because of U^{235} may be negative because resonances with higher than usual capture-to-fission ratio give negative contributions to the temperature coefficient of reactivity. These resonances are amplified in their effect because they are n arrow The capture width is nearly the same from resonance to resonance. Large capture-to-fission ratio means small fission width and therefore small total width.

In the study of fast reactors, it is found that the U^{235} by itself must have a positive Doppler temperature coefficient of reactivity. An admixture of sufficient U^{238} introduces a negative coefficient of reactivity, which balances the positive coefficient. Thus, one problem of interest is the determination of the minimum U^{238} to U^{235} ratio for which the temperature coefficient of reactivity is expected to be negative.

The detailed study of Doppler effect in intermediate reactors differs from that in fast reactors. In intermediate reactors the Doppler-broadened resonances are still quite narrow compared with their spacing for neutrons in the energy range of interest (from a few ev to several hundred ev) so that the effect of individual resonances can be studied and the result summed. Furthermore, the resonance parameters have been measured, at least over a significant part of the energy range.

A fundamentally more difficult problem arises when the self-shielding in energy, defined above, is coupled with effects arising from the lumping of the uranium in fuel elements embedded in a moderator. Much work on this question has been done at Knolls Atomic Power Laboratory by Glenn Roe and Henry Hurwitz. This subject which is of great importance in an intermediate reactor, will not be further treated in the present paper. Formulae for homogenous mixtures are in Section 5.

In a fast reactor, the important energy range lies near 100 kev. At such energies, there is no possibility of measuring the individual resonances. Furthermore, the Doppler-broadened resonances tend to overlap strongly, so that the effect cannot be characterized by a sum over individual resonances. The major portion of the Doppler effect will be found to arise from fluctuations in resonance strengths and spacings. Statistical considerations which permit an inference as to the order of magnitude of the Doppler effect in fast neutron reactors are given in Section 6.

DOPPLER-BROADENED RESONANCES

The Breit-Wigner formula, neglecting the interference of potential and resonance scattering, yields for the contribution to the total cross section from a single resonance

* Including work by H. Feshbach (now at MIT), G. Goertzel, and H. Yamauchi, Nuclear Development Associates, Inc.; and H. Hurwitz and G. Roe, Knolls Atomic Power Laboratory. (The work at KAPL concerned mainly intermediate reactors. The work at NDA was done as part of the fast reactor program of Atomic Power Development Associates, Inc.)

$$\sigma_{tR}(E) = \frac{\sigma_0\Gamma^2/4}{(E - E_0)^2 + \Gamma^2/4}$$

where E_0 is the resonance energy, Γ the total width of the resonance, and $\sigma_0\Gamma$ the strength of the resonance.

The total cross section of a given heavy nucleus may be written as

$$\sigma_t(E) = + \sum_R \sigma_{tR}(E)$$

The sum is over all resonances.

The contribution from a single resonance to the cross section for a reaction process x may be written as

$$\sigma_{xR}(E) = \frac{\sigma_{0x}\Gamma^2/4}{(E - E_0)^2 + \Gamma^2/4}$$

The above formulae for resonance shapes are valid in the absence of any Doppler effect (no nuclear motion). For a Maxwellian distribution of nuclear velocities,† the relation between a cross section at absolute temperature T, $\sigma(E,T)$ and the cross section without Doppler effect, $\sigma(\epsilon)$, is given by

$$\sigma(E,T) = \frac{\int_{-\infty}^{\infty} \sigma(\epsilon) e^{-(E-\epsilon)^2/\Delta^2}\, d\epsilon}{\int_{-\infty}^{\infty} e^{-(E-\epsilon)^2/\Delta^2}\, d\epsilon}$$

for $E \gg \Delta$. Here Δ, the Doppler width, is

$$\Delta = \sqrt{4EkT/A}$$

$$\Delta(u) = 1.2 \times 10^{-3} \sqrt{E(\text{ev})T}\ \text{ev}$$

where k is Boltzmann's constant and A the mass number of the struck nucleus.‡

From the above, it is clear that one may write for a Doppler-broadened resonance

$$\sigma_{xR} = \sigma_{0x}\psi\left(\frac{E - E_0}{\tfrac{1}{2}\Gamma}, \frac{\Delta^2}{\Gamma^2}\right)$$

where§

† A Maxwellian distribution is expected to occur for nuclei in a solid for temperatures above the Debye temperature (W. Lamb, Phys. Rev. *55*, 190 (1939)). For UO_2, the Debye temperature is 160°K (Jones et al., J. Chem. Phys. *20*, 695 (1952)).

‡ The precise relation is

$$\sqrt{E}\,\sigma(E,T) = \frac{\int_0^{\infty} \sqrt{\epsilon}\,\sigma(\epsilon)[e^{-(A/kT)(\sqrt{E}-\sqrt{\epsilon})^2} - e^{-(A/kT)(\sqrt{E}+\sqrt{\epsilon})^2}]\, d\epsilon}{\int_0^{\infty} [e^{-(A/kT)(\sqrt{E}-\sqrt{\epsilon})^2} - e^{-(A/kT)(\sqrt{E}+\sqrt{\epsilon})^2}]\, d\epsilon}$$

§ Tables of $\psi(x,\theta)$ are contained in M. E. Rose, W. Miranker, P. Leak, L. Rosenthal, and J. K. Hendrickson, A Table of the Integral

$$\psi(x,t) = \frac{1}{2\sqrt{\pi t}} \int_{-\infty}^{\infty} \frac{e^{-(x-y)^2/4t}}{1 + y^2}\, dy$$

WAPD-SR-506, October 1954, two volumes (Westinghouse Electric Corporation, Atomic Power Division, Pittsburgh, Pennsylvania).

$$\psi(x,\theta) = \frac{1}{2\sqrt{\pi\theta}} \int_{-\infty}^{\infty} \frac{1}{y^2 + 1} e^{-(x-y)^2/4\theta}\, dy$$

Similarly,

$$\sigma_{tR}(E) = \sigma_0\psi\left(\frac{E - E_0}{\tfrac{1}{2}\Gamma}, \frac{\Delta}{\Gamma}\right)$$

EFFECTIVE CROSS SECTIONS

In this paper transport of neutrons is neglected. In such a case, the neutron behavior in the system is determined by the specification of the neutron density per unit energy, $n(E)$, or by the flux $\phi(E) = v(E)n(E)$ where $v(E)$ is the speed of a neutron with energy E. If $\mu_t(E)$ is the total cross section per unit volume (total macroscopic cross section), $\psi(E) \equiv \mu_t\phi$ is the rate per unit energy at E of the removal of neutrons by all processes. This collision density $\psi(E)$ measures the outflow of neutrons from an energy range. Such an outflow must be compensated by an inflow, to which it is equal.

Such inflow processes include elastic scattering, inelastic scattering and fission. For each of these, the neutrons coming in are smoothly distributed in energy. Thus, in elastic scattering of a neutron of energy E by a nucleus of mass number A, the final neutron energy will be smoothly distributed over a range of energies starting at E and of width

$$\frac{4AE}{(A+1)^2} \simeq 4\frac{E}{A}$$

If $A = 238$ (U^{238}) and $E = 10^5$ ev, $4(E/A) \sim 1500$ ev. For lighter elements, more energetic neutrons, fission, or inelastic scattering, the neutrons coming in are spread smoothly over a wider range. Thus, under the conditions stated, $\psi(E) = \mu_t(E)\phi(E)$ is a smoothly varying function of energy over a range large compared with the spacing of resonances in heavy elements. If μ_t is not smoothly varying, $\phi = \psi/\mu_t$ is not.

By making use of the smoothness of the collision density, $\psi(E)$, an effective cross section and an effective smoothly varying flux may be defined. Effective values will be indicated by a tilde ($\sim$) above the quantity in question.

The criterion to be used in obtaining a suitable definition of "effective" is that the number of events of various types be unchanged when effective rather than actual cross sections are used.

Thus, suppose that ϵ is an energy range within which $\psi(E)$ may, to a good approximation, be taken as constant. The number of processes of type x which take place in such an energy range is given by

$$\int_E^{E+\epsilon} \frac{\mu_x}{\mu_t}\psi\, dE = \int_E^{E+\epsilon} \mu_x\phi\, dE$$

The effective values $\tilde{\mu}_x$, $\tilde{\mu}_t$, $\tilde{\phi}$, $\tilde{\psi}$ will be so defined that

$$\int_E^{E+\epsilon} \frac{\mu_x}{\mu_t}\psi\, dE = \frac{\tilde{\mu}_x}{\tilde{\mu}_t}\tilde{\psi}\epsilon = \tilde{\mu}_x\tilde{\phi}\epsilon$$

for each x. An additional requirement is that if μ_x is independent of energy, $\tilde{\mu}_x = \mu_x$. Then

$$\tilde{\mu}_x = \frac{\int_E^{E+\epsilon} \frac{\mu_x}{\mu_t}\, dE}{\int_E^{E+\epsilon} \frac{1}{\mu_t}\, dE}$$

The above definitions of effective cross sections, when introduced into reactor calculations, will properly take into account the fine-scale resonance structure of the cross sections.

In addition to $\tilde{\mu}_x$, defined as above, one may usefully introduce $\overline{\mu_x}$ defined as the average of μ_x over the energy interval ϵ.

$$\overline{\mu_x} = \frac{1}{\epsilon}\int_E^{E+\epsilon} \mu_x\, dE'$$

The self shielding factor, f, is defined by $\tilde{\mu}_x = f\overline{\mu_x}$.

Using $\overline{\mu_x}$, a simplified form for $\tilde{\mu}_x$ may be obtained. Thus, in particular, it may be that

$$\frac{\mu_t - \overline{\mu_t}}{\overline{\mu_t}} \ll 1$$

in which case the series expansions to be used below are valid.

Thus

$$\mu_t = \overline{\mu_t} + (\mu_t - \overline{\mu_t})$$

whence

$$\frac{\mu_x}{\mu_t} = \frac{\mu_x}{\overline{\mu_t} + (\mu_t - \overline{\mu_t})} \simeq \frac{\mu_x}{\overline{\mu_t}} - \frac{\mu_x(\mu_t - \overline{\mu_t})}{(\overline{\mu_t})^2} + \cdots$$

so that

$$\frac{1}{\epsilon}\int_E^{E+\epsilon} \frac{\mu_x}{\mu_t}\, dE' \simeq \frac{\overline{\mu_x}}{\overline{\mu_t}} - \frac{\overline{\mu_x\mu_t} - \overline{\mu_x}\,\overline{\mu_t}}{\overline{\mu_t}^2} + \cdots$$

To the same order

$$\frac{1}{\epsilon}\int_E^{E+\epsilon} \frac{1}{\mu_t}\, dE' \simeq \frac{1}{\overline{\mu_t}} - 0 + \cdots$$

Hence

$$\tilde{\mu}_x \simeq \overline{\mu_x} - \frac{\overline{\mu_x\mu_t} - \overline{\mu_x}\,\overline{\mu_t}}{\overline{\mu_t}} + \cdots$$

$$f = 1 - \left(\frac{\overline{\mu_x\mu_t}}{\overline{\mu_x}\,\overline{\mu_t}} - 1\right)$$

PERTURBATIONS

Effective cross sections change with temperature. In order to convert this to a change in reactivity, a result from reactor perturbation theory is needed.

There exists a suitably normalized weighting function $w(E)$ (the importance function) such that one has

$$\delta k = \nu w_H \int \delta\tilde{\mu}_f(E)\tilde{\phi}(E)\, dE - \int w(E)\delta\tilde{\mu}_a(E)\tilde{\phi}(E)\, dE$$

$$w_H = \int w(E) f(E)\, dE$$

where δk is the change in reactivity, $f(E)$ is the fission spectrum,

$$\int_0^\infty f(E)\, dE = 1$$

ν is the number of neutrons per fission, $\delta\tilde{\mu}_f$ is the change in effective macroscopic fission cross section, $\delta\tilde{\mu}_a$ is the change in effective macroscopic absorption (capture plus fission) cross section, and $\tilde{\phi}$ is the effective flux per unit energy.

INTERMEDIATE REACTORS

In intermediate reactors the individual resonances do not overlap.

The self-shielding factor for a single resonance is determined as follows. Let

$$\mu_t(E) = \mu t_N + \rho\sigma_0\psi\left(\frac{2}{\Gamma}(E - E_0), \frac{\Delta^2}{\Gamma^2}\right)$$

$$\sigma_{xR}(E) = \sigma_{0x}\psi\left(\frac{2}{\Gamma}(E - E_0), \frac{\Delta^2}{\Gamma^2}\right)$$

where μ_{tN} is the non-resonant part of the total cross section, and ρ is the atomic density of the nucleus in which the resonance occurs. It is assumed that other resonances are far enough away so that they do not contribute to $\mu_t(E)$.

Then one may write, with ΔE denoting an energy interval within which the major part of the resonance lies,

$$\tilde{\sigma}_{xR} = \frac{\int_{\Delta E} \frac{\sigma_{xR}}{\mu_t}\, dE}{\int_{\Delta E} \frac{1}{\mu_t}\, dE}$$

$$\overline{\sigma_{xR}} = \frac{1}{\Delta E}\int_{\Delta E} \sigma_{xR}\, dE$$

$$f = \frac{\tilde{\sigma}_{xR}}{\overline{\sigma_{xR}}} \simeq \frac{\int_{-\infty}^{\infty} \frac{\psi\left(\frac{2}{\Gamma}(E - E_0), \frac{\Delta^2}{\Gamma^2}\right)}{1 + \frac{\rho\sigma_0}{\mu_{tN}}\psi\left(\frac{2}{\Gamma}(E - E_0), \frac{\Delta^2}{\Gamma^2}\right)}\, dE}{\int_{-\infty}^{\infty} \psi\left(\frac{2}{\Gamma}(E - E_0), \frac{\Delta^2}{\Gamma^2}\right) dE}$$

Since

$$\int \sigma_{xR}\, dE = \frac{\pi}{2}\sigma_{0x}\Gamma$$

the contribution of a single resonance to the temperature coefficient is, using the results of Section 4,

$$\left(T\frac{\partial k}{\partial T}\right)_{resonance} = \frac{\pi}{2}\rho\sigma_{0a}\Gamma\tilde{\phi}w\left(\frac{\nu}{1+\alpha}\frac{w_H}{w} - 1\right)T\frac{\partial f}{\partial T}$$

where

$$\alpha = \frac{\sigma_{0c}}{\sigma_{0f}} = \frac{\sigma_{0a}}{\sigma_{0f}} - 1$$

is the capture-to-fission ratio. This, summed over all resonances, yields the temperature coefficient.

It is interesting to note that

$$\left(T\frac{\partial k}{\partial T}\right)_{resonance}$$

is negative if

$$\alpha > \nu\frac{w_H}{w} - 1$$

Furthermore, $T(\partial f/\partial T)$ emphasizes narrow resonances. Thus, if $\rho\sigma_0/\mu_{tN}$ is small, one finds for $T(\partial f/\partial T)$

$$T\frac{\partial f}{\partial T} = \frac{\rho\sigma_0}{2\mu_{tN}}\,\theta\,\frac{\partial}{\partial\theta}\,\psi(0,\theta)\,\Big|_{\theta=\frac{\Delta^2}{2\Gamma^2}}$$

If, further, Δ/Γ is small (not a practical case)

$$T\frac{\partial f}{\partial T} = \frac{\rho\sigma_0}{2\mu_{tN}}\,\frac{\Delta^2}{\Gamma^2}$$

One expects w_H/w to be of the order of ½ in an intermediate reactor so that the critical value of α is about 0.25. Thus there are indeed resonances in which $(\partial k/\partial T)_{resonance}$ is negative. The calculation indicates that the net Doppler effect of U^{235} may be negative for some reactors.

FAST-NEUTRON REACTORS

In the derivation to be presented here, we shall for simplicity neglect effects which reduce the Doppler effect at 10^5 ev by about a factor of 4 and which reduce the Doppler effect at 2 Mev by a factor of about 200. These effects are:

1. The decrease in level spacing (distance between resonances) with increasing energy.
2. The coming into importance, at higher energies, of the interactions of neutrons and nuclei with higher relative orbital angular momentum.
3. The interference between potential and resonance scattering.

Rather detailed predictions as to nuclear behavior (taken from Weisskopf's statistical model of the nucleus) were used in including the above effects. These considerations tend to obscure the Doppler effect itself. Furthermore, they probably reduce the U^{235} and U^{238} values by the same factor, so that one may predict the U^{238} to U^{235} concentration ratio required to obtain a negative temperature coefficient with some confidence. The strong reduction of Doppler effect at the higher energies means that in fairly dilute fast reactors one expects major contributions to the Doppler only from neutrons with energies of about 10^5 ev.

At such energies, the Doppler width Δ is equal to (at 625° K) 10 ev. This value is much larger than the distance between resonances in U^{235} and about the same as the distance between resonances in U^{238}. Furthermore, the mean energy change in slowing down in U is about 800 ev, so that $\tilde{\mu}_x$ may be calculated by averaging over many overlapping resonances.

The detailed values of the resonance parameters cannot be measured at present. Nevertheless, since there are so many resonances involved in the calculation of $\tilde{\mu}_x$, the energy averages involved in such a calculation may be thought of as a statistical average over a probability distribution from which the resonances have been selected. That is

$$\frac{1}{\epsilon}\int_E^{E+\epsilon} g(E')\,dE' \equiv \overline{g(E)}$$

is replaced by $\langle g(E)\rangle$.

The operation $\langle\ \rangle$ is defined by the following assumptions:

1. In a given nuclear species, the set of quantities σ_{0xk}, σ_{0k}, Γ_k characterizing the kth resonance are consistent with the assumption that the set has, for each k, been independently selected from a population of such parameters. This population is described by a probability density $p(\sigma_0,\sigma_{0x},\Gamma)$.
2. The set of resonance energies E_k are consistent with the assumption that the spacings between levels

$$S_k = E_k - E_{k-1}$$

have been independently selected from a population of such parameters. This population is described by a probability density $p(S)$.

Having been thus given the distribution of spaces, $p(S)$, it is straightforward to deduce the distribution for the kth energy $p_k(E)$.¶ We note that the probability that the kth energy will be E and the k'th will be E' is given by

$$p_{k,k'}(E,E') = p_k(E)\,p_{k'-k}(E'-E)$$

if $k' > k$.

The sum

$$\Omega(E) = \sum_{k=1}^{\infty} p_k(E)$$

defines the expected density of levels at E. If w is the mean density of levels, then $\Omega(E) \simeq w$ for $E \gg w$.

As a result of these remarks, it is clear that

$$\left\langle \sum_k g(\sigma_{0k},\sigma_{0xk},\Gamma_k,E_k) \right\rangle$$

$$= \iiiint \sum_k g(\sigma_0,\sigma_{0x},\Gamma,E)$$

$$x p(\sigma_0,\sigma_{0x},\Gamma)\,p_k(E)\,d\sigma_0\,d\sigma_{0x}\,d\Gamma\,dE$$

$$= w\left\langle \int_{-\infty}^{\infty} g\,dE \right\rangle_0 = w\int_{-\infty}^{\infty}\langle g\rangle_0\,dE$$

where

$$\langle g\rangle_0 = \iiint g(\sigma_0,\sigma_{0x},\Gamma,E)\,p(\sigma_0,\sigma_{0x},\Gamma)\,d\sigma_0\,d\sigma_{0x}\,d\Gamma$$

Similarly, one finds that

$$\left\langle \sum_{k,k'} g(\sigma_{0k},\sigma_{0xk},\Gamma_k,E_k)\,h(\sigma_{0k'},\sigma_{0xk'},\Gamma_{k'},E_{k'}) \right\rangle$$

$$= w\int_{-\infty}^{\infty}\langle g(\sigma_0,\sigma_{0x},\Gamma,E)\,h(\sigma_0,\sigma_{0x},\Gamma,E)\rangle_0\,dE$$

$$+ w\int_{-\infty}^{\infty}\int_{-\infty}^{\infty}\Omega(|E-E'|)$$

$$\times\langle g(\sigma_0,\sigma_{0x},\Gamma,E)\rangle_0\,\langle h(\sigma_0,\sigma_{0x},\Gamma,E')\rangle_0\,dE\,dE'$$

¶ $p_1(E) = p(E)$

$p_k(E) = \int_0^E p(\epsilon)\,p_{k-1}(E-\epsilon)\,d\epsilon$

The evaluation of $\tilde{\mu}_x$, $T(\partial\mu_x/\partial T)$, and thus $T(\partial k/\partial T)$ is straightforward. From Section 3

$$\tilde{\mu}_x = \langle\mu_x\rangle - \frac{\langle\mu_x\mu_t\rangle - \langle\mu_x\rangle\langle\mu_t\rangle}{\langle\mu_t\rangle}$$

Writing

$$\mu_x = \rho \sum_k \sigma_{0xk}\psi\left(\frac{2}{\Gamma_k}(E - E_k), \frac{\Delta^2}{\Gamma_k^2}\right)$$

and

$$\mu_t = \mu_{tN} + \mu_{tR} = \mu_{tN} + \rho \sum_k \sigma_{0k}\psi\left(\frac{2}{\Gamma_k}(E - E_k), \frac{\Delta^2}{\Gamma_k^2}\right)$$

one obtains directly $\left(\text{note that } \int_{-\infty}^{\infty} \psi\, dE = (\Gamma/2)\pi\right)$

$$\langle\mu_x\rangle = w\rho\left\langle\sigma_{0x}\int_{-\infty}^{\infty}\psi\left(\frac{2E}{\Gamma}, \frac{\Delta^2}{\Gamma^2}\right)dE\right\rangle_0 = w\rho\frac{\pi}{2}\langle\sigma_{0x}\Gamma\rangle_0$$

$$\langle\mu_x\mu_t\rangle - \langle\mu_x\rangle\langle\mu_t\rangle = \langle\mu_x\mu_{tR}\rangle - \langle\mu_x\rangle\langle\mu_{tR}\rangle$$

$$= \rho^2 w\left\langle\sigma_{0x}\sigma_0\int_{-\infty}^{\infty}\psi^2\, dE\right\rangle_0$$

$$+ \rho^2 w\int_{-\infty}^{\infty}\int_{-\infty}^{\infty}[\Omega(|E - E'|) - w]$$

$$\times\left\langle\sigma_{0x}\psi\left(\frac{2E}{\Gamma}, \frac{\Delta^2}{\Gamma^2}\right)\right\rangle\left\langle\sigma_0\psi\left(\frac{2E'}{\Gamma}, \frac{\Delta^2}{\Gamma^2}\right)\right\rangle dE\, dE'$$

Using $\Delta/\Gamma \gg 1$ so that

$$\psi\left(\frac{2E}{\Gamma}, \frac{\Delta^2}{\Gamma^2}\right) \simeq \frac{\sqrt{\pi}\,\Gamma}{2\Delta}e^{-E^2/\Delta^2}$$

$$\int_{-\infty}^{\infty}\psi^2\, dE = \frac{\Gamma^2}{2\Delta}\left(\frac{\pi}{2}\right)^{1/2}$$

one obtains

$$\langle\mu_x\mu_t\rangle - \langle\mu_x\rangle\langle\mu_t\rangle = \frac{S}{\Delta\sqrt{2\pi}}\langle\mu_x\rangle\langle\mu_{tR}\rangle$$

where

$$S = D - d$$

$$D = \frac{\langle\sigma_{0x}\sigma_0\Gamma^2\rangle_0}{w\langle\sigma_{0x}\Gamma\rangle_0\langle\sigma_0\Gamma\rangle_0}$$

$$d = \int_{-\infty}^{\infty}[1 - \Omega(|\eta|)/w]e^{-\eta^2/2\Delta^2}\, d\eta$$

Thus, since

$$T\frac{d}{dT}\frac{1}{\Delta} = -\frac{1}{2\Delta}$$

$$T\frac{\partial}{\partial T}\tilde{\mu}_x = \frac{S}{\sqrt{8\pi}\,\Delta}\frac{\langle\mu_x\rangle\langle\mu_{tR}\rangle}{\langle\mu_t\rangle}$$

This is the final result, which remains to be interpreted and applied. $\langle\mu_x\rangle$, $\langle\mu_t\rangle$ are the actual cross sections which go into the reactor calculations D is estimated from low-energy data thus: let there be r resonances in an energy range ΔE. Then

$$D = \frac{\sum_{\text{resonances}}\sigma_{0x}\sigma_0\Gamma^2}{\left(\sum_{\text{resonances}}\sigma_{0x}\Gamma\right)\left(\sum_{\text{resonances}}\right)\sigma_0\Gamma}\Delta E$$

For the energy range 12.5 to 35.3 ev one finds for U^{235} that $D^{25} = 6.4$ ev, and $n = 19$, $(\Delta E/n) = 1.20$ ev. For U^{238} up to about 120 ev, $D^{28} = 22$ ev, $(\Delta E/n) = 16.9$ ev.

The value of d depends on the assumption made as to the distribution of spaces, $p(S)$. Three cases have been evaluated.

1. Uniform spacing, for which

$$d = \frac{\Delta E}{n}.$$

2. Poisson distribution $p(S) = e^{-ws}w$, for which $d = 0$.

3. A distribution given by $p(S) = 4w^2Se^{-2ws}$ for which (if $w\Delta > 1$)

$$d = \frac{\Delta E}{2n}$$

This last case is suggested by experimental data on the distribution of low-energy resonances. Using the d values for this case gives

$$S^{25} = 5.8 \text{ ev}$$

$$S^{28} = 13.5 \text{ ev}$$

The contribution of U^{235} to $\partial k/\partial T$ is given by

$$\left(T\frac{\partial k}{\partial T}\right)_{25} = \left[\frac{v}{1+\alpha}\frac{w_H}{w} - 1\right]w\tilde{\phi}\rho_{25}{}^2\frac{\langle\sigma_a{}^{25}\rangle\langle\sigma_{tR}{}^{25}\rangle}{\langle\mu_t\rangle}\frac{S^{25}}{\sqrt{8\pi}\,\Delta}$$

The contribution of U^{238} is

$$\left(T\frac{\partial k}{\partial T}\right)_{28} = -w\tilde{\phi}\rho_{28}{}^2\frac{\langle\sigma_a{}^{28}\rangle\langle\sigma_{tR}{}^{28}\rangle}{\langle\mu_t\rangle}\frac{S^{28}}{\sqrt{8\pi}\,\Delta}$$

One expects $\langle\sigma_{tR}{}^{28}\rangle$ to be about the same as $\langle\sigma_{tR}{}^{25}\rangle$. Thus, the positive effect of 25 will be cancelled by the negative effect of 28 if

$$\frac{\rho_{28}{}^2}{\rho_{25}{}^2} \geq \left(\frac{v}{1+\alpha}\frac{w_H}{w} - 1\right)\frac{\langle\sigma_a{}^{25}\rangle S^{25}}{\langle\sigma_a{}^{28}\rangle S^{28}} \sim 1 \cdot \frac{2.2b}{0.27b}\frac{5.8}{13.5}$$

or, to obtain a negative temperature coefficient, $\rho_{28} > 1.87\rho_{25}$.

The Thermal Coefficient in a Heterogeneous Reactor

By A. D. Galanin, USSR

When calculating the thermal utilization factor (thermal coefficient) in a heterogeneous reactor, a method is generally used known in the theory of crystals as the Wigner-Zeitz cell method. The elementary cell, for instance a square one, is replaced by a circle with an equal area, in the centre of which a uranium cylinder is placed. The action of the remaining cells on the given one is accounted for by means of the boundary conditions: the flux of neutrons at the boundary of the cell equals zero.

Although such a method of calculation is in most cases sufficiently accurate, it is desirable to have a more detailed theory which could, first of all, confirm the correctness of the approximation method and, secondly, solve a number of problems which cannot be treated by the approximation method. Such problems include, for example, the dependence of the thermal utilization factor on the shape of the cell.

FORMULATION OF EQUATIONS

Consider a lattice with a cell area σ. In the lattice joints uranium cylinders (infinitely long) of radius ρ are located. The radius of the cylinder ρ is supposed to be sufficiently small. We shall ignore the resonance absorption of uranium. Then the uranium cylinder is characterized by two constants; the constant of multiplication η, which is the number of fast neutrons produced during the capture by the uranium cylinder of one thermal neutron, and the thermal constant γ representing the ratio of the flux of thermal neutrons falling upon the cylinder to the density of thermal neutrons on its surface. In the first approximation the thermal constant may be determined by using the elementary equation of diffusion:

$$\gamma = \frac{\pi\rho^2 D_U}{L_U^2} \cdot \frac{1}{Q} \tag{1}$$

where

$$Q = \frac{I_0\left(\frac{\rho}{L_U}\right)}{\frac{2L_U}{\rho} I_1\left(\frac{\rho}{L_U}\right)} \tag{2}$$

and D_U and L_U are the diffusion coefficient and diffusion length in uranium.

The differential equation for the thermal neutron density in the moderator appears as follows (in a stationary case):

$$D\,\Delta N(r) - \frac{N(r)}{T} + \eta\gamma \sum_k W(r,r_k)N(r_k) - \gamma \sum_k \delta(r - r_k)N(r)_k = 0 \tag{3}$$

where D is the diffusion coefficient of thermal neutrons in the moderator, T is the lifetime of thermal neutrons in the moderator, and $W(r,r_k)$ the probability that the fast neutron generated in the uranium cylinder number k, will become thermal at the point r. The latter term describes the absorption of thermal neutrons by uranium cylinders; r_k is the vector radius of number k cylinder. Wherever possible, the cylinder radius is considered equal to zero. Summation over k means a sum over two components k_1 and k_2. We shall consider a sufficiently large lattice. Then $W(r,r_k)$ equals (supposing that the equation of the age theory is justified):

$$W(r,r_k) = \frac{1}{4\pi\tau} e^{-\frac{(r-r_k)^2}{4\tau}} \tag{4}$$

Considering $N(r_k) \equiv N(k)$ to be given, it is easy to obtain with the help of the Fourier transformation the following solution of Equation 3 ($L^2 = DT$):

$$N(r) = \frac{\gamma}{2\pi D} \sum_k \left\{ \eta \int_0^\infty \frac{x e^{-x^2\tau} J_0(|r - r_k|x)}{x^2 + \frac{1}{L^2}}\, dx - K_0\left(\frac{|r - r_k|}{L}\right) \right\} N(k) \tag{5}$$

This solution may be expressed as follows*

* If

$$p(\tau) = \int_0^\infty \frac{x e^{-x^2\tau} J_0(xr)}{x^2 + 1/L^2}\, dx$$

then differentiating by τ, we obtain

$$\frac{\partial p}{\partial \tau} - \frac{p}{L^2} = -\frac{1}{2\tau} e^{-\frac{r^2}{4\tau}}$$

By solving this differential equation with the initial conditions

$$p(0) = \int_0^\infty \frac{x J_0(xr)\, dx}{x^2 + 1/L^2} = K_0\left(\frac{r}{L}\right) = \int_0^\infty \frac{dx}{2x} e^{-\left(x + \frac{r^2}{4L^2 x}\right)}$$

we obtain

$$p(\tau) = e^{\tau/L^2} \int_{\tau/L^2}^\infty \frac{dx}{2x} e^{-\left(x^2 + \frac{r^2}{4L^2 x}\right)}$$

Original language: Russian.

$$q_0 N(r) = \sum_k H(|r - r_k|)N(k) \tag{6}$$

where

$$q_0 = \frac{2\pi D}{\gamma} \cdot \frac{\sigma}{2\pi L^2} \tag{7}$$

$$H(|r|) = \frac{\sigma}{2\pi L^2}\left[\eta e^{\tau/L^2}\int_{\tau/L^2}^{\infty} - \int_0^{\infty}\right] e^{-\left(z+\frac{r^2}{4L^2 z}\right)}\frac{dz}{2z} \tag{8}$$

Equation 6 may be used to determine the critical dimensions of the reactor consisting of a small number of cells, provided it has an infinite reflector.[1]

Suppose in Equation 6 that $r \to r_k$. Then Equation 6 is an equation with regard to $N(k)$. We shall seek the solution in form:

$$N(k) = e^{i\vec{\kappa} r_k}$$

Inserting Equation 6, we obtain

$$q_0 = \sum_k H(|k|)e^{i\vec{\kappa} r_k} \tag{9}$$

Equation 9 is the characteristic equation of the lattice which determines the reactor Laplacian κ^2.

GENERAL CHARACTERISTIC EQUATION

We consider before the first part of the sum in Equation 9

$$\Sigma_1 = \frac{\sigma}{2\pi L^2}\eta e^{\tau/L^2}\int_{\tau/L^2}^{\infty}\frac{e^{-z}\,dz}{2z}\sum_k e^{i\vec{\kappa} r_k} e^{-\frac{r_k^2}{4L^2 z}} \tag{10}$$

Let us calculate this sum for a square lattice with spacing a. The sum over k appears as

$$\sum_k = \sum_{k_1,k_2} e^{i(\kappa_1 k_1 + \kappa_2 k_2)a - \frac{a^2}{4L^2 z}(k_1^2 + k_2^2)}$$

By transforming this sum with the help of Poisson's summation formula[2]

$$\sum_{n=-\infty}^{+\infty}\varphi(2\pi n) = \frac{1}{2\pi}\sum_{\nu=-\infty}^{+\infty}\int_{-\infty}^{+\infty}\varphi(k)e^{-i\nu k}\,dk \tag{11}$$

we obtain

$$\sum_k = \frac{1}{4\pi^2}\sum_{\nu}\int e^{i\frac{\vec{\kappa} ka}{2\pi} + \frac{a^2 k^2}{16\pi^2 L^2 z} + i\vec{\nu} k}\,dk$$

$$= \frac{4\pi L^2 z}{\sigma}\sum_{\nu} e^{-\frac{4\pi^2 L^2 z}{a^2}\left(\vec{\nu} + \frac{\vec{\kappa} a}{2\pi}\right)^2}$$

Inserting this result into Equation 10 and integrating by z we obtain

$$\Sigma_1 = \sum_{\nu} \frac{\eta e^{-\frac{4\pi^2\tau}{a^2}\left(\vec{\nu} + \frac{a}{2\pi}\vec{\kappa}\right)^2}}{1 + \frac{4\pi^2 L^2}{a^2}\left(\vec{\nu} + \frac{a\vec{\kappa}}{2\pi}\right)^2} \tag{21}$$

Under conditions

$$4e^{-\frac{4\pi^2\tau}{a^2}} \ll 1, \qquad \frac{\kappa a}{2\pi} \ll 1 \tag{13}$$

which in practically important cases are well fulfilled we obtain (in Equation 12 only one term with $\nu_1 = \nu_2 = 0$ is taken)

$$\Sigma_1 = \frac{\eta e^{-\kappa^2\tau}}{1 + \kappa^2 L^2} \tag{14}$$

When the conditions of Equation 13 are fulfilled, this result will remain for any shape of cell as well as when calculating the sum

$$\Sigma H(|r - r_k|)e^{i\vec{\kappa} r_k}$$

where r differs from the vector radius of any uranium cylinder.

The inequality in Equation 13 is the condition that the density of slowing down neutrons is constant throughout the cell.

The second part of the sum in Equation 9, Σ_2, we shall calculate for the cell as a parallelogram with sides a_1 and a_2 and an angle between the sides $\omega(\sigma = a_1 a_2 \sin\omega)$, remaining arbitrary

$$\Sigma_2 = -\frac{\sigma}{4\pi L^2}\int_0^{\infty}\frac{e^{-z}\,dz}{z}\sum_k e^{i\vec{\kappa}(r_k - r) - \frac{(\kappa_k - r)^2}{4L^2 z}} \tag{15}$$

In this case

$$(r_k - r)^2 = (a_1 k_1 - x)^2 + (a_2 k_2 - y)^2 + 2(a_1 k_1 - x)(a_2 k_2 - y)\cos\omega,$$

where x, y are oblique-angled coordinates of point r.

The application of the summation formula, Equation 11, with subsequent replacement of the variables

$$\frac{a_1 k_1}{2\pi} - x = u_1, \qquad \frac{a_2 k_2}{2\pi} - y = u_2$$

results in

$$\Sigma_2 = -\frac{1}{4\pi L^2}\int_0^{\infty}\frac{e^{-z}\,dz}{z}\sum_{\nu_1,\nu_2} e^{i2\pi\left(\frac{\nu_1 x}{a_1} + \frac{\nu_2 y}{a_2}\right)} \times \int_{-\infty}^{+\infty}$$

$$\int e^{-\frac{u_1^2 + u_2^2 + 2u_1 u_2\cos\omega}{4L^2 z} + i\left[u_1\left(\kappa_1 + \frac{2\pi\nu_1}{a_1}\right) + u_2\left(\kappa_2 + \frac{2\pi\nu_2}{a_2}\right)\right]} \sin\omega\,du_1\,du_2 \tag{16}$$

Coordinates u_1, u_2 are oblique-angled coordinates of the vector whose modulus is equal to

$$|\vec{F}| = \sqrt{u_1^2 + u_2^2 + 2u_1 u_2\cos\omega}$$

and $\kappa_1 + (2\pi\nu_1/a_1)$, $\kappa_2 + (2\pi\nu_2/a_2)$ are coordinates of vector f with modulus

$$|\vec{f}| = \frac{1}{\sin\omega}\sqrt{\left(\kappa_1 + \frac{2\pi\nu_1}{a_1}\right)^2 + \left(\kappa_2 + \frac{2\pi\nu_2}{a_2}\right)^2 - 2\left(\kappa_1 + \frac{2\pi\nu_1}{a_1}\right)\left(\kappa_2 + \frac{2\pi\nu_2}{a_2}\right)\cos\omega}$$

related to the basis of the inverse lattice. Then

$$u_1\left(\kappa_1+\frac{2\pi\nu_1}{a_1}\right)+u_2\left(\kappa_2+\frac{2\pi\nu_2}{a_2}\right)=Ff\cos\theta$$

$$du_1\,du_2=\frac{FdF}{\sin\omega}\,d\theta$$

and the integral by du_1, du_2 (in Equation 16) reduce to

$$\int_0^\infty Fe^{-\frac{F}{4L^2z}}\,dF\int_0^{2\pi}e^{iFf\cos\theta}\,d\theta$$

$$=2\pi\int_0^\infty Fe^{-\frac{F^2}{4L^2z}}J_0(fF)\,dF=4\pi L^2ze^{-L^2zf^2}$$

Consequently

$$\Sigma_2=-\sum_{\nu_1,\nu_2}\frac{e^{2\pi i\left(\frac{\nu_1x}{a_1}+\frac{\nu_2y}{a_2}\right)}}{1+4\pi^2L^2f_{\nu_1\nu_2}{}^2} \tag{17}$$

where

$$f_{\nu_1\nu_2}{}^2=\frac{1}{\sin^2\omega}\left[\left(\frac{\nu_1}{a_1}+\frac{\kappa_1}{2\pi}\right)^2+\left(\frac{\nu_2}{a_2}+\frac{\kappa_2}{2\pi}\right)^2-2\left(\frac{\nu_1}{a_1}+\frac{\kappa_1}{2\pi}\right)\left(\frac{\nu_2}{a_2}+\frac{\kappa_2}{2\pi}\right)\cos\omega\right] \tag{18}$$

If the conditions are fulfilled

$$\frac{4\pi L^2}{a_{1,2}{}^2}\gg 1 \tag{19}$$

$$\frac{a_{1,2}\kappa_{1,2}}{2\pi}\ll 1 \tag{20}$$

then

$$\Sigma_2=-\frac{1}{1+D^2\kappa^2}-q_1$$

where

$$\kappa_2=\frac{\kappa_1{}^2+\kappa_2{}^2-2\kappa_1\kappa_2\cos\omega}{\sin^2\omega}$$

$$q_1=\frac{\sin^2\omega}{4\pi^2L^2}\sum_{\nu_1,\nu_2}{}'\frac{\cos 2\pi\left(\frac{\nu_1x}{a_1}+\frac{\nu_2y}{a_2}\right)}{\left(\frac{\nu_1}{a_1}\right)^2+\left(\frac{\nu_2}{a_2}\right)^2-2\frac{\nu_1\nu_2}{a_1a_2}\cos\omega} \tag{21}$$

(The accent means the absence of the term $\nu_1=\nu_2=0$.) The characteristic equation of the lattice then appears as follows

$$q_0=\frac{\eta e^{-\kappa^2\tau}-1}{1+\kappa^2L^2}-q_1(0) \tag{22}$$

where $q_1(0)$ is obtained from Equation 21, if point x, y tends towards a point on the surface of the uranium cylinder.

Equation 22 may also be written as

$$1+\kappa^2L_p{}^2=ke^{-\kappa^2\tau};\qquad k=\frac{\eta}{1+q}$$

$$L_p{}^2=\frac{q}{1+q}L^2;\qquad q=q_0+q_1(0) \tag{23}$$

Quantity $q_1(0)$ characterizes the lump-effect in the thermal absorption due to non-uniformity in the distribution of thermal neutrons throughout the cell.

SQUARE LATTICE

Let us calculate q_1 for a square lattice

$$q_1=\frac{a^2}{4\pi^2L^2}\sum_{\nu_1,\nu_2}{}'\frac{\cos\frac{2\pi\nu_1x}{a}\cos\frac{2\pi\nu_2y}{a}}{\nu_1{}^2+\nu_2{}^2} \tag{24}$$

This series does not converge absolutely and therefore its sum depends on the order of summation. However, prior to integrating by z, the series converged absolutely. If we symmetrize there by ν_1 and ν_2, then the sum of the series in Equation 24 will also be independent of the order of summation. Therefore the sum over ν_1 and ν_2 can be written as follows

$$2\sum_{\nu=1}^{\infty}\frac{1}{\nu^2}\left(\cos\frac{2\pi\nu x}{a}+\cos\frac{2\pi\nu y}{a}\right)+2\sum_{\nu_1=1}^{\infty}\sum_{\nu_2=1}^{\infty}\frac{1}{\nu_1{}^2+\nu_2{}^2}\left[\cos\frac{2\pi\nu_1x}{a}\cos\frac{2\pi\nu_2y}{a}+\cos\frac{2\pi\nu_2x}{a}\cos\frac{2\pi\nu_1y}{a}\right]$$

The sum by one variable is calculated with the help of the formula

$$\sum_{k=1}^{\infty}\frac{\cos kx}{k^2+a^2}=\frac{\pi}{2\alpha}\frac{\operatorname{ch}\alpha(\pi-x)}{\operatorname{sh}\alpha\pi}-\frac{1}{2\alpha^2};$$

$$\sum_{k=1}^{\infty}\frac{\cos kx}{k^2}=\frac{\pi^2}{6}-\frac{\pi x}{2}+\frac{x^2}{4}$$

and we obtain

$$\frac{\pi^2}{3}-\frac{\pi}{a}(x+y)+\frac{\pi^2}{a^2}(x^2+y^2)+\pi\sum_{\nu=1}^{\infty}\frac{\operatorname{ch}\pi\nu_1\left(1-\frac{2y}{a}\right)\cos\frac{2\pi\nu_1x}{a}+\operatorname{ch}\pi\nu_1\left(1-\frac{2x}{a}\right)\cos\frac{2\pi\nu_1y}{a}}{\nu_1\operatorname{sh}\nu_1\pi}$$

In further transformations we consider and use the formula

$$\sum_{k=1}^{\infty}\frac{1}{k}\cos\beta k e^{-\alpha k}=-\frac{1}{2}\ln\left[1-2e^{-\alpha}\cos\beta+e^{-2\alpha}\right]$$

$$=\frac{\alpha}{2}-\frac{1}{2}\ln 4\left(\operatorname{sh}^2\frac{\alpha}{2}+\sin^2\frac{\beta}{2}\right)$$

and we get

$$q_1(x,y) = \frac{a^2}{4\pi L^2} \cdot \left\{ \frac{7\pi}{3} - \frac{\pi}{\alpha}(x+y) + \frac{\pi}{a^2}(a^2+y^2) - \frac{1}{2}\ln\left[4^4 f(x,y)f(y,x)f(x,a-y)f(y,a-x)\right] \right\} \quad (25)$$

where

$$f(x,y) = \sin^2\frac{\pi x}{a} + \mathrm{sh}^2\frac{\pi y}{a}$$

Now, supposing $x = \rho\cos\varphi$; $y = \rho\sin\varphi$ and expanding in powers of ρ/a we obtain

$$q_1(0) = \frac{a^2}{4\pi L^2}\left[\ln\frac{a^2}{\pi\rho^2} + \frac{\pi\rho^2}{a^2} - \ln 4\pi + \frac{\pi}{3}\right]$$

$$\ln 4\pi - \frac{\pi}{3} = 1.48 \quad (26)$$

As is known, the calculations by the Wigner-Zeitz cell method lead to the same formula, the only difference being that the coefficient 1.48 is replaced by ¾.

It should be noted that if allowance is made for the finiteness of radius ρ, Equation 7 should be changed to

$$q_0 = \frac{2\pi D}{\gamma} \cdot \frac{\sigma - \pi\rho^2}{2\pi L^2}$$

This will bring about a correct transition to the homogeneous case. Since from the very beginning the azimuthal dependence of the neutron density in the uranium cylinder has been ignored, the allowance for the next powers ρ/a in Equation 26 is not justified since in their presence there appears a factor depending on φ.

Estimate the errors caused by the conditions of Equations 19 and 20. If these conditions are not superimposed, then

$$q_1 = \sum_{\vec{\nu}} \frac{e^{2\pi i \frac{\vec{\nu}\vec{r}}{a}}}{1 + \frac{4\pi^2 L^2}{a^2}\left(\vec{\nu} + \frac{\vec{\kappa} a}{2\pi}\right)^2} \quad (27)$$

Rewrite Equation 27 as follows

$$q_1 = \frac{a^2}{4\pi^2 L^2}\sum_{\vec{\nu}}{}' \frac{e^{2\pi i \frac{\vec{\nu}\vec{r}}{a}}}{\nu^2} + \sum_{\vec{\nu}}{}' \left\{ \frac{e^{2\pi i \frac{\vec{\nu}\vec{r}}{a}}}{1 + \frac{4\pi^2 L^2}{a^2}\left(\vec{\nu} + \frac{\vec{\kappa} a}{2\pi}\right)^2} - \frac{e^{2\pi i \frac{\vec{\nu}\vec{r}}{a}}}{\frac{4\pi^2 L^2}{a^2}\nu^2} \right\}$$

In the second sum we may take $r = 0$. Then

$$q_1 = q_1(0) + \frac{a^2}{4\pi^2 L^2}\sum_{\vec{\nu}}{}' \left[\frac{1}{\frac{a^2}{4\pi^2 L^2} + \left(\vec{\nu} + \frac{\vec{\kappa} a}{2\pi}\right)^2} - \frac{1}{\nu^2} \right] \quad (28)$$

where $q_1(0)$ is expressed by Equation 26. In order to obtain an estimate, the sum over ν in Equation 28 may be replaced by an integral over the region outside circle with radius of order I.

Then, considering that we obtain

$$\frac{a^2}{4\pi^2 L^2} \ll 1, \qquad \frac{a^2\kappa^2}{4\pi^2} \ll 1$$

$$q_1 = q_1(0) - \frac{a^4}{16\pi^3 L^2 \epsilon^2}(1 + \kappa^2 L^2)$$

$$= \frac{a^2}{4\pi L^2}\left[\ln\frac{a^2}{\pi\rho^2} + \frac{\pi\rho^2}{a^2} - 1.48 - \frac{a^2}{4\pi^2 L^2 \epsilon^2}(1 + \kappa^2 L^2)\right]$$

where ϵ is the quantity of order I.

Most corrections analyzed here may be disregarded.

DISTRIBUTION OF THERMAL NEUTRON DENSITY IN THE CELL

Denote by $\epsilon(r)$ the ratio between the neutron density at point r (the origin of the coordinates is in one of the lattice joints) and the neutron density on the surface of the uranium cylinder. According to Equation 6 we have

$$q_0 N(r) = [\text{const} - q_1(r)]N(\rho)$$

and

$$q_0 N(\rho) = [\text{const} - q_1(0)]N(\rho)$$

Hence

$$\epsilon(r) = \frac{N(r)}{N(\rho)} = 1 + \frac{q_1(0) - q_1(r)}{q_0} \quad (29)$$

Consider the points located in the center of the cell and in the middle of the side. Using Equation 25, we obtain

$$q_1\left(\frac{1}{2},\frac{1}{2}\right) = \frac{a^2}{4\pi L^2}\left[\frac{11\pi}{6} - 4\ln 2\,\mathrm{ch}\frac{\pi}{2}\right] = -0.69\frac{a^2}{4\pi L^2}$$

$$q_1\left(0,\frac{1}{2}\right) = \frac{a^2}{4\pi L^2}\left[\frac{25\pi}{12} - 2\ln 4\,\mathrm{sh}\frac{\pi}{2} - \ln 4\,\mathrm{ch}\,\pi\right] = -0.34\frac{a^2}{4\pi L^2}$$

RECTANGULAR LATTICE

By taking in Equation 21

$$\omega = \frac{\pi}{2}, \qquad a_1 \neq a_2$$

we obtain

$$q_1 = \frac{1}{4\pi^2 L^2}\sum_{\nu_1,\nu_2}{}' \frac{\cos\frac{2\pi\nu_1 x}{a_1}\cos\frac{2\pi\nu_2 y}{a_2}}{\left(\frac{\nu_1}{a_1}\right)^2 + \left(\frac{\nu_2}{a_2}\right)^2} \quad (30)$$

By symmetrizing this series by ν_1 and ν_2 and performing a summation, it is possible to obtain the following

$$q_1(0) = \frac{a_1 a_2}{4\pi L^2}\left[\ln\frac{a_1 a_2}{\pi^2} + \frac{\pi\rho^2}{a_1 a_2} - \ln 4\pi + \frac{\pi}{6}\left(\frac{a_1}{a_2} + \frac{a_2}{a_1}\right)\right] \quad (31)$$

Hence, the difference $\delta q_1 = q(0)_{rect} - q(0)_{equ}$ equals (lattices with equal cell area are compared)

$$\delta q_1 = \frac{\sigma}{24L^2}\frac{(m-1)^2}{m} \tag{32}$$

where m is the ratio between the sides of the rectangular lattice. Thus, the square lattice is more effective than the rectangular one with $a_1 \neq a_2$.

COMPLEX LATTICE

Consider a lattice consisting of rods with different properties. Let r_k and r_l be vectors of rods of the first and second lattice. Both lattices are assumed square.

We shall consider such a special case when all the rods of the first and second lattices are in equal conditions. Analogous to Equation 6 we may write

$$N(r) = \frac{1}{q_0}\sum_k H_1(r - r_k)N(k) + \frac{1}{p_0}\sum_l H_1(r - r_l)N(l) \tag{33}$$

where

$$q_0 = \frac{2\pi D}{\gamma_1}\cdot\frac{\sigma_1}{2\pi L^2}; \qquad p_0 = \frac{2\pi D}{\gamma_2}\cdot\frac{\sigma_2}{2\pi L^2}$$

γ_1, γ_2 are the thermal constants of the lumps, and σ_1, σ_2 are the areas of the cells. Take in Equation 33 $r = r_k$ $(k = 0)$, $r = r_l$ $(l = 0)$ and

$$N(k) = N(r_0)e^{ikr_k}; \qquad N(r_l) = \epsilon N(r_0)e^{ikr_l}$$

where ϵ is a constant quantity, if, as we presume, the rods of the second lattice are placed at equivalent points of the first lattice. From Equation 33 we obtain

$$\begin{aligned} 1 &= \frac{G_1}{q_0} + \epsilon\frac{G_2 + \delta p_1}{p_0}, & G_1 &= \frac{\eta_1 e^{-\kappa^2\tau} - 1}{1 + \kappa^2 L^2} - q_1 \\ \epsilon &= \frac{G_1 + \delta q_1}{q_0} + \epsilon\frac{G_2}{p_0}, & G_2 &= \frac{\eta_2 e^{-\kappa^2\tau} - 1}{1 + \kappa^2 L^2} - p_1 \end{aligned} \tag{34}$$

where q_1 and p_1 are determined by Equation 26, $\delta q_1 = q_1 - \vec{q_1}(\alpha)$; $\delta p_1 = p_1 - \vec{p_1}(\beta)$, while $\vec{q_1}(\alpha)$, $\vec{p_1}(\beta)$ are determined by Equation 25, if we consider there x, y, as coordinates of the initial rod of one lattice relative to the other. Excluding ϵ from Equation 34 we obtain after simple transformations

$$1 + \kappa^2 L_p^2 = ke^{-\kappa^2\tau}$$

$$k = \frac{\eta_1(p - \vec{p_1}(\beta)) + \eta_2(q - \vec{q_1}(\alpha))}{qp + p - \vec{p_1}(\beta) + q - \vec{q_1}(\alpha) - \vec{q_1}(\alpha)\vec{p_1}(\beta)} \tag{35}$$

$$L_p^2 = L^2\cdot\frac{qp - \vec{q_1}(\alpha)\vec{p_1}(\beta)}{qp + p - \vec{p_1}(\beta) + q - \vec{q_1}(\alpha) - \vec{q_1}(\alpha)\vec{p_1}(\beta)}$$

The formulae obtained are fully symmetrical with regard to both lattices and pass into formulae of one lattice when $\gamma_2 \to 0$.

In case of a low lump effect, Equation 35 goes into the formulae which may be obtained by the homogeneous distribution of the material of the lumps in the moderator. Consider concretely a special case. Let

$$\frac{\gamma_2}{\gamma_1} = \zeta, \qquad \frac{\sigma_2}{\sigma_1} = n^2, \qquad n = 1.2$$

Both lattices are square; the lumps of the second lattice are inserted in the centers of the first

$$\left(\alpha_1 = \alpha_2 = \frac{1}{2}; \qquad \beta_1 = \beta_2 = \frac{1}{2n}\right)$$

Under these conditions

$$p_0 = q_0\frac{n^2}{\zeta}; \qquad p_1 = \frac{a^2n^2}{4\pi L^2}\left(\ln\frac{a^2}{\pi\rho^2} - 1.48 + \ln n^2\right);$$

$$\vec{q_1}(\alpha) = -0.69\frac{a^2}{4\pi L^2}$$

$$\vec{p_1}(\beta) = \frac{a^2n^2}{4\pi L^2}\left[\frac{7\pi}{3} + \frac{\pi}{n} + \frac{\pi}{2n^2} - \frac{1}{2}\ln \times\left\{256\left(\mathrm{sh}^2\frac{\pi}{2n} + \sin^2\frac{\pi}{2n}\right)^2\left(\mathrm{sh}^2\pi\left(1 - \frac{1}{2n}\right) + \sin^2\frac{\pi}{2n}\right)\times\left(\sin^2\pi\left(1 - \frac{1}{2n}\right) + \mathrm{sh}^2\frac{\pi}{2n}\right)\right\}\right]$$

$$= \begin{cases} -0.69\dfrac{a^2}{4\pi L^2} & \text{if} \quad n = 1 \\ +1.38\dfrac{a^2}{\pi L^2} & \text{if} \quad n = 2. \end{cases}$$

More complicated cases may be treated similarly.

RHOMBIC LATTICE

Consider a lattice with a cell in the shape of a rhombus with a side a and an angle 60 degrees [area of the cell $\sigma = (\sqrt{3}/2)a^2$]. From Equation 21 we have:

$$q_1 = \frac{3a^2}{8\pi^2L^2}\sum_{\nu_1,\nu_2}{}' \frac{\cos\frac{2\pi}{a}(\nu_1 x + \nu_2 y)}{\nu_1^2 + \nu_2^2 - \nu_1\nu_2}$$

When calculating this sum, some substitution of the variables should be made, which may lead to errors, due to the non-absolute convergence of the series. Therefore the necessary substitution of the variables should be done prior to the integration by z in Equation 15, and then the result so symmetrized that the change in the order of summation should not change the series. The substitution of the variables reduces to grouping, into even and odd ν_1 and ν_2. It is easy to see that q_1 may be written as follows (x, y are measured in a units).

$$q_1 = \frac{3a^2}{4\pi^2L^2}[I + II]$$

$$q_1 = \frac{3a^2}{4\pi^2L^2}[I + II]$$

$$I = \frac{1}{16}\sum_{m,n}{}'$$

$$\left\{\frac{\cos 2\pi[xm + n(x+2y)] + \cos 2\pi[ym + n(y+2x)]}{m^2 + 3n^2} + \frac{\cos 2\pi[xn + m(x+2y)]\cos 2\pi[xn + m(y+2x)]}{n^2 + 3m^2}\right\}$$

$$II = \frac{1}{4}\sum_{m,n}{}' \left\{\frac{\cos \pi[x(2m+1) + (x+2y)(2n-1)] + \cos \pi[y(2m+1) + (y+2x)(2n-1)]}{(2m+1)^2 + 3(2n-1)^2} + \frac{\cos \pi[x(2n+1) + (x+2y)(2m-1)] + \cos \pi[y(2n+1) + (y+2x)(2m-1)]}{(2n+1)^2 + 3(2m-1)^2}\right\}$$

The calculation of these sums is made in the same way as in the case of square lattices. As a result of the calculations, we obtain the following expressions for I and II (in this case we disregard expressions of the kind

$$e^{-2\sqrt{3}\pi},\ e^{-\frac{2\pi}{\sqrt{3}}}$$

as compared with 1)

For I:

$$I = \frac{\pi}{8}\left(\frac{52\pi}{9} + \frac{8\pi}{2}\rho^2\right) - \frac{\pi}{16\sqrt{3}}\ln\left\{4^{12} f(\sqrt{3}\,x\,x+2y) \times f(\sqrt{3}(1-x), x+2y) f(\sqrt{3}(1+x), x+2y) f(\sqrt{3}\,y, y+2x) \times f(\sqrt{3}(1-y), y+2x) f(\sqrt{3}(1+y), y+2x) f\left(\frac{x+2y}{\sqrt{3}}, x\right) \times f\left(\frac{1-x-2y}{\sqrt{3}}, x\right) f\left(\frac{1+x+2y}{\sqrt{3}}, x\right) f\left(\frac{y+2x}{\sqrt{3}}, y\right) \times f\left(\frac{1-y-2x}{\sqrt{3}}, y\right) f\left(\frac{1+y+2x}{\sqrt{3}}, y\right)\right\}$$

where

$$f(x,y) = \mathrm{sh}^2 \pi x + \sin^2 \pi y$$

When x, y are small we obtain:

$$I = \frac{\pi}{2\sqrt{3}}\left[\frac{\sqrt{3}\,\pi}{9} + \frac{\pi\rho^2}{\sigma} - \frac{1}{2}\ln\frac{\pi\rho^2}{\sigma} - \frac{1}{2}\ln 8\pi\right]$$

where $\rho^2 = a^2(x^2 + y^2 + xy)$ is the square of the distance from the origin of the coordinates to point x, y; σ is the area of the cell. For II we obtain:

$$II = \frac{\pi}{16\sqrt{3}}\ln\frac{A}{B}$$

where B is the product of functions f of the argument, half that in I, while A is the product of functions

$$f_1(x,y) = \mathrm{sh}^2 \pi x + \cos^2 \pi y$$

of the same arguments as in the case of f in B. With small x, y we obtain:

$$II = -\frac{\pi}{4\sqrt{3}}\ln\frac{\pi\rho^2}{2\sigma}$$

Thus the final formula for $q_1(0)$ appears as follows

$$q_1(0) = \frac{\sigma}{4\pi L^2}\left[\ln\frac{\sigma}{\pi\rho^2} + \frac{\pi\rho^2}{\sigma} - \ln 4\pi + \frac{\pi}{3} + \ln 2 - \left(1 - \frac{1}{\sqrt{3}}\right)\frac{\pi}{3}\right] \quad (36)$$

Hence the rhombic lattice produces a greater lump effect than the square one, of the magnitude:

$$\delta q_1 = \frac{\sigma}{4\pi L^2}\left[\ln 2 - \left(1 - \frac{1}{\sqrt{3}}\right)\frac{\pi}{3}\right] = 0.25\,\frac{\sigma}{4\pi L^2}$$

HEXAGONAL LATTICE

A hexagonal lattice is obtained if a rhombic-shaped lattice with a side a and angle 60 degrees is removed from a lattice also in the shape of a rhombus but with a side $\sqrt{3}\,a$. The cell areas are equal: that of the first lattice is $\sigma p_1 = (\sqrt{3}/2)\,a^2$; of the second $\sigma p_2 = (3\sqrt{3}/2)\,a^2$; and of the hexagonal lattice $\sigma_{hex} = (3\sqrt{3}/4)\,a^2$, where a is the side of the hexagon. The lump effect for such a lattice may be obtained on the bases of the formulae of the previous paragraph.

In the initial formulae earlier the sum over k_1, k_2 should be applied to the apexes of the rhombi with side a and from it must be subtracted the sum over the apexes of rhombi with side $\sqrt{3}\,a$. After calculating the sums, the coordinates x, y should be made to tend to the surface of the actually existing rod. Then we obtain from the first sum q_1 (rhombic) calculated earlier, and from the second sum q_1 for the rhombic lattice with the side $\sqrt{3}\,a$ but with $x = y = \frac{1}{3}$, i.e. (we disregard terms $\sim \pi\rho^2/a^2$):

$$q_1 = \frac{\sigma_{hex}}{\sigma_{p_1}}\frac{\sqrt{3}\,a^2}{8\pi L^2}\left(\ln\frac{\sqrt{3}\,a^2}{2\pi\rho^2} - \ln 2\pi + \frac{\pi}{3\sqrt{3}}\right) - \frac{\sigma_{hex}}{\sigma_{p_2}}\frac{3\sqrt{3}\,a^2}{8\pi^2 L^2}(I + II)$$

where

$$\frac{\sigma_{hex}}{\sigma_{p_1}} = \frac{\frac{3\sqrt{3}}{4}a^2}{\frac{\sqrt{3}}{2}a^2} = \frac{3}{2}, \qquad \frac{\sigma_{hex}}{\sigma_{p_2}} = \frac{\frac{3\sqrt{3}}{4}a^2}{\frac{3\sqrt{3}}{2}a^2} = \frac{1}{2}$$

Calculations I and II according to the formulae of the previous paragraph make I = −0.244, II = 0.158, and, hence

$$q_1 = \frac{\sigma}{4\pi L^2}\left(\ln\frac{\sigma}{\pi\rho^2} - 1.61\right) \quad (37)$$

It follows then that the hexagonal lattice is more effective than the square one:

$$\delta q_1 = q_{1sq} - q_{1hex} = 0.13\,\frac{\sigma}{4\pi L^2} \quad (38)$$

(The term $\pi\rho^2/\sigma$ in the formula for q_1 should be obtained from general considerations; in order to obtain it from the general formulae, x, y should be

replaced by the coordinates of the surface of the removed rod and not by the coordinates of its center $x = y = \frac{1}{8}$.)

NOTE ON THE CORRECTIONS FOR THE ELEMENTARY DIFFUSION EQUATION

Near the uranium cylinder that is intensively absorbing neutrons, allowance should be made for the deviation from the elementary diffusion equation. Suppose we know the exact (or approximate) solution of the problem of neutron density distribution near the intensively absorbing cylinder, inserted in an unlimited medium that has a slight absorption of neutrons. Incidentally, we know the distribution of neutrons inside the cylinder as well, and therefore it is possible to obtain the exact value of the thermal constant γ. Suppose the distribution of neutron density outside the cylinder is given by the formula

$$\varphi(r) = K_0\left(\frac{r}{L}\right) + F(r)$$

where $F(r)$ attenuates at distances of the order of the scattering mean free path. Then, making up the sum

$$\sum \varphi(|r - r_k|) = \sum K_0\left(\frac{|r - r_k|}{L}\right) + \sum F(|r - r_k|)$$

which determines q_1, we may confine ourselves in the second item to one term (if a is much greater than the scattering mean free path). Hence we have the following correction to Equation 26 for q_1

$$q_1 = q_1(0) + \frac{\sigma}{2\pi L^2} F(\rho)$$

where $q_1(0)$ is determined by Equation 26, i.e., by the elementary diffusion equation, and ρ is the radius of the cylinder.

REFERENCES

1. Galanin, A. D., *Critical dimensions of a heterogeneous reactor with a small number of lumps.*
2. Courant, R. and Gilbert, D., *Methods of mathematical physics*, vol. I, GTTI (1933).

Heterogeneous Methods for Calculating Reactors: Survey of Results and Comparison with Experiment

By S. M. Feinberg, USSR

When calculating the critical sizes of a reactor with a heterogeneous core and the spatial distribution of the neutron flux the homogenization rule is usually applied. In such calculations the heterogeneous lattice is substituted by a homogeneous multiplying medium possessing the same mean neutron parameters as a heterogeneous lattice of infinite dimensions.

Even in the case of a "large" reactor the need arises for a proof of the homogenization principle and for an evaluation of its possible error. In the case of a reactor composed of a comparatively small number of uranium slugs the use of the homogenization principle is, generally speaking, not justified.

In this connection direct methods of calculation of heterogeneous reactors were developed. The latter make possible the calculation of a reactor composed only of a few uranium slugs as well as the evaluation of errors introduced by the homogenization method.

It must be additionally stressed that the heterogeneous method enables us to study the neutron field near the active zone boundary in the vicinity of a separate absorbing rod introduced into the heterogeneous lattice and in composite lattices, that is, in lattices composed of slugs with different properties placed in an order of regular periodic alternation.

Thus the problem of the heterogeneous method is not limited to the proof of the homogenization method; in some cases it is the only possible and indispensable means of investigation of the neutron field.

1. THE PRINCIPLES OF THE HETEROGENEOUS METHOD

In the heterogeneous method the reactor is considered as a system of uranium slugs placed in a neutron-moderating medium. The uranium slugs are sources of fast neutrons and sinks for thermal and resonance neutrons.

The heterogeneous method is based on the following assumptions:

1. The thermal neutron field near the slugs possesses spheric or axial symmetry so that the sinks may be considered as of point or line configuration. This assumption is valid if the distance between the slugs is much greater than their dimensions. It should be noted that symmetrical structure of the reactor lattice favors fulfillment of the symmetry conditions in the neutron field in the vicinity of the slugs. Thus, the theory is applicable in the case of quite large slugs, if the lattice is sufficiently symmetrical.

2. An elementary diffusion equation may be used in describing thermal neutron diffusion between the slugs. This is justified when assuming that the absorption of thermal neutrons in the moderator is low and that the diffusion length is small in comparison with the distances between the slugs.

3. The value of the logarithmic derivative of a flux of thermal neutrons on the surface of the slug is a characteristic of the absorbing properties of the uranium slugs. When absorption of thermal neutrons inside the slug is great then conditions in the vicinity of the surface calling for the diffusion approximation are violated; in this case the logarithmic derivative should be given for the effective surface of the slug removed from its real surface to a distance of $\lambda_s/2$ (λ_s is the scattering mean free path in the moderator). A simple relation may be established between the intensity of the source and the sink. Let i_k be the intensity of the thermal neutron sink, i.e., the number of thermal neutrons absorbed by this sink in unit time, and let q_k be the intensity of the same source of fast neutrons, i.e., the number of fast neutrons emitted in unit time by the source. Then

$$q_k = \eta_k i_k \tag{1.1}$$

where η_k is the number of fission neutrons generated in the slug as a result of the absorption of one thermal neutron.

Besides the sources-sinks, the system may also contain outer sources of fast neutrons and sinks of thermal neutrons. Each source of fast neutrons generates a field of moderated neutrons, the spacial distribution of which are described by the following function

$$q_k j(E_1, E_0, |r - r_k|) \tag{2.1}$$

where $j(E_1, E_0, r)$ is the flux of the moderating neutrons, E_1 is the energy of the flux generated by a point (or line) source of fast neutrons of unit intensity and E_0 is the primary energy of the neutrons. The function j is determined by the values E_1, E_0 and the properties of the slowing-down medium. (In Equation 2.1 r is the radius-vector of the observation point, r_k the radius-vector of the position of the source.) Assuming that $E_1 = kT$ in Equation 2.1 and denoting $j(kT, E_0, r) = j_T^{E_0}(r)$, we get for k of that source the following

$$q_k j_T^{E_0}(|r - r_k|) \tag{3.1}$$

Original language: Russian.

Knowing the thermal neutron generating field, it is not difficult to define their spatial distribution ($\Phi = nv$), still disregarding the neutron absorption in the sinks (i.e., considering the moderator as free from point sinks for thermal neutrons). To find the distribution of the thermal neutrons it is sufficient to integrate (throughout the volume of the moderator) the product of the generation density of the thermal neutrons by the function of the influence of the point source. In diffusion approximation this function is expressed as follows:

For a point source of thermal neutrons, letting L be the diffusion length for thermal neutrons and Σ_c the macroscopic thermal neutron absorption cross section,

$$f(r) = e^{-r/L}/4\pi L^2\Sigma_c r \tag{4.1a}$$

and for a line source

$$f(r) = K_0(r/L)/2\pi L^2\Sigma_c \tag{4.1b}$$

where $K_0(x)$ is the modified Bessel function of the second kind. As a result of integration we obtain the distribution of the thermal neutron flux, generated in the moderating medium free from point sinks, by a single fast-neutron source.

This spatial distribution we denote as F and call it the Green function

$$F(|r - r_k|) = \int_\infty j_{T^{E_0}}(|r' - r_k|) f(|r - r'|)\, dr' \tag{5.1}$$

Evidently the Green function of the kth source may be written as:

$$q_k F(|r - r_k|) \tag{6.1}$$

Due to additivity properties of neutron sources placed in a moderator the field of thermal neutrons in a medium where there is no sink is described by

$$\Phi(r) = \sum_k q_k F(|r - r_k|) \tag{7.1}$$

where the sum is taken over all the fast-neutron sources in the reactor.

On the other hand, the influence of each kth point neutron sink decreases the thermal neutron flux by

$$i_k f(|r - r_k|) \tag{8.1}$$

Therefore, the spatial distribution of the thermal neutron flux in the reactor is:

$$\Phi(r) = \sum_k [q_k F(|r - r_k|) - i_k f(|r - r_k|)] \tag{9.1}$$

By employing the connection between q_k and i_k expressed in Equation 1.1 we find:

$$\Phi(r) = \sum_k i_k[\eta_k F(|r - r_k|) - f(|r - r_k|)] \tag{10.1}$$

As it may be assumed that the values of $F(r)$, $f(r)$, η_k are known, it is necessary to know i_k, the intensity of the thermal neutron sinks, to calculate the thermal neutron flux $\Phi(r)$.

If the distance between the slugs, the diffusion length and slowing-down length are much greater than the slugs themselves, then the thermal neutron flux in the vicinity of the nth slug may be designated approximately as

$$\Phi(|r - r_n|) \approx \sum_k{}' i_k[\eta_k F(d_{nk}) - f(d_{nk})]$$

$$+ i_n[\eta_n F(0) - f(\rho)] \equiv \sum_k i_k[\eta_k F(d_{nk}) - f(d_{nk})] \tag{11.1}$$

$$\rho = |r - r_n|; \quad d_{nk} = |r_n - r_k| \quad \text{when} \quad n \neq k$$
$$d_{nk} = \rho \quad \text{when} \quad n = k \tag{12.1}$$

In Equation 11.1 the sum $\sum_k{}'$ is extended over all the slugs except the nth. As the equations determining the thermal neutron flux are lineal the intensity of absorption of neutrons in the nth sink is proportional to the thermal neutron flux on the effective surface of the slug (taking $\rho = R_n$). The coefficient of proportionality γ_n between i_n and $\Phi(R_n)$ determined the absorbing properties of the slug

$$i_n = \frac{1}{\gamma_n}\Phi(R_n) \tag{13.1}$$

The value of γ_n may be determined either by experiment or by a non-diffusional calculation of the thermal neutron field in the vicinity of the slug. In a number of cases γ may be defined almost precisely from the elementary diffusion equation. From this and from Equation 11.1 we obtain:

$$\gamma_n i_n = \sum_k i_k[\eta_k F(d_{nk}) - f(d_{nk})] \tag{14.1}$$

Evidently, $d_{nn} = R_n$. Thus, we have a system of homogeneous line equations for the definition of i_k; this system may be briefly designated as:

$$\gamma_n i_n = \sum_{k=0}^{N-1} i_k \alpha_{kn} \tag{15.1}$$

where

$$\alpha_{kn} = \eta_k F(d_{kn}) - f(d_{kn}) \tag{16.1}$$

This system of equations may be solved when and only when its determinant equals zero; in this way we obtain the following conditions for the critical size of a reactor:

$$\begin{vmatrix} (\alpha_{00} - \gamma_0) & \alpha_{01} & \alpha_{02} \cdots & \alpha_{0,N-1} \\ \alpha_{10} & (\alpha_{11} - \gamma_1) & \alpha_{12} \cdots & \alpha_{1,N-1} \\ \cdots & \cdots & \cdots & \cdots \\ \cdots & \cdots & \cdots & \cdots \\ \alpha_{N-1,0} & \alpha_{N-1,1} & \alpha_{N-1,2} \cdots & (\alpha_{N-1,N-1} - \gamma_{N-1}) \end{vmatrix} = 0 \tag{17.1}$$

Equation 17.1 contains the values of η_i, γ_i, R_i, L, τ.* Each of these parameters may be the proper value of the problem.

Thus the calculation of a heterogeneous reactor composed of N uranium slugs is reduced to the solu-

* $6\tau = 4\pi \int_0^\infty r^4 j_{T^{E_0}}(r)\, dr$.

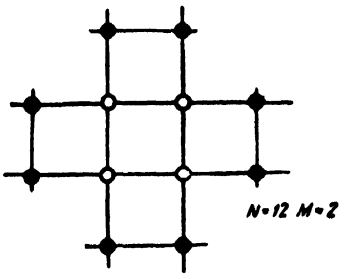

Figure 1. Scheme of an active zone consisting of N = 12 slugs; the number of unknown quantity M = 2

tion of a system of N uniform line equations. When the reactor is symmetrical and contains M groups of identically placed slugs, the number of equations decreases and becomes equal to $M < N$.

For instance, the reactor in Fig. 1 consists of $N = 12$ slugs; the number of groups of symmetrical slugs is $M = 2$.

Another case: an infinite lattice consisting of identical slugs; in this case $N = \infty$ and $M = 1$. If symmetry is taken into account, Equation 15.1 has the form:

$$\gamma_n i_n = \sum_{s=1}^{s=M} i_s \sum_{k'} \alpha_{nk'} \qquad (18.1)$$

where the index k' is extended over the values of the given group s (symmetrically placed rods).

For instance, the critical equation for an infinite lattice composed of identical slugs is:

$$\gamma_0 = \eta_0 \sum^{\infty} F(|r_k|) - \sum^{\infty}{}' f(|r_k|) - f(R_0) \qquad (19.1)$$

It should be noted that the function $f(R)$ when $R \to 0$ has a singularity:

For point slugs: $f(R) \to 1/4\pi\Sigma_c L^2 R$
For line slugs:

$$f(R) \to -\left(0.577 + \ln\frac{R}{2L}\right)/2\pi L^2\Sigma_c \quad \text{when } R \to 0 \qquad (20.1)$$

We have not as yet considered the resonance absorption in the slugs, occurring in the course of slowing down of neutrons. Resonance absorption may be calculated for one or several rather narrow levels—so narrow that the width of the "dangerous" zone is small in comparison with the average loss of energy in each collision.† This assumption made the resonance absorption (for a single level) equivalent to a monochromatic "negative" source, i.e., a neutron sink with the energy E_r equal the energy of the resonance level.

Thus the field of the slowing down neutrons (with $E < E_r$) appears to be generated by two sources: The actual fast neutrons source and the "negative" source, the energy of which is E_r. So when $E < E_r$ we have instead of Equation 3.1:

$$q_k j_T^{E_0}(|r - r_k|) - \psi_k j_T^{E_r}(|r - r_k|) \qquad (21.1)$$

† See I. I. Gurevich, I. Y. Pomeranchouk, P/649 "The Theory of Resonance Absorption in Heterogeneous Systems," this Session.

where ψ_k is the intensity of the resonance neutron sink. The value of ψ_k may be calculated by the following formula:

$$\psi_k = A_k \sum_p q_p j_{E_r}^{E_0}(|r_p - r_k|) \qquad (22.1)$$

where A_k is a constant which determines the absorption of resonance neutrons by the kth slug.

The scheme of heterogeneous calculation described above does not change if resonance absorption is considered. However, instead of Equation 5.1 the following expression, in which resonance absorption is taken into account, should be used:

$$q_k \int_\infty f(|r' - r|) j_T^{E_0}(|r' - r_k|)\, dr' - A_k \sum_p q_p j_{E_r}^{E_0}(|r_p - r_k|) \int_\infty f(|r' - r|) j_T^{E_r}(|r' - r_k|)\, dr'$$

Substituting the latter into Equation 14.1 after several transformations we have:

$$\gamma_n i_n = \sum_k^{N-1} \eta_k i_k F^*(r_n, r_k) - \sum_k^{N-1} i_k f(d_{nk}) \qquad (14.1^*)$$

where

$$F^*(r_n, r_k) = F(d_{nk}) - \sum_m^{N-1} F_T^{E_r}(d_{nm}) j_{E_r}^{E_0}(d_{km}) A_m$$

$$F_T^{E_r}(d_{nm}) = \int_\infty f(|r' - r_n|) j_T^{E_r}(|r' - r_m|)\, dr' \qquad (5.1^*)$$

Let us note that in distinction from $F(|r_n - r_k|)$ the function $F^*(r_n, r_k)$ is, generally speaking, dependent not only on the distance between points r_n and r_k.

Above, we have given a method for calculating a system of infinite cylindrical slugs, placed in an infinite neutron moderator. However, for a lattice, consisting of finite cylindrical slugs it is possible to evaluate the influence of the finiteness of the lattice.

For a reactor with line slugs placed parallel to the axis z, it is possible to solve the heterogeneous equation by separating the variables:

$$\Phi(r, z) = \Phi(r) \cos \kappa_z z \qquad (23.1)$$

The value κ_z is determined by this formula:

$$\kappa_z = \frac{\pi}{H + 2\Delta_z} \qquad (24.1)$$

In Equation 24.1 H is the height of the core, Δ_z is the reflector savings.

At the same time it is supposed that even in the presence of a reflector the density distribution of the neutrons along the z axis remains proportional to $\cos \kappa_z z$; thus, all the above-mentioned formulas turn out to be valid if we substitute for $1/L^2$,

$$\frac{1}{L^2} + \frac{\pi^2}{(H + 2\Delta_z)^2} = \frac{1}{L^2} + \kappa_z^2 \qquad (25.1)$$

and for η,

$$\eta e^{-\kappa_z^2 \tau}$$

Further we shall give a short survey of the results obtained by different authors from the heterogeneous method of solving certain reactor problems. It should be noted that this survey is not complete in consequence of space limitations; the author includes the most important works, from this point of view.

2. AN INFINITE LATTICE CONSISTING OF SIMILAR POINT OR LINE SLUGS

I. Y. Pomeranchouk and A. I. Akhiezer have investigated the problem of a heterogeneous lattice consisting of point (spherical) and line (cylindrical) slugs, placed periodically in an infinite moderator. The lattice was assumed to consist of identical slugs. Then, in agreement with Equations 19.1 and 20.1, the critical equation has the form:

$$\gamma = \eta \sum_k^{\infty} F(r_k) - \sum_k^{\infty\prime} f(r_k) - f(R) \qquad (19.1^*)$$

The problem consists of computing the sums in Equation 19.1*.

For the slowing down flux $j(E,r)$ from a point source the authors adopted an expression obtained from an age theory approximation for a monochromatic source of fast neutrons:

$$j(E_1,E_0,r) = \frac{e^{-r^2/4\tau(E_1,E_0)}}{(2\sqrt{\pi\tau(E_1,E_0)})^3} \qquad (1.2)$$

It is notable that the authors of all subsequent works used in this survey also proceeded from this expression, although it is not essential.

Substituting Equation 1.2 into Equation 5.1 and summing them up, we obtain the following expression (for point sources):

$$\sum_k^{\infty} F(r_k) = \sum_k^{\infty} \int \frac{e^{-r^2/4\tau}}{(2\sqrt{\pi\tau})^3} \frac{e^{-|r-r_k|/L}\,d\tau}{4\pi L^2\Sigma_c|r-r_k|} \qquad (2.2)$$

where $r_k = ak_1 + bk_2 + ck_3$, the k_i are integers, and a, b, c are basic lattice vectors.

By means of the Fourier transformation it is possible to show that:

$$\sum_k^{\infty} F(r_k) \approx \frac{1}{V\Sigma_c} \qquad (2.2^*)$$

if $e^{-4\pi^2\tau/a^2} \ll 1$. Here V is the volume of a cell in a periodic lattice, a being the largest period.

For the sum of the functions

$$\sum_k^{\infty\prime} f(r_k)$$

we have:

$$\sum_k^{\infty\prime} f(r_k) = \sum_k^{\infty\prime} e^{-r_k/L}/4\pi L^2\Sigma_c r_k \qquad (3.2)$$

If the resonance absorption of neutrons is taken into consideration and assumed to be due to one resonance level, the following expression may be obtained:

$$\sum_k^{\infty} F^*(r_k) = \sum_k^{\infty} \int_{\infty} \frac{e^{-r^2/4\tau}}{(2\sqrt{\pi\tau})^3} \frac{e^{-|r-r_k|/L}}{4\pi L^2\Sigma_c|r-r_k|}\,d\tau$$

$$- \frac{A}{V\Sigma_c} \sum_k^{\infty} \int_{\infty} \frac{e^{-r^2/4\tau_r}}{(2\sqrt{\pi\tau_r})^3} \cdot \frac{e^{-|r-r_k|/L}}{4\pi L^2\Sigma_c|r-r_k|}\,d\tau \qquad (4.2)$$

where $\tau \equiv \tau(E_0,kT)$, $\tau_r \equiv \tau(E_r,kT)$.

In the case of an infinite rectangular lattice consisting of line slugs in accordance with Equations 19.1* and 20.1, the critical condition is:

$$\gamma = \eta \sum_k^{\infty} F(r_k) - \sum_k^{\infty\prime} f(r_k) + \frac{0.577 + \ln\frac{R}{2L}}{2\pi L^2\Sigma_c} \qquad (5.2)$$

where

$$\sum_k^{\infty} F(r_k) = \sum_k^{\infty} \int_{\infty} \frac{e^{-\frac{r^2}{4\tau}}}{4\pi\tau} K_0\left(\frac{|r-r_k|}{L}\right) \frac{d\tau}{2\pi L^2\Sigma_c} \qquad (6.2)$$

$$\sum_k^{\infty\prime} f(r_k) = \sum_k^{\infty} \frac{K_0\left(\frac{r_k}{L}\right)}{2\pi L^2\Sigma_c} \qquad (7.2)$$

Using the Fourier transformation in the case of line slugs we get the following expressions:

$$2\pi L^2\Sigma_c F(r) = \int_{\infty} \frac{e^{-r_1^2/4\tau}}{4\pi\tau} K_0\left(\frac{|r-r_1|}{L}\right) dr_1$$

$$= \int_0^{\infty} \frac{xe^{-x^2\tau} I_0(xr)}{x^2 + 1/L^2}\,dx \qquad (8.2)$$

To calculate infinite sums in the case of a square lattice consisting of identical slugs with a spacing a, the Poisson summation formula may be applied; after a set of intermediate computations the following simple result evolves:

$$2\pi L^2\Sigma_c \sum_k^{\infty} F(r_k) = \frac{2\pi L^2}{a^2} \sum_{\nu}^{\infty} \frac{e^{-\frac{4\pi^2\tau\nu^2}{a^2}}}{1 + \frac{4\pi^2L^2}{a^2}\nu^2} \qquad (9.2)$$

If the condition $4\pi^2\tau/a^2 \gg 1$, is fulfilled, Equation 9.2 takes the form

$$2\pi L^2\Sigma_c \sum_k^{\infty} F(r_k) \approx \frac{2\pi L^2}{a^2}\left(1 + \frac{4e^{-4\pi^2\tau/a^2}}{1 + \frac{4\pi^2L^2}{a^2}}\right) \qquad (9.2^*)$$

Usually with sufficient precision,

$$\sum_k^{\infty} F(r_k) = \frac{1}{a^2\Sigma_c} \qquad (10.2)$$

It follows from this result that the slowing down density is almost constant if $e^{-4\pi^2\tau/a^2} \ll 1$. Furthermore, with this condition fulfilled, the slowing-down density does not depend on the configuration of the lattice cell.

A. D. Galanin‡ successfully replaced the slowly converging series $\sum_k^\infty f(r_k)$ by another with a more rapid convergence. This enabled him to estimate the accuracy of calculation of the thermal utilization θ by the method of equivalent cells and to find the dependence of θ on the form of the periodic lattice cell. Most important is the result of calculating $\sum_k^\infty f(r_k)$ for a lattice with a cell in the form of a parallelogram the sides of which are a_1 and a_2, the angle between them being ω.

When computing the sums of f the integral representation of $K_0(x)$ may be used.

$$2\pi L^2 \Sigma_c f(r) = K_0\left(\frac{r}{L}\right) = \int_0^\infty e^{-\left(z+\frac{r^2}{4L^2 z}\right)} \frac{dz}{2z} \quad (11.2)$$

Then, summing according to the Poisson rules gives§

$$\sum_k{}' K_0\left(\frac{|r - r_k|}{L}\right) = \frac{2\pi L^2}{\sigma} \sum_{\nu_1,\nu_2}^\infty \frac{e^{2\pi i\left(\frac{\nu_1}{a_1}x + \frac{\nu_2}{a_2}y\right)}}{\left[1 + \frac{4\pi^2 L^2}{\sin^2\omega}\left(\frac{\nu_1^2}{a_1^2} + \frac{\nu_2^2}{a_2^2} - \frac{2\nu_1\nu_2}{a_1 a_2}\cos\omega\right)\right]} \quad (12.2)$$

If the conditions $4\pi L^2/a_1 a_2 \sin^2\omega \gg 1$ are fulfilled, then

$$\sum_k{}' K_0\left(\frac{|r - r_k|}{L}\right) = \frac{2\pi L^2}{\sigma}\left(1 + \frac{\sin^2\omega}{4\pi^2 L^2}\right) \sum_{\nu_1,\nu_2}{}' \frac{e^{2\pi i\left(\frac{\nu_1}{a_1}x + \frac{\nu_2}{a_2}y\right)}}{\left(\frac{\nu_1^2}{a_1^2} + \frac{\nu_2^2}{a_2^2} - \frac{2\nu_1\nu_2}{a_1 a_2}\cos\omega\right)} \quad (13.2)$$

σ is the area of the lattice-cell; a prime means that the terms with $\nu_1 = \nu_2 = 0$ must be dropped.

Thermal utilization θ of an infinite lattice where $K_\infty = 1$, is the absence of resonance absorption in the moderating process, is, by definition:

$$\theta = \frac{\sum_k^\infty i_k}{\sum_k^\infty q_k} = \frac{\sum_k^\infty i_k}{\eta \sum_k^\infty i_k} = \frac{1}{\eta} \quad \text{or} \quad \frac{1-\theta}{\theta} = \eta - 1 \quad (14.2)$$

‡ A. D. Galanin, P/666 "The Thermal Coefficient in a Heterogeneous Reactor," this Session.

§ It must be noted that the following series are not absolutely convergent. For greater details see the work of A. D. Galanin.

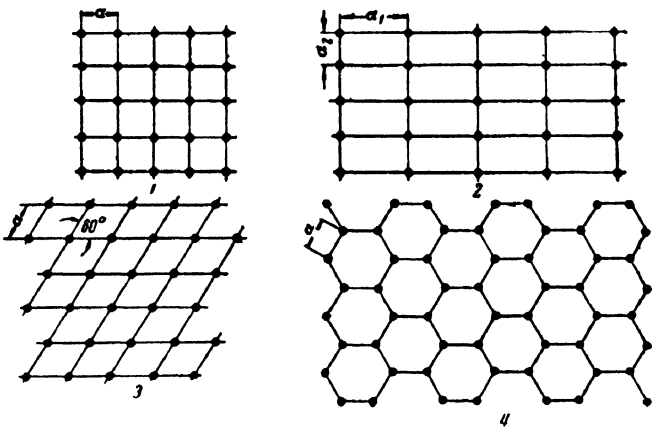

Figure 2. Scheme of lattices of the active zone of a reactor. 1. Square lattice with a spacing "a"; 2. Rectangular lattice with spacing "a" and "a_2"; 3. Rhomboid lattice with a spacing "a" and an angle $\omega = 60°$; 4. Hexagonal lattice with spacing "a"

From Equation 5.2, taking into account Equation 14.2, we get:

$$\frac{1-\theta}{\theta} = \eta - 1 = \frac{\gamma + \sum_k^\infty f(r_k)}{\sum_k^\infty F(r_k)} - 1 \quad (15.2)$$

In accordance with Equations 15.2 and 10.2 we further obtain:

$$\frac{1-\theta}{\theta} = \gamma a^2 \Sigma_c + \left(a^2\Sigma_c \sum_k^\infty f(r_k) - 1\right) = \gamma a^2 \Sigma_c + g \quad (16.2)$$

where g designates the value

$$g = a^2 \Sigma_c \sum_k^\infty f(r_k) - 1 \quad (17.2)$$

Remembering that

$$\sum_k^\infty f(r_k) = \frac{1}{2\pi L^2 \Sigma_c} \sum_k^\infty K_0\left(\frac{|\vec{\rho} - r_k|}{L}\right)$$

then

$$g = \frac{a^2}{2\pi L^2} \sum_k^\infty K_0\left(\frac{|r_k - \vec{\rho}|}{L}\right) - 1$$

In the case of the lattice under discussion we have for g:

$$g = \frac{\sin^2\omega}{4\pi^2 L^2} \sum_{\nu_1,\nu_2}^\infty \frac{\cos\left[2\pi\left(\frac{\nu_1}{a_1}x + \frac{\nu_2}{a_2}y\right)\right]}{\frac{\nu_1^2}{a_1^2} + \frac{\nu_2^2}{a_2^2} - \frac{2\nu_1\nu_2}{a_1 a_2}\cos\omega} \quad (18.2)$$

For a square lattice $a_1 = a_2 = a$; $\omega = \pi/2$; calculations lead to:

$$g = \frac{a^2}{4\pi L^2}\left[\ln\frac{a^2}{\pi R^2} + \frac{\pi R^2}{a^2} - \ln 4\pi + \frac{\pi}{3}\right] \quad (19.2)$$

$$\ln 4\pi - \pi/3 = 1.48$$

Calculation of θ by the equivalent cell method gives the same formula with substitution of 1.48 by 1.5. This shows that the calculation of θ by the equivalent cell method is precise enough.

For a rectangular lattice when $\omega = \pi/2$ and $a_1 \neq a_2$ we get:

$$g = \frac{a_1 a_2}{4\pi L^2}\left[\ln\frac{a_1 a_2}{\pi R^2} + \frac{\pi R^2}{a_1 a_2} - \ln 4\pi + \frac{\pi}{6}\left(\frac{a_1}{a_2} + \frac{a_2}{a_1}\right)\right] \quad (20.2)$$

For a rhomboid lattice with the side of the cell a and the angle $\omega = 60$ degrees

$$g = \frac{\sigma}{4\pi L^2}\left[\ln\frac{\sigma}{\pi R^2} + \frac{\pi R^2}{\sigma} - \ln 4\pi + \frac{\pi}{3} + \ln 2 - \frac{\pi}{3}\left(1 - \frac{1}{\sqrt{3}}\right)\right] \quad (21.2)$$

And lastly, for a hexagonal lattice with a side a:

$$g = \frac{\sigma}{4\pi L^2}\left[\ln\frac{\sigma}{\pi R^2} - 1.61\right] \quad (22.2)$$

The lattice schemes are given in Fig. 2.

If we compare a rhomboid and hexagonal lattice with a square lattice having identical cell areas σ we find that the rhomboid lattice suffers a loss in $\delta g = 0.25\sigma/4\pi L^2$, the hexagonal lattice shows an increase of $\delta g = 0.13\sigma/4\pi L^2$ in comparison to the square lattice.

Composite Lattices (Double and Triple)

S. M. Feinberg, E. P. Kunyegin and B. D. Slutskaya, and also independently A. D. Galanin, applied the heterogeneous method in calculating "multilattices," consisting of regularly alternating cylindrical slugs, differing from each other in their absorbing (γ_k,R_k) and multiplying properties (η_k).

Such composite lattices may be made up of enriched uranium slugs and control rods or slugs intended for the production of radioactive isotopes.

The composite lattice calculations enable us to evaluate the efficiency of the control rods system used in the reactor, the redistribution of heat generation in the uranium slugs due to the control rods, and the part of neutrons absorbed in slugs of different types.

Figures 3 and 4 represent "double" and "triple" lattices. It is not difficult to observe that composite lattices may be considered as regular lattices, inserted one into the other. For instance, the double lattice in Fig. 3 splits into three regular lattices inserted into each other. Each of these regular lattices is composed of slugs in identical conditions. Thus, the number of unknown M values in the system of Equation 18.1 is equal to the number of the above-mentioned regular lattices. The equation system in the case of a double lattice (Fig. 3) is as follows:

$$\gamma_n i_n = \sum_{s=1}^{s=3} i_s \sum_k^{\infty} (\eta_s F_{nk} - f_{nk}); \qquad n = 1, 2, 3 \ldots$$
$$\gamma_3 = \gamma_2 \neq \gamma_1, \qquad \eta_3 = \eta_2, \qquad \eta_1 = 0 \quad (23.2)$$

The infinite sums were extended over all the identical rods of one of the three regular lattices.

The sum $\sum_k^{\infty} f_{nk}$ were computed by a method analogical to the above-mentioned one. They are equal with sufficient precision to $1/a^2\Sigma_c$. In more complicated cases the next terms of the series in Equation 9.2 may be computed.

In the work by S. M. Feinberg, E. P. Kunyegin and B. D. Slutskaya the sums $\sum_k^{\infty} f_{nk}$ were calculated numerically. In the work by A. D. Galanin, as has been mentioned above, the rapidly converging series of Equations 12.2 and 13.2 were used (see Fig. 4).

The results of several typical calculations for composite lattices are given in Tables Ia and Ib.

In one case of a composite lattice when the number of unknown values $M = 2$, a simple analytical expression may be obtained for K_∞ and L^2 in such a lattice.

A method for calculating composite lattices has also been elaborated for a case, when the moderator does not absorb thermal neutrons. In this case the method of heterogeneous calculation described in the first section is not applicable in consequence of the

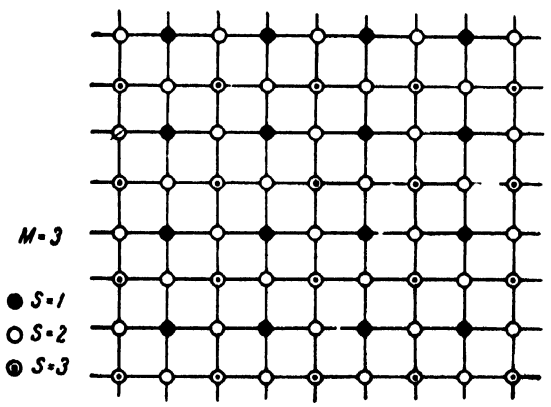

Figure 3. Scheme of a double lattice; the number of unknown quantities M = 3. 1. absorbing rods; 2, 3. multiplying slugs

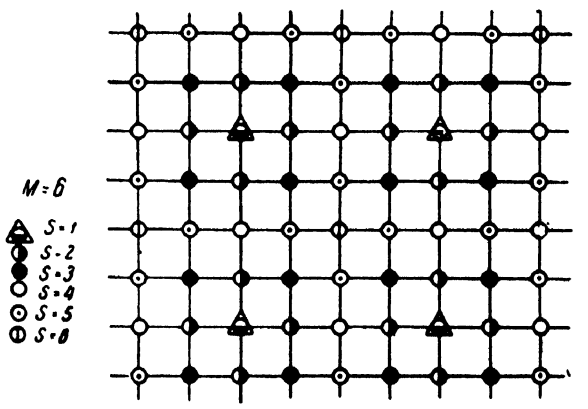

Figure 4. Scheme of triple lattice; the number of unknown quantities M = 6. 1. control rods; 2, 3, 5. multiplying slugs; 4, 6. slugs producing isotopes

Table Ia. For a "Double" Lattice, Fig. 3

$\frac{L^2}{\tau}$	$\frac{L}{a}$	$\frac{R}{a}$	$2\pi D\gamma_{2,3}$ $(D = \lambda_{tr}/3)$	$\gamma_{2,3}/\gamma_1$	$\eta_{2,3}$	η_1	Φ_1/Φ_2	Φ_2/Φ_3
10	2.74	0.107	4.75	0	1.17	0	1.41	1.03
10	2.74	0.107	4.75	0.5	1.36	0	1.17	1.01
10	2.74	0.107	4.75	1.0	1.49	0	1.00	1.00
10	2.74	0.107	4.75	1.5	1.60	0	0.873	0.992
10	2.74	0.107	4.75	2.0	1.68	0	0.775	0.985

divergence of $\sum_k^\infty f_{nk}$. Here use was made of the doubly-periodic solution of the Poisson equation $\Delta\Phi = \text{const.}$, possessing logarithmic singularities in the nodes of the lattice.

3. THE PROOF OF THE HOMOGENIZATION METHOD

A consequent derivation of formulas obtained by the homogenization method (i.e., the proof of this extensively applied rule) is of theoretical interest.

According to this method, as we know, at a distance from the boundary of the core of a large reactor the spatial distribution of a flux of neutrons Φ is described by superposition of the following expressions:

$$\Phi = e^{i\kappa r} \tag{1.3}$$

where κ^2 is the real root of the characteristic equation

$$K_\infty = e^{\kappa^2\tau}(1 + \kappa^2 L_c^2) \tag{2.3}$$

it being known that

$$K_\infty = \eta\theta, \qquad L_c^2 = L^2(1 - \theta) \tag{3.3}$$

Here κ^2 is the buckling, characterizing the effective critical dimension of the core of the reactor, i.e. the active zone increased by the reflector savings; θ is the thermal utilization coefficient in an infinite heterogeneous lattice with $\kappa = 0$.

The problem consists in defining the conditions at which Equations 1.3 and 2.3 are consequences of "heterogeneous" equations.

A. D. Galanin and V. V. Vladimirski have shown that for the spatial distribution of a flux of neutrons Φ similar to Equation 1.3 a characteristic equation, approximately coincident with Equations 2.3 and 3.3, follows from the heterogeneous Equations 17.1.

We shall proceed from equations 15.1. Noting that α_{rk} is a function of $\alpha_{nk}(|r_n - r_k|)$ we may write Equations 15.1 as follows:

$$\gamma i_n = \sum_k^\infty i_k \alpha(|r_n - r_k|)$$
$$\alpha_{nk} = \eta F(|r_n - r_k|) - f(|r_n - r_k|) \tag{4.3}$$

It is easy to discern that $i_n = e^{i\kappa r_n}$ is the solution of a system of Equations 4.3. Actually, the sum $\sum_k^\infty \alpha(|r_n - r_k|)e^{i\kappa r_k}$ may be transformed thus:

$$\sum_k^\infty \alpha(|r_n - r_k|)e^{i\kappa r_k} = e^{i\kappa r_n}\sum_k^\infty \alpha(|r_n - r_k|)e^{i\kappa(r_k - r_n)} \tag{5.3}$$

It is quite clear that for an infinite lattice

$$\sum_k^\infty \alpha(|r_n - r_k|)e^{i\kappa(r_n - r_k)} = \sum_k^\infty \alpha(|r_k|)e^{i\kappa r_k} \tag{6.3}$$

And so, we have:

$$\gamma e^{i\kappa r_n} = e^{i\kappa r_n}\sum_k^\infty \alpha(|r_k|)e^{i\kappa r_k} \tag{7.3}$$

From which

$$\gamma = \sum_k^\infty \alpha(|r_k|)e^{i\kappa r_k} = \eta\sum_k^\infty F(|r_k|)e^{i\kappa r_k} - \sum_k^\infty f(|r_k|)e^{i\kappa r_k} \tag{8.3}$$

Table Ib. For a "Triple" Lattice, Fig. 4

$\frac{L^2}{\tau}$	$\frac{L}{a}$	$\frac{R}{a}$	$2\pi D\gamma_1$ $(D = \lambda_{tr}/3)$	$\gamma/\gamma_{4,6}$	$\gamma_{2,3,5}/\gamma_1$	$\eta_{2,3,5}$	η_2	η_3	Φ_2/Φ_1	Φ_3/Φ_1	Φ_4/Φ_1	Φ_5/Φ_1	Φ_6/Φ_1
10	2.74	0.107	2.0	0.6	0	1.27	0	0	0.504	0.478	0.587	0.473	0.578
10	2.74	0.107	2.0	1.0	0	1.33	0	0	0.496	0.470	0.460	0.455	0.451
10	2.74	0.107	2.0	1.4	0	1.36	0	0	0.490	0.464	0.378	0.444	0.370
10	2.74	0.107	2.0	0.6	1	1.35	0	0	1.018	1.019	1.276	1.039	1.281
10	2.74	0.107	2.0	1.0	1	1.42	0	0	1.0	1.0	1.0	1.0	1.0
10	2.74	0.107	2.0	1.4	1	1.46	0	0	0.988	0.988	0.822	0.975	0.820
10	2.74	0.107	2.0	0.6	3	1.38	0	0	2.046	2.101	2.654	2.171	2.688
10	2.74	0.107	2.0	1.0	3	1.44	0	0	2.010	2.061	2.080	2.090	2.098
10	2.74	0.107	2.0	1.4	3	1.49	0	0	1.984	2.035	1.711	2.037	1.720
10	2.74	0.107	4.75	0.6	0	1.331	0	0	0.707	0.685	0.769	0.681	0.760
10	2.74	0.107	4.75	1.0	0	1.405	0	0	0.697	0.674	0.665	0.661	0.651
10	2.74	0.107	4.75	1.4	0	1.47	0	0	0.690	0.665	0.588	0.645	0.576
10	2.74	0.107	4.75	0.6	3	1.48	0	0	1.629	1.679	1.925	1.731	1.958
10	2.74	0.107	4.75	1.0	3	1.56	0	0	1.605	1.651	1.668	1.679	1.688
10	2.74	0.107	4.75	1.4	3	1.63	0	0	1.587	1.631	1.471	1.639	1.484

The first of the sums, written on the right side of the equation obtained, may be reduced to:

$$2\pi L^2\Sigma_c \sum_k^{\infty} F(|\gamma_k|)e^{i\kappa\gamma_k}$$

$$= \frac{2\pi L^2}{\sigma} \sum_{\nu}^{\infty} \frac{e^{-\frac{4\pi^2\tau}{a^2}\left(\vec{\nu}+\frac{\vec{a\kappa}}{2\pi}\right)^2}}{1+4\pi^2\frac{L^2}{a^2}\left(\vec{\nu}+\frac{\vec{a\kappa}}{2\pi}\right)^2} \approx \frac{2\pi L^2}{\sigma}\frac{e^{-\kappa^2\tau}}{1+\kappa^2L^2} \tag{9.3}$$

The latter expression is valid when $4\pi^2\tau \gg a^2$; $\kappa a \ll 1$.

The second sum in Equation 8.2 is defined by this formula:

$$2\pi L^2\Sigma_c \sum_k^{\infty} f(|\gamma_k|)e^{i\kappa\gamma_k}$$

$$= \frac{2\pi L^2}{\sigma} \sum_{\nu_1,\nu_2}^{\infty} \frac{e^{2\pi i\left(\frac{\nu_1}{a_1}x+\frac{\nu_2}{a_2}y\right)}}{1+\frac{4\pi L^2}{\sin^2\omega}\left[\left(\frac{\nu_1}{a_1}+\frac{\kappa_1}{2\pi}\right)^2+\left(\frac{\nu_2}{a_2}+\frac{\kappa_2}{2\pi}\right)^2 - 2\left(\frac{\nu_1}{a_1}+\frac{\kappa_1}{2\pi}\right)\left(\frac{\nu_2}{a_2}+\frac{\kappa_2}{2\pi}\right)\cos\omega\right]} \tag{10.3}$$

If $\kappa a \ll 2\pi$, then

$$2\pi L^2\Sigma_c \sum_k^{\infty} f(|\gamma_k|)e^{i\kappa\gamma_k} \approx -\frac{2\pi L^2}{\sigma}\left(g+\frac{1}{1+\kappa^2L^2}\right) \tag{10.3*}$$

where g is given in Equation 17.2. And so, when conditions $4\pi^2L^2 \gg a^2$, $4\pi^2\tau \gg a^2$ and $\kappa a \ll 2\pi$ are fulfilled, Equation 8.3 may be written as:

$$\Sigma_c \cdot \gamma \approx \eta\frac{e^{-\kappa^2\tau}}{1+\kappa^2L^2}\frac{1}{\sigma} - \left(\frac{1}{1+\kappa^2L^2}+g\right)\frac{1}{\sigma} \tag{11.3}$$

where g does not depend on $|\kappa|$ and is determined by Equation 18.2. The last equation may be written as follows:

$$K_\infty = e^{\kappa^2\tau}(1+\kappa^2L_{lattice}{}^2) \tag{12.3}$$

where

$$K_\infty = \frac{\eta}{1+\gamma\Sigma_c\sigma+g}, \qquad L^2{}_{lattice} = L^2\frac{\gamma\sigma\Sigma_c+g}{1+\gamma\Sigma_c\sigma+g} \tag{13.3}$$

It remains to be pointed out that in the case of $\kappa = 0$, as has been shown in Section 2 (Formula 16.2) the following relation is true:

$$\gamma\Sigma_c\sigma + g = \frac{1-\theta}{\theta} \tag{14.3}$$

Consequently,

$$K_\infty = \eta\theta, \qquad L_{lattice}{}^2 = L^2(1-\theta) \tag{15.3}$$

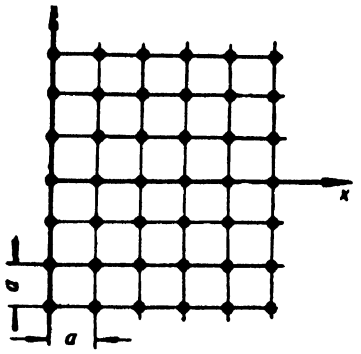

Figure 5. Scheme of a semi-infinite lattice with a spacing

It must be pointed out that if instead of a slowing down flux (j) of the form of Equation 1.2 another form of expression is used for "j", i.e., going over the limits imposed by the age approximation, then the function $e^{-\kappa^2\tau}$ in Equation 12.3 will be substituted by the Fourier-component j.

4. DEFINITION OF EFFECTIVE BOUNDARY CONDITIONS

In large multiplying systems near the core boundary or near the irregularities of the lattice (for instance, near the absorbing rod) a complicated irregular spatial distribution of the neutron flux is to be observed. On the contrary, far enough from the core boundary or the absorbing rod a regularly varying asymptotic spatial distribution of neutrons is established. To characterize the reactor as a whole this distribution is most important. If the variation of the neutron flux within one cell of the lattice be disregarded, the asymptotic dependence of i_n, when $|n|$ increases, may easily be found up to a certain quantity δ. This asymptotic dependence is not difficult to obtain from "homogeneous equations." With $k_\infty = 1$ the asymptotic dependence i on $|n|$ for a semi-infinite reactor has the form:

$$i_n \to \text{const}\ (an+\delta)$$

For an infinite reactor with spherical absorbing slugs:

$$i_n \to \text{const}\left(1-\frac{\delta}{r_n}\right)$$

The problem of determination of δ shall further on be designated as the problem of effective boundary conditions.

EFFECTIVE BOUNDARY CONDITIONS IN AN INFINITE REACTOR WITH A SEMI-INFINITE ACTIVE ZONE

A. M. Budker *et al.* considered a multiplying system in the form of an infinite moderator, in which a cubic lattice of point (spherical) slugs filling the half-space $x > 0$ (Fig. 5) was situated.

One shall proceed from the system of Equations 15.1, where $\gamma_n = \gamma = \text{const.}$:

$$\gamma i_n = \sum_{k=0}^{\infty} i_k\alpha_{nk}$$

Due to symmetry considerations for all slugs with fixed x the fluxes i_k are equal to each other and Equation 15.1 take the form:

$$\gamma i_n = \sum_{k=0}^{k=\infty} i_k \sum_{l=-\infty}^{+\infty} \sum_{m=-\infty}^{+\infty} \alpha_{n(k,l,m)} = \sum_{k=0}^{k=\infty} b_{nk} i_k \quad (1.4)$$

where

$$b_{nk} = \sum_{l=-\infty}^{+\infty} \sum_{m=-\infty}^{+\infty} \alpha_{n(k,l,m)} \quad (2.4)$$

This equation system has an infinite number of unknown quantities.

Since for a semi-infinite reactor a stationary solution of Equation 1.4 is possible only when $\kappa = 0$, at a far enough distance from the boundary of the active zone, that is, when $x_n \gg a$ the solution may be written as follows:

$$i_n = \underset{n\to\infty}{\text{const}}\ (na + \delta) \quad (3.4)$$

where the const. and δ are both constant.

Let us recall that the problem of effective boundary conditions consists in determining the value of δ. Calculation of the value l_{nk} in the first approximation leads to the following result:

$$b_{nk} \approx \eta\pi \frac{L}{a} e^{\tau/L^2} \left\{ e^{(n-k)\frac{a}{L}} \left[1 - \operatorname{erf}\left(\frac{n-k}{2\frac{\sqrt{\tau}}{a}} + \frac{\sqrt{\tau}}{L} \right) \right] + e^{-(n-k)\frac{a}{L}} \left[1 + \operatorname{erf}\left(\frac{n-k}{2\frac{\sqrt{\tau}}{a}} - \frac{\sqrt{\tau}}{L} \right) \right] \right\} - 2\pi \frac{L}{a} e^{-(n-k)\frac{a}{L}} \quad (4.4)$$

where

$$\operatorname{erf}(x) = \frac{2}{\sqrt{\pi}} \int_0^x e^{-t^2}\, dt$$

It should be noted that Equation 4.4 is approximate, since the last term is obtained by substituting an integral for the sums of singular functions, which is, generally speaking, unjustified. We should also note that b_{nk} depends on the absolute value of the difference $(|n - k|)$.

$$b_{nk} = b(|n-k|) = b_s; \qquad s = |n-k| \quad (5.4)$$

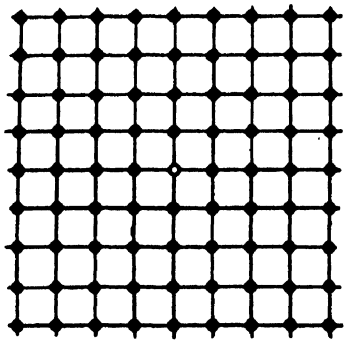

Figure 6. Scheme of an infinite lattice consisting of identical slugs; at the origin of the coordinates there is one slug with different properties

Then the developed system of Equation 1.4 has the form:

$$\begin{vmatrix} (b_{00}-\gamma) & b_{01} & b_{02} & \cdots \\ b_{10} & (b_{11}-\gamma) & b_{12} & \cdots \\ b_{20} & b_{21}, & (b_{22}-\gamma) & \cdots \\ \cdots & \cdots & \cdots & \cdots \\ \cdots & \cdots & \cdots & \cdots \end{vmatrix} = \begin{vmatrix} Mb_1b_2 & \cdots \\ b_1Mb_1 & \cdots \\ b_2b_1M & \cdots \\ \cdots & \cdots \\ \cdots & \cdots \end{vmatrix} = 0 \quad (6.4)$$

where

$$-M = \gamma - b_{nn} = \gamma - b_0 \quad (7.4)$$

To fulfill the stationary conditions for a semi-infinite reactor it is also necessary to fulfill them for an infinite reactor having a lattice identical to the first. This makes it possible to find the value of M. Indeed, for an infinite stationary lattice where $i_k = i_0 =$ const., Equations 15.1 take the form:

$$\gamma = \sum_{-\infty}^{+\infty} b_k = b_0 + 2\sum_{1}^{\infty} b_k \qquad \text{or} \qquad \gamma - b_0 = 2\sum_{1}^{\infty} b_k$$

Comparing with Equation 7.4 we get:

$$M = -2\sum_{1}^{\infty} b_k \quad (8.4)$$

Now the reflector savings δ may be evaluated. It is supposed that beginning from the mth slug there is an almost linear dependence of the neutron flux i_k on the number of the slug. Then for $k > m$

$$i_k = \frac{k+\delta}{m+\delta} i_m + \delta(i_k) \quad (9.4)$$

where $\delta(i_k)$ are presumably small.

Substituting Equation 9.4 into Equation 1.4 and using the above found value of M, we write:

$$i_n\left(2\sum_{1}^{\infty} b_k\right) = \sum_{k=1}^{k=m-1} i_k b_{n-k} + i_m \frac{1}{m+\delta} \sum_{k=m}^{\infty} (k+\delta) b_{n-k} + \sum_{k=m}^{\infty} \delta(i_k) b_{n-k} \quad (10.4)$$

The system of Equation 10.4 is "out of" at a certain value of m, i.e., it is assumed that the sum $\delta(i_k)$ may be disregarded. This gives us a homogeneous linear system of $m + 1$ equations. The eigenvalue of this system is the unknown quantity δ. The latter equals:

$$\frac{\delta}{a} =$$

$$\begin{vmatrix} -\left(2\sum_1^\infty b_k\right) & b_1 & b_2 \cdots & \left(\sum_m^\infty k b_k\right) \\ b_1 & -\left(2\sum_1^\infty b_k\right) & b_1 \cdots & \left(\sum_m^\infty k b_{k-1}\right) \\ \cdots & \cdots & \cdots & \cdots \\ b_m, & b_{m-1} \cdots & \left(\sum_{m+1}^\infty k b_{k-m} - 2m\sum_1^\infty b_k\right) & \end{vmatrix} \Bigg/ \begin{vmatrix} -\left(2\sum_1^\infty b_k\right) & b_1 & b_2 \cdots & \left(\sum_m^\infty b_k\right) \\ b_1 & -\left(2\sum_1^\infty b_k\right) & b_1 \cdots & \left(\sum_m^\infty b_{k-1}\right) \\ \cdots & \cdots & \cdots & \cdots \\ b_m & b_{m-1} \cdots & \left(\sum_{m+1}^\infty b_{k-m} - 2\sum_1^\infty b_k\right) & \end{vmatrix} \tag{11.4}$$

Taking various values for m beginning from $m = 1$, we find, generally speaking, various values for δ. The extent of dispersion of the found values of δ characterizes the error made in computing this value.

As an example let us consider a case when $\tau/L^2 = 0.12$; $a/L = 0.4$; $\eta = 1.22$. Calculation in accordance with Equation 11.5 gives such a result:

$m = 1$	2	3
$\delta/a = 3.2$	3.15	3.14

Effective Boundary Conditions in an Infinite Reactor with an Absorbing Rod

For an infinite lattice, consisting of identical point slugs in which only one slug is substituted by a neutron absorbing rod (Fig. 6) with a different absorptive and emissive capacity ($\eta \neq \eta_0 = \eta_k$; $\gamma \neq \gamma_0 = \gamma_k$), the problem of effective boundary conditions consists in finding the value of δ in the asymptotic expression for the dependence of the neutron flux i_k absorbed by the kth slug on the index k

$$i_k \to \text{const}\left(1 - \frac{\delta}{|r_k|}\right)$$
$$|k| \to \infty \tag{12.4}$$

A method of calculation analogous to the one described in the last section may be used in solving this problem. Thus, Equation 14.1 for the problem under consideration may be written:

$$n \neq 0: \quad \gamma_0 i_n = \sum_{-\infty}^{+\infty}{}' \alpha(|r_k - r_n|) i_k - i_0 f(|r_n|)$$
$$\equiv \sum_{-\infty}^{+\infty} \alpha(|r_k - r_n|) i_k - i_0 \eta F(|r_n|)$$
$$n = 0: \quad \gamma_\delta i_0 = \sum_{-\infty}^{+\infty}{}' \alpha(|r_k|) i_k - i_0 f(R_0)$$
$$\equiv \sum_{-\infty}^{+\infty} \alpha(|r_k|) i_k - i_0 \eta F(0) \tag{13.4}$$

where γ_0 is the absorption coefficient for the slugs of the lattice; γ_δ is the same quantity for a slug placed in the origin of the coordinates (with a radius R_0); $r_n = an$, n is an integer vector, and a is the spacing of the cubic lattice.

It is possible, beginning with any n to substitute for the flux i_n its asymptotic expression Equation 12.4 and further, disregarding small terms, to obtain for calculating δ a system consisting of $\sim n^3$ "out-of" equations.

However, it is more interesting to describe another method used in solving this problem.

If $|n|$ in Equation 13.4 would be infinitely large, then the member $i_0 \eta F(|r_n|) \to 0$ and therefore:

$$\gamma_0 i_n \to \sum_{-\infty}^{+\infty} \alpha(|r_k - r_n|) i_k \tag{14.4}$$

The solution of this asymptotic equation is: $i_n \to \text{const} = i_\infty$ i.e.,

$$\gamma_0 i_\infty = \sum_{-\infty}^{+\infty} \alpha(|r_k - r_n|) i_\infty \tag{15.4}$$

from which

$$\gamma_0 = \sum_{-\infty}^{+\infty} \alpha(|r_k|) \tag{16.4}$$

Subtracting separately from each term of Equation 15.4 the corresponding term of Equation 13.4 we find:

$$n \neq 0: \quad \gamma_0 i_n' = \sum_{-\infty}^{+\infty} \alpha(|r_k - r_n|) i_k' + i_0 \eta F(|r_n|)$$
$$n = 0: \quad \gamma_0 i_0' = \sum_{-\infty}^{+\infty} \alpha(|r_k|) i_k' + i_0 \eta F(0) + i_0 \Delta\gamma \tag{17.4}$$

where $i_n = i_\infty - i_n$ and $\Delta\gamma = \gamma_\delta - \gamma_0$.

From Equation 14.4 it is easy to see that $i_n \to 0$ when $|n| \to \infty$. Then $i_n'| \sim 1/a|n||$ decreases, as we shall see later.

Let us multiply each of Equations 17.4 by $e^{ia\kappa n}$ and summarize the results (κ is an arbitrary vector)

$$\gamma_0 \sum_{-\infty}^{+\infty} e^{i\vec{\alpha}\vec{n}} i_n' = \sum_{-\infty}^{+\infty} e^{i\vec{\alpha}\vec{n}} \sum_{-\infty}^{+\infty} \alpha(|r_k - r_n|) i_k' + i_0\eta \sum_{-\infty}^{+\infty} e^{i\vec{\alpha}\vec{n}} F(|r_n|) + i_0 \Delta\gamma \quad (18.4)$$

Changing the order of summation in the double sum, we write

$$\sum_{-\infty}^{+\infty}\sum_{-\infty}^{+\infty} = \sum_{-\infty}^{+\infty} i_k' \sum_{-\infty}^{+\infty} e^{i\vec{\alpha}\vec{n}} \alpha(|r_k - r_n|) = \sum_{-\infty}^{+\infty} i_k' e^{i\vec{\alpha}\vec{k}} \sum_{-\infty}^{+\infty} e^{i\vec{\alpha}\vec{n}} \alpha(|r_n|) \quad (19.4)$$

Now we introduce auxiliary periodic functions of the parameter $\vec{\kappa}$, defining them by the following Fourier series:

$$\tilde{i}(\vec{\kappa}) = \sum_{-\infty}^{+\infty} i_n' e^{i\vec{\alpha}\vec{n}} \quad \text{when} \quad |\vec{\kappa}| \neq 0,$$

$$\tilde{\alpha}(\vec{\kappa}) = \sum_{-\infty}^{+\infty} \alpha(|r_n|) e^{i\vec{\alpha}\vec{n}}, \quad (20.4)$$

$$\tilde{F}(\vec{\kappa}) = \sum_{-\infty}^{+\infty} F(|r_n|) e^{i\vec{\alpha}\vec{n}} \quad (21.4)$$

Note that the sum of Equation 20.4 converges at any $\kappa \neq 0$, but when $\kappa = 0$ it diverges. Using Equations 20.4, 21.4 and 19.4 Equation 18.4 may be written in the form

$$\kappa \neq 0: \quad \gamma_0 \tilde{i}(\vec{\kappa}) = \tilde{\alpha}(\vec{\kappa})\tilde{i}(\vec{\kappa}) + i_0(\eta\tilde{F}(\vec{\kappa}) + \Delta\gamma) \quad (22.4)$$

Noting from Equations 16.4 and 21.4 that $\gamma_0 = \tilde{\alpha}(0)$ we obtain

$$\vec{\kappa} \neq 0: \quad \tilde{i}(\vec{\kappa}) = i_0 \frac{\eta\tilde{F}(\vec{\kappa}) + \Delta\gamma}{\tilde{\alpha}(0) - \tilde{\alpha}(\vec{\kappa})} \quad (23.4)$$

Now i_n' may be computed from Equation 20.4 if the attention is paid to the fact that Equation 20.4 is an expression of the periodic function $\tilde{i}(\vec{\kappa})$ in the Fourier series. Thus the Fourier coefficient for this expansion is

$$i_n = \frac{i_0 a^3}{(2\pi)^3} \int_{\text{by the period}} \frac{\Delta\gamma + \eta\tilde{F}(\vec{\kappa})}{\tilde{\alpha}(0) - \tilde{\alpha}(\vec{\kappa})} e^{-i\vec{\alpha}\vec{n}} d\vec{\kappa} \quad (24.4)$$

Assuming that in Equation 24.4 n is equal to zero we obtain an equation connecting (i_∞/i_0) with γ_δ the coefficient of the absorbing slug:

$$\frac{i_\infty}{i_0} = 1 + \frac{a^3}{(2\pi)^3} \int_{\text{by the period}} \frac{\Delta\gamma + \eta\tilde{F}(\vec{\kappa})}{\tilde{\alpha}(0) - \tilde{\alpha}(\vec{\kappa})} d\vec{\kappa} \quad (25.4)$$

Thus the solution of a system of equations with an infinite number of unknown quantities is reduced to a quadrature.

To bring the solution to a numeric result it is necessary to calculate the integral on the right side of Equation 25.4 using the sums of Equation 21.4. The latter converge quite rapidly.

As has been pointed out in Part 2 this convergence may be made more rapid.

Now we return to the question of the behaviour of i_r' at infinity. When $|n| \to \infty$ in the integral of Equation 24.4 only the range $|\vec{\alpha}| \to 0$ is of essential value.

From Equation 21.4 it easily follows that

$$|\vec{\kappa}| \to 0: \quad \tilde{F}(\vec{\kappa}) \to \sum_{-\infty}^{+\infty} F(|r_k|) > 0$$

$$\tilde{\alpha}(0) - \tilde{\alpha}(\vec{\kappa}) \approx \frac{a^2\kappa^2}{2} \sum_{\infty}^{+\infty} k^2 \alpha(|r_k|) \cos^2(\vec{\kappa},\vec{k}) \quad (26.4)$$

Consequently, when $|n| \to \infty$

$$i_n' \to \frac{i_0}{|n|} \frac{\Delta\gamma + \eta \sum_{-\infty}^{\infty} F(|r_n|)}{\frac{1}{3} \sum_{-\infty}^{+\infty} k^2 \alpha(|r_n|)} \quad (27.4)$$

In the latter i_0 may be substituted by i_∞ from Equation 25.4. Comparing Equations 27.4 and 25.4 we find the connection existing between δ and i_0/i_∞ or the connection of δ and γ_δ

$$\delta = a \frac{3(\Delta\gamma + n \sum_k F_k)/\sum_k k^2\alpha_k}{1 + \frac{a^3}{(2\pi)^3} \int \frac{\Delta\gamma + \eta\tilde{F}(\vec{\kappa})}{\tilde{\alpha}(0) - \tilde{\alpha}(\vec{\kappa})} d\vec{\kappa}} \quad (28.4)$$

This problem has been studied previously by B. T. Geilikman, by another method for cases with spherical and cylindrical slugs. This author obtained

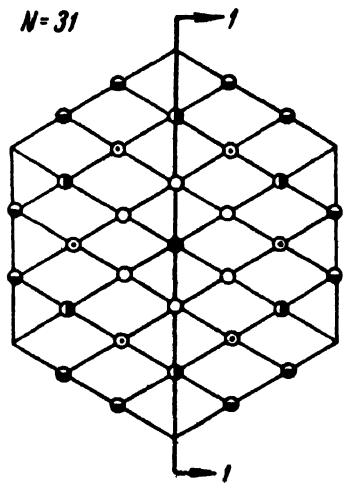

Figure 7. Scheme of a reactor with a small number of slugs ($N = 31$); the number of unknown quantities $M = 5$. Distribution of the neutron flux along the section 1-1 (see Fig. 9)

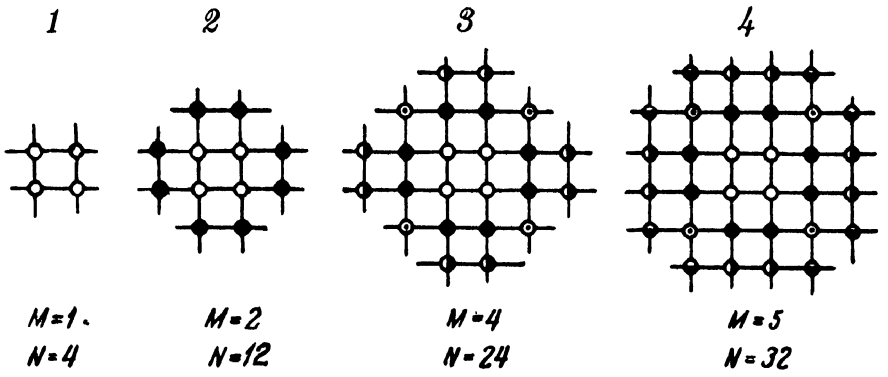

Figure 8. Scheme of a section with a small number of slugs. 1. Number of slugs N = 4; unknown quantities M = 1; 2. N = 12, M = 2; 3. N = 24, M = 2; 4. N = 32, M = 5

evaluations for δ assuming it possible to substitute integrals for infinite sums.

5. A REACTOR WITH A SMALL NUMBER OF SLUGS

For a reactor, the core of which consists of a small number of slugs, the application of the homogenization method is unjustified. The larger the number of slugs is the smaller is the difference between the calculations results for the heterogeneous and homogeneous methods. Comparison of the "homogeneous" and "heterogeneous" methods enables us to estimate the limits of validity and the error of the homogeneous method. The homogeneous method is especially unsatisfactory when applied to the calculation of the effect of an absorbing rod and the neutron field in a reactor in which the periodicity of the lattice has been violated.

The initial step for describing the stationary state of a reactor is again Equation 18.1.

$$\gamma_n i_n = \sum_{s=1}^{s=M} i_s \sum_{k'}^{N} (\eta_s F_{nk'} - f_{nk'}) \qquad (1.5)$$

For line slugs, in accordance with Equation 6.2

$$F_{kn} = F(d_{nk}) = \int_{\infty} (e^{-r^2/4\tau}/4\pi\tau) K_0\left(\frac{|r - d_{k,n}|}{L}\right) \frac{dr}{2\pi L^2 \Sigma_c}$$

$$f_{kn} = \frac{1}{2\pi L^2 \Sigma_c} K_0\left(\frac{d_{k,n}}{L}\right) \quad \text{when} \quad k \neq n;$$

$$\text{when} \quad k = n \quad f_{n,n} = \frac{1}{2\pi L^2 \Sigma_c} K_0\left(\frac{R_n}{L}\right)$$

where $d_{kn} = |r_k - r_n|$ is the distance between slugs k and n. G. A. Bat used the numerical method of calculating $F(d)$, representing this function as:

$$F_{kn} = F(d_{kn}) \equiv F\left(\frac{L^2}{4\tau}, \frac{d_{kn}}{L}\right) \qquad (2.5)$$

where

$$F(\beta,x) = K_0(x) \int_0^x y I_0(y) e^{-\beta^2 y^2} dy + I_0(x) \int_0^x y K_0(y) e^{-\beta^2 y^2} dy$$

A. D. Galanin independently pointed out that when $\tau/L^2 \ll 1$ the function $F(d)$ may be represented as a rapidly converging series.

Keeping the first terms of the series, we may write:

$$F(d) = \frac{e^{\tau/L^2}}{2\pi L^2 \Sigma_c} \int_{\tau/L^2}^{\infty} e^{-\left(z + \frac{d^2}{4L^2 z}\right)} \frac{dz}{2z} \approx \frac{e^{\tau/L^2}}{2\pi L^2 \Sigma_c} \left[K_0\left(\frac{d}{L}\right) + \frac{\tau}{2L^2} e^{-d^2/4\tau} + \frac{1}{2}\left(1 + \frac{d^2}{4L^2}\right) Ei(-d^2/4\tau) \right] \qquad (3.5)$$

Assuming the determinant of the system of Equation 1.5 to be equal to zero, we obtain the critical conditions for the reactor.

Several reactors were calculated according to this method; their schemes are shown in Figs. 7 and 8.

Results of the "heterogeneous" calculations were compared with the results of the respective "homogeneous" calculations; the latter were done by a two-group method, the quantities K_∞, θ and L were computed by formulae which follow from the homogeneization rule mentioned in Part 3.

The results of calculations for a reactor, the scheme of which is given in Fig. 7, show that the difference between the critical masses was quite small when calculated by the heterogeneous and homogeneous methods respectively; it was equal to ~15 per cent.

Table III shows the results of calculations done by A. D. Galanin** for the schemes on Fig. 8.

The multiplication factors shown in Table II have been calculated by the known formulae:

$$K_{hetero} = \frac{\eta}{1 + Q + g}; \qquad Q = 2\pi D\gamma \frac{d^2}{2\pi L^2} \qquad (4.5)$$

$$g = \frac{a^2}{4\pi L^2}\left(\ln \frac{a^2}{\pi R^2} + \frac{\pi R^2}{a^2} - 1.48\right) \qquad (4.5)$$

$$R_{reactor} = \sqrt{\frac{\overline{Na^2}}{\pi}}; \qquad \alpha^2 = -\frac{1}{2}\left(\frac{1}{L_{lattice}^2} + \frac{1}{\tau}\right) + \sqrt{\frac{1}{4}\left(\frac{1}{L_{lattice}^2} + \frac{1}{\tau}\right)^2 + \frac{K_\infty - 1}{L_{lattice}^2 \tau}} = \frac{5{,}76}{R_{reactor}^2} \qquad (5.5)$$

$$K_{homo} = e^{\alpha^2 \tau}(1 + \alpha^2 L_{lattice}^2) \qquad (6.5)$$

** For details see A. D. Galanin, P/663, "Critical Sizes of a Heterogeneous Reactor with a Small Number of Slugs," this Session.

Table II. For Fig. 4

$\frac{L^2}{\tau} = 10$; $\frac{L}{a} = 2.74$; $\frac{R}{a} = 0.107$; $\eta_1 = 0$; $\eta_{4,6} = 0$

$\frac{2\pi D\gamma_{2,3,5}}{D = \lambda_{tr}/3}$	$\gamma_{2,3,5}/\gamma_{4,6}$	$\gamma_{2,3,5}/\gamma_1$	$\eta_{2,3,5}$	Φ_2/Φ_1	Φ_3/Φ_1	Φ_4/Φ_1	Φ_5/Φ_1	Φ_6/Φ_1
2.0	0.6	0	1.27	0.504	0.478	0.587	0.473	0.578
2.0	1.0	0	1.33	0.496	0.470	0.460	0.455	0.451
2.0	1.4	0	1.36	0.490	0.464	0.378	0.444	0.370
2.0	0.6	1	1.35	1.018	1.019	1.276	1.039	1.281
2.0	1.0	1	1.42	1.0	1.0	1.0	1.0	1.0
2.0	1.4	1	1.46	0.988	0.988	0.822	0.975	0.820
2.0	0.6	3	1.38	2.046	2.101	2.654	2.171	2.688
2.0	1.0	3	1.44	2.010	2.061	2.080	2.090	2.098
2.0	1.4	3	1.49	1.984	2.035	1.711	2.037	1.720
4.75	0.6	0	1.331	0.707	0.685	0.769	0.681	0.760
4.75	1.0	0	1.405	0.697	0.674	0.665	0.661	0.651
4.75	1.4	0	1.47	0.690	0.665	0.588	0.645	0.576
4.75	0.6	3	1.48	1.629	1.679	1.925	1.731	1.958
4.75	1.0	3	1.56	1.605	1.651	1.668	1.679	1.688
4.75	1.4	3	1.63	1.587	1.631	1.471	1.639	1.484

Table III

Scheme No.	*Number of slugs N*	*R of reactor in unit a*	K_{II}	K_{hom}	K_{het}	$\frac{K_{het} - K_{II}}{K}$	$\frac{K_{het} - K_{hom}}{K}$
			1st variation slug radius $R = 0.1$				
			$a = \sqrt{\tau} = 1$; $L^2 = 49$; $Q = 0.015$; $g = 3.3 \times 10^{-3}$				
1	4	1.128	2.11	2.31	2.29	13.7%	−1.5%
2	12	1.954	1 48	1.51	1.53	9.8%	−3.4%
3	24	2.764	1.29	1.30	1.31	7.1%	+3.2%
4	32	3.192	1.23	1.24	1.25	6.4%	+3 2%
			2nd variation				
			$a = \sqrt{\tau} = 1$; $L^2 = 8$, $Q = 0.081$; $g = 0.020$				
1	4		2.41	2.86	2.97	28%	+5.6%
2	12		1.63	1.71	1.81	21.9%	+11.1%
3	24		1.38	1.41	1.47	18.5%	+12%
4	33		1.31	1.33	1.37	16.8%	+11.2%

For details see A. D. Galanin "Critical Sizes of a Heterogeneous Reactor with a Small Number of Slugs," this Session.

The results in Table III enable us to estimate the possibilities of "homogeneous" methods of calculating the critical K_∞.

It is interesting to compare the spatial distribution of the thermal neutron flux calculated by the heterogeneous and homogeneous methods. The distribution of the neutron flux in a reactor (scheme given in Fig. 7) is shown in Fig. 9.

The difference in the neutron flux in the reflector is fairly notable.

Of still greater interest are the results obtained by the heterogeneous method for altering the spatial distribution of the neutron flux when a neutron absorbing rod is inserted into the core.

Figure 10 shows the modification of the neutron field after insertion into the reactor of a central multiplying slug.

Figure 11 gives the modification of the neutron field and the values of η_{kp} of the slugs when a group of multiplying slugs is substituted by an absorbing group having other γ and R_0 (substitution of the group of slugs in Fig. 7).

Resonance Absorption in a Finite Lattice

In Part 1 of this survey we mentioned a method which enables us to estimate the resonance neutron capture in a heterogeneous system with an arbitrary number of slugs.

If the density of the neutrons above the resonance is constant in the system, or if it changes but slightly within the limits of one cell, then the resonance capture may be approximately computed by multiplying the quantity η by the factor φ†† which is defined by an empirical formula. This greatly simplifies the calculation, freeing us of the necessity of calculating double sums in Equation 14.1*.

However, for a system with a small number of slugs such a consideration is not valid; in this case a rigorous account of the influence of the resonance absorption is necessary (see Part 1). As has already been noted in Part 1, a strict account of the resonance absorption influence may be made if we assume that the energetic range of resonance absorption is sufficiently narrow.

†† The probability of resonance absorption of neutrons by uranium in an infinite lattice = $1 - \varphi$.

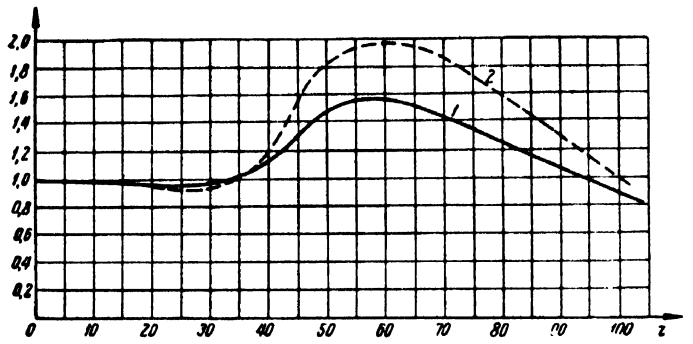

Figure 9. Spatial distribution of the thermal neutron flux in a reactor with a small number of slugs, the scheme of which is shown in Fig. 7. 1. $\Phi(r)$ was computed by the homogenization rule; 2. $\Phi(r)$ was calculated by the heterogeneous method; the intensity of neutrons in the core is averaged by the cell volume of the lattice

Actually two effects exist: (1) absorption at separate levels in the range of 6–100 ev; (2) a wide region of "unblocked absorption" extending to the energy fission neutron. The heterogeneous method of calculation is approximately valid only for estimation of the first effect. To estimate the influence of the position of the resonance level on the value of resonance absorption, S. M. Feinberg and B. D. Slutskaya calculated the heterogeneous system in Fig. 12. The calculation was made for $E_z \sim 10$ ev and $F_z \sim 400$; the computation results coincided within the range of calculation accuracy. This shows that the variation of the position of the resonance level in a wide range does not practically influence the calculation result. The dependence of the probability of resonance absorption on the number of slugs in a reactor may be clarified by the following example (see Fig. 12):

Figure 12 shows the scheme of successive increase of the number of slugs in the moderator.

The values of probability of resonance neutron capture depending on the number of slugs in the core are given in Table IV.

Thus resonance absorption in lattices consisting of a small number of slugs is essentially smaller than in infinite lattices with the same spacing and the same slugs. When the number of slugs is increased the resonance absorption quite rapidly approaches its value in infinite lattices.

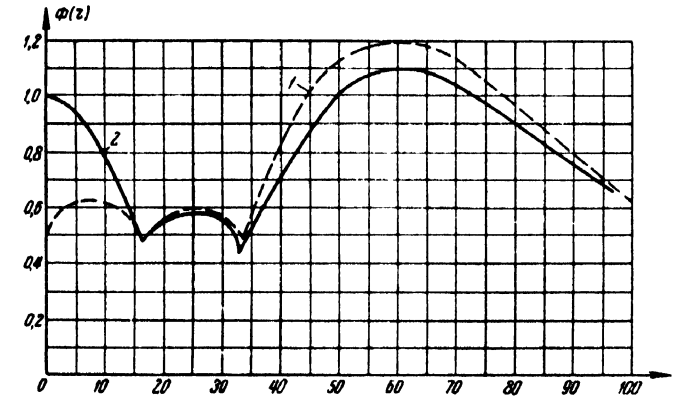

Figure 10. Change of the spatial distribution of the thermal neutron flux in a reactor (the scheme of which is given in Fig. 7) when the central slug is removed; 1. the reactor consists of 31 slugs; 2. the central slug is removed (the reactor consists of 30 slugs)

6. COMPARISON WITH EXPERIMENT

The correspondence of the results of heterogeneous calculations with experiment depends on the accuracy of the physical parameters applied in the calculation. To estimate the actual accuracy of the calculation and the dependence of the result on the variations of the physical parameters a special series of experiments has been made with a reactor‡‡ consisting of a small number of slugs.

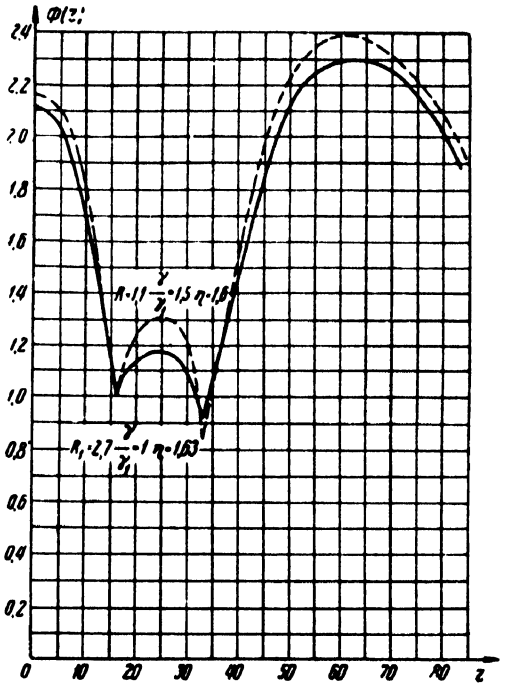

Figure 11. Change of the spatial distribution of the thermal neutron flux when γ is changed in the neutron absorbing rods (scheme shown in Fig. 7). R and γ correspond to the neutron absorbing slugs

As may be seen from Parts 1 and 5, the following physical parameters enter the calculation of a heterogeneous reactor with a small number of slugs:

$$\eta, L, \gamma, A, \tau, \tau_r, \Delta_z$$

If we build a number N of various critical systems containing identical slugs we get N connections between these seven parameters from the critical conditions. If $N \geq 7$ then the value of the parameters may be computed. However, if $N < 7$ then a part of the parameter must be given. Three critical reactors were consequently built in a large (practically infinite) graphite prism. Their schemes are shown in Fig. 13. The number of reactors is smaller than the number of values used in the calculation; consequently the values of four parameters must be picked beforehand.

(*a*) The reflector savings with respect to the height Δ_z may be estimated by means of the usual two or multi-group calculations. All the piles under consideration had a height considerably larger than the "diameter." Therefore the error in the given value $\Delta_z = 40$ cm may lead to a comparatively small error

‡‡ These experiments have been made on the suggestion of the author by a group of scientists at the Academy of Sciences of the USSR.

Table IV

Nos.	No. of slugs, N	Probability of resonance absorption $1 - \varphi\left(\frac{\eta_{A=0}}{\eta_A}\right)$
1	4	0.023
2	12	0.0374
3	16	0.0505
4	Infinite lattice	0.070

in computing the value of η. Thus, if $\delta\Delta_z = 10$ cm then this $\delta\eta_1 = 0.005$.

(*b*) A similar or even smaller error may be made in η if the position of the resonance level is wrong. Calculation shows that within reasonable limits, any choice of energy E_z (and therefore τ_z) leads to a change of not more than 0.005 in η. If we take $E_z = 15$ ev then $\tau_z = 100$ cm^2 and $\delta\eta_2 \sim 0.005$.

(*c*) A somewhat larger influence on the calculation results is exerted by the choice of the resonance absorption characteristic A. It was found by a semi-empirical formula and assumed to be equal to (40 ± 4) cm^2. The error contained in A is easy to define. Indeed in an infinite lattice with a spacing equal to 20 cm to the value of $A = (40 \pm 4)$ cm^2 corresponds the probability of the resonance absorption

$$1 - \exp\left(-\frac{40 \pm 4}{20^2}\right) = 0.1 \pm 0.01$$

In the piles under consideration the area of the moderator for one rod is on the average larger than in an infinite lattice with a spacing equal to 20 cm. For this reason the error in η is estimated as $\delta\eta_3 \sim 0.01$.

(*d*) An error in the given value of the age τ influences considerably the value of η. In accordance with the available experimental data τ is assumed to be

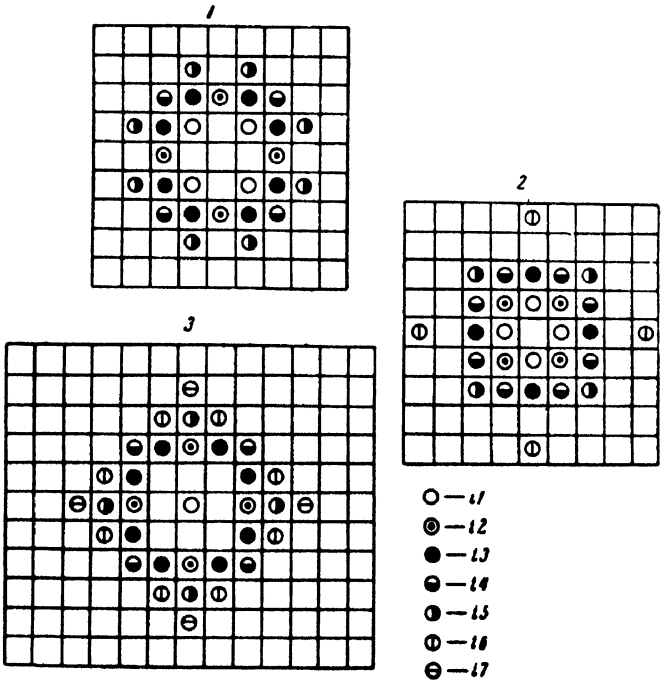

Figure 13. Scheme of reactors used in experiment. 1. Reactor consists of 28 rods; the number of unknown quantities 5. 2. Reactor consists of 28 rods; the number of unknown quantities 6. 3. Reactor consists of 33 rods· the number of unknown quantities 7

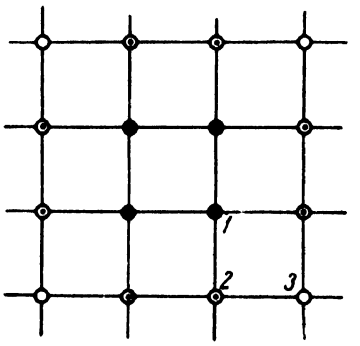

Figure 12. Schemes of lattices used for calculation of resonance absorption. 1. Lattice consists of four rods; 1 and 2. Lattice consists of 12 rods; 1, 2, 3. lattice consists of 16 rods

equal to (390 ± 10) cm^2 for the system under consideration; we may expect an error in $\delta\eta_4$ of about 0.015.

Thus the higher estimation of the error in η due to the uncertainty of the parameters Δ_z, E_r, A, τ, gives us the value $\delta\eta = \delta\eta_1 + \delta\eta_2 + \delta\eta_3 + \delta\eta_4 \leq 0.035$. It may be assumed that the actual error is not more than $\delta\eta = 0.02$ and does not exceed the error made when directly measuring η. Direct measurement made by B. G. Yerozolimsky using the method of measuring the effects from fissionable samples has given:

$$\eta = 1.647 \pm 0.017$$

The calculation results are given in Table V.§§

Calculation shows that there is no full correlation between the coincidences of η and the coincidences of i_k in calculation and experiment; however, the discrepancies are negligible and the precision attained is absolutely satisfactory from a practical point of view.

This is especially evident because in the accepted calculation scheme such factors as asymmetry in the neutron flux near the slug surface and also the dependence of the thermal neutron diffusion coefficient and the absorbing coefficient of the slug on the temperature of the neutron flux and several other factors are not accounted for.

The satisfactory agreement between the calculated and experimentally obtained values of the neutron flux distribution over slugs is quite notable. It confirms the assumption of the effectivity of the heterogeneous method especially for examining the spatial distribution of the neutron flux in the reactor.

Another point of interest is the application of the heterogeneous method for the calculation of the spatial distribution of a neutron field in a reactor with a rather large number of slugs and with considerable violations of the lattice.

A reactor employed for generation of radioactive isotopes had altogether about 240 channels. Part of them were loaded with uranium slugs, part with slugs for the generation of isotopes, and a part was used for the control system.

§§ See G. A. Bat, P/665, "Heterogeneous Calculations of Reactors with a Small Number of Slugs," this Session.

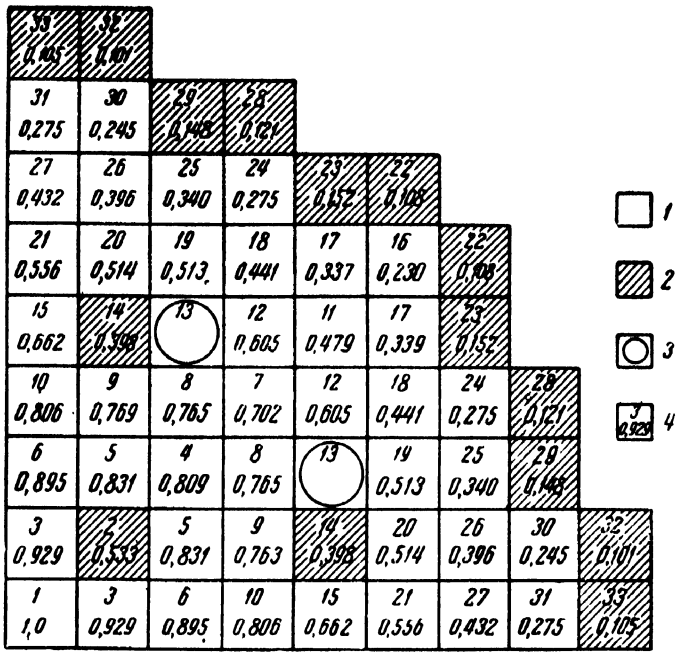

Figure 14. Cartogram of spatial distribution of a thermal neutron flux in a reactor. 1. Uranium slug cell; 2. cell of a slug producing isotopes; 3. cell of the control rod; 4. the upper number—number of the unknowns in the equations (18.1), the lower number—the neutron flux on the s-th slug (in relative units)

Owing to the symmetry in the position of the channels the problem has been reduced to solving the system of equations with 33 unknown quantities. This system of linear equations was calculated by means of

Figure 15. Radial distribution of the thermal neutron flux in a reactor. 1. Case of No. 2 position of slugs (see Table No. 6); 2. case of No. 3 position of slugs (see Table No. 6); 3. number of slugs "S"

computing machines. Various arrangements of the same rods producing isotopes and the control rods were considered. The use of rods producing isotopes with different degrees of "blackness" were also considered.

A typical cartogram of the spatial distribution of the neutron flux over the rods of the lattice and a scheme of the loading of the reactor are shown in Fig. 14.

The purpose of the calculations was to define the optimal position and optimal absorbing capacity of the slugs producing isotopes for obtaining the maximum quantity of radioactive isotopes with the minimum power of the reactor and, consequently, a minimum consumption of enriched uranium.

Table V

L = 52 cm; $2\pi D_\gamma$ = 3.3

Scheme		η	i_1	i_2	i_3	i_4	i_5	i_6	i_7	Average
1	Experiment	1.647 ± 0.017	1	0.96	0.84	0.80	0.79	—	—	0.86
	Calculation	1.63 ± 0.2	1	0.89	0.80	0.78	0.75	—	—	0.82
2	Experiment	1.647 ± 0.017	1	1.1	0.97	0.93	0.89	0.73	—	0.85
	Calculation	1.61 ± 0.02	1	1.1	0.98	0.93	0.87	0.74	—	0.85
3	Experiment	1.647 ± 0.017	1	0.70	0.66	0.59	0.54	0.51	0.49	0.59
	Calculation	1.64 ± 0.02	1	0.70	0.67	0.63	0.56	0.53	0.51	0.61

Table VI

No. of arrangement of different slugs in the active zone*	Number of cells with slugs producing isotopes†	Number of cells with control rods‡	Power by given i_{max}‡	Average density of neutrons along the radius $\sum_1^N i/Ni_{max}$	Absorption in the slugs producing isotopes	Absorption in the same slugs per power unit
2	2; 9	13	100	0.678	100	1
3	2; 9	1; 7	113	0.766	112	0.99
4	2; 9	12	103	0.697	102	0.99
5	2; 14	13	83.6	0.567	85.2	1.02
6	2; 14	1; 7	93.1	0.631	93.5	1
7	2; 20	13	89.7	0.608	93.1	1.04
8	2; 20	1; 7	96.6	0.655	98.8	1.02
9	2; 7; 9	13	82.4	0.572	82.4	1
10	2; 7; 14	13	71.4	0.496	72.6	1.02
11	2; 7; 20	13	72.8	0.505	75.4	1.04
12	2; 9; 12; 21	13	59.1	0.442	62.2	1.05
13	2; 9	13; 16; 24; 30	87.7	0.673	87.4	1

* The case of arrangement N 5 is given in Fig. 14.

† Total number of cells and their indications in all arrangements are the same as in Fig. 14; in all the arrangements the cells 22, 23, 28, 29, 32, 33 are occupied with slugs producing isotopes; all the other cells not mentioned here are occupied with uranium slugs.

‡ All the quantities are given in relative units.

The calculation results are given in Table VI.

The spatial distribution of the neutron flux is shown in Fig. 15. The calculation results were compared with experimental results obtained during the work of the reactor. The calculation prediction of the choice of an optimal loading of the reactor proved to be correct.

CONCLUSIONS

From the above-mentioned results the following conclusions may be made:

1. The application of the homogenization rule for the estimation of the critical size of a reactor is precise enough for practical purposes not only for a large reactor but also for a pile with a core consisting of a small ($\sim$20) number of slugs.

2. In order to determine the spatial distribution of the neutron flux within a reactor with a small number of slugs the heterogeneous method of calculation is necessary.

3. The heterogeneous method is necessary when examining neutron fields in composite lattices, in the vicinity of local violations of a regular lattice (the control rods, empty cells and so on) and near the boundary of the core.

4. Comparison of the results of calculating reactors by the heterogeneous method with experimental data showed a satisfactory agreement.

Natural Uranium – Beryllium and Natural Uranium Oxides–Metallic Beryllium Lattices: Computation of Cylindric Reactors

By Otto Gamba, L. A. Santalo, and F. Alsina,* Argentina

In the conventional nomenclature, the constants used are (See Table I):

$$\epsilon = 1.027 \qquad \eta = 1.32$$

Table I

	ρ	σ_a	σ_s	ξ	L	τ	χ (epithermal neutrons)
BeO	3	0.0092	11.1	0.17	29	133	0.138
Be	1.84	0.009	6.9	0.209	23.6	98	0.237
U	18.9	7.42	8.2	0.0084	123		0.42

The geometric characteristics adopted are: a = radius of the uranium rods = 1.25 cm; $c - a$ = thickness of the air (or coolant) annulus around the uranium rods = 1 cm; t = thickness of the aluminum cladding used on the uranium rods = 1 cm; and t_1 = aluminum thickness between the moderator and coolant = 1 cm.

With these characteristics, we followed, in the main, the usual computation method (as given in the Guggenheim-Pryce report for example), for (1) a natural uranium cylindrical reactor using beryllium oxide with non-absorbent coolant. Based on b, the radius of uranium rod right section (optimal value) = 8 cm; R, the radius of the reactor (without reflector) = 162 cm; U, the uranium tonnage (critical, without reflector) = 11.4 tons; and M(BeO), the beryllium oxide tonnage (critical, without reflector) = 69 tons, the tonnages needed to obtain a k_{eff} of 1.03 are, respectively: U = 24 tons (without reflector); M(BeO) = 144 tons (without reflector).

The tonnages with a BeO reflector are: U = 15.3 tons; M(BeO) = 92 tons; R(BeO) = 40 tons reflector (thickness, one scattering path).

For (2) a natural uranium cylindrical reactor using metallic beryllium with non-absorbent coolant and with b (optimal) = 7 cm, R = 164 cm (critical, without reflector), U = 15.5 tons (critical, without reflector), and M(Be) = 42 tons (critical, without reflector), the values to obtain a k_{eff} = 1.03 are: U = 46 tons (without reflector); M(Be) = 127 tons (without reflector). The tonnages with a Be reflector are: U = 33.5 tons; M(Be) = 92.5 tons; R(Be) = 26.5 tons reflector (thickness equal to one diffusion length).

For (3) a natural uranium cylindrical reactor using beryllium oxide with central channel having radius R_0 = 15 cm for experimental chamber purposes (with non-absorbent coolant), and with b (optimal) = 8 cm, R = outside radius = 165 cm (critical without reflector), U = 11.8 tons (critical without reflector), and M(BeO) = 71 tons (critical, without reflector), the tonnages to obtain a k_{eff} = 1.03 are: U = 24.4 tons (without reflector); M(BeO) = 146 tons (without reflector).

For (4) a natural uranium cylindrical reactor using metallic beryllium with central channel of radius R = 15 cm for experimental chamber purposes (non-absorbing coolant) taking b (optimal) = 7 cm, R = outside radius = 167 cm (critical, without reflector), U = 15.9 tons (critical, without reflector), and M(Be) = 43.5 tons (critical, without reflector), the tonnages to obtain a k_{eff} = 1.03 are: U = 47.8 tons (without reflector); M(Be) = 131 tons (without reflector).

CRITICAL SIZE OF A CYLINDRICAL REACTOR HAVING A CENTRAL CHANNEL

The results in cases (3) and (4) were obtained by applying the following theory for the computation of the critical size:

Let R_0 be the radius of the central channel and R the outside radius of the reactor (extrapolated). The flux equation

$$\Delta\phi + B^2\phi = 0$$

taking

$$\phi = \theta(r)Z(z)$$

yields

$$\frac{1}{\theta}\left(\frac{d^2\theta}{dr^2} + \frac{1}{r}\frac{d\theta}{dr}\right) = -\alpha^2; \qquad \frac{1}{z}\frac{d^2Z}{dz^2} = -\beta^2$$

Original language: Spanish.

* Comisión Nacional de la Energía Atómica, Argentina.

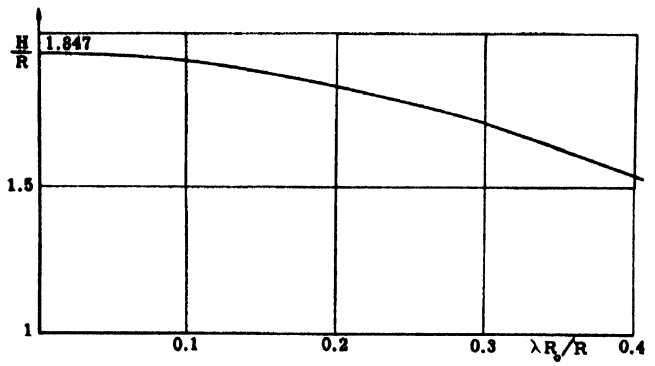

Figure 1

Taking $u = \alpha r$, the result is:

$$\theta(u) = AJ_0(u) - CY_0(u)$$

We assume, for the contour conditions:

(i) $$AJ_0(\alpha R) - CY_0(\alpha R) = 0 \qquad (1)$$

meaning zero flux over the extrapolated contour, and

(ii) $$\left(\frac{\partial \phi}{\partial r}\right)_{r=R_0} = 0$$

equivalent to the assumption that ϕ is constant inside the channel. This condition would be expressed

$$AJ_0'(\alpha R_0) - CY_0'(\alpha R_0) = 0 \qquad (2)$$

Applying Equations 1 and 2 we obtain:

$$J_0(\alpha R)Y_1(\alpha R_0) - Y_0(\alpha R)J_1(\alpha R_0) = 0$$

Taking

$$\frac{R_0}{R} = \lambda; \qquad \alpha R = x$$

we find the roots of the equation:

$$J_0(x)Y_1(\lambda x) - Y_0(x)J_1(\lambda x) = 0$$

By applying the Jahnke-Emde tables, the minimal roots for the several values of λ are:

λ	$x = \alpha R$
0	2.405
0.1	2.448
0.2	2.574
0.3	2.78
0.4	3.08

The equation for $Z(z)$ yields $Z = C \cos \beta z$ and, in order that $Z = 0$ for $z = H/2$, H being the height of the reactor, we should have

$$\beta = \pi/H$$

Therefore

$$\beta^2 = \alpha^2 + \beta^2 = \frac{x^2}{R^2} + \frac{\pi^2}{H^2}$$

in which the values of x/R for the several λ are given in Table I.

In order to obtain the minimum value, it is necessary to reduce to the minimum the expression $\pi(R^2 - R_0^2)H$ with the condition

$$\frac{x^2}{R^2} + \frac{\pi^2}{H^2} = \text{constant}$$

The condition:

$$\frac{H}{R} = \frac{\sqrt{2 \cdot \pi}}{x}$$

is easily derived, in which x assumes the values in Table I for the several values.

The following table thus is obtained:

λ	$\gamma(\lambda) = H/R$
0	1.847
0.1	1.815
0.2	1.726
0.3	1.60
0.4	1.44

Figure 1 was constructed with these values.

In order to obtain the critical dimensions of the reactor, we obtain, from the above expressions:

$$\alpha R = \frac{\sqrt{2} \cdot \pi}{H/R} = \frac{\sqrt{2} \cdot \pi}{\varphi^2 R^2}$$

and, therefore

$$B^2 = \alpha^2 + (\pi/H)^2 = \frac{3\pi^2}{\varphi^2 R^2}$$

and solving

$$R = \frac{\sqrt{3} \cdot \pi}{\varphi(\lambda) \cdot B}$$

Or: R = outside radius (extrapolated); R_0 = radius of the channel; height of reactor $H = \varphi R = \sqrt{3} \cdot \pi/B$.

Equation for the Importance of Neutrons, Reactor Kinetics and the Theory of Perturbation

By L. N. Ussachoff, USSR

1. EQUATION FOR A FLUX OF NEUTRONS IN A REACTOR AND DETERMINATION OF THE EFFECTIVE COEFFICIENT OF MULTIPLICATION

Before introducing the concept of importance of neutrons in a reactor and deriving an integro-differential equation for this value, let us write down the equation for a neutron flux.

The flux of neutrons whose energies are enclosed in a single interval near energy E and those velocities are directed along the vector $\boldsymbol{n}$ ($|\boldsymbol{n}| = 1$) inside a single solid angle depends on the point $\boldsymbol{r}$ and the moment t, and is defined by the function $F(\boldsymbol{r},E,\boldsymbol{n},t)$. The function $F(\boldsymbol{r},E,\boldsymbol{n},t)$ gives the number of the said neutrons traversing within a second the area of 1 cm^2, normal to vector $\boldsymbol{n}$.

By dividing the flux by the absolute value of velocity v we are sure to obtain the number of neutrons with energy E and direction of velocity $\boldsymbol{n}$ enclosed in 1 cm^3 near the point $\boldsymbol{r}$ at the moment t

$$\frac{F(\boldsymbol{r},E,\boldsymbol{n},t)}{v} = N(\boldsymbol{r},E,\boldsymbol{n},t)$$

For the sake of brevity let us say that the value is the number of neutrons of the beam $(E,\boldsymbol{n})$ at the point $\boldsymbol{r}$ at the moment t. Considering the balance of neutrons of the beam $(E,\boldsymbol{n})$ at the point $\boldsymbol{r}$ at the moment t, we obtain the following integro-differential equation*

$$\frac{1}{v}\frac{\partial F(\boldsymbol{r},E,\boldsymbol{n},t)}{\partial t} = -\frac{\partial F(\boldsymbol{r},E,\boldsymbol{n},t)}{\partial s} - \frac{F(\boldsymbol{r},E,\boldsymbol{n},t)}{l_{aifs}(\boldsymbol{r},E)}$$
$$+ \int_0^{E_0} dE' \int \frac{F(\boldsymbol{r},E',\boldsymbol{n},t)}{l_f(\boldsymbol{r},E')}\, \nu_{E'}(\boldsymbol{r}) \cdot \chi(E,E',\boldsymbol{n}\cdot\boldsymbol{n}',\boldsymbol{r})\, d\Omega'$$
$$+ \sum_i \frac{\lambda_i}{4\pi}\, \delta(E - E_i) \int_{-\infty}^{t} dt'\, e^{-\lambda_i(t-t')}$$
$$\int_0^{E_0} \int \frac{F(\boldsymbol{r},E',\boldsymbol{n}',t')}{l_f(\boldsymbol{r},E')}\, b_i(E',\boldsymbol{r})\, dE'\, d\Omega'$$
$$+ \int_0^{E_0} dE' \int w(E,E',\boldsymbol{n}\cdot\boldsymbol{n}',\boldsymbol{r})$$
$$F(\boldsymbol{r},E',\boldsymbol{n}',t)\, d\Omega' + q(\boldsymbol{r},E,\boldsymbol{n},t) \quad (1)$$

The value

$$\frac{\partial}{\partial t}\frac{F(\boldsymbol{r},E,\boldsymbol{n},t)}{v}$$

in the left part of the equation is according to the definition of the derivative, an increase in the number of neutrons of the beam $(E,\boldsymbol{n})$ at the point $\boldsymbol{r}$ at the moment t per second.

The right part shows the increases, in terms of algebra, of the number of neutrons of the same beam due to each of the physical processes under consideration, which, when summed up, represent the complete increase in this number per second.

The first term $-\partial F/\partial s$ is equal to the difference of the number of neutrons $(E,\boldsymbol{n})$ entering the cm^3 volume in question and emerging from it within a second.

The second term is equal to the number of neutrons ejected from the beam $(E,\boldsymbol{n})$ in a 1 cm^3 volume per second as a result of the radiative capture (index a), inelastic scattering (i), fission (f) and elastic scattering (s).

The value $1/l_{aifs}(\boldsymbol{r},E)$ is equal to the full macroscopic cross section of the above processes, $l_{aifs}(\boldsymbol{r},E)$ being the mean free path.

The third and fourth terms are equal respectively to the number of prompt and delayed neutrons of fission emitted in a second in the cm^3 volume under consideration and belonging to the beam $(E,\boldsymbol{n})$. For each fission caused by a neutron of the $(E',\boldsymbol{n})$ beam, $\nu_{E'}(\boldsymbol{r})$ prompt neutrons of fission are emitted and $b_i(E',\boldsymbol{r})$ fission fragments—carriers of delayed neutrons of the ith group—are produced. These disintegrate with the probability λ_i sec^{-1}, thereby emitting monoenergetic neutrons of energy E_i. If t' is the moment of formation of such a fragment, then at the moment t there will be $\lambda_i e^{-\lambda_i(t-t')}$ disintegrations per second.

The distribution of prompt neutrons of fission and delayed neutrons of the ith group depending on energies and angles is defined by function $\chi(E,E',\boldsymbol{n}\cdot\boldsymbol{n}',\boldsymbol{r})$ and function $\delta(E - E_i)/4\pi$ respectively. These functions are normalized in the following way:

$$\int_0^{E_0} \int \chi(E,E',\boldsymbol{n}\cdot\boldsymbol{n}',\boldsymbol{r})\, dE\, d\Omega = 1;$$
$$\int_0^{E_0} \int \frac{\delta(E - E_i)}{4\pi}\, dE\, d\Omega \quad (2)$$

The upper boundary of the spectrum of neutrons E_0 is the upper limit in all the integrals with respect to the energy. Σ signifies the summation of delayed neutrons of every group.

The fifth term of the right part is equal to the number of neutrons entering the $(E,\boldsymbol{n})$ beam from $(E',\boldsymbol{n}')$

Original language: Russian.

* Cf. for example references 1 and 2.

beams by elastic and inelastic scatterings, the value $w(E,E',\boldsymbol{n}\cdot\boldsymbol{n}',\boldsymbol{r})$ determining the corresponding probability of transition.

$$w(E,E',\boldsymbol{n}\cdot\boldsymbol{n}',\boldsymbol{r}) = \frac{S(E,E',\boldsymbol{n}\cdot\boldsymbol{n}',\boldsymbol{r})}{l_p(\boldsymbol{r},E')} + \sum_n \frac{f_n(E,E',\boldsymbol{n}\cdot\boldsymbol{n}',\boldsymbol{r})}{l_s^n(\mathbf{r},E')} \quad (3)$$

A more detailed determination of these functions is hardly required in this paper.

The last term $q(\boldsymbol{r},E,\boldsymbol{n},t)$ is equal to the number of neutrons entering the $(E,\boldsymbol{n})$ beam at point $\boldsymbol{r}$ at the moment t from the external neutron sources located at a given point and independent of the chain reaction. Spontaneous fissions, the cosmic background, photoneutron sources, specially placed into the reactor etc., may serve as such sources.

The flux of $F(\boldsymbol{r},E,\boldsymbol{n},t)$ is unambiguously determined by Equation 1 and a number of supplementary conditions expounded below.

It may be generally assumed that the reactor is limited by a convex surface and surrounded by a vacuum.

In this case at each point of the boundary $\boldsymbol{r}_{boundary}$ for all $\boldsymbol{n}$ directed from the vacuum into the reactor one should assume

$$F(\boldsymbol{r}_{boundary},E,\boldsymbol{n}_{interior},t) = 0 \quad (4)$$

unless there is a flux of neutrons from the vacuum.

The function $F(\boldsymbol{r},E,\boldsymbol{n},t)$ describing the flux of neutrons should be continuous, positive and finite†

$$F(\boldsymbol{r},E,\boldsymbol{n},t) \text{ is continuous} \quad (5)$$

$$0 \leq F(\boldsymbol{r},E,\boldsymbol{n},t) < \infty \quad (6)$$

throughout the volume of the reactor.

In a time-dependent case, it is necessary to assume the neutron flux $F(\boldsymbol{r},E,\boldsymbol{n},0)$ at the initial moment, as well as the number of carriers of delayed neutrons accumulated in the reactor by the moment $t = 0$.

When considering the self-sustaining chain reaction, one should assume

$$q(\boldsymbol{r},E,\boldsymbol{n},t) = 0 \quad (7)$$

If the configuration and composition of the reactor are fixed, all the quantities, except the neutron flux, forming part of Equation 1 and subsequently referred to as the reactor parameters, are time-independent. At the same time the neutron flux $F(\boldsymbol{r},E,\boldsymbol{n},t)$ proves to be stationary only at certain values of the reactor parameters, called critical. However, in the general case the neutron flux in the reactor either increases or decreases.

In such cases the reactor is called respectively supercritical or subcritical. However, at any value of the reactor parameters such a value of k_{eff} can be selected that Equation 1 will have a steady-state solution when dividing the third and fourth terms of the right part by this number. In this case Equation 1 is put down as follows:

$$0 = -\frac{dF(\boldsymbol{r},E,\boldsymbol{n})}{ds} - \frac{F(\boldsymbol{r},E,\boldsymbol{n})}{l_{actual}(\boldsymbol{r},E)} + \frac{1}{k_{eff}}\int_0^{E_0} dE' \int \frac{F(\boldsymbol{r},E',\boldsymbol{n}')}{l_f(\boldsymbol{r},E')}\left[\nu_{E'}(\boldsymbol{r})\chi(E,E',\boldsymbol{n}\cdot\boldsymbol{n}',\boldsymbol{r}) + \sum_i b_i(\boldsymbol{r},E')\frac{\delta(E-E_i)}{4\pi}\right]d\Omega' + \int_0^{E_0} dE' \int w(E,E',\boldsymbol{n}\cdot\boldsymbol{n}',\boldsymbol{r})F(\boldsymbol{r},E',\boldsymbol{n}')\,d\Omega' \quad (8)$$

The same conditions of Equations 4, 5 and 6 are imposed on the function $F(\boldsymbol{r},E,\boldsymbol{n})$. The introduction of k_{eff} appears to be equivalent to a change in the number of secondary neutrons by one fission.

In order to grasp more profoundly the physical meaning of the value k_{eff}, introduced as a formal mathematical aid, one should mentally break the continuous process of the chain reaction into individual neutron cycles which begin by emitting fission neutrons and end by the disappearance of all neutrons through absorption and leakage. As a result of absorption, a part of neutrons brings about fissions leading to the emission of neutrons which originate the next cycle.

We shall demonstrate that value k_{eff} is equal to the ratio between the number of fission neutrons emitted in the subsequent cycle and the corresponding number in the preceding one, i.e. that k_{eff} is the effective neutron multiplication factor for the reactor.

First of all we shall briefly designate the number of fission neutrons emitted at point $\boldsymbol{r}$ of the reactor in a second and entering the $(E,\boldsymbol{n})$ beam.

$$Q(\boldsymbol{r},E,\boldsymbol{n}) = \int_0^{E_0}\int\left[\nu_{E'}(\boldsymbol{r})\chi(E,E',\boldsymbol{n}\cdot\boldsymbol{n}',\boldsymbol{r}) + \sum b_i(E',\boldsymbol{r})\frac{\delta(E-E_i)}{4\pi}\right]\frac{F(\boldsymbol{r},E',\boldsymbol{n}')}{l_f(\boldsymbol{r},E')}\,dE'\,d\Omega' \quad (9)$$

Now let us proceed in accordance with the determination of the neutron cycle. Let us inject instantaneously $Q(\boldsymbol{r},E,\boldsymbol{n})/k_{eff}$ neutrons into a reactor of zero power at $t = 0$. The flux of $f(\boldsymbol{r},E,\boldsymbol{n},t)$ neutrons which originated directly from the neutrons of the said source obeys the time-dependent equation

$$\frac{1}{v}\frac{\partial f(\boldsymbol{r},E,\boldsymbol{n},t)}{\partial t} = -\frac{\partial f(\boldsymbol{r},E,\boldsymbol{n},t)}{\partial s} - \frac{f(\boldsymbol{r},E,\boldsymbol{n},t)}{l_{actual}(\boldsymbol{r},E)} + \int_0^{E_0} dE' \int w(E,E',\boldsymbol{n}\cdot\boldsymbol{n}',\boldsymbol{r})f(\boldsymbol{r},E',\boldsymbol{n}',t)\,d\Omega' \quad (10)$$

which is valid when $t > 0$ and the initial condition $f(\boldsymbol{r},E,\boldsymbol{n},0) = vQ(\boldsymbol{r},E,\boldsymbol{n})/k_{eff}$. By integrating this equation in time from 0 to ∞ and taking account of the initial condition and the decrease in the flux of neutrons $f(\boldsymbol{r},E,\boldsymbol{n},t)$ to zero at $t \to \infty$, we obtain for the integral flux

$$F(\boldsymbol{r},E,\boldsymbol{n}) = \int_0^{\infty} f(\boldsymbol{r},E,\boldsymbol{n},t)\,dt$$

† It is only in the presence of point sources of finite force that there is no finiteness.

the equation

$$0 = -\frac{dF(\mathbf{r},E,\mathbf{n})}{ds} - \frac{F(\mathbf{r},E,\mathbf{n})}{l_{a_i f_s}(\mathbf{r},E)} + \int_0^{E_0} dE' \int w(E,E',\mathbf{n}\cdot\mathbf{n}',\mathbf{r})F(\mathbf{r},E',\mathbf{n}')\,d\Omega' + \frac{Q(\mathbf{r},E,\mathbf{n})}{k_{eff}} \quad (11)$$

which coincides with Equation 8, allowance being made for Equation 9. Hence the number of neutrons emitted under the influence of the integral flux $F(\mathbf{r},E,\mathbf{n})$ equals $Q(\mathbf{r},E,\mathbf{n})$.

Thus it has been demonstrated that the ratio of the number of neutrons in the subsequent cycle to that of neutrons in the preceding one is equal to k_{eff}.

2. EQUATION FOR NEUTRON IMPORTANCE IN A REACTOR

Along with the distribution of neutrons in space, energies and directions of velocities, the concept of neutron importance may be introduced and an integro-differential equation formulated for it, which proves to be adjoint to Equation 8 for a neutron flux.‡

Consider a steady-state reactor in which the neutron flux is defined by Equation 8. The stationary properties of this reactor are ensured by a k_{eff}-fold decrease in the number of secondary neutrons per fission.

Suppose there are no neutrons in the reactor at the beginning, i.e., its power is equal to zero. If at some point $\mathbf{r}$ we inject N neutrons§ of energy E and direction $\mathbf{n}$, the neutrons are distributed in the reactor after some sufficiently long time according to their eigenfunction, and quite a definite level of power is established. This level evidently depends on the point $\mathbf{r}$, energy E and direction $\mathbf{n}$, and is proportional to the number of N neutrons injected.

Neutron importance is then a quantity proportionate to the said power level related to one neutron.

$$F^+(\mathbf{r},E,\mathbf{n}) = A\,\frac{\text{power level at } t\to\infty, \text{ if } N \text{ neutrons } (E,\mathbf{n}) \text{ are injected at point } \mathbf{r}}{N}$$

Neutron importance is determined with an accuracy up to the multiplication constant A which should be chosen for the sake of convenience in every specific case.

It follows from this definition of neutron importance that the integral importance of all neutrons which originated from initial neutrons is equal to the integral importance of initial neutrons. This is quite obvious, since the contribution of the initial neutrons to the chain reaction is fully dependent on the contribution of the neutrons originating from the initial ones.

By applying this consideration of the conservation of neutron importance in the analysis of physical processes which the neutrons of the $(E,\mathbf{n})$ beam undergo at the point $\mathbf{r}$ on the path ds, we obtain the integro-differential equation for neutron importance.

Now let N neutrons of energy E be injected at the point $\mathbf{r}_s$ in the direction $\mathbf{n}$, the importance of each neutron being $F^+(\mathbf{r}_s,E,\mathbf{n})$.

Of these neutrons evidently

$$N\left(1 - \frac{ds}{l_{a_i f_s}(\mathbf{r},E)}\right)$$

neutrons will reach the point $\mathbf{r}_{s+ds}$, the importance of each of these neutrons being equal (according to the definition) to $F^+(\mathbf{r}_{s+ds},E,\mathbf{n})$ of the $N\,\frac{ds}{l_{a_i f_s}(\mathbf{r},E)}$ neutrons which underwent collision, $NdsW(E',E,\mathbf{n}\cdot\mathbf{n}',\mathbf{r})$ neutrons will get into the $(E',\mathbf{n}')$ beam, if $W(E',E,\mathbf{n}\cdot\mathbf{n}',\mathbf{r})$ is a probability that a neutron from the $(E,\mathbf{n})$ beam will get into the $(E',\mathbf{n}')$ beam when passing the paths of unit length near the point $\mathbf{r}$. This probability according to the explanation given in Part 1 is expressed as follows:

$$W(E',E,\mathbf{n}\cdot\mathbf{n}',\mathbf{r}) = w(E',E,\mathbf{n}\cdot\mathbf{n}',\mathbf{r}) + \frac{1}{k_{eff}}\cdot\frac{1}{l_f(\mathbf{r},E)}\left[\nu_E(\mathbf{r})\chi(E',E,\mathbf{n}\cdot\mathbf{n}',\mathbf{r}) + \sum_i \frac{\delta(E'-E_i)}{4\pi}\,b_i(E,\mathbf{r})\right] \quad (13)$$

The importance of each neutron of the $(E',\mathbf{n}')$ beam, according to the definition, is $F^+(\mathbf{r}_{s+\epsilon ds},E',\mathbf{n}')(0 \le \epsilon \le 1)$. Taking into consideration that the integral importance of the initial neutrons $N\cdot F^+(\mathbf{r}_s,E,\mathbf{n})$ is equal to the integral importance of all neutrons which originated from the initial ones, we put down

$$N\cdot F^+(\mathbf{r}_s,E,\mathbf{n}) = N\left(1 - \frac{ds}{l_{a_i f_s}(\mathbf{r},E)}\right)F^+(\mathbf{r}_{s+ds},E,\mathbf{n}) + Nds\int_0^{E_0}\int W(E',E,\mathbf{n}\cdot\mathbf{n}',\mathbf{r})F^+(\mathbf{r}_{s+\epsilon ds},E',\mathbf{n}')\,dE'\,d\Omega \quad (14)$$

By transposing $NF^+(\mathbf{r}_s,E,\mathbf{n})$ into the right part, dividing both parts of the equation by Nds, reducing ds to zero and applying the ratio of Equation 13, we obtain the sought integro-differential equation for neutron importance

‡ The use of an adjoint equation when formulating the variation principle for kinetic equations was suggested by D. I. Blokhintsev (1951). An adjoint operator was introduced in A. Weinberg's article[3] in the case of a multi-group model in diffusion approximation, and it has been shown that the adjoint function defines neutron importance.[4] Early in 1953 a mathematical expression for neutron importance at age approximation for an intermediate naked reactor was suggested by A. S. Romanovich. The adjoint equation at age approximation has been used in an article by R. Ehrlich and H. Hurwitz.[5] The physical meaning of a time-dependent adjoint equation has been clarified by B. B. Kadomtsev (1955).

§ The values of N taken should be so high that fluctuations may be disregarded and that neutrons are distributed according to the corresponding distribution probabilities.

$$0 = \frac{dF^+(r,E,n)}{ds} - \frac{F^+(r,E,n)}{l_{eff}(r,E)} + \int_0^{E_0}\int w(E',E,n\cdot n',r)F^+(r,E',n')\,dE'\,d\Omega' + \frac{1}{k_{eff}}\cdot\frac{1}{l_f(r,E)}\int_0^{E_0}\int\left[\chi(E',E,n\cdot n',r)_E(r) + \sum_i \frac{\delta(E'-E_i)}{4\pi}b_i(E,r)\right]F^+(r,E',n')\,dE'\,d\Omega' \quad (15)$$

This equation differs from that for the flux of neutrons in the sign before the derivative in the direction n and the transposition of E and E' in $W(E,E',n\cdot n',r)$ (Cf. Equations 15, 14 and 13 with 8). This signifies that Equation 15 is adjoint to Equation 8. It should be stressed that the above deduction of Equation 15 lends to its terms a clear meaning in the physical sense.

Now we write down the boundary conditions imposed on $F^+(r,E,n)$. If the neutron is at the outer boundary of the system and its velocity is directed outwards, such a neutron cannot contribute to the chain reaction and, consequently, its importance equals zero. The condition at the outer boundary is

$$F^+(r_{boundary},E,n_{interior}) = 0 \quad (16)$$

The continuity conditions at any interface are likewise evident, i.e.

$$F^+(r,E,n) \text{ is continuous} \quad (17)$$

The conditions of finiteness and positiveness

$$0 \le F^+(r,E,n) < \infty \quad (18)$$

are likewise evident.

Equation 15 along with the conditions of Equations 16, 17 and 18 determines unambiguously (with an accuracy up to the multiplication constant) the importance function of neutrons $F^+(r,E,n)$.¶

3. DEDUCING THE EQUATION FOR THE PILE KINETICS AND THE FORMULA OF PERTURBATION

With Equation 1 available for the neutron flux in a nonsteady-state reactor and Equation 15 for neutron importance, it is easy to deduce the equation for pile kinetics. In the equation for the neutron flux, the magnitudes defining the composition and configuration of the reactor, generally speaking, depend on time t. The neutron importance equation should be expressed in the same values of these magnitudes for each t. In this case k_{eff}, figuring in the last equation, and function $F^+(r,E,n)$ depend on t as a parameter.

In order to deduce the equation for pile kinetics, Equation 1 is multiplied by $F^+(r,E,n,t)$, Equation 15 by $F^+(r,E,n,t)$, and the equations obtained should be subtracted from each other and integrated throughout the volume of the reactor including the reflector in all the energies and directions of neutron velocities.

This cancels the terms which take account of the transfer, absorption and slowing down of the neutrons, since these terms are adjoint in Equations 1 and 15, as well as of the boundary conditions of Equations 4 and 16. The following exact equation is obtained

$$\int dV\int d\Omega\int_0^{E_0} dE\,\frac{F^+(r,E,n,t)}{v}\cdot\frac{\partial F(r,E,n,t)}{\partial t} = \left(1-\frac{1}{k_{eff}(t)}\right)\int dV\int\int_0^{E_0} d\Omega\,dE\,F^+(r,E,n,t) \times\int_0^{E_0}\int\frac{F(r,E',n,t)}{l_f(r,E',t)}\cdot\left[\nu_{E'}(r)\chi(E,E',n\cdot n',t) + \sum_i b_i(r,E',t)\,\frac{\delta(E-E_i)}{4\pi}\right]dE'\,d\Omega' - \sum_i\int dV\int F^+(r,E_i,n,t)\,d\Omega\int_0^{E_0}\int\frac{F(r,E',n',t)}{l_f(r,E',t)}\cdot\frac{b_i(E',r,t)}{4\pi}\,dE'\,d\Omega' + \sum_i\int dV\int F^+(r,E_i,n,t)\,d\Omega \times\int_0^{E_0}\int dE'\,d\Omega'\int_{-\infty}^{t}\frac{F(r,E',n,t')}{l_f(r,E',t')}\cdot\frac{b_i(E',r,t')}{4\pi}\cdot\lambda_i e^{-\lambda_i(t-t')}\,dt' + \int_0^{E_0}\int\int q(r,E,n,t)F^+(r,E,n,t)\,dE\,d\Omega\,dV \quad (19)$$

If we are interested in the runaway or attenuation of the reactor as a whole, and not in the redistribution of the neutron density along the reactor, we may assume with approximation

$$F(r,E,n,t) \approx F(r,E,n)\varphi(t) \quad (20)$$

The latter assumption is precisely fulfilled when the parameters of the reactor are constant (for instance, at the expiration of some time after the jump of reactivity) and only approximately when the parameters and consequently $k_{eff}(t)$ change with the time. The most intensive redistribution of the neutron flux occurs in a thermal or intermediate reactor when an absorbing rod is inserted in it. In large reactors the said redistribution occurs only in a small part of the reactor volume, while in fast reactors no such intensive redistributions of the flux take place. By making yet another assumption that magnitude

$$\frac{b_i(E,r,t)}{l_f(r,E,t)}$$

is independent of time, supplanting Equation 20 into 19 and dividing both parts of Equation 19 by the integral value of all the fission neutrons which originate in the reactor to a second, i.e., by magnitude

$$\int dV\int\int_0^{E_0} d\Omega\,dE\,F^+(r,E,n,t)\int_0^{E_0}\int\frac{F(r,E',n')}{l_f(r,E',t)} \times\left[\nu_{E'}(r,t)\chi(E,E',n\cdot n',r,t) + \sum_i b_i(E',r,t)\,\frac{\delta(E-E_i)}{4\pi}\right]\times dE'\,d\Omega' = Ifn \quad (21)$$

¶ The above equations and conditions are set forth in the thesis by L. N. Ussachoff (1954).

(*Ifn* is "importance of fission neutrons") we obtain the known equation of pile kinetics

$$\frac{d\varphi(t)}{dt}\,T = \left[\frac{k_{eff}(t)-1}{k_{eff}(t)} - \sum_i \beta_i\right]\varphi(t) + \sum \beta_i\lambda_i \int_{-\infty}^{t} \varphi(t')e^{-\lambda_i(t-t')}\,dt' + q(t) \quad (22)$$

Here

$$T = \frac{\int_0^{E_0}\int\int \frac{F(r,E,n)}{v} F^+(r,E,n,t)\,dE\,d\Omega\,dV}{Ifn} = \frac{\text{Integral importance of all the neutrons in the reactor}}{Inf} = \text{the mean lifetime of the neutron in the reactor} \quad (23)$$

$$\beta_i = \frac{\int dV \int F^+(r,F_i,n,t)\,d\Omega \times \int\int_0^{E_0} \frac{F(r,E',n')}{l_f(r,E',t)}\,b_i(r,E',t)\,d\Omega'\,dE'}{Ifn} \quad (24)$$

$$= \frac{\text{The importance of all the delayed neutrons of the } i\text{th group emitted within a second}}{Ifn} = \left\{\begin{array}{l}\text{The effective fraction of the } i\text{th group of delayed neutrons with due allowance for their importance.}\end{array}\right.$$

$$q(t) = \frac{\int_0^{E_0}\int\int q(r,E,n,t) \times F^+(r,E,n,t)\,dE\,d\Omega\,dV}{Ifn} = \left\{\begin{array}{l}\text{The effective power of the introduced sources of neutrons with due allowance for their importance.}\end{array}\right. \quad (25)$$

It is worth noting that the expressions so obtained for the average lifetime of the neutrons, the effective fraction of the delayed neutrons and the effective power of the sources possess a clear physical meaning and are suitable for reactors of any configuration (in particular for those with reflectors) and any type (thermal, intermediate and fast).[6] Formula 23 yields known expressions for the average lifetime of neutrons in the specific cases of thermal (reference 4, p. 333) and intermediate** naked reactors.

Value $(k_{eff}-1)/k_{eff}$ forming part of Equation 22 and referred to as pile reactivity, determines its temporary behaviour. Very great accuracy is required in calculating the latter value to obtain reactivity through k_{eff}, with $k_{eff} \sim 1$. It is therefore expedient to have at our disposal a formula for direct calculation of reactivity. In order to obtain such a formula we shall, along with the reactor in question ($k_{eff} \neq 1$), in which the flux and importance are determined by Equations 8 and 15, consider a critical reactor ($k_{eff} = 1$) with parameters approximating those of the reactor in question. Let us write down the equation for neutron importance in the afore-mentioned critical reactor (the abbreviation *kp* is used for "critical.")

($k_{eff} = 1$)

$$0 = \frac{dF_{kp}^+(r,E,n)}{ds} - \frac{F_{kp}^+(r,E,n)}{l_{a_i f_s}^{kp}(E,r)} + \int_0^{E_0}\int w_{kp}(E',E,n\cdot n',r) \times F_{kp}^+(r,E',n')\,dE'\,d\Omega' + \frac{1}{l_f^{kp}(r,E)} \int_0^{E_0}\int \left[\chi_{kp}(E',E,n\cdot n',r)\nu_E^{kp}(r) + \sum_i \frac{\delta(E'-E_i)}{4\pi}\,b_i^{kp}(E,r)\right] F_{kp}^+(r,E',n')\,dE'\,d\Omega' \quad (26)$$

Let us multiply Equation 26 by the neutron flux $F(r,E,n)$ which obeys Equation 8, and Equation 8 by $F_{kp}^+(r,E,n)$, subtracting one from the other and integrating throughout the volume of the reactor, in all the energies and directions of neutron velocities, and finally, by dividing the result by *Ifn* expressed in

$$Ifn = \int dV \int_0^{E_0}\int F_{kp}^+(r,E,n)\,dE\,d\Omega \int_0^{E_0}\int \frac{F(r,E',n')}{l_f(r,E')} \times \left[\chi(E,E',n\cdot n',r)\nu_{E'}(r) + \sum_i \frac{\delta(E-E_i)}{4\pi}\,bi(E',r)\right] dE'\,d\Omega'$$

we obtain the expression for reactivity

$$\frac{k_{eff}-1}{k_{eff}} = -\frac{1}{Ifn}\int dV \int_0^{E_0} dE \left(\frac{1}{l_{a_i f_s}(r,E)} - \frac{1}{l_{a_i f_s}^{kp}(r,E)}\right) \int F_{kp}^+(r,E,n)F(r,E,n)\,d\Omega + \frac{1}{Ifn}\int dV \int_0^{E_0}\int\int_0^{E_0}\int F_{kp}^+(r,E,n)[w(E,E',n\cdot n,r) - w_{kp}(E,E',n\cdot n',r)]F(r,E',n') \times dE\,d\Omega\,dE'\,d\Omega' + \frac{1}{Ifn}\int dV \int_0^{E_0}\int\int_0^{E_0}\int F_{kp}^+(r,E,n) \left[\frac{\chi(E,E',n\cdot n',r)\nu_{E'}(r) + \sum_i \frac{\delta(E-E_i)}{4\pi}\,b_i(E',r)}{l_f(r,E')} - \frac{\chi^{kp}(E,E',n\cdot n',r)\nu_{E'}^{kp}(r) + \sum_i \frac{\delta(E-E_i)}{4\pi}\,b_i^{kp}(E',r)}{l_f^{kp}(r,E')}\right] \times F(r,E',n')\,dE\,d\Omega\,dE'\,d\Omega' \quad (27)$$

** As reported by V. Y. Pupko.

The physical meaning of each term of this formula is easy to perceive.

Equation 27 for reactivity is quite accurate, since nothing has been neglected during the deduction. In addition to the difference between the corresponding parameters of the two reactors, the expression comprises the neutron importance of the critical reactor, and the neutron flux of the reactor in question. If the difference between the parameters of the reactors under consideration is so small that the fluxes and importances of neutrons within these systems do not differ greatly, the values of the flux and the importance for any one of the reactors may be applied without any hazard of appreciable errors. With such an approximation Equation 27 may be termed the formula of the theory of perturbation. It is convenient, notably, to calculate by means of this formula any change in the reactivity of the system by placing at any point of the core and reflector a substance which depends in any way on the energy of the cross sections of capture, fission, and elastic and inelastic scattering.

The same functions which define the flux and importance of neutrons may be used to compute the mean lifetime T and the effective fraction of the delayed neutrons β_i of the ith group according to Equations 23 and 24.

The theory of perturbation within the multi-group model in a diffusion approximation has been given in the article[3] and the book.[4] In the age approximation, the theory of perturbation for an intermediate naked reactor was elaborated early in 1953 by A. S. Romanovich and generalized by L. N. Ussachoff and G. I. Marchuk (1954) for a reactor with a reflector.

The theory of perturbation based on a kinetic equation within the limits of a one-group model, was developed by N. A. Dmitriev (1948) and independently by K. Fuchs.[7]

Equation 27 is a generalization of the corresponding findings of the afore-mentioned works. The results are derived from Equation 27 for specific cases.

4. DETERMINATION OF k_{eff} BY THE METHOD OF SUCCESSIVE APPROXIMATIONS AND THE CONVERGENCE OF THIS METHOD

The experience of computation work has shown that determining k_{eff} by the method of successive approximations is the most universal and effective method of reactor computations.†† It is therefore of considerable interest to investigate the convergence of the process of successive approximations.

The proof of convergence and an estimate of its rapidity in the case of an intermediate naked reactor was supplied by G. I. Marchuk (1954).

Below is outlined the proof of convergence in the general case under consideration, and expressions are derived to estimate the rapidity of convergence.

To begin with, let us make some simplifying suppositions. First of all, let us assume that not only delayed but prompt fission neutrons as well are emitted isotropically.

$$\chi(E,E',\boldsymbol{n}\cdot\boldsymbol{n}',\boldsymbol{r}) = \frac{\chi(E,E',\boldsymbol{r})}{4\pi}$$

Secondly, suppose that the spectrum of the fission neutrons (prompt and delayed taken together) are independent of the variables $\boldsymbol{r},E'$. These assumptions§§ lead to replacement in Equations 8 and 15.

$$\left[\chi(E,E',\boldsymbol{n}\cdot\boldsymbol{n}',\boldsymbol{r})\nu_{E'}(\boldsymbol{r}) + \sum_i \frac{\delta(E-E_i)}{4\pi} b_i(E',\boldsymbol{r})\right] \rightarrow \left[\nu_{E'}(\boldsymbol{r}) + \sum_i b_i(E',\boldsymbol{r})\right]\frac{\chi(E)}{4\pi} \quad (28)$$

Here $\nu_{E'}(\boldsymbol{r}) + \sum_i b_i(E',\boldsymbol{r})$ is the number of prompt and delayed neutrons emitted in a fission, caused by a neutron of energy E' at the point $\boldsymbol{r}$, and $\chi(E)$ is the spectrum of the fission neutrons, including the delayed neutrons normalized per unit

$$\int_0^\infty \chi(E)\,dE = 1 \quad (29)$$

The number of fission neutrons emitted at the point $\boldsymbol{r}$ of the reactor within a second and entering the $(E,\boldsymbol{n})$ beam[9] is now expressed as follows:

$$Q(\boldsymbol{r},E,\boldsymbol{n}) = Q(\boldsymbol{r})\frac{\chi(E)}{4\pi} \quad (30)$$

where

$$Q(\boldsymbol{r}) = \int_0^{E_0} \frac{\int F(\boldsymbol{r},E',\boldsymbol{r}')\,d\Omega'}{l_f(\boldsymbol{r},E')}\left[\nu_{E'}(\boldsymbol{r}) + \sum_i b_i(E',\boldsymbol{r})\right]dE' \quad (31)$$

is the complete number of fission neutrons emitted at the point $\boldsymbol{r}$ within a second.

The method of successive approximation employed to find k_{eff} and the neutron flux in the reactor consists of the following: when solving Equation 8 the value $Q(\boldsymbol{r},E,\boldsymbol{n})/k_{eff}$ is considered to be known and is assumed as being equal to $\chi(E)Q^{(0)}(\boldsymbol{r})$, where $Q^{(0)}(\boldsymbol{r})$ is an arbitrarily assumed distribution of the number of fission neutrons emitted. As a result of solving Equation 8, the neutron flux $F^{(0)}(\boldsymbol{r},E,\boldsymbol{n})$ is found, by means of which $Q^{(1)}(\boldsymbol{r})$ is obtained according to Equation 31. Then the problem of finding the neutron flux from the assumed sources of neutrons of the fission spectrum is solved again, but this time $Q(\boldsymbol{r},E,\boldsymbol{n})/k_{eff}$ in Equation 8 is replaced by $\chi(E)Q^{(1)}(\boldsymbol{r})$.

On the basis of $F^{(1)}(\boldsymbol{r},E,\boldsymbol{n})$ so obtained, according to

†† This method was suggested[8] and later utilized and elaborated by A. S. Romanovich (1952), L. N. Ussachoff (1953) and G. I. Marchuk (1954) as well as in an article.[5]

The numerical methods evolved by G. I. Marchuk (1954) as well as by R. Ehrlich and H. Hurwitz[6] proved the most effective. The common method of searching for the critical dimension within the multigroup model which leads to a computation of determinants (see reference 4, p. 268, 278) can compete successfully, as far as labor-saving is concerned, with the above method only in problems no more complex than a two-group calculation of a reactor with a reflector, in a diffusion approximation.

§§ These assumptions are at present commonly accepted.

Equation 31, $Q^{(2)}(r)$ is computed, etc. This process can be continued until $Q^{(n)}(r)$ proves to be proportionate to $Q^{(n-1)}(r)$. The ratio factor is the value k_{eff} sought.

$$k_{eff} = \lim_{n\to\infty} \frac{Q^{(n)}(r)}{Q^{(n-1)}(r)}$$

The algorithm of the computation $Q^{(n)}(r)$ according to $Q^{(n-1)}(r)$ can be briefly expressed with the help of an integral operator whose kernel is Green's function $P(r \to r')$ equal to the number of neutrons appearing at the point r' as a result of fissions induced by neutrons which originated from one neutron of the fission spectrum, emitted at the point r. ¶¶ From the definition $P(r \to r')$ it is clear that

$$Q^{(n)}(r') = \int P(r \to r')Q^{(n-1)}(r)\, dV \qquad (32)$$

The distribution of neutron sources of the fission spectrum so established, $Q(r)$, appears to obey the integral equation

$$\int P(r \to r')Q(r)\, dV = k_{eff}Q(r') \qquad (33)$$

Now let us deduce an equation for the importance of a fission spectrum neutron $M(r)$ related to $F^+(r,E,n)$ by the formula:

$$M(r) = \int\int \frac{\chi(E)}{4\pi} F^+(r,E,n)\, dE\, d\Omega$$

As before, let us consider a steady-state reactor whose steadiness is provided by reducing the number of fission neutrons by k_{eff} times. Let us place one neutron of the fission spectrum at the point r, its importance being $M(r)$. This leads to the emission of neutrons at each point r' in the next cycle $\frac{P(r \to r')}{k_{eff}}$. The importance of each neutron is $M(r')$. As has been explained in Part 2, the integral importance of neutrons which originated at the steady-state reactor from an initially emitted neutron must be preserved. Hence the following equation

$$M(r) = \frac{1}{k_{eff}} \int P(r \to r')M(r')\, dV' \qquad (34)$$

should take place, which is the integral equation for the importance of the fission spectrum neutrons. This equation is adjoint to Equation 33. The process of successive approximations for solving Equation 34 follows the pattern below similarly to (32):

$$M^{(n)}(r) = \int P(r \to r')M^{(n-1)}(r')\, dV' \qquad (35)$$

Finally, let us consider the convergence of the process of successive approximations.

Suppose that integral Equations 33 and 34 possess an infinite spectrum of eigenvalues $k_{eff\,n} \equiv k_n$ diminishing with the growth of n and that the eigenfunctions corresponding to these eigenvalues form a complete system.

The orthogonality of the eigenfunctions $Q_\alpha(r)$ and $M_\beta(r)$ belonging to various eigenvalues k_α and k_β is proved by a cross multiplication of the equations for $Q_\alpha(r)$ and $M_\beta(r)$, integration throughout the space and subtraction of one equation from the other. As a result, the right parts are eliminated, the equation

$$(k_\alpha - k_\beta)\int Q_\alpha(r)M_\beta(r)\, dV = 0 \qquad (36)$$

is obtained and orthogonality becomes evident.

Let us assume some functions $Q^{(0)}(r)$ and $M^{(0)}(r)$ as a zero approximation for the distribution of the fission neutrons and their importance. Now let us represent these functions as a series:

$$Q^{(0)}(r) = \sum_{\alpha=1}^{\infty} q_\alpha Q_\alpha(r); \qquad q_\alpha = \frac{\int Q^{(0)}(r)M_\alpha(r)\, dV}{\int Q_\alpha(r)M_\alpha(r)\, dV} \qquad (37)$$

$$M^{(0)}(r) = \sum_{\alpha=1}^{\infty} m_\alpha M_\alpha(r); \qquad m_\alpha = \frac{\int M^{(0)}(r)Q_\alpha(r)\, dV}{\int Q_\alpha(r)M_\alpha(r)\, dV} \qquad (38)$$

Using the Equations 32, 35, 37 and 38 and bearing in mind that

$$\int P(r \to r')Q_\alpha(r)\, dV = k_\alpha Q_\alpha(r')$$

$$\int P(r \to r')M_\alpha(r')\, dV' = k_\alpha M_\alpha(r)$$

we obtain for $Q^{(n)}(r)$ and $M^{(p)}(r)$ the following formulae

$$Q^{(n)}(r) = \sum_{\alpha=1}^{\infty} q_\alpha k_\alpha{}^n Q_\alpha(r) = q_1 k_1{}^n \left[Q_1(r) + \sum_{\alpha=2}^{\infty} \frac{q_\alpha}{q_1}\left(\frac{k_\alpha}{k_1}\right)^n Q_\alpha(r)\right] \qquad (39)$$

$$M^{(p)}(r) = \sum_{\alpha=1}^{\infty} m_\alpha k_\alpha{}^p M_\alpha(r) = m_1 k_1{}^p \left[M_1(r) + \sum_{\alpha=2}^{\infty} \frac{m_\alpha}{m_1}\left(\frac{k_\alpha}{k_1}\right)^p M_\alpha(r)\right] \qquad (40)$$

These formulae show the convergence of $Q^{(n)}(r)$ and $M^{(p)}(r)$ when $n, p \to \infty$ to eigenfunctions corresponding to the first eigenvalue: $Q_1(r)$ and $M_1(r)$.

If $Q^{(n)}(r)$ and $M^{(p)}(r)$, are derived, the magnitude of

---

¶¶ The function $P(r \to r')$ is obtained from the formula

$$P(r \to r') = \int \frac{\int p(r',E,n')\, d\Omega'}{l_f(r',E')} \cdot [\nu_{E'}(r') + \sum_i b_i(E',r')]\, dE',$$

the function $p(r',E,n)$ being determined by the equation

$$0 = -\frac{dp(r',E,n)}{ds} - \frac{p(r',E,n)}{l_{a+s}(r',E)} + \int w(E,E',n\cdot n',r')p(r',E',n')\, dE'\, d\Omega' + \chi(E)\frac{\delta(r'-r)}{4\pi}$$

and conditions of the kind given in Equations 4, 5 and 6.

the effective multiplication factor k_{eff}, equal to the first eigenvalue K_1, should be sought for from the formula:

$$k_{eff}^{(n+p)} = \frac{\int Q^{(n)}(r) M^{(p)}(r)\, dV}{\int Q^{(n-1)}(r) M^{(p)}(r)\, dV} = \frac{\int Q^{(n)}(r) M^{(p)}(r)\, dV}{\int Q^{(n)}(r) M^{(p-1)}(r)\, dV}$$

$$= k_1 \frac{1 + \sum_{\alpha=2}^{\infty} \frac{q_\alpha m_\alpha}{q_1 m_1} \left(\frac{k_\alpha}{k_1}\right)^{n+p}}{1 + \sum_{\alpha=2}^{\infty} \frac{q_\alpha m_\alpha}{q_1 m_1} \left(\frac{k_\alpha}{k_1}\right)^{n+p-1}} \quad (41)$$

If one proceeds from the above assumptions, Equation 41 proves the convergence of $k_{eff}^{(n+p)} \to k_1$ when $(n + p) \to \infty$ and furnishes the estimate of error at $(n + p)$ approximation.

A number of features of Equation 41 are worth noting.[5] Inasmuch as the expression for the magnitude of error includes the sum $(n + p)$, the error is determined by the total number of successive approximations for $Q(r)$ and $M(r)$.*** The reasonable choice of $Q^{(0)}(r)$ and $M^{(0)}(r)$ very substantially affects the error. For example, if one of the functions coincides with the eigenfunction belonging to K_1, all the q_α's or m_α's are equal to zero at $\alpha \geq 2$. In this case the calculation of the first approximation for $M(r)$ or $Q(r)$ already produces quite an exact value of k_{eff}. If the functions of $Q^{(0)}(r)$ and $M^{(0)}(r)$ approach $Q_1(r)$ and $M_1(r)$, all the q_α's and m_α's are small at $\alpha \geq 2$ as compared with q_1 and m_1 and so much the more are the products $q_\alpha m_\alpha$ in comparison with $q_1 m_1$. Therefore, having some experience regarding the behaviour of $Q_1(r)$ and $M_1(r)$, it is possible to determine k_{eff} with sufficient accuracy already after computing $Q^{(1)}(r)$ or $M^{(1)}(r)$, or, at the worst, after computing both $Q^{(1)}(r)$ and $M^{(1)}(r)$.

It should be noted that the simplest way of becoming familiar with values of the order of $k_2, k_3, \ldots, k_\alpha, \ldots$, as well as $q_2, q_3, \ldots, q_\alpha, \ldots, m_2, m_3, \ldots, m_\alpha, \ldots$, which are included in Equation 41 is to solve a problem which is close in a physical aspect to the real problem but with separable variables.

*** Since it is useful to know the functions of both $Q(r)$ and $M(r)$, it is expedient to calculate either of them with equal accuracy, i.e., to assume $n \sim p$.

REFERENCES

1. Marshak, R., Rev. Mod. Phys. *19*, 185 (1947).
2. Akhiezer, A. I. and Pomeranchuk, I. Y., *Nekotorye Voprosy teorii Yadra*, Moscow-Leningrad, GITTL (1950).
3. Weinberg, A., A. Journ. Phys., *20*, 401 (1952).
4. Glasstone, S. and Edlund, M., *Elements of the theory of nuclear reactors*. Moscow IL (1954).
5. Ehrlich, R. and Hurwitz, H., Nucleonics, *12*, No. 2, 23 (1954).
6. Hurwitz, H., Nucleonics, *5*, No. 1, 62 (1949).
7. Fuchs, K., Proc. Phys. Soc. A. *62*, 791 (1949).
8. Thompson, A., Journ. Appl. Phys. *22*, 1223 (1951).

The Thermal Reactor Regulators' Efficiency

By A. D. Galanin, USSR

1. DETERMINATION OF REGULATOR EFFICIENCY ON THE BASIS OF PERTURBATION THEORY

In order to determine the efficiency of a regulator, (by a regulator we mean a cylinder absolutely black for thermal neutrons and transparent for moderating neutrons) one may use the perturbation theory. As a matter of fact, however great the perturbation caused by a regulator in close proximity to it, this perturbation spreads to an area whose volume is small in comparison with that of the whole reactor. A comparison of the results obtained with the help of the perturbation theory with those obtained by means of an accurate solution (when such is possible) proves that the application of the perturbation theory is correct if the change in the multiplication factor Δk caused by the regulator meets the requirement

$$\Delta k \ll k - 1$$

Let us consider a cylindrical reactor with a regulator lowered parallel to the reactor axis along the whole of its height. The application of the perturbation theory to the equation (N = density of thermal neutrons)

$$\Delta N + \alpha^2 N = 0 \tag{1}$$

leads to the following result

$$\frac{\Delta k}{k} = \frac{2(L^2 + \tau) N_0 \dfrac{\partial N}{\partial \rho} \rho}{R^2 \mu_2 N_{max}^2} \tag{2}$$

Here L is the diffusion length, $\sqrt{\tau}$ is the slowing down length, $M = \sqrt{L^2 + \tau}$ is the migration length, R is the reactor radius, N_0 and N are the unperturbed and perturbed densities at the point where the regulator is placed, $\partial N/\partial \rho$ means $\partial N(r)/\partial r\,|_{r=\rho}$, where ρ is the effective radius of the black cylinder and, at last,

$$\mu_2 = \frac{\int N^2(r)\, dS}{\pi R^2 N_{max}^2} \tag{3}$$

is the averaging coefficient of the neutron density square (below N_{max} is accepted as 1).

The application of Equation 1, is, however, not true since Equation 1 is justified when the change in the neutron density at lengths of the order of $\sqrt{\tau}$ is not great. In our case, however, large gradients arise near the regulator at distances which, generally speaking, are comparable with $\sqrt{\tau}$.

Let us apply the perturbation theory to an integral equation which is precise within the limits of the age theory (we leave out errors related to the departure from the elementary equation of diffusion near the black cylinder; it is supposed that these departures are fully taken account of by inserting the effective radius of the cylinder).

$$\Delta N(r) - \frac{N(r)}{L^2} + \frac{k}{L^2} \int W(r,r') N(r')\, dr' = 0 \tag{4}$$

where $W(r,r')$ is the probability that the fast neutron generated in point r' will slow down to the rate of the thermal neutrons at point r.

As a result we obtain

$$\frac{\Delta k}{k} = \frac{2\pi\rho L^2 N_0 \dfrac{\partial N}{\partial \rho}}{\int (N_0 - L^2 \Delta N_0) N_0\, dv} \approx \frac{2L^2 N_0 \dfrac{\partial N}{\partial \rho} \rho}{R^2 \mu_2 (1 + \alpha^2 L^2)} \tag{5}$$

where it is supposed that in practically the whole volume of the reactor the equation

$$\Delta N_0 + \alpha^2 N_0 = 0$$

can be used. Equation 5 differs in the main from Equation 2 in that M^2 is substituted by L^2. Such a substitution is quite natural, since the regulator absorbs only thermal neutrons and its efficiency cannot depend on the value of moderation length.

2. DETERMINATION OF THE DENSITY GRADIENT OF NEUTRONS CLOSE TO THE REGULATOR

If we determined the density gradient of neutrons near the regulator proceeding from Equation 1, we would obtain as a result

$$\rho \frac{\partial N}{\partial \rho} = -\frac{2}{\pi Y_0(\alpha\rho)} \approx \frac{1}{\ln \dfrac{2}{\gamma \alpha \rho}} \tag{6}$$

where $\gamma = 1.78 \ldots$, $\alpha = 2.4/R$ and R is the reactor radius. However, the application of Equation 1, as we have already pointed out, is unjustified and therefore we shall consider Equation 4. Let us insert into it a regulator in the form of a point singularity

$$\Delta N(r) - \frac{N}{L^2} + \frac{k}{L^2} \int W(r,r') N(r')\, dr' - A\delta(r - r_0) = 0 \tag{7}$$

Original language: Russian.

where A defines the value of the neutron flux falling upon the regulator. The kernel $W(r,r')$ for a sufficiently large reactor (far from its boundaries) has the form (r is everywhere a two-dimensional vector)

$$W(r,r') = \frac{1}{4\pi\tau} e^{-(r-r')^2/4\lambda}$$

Equation 7 may be solved by the Fourier transformation:

$$N(r) = C(r) - A \int \frac{e^{i(r-r_0)s}\, ds}{\frac{1}{L^2} + s^2 - \frac{k}{L^2} e^{-s^2\tau}}$$

where $C(r)$ is the solution of Equation 7 without term $A\delta(r - r_0)$ (i.e., having no singularity in point $r = r_0$).

Let us define

$$\int_0^\infty \frac{sJ_0(|r - r_0|s)\, ds}{\frac{1}{L^2} + s^2 - \frac{k}{L^2} e^{-s^2\tau}} P(r - {}_0) \qquad (8)$$

Using the condition $N = 0$ we obtain on the regulator surface

$$N(r) = C(r) - C(r_0) \frac{P(|r - r_0|)}{P(\rho)} \qquad (9)$$

Using the relation

$$\int_0^\infty \frac{sJ_0(\rho s)\, ds}{\frac{1}{L^2} + s^2} = K_0\left(\frac{\rho}{L}\right) \qquad (10)$$

we obtain ($\rho \to 0$)

$$P(\rho) = K_0\left(\frac{\rho}{L}\right) + \frac{k}{L^2} \int_0^\infty \frac{e^{-s^2\tau}\, ds}{\left(\frac{1}{L^2} + s^2 - \frac{k}{L^2} e^{-s^2\tau}\right)\left(\frac{1}{L^2} + s^2\right)} \qquad (11)$$

As ($\rho \ll L$)

$$\frac{d}{d\rho} K_0\left(\frac{\rho}{L}\right) \approx -\frac{1}{\rho}$$

[$C(r)$ is not differentiated in this case, since the unperturbed density is considered almost constant]

$$\left(r \frac{\partial N}{\partial r}\right)_{r=\rho} = \frac{N_0}{P(\rho)} \qquad (12)$$

where N_0 is the unperturbed neutron density at the point r_0.

Thus, Equation 5 now assumes the following form (we consider that $\alpha^2 L^2 \ll 1$)

$$\frac{\Delta k}{k} = \frac{2L^2 N_0^2}{R^2 \mu_2 P(\rho)} \qquad (13)$$

Now it is necessary to analyze the integral $P(\rho)$. Let us consider the case ($\tau \to 0$):

$$P(\rho)_{\tau \to 0} = \int_0^\infty \frac{J_0(\rho s) s\, ds}{s^2 - \alpha^2} \quad \text{and} \quad \alpha^2 = \frac{k-1}{L^2}$$

With $k > 1$ the integrand has a pole at the points $s = \pm\alpha$. If this integral is understood in terms of the principal value, we obtain ($\alpha\rho \to 0$).*

$$P(\rho)_{\tau \to 0} = -\frac{\pi}{2} Y_0(\alpha\rho) \approx \ln \frac{2}{\gamma\alpha\rho}$$

which coincides with Equation 6, as it should be in the case of ($\tau \to 0$). Hence we conclude that with $\tau \neq 0$ integral $P(\rho)$ should be understood in terms of the principal value.

In further analysis we shall assume that $K - 1 \ll 1$. In Equation 11 from $P(\delta)$ a part not depending on P in $P \to 0$ is removed. This term however, goes to infinity logarithmically, when $k \to 1$. The removal from it of a term of the kind $\ln \alpha^2\tau (\alpha^2 = (k-1)/(L^2 + \tau))$ can be effected if we divide the integration interval into two: $0 < s^2\tau < \delta$; $\delta < s^2\tau < \infty$ with $\alpha^2\tau \ll \delta \ll 1$.

The result of the calculation is as follows:

$$P(\rho) = K_0\left(\frac{\rho}{L}\right) + \frac{L^2}{2(L^2+\tau)} \ln \frac{1}{\gamma\tau\alpha^2} - \frac{1}{2} \ln \frac{L^2+\tau}{\gamma\tau} + \frac{1}{2\left(1 + \frac{L^2}{\tau}\right)} \int_0^\infty \frac{(1 - z - e^{-z})e^{-z}\, dz}{z\left(1 + z\frac{L^2}{\tau} - e^{-z}\right)}$$

Here the remaining integral is approximately equal to

$$-\frac{1}{2}\left(1 + \frac{L^2}{\tau}\right)^{-1}$$

with error under 0.04 in $\frac{1}{4} < \frac{L^2}{\tau} < 4$. Thus approximately

$$P(\rho) = \ln \frac{2L}{\gamma\rho} + \frac{L^2}{2(L^2+\tau)} \ln \frac{1}{\gamma\tau\alpha^2} - \frac{1}{2} \ln \frac{L^2+\tau}{\gamma\tau} - \left(\frac{\tau}{2(L^2+\tau)}\right)^2 \qquad (14)$$

In most cases only the first term of Equation 14 may remain in the calculations.

3. ABSORBING ROD LATTICE IN A HOMOGENEOUS MULTIPLYING MEDIUM

In a number of cases a great number of absorbing rods have to be inserted. In this case interference occurs between separate rods, and their summary effect is not equal to the net sum of effects of each rod. In order to determine the possible values of the interference coefficient we shall consider the limiting case of a whole lattice of absorbing rods occupying the whole reactor. For the sake of simplicity, we shall

* We have

$$\int_0^\infty \frac{xJ_0(ax)}{x^2-1} dx = \frac{2}{\pi} \int_1^\infty \frac{dt}{\sqrt{t^2-1}} \int_0^\infty \frac{x \sin axt}{x^2-1} dx = \int_1^\infty \frac{\cos at}{\sqrt{t^2-1}} dt = -\frac{\pi}{2} Y_0(a)$$

in which the integral is understood in terms of the principal value. See Ryzhik and Gradstein. "Table of integrals, sum of series and products" formulae 6.413,2; 3.523,4; 3.528,4.

consider first a homogeneous reactor, and then evaluate the inaccuracies arising from the homogenization of the heterogeneous reactor.

We obtain a characteristic equation of absorbing rod lattice inserted into a homogeneous multiplying medium.

The equation for neutron density is as follows:

$$\Delta N - \frac{N}{L^2} + \frac{k}{L^2}\int W(r,r')N(r')\,dr' - \frac{\gamma}{D}\sum_k N(k)\delta(r - r_k) = 0 \qquad (15)$$

where γ is the thermal constant (I), $N(k)$ is the neutron density on the surface of rod number k (below $\gamma \to \infty$, $N(k) \to 0$). Solving by the Fourier transformation, we obtain

$$N(r) = \frac{\gamma}{D}\int \frac{\sum_k N(k)e^{i\kappa(r-r_k)}\,d\kappa}{\frac{k}{L^2}e^{-\kappa^2\tau} - \kappa^2 - \frac{1}{L^2}}$$

Now let r be tended towards a point on the surface of the zero absorbing rod. Supposing

$$N(k) = N(0)e^{-ika}$$

where a is the lattice spacing, α^2 is the Laplacian of the reactor with a lattice of absorbing rods. Then

$$1 = \frac{\gamma}{D}\int \frac{\sum_k e^{i(\kappa-\alpha)ka}}{\frac{k}{L^2}e^{-\kappa^2\tau} - \kappa^2 - \frac{1}{L^2}}\,d\kappa$$

We transform the sum over k in the following way (the equation may be checked by using the Poisson formula)

$$\sum_k e^{i(\kappa-\alpha)ka} = \sum_\nu \delta\left[\nu - \frac{a}{2\pi}(\alpha - \kappa)\right]$$

and hence instead of Equation 16 we obtain

$$1 = \frac{\gamma}{D}\frac{4\pi^2L^2}{d^2}\sum_\nu \left[ke^{\left(\frac{2\pi\nu}{a}-\alpha\right)^2\tau} - \left\{1 + \left(\frac{2\pi\nu}{a} - \alpha\right)^2 L^2\right\}\right]^{-1} \qquad (17)$$

Equation 17 should be specified by taking as numerator $e^{\frac{2\pi\nu\rho}{a}}$ where ρ is the radius (efficient) of the absorbing rod (in agreement with the fact that r tends to the point on the surface of the rod, not in its centre).

Then turning to absolutely absorbing rods, i.e., considering $\gamma \to \infty$, we obtain

$$\sum_\nu e^{\frac{2\pi\nu\rho}{a}i}\left\{ke^{-\left(\frac{2\pi\nu}{a}-\alpha\right)^2\tau} - \left[1 + \left(\frac{2\pi\nu}{a} - \alpha\right)^2 L^2\right]\right\}^{-1} = 0 \qquad (18)$$

Further under conditions that

$$4e^{-\frac{4\pi^2\nu^2}{a^2}\tau} \ll 1; \qquad \nu \geq 1$$

$$\frac{4\pi^2\nu^2}{a^2} \gg \alpha^2; \qquad \nu \geq 1$$

we have

$$ke^{-\alpha^2\tau} - (1 + \alpha^2L^2) = \frac{1}{q_1} \qquad (19)$$

where

$$q_1 = \sum_{\nu\neq 0} \frac{e^{\frac{2\pi\nu\rho}{a}i}}{1 + \frac{4\pi^2L^2}{a^2}\nu^2} \qquad (20)$$

A sum of this form always appears in the lump effect theory in thermal neutron absorption.[1] It is equal to

$$q_1 = \frac{a^2}{4\pi L^2}\left(\ln\frac{a^2}{\pi\rho^2} + \frac{\pi\rho^2}{a^2} - 1.48\right) \qquad (21)$$

on the condition that

$$\frac{a^2}{4\pi^2L^2} \ll 1 \quad \text{and} \quad \frac{\pi\rho^2}{a^2} \ll 1$$

Equation 19 may be written as follows:

$$\frac{kq_1}{1+q_1}e^{-\alpha^2\tau} = 1 + \frac{q_1L^2}{1+q_1}\alpha^2 \qquad (22)$$

i.e.,

$$k_p = \frac{kq_1}{1+q_1}; \qquad L_p = \sqrt{\frac{q_1}{1+q_1}}L \qquad (23)$$

the multiplication factor and the diffusion length in the reactor, in the presence of a lattice of the absorbing rods.

If $p \to 0$ then $q_1 \to \infty$ and $k_p \to k$. Similarly a characteristic equation can be formulated in case the lattice consists of multiplying rods.

4. INTERFERENCE COEFFICIENT OF REGULATING RODS

Let us consider a homogeneous reactor with a lattice of absorbing rods. The absorbing rod efficiency may be calculated on the one hand by Equation 13, and on the other, by Equation 23. It is precisely, according to Equation 23,

$$\frac{\Delta k}{k} = \frac{1}{1+q_1} \qquad (24)$$

while according to Equation 13

$$\frac{\Delta k}{k} = \frac{2L^2\zeta}{R^2\mu_2P(\rho)}\sum_k N_0^2(r_k) \qquad (25)$$

where ζ is the unknown interference coefficient, r_k – the vector radius of the absorbing rod. By replacing the sum of Equation 25 by the integral

$$\sum_k N_0^2(r_k) = \frac{1}{a^2}\int N_0^2(r)\,dS = \frac{\mu_2 \pi R^2}{a^2}$$

and comparing Equation 24 with Equation 25, we obtain

$$\zeta = \frac{a^2}{2\pi L^2}\frac{P(\rho)}{1+q_1} \tag{26}$$

where $P(\rho)$ is given by Equation 14, and q_1 by 21. It is easy to see that in $a^2 \to 0$ the interference coefficient $\zeta \to 1$, remains under 1. In another limiting case $a^2 \to \infty$ Equation 26 is not justified since it has been supposed that $a^2/4\pi^2L^2 \ll 1$. The estimation of the sum in Equation 20 may be made with $a^2/4\pi^2L^2 \gtrsim 1$.

Such an estimation shows that in this case

$$q_1 = \frac{a^2}{2\pi L^2}\left[\ln\frac{2L}{\gamma\rho} + \text{a term of the order of } e^{-\frac{a^2}{2\pi L^2}}\right]$$

If in $P(\rho)$ Equation 14, only the first term $\ln 2L/\gamma\rho$ is left, then with the increase of a, the screening coefficient tends to 1 exponentially. If in Equation 14 the term with $\ln(1/\tau\alpha^2)$ is also taken into consideration, it may happen that ζ will be greater than 1, however, as can be shown, the application of the perturbation theory requires that $\ln(2L/\gamma\rho) \gg \ln(1/\tau\alpha^2)$. If however Equation 25 contains errors related to inaccuracy of the perturbation theory, then ζ is not only the interference coefficient, but it also includes corrections to the theory of perturbations. Then it may happen that $\zeta > 1$.

5. HOMOGENIZATION COEFFICIENT

Now let us consider a heterogeneous reactor in which an absorbing rod lattice is inserted. The action of the lattice on the reactor reactivity may be calculated by using the theory of a complex lattice,[1] on one hand, and by homogenization of the reactor and using Equation 24, on the other.

In the complex lattice theory, simple formulae are obtained if the absorbing rods are inserted either in every cell, or in every other cell. Let us denote

$$\xi = \frac{\left(\frac{\Delta k}{k}\right)_{hom}}{\left(\frac{\Delta k}{k}\right)_{hetero}}$$

Using the formulae of reference 1 we may obtain the following result:

$$\xi = 1 - \frac{sq_1 - \epsilon\dfrac{a^2}{4\pi L^2}}{(1+q_1)(1+s)} \tag{27}$$

Here, q_1 has been determined in section 3, L is diffusion length in the lattice, $\epsilon = +0.69$, if the absorbing rods are in the centre of every cell, and $\epsilon = 0.18$, if the distance between the absorbing rods a is equal to a double spacing of the lattice and value s is determined in the following way

$$s = 0.69\frac{a_0^2}{4\pi L_0^2}\frac{1}{q_u}$$

where L_0 is the diffusion length in the moderator, a_0 is the spacing of the uranium rod lattice, and q_u determines the thermal absorption in the uranium lattice[1]

$$q_u = q_0 + \frac{a_0^2}{4\pi L_0^2}\left(\ln\frac{a_0^2}{\pi\rho_U^2} - \frac{3}{2}\right)$$

where ρ_U is the radius of uranium rods, and q_0 the homogeneous part of thermal absorption. Usually s amounts to several per cent. If $s \ll 1$, and $q_1 \gg 1$ then assuming that

$$\frac{a^2}{4\pi^2L^2} \ll 1, \qquad \ln\frac{a^2}{\pi\rho^2} \gg 1$$

$$\xi = 1 - s \tag{28}$$

i.e.,

$$\left(\frac{\Delta k}{k}\right)_{hom} < \left(\frac{\Delta k}{k}\right)_{hetero}$$

Such a sign accords with the fact that we insert in the heterogeneous reactor absorbing rods in the centre of the cells where the neutron density is above average.

Equations 27 and 28 show that the homogenization coefficient for the models in question approximates unity. Both cases under discussion produce the same homogenization coefficient, provided

$$\ln\frac{a^2}{\pi\rho^2} \gg 1$$

If the absorbing rods are placed in a different way, for instance, not in the centres of the cells, but replace uranium rods in some cells, then the homogenization coefficient will differ from Equation 28. In this case, ξ may be evaluated in accordance with the theory of complex lattices outlined in reference 1.

REFERENCES

1. Galanin, A. D., *Calculation of the thermal coefficient in a heterogeneous reactor.* Report at the International Conference of Peaceful Use of Atomic Energy, this Session.

The Cylindrically Symmetrical Solution of Milne's Problem Using Spherical Harmonic Analysis

By Ladislav Trlifaj,* Czechoslovakia

In neutron diffusion theory, the following common problem is known as Milne's problem: an infinite space scatters neutrons isotropically, but neither absorbs them, nor modifies their energy. In this space, a black body is assumed to be present, which absorbs all neutrons impinging on it. It is further assumed that, in this space, there are no sources of neutrons with the exception of a neutron stream of constant density coming from infinity. Determine the neutron flux in said space.

This problem has been solved by means of different methods, and for different shapes of the black body.[1,2] Its solution is important for the accurate determination of the dimensions of the control assemblies in a reactor. For this reason, we have chosen to solve for the case of a black body shaped as an infinite cylinder of radius a.

However, in the next part of the calculations, we assume that the infinite space does scatter neutrons with a cross section of:

$$\Sigma_s\{1 + 3fP_1^0(\omega)\} \tag{1}$$

which is a function of the cosine of neutron scattering angle ω. The quantity f is known as the average cosine of the neutron scattering angle; Σ_s is the macroscopic cross-section for the isotropic scattering of neutrons. The functions P_r^m are the ordinary (related) Legendre polynomials. We also will assume that the space absorbs neutrons with a cross-section Σ_a and we will also use the expression $d = \Sigma_a \cdot \Sigma_s$.

The cylindrical symmetry of the problem indicates that the function of neutron distribution in space, and in the directions of their constant velocity, depends only on distance ρ from the axis of the cylindrical black body. Naturally, it also depends on the cosine of the angle included between the (constant) neutron velocity vector $\vec{v}$, and the distance from the cylinder axis vector $\vec{\rho}$; as well as on the cosine of angle φ which is included between the surface of vectors $\vec{v}$, $\vec{\rho}$, and the surface perpendicular to the black body cylinder axis. Let us designate these cosines as ϑ, μ and express them in cylindrical and rectangular coordinates, as follows:

$$\vartheta = \frac{\vec{\rho}\,\vec{v}}{\rho v}, \qquad \mu = \frac{\vec{\rho} \times \vec{v}}{\rho v \sqrt{1-\vartheta^2}} \cdot \frac{\vec{\kappa}}{|\vec{\kappa}|} = \frac{1}{v\sqrt{1-\vartheta^2}\cdot\rho}$$

$$(xv_y - yv_x) = \cos\varphi \tag{2}$$

The usual Boltzmann equation, which governs the neutron distribution function $\psi(\rho,\vartheta,\mu)$ in the space outside the black body, can then be expressed as

$$(P_1^0(\omega) = P_1^0(\vartheta)P_1^0(\vartheta') + P_1^1(\vartheta)P_1^1(\vartheta')\cos(\varphi - \varphi'))$$

$$\vartheta\frac{\partial}{\partial\rho}\psi(\rho,\vartheta,\mu) + \frac{(1-\vartheta^2)\mu^2}{\rho}\frac{\partial}{\partial\vartheta}\psi(\rho,\vartheta,\mu)$$

$$- \frac{\vartheta\mu(1-\mu^2)}{\rho}\frac{\partial}{\partial\mu}\psi(\rho,\vartheta,\mu) + \Sigma_s(1+\alpha)\psi(\rho,\vartheta,\mu)$$

$$= \frac{\Sigma_s}{4\pi}\int_{-1}^{1} d\vartheta' \int_{-\pi}^{\pi} d\varphi' \,[1 + 3fP_1^0(\omega)]\psi(\rho,\vartheta',\mu') \tag{3}$$

This equation may be solved by means of the familiar method of spherical harmonic analysis. This method consists of expanding the unknown function ψ into a series of functions in rectangular coordinates, in this case $P_n^m(\vartheta)\cdot\cos m\varphi$, terminating the theoretically infinite series at the finite number of terms of this series. We further use an approximation of P_3 and may therefore write,

$$\psi(\rho,\vartheta,\mu) = \psi_{00}(\rho)P_0^0(\vartheta) + \psi_{10}(\rho)P_1^0(\vartheta)$$
$$+ \psi_{20}(\rho)P_2^0(\vartheta) + \psi_{22}(\rho)P_2^2(\vartheta)(2\mu^2 - 1)$$
$$+ \psi_{30}(\rho)P_3^0(\vartheta) + \psi_{32}(\rho)P_3^2(\vartheta)(2\mu^2 - 1) \tag{4}$$

The choice of even harmonics P_n^{2m} is dictated by the symmetrical nature of the problem relative to a surface passing through the axis of the black body cylinder.

Differential Equation 3 then breaks up into a system of linear differential equations

$$5\psi_{00}'(\rho) + 5\psi_{10}(\rho) + 2\psi_{20}'(\rho) + \frac{3}{\rho}\psi_{20}(\rho) - \frac{6}{\rho}\psi_{22}(\rho)$$
$$+ 5\alpha\psi_{10}(\rho) - 5f\psi_{10}(\rho) = 0 \tag{5.1}$$

$$\psi_{10}'(\rho) + \frac{1}{\rho}\psi_{10}(\rho) + 3\alpha\psi_{00}(\rho) = 0 \tag{5.2}$$

Original language: Russian.

* Science Associate of the Institute of Nuclear Physics.

$$14\psi_{10}'(\rho) - \frac{7}{\rho}\psi_{10}(\rho) + 21\psi_{20}(\rho) + 9\psi_{30}'(\rho) + \frac{18}{\rho}\psi_{30}(\rho) - \frac{90}{\rho}\psi_{32}(\rho) + 21\alpha\psi_{20}(\rho) = 0 \quad (5.3)$$

$$3\psi_{20}'(\rho) - \frac{3}{\rho}\psi_{20}(\rho) + \frac{6}{\rho}\psi_{22}(\rho) + 5\psi_{30}(\rho) + 5\alpha\psi_{30}(\rho) = 0 \quad (5.4)$$

$$2\psi_{22}'(\rho) - \frac{2}{\rho}\psi_{22}(\rho) + \frac{1}{\rho}\psi_{20}(\rho) + 10\psi_{32}(\rho) + 10\alpha\psi_{32}(\rho) = 0 \quad (5.5)$$

$$30\psi_{32}'(\rho) + \frac{60}{\rho}\psi_{32}(\rho) + \frac{7}{\rho}\psi_{10}(\rho) - \frac{3}{\rho}\psi_{30}(\rho) + 42\psi_{22}(\rho) + 42\alpha\psi_{22}(\rho) = 0 \quad (5.6)$$

The black body absorbs all the neutrons impinging on it. Accordingly, the current density of neutrons moving from the body into the scattering space must equal zero:

$$j_+(\rho) = 2\int_0^1 d\vartheta \int_{-1}^1 \frac{d\mu}{\sqrt{1-\mu^2}}\,\vartheta\psi(a,\vartheta,\mu) = 0 \quad (6)$$

However, it is known that this boundary condition is less stringent than the conditions which should, in fact, exist at the boundaries of the black body. Boundary conditions of Equation 6 may be rewritten with the help of the expansion of Equation 4 in the following form:

$$12\psi_{00}(a) + 8\psi_{10}(a) + 3\psi_{20}(a) = 0 \quad (7)$$

Further examination of Equations 5 and 7 will rest on subdivision into two situations: We will first make $\alpha = f = 0$; in the second case we will assume that α, f are sufficiently small, so that we can use the perturbation theory. This case is met quite often in practice.

THE CASE WHERE $\alpha = f = 0$

When the space outside the black body scatters neutrons isotropically without absorbing them, it can be easily shown that the expression

$$j(\rho) = 2\int_{-1}^1 d\vartheta - \int_{-1}^1 \frac{d\mu}{\sqrt{1-\mu^2}}\,\vartheta\psi(\rho,\vartheta,\mu)$$

is equal to const: ρ. Let us multiply Equation 3 by the expression $(1-\mu^2)^{-1/2}$ and integrate with respect to ϑ and μ: After a few calculations we arrive at equation

$$\frac{\partial}{\partial\rho}j(\rho) + \frac{1}{\rho}j(\rho) = 0$$

the solution of which is the expression shown before. The quantity $j(\rho)$ is the current density of the neutrons arriving from the infinitely distant source (neutron current being logarithmic at infinity). When its power has the value 2π, then const $= -1$.

The expression $-1/\rho$ also is a solution of Equation 5.2. Solving the other equations is a painstaking but not complicated operation; we will therefore put down the final result directly (choosing a unit length so that $\Sigma_s = 1$):

$$\psi_{00}(\rho) = \log\rho + \frac{32}{3\lambda_1}g_1K_0(\lambda_1\rho) + C \quad (8.1)$$

$$\psi_{10}(\rho) = -\frac{1}{\rho} \quad (8.2)$$

$$\psi_{20}(\rho) = -\frac{1}{\rho^2} - \frac{20}{3\lambda_1}g_1K_0(\lambda_1\rho) - \frac{20}{\lambda_1}g_1K_2(\lambda_1\rho) + \frac{20}{\lambda_2}g_2K_0(\lambda_2\rho) - \frac{20}{\lambda_2}g_2K_2(\lambda_2\rho) \quad (8.3)$$

$$\psi_{22}(\rho) = \frac{1}{6\rho^2} - \frac{10}{3\lambda_1}g_1K_0(\lambda_1\rho) + \frac{10}{3\lambda_1}g_1K_2(\lambda_1\rho) + \frac{10}{\lambda_2}g_2K_0(\lambda_2\rho) + \frac{10}{3\lambda_2}g_2K_2(\lambda_2\rho) \quad (8.4)$$

$$\psi_{30}(\rho) = -\frac{2}{\rho^3} - 6g_1K_1(\lambda_1\rho) - 10g_1K_3(\lambda_1\rho) + 10g_2K_1(\lambda_2\rho) - 10g_2K_3(\lambda_2\rho) \quad (8.5)$$

$$\psi_{32}(\rho) = \frac{1}{5\rho^3} - g_1K_1(\lambda_1\rho) + g_1K_3(\lambda_1\rho) + \frac{5}{3}g_2K_1(\lambda_2\rho) + g_2K_3(\lambda_2\rho) \quad (8.6)$$

Functions K_n are forms of the well-known Bessell functions of the second order; and quantities λ_1, λ_2 which do not depend on shape, are

$$\lambda_1 = \frac{\sqrt{35}}{3}, \qquad \lambda_2 = \sqrt{7} \quad (9)$$

Equations 8 are the only solution of Equations 5 which are logarithmic only at infinity [for $\psi_{00}(\rho)$]. Function $\psi_{00}(\rho)$ is the neutron current and $\psi_{10}(\rho)$ the neutron current density.

In the solutions shown, there are three unknown integration constants g_1, g_2, C; the fourth factor was determined during normalizing of the source. To enable us to determine values of g_1, g_2, C, we must, in addition to the boundary condition of Equation 7, choose two additional similar conditions. Usually, conditions of the following type are chosen:

$$\int_0^1 d\vartheta \int_{-1}^1 \frac{d\mu}{\sqrt{1-\mu^2}}P_3^0(\vartheta)\psi(a,\vartheta,\mu) = 0$$

$$\int_0^1 d\vartheta \int_{-1}^1 \frac{d\mu}{\sqrt{1-\mu^2}}P_3^2(\vartheta)(2\mu^2-1)\psi(a,\vartheta,\mu) = 0 \quad (10)$$

Since, following the substitution of Expansion 4 into Equation 3, one should really make $\psi_{32}(\rho) = 0$, $\psi_{22}(\rho) = 0$, we will choose the following two as the additional conditions:

$$\psi_{32}(a) = 0 \qquad \psi_{22}(a) = 0 \quad (11)$$

which express the indicated condition approximately and at the most sensitive point $\rho = a$. Equations 11 together with 7 determine values and signs of g_1, g_2, C.

However, direct determination of the linear (asymptotic) length of extrapolation is a more interesting problem. In the present case, this length is given by the equation

$$d = aC + a \log a \tag{12}$$

Somewhat detailed, but in general quite simple, calculations by means of Equations 7 and 11 show that length of extrapolation may be expressed by the following equation:

$$d = \frac{2}{3} + \frac{16}{g\lambda_1} \cdot \frac{1}{a\Delta(a)} K_0(\lambda,a)K_1(\lambda_2 a) - \frac{64}{3\lambda_1\lambda_2} \cdot \frac{1}{a_2\Delta(a)} K_0(\lambda_1 a)K_0(\lambda_2 a) \tag{13}$$

and the quantity $\Delta(a)$ is given by the expression

$$\Delta(a) = \frac{32}{7a} K_1(\lambda_1 a)K_1(\lambda_2 a) - \frac{40}{3\lambda_1\lambda_2 a} K_0(\lambda_1 a)K_2(\lambda_2 a) \frac{40}{\lambda_1\lambda_2 a} K_0(\lambda_2 a)K_2(\lambda_1 a) \tag{14}$$

In order to show more closely the relationship between the length of extrapolation and the radius of the cylindrical black body, we will make two liminal transitions in Equation 13. In the first transition, we will assume that radius a is small, so that we can replace Bessell functions K_n with Laurent series. Then,

$$d = \frac{2}{3} - \frac{7}{8} a \log a - \frac{7}{8} \left\{ - \frac{5}{48} + \frac{27}{32} \log \frac{\lambda_1}{\lambda_2} + \log \frac{\lambda_2 B}{2} \right\} a + \cdots \tag{15.1}$$

where $B = e^{\gamma}$, λ is Euler's constant, $\gamma = 0.57721$.

In the second transition, we will assume that radius a is sufficiently large so that, for functions K_n we can utilize their asymptotic expansions.

$$d = \frac{2}{3} - \frac{\sqrt{7}\,(5 + \sqrt{5})}{120} + \left(\frac{23}{40} + \frac{3\sqrt{5}}{20}\right)\frac{1}{a} - \frac{\sqrt{7}\,(2245 + 1209\sqrt{5})}{11200} \frac{1}{a^2} + \cdots \tag{15.2}$$

Both Equations 15 differ from Davison's exact equation[2] which was obtained by consecutive solution of Peierls' integral equation, corresponding to the given problem. However, Reference 2 also utilizes the graph of the relation between extrapolation length d and radius a, which corresponds to the approximation P_3 calculated by means of spherical harmonic analysis. In general, this is comparable to Equation 13. Reference 2 does not show calculations; we need them for the second case when $\alpha \neq 0, f \neq 0$.

The difference between the results obtained by integral equations, as in Reference 2, and those obtained by spherical harmonic analysis can be explained by the difference in the two methods for small values of radius ρ. Results of the first method are more accurate. Despite this, the spherical harmonic method is not without value, since, in a certain sense, it is broader, and it permits several interesting conclusions when $\alpha \neq 0, f \neq 0$. We will therefore consider this case next.

THE CASE WITH A SMALL α, f

In this case we will use the previous Equations 5; however, we will identify their solution as capital Ψ. Since we have assumed that values α, f are sufficiently small, we can break these functions down into a series in α, f, and we will limit ourselves to the terms of an order not higher than α^2, αf, f^2

$$\Psi(\rho) = \psi(\rho) + \alpha\psi_{(\rho)}{}^{(\alpha)} + f\psi_{(\rho)}{}^{(f)} + \alpha^2\psi_{(\rho)}{}^{(\alpha^2)} + \alpha f\psi_{(\rho)}{}^{(\alpha f)} + f^2\psi_{(\rho)}{}^{(f^2)} + \cdots \tag{16}$$

So far, we have not assigned subscripts 00, 10, 20, 22, 30, 32, to the corresponding functions of Ψ, ψ.

As Expansion 16 indicates, we will seek individual terms of this expansion by means of the simple perturbation theory. Thus, the zero-order approximations are solutions to Equation 8 in which we make $g_1 = g_2 = 0$. Otherwise, Equations 5 would be incompatible upon solving them for a higher order. Using similar reasoning, we will always omit solutions of homogeneous equations for higher orders corresponding to $g_1 \neq 0$, $g_2 \neq 0$. We will also omit those solutions of homogeneous equations which would only lead to the re-evaluation of the factor as const $= -1$; re-evaluation of this sort is a concomitant of the theory of perturbation, and not a physical phenomenon.

Zero order solutions then have the following form (assuming all $\Sigma_s = 1$):

$$\psi_{00}(\rho) = \log \rho + C \qquad \psi_{10}(\rho) = \frac{1}{\rho} \tag{17.1}$$

$$\psi_{20}(\rho) = -\frac{1}{\rho^2} \qquad \psi_{30}(\rho) = -\frac{2}{\rho^3} \tag{17.2}$$

$$\psi_{22}(\rho) = \frac{1}{6\rho^2} \qquad \psi_{32}(\rho) = \frac{1}{5\rho^3} \tag{17.3}$$

A solution of the next order for $\psi^{(\alpha)}$, $\psi^{(f)}$ now is easily obtained by means of Equations 5 and 16. After a few calculations we have:

$$\psi_{00}{}^{(\alpha)}(\rho) = \tfrac{1}{6} \log \rho + \tfrac{3}{4}\rho^2 \log \rho + (\tfrac{3}{4}C - \tfrac{3}{4})\rho^2 \tag{18.1}$$

$$\psi_{10}{}^{(\alpha)}(\rho) = -\tfrac{3}{2}\rho \log \rho + (\tfrac{3}{4} - \tfrac{3}{2}C)\rho \tag{18.2}$$

$$\psi_{20}{}^{(\alpha)}(\rho) = \frac{8}{35}\frac{1}{\rho^2} + \frac{1}{2} \log \rho + \left(\frac{3}{4} + \frac{1}{2}C\right) \tag{18.3}$$

$$\psi_{22}{}^{(\alpha)}(\rho) = -\frac{4}{105}\frac{1}{\rho^2} + \frac{1}{4} \log \rho + \left(-\frac{1}{8} + \frac{1}{4}C\right) \tag{18.4}$$

$$\psi_{30}{}^{(\alpha)}(\rho) = \frac{86}{35}\frac{1}{\rho^3} + \frac{3}{10}\frac{1}{\rho} \tag{18.5}$$

$$\psi_{32}{}^{(\alpha)}(\rho) = -\frac{43}{175}\frac{1}{\rho^3} - \frac{3}{20}\frac{1}{\rho} \tag{18.6}$$

and

$$\psi_{00}^{(f)}(\rho) = -\log\rho \tag{19.1}$$

$$\psi_{10}^{(f)}(\rho) = \psi_{20}^{(f)}(\rho) = \psi_{22}^{(f)}(\rho) = \psi_{30}^{(f)}(\rho) = \psi_{32}^{(f)}(\rho) = 0 \tag{19.2}$$

These solutions fully describe second-order solutions for $\psi^{(\alpha^2)}(\rho)$, $\psi^{(\alpha f)}(\rho)$, $\psi^{(f^2)}(\rho)$. Again utilizing Equations 5 and 16, we will have, for these functions, the following expressions:

$$\psi_{00}^{(\alpha^2)}(\rho) = -\frac{4}{175}\log\rho + \frac{3}{10}\rho^2\log\rho + \left(\frac{3}{20}C - \frac{3}{10}\right)\rho^2 + \frac{9}{64}\rho^4\log\rho + \left(\frac{9}{64}C - \frac{27}{128}\right)\rho^4 \tag{20.1}$$

$$\psi_{10}^{(\alpha^2)}(\rho) = -\frac{3}{10}\rho\log\rho + \frac{3}{20}\rho - \frac{9}{16}\rho^3\log\rho + \left(\frac{45}{64} - \frac{9}{16}C\right)\rho^3 \tag{20.2}$$

$$\psi_{20}^{(\alpha^2)}(\rho) = \frac{692}{1225}\frac{1}{\rho^2} - \frac{1}{70}\log\rho + \left(-\frac{3}{140} - \frac{4}{35}C\right) + \frac{15}{16}\rho^2\log\rho + \left(-\frac{51}{64} + \frac{15}{16}C\right)\rho^2 \tag{20.3}$$

$$\psi_{22}^{(\alpha^2)}(\rho) = -\frac{346}{3675}\frac{1}{\rho^2} - \frac{1}{140}\log\rho + \left(\frac{1}{280} - \frac{2}{35}C\right) + \frac{3}{32}\rho^2\log\rho + \left(-\frac{15}{128} + \frac{3}{32}C\right)\rho^2 \tag{20.4}$$

$$\psi_{30}^{(\alpha^2)}(\rho) = -\frac{1626}{1225}\frac{1}{\rho^3} - \frac{54}{175}\frac{1}{\rho} - \frac{27}{40}\rho\log\rho + \left(\frac{9}{160} - \frac{27}{40}C\right)\rho \tag{20.5}$$

$$\psi_{32}^{(\alpha^2)}(\rho) = \frac{813}{6125}\frac{1}{\rho^3} + \frac{27}{175}\frac{1}{\rho} - \frac{9}{80}\rho\log\rho + \left(\frac{27}{320} - \frac{9}{80}C\right)\rho \tag{20.6}$$

and

$$\psi_{00}^{(\alpha f)}(\rho) = \frac{4}{5}\log\rho - \frac{3}{2}\rho^2\log\rho + \left(\frac{3}{2} - \frac{3}{4}C\right)\rho^2 \tag{21.1}$$

$$\psi_{10}^{(\alpha f)}(\rho) = \frac{3}{2}\rho\log\rho - \frac{3}{4}\rho \tag{21.2}$$

$$\psi_{20}^{(\alpha f)}(\rho) = \frac{27}{35}\frac{1}{\rho^2} - \frac{1}{2}\log\rho - \frac{3}{4} \tag{21.3}$$

$$\psi_{22}^{(\alpha f)}(\rho) = -\frac{9}{70}\frac{1}{\rho^2} - \frac{1}{4}\log\rho + \frac{1}{8} \tag{21.4}$$

$$\psi_{30}^{(\alpha f)}(\rho) = \frac{54}{35}\frac{1}{\rho^3} - \frac{3}{10}\frac{1}{\rho} \tag{21.5}$$

$$\psi_{32}^{(\alpha f)}(\rho) = -\frac{27}{175}\frac{1}{\rho^3} + \frac{3}{20}\frac{1}{\rho} \tag{21.6}$$

However,

$$\psi_{00}^{(f^2)}(\rho) = \psi_{10}^{(f^2)}(\rho) = \psi_{20}^{(f^2)}(\rho) = \psi_{22}^{(f^2)}(\rho) = \psi_{30}^{(f^2)}(\rho) = \psi_{32}^{(f^2)}(\rho) = 0 \tag{22}$$

The only unknown integration constant C, in solutions 17 to 21, must be determined from the boundary condition, Equation 7. However, here again, the determination of extrapolation length a is of more interest. If this length be determined as

$$d = \left\{C + \log a + \frac{1}{5}\alpha\log a - f\log a - \frac{4}{175}\alpha^2\log a + \frac{4}{5}\alpha f\log a\right\} : \frac{1}{a}\left\{1 + \frac{1}{5}\alpha - f - \frac{4}{175}\alpha^2 + \frac{4}{5}\alpha f\right\}$$

then from the condition of Equation 7, it follows that

$$d = \frac{2}{3}\left\{1 + \frac{1}{5}\alpha - f + \frac{4}{5}\alpha f - \frac{4}{175}\alpha^2\right\}^{-7} + \cdots \tag{23}$$

in which we will ignore terms which are functions of radius a. We have done this since spherical harmonic analysis, which we are using, does not give a very good evaluation (which, incidentally, also follows from the preceding part of Reference 2).

If we now change from a unit length for which $\Sigma_s = 1$ to normal unit lengths, we can rewrite Equation 23 in the following form:

$$D = \frac{1}{3}\frac{1}{\Sigma(1-f)}\cdot\left\{1 - \frac{4}{5}\frac{\Sigma_a}{\Sigma} + \frac{\Sigma_a\cdot f}{\Sigma(1-f)} - \frac{4}{175}\frac{\Sigma_a^2}{\Sigma\Sigma_s(1-f)}\right\}^{-7} \tag{24}$$

Here we have introduced the term $\Sigma = \Sigma_s + \Sigma_a$. From this equation, it further follows that, for practical purposes, the extrapolation length in a cylindrical black body may be calculated from the equation

$$d = \lambda(\Sigma_s a)\cdot 3D \tag{25}$$

in which function $\lambda(\Sigma_s a)$ is determined from curve 2 of Reference 2, and D is the diffusion coefficient in the subject space whose cross sections for neutrons are Σ_s, Σ_a, and whose average cosine of the scattering angle for neutrons is f. For small values of α, f, constant D is determined by the equation

$$d = \frac{2}{3}\cdot\frac{1}{\Sigma(1-f)}\cdot\left\{1 - \frac{4}{5}\frac{\Sigma_a}{\Sigma} + \frac{\Sigma_a}{\Sigma}\frac{f}{1-f} - \frac{4}{175}\frac{\Sigma_a^2}{\Sigma\Sigma_s(1-f)}\right\}^{-7} \tag{26}$$

which also agrees with the diffusion coefficient determined in Reference 3.

REFERENCES

1. Marshak, R. E., Phys. Rev. *71*, 443 (1947).
2. Davison, B., Phys. Soc. Proc. A 64, 881 (1951).
3. Glasstone, S., Edlund, M. C., *The elements of nuclear reactor theory*, Toronto-New York-London (1952).

Solution of the Generalized Milne Problem

By G. A. Bat and D. F. Zaretsky, USSR

The subject studied is the density distribution of monochromatic neutrons in two halfspaces divided by a plane boundary. Media with arbitrary capture and multiplication, scattering neutrons according to the law $1 + f\mu_0$ are considered. An integral equation for determining neutron density is deduced. An exact analytical solution of that equation is found by means of the Wiener-Hopf method.

I

In a great number of neutron-diffusion problems one needs knowledge of the neutron-density distribution near the interface of two media, the effective boundary conditions, the albedo, etc.

The anisotropy of the elementary act of neutron scattering makes calculations very difficult.

For solving kinetic equations with anisotropy one generally uses the approximative method of Wick or the method of spherical harmonics. In the last method both the function of neutron distribution in the space and directions of flight, and the scattering function determining the anisotropy in the act of collision of the neutron with the nucleus are expanded into the Legendre series.

Moreover, the kinetic equation becomes equivalent to an infinite system of recurrent differential equations for angle moments of the distribution function. To secure an approximate solution of this system, one leaves a finite number of polynomials in the expansion and considers a finite number of equations together with boundary conditions.

In order to verify such approximate methods it is interesting to find a more exact method of solving problems with anisotropy.

But the analytical methods of finding the neutron density distribution have been developed, as far as we know, only for the case of two halfspaces divided by a plane boundary. For geometrically more complex problems it is necessary to develop effective quantitative methods which make it possible to determine interesting practical quantities with a sufficient degree of accuracy.

This paper deals with problems with a function of distribution depending on one angle variable. The method of deducing an integral equation for the neutron density shown here is applicable in a case when the scattering function is given by a sum of a finite number of Legendre polynomials. An exact solution for the density of neutrons is found for the case of two halfspaces with an arbitrary absorption, arbitrary multiplication and with a scattering law $1 + f\mu_0$.

II

The kinetic equation for the function of distribution $\Psi(\vec{r},\vec{\Omega})$ of monochromatic neutrons may be written from the balance of particles for the whole of volume V which is under consideration:

$$\Psi(\vec{r},\vec{\Omega}) = \int e^{-\rho}\, d\rho \left\{ \frac{\nu}{\lambda_c} \int \Psi(\vec{r}',\vec{\Omega}') \frac{d\vec{\Omega}'}{4\pi} + \frac{1}{\lambda_s} \int \Psi(\vec{r},\vec{\Omega}') \cdot F(\vec{\Omega},\vec{\Omega}') \frac{d\vec{\Omega}'}{4\pi} \right\} \quad (1)$$

In Equation 1 all lengths are measured in units λ of the total length of the free neutron path. The total length, as well as all the other characteristics of the media, in question, may be different in different regions of the volume V. That is why the space intervals $\rho = |r - r'|$ in regions with different paths λ, are measured in units of suitable total lengths.

In the following we will use notations: λ_c and λ_s are the lengths of free neutron path correspondingly for capture and multiplication,

$$\frac{1}{\lambda} = \frac{1}{\lambda_c} + \frac{1}{\lambda_s}$$

ν is the coefficient of multiplication (the average number of neutrons appearing in one act of capture); and $F(\vec{\Omega},\vec{\Omega}')$ the scattering function determining the probability, that in the process of scattering the direction of flight of the neutron will change from $\vec{\Omega}'$ to $\vec{\Omega}$.

The scattering function is normalized by the condition

$$\int F(\vec{\Omega},\vec{\Omega}') \frac{d\vec{\Omega}'}{4\pi} = \int F(\vec{\Omega},\vec{\Omega}') \frac{d\vec{\Omega}}{4\pi} = 1 \quad (2)$$

in virtue of which in the expansion

$$F(\vec{\Omega},\vec{\Omega}') = F(\mu_0) = \sum_l (2l + 1) f_l P_l(\mu_0) \quad (3)$$

the coefficient $f_0 = 1$.

Original language: Russian.

Let us introduce notations:

$$\mu = \cos\Theta$$
$$\mu' = \cos\Theta'$$
$$h = \lambda\left(\frac{\nu}{\lambda_c} + \frac{1}{\lambda_s}\right)$$
$$f_0' = 1$$
$$f_l' = \frac{f_l}{1 + \nu\dfrac{\lambda_s}{\lambda_c}}$$

when $l > 0$. Using the relation

$$P_l(\mu_0) = P_l(\mu)P_l(\mu') + 2\sum_{m=1}^{l}\frac{(l-m)!}{(l+m)!}P_l^{(m)}(\mu), \qquad P_l^{(m)}(\mu')\cos(\varphi - \varphi')$$

for problems, where $\Psi(r,\vec{\Omega}) \equiv \Psi(r,\mu)$, we will have

$$\Psi(r,\mu) = \tfrac{1}{2}\sum_l (2l+1)P_l(\mu) \int f_l' h \cdot e^{-\rho}\, d\rho \times \Psi_l(r') \quad (4)$$

it being known that

$$\Psi_l(r) = \int P_l(\mu)\Psi(r,\mu)\, d\mu \quad (5)$$

Integrating Equation 4 with μ as a variable we will have for the zero moment the expression

$$\Psi_0(r) = \tfrac{1}{2}\sum_l (2l+1)\iint f_l' h \Psi_l(r')P_l(\mu)e^{-\rho}\, d\rho\, d\mu \quad (6)$$

Equation 6 gives the relation between the neutron density $\Psi_0(r)$ and higher moments of the distribution function. It is obvious that the sum in the right part contains the same quantity of terms as Equation 3.

Another relation between moments may be found from Boltzmann's kinetic equation. Having in mind to use the results of this section farther, we will discuss circumstantially the case of two halfspaces, divided by a flat boundary. Boltzmann's equation may be written as follows:

$$\mu\frac{\partial\Psi(z,\mu)}{\partial z} + \Psi(z,\mu) = \frac{\nu}{2\lambda_c}\int \Psi(z,\mu')\, d\mu' + \frac{1}{\lambda_s}\int \Psi(z,\mu')F(\vec{\Omega},\vec{\Omega}')\frac{d\vec{\Omega}'}{4\pi} \quad (7)$$

If we write down the expansion of the distribution function into Legendre series

$$\Psi(z,\mu) = \tfrac{1}{2}\sum_{l=0}^{\infty}\Psi_l(z)(2l+1)\cdot P_l(\mu) \quad (8)$$

then Equation 7 may be substituted by an infinite system of differential equations:

$$k\frac{d\Psi_{k-1}(z)}{dz} + (k+1)\frac{d\Psi_{k+1}(z)}{dz} = (2k+1)\cdot(f_k'h - 1)\Psi_k(z) \quad (9)$$

Then Equation 6 for our case may be written as follows:

$$\Psi_0(z) = \frac{h_2}{2}\sum_l (2l+1)f_{l2}'\int_{-\infty}^{0}\Psi_l(z')K_l(z,z')\, dz' + \frac{h_1}{2}\sum_l (2l+1)f_{l1}'\int_0^{\infty}\Psi_l(z')K_l(z,z')\, dz' \quad (10)$$

where

$$K_l(z,z') = \int_{z-z'}^{\infty} e^{-\rho}P_l\left(\frac{z-z'}{\rho}\right)\frac{d\rho}{\rho} \quad (11)$$

Integrating Equation 10 by parts and using Equation 9 we can express the moments Ψ_l in terms of neutron density and obtain an equation for Ψ_0. This equation becomes rapidly cumbersome when the quantity of terms left in the expansion of Equation 3 increases. As we intend in obtaining an analytical solution to consider only the law $1 + f\mu_0$ of the anisotropy of scattering, it is enough to write the equation with $f_l = 0$ when $l \geq 2$;

$$\Psi_0(z) = \frac{h_2}{2}\int_{-\infty}^{0} dz'\Psi_0(z')E_1(|z-z'|) + \frac{h_1}{2}\int_0^{\infty} dz'\Psi_0(z')E_1(|z-z'|) + \frac{3h_2}{2}(1-h_2)f_2' \int_{-\infty}^{0} dz'\Psi_0(z')E_3(|z-z'|) + \frac{3h_1}{2}(1-h_1) \times f_1'\int_0^{\infty} dz'\Psi_0(z')E_3(|z-z'|) - \frac{3}{2}\Psi_1(0)[h_1f_1' + h_2f_2']E_3(|z|) \quad (12)$$

where

$$E_n(x) = \int_1^{\infty}\frac{e^{-xt}}{t^n}\, dt \quad (13)$$

III

We shall make the Laplace transformation of Equation 12, introducing functions:

$$F_0^+(w) = \int_0^{\infty}\Psi_0(z)e^{-wz}\, dz \qquad F_0^-(w) = \int_{-\infty}^{0}\Psi_0(z)e^{-wz}\, dz \quad (14)$$

Then we shall have

$$F_0^+(w) + F_0^-(w) = h_1\frac{\operatorname{arc\,th} w}{w}F_0^+(w) + h_2\frac{\operatorname{arc\,th} w}{w}F_0^-(w) - \frac{3h_1(1-h_1)f_1'}{w^2}\left(1 - \frac{\operatorname{arc\,th} w}{w}\right)F_0^+(w) - \frac{3h_2(1-h_2)f_2}{w^2}\times\left(1 - \frac{\operatorname{arc\,th} w}{w}\right)F_0^-(w) + \frac{3(h_1f_1' + h_2f_2')}{w^2}\left(1 - \frac{\operatorname{arc\,th} w}{w}\right)\Psi_1(0) \quad (15)$$

Obviously, the transformation is possible only in the region $\kappa_1 < |\mathrm{Re}\ w < \kappa_2$, where $\kappa_{1,2}$ are the first roots of the transcendental equations:

$$K_{1,2}(w) = 0$$

$$K_{1,2} = 1 - h_{1,2}\frac{\operatorname{arc\,th} w}{w} + \frac{3h_{1,2}(1-h_{1,2})f_{1,2}'}{w^2}\left(1 - \frac{\operatorname{arc\,th} w}{w}\right) \quad (16)$$

The quantities $\kappa_{1,2}$ determine the behaviour of the function $\Psi_0(z)$ in the region far from the interface. If the neutron flux falls from infinity in medium "1", then

$$\Psi_0^{ac} \underset{z>0}{\sim} C_1^+ e^{\kappa_1 z} + C_1^- e^{-\kappa_1 z}$$

$$\Psi_0^{ac} \underset{z<0}{\sim} C_2^+ e^{\kappa_2 z} \quad (17)$$

We hold that $h_1 > h_2$ because in that case there is one common region where both functions $F_0^-(w)$ and $F_0^+(w)$ are regular. The case $h_1 < h_2$ shall be considered separately. We may note that $F_0^+(w)$ is regular, when $\mathrm{Re}\ w > \kappa_1$ and $F_0^-(w)$ is regular, when $\mathrm{Re}\ w < \kappa_2$. Equation 15 may be written down as follows:

$$\Phi^+(w)K_1(w) = -\Phi^-(w)K_2(w) \quad (18)$$

where

$$\Phi^+(w) = F_0^+(w)\{h_1(1-h_2)[w^2 + 3f_1'(1-h_1)] - h_2(1-h_1)[w^2 + 3f_2'(1-h_2)]\} - 3\Psi_1(0)(1-h_2)(h_1f_1' + h_2f_2') \quad (19)$$

$$\Phi^-(w) = F_0^-(w)\{h_1(1-h_2)[w^2 + 3f_1'(1-h_1)] - h_2(1-h_1)[w^2 + 3f_2'(1-h_2)]\} + 3\Psi_1(0)(1-h_2)(h_1f_1' + h_2f_2') \quad (20)$$

Relations for Laplace transforms may be also deduced immediately from Boltzmann's Equation 7.

When $z > 0$, we may write for the chosen scattering function, as follows

$$F^+(w,\mu) = \frac{1}{1+\mu w}\left\{\frac{h_1}{2}F_0^+(w) + \mu\Psi(0,\mu) + \frac{3}{2}f_1'\frac{\mu}{w}h_1 \times [\Psi_1(0) - (1-h_1)F_0^+(w)]\right\} \quad (21)$$

where

$$F^+(w,\mu) = \int_0^\infty \Psi(z,\mu)e^{-wz}\,dz$$

If we integrate Equation 21 with μ as a variable, in the interval $1 \geq \mu \geq -1$, then

$$F^+(w)\left\{1 - h_1\frac{\operatorname{arc\,th} w}{w} + \frac{3h_1(1-h_1)f_1'}{w^2}\left(1 - \frac{\operatorname{arc\,th} w}{w}\right)\right\} - \frac{3h_1f_1'\Psi_1(0)}{w^2}\left(1 - \frac{\operatorname{arc\,th} w}{w}\right) = \int_{-1}^{+1}\frac{\mu\Psi(0,\mu)}{1+\mu w}\,d\mu \quad (22)$$

An absolutely analogous expression may be written for the function $F_0^-(w)$.

Comparing Equations 22 and 15 we find that

$$-\Psi_1(0) \equiv -\int_{-1}^{+1}\mu\Psi(0,\mu)\,d\mu = F_0^-(0)[(1-h_2) - h_2(1-h_2)f_2'] + h_2f_2'\Psi_1(0)$$

$$F_0^-(0) = \frac{\Psi_1(0)(1+h_2f_2')}{(1-h_2)(1-f_2f_2')} \quad (23)$$

IV

Let us use the Wiener-Hopf method for solving Equation 18. We will introduce auxiliary functions:

$$\tau_1(w) = \frac{w^2-1}{w^2-\kappa^2}K_1(w) \qquad \tau_2(w) = \frac{w^2-1}{w^2-\kappa^2}K_2(w) \quad (24)$$

The functions $\tau_{1,2}$ cannot be equal to zero in the interval $-1 < \mathrm{Re}\ w < 1$ and tend to become equal to 1 in the same interval when $|w| \to \infty$.

Let us choose the branch of the function $\ln \tau(w)$, for which $\ln 1 = 0$. Therefore $\ln \tau(w) \to 0$ when $|w| \to \infty$ in the interval $-1 < \mathrm{Re}\ w < 1$ and is regular in that interval, then according to Cauchy's theorem

$$\ln \tau(w) = \frac{1}{2\pi i}\int_{\beta-i\infty}^{\beta+i\infty}\frac{\ln\tau(z)}{z-w}\,dz - \frac{1}{2\pi i}\int_{-\beta-i\infty}^{-\beta+i\infty}\frac{\ln\tau(z)}{z-w}\,dz \qquad 0 < \beta < 1 \quad (25)$$

Let us introduce two functions τ_+ and τ_-

$$\tau_-(w) = \exp\left[\frac{1}{2\pi i}\int_{-\beta-i\infty}^{-\beta+i\infty}\frac{\ln\tau(z)}{z-w}\,dz\right]$$

$$\mathrm{Re}\ w > -\beta \qquad \tau_+(w) = \exp\left[\frac{1}{2\pi i}\int_{\beta-i\infty}^{\beta+i\infty}\frac{\ln\tau(z)}{z-w}\,dz\right] \qquad \mathrm{Re}\ w < \beta \quad (26)$$

Then we shall have

$$\ln\tau(w) = \ln\tau_+(w) - \ln\tau_-(w) \qquad \tau(w) = \frac{\tau_+(w)}{\tau_-(w)} \quad (27)$$

The function $\tau_-(w)$ is regular when $\mathrm{Re}\ w > -\beta$ and $|\tau_-(w)| > 0$ when $\mathrm{Re}\ w > -\beta' > -\beta$. Accordingly $\tau_+(w)$ is regular when $\mathrm{Re}\ w < \beta$ and $|\tau_+(w)| > 0$ when $\mathrm{Re}\ w < \beta' < \beta$.

Consequently we may write instead of Equation 18

$$\Phi^+(w)\frac{w^2-\kappa_1^2}{w+\kappa_2}\frac{\tau^{(2)}(w)}{\tau^{(1)}(w)} = -\Phi(w)(w-\kappa_2)\frac{\tau_+^{(2)}(w)}{\tau_+^{(1)}(w)} \quad (28)$$

It follows from the definition of the functions that form Equation 28 that the left part of the equation is

regular when Re $w > \kappa_1$ and the right part is regular when Re $w < \kappa_2$. As we have $\kappa_2 > \kappa_1$ these halfplanes overlap in the region $\kappa_1 < \text{Re } w < \kappa_2$ and it follows that the left part of Equation 28 is the analytical continuation of the right and vice versa. That means that the right and left parts are expressions of only one function, regular in all the plane w.

If we take into account that functions $F^+(w)$ and $F^-(w)$ behave as $1/w$, when $|w| \to \infty$ and that $\tau_+(w)$ and $\tau_-(w)$ are nowhere equal to zero, then according to the theorem of Liouville we shall have

$$\Phi^+(w)\frac{w^2-\kappa_1^2}{w-\kappa_2}\frac{\tau_-^{(2)}(w)}{\tau_-^{(1)}(w)} = -\Phi^-(w)(w-\kappa_2)\frac{\tau_+^{(2)}(w)}{\tau_+^{(1)}(w)} = c_0 + c_1 w + c_2 w^2 \quad (29)$$

The inverse transformation from the variable w to z gives us

$$\underset{\substack{z>0\\ \sigma_1>\kappa_1}}{\Psi_0(z)} = \frac{1}{2\pi i}\int_{\sigma_1-i\infty}^{\sigma_1+i\infty} e^{wz}\,dw\,\Lambda(w)\left\{(c_0+c_1w+c_2w^2)\frac{\tau_-^{(1)}(w)}{\tau_-^{(2)}(w)}\frac{w+\kappa_2}{w^2-\kappa_1^2} + 3\Psi_1(0)(1-h_2)(h_1f_1'+h_2f_2')\right\} \quad (30)$$

$$\underset{\substack{z<0\\ \sigma_1<\kappa_1}}{\Psi_0(z)} = \frac{1}{2\pi i}\int_{\sigma_1-i\infty}^{\sigma_1+i\infty} e^{wz}\,dw\,\Lambda(w)\left\{(c_0+c_1w+c_2w^2)\frac{\tau_+^{(1)}(w)}{\tau_+^{(2)}(w)}\frac{1}{w-\kappa_2} + 3\Psi_1(0)(1-h_2)(h_1f_1'+h_2f_2')\right\} \quad (31)$$

where

$$\Lambda(w) = \{h_1(1-h_2)[w^2-3f_1'(1-h_1)] - h_2(1-h_1)[w^2+3f_2'(1-h_2)]\}^{-1} \quad (32)$$

V

We shall now proceed to determine the coefficients c_0, c_1 and c_2. First of all let us surmise that $w = 0$ in Equation 29 and let us compare the result with Equation 23. Using the definition (Equation 19) of the function $\Phi^-(w)$ we shall have

$$c_0 = \kappa_2\frac{\tau_+^{(2)}(0)}{\tau_+^{(1)}(0)}\,6\Psi_1(0)(1-h_1)h_2f_2'\,\frac{1-h_1f_1'}{1-h_2f_2} \quad (33)$$

If we note the known properties of the functions $\tau, \tau_\pm$:

$$\tau_+(w)\tau_-(-w) = 1 \qquad \tau_-(-w) = \frac{1}{\tau_+(w)} = \frac{1}{\tau(w)\tau_-(w)} \quad (34)$$

$$\tau(0) = \frac{(1-h)(1-hf')}{\kappa^2} \qquad \tau_+(0) = \sqrt{\tau(0)} \qquad \tau_-(0) = \frac{1}{\sqrt{\tau(0)}} \quad (35)$$

and introduce Equation 35 in the expression for c_0, then

$$c_0 = \frac{\kappa_1^2}{\kappa_2}\,6h_2f_2'(1-h_2)\Psi_1(0) \quad (36)$$

Let us further note that with $|z| \gg 1$ the asymptotical expressions for $\Psi_0(z)$ may contain only terms of the form $e^{\kappa z}$. That is why residues of the integrants in Equations 30 and 31 have to be equal to zero, when

$$w = \pm\sqrt{-\frac{3(1-h_1)(1-h_2)(h_1f_1'-h_2f_2')}{h_1-h_2}} \equiv \pm i\gamma \quad (37)$$

Therefore we have two pairs of equations for determining the coefficients c_1 and c_2. It is easy to prove that these two pairs are self-equivalent. Using Equation 30 we shall have

$$(i\gamma)c_1 = \frac{3}{2}\Psi_1(0)(1-h_2)(h_1f_1'+h_2f_2')(\gamma^2+\kappa_1^2) \times\left[\frac{\tau_-^{(2)}(i\gamma)}{\tau_-^{(1)}(i\gamma)}\frac{1}{i\gamma+\kappa_2} - \frac{\tau_-^{(2)}(-i\gamma)}{\tau_-^{(1)}(-i\gamma)}\frac{1}{-i\gamma+\kappa_2}\right]$$

$$(i\gamma)^2c_2 = -6\Psi_1(0)(1-h_2)\left\{h_2f_2'\frac{\kappa_1^2}{\kappa_2} - \frac{1}{4}(h_1f_1'+h_2f_2')(\kappa^2+\kappa_1^2) \times\left[\frac{\tau_-^{(2)}(i\gamma)}{\tau_-^{(1)}(i\gamma)}\frac{1}{i\gamma+\kappa_2} + \frac{\tau_-^{(2)}(-i\gamma)}{\tau_-^{(1)}(-i\gamma)}\frac{1}{-i\gamma+\kappa_2}\right]\right\} \quad (38)$$

We shall find the asymptotical expressions for $\Psi_0(z)$ by computing the residues of the integrants in Equations 30 and 31 corresponding to $w = \kappa_2, \kappa_1, -\kappa_1$

$$\underset{z>0}{\Psi_0^{ac}(z)} = \frac{\Lambda(\kappa_1)}{2\kappa_1}\left\{(\kappa_1+\kappa_2)\frac{\tau_-^{(1)}(\kappa_1)}{\tau_-^{(2)}(\kappa_1)}(c_0+c_1\kappa_1+c_2\kappa_1^2)e^{\kappa_1 z} + (\kappa_1-\kappa_2)\frac{\tau_-^{(1)}(-\kappa_1)}{\tau_-^{(2)}(-\kappa_1)}(c_0-c_1\kappa_1+c_2\kappa_1^2)e^{-\kappa_1 z}\right\} \equiv C_{11}^+e^{\kappa_1 z} + C_{11}^-e^{-\kappa_1 z} \quad (39)$$

$$\underset{z<0}{\Psi_0^{ac}} = \Lambda(\kappa^2)\frac{\tau_+^{(1)}(\kappa_2)}{\tau_+^{(2)}(\kappa_2)}(c_0+c_1\kappa_2+c_2\kappa_2^2)e^{\kappa_2 z} \equiv C_{12}^+e^{\kappa_2 z} \quad (40)$$

VI

Equations 30 and 31 give the solution of the problem for the considered case $h_1 > h_2$. If the neutron flux falls from a medium less active in a medium more active ($h_1 < h_2$) then there is no common region, where functions $F^+(w)$ and $F^-(w)$ are regular, and our analysis, in general, is not applicable.

One can show, however, that the solution of the problem even when $h_1 < h_2$ may be written down in the form of Equations 30 and 31.

We shall use the following theorem:

Let us assume that $\xi(w)$ is regular in the band $a_1 \le \text{Re } w \le a_2$ and tends to become zero when $|w| \to \infty$ in that band and that $\zeta(w)$ has analogous properties in the band $b_1 \le \text{Re } w \le b_2$, $b_2 < a_1$. If

$$\int_{a-i\infty}^{a+i\infty}\xi(w)e^{wz}\,dw + \int_{b-i\infty}^{b+i\infty}\zeta(w)e^{wz}\,dw = 0$$

for any Z and for $a_1 < a < a_2$, $b_1 < b < b_2$, then

$\xi(w)$ and $\zeta(w)$ are regular in the band $b_1 < \mathrm{Re}\, w < a_2$, the sum of these functions is equal to zero in this band and with $|w| \to \infty$ they tend to zero uniformly in each internal band.

Let us now express Equation 12 in a form suitable for using the theorem above mentioned. We shall make the Laplace transformation of the integrals in the right part of the equation. After the transformation we shall have in the region "1"

$$F_0^+(w)[1 - K_1(w)] + \frac{3\Psi_1(0)f_1'}{w^2 + 3f_1'(1 - h_1)}[K_1(w) - (1 - h_1)]$$

and in the region "2"

$$F_0^-(w)[1 - K_2(w)] + \frac{3\Psi_1(0)f_2'}{w^2 + 3f_2'(1 - h_2)}[K_2(w) - (1 - h_2)]$$

According to the definition of functions $F^{\pm}(w)$ and $K_{1,2}(w)$ the first transformation is possible only in the band $\kappa_1 < \mathrm{Re}\, w < 1$ and the second in the band $-1 < \mathrm{Re}\, w < \kappa_2$.

We may now write down Equation 12 in the form

$$\int_{\sigma_1-i\infty}^{\sigma_1+i\infty} \left\{F_0^+(w)K_1(w) - \frac{3\Psi_1(0)f_1'}{w^2 + 3f_1'(1 - h_1)}[K_1(w) - (1 - h_1)]\right\} e^{wz}\, dw$$

$$= -\int_{\sigma_1-i\infty}^{\sigma_1+i\infty} \left\{F_0^-(w)K_2(w) - \frac{3\Psi_1(0)f_1'}{w^2 + 3f_2'(1 - h_2)}[K_2(w) - (1 - h_2)]\right\} e^{wz}\, dw$$

where $\kappa_1 < \sigma_1 < 1$; $-1 < \sigma_2 < \kappa_2$.

The conditions of the theorem above mentioned are fulfilled when $|w| \to \infty$ and accordingly

$$F_0^+(w)K_1(w) - \frac{3\Psi_1(0)f_1'}{w^2 + 3f_1'(1 - h_1)}[K_1(w) - (1 - h_1)]$$

$$= -F_0^-(w)K_2(w) + \frac{3\Psi_1(0)f_2'}{w^2 + 3f_2'(1 - h_2)}[K_2(w) - (1 - h_2)] \quad (41)$$

$$\kappa_2 \leq \mathrm{Re}\, w \leq \kappa_1$$

It is easy to remark that using functions $\Phi^{\pm}(w)$ and $\tau(w)$ we may easily express Equation 41 in the form of Equation 28 and that according to the same theorem the left and right parts of the equation will have a common region of regularity.

Accordingly, the form of the solution is suitable for any relation between h_1 and h_2.

VII

We have considered the case when the neutron flux is directed from the medium "1" to the medium "2." The solution may be written for the case when the flux falls from medium "2" to medium "1," simply by transposing the indexes of the media.

A general solution is a linear combination of these two solutions.

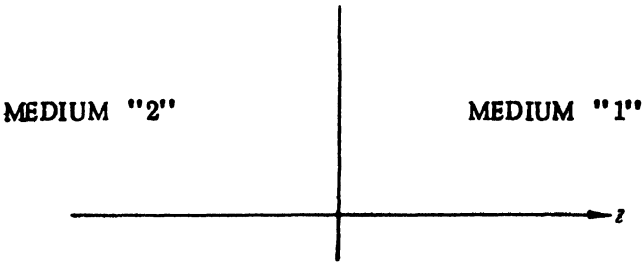

Figure 1

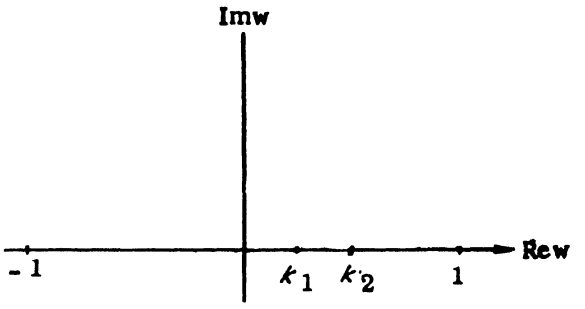

Figure 2

We may write down the asymptotical solution in the form

$$\underset{z>0}{\Psi_0^{ac}(z)} = C_{11}^+ e^{\kappa_1 z} + C_{11}^- e^{-\kappa_2 z} \quad \text{and}$$

$$\underset{z<0}{\Psi_0^{ac}(z)} = C_{21}^+ e^{\kappa_2 z}$$

if the flux is directed from the medium "1" to the medium "2," and in the form

$$\underset{z>0}{\Psi_0^{ac}(z)} = C_{12}^- e^{-\kappa_1 z} \quad \text{and}$$

$$\underset{z<0}{\Psi_0^{ac}(z)} = C_{22}^+ e^{\kappa_2 z} + C_{22}^- e^{-\kappa_2 z}$$

if the flux is directed from the medium "2" to the medium "1."

Then the general solution may be expressed as follows:

$$\underset{z>0}{\Psi_0^{ac}(z)} = C_1' C_{11}^+ e^{\kappa_1 z} + \{C_1' C_{11}^- + C_2' C_{21}^-\} e^{-\kappa_1 z}$$

$$\underset{z<0}{\Psi_0^{ac}(z)} = \{C_1' C_{21}^+ + C_2' C_{22}^+\} e^{\kappa_2 z} + C_2' C_{22}^- e^{-\kappa_2 z} \quad (42)$$

where C_1', C_2' are arbitrary constants.

Let us note that

$$C_{12}^- = \frac{2C_{11}^-}{1 - \frac{\kappa_2}{\kappa_1}} \quad \text{and} \quad C_{21}^+ = \frac{2C_{22}^+}{1 - \frac{\kappa_1}{\kappa_2}} \quad (43)$$

and rewrite Equation 42 in the form

$$\underset{z>0}{\Psi_0^{ac}(z)} = \varphi_1 \left[A \operatorname{ch} \kappa_1(z - z_1) + \frac{B}{\kappa_1} \operatorname{sh} \kappa_1(z - z_1)\right]$$

$$\underset{z<0}{\Psi_0^{ac}(z)} = \varphi_2 \left[A \operatorname{ch} \kappa_2(z + z_2) + \frac{B}{\kappa_2} \operatorname{sh} \kappa_2(z + z_1)\right] \quad (44)$$

where

$$A = C_1' + C_2' \quad \text{and} \quad B = C_1'\kappa_2 - C_2'\kappa_1$$

$$\varphi_1^2 = \frac{C_{11}^+ - C_{11}^-}{1 - \left(\frac{\kappa_2}{\kappa_1}\right)^2} \quad \text{and} \quad \varphi_2^2 = \frac{C_{22}^+ C_{22}^-}{2 - \left(\frac{\kappa_1}{\kappa_2}\right)^2} \tag{45}$$

$$z_1 = \frac{1}{2\kappa_1} \ln \frac{C_{11}^-}{C_{11}^+} \quad \text{and} \quad z_2 = \frac{1}{2\kappa_2} \ln \frac{C_{22}^-}{C_{22}^+} \tag{46}$$

Excluding A and B we shall have boundary conditions for the asymptotic functions in the form:

$$\left.\frac{\Psi_0^{ac}(z)}{\varphi_1}\right|_{z=z_1} = \left.\frac{\Psi_0^{ac}(z)}{\varphi_2}\right|_{z=-z_2} \tag{47}$$

$$\left.\frac{d \ln \Psi_0^{ac}(z)}{dz}\right|_{z=z_1} = \left.\frac{d \ln \Psi_0^{ac} z)}{dz}\right|_{z=-z_2} \tag{48}$$

The condition of Equation 47 depicts the jump of the asymptotic neutron densities in "extrapolated points" z_1 and $-z_2$, the condition of Equation 48 depicts the fact that the logarithmic derivatives in these points are equal.

VIII

We shall use the properties of the functions $\tau_+(w)$ to compute the quantities $z_{1,2}$, $\varphi_{1,2}$. The function $\tau_-(w)$ may be expressed for the case, when Re $w > 0$, as an integral taken along the real axis. Displacing the line of integration in the first of the formulas (Equation 26) in the direction of the imaginary axis ($\beta = 0$) and making the substitution $z = it$, we shall have

$$\underset{\mathrm{Re}\, w>0}{\ln \tau_-(w)} = \frac{w}{\pi} \int_0^\infty \frac{dt}{t^2 + u^2} \ln \left\{ \frac{t^2 + 1}{t^2 + \kappa^2} \left[1 - h \frac{\operatorname{arc\,tg}\, t}{t} - \frac{3h(1-h)f'}{t^2} \left(1 - \frac{\operatorname{arc\,tg}\, t}{t} \right) \right] \right\} \tag{49}$$

For imaginary quantities, $w = is$, one must take the principal value of the integral (Equation 49) adding a halfcircuit above the point $t = s$.

Using the relations of Equation 34, we may express $\tau_-(-w)$ and $\tau_+(w)$ through $\tau_-(w)$.

Thus, the problem of finding effective boundary conditions is reduced to the computing of integrals.

In conclusion we should like to state the following:

We find the asymptotic neutron density Ψ_0^{ac} as a solution for an equation of the diffusive type

$$\Delta \Psi_0^{ac} - \kappa_{1,2}^2 \Psi_0^{ac} = 0 \tag{50}$$

with boundary conditions given in Equations 47 and 49. The constants $\kappa_{1,2}$ determining the behaviour of the asymptotic density, are found as the roots of Equation 16 and are nothing else than inverse lengths of diffusion measured in units of the total free path length λ.

For small absorptions we have

$$\kappa \simeq \sqrt{3(1-h)(1-f)}$$

a result known in the diffusion theory.

Accepting one of the halfspaces as "absolutely black" and the other as nonabsorbing, we shall also have a known result; the asymptotic neutron density becomes equal to zero on the distance $0.71\lambda_{tr}$ from the interface (λ_{tr} is the transport free path length).

We may also note that we left only two terms in the expansion of the scattering function merely in order to simplify calculations. The method may be generalized for any quantity of terms in Equation 3.

Effective Boundary Conditions for "Grey" Bodies

By D. F. Zaretsky, USSR

INTRODUCTION

"Grey" bodies are called here those which unlike "black" ones do not absorb all the neutrons incident on their surface.

"Greyness" may be due to two reasons:

1. Neutrons scattering inside the body; then part of the neutrons falling on the body from the surrounding medium return to that medium.

2. Passage of the neutrons through the absorbing body, if its diameter is not too large compared with the total mean free path in the body substance.

We shall examine here only the second effect and shall neglect scattering in the body compared with capture.

Most interesting from the practical standpoint are the spherical and cylindrical bodies. And the present paper examines approximate methods of finding effective boundary conditions for these cases. It will be assumed that the body is placed in an infinite isotropically scattering nonabsorbing medium in which a stationary flux of monochromatic neutrons is maintained. Our examination begins with the simplest case of spherical geometry.

1. EFFECTIVE BOUNDARY CONDITIONS FOR A "GREY" SPHERE

The Peierls neutron density equation will in this case have the following form:

$$n(r) = \frac{1}{2\lambda_s^{cp}} \int_a^\infty n(r')r'^2\,dr' \times \int_0^{\arccos a/r + \arccos a/r'} \exp\left[-\frac{\sqrt{r'^2 + r^2 - 2rr'\cos\theta}}{\lambda_s^{cp}}\right] \frac{\sin\theta\,d\theta}{r'^2 + r^2 - 2rr'\cos\theta} + \frac{1}{2\lambda_s^{cp}} \int_a^\infty n(r')r'^2\,dr' \int_{\arccos a/r + \arccos a/r'}^{\pi} \exp\left[-\frac{\sqrt{r'^2 + r^2 - 2rr'\cos\theta}}{\lambda_s^{cp}} - 2\left(\frac{1}{\lambda} - \frac{1}{\lambda_s^{cp}}\right)\sqrt{a^2 - \frac{r^2r'^2\sin^2\theta}{r'^2 + r^2 - 2rr'\cos\theta}}\right] \frac{\sin\theta\,d\theta}{r'^2 + r^2 - 2rr'\cos\theta} \quad (1)$$

where λ_s^{cp} is the scattering mean free path in the medium, and λ is the neutron total mean free path in the sphere.

Original language: Russian.

It will be noted that the first term on the right-hand side of Equation 1 takes into account the "shadow" effect of the absorbing sphere, and the second term the neutron passage through the sphere. Substituting $\sqrt{r^2 + r'^2 - 2r'r\cos\theta} = x$ Equation 1 may readily be reduced to (all mean free paths in Equation 1 are measured by λ_s^{cp}):

$$N(r) = \frac{1}{2}\int_a^\infty N(r')\,dr'\{E_1(|r - r'|) - E_1(\sqrt{r^2 - a^2} + \sqrt{r'^2 - a^2})\} + \frac{1}{2}\int_a^\infty N(r')\,dr' \int_{\sqrt{r'^2 - a^2} + \sqrt{r^2 - a^2}}^{r + r'} \frac{dx}{x} \exp\left[-x - \frac{1 - \lambda}{\lambda x}\sqrt{(r^2 + x^2 - r'^2)^2 - 4x^2(r^2 - a^2)}\right] \quad (2)$$

where $N(r) = rn(r)$ and $E_1(t)$ is the integral exponent.

Denoting the kernels of the integral Equation 2 by $K(r,r')$ we obtain:

$$N(r) = \int_a^\infty N(r')K(r,r')\,dr' \quad (3)$$

The solution of Equation 3 should be sought in the form $N(r) = r - Q(r)$.

It is evident from the above that $Q(\infty) - Q(r)$ is fast tending to zero with $r \to \infty$ (at least not slower than e^{-r}).

For $Q(r)$ we have

$$Q(r) = \tfrac{1}{2}\int_a^\infty Q(r')K(r,r')\,dr' + f(r)$$

where

$$f(r) = r - \int_a^\infty K(r,r')r'\,dr' = \tfrac{1}{2}\left[aE_2(r - a) + E_3(\sqrt{r^2 - a^2}) - E_3(r - a) - \int_{\sqrt{r^2 - a^2}}^{r} dx\, e^{-x - \left(\frac{r}{\lambda} - 1\right)\sqrt{a^2 - r^2 + x^2}}\right] \quad (4)$$

Further on a relation will be needed between $Q(\infty)$ and

$$\int_a^\infty Q(r)f(r)\,dr$$

To obtain this relation we introduce the auxiliary equation

$$Q(r) = \int_a^\infty dr'Q(r')K_1(r,r') + \varphi(r) \quad (5)$$

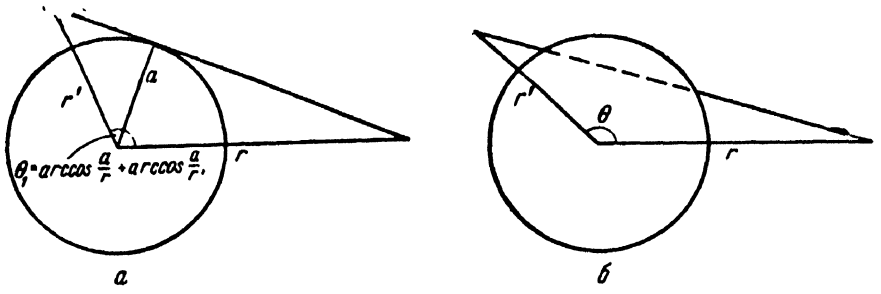

Figure 1

where

$$K_1(r,r') = \begin{cases} K(r,r') \text{ over the entire shaded part in Fig. 2.} \\ \tfrac{1}{2}[E_1(|r-r'|) - E_1(r+r')] \text{ over the entire unshaded part.} \end{cases}$$

Equation 5 may be transcribed as follows:

$$Q(r) = \int_0^\infty dr' Q(r') K_1(r,r') - \tfrac{1}{2}\int_0^a dr' Q(r')[E_1(|r-r'|) - E_1(r+r')] + \varphi(r)$$

or

$$Q(r) = \tfrac{1}{2}\int_0^\infty Q(r')[E_1(|r-r'|) - E_1(r+r')]\,dr' - \tfrac{1}{2}\int_0^a Q(r')[E_1(|r-r'|) - E_1(r+r')]\,dr' + \int_a^\infty Q(r')\{K_1(r,r') - \tfrac{1}{2}[E_1(|r-r'|) - E_1(r+r')]\}\,dr' + \varphi(r) \quad (6)$$

Equation 6 will be written thus

$$Q(r) = \tfrac{1}{2}\int_0^\infty Q(r')[E_1(|r-r'|) - E_1(r+r')]\,dr' + F(r) \quad (7)$$

where $F(r)$ is the sum of all right-hand side terms of Equation 6, except the first. It is seen that $F(r)$ is a function ($\sim e^{-r}$) decreasing rapidly with distance.

Formally Equation 7 coincides with the Peierls equation for neutron density in an infinite non-absorbing medium with spherically symmetric distribution of source $F(r)/r$. Applying Gauss's theorem to sufficiently large distances we obtain ($r \gg 1$):

$$-\frac{4\pi}{3}\left[\frac{Q(r)}{r}\right]' r^2 = 4\pi\int_0^r F(r')r'\,dr'$$

or in the limit, with $r \to \infty$:

$$Q(\infty) = 3\int_0^\infty F(r) r\,dr \quad (8)$$

Substituting in Equation 8 the expression for $F(r)$ and carrying out simple transformations, we obtain

$$Q(\infty) = 3\int_a^\infty r\,dr\,f(r) - 3\int_a^\infty Q(r)f(r)\,dr \quad (9)$$

Thus, the relation between $Q(r)$ and

$$\int_a^\infty Q(r)f(r)\,dr$$

has been found. The integral

$$\int_a^\infty r\,dr\,f(r)$$

is readily taken:

$$\int_a^\infty r\,dr\,f(r) = \frac{a^2}{4} - \frac{3\lambda^2}{4}\left[\frac{1}{2} - e^{-2\frac{a}{\lambda}}\left(\frac{1}{2} + \frac{a}{\lambda}\right)\right] \quad (10)$$

If the diameter of the absorbing sphere is small compared to the scattering mean free path in the medium ($2a \ll 1$), then the region defined by r, in which $Q(r)$ may appreciably differ from its asymptotic value $Q(\infty)$, is, apparently, of the order of the sphere's diameter ($\sim 2a$).

Indeed in this case the values of neutron density near the sphere's surface will be determined only by the "shadow" effect, and the latter is essential only at distances from the surface of the sphere of the order of its diameter, while the scale factor governing the variation of the function $f(r)$ is a quantity of the order of unity (i.e. $\sim \lambda_s^{op}$). It should therefore be no great error to substitute in the integral

$$\int_a^\infty Q(r)f(r)\,dr$$

the asymptotic value of $Q(r)$, i.e. $Q(\infty)$. Then for $Q(\infty)$ we obtain the following approximate relationship:

$$Q(\infty) = \frac{\frac{3a^2}{4} - \frac{3\lambda^2}{4}\left[\frac{1}{2} - e^{-2\frac{a}{\lambda}}\left(\frac{1}{2} + \frac{a}{\lambda}\right)\right]}{1 + 3\int_a^\infty f(r)\,dr} \quad (11)$$

To use Equation 11 it is necessary to find the error

Table I.

λ	a = 0.05	0.1	0.2	0.3	0.4
0	0.00187	0.00738	0.0286	0.0620	0.106
0.1	0.000882	0.00521	0.0255	—	—
0.2	0.000521	0.00351	0.0204	0.0517	—
0.3	—	0.00262	—	0.0447	—
0.4	—	0.00208	0.0438	—	0.0771

it gives for various cases. This error will be the highest when the sphere is "black." Due to the partial transparency of the "grey" sphere, the function $Q(r)$ should in this case be relatively closer to its asymptotic value $Q(\infty)$ than in the case of the "black" sphere. We should therefore verify the correctness of our approximation for the case of the "black" sphere. It is known that in the case of an infinitely small radius of a "black" sphere or cylinder, the value:

$$\gamma = \frac{n_\infty}{\frac{\partial n_\infty}{\partial r}} \to \frac{4}{3}$$

where n_∞' is the asymptotic density with $r = a \to 0$. In our case

$$\gamma = \frac{a^2}{Q(\infty)} - a$$

On the other hand, the expression for $Q(\infty)_{\text{black}}$ is derived from Equation 11 with $\lambda \to 0$:

$$Q(\infty)_{\text{black}} = \frac{a^2}{\frac{2}{3} + a + 2\int_a^\infty E_3(\sqrt{r^2 - a^2})\, dr} \tag{12}$$

Consequently

$$\gamma_{\text{black}} = \tfrac{2}{3} + 2\int_a^\infty E_3(\sqrt{r^2 - a^2})\, dr$$

But

$$\lim_{a\to 0} \int_a^\infty E_3(\sqrt{r^2 - a^2})\, dr = \tfrac{1}{2}$$

therefore

$$\gamma_{\text{black}} \to \tfrac{4}{3} \text{ with } a \to 0$$

Thus, Equation 12 obtained by substituting $Q(r)$ for $Q(\infty)$ yields the correct limiting result for the "black" sphere with $a \to 0$.

We further see that when $a \to \infty$, Equation 12 yields a meaningful result. The precise value of γ_{black} in this case should be 0.71. According, however, to the approximate formula Equation 12 we obtain $\gamma_{\text{black}} \to \frac{4}{3}$ with $a \to 0$. This value is only 5.5 per cent less than the precise value. At the intermediate point $a = 0.5$ Equation 12 yields $\gamma_{\text{black}} = 1.08$ which is identical with the value obtained for the same radius by A. L. Brudno (1951) by a different method. Consequently, it may be expected that Equation 12 is practically exact for spheres with small radii, and yields a comparatively small error in the case of $a \sim 1$.

Returning to our problem of the "grey" sphere, Equation 11 may be written as:

$$Q(\infty)_{\text{grey}} = \frac{1 - \frac{\lambda^2}{a^2}\left[1 - e^{-2\frac{a}{\lambda}}\left(\frac{1}{2} + \frac{a}{\lambda}\right)\right]}{A}$$

$$A = \frac{1}{Q(\infty)_{\text{black}}} - \frac{\lambda^2}{2a^3} + \frac{\lambda}{a^2}\left(1 - \frac{\lambda}{2a}\right)e^{-2\frac{a}{\lambda}} + \frac{2}{a}\int_0^1 x\,dx\, e^{-a\left(\frac{2}{\lambda}-1\right)x}\int_0^1 dz\, e^{-\frac{a}{z}\sqrt{1-z^2(1-x^2)}} \tag{13}$$

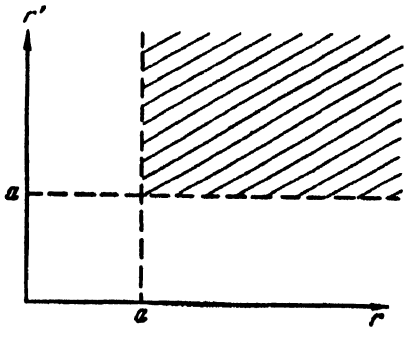

Figure 2

The limiting values for γ, deduced from this formula, correspond to the meaning of the problem

$\gamma_{\text{grey}} \to \infty$ with $a \to 0$ and $\gamma_{\text{grey}} \to \frac{4}{3}$ with $a \to \infty$

The following table gives the values of $Q(\infty)_{\text{grey}}$, computed for certain quantities of a and λ.

Another way of determining the accuracy of Equation 13, besides the above analysis of the results for the "black" sphere, is a comparison with data obtained by other methods. Such for example, is the variation method for evaluating $Q(\infty)_{\text{grey}}$. Examine the equation:

$$I(Q) = \frac{\int_a^\infty dr\, Q(r)\left\{Q(r) - \int_a^\infty dr' K(r,r') Q(r')\right\}}{\left[\int_a^\infty dr\, Q(r) f(r)\right]^2} \tag{14}$$

where $K(r,r')$ is the kernel of Equation 4, and $f(r)$ is the free term. When the trial function $Q(r)$ equals the exact solution of Equation 4, Equation 14 assumes its smallest value determined by

$$\frac{1}{\int_a^\infty dr\, Q(r) f(r)}$$

But according to Equation 8

$$\frac{1}{\int_a^\infty dr\, Q(r) f(r)} = \frac{3}{C(a,\lambda) - Q(\infty)}$$

where in our case

$$C(a,\lambda) = \frac{3a^2}{4} - \frac{3\lambda^2}{4}\left[\frac{1}{2} - e^{-2\frac{a}{\lambda}}\left(\frac{1}{2} + \frac{a}{\lambda}\right)\right]$$

Selecting the trial function in the simplest way $Q(r) = \text{const}$, we obtain an approximate expression for $Q(\infty)_{\text{grey}}$:

$$\frac{3}{C(a,\lambda) - Q(\infty)_{\text{grey}}} = \frac{\int_a^\infty dr\left[1 - \int_a^\infty dr' K(r,r')\right]}{\left[\int_a^\infty dr f(r)\right]^2} \tag{15}$$

In the case of "black" spheres this choice of trial function yields a negligible error in $Q(\infty)$. It is to be expected that for "grey" spheres, the error will be still smaller.

The value $Q(\infty)_{\text{grey}}$ obtained by Equation 15 for $a = \frac{1}{3}$ and $\lambda = \frac{1}{3}$ equals 0.0233, whereas the value $Q(\infty)_{\text{grey}}$ for the same parameters obtained from Equation 13 equals 0.0235. Thus, the difference

does not exceed one per cent. The negligible difference in the values of $Q(\infty)_{grey}$ obtained by different methods yields additional proof of the practical applicability of the relatively simple Equation 13.

2. EFFECTIVE BOUNDARY CONDITIONS FOR "GREY" CYLINDER

For practical purposes it is more important to know the effective boundary conditions for cylinders. In this case, however, the kernel of the Peierls equation is more involved than in the case of spherical geometry and, consequently, makes it also more complicated to find asymptotic density. Therefore, of practical interest in this case is the deduction of a simple formula for effective boundary conditions, which at the same time, would also ensure the necessary accuracy.

The given problem is considered in the same way as in the case of the "grey" sphere: a cylinder of infinite height is placed in an isotropically scattering non-absorbing medium in which a steady flux of monochromatic neutrons is maintained.

The Peierls equation for neutron density in the medium surrounding the cylinder is written thus (all dimensions are measured in units of mean free path in the medium):

$$n(r) = \frac{1}{\pi}\int_a^\infty n(r')r'dr' \times \int_0^{\arccos\frac{a}{r}+\arccos\frac{a}{r'}} d\varphi \int_0^\infty \frac{e^{-\sqrt{r'^2+r^2+z^2-2rr'\cos\varphi}}}{r'^2+r^2+z^2-2rr'\cos\varphi}dz + \frac{1}{\pi}\int_a^\infty n(r')r'\,dr' \times \int_{\arccos\frac{a}{r}+\arccos\frac{a}{r'}}^{\pi} d\varphi \int_0^\infty dz \frac{\exp B}{r'^2+r^2+z^2-2rr'\cos\varphi} \quad (16)$$

where

$$B = -\sqrt{r^2+r'^2+z^2-2rr'\cos\varphi}\left[1+2\left(\frac{1}{\lambda}-1\right)\times\frac{\sqrt{a^2(r^2+r'^2-2rr'\cos\varphi)-r^2r'^2\sin^2\varphi}}{r^2+r'^2-2rr'\cos\varphi}\right]$$

where λ is the mean free path in the cylinder, and a is the cylinder radius. The first integral in the right-hand side of Equation 16 contributes to the density of all neutrons incident at the given point, without passing through the cylinder. The second integral refers to the part of neutrons incident at the given point, having passed through the cylinder. Examine in greater detail how the last integral is obtained. The neutron scattered at point A traverses the paths AB and CD in the medium and the path BC in the cylinder (Fig. 3).

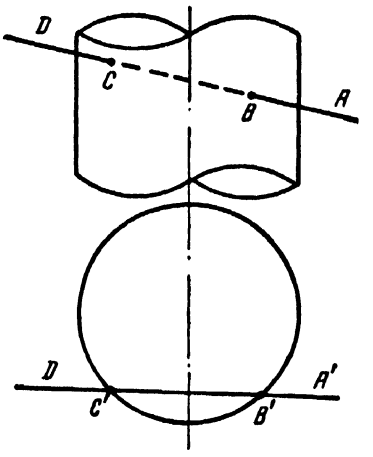

Figure 3

The path traversed in the medium:

$$AB + CD = AD - BC = AD - \frac{B'C'}{\cos(\widehat{AD;A'D})}$$

where

$$\cos(\widehat{AD;A'D})$$

is the cosine of the angle between the section AD and its projection on the plane perpendicular to the cylinder axis and passing through point D. From elementary geometrical considerations it follows that

$$BC = 2\cdot\frac{(\sqrt{a^2(r^2+r'^2-2rr'\cos\varphi)-r^2r'^2\sin^2\varphi} \times \sqrt{r^2+r'^2+z^2-2r'r\cos\varphi})}{r^2+r'^2-2rr'\cos\varphi}$$

At the same time the total "optical" path traversed by the neutron from point A, where scattering took place to point r, is determined by the expression

$$AB + CD + \frac{BC}{\lambda} = \sqrt{r^2+r'^2+z^2-2rr'\cos\varphi}\left[1+2\left(\frac{1}{\lambda}-1\right)\times\frac{\sqrt{a^2(r^2+r'^2-2rr'\cos\varphi)-r^2r'^2\sin^2\varphi}}{r^2+r'^2-2rr'\cos\varphi}\right]$$

Thus, the structure of the second term in the right-hand side of Equation 16 is now apparent.

Using the relationship known from the Bessel function theory and substituting $\sqrt{r^2+r'^2-2rr'\cos\varphi} = t$, Equation 16 becomes

$$n(r) = \frac{2}{\pi}\int_a^\infty n(r')r'\,dr' \int_{|r-r'|}^{\sqrt{r^2-a^2}+\sqrt{r'^2-a^2}} \frac{dt\cdot K_s(t)}{\sqrt{4r^2r'^2-(r^2+r'^2-t^2)^2}} + \frac{2}{\pi}\int_a^\infty n(r')r'\,dr' \int_{\sqrt{r^2-a^2}+\sqrt{r'^2-a^2}}^{r+r'} \frac{dt\cdot K_s[t+I(t)]}{\sqrt{4r^2t^2-(r^2+r'^2-t^2)^2}}$$

where

$$I(t) = \left(\frac{1}{\lambda} - 1\right)\sqrt{4a^2 - \frac{4r^2r'^2 - (r^2 + r'^2 - t^2)^2}{t^2}}$$

and

$$K_i(t) = \int_t^\infty K_0(x)\,dx$$

The solution of Equation 17 at a large distance from the cylinder boundary should tend towards the function whose form is determined by the solution of the corresponding diffusion equation

$$n(r) \underset{r\to\infty}{\longrightarrow} A[1 + Q(\infty)\ln r] \tag{17}$$

Making the non-essential constant A equal to unity, the solution of Equation 17 may be represented by $n(r) = 1 + Q(r)$ where $|Q(r) - Q(\infty)\ln r| \to 0$ with $r \to \infty$. For $Q(r)$ we obtain

$$Q(r) = \int_a^\infty Q(r')K(r,r')r'\,dr' + f(r) \tag{18}$$

where

$$K(r,r') = \frac{2}{\pi}\int_{|r-r'|}^{\sqrt{r^2-a^2}+\sqrt{r'^2-a^2}} \frac{dt\,K_i(t)}{\sqrt{4r^2r'^2 - (r^2 + r'^2 - t^2)^2}} + \frac{2}{\pi}\int_{\sqrt{r^2-a^2}+\sqrt{r'^2-a^2}}^{r+r'} \frac{dt\,K_i[t + I(t)]}{\sqrt{4r^2t^2 - (r^2 + r'^2 - t^2)^2}}$$

$$f(r) = \int_a^\infty K(r,r')\,dr' - 1$$

The following relationship for the cylinder can be found in the same way as in the case of the sphere:

$$Q(\infty) = -3\int_a^\infty Q(r)f(r)r\,dr - 3\int_a^\infty f(r)r\,dr \tag{19}$$

By the same discussion as in the case of the sphere we reach the conclusion that for thin cylinders ($2a \ll 1$) $Q(r)$ in the right-hand side of Equation 19 can without particular error be replaced by its asymptotic quantity $Q(\infty)\ln r$. Then

$$Q(\infty) = -\frac{\int_a^\infty f(r)r\,dr}{\frac{1}{3} + \int_a^\infty \ln r f(r) r\,dr} \tag{20}$$

To get an idea of the error given by Equation 20 it will be applied for the case of the "black" cylinder. Then

$$f(r)_{\text{black}} = \frac{2}{\pi}\int_a^\infty r'\,dr' \int_{r-r'}^{\sqrt{r^2-a^2}+\sqrt{r'^2-a^2}} \frac{dt\,K_i(t)}{\sqrt{4r'^2r^2 - (r^2 + r'^2 - t^2)^2}} - 1$$

or after simple transformations:

$$f(r)_{\text{black}} = \frac{1}{\pi}\int_{r-a}^{\sqrt{r^2-a^2}} dt \arcsin\frac{r^2 + t^2 - a^2}{2rt} K_i(t) + \frac{1}{\pi}\arcsin\frac{\sqrt{r^2 - a^2}}{r}\int_{\sqrt{r^2-a^2}}^\infty dt\,K_i(t) - \frac{1}{2}\int_{r-a}^\infty dt\,K_i(t) \tag{21}$$

In the case of cylindrical geometry:

$$\gamma = \frac{1 + Q(\infty)\ln a}{Q(\infty)/a} \tag{22}$$

For the "black" cylinder

$$\gamma_{\text{black}} = \frac{a\int_a^\infty [\ln a - \ln r] f(r)_{\text{black}} r\,dr - \frac{a}{3}}{\int_a^\infty f(r)_{\text{black}} r\,dr} \tag{23}$$

In the limiting case of small radii ($a \ll 1$) it may be shown by Equation 23 that $\gamma_{\text{black}} \to \frac{1}{3}$ when $a \to 0$. In the other limiting case: $\gamma_{\text{black}} \to \frac{2}{3}$ when $a \to \infty$. For the intermediate value a the error yielded by the above approximate method is determined by comparison with γ_{black} obtained by direct numerical solution of the kinetic equation. Results appear in Table II.

Table II.

a	γ_{black} *by numerical methods*	γ_{black} *by Equation 23*	*Difference* %
0.5	0.99	0.963	2.7
1	0.889	0.864	2.8

The author found the value of γ_{black} in the second column for $a = 0.5$ by the variation method (in 1951); and Sobolev found the value for $a = 1$ by the lattice method (1951).

Thus, the error in determining γ_{black} by Equation 23 does not exceed 2–3 per cent in the interval a under consideration. This accuracy is quite adequate for practical purposes. By the considerations expressed in the preceding section one may expect that for the "grey" cylinders the accuracy of the method will be greater. In this case:

$$f(r)_{\text{grey}} = \frac{1}{\pi}\int_{r-a}^{\sqrt{r^2-a^2}} dt \arcsin\frac{r^2 + t^2 - a^2}{2rt} K_i(t) + \frac{1}{\pi}\int_{\sqrt{r^2-a^2}}^{r+a} dt \arcsin\frac{r^2 + t^2 - a^2}{2rt} K_i[Z(t)] + \frac{1}{2}\int_{r+a}^\infty dt\,K_i\left[t + 2a\left(\frac{1}{\lambda} - 1\right)\right] \tag{24}$$

where

$$Z(t) = \frac{t}{\lambda} - \left(\frac{1}{\lambda} - 1\right)\frac{r^2 - a^2}{t}$$

and the γ_{grey} will be determined by

$$\gamma_{\text{grey}} = \frac{a\int_a^\infty [\ln a - \ln r] f(r)_{\text{grey}} r\,dr - \frac{a}{3}}{\int_a^\infty f(r)_{\text{grey}} r\,dr} \tag{25}$$

As in the case of the "grey" sphere $\gamma_{\text{grey}} \to \infty$ with $a \to 0$ and $\gamma_{\text{grey}} \to \frac{2}{3}$ with $a \to \infty$, which corresponds to the physical conditions of the problem.

But Equation 25 is still too involved for practical calculations. Therefore, a simpler formula which at

Table III.

a/λ	γ_{grey} by Equation 25	λ_{grey} by Equation 30	Deviation %
¼	3.26	3.20	2
½	1.92	1.89	1.5
1	1.29	1.29	0
2	1.06	1.06	0

Table IV.

a/λ \ a	0.1	0.2	0.3	0.4	0.5
2	1.31	1.23	1.16	1.11	1.06
⅜	1.39	1.31	1.24	1.18	1.13
1	1.57	1.49	1.41	1.35	1.29
⅝	1.89	1.81	1.53	1.66	1.58
½	2.22	2.15	2.06	1.99	1.89
¼	3.66	3.60	3.48	3.36	3.20

the same time would not introduce a big error is desirable for evaluations. Such a formula can be deduced by the following considerations: if the cylinder is thin ($2a \ll 1$) then the one-sided flux incident on its surface from the medium is isotropically distributed in the angles. On the other hand, there is very little probability that the neutron having passed through the cylinder will again return to its surface, i.e., the solid angle at which the cylinder is seen from the point where scattering will occur is small. If the medium does not capture then the total flux of neutrons through the surface surrounding the cylinder is preserved. The quantity of the flux can be found if the asymptotic density is known:

$$j = -\frac{1}{3}\frac{\partial n_\infty}{\partial r}$$

In the case of the cylinder: $n_\infty = 1 + Q(\infty) \ln r$. The total flux through the cylinder surface is equal to $j 2\pi r = -\frac{2\pi}{3} Q(\infty)$. By the above considerations the total one sided flux incident from the medium on the thin "grey" cylinder is proportional to $Q(\infty)_{black}$. Then the difference between the total fluxes in the medium:

$$j_{black} - j_{grey} = D j_{black} \tag{26}$$

where D is the escape probability of the neutron incident on the "grey" cylinder and Equation 26 can be written in the following form:

$$\frac{Q(\infty)_{black} - Q(\infty)_{grey}}{Q(\infty)_{black}} = D \tag{27}$$

The coefficient D is readily computed for the "grey" cylinder, as the one sided flux incident on it from the medium can be regarded to be isotropic:

$$D = \frac{\int_0^\pi d\varphi \int_0^\pi \sin^2\theta \, d\theta \, e^{-\frac{2a}{\lambda}\frac{\cos\varphi}{\sin\theta}} \cos\varphi}{\int_0^\pi d\varphi \cos\varphi \int_0^\pi \sin^2\theta \, d\theta} \tag{28}$$

Using the integral representation for the Bessel functions Equation 28 may be reduced to:

$$D = 1 - \frac{16a^2}{\pi\lambda^2}\int_0^1 \sqrt{1-x^2}\, x\, dx \left[K_1\left(\frac{2a}{\lambda}x\right) - \int_{2ax/\lambda}^\infty K_0(z)\, dz\right] \tag{29}$$

Consequently:

$$Q(\infty)_{grey} = Q(\infty)_{black}\frac{16a^2}{\pi\lambda^2}\int_0^1 \sqrt{1-x^2}\, x\, dx \left[K_1\left(\frac{2ax}{\lambda}\right) - \int_{2ax/\lambda}^\infty K_0(z)\, dz\right] \tag{30}$$

Equation 30 permits ready evaluation of $Q(\infty)_{black}$ and, hence, also γ_{grey} for thin "grey" rods. The error from Equation 30 can be evaluated by comparing the quantities obtained by Equation 30 and 25. Such a comparison for γ_{grey} in the case of $a = 0.5$ is given in Table III.

It is seen from this table that in our interval a/λ the values of γ_{grey} calculated by Equations 25 and 30 differ little (2 %) from each other. When $a < 0.5$, the error in determining γ_{grey} by Equation 30 should be still smaller. In case of large cylinder radii, Equation 30 cannot be applied. For $a = 1$ and $\lambda = 2$, γ_{grey}, determined by corresponding formulae, differ by 15 per cent. That is why Equation 30 can be applied without much error for $a \leq 0.5$. The following table gives the values of γ_{grey} obtained by Equation 30 for several a in the interval $0 < a \leq 0.5$ and for various values of the ratio a/λ (see Table IV).

The values γ_{black}, required for computing γ_{grey} in Table IV have been calculated by Equation 20.

In conclusion it will be noted that the considerations whereby Equation 30 has been obtained are valid not only for solid cylinders, but also for hollow ones. Knowledge of effective boundary conditions for "grey" cylinders is important for the computation of the thermal utilization coefficient O in calculating enriched uranium reactors, also for finding the controlling ability of control rods.

REFERENCE

1. Marshak, R. E., Phys. Rev. *71*, 688 (1947).

Record of Proceedings of Session 23A

SATURDAY MORNING, 20 AUGUST, 1955

Chairman: Mr. C. Salvetti (Italy)
Vice Chairman: Mr. A. Soltan (Poland)
Scientific Secretaries: Messrs. M. Trocheris and J. Leite Lopes

PROGRAMME

P/611 Survey of neutron thermalization theories.....E. R. Cohen
P/433 Calculation of the fine structure of the thermal neutron flux in a pile by the spherical harmonics method.....J. H. Tait

DISCUSSION

P/608 Comparison of theory and experiment for intermediate assemblies.....H. Hurwitz and R. Erlich
P/430 Method for calculating the critical mass of an intermediate reactor.....M. E. Mandl and J. Howlett
P/664 Application of the method of effective boundary conditions for calculating the critical dimensions of reactors.....A. D. Galanin

DISCUSSION

P/669 Heterogeneous methods of reactor calculations. Survey of results and comparison with experiments.....S. M. Feinberg
P/649 Theory of resonance absorption in heterogeneous systems...I. I. Gurevich and I. Y. Pomeranchouk
P/666 The thermal utilization factor in a heterogeneous reactor.....A. D. Galanin
P/1003 Lattice calculations on natural uranium-beryllium oxide and natural uranium-beryllium metal in a cylindrical reactor.....O. Gamba, *et al.*

DISCUSSION

P/656 Equation for the importance of neutrons, reactor kinetics, and the theory of perturbation.....L. N. Ussachoff
P/796 Remarks about the Milne problem with cylindrical symmetry.....L. Trlifaj
P/667 Effective boundary conditions for "grey" bodies.....D. F. Zaretsky

DISCUSSION

Mr. E. R. COHEN (USA) presented paper P/611 as follows: In elementary reactor theory thermal neutrons are often represented as a monoenergetic group. The cross sections to be applied to this group can be defined in terms of integrals over the assumed Maxwellian spectrum of neutron velocities, but the "energy" of the group is not well defined and in fact may be different depending on the purpose for which this energy is to be used. For the determination of mean free paths or absorption rates, the temperature of the assumed Maxwell distribution is appropriate, but the energy at which neutrons can be considered to make a transition from the slowing down region into the thermal group is certainly a much higher energy than this.

In addition the temperature which defines the neutron Maxwell distribution need not be the same as the temperature of the moderator. If equilibrium is established the two temperatures will of course be the same; however, since neutron absorption is present complete equilibrium cannot be established. If the absorption cross section has an inverse velocity dependence so that the absorption lifetime is independent of energy, this absorption cannot, *per se*, be responsible for the non-equilibrium. Thus, if the neutron source is itself an equilibrium distribution, this distribution will be maintained. Also, if the course of neutrons is a pulse at time $t = 0$, the effect of absorption is to deplete the neutron density uniformly, without otherwise altering the neutron spectrum. If λ is the constant capture probability for neutrons per unit time and $N(v,t)$ is the neutron velocity distribution at time t after a pulse source, $N(v,t)e^{\lambda t}$ will be the solution of the problem without absorption. Hence $N(v,t)$ will asymptotically approach an equilibrium distribution as $t \to \infty$.

The steady-state neutron distribution in the presence of absorption is therefore complicated not by absorption itself but by the fact that the neutron source does not produce an equilibrium distribution and the neutrons are absorbed before this neutron distribution is established.

In a reactor the neutrons are produced with energies which are large with respect to the energy of thermal motion of the moderator, kT_0. In this case the neutrons slow down into the thermal region, and in the initial stages of this process the thermal motion of the moder-

ator can be neglected. The slowing down of fast neutrons has been treated by Placzek and by Marshak. These analyses are primarily interested in the slowing down process itself rather than the thermalization process and concern themselves with a stationary moderator—that is, one whose temperature is negligible.

As long as the neutron source energies are sufficiently high an equilibrium slowing down distribution will be established before the effects of the thermal motion of the moderator become important. If this restriction is satisfied, then the details of the source distribution are unimportant and the specification of the source can be replaced by a condition on the asymptotic neutron distribution for large velocities, which can in turn be determined from the asymptotic behavior of the slowing down in a stationary moderator.

The general description of the kinetic behavior of a mixture of two gases is complicated by the nonlinearity of the Boltzmann equation. Thus a completely general discussion of the diffusion of neutrons into a medium with which they exchange energy is a problem not easily treated. It is, however, possible to linearize the equation if we are dealing with neutron densities to be expected in reactors. In a neutron flux of 10^{13} neutrons/sec/cm^2 and a moderator with a scattering cross section of 10 barns, any given atom suffers a collision once every 10^{10} seconds—once every 300 years. These times are obviously quite long compared to the atom-atom collision rates in a gas or to the natural vibration frequencies in a solid and hence the moderator may validly be assumed to be unaffected by the neutrons, and in addition the neutron-neutron collisions themselves are even more completely negligible.

As usual with the equations of kinetic theory, the completely general equations have been treated only in general terms. The time-dependent equation has been considered in an approximate manner by von Dardel, but extensive numerical calculations have apparently been done only for the steady-state, space-independent problem. The equation in this case reduces to the form given in Equation 2 of paper P/611.

In the case of a monatomic gaseous moderator, the calculation of $G_s(v \rightarrow v')$ is the classical one of kinetic theory.

For gaseous and liquid moderators the neutron will still collide with the individual atom at high energies where there is enough energy to break through the molecular bond.

In the region of neutron energies below 1 ev the neutron does not collide with individual atoms but rather with the molecule as a whole. If the energy is high enough the vibrational states of the molecule can be excited by the collision; in the region of major interest for the thermalization of neutrons, however, only the rotational states of the atom can be excited. For H_2O vibrational states can be excited only above 0.20 ev. In describing the collisions of a neutron with a water molecule it will therefore be adequate to consider only the rotational states of the molecule. Sachs and Teller have shown that the hydrogen atom in a molecule can be described in terms of an equivalent free-mass point whose mass is described by a tensor. Such a description is quite plausible. If the neutron collides with the hydrogen atom in a direction perpendicular to the plane of the water molecule, the hydrogen atom will be effectively free and its effective mass is 1; if the neutron strikes the hydrogen in the line joining the atom to the center of gravity of the molecule, the system recoils as a whole and the effective mass is 18. For the incident neutron in the direction perpendicular to these two directions, the effective mass has some intermediate value.

Brown and St. John have used the results of Sachs and Teller's analysis in a calculation of the neutron distribution in D_2O. For the molecule the effective mass tensor has principal components (2, 3.517, 20). If we define the effective mass in terms of the trace of the inverse mass tensor the effective mass of the deuterium atom in the D_2O molecule is 3.596 mass units. The effective mass of the oxygen, on the other hand, is 17.607 and it is a valid first approximation to consider oxygen as an infinitely heavy atom and neglect any energy transfer in collisions between it and a neutron. This is not as good an approximation as the equivalent assumption for H_2O, both because of the larger difference in mass and because of the larger hydrogen scattering cross section.

Crystalline Moderators

For a crystalline moderator such as graphite or beryllium, it is necessary to consider the detailed structure of the crystal lattice. The theory of neutrons scattered by crystalline lattices has been discussed by various authors.

Brockhouse and Hurst [*Phys. Rev.* 88, 542 (1952)] at Chalk River have investigated the problem experimentally and show that for scatterers heavier than aluminum it is approximately valid to treat the scatterer as a free gas. This can be seen from the following simple argument.

The kinetic energy of the equivalent oscillators in the crystal will be $\frac{1}{2}kT$. The energy transferred in a collision will therefore have a distribution with a spread in energy of approximately

$$\Delta E \approx \left(\sqrt{E} + \frac{kT}{2m}\right)^2 - \left(\sqrt{E} - \sqrt{\frac{kT}{2m}}\right)^2 = \sqrt{\frac{8kTE}{m}}$$

If this energy is large compared to $K\theta$, where θ is the Einstein temperature of the oscillator, there will be several values of n for which the probability of transferring an energy equal to $nk\theta$ will be important and these probabilities will form a histogram approximation to the energy loss distribution in an equivalent Maxwell gas. This approximation will be better as the number of states involved increases. Hence the criterion for the validity of replacing an Einstein crystal by a free gas is

$$E/kT \gg (m/8)(\theta/T)^2$$

The same criterion can be applied to a Debye oscillator; in this case the approximation to a free gas

should be somewhat better since there is a continuum of oscillators.

We can conclude that, in general, the approximation of a free gas tends to be better for heavier elements where the Einstein or Debye temperature is low and breaks down for crystals in which the Einstein temperature, and hence the level spacing, is large. Unfortunately, graphite is in this latter class. For graphite and beryllium it may be necessary either to carry out a detailed quantum mechanical analysis of the scattering process or to determine experimentally the differential inelastic scattering cross section for slow neutrons as a function of neutron energy and angle of scattering.

In neutron slowing down in hydrogen the equations can be solved analytically by reducing the integral equation to a differential equation. This is one of the few special cases in which this is possible. These cases shall now be mentioned. All of them are restricted to a scattering cross section which is independent of velocity.

One considers a hypothetical monatomic hydrogen moderator, as was done by Wigner and Wilkins, for which the scattering cross section is independent of velocity. The results are shown in Slide 1 (Fig. 1 of P/611). Also shown on the slide are the asymptotic distributions for a stationary moderator without absorption and with absorption. We see that the absorption rather than the moderator motion is initially the important effect as the neutrons slow down.

For moderators of intermediate mass, or for which the cross sections are not simple analytic expressions, recourse must be made to numerical methods of solution. There are two different approaches which have been used. One method involves the iteration of the integral equation; the other, which has a more direct physical appeal, involves following the history of individual neutrons from collision to collision.

High speed electronic digital computers have been used to carry out a numerical integration of the equations. Results of these calculations for D_2O moderators are shown in Slide 2 (Fig. 2 of P/611).

A quite different numerical approach has been followed at Oak Ridge National Laboratory by Osborn, Bate and Coveyou. This method consists of calculating the detailed behavior of a representative neutron as it loses or gains energy in successive collisions until it is absorbed. Several thousand neutron "histories" are assembled in this way and from them the neutron density is determined. The calculation was directly designed to take full advantage of the unique capacity of the ORACLE for performing an enormous number of simple operations in a short time.

A neutron at a preassigned source speed is considered to be released into the moderating medium. Since the cross sections are known the probabilities of absorption and capture are determined. A selection is made from a table of random numbers to determine whether the collision is an absorption or a scattering. If the event is an absorption, that fact is recorded and a new neutron is introduced at the source speed. If the event is a scattering, a decision must be made regarding the speed of the target nucleus and the angle of approach between neutron and target. Having made this selection it is then a simple matter, on the assumption of isotopic scattering in the center-of-mass system to select a new speed for the neutron. This new neutron now repeats the same sequence until it is finally absorbed, thus terminating a history.

The results of a calculation are obtained from the machine in the form of a histogram of the number of scattering events and the number of absorptions which occur in each of a set of intervals into which the range of the velocity variable has been subdivided. A single calculation may involve as many histories as might be required to provide a total of at least 65,000 scattering events.

Two cases were calculated which duplicate Wigner and Wilkins' calculation for hydrogen. The comparison of the results are shown in Slide 3 (Fig. 3 of P/611). The solid lines are the same curves as in the previous slide; the points represent the results of the machine calculation on the ORACLE. The only adjustment is to the scale of the plot. The results agree quite well.

It is also possible to take the results of these analyses of neutron slowing down and apply them to the calculation of neutron age and neutron temperature. The usual Fermi age theory expresses the migration area of thermal neutrons. The integral (the Fermi age) is usually written with a lower limit equal to kT_0. It is obvious that this lower limit cannot be correct. The correct lower limit should be deducible from a consistent model which relates absorption to slowing down.

Mr. Cohen then reviewed the mathematical formulation in paper P/611 under the heading "Neutron Age" and concluded by showing Fig. 4 of P/611.

Mr. J. H. TAIT (UK) presented paper P/433, concluding as follows: In conclusion, it should be stated that certain approximations can be made to the correct application of the spherical harmonics methods, which reduce the number of equations needed for the solution. The formulae for the various moments in the P_s approximation contain two and sometimes three terms. One term in the flux corresponds to the diffusion approximation and the other two terms take into account any divergences from the diffusion theory at points near to a boundary. The formulae for the transient terms in the moderator are given as the sum of a Bessel function of the first kind and one of the second kind.

To end, I will just state that one can justify including all the I functions in the solution in the moderator, and this enables us in the P_3 approximation to reduce the number of equations from nine to seven.

DISCUSSION OF P/611, P/433

Mr. E. P. WIGNER (USA): I am wondering if we could have a bit of a summary of the experimental information on the thermalization of neutrons—in particular as regards the temperature of the distribution and diffusion therefrom.

Mr. E. R. COHEN (USA): There is a little experimental work, but most of it is contradictory. The figures we listed in the published paper are not complete, but let me quickly review them. Taylor at BEPO measured no temperature at all at the Harwell reactor; he used a crystal spectrometer, and I mention this because there may be the argument that the method used to detect temperature might be involved in the type of answer you get. Gavin in the thermal test reactor at the Knolls Atomic Power Laboratory found no increase in temperature, using foil techniques to determine temperature. Zinn analyzed the neutron beam of the Argonne reactor with a crystal spectrometer and found a temperature increase of 90°C. Branch measured an increase of 140°C in the Oak Ridge reactor. I believe Branch used foil techniques.

These are four items of data that I included in the published paper. There are other data, equally discordant, indicated by Hughes in his book on pile neutron physics.

Mr. BUSSAC (France): I would like to ask Mr. Cohen whether he has studied the effect of the diffusion of neutrons on thermalization, or whether a study of that kind is now in progress?

Mr. E. R. COHEN (USA): Do you mean the effect of finite buckling on the neutron distribution? This was treated rather crudely by considering the diffusion constant times the buckling as an additional absorption term, and the results are rather consistent with the curves shown for essentially the zero buckling limit. I am not sure, however—it depends what your definition of terms is and whether the dependence on buckling is significant or not—whether you want to include that as part of the change in migration area or consider it in a different way, but it can I think easily be neglected in the theory.

Mr. V. P. DUGGAL (India): I want to ask if Mr. Cohen has any experimental figures on the slowing-down age. In a moderator with quite a high absorption coefficient, how will the slowing-down age be affected?

Mr. E. R. COHEN (USA): Some measurements were made, which I reported yesterday, in which we poisoned a heavy-water natural-uranium lattice with 150 mg/l of B_2O_3 and, assuming that this change in the absorption of the moderator affected only the thermal properties and did not change the nonthermal properties of the multiplication, and by comparing the measured bucklings in the poisoned and unpoisoned lattices, assuming that we knew everything except the age, which was unchanged in the two cases, we defined an age of 107 cm^2. The usually reported age—at least in United States literature—from a fission spectrum to the indium resonance is approximately 100 cm^2. We estimated that this is corrected to 102 by the presence of the uranium in our lattice, leaving an effective age for a two-group calculation from indium to thermal of about 5 cm^2. Now, this corresponds to my limit of the effective age that you would use in a two-group calculation in which there is no absorption at all in the fast group, so that you have to adjust the age to account for the decreased migration of those neutrons that are absorbed in the pile and the $1/v$ absorption—that is, the 16 kT limit, which gives about the same value.

Mr. V. P. DUGGAL (India): Do you know of any experimental figures in the case of graphite?

Mr. E. R. COHEN (USA): No.

Mr. J. HOROWITZ (France): Do you know whether it is proposed to use the same method in the United States for making measurements in respect of graphite?

Mr. E. R. COHEN (USA): We are not planning them at the moment. It is a little more difficult to poison graphite uniformly with boron than it is to poison water with boron, and I am not quite sure how you would achieve the same type of experiment with a solid moderator.

Mr. HOROWITZ (France): We intend to perform a graphite experiment reducing the graphite diffusion length not by poisoning but by means of a moderator.

Mr. H. HURWITZ (USA) presented paper P/608 as follows: The early measurements of the thermal neutron cross sections of plutonium showed that the prospects of a plutonium breeding cycle utilizing thermal neutrons were marginal. At the time it was felt that the high thermal capture-to-fission ratio in plutonium might be ascribed to an abnormally low fissionability in the 0.3 ev resonance. Hence if a reactor were designed to have a neutron spectrum above the 0.3 ev plutonium resonance it was thought that the average capture-to-fission ratio might be small. Accordingly, an extensive program of critical experiments and calculations was undertaken at the Knolls Atomic Power Laboratory to investigate the properties of intermediate assemblies. As a result of this and related programs it was learned that the 0.3 ev resonance is by no means unique in its high capture-to-fission ratio. Although this unfavorable result decreased engineering interest in intermediate breeders, the experimental and theoretical studies of the intermediate assemblies provided a great deal of valuable reactor physics information which is relevant to other types of reactors as well.

The investigation of critical mass as a function of reactor composition, which was one of the objectives of the program, actually comprised only a small part of the studies. There were also extensive investigations of the spatial distribution of fissions; the distributions of neutron flux in energy and position, and reactivity coefficients.

The characteristic feature of intermediate assemblies is that the fissions are caused by neutrons whose energies cover a very wide range. Since the neutron cross sections are strongly dependent on energy, it is necessary to consider in detail the spatial variation of neutrons having many different energies. These spatial distributions may be entirely different in the high and low energy parts of the neutron spectrum.

The starting point of most theoretical calculations on intermediate assemblies is the Fermi age-diffusion equation. This equation is a satisfactory first ap-

proximation to the rigorous Boltzmann equation in most cases of interest since the assembly dimensions are usually large compared to a neutron mean free path. Corrections may be made for the effects of inhomogeneous structure in the core and reflection, and the errors in the age-diffusion equation itself by slightly modifying the cross sections used in the calculations.

The form of the age diffusion equation is

$$-\nabla \frac{1}{3\sigma_{tr}} \nabla nv + \sigma_a nv = -\frac{\partial a}{\partial u} + \nu Z(u) \int nv\sigma_f \, du'$$

where nv is the neutron flux per unit range in the logarithmic energy variable, u $(= \ln E_0/E)$. The source density is the spatial fission distribution times the spectrum of neutrons emitted in fission, $Z(u)$. The relationship shown between the slowing-down density, q $(= \xi\sigma_p nv)$, and the neutron flux is valid for heavy moderators for which the neutron slowing down occurs in many small collisions. When hydrogen is present in substantial quantities, it is possible to take into account the large energy loss per collision between a neutron and a proton, but not the correlation between energy loss and scattering angle, by introducing a differential relation between slowing-down density and neutron flux instead of the direct proportionality relation shown here.

The equation adjoint to the age-diffusion equation is

$$-\nabla \frac{1}{3\sigma_{tr}} \nabla F + \sigma_a F = + \xi\sigma_s \frac{\partial F}{\partial u} + \nu\sigma_f(u) \int ZF \, du'$$

The variable F is the neutron importance function which is needed for perturbation theory. Like the flux, it is taken to be a function of position and energy. This function strictly depends also on the direction of the neutron motion. However, when the neutron mean free path is small, the angular dependence is also small so that the average over angle has physical significance. The relation between the differential equation for the angular average of F and the adjoint to the Boltzmann equation is entirely analogous to the relation between the diffusion equation for neutron flux and the Boltzmann equation itself.

The age-diffusion equation and its adjoint can be solved analytically for several types of simplified models. However, in the cases of practical interest in which cross sections in different regions of the assembly depend on energy in different ways, an analytic solution is not feasible. Hence numerical methods must be employed. Most of these methods have the common feature that the spatial distribution of fissions is assumed, and the flux resulting from the neutrons emitted in these fissions is calculated. From the calculated flux a new fission distribution may be obtained. If the proper fission distribution has been assumed, the new distribution will have the same shape as the assumed distribution, and the ratio of calculated fissions to assumed fissions will give the reactivity of the assembly.

A natural way to integrate numerically the age-diffusion equation would seem to be to use the neutron flux evaluated at one energy to calculate the flux derivative with respect to energy, and then to use this to extrapolate to a slightly lower energy. This so-called "explicit" integration scheme has the disadvantage of being unstable unless a very large number of energy intervals are employed. This type of unstability can be avoided if so-called "implicit" schemes are employed in which the energy derivative is expressed in terms of the flux at the new energy. The difference equations in the energy variable which are obtained in this manner have the form of coupled differential equations in the space variables. These are known as multigroup equations because they can be interpreted physically as describing the migration of groups of neutrons with several distinct energies.

A description of the derivation of the multigroup equations is given in the paper submitted to this Conference by Mandl and Howlett (P/430, this Session) who also discuss in detail the stability of conditions.

The general form of the multigroup is

$$-\nabla D_i \nabla N V_i + \Big(\Sigma_{a_i} + \sum_{j>i} T_{i\to j}\Big) N V_i = \sum_{j<i} N V_j T_{j\to i} + S_i$$

$$S_i = Z_i \sum_j N V_j \Sigma_{f_j}$$

where Σ_{a_i}, Σ_{f_i}, $T_{i\to j}$ and D_i are obtained from appropriate group averages of cross section combinations.

The coefficients $T_{i\to j}$ represent effective cross sections for neutron transfer between the groups. Since we customarily number the groups starting at the highest energy, $T_{i\to j}$ is only different from zero when j is greater than i. When the neutron slowing down occurs only through collisions with heavy moderator atoms, there is transfer from one group to the next lower energy group. However, when there is slowing down by hydrogen or inelastic scattering, the transfer may occur between non-adjacent groups.

Although the multigroup equations may in principle be solved analytically in one-dimensional problems, it is again more convenient to replace the spatial differential equations by difference equations which are solved numerically.

It is feasible to integrate numerically one-dimensional problems involving several spatial regions and up to about ten energy groups with desk calculating machines. However, the calculations are greatly facilitated by the use of automatic electronic computing machines.

A very important advantage of the electronic computing machines is that they have made it possible to solve multigroup problems in two space dimensions. This is opening the way to a considerably greater accuracy in the comparison of theory and experiment, and to the attainment of far more detailed engineering design information than has been practical with hand calculations.

The most practical procedure for solving the two-dimensional difference equations for a group is to make

use of relaxation techniques. Even with the fastest automatic computing machines it is necessary to choose the iteration procedures with considerable care so that when the dimensions of the spatial mesh are small, the convergence ratio will not be inconveniently slow. The two-dimensional multigroup codes which are now in use all employ some modifications of the extrapolated Liebmann procedure.

The adjoint equation to the age-diffusion equation can be converted to multigroup form in a manner closely analogous to the procedure used for the flux equation. In solving the adjoint multigroup equations one proceeds from the lowest energy group successively upward in energy instead of from the highest energy group downward as is the case with the flux multigroup equations. This is because the equation for the neutron value in essence traces the history of the neutrons backwards from the energies and positions at which they cause fissions to the energies and positions at which they are introduced into the assembly.

I will now illustrate the comparison of results calculated by the multigroup method with experiment for four assemblies with beryllium moderator. Two of these assemblies were studied at the Knolls Atomic Power Laboratory, and two were studied at Oak Ridge. The experiments are described in some detail in the paper of T. M. Snyder (P/602, Session 21A, this Volume).

The assembly on which most extensive measurements were made is known as SAPL PPA-5. It consisted of a hexagonal core of 85 liters volume, a beryllium reflector about 8 in. thick, and a natural uranium blanket about 30 in. thick. The core contained 58 kg of U^{235} and 34 moles of beryllium per mole of U^{235}.

The structure of the assembly is indicated on Slide 3 (Fig. 3 of P/602, Session 21A). There were two halves, each consisting of a close-packed matrix of thin walled 2-inch metal tubes. Fuel elements in the form of ½ millimeter thick discs of uranium interspersed with discs of beryllium, sodium and iron were inserted into the matrix tubes. The two halves of the assembly could be separated for loading and then brought together to approach criticality.

Multigroup calculations for the neutron flux and adjoint functions were performed using a 27.6 cm radius equivalent spherical core. The flux and adjoint calculations indicated that the assembly was about 4 per cent over critical. It is believed that the equivalent sphere model which was employed overestimates reactivity by a few per cent so that a calculation by the two-dimensional techniques which are now available would presumably give very nearly the correct reactivity.

The relation between the theoretical and experimental fission distributions is shown in Slide 4 (Fig. 1 of P/608). The spherical model is inadequate to predict the power distribution in a quantitative way, but the calculated distribution appears qualitatively correct. The calculated distribution is intermediate in shape between experimental fission distribution traverses taken to the sides and edges of the core.

The neutron spectrum in the assembly was measured by the activation of manganese, gold, and indium foils and by determining the sub-cadmium fission fraction. The comparison of the calculated and measured neutron spectra at the center of the core is shown in Slide 5 (Fig. 3 of P/608).

The major discrepancy between theory and experiment is a somewhat greater experimental sub-cadmium flux.

Extensive experimental measurements were made of the neutron importance function—i.e., the iterated fission probability—for application to studies of the capture-to-fission ratio in U^{235} and Pu^{239}. The importance for low-energy neutrons may be obtained by comparing the reactivity coefficient of a resonance absorber such as gold with the number of absorptions in the foil as determined by activation techniques. To obtain the fast neutron importance function experimentally it is necessary to change the number of fast neutrons produced in the assembly without changing the number of thermal absorptions. One means of accomplishing this is a foil inversion technique in which two foils of fissionable material are first exposed between two foils of an absorber and then the foil stack is rearranged so that the fissionable foils are on the outside. The fast neutron importance is then proportional to change in reactivity caused by the inversion divided by the change in fission rate in the foils.

The experimental results for neutron importance and the calculated values at the center and edge of the SAPL V core are shown in Slide 6 (Figs. 3 and 4 of P/108). The values of F_L for thick gold foils are slightly smaller than those for the thin foils since in the former case more of the absorptions occur in the higher energy resonances. Note that the results are expressed in units of dollars, which represent the reactivity contribution of delayed neutrons. For SAPL V, calculations indicate that the dollar is 0.0087 in absolute units. This is about 12 per cent greater than the delayed neutron fraction of 0.0755 due to the lower energy of the delayed neutrons.

Another experimental test of the theoretical neutron importance calculations is the reactivity coefficient of U^{235} as a function of position in the core—i.e., the statistical weight of the fuel. In contrast to the situation in assemblies where a one-group theory is a good approximation, the statistical weight in SAPL V is not directly proportional to the square of the fission density. As in the case of the flux calculations, the agreement between calculated and measured statistical weights is as good as could be expected considering that the calculations were performed for a sphere.

After the investigations on SAPL V were concluded, some studies were undertaken on assemblies with considerably higher neutron spectra. One of the assemblies, known as PPA-11, had almost no beryllium in the core, but had a beryllium reflector. The critical mass was 124 kg of U^{235}. A multigroup calculation which was performed in spherical geometry gave a critical mass of about 113 kg. This is in good agreement with the experiment since the critical mass should be

Table 1. Criticality Results

Assembly	kg U^{235}	Core Be/U^{235} atomic ratio	Reflector	"Best" $\frac{k_{obs.}}{k_{calc.}}$
SAPL-PPA-5	58.1	33.8	Be	0.975 (a)
SAPL-PPA-11	123.7	1.74	Be	0.997 (b)
CA-1	18.08	390	—	1.044
CA-18	7.65	1560	—	1.030

(a) Geometrical error in $k_{calc.}$ could be $\sim+0.05$.
(b) Calculation for 114 kg U^{235} in sphere.

about 10 per cent larger in the actual hexagonal geometry than in the assumed spherical geometry.

The two final assemblies which I will mention were studied at Oak Ridge National Laboratory with the primary purpose of testing the agreement of theory and experiment for beryllium-moderated assemblies. The cores in these assemblies were approximately cubical in shape and there was no reflector. The experimental facilities were similar to those at the Knolls Atomic Power Laboratory except that the aluminum matrix tubes were square rather than round.

Slide 7 (Fig. 11 of P/602, Session 21A) shows the critical assembly at Oak Ridge. Some of the properties of these assemblies are shown in Table 1 on this page.

The Oak Ridge bare assemblies, known as CA-1 and CA-18, had low critical masses because of the large core dimensions.

The theoretical calculations referred to on the slides were performed at Oak Ridge by a simplified procedure which was made possible by the absence of a reflector. In this method the spatial flux distribution at each energy was assumed to consist of a single harmonic having an extrapolation distance proportional to the transport mean free path at the particular energy. Several different calculations were performed to investigate the effect of various factors on reactivity. It was found, for example, that self-shielding of the fuel elements decreases the reactivity by 1 per cent in CA-1 and 5 per cent in CA-18. The reflection of neutrons by the empty aluminium matrix tubes outside the core increases reactivity by about 4 per cent in the two assemblies. The Oak Ridge calculations indicated that the anisotropy in the beryllium scattering reduces reactivity by about 8 per cent. However, more recent calculations by Mr. Bulmer at the Knolls Atomic Power Laboratory give a lower correction for anisotropic scattering, i.e., 3½ per cent for CA-1.

With this smaller anisotropy correction, the best theoretical calculations give slightly too high a reactivity. This is in contrast to the earlier data for CA-1 presented in Table I, but is similar to our experience with calculations for water-moderated assemblies in which the calculated reactivity is also slightly too high. This is even more the case if the 5–10 per cent neutron multiplication in Be, mentioned by Sanders of the UK in Session 19A is correct. In any case, the agreement between theory and experiment is well within the limits which would be expected in view of the remaining uncertainties in the beryllium transport cross section, and cross section for Be(n,2n) reaction.

We have seen from the above discussion that the multigroup calculations based on the Fermi age-diffusion equation give descriptions of the properties of beryllium moderated assemblies with neutron spectra ranging from that of CA-18, which 85 per cent of the fissions are due to sub-cadmium neutrons, to that of SAPL PPA-11, in which 50 per cent of the fission is caused by neutrons above 125 kev. The theory not only provides good values of reactivity but also predicts the detailed features of neutron flux and adjoint function variation with position and energy. It may be anticipated that the correlation between theory and experiment will become still better as improved experimental information on the beryllium cross sections at high energy and the U^{235} resonance structure are utilized in the calculations. The multigroup technique, particularly when used in conjunction with high-speed digital computing machines, which can conveniently handle problems in more than one space dimension, is therefore an increasingly valuable tool for use in the design and analysis of nuclear reactors.

Mr. A. P. RUDIK (USSR) presented paper P/664 as follows: This paper deals with the application of the method of effective boundary conditions for calculating the critical dimensions of reactors.

In cases where the reactor dimensions are substantially greater than the neutron moderation length $\sqrt{\tau}$, the thermal-neutron density distribution $N(\vec{r})$ in a homogeneous multiplying medium may be described by the single-group equation:

$$\Delta N(\vec{r}) + \alpha^2 N(\vec{r}) = 0 \qquad (1)$$

where the Laplacian or buckling

$$\alpha^2 = \frac{k-1}{L^2 + k_\tau}$$

in which k is the multiplication factor and L the reactor diffusion length.

Equation 1 can be obtained most readily from the following equation for the thermal neutron density:

$$\Delta N(\vec{r}) - \frac{N(\vec{r})}{L^2} + \frac{k}{L^2}\int W(r,r')N(r')\,dr' = 0 \qquad (2)$$

where $W(r,r')$ is the probability that a fast neutron produced by thermal neutron capture at a point $\vec{r}'$ will be slowed down to thermal energy at a point $\vec{r}$.

In order to derive Equation 1 from Equation 2, we must note that the thermal-neutron density $N(\vec{r})$ changes substantially over distances of the order of the dimensions of the reactor, whereas the probability $W(r,r')$ changes substantially over distances of the order of $\sqrt{\tau}$. Taking advantage of this, we expand the integral $N(r')$ by the powers of the modulus $(r - r')$, restricting ourselves to 3 terms of the expansion.

Considering that the probability normalization

$$\int W(\vec{r},\vec{r}')\,d\vec{r}' = 1$$

and the definition of τ in terms of the square of the mean distance

$$= \tfrac{1}{6}\overline{r^2} = \tfrac{1}{2}\overline{x^2} = \tfrac{1}{2}\int W(r,r')(x - x')^2 \, dr'$$

we then arrive at Equation 1.

This result at once indicates that any deviations of the properties of the system from those given by Equation 1 will be substantial only close to the boundary between the multiplying medium and the reflector. It is therefore worth while to consider separately the area of the order of $\sqrt{\tau}$ close to the boundary between the multiplying medium and the reflector and by so doing establish an effective boundary condition such that Equation 1, taken in conjunction with this boundary condition, would give correct values for the critical dimensions and a correct neutron density distribution for the systems under consideration. Since the thickness of the layer which we are to consider is considerably less than the dimensions of the multiplying medium, we shall be able to arrive at the boundary condition by considering the neutron density distribution for a plane problem by the two-group theory.

Thus, the problem may be formulated as follows. The two-group theory is used to determine the thermal-neutron density distribution close to the boundary between the reflector and an infinite multiplying medium with properties that coincide with the properties of an actual system, but where the multiplication factor is equal to unity, $k = 1$. We then define the boundary condition

$$\lambda = -\left(\frac{1}{N}\frac{\partial N}{\partial x}\right)_{x=0}$$

where N is the neutron density in the multiplying medium, at a distance from the boundary line $x = 0$.

The thermal-neutron density distribution in the reactor and its critical dimensions are then found by solving Equation 1 with the boundary condition

$$\lambda = -\frac{1}{N}\frac{\partial N}{\partial \nu}$$

where ν is the normal to the surface of the multiplying medium. I shall not give the two-group theory equations and their solutions, as they are in the paper.

Since λ is known, the boundary conditions for the fundamental Equation 1 can be determined. Depending on the geometry, they have the following forms:

For plane geometry:

$$\lambda = -\frac{1}{N}\frac{\partial N}{\partial z}$$

For spherical geometry:

$$\lambda = -\left(\frac{1}{N}\frac{\partial (Nr)}{\partial r}\right)_{r=R}$$

where r is the radius of the sphere;

For cylindrical geometry:

$$\lambda = -\left(\frac{1}{N\sqrt{r}}\frac{\partial (N\sqrt{r})}{\partial r}\right)_{r=R}$$

where r is the radius of the cylinder.

By substituting (rN) and $\sqrt{rN}$ for N in the expressions for the boundary conditions for the sphere and the cylinder respectively, we can make an approximate correction for surface curvature.

By means of these boundary conditions, we arrive at the following characteristic equations for determining the critical size of the reactor:

1. Slab reactor $2H$ high with similar reflectors at its bases: $\alpha \tan \alpha H = \lambda$.
2. Spherical reactor of radius R: $\alpha \cot \alpha R = -\lambda$.
3. Cylindrical reactor of radius R:

$$\frac{\alpha J_1(\alpha R)}{J_0(\alpha R)} = \lambda + \frac{1}{2R}$$

where J_0 and J_1 are Bessel functions.

Let us consider in more detail the determination of the critical size of a cylindrical reactor surrounded on all sides by its reflector. We shall approach this by considering that the boundary condition at the surface of the side of the cylinder does not depend on density distribution along the height, and similarly for the boundary condition at the ends. We then have the following characteristic equations:

$$\frac{\alpha_z J_1(\alpha_z R)}{J_0(\alpha_z R)} = \lambda_r + \frac{1}{2R}$$

$$\alpha_z \tan \alpha_z H = \lambda_z, \qquad \alpha_z^2 + \alpha_r^2 = \alpha^2$$

where λ_r, λ_z are given. α^2 is also given, being determined by the properties of the system. By solving these equations, we can get R as a function of H, and hence, *inter alia*, determine the optimum shape for the cylindrical reactor from it.

The accuracy of this method of solving the problem can be substantially increased by taking into account the dependence of the boundary conditions at the lateral surface on the neutron density distribution along the height, i.e., on L_z^2, and on the boundary conditions at the ends, i.e. on α_r^2. This examination can easily be done under the two-group theory. λ_r is then a function of α_z, and λ_z is a function of α_r. Given the radius and height of the system we can then use the characteristic equations to express α_r as a function of α_z (from Equation 21 of P/664) and α_z as a function of α_r (from Equation 22 of P/664).

The intersection of these curves yields α^2, which is equivalent to the Laplacian describing the properties of the system. By interchanging R and N, a situation in which a given system will be critical can be achieved.

A comparison of the effective boundary conditions method with the accurate solution of the two-group equations shows that the error in the effective boundary conditions method does not exceed 5–10 per cent.

DISCUSSION OF P/608 AND P/664

Mr. H. Hurwitz (USA): Ideas similar to those which have been described by Mr. Rudik have been extensively applied in many laboratories. One of the most comprehensive investigations of reflector savings concepts was made by G. D. Volkoff of Canada. Particularly illuminating results have been obtained for

the situation in which the core is the same as the reflector except for the presence of fissionable material which is assumed to absorb only thermal neutrons. In this case, a spherical reactor with an infinite reflector is equivalent to a plane slab assembly with infinite reflector on both sides and a thickness equal to the sphere diameter, provided that the antisymmetrical solution for the flux in the slab is considered. Therefore, if the interaction between the opposite faces of the equivalent slab can be neglected, the reflector saving for the sphere is identical to that which exists in plane geometry. Under these assumptions it is possible to calculate the reflector savings by the Wiener-Hopf technique.

As I discussed in Session 20A, the reflector savings may then be expressed as an integral involving the Fourier transform of the slowing down density. The integral can be numerically evaluated if numerical results for the slowing down Fourier transform have been calculated. This procedure has been used in the theory of the water-moderated assemblies investigated by Callihan.

It is also possible to apply variational procedures to calculate the reflector savings. In this way, an accurate expression for the reflector savings can be obtained, which, when the buckling is small, involves only the first three moments of the kernel in a displacement-type integral equation which can be derived for the reactor power. These procedures have been discussed by Marshak and myself in the *Physical Review*.

I would like to ask one small question. In the cylindrical case, you have, in addition to λ, a term $1/R$ which is equal to the ratio of the vessel function. You have J_1/J_0 is $\lambda + 1/R$. Would this hold if you had just the one-velocity theory?

Mr. A. P. RUDIK (USSR): I did not quite understand the question as interpreted, so I would prefer to meet you in the corridor afterwards, where you will perhaps be able to clarify your question for me.

Mr. T. N. ZUBAREV (USSR) presented paper P/669.

Mr. A. P. RUDIK (USSR) presented papers P/649 and P/666. In connection with the former, he said: As is well known, resonance absorption in systems consisting of a mixture of uranium and moderator can be reduced by distributing the neutron-absorbing substance, i.e., the uranium, non-uniformly as concentrations or slugs separated by the moderator.

A substantial reduction in resonance absorption in heterogeneous systems, as compared with homogeneous systems with the same concentration ratio of uranium nuclei to moderator nuclei, is achieved when the following conditions exist simultaneously (it should be noted that neither of these is sufficient by itself). First, the neutron mean free path in the moderator cell must be much longer than the scattering length in the moderator, i.e., $L - \bar{l}\omega > \lambda_s$, where ω is the ratio of the volumes of moderator and uranium; under these conditions, a resonance-energy neutron which has escaped capture in one slug will reach the next uranium slug with its energy reduced below the resonance level. If this condition is not fulfilled, i.e., if there are a large number of uranium slugs on a single scattering length λ_s, the resonance absorption will be the same as for a homogeneous system. Secondly, the neutron mean free path in a slug must be considerably greater than the resonance absorption length for a neutron of energy E_0 in the uranium; i.e., $\bar{l} > \lambda_s(E_0)$.

Under this condition, the U^{238} atoms inside the slug are shielded and resonance absorption is reduced. If this condition is not fulfilled, i.e., if the slugs are transparent to neutrons, the resonance absorption is the same as for a homogeneous system, which means that it is proportional to the concentration in the specific case.

We shall determine resonance absorption in a heterogeneous system by making the following assumptions.

First, we shall consider that the resonance-neutron density per cell is constant. This condition is not essential, but it simplifies the calculations. We may note that the neutron density self-absorption for the slugs, which exists in reality results in the calculated resonance absorption in a constant field of neutrons being greater than the actual resonance absorption.

The assumption that the neutron density in each cell is constant is known to be fulfilled in the case where the average slug size is less than the neutron scattering length in the moderator. However, even in the case where the slug size is greater than the scattering length in the moderator, the resonance neutron field is only slightly disturbed if the neutron energy loss per collision is greater than the width of the danger-zone for resonance absorption.

Second, it is assumed that the length of the neutron free path in the slug coincides with the length in the absence of scattering. This is true in the case of small absorptions by particular levels.

We shall refer to slugs to which both assumptions apply as "small slugs."

In the case of small slugs, the resonance escape probability in the moderation process—ϕ—can be computed by the kinetic theory of gases, the uranium slugs themselves serving as "molecules."

The free path of a neutron of energy E in respect of capture in uranium slugs is:

$$\Lambda_c = \frac{L}{\zeta(E)}$$

where L is the neutron free path in respect of collision with uranium slugs, which is equal to: $L = \bar{l}\omega$ while $\zeta(E)$, the so-called "sticking probability" coefficient, the probability that the neutron will stick to the slug, is equal to:

$$\zeta(E) = \int (1 - e^{-\frac{l}{\lambda_s(E)}}) f(l)\, dl$$

where $f(l)$ is a function of the neutron path distribution in the slug. It is clear that the sticking probability coefficient depends on the shape of the uranium slugs.

By means of the quantities which have been intro-

duced, it is easy to determine the relative probability of neutron capture by a slug, $W(E)$, which can be represented in the following form:

$$W(E) = \frac{\frac{1}{\Lambda_c}}{\frac{1}{\Lambda_c} + \frac{1}{\lambda_s}} = \frac{\zeta(E)}{\zeta(E) + \frac{L}{\lambda_s}}$$

As is well known, the resonance escape probability, if close to unity, is related to the relative probability of neutron capture by the slug in the following way:

$$-\ln \phi = \frac{1}{\xi} \int W(E) \frac{dE}{E}$$

where ξ is the average logarithmic energy loss in the moderator.

As we have already noted, in the case of very small slugs the expression for ϕ gives the correct transition to the homogeneous case. It is interesting to observe that the transition to homogeneity takes place in the case of slugs with a size of $l \sim \lambda_s/\omega$, for which the self-shielding effect of the uranium may still be very strongly evident if the size of the slug is considerably larger than the resonance-neutron absorption free path in the uranium.

In the case of relatively large slugs, with which we are mainly concerned, the condition that applies is the reverse of that in which homogenization occurs, i.e., the slug size is considerably larger than the scattering free path in a moderator divided by ω: $l \gg \lambda_s/\omega$. In that case, we can neglect the sticking probability coefficient in the denominator of the expression for the probability of neutron capture by a slug, $W(E)$, so that the expression for $\ln \phi$ appears in the simple form

$$-\ln \phi = \frac{1}{\xi} \int \frac{\lambda_s}{L} \zeta(E) \frac{dE}{E}$$

This formula for resonance absorption is applicable to any absorption band structure.

We shall carry out a further analysis of ϕ by dividing the U^{238} levels into two groups. The first (lower) blocked group will include strong, not overlapping levels for which the resonance capture cross section is large, and the second, unblocked, group will consist of high levels (there may be many of them and they may overlap) for which the resonance cross sections are not large. We shall use the Breit-Wigner formula for the levels in the blocked group. We then obtain for ϕ the following general formula, which applies to slugs of any geometrical shape:

$$-\ln \phi = \frac{\lambda_s}{\xi L} \left[\sqrt{\pi N} \sqrt{l} \sum_{(i)} \frac{\sqrt{\sigma_{0i} \Gamma_i^2}}{E_{0i}} + N l \int_{(E)} \sigma'(E) \frac{dE}{E} \right]$$

where N is the number of U^{238} nuclei in 1 cm^3 of the uranium slug; σ_{0i} is the absorption cross section at the center of the level line i; Γ_i is the level line width, and E_{0i} is the energy of level i.

The first term of this formula represents the blocked absorption. The summation is done for each of the U^{238} resonance levels placed in the first group. This term depends on the geometrical shape of the slugs.

The second term of the formula represents unblocked absorption. It is integrated with respect to that portion of the energy spectrum in which the U^{238} resonance levels placed in the second group are distributed. This term is not dependent on the geometric shape of the slugs but depends only on the concentration of U^{238} nuclei in relation to the moderator nuclei.

Let us consider as an example an infinite uniform lattice made up of long cylindrical uranium rods of diameter α. The expression for ϕ in the case of a square lattice of mesh α then has the form:

$$-\ln \phi = \frac{\lambda_s}{\xi} \frac{\alpha d^{3/2} + \beta d^2}{\alpha^2 - \frac{\pi d^2}{4}}$$

where α and β are constants determined by the U^{238} levels. The expressions for α and β are set out in the printed text of this paper.

Let us now make allowance for the Doppler line-broadening effect. The Doppler broadening results in an increase in resonance absorption $(1 - \phi)$ and makes resonance absorption dependent on the temperature of the uranium. The Doppler effect has no influence on the unblocked portion of resonance absorption. This is because the unblocked portion of resonance absorption is determined by the sum of the areas of the levels, and these areas i.e., the integrals from the energy cross sections, do not depend on Doppler broadening.

On the other hand, the Doppler effect must not affect resonance capture due to the first levels of the blocked group. In the case of the lower levels, where the resonance absorption length is very short, almost all the neutrons in the energy interval, which is considerably greater than the Doppler width, "corroded out" of the neutron spectrum incident on the slug, and the absorption curve is therefore practically of the Breit-Wigner type. The Doppler effect can play a substantial part only in the case of relatively high blocked-group levels, i.e., for levels immediately adjoining the unblocked group.

Let us, therefore, divide the blocked resonance capture into two components. The first component will include absorption due to the lower U^{238} resonance levels. These are not influenced by the Doppler effect. The second component will consist of absorption due to the levels of intermediate energy with the Doppler form of resonance curve.

In our calculations we shall use the formula for Doppler broadening in a gas. By making the rough assumption that all levels of the second component of the blocked group have the pure Doppler form, we

obtain the following formula for resonance capture, taking the Doppler effect into account:

$$-\ln \phi = \frac{1}{\xi}\frac{\lambda_s}{L}\left[\sqrt{\pi N}\,\sqrt{\bar{l}}\sum_{(i)}\frac{\sqrt{\sigma_{0i}\Gamma_i^2}}{E_{0i}} + 2\sum_{(k)}\frac{\Delta_k}{E_{0k}}\sqrt{\ln\left(\frac{\sqrt{\pi}}{2}\cdot\frac{\Gamma_k}{\Delta}N\sigma_0\bar{l}\right)} + N\bar{l}\int_{(E)}\sigma\frac{dE}{E}\right]$$

The first and third terms in this formula describe the levels which do not change under the influence of the Doppler effect. The second term gives the blocked resonance absorption in the range of levels which show the Doppler form of resonance curve. Here, Δ is the Doppler width.

A quantitative examination of resonance capture by slugs, allowing for Doppler line broadening, was carried out by F. L. Shapiro. The results of his calculations are given in the printed text of the paper.

Finally, there is a brief observation on the allowance to be made for the influence on resonance absorption of neutron scattering by uranium in large slugs. The theory of this effect has been developed by A. D. Galanin. The fundamental purpose of these calculations was to delimit the field of application of the small-slug theory. It was established that the small-slug theory of resonance absorption remained applicable until the slug radii approached the order of magnitude of the scattering length in uranium, when the actual value for resonance absorption would be less than the value given by the small-slug theory.

Mr. O. GAMBA (Argentina) presented paper P/1003, concluding with the following remarks: It can be shown as the conclusion of these calculations that beryllium and beryllium oxide are materials of real value in natural-uranium nuclear reactor technology for use as moderator and/or reflector. The picture becomes even more favorable if you consider the figures for effective absorption cross sections mentioned by the Russian research workers, which are significantly less than the 9 and 9.2 millibarns used here. The prospects that they will be used are not, however, very bright. The importance of attaining high temperatures in power reactors is not of first priority in view of the low incidence of the fuel-cost component of the total cost per kilowatt-hour of nuclear electricity, unless the gas turbine should come to be used. Furthermore, the prices ruling at present for these materials do not favor their use in ordinary engineering. This is another of those cases in which the prospects of this new nuclear reactor technology are restricted by conventional technologies.

DISCUSSION OF P/669, P/649, P/666, AND P/1003

Mr. P. F. GAST (USA): A method for calculating heterogeneous reactors was developed by Dr. Horning and his calculations are reported in declassified report HW-34021. The equations which he developed are similar to those of Mr. Feinberg, with the following exceptions.

We have defined a parameter h, which is simply the relationship between the source and the sink; in other words, h is the number of fast neutrons produced in the fuel element for each thermal neutron and absorbed. In the case of a bare uranium rod, h becomes equivalent to $\eta\epsilon$, but with more complicated effects. For example, a uranium slug surrounded by cooling water and then a tube results in h being less than $\eta\epsilon$ because of the capture of the neutrons in these other materials. We have adopted the view that h is a characteristic of the entire fuel assembly and can be measured experimentally or calculated.

The other parameter is the parameter β defined by this equation, $Q = \beta\int J\,dS$, in which the sink of thermal neutrons is given as β times the integral of the neutrons incident over the surface of the fuel element. β has been given the name "blackness" in the United States because it represents the fraction of the incident neutrons which are absorbed. For the incident neutrons we have taken the standard form from diffusion theory, equal to the neutron flux ϕ divided by 4 plus the diffusion coefficient D divided by 2 times the normal gradient of the flux on the surface of the fuel assembly, $d\phi/dm$.

From this point on, the development of the equation is very similar to that of Dr. Feinberg.

I should like to say a little about the measurement, experimentally, of these parameters as it has been carried out. If one has a large rectangular stack of graphite in an artificial neutron source and measures the neutron distribution along the center of this pile, first, with just the source and the detectors present and, secondly, by inserting a fuel tube, the comparison of these two measurements will allow a determination of parameters h and β experimentally and then a check of the theory. We have repeated these measurements with two additional fuel tubes in central locations to find out whether, repeating the experiment, we get the same numbers h and β characteristic of the slug; and we do, in fact, get good agreement.

Similar parameters can be defined in the case of resonance absorption and determined by similar experiment in which, now, the detectors are covered with cadmium, so that only the resonance flux is measured.

We have made so far only one application of the method to an actual reactor. The reactor which I described yesterday in paper P/607 (Session 21A) was designed by using this type of method. Since this reactor has not yet gone critical, I am unable to report on the calculations. In the case of a simple cylindrical fuel element, the parameter β, the blackness, may be computed by the method developed by Stewart, which is also outlined in paper P/607.

The CHAIRMAN: We have another comment, on paper P/649.

Mr. L. M. BARKOV (USSR): I should like to speak briefly about the experimental work on the measurement of resonance absorption in uranium-graphite lattices.

M. B. Egizarov, V. C. Dikarev and V. G. Madeyev

have carried out a number of experiments on the uranium-graphite reactor of the Academy of Sciences of the USSR, to study resonance absorption in uranium cylindrical slugs as a function of slug diameter and temperature. The results of their work agree with those inferred from the theory of resonance absorption in heterogeneous systems developed by I. I. Gurevich and I. Y. Pomeranchouk.

In the neutron field of the reactor, between the two halves of the slug being investigated, which was surrounded by a cadmium shield, a thin uranium disc with a radius equal to that of the slug was irradiated. The β-activity of the uranium-239 accumulated in the uranium disc was taken as a measure of the quantity of resonance neutrons absorbed by the uranium-238.

The results of experiments with cylindrical slugs with a diameter of 5 to 0.045 cm definitely prove that the full resonance absorption consists of blocked and unblocked sections.

From these experiments, and also from measurements of the absolute value for resonance absorption probability for a single specific uranium-graphite lattice, the following semi-empirical formula was obtained for the dependence of resonance absorption probability on the lattice parameters:

$$-\ln \phi = \frac{\lambda_s}{\xi} \frac{0.357 \times D^{3/2} + 0.184 \times D^2}{S} \pm 5\%$$

which remains true for all diameters between 0.01 cm and 5 cm.

In this expression, λ_s/ξ represents the moderating characteristics, S the area of the moderator in the cell, and D the diameter of the slug.

The dependence of $-\ln \phi$ on the diameter of the slug and on the lattice spacing given by the semi-empirical formula was also confirmed by experiments to study resonance capture in heterogeneous systems with ordinary-water moderator, where the lattice spacing was identical with the diameter of the slug.

This semi-empirical formula of M. B. Egizarov is used in the Soviet Union to calculate the ϕ of uranium-graphite and uranium-water reactors.

The resonance absorption ϕ has also been studied by Barkov and Frank and their associates.

The temperature dependence has been studied by Egizarov and his associates and Frank and his associates.

All these experiments were described in detail by their authors at the session of the Academy of Sciences of the USSR devoted to the problems of the peaceful uses of atomic energy.

The CHAIRMAN: On the same paper on the theory of resonance absorption, we have a question from Mr. Spinrad.

Mr. B. I. SPINRAD (USA): I had two questions, but I believe the second one was just answered.

The first is that, inasmuch as the formulae used in calculating resonance escape for uranium systems differ between the Soviet Union and the United States and I am rather used to thinking in terms of the simple physical explanation of absorption on a surface with further absorption in a volume, I find it rather hard to get a physical picture for the surface term used in the Soviet Union, which is the square root of surface and mass—if I understood correctly. I was wondering if there is a simple physical picture which one might use to explain this term.

Mr. A. P. RUDIK (USSR): As far as I am concerned, this is the ordinary concept. I do not know how to explain it any more clearly. It is the same thing that occurs in optics in resonance line capture. It can all be looked up in the old but good book of B . . . .

Mr. E. P. WIGNER (USA): I think the main physical difference between the concepts used in the United States and those in the paper reported by Mr. Rudik is that the effect of the collision of the neutrons with the uranium atoms is disregarded in Mr. Pomeranchouk's paper. The collisions with the uranium atoms lead to a specific change in energy. These changes are very large as compared with the distance between the various resonances concerned, which are at high values. This is due to the fact which we consider absorption and not to the fact that Mr. Rudik described, namely, the thinness of the sample. The collision with the uranium atoms is significant, as is borne out by two experiments.

The first is a very old observation which prompted many of the investigations by Creutz, and it is the following. We had a uranium sphere and surrounded part of the uranium sphere with a cadmium absorber and we measured the activity of the uranium in the cadmium absorber. This activity depended on the thickness of the cadmium and it depended in such a way that when the cadmium absorber thickness was increased, the absorption also increased. This was soon attributed to the increased scattering within the uranium which caused energy changes and thus threw neutrons into resonance lines of the uranium.

The second observation was that made by Mitchell. Mitchell plotted the volume absorption as a function of the admixture of the uranium. He found, as has been reported, that as far as heavy water, carbon and bismuth were concerned—and I believe also heavier materials—that the absorption was a direct function of the scattering cross section also. You will remember the slide which I showed and that it extrapolated due to scattering cross section of 8.3 to the value observed for pure uranium?

I should mention perhaps that Mr. Shapiro told me yesterday that there are experiments carried out in the Soviet Union which directly contradict this observation. These experiments were carried out in the following way. A uranium tube was taken and put into a reactor and the resonance absorption of it was measured. Then, the uranium tube was filled with lead and the resonance absorption again was measured. The resonance absorption did not change. This shows that, according to this experiment, a good deal of scattering material introduced right at the center of the uranium did not change the resonance

absorption. There is, therefore, direct experimental conflict between the two measurements which, of course, I am unable to explain, not being able to repeat any of the experiments right now.

Mr. A. P. RUDIK (USSR): I am tremendously grateful to Mr. Wigner for his very interesting ideas on this subject. Nevertheless, we ourselves consider, on the basis of the experiments carried out in Kh . . . . Generally speaking, scattering by uranium influences resonance absorption only for higher levels, which affect only one-third of the total absorption. Attempts have been made to take the scattering into account, but this leads to very complicated calculations.

Mr. E. P. WIGNER (USA): I should mention perhaps that we are well aware of the significance of the higher levels. In fact, we attribute most of the resonance absorption to the higher levels. According to our views, the resonance absorption extends from the lowest level at 6 v to several thousand volts, and much of the absorption is caused at the higher levels. However, absorption at these higher levels is fundamentally influenced by the scattering of uranium which throws neutrons, originally between the levels, into the levels.

Mr. A. P. RUDIK (Union of Soviet Socialist Republics): In this connection I should like to mention briefly that we made attempts to elucidate the size of the blocked part of the resonance absorption using the experimental data for the U^{238} levels: the first three levels are quite sufficient for this purpose; evidently higher levels make some contribution to the unblocked part of the resonance absorption.

Mr. A. M. WEINBERG (USA): I should like to make a very brief comment with respect to paper P/669. I should simply like to state for the record the fact that calculations very similar to those reported by Mr. Zubarev were made in the United States by Professor Teller and Professor Christie in the early part of the war. I simply state this for the record.

Mr. D. V. BLOKHINTSEV (USSR) presented paper P/656.

Mr. L. TRLIFAJ (Czechoslovakia) presented paper P/796 as follows: The work of Davison and other authors has made us familiar with formulae for the extrapolation distance in the case of a non-absorbent medium as a function of the radius of the black body. We should therefore like to explain how these formulae can be adapted to allow for a weak absorption of neutrons in the medium. To do so rapidly and simply, we solved Milne's problem by means of the spherical harmonics method, and it proved possible to estimate the part played by absorption in the formula for the extrapolation distance.

I will now remind you of Milne's problem in neutron diffusion theory.

An infinite medium scatters neutrons isotropically but does not absorb them and does not change their energy. In the medium there is a black body which absorbs all the neutrons incident upon it. It is also assumed that there are no neutron sources in the medium but there is a constant flux density of neutrons which come in from infinity. Determine the neutron flux in this medium.

We are going to solve the problem for the case where the black body has the form of an infinite cylinder of radius a.

In subsequent calculations, however, we shall assume the further possibility that the infinite medium scatters neutrons with a cross section of

$$\Sigma_s\{1 + 3fP_1^0(\omega)\} \qquad \text{(I)}$$

which is dependent on the cosine of the neutron-scattering angle ω. The quantity f is known to be the mean cosine of the neutron-scattering angle and Σ_s is the macroscopic cross section for isotropic neutron scattering. We assume further that the medium absorbs neutrons with a cross-section of Σ_a, and from now on we shall use the expression $\alpha \equiv \Sigma_a/\Sigma_s$.

The cylindrical symmetry of the problem shows that the neutron distribution function in space and along their direction of constant velocity depends only on the distance ρ from the axis of the cylindrical black body. Of course, it also depends on the cosine of the angle formed by the neutron velocity vector $\vec{v}$ and the vector of the distance from the cylinder axis $\vec{\rho}$, and on the cosine of the angle ϕ between the plane of the vectors $\vec{v}$, $\vec{\rho}$ and the plane which is horizontal to the cylinder axis of the black body. We shall denote these cosines by the symbols θ and μ, and we can express them in cylindrical or orthogonal co-ordinates as follows:

$$\theta = \frac{(\vec{\rho}\vec{v})}{\rho v}, \qquad \mu = \frac{[\vec{\rho} \times \vec{v}]}{\rho v \sqrt{1-\theta^2}} \cdot \frac{\vec{z}}{|\vec{z}|}$$

$$= \frac{1}{v\sqrt{1-\theta^2}\cdot\rho}(xv_y - yv_x) = \cos\phi \qquad \text{(II)}$$

The ordinary Boltzmann equation, to which the function of the neutron distribution in the medium outside the black body is subordinate, will then be written as follows:

$$\theta\frac{\partial}{\partial\rho}\psi(\rho,\theta,\mu) + \frac{(1-\theta^2)\mu^2}{\rho}\cdot\frac{\partial}{\partial\theta}\psi(\rho,\theta,\mu)$$

$$- \frac{\theta\mu(1-\mu^2)}{\rho}\frac{\partial}{\partial\mu}\psi(\rho,\theta,\mu) + \Sigma_s(1+\alpha)\psi(\rho,\theta,\mu)$$

$$= \frac{\Sigma_s}{4\pi}\int_{-1}^{1}d\theta'\int_{-\pi}^{\pi}d\phi'\{1 + 3fP_1^0(\omega)\}\psi(\rho,\theta',\mu') \qquad \text{(III)}$$

A well-known method by which this equation can be solved is the spherical harmonics method. In our further calculations we shall use the approximation P_3 and therefore we shall write

$$\psi(\rho,\theta,\mu) = \psi_{00}(\rho)P_0^0(\theta) + \psi_{10}(\rho)P_1^0(\theta)$$

$$+ \psi_{20}(\rho)P_2^0(\theta) + \psi_{22}(\rho)P_2^2(\theta)(2\mu^2-1)$$

$$+ \psi_{30}(\rho)P_3^0(\theta) + \psi_{32}(\rho)P_3^2(\theta)(2\mu^2-1) \qquad \text{(IV)}$$

The selection of the even harmonics P_n^{2m} is indicated by the symmetry of the problem in relation to the plane which passes through the cylinder axis of the black body.

Differential Equation 3 then breaks down into a series of linear differential equations, Equations 5 in the text of the paper.

All neutrons incident on the black body are absorbed in it. Hence the resulting flux density of the neutrons emerging from the body into the scattering medium must be equal to zero. This boundary condition is well known and may be expressed by means of the transformation of Equation 4 in the form:

$$12\psi_{00}(a) + 8\psi_{10}(a) + 3\psi_{20}(a) = 0 \qquad (V)$$

We divided our further consideration of Equations 5 in the text and the equation we have just written into two cases. First, we wrote $\alpha = f = 0$, and in the second case we considered that the quantities α and f were small enough to enable us to use the perturbation theory. In practice, we encounter this case quite often.

In the case where $\alpha = f = 0$, it can easily be shown that the neutron flux density $j(\rho) = \text{const.}/\rho$. This expression governs the "non-uniform" part of the solution to Equations 5 in the text, while the uniform part of this solution corresponds to a specific problem of characteristic values. A more detailed solution of this is given in the text. The text in the paper also calculates the asymptotic extrapolation distance, the dependence of which on the radius of the cylinder a looks very similar to the corresponding graph of Davison.

The case where α and f are not equal to zero may also be solved quite similarly to the case where $\alpha = f = 0$. This method of calculation leads to the following result (we shall now denote the solution of Equations 5 in the text by the large Ψ):

$$\Psi_{n,m}(\rho) = \sum_{i=1,2} \sum_{(l)} \{a_i G_{nm}^{(l)}(|x_i|) K_l(|x_i|\rho) + f_i F_{nm}^{l}(|x_i|) I_l(|x_i|\rho)\} + H_{nm}(\rho) \qquad (VI)$$

where the symbol l of the summation $\sum_{(l)}$ passes through the values $l = 0.2$ when $n = 0.2$, $l = 1.3$ when $n = 1.3$. The quantities x_i are the roots of the quadratic equation:

$$9x - [27d(1 + d - f) + 35(1 + d)^2 + 28d(1 + d)]x^2 + 105d(1 + d)^2(1 + d - f) = 0 \qquad (VII)$$

The symbol $H_{nm}(\rho)$ represents the uniform part of the solution, which is similar in form to the part of solution (8) in the text which corresponds to the root $\lambda = \sqrt{7}$. In this case, however, the expression $\lambda = \sqrt{7}\,(1 + d)$ is the root, and there are two unknown constants corresponding to solutions with the Bessel functions K and I.

It is convenient to use the solution indicated in the case where the cylindrical body is semi-transparent to thermal neutrons or in calculating the reactor lattice. For the sake of brevity and simplicity of presentation, the text of the paper did not include this solution, but it is similar to the solution given by Tait, whose paper was presented at today's session.

The problem for α and f not equal to zero was solved in the text in a simpler way which completely answered the purpose we had set ourselves. We assumed that α and f were small quantities, and the results of the calculations made it clear that for practical purposes it is convenient to determine the extrapolation distance in a cylindrical black body by the formula

$$\alpha = \lambda(\Sigma_s a) \cdot 3D \qquad (VIII)$$

in which the value of the function $\lambda(\Sigma_s a)$ is determined by graph 2 of Davison's paper, and the diffusion coefficient in the medium under consideration, which is characterized by the cross sections Σ_s, Σ_a for neutrons and by the mean cosine of the neutron scattering angle f, appears as the quantity D. The coefficient D is determined for small values of α and f by the normal expression, which agrees with the determination of the diffusion coefficient in the book by Glasstone and Edlund, etc.

DISCUSSION OF P/656 AND P/796

Mr. H. HURWITZ (USA): I want to make a very minor point about the normalization of the adjoint functions which we use as compared to those described by you. You define your adjoint as the power resulting from the insertion of a neutron, whereas in some laboratories in the United States we define the adjoint as the number of resulting fissions per generation. The difference in the two normalizations is the reactor generation time. We use our normalization because it gives a dimensionless quantity for the adjoint function and does not introduce the ambiguity as to whether or not one considers the delayed neutrons in defining generation time.

Mr. D. V. BLOKHINTSEV (USSR) presented paper P/667.

DISCUSSION OF P/667

Mr. A. M. WEINBERG (USA): I would just like to say this. Mr. Blokhintsev seems to attribute some of this to Mr. Weinberg. I must correct him by saying that adjoints were introduced into the United States reactor calculations by our good friend Professor Wigner.

Mr. D. V. BLOKHINTSEV (USSR): I do not see that there is any disagreement between us, but certainly the way indicated by Mr. Gurevich and Mr. Weinberg is also possible.

Mr. A. M. WEINBERG (USA): I should say that in the published literature Mr. Wigner introduced adjoints in 1944. The first public disclosure was in the *Physical Review* in 1946 in a short statement by Professor Nordheim.

Mr. D. V. BLOKHINTSEV (USSR): We had known the adjoint equation for a long time, but came to ap-

preciate its value more recently, and in that connection the work done in the USA has been very important to us.

Mr. J. E. WILKINS, JR. (USA): I worked with Mr. Wigner during the war and had occasion to use some of this theory. As a mathematician, I was greatly interested in the proof of convergence that was given in section 4 of the paper. I made some arguments myself during the war but was always perplexed by the necessity of verifying that no eigenfunction can be orthogonal to its own adjoint eigenfunction. This proof usually follows from some sort of symmetry property of the operator. Do the authors possess any information on this point in the very general framework of their paper?

Mr. BLOKHINTSEV (USSR): I must say that I do not quite understand to which functions and equations you are referring.

Mr. J. E. WILKINS (USA): Perhaps we can discuss this privately. If you want a specific reference, it is to Equation 37 in the paper, where the coefficients involve the division of an integral which will vanish unless one can prove it does not vanish.

Mr. D. V. BLOKHINTSEV (USSR): I think it would be better to discuss this with the paper before us, and to discuss this privately.

PEACEFUL USES OF ATOMIC ENERGY:

Proceedings of the International Conference in Geneva, August 1955.

The following is a complete listing of the sixteen volumes which comprise this publication, together with the main subjects covered by each volume.

VOLUME 1

The World's Requirements for Energy: The Role of Nuclear Power

World Energy Needs
Capital Investment Required for Nuclear Energy
The Role of Thorium
The Role of Nuclear Power in the Next 50 Years
Education and Training of Personnel in Nuclear Energy
Economics of Nuclear Power

VOLUME 2

Physics, Research Reactors

Special Topics in Nuclear Physics
Fission Physics
Research Reactors
Research Reactors and Descriptions

VOLUME 3

Power Reactors

Experience with Nuclear Power Plants
Fuel Cycles
Design of Reactors for Power Production
Power Reactors, Prototypes

VOLUME 4

Cross-Sections Important to Reactor Design

Equipment and Techniques Used in Measuring Cross-Sections Important to Reactor Design
Cross-Sections of Non-Fissionable Materials: Delayed Neutrons
Cross-Sections of Fissionable Materials
Properties of Fissionable Materials

VOLUME 5

Physics of Reactor Design

Integral Measurements
Resonance Integrals
Fission Product Poisoning
Criticality in Solutions
Zero Energy and Exponential Experiments
Zero Energy Experiments on Fast Reactors and Reactor Kinetics
Reactor Theory

VOLUME 6

Geology of Uranium and Thorium

Occurrence of Uranium and Thorium
Prospecting for Uranium and Thorium

VOLUME 7

Nuclear Chemistry and the Effects of Irradiation

The Fission Process
Facilities for Handling Highly Radioactive Materials
Chemistry of Fission Products
Heavy Element Chemistry
Effects of Radiation on Reactor Materials
Effects of Radiation on Liquids
Effects of Radiation on Solids

VOLUME 8

Production Technology of the Materials Used for Nuclear Energy

Treatment of Uranium and Thorium Ores and Ore Concentrates
Production of Metallic Uranium and Thorium
Analytical Methods in Raw Material Production
Production Technology of Special Materials

VOLUME 9

Reactor Technology and Chemical Processing

Waste Disposal Problems
Metallurgy of Thorium, Uranium and their Alloys
Fabrication of Fuel Elements
Liquid Metal Technology
Chemical Aspects of Nuclear Reactors
Chemical Processing of Irradiated Fuel Elements
Waste Treatment and Disposal
Separation and Storage of Fission Products

VOLUME 10

Radioactive Isotopes and Nuclear Radiations in Medicine

Isotopes in Medicine and Biology
Therapy
Diagnosis and Studies of Disease

VOLUME 11

Biological Effects of Radiation

Modes of Radiation Injury and Radiation Hazards
Mechanisms of Radiation Injury
Protection and Recovery
Genetic Effects
Human Implications

VOLUME 12

Radioactive Isotopes and Ionizing Radiations in Agriculture, Physiology, and Biochemistry

Isotopes in Agriculture
Radiation-induced Genetic Changes and Crop Improvement
Tracer Studies in Agriculture
Animal Physiology
Plant Biochemistry
General Biochemistry

VOLUME 13

Legal, Administrative, Health and Safety Aspects of Large-Scale Use of Nuclear Energy

Legal and Administrative Problems
Reactor Safety and Location of Power Reactors
Safety Standards and Health Aspects of Large-Scale Use of Atomic Energy

VOLUME 14

General Aspects of the Use of Radioactive Isotopes: Dosimetry

Isotopes in Technology and Industry
General Uses, Production and Handling of Radioactive Isotopes
Dosimetry

VOLUME 15

Applications of Radioactive Isotopes and Fission Products in Research and Industry

Radioactive Isotopes in Research
Radioactive Isotopes in Control and Technology
Fission Products and their Applications

VOLUME 16

Record of the Conference

Opening of the Conference and the Presidential Address
International Co-operation in the Peaceful Uses of Atomic Energy
Closing Presidential Address
Evening Lectures
Author Index and Paper Index

SALES AGENTS FOR UNITED NATIONS PUBLICATIONS

ARGENTINA
Editorial Sudamericana S.A., Alsina 500, Buenos Aires.

AUSTRALIA
H. A. Goddard, 255a George St., Sydney; 90 Queen St., Melbourne.
Melbourne University Press, Carlton N.3, Victoria.

AUSTRIA
B. Wüllerstorff, Markus Sittikusstrasse 10, Salzburg.
Gerold & Co., Graben 31, Wien.

BELGIUM
Agence et Messageries de la Presse S.A., 14-22 rue du Persil, Bruxelles.
W. H. Smith & Son, 71-75, boulevard Adolphe-Max, Bruxelles.

BOLIVIA
Librería Selecciones, Casilla 972, La Paz.

BRAZIL
Livraria Agir, Rio de Janeiro, Sao Paulo and Belo Horizonte.

CAMBODIA
Papeterie-Librairie Nouvelle, Albert Portail, 14 Avenue Boulloche, Pnom-Penh.

CANADA
Ryerson Press, 299 Queen St. West, Toronto.
Periodica, Inc., 5112 Ave. Papineau, Montreal.

CEYLON
Lake House Bookshop, The Associated Newspapers of Ceylon, Ltd., P. O. Box 244, Colombo.

CHILE
Librería Ivens, Casilla 205, Santiago.
Editorial del Pacífico, Ahumada 57, Santiago.

CHINA
The World Book Co., Ltd., 99 Chungking Road, 1st Section, Taipeh, Taiwan.
Commercial Press, 211 Honan Rd., Shanghai.

COLOMBIA
Librería América, Medellín.
Librería Nacional Ltda., Barranquilla.
Librería Buchholz Galería, Bogotá.

COSTA RICA
Trejos Hermanos, Apartado 1313, San José.

CUBA
La Casa Belga, O'Reilly 455, La Habana.

CZECHOSLOVAKIA
Ceskoslovensky Spisovatel, Národní Trída 9, Praha 1.

DENMARK
Einar Munksgaard, Ltd., Norregade 6, Kobenhavn, K.

DOMINICAN REPUBLIC
Librería Dominicana, Mercedes 49, Ciudad Trujillo.

ECUADOR
Librería Científica, Guayaquil and Quito.

EGYPT
Librarie "La Renaissance d'Egypte," 9 Sh. Adly Pasha, Cairo.

EL SALVADOR
Manuel Navas y Cía., 1a. Avenida sur 37, San Salvador.

FINLAND
Akateeminen Kirjakauppa, 2 Keskuskatu, Helsinki.

FRANCE
Editons A. Pedone, 13, rue Soufflot, Paris V.

GERMANY
Elwert & Meurer, Hauptstrasse 101, Berlin-Schoneberg.
W. E. Saarbach, Gereonstrasse 25-29, Köln (22c).
Alexander Horn, Spiegelgasse 9, Wiesbaden.

GREECE
Kauffmann Bookshop, 28 Stadion Street, Athens.

HAITI
Librairie "A la Caravelle," Boîte postale 111-B, Port-au-Prince.

HONDURAS
Librería Panamericana, Tegucigalpa.

HONG KONG
The Swindon Book Co., 25 Nathan Road, Kowloon.

ICELAND
Bokaverzlun Sigfusar Eymundssonar H. F., Austurstraeti 18, Reykjavik.

INDIA
Orient Longmans, Calcutta, Bombay, and Madras.
Oxford Book & Stationery Co., New Delhi and Calcutta.
P. Varadachary & Co., Madras.

INDONESIA
Pembangunan, Ltd., Gunung Sahari 84, Djakarta.

IRAN
"Guity", 482 Avenue Ferdowsi, Teheran.

IRAQ
Mackenzie's Bookshop, Baghdad.

ISRAEL
Blumstein's Bookstores Ltd., 35 Allenby Road, Tel-Aviv.

ITALY
Librería Commissionaria Sansoni, Via Gina Capponi 26, Firenze.

JAPAN
Maruzen Company, Ltd., 6 Tori-Nichome, Nihonbashi, Tokyo.

LEBANON
Librairie Universelle, Beyrouth.

LIBERIA
J. Momolu Kamara, Monrovia.

LUXEMBOURG
Librairie J. Schummer, Luxembourg.

MEXICO
Editorial Hermes S.A., Ignacio Mariscal 41, México, D.F.

NETHERLANDS
N.V. Martinus Nijhoff, Lange Voorhout 9, 's-Gravenhage.

NEW ZEALAND
United Nations Association of New Zealand, C.P.O. 1011, Wellington.

NORWAY
Johan Grundt Tanum Forlag, Kr. Augustsgt. 7A, Oslo.

PAKISTAN
Thomas & Thomas, Karachi.
Publishers United Ltd., Lahore.
The Pakistan Cooperative Book Society, Dacca and Chittagong (East Pak.).

PANAMA
José Menéndez, Plaza de Arango, Panamá.

PARAGUAY
Agencia de Librerías de Salvador Nizza, Calle Pte. Franco No. 39-43, Asunción.

PERU
Librería Internacional del Peru, S. A., Lima and Arequipa.

PHILIPPINES
Alemar's Book Store, 749 Rizal Avenue, Manila.

PORTUGAL
Livraria Rodrigues, 186 Rua Aurea, Lisboa.

SINGAPORE
The City Book Store, Ltd., Winchester House, Collyer Quay.

SPAIN
Librería Bosch, 11 Ronda Universidad, Barcelona.
Librería Mundi-Prensa, Lagasca 38, Madrid.

SWEDEN
C. E. Fritze's Kungl. Hovbokhandel A-B, Fredsgatan 2, Stockholm.

SWITZERLAND
Librairie Payot S.A., Lausanne, Genève.
Hans Raunhardt, Kirchgasse 17, Zurich 1.

SYRIA
Librairie Universelle, Damas.

THAILAND
Pramuan Mit Ltd., 55 Chakrawat Road, Wat Tuk, Bangkok.

TURKEY
Librairie Hachette, 469 Istiklal Caddesi, Beyoglu, Istanbul.

UNION OF SOUTH AFRICA
Van Schaik's Bookstore (Pty.), Ltd., Box 724, Pretoria.

UNITED KINGDOM
H.M. Stationery Office, P. O. Box 569, London, S.E. 1 (and at H.M.S.O. Shops).

UNITED STATES OF AMERICA
International Documents Service, Columbia University Press, 2960 Broadway, New York 27, N. Y.

URUGUAY
Representación de Editoriales, Prof. H. D'Elía, Av. 18 de Julio 1333, Montevideo.

VENEZUELA
Librería del Este, Av. Miranda No. 52, Edf. Galipan, Caracas.

VIET-NAM
Papeterie-Librairie Nouvelle, Albert Portail, Boîte Postale 283, Saigon.

YUGOSLAVIA
Drzavno Preduzece, Jugoslovenska Knjiga, Terazije 27/11, Beograd.
Cankarjeva Zalozba, Ljubljana, Slovenia.

Orders and inquiries from countries where sales agents have not yet been appointed may be sent to: Sales and Circulation Section, United Nations, New York, U.S.A.; or Sales Section, United Nations, Palais des Nations, Geneva, Switzerland.